Application of the Monooxygenase Enzymes CYP101B1 and CYP101C1 from *Novosphingobium aromaticivorans* for Selective and Efficient Functionalisation of Inert C-H bonds

Md Raihan Sarkar

A Thesis Submitted in Fulfilment of the Requirements
for the Degree of Doctor of Philosophy
30th May 2019

Supervisor: Assoc. Prof. Stephen G. Bell

Department of Chemistry
The University of Adelaide
North Terrace Campus
Adelaide, South Australia 5005

Contents

Abstract ..... **XVI**
Statement of Originality ..... **XVIII**
Acknowledgements ..... **XIX**
Abbreviations ..... **XX**

Chapter 1 ..... **1**
1. Introduction **1**
1.1. General Overview of Cytochrome P450s 1
1.2. The Catalytic Cycle of Cytochrome P450s 3
1.3. Mechanistic Probes of Cytochrome P450s 9
1.4. Applications of Cytochrome P450s 12
1.5. P450 Enzymes from *Novosphingobium aromaticivorans* 19
1.6. Thesis Aims 23

Chapter 2 ..... **25**
2. Experimental **25**
2.1. General 25
2.2. Media Solution 25
2.3. Enzyme Purification 28
2.3.1. Purification of CYP101B1 and CYP101C1 28
2.3.2. Carbon Monoxide Binding Assays of Purified P450 and Mutant P450 29
2.3.3. Purification of Ferredoxin Reductase (ArR) 29
2.3.4. Purification of Ferredoxin (Arx) 30
2.4. Whole-cell Biotransformation 31
2.5. Spin-state Shift 32
2.6. Substrate Binding Assays 33
2.7. *In Vitro* NADH Turnover Assays 34
2.8. Hydrogen Peroxide Assays 35
2.9. Synthesis of Ester Substrates 36

Chapter 3 ..... **39**

3. Biocatalytic Oxidation of Saturated Hydrocarbons by CYP101B1 and CYP101C1 ..... **39**

3.1. Introduction 39

3.2. Results 41

3.3. Discussion 113

Chapter 4 ..... **116**

4. The Selective and Efficient Biocatalytic Oxidation of Unactivated C-H Bonds of Adamantyl Derivatives **116**

4.1. Introduction 116

4.2. Results 116

4.3. Discussion 142

Chapter 5 ..... **145**

5. The Efficient Oxidation of Hydrophobic Aromatic Substrates Using Site-directed Mutagenesis of CYP101B1 ..... **145**

5.1. Introduction 145

5.2. Protein Engineering 145

5.3. Results 147

5.4. Discussion 197

Chapter 6 ..... **200**

6. The Selective Oxidation of Alkyl-Substituted Cubanes Using CYP101B1 ..... **200**

6.1. Introduction 200

6.2. Results 205

6.3. Discussion 217

Chapter 7 ..... **221**

7. Futile Redox Cycling in Cytochrome P450 Electron Transfer Systems Induced by Oxygenated Aromatics **221**

7.1. Introduction 221

7.2. Results 223

7.3. Discussion 240

Chapter 8 Conclusion and Future Direction.....243

Chapter 9 References.....249

List of Publications Arising From This Thesis……...508

Figures

Figure 1. 1 UV-Vis absorbance spectrum of the ferric resting state of a P450 enzyme 1
Figure 1. 2 A selection of reactions catalysed by cytochrome P450 enzymes. 3
Figure 1. 3 The catalytic cycle of cytochrome P450 enzymes.....5
Figure 1. 4 UV-Vis absorbance spectrum of the P450 enzyme upon substrate binding.....6
Figure 1. 5 Example of the different types of electron transfer proteins. 7
Figure 1. 6 The insertion and radical rebound mechanisms of P450-mediated hydroxylation reactions 9
Figure 1. 7 Several pathways for cyclohexene oxidation by an oxoiron (1V) species 10
Figure 1. 8 Proposed hydroxylation via the P450 hydroperoxo-iron species 11
Figure 1. 9 P450s catalysed the metabolism of progesterone and vitamin D_3.....13
Figure 1. 10 Different chemical approaches to activate inert C-H bonds.....14
Figure 1. 11 P450 mediated selective oxidation of different substrates 15
Figure 1. 12 The activities of wild-type CYP101D1 and CYP101A1 which have been improved by protein engineering 16
Figure 1. 13 P450 activity has been improved through using type II P450 ligands. 17
Figure 1. 14 Drug metabolites which have been synthesised in larger yield using different P450s to assess toxicity and biological activity. 18
Figure 1. 15 Enzymatic regeneration of expensive redox cofactor.....19
Figure 1. 16 The products reported from camphor oxidation by CYP101D1, CYP101D2, CYP101A1 and CYP101B1.....20
Figure 1. 17 CYP101B1 catalysed the oxidation of different class of substrates. 21
Figure 1. 18 Oxidation of aromatic substrates by CYP101B1.....22
Figure 1. 19 Oxidation of *β*-ionone by CYP101C1. 22

Figure 2. 1 An example of ferrous-carbon monoxide assay of purified P450s. 29
Figure 2. 2 The spin-state shifts of CYP101A1 ($P450_{cam}$) induced by camphor.. 32
Figure 2. 3 The *in vitro* turnover of CYP101B1 with cyclooctyl acetate 34
Figure 2. 4 The synthesis of ester derivatives.....37

Figure 3. 1 The cyclic compounds screened with CYP101B1 and CYP101C1……. 41
Figure 3. 2 The spin-state shifts of CYP101B1 after addition of cyclic alkanes 43
Figure 3. 3 Dissociation constant analysis with cyclooctane.....44
Figure 3. 4 GC analysis of the turnover of cyclohexane by CYP101B1 47

Figure 3. 5 ^{13}C NMR of a mixture of 1,7-cyclododecanediol, 1,6-cyclododecanediol and an unknown metabolite. 48
Figure 3. 6 GC-MS analysis of cyclododecane *in vitro* turnovers by CYP101B1 50
Figure 3. 7 The overall product formation rates of CYP101B1 and CYP101C1 with cyclic alkanes and alcohols. 51
Figure 3. 8 The spin-state shifts of CYP101B1 after addition of cyclooctanone and cyclononanone.. 52
Figure 3. 9 GC-MS analyses of the *in vitro* turnovers of cyclononanone by CYP101B1 and CYP101C1.. 55
Figure 3. 10 ^{1}H NMR of 2-hydroxycyclononanone 56
Figure 3. 11 The spin-state shift of CYP101B1 after addition of cyclodecanone. 57
Figure 3. 12 GC-FID analyses of the *in vitro* turnovers of cyclodecanone by CYP101B1 and CYP101C1.. 58
Figure 3. 13 ^{1}H NMR of 2-hydroxycyclodecanone 61
Figure 3. 14 The spin-state shift of CYP101B1 after addition of cycloundecanone. 62
Figure 3. 15 GC-MS analysis of the *in vitro* turnover of cycloundecanone by CYP101B1 and CYP101C1. 63
Figure 3. 16 ^{1}H NMR of 2-hydroxycycloundecanone 65
Figure 3. 17 The spin-state shift of CYP101B1 after addition of cyclododecanone. 66
Figure 3. 18 GC-MS analyses of the *in vitro* turnovers of cyclododecanone by CYP101B1 and CYP101C1 67
Figure 3. 19 ^{1}H NMR of 2-hydroxycyclododecanone. 69
Figure 3. 20 The spin-state shift of CYP101B1 after addition of cyclopentadecanone. 70
Figure 3. 21 GC-MS analysis of the *in vitro* turnover of cyclopentadecanone by CYP101B1 and CYP101C1 71
Figure 3. 22 ^{1}H NMR of 8-hydroxycyclopentadecanone 73
Figure 3. 23 An overview of product formation rates of CYP101B1 and CYP101C1 with cycloalkanones. 74
Figure 3. 24 Substrates with ester directing groups were screened with both enzymes. 75
Figure 3. 25 The spin-state shift of CYP101B1 after addition of cyclohexyl acetate. 77
Figure 3. 26 GC-MS analysis of the turnover of cyclohexyl acetate by CYP101B1.. 77
Figure 3. 27 ^{1}H NMR of *trans*-4-hydroxycyclohexyl acetate. 78
Figure 3. 28 The spin-state shift of CYP101B1 after addition of cyclohexyl butyrate. 80
Figure 3. 29 GC-MS analysis of turnover of cyclohexyl butyrate by CYP101B1.. 81

Figure 3. 30 The spin-state shift of CYP101B1 after addition of cyclohexyl isobutyrate.....82
Figure 3. 31 GC-MS analysis of turnover of cyclohexyl isobutyrate by CYP101B1.....83
Figure 3. 32 The spin-state shift of CYP101B1 after addition of 4-*tert*-butylcyclohexyl acetate.. 84
Figure 3. 33 GC analysis of the *in vitro* turnover of 4-*tert*-butylcyclohexyl acetate (*cis* and *trans* mixture) by CYP101B1. 85
Figure 3. 34 The spin-state shift of CYP101B1 after addition of methylcyclohexyl acetate. 87
Figure 3. 35 GC analyses of *in vitro* turnovers of methylcyclohexyl acetate by CYP101B1 and CYP101C1. 88
Figure 3. 36 ^{1}H-^{1}H ROESY NMR of methyl-2-*(trans*-4-hydroxycyclohexyl)acetate.....89
Figure 3. 37 The spin-state shift of CYP101B1 after addition of ethylcyclohexyl acetate. ...90
Figure 3. 38 GC analyses of the *in vitro* turnovers of ethylcyclohexyl acetate by CYP101B1 and CYP101C1. 91
Figure 3. 39 ^{1}H and ^{13}C NMR of ethyl-*trans*-2-(4-hydroxycyclohexyl)acetate. 92
Figure 3. 40 ROESY NMR of ethyl-*trans*-2-(4-hydroxycyclohexyl)acetate. 93
Figure 3. 41 The spin-state shifts of CYP101B1 with cyclooctyl acetate. 94
Figure 3. 42 GC-MS analysis of *in vitro* turnover of cyclooctyl acetate by CYP101B1 and CYP101C1.. 95
Figure 3. 43 ^{1}H NMR of 5-hydroxycyclooctyl acetate. 96
Figure 3. 44 GC-MS analyses of the *in vitro* turnovers of cyclooctyl isobutyrate by CYP101B1 and CYP101C1. 97
Figure 3. 45 ^{1}H NMR of 5-hydroxycyclooctyl isobutyrate 98
Figure 3. 46 The spin-state shift of CYP101B1 after addition of cyclododecyl acetate.....99
Figure 3. 47 GC-MS analyses of *in vitro* turnovers of cyclododecyl acetate by CYP101B1 and CYP101C1. 100
Figure 3. 48 ^{1}H NMR of 7-hydroxycyclododecyl acetate 101
Figure 3. 49 GC analysis of the *in vitro* turnover of *α*-terpinyl acetate by CYP101B1 and CYP101C1.. 103
Figure 3. 50 ^{1}H NMR of the 3-cyclohexene-1-methanol, 5-hydroxy-*α*,*α*,4-trimethyl-, *α*-acetate.. 103
Figure 3. 51 The linear alkyl ketones and esters which were screened with CYP101B1 and CYP101C1. 105
Figure 3. 52 The spin-state shifts of CYP101B1 after addition of 2-nonanone and 2-undecanone. 106

Figure 3. 53 GC-MS analyses of *in vitro* turnovers of 2-nonanone by CYP101B1. 108
Figure 3. 54 GC analyses of *in vitro* turnovers of 2-undecanone by CYP101B1.....110
Figure 3. 55 *In vitro* turnover of citronellyl acetate by CYP101B1 and CYP101C1 coeluted with a synthesised epoxide in GC.....111
Figure 3. 56 GC-MS analysis of *in vitro* turnover of linalyl acetate by CYP101C1.....112
Figure 3. 57 An overview of Product formation rates (PFR) of CYP101B1 and CYP101C1 with best substrates investigated in this chapter 114

Figure 4. 1 The adamantane substrates screened with CYP101B1…….. 117
Figure 4. 2 The products formed from CYP101B1 turnovers of adamantane, adamantanols and 2-adamantanone 119
Figure 4. 3 Spin-state shifts and dissociation constants of CYP101B1 with 1-adamantyl methyl ketone and methyl-2-(1-adamantyl acetate).....120
Figure 4. 4 GC-MS analysis of the *in vitro* turnover of 1-adamantylmethyl ketone by CYP101B1.. 123
Figure 4. 5 ^{1}H NMR of *trans*-4-hydroxy-1-adamantylmethyl ketone 124
Figure 4. 6 ^{1}H NMR of methyl-2-(*trans*-4-hydroxy-1-adamantyl) acetate.. 125
Figure 4. 7 The products generated from CYP101B1 turnovers of 1-adamantylmethyl ketone and methyl-2-(1-adamantyl) acetate 126
Figure 4. 8 Spin-state shifts of CYP101B1 after addition of 1-adamantyl acetate.....127
Figure 4. 9 GC-MS analysis of the *in vitro* and whole-cell turnovers of 1-adamantyl acetate by CYP101B1. 128
Figure 4. 10 ^{1}H NMR of *trans*-4-hydroxy-1-adamantyl acetate.....129
Figure 4. 11 GC-MS analyses of the *in vitro* and whole-cell turnovers of 1-adamantyl isobutyrate by CYP101B1. 130
Figure 4. 12 ^{1}H NMR of *trans*-4-hydroxy-1-adamantyl isobutyrate. 131
Figure 4. 13 The metabolites generated from CYP101B1 turnovers of 1-adamantyl acetate and 1-adamantyl isobutyrate.....132
Figure 4. 14 Spin-state shifts of CYP101B1 after addition of 2-adamantyl acetate and 2-adamantyl isobutyrate.. 133
Figure 4. 15 GC-MS analysis of the *in vitro* and whole-cell turnovers of 2-adamantyl acetate by CYP101B1. 134
Figure 4. 16 ^{1}H NMR of 5-hydroxy-2-adamantyl acetate. 135

Figure 4. 17 GC-MS analysis of the *in vitro* and whole-cell turnovers of 2-adamantyl isobutyrate by CYP101B1 136
Figure 4. 18 The products formed from CYP101B1 turnovers of 2-adamantyl acetate and 2-adamantyl isobutyrate. 137
Figure 4. 19 ^{1}H NMR of 5-hydroxy-2-adamantyl isobutyrate. 137
Figure 4. 20 Spin-state shifts of CYP101B1 after addition of 1-adamantylamine and N-(1-adamantyl)acetamide 138
Figure 4. 21 GC-MS analysis of the turnover of 1-adamantylamine by CYP101B1. 140
Figure 4. 22 ^{1}H NMR of 4-hydroxy-N-(1-adamantyl)acetamide.. 141
Figure 4. 23 The products formed from turnovers of N-(1 adamantyl)acetamide. 142

Figure 5. 1 The crystal structure of camphor bound CYP101D1 146
Figure 5. 2 Spin-state shifts of CYP101B1 after addition of *β*-ionone 147
Figure 5. 3 GC-MS analysis of the turnover of *β*-ionone by H85F CYP101B1 149
Figure 5. 4 GC-MS analysis of the turnover of *p*-cymene by H85F CYP101B1 150
Figure 5. 5 The substrates screened with WT CYP101B1 and H85F CYP101B1 151
Figure 5. 6 Spin-state shifts of H85F and WT CYP101B1 after addition of toluene. 152
Figure 5. 7 GC analyses of the turnovers of toluene by H85F CYP101B1 and CYP101B1..152
Figure 5. 8 Spin-state shifts of H85F CYP101B1 after addition of *p*-xylene. 153
Figure 5. 9 The products identified from the WT CYP101B1 and H85F CYP101B1 turnovers with toluene. 154
Figure 5. 10 GC-MS analysis of the turnover of *o*-xylene by H85F and WT CYP101B1 ..155
Figure 5. 11 Spin-state shifts of H85F CYP101B1 and WT CYP101B1 after addition of ethylbenzene. 156
Figure 5. 12 GC-MS analysis of the turnover of ethylbenzene by CYP101B1 157
Figure 5. 13 Spin-state shifts of H85F CYP101B1 and WT CYP101B1 upon addition of 2-ethyltoluene. 159
Figure 5. 14 GC-MS analyses of the turnovers of 2-ethyltoluene by H85F CYP101B1 and CYP101B1. 159
Figure 5. 15 ^{1}H NMR of (2-ethylphenyl)methanol. 160
Figure 5. 16 The products identified from the CYP101B1 and H85F CYP101B1 turnovers of ethylbenzene, 2-ethyltoluene and 3-ethyltoluene 160
Figure 5. 17 Spin-state shifts of H85F CYP101B1 and WT CYP101B1 upon addition of 3-ethyltoluene. 161

Figure 5. 18 GC-MS analyses of the turnovers of 3-ethyltoluene by H85F CYP101B1 and CYP101B1 162
Figure 5. 19 ^{1}H NMR of 1-(3-methylphenyl)ethanol. 163
Figure 5. 20 Spin-state shifts of H85F CYP101B1 and WT CYP101B1 after addition of *n*-propylbenzene.. 164
Figure 5. 21 GC analyses of the turnovers of *n*-propylbenzene by H85F CYP101B1 and CYP101B1 166
Figure 5. 22 Spin-state shifts of H85F CYP101B1 and WT CYP101B1 upon addition of isopropylbenzene. 167
Figure 5. 23 Spin-state shifts of H85F CYP101B1 and WT CYP101B1 upon addition of isobutylbenzene. 168
Figure 5. 24 GC-MS analyses of the turnovers of isobutylbenzene by H85F CYP101B1 and WT CYP101B1 169
Figure 5. 25 The products identified from the CYP101B1 and H85F CYP101B1 turnovers of isopropylbenzene and isobutylbenzene.....169
Figure 5. 26 Spin-state shifts of H85F and WT CYP101B1 after addition of indane. 170
Figure 5. 27 GC analysis of the *in vitro* turnover of indane by H85F CYP101B1 and CYP101B1. 171
Figure 5. 28 Spin-state shifts of H85F CYP101B1 and WT CYP101B1. 172
Figure 5. 29 GC-MS analysis of the turnover of styrene by H85F and WT CYP101B1 173
Figure 5. 30 Dissociation constant analyses of 2-methylstyrene H85F variant. 174
Figure 5. 31 GC-MS analyses of the turnover of 2-methylstyrene by H85F CYP101B1 and CYP101B1. 175
Figure 5. 32 GC-MS analyses of the turnovers of *β*-methylstyrene by H85F CYP101B1 and CYP101B1 176
Figure 5. 33 The products identified from the CYP101B1 and H85F CYP101B1 turnovers of the styrene, 2-methylstyrene and *β*-methylstyrene. 177
Figure 5. 34 The naphthalene derivatives and related substrates screened with WT and H85F CYP101B1. 178
Figure 5. 35 Spin-state shifts of H85F variant after addition of 1-methylnaphthalene. 179
Figure 5. 36 Dissociation constant analysis with 1-methylnaphthalene 180
Figure 5. 37 GC-MS analyses of the turnovers of 1-methylnaphthalene by H85F CYP101B1 and CYP101B1. 180

Figure 5. 38 GC-MS analyses of the turnovers of 2-methylnaphthalene by H85F CYP101B1 and CYP101B1 181
Figure 5. 39 Spin-state shifts after addition of 1,2-dimethylnaphthalene to H85F CYP101B1 and WT CYP101B1. 182
Figure 5. 40 GC-MS analyses of the turnovers of 1,2-dimethylnaphthalene by H85F and WT CYP101B1.. 184
Figure 5. 41 Spin-state shifts H85F variant and WT CYP101B1 after addition of 1,5-dimethylnaphthalene. 185
Figure 5. 42 GC analyses of the turnovers of 1,5-dimethylnaphthalene by CYP101B1. 186
Figure 5. 43 The products identified from the WT and H85F CYP101B1 turnovers with alkylnaphthalenes.....187
Figure 5. 44 Spin-state shifts of H85F and WT variant after addition of 2,6-dimethylnaphthalene. 187
Figure 5. 45 GC-MS analyses of the turnovers of 2,6-dimethylnaphthalene by H85F CYP101B1 and CYP101B1. 188
Figure 5. 46 Spin-state shifts of H85F and WT CYP101B1 after addition of 2,7-dimethylnaphthalene. 189
Figure 5. 47 GC-MS analysis of the turnover of 2,7-dimethylnaphthalene by H85F CYP101B1 and WT CYP101B1.....189
Figure 5. 48 Spin-state shifts and dissociation constants of H85F and WT CYP101B1 with acenaphthene.. 190
Figure 5. 49 GC-MS analyses of the *in vitro* turnovers of acenaphthene by H85F and WT CYP101B1. 191
Figure 5. 50 Spin-state shifts of CYP101B1 variants after addition of phenylcyclohexane.192
Figure 5. 51 GC-MS analyses of the turnover of phenylcyclohexane by H85F and WT CYP101B1. 192
Figure 5. 52 Spin-state shifts of H85F CYP101B1 and WT CYP101B1 after addition of biphenyl.....193
Figure 5. 53 Spin-state shifts of H85F CYP101B1 after addition of 2-methylbiphenyl 194
Figure 5. 54 GC-MS analyses of the turnovers of 2-methylbiphenyl by H85F and WT CYP101B1.. 196
Figure 5. 55 The products identified from the CYP101B1 and H85F CYP101B1 turnovers with phenylcyclohexane and biphenyl substrates 197

Figure 6. 1 Three-dimensional views of cubane 200
Figure 6. 2 Cubane as a bioisostere for benzene. 201
Figure 6. 3 Potential radical and cationic rearrangement products which could arise from P450 oxidation reactions 203
Figure 6. 4 The reactions of various methane monooxygenase (MMO) and cytochrome P450 (CYP) enzymes with methylcubane and their product distributions.. 204
Figure 6. 5 Cubane derivatives used in this study with CYP101B1. 205
Figure 6. 6 Spin-state shift of CYP101B1 with 4-methylcubane-1-methoxy carbonyl. 206
Figure 6. 7 GC-MS analysis of the *in vitro* turnover of 4-methylcubane-1-methoxy carbonyl by CYP101B1. 208
Figure 6. 8 ^{1}H NMR of 4-hydroxymethylcubane-1-methoxy carbonyl 209
Figure 6. 9 Products identified after the oxidation of the substrates 4-methylcubane-1-methoxy carbonyl, 4-ethylcubane-1-methoxy carbonyl and 4-methylcubane-1-acetic acid methyl ester by CYP101B1. 209
Figure 6. 10 Spin-state shift of CYP101B1 with the 4-ethylcubane-1-methoxy carbonyl. ..210
Figure 6. 11 GC-MS analysis of the *in vitro* turnover of 4-ethylcubane-1-methoxy carbonyl by CYP101B1. 211
Figure 6. 12 The spin-state shift of CYP101B1 with 4-methylcubane-1-acetic acid methyl ester. 212
Figure 6. 13 The GC-MS analysis of the small-scale turnover of 4-methylcubane-1-acetic acid methyl ester by CYP101B1. 213
Figure 6. 14 ^{1}H NMR of 4-hydroxymethylcubane-1-acetic acid methyl ester 214
Figure 6. 15 Spin-state shifts of CYP101B1 with 4-methylcuban-1-yl acetate, 4-methylcubane-1-methyl ketone and 4-methylcubane-1-carboxylic acid. 215
Figure 6. 16 GC-MS analysis of the turnover of 4-methylcuban-1-yl-acetate. 216
Figure 6. 17 Barton-McCombie deoxygenations and Barton decarboxylation to monitor radical rearrangement.. 217
Figure 6. 18 Barton decarboxylation approach to synthesise 4-ethylcubane-1-methoxy carbonyl.....218
Figure 6. 19 The proposed mechanism of hydroxylation reaction of CYP101B1 with the methylcubane derivatives.....219
Figure 6. 20 An overview of the in-cage radical recombination and diffusive case escape..220

Figure 7. 1 Oxygenated aromatics used in the current study. 222
Figure 7. 2 UV-Vis NADH oxidation assays of CYP101B1 with naphthalene 223
Figure 7. 3 NADH oxidation assays of CYP101B1 with 1-naphthol 224
Figure 7. 4 GC analysis of the turnover of 1-naphthol 225
Figure 7. 5 Enzyme mediates chemical redox cycling.....227
Figure 7. 6 GC-MS analyses of the *in vitro* turnovers of 2-adamantyl acetate with CYP101B1/ArR/Arx system in the presence of different concentrations 1-naphthol.....229
Figure 7. 7 GC-MS analyses of *in vitro* turnovers of 2-adamantyl acetate with the CYP101B1 system in the presence of different concentrations 1,4-naphthoquinone. 230
Figure 7. 8 The GC-MS analyses of *in vitro* turnovers of 2-adamantyl acetate with CYP101B1/ArR/Arx system in the presence of different concentrations menadione.....233
Figure 7. 9 GC-MS analyses of the *in vitro* turnovers of 2-adamantyl acetate with the CYP101B1 system in the presence of different concentrations 2,6-dihydroxynaphthalene. 236
Figure 7. 10 An overview of how 1,4-naphthoquinone could interrupt electron transfer to P450 during naphthalene or 1-naphthol metabolism. 241

Tables

Table 2. 1 Instrument operating conditions.....27

Table 2. 2 NMR analysis of synthesised of ester derivatives 38

Table 3. 1 Substrate binding, turnovers and coupling efficiency data for CYP101B1 and CYP101C1 with cyclic alkanes and alcohols. 46

Table 3. 2 The assignments of cyclododecanol metabolites using ^{13}C NMR. 49

Table 3. 3 Substrate binding, turnovers and coupling efficiency data for CYP101B1 and CYP101C1 with cycloalkanones.. 54

Table 3. 4 ^{1}H and ^{13}C NMR signals of the HC-OH and HC-O groups which have been reported ($CDCl_3$) 60

Table 3. 5 Substrate binding, turnovers and coupling efficiency data for CYP101B1 and CYP101C1 with a series of substrates containing the ester directing group. 79

Table 3. 6 Substrate binding, turnovers and coupling efficiency data for CYP101B1 and CYP101C1 with linear ketones and terpene esters. 107

Table 4. 1 Substrate binding, turnovers and coupling efficiency data for CYP101B1 with adamantane, 2-adamantanone, 1- and 2-adamantanol.....118

Table 4. 2 Substrate binding, turnovers and coupling efficiency data for CYP101B1 with 1-adamantylmethyl ketone, methyl-2-(1-adamantyl acetate), 1- and 2-adamantyl acetate, and 1- and 2-adamantyl isobutyrate. 122

Table 4. 3 Substrate binding, turnovers and coupling efficiency data for CYP101B1 with 1-adamantylamine and N-(1-adamantyl)acetamide.. 139

Table 4. 4 The metabolites formed from CYP101B1 turnovers of adamantane substrates... 144

Table 5. 1 Substrate binding, turnovers and coupling efficiency data for CYP101B1 (WT and the H85F variant) with *β*-ionone and *p*-cymene.....148

Table 5. 2 Substrate binding, turnovers and coupling efficiency data for CYP101B1 (WT and the H85F variant) with toluene, *o*-, *m*- and *p*-xylene.. 154

Table 5. 3 Substrate binding, turnovers and coupling efficiency data for CYP101B1 (WT and the H85F variant) with ethylbenzene, 2- and 3-ethyltoluene. 158

Table 5. 4 Substrate binding, turnovers and coupling efficiency data for CYP101B1 (WT and the H85F variant) with *n*-propylbenzene, isopropylbenzene and isobutylbenzene. 165
Table 5. 5 Substrate binding, turnovers and coupling efficiency data for CYP101B1 (WT and the H85F) with styrene, *β*-methylstyrene and 2-methylstyrene. 173
Table 5. 6 Substrate binding, turnovers and coupling efficiency data for CYP101B1 (WT and the H85F variant) with 1- and 2-methylnaphthalene.. 179
Table 5. 7 Substrate binding, turnovers and coupling efficiency data for CYP101B1 (WT and the H85F variant) with alkyl substituted naphthalenes 183
Table 5. 8 Substrate binding, turnovers and coupling efficiency data for CYP101B1 (WT and the H85F) with phenylcyclohexane and substituted biphenyls.....195

Table 6. 1 C-H Bond Dissociation Energies (BDE) and s orbital character of different substrates……202
Table 6. 2 Substrate binding, turnover and coupling efficiency data for CYP101B1 with cubane derivatives 207

Table 7. 1 The NADH oxidation rates of CYP101B1/Arx/ArR system and only Arx/ArR with naphthalene, 1-naphthol and 2-naphthol……..……. 225
Table 7. 2 The NADH oxidation rates of CYP101B1/Arx/ArR system and only Arx/ArR with 1,4-naphthoquinone.. 227
Table 7. 3 The NADH oxidation rates of CYP101B1 with 2-adamantyl acetate in the presence of 1-naphthol. 228
Table 7. 4 The NADH oxidation rates of CYP101B1 with 2-adamantyl acetate in the presence of 1,4-naphthoquinone. 230
Table 7. 5 The NADH oxidation rates of CYP101B1/Arx/ArR system and only Arx/ArR with menadione. 231
Table 7. 6 The NADH oxidation rates of CYP101B1 with 2-adamantyl acetate in the presence of menadione. 232
Table 7. 7 The NADH oxidation rates of CYP101B1/Arx/ArR system and only Arx/ArR with vitamin K1. 234
Table 7. 8 The NADH oxidation rates of CYP101B1/Arx/ArR system and only Arx/ArR with 2,6-dihydroxynaphthalene. 235

Table 7. 9 The NADH oxidation rates of Arx/ArR with 3-methoxyphenol and 6-methoxy-1-tetralone.....237
Table 7. 10 The NADPH oxidation rates of Adx/AdR system with 1-naphthol.....238
Table 7. 11 The NADPH oxidation rates of Adx/AdR system with different oxygenated aromatics.. 239
Table 7. 12 The NADPH oxidation rates of CPR system with 1-naphthol.....240

Appendix 269

Appendix A Supplementary Data for Chapter 2 269
Appendix B Supplementary Data for Chapter 3 284
Appendix C Supporting information for Chapter 4 411
Appendix D Supporting information for Chapter 5 454
Appendix E Supplementary Data for Chapter 6 479

Abstract

The cytochrome P450 enzymes CYP101B1 and CYP101C1, which are from the aromatic hydrocarbon degrading bacterium *Novosphingobium aromaticivorans* DSM12444, can hydroxylate norisoprenoids with high activity and selectivity. With the aim of further understanding their substrate range, a selection of cyclic alkanes, ketones and alcohols were studied. Cycloalkanes were oxidised, but both enzymes displayed low binding affinity and productive activity. The presence of a ketone moiety in the cycloalkane skeleton significantly improved the substrate binding affinity and the oxidation activity. CYP101C1 catalysed the oxidation of the cycloalkanones at the C-2 position with high regioselectivity. The regioselectivity of CYP101B1 was different. It oxidised cycloalkanones at positions remote from the carbonyl group. This indicated that the binding orientation of the cyclic ketones in the active site of each enzyme must be different. Cyclic alcohols and cyclohexylacetic acid showed little to no activity with either enzyme. The introduction of an ester protecting group to these substrates significantly enhanced the monooxygenase activity. These substrates were oxidised regioselectively on the opposite side of the ring system to the ester directing group. For example, both enzymes preferentially oxidised the C-H bond at the C4, C5 and C7 position of the cyclohexyl, cyclooctyl and cyclododecyl ester compounds, respectively. In addition, certain linear ketones and esters were also found to be suitable substrates for these biocatalysts.

CYP101B1 mediated metabolism of the tricyclic compounds adamantane, 1- and 2-adamantanol and 2-adamantanone proceeds with low oxidation activity and multiple metabolites were identified. Insertion of a directing group (acetate/isobutyrate) at the alcohol of these adamantanols significantly increased the affinity, activity and coupling efficiency (productive use of reducing equivalents) of CYP101B1 compared to the parent compounds. This substrate engineering approach with these adamantyl derivatives led to a 65 to 122-fold higher product formation activity. The turnovers were also regioselective and in some instances stereoselective. Additionally, the amide N-(1-adamantyl)acetamide was oxidised efficiently by CYP101B1, whereas 1-adamantylamine was not. Whole-cell biotransformation systems were used to generate the metabolites in good yield (g/L scale). Overall, the use of ester directing groups and the modification of the amine to an amide enabled CYP101B1 to oxidise the adamantane skeleton more efficiently and selectively.

Wild-type (WT) CYP101B1 can catalyse the oxidation of aromatic substrates such as alkylbenzenes, alkylnaphthalenes and acenaphthene, but the binding affinities and the oxidation activities were low. Both the binding affinity and product formation activity of this enzyme for these hydrophobic substrates were enhanced using site-directed mutagenesis. The Histidine 85 (H85) of CYP101B1 aligns with tyrosine 96 of CYP101A1 ($P450_{cam}$), which, in the latter enzyme forms the only hydrophilic interaction with its natural substrate, camphor. The H85 residue of CYP101B1 was therefore replaced with phenylalanine (F), and this H85F variant exhibited greater affinity and activity towards hydrophobic substrates. For instance, the product formation activity of the H85F variant for acenaphthene oxidation was increased six-fold to 245 nmol.nmol-CYP^{-1}.min^{-1}. This indicated that this residue is in the substrate binding pocket or the access channel of the enzyme.

Methylcubanes have been used as mechanistic probes to differentiate between radical and cationic pathways in cytochrome P450 oxidation. A series of methylcubanes were designed which would place the methyl group close to reactive heme iron centre of CYP101B1. CYP101B1 efficiently oxidised the substituted methylcubane derivatives yielding the equivalent cubylmethanol in 93 ± 7 % yield. The cube was found to be intact in all the turnover products, and no methylcubanols or any other rearranged metabolites containing homocubyl were detected. These results were consistent with a rapid radical rebound step in these oxidations and argued against the involvement of any carbocation-based intermediates during the oxidation.

The CYP101B1 system, which also combines a FAD-containing ferredoxin reductase and a [2Fe-2S] ferredoxin, was investigated with oxygenated aromatics including naphthols, naphthoquinones, dihydroxynaphthalene and phenols. *In vitro* NADH oxidation rates in both the presence and absence of CYP101B1 were fast with these substrates (≥800 min^{-1}). Minimal metabolite formation was detected, and the majority of reducing equivalents were transformed into hydrogen peroxide. Large amount of H_2O_2 in these reactions in the absence of P450 indicated that the ferredoxin (Arx) and ferredoxin reductase (ArR) catalysed futile redox cycling with naphthoquinones giving rise to the uncoupling of the reducing equivalents. Further examination of naphthols and naphthoquinones together with 2-adamantyl acetate in the fully reconstituted CYP101B1 turnovers demonstrated that the presence of naphthoquinones led to diminished product formation as they interfere with the electron transfer process. This type of uncoupling in the bacterial P450 electron transfer partners containing ferredoxin system would be considered an additional form of uncoupling over those which arise in the P450 active site.

Statement of Originality

I certify that this research work contains no material which has been accepted for the award of any other degree or diploma in my name in any university or other tertiary institution and, to the best of my knowledge and belief, contains no material previously published or written by another person, except where due reference has been made in the text. In addition, I certify that no part of this work will, in the future, be used in a submission in my name for any other degree or diploma in any university or other tertiary institution without the prior approval of the University of Adelaide and where applicable, any partner institution responsible for the joint award of this degree.

I give consent to this copy of my thesis when deposited in the University Library, being made available for loan and photocopying, subject to the provisions of the Copyright Act 1968.

The author acknowledges that copyright of published works contained within this thesis resides with the copyright holder(s) of those works.

I also give permission for the digital version of my thesis to be made available on the web, via the University's digital research repository, the Library Search and also through web search engines, unless permission has been granted by the University to restrict access for a period.

I acknowledge the support I have received for my research through the provision of an Australian Government Research Training Program Scholarship.

Md Raihan Sarkar

30th May 2019

Acknowledgements

My biggest thanks have to go to my supervisor Associate Professor Stephen Bell for his tireless dedication towards supervising my project and his endless patience in editing drafts of this thesis.

I am also grateful to Professor Simon Pyke for always having an open and welcoming door throughout my time with this project. Thanks also to the past and present members of the Bell group. Everyone has been incredibly supportive and fantastic of having around. Thanks to Tom, Stella, Sherry, Joel, Matthew, Saurabh, Daniel, Cameron, Natasha, Emma, Sarah, Sam, Rebecca, Ian, Samarat, Heba and Kai. I wish all of you the best in your future endeavours. I am also grateful to Tom, Daniel, Sherry, Saurabh, Joel and Matthew for proofreading and Phil Clements for NMR. I would like to thank our collaborator Sevan D. Houston, James J. De Voss, G. Paul Savage, Craig M. Williams from the University of Queensland and Robert Tuckey from The University of Western Australia

Finally, I must express my very profound gratitude to my parents, spouse Akhi, son Ehan as well as all the well wisher Professor ABM Faroque, Rifat, Soma, Dr Akm Shaheduzzaman, Dr Nazrul, Saiful, Shiplu, Alif, Monjur, Atiq and Mamun for providing me with unfailing support and continuous encouragement throughout my years of study.

Finally, if you are reading this, thank you for taking the time to do so.

Abbreviations

AdR	Adrenodoxin reductase
Adx	Adrenodoxin
ArR	Ferredoxin reductase
Arx	Ferredoxin
$CDCl_3$	Deuterated chloroform
CO	Carbon monoxide
Cpd I	Compound I
CYP	Cytochrome P450
DCM	Dichloromethane
DFT	Density Functional Theory
DTT	Dithiothreitol
DMSO-d_6	Dimethyl sulfoxide-d_6
EMM	*E. coli* Minimal Media
EtOH	Ethanol
EtOAc	Ethyl acetate
FMN	Flavin mononucleotide
FAD	Flavin adenine dinucleotide
GC	Gas Chromatography
GC-MS	Gas Chromatography-Mass Spectrometry
HCl	Hydrochloric acid
HPLC	High-Performance Liquid Chromatography
HRP	Horseradish Peroxidase
hr	Hour (s)
H85F	Histidine 85 Phenylalanine
IPTG	Isopropyl-*β*-D-thiogalactoside
IS	Internal Standard
LB	Lysogeny Broth
LS	Low Spin
Min	Minute
MS	Mass Spectrometry
Multiplicities	s= singlet, d= doublet, *t*= triplet, *q*= quartet, m= multiplet, quin= quintet, sext= sextet, sep= septet, br= broad
NADH	Reduced form of nicotinamide adenine dinucleotide
NMR	Nuclear Magnetic Resonance
PDB	Protein Data Bank
PFR	Product Formation Rate
TIC	Total Ion Count
RT	Retention Time
SOC	Super Optimal Broth with catabolite repression
WT	Wild-Type

Chapter 1

1. Introduction

1.1. General Overview of Cytochrome P450s

Cytochrome P450 enzymes (P450s or CYPs) are a superfamily of monooxygenase metalloproteins which are found in all kingdoms of life, including animals, plants, bacteria and fungi [1]. The name "P450" is derived due to its red pigmentation (P) and the enzyme has a characteristic absorption peak at 450 nm when it is reduced and bound with carbon monoxide (Figure 1. 1) [2]. P450 systems were first recognised in 1958. Klingenberg and Garfinkel independently identified and reported a unique CO-bound red pigment, which exhibits a Soret absorption peak at 450 nm, in rat and pig liver microsomes [3, 4]. Omura and Sato first described the hemoprotein nature of this pigment in 1964 [5]. The protoporphyrin (heme) centre is attached to the enzyme via coordination of the ferric ion with a proximal cysteine thiolate ligand (I; Figure 1. 1 and Figure 1. 3) [1, 6]. This thiolate ligand is significant for enzymatic activity and contributes to the unique Soret absorption peak of the carbon monoxide reduced enzyme (450 nm) [6, 7].

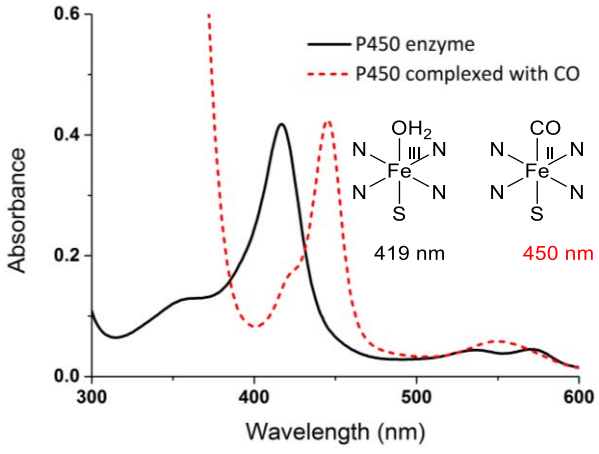

Figure 1. 1 UV-Vis absorbance spectrum of the ferric resting state of a P450 enzyme (black). The Soret absorbance peak at ~450 nm is observed upon binding the ferrous form with a CO ligand (dashed red) [2].

The P450 superfamily is currently comprised of more than 300,000 (as of January 2018) cytochrome P450 sequences and among these nomenclature has been assigned to 41,000 [8]. For instance, the human genome has 57 unique P450 systems, while the *Mycobacterium tuberculosis* bacterium contains 20 P450 genes [9, 10]. Other examples include 458 different P450s are found in rice, and the carnivorous mushroom (*Laccaria bicolor*) has 91 P450 sequences [11, 12]. However, the bacterium *Escherichia. coli* contains no P450 system [13].

The systematic naming of each member of this superfamily is based on their sequence similarity and function [14, 15]. Each member of this superfamily is grouped according to amino acid sequence similarity into a specific family (≥40% similarity) and subfamily (≥55% similarity) [8, 16-18]. The name of a P450 enzyme is designated by its family number and subfamily letter following the prefix CYP. Families are denoted with a numerical identifier such as CYP1–CYP49, CYP301–CYP499, CYP3001–CYP4999 for mammalian, CYP51–CYP69 for fungal, CYP501–CYP699, CYP5001–CYP6999 for lower eukaryotes, CYP71–CYP99, CYP701–CYP999 for plant and CYP101–CYP299, CYP1001–CYP1050 for bacterial P450 enzymes families [1, 8, 19, 20]. The subfamily is expressed by a letter, for instance, A and a number such as 1, which catalogues the P450 enzyme within the subfamily. For example, CYP102A1 from the bacterium *Bacillus megaterium* is the first identified P450 enzyme in the subfamily "A" of the family "102" [21-23].

These P450 enzymes are capable of introducing one oxygen atom into chemically inert C-H bonds with high chemo-, regio- and stereo-selectivity (Equation 1. 1) [1, 13]. The primary activity which they perform is hydroxylation, but P450 enzymes can also catalyse a wide range of reactions including alkene epoxidation, heteroatom oxidation, desaturation, oxidative ester cleavage, isomerisation, rearrangement, ring expansion and ring formation. These make P450s one of the most versatile biological catalyst superfamilies (Figure 1. 2) [13, 24-31].

$$R\text{-}H + NAD(P)H^{+} + H^{+} + O_2 \longrightarrow NAD(P)^{+} + H_2O + R\text{-}OH \qquad (1.\ 1)$$

where R-H is the substrate and R-OH is the metabolite generated by the P450 enzyme.

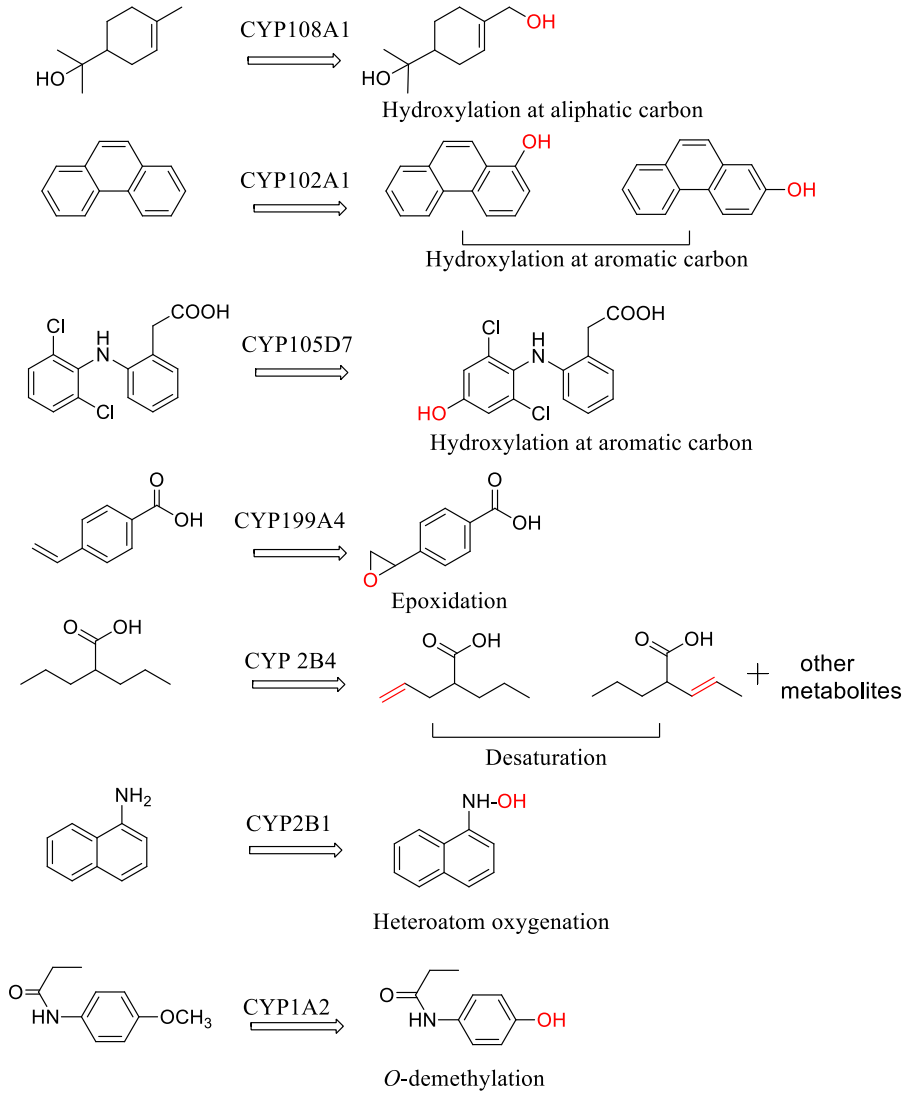

Figure 1. 2 A selection of reactions catalysed by cytochrome P450 enzymes [13, 24-31].

1.2. The Catalytic Cycle of Cytochrome P450s

The catalytic cycle for the majority of the members of the P450 superfamily is believed to be predominantly the same (Figure 1. 3) [9, 13]. However, substrate selectivity and activity of individual P450 enzymes depend on the sequential and structural differences in the active site [1]. $P450_{cam}$ (CYP101A1), isolated from the bacterium *Pseudomonas putida*, was one of the first and hence most well-known P450 to be purified in soluble and crystalline form, and its three-dimensional structure has been determined [32-34]. CYP101A1 has been therefore used as a model system to gain a detailed understanding of the P450 catalytic cycle [32-34].

In the resting state, the 6th distal coordination site of the heme centre is usually occupied by a water molecule (I) and this ligand can be observed in the substrate-free crystal structure of P450 enzymes (Figure 1. 3) [9]. The water ligand is displaced by the substrate which initiates the catalytic cycle (II), and this step can be monitored by UV-Vis spectrophotometry as the enzyme gives a characteristic shift from the low spin resting state (I; ~418-419 nm) to a high spin-state (II) which absorbs at ~390 nm (Figure 1. 3 and Figure 1. 4). The high spin form (II) of the ferric centre then accepts an electron from NADPH (or NADH), delivered by electron transfer partners to generate the ferrous form (III). The ferrous ion can bind molecular dioxygen to form a ferrous-dioxygen complex (IV) [9]. This complex (IV) receives another electron to yield the ferric-peroxy anion complex (V) [35]. The ferric-peroxy anion complex undergoes protonation (VI) at the distal oxygen of the complex (V) to give compound 0 (VI) followed by cleavage of the O-O bond to generate a highly reactive species called compound I (Cpd I) [36, 37]. Cpd I is considered as the primary oxidant in the majority of P450 reactions and is capable of abstracting a hydrogen atom from a substrate C-H bond [38]. This is followed by the introduction of the oxygen atom to the substrate via a radical rebound mechanism (Figure 1. 3) [36].

The characterisation of compound I is difficult due to its extremely short lifetime. However, recently it was characterised under cryogenic conditions which confirmed its nature and identification as a key intermediate [36, 39]. The iron centre of Cpd I has two unpaired electrons in the 3d π* orbital of the iron and one in the porphyrin a_{2u} π* orbital (Figure 1. 3) [40-42]. It can exist in a high spin quartet state, $^4A_{2u}$, in which all electrons have parallel spin or in the low-spin doublet state with the electron in porphyrin orbital inverted ($^2A_{2u}$) [40-42]. A pair of sextet and quartet excited states has also been described which are higher in energy than the doublet and quartet ground states of Cpd I [41].

Cpd I breaks the substrate C-H bond homolytically, resulting in a substrate radical ($^{\cdot}$R) and forms an intermediate iron-hydroxy species [Fe^{IV}–**OH**] (Figure 1. 3). The substrate radical recombines with the iron bound hydroxy group to generate the product (R-OH; Figure 1. 3). Once the product (R-OH) formation is complete, it dissociates from the active site of the enzyme. A water ligand then binds to the iron centre of the enzyme to reform the resting state (I).

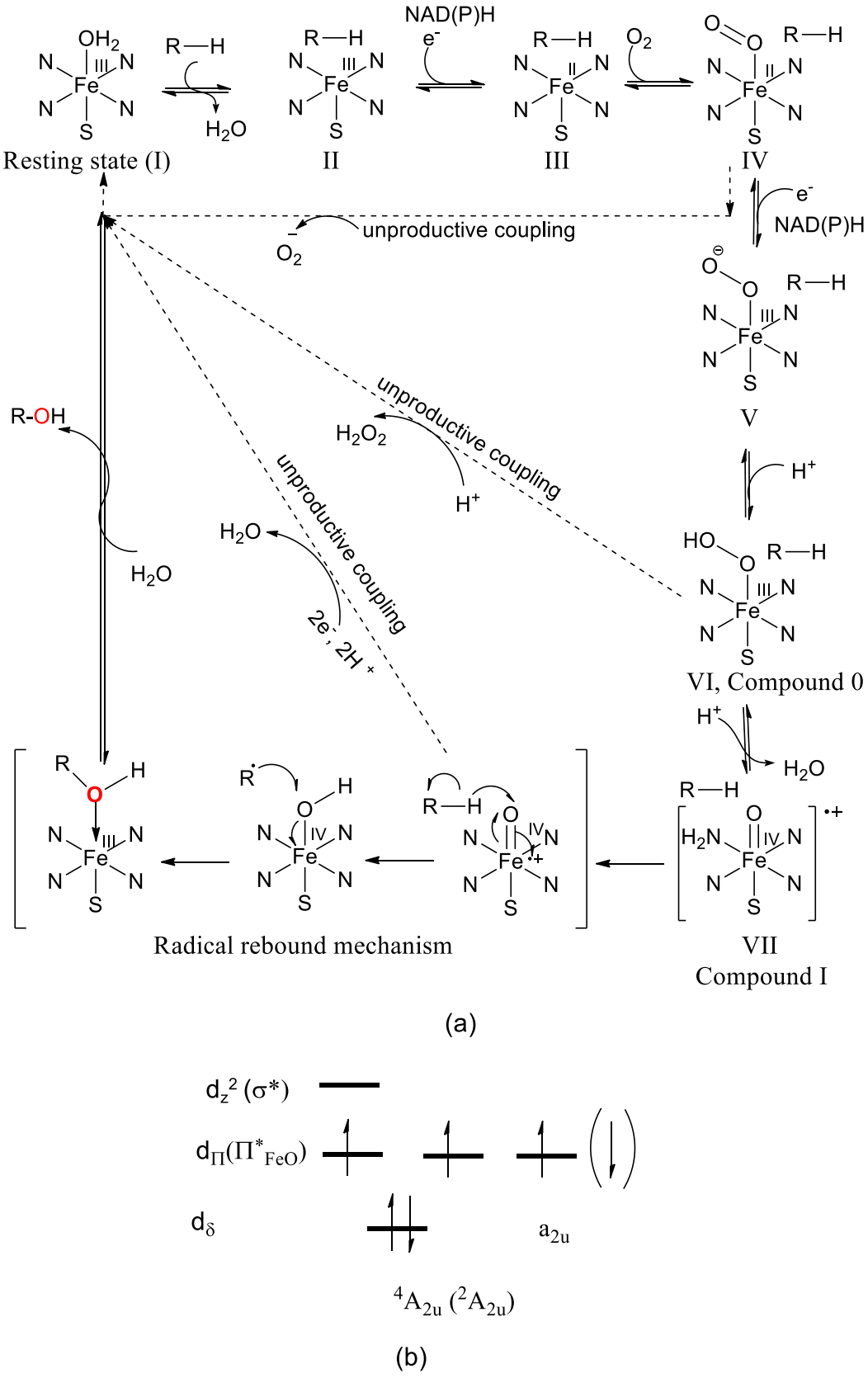

Figure 1. 3 (a) The catalytic cycle of cytochrome P450 enzymes. **(b)** The electronic structure of Cpd I [38, 40-42].

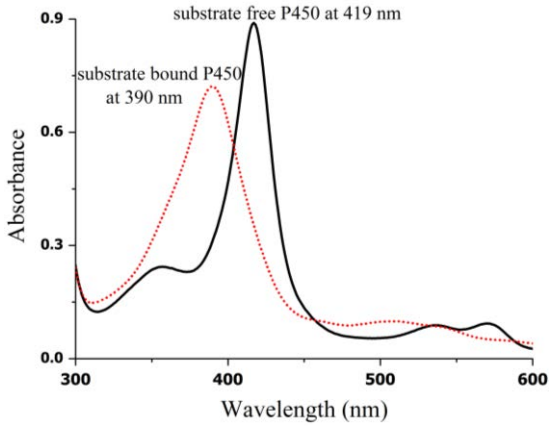

Figure 1. 4 UV-Vis absorbance spectrum of the resting state of the P450 enzyme (I; black). The Soret absorbance peak is at ~419 nm, and this absorbance peak shifted to ~390 nm upon binding of a substrate (II; dashed red).

The catalytic cycle of P450 enzymes requires two electron transfer steps II to III and IV to V (Figure 1. 3). These reducing equivalents are usually derived from NADH or NADPH and are shuttled to the P450 via electron transfer proteins [43]. The P450 enzyme must form a complex with one of its redox partners. During the early stage of P450 discovery, two prime classes of redox partners were described, class I and class II [44, 45]. Many bacterial P450s such as CYP101A1 from *P. putida* receives electrons from NADH via a class I redox partner system, which consists of an iron-sulfur protein (ferredoxin) and a flavin-containing reductase (ferredoxin reductase) [46-50]. Most of the mitochondrial P450s such as CYP11B1 accept reducing equivalents from NADPH through NADPH-adrenodoxin reductase and adrenodoxin which are similar to these bacterial systems (Figure 1. 5) [44, 45, 51, 52]. In both ferredoxin/adrenodoxin reductase first gains two electrons from NAD(P)H. These electrons are then transported one at a time to the second component of the system, a ferredoxin/ adrenodoxin and which then delivered individually to the target P450 enzyme (Figure 1. 5) [53]. The most studied ferredoxins in this class of redox partners contain iron-sulfur [2Fe-2S] clusters [44, 54]. However, there are few other cluster types which have also been reported [44, 55-57]. For example, CYP105D1 from *Streptomyces griseus* receives the reducing equivalents from ferredoxins which contains a [3Fe–4S] and a [4Fe–4S] cluster [55-57].

The membrane-bound and eukaryote microsomal monooxygenases, e.g. CYP2C5 and CYP3A4 typically belong to the class II system, which is associated with a single membrane-bound NADPH reductase containing FAD and flavin mononucleotide (FMN) domains (Figure

1. 5) [46, 50, 58-60]. Several other redox partner systems have been identified for P450s. These have been divided into a total of ten different classes including the class I and class II system discussed above [44].

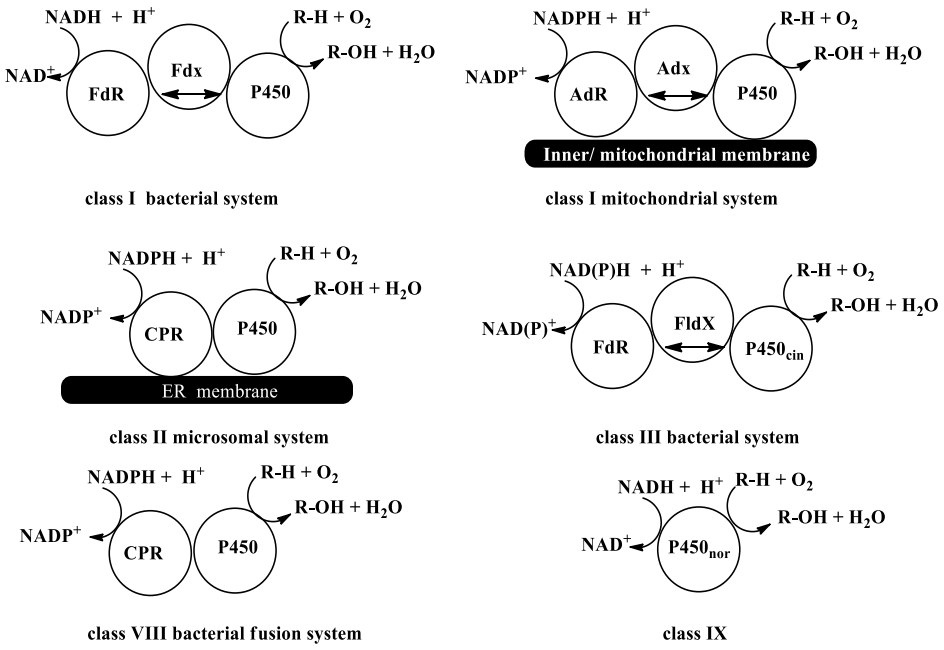

(a)

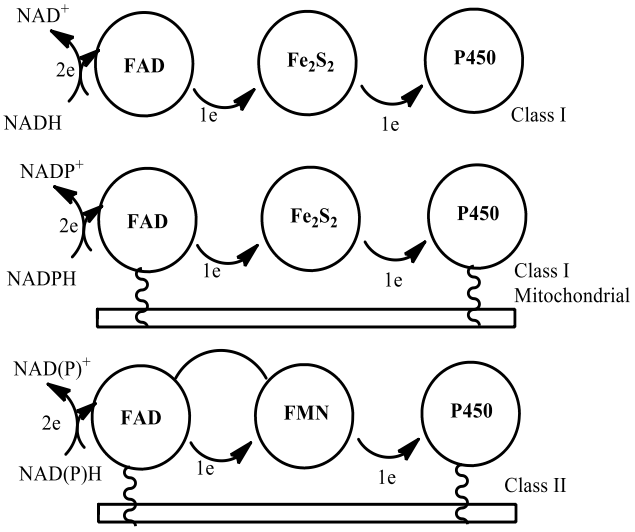

(b)

Figure 1. 5 (a) Example of the different types of electron transfer proteins used by P450s including class I, class II, class III, class VIII and class IX [44]. CPR: Cytochrome P450 reductase. **(b)** Class I and class II electron transfer process from NAD(P)H to the P450 enzymes [44, 53].

Other examples of electron transfer partners for P450 enzymes include class III P450 systems, e.g. CYP176A1 ($P450_{cin}$). This has two separate redox partners like the class I system, but instead of an iron-sulfur protein, it uses a second mediator protein, a flavodoxin (FMN), which is similar to the class II systems (Figure 1. 5) [44, 46, 61]. CYP102A1 ($P450_{BM3}$) from *Bacillus megaterium* belongs to the class VIII catalytically self-sufficient P450 system. In this system, the P450 domain is fused to a reductase, which contains both FAD and FMN domains (Figure 1. 5) [21, 44, 62]. The class VI P450 system stands somewhere between the self-sufficient $P450_{BM3}$ (Class VIII) and $P450_{cin}$ (Class III) systems. It consists of a putative NAD(P)H-dependent flavoprotein reductase and a flavodoxin-P450-fusion protein [44, 63-65]. The class IX system, such as the soluble eukaryotic $P450_{nor}$ or CYP55 from the fungus *Fusarium oxysporum*, has been shown not to require a flavoprotein to supply the reducing equivalents and it can use NADH directly for the reduction process (Figure 1. 5) [66-68].

The product formation activity and efficiency of substrate oxidation by P450 enzymes depend on several factors including the rates of electron and proton transfer within the catalytic cycle of the enzyme. In theory, each molecule of NADH/NAD(P)H and oxygen consumed during a turnover of the catalytic cycle, should produce one molecule of product. However, this complete utilisation of redox equivalents for product formation is rarely observed due to uncoupling reactions. These processes can arise if a particular step of the catalytic cycle occurs too slowly (Figure 1. 3) [69]. If the second electron transfer step is inefficient, superoxide may be released from the ferrous-dioxygen complex (IV) which reverts to the ferric state [70]. A second possible uncoupling event originates if the second protonation of the distal oxygen of ferric-hydroperoxide (VI) occurs too slowly and instead a proton is transferred to the proximal oxygen. Hydrogen peroxide is then released as a by-product (Figure 1. 3). Excess H_2O in the P450 active site can accelerate this peroxide forming uncoupling process [70]. The third uncoupling pathway is due to the unproductive two-electron reduction of compound I (VII) to water. This can occur when the substrate does not bind in the active site of the P450 in an orientation where Cpd I can attack a C-H bond. In general, if the substrate does not have favourable active site interactions, the uncoupling processes are increased [71, 32, 72, 73].

In some cases, the product may act as an inhibitor by reversibly binding to the active site of the P450 enzyme and preventing productive substrate binding and oxygenation. Uncoupling in the electron-transport chain has also been reported for the P450s that accept reducing equivalents

from electron-transport chains [71, 74-78]. Therefore, the electron transfer between the redox proteins and the P450 enzyme has to be fine-tuned to minimise the uncoupling, which is vital for efficient P450 activity [79]. Certain aromatic compounds, such as polycyclic aromatic hydrocarbons, arylamines and quinones can inhibit the activity of mammalian cytochrome P450s by interfering with electron transfer to the heme through futile redox cycling and this can be considered another type of uncoupling process [80, 81-83].

1.3. Mechanistic Probes of Cytochrome P450s

The majority of the steps in P450 catalytic oxidation cycle are well characterised, including the steps involving the binding of the substrate, reduction of ferric ion, ferrous-dioxygen complex formation and the second reduction step (Figure 1. 3) [84]. However, an understanding of the final oxidation mechanism is still not complete. This step dictates the resulting metabolite distribution in P450 catalysed oxidation reactions [84, 85]. There are numerous proposed mechanisms for the final product determining step.

The C-H hydroxylation step was hypothesised to be carried out by a high-valent iron-oxo species which transferred oxygen in the C-H bonds via a direct insertion mechanism (Figure 1. 6 (a)) [25, 86-89]. This was later replaced by a "radical rebound" mechanism based on studies with mechanistic probes of Groves and co-workers (Figure 1. 6 (b)) [84, 86, 90-92].

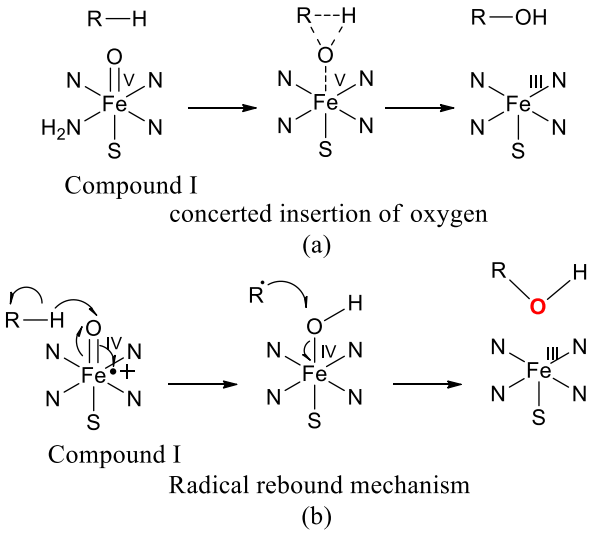

Figure 1. 6 The **(a)** insertion and **(b)** radical rebound mechanisms of P450-mediated hydroxylation reactions [38].

Mechanistic probes have the potential to differentiate between radical and cationic intermediates formed during the oxidation which make them useful in the mechanistic investigation of hydroxylation reaction of P450s [84 85, 86, 93]. Groves and co-workers described the oxidation of norbornane, 3,3,6,6-tetradeuteriocyclohexene, methylenecyclohexane and *β*-pinene with P450 systems and suggested hydroxylation occurs through the radical rebound mechanism [74-76]. For example, different mechanisms can be validated using the intermediates formed during the P450 mediated oxidation of cyclohexene. The concerted insertion of oxygen (A) could explain why the hydroxylation occurs at the allylic site of cyclohexene, but this mechanism could not justify the allylic rearrangement products that were observed with hydroxylation (Figure 1. 7) [92]. The mechanism 'D'predicts that the hydroxylation at allylic C-H bond should occur with the rearrangement of the π bond, but this path is unable to explain hydroxylation metabolites formed without rearrangement (Figure 1. 7) [92]. The mechanism "C" is a preferential path for epoxidation of cyclohexene, but allylic hydroxylation of cyclohexene without rearrangement is unlikely to arise by this mechanism either as the oxidant should interact initially with the π bond (Figure 1. 7). The hydroxylation of cyclohexene both with or without rearrangement can be validated with a two-step radical rebound mechanism (B; Figure 1. 6 and Figure 1. 7) [92, 84, 90].

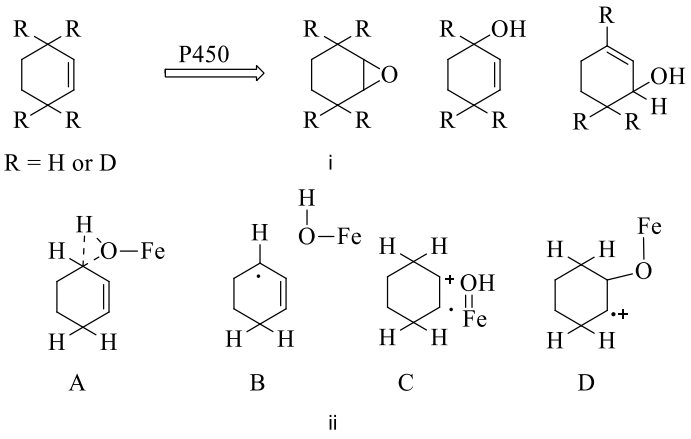

Figure 1. 7 (i) P450 mediated oxidation of cyclohexene [92]. **(ii)** Several pathways for cyclohexene oxidation by an oxoiron (IV) species. (A) Concerted oxygen insertion, (B) radical recombination, (C) electron transfer from alkene to generate π-cation radical which later loses an allylic hydrogen atom, (D) addition of iron-bound oxygen to π bond followed by elimination of proton [92].

Cpd I is widely recognised as the main oxidising species. However, observations during several studies have been interpreted as evidence of multiple oxidants, also including the

ferric peroxy anion (V) and ferric-hydroperoxy species Cpd 0 (VI; Figure 1. 3) [94-96]. For illustration, Newcomb and co-workers studied the two hypersensitive mechanistic probes *trans,trans*-2-methoxy-3-phenylmethylcyclopropane and methylcubane which were capable of distinguishing between potential radical and cation intermediates by rearranging to give distinct products based on the intermediate formed during the P450 product formation steps [84]. Oxidation of these probes by P450s generated different rearrangement products resulting from cationic and radical intermediates (Figure 1. 8) [84]. These results have been rationalised via a concerted "non-synchronous" mechanism, and the cationic intermediate rearrangement products were hypothesised to arise from the reaction with the hydroperoxo-iron intermediate (Fe-O-OH; Figure 1. 8) [84].

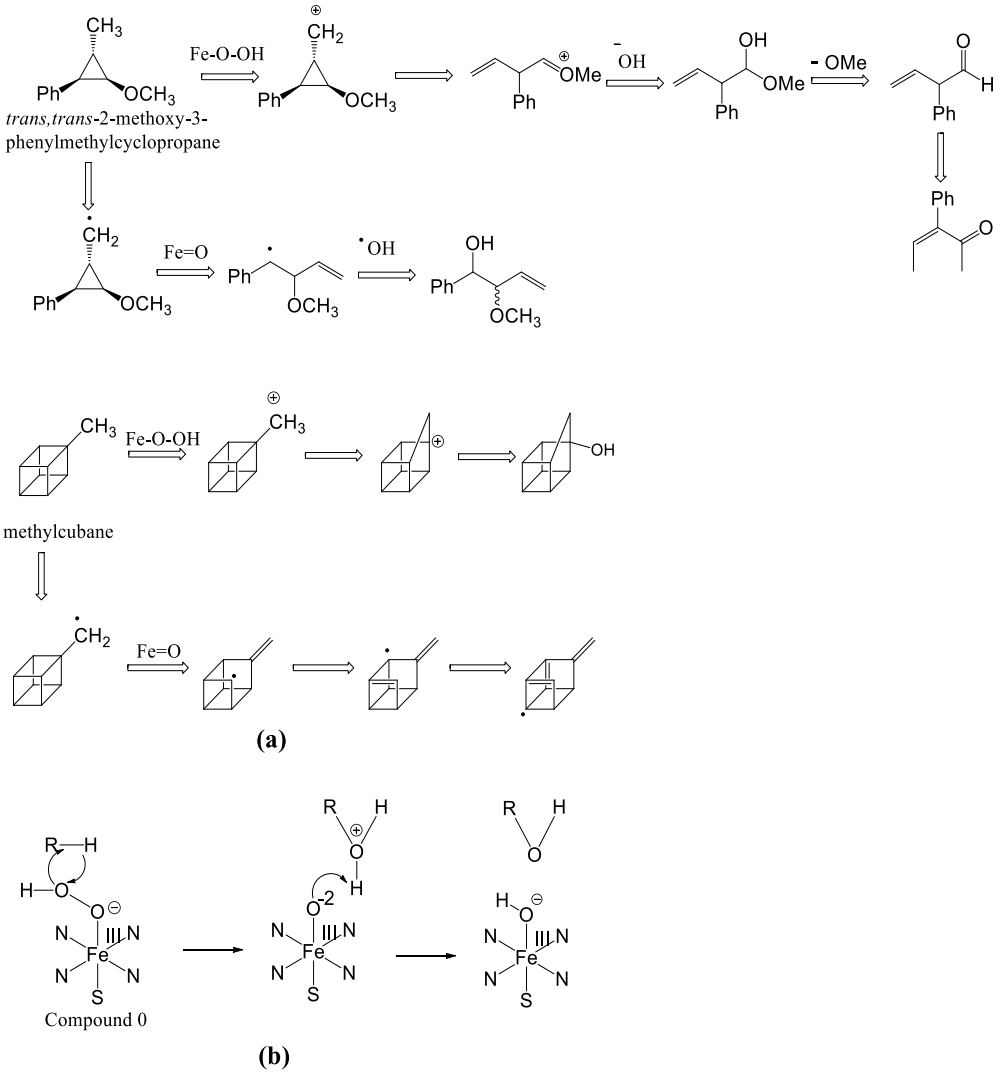

Figure 1. 8 (a) Products generated by P450s which can be used for differentiating between cationic and radical intermediates formed during hydroxylation [84]. **(b)** Newcomb *et al*. proposed the hydroxylation via the P450 hydroperoxo-iron species [84].

However, DFT investigations disagree with the involvement of the hydroperoxo-iron intermediate (Cpd 0) as the redox potential of this is inadequate for C-H bond abstraction [97-99]. Other experimental studies were also in agreement with this theoretical observation [100]. Recently a "two-state" reactivity model has been proposed based on theoretical studies which hypothesised the radical or cationic intermediates formed are controlled by the spin-state of compound I [98].

In the two-state model, reactive intermediates can be present in doublet and quartet states (Figure 1. 3) [101, 102]. Calculations predict that the oxygenation pathways undertaken via doublet state proceed in a barrierless fashion, whereas the quartet state has a significant rebound barrier extending the lifetime of the intermediate [101, 103]. Many experimental observations have been interpreted using this theory and by assuming that the longer lived intermediate of the quartet state undertakes alternative pathways involving radical rearrangements or electron transfer reactions to give the cation.

Further investigation is required to fully characterise of the product formation step and to understand the product distribution of P450 catalysed metabolism of a wide range of natural and non-natural substrates [104].

1.4. Applications of Cytochrome P450s

Cytochrome P450 enzymes play various roles in the synthesis of natural products and are involved in the breakdown of xenobiotic compounds. They are engaged in a range of oxidative processes as part of the biosynthesis of hormones, vitamins and secondary metabolites as well as the metabolism and degradation of cholesterol, environmental chemicals, pollutants and a wide variety of organic compounds [105-108]. For example, CYP17A1, CYP21B1, CYP3A4, CYP3A5 and CYP105A1 catalyse the synthesis of cholesterol, vitamins, steroids and other lipids, and are also capable of the oxidation of drug molecules (Figure 1. 9) [105-108].

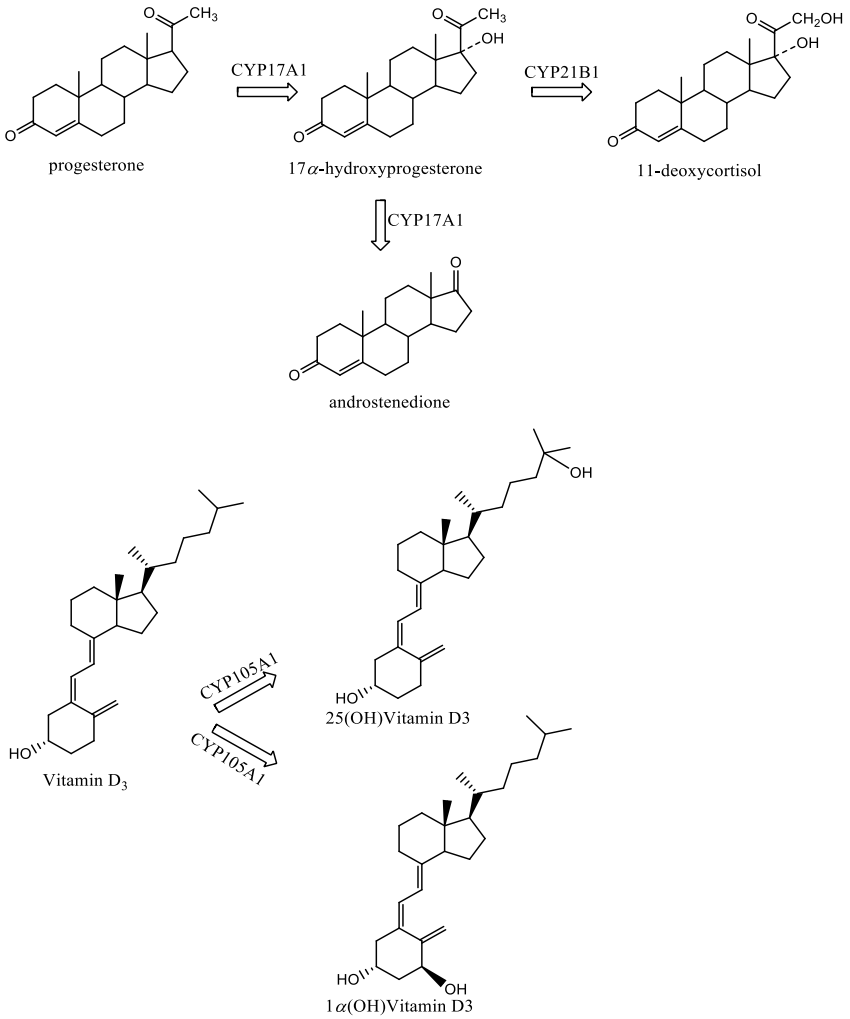

Figure 1. 9 P450s catalysed the metabolism of progesterone and vitamin D_3 [107, 108].

In the last few decades, notable progress has been made in the development of chemical strategies to functionalise inert C-H bonds [109]. Transition metal-containing catalysts and directing groups have been collectively applied to favour oxidation of an sp^3 or sp^2 C-H bond [110-112]. Other approaches such as the use of non-heme iron hydroxylation catalysts, peptide-embedded trifluoromethyl ketone catalysts and iron (Fe)-based small molecule catalysts have been used to oxidise electronically activated (typically tertiary or heteroatom-bearing) C-H bonds with high selectivity over less reactive secondary and primary C-H bonds [105, 113-115]. For example, the selective oxidation of *cis*-1,2-dimethylcyclohexane and 2,6-dimethyloctane using different non-heme iron complexes were reported (Figure 1. 10) [113]. Regioselectivity in C-H bond oxidation has also been improved through "biomimetic" supramolecular approaches, for instance, regio- and stereoselective functionalisation of 4-methylcyclohexyl acetic acid by a catalytic Mn-oxo complex (Figure 1. 10) [116-118]. Manganese-porphyrin catalysts containing 2′,4′,6′-triphenyl phenyl groups showed better activity on primary C-H bonds over secondary,

and the selectivity of oxidation was improved for N-alkylpyrrolidines C(sp^3)-H bonds without the requirement for directing groups by utilising Pt-catalyst (Figure 1. 10) [116, 119, 120]. The supramolecular (manganese and iron) porphyrins combined with structural elements to bind and hold the substrate in a specific orientation/position above a metal centre to oxidise the C-H bond selectively, has also been reported [105, 116-118].

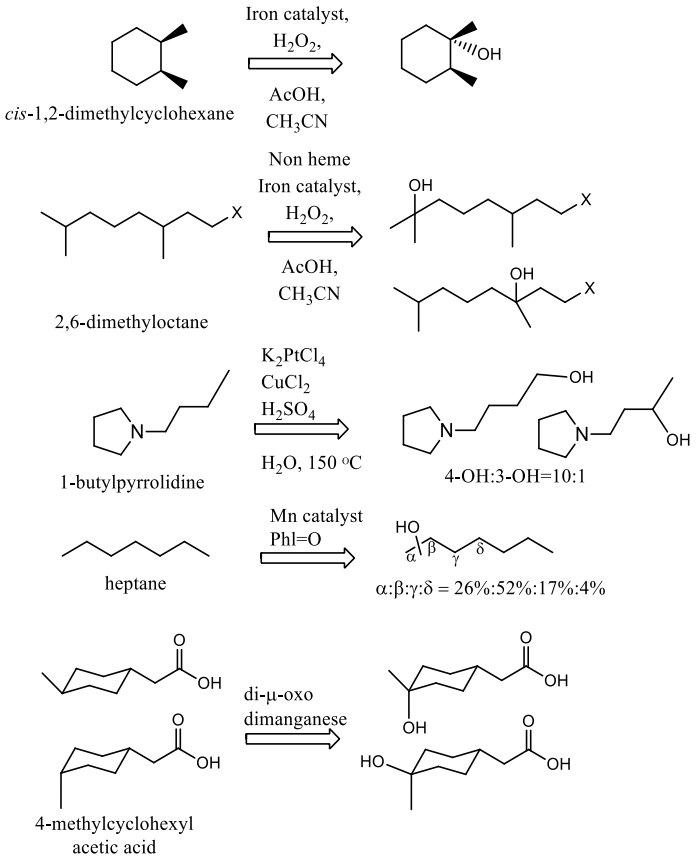

Figure 1. 10 Different chemical approaches to activate inert C-H bonds [116, 117, 119, 121, 122].

Despite this progress, conventional chemical strategies for inert C-H bond oxidation are not devoid of drawbacks. The regioselectivity of chemical reagents/catalysts to the most reactive C-H bond over the other bonds due to electronic or stereoelectronic effects is still the most limiting aspect [105]. Moreover, harsh or toxic chemical reactants are required to functionalise the inert C-H bonds, and these often result in low product yields or unwanted side-products. In this context, cytochrome P450 enzymes have emerged as an attractive strategy, which can catalyse the reactions under mild ambient conditions [105]. It is also a valuable methodology for green chemistry because these catalysts utilise natural molecular oxygen, which is abundant, inexpensive and non-toxic to the environment [123, 124]. P450s are capable of oxidising inactive C-H bond with high chemo-, regio- and stereo-selectivity in the presence of multiple other C-

H bonds of similar or higher reactivity. For examples, the regioselective oxidation of quinoline-6-carboxylic acid and *α*-irone by CYP199A2 and CYP267B1, respectively and the enantioselective hydroxylation of 2-arylacetic acid in the '*α*' C-H bond using CYP102A1 highlighted the advantages of using biocatalytic systems in selective oxidation (Figure 1. 11) [125, 126]. Another example, the P450 enzyme CYP154E1 from bacterium *Thermobifida fusca YX*, catalysed the double hydroxylation of (*E*)-stilbene efficiently and selectively [127]. Therefore, the biocatalytic production of fine chemicals in larger scale using P450 enzyme would be attractive [128-131]. For instance, pravastatin, a cholesterol-lowering drug was synthesised on an industrial scale by a bioconversion process using a water-soluble P450 named CYP105A3 from *Streptomyces carbophilus* (Figure 1. 11) [132, 133].

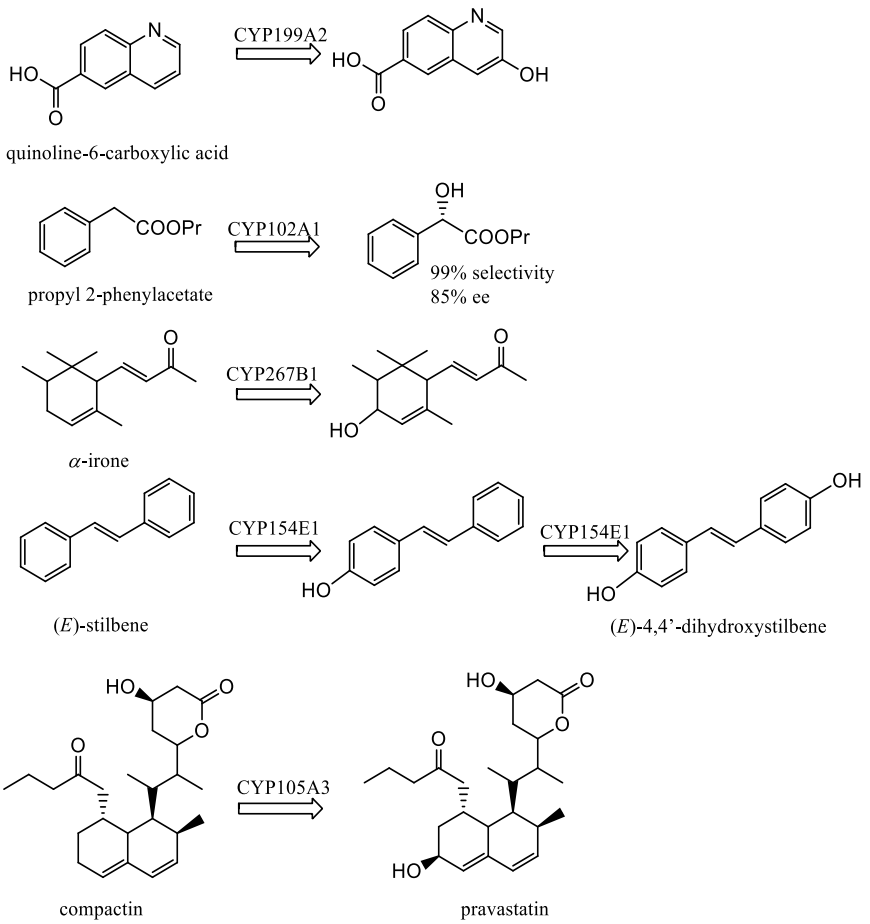

Figure 1. 11 P450 mediated selective oxidation of different substrates [125, 127, 133, 134].

Whole-cell biotransformation using P450s is also a valuable approach to produce drugs, vitamins, flavours, fragrances and pesticides [133]. Application of P450s in the field of bioremediation has generated significant interest as P450s can catalyse the degradation of chlorinated dibenzo-*p*-dioxin, polychlorinated biphenyl (PCB) and other pollutants which are

formed by different industrial processes [133, 135-137]. However, practical applications of P450 enzymes are still limited because of their low affinity and activity towards non-natural substrates [76, 138, 139]. Some P450s suffer from low stability and activity, and the desired substrates and products can be toxic to cells [76, 138, 139].

To address these issues, different approaches have been taken to improve P450 enzymes for use on a larger scale. Protein engineering of P450 enzymes including site-directed mutagenesis, random mutagenesis, construction of chimeric P450s and DNA shuffling methods have been used to improve their activity towards a broad range of non-physiological substrates [133, 140, 141]. For example, $P450_{BM3}$ from *Bacillus megaterium* is capable of oxidising *β*-ionone but exhibits weak binding and low product formation activity [142]. By using site-directed mutagenesis, the performance of $P450_{BM3}$ (F87V mutant) was increased towards *β*-ionone, resulting in a 115-fold increased product formation rate when compared to the wild-type (Figure 1. 12) [142]. The catalytic activity of CYP101A1 and CYP101D1 have also been enhanced via protein engineering approaches to enable the oxidation of hydrophobic substrates which were not generally accepted by the WT enzymes (Figure 1. 12) [143, 144].

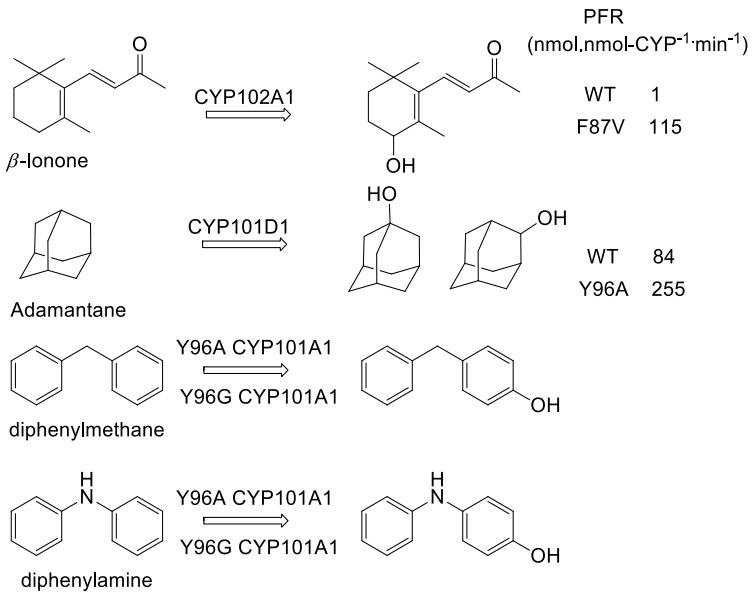

Figure 1. 12 The activities of wild-type CYP101D1 and CYP101A1 ($P450_{cam}$) which have been improved by protein engineering [143, 144]. No or little product was reported in the turnover of wild-type CYP101A1 enzyme with diphenylmethane and diphenylamine. However, Y96A and Y96G CYP101A1 variants catalysed the oxidation of these substrates efficiently.

The activity of different P450s such as CYP2A6 and CYP102A1 were expanded via random mutagenesis [145, 146]. For example, the F209T mutant of CYP2A6 displayed 13-fold higher activity over the wild-type in the oxidation of coumarin, and different variants of CYP102A1 such as F81I, E267V and L86I increased the catalytic activity of this enzyme with dextromethorphan and 3,4-methylenedioxy-methylamphetamine [145, 146]. Effective shuffling of P450 enzyme sequences could be another way to improve catalytic activities [147]. For example, a shuffled library of mammalian CYP2C9, CYP2C11 and CYP2C19 genes, was constructed using a modified DNA family shuffling approach and these enzymes displayed higher indole oxidation activity than the parental P450s [147].

Instead of protein modification, substrate engineering represents another useful strategy to enhance the efficacy of these enzymes for synthetic applications [138, 148-150]. This can be done via the installation of a functional group in a specific position of the substrate or the introduction of a chemical moiety to the substrate which then anchors the substrate in the active site of the enzyme in a place so that P450-mediated oxidation occurs efficiently [105]. This approach using a chemical auxiliary was successfully implemented to afford predictable oxidation of small hydrocarbon substrates and improve the activity of various P450s such as CYP102A1, CYP3A4 and CYP2E1 toward these non-natural substrates (Figure 1. 13) [105, 150-155]. Structural analysis by X-ray crystallography enables a better understanding of the substrate selectivity of the enzyme, and this information can be used to expand P450 activity [156].

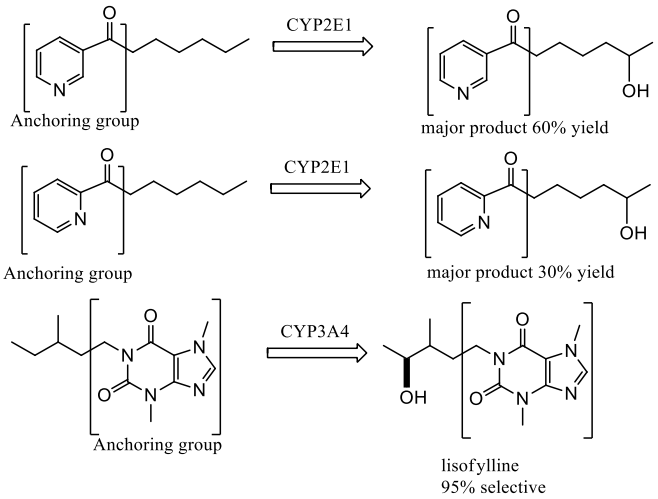

Figure 1. 13 P450 activity and selectivity has been improved through using type II P450 ligands [105, 151, 153]. These chemical auxiliaries allow P450s to oxidise inert C-H bonds with high regio-, chemo- and stereo-selectively.

As the performance of the P450 enzymes usually depend on the electron transfer, the requirement for appropriate redox partners and the expensive co-factor (NAD(P)H) for catalysis are still major limiting factors to utilise them in larger scale synthesis [157-159]. To overcome the 'cofactor challenge' different approaches have been developed including whole-cell biotransformation, biomimetic systems containing enzymatic cofactor regeneration systems and alternative nonenzymatic regeneration methods [160, 161].

Whole-cell biotransformation systems containing the desired P450 and electron transfer partner genes, can be used to regenerate the expensive reducing equivalents. These systems can be scaled up to larger-scale production [76, 139]. For example, different drug metabolites were generated in large-scale to support toxicity and biological activity assays using human P450s, e.g. CYP3A4, CYP2C9 and CYP1A2 which are expressed in *Escherichia coli* (Figure 1. 14) [162].

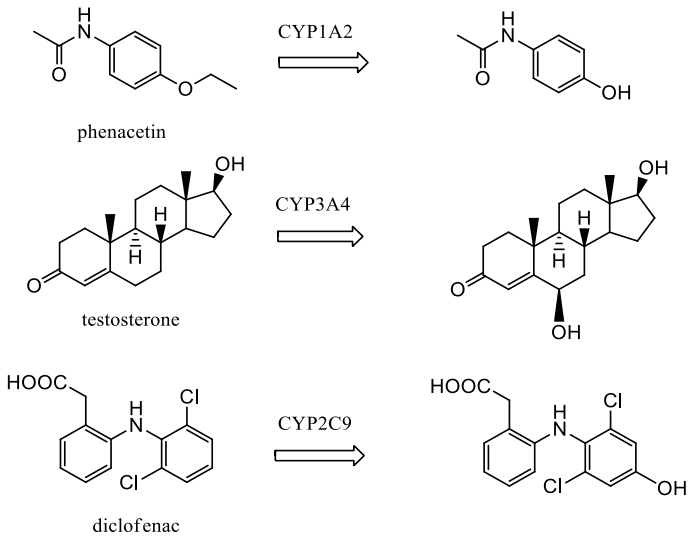

Figure 1. 14 Drug metabolites which have been synthesised in larger yield using different P450s to assess toxicity and biological activity [162].

Theoretically, the oxidised coenzyme $NAD(P)^+$ requires two electrons and a hydrogen ion to be reduced to NAD(P)H [163]. Different enzymatic systems for cofactor regeneration have been reported such as glucose dehydrogenase, phosphite dehydrogenase, alcohol dehydrogenase, amino acid dehydrogenase, formate dehydrogenase and NAD(P) oxidase [160, 161, 164, 165]. Many of these have been successfully applied in larger-scale syntheses [165]. There are some advantages to using glucose dehydrogenase such as it is commercially available, inexpensive and stable under aerobic conditions [166]. However, isolation of the generated P450 metabolites becomes

challenging due to the presence of glucose and gluconolactone [167]. To overcome this, formate dehydrogenase (FDH) can be used which uses formate as a substrate and catalyses NAD^+-mediated oxidation to form CO_2 and NADH (Figure 1. 15) [159]. Kragl and co-workers have reported a mutated FDH suitable for NADPH dependent P450s [159].

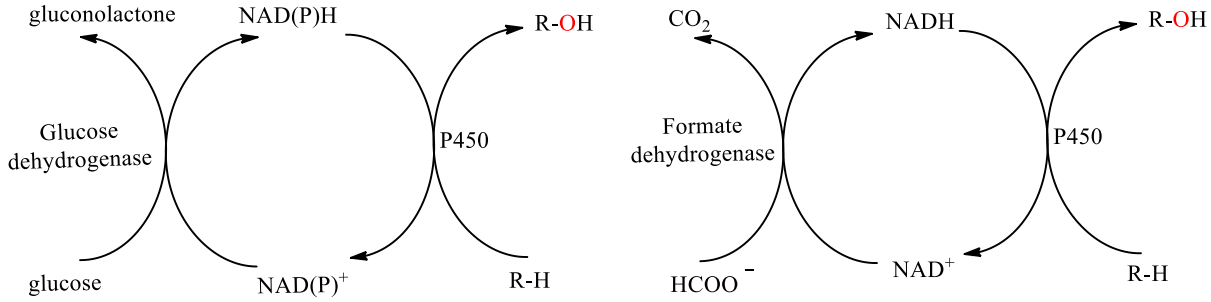

Figure 1. 15 Enzymatic regeneration of expensive redox cofactor [160, 168].

Electrochemical regeneration of either NADH or NADPH has the advantage which does not require a second enzyme and co-substrate, thereby avoiding the production of unwanted by-product(s) [160, 164]. Chemical catalysts such as organometallic complex $[Cp^*Rh(bpy)(H_2O)]^{2+}$ have also been reported to regenerate NADH and NADPH in monooxygenase turnovers [163, 169]. In this NAD(P)H regeneration approach the organometallic complex act as a hydride transfer reagent, and a cathode is used as a source of reducing equivalents [169].

1.5. P450 Enzymes from *Novosphingobium aromaticivorans*

Novosphingobium aromaticivorans DSM12444 is an oligotrophic bacterium first isolated from coastal plain subsurface sediments (at a depth of 410 m below land surface) in the USA [170, 171]. It is believed that the bacterium is capable of utilising different aromatic hydrocarbons including toluene, *p*-cresol, naphthalene, salicylate and xylenes as the sole carbon and energy source [170]. The genome of this bacteria contains sixteen P450 enzyme-encoding genes [48]. A large number of P450 and other monooxygenase and dioxygenase genes within the bacterium allow it to metabolise a wide variety of compounds and enable it to survive in an environment that offers very little support for life [171]. The sixteen P450s from this bacterium belong to ten different families, and among those, four enzymes (B1, C1, D1 and D2) are from the CYP101 family. These and one other from the CYP111 family (A2) use a common class I electron

transfer system consisting of a flavin-dependent ferredoxin reductase, ArR, and a [2Fe-2S] ferredoxin, Arx (Figure 1. 5) [30, 48-50, 172]. These five enzymes have been cloned with these physiological electron transfer partners in *Escherichia coli* cells to generate whole-cell biotransformation systems [48, 49, 172].

CYP101D1 and CYP101D2 have both been shown to selectively oxidise camphor to 5-*exo*-hydroxycamphor (Figure 1. 16) [48, 49]. This is the same metabolite formed with CYP101A1 ($P450_{cam}$) [25, 33, 48, 49, 173, 174]. CYP101B1 was found to oxidise camphor [48]. Unlike CYP101A1, CYP101D1 and CYP101D2, it was unselective, generating four different products (Figure 1. 16) [48, 49]. However, it displayed high activity and selectivity, when oxidising norisoprenoids such as α- and β-ionone. Furthermore, CYP101B1 exhibited high binding affinity with both α- and β-ionone (≥95% spin-state shift, K_d = 0.23 µM and 0.26 µM, respectively) and a fast product formation rate was observed in each substrate turnover. CYP101B1 catalysed the oxidation of these substrates efficiently and generated a 3-hydroxy α/β- ionone as a significant metabolite alongside a minor 4-hydroxy product (Figure 1. 17) [175]. This indicated that these norisoprenoids could closely resemble the natural substrates of this enzyme [175].

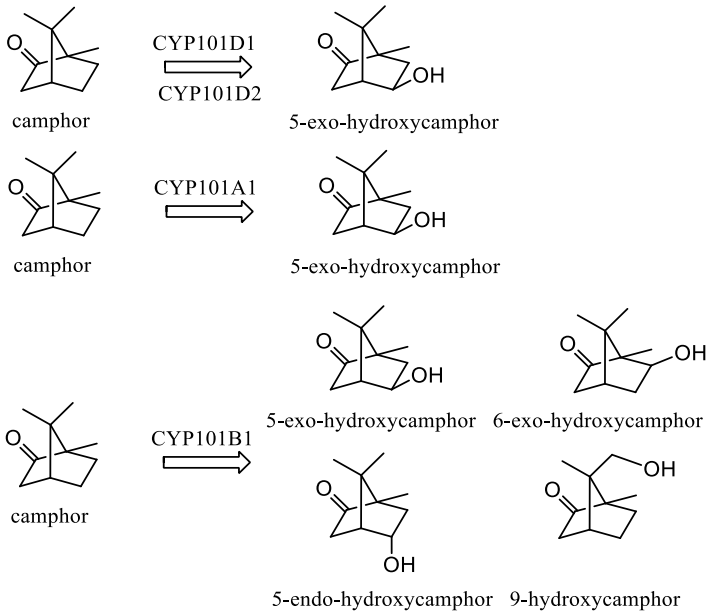

Figure 1. 16 The products reported from camphor oxidation by CYP101D1, CYP101D2, CYP101A1 and CYP101B1 [48, 49].

Further investigation of CYP101B1 has been carried out with a variety of other norisoprenoids such as β-damascone, which also bound to the enzyme with high affinity (≥80% HS, K_d = 8.3

µM). This was oxidised to two metabolites 3-hydroxy-*β*-damascone and 4-hydroxy-*β*-damascone (Figure 1. 17). When screened with monoterpenoids, CYP101B1 was found to be capable of oxidation, but levels of product formation activity and selectivity were lower when compared to norisoprenoids [176]. For instance, CYP101B1 catalysed the oxidation of (+)-fenchone to generate three hydroxylated metabolites with poor product formation activity compared to *α*- and *β*-ionone (Figure 1. 17) [176]. The efficiency and selectivity of oxidation of monoterpenoid substrates have been improved using their ester derivatives [176]. For example, CYP101B1 catalysed the oxidation of monoterpenoid esters such as myrtenyl acetate, bornyl acetate and fenchyl acetate with high product formation activities and selectivity. The turnovers of borneol, myrtenol and isoborneol generated multiple products at low yields [176].

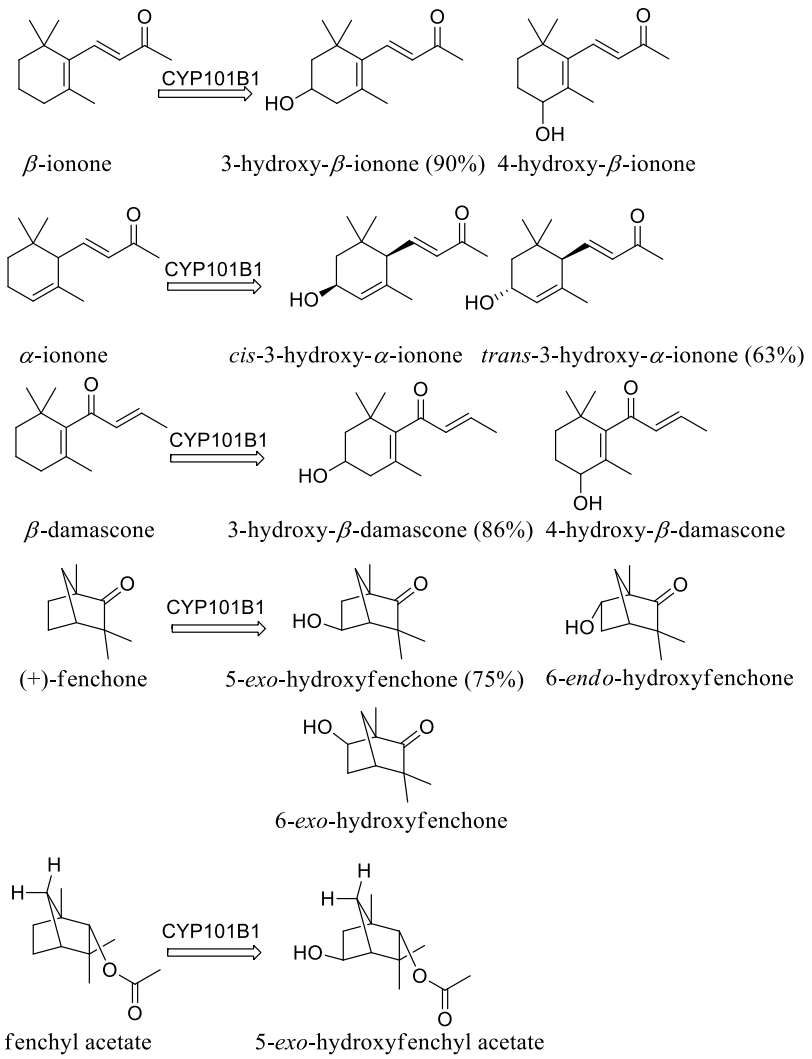

Figure 1. 17 CYP101B1 catalysed the oxidation of different classes of substrates [175, 176].

CYP101B1 was also able to bind and oxidise aromatic substrates including *p*-cymene and phenylcyclohexane (Figure 1. 18) [175]. These aromatic substrates induced a minimal spin-state shift in CYP101B1. The enzyme also exhibited weaker binding affinities for these substrates than norisoprenoids. The reactions were selective, but the product formation activities were lower suggesting that they are less effective substrates for CYP101B1 than those outlined above (Figure 1. 18) [175].

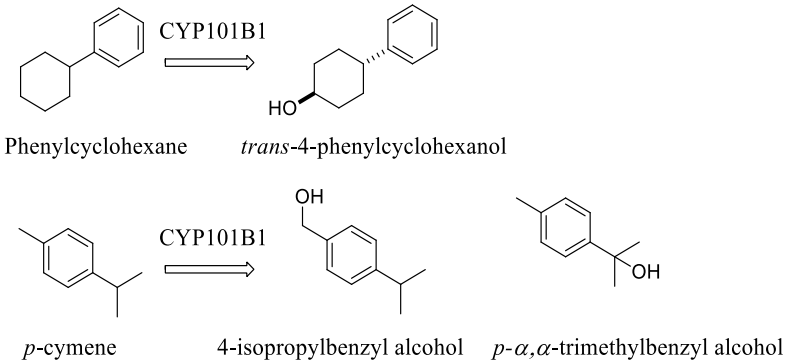

Figure 1. 18 Oxidation of aromatic substrates by CYP101B1 [175].

CYP101C1 from *Novosphingobium aromaticivorans* is a homologue of the CYP101B1 enzyme, also accepts electrons from the ArR/Arx class I electron transfer system [47]. CYP101C1 displays no activity for camphor oxidation [47]. CYP101C1 can oxidise norisoprenoid substrates, e.g. *β*-ionone with high activity. Interestingly only marginal changes in the heme spin-state shifts have been observed on substrate binding to CYP101C1 with any of these compounds [47, 48]. While CYP101C1 oxidised *β*-ionone to the same metabolites as CYP101B1, but the selectivity was different (Figure 1. 19). The major metabolite for CYP101C1 arises from C4 (75%) oxidation while CYP101B1 oxidised the substrate predominantly at the C3 (90%) position (Figure 1. 19) [47].

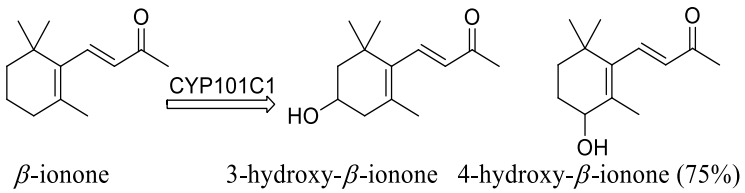

Figure 1. 19 Oxidation of *β*-ionone by CYP101C1 [47].

Whole-cell oxidation systems of both CYP101B1 and CYP101C1 have been generated, and these systems enabled the production of oxidised metabolites on a gram-per-litre scale which indicated they were viable for use in the production of metabolite for further characterisation [47, 176].

1.6. Thesis Aims

CYP101B1 and CYP101C1 exhibit activity for norisoprenoid oxidation resulting in different metabolite selectivity in *β*-ionone oxidation. CYP101B1 also shows interesting activity with monoterpenoid esters. To further explore the potential of both enzymes as biocatalysts for valuable chemical or drug metabolite synthesis, they will be tested with a series of compounds (C_6–C_{15}) which contain an alcohol, ester, or ketone functional group. These investigations will allow us to explore the substrate range of these enzymes in more detail and will generate valuable information about the activity with different sized substrates. Substrate engineering techniques will be implemented to improve the acceptance of alcohol substrates which show little or no affinity with the enzymes. It was hypothesised that introduction of a directing group, mimic to the butenone side chain of *β*-ionone, to cyclic alcohols, could enable more efficient and selective catalytic oxidation by both enzymes. A similar approach will be applied for tricyclic adamantane substrates to allow efficient oxidation of the inert tricyclic hydrocarbon skeleton of these substrates, and the regio and stereoselectivity will be assayed. Turnovers will be scaled up using whole-cell biotransformation systems and the products will be isolated for characterisation.

CYP101B1 has been shown to oxidise aromatic compounds like *p*-cymene and phenylcyclohexane, but the efficiency is low. To expand the substrate range, site-directed mutagenesis of CYP101B1 will be carried out with the intention of improving the activity towards these hydrophobic aromatic substrates. A variety of hydrophobic alkylbenzenes and naphthalenes will be screened with both wild-type and mutant CYP101B1 to determine if any hydroxy compounds can be generated. The whole-cell system will also be used to synthesise the metabolites on a larger-scale.

Cubane can act as bioisostere for benzene due to its similar size and shape, and it can be used to develop new drugs and agrochemicals with improved characteristics over existing candidates. Cubane derivatives can be synthesised using different chemical techniques, but new methodologies for functionalising these substrates are required. Methylcubane has also been used as a probe to elucidate the mechanism of the methane monooxygenase (MMO) from *Methylosinus trichosporium OB3b* and various P450 enzymes [177]. A series of 4-methylcubane derivatives will be designed and screened with CYP101B1 to assess how efficiently and selectively these cubane derivatives are oxidised. These reactions may be useful as mechanistic probes for CYP101B1 mediated hydroxylation of inert C-H bonds. This could determine if any rearrangement reactions arise from a radical or cationic intermediate which are formed during the hydroxylation process.

Finally, an additional form of uncoupling of the reducing equivalents by P450 systems in the presence of oxygenated aromatics will be investigated. Different electron transfer partners (ET) including those of the CYP101B1 system (ArR and Arx) will be used to provide a better understanding of this form of uncoupling in these systems.

Chapter 2

2. Experimental

2.1. General

General reagents, substrates, laboratory solvents, HPLC solvents were purchased from Sigma-Aldrich, Tokyo Chemical Industry (TCI), Alfa Aesar and Acros Organics. Antibiotics (ampicillin and kanamycin), isopropyl *β*-D-1-thiogalactopyranoside (IPTG), detergent (Tween 80) and dithiothreitol (DTT) were supplied by Astral Scientific (Australia).

2.2. Media Solution

The different media used for bacterial growth and whole-cell turnovers were as follows (all per litre of media) [233]:

Lysogeny Broth (LB)

- Yeast extract (5 g)
- Tryptone (10 g)
- NaCl (10 g)

2 x YT broth

- Yeast extract (10 g)
- Tryptone (16 g)
- NaCl (5 g)

Trace elements solution

- $FeCl_3$ ($6H_2O$) (16.7 g)
- Na_2EDTA (20.1 g)
- $CoCl_2$ ($6H_2O$) (0.25 g)
- $CaCl_2$ (H_2O) (0.74 g)

- $ZnSO_4$ ($7H_2O$) (0.18 g)
- $CuSO_4$ ($5H_2O$) (0.10 g)
- $MnSO_4$ ($4H_2O$) (0.132 g)

Super Optimal broth with Catabolite repression (SOC)

- Yeast extract (5 g)
- Tryptone (20 g)
- NaCl (0.5 g)
- $MgCl_2$ (1 g)
- KCl (0.2 g)
- Glucose (0.2% w/v)

E. coli minimal media (EMM)

- K_2HPO_4 (7 g)
- KH_2PO_4 (3 g)
- $(NH_4)_2SO_4$ (1 g)
- $Na_3C_6H_5O_7$ (Trisodium citrate**)** (0.5 g)
- $MgSO_4$ (0.1 g)
- 20% D-glucose (40 ml)

The required antibiotics such as ampicillin (100 µg ml^{-1}) and kanamycin (30 µg ml^{-1}) were added to LB and 2 x YT media as required.

UV/Vis spectroscopy was performed on a Varian Cary 60 or 5000 spectrophotometer, and these assays were recorded at 30 ± 0.5 ºC. The details of Gas Chromatography-Mass Spectrometry (GC-MS) and Gas Chromatography (GC) analyses, methods, columns and instrument conditions are provided in Table 2. 1. HPLC analyses were performed using an Agilent 1260 Infinity pump equipped with an Agilent Eclipse Plus C18 column (250 mm x 4.6 mm x 5 µm) and coupled with a UV detector (monitored at 280 nm for naphthalene, acenaphthene turnovers and 254 nm for biphenyls assays). A gradient of 20-95% acetonitrile (with trifluoroacetic acid, 0.1%) in water (TFA, 0.1%) was used.

Table 2. 1 Instrument Operating Conditions

GC-MS	**Shimadzu GC-17A instrument attached to a QP5050A MS detector**
Column	ZebronDB-5 MS fused silica column (30 m x 0.25 mm x 0.25 µm)
Column carrier gas Injector and interface temperature	Helium; flow rate 1.3 ml min^{-1} 250 °C and 280 °C
Methods for cyclic alkanes, cyclic ketones, cyclic esters, cubane, aromatic and adamantane compounds	140 °C (hold 3 min), 10 °C/ min to 220 °C (hold 7 min.)
Methods for cyclic alkanes (C6-C8) and small aromatic compounds	120 °C (hold 3 min), 10 °C/ min to 220 °C (hold 7 min.)
GC-MS	**Shimadzu GC-2010 coupled to a GC-MS-QP2010S detector**
Column	DB-5 MS fused silica column (30 m x 0.25 mm x 0.25 µm)
Column carrier gas Injector and interface temperature	Helium; flow rate 1.3 ml min^{-1} 250 °C and 280 °C
Methods for cyclic alkanes, ketones, esters, cubane, aromatic compounds	140 °C (hold 3 min), 10 °C min^{-1} to 220 °C (hold 7 min)
Methods for cyclic alkanes (C6-C8) and small aromatic compounds	120 °C (hold 3 min), 10 °C min^{-1} to 220 °C (hold 7 min)
GC	**Shimadzu Tracera GC coupled to Barrier Discharge Ionization Detector (BID)**
Column	Supelcowax column (Shimadzu Supelco, 30 m x 0.32 mm x 0.25 µm)
Column carrier gas Injector and BID temperatures	Helium and flow rate 1.3 ml min^{-1} 250 °C
Methods for cyclic alkanes, ketones, esters, cubane, aromatic compounds	120 °C (hold 3 min), 5 °C min^{-1} to 220 °C (hold 3 min)
Methods for cyclic alkanes (C6-C8) and small aromatic compounds	80 °C (hold 3 min), 5 °C min^{-1} to 220 °C (hold 3 min)
GC	**Shimadzu Tracera GC coupled to Barrier Discharge Ionization Detector (BID)**
Chiral Column	RT®- BDEXse chiral silica column (Restek; 30 m x 0.32 mm x 0.25 µm)
Column carrier gas Injector and BID temperatures	Helium and flow rate 3 ml min^{-1} 230 °C
Methods for cyclic alkanes, ketones, esters, cubane, aromatic compounds	100 °C (hold 3 min), 5 °C min^{-1} to 200 °C (hold 3 min)
Methods for cyclic alkanes (C6-C8) and small aromatic compounds	80 °C (hold 3 min), 5 °C min^{-1} to 200 °C (hold 3 min)

2.3. Enzyme Purification

2.3.1. Purification of CYP101B1 and CYP101C1

BL21 (DE3) *E. coli* competent cells were transformed with a plasmid vector (pET26; Merck Millipore) harbouring the appropriate CYP101B1 or CYP101C1 gene and grown on LB_{kan} plate. A single colony was added to each flask of $2xYT_{kan}$ or LB_{kan} (500 mL in each 2 L flask and a total of 3-4 L of media). These were grown at 37 ºC with shaking at 110 RPM for 10 hours. The temperature was decreased to 18 ºC, and 30 min later, ethanol (2% v/v) and benzyl alcohol (0.02% v/v) were added. Protein production was facilitated by adding 0.1 mM of IPTG from a 0.5 M stock solution. The culture was grown for a further 48 to 72 hours at 18 ºC and 90 rpm. The cell pellets were harvested by centrifugation (5000 *g*, 20 min at 4 ºC) and stored at -20 ºC before extraction. The pellets were resuspended in 200 mL Tris buffer (50 mM, pH 7.4) containing 1 mM DTT (Buffer T). The resuspended cells were lysed by sonication using an Autotune CV334 Ultrasonic Processor equipped with a standard probe (136 mm x 13 mm; Sonics and Materials, US). Pulses (40 x 20s on with 40 s intervals) were used to lyse the cells. The cell debris was discarded by centrifugation (37 000 *g*, 20 min, 4 ºC). The suspended protein was loaded onto a DEAE Sepharose column (XK50, 200 mm x 40 mm; GE Healthcare), and purified using a gradient from 100 to 250 mM KCl in buffer T at a flow rate of 6 mL min^{-1}. The red coloured protein containing fractions were combined and concentrated by ultrafiltration (10 kDa exclusion membrane). The concentrated protein was desalted by Sephadex G-25 coarse grain column (200 mm x 40 mm) using Buffer T.

The desalted protein was concentrated and loaded onto a Source-Q ion-exchange column (XK26, 80 mm x 30 mm; GE Healthcare) linked to an AKTA Pure (GE Healthcare), and eluted using a linear gradient from 50 to 400 mM KCl in Buffer T. The fractions containing pure protein, which had an absorbance ratio A_{419}/A_{280} >1, were combined and concentrated via ultrafiltration (10 kDa exclusion membrane). The concentrated protein was then centrifuged (7000 *g*, 10 min at 4 ºC) to remove solid debris. The protein was filtered using a 0.22 µm syringe filter after mixing with an equal volume of 80% glycerol and stored at -20 ºC. The extinction coefficients of CYP101B1 and CYP101C1 were reported as ε_{417} = 113 mM^{-1} cm^{-1}

and ε_{417} = 121 mM^{-1} cm^{-1} respectively, which were henceforth used to determine the concentration of the enzymes [5, 49].

2.3.2. Carbon Monoxide Binding Assays of Purified P450s

The ferrous- carbon monoxide (CO) spectrum was recorded to check the purified P450s and their mutant forms were functional. The P450 enzyme was diluted to ≈ 1 µM, and its spectrum was recorded from 700 nm to 250 nm using a UV-visible spectrophotometer. Sodium dithionite (~1 mg) was then added to the enzyme and the spectrum recorded. Carbon monoxide was gently bubbled through the enzyme solution, and the spectrum was re-recorded to generate ferrous-CO bound spectrum (Figure 2. 1) [5].

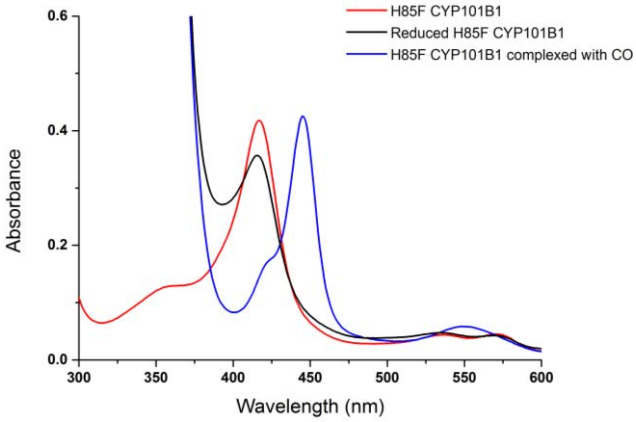

Figure 2. 1 An example of ferrous-carbon monoxide assay of purified P450.

2.3.3. Purification of Ferredoxin Reductase (ArR)

BL21 (DE3) *E. coli* competent cells (25 µL) were transformed with pET26 vector containing the ArR gene and grown on a LB_{kan} plate overnight [49, 175]. Colonies were added to LB_{kan} (6 x 500 mL) solutions and grown at 37 ºC at 120 rpm for 10 hours. The temperature was reduced to 18 ºC, and half an hour later, 10 mL ethanol and 200 µL benzyl alcohol were added to each flask. IPTG (0.1 mM) was added to induce the protein production, and the culture was grown for a further 72 h at 18 ºC and 90 rpm. The cell pellets were harvested by centrifugation (5000

g, 20 min at 4 ºC) and resuspended in 200 mL 50 mM buffer T, pH 7.4. The cells were lysed via sonication using 40 x 20 s with 40 s intervals. The resulting suspension was centrifuged to discard cell debris (37 000 *g*, 20 min, 4 ºC). The protein containing supernatant was loaded onto a DEAE Sepharose column (XK50, 200 mm x 40 mm; GE Healthcare) and purified using a salt gradient of 100 to 300 mM KCl in buffer T at a flow rate of 6 mL min^{-1}. The yellow coloured fractions combined and concentrated by ultrafiltration (10 kDa exclusion membrane). The concentrated protein was then desalted via a Sephadex G-25 medium grain column (250 mm x 40 mm; GE Healthcare). The desalted protein was further purified using Source-Q ion-exchange column (XK26, 80 mm x 30 mm; GE Healthcare) as described previously with elution using a linear gradient from 50 to 400 mM KCl in Buffer T. The ferredoxin reductase containing fractions with A_{280}/A_{458} <8, were combined and concentrated using ultrafiltration. The concentrated protein was centrifuged (7000 *g*, 10 min at 4 ºC) to remove particulate matter and protein was diluted with an equal volume of 80% glycerol. The diluted protein was further purified via a 0.22 µm syringe filter and stored at -20 ºC. The ArR concentration was estimated using extinction coefficient, ε_{458} = 10 mM^{-1} cm^{-1} [49].

2.3.4. Purification of Ferredoxin (Arx)

A pRSFDuet plasmid harbouring the gene encoding the ferredoxin (Arx) was transformed into BL21 (DE3) *E. coli* competent cells, and cells were grown on a LB_{kan} plate overnight [49]. The colonies from LB_{kan} plate were added to LB_{kan} (5 x 500 mL) media and grown at 37 ºC with continuous shaking at 120 rpm for 10 hours. The temperature was decreased to 18 ºC, and after half an hour 10 mL ethanol and 200 µL benzyl alcohol were added in each flask (500 mL growth media). Protein production was facilitated by adding 0.1 mM IPTG (from a 0.5 M stock solution), and the culture was grown for a further 72 hours at 90 rpm. The cell pellets were harvested by centrifugation (5000 *g*, 20 min at 4 ºC) and resuspended in 300 mL 10 mM, pH 7.4 Tris buffer solution (containing 1 mM DTT, 20% v/v glycerol, 1% v/v 2-mercaptoethanol, 300 mg lysozyme, 2 mL Triton X-100 and 2 mL Tween 20). The resuspended cells were stirred for 30 minutes on ice before sonication (see above).

The resulting solution was centrifuged to separate the cell debris from the soluble protein (37 000 *g*, 20 min, 4 ºC). The brown supernatant was loaded onto a DEAE Sepharose column

(XK50, 200 mm x 40 mm; GE Healthcare) and protein was eluted using a salt gradient of 100 to 600 mM KCl in Buffer T at a rate 6 mL min^{-1}. The brown fractions containing the ferredoxin were combined and concentrated using by ultrafiltration (3 kDa exclusion membrane). The concentrated protein was desalted using Sephadex G-25 medium grain column (200 mm x 40 mm) pre-equilibrated with Buffer T. The desalted protein was further purified using a Source-Q ion-exchange column (XK26, 80 mm x 30 mm; GE Healthcare) with elution using a linear gradient from 100 mM to 600 mM KCl in buffer T at a rate 6 mL min^{-1}. The fractions which had an absorbance A_{415}/A_{280} >0.6, were combined and concentrated using ultrafiltration (3 kDa exclusion membrane). The concentrated protein was centrifuged (7000 *g*, 10 min at 4 ºC) to remove any particulate matter before adding an equal amount of 80% glycerol. The protein was sterilised via a 0.22 µm syringe filter and stored at -20 ºC. The Arx concentration was calculated using the extinction coefficient, ε_{415} = 9.2 mM^{-1} cm^{-1} [49].

2.4. Whole-cell Biotransformation

The DNA vectors pETDuet harbouring the genes of the ferredoxin (Arx) and ferredoxin reductase (ArR), and the pRSFDuet containing the relevant P450 and Arx genes, were transformed together into BL21 (DE3) *E. coli* competent cells [49]. The transformed cells were grown on a $LB_{kan/amp}$ plate overnight at 37 ºC. A single colony from the plate was added to $LB_{kan/amp}$ (500 mL) media and allowed to grow for another 10 hours at 37 ºC with shaking (120 rpm). Protein production was induced as described in the previous sections and the culture was grown at 18 ºC and 90 rpm overnight (Figure 2. 2). The cell pellets were harvested from the growth media by centrifugation (5000 *g*, 20 min at 4 ºC), and cells were resuspended in 1 L *E. coli* minimal media (EMM).

The resuspended cells (200-250 mL) were transferred to 2 L baffled flasks and 0.5 to 1 mM substrate was added (the amount depended on substrate solubility). The flasks were shaken at 30 ºC and 150 rpm for 4 h. Further aliquots of the substrate (0.5 to 2 mM) were added along with additional glucose (2 mL from 20% solution) and phosphate-buffered saline (PBS, 2.5% v/v). The reactions were continued overnight before the cells were removed from the supernatant by centrifugation (5000 *g*, 20 min, 4 ºC). Products were extracted from the supernatant by liquid-liquid extraction using ethyl acetate or dichloromethane (3 x 100 mL),

washed with brine and dried with anhydrous magnesium sulphate. The extracted products were isolated by silica column chromatography with a gradient from 90:10 to 50:50 hexane to ethyl acetate, using a 5% increase in every 50 to 100 mL. The purified metabolites were characterised by NMR in deuterated chloroform or DMSO. NMR spectra were acquired on an Agilent DD2 or a Varian Inova spectrometer, operating at 500 or 600 MHz for ^{1}H and 126 or 151 MHz for ^{13}C. A combination of ^{1}H, ^{13}C, COSY, HSQC, HMBC and ROESY experiments were used to determine the structure of the metabolites.

2.5. Spin-State Shift

The relevant P450 enzyme was diluted to ~ 3 µM with 50 mM Tris buffer (pH 7.4). The UV-Vis spectrum was recorded from 700 nm to 250 nm. Aliquot of the substrate (1 µL from 100 mM stock solution in ethanol or DMSO) was added to 500 µL of the enzyme solution, and the spectrum was recorded. Further aliquots of the substrate were added until the shift from low-spin (420 nm) to high-spin (390 nm) did not change. The percentage of high-spin (HS) state shift induced by the substrate was estimated by comparing with the spectra of camphor-free and camphor-bound $P450_{cam}$ (CYP101A1; Figure 2. 2).

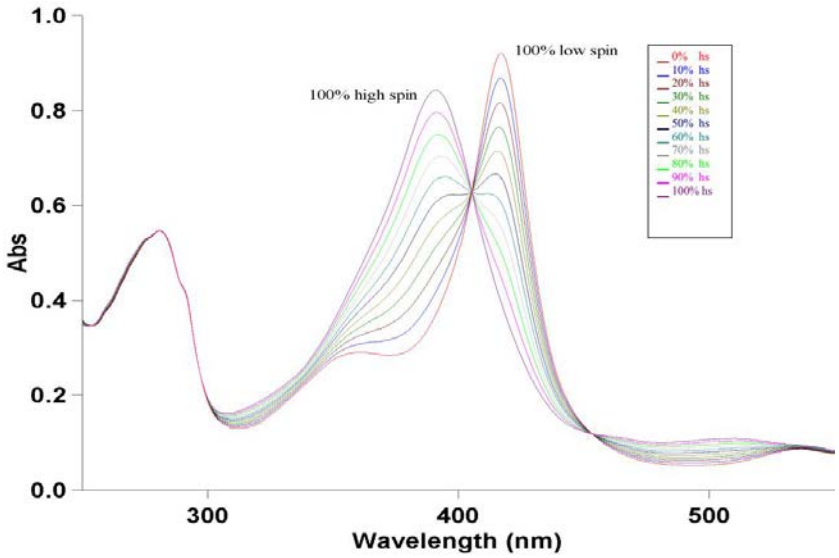

Figure 2. 2 The spin-state shifts of CYP101A1 ($P450_{cam}$) induced by camphor. This set of spectra was used to determine the heme spin-state change of substrate-bound P450 enzyme.

2.6. Substrate Binding Assays

Dissociation constants (K_d) were determined to measure how tightly the substrates bind to the enzymes. The P450 enzymes were diluted to ~1 μM with 50 mM Tris buffer pH 7.4. The UV-Vis spectrum of 2.5 mL of the enzyme was recorded between 600 nm to 300 nm, and the spectrophotometer was baselined. Successive aliquots of the substrate (cumulative volumes from 0.5 to 10 μL from 1 mM stock solution in ethanol/DMSO) were added, and the different spectra were recorded. Further aliquots (1 to 10 μL) of the substrate from 10 mM stock solution were then added. Finally, aliquots from 100 mM stock solution were added until the peak to trough absorbance difference remained constant. The peak to trough absorbance differences were plotted against the substrate concentration to determine the dissociation constant of the substrate and fitted to hyperbolic function (Eqn 2. 1) [178, 179]:

$$\Delta A = \frac{\Delta A_{\max} \times [\mathrm{S}]}{K_d + [\mathrm{S}]} \qquad \textbf{Eqn 2. 1}$$

Where ΔA represents the peak to trough absorbance difference, ΔA_{max} is the maximum absorbance difference, [S] represents substrate concentration, and K_d is the dissociation constant.

If substrates exhibited tight binding, defined as having a dissociation constant less than five times that of the enzyme concentration (K_d < 5[E]), the data was instead fitted to the tight binding quadratic equation (Morrison) (Eqn 2. 2) [180].

$$\frac{\Delta A}{\Delta A_{\max}} = \frac{([E]+[S]+K_d) - \sqrt{\{([E]+[S]+K_d)^2 - 4[E][S]\}}}{2[E]} \qquad \textbf{Eqn 2. 2}$$

where ΔA is the peak-to-trough absorbance difference, ΔA_{max} represents the maximum absorbance difference, [S] is the substrate concentration and [E] represents the enzyme concentration [180].

2.7. *In Vitro* NADH Turnover Assays

NADH turnover/consumption rates were measured by preparing a 1.2 mL mixture containing 0.5 µM of P450 enzyme, 5 µM ferredoxin (Arx), 1 µM ferredoxin reductase (ArR), 12 µL bovine liver catalase and oxygenated 50 mM Tris buffer, pH 7.4, in a cuvette. This was allowed to reach 30 ºC, and NADH was added to a concentration ~ 320 µM (A_{340}~ 2). The absorbance was monitored at 340 nm by a UV-Vis spectrophotometer (Figure 2.3). After one minute, 0.2 -1 mM of the substrate from a 100 mM stock solution in ethanol or DMSO was then added and mixed by inversion (the amount of substrate added was dependent on the substrate solubility). The NADH oxidation rate was calculated by recording the gradient of the absorbance at 340 nm versus time and using the extinction coefficient of NADH, ε_{340} = 6.22 mM^{-1} cm^{-1} (Figure 2. 3).

The *in vitro* turnovers were analysed via GC, GC-MS and HPLC to assess product formation (Table 2. 1). Co-elution experiments were used to identify the products generated in turnovers with authentic standards in GC, GC-MS, and HPLC. If standards were not available, the metabolites were synthesised in larger yield using a whole-cell oxidation system for characterisation. For GC and GC-MS analysis, 990 µL of the reaction mixture was taken and mixed with 10 µL of internal standard (20 mM *p*-cresol in ethanol). The mixture was then extracted with 400 µL of ethyl acetate. The organic extracts were analysed directly by GC/GC-MS. For HPLC, 150 µL of the reaction mixture was mixed with 2 µL internal standard (9-hydroxyfluorene in ethanol) and 100 µL of acetonitrile (AcCN). This sample was then analysed in HPLC.

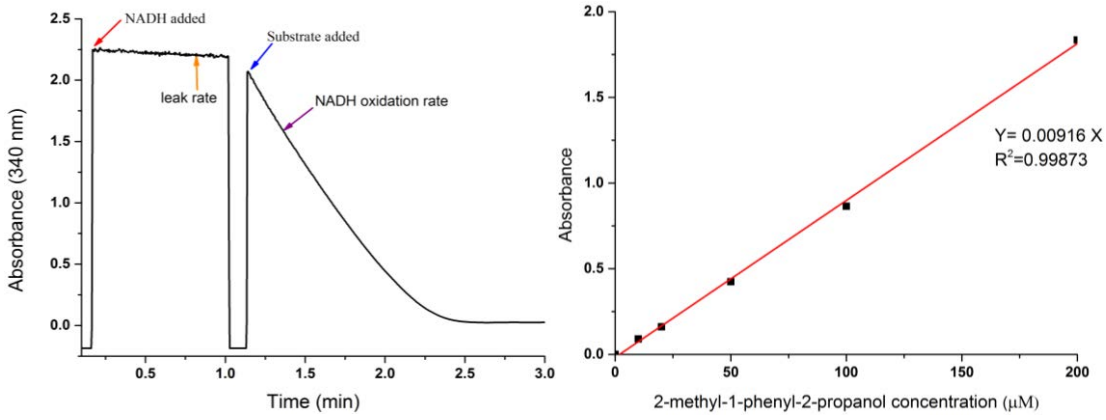

(a) (b)

Figure 2. 3 (a) The *in vitro* turnover of CYP101B1 with cyclooctyl acetate monitored at 340 nm. **(b)** Calibration curve of 2-methyl-1-phenyl-2-propanol.

The ratio of total area of product(s) and internal standard was used to calculate the product concentration. Metabolites were calibrated using the authentic product standard or isomers of the product or substrates where authentic products not available. These standards, at different concentrations (10 µM to 200 µM), were combined with an internal standard (500 µM) as described above for sample preparation. These were then analysed via HPLC/GC/GC-MS using the same method as for the turnovers. Product and internal standard area ratios were plotted against the concentrations to create the calibration curve which was used to measure the amount of metabolite generated in the turnovers (Figure 2. 3). To calculate the productive use of reducing equivalents (coupling efficiency), the concentration of the product formed in the turnover was divided by the concentration of NADH that was added (calculated from the absorbance at 340 nm). The proportion of product formed per NADH molecule oxidised (the coupling efficiency) was used with the NADH oxidation rate to give the product formation rate.

The total turnover number (TTN) was determined with the best substrates to monitor the efficiency and activity of the enzyme over an extended period. These were determined using a ArR:Arx:CYP101B1 concentration ratio of 1:10:1. The CYP enzyme (0.1 µM) was combined with ArR (0.1 mM), Arx (1 µM), 2 mM substrate and 4 mM NADH. Oxygenated 50 mM Tris buffer, pH 7.4, was added to the mixture to a final volume of 1.2 mL. The turnover mixture was kept at room temperature for 2 hours before extraction with 400 µL of ethyl acetate. The organic extracts were analysed directly by GC/GC-MS.

2.8. Hydrogen Peroxide Assays

The concentration of hydrogen peroxide (H_2O_2), generated from the uncoupling of NADH during *in vitro* turnovers, was determined using horseradish peroxidase (HRP), phenol and aminoantipyrine (4-AP) [181]. The turnover incubation mixture (400 µL) was combined with 200 µL of a solution of 50 mM phenol (in Tris buffer, pH 7.4) and 200 µL aminoantipyrine (5 mM stock solution in 50 mM Tris buffer, pH 7.4). The absorbance of the resulting mixture at 510 nm (λ_{max} of the quinoneimine coupling product, ε_{510} = 6580 $M^{-1}cm^{-1}$) was set to zero, and 1 µL of horseradish peroxidase (20 mg mL^{-1} HRP in water) was then added. The absorbance at 510 nm was recorded. The concentration of resulting quinoneimine, which arises from the

reaction between peroxidase-mediated oxidation of phenol by hydrogen peroxide and 4-AP, was calculated in µM, using equation Eqn 2. 3:

$$[\boldsymbol{quinoneimine}] = \frac{\boldsymbol{A_{510}\ \mathrm{X}\ 10^6}}{\boldsymbol{6580}} \qquad \textbf{Eqn 2. 3}$$

As the incubation mixture was diluted 2-fold (400 µL to 800 µL) and two molecules of hydrogen peroxide (H_2O_2) are required to form the quinone, the concentration of hydrogen peroxide formed was then calculated using equation Eqn 2. 4:

$$[\boldsymbol{H_2O_2}] = \mathbf{4\ x}\ \frac{\boldsymbol{A_{510}\ \mathrm{X}\ 10^6}}{\boldsymbol{6580}} \qquad \textbf{Eqn 2. 4}$$

2.9. Synthesis of Ester Substrates

The cyclic alcohols (cyclohexanol, cyclooctanol, cyclododecanol and adamantanol) substrates (~0.5 g, 1.0 eq) were dissolved in dichloromethane (~20 mL), and trimethylamine (~2.0 eq) was added at 0 °C and stirred for 5.0 minutes. Isobutyryl chloride (~1.2 eq) or acetyl chloride (~1.2 eq) was then added dropwise at 0 °C, and the reaction was subsequently stirred at room temperature for 3.0 hours (Figure 2. 4).

Adamantyl derivatives were synthesised by Samrat Dasgupta using the following method [182]. For 1-adamantyl acetate synthesis, pyridine (~0.65 mL, 3.0 eq) was added to a solution of 1-adamantanol (500 mg, 1.0 eq) in dichloromethane (~20 mL) at 0 °C and stirred for 5 minutes. Acetyl chloride (~0.3 mL, 1.5 eq) was added dropwise at 0 °C, and the reaction was stirred at room temperature (RT) for two to four hours. The progress of the synthesis was monitored by TLC or GC/GC-MS.

On completion, the reaction mixtures were washed with a saturated sodium bicarbonate solution. The organic layer was isolated and washed with brine solution, dried over anhydrous Na_2SO_4 or $MgSO_4$, filtered and concentrated under vacuum to obtain the crude product. The products were separated by silica chromatography using a 5% ethyl acetate/petroleum benzine mixture, and the acetate/isobutyrate products were obtained as colourless oils. Similar methods were used to synthesise cyclohexyl isobutyrate, cyclooctyl acetate, cyclooctyl isobutyrate and

cyclododecyl acetate but in all cases, trimethylamine was used instead of pyridine. The synthesised substrates were characterised using NMR spectroscopy and mass spectrometry (Table 2. 2 and Figure A. 1 to Figure A. 17).

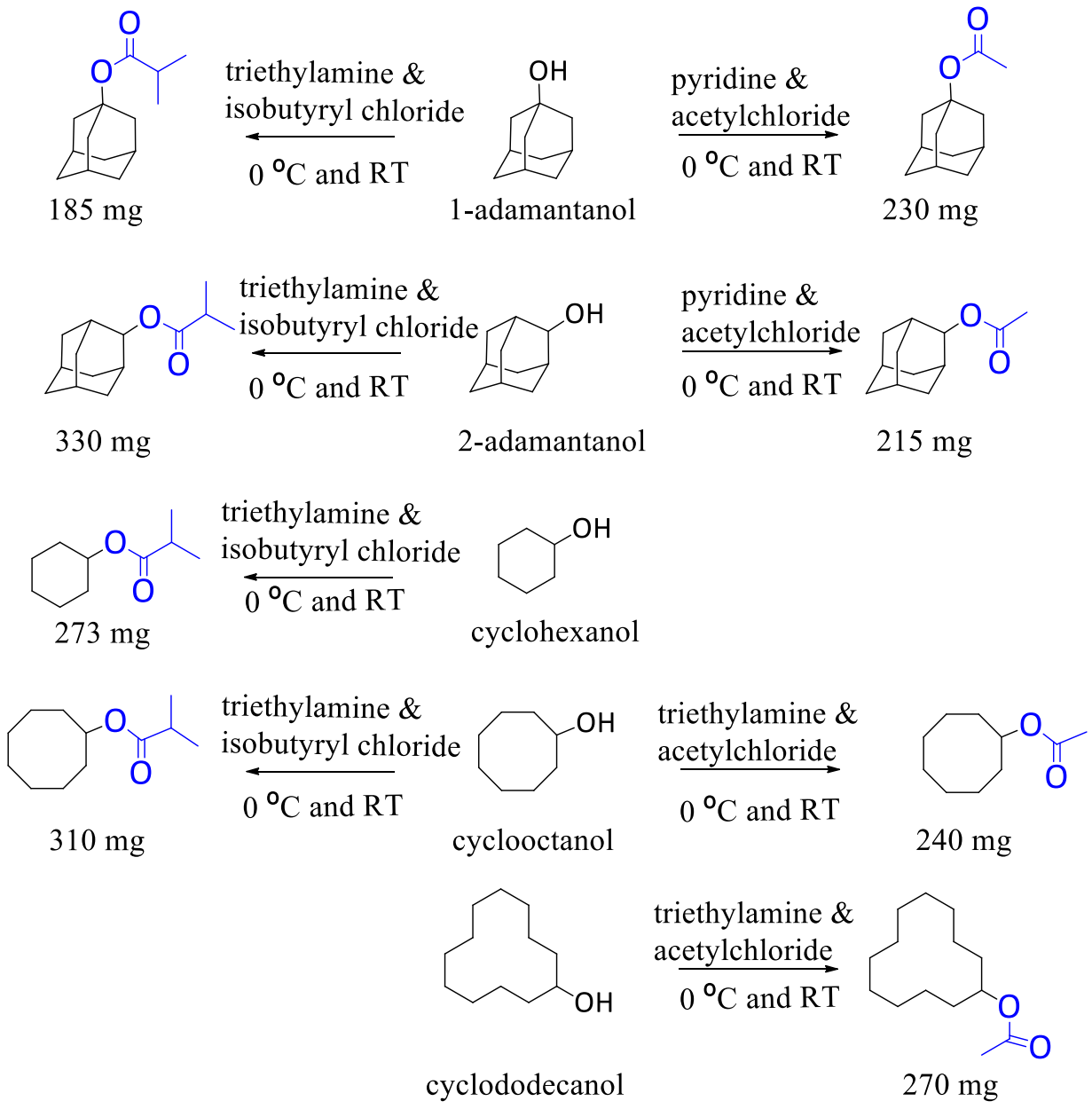

Figure 2. 4 The synthesis of 1-adamantyl acetate, 2-adamantyl acetate, 1-adamantyl isobutyrate, 2-adamantyl isobutyrate, cyclohexyl isobutyrate, cycooctyl acetate, cyclooctyl isobutyrate and cyclododecyl acetate.

Table 2. 2 NMR analysis of synthesised ester derivatives (Full data in Appendix A; # synthesised by Samrat Dasgupta).

Substrates	Confirmation (NMR)
1-adamantyl acetate # Conversion and Yield (44% and 230 mg)	^{1}H NMR (500 MHz, $CDCl_3$) [182] δ 2.18-2.13 (m, 3H, H3, H5 & H7), 2.11-2.08 (m, 6H, 2xH2, 2xH9 & 2xH10), 1.96 (s, 3H, 3xH12), 1.70-1.61 (m, 6H, 2xH4, 2xH6 & 2xH8). ^{13}C NMR (126 MHz, $CDCl_3$) δ 172.92 (C11), 82.65 (C1), 43.68 (C2, C9 & C10), 38.65 (C4, C6 & C8), 33.31 (C3, C5 & C7), 25.47 (C12).
2-adamantyl acetate # Conversion and Yield (43% and 215 mg)	^{1}H NMR (500 MHz, $CDCl_3$) [182] δ 4.96-4.83 (m, 1H, H2), 2.07 (s, 3H, 3xH12), 2.05-1.97 (m, 4H, H1, H3, H8 & H10), 1.88-1.82 (m, 4H, H4, H5, H7 & H9), 1.80-1.73 (m, 4H, H4, 2xH6 & H9), 1.56 (d, J = 10.6 Hz, 2H, H8 & H10). ^{13}C NMR (126 MHz, $CDCl_3$) δ 173.50 (C11), 79.54 (C2), 40.04 (C6), 39.01 (C4 & C9), 34.65 (C1 & C3), 34.37 (C8 & C10), 29.88/29.69 (C5/C7), 24.23 (C12).
1-adamantyl isobutyrate # Conversion and Yield (36% and 185 mg)	^{1}H NMR (500 MHz, $CDCl_3$) [182] δ 2.43 (*septet*, J = 7.0 Hz, 1H, H12), 2.19-2.14 (m, 3H, H3, H5 & H7), 2.13-2.05 (m, 6H, 2xH2, 2xH9 & 2xH10), 1.72-1.63 (m, 6H, 2xH4, 2xH6 & 2xH8), 1.11 (d, J = 7.0 Hz, 6H, 3xH13 & 3xH14).
2-adamantyl isobutyrate Conversion and Yield (66% and 330 mg)	^{1}H NMR (500 MHz, $CDCl_3$) [182] δ 4.93-4.87 (m, 1H, H2), 2.57 (*septet*, J = 7.0 Hz, 1H, H12), 2.05-1.96 (m, 4H, H1, H3, H8 & H10), 1.87-1.81 (m, 4H, H4, H5, H7 & H9), 1.79-1.41 (m, 4H, H4, 2xH6 & H9), 1.56 (d, J = 11.9 Hz, 2H, H8 & H10), 1.19 (d, J = 7.0 Hz, 6H, 3xH13 & 3xH14). ^{13}C NMR (126 MHz, $CDCl_3$) δ 179 (C11), 79.04 (C2), 40.04 (C6), 38.98 (C4 & C9), 37.06 (C12), 34.49 (C1 & C3), 34.44 (C8 & C10), 29.91/29.66 (C5/C7), 21.70 (C13 & C14).
cyclohexyl isobutyrate # Conversion and Yield (55% and 273 mg)	^{1}H NMR (500 MHz, $CDCl_3$) δ 4.82-4.66 (m, 1H, H1), 2.52 (*septet*, J = 7.0 Hz, 1H, H8), 1.88-1.66 (m, 10H), 1.16 (d, J = 7.0 Hz, 6H, 3xH9 & 3xH10).
cyclooctyl acetate Conversion and Yield (48% and 240 mg)	^{1}H NMR (500 MHz, $CDCl_3$) δ 4.95-4.85 (m, 1H, H1), 1.99 (s, 3H, 3xH10), 1.83-1.42 (m, 14H).
cyclooctyl isobutyrate Conversion and Yield (62% and 310 mg)	^{1}H NMR (500 MHz, $CDCl_3$) δ 4.99-4.84 (m, 1H, H1), 2.49 (*septet*, J = 7.0 Hz, 1H, H10), 1.85-1.43 (m, 14H), 1.15 (d, J = 7.0 Hz, 6H, 3xH11 & 3xH12).
cyclododecyl acetate Conversion and Yield (50% and 270 mg)	^{1}H NMR (500 MHz, $CDCl_3$) δ 5.05-4.95 (m, 1H, H1), 2.03 (s, 3H, 3xH14), 1.76-1.63 & 1.53-1.26 (m, 22H).

Chapter 3

3. Biocatalytic Oxidation of Saturated Hydrocarbons by CYP101B1 and CYP101C1

3.1. Introduction

Alicyclic compounds, which constitute a large class of organic compounds including monocyclic cycloalkanes, cycloalkanones and cycloalkyl esters, are used in manufacturing perfumes, flavours, essential oils, tobacco products, herbicides, insecticides and serve as intermediates in the pharmaceutical industry [183, 184]. They are the main constituents of petroleum; for example, *n*-alkanes, branched alkanes, monocyclic substrates like cyclopentane and cyclohexane compounds are the most predominant. They are also commonly used as solvents and found as secondary metabolites in microbes and plants such as terpenoids [183-188]. Functionalisation of the C-H bonds of alicyclic compounds would have an enormous impact on the field of chemical synthesis [189-193]. Indeed, selective C-H bond activations could pave the way for preparing more complex molecular skeletons [194, 195]. Unfortunately, selective C-H bond functionalisation is one of the most challenging chemical processes due to the low reactivity of the bond and overoxidation issues [193, 196]. The selective hydroxylation of alicyclic hydrocarbons using mild conditions is a primary goal for synthetic chemistry [196-198]. Different metal catalysts and oxidising reagents have been reported to oxidise the inert C-H bonds of alicyclic compounds [199-203]. For instance, cyclohexanone and cyclohexanol, which are essential chemical intermediates for the synthesis of polyamide and plastics, are synthesised using various cyclohexane oxidation processes including H_2O_2-based hydroxylation, Au-Pd bimetallic catalysts and homogeneous transition-metal salt catalysts which are designed to reduce the occurrence of overoxidation products [193, 204-206]. However, despite an enormous effort over the last few decades, several challenges remain [196]. The main concern is that harsh chemicals, heavy metals and toxic solvents are used in most of these chemical oxidation approaches [207].

The use of an enzyme biocatalyst instead of the toxic chemical catalyst could be an alternative and efficient approach to avoid the issues discussed above. Many bacterial and fungal species have been shown to oxidise cyclic compounds C-H bonds [187]. For examples, Fonken *et al.*

reported oxidation of C12-, C13- and C14- macrocyclic compounds using *Sporotrichum sulfurescens* (*Beauveria sulfurescens* ATCC7159) and Ashton *et al.* described the oxidation of cyclododecanone and cyclopentadecanone by different fungi such as *Calonectria decora*, *Daedalea rufescens*, *Ophiobolus herpotrichus* and *Rhizopus nigricans* [208, 209]. CYP153A6 from a *Mycobacterium* sp. hydroxylates medium-chain-length alkanes and cyclic alkanes (C6 to C11) [210]. CYP153A13a from *Alcanivorax borkumensis* SK2 was fused to RhFred to improve the activity towards alkane hydroxylation. The oxidation of different length alkanes and cyclic alkanes were also catalysed with high regioselectively at the terminal carbon by membrane-bound P450s such as rabbit CYP4B1 and CYP52A3 from *Candida maltosa* [211, 212]. Self-sufficient P450 BM3 and some of its mutants have been reported to oxidise C8-C12 cycloalkanes [213]. However, in most of the above cases, product formation activity or selectivity was low. For example, the turnover rate for CYP4B1 was 11-33 min^{-1} with C7 to C10 *n*-alkyl hydrocarbons and in other instance, the oxidation of cyclic and linear alkanes by wild type CYP102A1 proceeded with low activity and selectivity [211-213].

CYP101B1 and CYP101C1 can oxidise *β*-ionone and other norisoprenoids, and CYP101B1 has been shown to be a highly efficient biocatalyst for other related substrates including monoterpenoids acetates [47, 175, 176]. CYP101B1 oxidises *β*-ionone preferentially hydroxylating at the C-3 (90%) position while CYP101C1 can efficiently hydroxylate at the C-4 (75%) [47, 175]. The butenone side chain of *β*-ionone is an important structural feature enabling the substrate to bind effectively to CYP101B1 [175]. It is hypothesised that this butenone side chain holds the substrate in a place for efficient and selective oxidation. This is one of the key features which allows these oxidation reactions to proceed with high catalytic activity, turnover number and coupling efficiency [175]. Previous studies have shown that when an acetate ester directing group was added to monoterpenoid structures the binding affinity and oxidation activity with CYP101B1 increased dramatically [176]. With these bicyclic terpenoids the regioselectivity of oxidation also improved with the site of C-H bond abstraction being on the opposite side of the ring system to the ester group. This is in agreement with the regioselectivity of norisoprenoid oxidation by CYP101B1. The substrates chosen here would test the directing capability of the ester group on more flexible cycloalkyl rings. With this in mind, it was decided to investigate a series of cyclic substrates, ranging in ring size from 6 to 15 carbons including their alcohols and ketones, with CYP101B1 and CYP101C1 (Figure 3. 1). Both enzymes were tested with a range of compounds containing an ester directing group, such as acetate and isobutyrate which

would mimic the butenone side chain of *β*-ionone, to assess this effect on the catalytic activity of these two enzymes (Figure 3. 24).

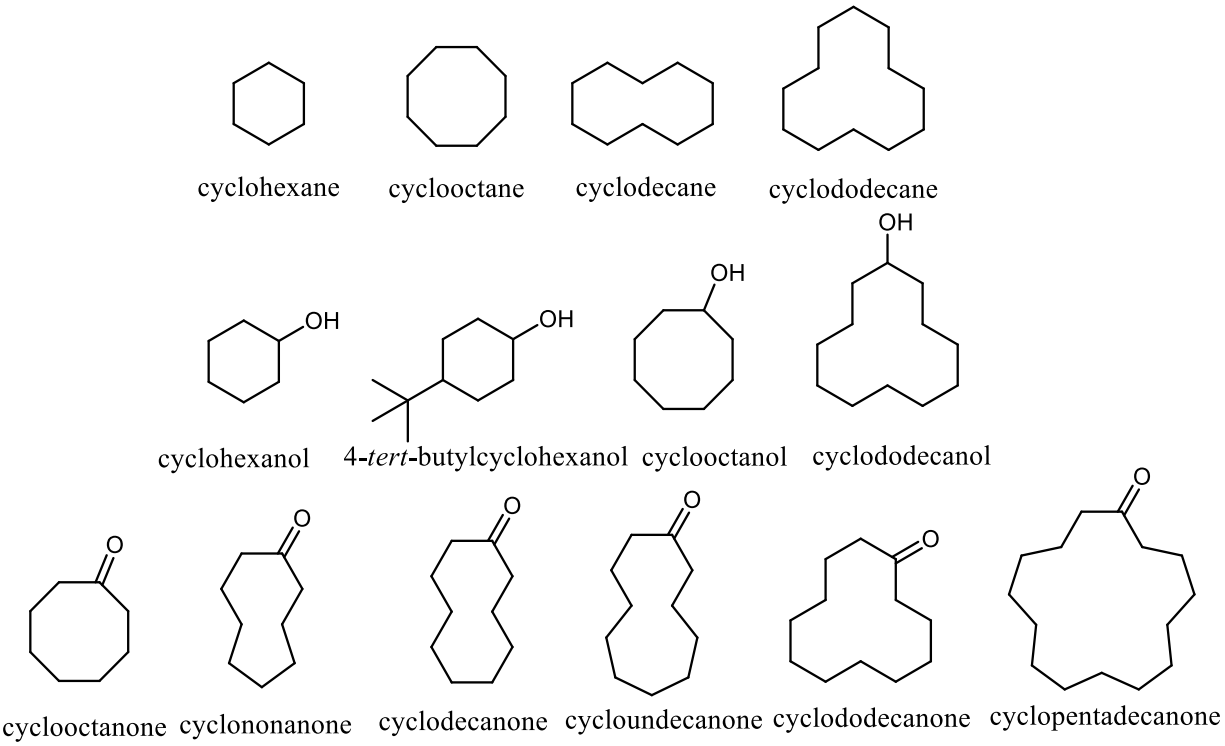

Figure 3. 1 The cyclic compounds screened with CYP101B1 and CYP101C1.

3.2. Results

3.2.1 The oxidation of cyclic alkanes, alcohols and ketones by CYP101B1 and CYP101C1

The spin-state shift induced by substrate binding gives a general indication of the ability of the substrates to replace the water ligand bound to the heme iron and hence if it fits into the active site. The spin-state shift of CYP101B1 was analysed with each substrate (Figure 3. 1). None of the previous substrates investigated with CYP101C1 induced a substantial change of the spin-state from the low spin form. None of the substrates studied here significantly altered the spin-state of CYP101C1 either. This could be due to this enzyme having a very specific active site or other reasons as described previously [47].

Cyclohexane induced a shift to 15% high spin in CYP101B1 (henceforth % will be assigned to the proportion of high spin (HS) heme-induced by substrate binding). Cyclooctane shifted the spin-state by a greater degree than cyclohexane (35%; Table 3. 1 and Figure 3. 2). The larger

cycloalkanes cyclodecane and cyclododecane displayed similar heme spin-state shifts to that of cyclooctane (30-40%; Table 3. 1 and Figure 3. 2). These results indicated that these hydrocarbon substrates were not well accommodated in the active site of CYP101B1. The substrate binding affinity of cyclooctane, cyclodecane and cyclododecane was analysed. With cyclodecane and cyclododecane, the binding affinity was tighter with a low dissociation constant K_d = 0.88 ± 0.04 µM and K_d = 0.16 ± 0.03 µM, respectively, while cyclooctane bound with the enzyme more weakly (K_d = 31 ± 4 µM; Figure 3. 3).

The cyclic alcohols cyclohexanol and cyclooctanol shifted the spin-state to less than 5%, suggesting these are poor substrates for the CYP101B1 enzyme (Table 3. 1 and Figure 3. 2). 4-*tert*-Butylcyclohexanol induced the heme spin-state shift to 15% high spin upon addition to CYP101B1 (Figure 3. 2). However, cyclododecanol altered 90% of the heme iron spin to high spin-state and exhibited a tight binding with a dissociation constant K_d of 1.5 µM (Figure 3. 3).

The NADH oxidation and product formation rates give a general indication of P450 activity; these were observed to be low for CYP101B1 with cyclohexane, 61 nmol.(nmol-P450)$^{-1}$ .min^{-1} and 2 nmol.(nmol-P450)$^{-1}$.min^{-1}, respectively (henceforth abbreviated to min^{-1}; Table 3. 1). The coupling efficiency which is the productive use of reducing equivalent was also minimal (3%; Table 3. 1). These results were in agreement with the small spin-state shift induced by cyclohexane. CYP101C1 showed even lower product formation activity with cyclohexane (Table 3. 1). The conversion of cyclohexane by both enzymes yielded to a single metabolite, which was identified as cyclohexanol by a GC coelution experiment with an authentic standard (Figure 3. 4). The turnover of cyclohexanol with CYP101B1 also displayed a slow NADH oxidation rate (53 min^{-1}), and no product was detected in GC/GC-MS analysis (Table 3. 1). Although CYP101B1 exhibited high NADH oxidation activity for 4-*tert*-butylcyclohexanol, no product was observed in the turnovers (Table 3. 1). These results indicated that cyclohexanol and 4-*tert*-butylcyclohexanol were not accepted by CYP101B1 and CYP101C1 at all.

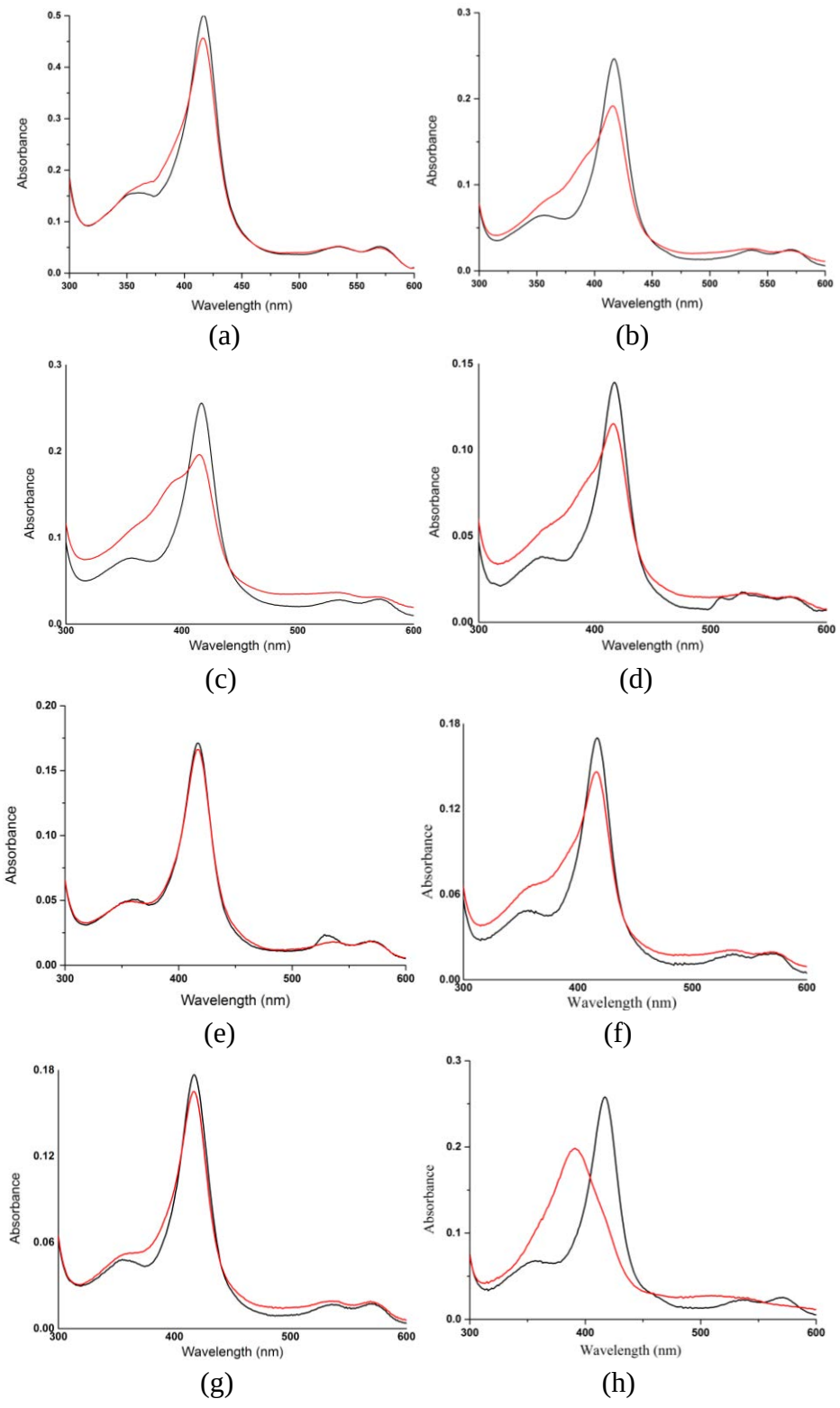

Figure 3. 2 The spin-state shifts (red) of CYP101B1 after addition of **(a)** cyclohexane, **(b)** cyclooctane, **(c)** cyclodecane, **(d)** cyclododecane, **(e)** cyclohexanol, **(f)** 4-*tert*-butylcyclohexanol, **(g)** cyclooctanol and **(h)** cyclododecanol.

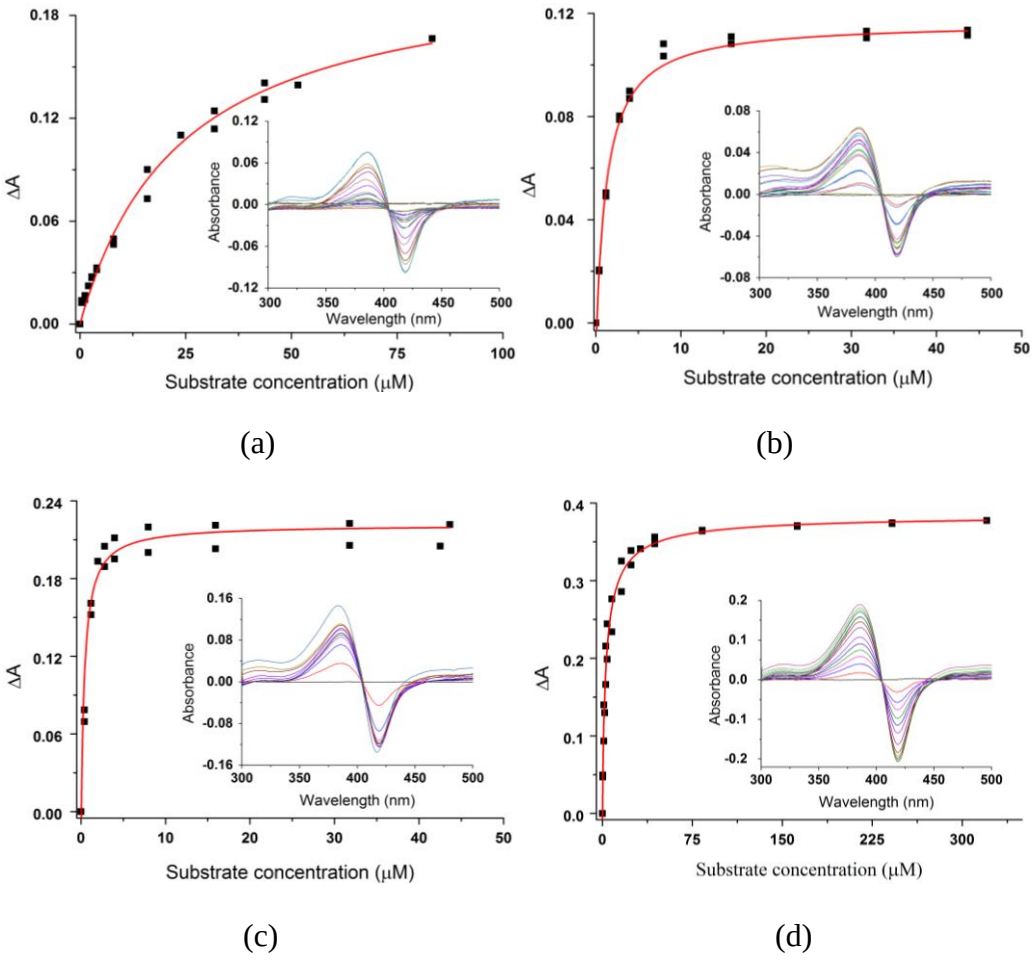

Figure 3. 3 Dissociation constant analysis with **(a)** cyclooctane (2.19 μM CYP101B1/ K_d 31 ± 4 μM), **(b)** cyclodecane (1.23 μM CYP101B1/K_d 0.88 ± 0.04 μM), **(c)** cyclododecane (2.37 μM CYP101B1/ K_d 0.16 ± 0.03 μM), and **(d)** cyclododecanol (2.37 μM CYP101B1/ K_d 1.5 ± 0.3 μM). The concentration of enzyme used in the analyses and the dissociation constants (K_d) are provided in brackets. The dissociation constant for cyclohexane was not measured due to the low response of the spin-state to substrate addition.

Addition of cyclooctane to CYP101B1 induced a six-fold faster NADH oxidation rate (391 min^{-1}) than that observed with cyclohexane (Table 3. 1). Higher levels of product formation activity compared to the cyclohexane turnovers were detected, and this was reflected in the coupling efficiency of the turnover (49% versus 3%; Table 3. 1). Cyclooctane displayed lower NADH oxidation activity (90 min^{-1}) and product formation rate (18 min^{-1}) in the CYP101C1 system than the CYP101B1 (Table 3. 1). A significant metabolite (99% selectivity) was detected in the GC-MS analyses of the *in vitro* turnovers of both CYP101B1 and CYP101C1 with cyclooctane. This metabolite was identified as cyclooctanol by GC-MS coelution

experiment with an authentic cyclooctanol standard (m^+/z = 128.05; Figure 3. 4 and Figure B. 1). A minor peak was also detected in the GC-MS analysis that had a different mass spectrum (1%; m^+/z = 126.05; Figure B. 1). This product was confirmed as cyclooctanone by GC-MS coelution experiment with an authentic standard (Figure 3. 4). The oxidation of cyclooctanol by CYP101B1 resulted in little or no detectable product formation activity despite having a NADH oxidation rate of 158 min^{-1} (Table 3. 1). Overall, both enzymes oxidised cyclooctane more efficiently when compared with cyclohexane, but CYP101B1 was a better system than CYP101C1.

CYP101B1 displayed a higher NADH oxidation rate (397 min^{-1}) upon addition of cyclodecane than the CYP101C1 system (164 min^{-1}, Table 3. 1). However, the product formation rates with both enzymes were lower than the cyclooctane. In the case of CYP101B1, this was predominantly due to a reduced coupling efficiency (11% versus 49%; Table 3. 1). CYP101B1 also exhibited a lower total turnover number with cyclodecane than the cyclooctane (420 versus 3400; Table 3. 1). This could be due to the lower water solubility of cyclodecane. The *in vitro* turnovers of cyclodecane by both enzymes generated two monooxygenase metabolites. The minor product (5% for CYP101B1 and 25% for CYP101C1) was identified as cyclodecanone (m^+/z = 154.20) by GC-MS coelution experiments with a commercial standard (Figure 3. 5 and Figure B. 1). The other metabolite was confirmed as cyclodecanol (m^+/z = 156.20) by coeluting the product generated from the reduction of cyclodecanone with sodium borohydride ($NaBH_4$) using a standard method (Figure 3. 4 and Figure B. 1) [214].

Cyclododecane induced a faster NADH oxidation activity (174 min^{-1}) in CYP101B1 than CYP101C1 (84 min^{-1}; Table 3. 1). The product formation rates of CYP101B1 and CYP101C1 with cyclododecane were slower compared to cyclooctane (Table 3. 1). Despite the low product formation activity and coupling efficiency, both enzymes catalysed the oxidation of cyclododecane and formed a single major metabolite (92% for CYP101B1 and 60% for CYP101C1; based on GC peaks area) alongside two minor products. The metabolites detected in the GC-MS analyses of the *in vitro* turnovers of both enzymes did not coelute with a cyclododecanol standard (Figure 3. 6). In order to identify these products, cyclododecanol was investigated as a substrate with both enzymes. Cyclododecanol changed the heme spin-state to 90% high spin upon addition to CYP101B1. The product formation rate (41 min^{-1}) and the coupling efficiency (21%) were superior to those of the parent cycloalkane (Table 3. 1).

CYP101C1 had a slightly higher NADH oxidation activity (280 min^{-1}) than the CYP101B1 system, but the product formation rate was lower due to a coupling efficiency of only 11% (Table 3. 1).

Table 3. 1 Substrate binding, turnover and coupling efficiency data for CYP101B1 and CYP101C with cyclic alkanes and alcohols. The *in vitro* turnover activities were measured using a ArR: Arx: P450 concentration ratio of 1:10:1 (0.5 µM CYP enzyme, 50 mM Tris, pH 7.4). TTN, the total turnover numbers, were determined using assays set up with the same ratio of enzymes as used *in vitro* turnovers but with 0.1 µM CYP enzyme, 1 to 2 mM substrate and 4 mM NADH (theoretical maximum value 20,000 for 2 mM substrate). N is the NADH oxidation rate, PFR the product formation rate and C is the coupling efficiency, which is the percentage of NADH utilised for the formation of products. The data are reported as mean ± S.D. (n = 3). Rates are given in nmol.nmol-CYP^{-1}.min^{-1}. - not measured or not able to be determined accurately.

Substrate	CYP101B1/ CYP101C1	%HS heme	N (Min^{-1})	PFR (Min^{-1})	C (%)	TTN
cyclohexane	CYP101B1	15	61 ± 9	2 ± 1	3	-
	CYP101C1	**-**	**42 ± 4**	**<1**	**<1**	**-**
cyclohexanol	CYP101B1	5	53 ± 2	-	-	-
4-*tert*-butylcyclohexanol	CYP101B1	15	363 ± 9	-	-	-
cyclooctane	CYP101B1	35	391 ± 11	209 ± 17	49	3400 ± 150
	CYP101C1	**-**	**90 ± 13**	**18 ± 7**	**20**	**-**
cyclooctanol	CYP101B1	10	158 ± 2	-	-	-
cyclodecane	CYP101B1	40	397 ± 15	42 ± 34	11	420 ± 75
	CYP101C1	**-**	**164 ± 5**	**17 ± 7**	**13**	**-**
cyclododecane	CYP101B1	30	174 ± 5	15 ± 3	9	-
	CYP101C1	**-**	**84 ± 10**	**2 ± 1**	**2**	**-**
cyclododecanol	CYP101B1	90	198 ± 7	41 ± 1	21	1360 ± 90
	CYP101C1	**-**	**280 ± 5**	**31 ± 20**	**11**	**650 ± 40**

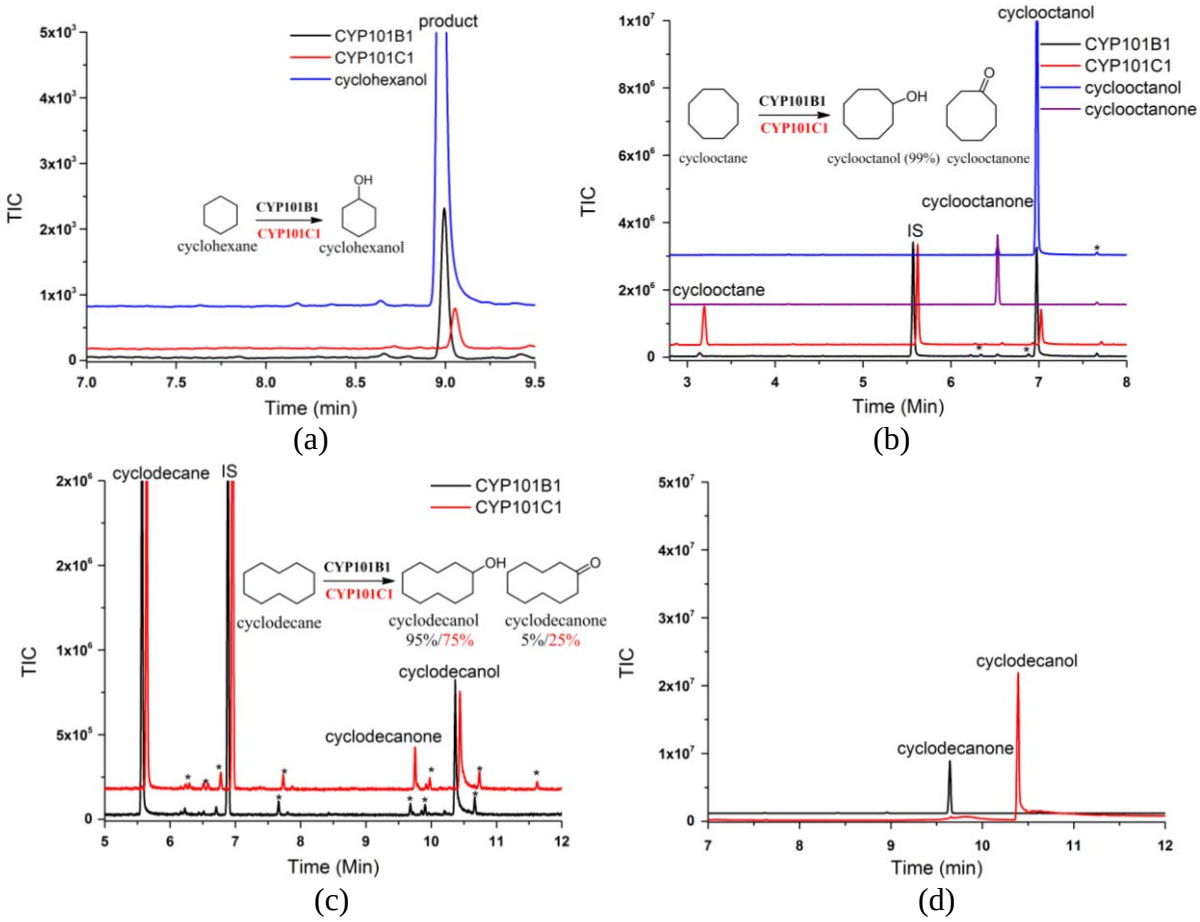

Figure 3. 4 (a) GC analysis of the turnover of cyclohexane by CYP101B1 (black) and CYP101C1 (red). Cyclohexane (RT 2.05 min, not shown) and the product; cyclohexanol (8.9 min). **(b)** GC-MS analysis of the turnovers of cyclooctane by CYP101B1 (black) and CYP101C1 (red). Cyclooctane (RT 3.2 min) and the products; cyclooctanone (6.6 min) and cyclooctanol (6.9 min). **(c)** GC-MS analysis of the turnovers of cyclodecane by CYP101B1 (black) and CYP101C1 (red). Cyclodecane (RT 5.1 min) and the products; cyclodecanone (9.7 min) and cyclodecanol (10.45 min). **(d)** The control of cyclodecanone, and cyclodecanol generated from the reduction of cyclodecanone by $NaBH_4$. Impurities are labelled (*). The chromatograms (a, b, c) were offset along the x and y-axes for clarity (CYP101C1; red).

The GC-MS/GC analysis of CYP101B1 *in-vitro* turnover with cyclododecanol showed a primary product (90% based on GC peaks area; m^+/z = 200.10) alongside two minor metabolites. The metabolites were generated by whole-cell biotransformation resulting in a total conversion of substrate into the products (Figure 3. 6). The metabolites (total ~25 mg) were difficult to separate from each other. However, the products were identified via ^{13}C NMR carbon signals and their relative intensities (Figure 3. 5). The major product (at RT 19.6 min; 90%) was characterised as 1,7-cyclododecanediol which showed four carbon signals 71.48

(C1, C7), 35.21 (C2, C6, C8, C12), 26.86 (C4, C10) and 23.72 (C3, C5, C9, C11) in the ^{13}C NMR with an intensity ratio 2:4:2:4 (Figure 3. 5, Table 3. 2 and Figure B. 2-B. 6) [215]. One of the minor (6%; RT 19.65 min) metabolites was characterised as 1,6-cyclododecanediol due to six equal intensity carbon signals 71.25 (C2, C6), 35.40 (C2, C5), 35.31 (C7, C12), 26.26 (C3, C4), 24.79 (C8, C11), 23.5 (C9, C10) in the ^{13}C NMR (Table 3. 2 and Figure B. 2-B. 6). The other minor product (RT 9.7 min) was presumed to be either the other diastereomer of 1,6-cyclododecanediol or 1,4-cyclododecanediol as the ^{13}C NMR also had additional six carbon signals of equal intensity.

The metabolites of the cyclododecane *in vitro* turnovers by CYP101B1 and CYP101C1 were then confirmed by GC-MS coelution experiments with the cyclododecanol turnover (Figure 3. 6). The main (~92%) and minor metabolites of cyclododecane turnovers by CYP101B1 were 1,7-cyclododecanediol and 1,6-cyclododecanediol, respectively as the retention time matched with the major and minor products of the cyclododecanol turnover (Figure 3. 6). The selectivity of cyclododecane and cyclododecanol oxidation was reduced for CYP101C1. This generated the same major metabolite (60%) which was observed in the GC-MS analysis of CYP101B1 turnover, alongside two minor products accounted for the remaining 40% of the total turnover products formed. It is assumed that both enzymes converted the cyclododecane into cyclododecanol, which is then further oxidised to 1,7-cyclododecanediol and 1,6-cyclododecanediol (Figure 3. 6).

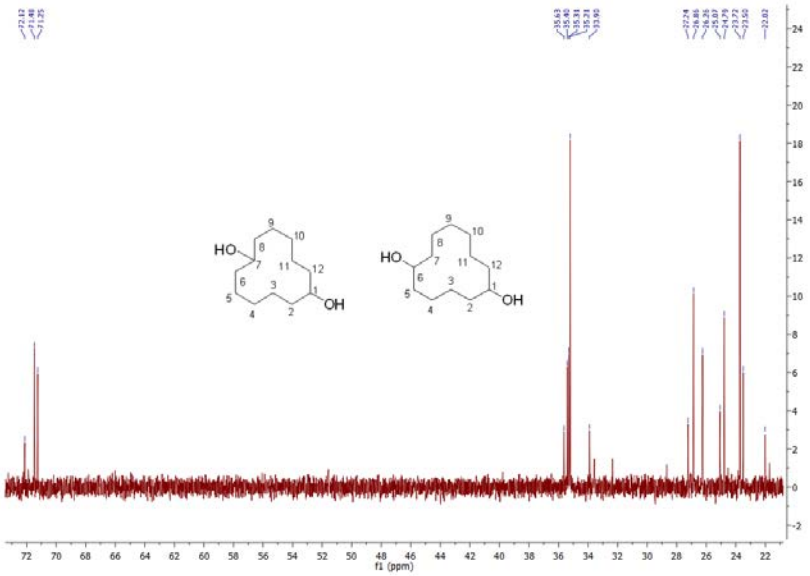

Figure 3. 5 ^{13}C NMR of a mixture of 1,7-cyclododecanediol, 1,6-cyclododecanediol and an unknown metabolite. The details of assignment of the carbon peaks see Table 3. 2. Full data are given in Appendix B (Figure B. 2-B. 6).

Table 3. 2 The assignments of cyclododecanol metabolites using ^{13}C NMR.

		1,7-cyclododecanediol [215] (4 signals) 2:4:2:4 intensity	1,6-cyclododecanediol (6 signals) equal intensity	Remaining (6 signals) Equal intensity
Carbons	**Intensity**	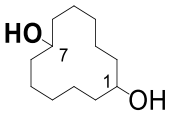	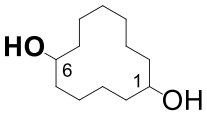	Either diastereomer of C6 or C4 as six signals
72.12	1			
71.48	2	C1, C7		
71.25	2		C1, C6	
35.63	1			
35.40	2		C2, C5	
35.31	2		C7, C12	
35.21	4	C2, C6, C8, C12		
33.90	1			
27.24	1			
26.86	2	C4, C10		
26.26	2		C3, C4	
25.07	1			
24.79	2		C8, C11	
23.72	4	C3, C5, C9, C11		
23.5	2		C9, C10	
22.02	1			

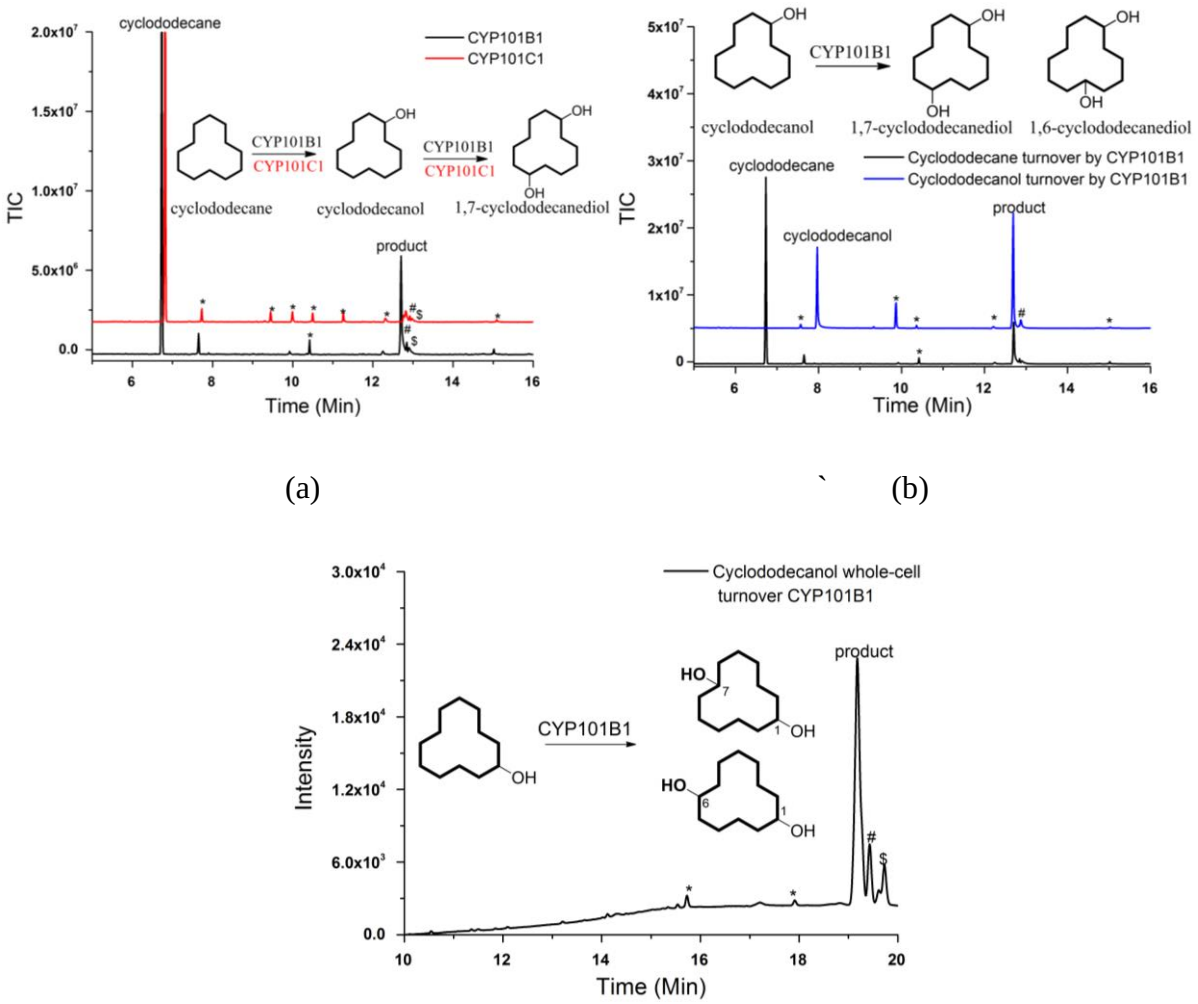

Figure 3. 6 (a) GC-MS analysis of cyclododecane *in vitro* turnovers by CYP101B1 (black) and CYP101C1 (red). Cyclododecane (RT 6.8 min) and the products; 1,7-cyclododecanediol (RT 12.9 min), 1,6-cyclododecanediol and unknown metabolite (RT 12.95 min and RT 13.0 min) labelled as # and $. The chromatogram (CYP101C1) was offset along the x and y-axis for clarity. **(b)** GC-MS analysis of cyclododecanol turnover with CYP101B1. Cyclododecanol (RT 7.9 min) and the products; 1,7-cyclododecanediol (RT 12.9 min) and 1,6-cyclododecanediol (RT 12.95 min) labelled as #. **(c)** The GC analysis of the whole-cell turnover of cyclododecanol. Cyclododecanol (RT 10.2 min) and the product; 1,7-cyclododecanediol (RT 19.6 min) and the minor metabolites; 1,6-cyclododecanediol and an unknown (RT 19.65 min$^{\#}$ and RT 19.7 min$^{\$}$). Impurities are marked (*).

Overall, the spin-state shifts of CYP101B1 with smaller C6 cycloalkane and cyclic alcohols were lower compared to C8 to C12 cycloalkane substrates. Cyclooctane, cyclodecane and cyclododecane induced almost similar spin-state changes upon addition to the CYP101B1 enzyme. CYP101C1 and CYP101B1 are capable of metabolising cycloalkanes, and the later enzyme showed higher product formation activity (Figure 3. 7). Neither enzyme showed little to no activity with cyclohexanol and cyclooctanol, but they both can oxidise cyclododecanol.

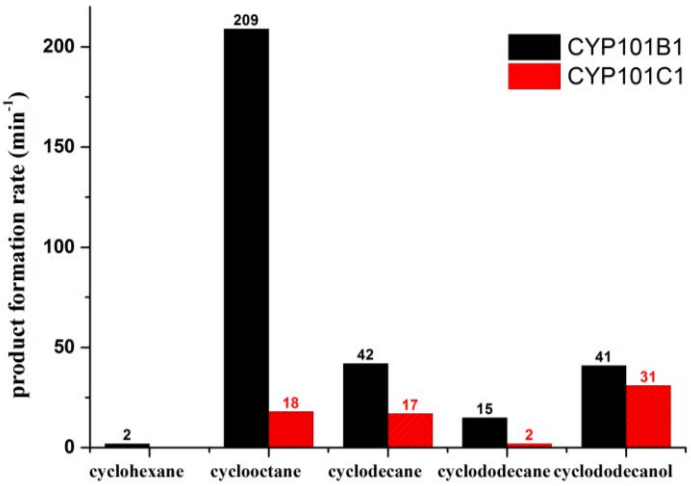

Figure 3. 7 The overall product formation rates of CYP101B1 and CYP101C1 with cyclic alkanes and alcohols. Product formation rates are given in nmol.nmol-CYP^{-1}.min^{-1}.

Different cycloalkanones were screened with both enzymes to explore the binding affinity and catalytic activity with substrates containing a ketone moiety. Cyclooctanone induced a 10% heme spin-state shift in CYP101B1, which was even lower than cyclooctane (Figure 3. 8 and Table 3. 3). Both enzymes displayed low activity, and there was no evidence of any product formation with cyclooctanone.

Addition of cyclononanone shifted the heme spin-state of CYP101B1 to 30% high spin form (Figure 3. 8). The dissociation constant (K_d) of CYP101B1 with cyclononanone was determined 46 ± 21 µM (Figure 3. 8 and Table 3. 3). The NADH oxidation rate for CYP101B1 and CYP101C1 was 308 min^{-1} and 289 min^{-1}, respectively (Table 3. 3). In the case of CYP101B1, the product formation activity measured 131 min^{-1} which was higher than that observed for CYP101C1 (75 min^{-1}; Table 3. 3). This was due to the greater coupling efficiency

of 43% for CYP101B1. The improved product formation rates and coupling efficiencies of CYP101B1 and CYP101C1 with cyclononanone compared to the C10 and C12 cycloalkanes illustrated that the ketone group might play an important role in enhancing substrate binding and oxidation activity.

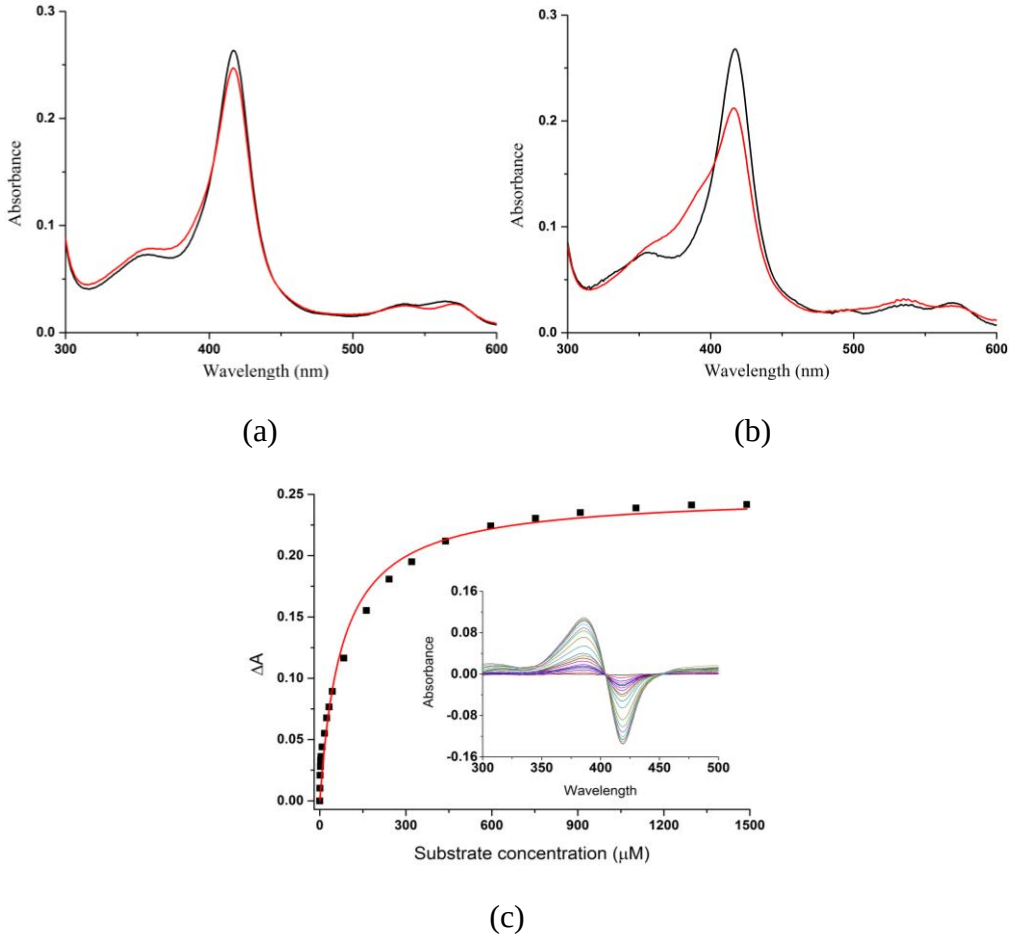

Figure 3. 8 The spin-state shifts (red) of CYP101B1 after addition of **(a)** cyclooctanone and **(b)** cyclononanone. **(c)** The dissociation constant analysis with cyclononanone (2.11 μM CYP101B1/ K_d 46 μM). The concentration of the enzyme used in the binding assay and the dissociation constant (K_d) are provided in brackets.

The GC-MS analyses of the *in vitro* turnovers of CYP101B1 and CYP101C1 with cyclononanone showed different regioselectivity (Figure 3. 9). Both transformed the cyclononanone to monooxygenase metabolites, and whole-cell turnovers were carried out to generate each metabolite in a sufficient amount for identification (Figure B. 1). Each product

was purified via silica column chromatography and identified by NMR and their mass spectra (Figure 3. 9, Figure B. 1 and Figure B. 7-B. 16).

The primary metabolite (98%; at RT 12.2 min) generated by CYP101C1 was assigned as 2-hydroxycyclononanone by NMR analysis [216, 221]. It contained a multiplet peak at 4.28-4.21 (H2) and a distinct peak of -CO**H** proton (C2) at 3.7-3.72 ppm in ^{1}H NMR, which is observed due to the interaction with C=O (Figure 3. 9 and Figure B. 7-B. 10) [216, 221]. The mass spectrum also matched with that reported in the literature (m^{+}/z = 156.15; Figure B. 1) [216, 221]. This product was the minor metabolite in the CYP101B1 turnover (4%; Figure 3. 9). The chiral GC analysis of the *in vitro* turnover of CYP101C1 displayed a mixture of 2-hydroxycyclononanone enantiomers in a distribution of 30 to 70 % (Figure 3. 9). Further investigation is required to find out which enantiomer is in excess.

The main product (87%; at RT 11.2 min) from the CYP101B1 *in vivo* turnover was purified (~22 mg) by silica column chromatography. The ^{1}H NMR spectrum had a multiplet signal at δ 4.04-4.17 ppm (Figure 3. 10). However, in the ^{13}C spectrum C1 (C=O) peak was not detectable and a distinct signal at 100.36 ppm was present (Figure B. 12). The HMBC NMR spectrum showed a strong correlation of C1 (100.36 ppm) to H5 δ (4.04-4.17 ppm), which indicated a cyclisation connecting C1 to C5 (Figure B. 11-B. 16 and Table 3. 4). This metabolite was assigned as 1-hydroxy-10-oxabicyclo[4.3.1]decane (Figure 3. 10, Table 3. 4, and Figure B. 11-B. 16) [217, 218]. The NMR and mass spectrum were also in agreement with those reported in the literature (m^{+}/z = 156.15; Figure B. 11-B. 16 and Figure B. 1) [217]. Initially, hydroxylation occurred at C5, which converts to the corresponding cyclic hemiacetal through intramolecular nucleophilic attack of the C5 hydroxyl group to the electrophilic carbonyl group. The mechanism leading to the formation of this cyclic metabolite is given in Figure 3. 10.

The NMR displayed that a minor metabolite was also present (~9% from the NMR integration of **H**C5(OH) and **H**C5O) with 1-hydroxy-10-oxabicyclo[4.3.1]decane [218]. It was predicted to be the corresponding 5-hydroxycycloalkanone precursor to the 1-hydroxy-10-oxabicyclo[4.3.1]decane hemiacetal which could be present in equilibrium. This was confirmed by comparing the ^{1}H NMR spectrum peak of H5 at 3.79-3.73 ppm with that reported in the literature (Table 3. 4 and Figure 3. 10 (b)) [218]. The minor product from the CYP101C1 turnover coeluted with the primary product (1-hydroxy-10-oxabicyclo[4.3.1]decane) of CYP101B1 in GC-MS (~2%; at RT 11.2 min, Figure 3. 9).

Table 3. 3 Substrate binding, turnover and coupling efficiency data for CYP101B1 and CYP101C with cycloalkanones. The *in vitro* turnover activities were measured using a ArR:Arx: CYP101B1/CYP101C1 concentration ratio of 1:10:1 (0.5 mM CYP enzyme, 50 mM, pH 7.4). N is the NADH oxidation rate, PFR the product formation rate, C is the coupling efficiency and TTN, total turnover number. The data are reported as mean ± S.D. (n = 3), and rates are given in nmol.nmol-CYP^{-1}.min^{-1}. - Not measured or not able to be determined accurately. n.p: no product.

Substrate	CYP101B1/ CYP101C1	K_d (µM)	N	PFR	C (%)	TTN
cyclooctanone	CYP101B1	-	93.4 ± 9	n.p	n.p	-
	CYP101C1	**-**	**88 ± 2**	**n.p**	**n.p**	**-**
cyclononanone	CYP101B1	46 ± 21	308 ± 10	131 ± 11	43	886 ± 77
	CYP101C1	**-**	**289 ± 16**	**75 ± 4**	**26**	**226 ± 36**
cyclodecanone	CYP101B1	46 ± 2	323 ± 38	149 ± 54	45	1728 ± 48
	CYP101C1	**-**	**531 ± 75**	**113 ± 13**	**22**	**1185 ± 91**
cycloundecanone	CYP101B1	8.4 ± 0.3	409 ± 11	222 ± 14	54	3481 ± 293
	CYP101C1	**-**	**660 ± 53**	**141 ± 18**	**22**	**3301 ± 332**
cyclododecanone	CYP101B1	2.4 ± 0.4	391 ± 11	283 ± 38	72	5750 ± 276
	CYP101C1	**-**	**853 ± 24**	**239 ± 31**	**28**	**543 ± 62**
cyclopentadecanone	CYP101B1	0.5 ± 0.1	126 ± 4	47 ± 3	38	-
	CYP101C1	**-**	**217 ± 4**	**14 ± 3**	**7**	**-**

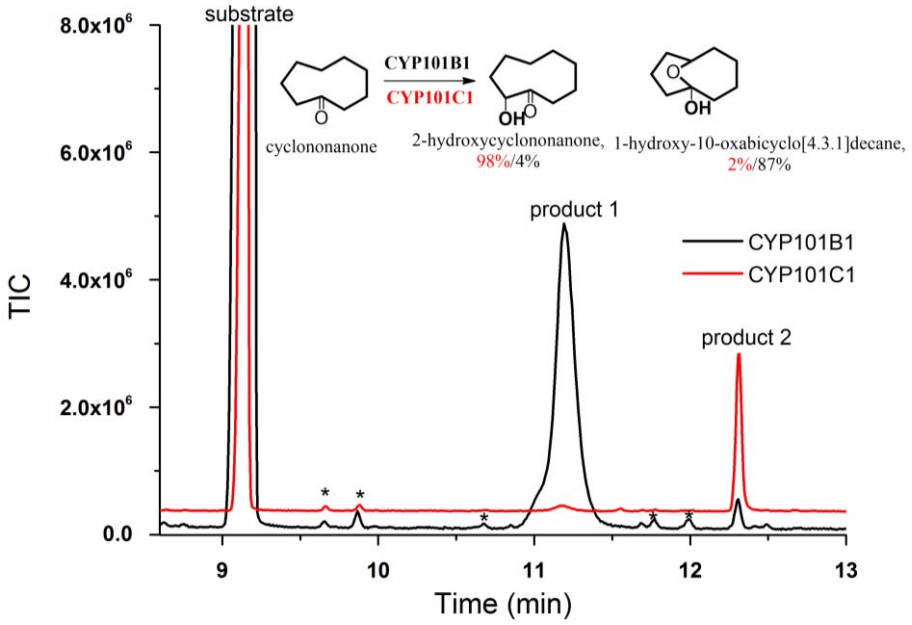

(a)

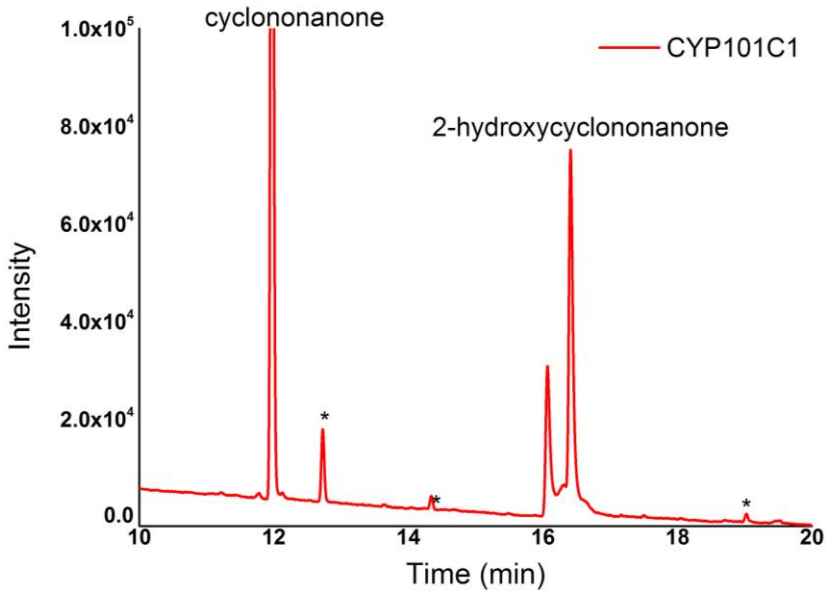

(b)

Figure 3. 9 (a) GC-MS analyses of the *in vitro* turnovers of cyclononanone by CYP101B1 and CYP101C1. Cyclononanone (RT 9.1 min) and the products; 1-hydroxy-10-oxabicyclo[4.3.1]decane in equilibrium with 5-hydroxycyclononanone (RT 11.2 min) and 2-hydroxycyclononanone (RT 12.2 min). **(b)** The chiral GC analysis of the *in vitro* turnover of cyclononanone by CYP101C1. Cyclononanone (RT 12.0 min) and the product 2-hydroxycyclononanone (two enantiomers: RT 16.4 min and RT 16.5 min). Impurities are labelled (*).

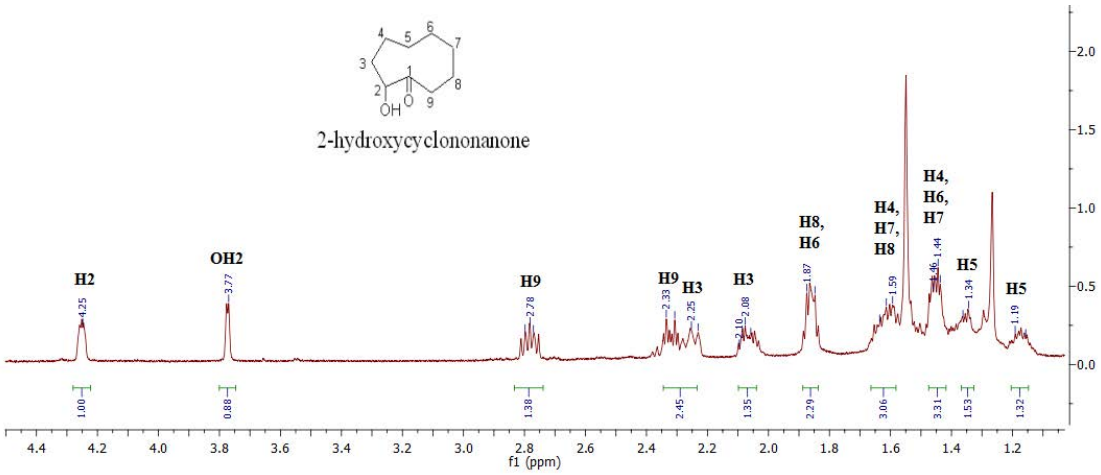

(a)

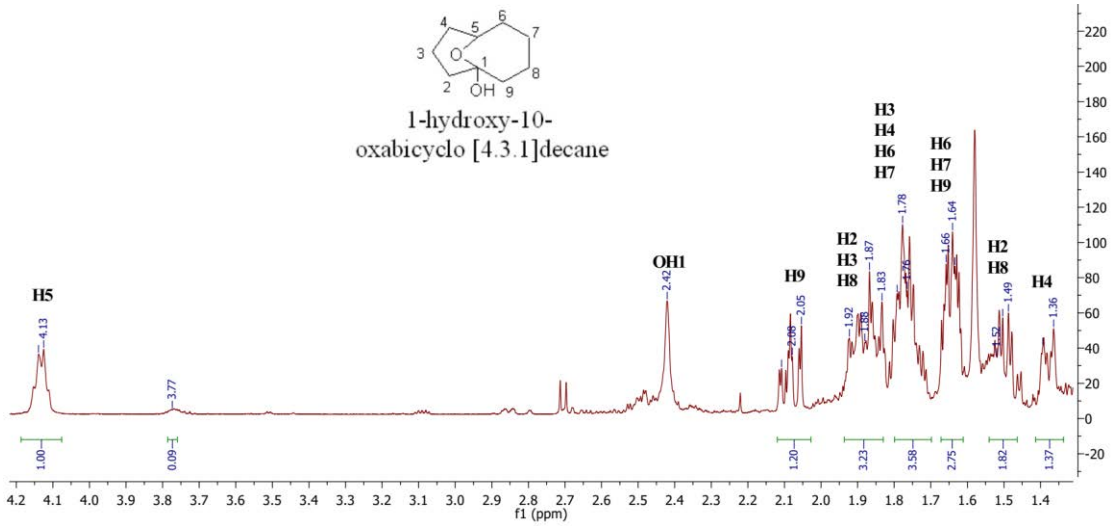

(b)

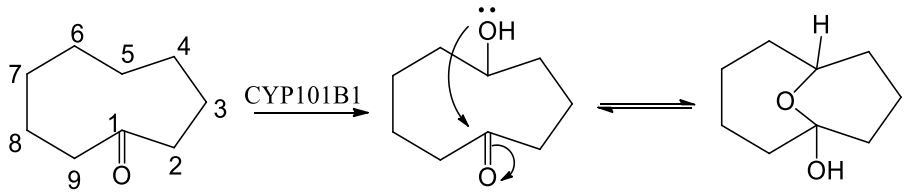

(c)

Figure 3. 10 (a) ^{1}H NMR of 2-hydroxycyclononanone (CYP101C1). **(b)** ^{1}H NMR of 1-hydroxy-10-oxabicyclo[4.3.1]decane and 5-hydroxycyclononanone (9%). Full data are given in appendix B (Figure B. 7-B. 16). **(c)** The proposed mechanism of 1-hydroxy-10-oxabicyclo[4.3.1]decane formation [218].

Addition of cyclodecanone generated a 50% shift to the high spin form in CYP101B1 (Figure 3. 11). The binding affinity for cyclodecanone (K_d = 46 µM) was similar to that of cyclononanone (Table 3. 3 and Figure 3. 11). When cyclodecanone was added to both the CYP101B1 and CYP101C1 turnover system, a higher oxidation activity was observed in each case compared to cyclononanone (Table 3. 3). Although the CYP101C1 system displayed a greater NADH oxidation rate (531 min^{-1}) than CYP101B1 (323 min^{-1}), the product formation rate was reduced due to a low coupling efficiency (22% versus 45%, Table 3. 3).

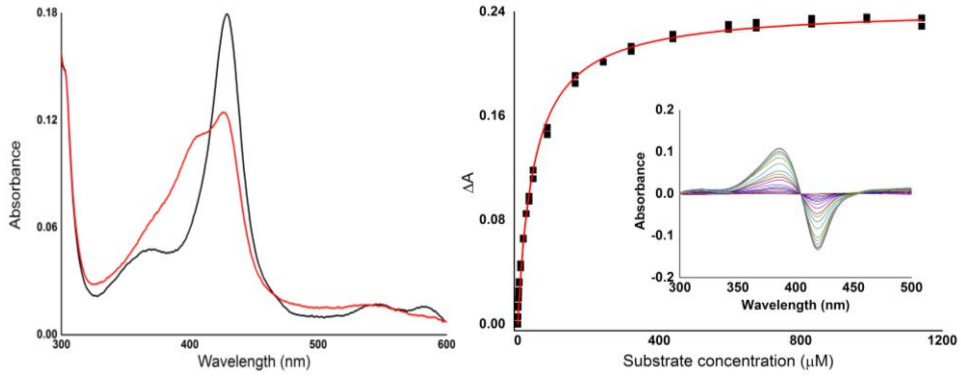

(a) (b)

Figure 3. 11 (a) The spin-state shift (red) of CYP101B1 after addition of cyclodecanone. **(b)** The dissociation constant analysis with cyclodecanone (2.35 µM CYP101B1/ K_d 46 µM). The concentration of the enzyme used in the study and the dissociation constant (K_d) are provided in brackets.

Turnovers of each enzyme with cyclodecanone showed the formation of monooxygenase products in the GC-MS analyses (m^+/z = 170.2 and m^+/z = 170.1; Figure 3. 12 and Figure B. 1). The GC-FID analysis of both *in vitro* and *in vivo* turnover of CYP101B1 indicated that CYP101B1 generated two major metabolites in a 3:2 ratio (RT 10.0 min and RT 10.9 min; Figure 3. 12). A minor metabolite, which eluted earlier, was also formed (RT 7.2 min; m^+/z =170.20; Figure 3. 12 and Figure B. 1). But in the case of CYP101C1, the GC/GC-MS analyses of the turnovers displayed one major metabolite (90%; at RT 7.2 min) which coeluted with the minor product from CYP101B1 oxidation. The minor metabolites of CYP101C1 turnovers coeluted with the main metabolites of the CYP101B1 turnover and made up the remainder (10%; RT 10.0 min and RT 10.9 min; Figure 3. 12).

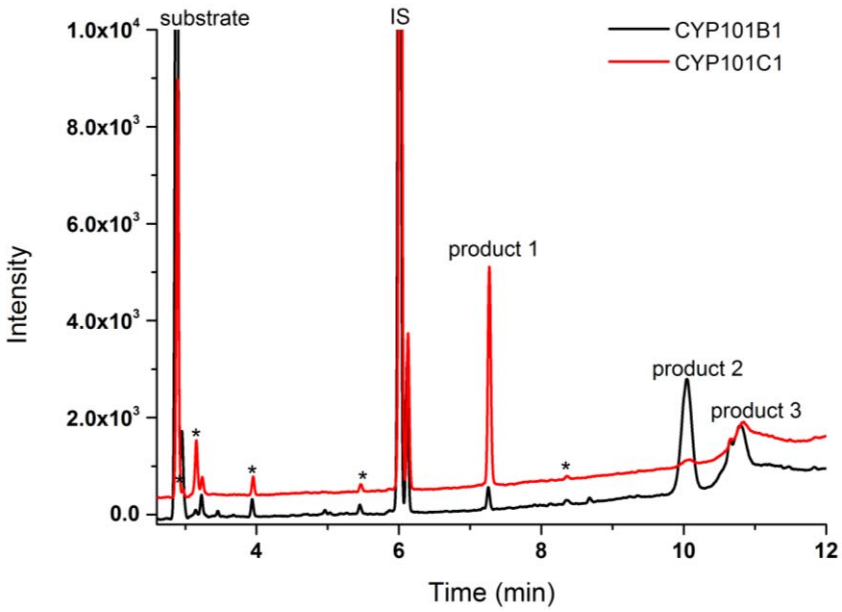

(a)

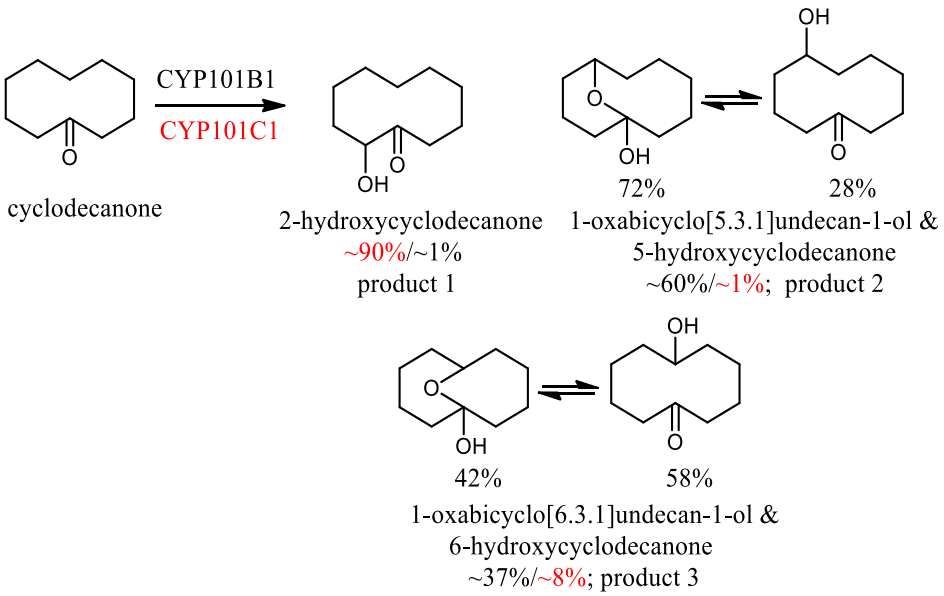

(b)

Figure 3. 12 (a) GC-FID analyses of the *in vitro* turnovers of cyclodecanone by CYP101B1 and CYP101C1. Cyclodecanone (RT 2.9 min) and the products; 2-hydroxycyclodecanone (RT 7.2 min); 1-oxabicyclo[5.3.1]undecan-1-ol and 5-hydroxycyclodecanone (RT 10.0 min); a mixture of 1-oxabicyclo[6.3.1]undecan-1-ol and 6-hydroxycyclodecanone (RT 10.9 min). Impurities are labelled (*). **(b)** The metabolites generated in the turnovers of CYP101B1 and CYP101C1 with cyclodecanone. The product distributions are given as percentages.

Both major metabolites from CYP101B1 *in vivo* turnovers of cyclodecanone were purified by silica column chromatography. The main product (60%; at RT 10.0 min) was characterised using NMR. It was isolated as an equilibrium mixture but was confirmed as 1-oxabicyclo[5.3.1]undecan-1-ol [218]. The expected C1 (C=O) signal in the ^{13}C NMR spectrum was not present, but a peak was observed at 98.80 ppm (Figure 3. 13 and Figure B. 21-B. 26). The ^{1}H-^{13}C HMBC NMR spectrum showed a correlation of C1 with H5 which demonstrated a cyclisation product (Figure 3. 13, Table 3. 4 and Figure B. 21-B. 26) [218]. The minor peaks in the NMR spectrum of 1-oxabicyclo[5.3.1]undecan-1-ol were consistent with 5-hydroxycyclodecanone and the ^{1}H NMR peak of H5 (3.83-3.78 ppm) was in agreement with the NMR reported in the literature (Table 3. 4 and Figure B. 21-B. 26) [218]. 1-Oxabicyclo[5.3.1]undecan-1-ol has been demonstrated to co-exist in a transannular tautomeric equilibrium with 5-hydroxycyclodecanone (Figure 3. 13 (b)) [218]. The ^{1}H NMR signals of the methine protons **H**C5(OH) (3.81-3.72 ppm) and **H**C5O (3.97-4.07 ppm) were used to determine the concentration/percentage of 1-oxabicyclo[5.3.1]undecan-1-ol (~72%) and 5-hydroxy cyclodecanone (~28%) metabolites in $CDCl_3$ [218].

The other metabolite (37%; at RT 10.9 min) was purified (~12 mg). The NMR analysis confirmed that it was a mixture of 1-oxabicyclo[6.3.1]undecan-1-ol (~42%) and 6-hydroxycyclodecanone. Both displayed symmetry and a reduced number of carbon peaks in the ^{13}C NMR and the characteristic proton peaks at 4.13-4.01 (**H**C6O) and 3.90-3.79 (**H**C6(OH)) in the ^{1}H NMR spectrum, enabling their identification (Figure 3. 13, Table 3. 4 and Figure B. 27-B. 31) [218]. These assignments were also in agreement with the NMR reported in literature [218]. The percentage of each product isomer was determined using these ^{1}H NMR methine proton integrations [218]. The mechanism of 1-oxabicyclo[5.3.1]undecan-1-ol and 1-oxabicyclo[6.3.1]undecan-1-ol formation was assumed to be similar to 1-hydroxy-10-oxabicyclo[4.3.1]decane formation (Figure 3. 10).

The other minor product (1%; at RT 7.2 min) of CYP101B1 coeluted with the main metabolite (2-hydroxycyclodecanone) of CYP101C1 (Figure 3. 12 and Figure 3. 13). Additional carbon peaks were also noticed in the ^{13}C NMR spectrum of 1-oxabicyclo[6.3.1]undecan-1-ol and 6-hydroxycyclodecanone which indicated another minor product (~2%) was also present. This was presumed to be a 4-hydroxy metabolite due to the correlation of 72.83 ppm (C4) with the

protons of 2.41-2.33 (H2) and 2.01-1.87 (H3) in the HMBC NMR spectrum, but the product was not able to be fully characterised due to noise (Figure B. 32).

The regioselectivity of CYP101C1 was different. This system generated a single major hydroxylated metabolite (m^+/z = 170.2, Figure 3. 12 and Figure B. 1). This product was synthesised in large-scale by a CYP101C1 whole-cell biotransformation system. The metabolite from the *in vivo* turnover was extracted and purified (~15 mg) using silica column chromatography. The ^{1}H NMR spectrum of the isolated product had two distinct peaks of H2 at 4.29-4.17 ppm and C2O**H** at 3.88-3.76 ppm. In the ^{13}C NMR spectrum, the signal of C2 carbon (79.11 ppm) which would be adjacent to the carbonyl group displayed significant deshielding. The data was in agreement with that in the literature for 2-hydroxycyclodecanone [219]. Therefore, the hydroxylation was assigned at C-2 (Figure 3. 13 and Figure B. 17-B. 20). The mass spectrum analysis also confirmed this assignment (Figure B. 1) [219]. Coelution of the minor metabolites (~10%) of CYP101C1 turnover with the major products of CYP101B1 in GC showed an identical retention time (Figure 3. 12).

Table 3. 4 ^{1}H and ^{13}C NMR signals of the HC-OH and HC-O groups which have been reported ($CDCl_3$) [218].

Hydroxy ketone	HC-OH (C) (*δ*)	Hemiacetal	HC-O (C) (*δ*)
5-hydroxycyclononanone	3.70 (71.3)	1-hydroxy-10-oxabicyclo [4.3.1]decane	4.08 (73.7)
5-hydroxycyclodecanone	3.75 (69.9)	1-oxabicyclo[6.3.1] undecan-1-ol	4.0 (73.6)
6-hydroxycyclodecanone	3.83 (69.9)	1-oxabicyclo[6.3.1] undecan-1-ol	4.07 (76.6)

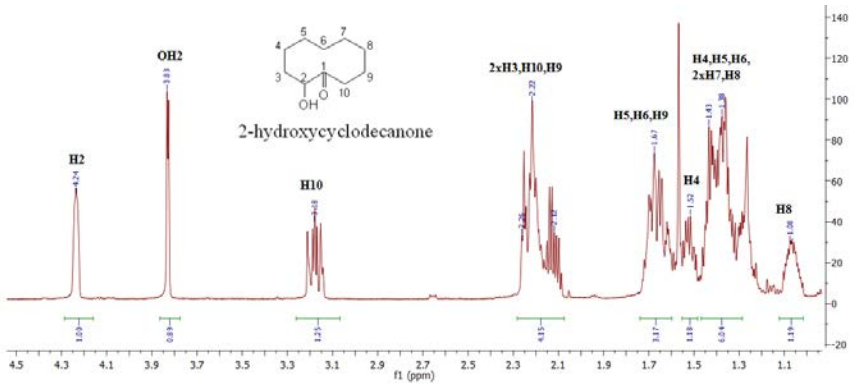

(a)

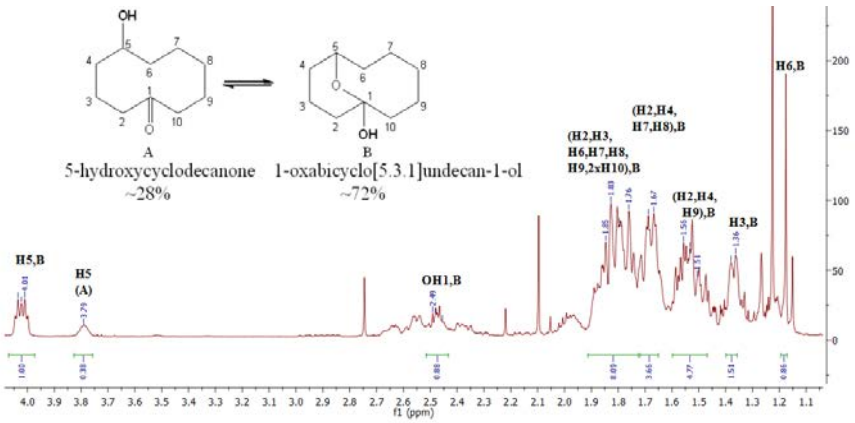

(b)

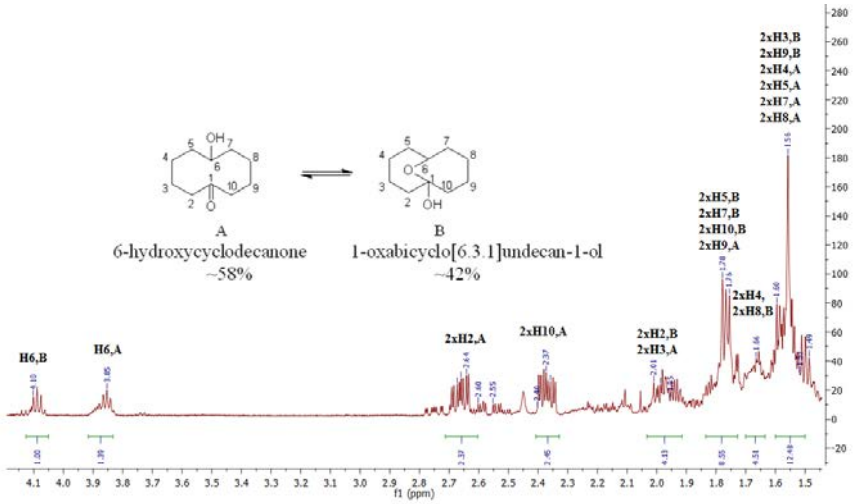

(c)

Figure 3. 13 (a) ^{1}H NMR spectrum of 2-hydroxycyclodecanone (CYP101C1). **(b)** ^{1}H NMR spectrum of 1-oxabicyclo[5.3.1]undecan-1-ol and 5-hydroxycyclodecanone (CYP101B1). **(c)** ^{1}H NMR spectrum of a mixture of 1-oxabicyclo[6.3.1]undecan-1-ol (~42%) and 6-hydroxycyclodecanone (CYP101B1). A small amount of potential 4-hydroxy metabolite was also present. Full data are provided in Appendix B (Figure B. 17-B. 32).

The spin-state shift of CYP101B1 after addition of cycloundecanone was higher than that observed with cyclodecanone and cyclononanone (80%; Figure 3. 14 and Table 3. 3). This substrate also bound several times more tightly than the smaller cycloalkanones (Table 3. 3). The dissociation constant was 8.4 µM which signified that cycloundecanone was well accommodated in the active site of the CYP101B1 enzyme (Figure 3. 14). In the presence of cycloundecanone, NADH was oxidised by CYP101B1 at a rate of 409 min^{-1}, and the product formation rate was 222 min^{-1} (Table 3. 3). CYP101C1 exhibited a faster NADH oxidation rate of 660 min^{-1} than CYP101B1 (Table 3. 3). However, the product formation rate was slower compared to CYP101B1 due to the recurring lower coupling efficiency observed with this system (22%; Table 3. 3). CYP101B1 displayed an improved coupling efficiency (54%) with cycloundecanone compared to cyclononanone and cyclodecanone. The rates and coupling efficiency followed the trend in the improvement of the binding affinity and magnitude of the heme spin-state induced in CYP101B1 with cycloundecanone.

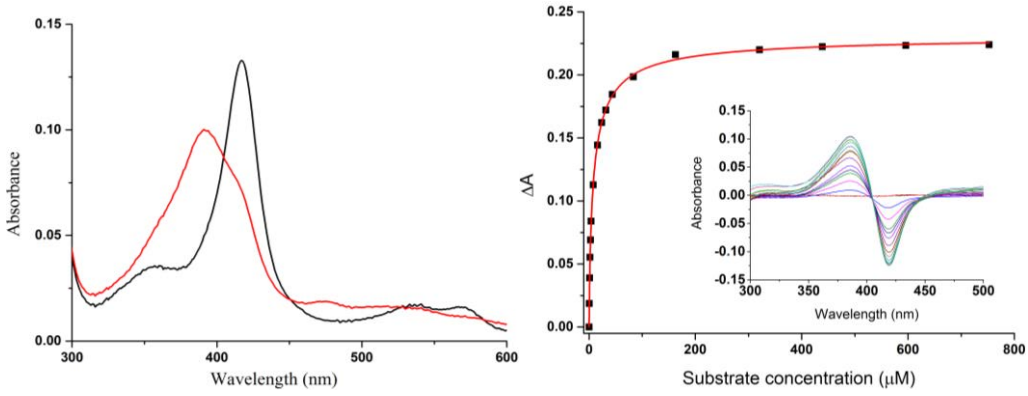

(a) (b)

Figure 3. 14 (a) The spin-state shift (red) of CYP101B1 after addition of cycloundecanone. **(b)** The dissociation constant analysis with cycloundecanone (2.0 µM CYP101B1/K_d 8.4 µM). The concentration of enzyme used in the binding assay and the dissociation constant (K_d) are provided in brackets.

The GC-MS analysis of the extract obtained following *in vitro* turnover of CYP101C1 with cycloundecanone revealed a single major hydroxylated product (~92%; RT 8.4 min; m^+/z = 184.40) with three minor metabolites making up the remainder (Figure 3. 15 and Figure B. 1). The primary metabolite of this substrate was generated in a higher yield using a CYP101C1 whole-cell oxidation system and was isolated (~20 mg) via silica column chromatography. The ^{1}H NMR spectrum of this metabolite had two distinct multiplet peaks for H2 at (4.30-4.24 ppm) and C2-O**H** at (3.6-3.44 ppm). In the HMBC NMR, the carbonyl C1 showed strong correlations

with C2-O**H** (3.6-3.44 ppm), H3, H10 and H11, indicating hydroxylation occurred at the C2 position (Figure B. 33-B. 38). The product was thus assigned as 2-hydroxycycloundecanone and confirmed by comparing the ^{1}H and ^{13}C NMR signals with the NMR reported previously (Figure 3. 16 and B. 33-B. 38) [220]. The mass spectrum analysis was also in agreement of this assignment (Figure B. 1) [220]. Chiral-GC analysis showed that this turnover generated two enantiomers of 2-hydroxycycloundecanone an almost equal amount (46:54; Figure 3. 15). Two of the minor products were identified by GC-MS coelution experiment with the metabolites of CYP101B1 (Figure 3. 15).

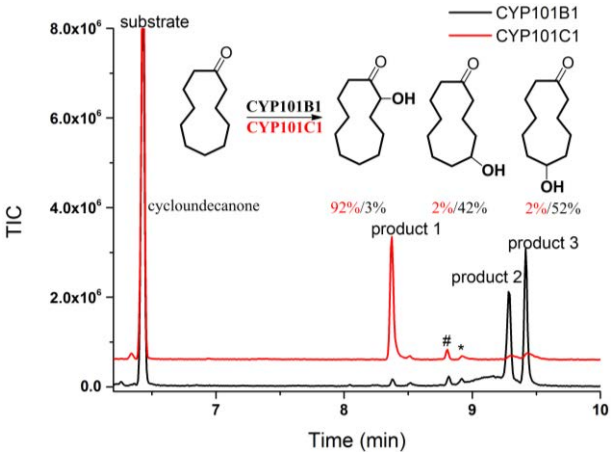

(a)

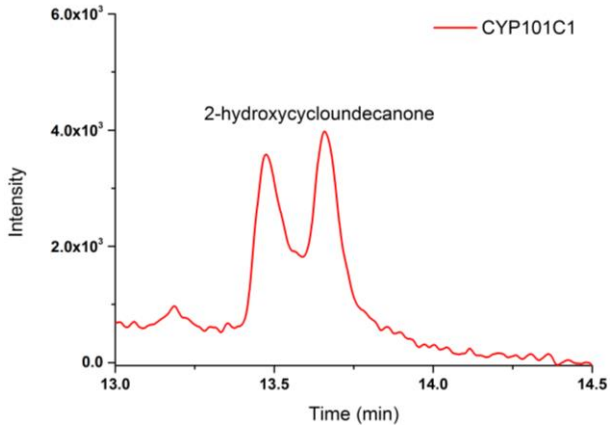

(b)

Figure 3. 15 (a) GC-MS analyses of the *in vitro* turnovers of cycloundecanone by CYP101B1 and CYP101C1. Cycloundecanone (RT 6.4 min) and product 1; 2-hydroxycycloundecanone (RT 8.4 min), product 2; 5-hydroxycycloundecanone (RT 9.3 min) and product 3; 6-hydroxycycloundecanone (RT 9.45 min). There is minor (≤4%) unidentified product[#] in both enzymes turnover at RT 8.8 min. **(b)** The chiral GC analysis of *in vitro* turnover of cycloundecanone by CYP101C1. Cycloundecanone (RT 9.4 min; not shown) and the product; 2-hydroxycycloundecanone (two enantiomers RT 13.5 min and RT 13.6 min). Impurities are labelled (*).

GC-MS analyses of the *in vitro* turnovers of CYP101B1 indicated two metabolites were generated in significant yield (~42%; m^+/z = 184.30 and ~52%; m^+/z = 184.20) alongside two minor hydroxylated metabolites (Figure 3. 15 and Figure B. 1). *In vivo* turnovers were used to generate the products in larger-scale for characterisation and the metabolites were isolated by silica column chromatography (~10 mg and ~15 mg). The ^{1}H NMR of the metabolite at RT 9.3 min in GC-MS, had a multiplet peak at 3.76-3.70 ppm suggesting a hydroxylated product (Figure 3. 16 and Figure B. 40-B. 44). The correlations of C1 (216.69 ppm) with H2, H11 (2.55-2.42 ppm), H3 (1.89-1.82 ppm) and H10 (1.81-1.74 ppm) in ^{1}H-^{13}C HMBC NMR spectrum, were used to assign these proton peaks. The C4 (44.97 ppm) signal was confirmed using its interaction with H2 (2.55-2.42 ppm) in the HMBC NMR (Figure B. 40-B. 44). The product was identified as the 5-hydroxy metabolite due to the **C**HOH carbon signal (72.36 ppm) displaying strong correlations with H3 (1.89-1.82 ppm), H4 (1.73-1.63 ppm) and H6 (1.54-1.50 ppm) in the HMBC NMR (Figure B. 40-B. 44). Some additional minor peaks in the ^{1}H and ^{13}C NMR of this product indicated that another metabolite (~1) was also present as an impurity, but this was not able to be characterised (Figure 3. 16 and Figure B. 40-B. 44).

The ^{1}H NMR spectrum of the other major metabolite (RT 9.45 min in GC-MS) had a multiplet peak at 3.72-3.66 ppm demonstrating a monohydroxylated product (Figure 3. 16). The ^{13}C-^{1}H HMBC NMR spectrum analysis revealed the correlations of C1 (216.91 ppm) with the H2, H11 (2.60-2.36 ppm) and H3, H10 (1.84-1.72 ppm) proton signals. C4 (24.42 ppm) and C5 (34.79 ppm) were assigned using the interactions with H2 (2.60-2.36 ppm) and H3 (1.84-1.72 ppm), respectively in the HMBC NMR (Figure B. 45-B. 49). The **C**HOH carbon signal (72.73 ppm) displayed strong correlations with H4 (1.47-1.42 ppm), H5 (1.63-1.56 ppm), H7 (1.47-1.42 ppm) and H8 (1.41-1.33 ppm) in the HMBC NMR spectrum (Figure B. 45-B. 49). The metabolite was therefore identified as 6-hydroxycycloundecanone. Some additional minor signals in the proton and carbon NMR of this product indicated that an unidentified metabolite (~1) was also present as an impurity (Figure 3. 16, Figure B. 45-B. 49).

One of the minor (~3%; RT 8.4 min) metabolites coeluted with 2-hydroxycycloundecanone in GC-MS (Figure 3. 15). The other product (RT 8.8 min in GC-MS, ≤4%) for both CYP101B1 and CYP101C1 turnovers was unidentified as it was not generated in large enough quantity for NMR characterisation (Figure 3. 15). However, the mass spectrum suggested it may be a further oxidation product with a mass, m^+/z = 182.30 (Figure B. 1).

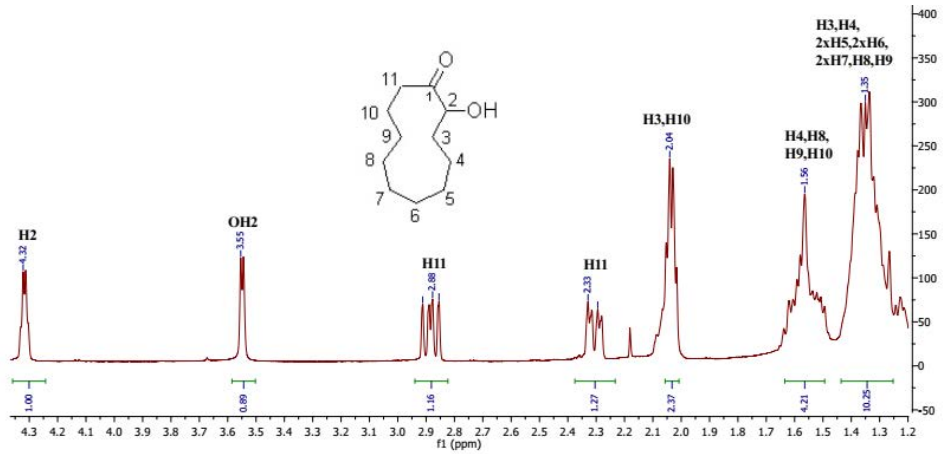

(a)

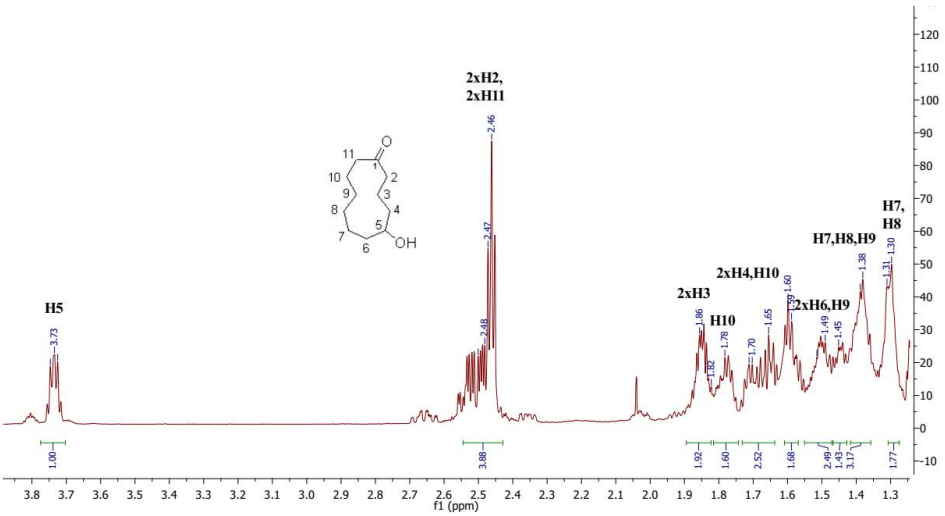

(b)

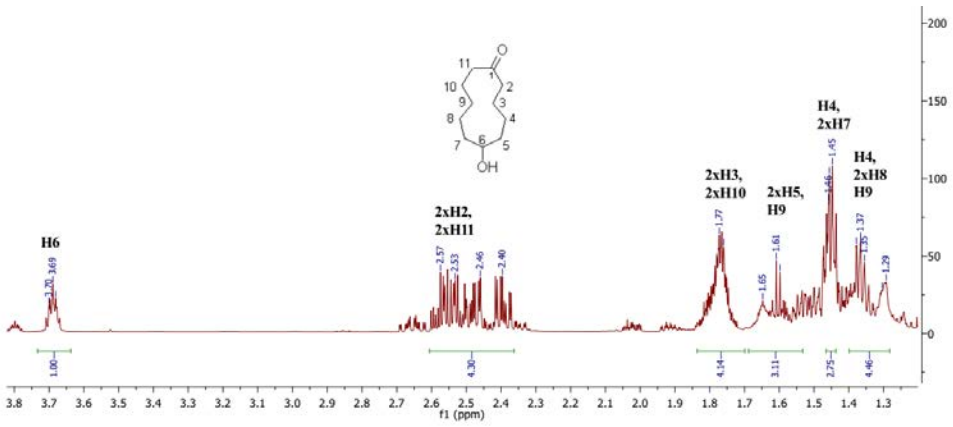

(c)

Figure 3. 16 (a) ^{1}H NMR spectrum of 2-hydroxycycloundecanone (CYP101C1) [220, 221]. **(b)** ^{1}H NMR of 5-hydroxycycloundecanone (CYP101B1). **(c)** ^{1}H NMR spectrum of 6-hydroxycycloundecanone (CYP101B1). In NMR of both 5-hydroxycycloundecanone and 6-hydroxycycloundecanone, a small unidentified metabolite or impurity was present. Complete NMR spectra are provided in Appendix B (Figure B. 33-B. 49).

Cyclododecanone altered the heme spin-state of CYP101B1 almost entirely to the high spin form (90%), and the enzyme bound tightly with a higher affinity than cycloundecanone (K_d = 2.4 µM; Table 3. 3 and Figure 3. 17). The rate of NADH oxidation of CYP101B1 with cyclododecanone was 391 min^{-1}, which was in-between those observed for cyclodecanone and cycloundecanone (Table 3. 3). The majority of the NADH reducing equivalents were used for product formation, leading to a higher product formation activity, 283 min^{-1}, compared to cycloundecanone (coupling efficiency; 72% versus 54%; Table 3. 3). The total turnover number was significantly greater compared to other cycloalkanones investigated here (TTN 5750; Table 3. 3). Interestingly CYP101C1 showed an even higher NADH oxidation activity (853 min^{-1}) in the presence of cyclododecanone (Table 3. 3). However, the product formation rate and efficiency of productive NADH utilisation for the oxidation of this substrate were lower; 239 min^{-1} and 28%, respectively (Table 3. 3).

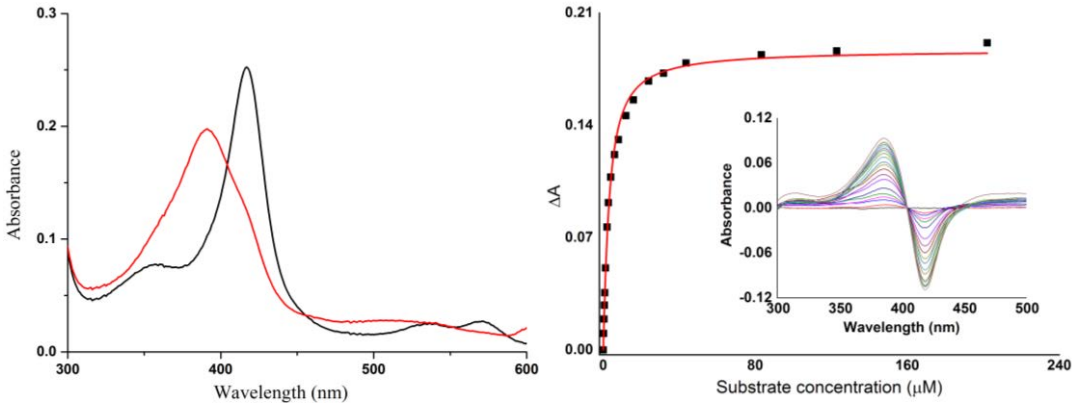

(a) (b)

Figure 3. 17 (a) The spin-state shift (red) of CYP101B1 after addition of cyclododecanone. **(b)** Dissociation constant analysis with cyclododecanone (1.58 µM CYP101B1/K_d 2.4 µM). The concentration of enzyme used in the binding assay and the dissociation constant (K_d) are provided in brackets.

GC-MS analysis of the turnovers of cyclododecanone by CYP101C1 displayed a single major metabolite (98%; RT 15.5 min) with one other minor (RT 17.7 min) product (Figure 3. 18). The mass spectra of both these products were consistent with monooxygenase metabolites (m^+/z = 198.25 and m^+/z = 198.05; Figure 3. 18 and Figure B. 1).

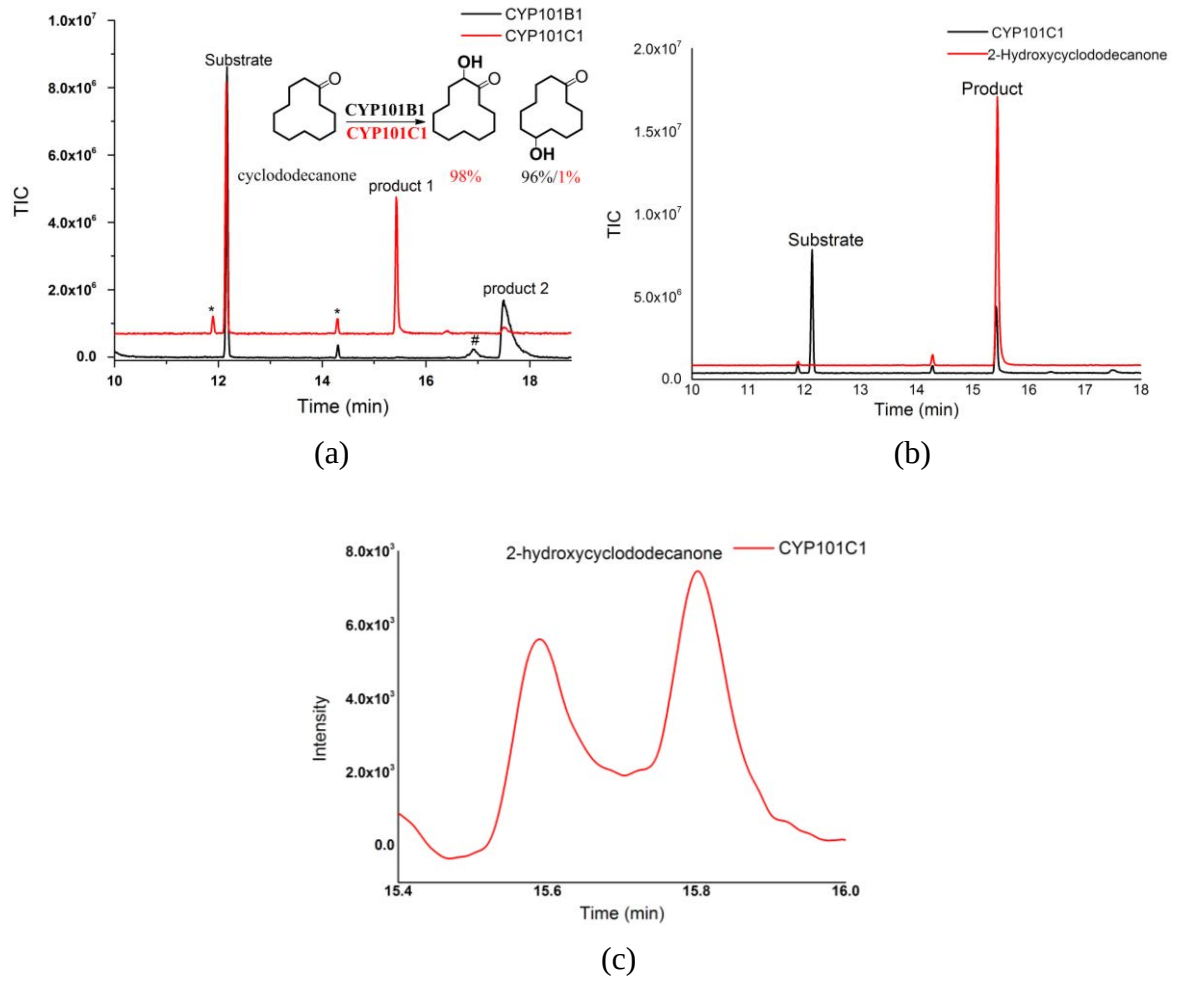

Figure 3. 18 (a) GC-MS analyses of the *in vitro* turnovers of cyclododecanone by CYP101B1 (black) and CYP101C1 (red). Cyclododecanone (RT 12.1 min) and the product 1; 2-hydroxycyclododecanone (RT 15.5 min), product 2; 7-hydroxycyclododecanone (RT 17.7 min). There is a minor product[#] in CYP101B1 enzyme turnover at RT 16.9 min. **(b)** The authentic commercial standard (red) coeluted with CYP101C1 turnover (black) in GC-MS**. (c)** Chiral GC analysis of the *in vitro* turnover of cyclododecanone by CYP101C1. Cyclododecanone (RT 10.2 min; not shown) and the product; 2-hydroxycyclododecanone (two enantiomers; RT 15.6 min and 15.8 min). Impurities are labelled (*).

The primary metabolite of cyclododecanone turnover was generated using the CYP101C1 *in vivo* turnover system for characterisation. The metabolite was purified (~29 mg) by column chromatography and assigned as 2-hydroxycyclododecanone by NMR analysis (Figure 3. 18, Figure B. 50-B. 55) [219, 220]. The ^{1}H NMR spectrum of this product had two characteristic peaks for H2 (4.44-4.34 ppm) and C2O**H** (3.58-3.50 ppm). The latter peak is observed due to the

correlation with the carbonyl oxygen (Figure 3. 19). ^{1}H-^{1}H gCOSY NMR also showed strong interaction between the H2 and C2O**H** (Figure B. 53). The HMBC NMR spectrum analysis displayed the correlation of C1 (215.55 ppm) with C2O**H** proton indicating hydroxylation occurred at C2 (Figure 3. 19 and Figure B. 50-B. 55). The product was further confirmed by GC-MS coelution experiment with a commercial standard. The ^{1}H NMR spectrum of the standard matched with the isolated product proton NMR (Figure 3. 18 and Figure B. 50). The chiral GC analysis revealed that the turnover of CYP101C1 generated a mixture of enantiomers (45%:55%) of 2-hydroxycyclododecanone (Figure 3. 18).

One major product (96%; RT 17.7 min) and a minor metabolite (RT 16.9 min) were detected in the GC-MS analyses of the *in vitro* and *in vivo* turnovers of CYP101B1 with cyclododecanone (Figure 3. 18). The mass spectra suggested that both were monohydroxylated products (m^{+}/z = 198.35 and m^{+}/z = 198.50; Figure 3. 18 and Figure B. 1). The primary metabolite from a CYP101B1 *in vivo* turnover was isolated (~27 mg) using silica column chromatography and identified as 7-hydroxycyclododecanone by NMR analysis (Figure 3. 19 and Figure B. 56-B. 60) [208]. The ^{13}C NMR spectrum of this metabolite exhibited seven carbon signals demonstrating the hydroxylation took place at the C7 position generating a symmetrical metabolite (Figure 3. 19 and Figure B. 57). Five out of seven signals displayed double the intensity of the others, representing pairs of equivalent carbons, which is in agreement with this metabolite assignment.

The primary product of the CYP101B1 turnovers coeluted in GC-MS with the minor metabolite of the CYP101C1 turnover, confirming the identity of this minor product as 7-hydroxycyclododecanone (m^{+}/z = 198.05). The minor metabolite (~4%) of CYP101B1 with the retention time 16.9 min, was unable to be generated in a large enough quantity for characterisation by NMR. However, the mass spectrum suggested that this was consistent with a monooxygenase product with a mass, m^{+}/z 198.35 (Figure B. 1).

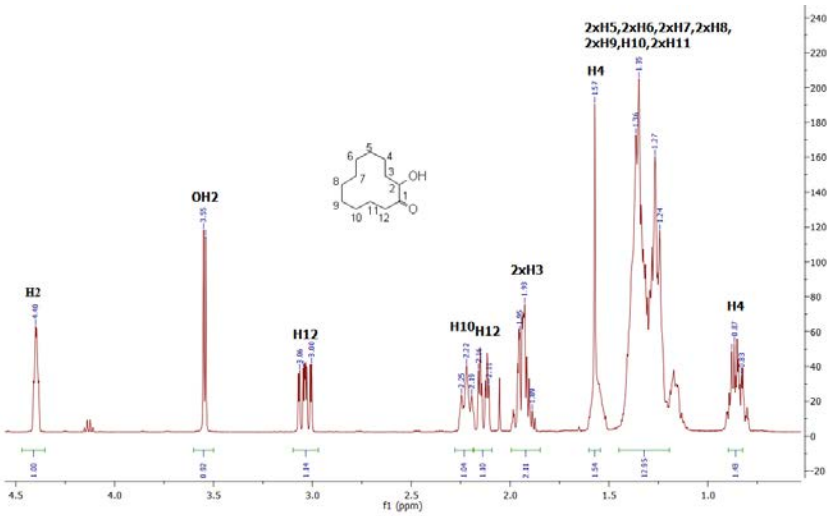

(a)

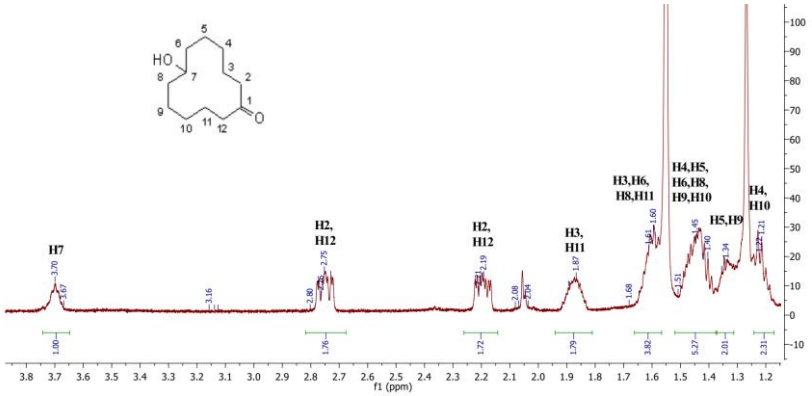

(b)

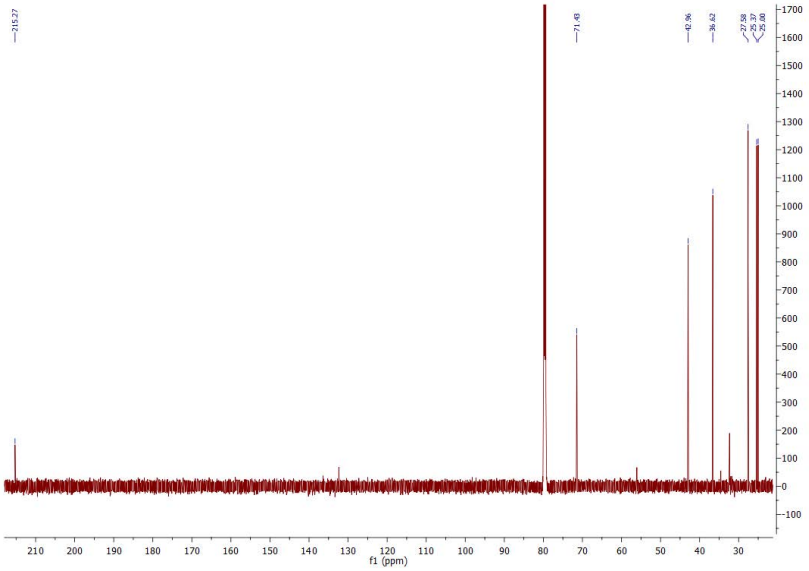

(c)

Figure 3. 19 (a) ^{1}H NMR of 2-hydroxycyclododecanone (CYP101C1). **(b)** ^{1}H NMR of 7-hydroxycyclododecanone (CYP101B1). **(c)** ^{13}C NMR of 7-hydroxycyclododecanone (CYP101B1). Full data are presented in Appendix B (Figure B. 50-B. 60).

The fifteen-carbon containing alicyclic ketone cyclopentadecanone induced a 75% spin-state shift in CYP101B1 (Figure 3. 20). It displayed very tight binding to CYP101B1 (K_d = 0.45 µM; Figure 3. 20 and Table 3. 3). This suggested the active site of the enzyme can accommodate these larger substrates. CYP101B1 exhibited increased product formation activity toward cyclopentadecanone with a rate of 47 min^{-1} compared to CYP101C1 (14 min^{-1}; Table 3. 3). However, these rates were slower than those with cyclododecanone and cycloundecanone (Table 3. 3). The productive utilisation of NADH was reduced for CYP101C1 (7% versus 38%; Table 3. 3).

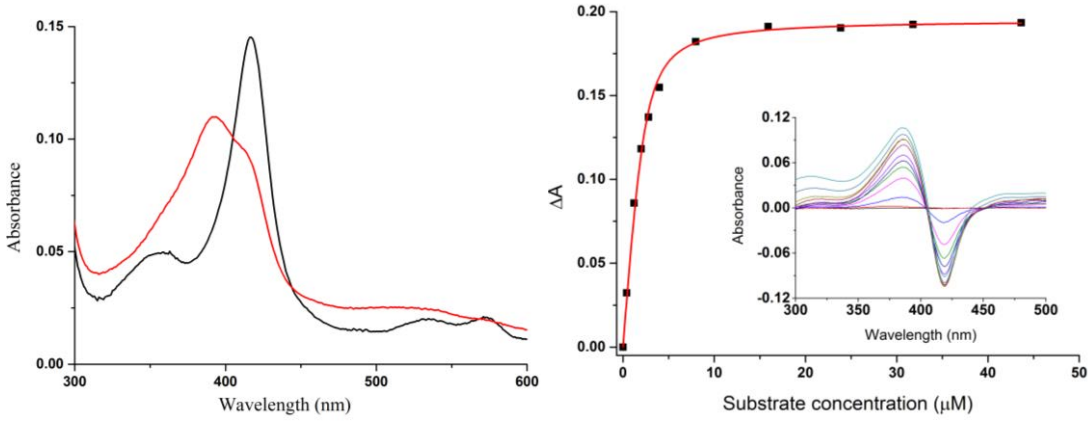

(a) (b)

Figure 3. 20 (a) The spin-state shift (red) of CYP101B1 after addition of cyclopentadecanone. **(b)** The dissociation constant analysis with cyclopentadecanone (2.3 µM CYP101B1/K_d 0.45 µM). The concentration of enzyme used in the binding study and the dissociation constant (K_d) are provided in brackets.

CYP101C1 oxidised this substrate into two metabolites, and GC-MS analysis revealed that both of these were monohydroxylated products (m^+/z = 240.25, m+/z = 240.25; Figure 3. 21 and Figure B. 1). Whole-cell turnover containing CYP101C1 enzyme was used to generate the metabolites of cyclopentadecanone in larger yield for NMR characterisation. However, neither was generated in sufficient quantity for NMR analysis. The primary metabolite (64%; RT 14.6 min) was confirmed by comparing its mass spectrum with the reported mass spectrum of 2-hydroxycyclopentadecanone in the literature (Figure B. 1) [219, 222]. Hence the product was consistent with a 2-hydroxy metabolite as found for other cycloalkanones tested above with CYP101C1.

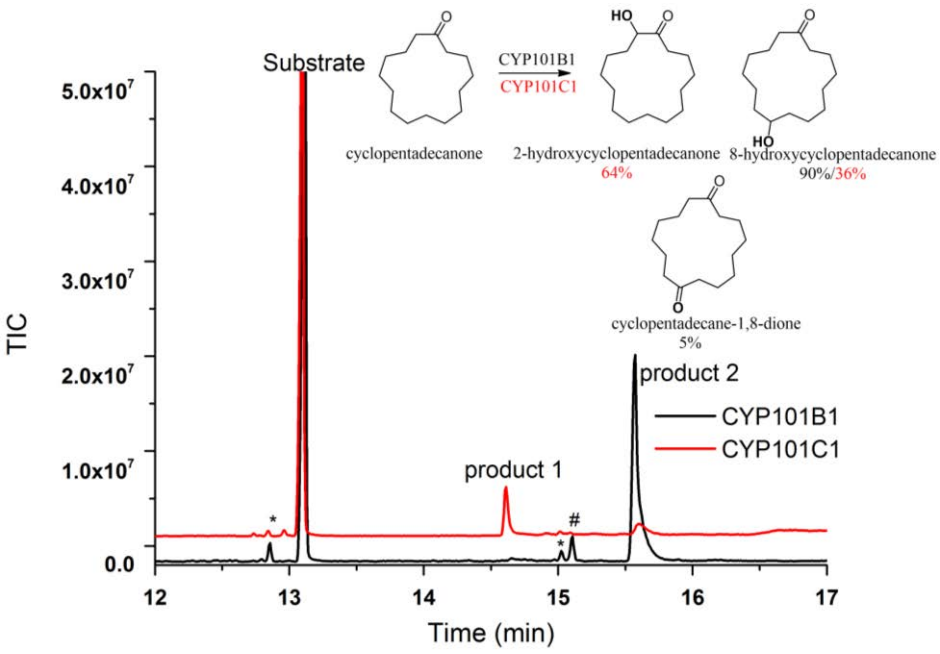

(a)

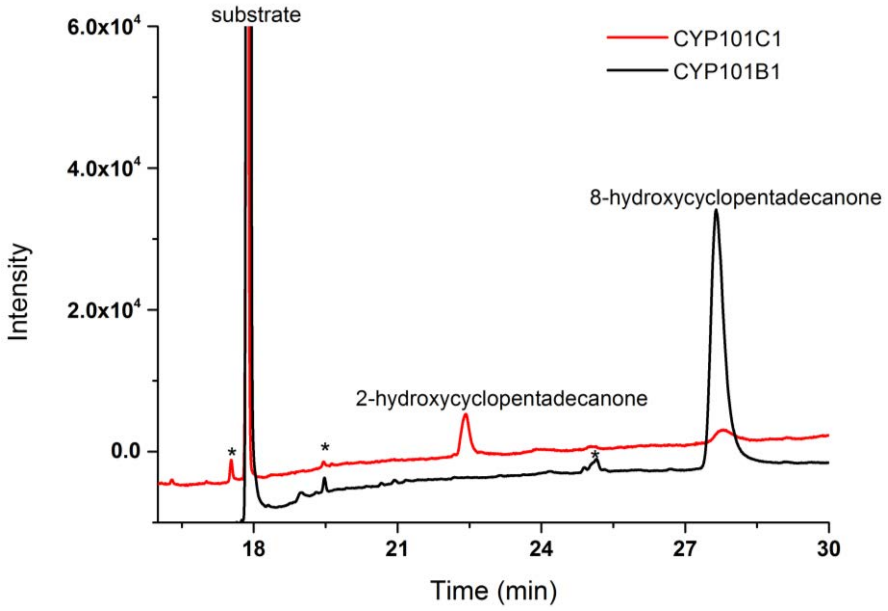

(b)

Figure 3. 21 (a) GC-MS analysis of the *in vitro* turnover of cyclopentadecanone by CYP101B1 and CYP101C1. Cyclopentadecanone (RT 13.1 min) and the product 1; 2-hydroxycyclopentadecanone (RT 14.6 min), product 2; 8-hydroxycyclopentadecanone (RT 15.6 min) [208]. There is a minor product[#] in CYP101B1 enzyme turnover at RT 15.1 min was assigned as cyclopentadecane-1,8-dione (≤5%) [208]. **(b)** The chiral GC analysis of *in vitro* turnover of cyclopentadecanone by CYP101C1 and CYP101B1. Impurities are labelled (*).

CYP101B1 mediated oxidation of cyclopentadecanone generated a single major hydroxylated product, which was detected in the GC-MS analysis (90%; RT 15.6 min; m^+/z = 240.25; Figure 3. 21). To confirm the identity of the metabolite, it was synthesised in higher yield using a CYP101B1 whole-cell turnover system, purified (~24 mg) via silica column chromatography. The metabolite was assigned as 8-hydroxycyclopentadecanone by NMR analysis (Figure 3. 22 and Figure B. 61-B. 68) [208]. In the ^{1}H NMR, a multiplet peak at 3.71-3.64 ppm confirmed a monohydroxylated product. HMBC correlations were used to assign the metabolite (Figure 3. 22 and Figure B. 61-B. 68). The interactions of C1 (215.30) with H2, H15 (2.47-2.33 ppm) and H3, H14 (1.74-1.60 ppm) were used to determine these proton peaks. C4 (29.64 ppm) and C5 (30.18 ppm) were identified using the HMBC correlations with H2 (2.47-2.33 ppm) and H3 (1.74-1.60 ppm), respectively. C5 (30.18) did not show any interaction with the C**H**(OH) peak (3.71-3.64 ppm), indicating hydroxylation did not occur in C6 or C7. C6 (25.90) was assigned via the correlation of H5 (1.40-1.25), and C6 displayed a weak interaction with the peak at 3.71-3.64 ppm, demonstrating the insertion of oxygen likely occurred at C8 (72.70 ppm; Figure 3. 22 and Figure B. 61-B. 68). The mass spectrum was also in agreement with this assignment (Figure B. 1) [208]. The ^{13}C NMR of 8-hydroxycyclopentadecanone also had some small peaks suggesting minor unidentified metabolites were also present (≤5%; Figure B. 62).

The 8-hydroxycyclopentadecanone coeluted with the minor product (36%) of CYP101C1 in GC-MS (Figure 3. 21). There was also a small amount of further oxidation product (5%) observed in the GC-MS analysis of the CYP101B1 turnovers (m^+/z = 238.20; Figure 3. 21 and Figure B. 1). This minor product was presumed to be cyclopentadecane-1,8-dione by comparing its mass spectrum with that reported in the literature, m^+/z 238.20, 220.20, 181.20, 125.15, 112.10, 111.15, 98.15, 84.15, 83.10, 69.10, 55.10 and 43.10. (Figure B. 1) [208]. The chiral GC analyses of both CYP101B1 and CYP101C1 *in vitro* turnovers did not display any chiral separation of the metabolites (Figure 3. 21).

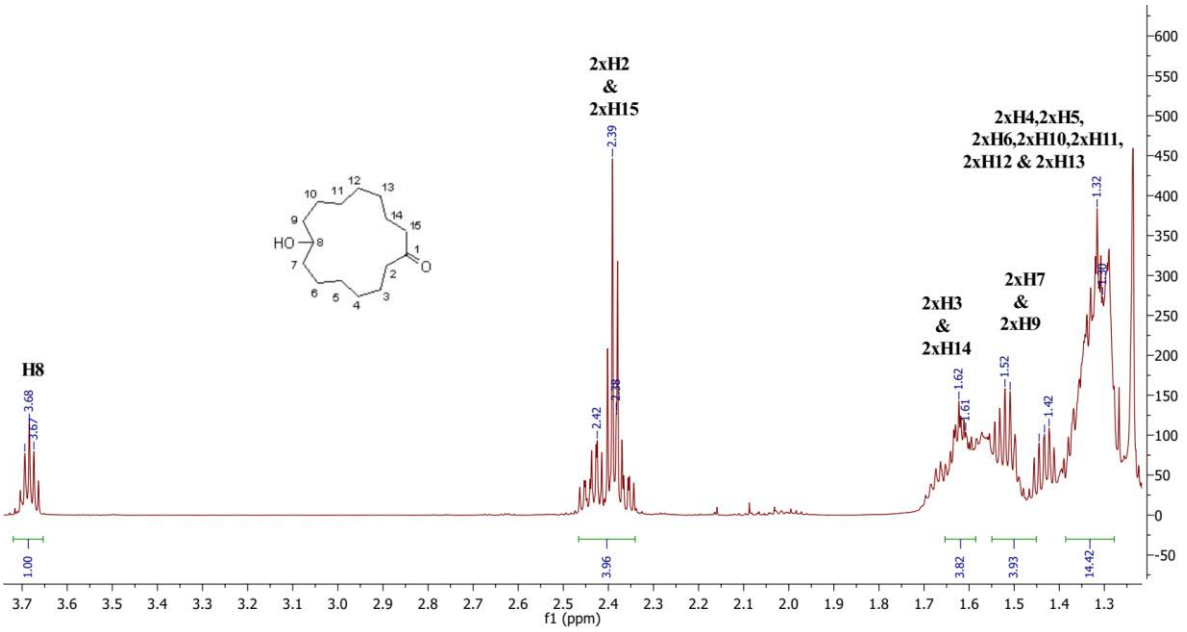

(a)

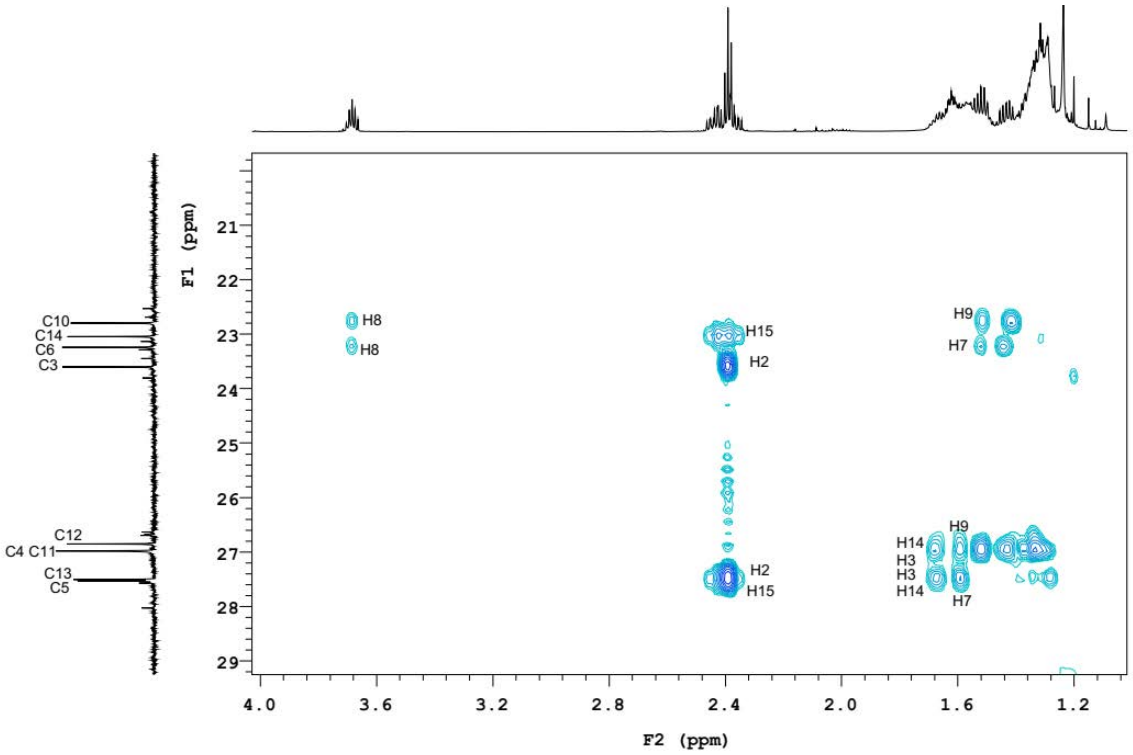

(b)

Figure 3. 22 (a) ^{1}H NMR spectrum of 8-hydroxycyclopentadecanone (CYP101B1). **(b)** Zoomed in (20 to 30 ppm region) version of HMBC NMR spectrum of 8-hydroxycyclopentadecanone, which highlighted the correlations of carbons with the protons. Full data are provided in Appendix B (Figure B. 61-B. 68).

In summary, the oxidative activities of both enzymes were better with the cycloalkanones compared to the cyclic alkanes and alcohols. Substrate profiling indicated that CYP101B1 and CYP101C1 were able to accommodate and oxidise different size of cyclic compounds with these of the ketones ranging from C9 to C15 being the most efficient (Figure 3. 23).

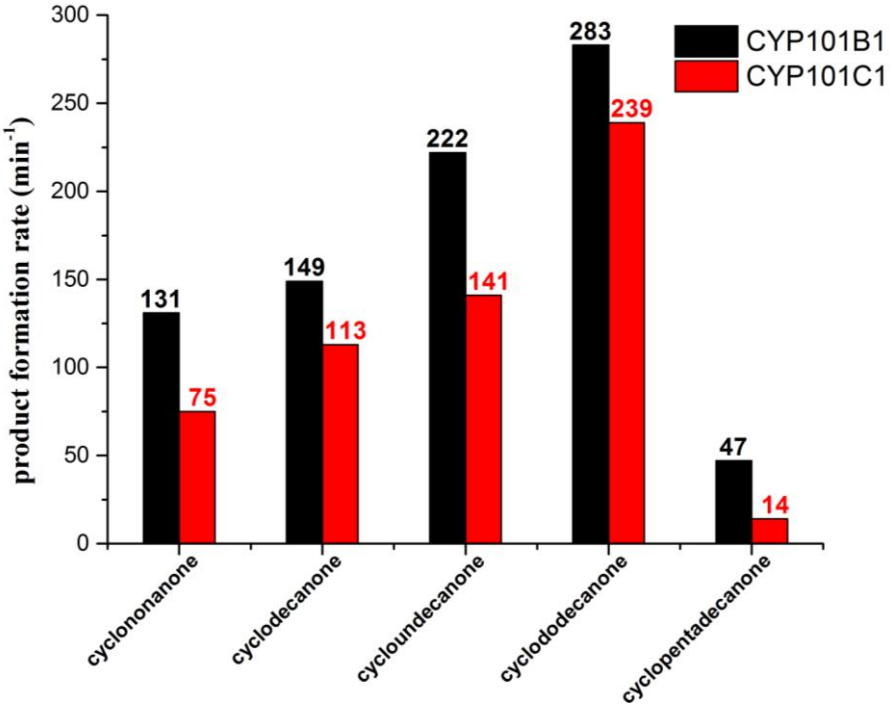

Figure 3. 23 An overview of product formation rates of CYP101B1 and CYP101C1 with cycloalkanones. Product formation rates are given in nmol.nmol-CYP^{-1}.min^{-1}.

The CYP101C1 predominantly hydroxylated at C2 while CYP101B1 was more selective for C-H bond abstraction at carbons on the remote sites of the ring to the ketone.

3.2.2 Use of Directing Groups to Improve the Activity of CYP101B1 and CYP101C1 for Cyclic Alcohols

Both CYP101B1 and CYP101C1 were able to oxidise certain cyclic alkanes and cycloalkanones, in some instances with high selectivity. CYP101B1 and CYP101C1 oxidised *β*-ionone and other norisoprenoid class of compounds efficiently (Figure 1. 17 and Figure 1. 19) [47, 175]. It has also been shown that ester directing groups can help to hold certain substrates in a suitable position of CYP101B1 in the active site for efficient and selective oxidation [175, 176]. Cyclohexanol and cyclooctanol did not show any activity with CYP101B1 and CYP101C1 (Table 3. 1). However, cyclododecanol exhibited higher activity compared to cyclohexanol and cyclooctanol. Both enzymes oxidised cyclododecanol unselectively and with a low coupling efficiency. In order to assess if a directing group could improve the catalytic activity and selectivity of both enzymes, different ester derivatives of cyclic alcohols were synthesised and investigated (Figure 3. 24). First, a range of cyclohexanol derived esters (acetate, isobutyrate and butyrate), as well as the ethyl and methyl esters of cyclohexylacetic acid were tested to assess if the oxidation of cyclohexane rings could be improved (Figure 3. 24). Cyclooctanol and cyclododecanol derived esters were also evaluated. The synthesis of these ester substrates was described in Chapter 2.

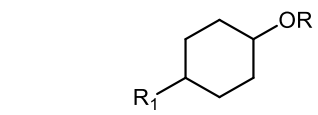

R=-$COCH_3$, R_1=H, cyclohexyl acetate
R=-$COCH(CH_3)_2$, R_1=H, cyclohexyl isobutyrate
R=-$COCH_2CH_2CH_3$, R_1=H, cyclohexyl butyrate
R=-$COCH_3$, R_1=-$C(CH_3)_3$, 4-*tert*-butyl-cyclohexyl acetate

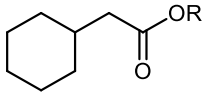

R=-CH_2CH_3, ethylcyclohexylacetate
R=-CH_3, methylcyclohexylacetate

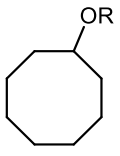

R=-$COCH_3$, cyclooctyl acetate
R=-$COCH(CH_3)_2$, cyclooctyl isobutyrate

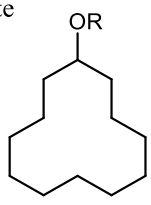

R=-$COCH_3$, cyclododecyl acetate

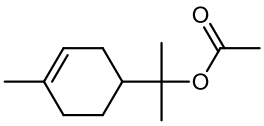

α-terpinyl acetate

Figure 3. 24 Substrates with ester directing groups were screened with both enzymes.

Addition of cyclohexyl acetate induced a spin-state shift of 25% in CYP101B1, which was only a minor improvement over cyclohexane and the parent alcohol cyclohexanol (Figure 3. 25, Table 3. 5 and Table 3. 1). The binding affinity was low, K_d = 544 µM (Figure 3. 25). The NADH oxidation rate for turnovers of this substrate with CYP101B1 and CYP101C1 were 415 min^{-1} and 173 min^{-1}, respectively. Little or no product formation activity was detected for CYP101C1. The CYP101B1 turnover generated a single metabolite with a low product formation rate (56 min^{-1}) and a coupling efficiency of 14% (Table 3. 5 and Figure 3. 26).

A larger scale *in vivo* turnover was carried out to generate the metabolite in adequate yield, which was then purified (~29 mg) via silica column chromatography, and characterised by NMR and mass spectrum analysis (m^+/z 158.0; Figure 3. 26, Figure B. 1, Figure B. 69-B. 74). A characteristic multiplet peak at 3.76-3.72 ppm in the ^{1}H NMR spectrum indicates a hydroxy metabolite (Figure 3. 27). The identity of this metabolite was determined to be 4-hydroxycyclohexyl acetate [223]. The main reason for this assignment was that the ^{13}C NMR spectrum has six signals, two of which 34.94 (C3 and C5) and 31.27 (C2 and C6) can be attributed from their intensity to pairs of identical carbons indicating hydroxylation took place at C4 (Figure B. 69-B. 74). The product was further confirmed from the correlations of C1 (74.38 ppm) and C4 (73.25 ppm) with the protons at δ 2.02-1.93 (H2, H3, H5 and H6) and δ 1.54-1.36 (H2, H3, H5 and H6) in HMBC NMR spectrum (Figure B. 69-B. 74).

^{1}H-^{1}H ROESY NMR was carried out to determine the stereoselectivity (Figure B. 69-B. 74). However, this assignment was hindered due to overlapping signals of the axial and equatorial protons of C2, C3, C5 and C6. The stereoselectivity was assigned using the ^{1}H NMR signals of the H1 and H4 protons. The splitting patterns of H1 and H4 peaks are similar (triplet of triplets) suggesting they have the same environment in relation to the ring system. The coupling constants, J_{H4} = 3.4, 9.2 Hz and J_{H1} = 3.4, 9.5 Hz demonstrated that they are in the same orientation (both axial based on the higher coupling constants; Figure B. 69 and Figure 3. 27). Therefore, the product was assigned as the *trans* isomer.

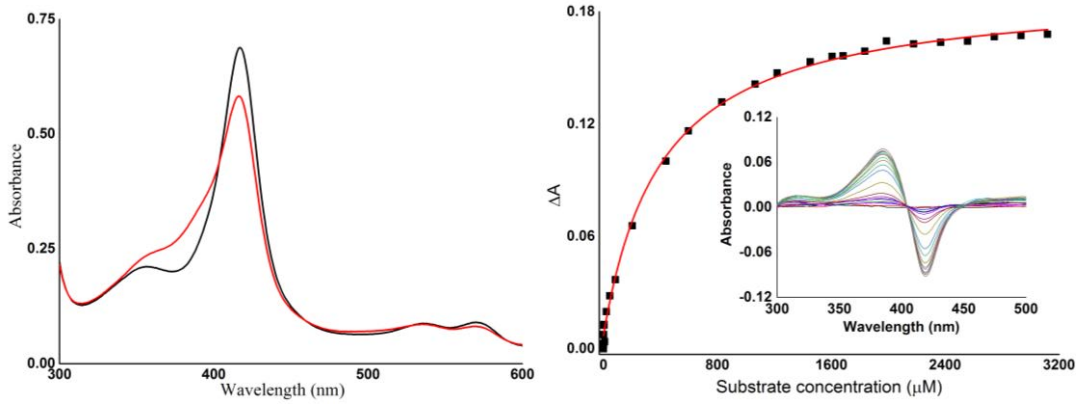

(a) (b)

Figure 3. 25 (a) The spin-state shift (red) of CYP101B1 after addition of cyclohexyl acetate. **(b)** The dissociation constant analysis with cyclohexyl acetate (1.74 μM CYP101B1/K_d 544 μM). The concentration of enzyme used in the binding assay and the dissociation constant (K_d) are provided in brackets.

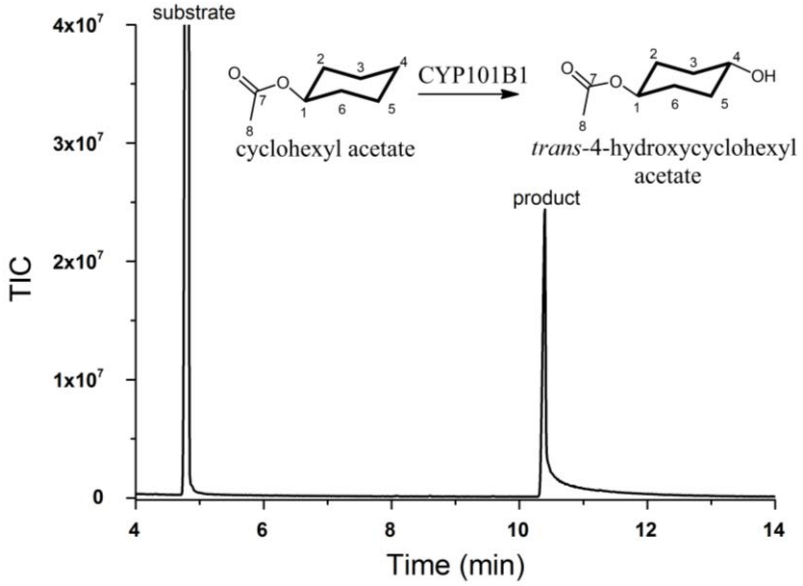

Figure 3. 26 GC-MS analysis of the *in vitro* turnover of cyclohexyl acetate by CYP101B1. Cyclohexyl acetate (RT 4.9 min) and the product; *trans*-4-hydroxycyclohexyl acetate (RT 10.6 min).

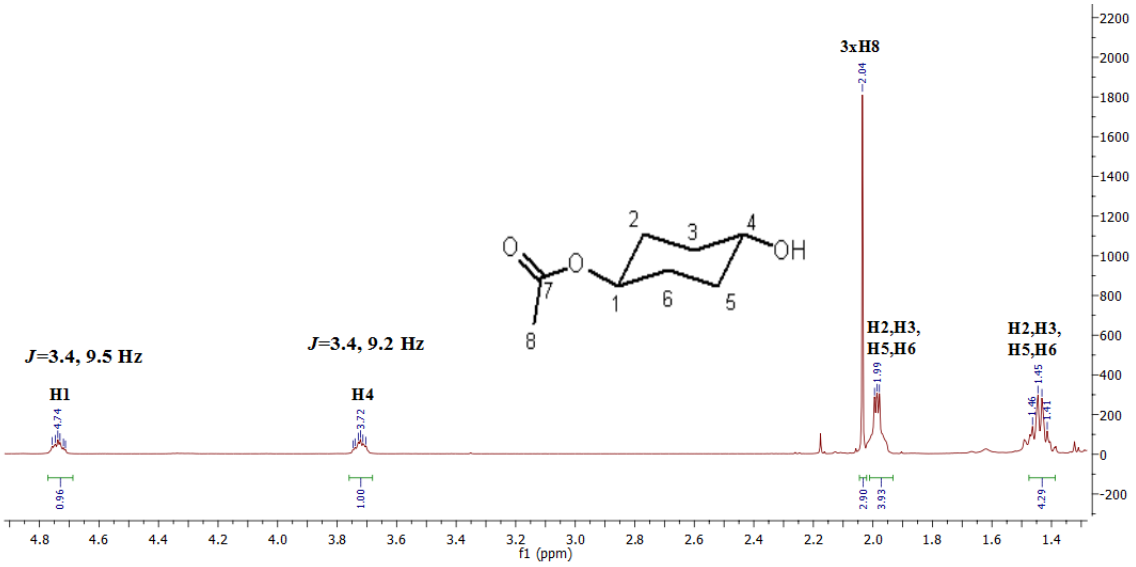

(a)

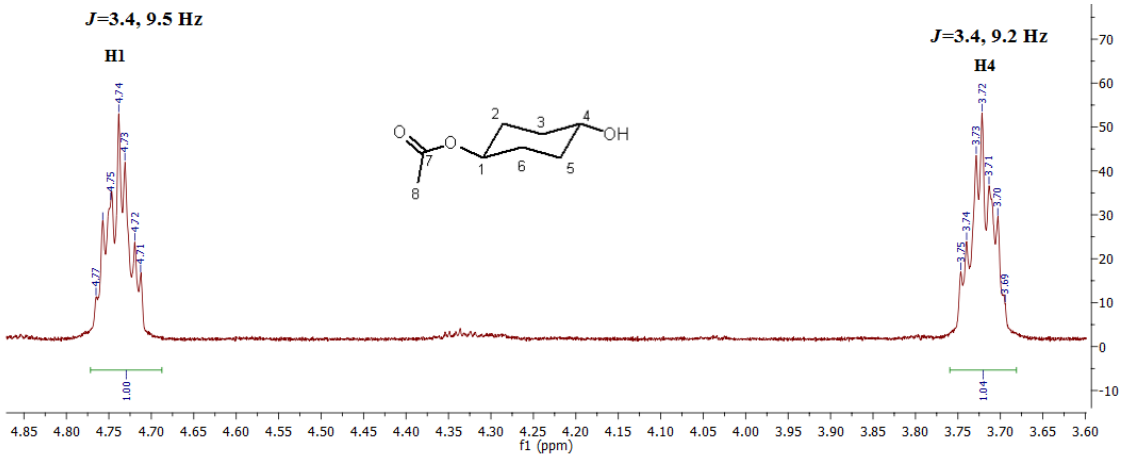

(b)

Figure 3. 27 (a) ^{1}H NMR spectrum of *trans*-4-hydroxycyclohexyl acetate (CYP101B1). **(b)** Zoomed in H1 and H4 peaks to highlight their splitting pattern. Full data are provided in Appendix B (Figure B. 69-B. 74).

Table 3. 5 Substrate binding, turnover and coupling efficiency data for CYP101B1 and CYP101C with a series of substrates containing the ester directing group. The turnover activities were measured as described in Table 3. 3. The data are reported as mean ± S.D. (n = 3). Rates are given in nmol.nmol-CYP^{-1}.min^{-1}. - not measured or not able to be determined accurately. n.p no product.

Substrate	CYP101B1/ CYP101C1	K_d (µM)	NADH	PFR	Coupling (%)	TTN
cyclohexyl acetate	CYP101B1	544 ± 40	415 ± 56	56 ± 6	14	910 ± 385
	CYP101C1	**-**	**173 ± 13**	**n.p**	**-**	**-**
cyclohexyl butyrate	CYP101B1	114 ± 4	603 ± 32	310 ± 62	51	9580 ± 530
	CYP101C1	**-**	**188 ± 16**	**25 ± 10**	**13**	**741 ± 48**
cyclohexyl isobutyrate	CYP101B1	61 ± 5	383 ± 26	220 ± 62	57	3230 ± 65
	CYP101C1	**-**	**106 ± 11**	**20 ± 2**	**19**	**144 ± 10**
4-*tert*-butyl-cyclohexyl acetate	CYP101B1	1.1 ± 0.04	766 ± 70	208 ± 50	27	5640 ± 740
methylcyclohexyl acetate	CYP101B1	31 ± 1.5	736 ± 26	261 ± 20	34	9460 ± 535
	CYP101C1	**-**	**257 ± 8**	**36 ± 11**	**14**	**288 ± 21**
ethylcyclohexyl acetate	CYP101B1	40 ± 1	667 ± 29	274 ± 15	42	7250 ± 1720
	CYP101C1	**-**	**284 ± 35**	**56 ± 12**	**21**	**421 ± 60**
cyclooctyl acetate	CYP101B1	1.6 ± 0.2	722 ± 16	223 ± 20	31	8180 ± 1100
	CYP101C1	**-**	**961 ± 23**	**268 ± 24**	**28**	**3334 ± 686**
cyclooctyl isobutyrate	CYP101B1	1.3 ± 0.2	732 ± 11	626 ± 30	75	4660 ± 1700
	CYP101C1	**-**	**301 ± 2**	**25 ± 5**	**9**	**186 ± 75**
cyclododecyl acetate	CYP101B1	0.05 ± 0.01	394 ± 8	94 ± 7	23	2990 ± 773
	CYP101C1	**-**	**587 ± 7**	**50 ± 8**	**9**	**797 ± 100**
α-terpinyl acetate	CYP101B1	**-**	178 ± 20	**-**	**-**	
	CYP101C1	**-**	**898 ± 16**	**497 ± 20**	**55**	**2810 ± 158**

Increasing the size of the ester directing group, for example, butyrate and isobutyrate instead of acetate, improved the binding affinity of the cyclohexyl substrates for CYP101B1. Cyclohexyl butyrate shifted the spin-state of CYP101B1 to 60% and showed a dissociation constant of K_d = 114 µM (Figure 3. 28 and Table 3. 5). CYP101B1 catalysed the oxidation of this substrate with a high NADH consumption rate of 603 min^{-1} and a coupling efficiency of 51% which resulted in a product formation rate of 310 min^{-1} (Table 3. 5). The total turnover

number (9580) was also significantly increased compared to cyclohexyl acetate (910). In comparison with CYP101B1, CYP101C1 had substantially lower product formation rates and coupling efficiencies (Table 3. 5). Both enzymes oxidised cyclohexyl butyrate to the same single metabolite (Figure 3. 29). Using an *in vivo* turnover system of CYP101B1, the metabolite was generated in sufficient yield for NMR characterisation. The metabolite was isolated (~26 mg) using silica column chromatography and characterised by NMR analysis (Figure 3. 29 and Figure B. 75-B. 79). ^{1}H NMR spectrum had a distinct multiplet peak of hydroxylation at 3.71-3.60 ppm. The product has eight ^{13}C NMR signals, and HSQC NMR spectrum displays the connections of 34.80 (C3 and C5), 31.25 (C2 and C6) with the protons of 1.99-1.88 ppm and 1.47-1.33 ppm regions indicating hydroxylation occurred at the C-4 position resulting in a symmetrical metabolite (Figure 3. 29 and Figure B. 75-B. 79). gCOSY NMR spectrum analysis was also in agreement with this assignment. The splitting patterns and coupling constants of the H1 and H4 protons, J_{H1} = 3.1, 9.4 Hz and J_{H4} = 3.1, 9.2 Hz were similar, indicating their axial orientations (Figure 3. 29). Therefore, this metabolite was confirmed as *trans*-4-hydroxycyclohexyl butyrate.

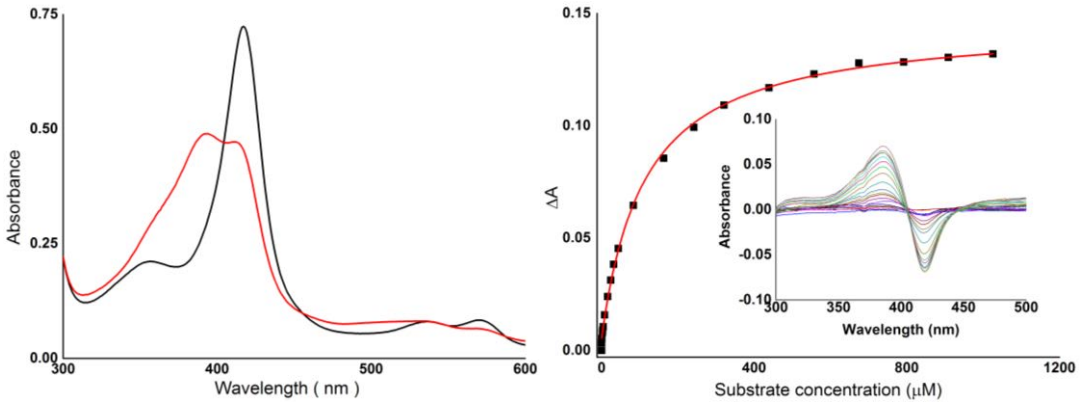

(a) (b)

Figure 3. 28 (a) The spin-state shift (red) of CYP101B1 after addition of cyclohexyl butyrate. **(b)** The dissociation constant analysis with cyclohexyl butyrate (1.33 µM CYP101B1/K_d 114 µM). The concentration of enzyme used in the binding assay and the dissociation constant (K_d) are provided in brackets.

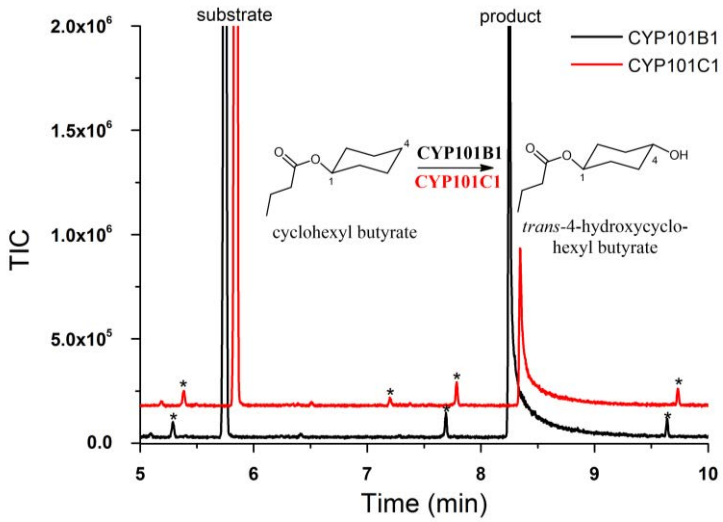

(a)

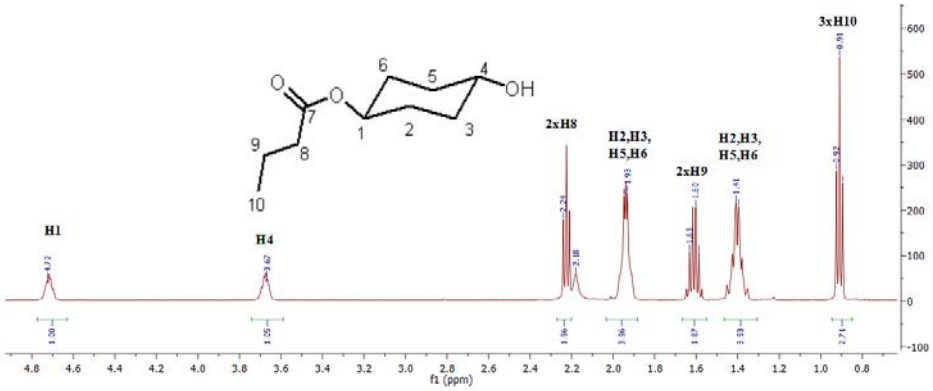

(b)

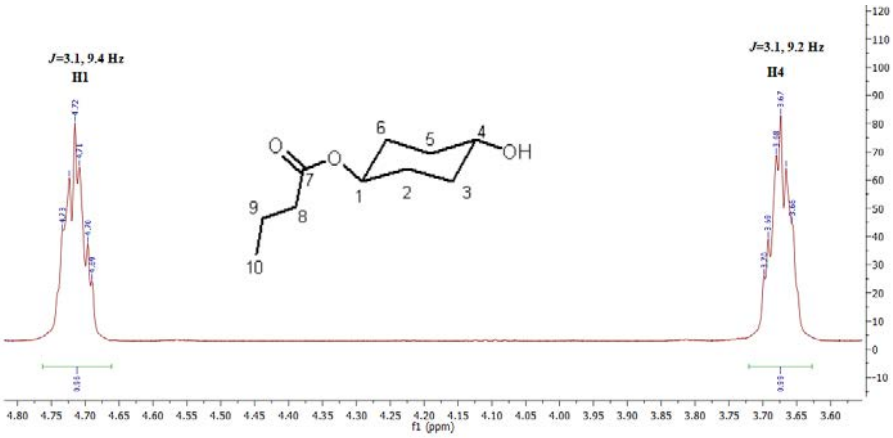

(c)

Figure 3. 29 (a) GC-MS analysis of *in vitro* turnover of cyclohexyl butyrate by CYP101B1 and CYP101C1. Cyclohexyl butyrate (RT 5.7 min) and the product; *trans*-4-hydroxycyclohexyl butyrate (RT 8.5 min). The chromatogram (CYP101C1) was offset along the x and y-axes for clarity. **(b)** ^{1}H NMR spectrum of *trans*-4-hydroxycyclohexyl butyrate (CYP101B1). **(c)** Zoomed in version of ^{1}H NMR spectrum to highlight the peaks of H1 and H4. Full data are provided in Appendix B (Figure B. 75-B. 79).

Addition of cyclohexyl isobutyrate also changed the spin-state of CYP101B1 to 60% and bound with a dissociation constant of 61 µM (Figure 3. 30 and Table 3. 5). Cyclohexyl isobutyrate caused the CYP101B1 turnover system to oxidise NADH at a rate of 383 min^{-1} which was less than the other substrates tested above, but a faster product formation rate was observed compared to cyclohexyl acetate due to improved coupling efficiency (57%; Table 3. 5). The total turnover number of CYP101B1 with cyclohexyl isobutyrate was in between the cyclohexyl acetate and cyclohexyl butyrate (3226; Table 3. 5). CYP101C1 oxidation of cyclohexyl isobutyrate proceeded with a low NADH oxidation activity of 106 min^{-1}, product formation rate of 20 min^{-1} and coupling efficiency of 19% (Table 3. 5). Both *in vitro* and *in vivo* turnovers of this substrate with these enzymes generated the same product with high selectivity (≥99%), which was detected in GC-MS analysis (Figure 3. 31). The CYP101B1 whole-cell system was used to generate the metabolite in the required yield for characterisation. The product was isolated by silica column chromatography and characterised by NMR analysis (~10 mg; Figure 3. 31 and Figure B. 80-B. 83). The ^{1}H NMR had a characteristic signal at 3.78-3.70 ppm, which is an indication of a hydroxylation metabolite (Figure 3. 31). The ^{1}H-^{13}C HSQC NMR analysis displayed the correlations of carbons at 34.75 ppm (C3 and C5) and 31.04 ppm (C2 and C6) with the protons at δ 2.04-1.89 (H2, H4, H5 and H6) and δ 1.51-1.43 (H2, H4, H5 and H6), confirming the hydroxylation occurred at the C4 position, which is the only position equidistant to the C2, C6 and C3, C5 carbons (Figure B. 82). The ^{1}H, ^{13}C, ^{1}H-^{1}H gCOSY NMR spectra were also in agreement with this assignment. The stereoisomer of this metabolite was confirmed as *trans* due to the high coupling constants of J_{H4} = 3.3, 8.8 Hz and J_{H1} = 4.7, 9.1 Hz, demonstrating their axial orientations (Figure 3. 31 and Figure B. 80-B. 83).

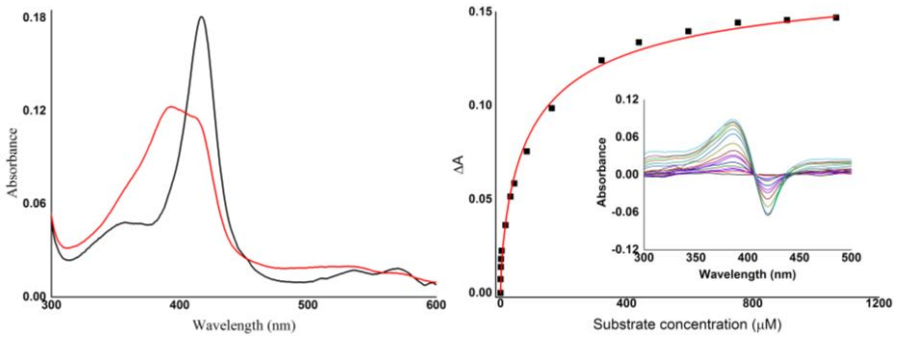

(a) (b)

Figure 3. 30 (a) The spin-state shift (red) of CYP101B1 after addition of cyclohexyl isobutyrate. **(b)** Dissociation constant analysis with cyclohexyl isobutyrate (1.65 µM CYP101B1/K_d 61 µM). The concentration of enzyme used in the study and the dissociation constant (K_d) are provided in brackets.

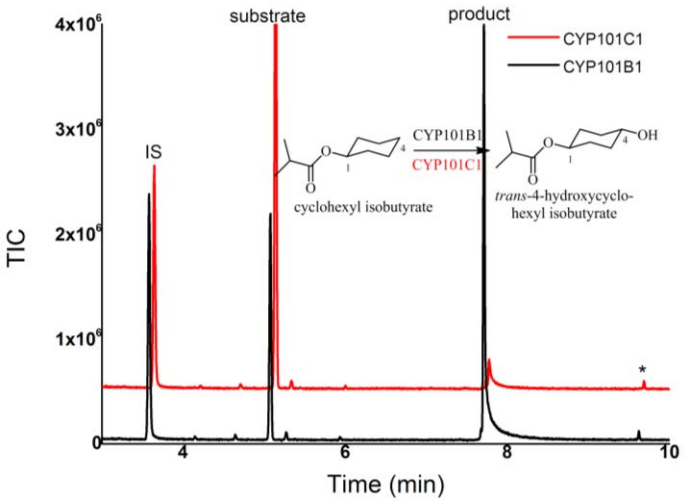

(a)

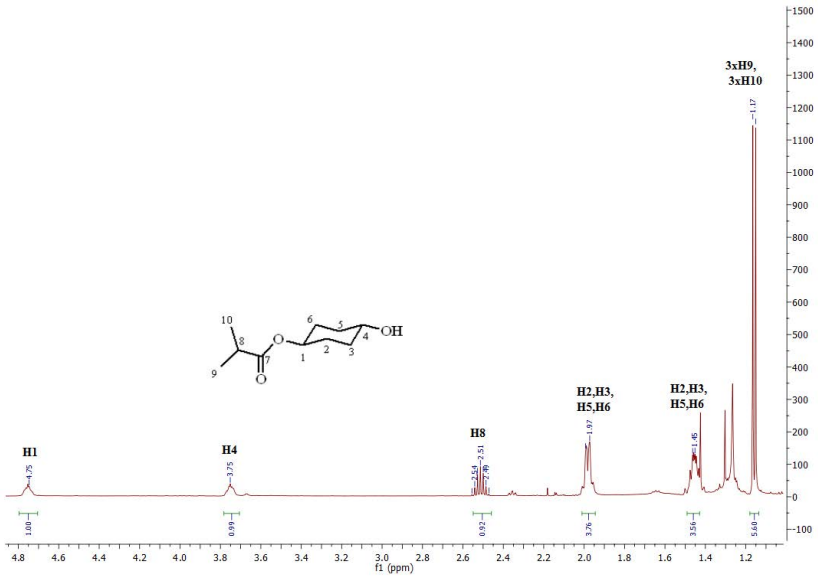

(b)

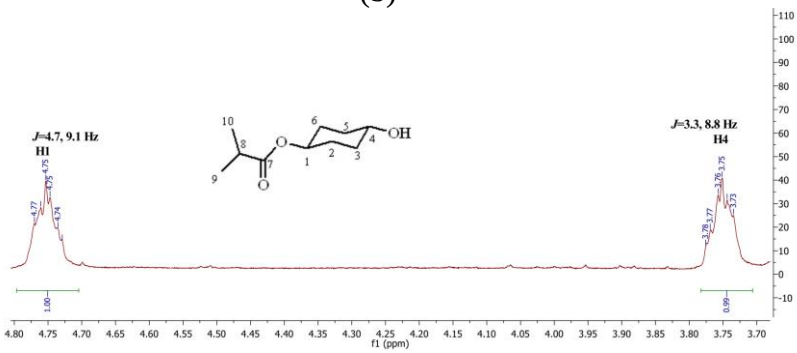

(c)

Figure 3. 31 (a) GC-MS analysis of *in vitro* turnover of cyclohexyl isobutyrate by CYP101B1 and CYP101C1. Cyclohexyl isobutyrate (RT 5.1 min) and the product; *trans*-4-hydroxycyclohexyl isobutyrate (RT 7.9 min). The chromatogram (CYP101C1) was offset along the x and y-axes for clarity. **(b)** ^{1}H NMR spectrum of *trans*-4-hydroxycyclohexyl isobutyrate (CYP101B1). **(c)** Zoomed in version of ^{1}H NMR spectrum to highlight the H1 and H4 peaks splitting patterns. Full data are presented in Appendix B (Figure B. 80-B. 83).

The cyclohexyl ester derivative containing a *tert*-butyl group in the *para* position was also examined with CYP101B1. The spin-state shift induced by a mixture of the *cis/trans* isomers of 4-*tert*-butylcyclohexyl acetate was significantly higher than the 4-*tert*-butylcyclohexanol (~85% versus 15%, Figure 3. 32 and Figure 3. 2). The binding affinity was tighter compared to other cyclohexanol derived esters tested above, indicating this substrate was better accommodated in the active site of the enzyme (Figure 3. 32 and Table 3. 5).

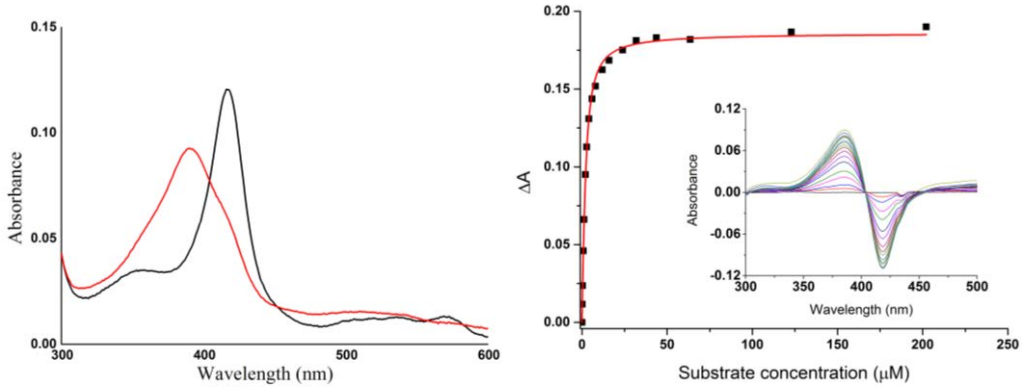

(a) (b)

Figure 3. 32 (a) The spin-state shift (red) of CYP101B1 after addition of 4-*tert*-butylcyclohexyl acetate. **(b)** Dissociation constant analysis with 4-*tert*-butylcyclohexyl acetate (1.75 µM CYP101B1/K_d 1.1 µM). The concentration of enzyme used in the binding assay and the dissociation constant (K_d) are provided in brackets.

4-*tert*-Butylcyclohexyl acetate induced a faster NADH oxidation activity in the CYP101B1 system (766 min^{-1}; Table 3. 5). It catalysed the turnover of this substrate with a product formation rate of 208 min^{-1} and a coupling efficiency of 27% (Table 3. 5). The *in vitro* CYP101B1 turnovers of *cis* and *trans* isomers of 4-*tert*-butylcyclohexyl acetate were analysed by GC/GC-MS, which indicated that each diastereomer was transformed to a monohydroxylated metabolite (GC-MS RT 13.2 min; m^+/z = 214.10 and RT 14.1 min; m^+/z = 214.20; Figure 3. 33 and Figure B. 1). The products were generated in a sufficient amount using the CYP101B1 whole-cell biotransformation system for characterisation. One of the metabolites (RT 14.1 min in GC) was isolated (~15 mg) using silica column chromatography, and this was characterised by NMR analysis. The metabolite was identified as 4-(1-hydroxy-2-methylpropan-2-yl)cyclohexyl acetate (*trans*; J_{H1} = 4.5, 11.2 Hz and J_{H4} = 2.9, 12.1 Hz) using the distinct methyl hydroxylation peak which was observed at 3.39 (2H, 2xH8) in the ^{1}H NMR spectrum (Figure 3. 33 and Figure B. 85). The ^{13}C, gCOSY, HSQC NMR spectra were also in

agreement with this assignment (Figure B. 84-B. 88). The other product was not isolated, but it was presumed to be the hydroxylated metabolite of the *cis* diastereomer (m^+/z = 214.10, Figure B. 1 and Figure B. 85). Further confirmation is required, which could be done using NMR. The substrate *tert*-butyl side chain must, therefore, be held in close proximity to the heme centre which inserted the hydroxyl group in one of the methyl groups instead of cyclohexane skeleton.

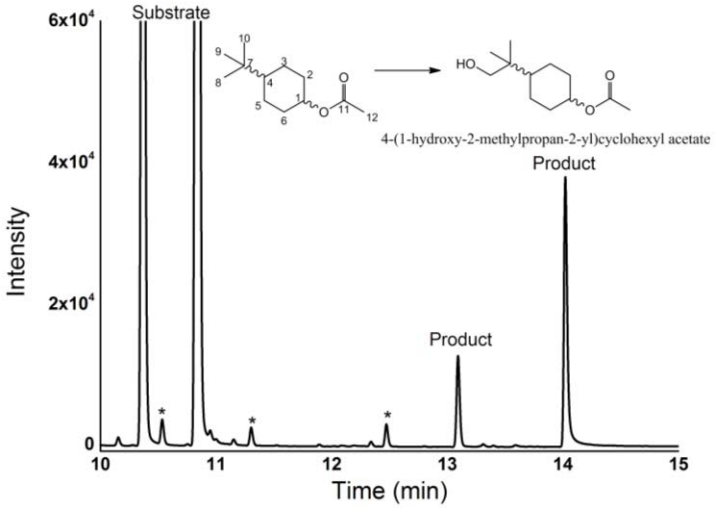

(a)

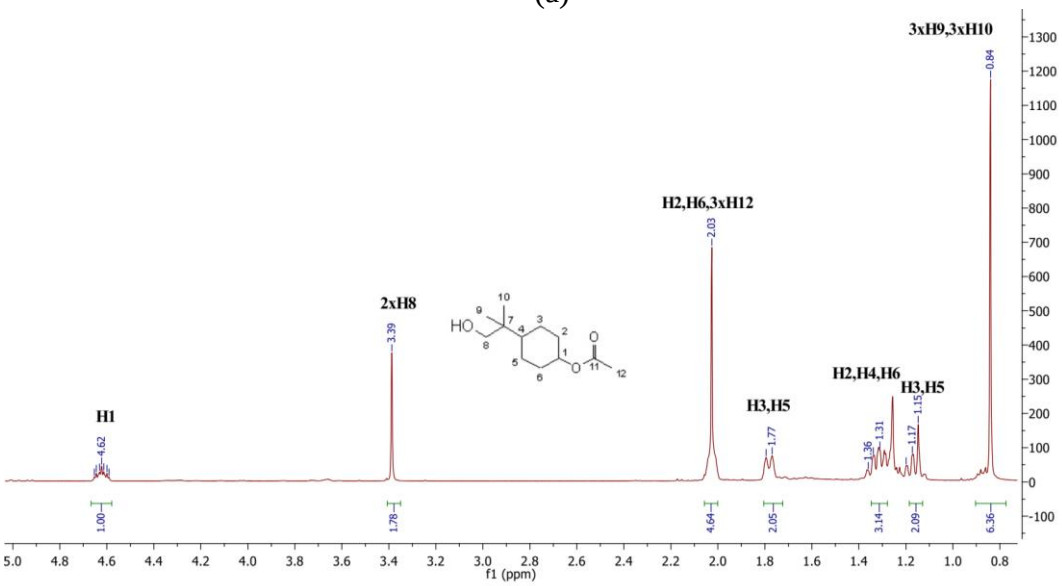

(b)

Figure 3. 33 (a) GC analysis of the *in vitro* turnover of 4-*tert*-butylcyclohexyl acetate (*cis* and *trans* mixture) by CYP101B1. *Cis* and *trans*-4-*tert*-butylcyclohexyl acetate (RT 10.45 min and 10.90 min) and the product 4-(1-hydroxy-2-methylpropan-2-yl)cyclohexyl acetate (RT 13.2 min (*cis*) and 14.1 min (*trans*)). **(b)** ^{1}H NMR spectrum *trans*-4-(1-hydroxy-2-methylpropan-2-yl)cyclohexyl acetate. Full data are provided in Appendix B (Figure B. 84-B. 88).

The above results demonstrate that the catalytic activity of both enzymes was improved for cyclohexyl derived esters. Cyclohexylacetic acid was also investigated as a substrate. It did not induce the heme spin of the CYP101B1 enzyme to high spin-state, and no product was detectable when this substrate was added to either the CYP101B1 or CYP101C1 system (Figure not shown). However, the methyl and ethyl esters of cyclohexylacetic acid showed better binding characteristics.

A substantial heme spin-state alteration was noticed when methylcyclohexyl acetate was added to CYP101B1. This substrate gave a 95% shift to the high spin form, and the binding affinity was improved with a K_d of 31 µM (Figure 3. 34 and Table 3. 5). This was tighter than the binding affinities of cyclohexanol derived esters investigated above (Figure 3. 34). The NADH oxidation and product formation activity were also enhanced for both enzymes (Table 3. 5). Compared to CYP101C1, CYP101B1 showed a better NADH oxidation activity of 736 min^{-1} and product formation rate of 261 min^{-1} with a two-fold greater coupling efficiency (Table 3. 5).

The same monooxygenase metabolite was detected in the GC/GC-MS analyses of the *in vitro* turnovers of this substrate with CYP101B1 and CYP101C1 (m^+/z = 172.0; Figure 3. 35 and Figure B. 1). A larger-scale whole-cell oxidation of methylcyclohexyl acetate with the CYP101B1 system was carried out to generate the metabolite in sufficient amount (Figure 3. 35). The product was isolated (~32 mg) by silica column chromatography and identified via NMR analysis. In ^1H NMR spectrum, a characteristic multiplet peak at 3.59-3.52 ppm is present, demonstrating a hydroxylation metabolite was formed (Figure 3. 35 and Figure B. 89-B. 95). The product was identified as the 4-hydroxy metabolite based on ^1H-^{13}C HMBC NMR correlations of C4 (73.25 ppm) with the protons of H3, H5 (1.36-1.28 ppm) and H2, H6 (1.84-1.74 ppm). This assignment was further confirmed by ^1H-^{13}C HSQC NMR spectrum analysis where two equal intensity of carbon peaks at 37.86 ppm (C3 & C5) and 33.61 ppm (C2 & C6) showed connections with the protons in the region of 2.02-1.94 ppm, 1.84-1.74 ppm, 1.36-1.28 ppm and 1.12-1.00 ppm, which are only possible if hydroxylation took place at C4 position to form a symmetrical product (Figure B. 89-B. 95).

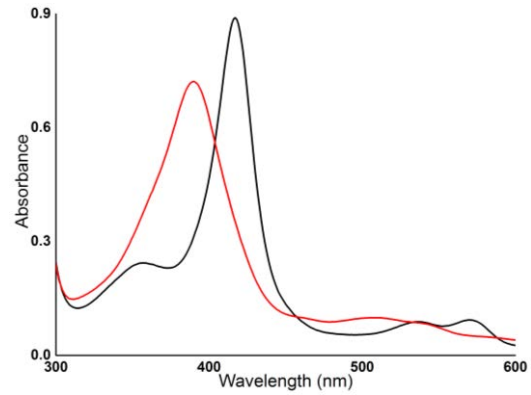

(a)

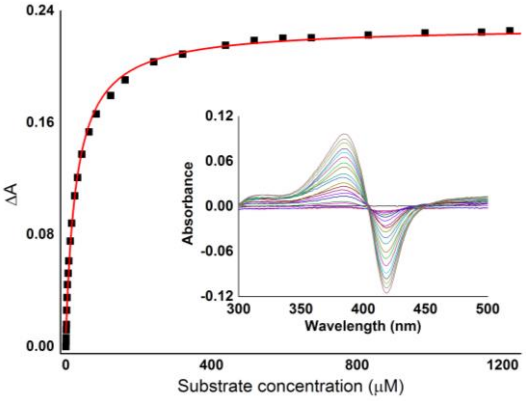

(b)

Figure 3. 34 (a) The spin-state shift (red) of CYP101B1 after addition of methylcyclohexyl acetate. **(b)** The dissociation constant analysis with methylcyclohexyl acetate (1.70 µM CYP101B1/K_d 31 µM). The concentration of enzyme used in the binding assay and the dissociation constant (K_d) are provided in brackets.

The stereoselectivity of this metabolite was confirmed using ^{1}H-^{1}H ROESY NMR spectrum analysis (Figure 3. 36 and Figure B. 94-B. 95). H4 showed a characteristic interaction with $H_{2/6ax}$ (1.12-1.00 ppm) indicating the axial orientation of this proton. The axial orientation of H4 and H1 were confirmed by their axial-axial and axial-equatorial coupling constants of J_{H4} = 10.8, 4.1 Hz and J_{H1} = 3.8, 7.4 Hz (Figure 3. 35). The H7 displayed a strong correlation with $H6_{eq}$ and a weak interaction with $H6_{ax}$ in ROESY NMR spectrum that also indicates the axial orientation of H1. Therefore, the product was assigned as methyl-2-*(trans*-4-hydroxycyclohexyl)acetate (Figure 3. 36 and Figure B. 94-B. 95).

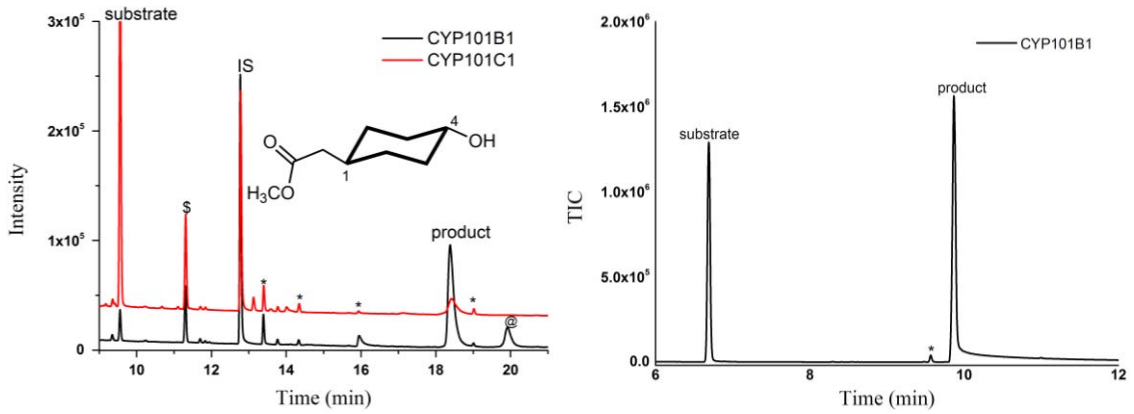

(a) (b)

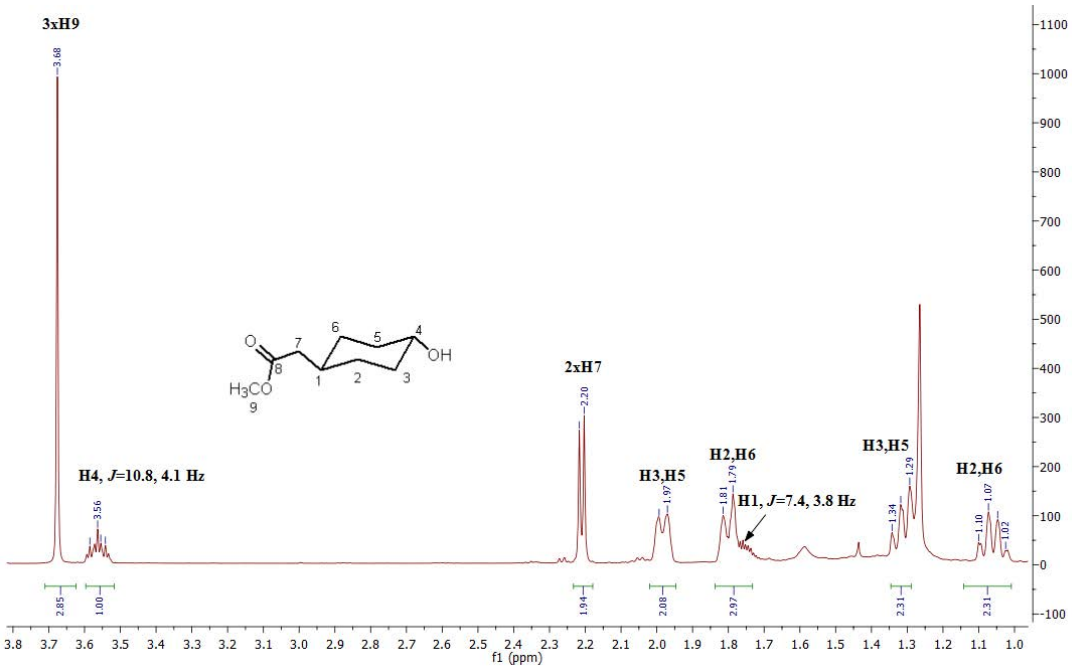

(c)

Figure 3. 35 (a) GC analyses of *in vitro* turnovers of methylcyclohexyl acetate by CYP101B1 and CYP101C1. Methylcyclohexyl acetate (RT 9.8 min) and the product; methyl-2-(*trans*-4-hydroxycyclohexyl)acetate (RT 18.5 min), and a peak for esterification of the substrate to ethylcyclohexyl aceate[$] (RT 11.5 min) and product of ethylcyclohexyl acetate oxidation[@] (RT 19.9 min). **(b)** GC-MS analysis of the *in vivo* turnover of methylcyclohexyl acetate by CYP101B1. Methylcyclohexyl acetate (RT 6.7 min) and the product; methyl-2-(*trans*-4-hydroxycyclohexyl)acetate (RT 9.9 min). **(c)** ^{1}H NMR spectrum of methyl-2-(*trans*-4-hydroxycyclohexyl)acetate (CYP101B1). Full data are provided in Appendix B (Figure B. 89-B. 95).

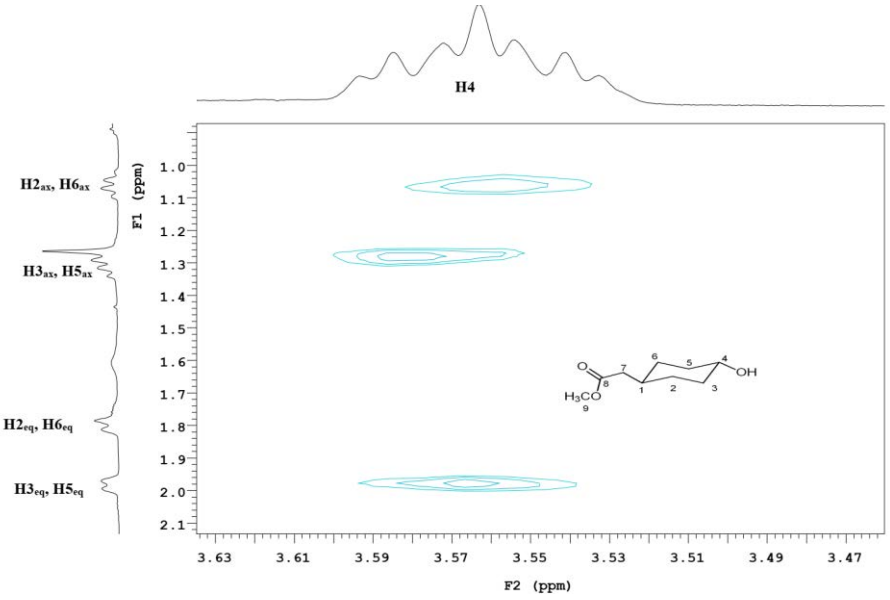

(a)

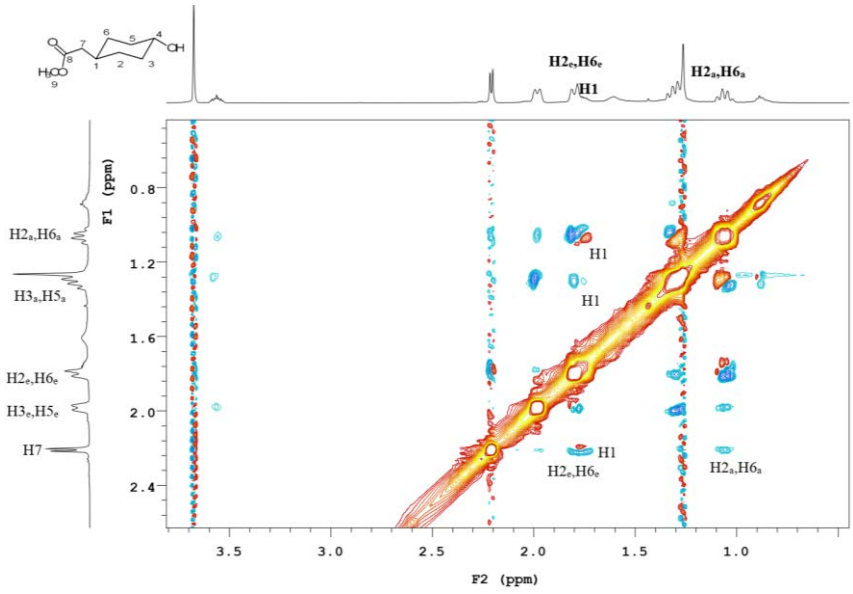

(b)

Figure 3. 36 ^{1}H-^{1}H ROESY NMR spectrum of methyl-2-*(trans*-4-hydroxycyclohexyl)acetate showed the interactions of **(a)** H4 (axial) with the $H_{2/6ax}$ protons, and **(b)** H7 (equatorial side chain) displayed correlations with the protons of $H6_{ax/eq}$.

Ethylcyclohexyl acetate shifted the spin-state of CYP101B1 to ~85% high spin form (Figure 3. 37), and it displayed slightly lower binding affinity than methylcyclohexyl acetate (K_d = 40 µM versus K_d = 31 µM; Figure 3. 37 and Table 3. 5). Addition of this substrate in the *in vitro* turnover assay of CYP101B1 induced a fast NADH oxidation rate (667 min^{-1}), indicative of

efficient product formation rate (274 min^{-1}; Table 3. 5). The oxidation of this substrate by CYP101C1 progressed at a slower NADH oxidation activity and a product formation rate of 284 and 56 min^{-1}, respectively. The coupling efficiency was also lower for the CYP101C1 system (42% versus 21%; Table 3. 5). CYP101B1 exhibited a significantly higher total turnover number compared to CYP101C1 (7250 versus 421; Table 3. 5).

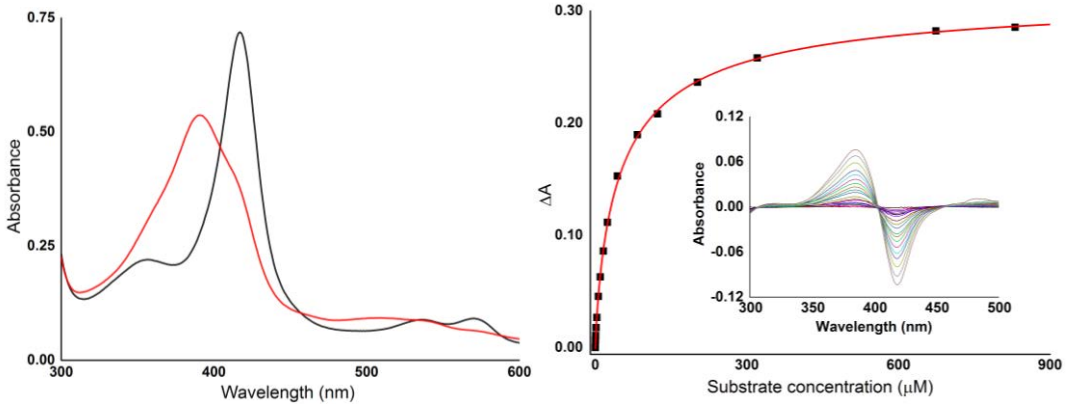

(a) (b)

Figure 3. 37 (a) The spin-state shift (red) of CYP101B1 after addition of ethylcyclohexyl acetate. **(b)** The dissociation constant analysis with ethylcyclohexyl acetate (1.65 µM CYP101B1/K_d 40 µM). The concentration of enzyme used in the binding study and the dissociation constant (K_d) are provided in brackets.

The GC-MS analyses of the *in vitro* turnovers of both CYP101B1 and CYP101C1 indicated that same major monohydroxylated metabolite was formed, which accounted for 99% of the total turnover products (m^+/z = 186.15; Figure 3. 38 and Figure B. 1). This metabolite was generated using the CYP101B1 *in vivo* turnover system, and then extracted and isolated for NMR analysis (~24 mg; Figure 3. 38 and Figure B. 96-B. 102). The H2 and H6 proton peaks (1.84-1.71 and 1.11-1.01 ppm) were determined via ^1H-^1H coupling with H1 in gCOSY NMR (Figure B. 98). These proton peaks were further confirmed via the ^1H-^{13}C HMBC NMR correlations of C2 and C6 (33.59 ppm) with H7 (2.19 ppm) (Figure 3. 37 and Figure B. 96-B. 102). The HMBC NMR interactions of C2 and C6 with the H3 and H5 (1.3-1.23 ppm) protons were used to assign the C3 and C5 (37.87 ppm) carbon signals (Figure 3. 39). Two carbon signals 37.87 (C3 & C5) and 33.59 (C2 & C6) in the ^{13}C NMR spectrum showed double the intensity compared to the other peaks, suggesting each signal represented two equivalent carbons. Hence, the hydroxylation occurred at the C4 position, resulting in a symmetrical metabolite (Figure 3. 39 and Figure B. 96-B. 102).

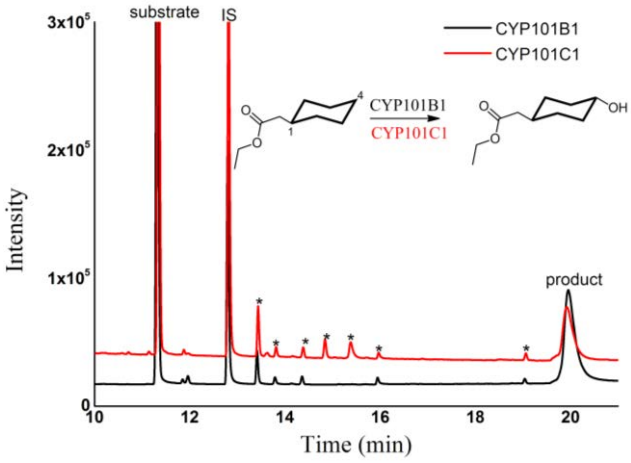

(a)

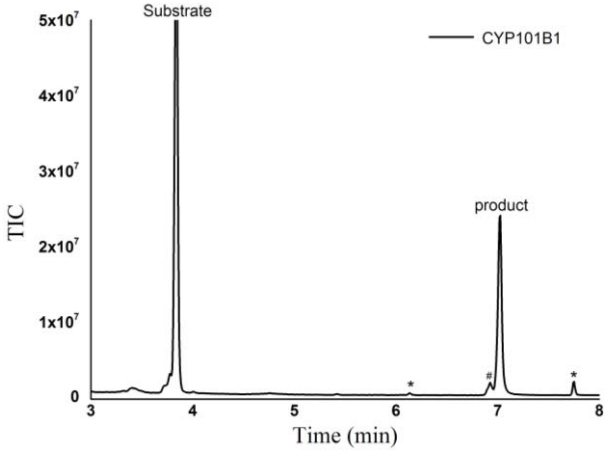

(b)

Figure 3. 38 (a) GC analyses of the *in vitro* turnovers of ethylcyclohexyl acetate by CYP101B1 and CYP101C1. Ethylcyclohexyl acetate (RT 11.5 min) and the product; ethyl-*trans*-2-(4-hydroxycyclohexyl)acetate (RT 20.1 min). **(b)** GC-MS analysis of the *in vivo* turnover of ethylcyclohexyl acetate by CYP101B1. Ethylcyclohexyl acetate (RT 3.9 min) and the product; ethyl-*trans*-2-(4-hydroxycyclohexyl)acetate (RT 7.0 min) and a further oxidation metabolite at RT 6.9 min$^{\#}$ (1%; m^+/z =184.25, Figure B. 1).

The stereoselectivity was confirmed by ^{1}H-^{1}H ROESY NMR analysis (Figure 3. 40 and Figure B. 101-B.102). The interaction of H4 with $H_{2/6ax}$ in ROESY NMR spectrum indicated its axial orientation. The correlations of H7 with $H_{6ax/eq}$ in the ROESY NMR suggested the axial orientation of H1. The axial-axial and axial-equatorial coupling constants of H4, J_{H4} = 10.9, 4.1 Hz and H1, J_{H1} = 7.7, 3.7 Hz, were also confirmed their axial orientation (Figure 3. 40 and Figure B. 101-B. 102). Therefore, the diastereomer was assigned as a *trans* isomer of ethyl-2-(4-hydroxycyclohexyl)acetate (Figure 3. 40 and Figure B. 101-B. 102).

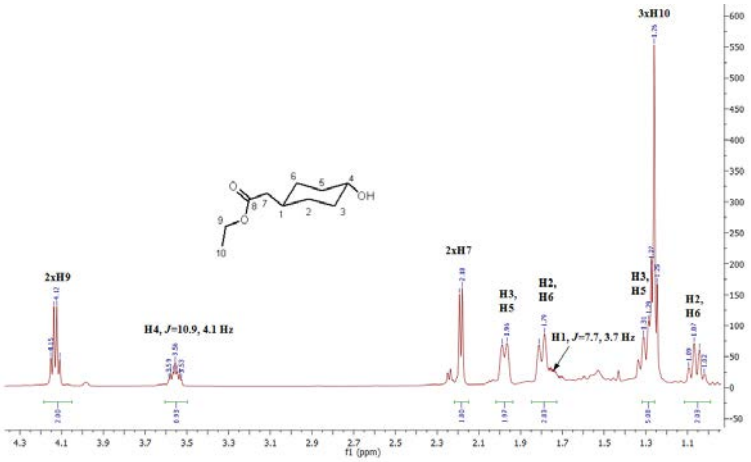

(a)

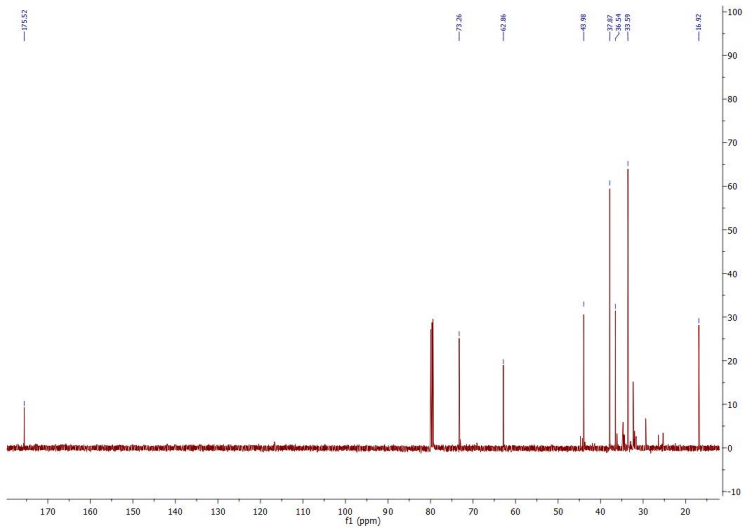

(b)

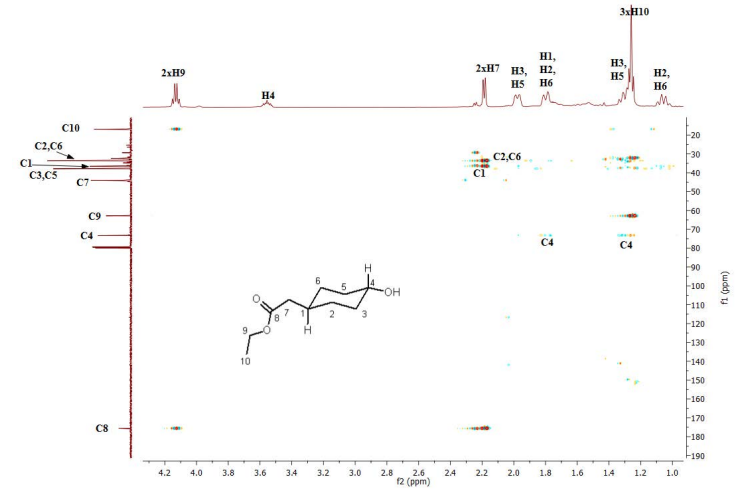

(c)

Figure 3. 39 (a and b) ^{1}H and ^{13}C NMR spectrum of ethyl-*trans*-2-(4-hydroxycyclohexyl)acetate (CYP101B1). **(c)** HMBC NMR spectrum of ethyl-*trans*-2-(4-hydroxycyclohexyl)acetate. Full data are in Appendix B (Figure B. 96-B. 102).

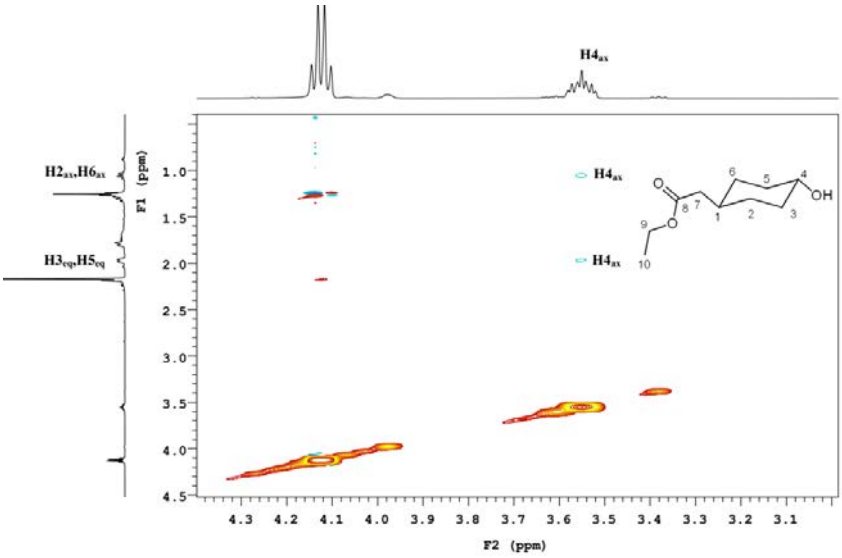

(a)

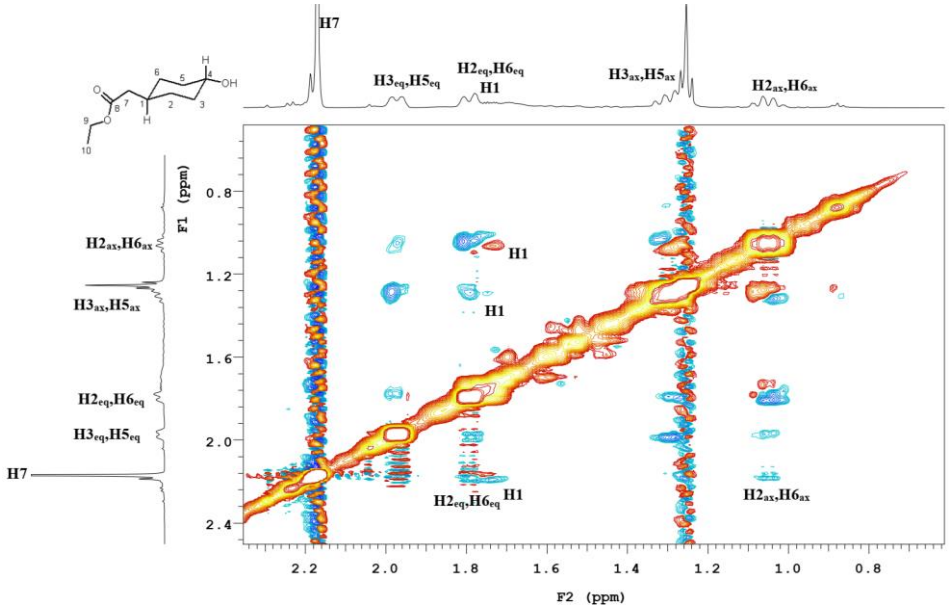

(b)

Figure 3. 40 Zoomed in version of ROESY NMR (600 MHz) spectrum of ethyl-*trans*-2-(4-hydroxycyclohexyl)acetate, which highlighted the interactions of **(a)** H4 (axial) with the $H_{2/6ax}$ protons, and **(b)** H7 (equatorial side chain) showed correlations with the $H6_{ax/eq}$ protons.

Cyclooctyl acetate and cyclooctyl isobutyrate both generated a significantly higher spin-state shift (~85 to 95%) upon addition to CYP101B1 when compared to cyclooctane (35%) and their parent alcohol cyclooctanol (5%; Figure 3. 41 and Figure 3. 2). The dissociation constants of CYP101B1 with both substrates were investigated to determine how tightly each substrate bound in the active site. CYP101B1 had tighter binding affinities with both of these substrates than the cyclic (C6) ester derivatives (K_d 1.3 µM and 1.6 µM; Figure 3. 41 and Table 3. 5).

Compared to cyclooctane and cyclooctanol, cyclooctyl acetate and isobutyrate induced faster NADH oxidation rates in CYP101B1 system. Among these two ester substrates, higher product formation activity and coupling efficiency were observed with cyclooctyl isobutyrate (Table 3. 5). CYP101C1 catalysed the oxidation of cyclooctyl acetate with greater NADH oxidation activity (961 min^{-1}) and marginally faster product formation rate than the CYP101B1 (268 min^{-1} versus 223 min^{-1}; Table 3. 5). However, for cyclooctyl isobutyrate, CYP101C1 had a slower product formation rate compared to CYP101B1, due to a significant reduction in the coupling efficiency (9% versus 75%). Total turnover number of CYP101B1 with cyclooctyl acetate was 3-fold higher than the CYP101C1 system (Table 3. 5). TTNs with cyclooctyl isobutyrate were reduced in both systems, and this may be due to the lower water solubility of this substrate (Table 3. 5).

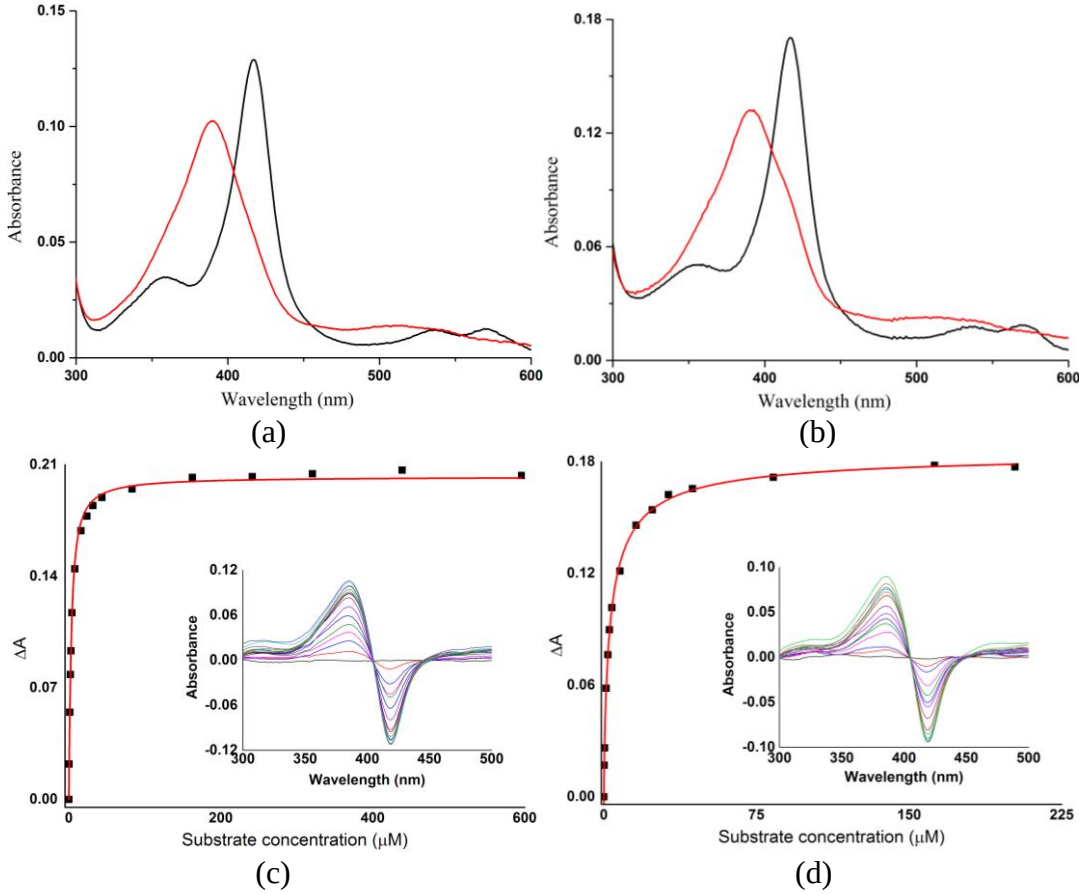

Figure 3. 41 The spin-state shifts (red) of CYP101B1 with **(a)** cyclooctyl acetate and **(b)** cyclooctyl isobutyrate. Dissociation constants with **(c)** cyclooctyl acetate (1.59 μM CYP101B1/ K_d 1.6 μM) and **(d)** cyclooctyl isobutyrate (1.50 μM CYP101B1/K_d 1.3 μM). The concentration of enzyme used in the binding assays and the dissociation constants (K_d) are provided in brackets.

Cyclooctyl acetate, when turned over by CYP101B1, formed a single metabolite, and the mass spectrum analysis indicated that it was a hydroxylated metabolite with a mass, m^+/z = 186.20 (98%; Figure 3. 42 and Figure B. 1). CYP101C1 generated the same metabolite (80%) observed in the GC-MS analysis of CYP101B1 turnover, alongside a minor product which accounted for the remaining 20% of the total turnover products formed (Figure 3. 42 and Figure B. 1).

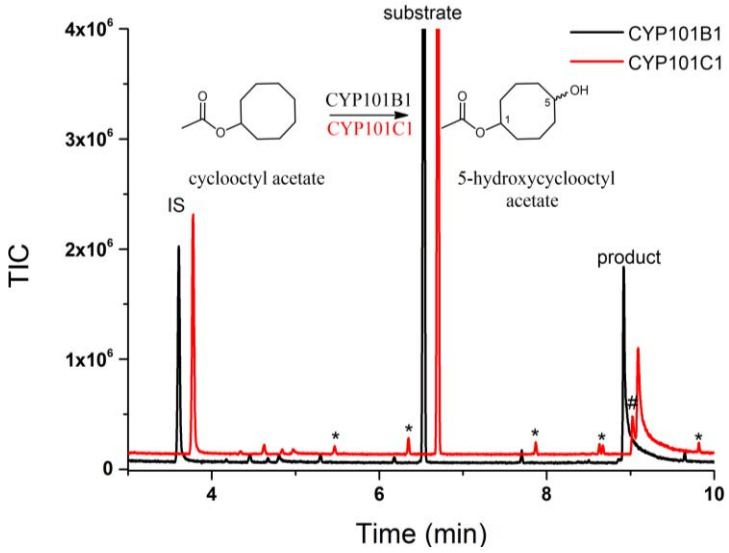

Figure 3. 42 GC-MS analyses of *in vitro* turnovers of cyclooctyl acetate by CYP101B1 and CYP101C1. Cyclooctyl acetate (RT 6.5 min) and the product; 5-hydroxycyclooctyl acetate (RT 8.95 min), and a minor peak at RT 8.8 min[#] with CYP101C1 turnover which was not formed in large enough yield to be identified using NMR but that was assigned as a further oxidation product based on its spectrum (m^+/z = 184.10; Figure B. 1). The chromatogram (CYP101C1) was offset along the x and y-axes for clarity.

The primary metabolite of the CYP101B1 turnover was generated using a whole-cell oxidation system, extracted and purified by silica column chromatography. Sufficient amount (~31 mg) of the metabolite was obtained for NMR characterisation (Figure 3. 43 and Figure B. 103-B. 108). The ^{13}C NMR spectrum had six carbon signals between the region 20-80 ppm, three of which 37.87 ppm (C4 & C6), 34.93 ppm (C2 & C8) and 21.55 ppm (C3 & C7) displayed almost double the intensity of the other three carbons peaks at 76.61 ppm (C1), 73.88 ppm and 24.13 (C10) (Figure B. 103-B. 108). This could only be possible if hydroxylation occurs at C5 to generate a symmetrical product. The HSQC and HMBC NMR spectra were also in agreement with the assignment (Figure B. 103-B. 108). The stereoselectivity was not able to be confirmed using ^1H-^1H ROESY NMR spectrum due to overlapping proton peaks in the ^1H NMR (Figure

3. 43 and Figure B. 108). However, the coupling constants of H1 (3.6 and 8.6 Hz), H5 (3.7 and 8.3 Hz) and their splitting patterns (*tt*) indicated their similar orientation (both axial; Figure B. 103). Hence, the product was presumed to be a *trans* isomer (Figure 3. 43 and Figure B. 103).

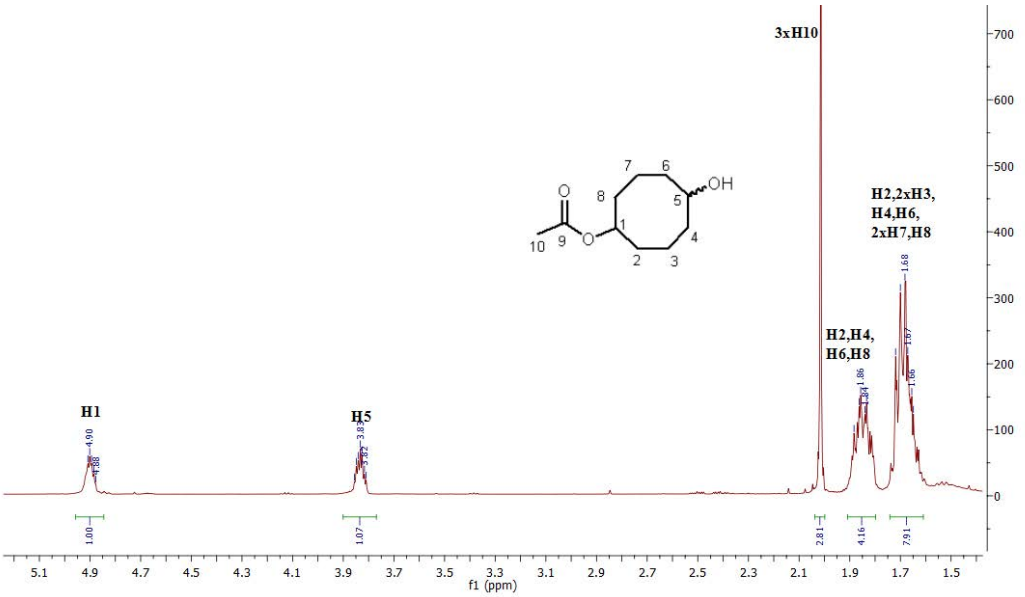

(a)

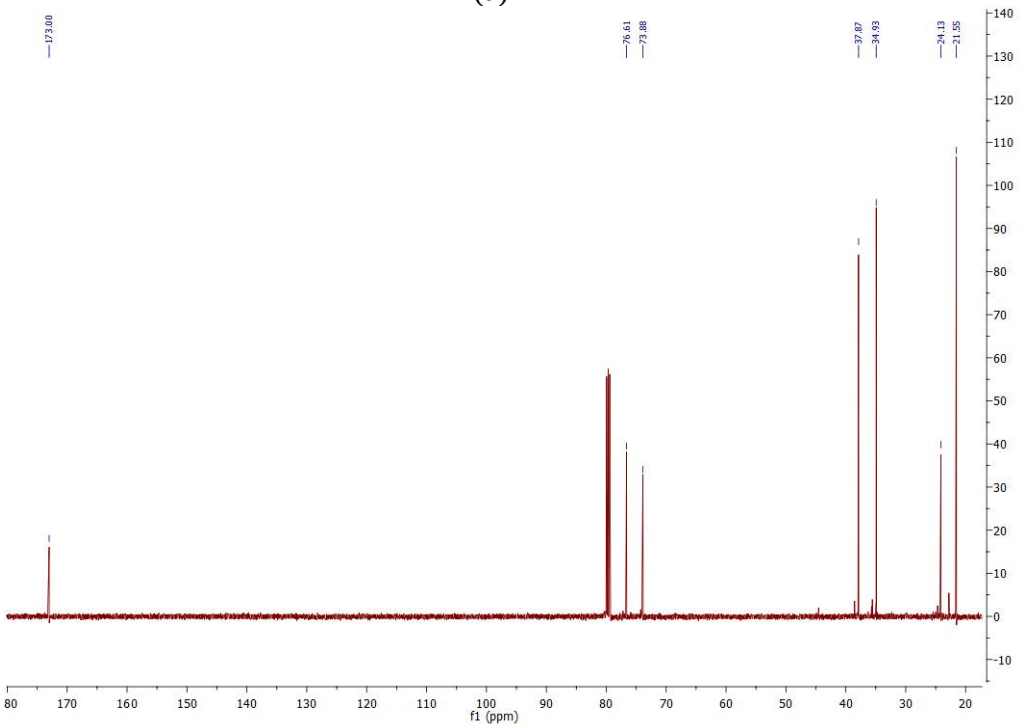

(b)

Figure 3. 43 (a) ^{1}H NMR spectrum of 5-hydroxycyclooctyl acetate (*trans*). **(b)** ^{13}C NMR spectrum of 5-hydroxycyclooctyl acetate (*trans*). Full data are presented in appendix B (B. 103-B. 108). The detail of minor signals of the ^{13}C NMR is given in Figure B. 104.

In the turnovers of cyclooctyl isobutyrate by CYP101B1 and CYP101C1, a single major metabolite was detected in the GC-MS analyses (m^+/z = 214.9; Figure 3. 44 and Figure B. 1). A whole-cell oxidation system containing CYP101B1 enzyme was used to generate this metabolite in larger yield for NMR characterisation. The metabolite was extracted and purified (~25 mg) using silica column chromatography. The presence of a characteristic multiplet peak at 3.88-3.74 ppm in ^{1}H NMR spectrum indicated a hydroxylated metabolite (Figure 3. 45 and Figure B. 109-B. 114). The ^{13}C NMR spectrum had eight carbon signals among these four signals 37.85 ppm, 34.92 ppm, 21.59 ppm and 21.53 ppm showed approximately two-fold higher intensity compared to 76.10 ppm (C1), 73.92 ppm, 36.81 ppm (C10) as observed in cyclooctyl acetate, which demonstrated each signal represents the pair of equivalent carbons, and that indicated hydroxylation at C5 to form a symmetrical metabolite (Figure B. 109-B. 114). The ^{1}H-^{13}C interactions in HSQC and HMBC NMR spectra were also in agreement with this assignment (Figure B. 109-B. 114). ^{1}H-^{1}H ROESY NMR spectrum was carried out to determine the stereoselectivity, however, overlapping of the proton peaks hampered identification. The coupling constants of H5 (J_{H5} = 3.8, 8.0 Hz) and H1 (J_{H1} = 3.5, 8.1 Hz) demonstrating their similar orientation (both axial). Therefore, the metabolite was proposed as a *trans* isomer. Some additional minor peaks in the ^{13}C NMR spectrum of this product indicated that two other metabolites were also present as impurities, but these were not able to be fully characterised (B. 110).

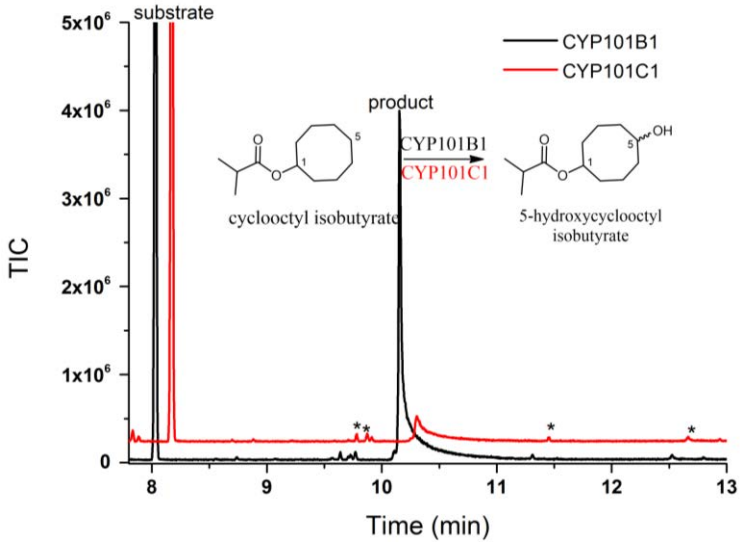

Figure 3. 44 GC-MS analyses of the *in vitro* turnovers of cyclooctyl isobutyrate by CYP101B1 and CYP101C1. Cyclooctyl isobutyrate (RT 8.0 min) and the product; 5-hydroxycyclooctyl isobutyrate (RT 10.2 min; *trans*). The chromatogram (CYP101C1) was offset along the x and y-axes for clarity.

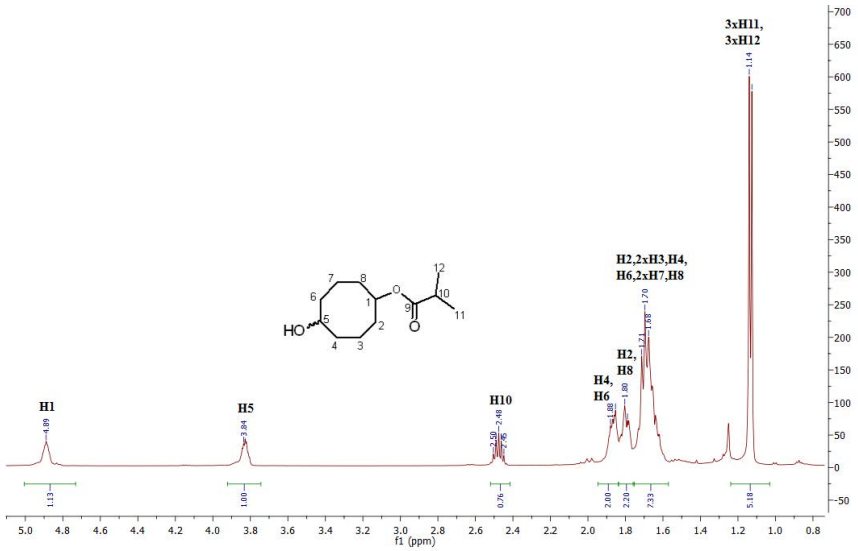

(a)

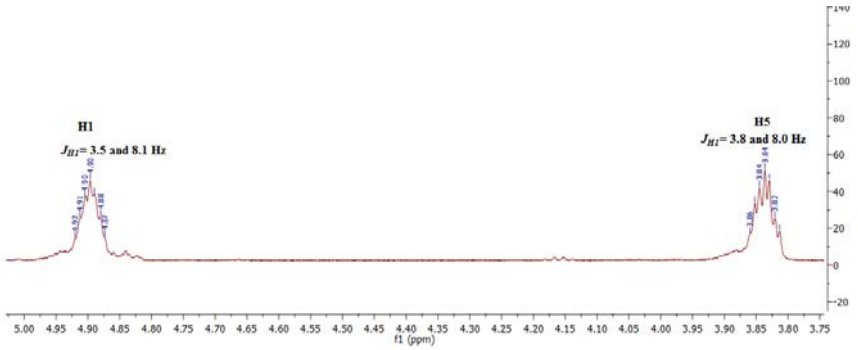

(b)

Figure 3. 45 (a) ^{1}H NMR spectrum of 5-hydroxycyclooctyl isobutyrate (*trans*). **(b)** Zoomed in version of ^{1}H NMR spectrum to highlight the H1 and H5 peaks splitting patterns. Full data are provided in Appendix B (Figure B. 109-B. 114).

Cyclododecyl acetate induced a complete shift of heme spin-state to the high spin form (~ 95%) in CYP101B1 (Figure 3. 46). The enzyme also bound tightly to the substrate (K_d = 0.05 µM; Figure 3. 46). The rates of NADH oxidation of CYP101B1 and CYP101C1 with this substrate were 394 and 587 min^{-1}, respectively and these were significantly faster compared to cyclododecane and cyclododecanol (Table 3. 5). However, both enzymes displayed low coupling efficiencies (≤23%), that resulted in reduced product formation rates (≤94 min^{-1}; Table 3. 5). These were lower than those of cyclododecanone and cyclooctyl acetate (Table 3. 5).

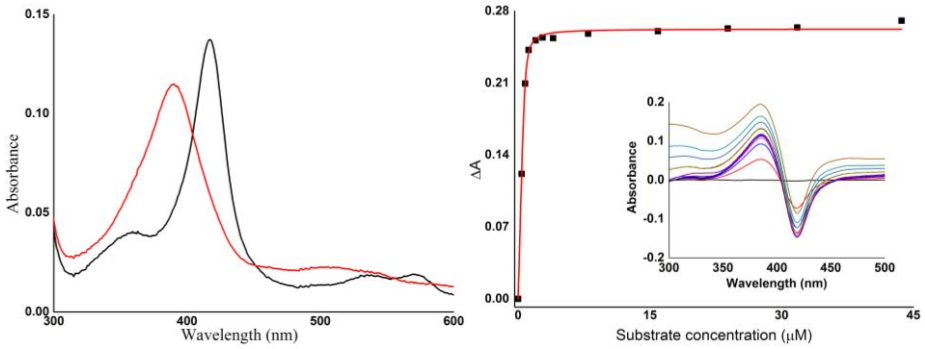

(a) (b)

Figure 3. 46 (a) The spin-state shift (red) of CYP101B1 after addition of cyclododecyl acetate. **(b)** The dissociation constant analysis with cyclododecyl acetate (2.1 μM CYP101B1/K_d 0.05 μM). The concentration of enzyme used in the binding assay and the dissociation constant (K_d) are provided in brackets.

CYP101B1 catalysed the oxidation of cyclododecyl acetate and generated one significant (74%) product alongside three minor metabolites (Figure 3. 47). These products were generated in larger quantity for characterisation using the CYP101B1 whole-cell system. The major metabolite (at RT 17.3 min in GC) was purified (~21 mg) and identified as a 7-hydroxycyclododecyl acetate by NMR analysis (Figure 3. 48 and Figure B. 115-B. 118) [150]. The **H**COH signal was observed at 3.89-3.80 ppm in the ^{1}H NMR (Figure 3. 48). The ^{13}C NMR displayed nine carbon signals, five of which were double the height of the other peaks, representing pairs of equivalent carbons (Figure B. 116 and Table B. 1). The carbons and hydrogens were assigned via ^{1}H-^{13}C HSQC analysis and the metabolite was identified as a 7-hydroxycyclododecyl acetate (Figure B. 118 and Figure 3. 48) [150]. This metabolite was confirmed as a single diastereomer by comparing the ^{13}C NMR signals and ^{1}H NMR spectrum protons peaks of **H**C1(OAC) (δ 4.91, J = 5.5, 8.1 Hz, H1) and **H**C7OH (δ 3.89-.380 ppm; J = 5.0, 8.0 Hz, H7) with the NMR reported previously (Table B. 1, Figure 3. 48 and Figure B. 115-B. 118) [150]. The splitting patterns of H1 and H7, and similar coupling constants suggested their orientation must be in the same direction (both axial; Figure 3. 48). Therefore, the product was assigned as the *trans* isomer [150]. This metabolite was also detected in CYP101C1 turnover as a minor metabolite (~5%; Figure 3. 47). The other products of CYP101B1 turnover were not generated in sufficient quantity for characterisation by NMR. However, the ^{1}H and ^{13}C NMR spectra of the primary metabolite had some additional signals, which indicated these minor products were also present in the NMR sample (Table B. 1, Figure B. 115-B. 123). The detail of the ^{13}C NMR signals is provided in Table B. 1.

One of the minor metabolites (at RT 16.5 min; 2%) was assigned as the other diastereomer of 7-hydroxycyclododecyl acetate (*cis*) via the carbon signals (Figure B. 116 and Figure B. 123). These ^{13}C NMR signals (71.73, 68.75, 32.43, 29.14, 24.07, 21.36, 20.97, 20.94, 18.97 ppm; carbonyl signal not detected) were in good agreement with the reported NMR carbon signals (71.6, 68.7, 32.4, 29.1, 24.0, 21.3, 21.0, 20.9, 18.6; Table B. 1, Figure B. 116) [150]. This metabolite coeluted in GC with the major product (80%; RT 16.5 min) of CYP101C1 (Figure B. 123) [150].

Another minor metabolite (at RT 16.2 min) was not able to be purified in sufficient yield. However, the NMR of the mixture of metabolites suggested that this was a 5-hydroxy metabolite (Figure B. 119-B. 122, Table B. 1). The correlations of H1 (5.05-4.95 ppm) with carbons in the ^{1}H-^{13}C HMBC NMR were used to assign the signals C2 (29.69), C3 (20.32), C11 (20.70) and C12 (29.56). The product was confirmed as 5-hydroxycyclododecyl acetate as C3 (20.70) displayed a strong correlation with the multiplet H5 (3.72-3.88 ppm) in the HMBC NMR (Figure B. 119-B. 122). The high coupling constants of H1 (J_{H1} = 6.4, 11.9 Hz) and H5 (J_{H5} = 6.4, 12.4 Hz) indicated their axial orientation, hence the product was proposed a *trans* isomer of 5-hydroxycyclododecyl acetate (Figure B. 119). The minor product peak at RT 16.4 min (GC) was thought to be another alcohol or the other diastereomer of 5-hydroxycyclododecyl acetate as additional twelve minor carbon signals were present in ^{13}C NMR of 5-hydroxycyclododecyl acetate (Table B. 1, Figure B. 120 and Figure 3. 47). However, full characterisation of this metabolite was not possible due to inadequate yield. These two minor metabolites were also observed in the CYP101C1 turnovers (Figure 3. 47).

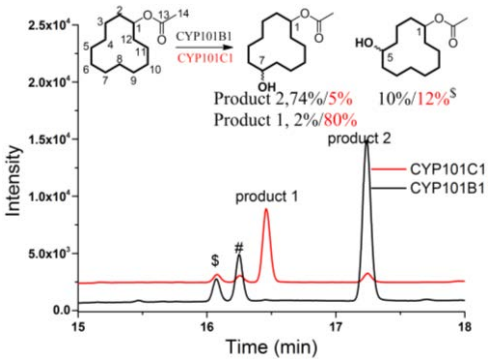

Figure 3. 47 GC analyses of *in vitro* turnovers of cyclododecyl acetate by CYP101B1 and CYP101C1. Cyclododecyl acetate (RT 5.6 min; not shown) and the products; proposed 5-hydroxycyclododecyl acetate$ (RT 16.2 min) and unidentified metabolite# (RT 16.4 min); product 1; 7-hydroxycyclododecyl acetate (RT 16.5 min; *cis* isomer) [150]; product 2; 7-hydroxycyclododecyl acetate (RT 17.3 min; *trans* isomer) [150].

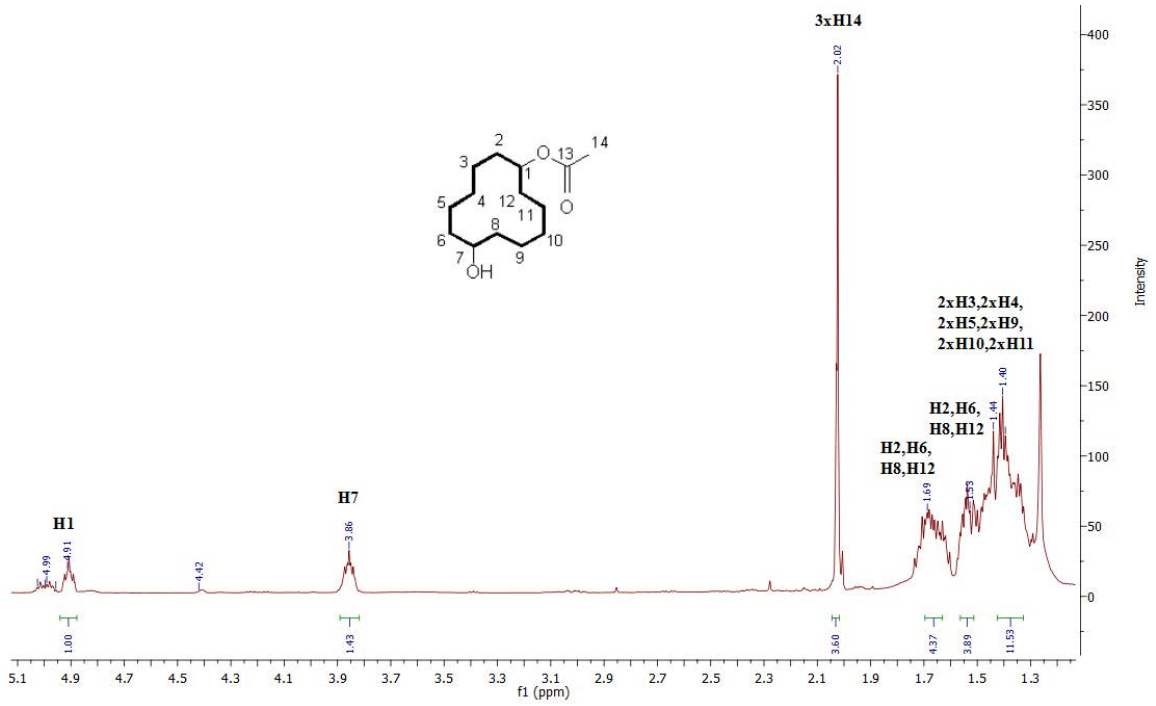

(a)

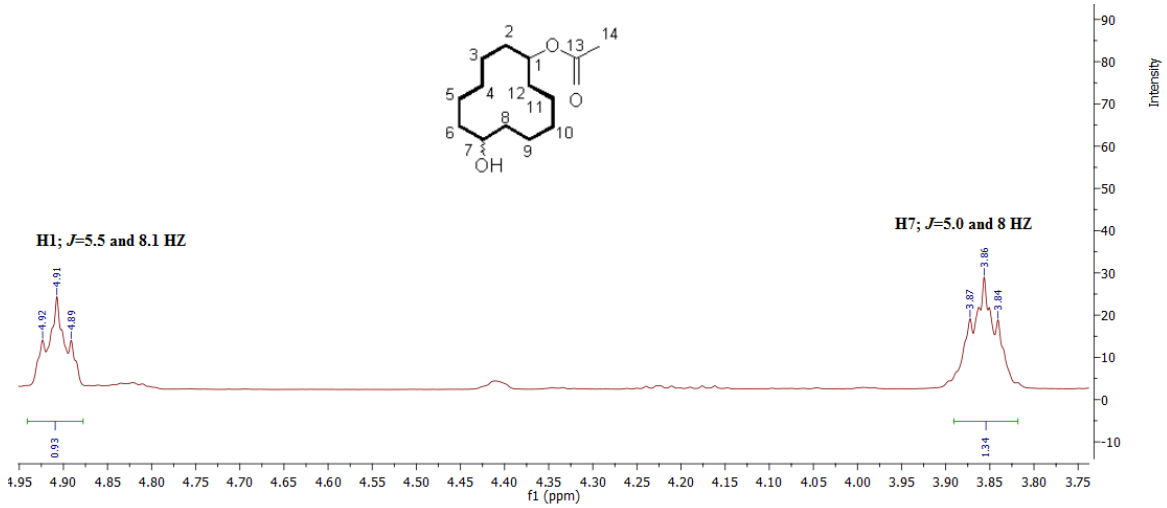

(b)

Figure 3. 48 (a) ^{1}H NMR spectrum of 7-hydroxycyclododecyl acetate (RT 13.6 min; *trans*) [150]. **(b)** Zoomed in version of ^{1}H NMR spectrum of 7-hydroxycyclododecyl acetate which highlighted the splitting patterns of H1 and H7 peaks, and this product was presumed to be a *trans* isomer of 7-hydroxycyclododecyl acetate. Full data are presented in Appendix B (Table B. 1, Figure B. 115-B. 123).

α-Terpinyl acetate containing *p*-menthane backbone was also screened to find out the effect of the presence of a double bond in the ring on the activity of both enzymes. Oxidation of *α*-terpinyl acetate by CYP101C1 proceeded with a significantly higher NADH oxidation rate than that measured for CYP101B1 (898 min^{-1} versus 178 min^{-1}; Table 3. 5). CYP101B1 did not oxidise this substrate with no product detected in the GC-MS analysis of the *in vitro* turnover [233]. CYP101C1 oxidised the *α*-terpinyl acetate efficiently with a product formation rate of 497 min^{-1} and a coupling efficiency of 55% (Table 3. 5). The GC analysis of the CYP101C1 *in vitro* turnover revealed a primary (82%) alongside a minor metabolite (Figure 3. 49). The epoxide of *α*-terpinyl acetate was synthesised by *m*CPBA using a standard method (Figure not shown) [230]. *m*-Chloroperbenzoic acid (1.2 equivalent) was mixed with the *α*-terpinyl acetate in dichloromethane (DCM) at 0 ºC, and the mixture was stirred for two hours to generate the epoxide [230]. The progress of the reaction was monitored in GC-MS. However, this did not coelute with the metabolite generated by CYP101C1 (at RT 15.25 min in GC-MS).

The CYP101C1 whole-cell system was used to generate the metabolite in the required yield for characterisation. The major metabolite was extracted and isolated using silica column chromatography and characterised by NMR analysis (~10 mg; Figure 3. 49 and Figure B. 124-B. 131). The presence of a broad peak at 4.20 ppm in ^{1}H NMR confirmed a hydroxylated metabolite (Figure 3. 49). The H6 signal was assigned via the correlations of C1 (44.56 ppm) with the protons of 1.48-1.41 (H9 and H10), 2.19-2.13 (H6) and 1.35-1.20 (H6) in the ^{1}H-^{13}C HMBC NMR (Figure B. 124-B. 131). The H2 peaks (2.02-1.97 and 1.92-1.85 ppm) also showed interaction with the π-bond proton H3 (5.48 ppm) in the gCOSY NMR. The product was identified as 3-cyclohexene-1-methanol, 5-hydroxy-*α*,*α*,4-trimethyl-,*α*-acetate due to the correlations of H5 (4.20 ppm) with both hydrogens on C6 (H6 (2.19-2.13 ppm) and H6 (1.35-1.20)) in ^{1}H-^{1}H gCOSY NMR (Figure B. 126).

The minor metabolite (at RT 12.5 min) was not generated and purified in high enough yield for NMR characterisation. However, by using the small peaks in the ^{1}H and ^{13}C NMR spectra of the major metabolite, this minor product was assigned to be the other diastereomer of 3-cyclohexene-1-methanol, 5-hydroxy-*α*,*α*,4-trimethyl-,*α*-acetate. The minor signal at 71.25 ppm (C5) in the ^{13}C NMR spectrum of the primary product displayed a correlation with (H7) in the HMBC NMR, as well as the presence of the two alkene carbons peaks at 120 to 140 ppm region, were in agreement with this assignment (Figure B. 131).

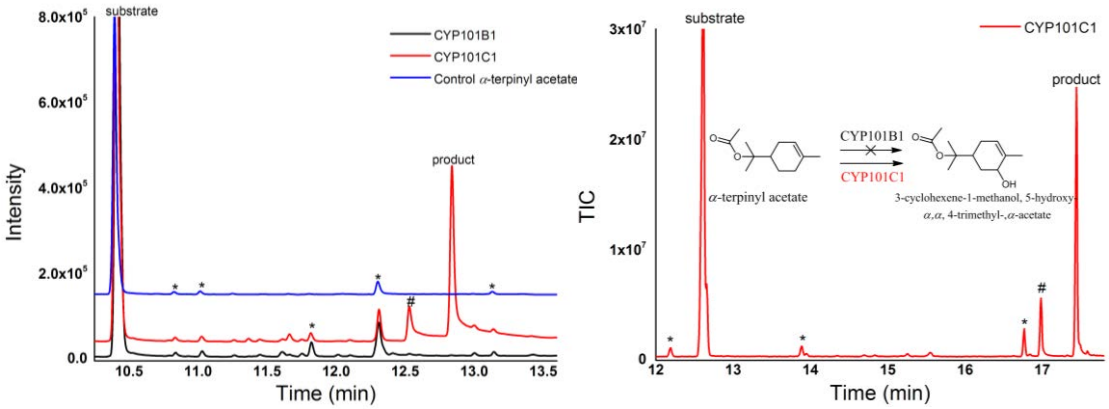

(a) (b)

Figure 3. 49 (a) GC analysis of the *in vitro* turnover of *α*-terpinyl acetate by CYP101B1 and CYP101C1. *α*-Terpinyl acetate (RT 10.4 min) and the products; 3-cyclohexene-1-methanol, 5-hydroxy-*α*,*α*,4-trimethyl-,*α*-acetate (RT 12.8 min; CYP101C1) and its other diastereomer[#] (RT 12.5 min). **(b)** GC-MS analysis of the *in vitro* turnover of *α*-terpinyl acetate by CYP101C1. *α*-Terpinyl acetate (RT 12.6 min) and the products; 3-cyclohexene-1-methanol, 5-hydroxy-*α*,*α*,4-trimethyl-,*α*-acetate (RT 17.4 min; CYP101C1) and its other diastereomer[#] (RT 17.0 min). The impurities are marked (*).

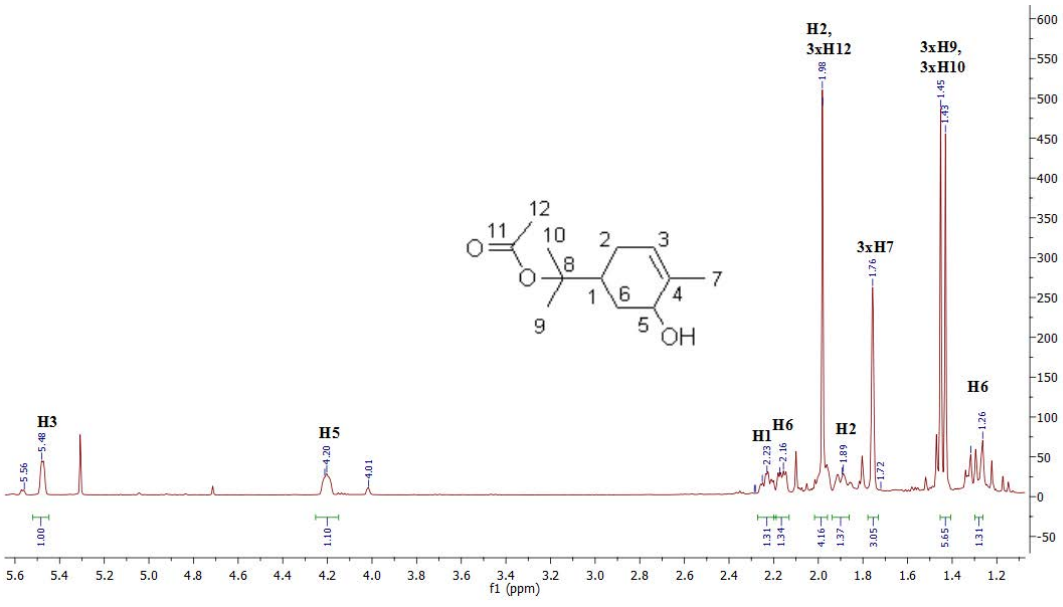

Figure 3. 50 [1]H NMR spectrum of the 3-cyclohexene-1-methanol, 5-hydroxy-*α*,*α*,4-trimethyl-,*α*-acetate. Full data are presented in Appendix B (Figure B. 124-B. 131).

In summary, introduction of an ester directing group to the cycloalkanols or cyclohexylacetic acid significantly improved the activity of CYP101B1 toward these cyclic substrates. The cyclohexyl derivatives possess a similar ring system to the ionones, and the ester moieties could mimic the butenone chain of the norisoprenoids. These two factors are likely to contribute to improving the activity and better binding of these substrates, especially with CYP101B1. The oxidation of cyclic esters by CYP101B1 and CYP101C1 occurred predominantly at the C-H bonds on the opposite side of the ring to the ester group, for example, C4 for cyclohexyl derivatives, and C5, and C7 for the cyclooctyl and cyclododecyl derivatives, respectively. CYP101B1 displayed superior product formation rates and total turnover number than the CYP101C1 system for most substrates. Both enzymes preferentially formed the *trans* diastereomer, however, for 7-hydroxycyclododecyl acetate CYP101C1 generated the *cis* isomer.

3.2.3 The Oxidation of Linear Ketones and Terpene Esters by CYP101B1 and CYP101C1

To further explore the substrate range of CYP101B1 and CYP101C1, they were studied with linear substrates containing a ketone moiety such as 2-nonanone, 2-undecanone, and monoterpenoid esters (Figure 3. 51). These are commonly used as fragrance, flavouring and insect repellent agents [224-227]. Functionalisation of the C-H bonds of these compounds are highly sought-after intermediates within chemical industries [224-227].

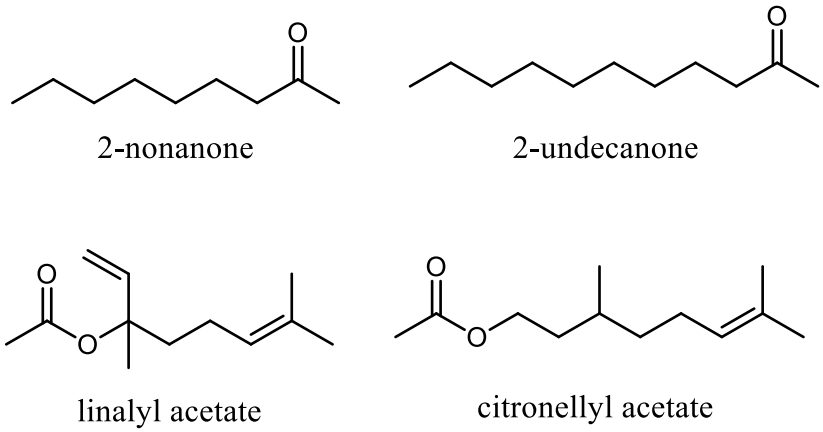

Figure 3. 51 The linear alkyl ketones and esters which were screened with CYP101B1 and CYP101C1.

2-Nonanone and 2-undecanone induced 20% and 30% heme spin-state shift in CYP101B1, respectively (Figure 3. 52). 2-Nonanone bound with a lower affinity to CYP101B1 than 2-undecanone (140 µM versus 44 µM; Figure 3. 52). 2-Nonanone and 2-undecanone mediated spin-state shifts and binding affinities of CYP101B1 were weaker when compared with their cyclic counterparts cyclononanone and cycloundecanone (Figure 3. 52 and Table 3. 3).

CYP101B1 oxidised 2-nonanone with a faster NADH oxidation activity (552 min^{-1} versus 270 min^{-1}), product formation (219 min^{-1} versus 92 min^{-1}) rate and higher coupling efficiency than the CYP101C1 system (40% versus 34%; Table 3. 6). GC-MS analyses of the *in vitro* turnovers of 2-nonanone by CYP101B1 revealed one single major metabolite peak at RT 11.25 min, accounted 98% of total turnover products arising from the enzymatic oxidation (Figure 3. 53). The mass spectrum indicated that is a monooxygenase metabolite (m^+/z = 158.20; Figure B. 1). With an aim to identify this metabolite, a whole-cell turnover containing CYP101B1

enzyme was used to generate the product in sufficient yield for NMR characterisation. The ^{1}H NMR spectrum had a multiplet peak at 3.86-3.73 ppm, confirming a hydroxylation metabolite (Figure 3. 53). The product was assigned as 8-hydroxy due to the correlation of C8 (70.71 ppm) with the doublet peak of the H9 methyl protons at 1.19 ppm in the ^{1}H-^{13}C HMBC NMR spectrum (Figure B. 132-B. 136) [228]. The metabolite was confirmed as hydroxylation at H8 by the strong interaction with the protons of C9 in gCOSY NMR spectrum (Figure B. 134).

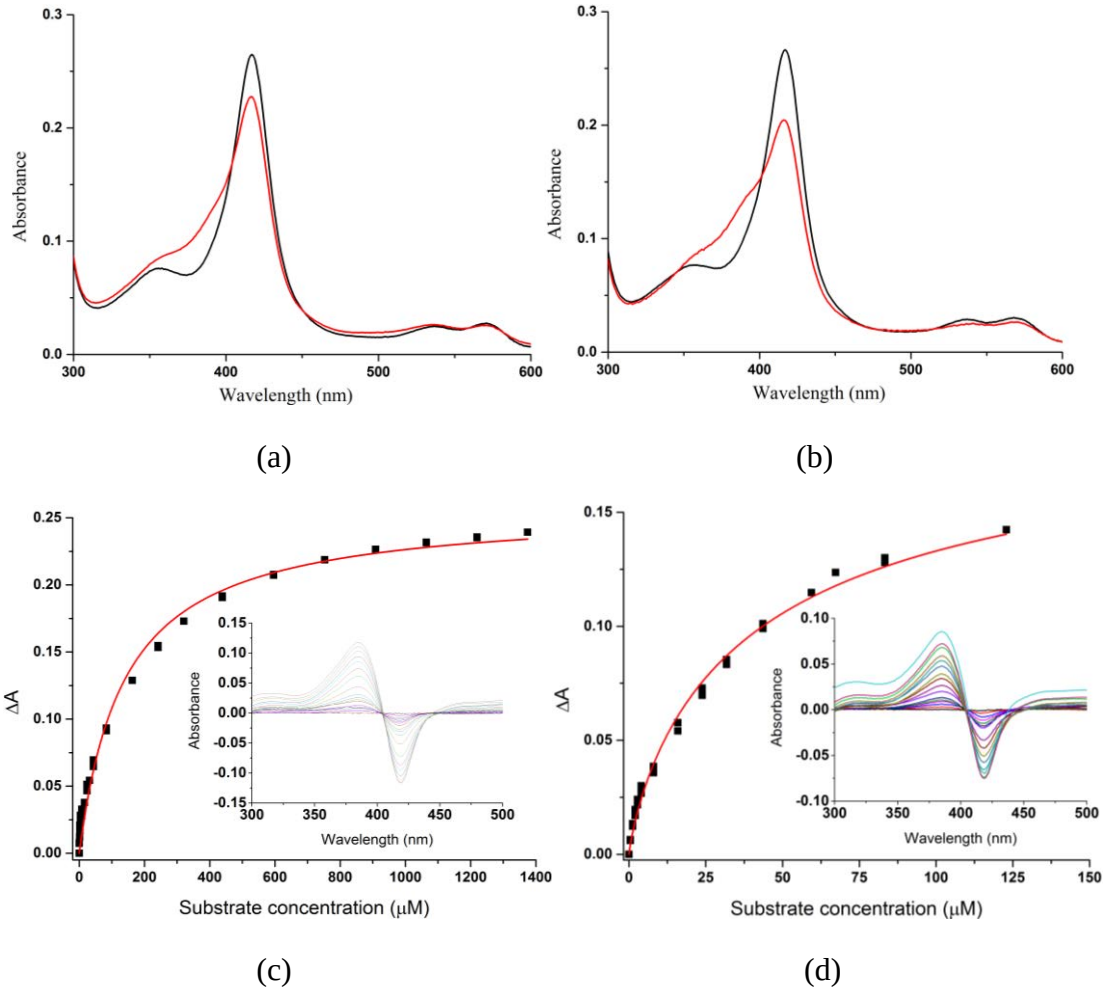

Figure 3. 52 The spin-state shifts (red) of CYP101B1 after addition of **(a)** 2-nonanone and **(b)** 2-undecanone. The dissociation constants analysis with **(c)** 2-nonanone (2.63 μM CYP101B1/K_d 140 μM) and **(d)** 2-undecanone (2.11 μM CYP101B1/K_d 44 μM). The concentration of enzyme used in the binding studies and the dissociation constants (K_d) are provided in brackets.

The selectivity of oxidation completely changed in the case of CYP101C1 system as it oxidised the 2-nonanone to one different major product (~93%; at RT 8.5 min) alongside with a minor metabolite. The mass spectra suggested that both these were monohydroxylated metabolites (m^+/z = 158.65, m^+/z = 158.20; Figure B. 1). The minor product (at RT 11.25 min) was confirmed as 8-hydroxy-2-nonanone by coeluting with the turnover metabolite of CYP101B1 using GC-MS (Figure 3. 53). The CYP101C1 whole-cell turnover was carried out to generate the primary metabolite for NMR characterisation, however, it was not generated in enough yield. The product was identified as 3-hydroxy-2-nonanone based on its mass spectrum fragmentation patterns (158.65, 115.15, 97.15, 85.10, 71.15, 69.15, 55.10, 43.10; Figure B. 1). Fragments detected at m^+/z 115.15, 97.15 and 85.10, corresponding to the elimination of -$COCH_3$ (43), -OH, -H3 (18) and -C3 (12), respectively, enabling the identification of this metabolite.

Table 3. 6 Substrate binding, turnover and coupling efficiency data for CYP101B1 and CYP101C1 with linear ketones and terpene esters. The *in vitro* turnover activities were measured as described in Table 3. 1 and Table 3. 3. The data are reported as mean ± S.D. (n = 3) and rates are given in nmol.nmol-CYP^{-1}.min^{-1}. - not measured or not able to be determined accurately.

Substrate	CYP101B1/ CYP101C1	NADH	PFR	Coupling (%)	TTN
2-nonanone	CYP101B1	552 ± 11	219 ± 34	40	5700 ± 85
	CYP101C1	**270 ± 12**	**92 ± 15**	**34**	-
2-undecanone	CYP101B1	568 ± 3	340 ± 50	60	1660 ± 95
	CYP101C1	**311 ± 12**	**59 ± 25**	**19**	-
citronellyl acetate	CYP101B1	418 ± 4	115 ± 1	28	-
	CYP101C1	**654 ± 8**	**304 ± 11**	**47**	**1540 ± 216**
linalyl acetate	CYP101B1	205 ± 8	8 ± 1	4	-
	CYP101C1	**200 ± 2**	**50 ± 2**	**25**	-

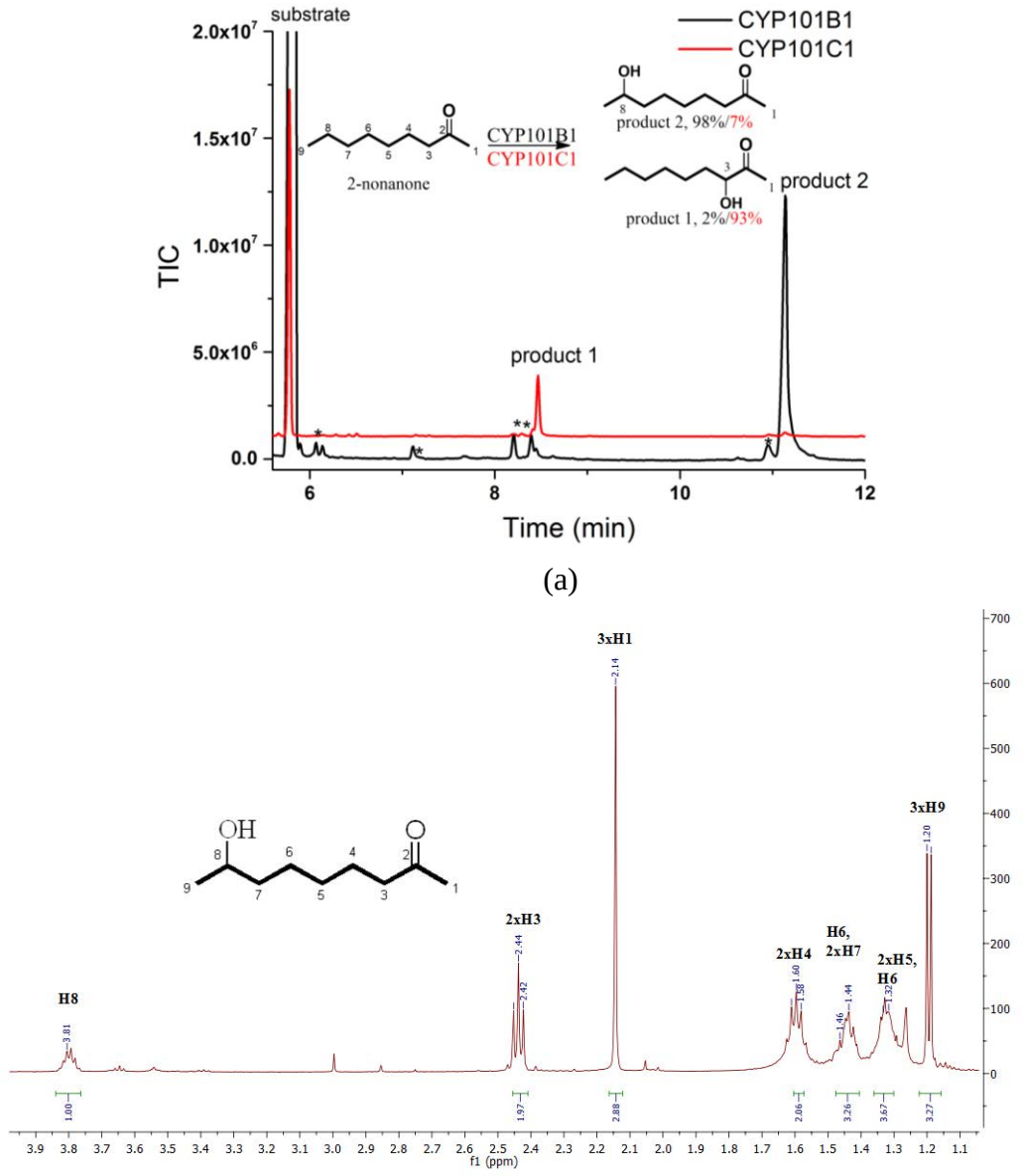

Figure 3. 53 (a) GC-MS analyses of the *in vitro* turnovers of 2-nonanone by CYP101B1. 2-Nonanone (RT 5.8 min); the major products 8-hydroxy-2-nonanone (RT 11.25 min; m^+/z =158.20) and 3-hydroxy-2-nonanone (RT 8.5 min; m^+/z =158.65). The chromatogram (CYP101C1) was offset along the x and y-axes for clarity. **(b)** ^{1}H NMR spectrum of 8-hydroxy-2-nonanone (RT 11.25 min). Full data are given in Appendix B (Figure B. 132-B. 136).

CYP101B1 exhibited a lower binding affinity with 2-undecanone than cycloundecanone, despite this the *in vitro* turnovers of 2-undecanone by CYP101B1 induced at a faster oxidation activity (568 min^{-1}) and a higher product formation rate (340 min^{-1}) as well as a high coupling efficiency of 60% (Table 3. 3 and Table 3. 6). CYP101C1 catalysed the oxidation of this

substrate with slower NADH oxidation rate, and that resulted in a reduced product formation activity of 59 min^{-1} (Table 3. 6). These lower rates could be rationalised due to the lower coupling efficiency of CYP101C1 (19%; Table 3. 6).

CYP101B1 catalysed the oxidation of 2-undecanone to form one major product (80%) alongside three minor metabolites (Figure 3. 54). A larger scale *in vivo* turnover of CYP101B1 was carried out to generate the metabolites sufficient quantity for characterisation. The major product (RT 14.95 min) was isolated (~18 mg) using silica column chromatography and characterised by NMR (Figure 3. 54, Figure B. 1 and Figure B. 137-B. 142). The characteristic multiplet peak at 3.63-3.53 ppm in ^{1}H NMR spectrum indicated a hydroxylated metabolite (Figure 3. 54). The 2xH10 protons were assigned using the interaction with H11 (0.96-0.88 ppm) in ^{1}H-^{1}H gCOSY NMR spectrum (Figure B. 138). The C6 (28.06), C7 (39.90) and C9 (42.38) were assigned using correlations with protons in the ^{1}H-^{13}C HMBC and HSQC NMR. The interactions of carbon (74.26 ppm) with the protons of 1.52-1.37 ppm (H6, H7, H9, and H10) in the HMBC NMR spectrum suggested that the hydroxylation took place at the C8 position (Figure B. 137-B. 142).

The two minor metabolites (at RT 15.2 min and 15.9 min) were not generated in large enough yield for NMR identification. However, the ^{13}C NMR of the major metabolite displayed minor carbon signals **C**H(OH) at 75.92 ppm and 74.34 ppm. In the HMBC NMR spectrum, the carbon signal (75.92 ppm) correlated strongly with H11 (0.96-0.88 ppm) and this metabolite was identified as 9-hydroxy-2-undecanone, not the 10-hydroxy product (Figure B. 137-B. 142). If hydroxylation took place at C10, the chemical shift (doublet peak) of the protons on carbon C11 would move further downfield (Figure B. 142). The other carbon signal at 74.34 ppm showed the correlation with the protons at 1.52-1.1.28 ppm, and the detail of this product assignment is presented in Appendix B (Figure B. 142) [229]. The third minor metabolite at RT 6.2 min was identified by coelution experiment in GC-MS with the main product of CYP101C1 (Figure 3. 54).

CYP101C1 metabolised 2-undecanone into three metabolites with a ratio of 70:20:10 (Figure 3. 54 and Figure B. 1). The major (70%; RT 6.2 min) metabolite was assigned as 3-hydroxy-2-undecanone by matching its mass spectrum with the published data (Figure B. 1) [219]. The experimental mass spectrum (m^{+}/z = 186.25, 143.20, 125.25, 111.50, 97.15, 83.10, 69.15, 55.10, 43.05) closely matched with the reported mass spectrum m^{+}/z = 186, 143, 125, 111, 97,

83, 69, 55 and 43 (Figure B. 1) [219]. The minor metabolites of CYP101C1 turnovers were confirmed by coeluting the products of CYP101B1 in GC-MS (Figure 3. 54 and Figure B. 1).

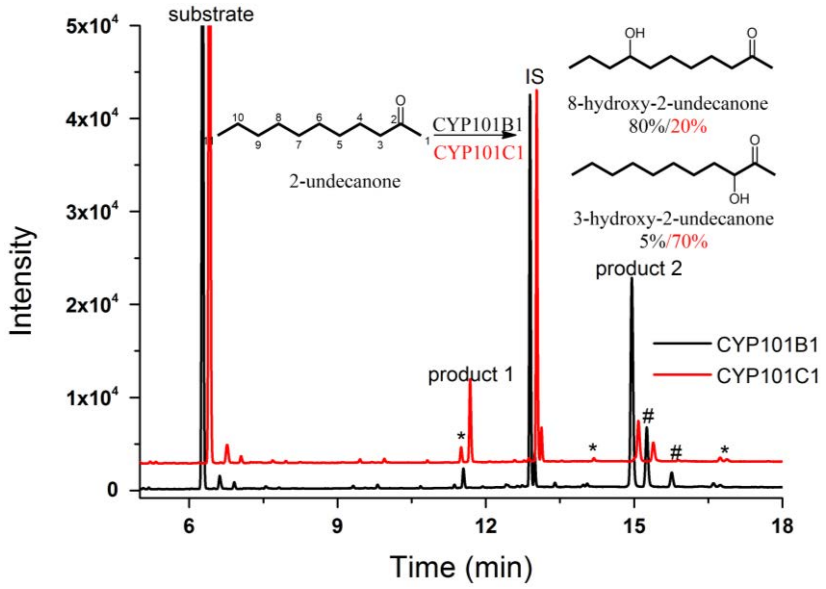

(a)

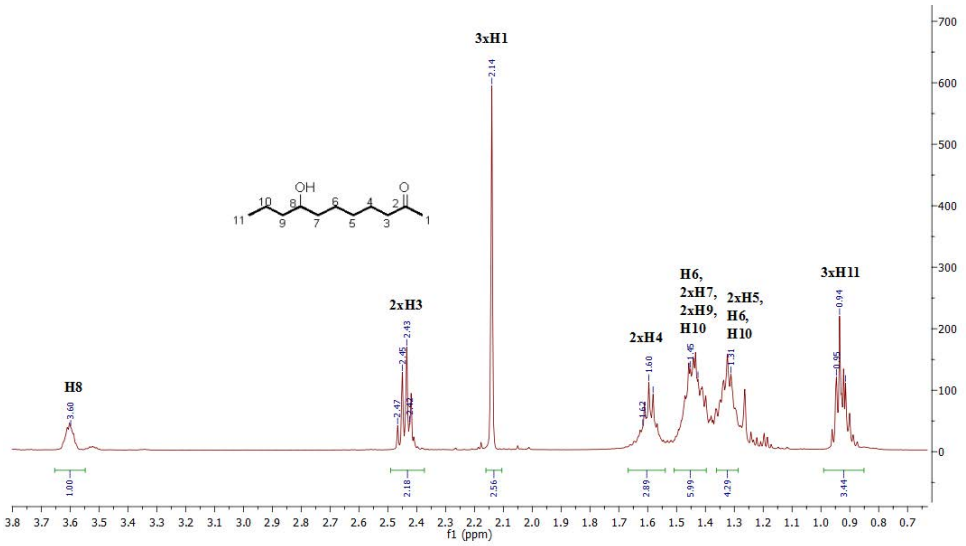

(b)

Figure 3. 54 (a) GC analyses of *in vitro* turnovers of 2-undecanone by CYP101B1 (black) and CYP101C1 (red). 2-Undecanone (RT 6.2 min) and the product 1: 3-hydroxy-2-undecanone (RT 11.5 min), product 2: 8-hydroxy-2-undecanone (RT 14.95 min), and proposed 7-hydroxy-2-undecanone[#] (RT 15.2 min; based on carbon signal (74.92 ppm) intensity in ^{13}C NMR) and 9-hydroxy-2-undecanone[#] (RT 15.9 min, based on C9 (75.92 ppm) carbon signal intensity in the ^{13}C NMR). The chromatogram (CYP101C1) was offset along the x and y-axes for clarity. **(b)** ^{1}H NMR of 8-hydroxy-2- undecanone (RT 14.95 min). Full data are given in Appendix B (Figure B. 137-B. 142).

CYP101C1 catalysed the oxidation of linear esters such as citronellyl acetate and linalyl acetate with significantly faster NADH oxidation activity than the CYP101B1 system (Table 3. 6). The turnover of citronellyl acetate with CYP101C1 resulted in higher levels of product formation activity. This was also due to the greater coupling efficiency of the turnover (47% versus 28%; Table 3. 6)

GC analysis revealed that a single product was generated in both the CYP101B1 and CYP101C1 *in vitro* turnovers of citronellyl acetate (Figure 3. 55). The product was confirmed as citronellyl acetate epoxide by coeluting with a standard, which was synthesised via the oxidation of citronellyl acetate with *m*-chloroperbenzoic acid (Figure 3. 55) [230, 231]. *m*-Chloroperbenzoic acid (1.2 equivalent) was mixed with the citronellyl acetate in dichloromethane (DCM) at 0 ºC, and the mixture was stirred for one hour to generate the epoxide (Figure 3. 55). The progress of the reaction was monitored in GC-MS.

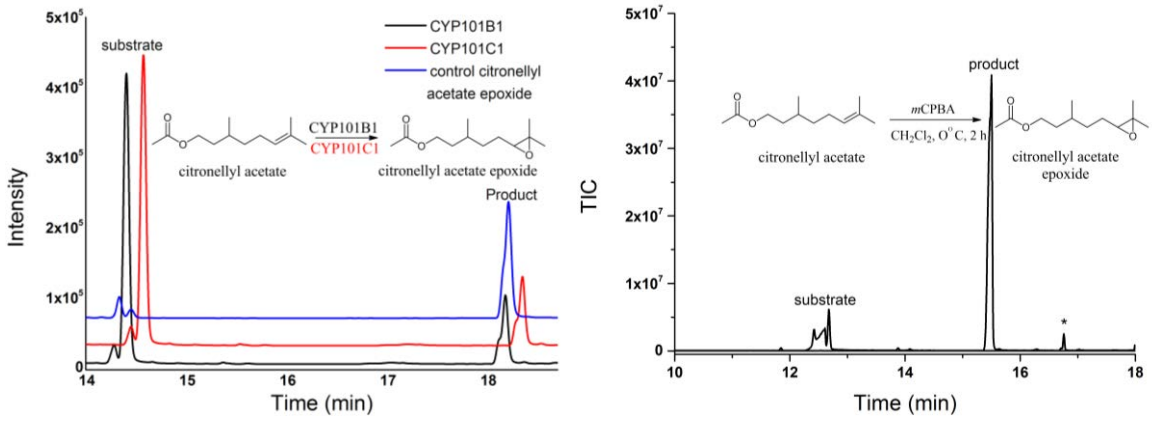

(a) (b)

Figure 3. 55 (a) *In vitro* turnover of citronellyl acetate by CYP101B1 and CYP101C1, coeluted with a synthesised epoxide in GC. Citronellyl acetate (RT 14.4 min) and the product; citronellyl acetate epoxide (RT 18.3 min). The chromatogram (CYP101C1) was offset along the x and y-axes for clarity. **(b)** GC-MS analysis of epoxide synthesis reaction of citronellyl acetate. Citronellyl acetate (RT 12.7 min) and the product; citronellyl acetate epoxide (RT 15.5 min). Mass spectrum is provided in Appendix B (Figure B. 1). The impurities are marked (*).

CYP101B1 and CYP101C1 oxidised linalyl acetate with lower NADH oxidation and product formation rates compared to citronellyl acetate (Table 3. 6). The NADH oxidation rates of

CYP101C1 (200 min^{-1}) and CYP101B1 (205 min^{-1}) were similar (Table 3. 6). The product formation rate was six-fold faster for CYP101C1 (50 min^{-1} versus 8 min^{-1}) due to the better coupling efficiency of this system (25% and 4%; Table 3. 6). The *in vitro* turnovers of CYP101C1 and CYP101B1 with this substrate generated a single major metabolite 90% and 60%, respectively with a second product making up the remainder (Figure 3. 56). The products were proposed as 6,7-epoxy-3,7-dimethyl-1-octen-3-yl acetate [231] (RT 12.5 min) and 1,2-epoxy-3,7-dimethyl-6-octen-3-yl acetate by coeluting with standards synthesised via the oxidation of linalyl acetate using *m*-CPBA (Table 3. 6 and Figure 3. 56) [230, 231]. However, NMR analysis is required to fully confirm the identity of the metabolites.

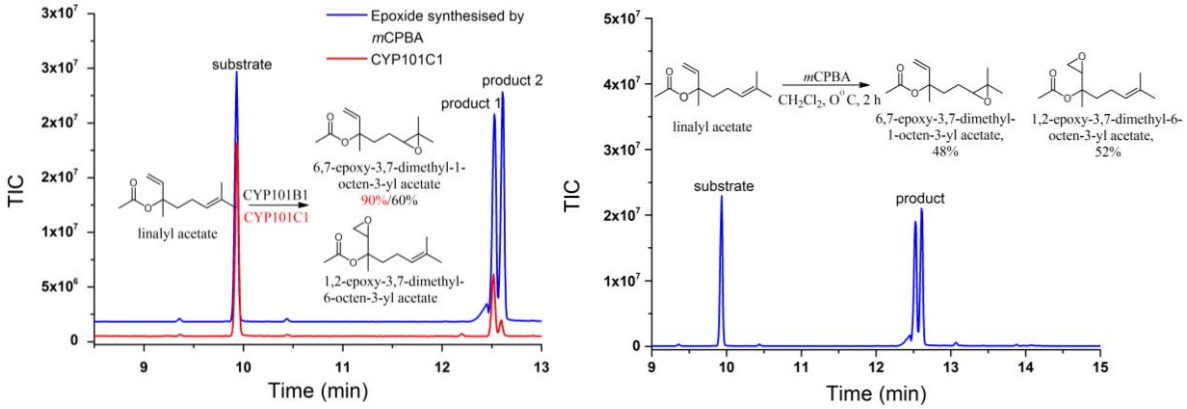

(a) (b)

Figure 3. 56 (a) GC-MS analysis of the *in vitro* turnover of linalyl acetate by CYP101C1 (red), which coeluted with the epoxidation reaction of linalyl acetate with *m*CPBA (blue). Linalyl acetate (RT 9.9 min) and the products; 6,7-epoxy-3,7-dimethyl-1-octen-3-yl acetate (RT 12.5 min) and 1,2-epoxy-3,7-dimethyl-6-octen-3-yl acetate (RT 12.6 min). **(b)** The GC-MS analysis of epoxide synthesise reactions of linalyl acetate. Linalyl acetate (RT 9.9 min) and products; 6,7-epoxy-3,7-dimethyl-1-octen-3-yl acetate, 48% (RT 12.5 min) [232]; 1,2-epoxy-3,7-dimethyl-6-octen-3-yl acetate, 52% (RT 12.6 min). Mass spectra are provided in Appendix B (Figure B. 1).

3.3. Discussion

CYP101B1 and CYP101C1 exhibited low oxidation and product formation activities with cyclic alkanes (C_6 to C_{12}). Despite this, both enzymes were able to oxidise these substrates. The smallest substrate tested, cyclohexane induced a low spin-state shift in CYP101B1, and a hydroxylated product was detected. The larger cyclic alkanes cyclooctane, cyclodecane and cyclododecane bound better to CYP101B1. The product formation rates for both enzymes with these larger substrates were improved compared to that of cyclohexane. One major hydroxylated product alongside a small amount of ketone further oxidation metabolite was detected in the turnovers of these enzymes with most of the cyclic alkanes. The majority of the cyclic alcohols did not show any significant binding affinity with CYP101B1 and CYP101C1, and little or no product formation was observed in GC/GC-MS analyses. The exception was cyclododecanol, which was oxidised by both enzymes and generated the 1,7-cyclododecanediol metabolite alongside two other minor products.

Cycloalkanones (C_9 to C_{15}) induced higher spin-state shifts in the CYP101B1 compared to their cyclic alkanes and alcohol equivalents. With these substrates, CYP101B1 displayed faster product formation rates than the CYP101C1. In particular, CYP101B1 oxidation activity was highest with cycloundecanone and cyclododecanone. CYP101B1 oxidised cyclononanone and cyclodecanone yielding 1-hydroxy-10-oxabicyclo[4.3.1]decane, 1-oxabicyclo[5.3.1]undecan-1-ol and 1-oxabicyclo[6.3.1]undecan-1-ol. These exist in a transannular tautomeric equilibrium with their corresponding hydroxy cycloalkanones. The regioselectivity of CYP101C1 oxidation with these cyclic ketones was different, and it predominantly generated 2-hydroxy metabolites irrespective of the size of the ring. The improved activity of CYP101B1 and CYP101C1 with these cycloalkanone structures is likely due to the presence of the ketone moiety. This enables more favourable binding in the active site of the enzyme and therefore more efficient turnover. Note that the binding orientation of these substrates in CYP101B1 and CYP101C1 must be significantly different to account for these observed regioselectivity differences.

Cyclic compounds containing ester directing groups displayed greater binding affinities with CYP101B1 than their cyclic alcohol and acid counterparts. Cyclohexanol derivatised with acetate, butyrate and isobutyrate directing groups were oxidised by CYP101B1 efficiently whereas no product formation was observed with cyclohexanol. The enzyme metabolised these

substrates regioselectively at C4 with the *trans* diastereomer being favoured. Introducing an ester directing group to cyclohexylacetic acid, significantly increased the binding affinity with CYP101B1 and resulted in high product formation activities. CYP101C1 was able to oxidise the majority of these substrates, but the catalytic performance was lower due to the poor productive utilisation of the reducing equivalents compared to the CYP101B1 system. The total turnover number was higher for these ester derivatives with CYP101B1 than the CYP101C1. The use of ester directing groups significantly increased the activity of CYP101B1 with cyclooctanol ester derivatives. Cyclooctyl acetate and cyclooctyl isobutyrate displayed tight binding with CYP101B1 as well as high product formation rates. Both substrates were oxidised regioselectively at the C5 (*trans*-isomer) position by CYP101B1. CYP101C1 also preferred to insert the hydroxyl group into the C5 position of both substrates but the activity was significantly reduced for cyclooctyl isobutyrate when compared to its acetate counterpart, and in both cases, further oxidation metabolite was also detected as minor products. CYP101B1 bound tightly with cyclododecyl acetate. The product formation rate and coupling efficiency were lower than the smaller cyclic acetate esters. CYP101B1 favoured hydroxylation at the C7 position of cyclododecyl acetate and generated mainly *trans* isomer of 7-hydroxycyclododecyl acetate, while CYP101C1 preferred to form the other C7 hydroxy diastereomer. Both enzymes also formed 5-hydroxycyclododecyl acetate as a minor metabolite in these turnovers. In the case of α-terpinyl acetate, CYP101B1 did not show any catalytic activity while CYP101C1 oxidised this substrate effectively. It was oxidised principally at the C5 position by CYP101C1.

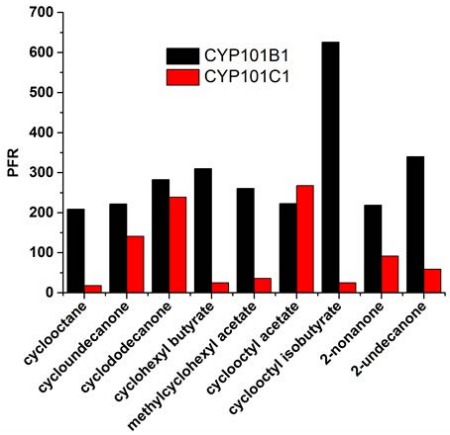

Figure 3. 57: An overview of Product formation rates (PFR) of CYP101B1 and CYP101C1 with best substrates investigated in this chapter. PFRs are given in nmol.nmol-CYP^{-1}.min^{-1}.

Linear ketones were oxidised with low to moderate activity by CYP101B1. In contrast to the cyclic compounds, several linear substrates exhibited higher activity with CYP101C1. CYP101B1 oxidised 2-nonanone and 2-undecanone predominantly at the C8 position. A

significant amount of 3-hydroxy metabolite in addition to the 8-hydroxy product was also observed in the turnovers of CYP101C1 with 2-nonanone and 2-undecanone. CYP101C1 oxidised citronellyl acetate and linalyl acetate to their epoxides with higher activities than the CYP101B1 system.

In summary, the screening of different cyclic ketones and esters as well as linear ketones and esters with the enzymes demonstrated that CYP101B1 and CYP101C1 are capable of generating metabolites in good yield and often with high selectivity. The regioselectivity achieved for cyclic alkanes, ketones and specially for esters are impressive given the lack of other distinguishing features on these cyclic molecules. CYP101B1 catalysed the oxidation of compounds containing ester directing group with high regio- and stereoselectively. The high product formation rates and TTNs for the optimal substrates combined with the levels of selectivity are favourable compared to other systems such as the monooxygenase system PikC from *Streptomyces venezuelae* [369, 370]. Previously this monooxygenase system was shown to be capable of oxidising cyclic substrates including cycloalkyls, macrolides and macrolactones substituted with desosamine and related dimethylamine containing synthetic anchoring groups (TTN approx. 500) [369, 370, 371]. However the selectivity of these oxidation reactions was reduced for cycloalkyl substrates compared to more functionalised macrolides and macrolactones; e.g., 7 products were generated with the protected cyclododecanol [369, 371]. Generally, the addition of double bonds or other functional groups to larger ring structures has been shown to improve the selectivity of P450 catalysed oxidations. For instance, the activity and selectivity of the CYP102A1 catalysed oxidation of cembrenoid derivatives has been optimised with multiple rounds of mutagenesis and substrate engineering resulting in the formation multiple products at allylic and non-activated C-H bonds but more saturated analogues displayed lower selectivity [369, 372, 373]. The cytochrome P450 monooxygenase enzyme CYP101B1 and CYP101C1 when combined with its physiological electron transfer partner Arx and ArR can efficiently oxidise cyclic hydrocarbon derivatives [369]. The C-H bond abstraction and selectivity of oxidation for a given methylene group was high and this could be made almost totally selective by modifying the ester protecting group or functional group on the ring system and these P450 enzymes are therefore ideal candidates for study to generate biocatalysts for the selective functionalisation of more complex substrates [369]. Further studies of these P450 enzymes would be needed to expand the substrate range and enhance the monooxygenase activity and selectivity towards these alicyclic substrates.

Chapter 4

4. The Selective and Efficient Biocatalytic Oxidation of Unactivated C-H Bonds of Adamantyl Derivatives

4.1. Introduction

CYP101B1 has been shown to be a highly efficient biocatalyst for the oxidation of *β*-ionone, other norisoprenoids and monoterpenoid acetates [175, 176]. The butenone side chain of *β*-ionone is an important structural feature, enabling the substrate to bind with the enzyme. It is hypothesised that the chain holds the substrate in a place for efficient and selective oxidation. This is one of the main features which allows these oxidation reactions to proceed with high catalytic activity, turnover number and coupling efficiency [175]. Adamantane and adamantanols have been demonstrated to be poor substrates for CYP101B1 [233]. CYP101B1 catalysed the oxidation of different cyclic alcohol compounds more efficiently when an ester directing group was inserted in these substrates (Chapter 3). With an aim of improving the activity of CYP101B1 towards inert tricyclic adamantyl substrates, ester protecting groups were introduced to the adamantanols via esterification reactions, and these substrates were investigated (Chapter 2 and Figure A. 1-A. 14). This modification, by inserting an ester directing group which is simple to add to and remove from alcohols, could allow CYP101B1 to oxidise these substrates more efficiently. The amide equivalent of an adamantyl amine was also evaluated to see if this could act as a chemical auxiliary to enable the oxidation of this substrate.

4.2. Results

Biocatalytic Oxidation of Unactivated Adamantyl C-H Bonds

Tricyclic adamantane compounds are considered vital for the production of functional materials, polymers and pharmaceuticals [234-237]. Current chemical methods to activate or functionalise the inert C-H bonds of adamantane substrates require harsh oxidants, are poorly

selective and prone to over-oxidation [234-236]. Different microbial strains have been reported, which can oxidise adamantane and its derivatives, and several cytochrome enzymes including CYP101A1 are capable of hydroxylating adamantane and 2-adamantanone [143, 234-236, 238-240]. However, in most instances the activity is low. In this study, a range of substrates with an adamantane skeleton was screened with CYP101B1 for biocatalytic oxidation (Figure 4. 1).

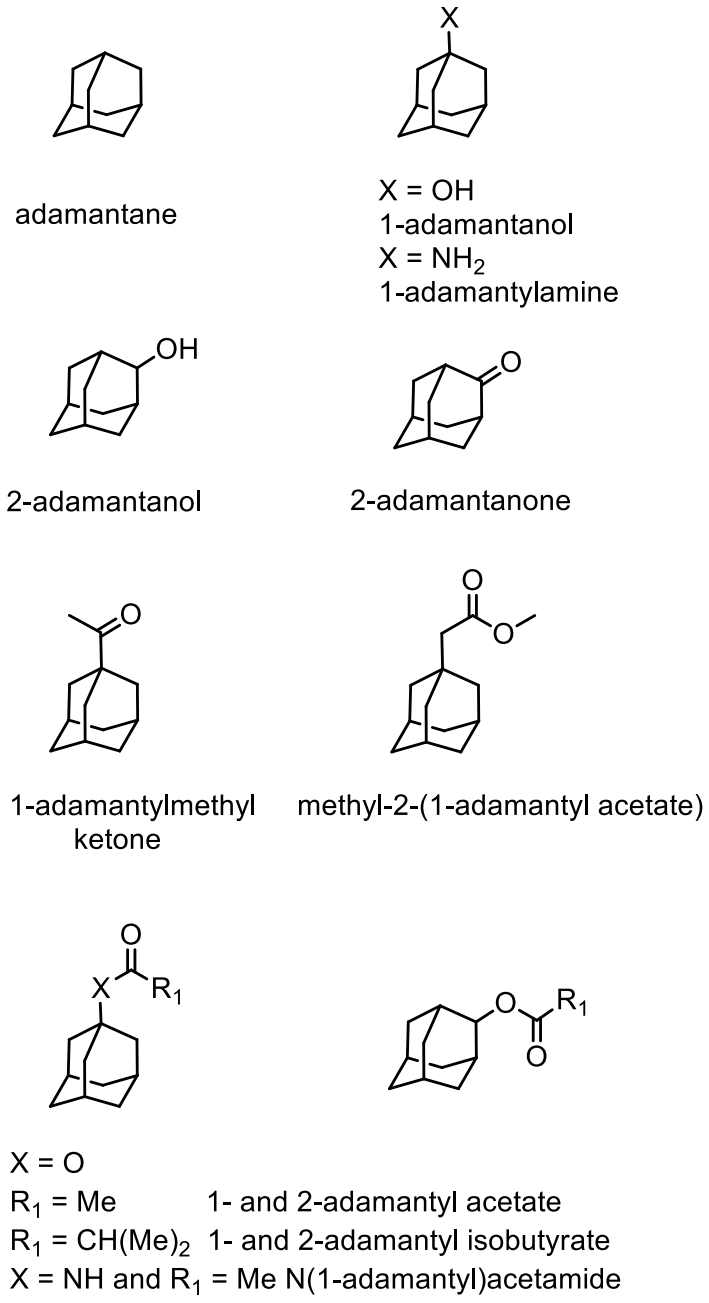

Figure 4. 1 The adamantane substrates screened with CYP101B1 [182].

Previous studies have demonstrated that the heme spin-state shifts of CYP101B1 upon addition of adamantane and adamantanone were 30-35%, and these were lower than the spin-state shifts induced by 1- and 2-adamantanol (55-60%) [182, 233]. The dissociation constants of CYP101B1 with 1-adamantanol (K_d = 711 µM) and 2-adamantanone (548 µM) indicated a weak binding affinity [182, 233]. The NADH oxidation rate of CYP101B1 in the presence of adamantane was only 140 min^{-1}, while this rate was reported to be faster for 1-adamantanol (415 min^{-1}) and 2-adamantanol (563 min^{-1}) [233]. In the case of 2-adamantanone, the rate of NADH oxidation was higher compared to the adamantanols. Despite these high NADH oxidation activities, the productive use of reducing equivalents by CYP101B1 with all these substrates were minimal which resulted in low product formation activities (Table 4. 1) [233]. The product formation activity of CYP101B1 with 2-adamantanone was the highest (104 min^{-1}) which was hypothesised to be due to the presence of a ketone moiety [233]. Repeating these turnovers showed similar results to those reported previously [233].

Table 4. 1 Substrate binding, turnover and coupling efficiency data for the CYP101B1 with adamantane, 2-adamantanone, 1- and 2-adamantanol [233]. The *in vitro* turnover activities were measured using a ArR:Arx:CYP101B1 concentration ratio of 1:10:1 (0.5 µM CYP enzyme, 50 mM Tris, pH 7.4). N is the NADH oxidation rate, PFR is the product formation rate and C is the coupling efficiency. - Not calculated due to low detector response to the addition of substrate or low substrate solubility interfered with the titration. Data are reported as mean ± S.D. (n = 3). Rates are given in nmol.nmol-CYP^{-1}.min^{-1}

substrate	%HS heme	K_d (µM)	N (min^{-1})	PFR (min^{-1})	C %
adamantane	30%	-	140 ± 10	0.2 ± 0.1	0.11
1-adamantanol	60%	711 ± 26	415 ± 55	11 ± 4	3
2-adamantanol	55%	-	563 ± 10	11 ± 3	2
2-adamantanone	35%	548 ± 15	669 ± 7	104 ± 9	16

Adamantane and 1-adamantanol were oxidised by CYP101B1 to generate a major and minor monooxygenase product while 2-adamantanone was hydroxylated to give two metabolites in almost equal amounts (Figure 4. 2). The oxidation of 2-adamantanol was unselective generating up to six products (Figure 4. 2).

Overall, CYP101B1 showed low product formation activity and coupling efficiency with adamantane, 2-adamantanone, 1- and 2- adamantanol compared to norisoprenoid substrates [176, 233].

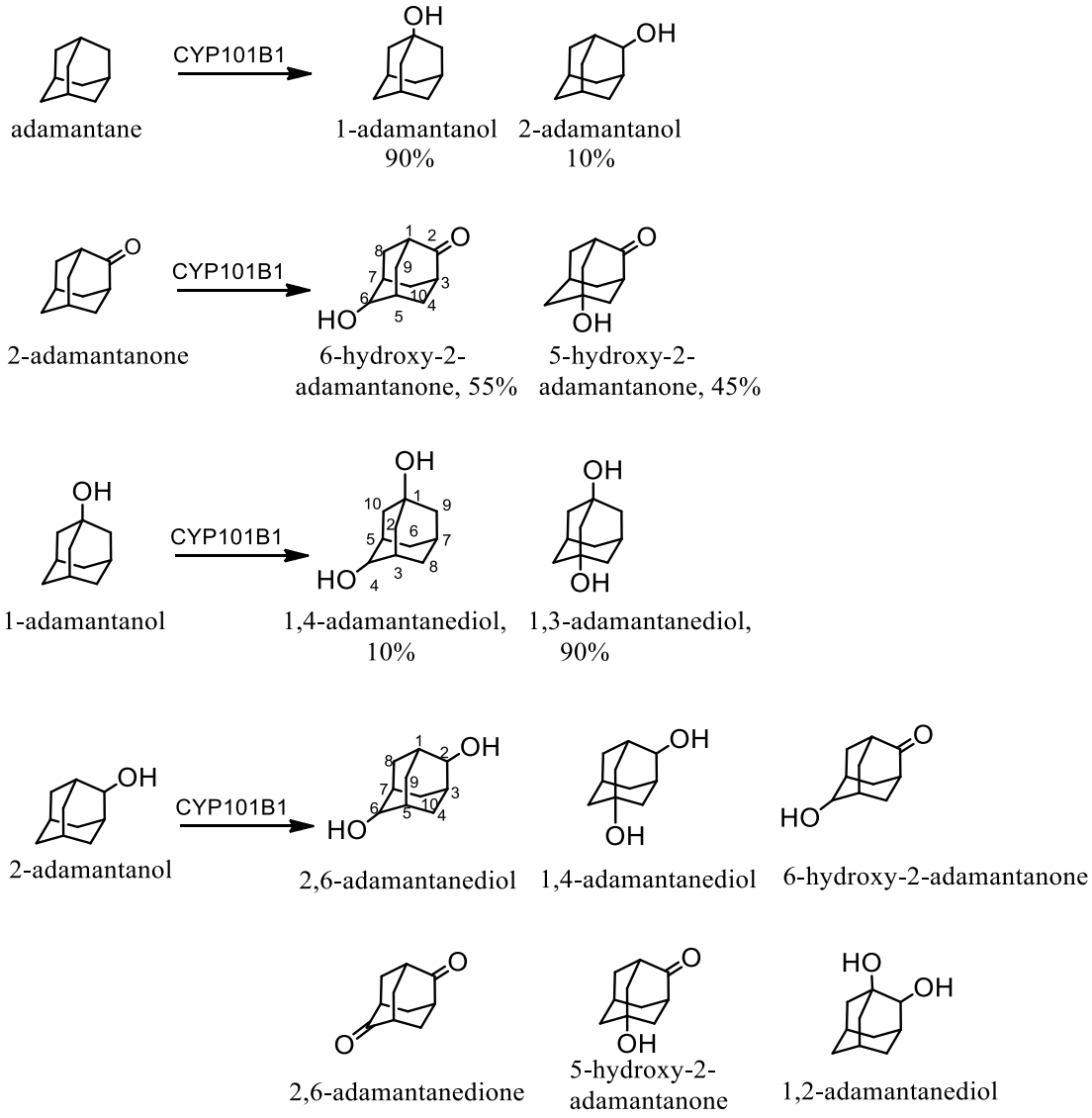

Figure 4. 2 The products formed from CYP101B1 turnovers of adamantane, adamantanols and 2-adamantanone [182, 233]. The product distributions are given as percentages.

Addition of 1-adamantylmethyl ketone in CYP101B1 shifted the spin-state to the ~70% high-spin form (Figure 4. 3). This was a relatively small increase compared to the shift induced by 1-adamantanol (60%), but the binding affinity was an order of magnitude higher (K_d = 32 µM versus 711 µM; Figure 4. 3). The NADH oxidation (923 min^{-1}) and product formation (473 min^{-1}) rates of CYP101B1 with this substrate were also faster compared to the adamantanols and 2-adamantanone (Table 4. 2).

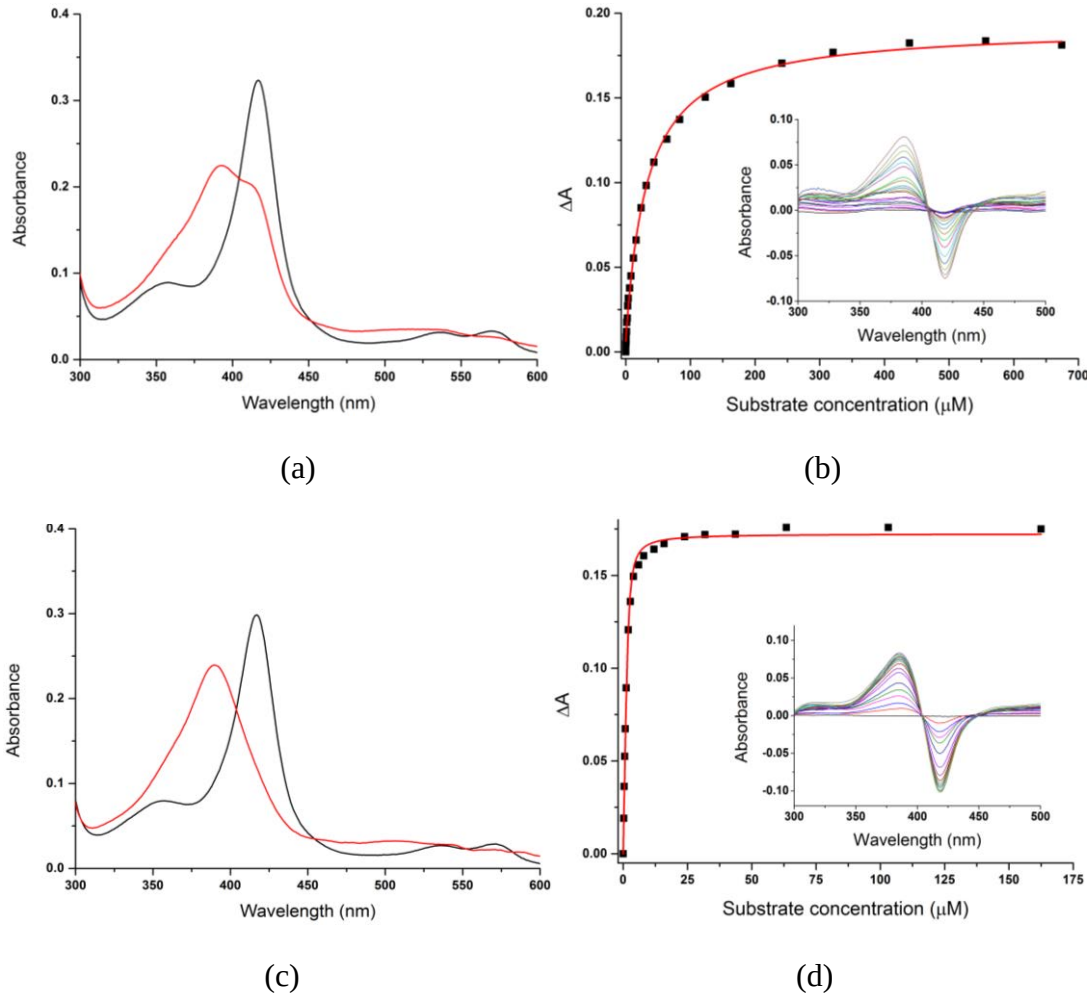

Figure 4. 3 Spin-state shifts (left) and dissociation constants (right) of CYP101B1 with 1-adamantylmethyl ketone and methyl-2-(1-adamantyl acetate). Spin-state shifts (red) of CYP101B1 after addition of **(a)** 1-adamantylmethyl ketone and **(c)** methyl-2-(1-adamantyl acetate). Dissociation constants analysis with **(b)** 1-adamantylmethyl ketone (2.1 µM CYP101B1/K_d 32 µM) and **(d)** methyl-2-(1-adamantylacetate) (2.0 µM CYP101B1/K_d 0.2 µM). The concentration of enzyme used in binding assays and the dissociation constant are provided in brackets.

A significant increase in the coupling efficiency (51%) was also observed with 1-adamantylmethyl ketone and therefore the levels of metabolite formation (473 min^{-1}; Table 4. 2). Two products, in an approximate 3:1 ratio, were detected in the GC-MS analyses of both the *in vitro* and whole-cell turnovers (MS of both m^+/z = 194.05; Figure 4. 4 and Figure C. 1, Figure C. 2-C. 13). These metabolites were generated by the whole-cell oxidation system for characterisation. The *in vivo* turnover products were extracted and purified by silica column chromatography, and the yield of main and minor metabolite after purification was ~31 mg and ~20 mg, respectively.

NMR spectroscopy was used to identify the metabolites (Figure 4. 5, Figure 4. 7 and Figure C. 2-C. 13) [182]. The H2, H9 and H10 proton peaks of major metabolite (RT 10.2 min) were assigned using the correlations with C11 (216.17 ppm) in ^{13}C-^{1}H HMBC NMR spectrum (Figure C. 6). H5 was determined from the interaction with H10 in gCOSY NMR spectrum (Figure C. 4). The primary product was identified as a 4-hydroxy-1-adamantylmethyl ketone due to the carbon signal at 76.15 ppm (C4) showed correlations with H3, H5 (2.02-1.95); H2, H10 (1.90-1.83); H2, H10 (1.82-1.75) and H6, H8 (1.45) in the HMBC NMR spectrum (Figure C. 6) [182]. The enzyme selectively generated the *trans* isomer of 4-hydroxy-1-adamantylmethyl ketone, which was confirmed by characteristic interactions of H4 (δ 3.88-3.84) with H5 (δ 2.02-1.95) and H10 (δ 1.82-1.75) in the ^{1}H-^{1}H ROESY NMR spectrum (Figure 4. 5 and Figure C. 7-C. 8).

The minor product was assigned 3-hydroxy-1-adamantylmethyl ketone as the absence of characteristic multiplet peak for hydroxylation at a methylene group (C**H**-OH) in the ^{1}H NMR spectrum. The carbon signal 71.21 ppm (C3) displayed strong correlations with H2 (1.78-1.74), H4, H8 (1.73-1.67) and weak interactions with H5, H7 (2.34-2.27) in the ^{1}H-^{13}C HMBC NMR spectrum, which suggested hydroxylation at a more reactive bridgehead position (COH; Figure C. 13) [182]. The ^{13}C NMR spectrum showed three distinct carbon signals at 47.03 ppm (C4 & C8), 39.76 ppm (C9 & C10), 32.92 ppm (C5 & C7), their intensities were almost double than the other peaks, indicating hydroxylation took place at the symmetrical C3 position (Figure C. 10).

Table 4. 2 Substrate binding, turnover and coupling efficiency data for the CYP101B1 with 1-adamantylmethyl ketone, methyl-2-(1-adamantyl acetate), 1- and 2-adamantyl acetate and 1- and 2-adamantyl isobutyrate. The *in vitro* turnover activities were measured as described in Table 4. 1. TTN (total turnover number) was determined using assays set up with the same ratio of enzymes as used in Table 4. 1 but with 0.1 μM CYP enzyme, 2 mM substrate and 4 mM NADH (theoretical maximum value 20,000). The other data and rates are given as described in Table 4. 1.

substrate	%HS heme	K_d (μM)	N (min^{-1})	PFR (min^{-1})	C %	TTN
1-adamantylmethyl ketone	70%	32 ± 1.0	923 ± 31	473 ± 22	51	6690
methyl-2-(1-adamantyl acetate)	95%	0.2 ± 0.03	1120 ± 4	704 ± 28	63	16500
1-adamantyl acetate	90%	3.9 ± 0.1	1300 ± 16	821 ± 27	63	6050
2-adamantyl acetate	90%	1.9 ± 0.1	1170 ± 11	877 ± 18	75	11500
1-adamantyl isobutyrate	95%	1.6 ± 0.1	1360 ± 7	1350 ± 22	99	4130
2-adamantyl isobutyrate	90%	0.6 ± 0.04	1060 ± 6	722 ± 10	68	7090

Given the improvement observed in the binding affinity and activity of CYP101B1 with 1-adamantylmethyl ketone over the adamantanols, other adamantyl substrates which contain carbonyl ester groups were investigated. Methyl-2-(1-adamantyl acetate) induced an almost complete heme spin-state shift of CYP101B1 to the high-spin form (95%), and the enzyme bound this substrate very tightly (K_d = 0.2 μM; Table 4. 2). CYP101B1 oxidised methyl-2-(1-adamantyl acetate) with a faster NADH oxidation activity of 1120 min^{-1} and product formation rate of 704 min^{-1} compared to 1-adamantylmethyl ketone (Table 4. 2). The coupling efficiency was 63%. It was oxidised to form two products with a ratio of 84:16 (Figure 4. 4).

These metabolites were generated on a larger scale by a whole-cell turnover system and isolated by silica column chromatography. After isolation, the major product (~25 mg) was identified via NMR analysis as methyl-2-(*trans*-4-hydroxy-1-adamantyl) acetate, and the minor metabolite (~5 mg) was characterised as methyl-2-(3-hydroxy-1-adamantyl) acetate using the same process as that used to identify the 1-adamantylmethyl ketone metabolites

(Figure 4. 4, Figure 4. 6, Figure 4. 7 and Figure C. 14-C. 23) [182]. The MS spectra supported these metabolite assignments (both m^+/z = 224.05, Figure C. 1). The methyl-2-(*trans*-4-hydroxy-1-adamantyl) acetate was assigned as the *trans* isomer due to the characteristic interactions of H4 (δ 3.88-3.83) with H5 (δ 1.96-1.88) and H2, H10 (δ 1.72-1.66) in the ^{1}H-^{1}H ROESY NMR (Figure 4. 4 and Figure 4. 6).

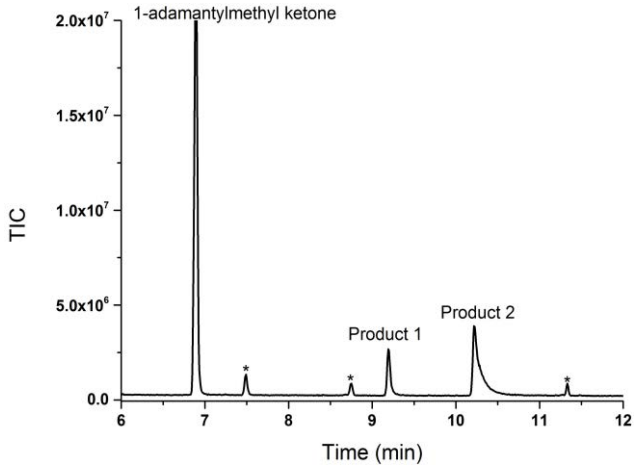

(a)

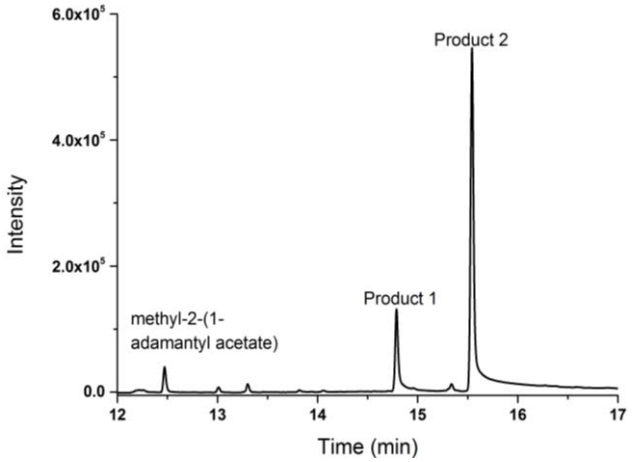

(b)

Figure 4. 4 (a) GC-MS analysis of the *in vitro* turnover of 1-adamantylmethyl ketone by CYP101B1. 1-Adamantylmethyl ketone (RT 6.9 min) and the products: 3-hydroxy-1-adamantylmethyl ketone (product 1; RT 9.2 min) and *trans*-4-hydroxy-1-adamantylmethyl ketone (product 2; RT 10.2 min). **(b)** GC analysis of the *in vitro* turnover of methyl-2-(1-adamantyl acetate) by CYP101B1. Methyl-2-(1-adamantyl acetate) (RT 13.0 min) and the products: methyl-2-(3-hydroxy-1-adamantyl) acetate (product 1; RT 14.8 min) and methyl 2-(*trans*-4-hydroxy-1-adamantyl) acetate (product 2; RT 15.6 min). Impurities are marked (*).

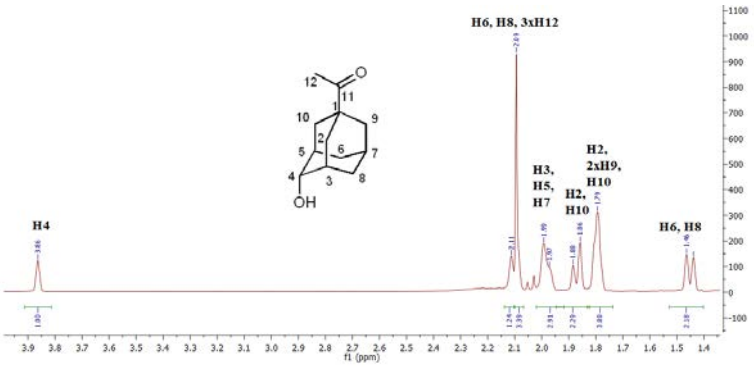

(a)

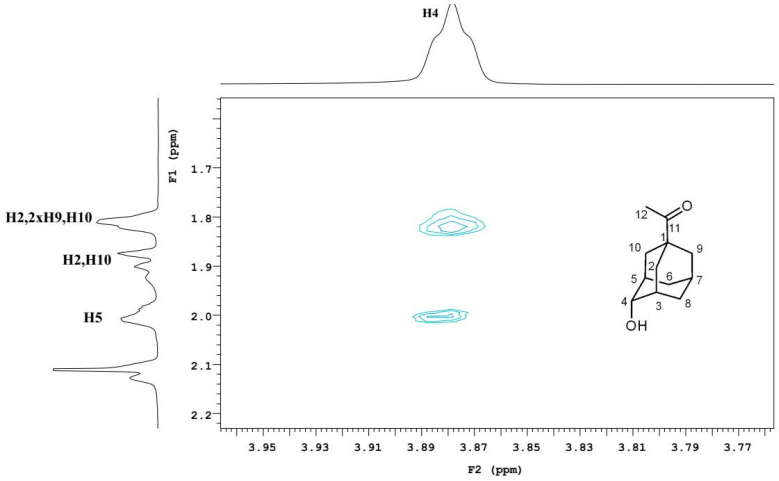

(b)

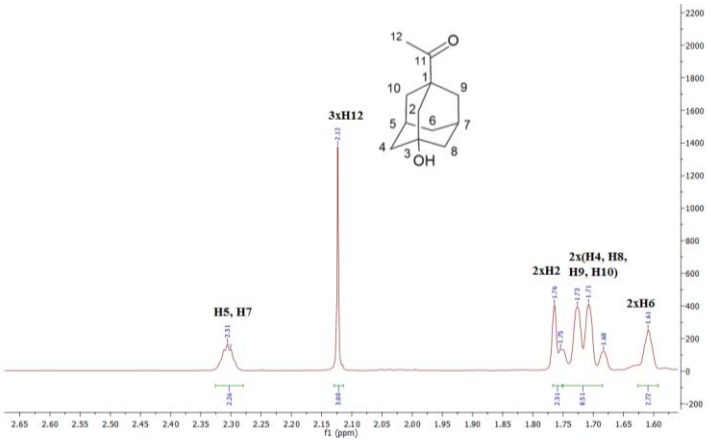

(c)

Figure 4. 5 (a) ^{1}H NMR spectrum of *trans*-4-hydroxy-1-adamantylmethyl ketone. **(b)** ROESY NMR spectrum of *trans*-4-hydroxy-1-adamantylmethyl ketone highlighting the interactions of H4 with H2, H5 and H10. **(c)** ^{1}H NMR spectrum of 3-hydroxy-1-adamantylmethyl ketone. Full data are presented in Appendix C (Figure C. 2-C. 13).

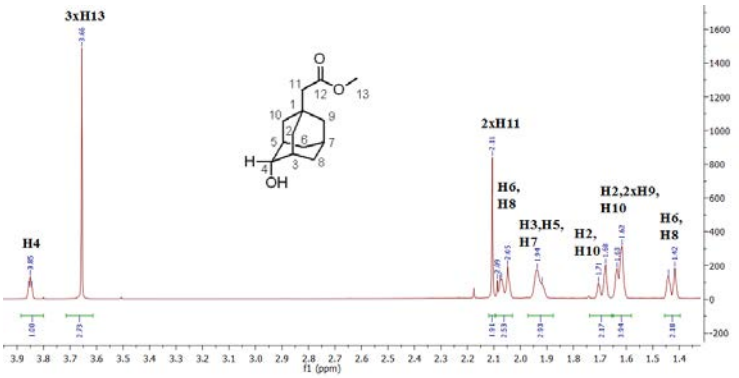

(a)

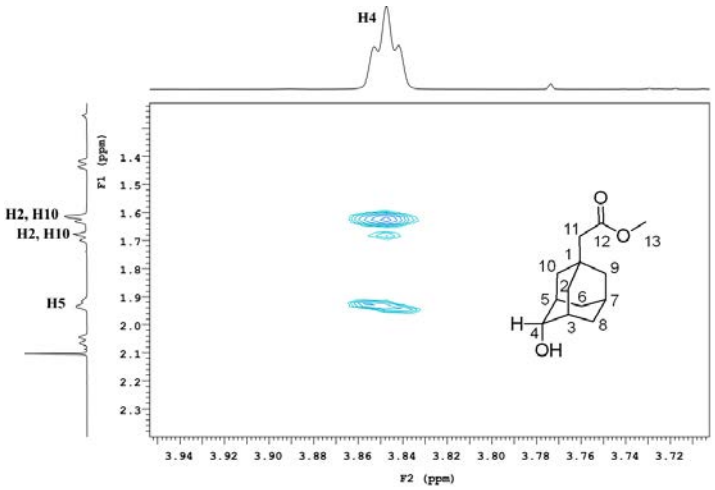

(b)

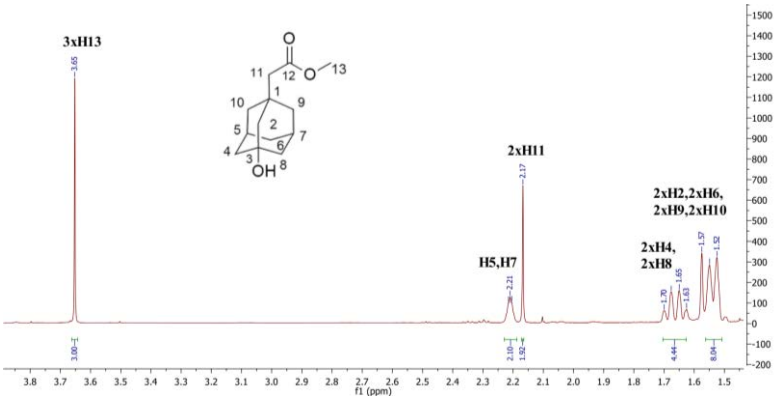

(c)

Figure 4. 6 (a) ^{1}H NMR spectrum of methyl-2-(*trans*-4-hydroxy-1-adamantyl) acetate. **(b)** ROESY NMR spectrum of methyl-2-(*trans*-4-hydroxy-1-adamantyl) acetate which highlighted the interactions of H4 with H2, H5 and H10. **(c)** ^{1}H NMR spectrum of methyl-2-(3-hydroxy-1-adamantyl) acetate. Full data are provided in Appendix C (Figure C. 14-C. 23).

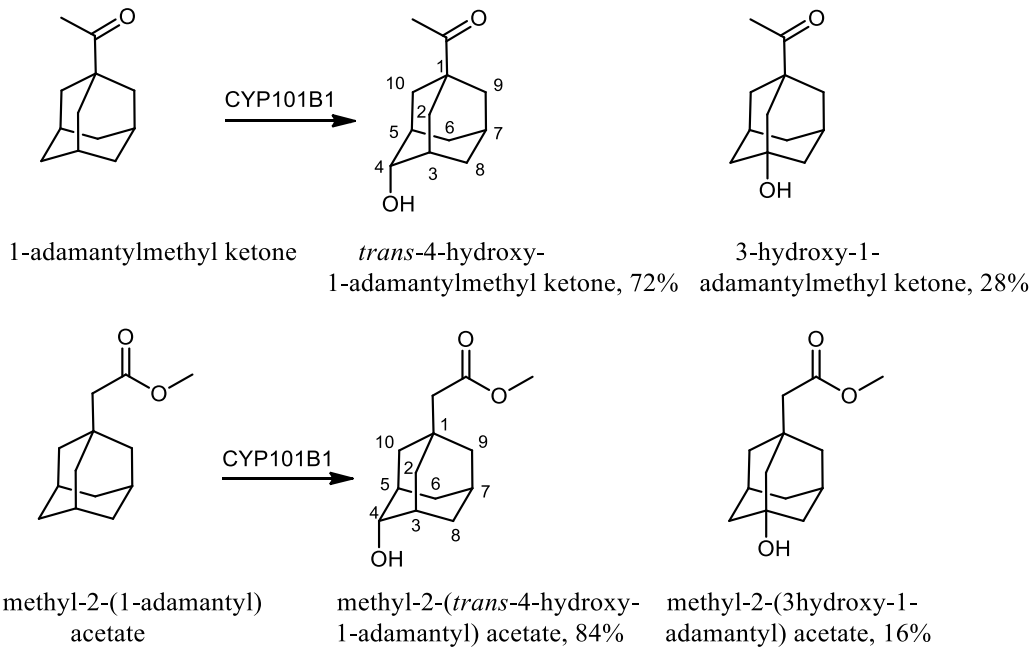

Figure 4. 7 The products generated from CYP101B1 turnovers of 1-adamantylmethyl ketone and methyl-2-(1-adamantyl) acetate [182]. The product distributions are given as percentages.

The acetate and isobutyrate esters of 1-and 2-adamantanol were synthesised using standard methodologies. These were tested as substrates with the intention of observing the activity of CYP101B1 for 1- and 2-adamantyl derivatives containing ester protecting groups (Chapter 2 and Figure A. 1-A. 14) [182].

The addition of 1-adamantyl acetate and 1-adamantyl isobutyrate induced an almost complete heme spin shift of CYP101B1 to the high spin form (90% versus 95%; Figure 4. 8). The substrate binding was found to be tighter with both 1-adamantyl acetate and 1-adamantyl isobutyrate than for the majority of the adamantane derivatives assessed with CYP101B1 above. The binding affinity of CYP101B1 with the isobutyrate ester, 1.6 µM (K_d) exceeded that of the acetate, 3.9 µM (K_d).

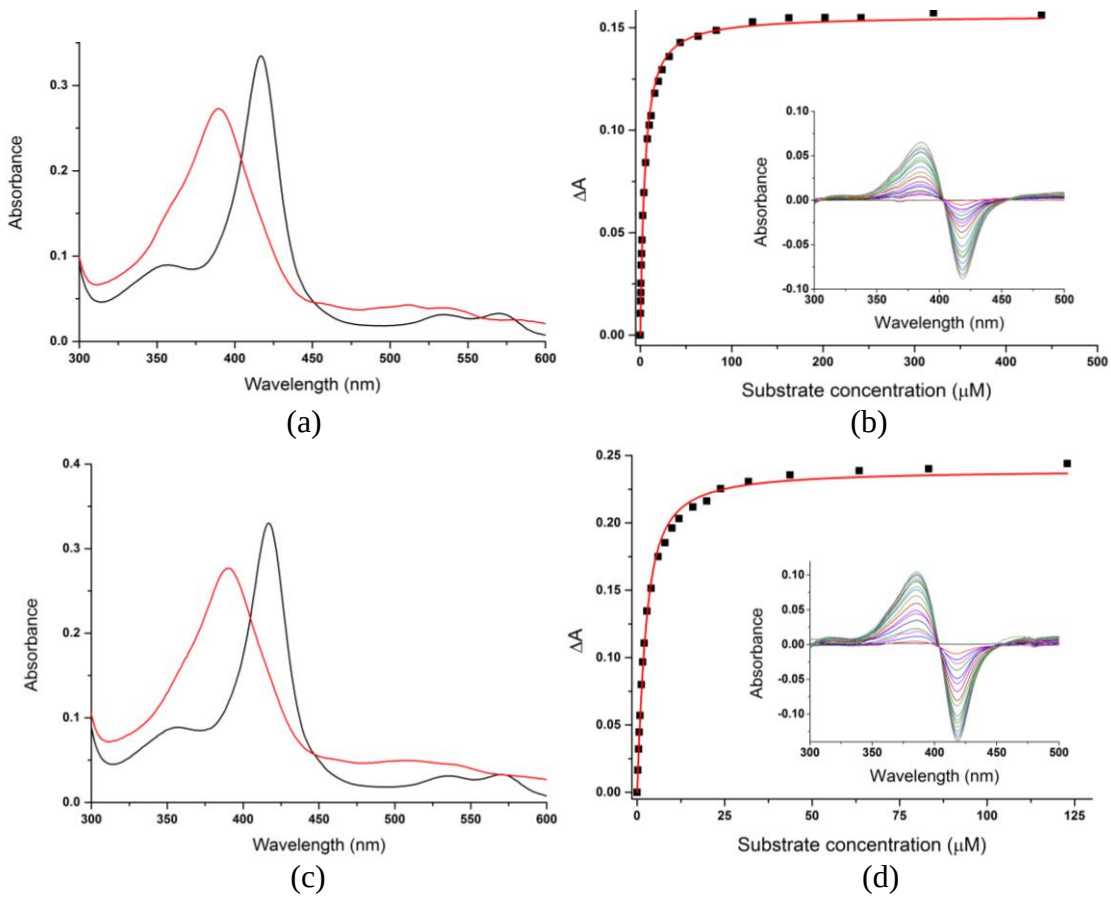

Figure 4. 8 Spin-state shifts (red) of CYP101B1 after addition of **(a)** 1-adamantyl acetate and **(c)** 1-adamantyl isobutyrate. Dissociation constants analysis with **(b)** 1-adamantyl acetate, (2.0 μM CYP101B1/K_d 3.9 μM) and **(d)** 1-adamantyl isobutyrate (1.9 μM CYP101B1/K_d 1.6 μM). The concentration of enzyme used in binding studies and the dissociation constants are provided in brackets.

The NADH oxidation and product formation rates of CYP101B1 with 1-adamantyl acetate and isobutyrate were faster than those of 1-adamantylmethyl ketone and methyl-2-(1-adamantyl acetate) (Table 4. 2). The NADH oxidation rates of both were comparable, 1300 and 1360 min^{-1}, but the coupling efficiency of 1-adamantyl isobutyrate was greater than 1-adamantyl acetate, 99% versus 63%. Due to a higher efficiency of NADH utilisation, the oxidation of 1-adamantyl isobutyrate by CYP101B1 proceeded with a faster product formation rate than 1-adamantyl acetate (1350 versus 821 min^{-1}; Table 4. 2). The turnover of 1-adamantyl acetate generated two hydroxylated products (MS, m^+/z = 210.10 and m^+/z = 210.0) in an approximate 4:1 ratio (Figure 4. 9 and Figure C. 1). The primary product was isolated (~26 mg) by silica column chromatography after generation using a whole-cell biotransformation system. This metabolite was characterised by NMR (Figure 4. 10, Figure 4. 13 and Figure C. 24-C. 30) [182]. The H2, H3, H5, H7, H9 and H10 protons were determined via the correlations with C1 (81.76 ppm) in

^{1}H-^{13}C HMBC NMR spectrum (Figure 4. 10). The product was identified as 4-hydroxy-1-adamantyl acetate due to the strong interactions of the carbon peak at 75.74 ppm (C4) with the proton peaks of H2, H3, H5, H6, H8 and H10 in the HMBC NMR spectrum (Figure C. 28). The orientation of the hydroxy group at C4 position was confirmed through ^{1}H-^{1}H ROESY spectrum analysis, and the metabolite was assigned as a *trans* isomer due to the distinctive interactions of H4 (δ 3.96-3.92) with H5 (δ 2.09-2.01), H2 and H10 (δ 2.16-2.09) (Figure 4. 10 and Figure C. 29-C. 30) [182]. The minor product was not isolated as a pure compound, but the ^{1}H NMR and mass spectrum indicated it was a 3-hydroxy metabolite (m^{+}/z = 210.0; Figure 4. 10, Figure 4. 13, Figure C. 1 and Figure C. 31).

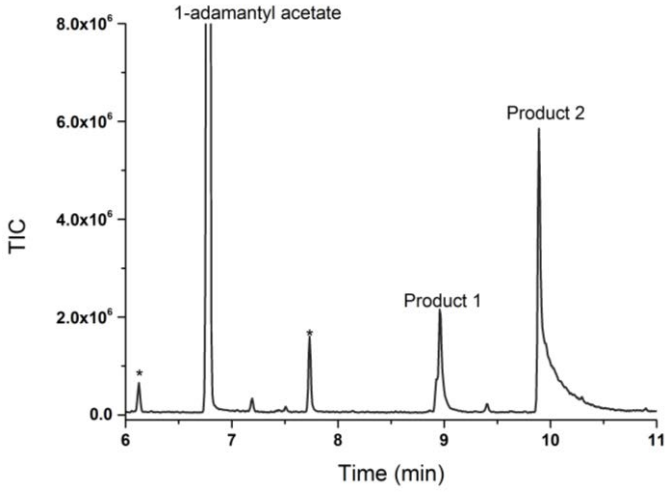

(a)

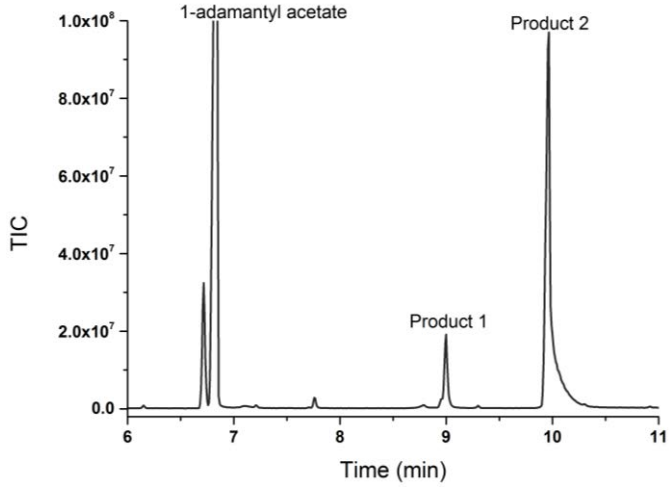

(b)

Figure 4. 9 GC-MS analysis of the **(a)** *in vitro* and **(b)** whole-cell turnovers of 1-adamantyl acetate by CYP101B1. 1-Adamantyl acetate (RT 6.8 min) and the products; 3-hydroxy-1-adamantyl acetate (Product 1; RT 8.9 min) and *trans*-4-hydroxy-1-adamantyl acetate, (Product 2; RT 9.9 min). Impurities are marked (*).

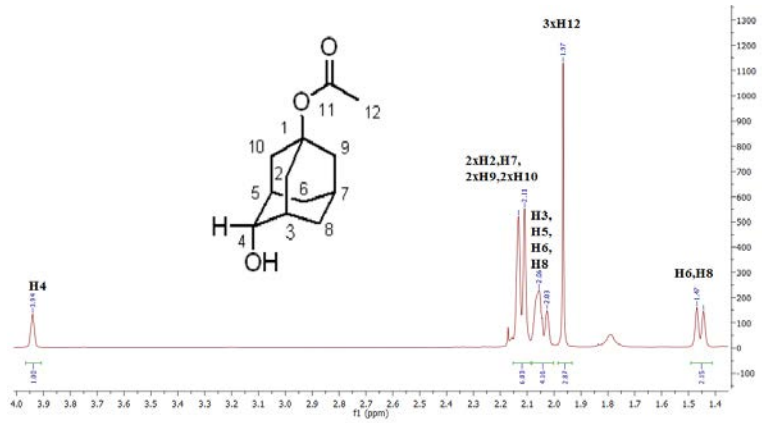

(a)

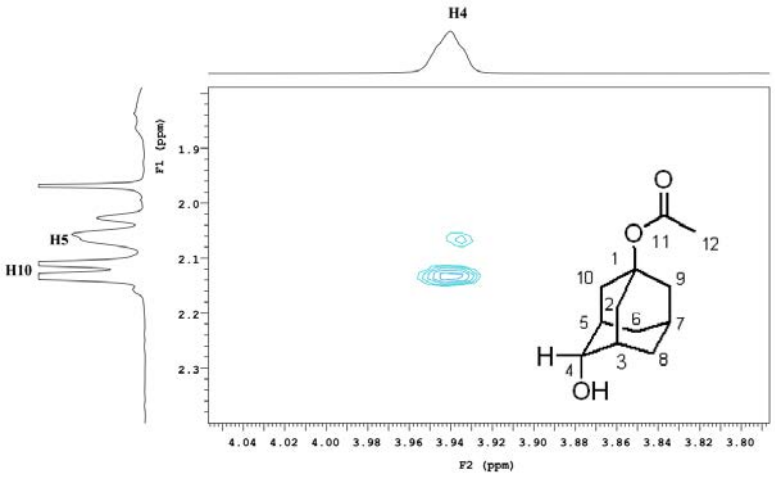

(b)

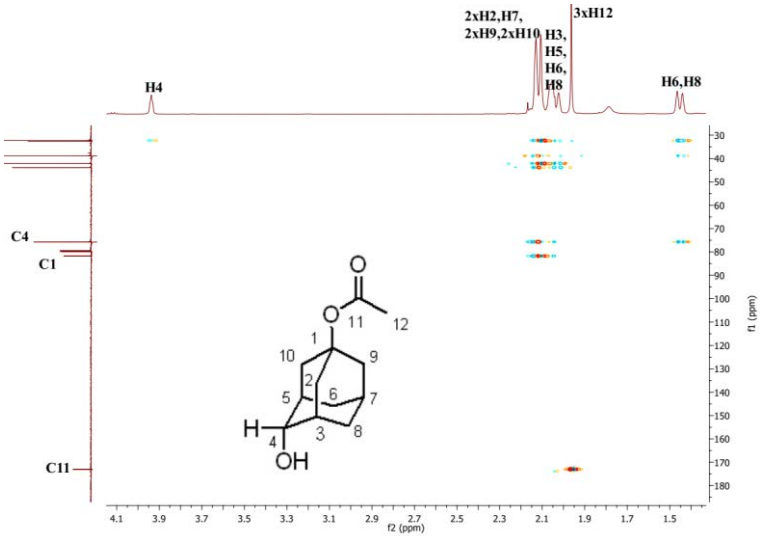

(c)

Figure 4. 10 (a) ^{1}H NMR spectrum of *trans*-4-hydroxy-1-adamantyl acetate. **(b)** ROESY NMR of *trans*-4-hydroxy-1-adamantyl acetate which highlighted the interactions of the H4 with H5 and H10. **(c)** The HMBC NMR spectrum of *trans*-4-hydroxy-1-adamantyl acetate. Full data are given in Appendix C (Figure C. 24-C. 30).

CYP101B1 catalysed the oxidation of 1-adamantyl isobutyrate regioselectively and generated one monooxygenase metabolite, 97% (GC-MS; m^+/z = 238.05; Figure 4. 11 and Figure C .1). This was purified (~35 mg) via silica column chromatography and characterised by NMR analysis (Figure 4. 12 and Figure 4. 13). The distinct multiplet peak at 3.96-3.92 ppm in ^{1}H NMR spectrum confirmed a hydroxylated metabolite. The correlations of C1 (81.76 ppm) with protons in HMBC NMR spectrum were used to assign H3, H5, H9 and H10 (Figure C. 36) [182]. H6 and H8 were identified via the characteristic interactions with H5, H3 and H7 in ^{1}H-^{1}H gCOSY NMR spectrum (Figure C. 34). The product was confirmed as 4-hydroxy-1-adamantyl isobutyrate due to the correlations of C4 (75.82 ppm) with H3, H5, H6 and H8 in HMBC NMR spectrum (Figure C. 36). The stereochemistry of this metabolite was determined by the strong interactions of H4 (δ 3.96-3.92) with H5 (δ 2.08-2.01) and H10 (δ 2.17-2.09) in ^{1}H-^{1}H ROESY NMR spectrum, and therefore the product was confirmed as a *trans* isomer (Figure 4. 12 (b), Figure C. 37-C. 38). A small peak was also detected in the GC-MS analysis of the turnover, which had a mass spectrum and retention time consistent with that of 3-hydroxy-1-adamantyl isobutyrate (m^+/z = 238.05) but was not isolated in sufficient yield from the whole-cell turnover to be fully characterised (Figure 4. 11, Figure 4. 13 and Figure C. 1).

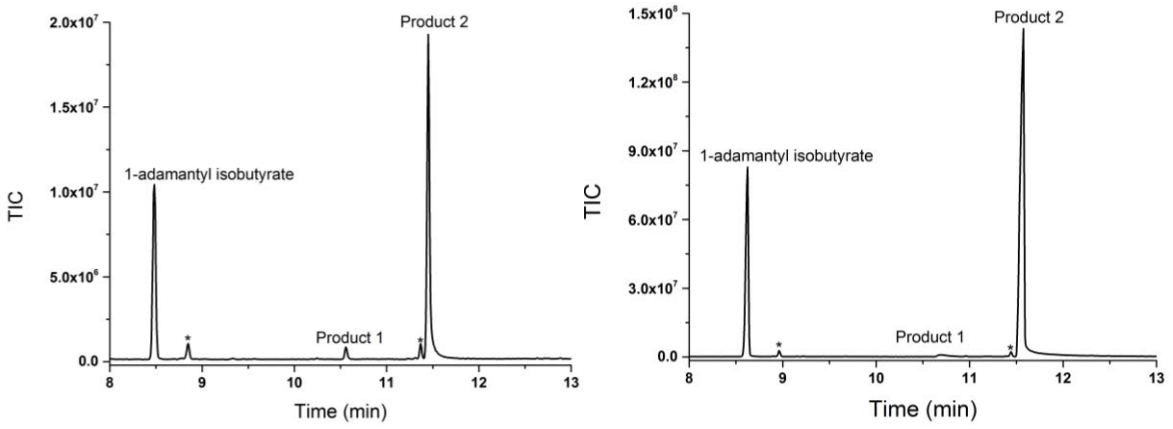

Figure 4. 11 GC-MS analyses of the **(a)** *in vitro* and **(b)** whole-cell turnovers of 1-adamantyl isobutyrate by CYP101B1. 1-Adamantyl isobutyrate (Product 1; RT 8.6 min) and the product; *trans*-4-hydroxy-1-adamantyl isobutyrate (Product 2; RT 11.5 min). The minor peak (3%) at 10.6 min has a MS and retention time consistent with it being 3-hydroxy-1-adamantyl isobutyrate. Impurities are labelled (*).

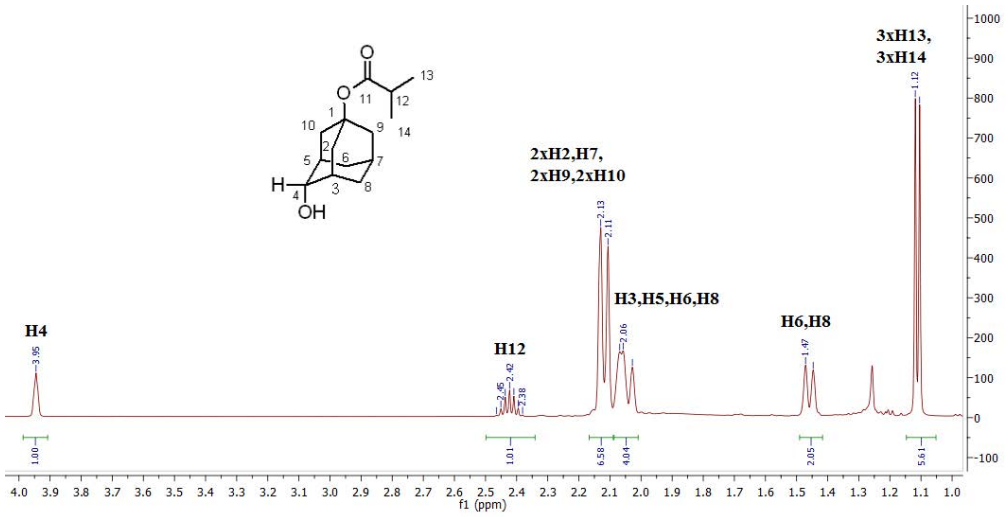

(a)

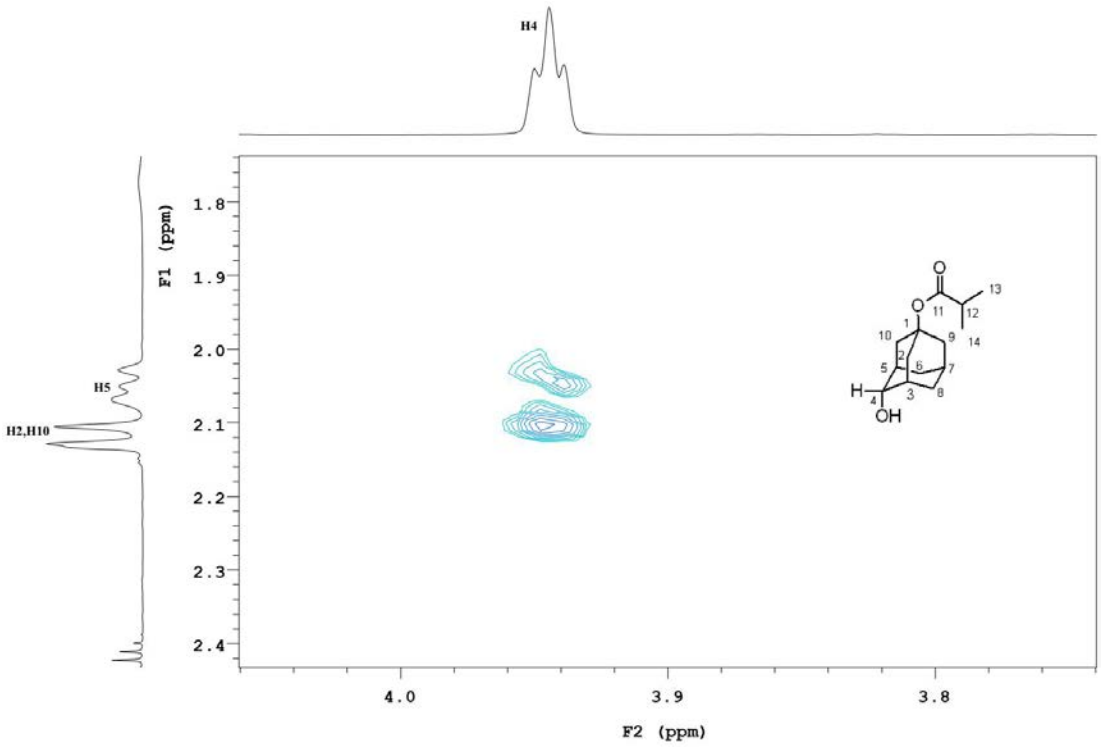

(b)

Figure 4. 12 (a) ^{1}H NMR spectrum of *trans*-4-hydroxy-1-adamantyl isobutyrate. **(b)** ROESY NMR spectrum of *trans*-4-hydroxy-1-adamantyl isobutyrate acetate which highlighted the interactions of the H4 with H2, H5 and H10. Full data are presented in Appendix C (Figure C. 32-C. 38).

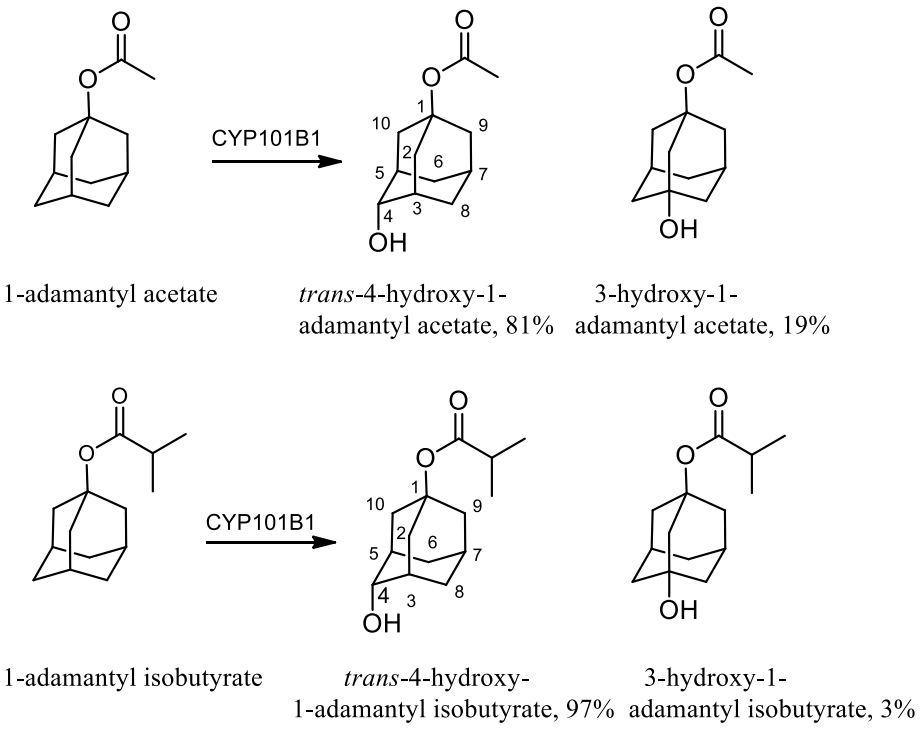

Figure 4. 13 The metabolites generated from CYP101B1 turnovers of 1-adamantyl acetate and 1-adamantyl isobutyrate. The product distributions are given as percentages.

To further evaluate the enzyme binding affinity and activity, 2-adamantyl acetate and isobutyrate were investigated as potential substrates. The addition of 2-adamantyl acetate and 2-adamantyl isobutyrate to CYP101B1 both induced a spin-state shift of ~90% high-spin (Figure 4. 14). In line with the substantial spin-state changes, the enzyme also bound tightly with both substrates. The binding affinities were tighter than their 1-adamantyl ester counterparts (K_d: 1.9 µM and 0.6 µM; Table 4. 2 and Figure 4. 14).

CYP101B1 catalysed the oxidation of these substrates efficiently. The NADH oxidation rates with 2-adamantyl acetate and 2-adamantyl isobutyrate were comparable, 1170 min^{-1} and 1060 min^{-1} (Table 4. 2) The coupling efficiency of the turnover of 2-adamantyl acetate was greater resulting in a product formation rate of 877 min^{-1} (Table 4. 2). The oxidation of 2-adamantyl isobutyrate by CYP101B1 proceeded with a slower product formation rate than that of 1-adamantyl isobutyrate predominantly due to a reduced coupling efficiency (68% versus 99%; Table 4. 2).

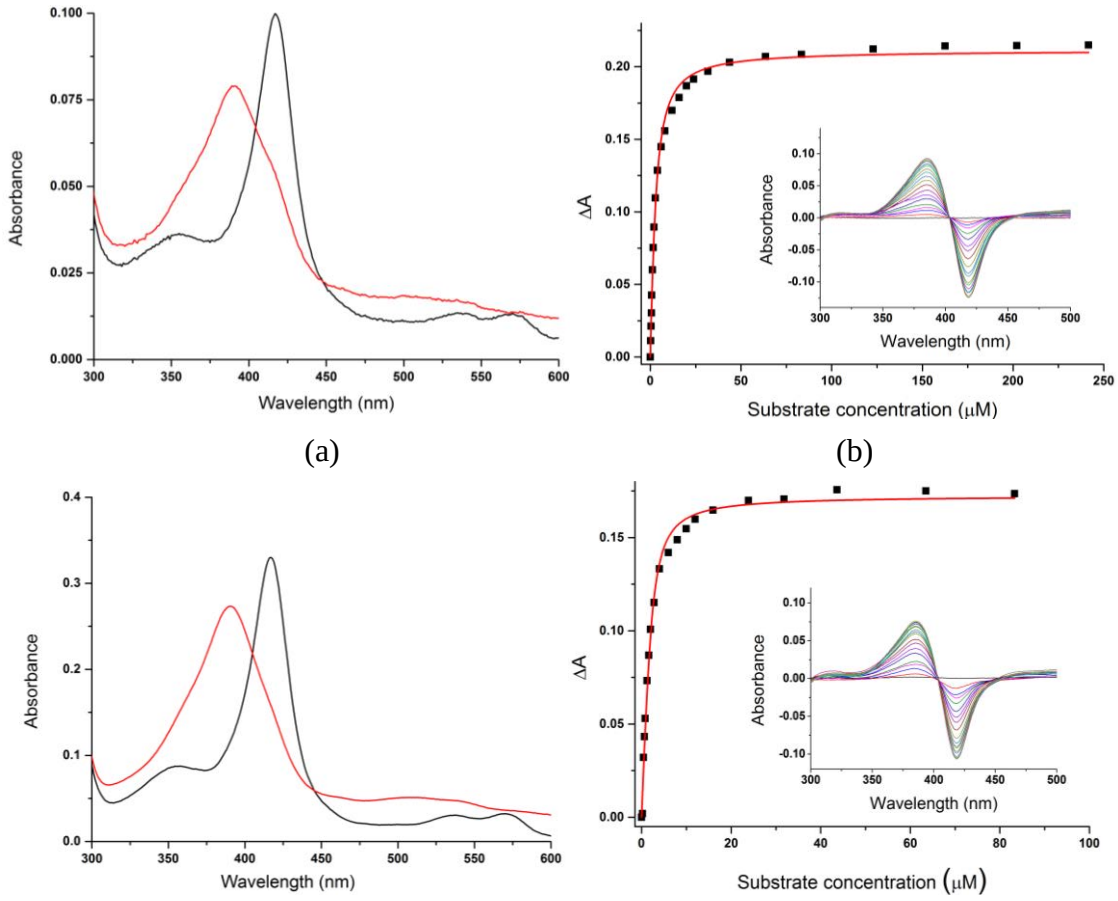

Figure 4. 14 Spin-state shifts (red) of CYP101B1 after addition of **(a)** 2-adamantyl acetate and **(c)** 2-adamantyl isobutyrate. Dissociation constant analysis with **(b)** 2-adamantyl acetate (1.8 µM CYP101B1/K_d 1.9 µM) and **(d)** 2-adamantyl isobutyrate (2.1 µM CYP101B1/K_d 0.6 µM). The concentration of the enzyme used in binding studies, and the dissociation constant are provided in brackets.

CYP101B1 oxidised 2-adamantyl acetate into a single hydroxylated metabolite (GC-MS; m^+/z = 210.10, Figure 4. 15 and Figure C. 1). A CYP101B1 whole-cell oxidation system was used to generate this metabolite in sufficient yield for NMR characterisation (Figure 4. 15). The product was extracted and isolated (~25 mg) using silica column chromatography and identified via NMR analysis (Figure 4. 16, Figure 4. 18 and Figure C. 39-C. 43). The H1 and H3 were determined via the interactions with H2 in gCOSY NMR spectrum (Figure C. 44). gCOSY was also used to confirm the H4 and H9 peaks through the correlations with H3 and H1, respectively (Figure C. 41). The peaks of H1, H3, H4, H8 and H9 were further confirmed using the interactions with C2 (78.25 ppm) in the HMBC NMR spectrum (Figure 4. 16 and Figure C. 43). The product was identified as 5-hydroxy-2-adamantyl acetate using the

correlations of C5 (70.12 ppm) with the protons at δ 1.86-1.80 (H4 and H9) and δ 1.78-1.70 (H4, 2xH6 and H9) in HMBC NMR spectrum (Figure 4. 16 and Figure C. 39-C. 43) [182]. A minor metabolite was also observed in the turnover, <3%, (RT 10.3 min; Figure 4. 15) which had a mass spectrum (m^+/z = 210.20) consistent with a hydroxylation product but this was not isolated in high enough yield to be characterised in more detail (Figure 4. 15, Figure 4. 18 and Figure C. 1) [182].

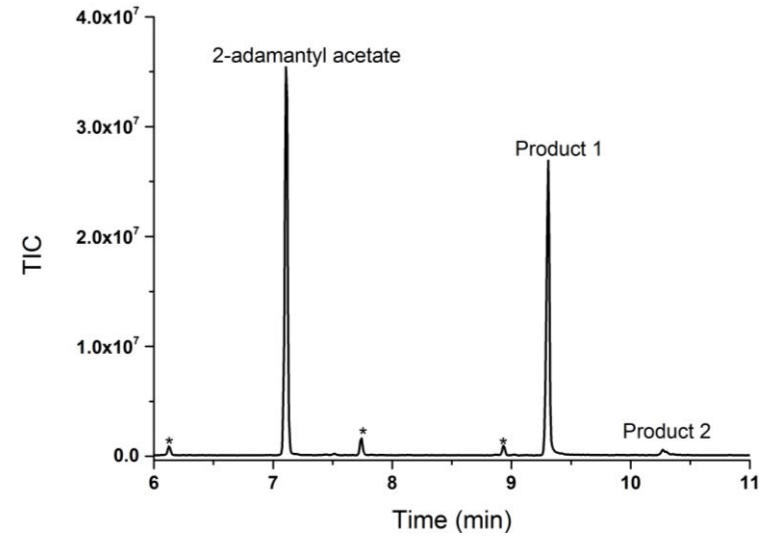

(a)

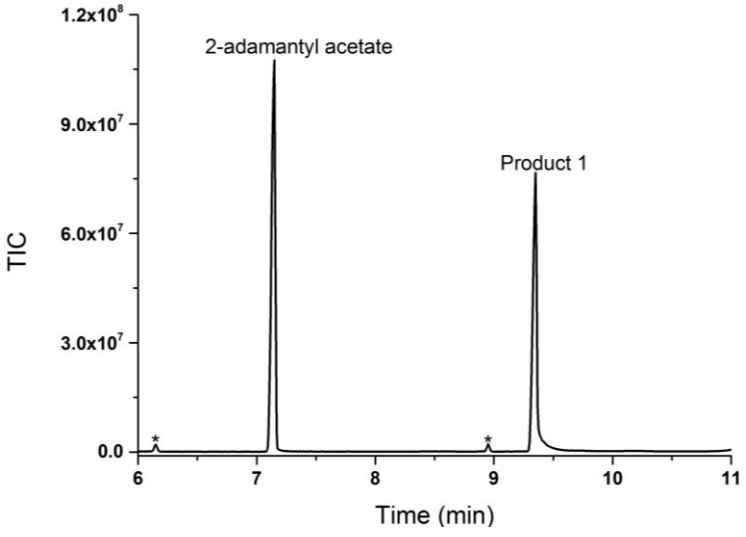

(b)

Figure 4. 15 GC-MS analysis of the **(a)** *in vitro* and **(b)** whole-cell turnovers of 2-adamantyl acetate by CYP101B1. 2-Adamantyl acetate (RT 7.1 min) and the product; 5-hydroxy-2-adamantyl acetate (product 1; RT 9.4 min), and a minor metabolite (product 2; RT 10.1 min) whose MS was consistent with a hydroxylation product. Impurities are labelled (*).

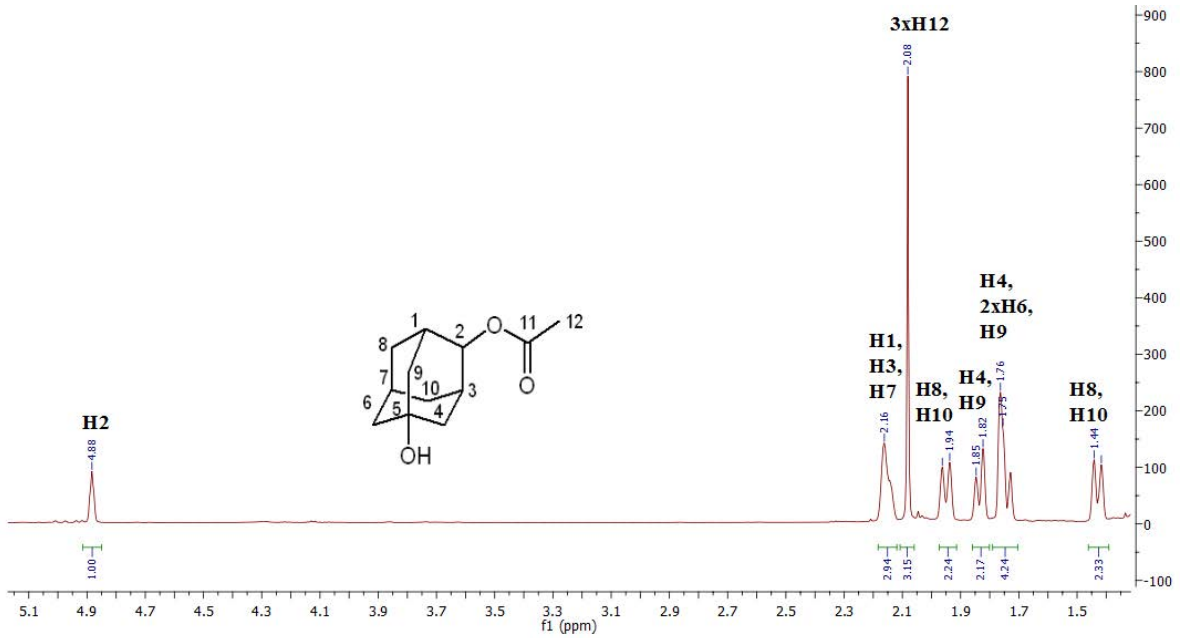

(a)

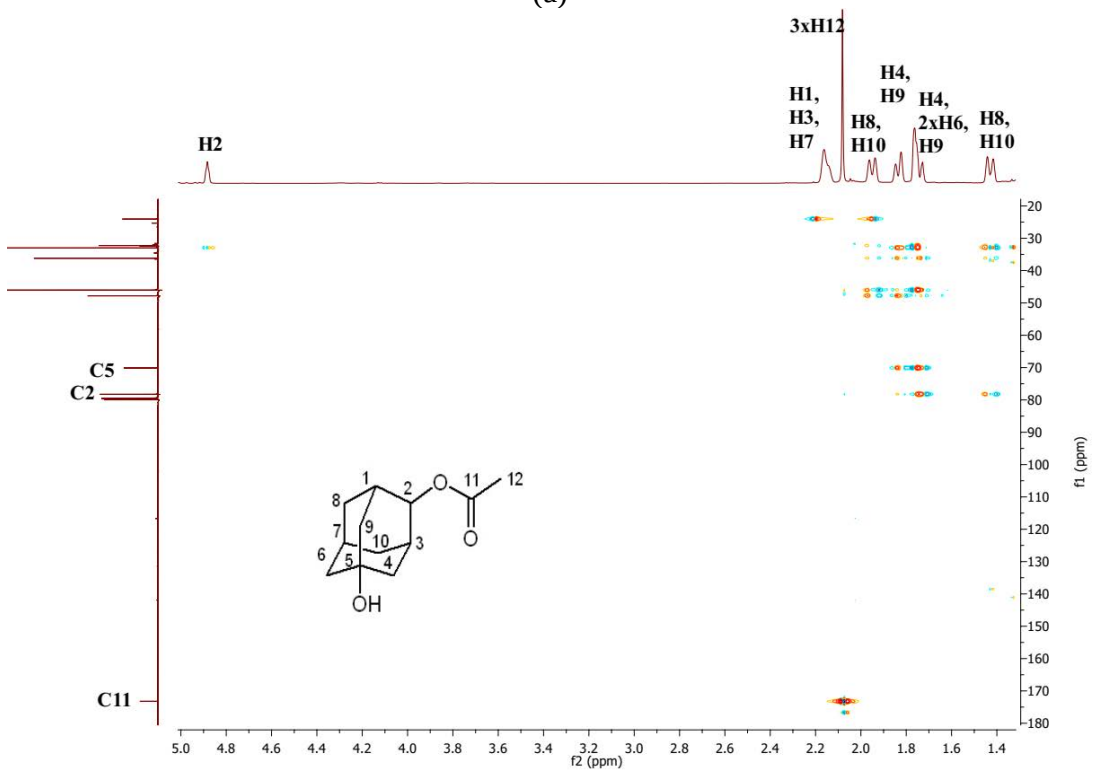

(b)

Figure 4. 16 (a) ^{1}H NMR spectrum of 5-hydroxy-2-adamantyl acetate. **(b)** The HMBC NMR spectrum of 5-hydroxy-2-adamantyl acetate which highlighted the correlations of C5 with the protons H4, H6 and H9. Full data are in Appendix C (Figure C. 39-C. 43).

GC and GC-MS analysis of the *in vitro* turnovers of 2-adamantyl isobutyrate showed the presence of a single monooxygenase product, ≥97% (m^{+}/z = 238.10; Figure 4. 17 and Figure C. 1). A larger scale whole-cell turnover of CYP101B1 was carried out to generate the sole

metabolite for NMR characterisation. The product was isolated (~40 mg) using silica column chromatography and identified as 5-hydroxy-2-adamantyl isobutyrate by NMR analysis via the same process as that used to assign the 2-adamantyl acetate metabolite (Figure 4. 18, Figure 4. 19 and Figure C. 44-C. 48) [182]. There was a minor product (≤3%) observed at a higher retention time which had mass spectrum (m^+/z = 238.25) consistent with a hydroxylation product but was not isolated in large enough yield to be characterised further (Figure 4. 17 and Figure C .1).

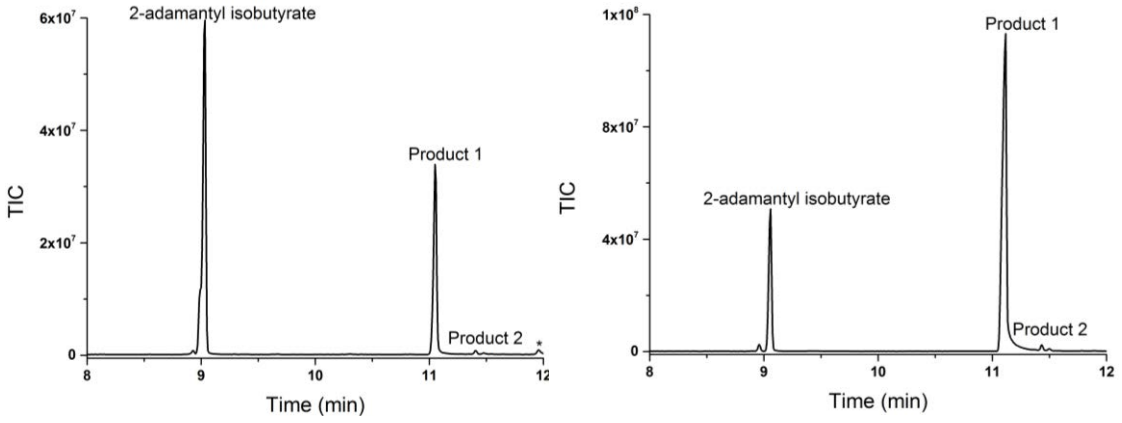

Figure 4. 17 GC-MS analysis of the **(a)** *in vitro* and **(b)** whole-cell turnovers of 2-adamantyl isobutyrate by CYP101B1. 2-Adamantyl isobutyrate (RT 8.9 min) and the products; 5-hydroxy-2-adamantyl isobutyrate (product 1; RT 11.1 min) and minor (product 2; RT 11.4 min), whose MS was consistent with a hydroxylation product. Impurities are labelled (*).

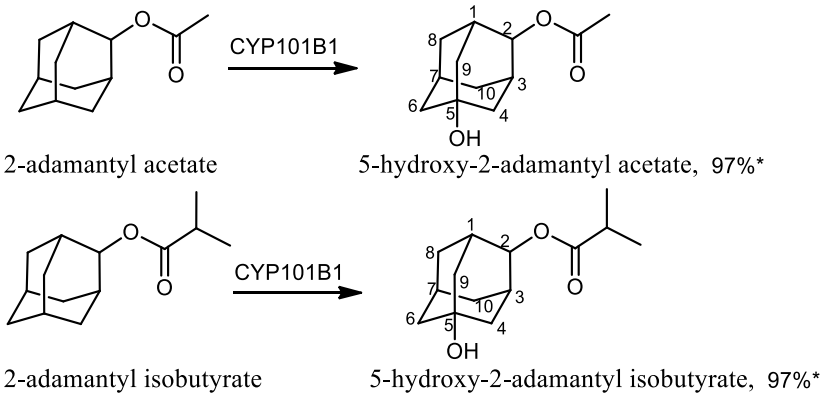

Figure 4. 18 The products formed from CYP101B1 turnovers of 2-adamantyl acetate and 2-adamantyl isobutyrate. *There is a small, ≤3%, amount of an uncharacterised minor metabolite with a MS consistent of a hydroxylation product detected in these turnovers. The product distributions are given as percentages.

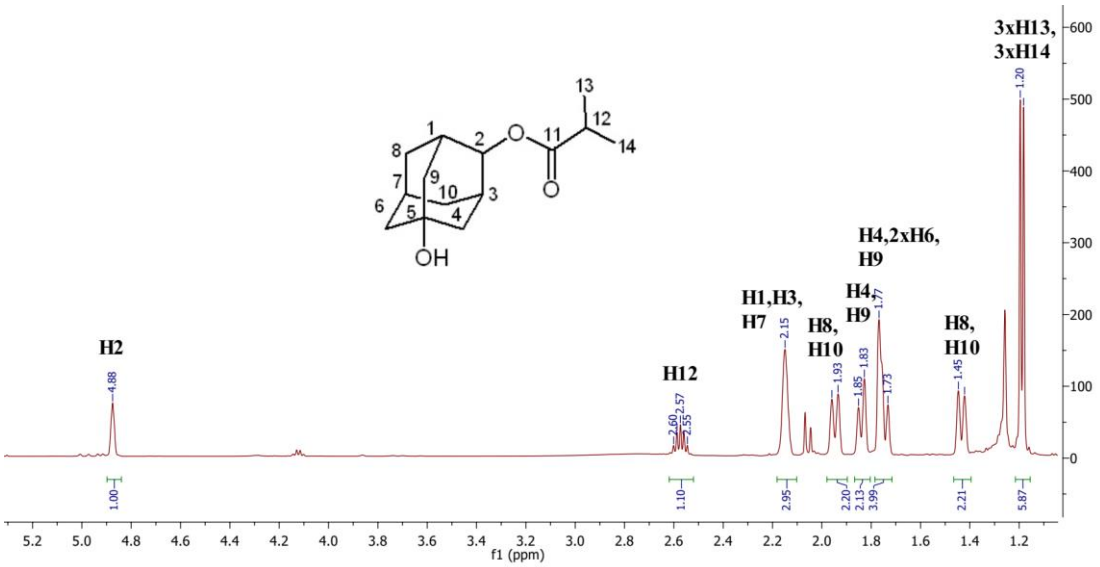

(a)

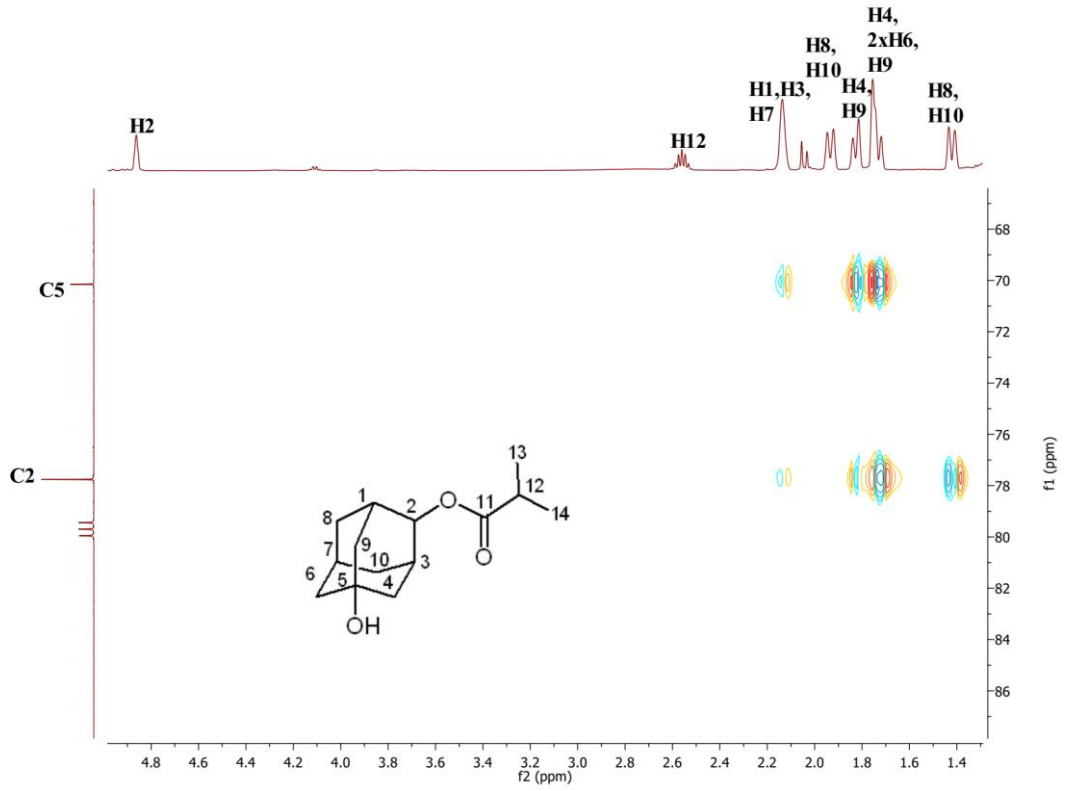

(b)

Figure 4. 19 (a) ^{1}H NMR spectrum of 5-hydroxy-2-adamantyl isobutyrate. **(b)** Zoomed in version of HMBC NMR spectrum of 5-hydroxy-2-adamantyl isobutyrate to highlight the correlations of C2 and C5 with the protons (H4, H8, H9, H10) and (H1, H3, H4, H6, H7, H9), respectively. Full data are provided in Appendix C (Figure C. 44-C. 48).

Addition of 1-adamantylamine to CYP101B1 induced a spin-state shift of <5% (Figure 4. 20). The rate of NADH oxidation was slow (35 ± 0.3 min^{-1}; Table 4. 3). No product could be detected for *in vitro* turnovers of 1-adamantylamine in GC-MS analysis (Figure 4. 21 and Figure 4. 22).

Converting 1-adamantylamine to the acetamide resulted in a substantial increase in the spin-state of CYP101B1 upon substrate addition. N-(1-adamantyl)acetamide induced a spin-state shift to 50% high spin form in CYP101B1 (Figure 4. 20). However, the binding affinity, as measured by the dissociation constant (K_d = 55 µM), was lower than those of the adamantyl ester derivatives and 1-adamantylmethyl ketone (Figure 4. 20, Table 4. 2 and Table 4. 3). The rate of NADH oxidation (955 min^{-1}) was fast, but the product formation activity was lower 166 min^{-1} when compared to other adamantyl ester derivatives. This is likely due to the minimal productive utilisation of reducing equivalents to metabolite formation (17%; Table 4. 3).

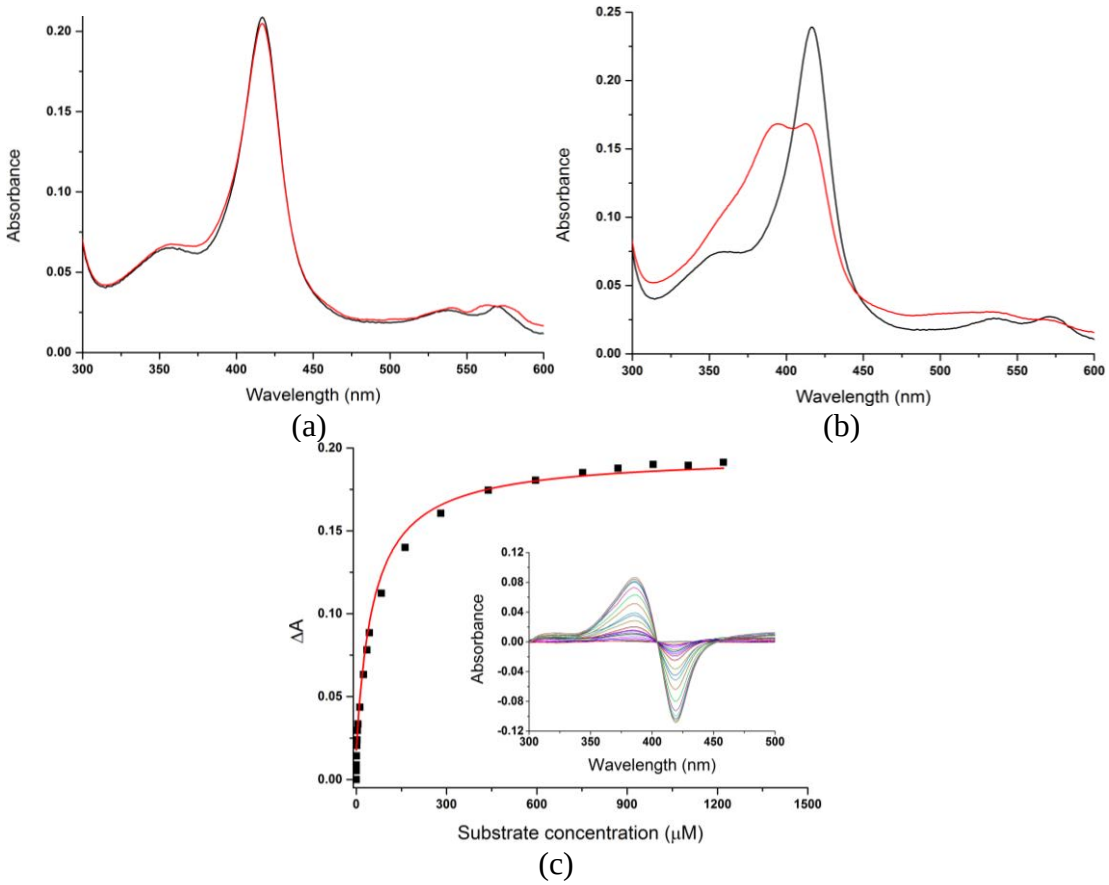

Figure 4. 20 Spin-state shifts (red) of CYP101B1 after addition of **(a)** 1-adamantylamine and **(b)** N-(1-adamantyl)acetamide. **(c)** Dissociation constant analysis with N-(1-adamantyl)acetamide (1.7 µM CYP101B1/K_d 55 µM). The concentration of the enzyme used in the binding assay and the dissociation constant are given in brackets.

Table 4. 3 Substrate binding, turnover and coupling efficiency data for the CYP101B1 with 1-adamantylamine and N-(1-adamantyl)acetamide. The *in vitro* turnover activities were measured as described in Table 4. 1. The Data and rates are provided as described in Table 4. 1 and Table 4. 2. n.p: no product. - Not calculated due to low detector response to the addition of substrate or low substrate solubility interfered with the titration.

substrate	%HS heme	K_d (μM)	N (min^{-1})	PFR (min^{-1})	C %	TTN
1-adamantylamine	<5%	-	35 ± 0.3	n.p	n.p	n.p
N-(1-adamantyl)acetamide	50%	55 ± 5	955 ± 25	166 ± 9	17	780

CYP101B1 oxidised N-(1-adamantyl)acetamide into two hydroxylated products (GC-MS; both m^+/z = 209.1) in an approximate 3:1 ratio (Figure 4. 21 and Figure C. 1). These were generated in more significant quantities via the whole-cell oxidation system, and both were extracted and isolated using silica gel chromatography (note; as the products are highly soluble in aqueous solution, dichloromethane and petroleum benzine were used instead of ethyl acetate during liquid-liquid extraction) [241]. The major metabolite was identified as 4-hydroxy-N-(1-adamantyl)acetamide (isolated ~15 mg) due to distinct peak at δ 3.98-3.84 in ^{1}H NMR spectrum, and the correlations of C4 (75.98) with H6 and H8 in HMBC NMR spectrum (Figure 4. 22 and Figure C. 49-C. 55) [182]. The minor metabolite was assigned as the 3-hydroxy product (~3 mg) using its NMR spectra (Figure 4. 21, Figure 4. 23 and Figure C. 56-C. 57) [182]. Due to overlapping proton peaks in ROESY NMR spectrum, the stereochemistry could not be determined for the 4-hydroxy metabolite (Figure C. 54-C. 55).

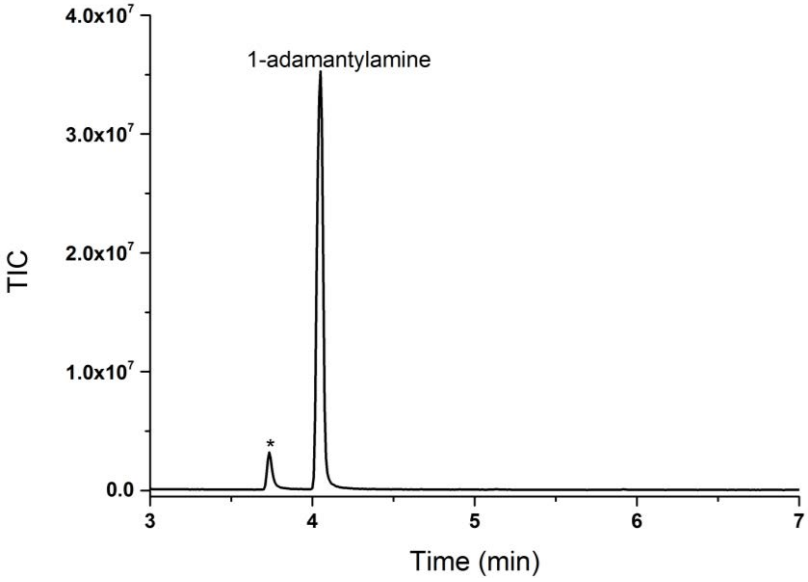

(a)

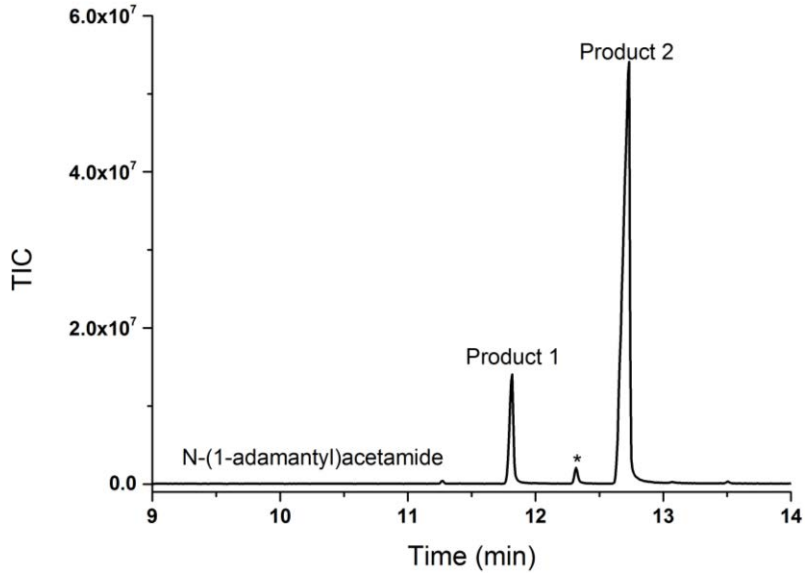

(b)

Figure 4. 21 (a) GC-MS analysis of the *in vitro* turnover of 1-adamantylamine by CYP101B1. 1-Adamantylamine (RT 4.05 min). **(b)** GC-MS analysis of the whole-cell turnover of N-(1-adamantyl)acetamide by CYP101B1. N-(1-adamantyl)acetamide (RT 9.75 min) and the minor product; 3-hydroxy-N-(1-adamantyl)acetamide (product 1; RT 11.8 min) and major product; 4-hydroxy-N-(1-adamantyl)acetamide (product 2; RT 12.8 min). Impurities are labelled (*).

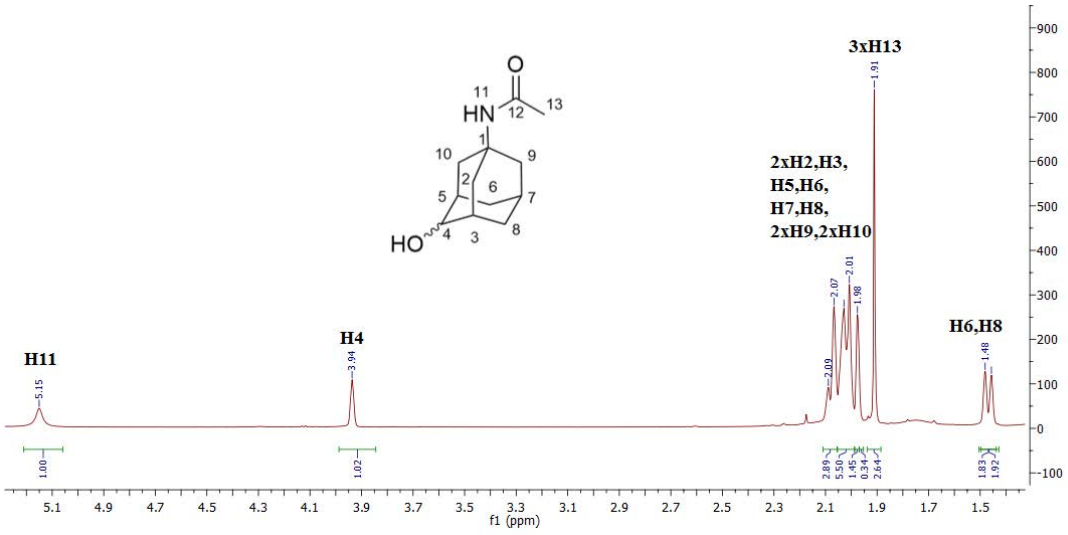

(a)

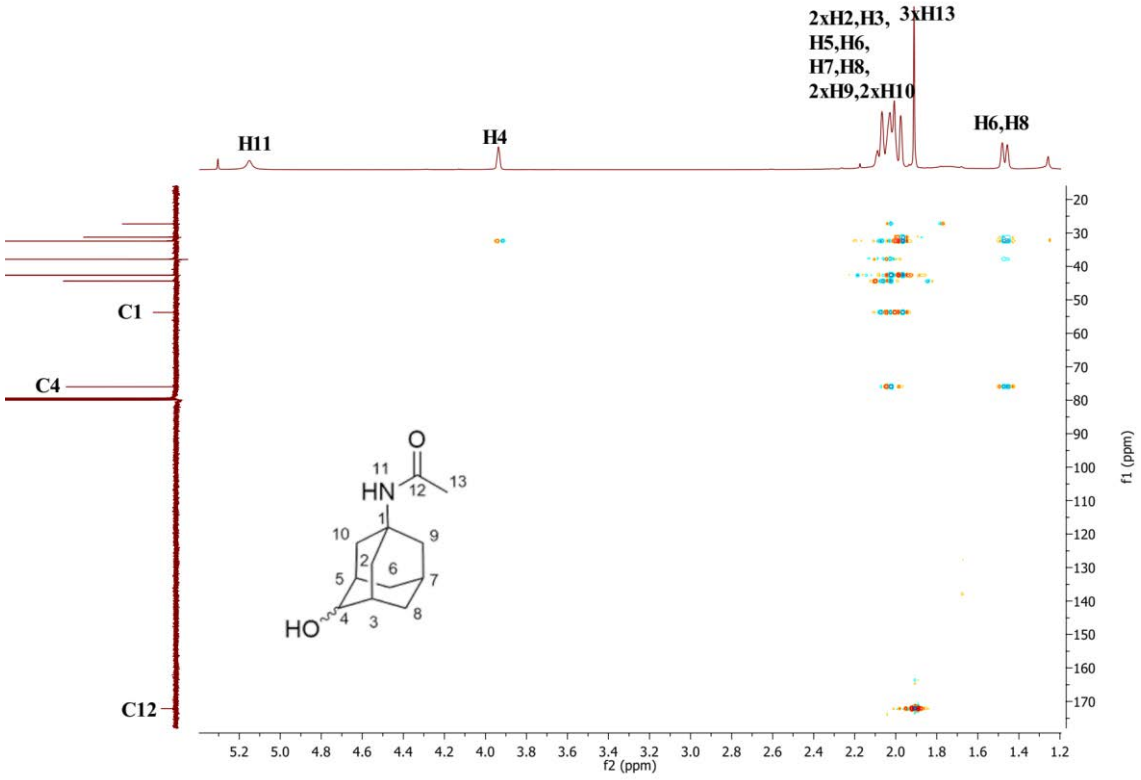

(b)

Figure 4. 22 (a) ^{1}H NMR spectrum of 4-hydroxy-N-(1-adamantyl)acetamide. **(b)** The HMBC NMR spectrum of 4-hydroxy-N-(1-adamantyl)acetamide which highlighted the correlations of C4 with the protons including H6 and H8. Full data are given in Appendix C (Figure C. 49-C. 57).

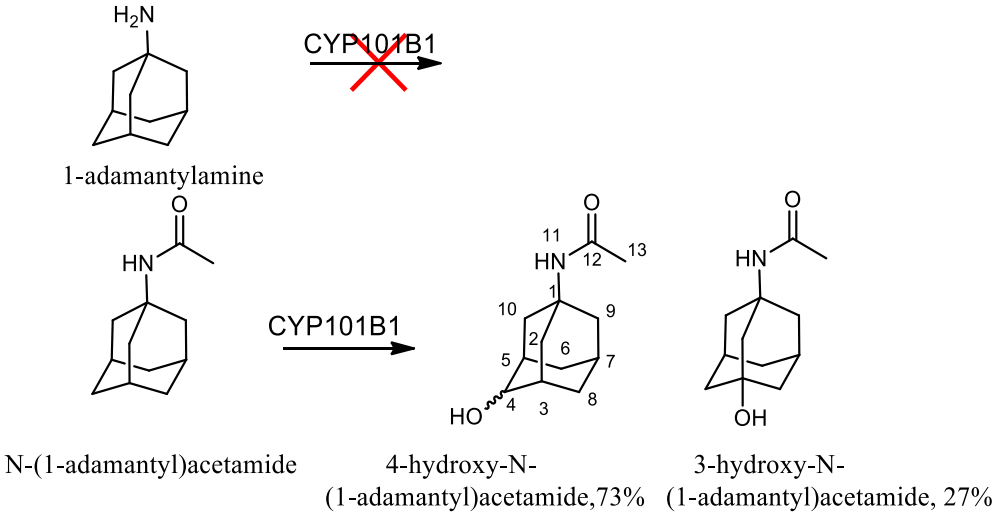

Figure 4. 23 The products generated from CYP101B1 turnovers of N-(1 adamantyl)acetamide. No product was detected in the turnovers with 1-adamantylamine. The product distributions are given as percentages.

4.3. Discussion

CYP101B1 has been reported to oxidise a broad range of substrates, and optimal catalytic efficiency was achieved for norisoprenoids and monoterpenoid acetates. All of these substrates contain a carbonyl group on a side chain attached to substituted ring systems. These substrates are hydroxylated with high activity, total turnover numbers and regioselectivity. The oxidation of adamantane derivatives are of interest as they are used as building blocks for many complex drug molecules and polymers [234, 236, 237]. Microbial oxidative bio-transformations of adamantane, 2-adamantanone, adamantanols and related substrates including the acetate esters are possible using different bacteria, including *Streptomyces*, and fungi including *Basidiomycota, Absidia cylindrospora* and *Beauveria* (*Sporotrichum*) *sulfurescens* [234-236, 239, 241, 242]. Certain P450 enzymes such as CYP101A1 and CYP101D2 including their mutants have also been reported to oxidise adamantane based substrates, however at lower activities than the turnovers of the esters reported here with CYP101B1 [143, 238, 240].

CYP101B1 showed poor affinity and activity for adamantane, 2-adamantanone and adamantanols. The importance of the ketone-containing side chain for efficient biocatalysis with CYP101B1 can be clearly seen by comparing the binding properties and activities of adamantyl acetates and isobutyrates with adamantane, 2-adamantanone, and both

adamantanols. The oxidation of the esters proceeded more efficiently and was more selective with improved binding and catalytic properties.

1-adamantylmethyl ketone bound tightly to CYP101B1 and gave a faster product formation rate compared to 1-adamantanol. Methyl-2-(1-adamantyl acetate) bound to CYP101B1 with the highest affinity. This substrate has the highest total turnover number (16500). CYP101B1 had a higher affinity for the adamantyl isobutyrates than the equivalent acetates. The turnovers of 1-adamantyl isobutyrate were selective for the formation of the *trans*-4-hydroxy product (97%). Other substituents at the equivalent position led to the production of the 3-hydroxy metabolite as a significant minor product (16-28%) in addition to the 4-hydroxy metabolite. The selectivity of ester oxidation was different to 1-adamantanol oxidation which favoured oxidation to 1,3-adamantanediol. In the case of 1-adamantyl acetate and isobutyrate, hydroxylation was preferred at C4 over the more reactive tertiary position, and the lack of product corresponding to a *cis*-4-hydroxy species must be due to the orientation of the substrate in the enzyme active site. Overall, the ketone-containing side chain appeared to hold the adamantyl tricyclic ring in such a position that allows only certain C-H bonds to be attacked compared to the parent adamantanols which presumably bind in multiple orientations in the active site or are highly mobile.

2-Adamantyl isobutyrate bound more strongly to CYP101B1 than the equivalent acetate but was oxidised with low activity. For 2-adamantyl acetate and isobutyrate, hydroxylation occurs predominantly at the more reactive bridgehead position to produce the 5-hydroxy metabolite whereas for 2-adamantanone and 2-adamantanol a significant level of oxidation was also observed at the methylene group at C6. The lower total turnover numbers of the isobutyrate esters despite the higher product formation activity may be due to lower solubility and requires further optimisation.

The 1-adamantylamine and N-(1-adamantyl)acetamide frameworks are found in many drugs molecules, e.g. rimantadine, adapromine and tromantadine [243-245]. The selective functionalisation of the acetamide derivative could be used to generate drug metabolites for activity studies or to add functional groups for the development of new drugs with improved properties. The reduced product formation activity and total turnover number due to a poor coupling efficiency of the acetamide versus the ester, require further investigation but could be due to an alternative binding mode as reflected in the lower spin-state shift induced by the

acetamide. Despite the lower turnover activity, the substrate was efficiently metabolised, and a large amount of product was generated using the whole-cell biotransformation system.

The selective oxidation of the adamantyl esters with high activity by CYP101B1 could be useful for synthetic chemistry [182, 234-236, 238-240]. Acetate, acetamide, isobutyrate and other ester or amide groups could be used as directing groups to improve catalytic performance and tune the selectivity without protein engineering. The *in vitro* activity and total turnovers achieved with CYP101B1 are significantly higher than those reported for the majority of other P450 systems (Table 4. 4). Large quantities of the products were generated (up to 3 mM conversion of all of the added substrate, ~680 mg L^{-1}) using the whole-cell *E. coli* oxidation system at low cell densities in shake flasks without optimisation. This is encouraging for the scale-up of enzyme activity in the future.

Table 4. 4. The metabolites formed from CYP101B1 turnovers of adamantane substrates. n.p no product.

Adamantane substrates	Products and Yield (mg)	PFR (min^{-1})
1-adamantylmethyl ketone	3-hydroxy-1-adamantylmethyl ketone (~20) *trans*-4-hydroxy-1-adamantylmethyl ketone (~31)	473 ± 22
Methyl-2-(1-adamantyl acetate)	methyl-2-(3-hydroxy-1-adamantyl)acetate (~5) methyl-2-(*trans*-4-hydroxy-1-adamantyl)acetate (~25)	704 ± 28
1-adamantyl acetate	3-hydroxy-1-adamantyl acetate *trans*-4-hydroxy-1-adamantyl acetate (~26)	821 ± 27
1-adamantyl isobutyrate	3-hydroxy-1-adamantyl isobutyrate *trans*-4-hydroxy-1-adamantyl isobutyrate (~35)	1350 ± 22
2-adamantyl acetate	5-hydroxy-2-adamantyl acetate (~25)	877 ± 18
2-adamantyl isobutyrate	5-hydroxy-2-adamantyl isobutyrate (~40)	722 ± 10
1-adamantylamine	n.p	n.p
N-(1-adamantyl)acetamide	3-hydroxy-N-(1-adamantyl)acetamide (~3) 4-hydroxy-N-(1-adamantyl)acetamide (~15)	166 ± 9

Chapter 5

5. The Efficient Oxidation of Hydrophobic Aromatic Substrates Using Site-directed Mutagenesis of CYP101B1

5.1. Introduction

The CYP101B1 enzyme can bind and oxidise a broad range of substrates including monoterpenoids and adamantyl esters as well as hydrophobic aromatic compounds such as indole, phenylcyclohexane and *p*-cymene [175, 182, 233]. As CYP101B1 is able to oxidise certain aromatic hydrocarbons, it could, therefore, have applications as a biocatalyst for their oxidation [175, 233]. Compared to the norisoprenoids and ester substrates, most of the hydrophobic substrates induce a smaller heme spin-state shift when added to CYP101B1 and bind with a lower affinity. They are also oxidised at slower product formation rates. Protein engineering of CYP101B1 could improve the activity and selectivity of this enzyme for the hydrophobic aromatic substrates.

5.2. Protein Engineering

The crystal structure of CYP101B1 has not been solved, but structures of the related P450s CYP101C1, CYP101D1 and CYP101D2 from the same bacterium have been reported [47, 143, 175, 246, 247]. One of the best-characterised cytochrome P450 enzymes CYP101A1 ($P450_{cam}$) oxidised (*R*)-camphor to 5-*exo*-hydroxycamphor with 100% stereoselectivity [248, 249]. CYP101D1 and CYP101D2, which belong to the same family as CYP101A1, also selectively oxidise camphor to 5-*exo*-hydroxycamphor [49, 143, 250]. The tyrosine residue (Y96) of CYP101A1 has been shown to be important in determining the substrate specificity [144, 251-253]. This residue is also conserved in CYP101D1 and CYP101D2 [143]. These CYP101 family members were used as model systems to facilitate the residue to target for mutagenesis [72, 144, 254-258]. The analysis of the camphor bound crystal structures of CYP101A1 (PDB: 2CPP) and CYP101D1 (PDB: 3LXI) demonstrated that in both a tyrosine residue forms a hydrogen bond with the carbonyl group of the camphor molecule (Figure 5. 1) [248, 250]. This helps to hold the substrate in a suitable

position for selective hydroxylation [248, 250]. Modification of the active site, by replacing the tyrosine residue with phenylalanine and alanine enhanced the affinity of CYP101A1 and CYP101D2 for hydrophobic substrates such as naphthalene, pyrene, styrene, phenylcyclohexane, cyclooctane, adamantane and 2-methylpentane [143, 144, 255, 259-261]. This residue, therefore, plays a role in determining the substrate range of these P450 enzymes [143, 255].

The active site of CYP101B1 was modelled by Swiss-Model using the camphor-bound CYP101D1 (PDB ID: 3LXI) crystal structure (Figure 5. 1) [50, 262, 263, 264, 265]. Aligning the amino acid sequences of the CYP101B1, CYP101D1, CYP101D2, CYP101A1 enzymes show that the tyrosine (Y) 96 residue of CYP101A1, is conserved in CYP101D1 and CYP101D2 but not in CYP101B1 [47, 49, 175, 250]. In CYP101B1 a histidine residue aligns sequentially with Y96 of CYP101A1. It was hypothesised that H85 of CYP101B1 might play a similar role interacting with norisoprenoid and ester substrates potentially through the substrate carbonyl group [175, 176]. Replacing H85 with a hydrophobic residue, such as phenylalanine, could, therefore, improve the affinity of CYP101B1 towards hydrophobic substrates.

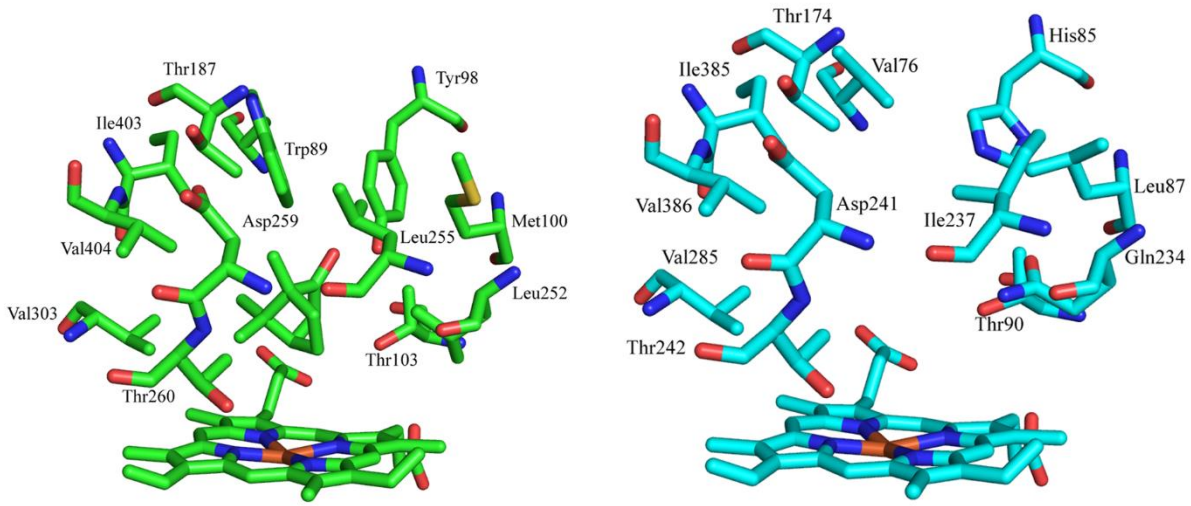

Figure 5. 1 (Left) The crystal structure of camphor-bound CYP101D1 (PDB 3LXI) highlighting the hydrogen bond interaction between the camphor carbonyl and the conserved tyrosine residue (Y98). This is the equivalent residue to Y96 in CYP101A1. CYP101D1 was the closest homologue of CYP101B1 in the Protein Data Bank PDB. **(Right)** The modelled structure of CYP101B1 created by Swiss-Model highlighting the potential location of histidine 85 (H85) [50, 264, 265]. The modelled structure of CYP101B1 was designed by Joel Lee [264].

5.3. Results

5.3.1 The oxidation of alkylbenzenes by CYP101B1 and the H85F variant

CYP101B1 has a high affinity for *β*-ionone (K_d = 0.23 ± 0.1 µM, ≥95% spin state shift), which it oxidises into two products 3-hydroxy-*β*-ionone and 4-hydroxy-*β*-ionone with a ratio 90:10 (Table 5. 1, Figure 5. 2 and Figure 5. 3) [175]. The NADH consumption rate, product formation activity and coupling efficiency were high, indicating that *β*-ionone might be closely related to the natural substrate for wild-type CYP101B1 [48, 49, 250]. When *β*-ionone was tested with the H85F variant of CYP101B1 it induced a 50% high spin (HS) state shift and bound less tightly, K_d = 5.8 ± 2 µM compared to WT CYP101B1 (Table 5. 1, Figure 5. 2 and Figure 5. 3) [233].

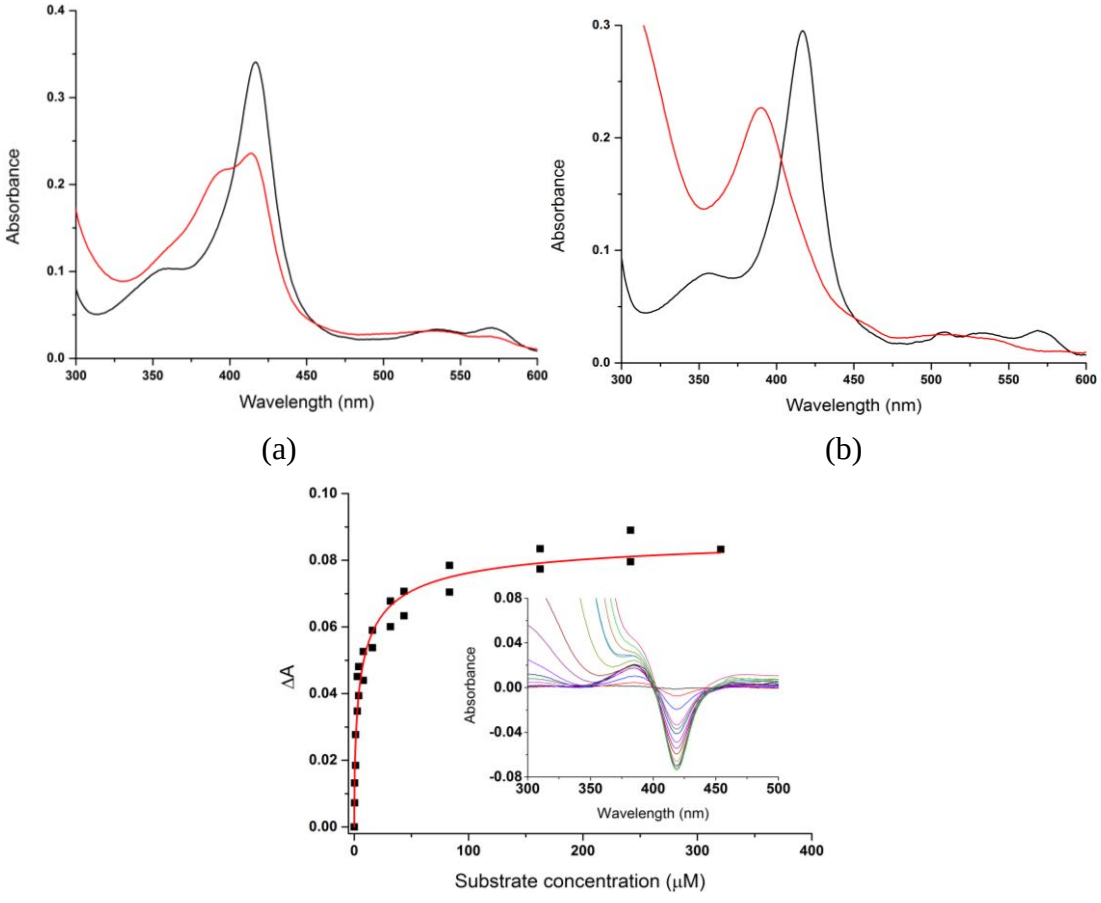

Figure 5. 2 Spin-state shifts (red) of **(a)** H85F CYP101B1 and **(b)** WT CYP101B1 after addition of *β*-ionone [233]. **(c)** Dissociation constant analysis with *β*-ionone (1.27 µM H85F CYP101B1/K_d 5.8 µM). The difference between A_{420} and A_{600} nm was used due to the interference of absorbance of the substrate with the analysis below 400 nm. The concentration of enzyme used in the binding assay and the dissociation constant (K_d) are provided in brackets.

The weaker binding and lower spin-state shift suggest that the interactions of this substrate in the binding pocket of H85F CYP101B1 are less favourable. The oxidation activity was also reduced, with a slower NADH oxidation activity (412 versus 1600 nmol.nmol-CYP^{-1}.min^{-1}; henceforth abbreviated to min^{-1}), product formation rate (140 min^{-1} versus 1010 min^{-1}) and lower coupling efficiency (34% versus 63%; Table 5. 1).

Table 5. 1. Substrate binding, turnover and coupling efficiency data for CYP101B1 (WT and the H85F variant) with *β*-ionone and *p*-cymene. The *in vitro* turnover activities were measured using a ArR:Arx:CYP101B1 concentration ratio of 1:10:1 (0.5 μM CYP enzyme, 50 mM Tris, pH 7.4). N is the NADH oxidation rate, PFR the product formation rate and C is the coupling efficiency, which is the percentage of NADH utilised for the formation of products. The data are reported as mean ± S.D. (n = 3) and rates are given in nmol.nmol-CYP^{-1}.min^{-1}. - not measured or not able to be determined accurately.

substrate	CYP101B1	%HS heme	K_d (μM)	N (min^{-1})	PFR (min^{-1})	C %
β-ionone	WT [175]	≥95%	0.23 ± 0.1	1600 ± 100	1010 ± 60	63
	H85F	**50%**	**5.8 ± 2**	**412 ± 36**	**140 ± 11**	**34**
p-cymene	WT [175]	5%	-	197 ± 27	25 ± 6	13
	H85F	**10%**	**-**	**272 ± 11**	**95 ± 7**	**35**

The *in vitro* oxidation of *β*-ionone by the H85F mutant was found to generate the same two metabolites as WT CYP101B1. These were identified using GC-MS coelution experiment with the turnover products of WT CYP101B1. However, the selectivity of oxidation was altered. While the WT enzyme favoured the generation of the 3-hydroxy metabolite, the H85F mutant enzyme catalysed hydroxylation mainly at the more reactive allylic C-H bond to form 4-hydroxy-*β*-ionone (Figure 5. 3). The ratio of the two products 3-hydroxy to 4-hydroxy-*β*-ionone was observed 9:1 with WT CYP101B1, but in the case of H85F variant of CYP101B1, this was changed to 1:9 (Figure 5. 3).

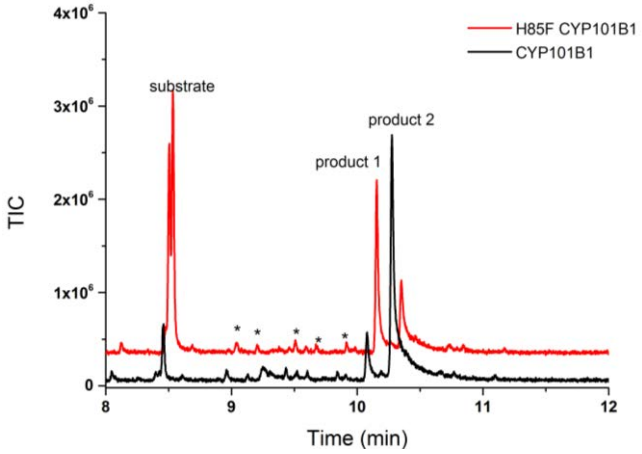

(a)

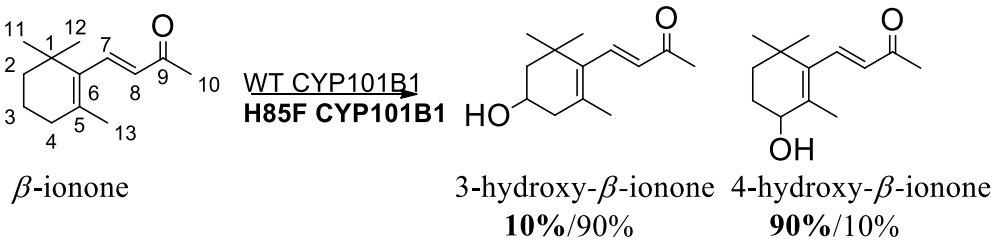

β-ionone 3-hydroxy-*β*-ionone **10%**/90% 4-hydroxy-*β*-ionone **90%**/10%

(b)

Figure 5. 3 (a) GC-MS analysis of the turnover of *β*-ionone by H85F CYP101B1 (red) and CYP101B1 (black). *β*-Ionone (RT 8.5 min), products were identified as 4-hydroxy-*β*-ionone (10.2 min, product 1) and 3-hydroxy-*β*-ionone (RT 10.3 min, product 2) by co-elution with the WT CYP101B1 turnovers [233]. The chromatogram (H85F) was offset along the x and y-axes for clarity. **(b)** The products generated from the CYP101B1 and H85F CYP101B1 turnovers with *β*-ionone. The product distributions are given as percentages (H85F variant in bold) [175, 265, 266].

WT CYP101B1 can oxidise small aromatic compounds like *p*-cymene and indole [175]. *p*-Cymene induced only 5% heme spin-state shift in WT CYP101B1. The NADH oxidation rate, 197 min^{-1}, and the product formation rate, 25 min^{-1} were low (Table 5. 1). *p*-Cymene only induced a 10% spin-state shift with H85F CYP101B1. The NADH turnover frequency increased to 272 min^{-1}, and the product formation rate (95 ± 7 min^{-1}) was nearly 4-fold faster than that of wild-type enzyme (Table 5. 1). The coupling efficiency of the *p*-cymene turnover was more significant for the H85F CYP101B1 variant than the WT enzyme (35% versus 13%). *In vitro* oxidation of this substrate by the mutant enzyme generated two products in a similar ratio to the WT enzyme (Figure 5. 4 and Figure 5. 3). The minor metabolite was *p*-*α,α*-trimethylbenzyl alcohol alongside with 4-isopropylbenzyl alcohol as the primary metabolite.

These metabolites were confirmed by coeluting the turnover products of CYP101B1 which were previously identified via coelution experiments in GC-MS with authentic standards (Figure 5. 3 and Figure 5. 4) [175].

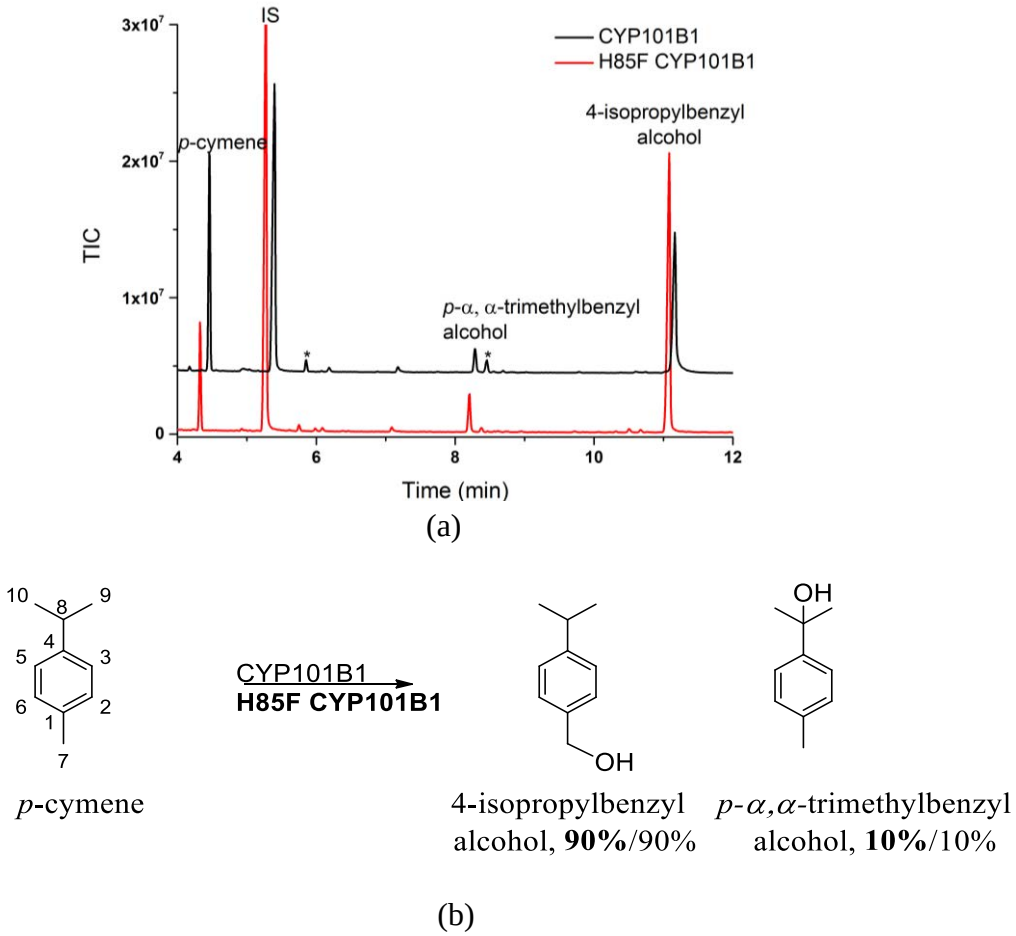

Figure 5. 4 (a) GC-MS analysis of the turnover of *p*-cymene by H85F CYP101B1 (red) and CYP101B1 (black). *p*-Cymene (RT 4.4 min) and the products; *p*-*α*,*α*-trimethylbenzyl alcohol (8.2 min) and 4-isopropylbenzyl alcohol (RT 11.1 min). The chromatogram (CYP101B1) was offset along the x and y-axes for clarity. Impurities are labelled (*). **(b)** The products generated from the CYP101B1 and H85F CYP101B1 turnovers with *p*-cymene. The product distributions are given as percentages (H85F variant in bold) [175, 265, 266].

A range of similarly sized alkylbenzene substrates such as toluene, *o*-, *m*- and *p*-xylene were then screened with H85F and WT variants (Figure 5. 5). The effect of size of substrates and position of the alkyl substituent on binding and activity parameters of enzymes were investigated using isobutylbenzene, *n*-propylbenzene, isopropylbenzene, indane and 2- and 3-

ethyltoluene. Styrene, 2-methylstyrene and *β*-methylstyrene were used to examine the effect of the planar and more reactive vinyl substituent on the activity of both variants (Figure 5. 5).

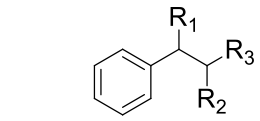

R_3 = Me, R_1 & R_2 = H, *n*-propylbenzene
R_1 = H, R_2 & R_3 = Me, isobutylbenzene
R_1 = Me, R_2 & R_3 = H, isopropylbenzene

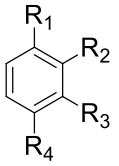

R_1 = Me, R_2, R_3 & R_4 = H, toluene
R_1 & R_2 = Me, R_3 & R_4 = H, *o*-xylene
R_1 & R_3 = Me, R_2 & R_4 = H, *m*-xylene
R_1 & R_4 = Me, R_2 & R_3 = H, *p*-xylene
R_1, R_2 & R_4 = H, R_3 = Et, ethylbenzene
R_1 = Me, R_3 & R_4 = H, R_2 = Et, 2-ethyltoluene
R_2 & R_4 = H, R_1 = Me, R_3 = Et, 3-ethyltoluene

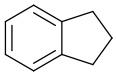

indane

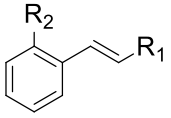

R_1 = H, R_2 = H, styrene
R_1 = Me, R_2 = H, *β*-methylstyrene
R_1 = H, R_2 = Me, 2-methylstyrene

Figure 5. 5 The substrates screened with WT CYP101B1 and H85F CYP101B1 [265].

Compared to *p*-cymene, a smaller heme spin-state shift (5%) to both the wild-type and mutant enzyme was observed with toluene (Figure 5. 6). The NADH oxidation (69 ± 7 min^{-1} versus 40 ± 6 min^{-1}) and product formation (3 min^{-1} versus 1 min^{-1}) rates were slower with the WT and mutant enzyme (Table 5. 2). The smaller shift and lower oxidation activity observed with toluene, which can be related to *p*-cymene, by removal of the isopropyl group from the latter, suggest that binding of the smaller substrate is suboptimal. The coupling efficiency was also minimal, 4% for the mutant enzyme and 2% for WT CYP101B1. *In vitro* oxidation of toluene by WT and H85F mutant variants generated a single metabolite. The mass spectrum analysis revealed that it was a hydroxylation product (m^+/z = 108.10; Figure 5. 7 and Figure D. 1). The metabolite was identified as benzyl alcohol by coelution experiment in GC-MS with an authentic standard (Figure 5. 7 and Figure 5. 9).

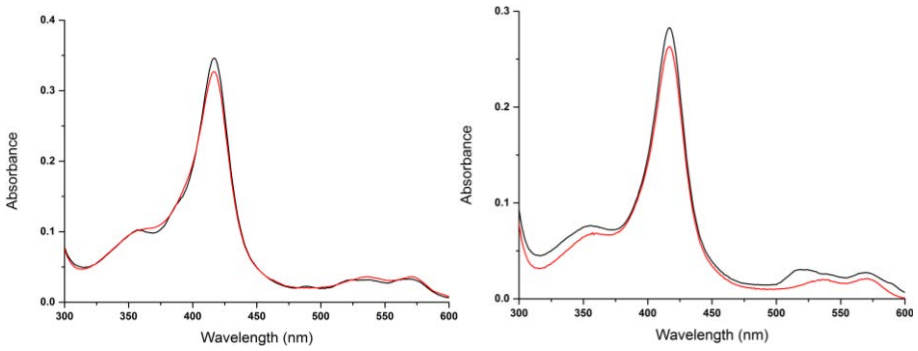

(a) (b)

Figure 5. 6 Spin-state shifts (red) of **(a)** H85F CYP101B1 and **(b)** WT CYP101B1 after addition of toluene.

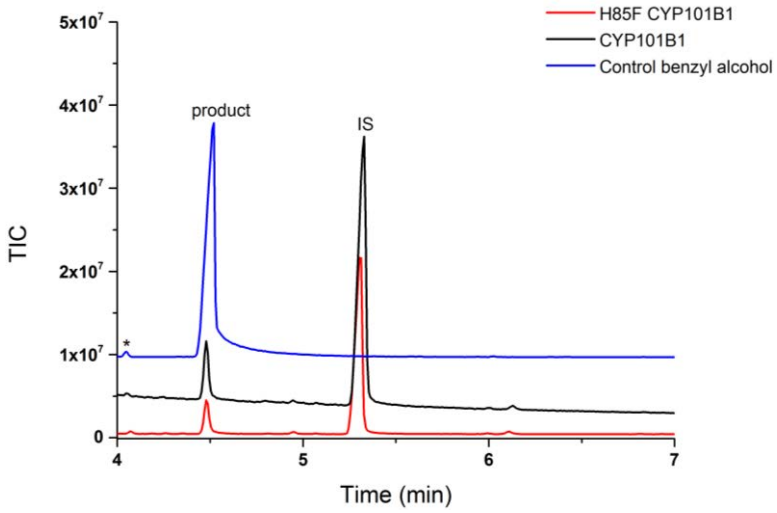

Figure 5. 7 GC-MS analyses of the turnovers of toluene by H85F CYP101B1 (red) and CYP101B1 (black). Toluene (RT 1.8 min, not shown) and the product; benzyl alcohol (4.5 min).

To assess the effect of altering the position of the methyl group on binding and activity, the isomers of xylene were investigated. Addition of *o*-, *m*- and *p*-xylene to CYP101B1 induced spin-state shifts of ≤5% which are similar to *p*-cymene and toluene (Figure 5. 8). These substrates effected 10 to 15% heme spin-state shifts in H85F CYP101B1 (Table 5. 2 and Figure 5. 8). The rates of NADH oxidation of H85F and WT enzymes with *o*-xylene were 286 ± 4 min^{-1} and 55 ± 14 min^{-1}, respectively (Table 5. 2). These values were significantly higher than that observed with *m*- and *p*-xylene (Table 5. 2). In all instances, H85F showed improved activity compared to the WT enzyme.

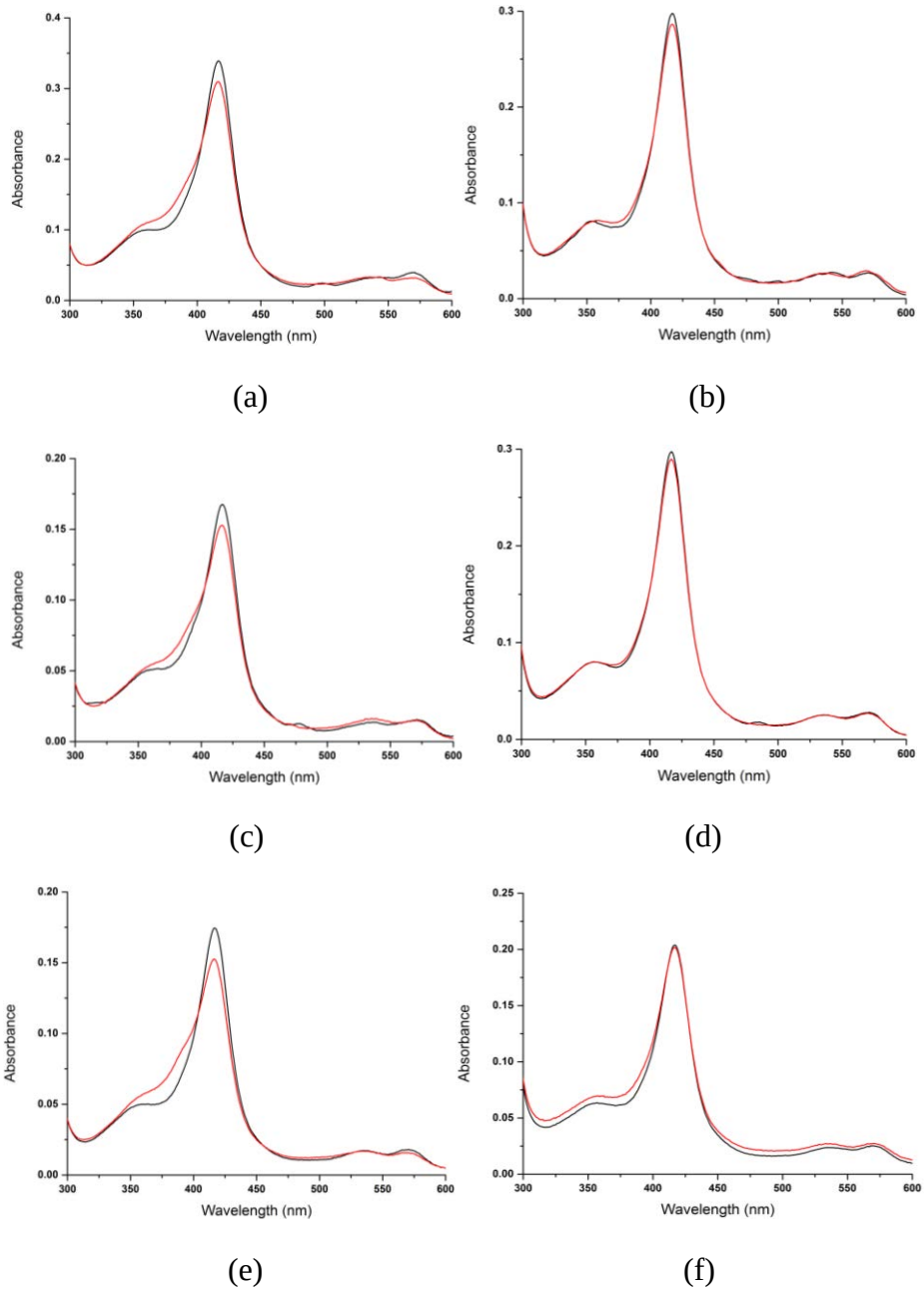

Figure 5. 8 Spin-state shifts (red) of H85F CYP101B1 after addition of **(a)** *p*-xylene, **(c)** *m*-xylene **(e)** *o*-xylene, and spin-state shifts (red) of WT CYP101B1 after addition of **(b)** *p*-xylene, **(d)** *m*-xylene and (f) *o*-xylene.

The product formation rates observed with H85F mutant for *o*-xylene (70 ± 3 min^{-1}), *m*-xylene (21 ± 7 min^{-1}) and *p*-xylene (13 ± 5 min^{-1}) were greater than the WT (Table 5. 2). Poor coupling of the redox equivalents to product formation (≤4%) resulted in low levels of metabolites in the turnovers of all the xylenes with WT CYP101B1 (Table 5. 2). H85F mutant system

displayed higher coupling efficiencies with *o*-xylene (25% versus 4%), *m*-xylene (20% versus 4%) and *p*-xylene (12% versus 3%) than the WT (Table 5. 2).

Table 5. 2. Substrate binding, turnover and coupling efficiency data for CYP101B1 (WT and the H85F variant) with toluene, *o*-, *m*- and *p*-xylene. The turnover activities were measured as described in Table 5. 1. The data are reported as mean ± S.D. (n = 3) and rates are given in nmol.nmol-CYP^{-1}.min^{-1}.

substrate	CYP101B1	%HS heme	N (min^{-1})	PFR (min^{-1})	C %
toluene	WT	5%	40 ± 6	1 ± 1	2
	H85F	**5%**	**69 ± 7**	**3 ± 1**	**4**
o-xylene	WT	≤5%	55 ± 14	3 ± 1	4
	H85F	**15%**	**286 ± 4**	**70 ± 3**	**25**
m- xylene	WT	≤5%	5 ± 3	2 ± 3	4
	H85F	**10%**	**109 ± 8**	**21 ± 7**	**20**
p- xylene	WT	≤5%	42 ± 5	1.2 ± 3	3
	H85F	**10%**	**109 ± 10**	**13 ± 5**	**12**

Both the WT enzyme and the H85F variant selectively oxidised these substrates into a single metabolite with the hydroxylation occurring at a benzylic C-H bond in all cases (Figure 5. 9 and Figure 5. 10). The products were identified as 2-methylbenzyl alcohol, 3-methylbenzyl alcohol and 4-methylbenzyl alcohol after coeluting with authentic standards in GC-MS (Figure 5. 9 and Figure 5. 10). Mass spectra analyses also supported to these assignments (all mass; m^+/z= 122.1; Figure D. 1).

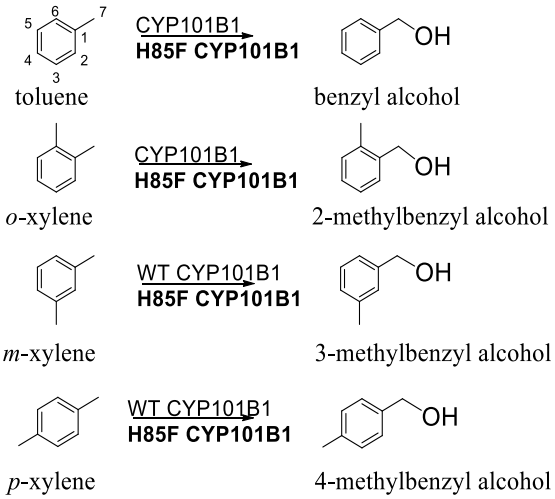

Figure 5. 9 The products identified from the WT CYP101B1 and H85F CYP101B1 turnovers with toluene, *o*-, *m*- and *p*-xylene [265].

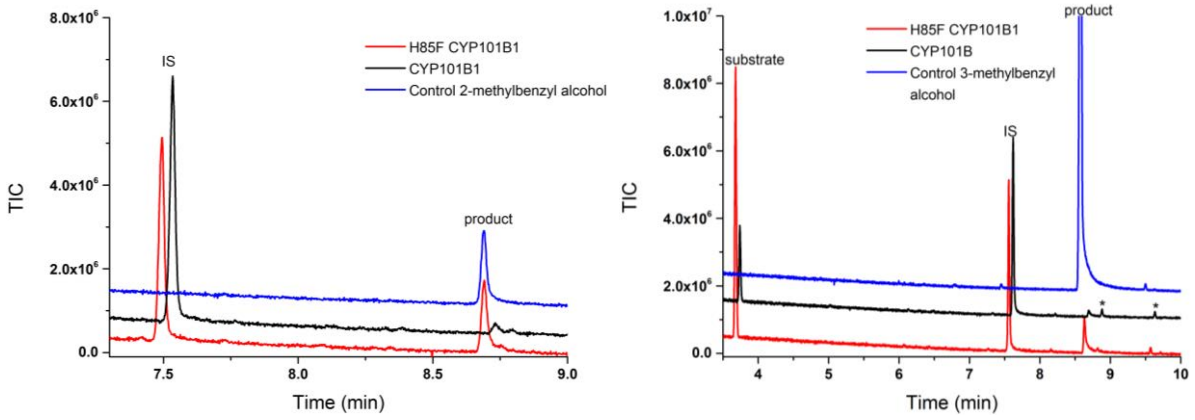

(a)

(b)

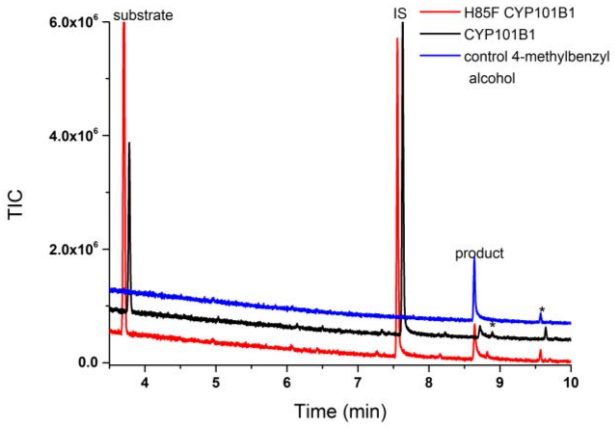

(c)

Figure 5. 10 (a) GC-MS analysis of the turnover of *o*-xylene by H85F CYP101B1 (red) and CYP101B1 (black). *o*-Xylene (RT 4.05 min, not shown) and the product; 2-methylbenzyl alcohol (8.7 min). **(b)** GC-MS analysis of the turnover of *m*-xylene by H85F CYP101B1 (red) and CYP101B1 (black). *m*-Xylene (RT 3.65 min) and the product; 3-methylbenzyl alcohol (8.6 min). **(c)** GC-MS analysis of the turnover of *p*-xylene by H85F CYP101B1 (red) and CYP101B1 (black). *p*-Xylene (RT 3.75 min) and the product; 4-methylbenzyl alcohol (8.8 min). The chromatograms (CYP101B1, a, b, c) were offset along the x and y-axes for clarity Impurities are marked (*).

The spin-state shift of the H85F mutant upon addition of the ethylbenzene was 30% versus ≤5% with the WT enzyme (Figure 5. 11). Ethylbenzene also bound more tightly to the H85F variant (K_d = 2.5 µM versus 520 µM; Figure 5. 11). The rate of NADH oxidation by H85F CYP101B1 upon the addition of ethylbenzene was 4-fold faster than that of WT CYP101B1 (201 ± 22 min^{-1} versus 47 ± 2 min^{-1}; Table 5. 3). The product formation rate was also greater for the mutant (43 ± 4 min^{-1}) due to a higher coupling efficiency than the WT system (21% versus 13%; Table 5. 3). Both variants oxidised ethylbenzene into a major single metabolite (Figure 5. 12). This was confirmed as 1-phenylethanol by coelution experiment in GC-MS with an authentic standard and mass spectrum analysis (m^+/z = 122.05; Figure 5. 12, Figure 5. 16, and Figure D. 1). Chiral GC analysis of the *in vitro* turnovers displayed a mixture of enantiomers; (*S*)-(-)-1-phenylethanol and (*R*)-(+)-1-phenylethanol in both turnovers (Figure 5. 12 and Figure 5. 16). The distribution of the enantiomers with the WT enzyme was 55 to 45 % (excess (*S*)-(-)-1-phenylethanol), and the H85F variant also generated more (*S*)-(-)-1-phenylethanol (77%; Figure 5. 12 and Figure 5. 16).

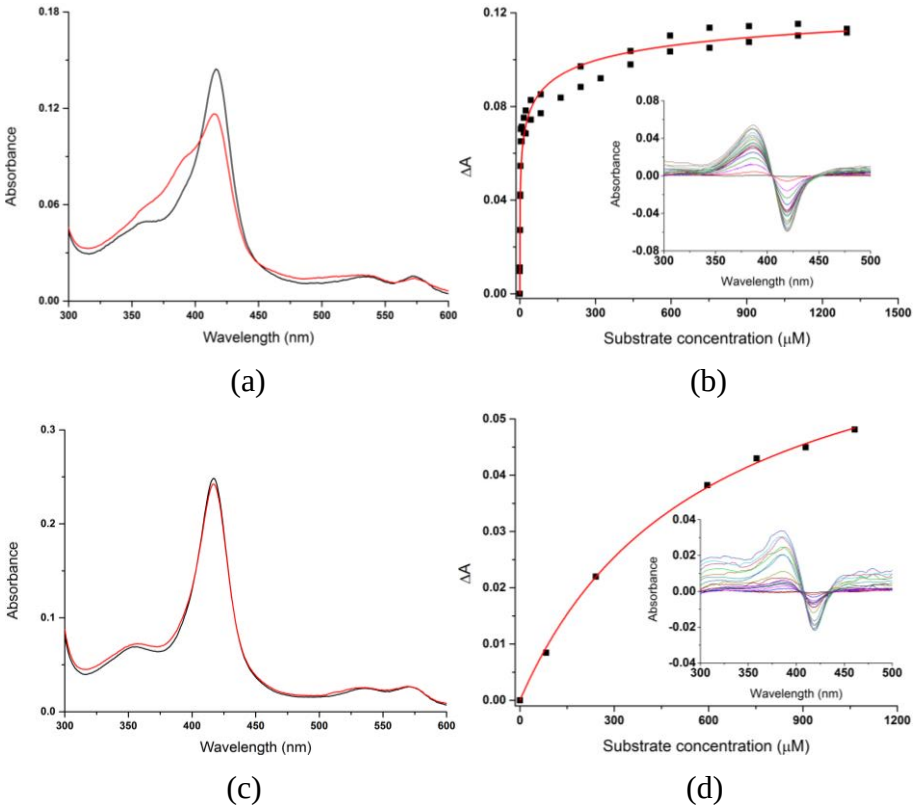

Figure 5. 11 Spin-state shifts (red) of **(a)** H85F CYP101B1 and **(c)** WT CYP101B1 after addition of ethylbenzene. The dissociation constant analysis of **(b)** H85F 1.56 µM/K_d 2.5 µM and **(d)** WT CYP101B1 1.31 µM/K_d 520 µM with ethylbenzene. The concentration of the enzyme used in the binding studies and the dissociation constants (K_d) are provided.

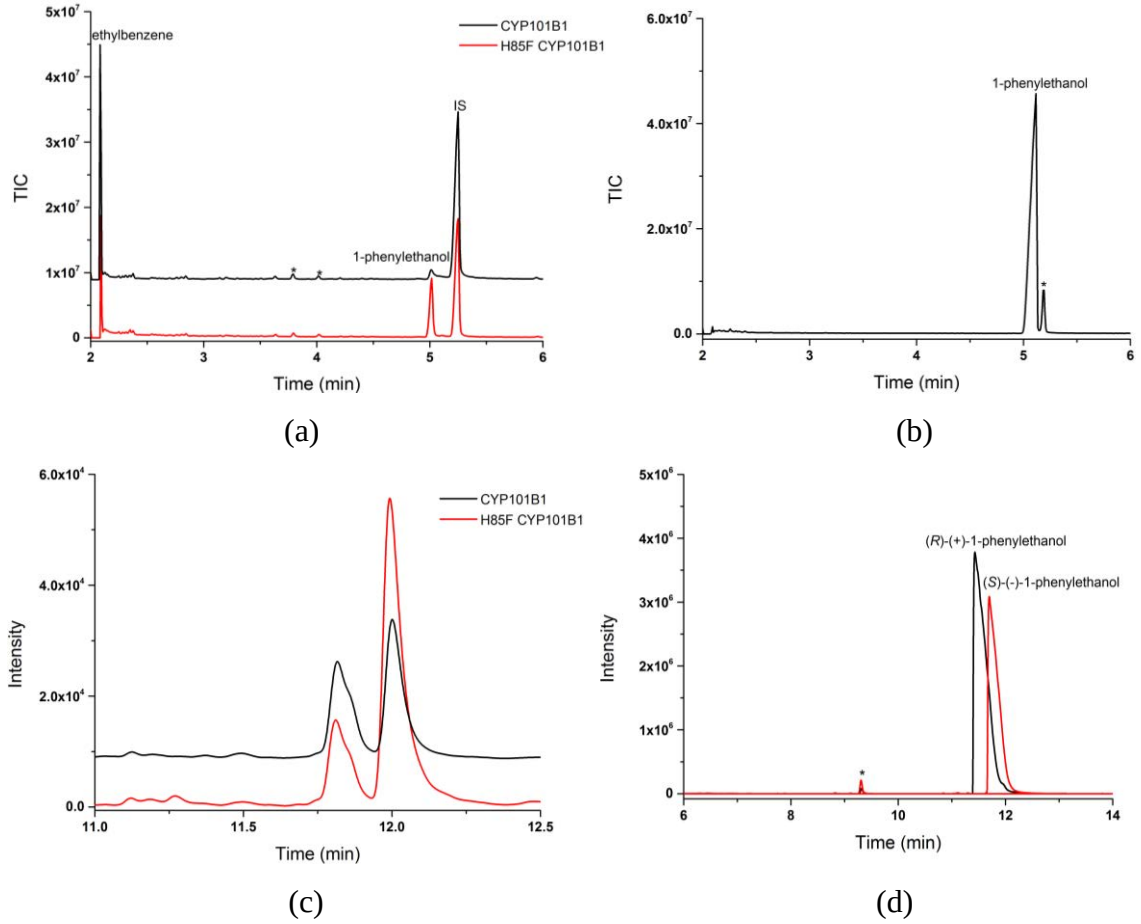

Figure 5. 12 (a) GC-MS analysis of the turnover of ethylbenzene by H85F CYP101B1 (red) and CYP101B1 (black). Ethylbenzene (RT 2.1 min) and the product; 1-phenylethanol (RT 5.05 min). **(b)** GC-MS control 1-phenylethanol (RT 5.05 min). **(c)** Chiral GC analysis of the turnover of ethylbenzene H85F CYP101B1 (red) and CYP101B1 (black); (*R*)-(+)-1-phenylethanol (RT 11.85 min) and (*S*)-(-)-1-phenylethanol (RT 12.0 min). **(d)** Chiral GC control of enantiomers (*R*)-(+)-1-phenylethanol (RT 11.85 min) and (*S*)-(-)-1-phenylethanol (RT 12.0 min). Impurities are labelled (*).

2-Ethytoluene altered the low heme spin-state to 30% high spin form upon addition to H85F CYP101B1. In comparison, it changed only 10% in the WT enzyme (Figure 5. 13). The NADH oxidation rate (496 min^{-1}) and product formation activity (262 min^{-1}) were also significantly faster for the mutant and the coupling efficiency was greater (53% versus 35%; Table 5. 3). Both the WT and H85F variants oxidised 2-ethyltoluene into one major metabolite (70% and 90%, respectively; m^+/z = 135.95) alongside two minor products (Figure 5. 14 and Figure D. 1). The major metabolite was generated using a whole-cell biotransformation system and identified after isolation as (2-ethylphenyl)methanol via NMR analysis (Figure 5. 15, Figure 5. 16, Figure D. 2-D. 3) [265]. The product was assigned as all the aromatic hydrogens and those of the ethyl group remained intact (Figure 5. 15). The peak at 4.74 ppm in the ^1H NMR ($CDCl_3$), indicated the hydroxylation occurred at the methyl group (Figure 5. 15 and Figure D. 2-D. 3). One of the minor metabolites 1-(2-methylphenyl)ethanol (m^+/z = 136.05), was identified by coelution with a standard in GC-MS (RT 7.9 min; Figure 5. 14). The other minor metabolite was assigned as 2-ethylbenzaldehyde (m^+/z = 136.10), based on its MS fragmentation pattern (RT 7.1 min; Figure 5. 14, Figure 5. 16 and Figure D. 1). Chiral GC analysis revealed a roughly equal mixture of (*S*)-1-(2-methylphenyl)ethanol and (*R*)-1-(2-methylphenyl)ethanol was generated by WT CYP101B1 (Figure 5.14 and Figure 5.16). The H85F mutant was more selective and gave a 70% of (*S*)-1-(2-methylphenyl)ethanol (Figure 5. 14 and Figure 5. 16) [265].

Table 5. 3 Substrate binding, turnover and coupling efficiency data for the turnovers of CYP101B1 (WT and the H85F variant) with ethylbenzene, 2- and 3-ethyltoluene. The turnover activities were measured as described in Table 5. 1. -not measured. The data are reported as mean ± S.D. (n = 3) and rates are given in nmol.nmol-CYP^{-1}.min^{-1}.

substrate	CYP101B1	%HS heme	K_d (μM)	N (min^{-1})	PFR (min^{-1})	C %
ethylbenzene	WT	≤5%	520 ± 70	47 ± 2	6 ± 6	13
	H85F	**30%**	**2.5 ± 1**	**201 ± 22**	**43 ± 4**	**21**
2-ethyltoluene	WT	10%	-	156 ± 7	55 ± 1	35
	H85F	**30%**	**-**	**496 ± 16**	**262 ± 15**	**53**
3-ethyltoluene	WT	≤5%	-	90 ± 13	15 ± 1	16
	H85F	**5%**	**-**	**228 ± 5**	**100 ± 3**	**44**

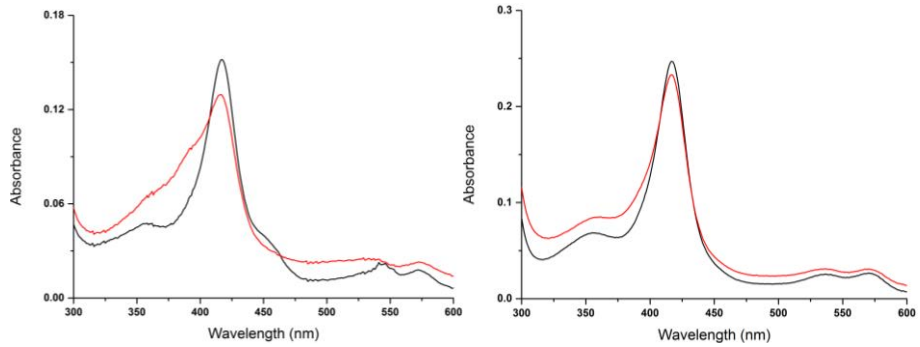

(a) (b)

Figure 5. 13 Spin-state shifts (red) of **(a)** H85F CYP101B1 and **(b)** WT CYP101B1 upon addition of 2-ethyltoluene.

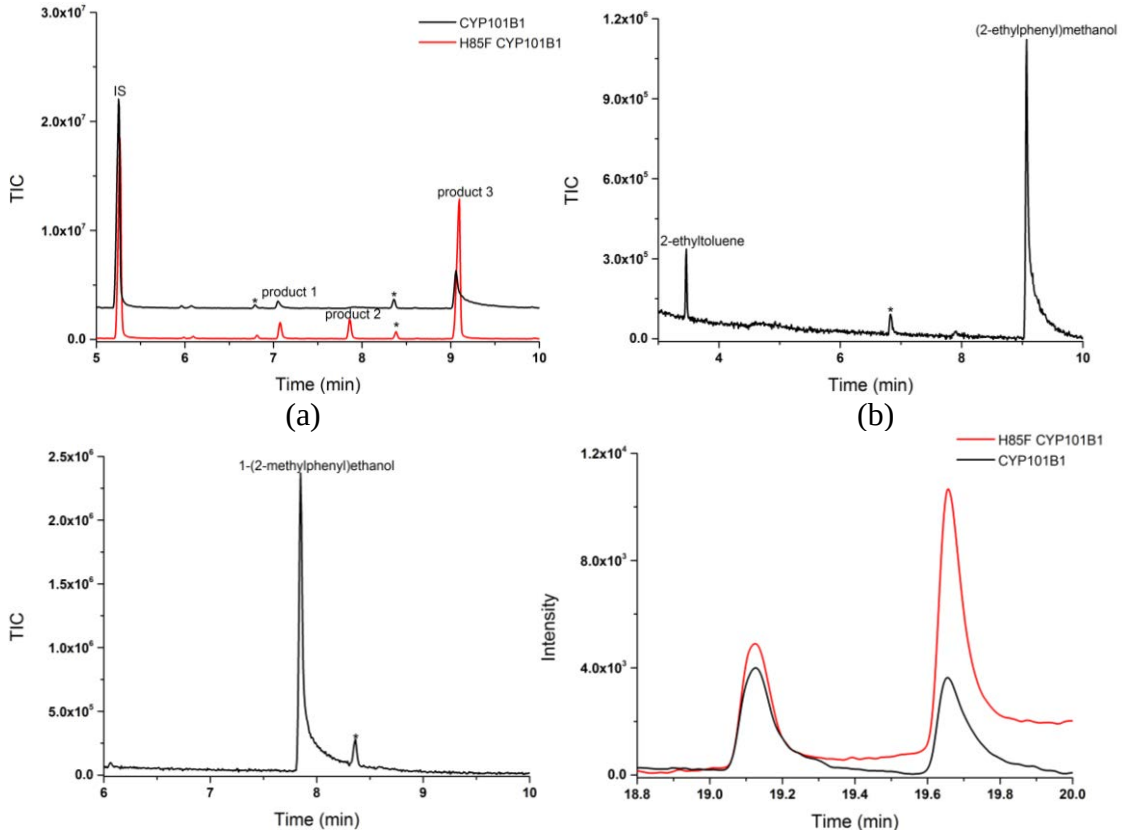

(a) (b) (c) (d)

Figure 5. 14 (a) GC-MS analyses of the turnovers of 2-ethyltoluene by H85F CYP101B1 (red) and CYP101B1 (black). The products 2-ethylbenzaldehyde (RT 7.1 min, product 1), 1-(2-methylphenyl)ethanol (RT 7.9 min, product 2) and (2-ethylphenyl)methanol (RT 9.1 min, product 3). **(b)** GC-MS analysis of whole-cell turnover of 2-ethyltoluene with WT CYP101B1. 2-Ethyltoluene (RT 3.5 min) and the only product detected was (2-ethylphenyl)methanol (RT 9.1 min). **(c)** GC-MS control 1-(2-methylphenyl)ethanol (RT 7.9 min). **(d)** Chiral GC analyses of the *in vitro* turnovers of WT and mutant CYP101B1. A mixture of enantiomers was observed; (*R*)-(+)-1-(2-methylphenyl)ethanol (RT 19.1 min) and (*S*)-(-)-1-(2-methylphenyl)ethanol (RT 19.6 min) [265]. Impurities are labelled (*).

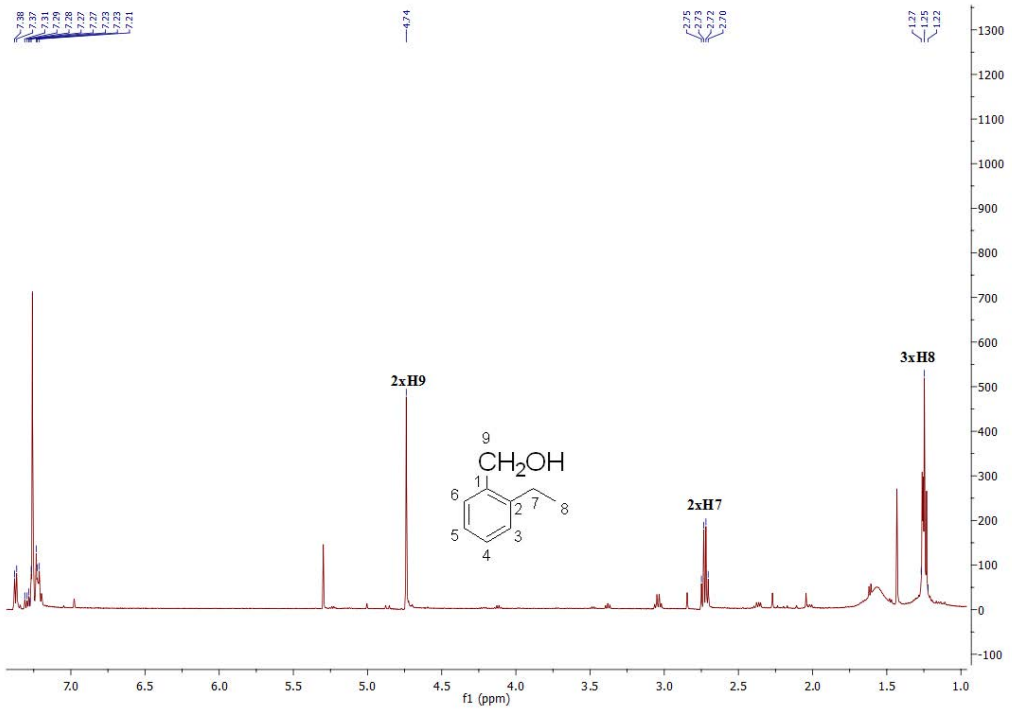

Figure 5. 15 ^{1}H NMR of (2-ethylphenyl)methanol ($CDCl_3$) [265]. Full data are in Appendix D (Figure D. 2-D. 3). There is a small amount of impurity present in the NMR sample.

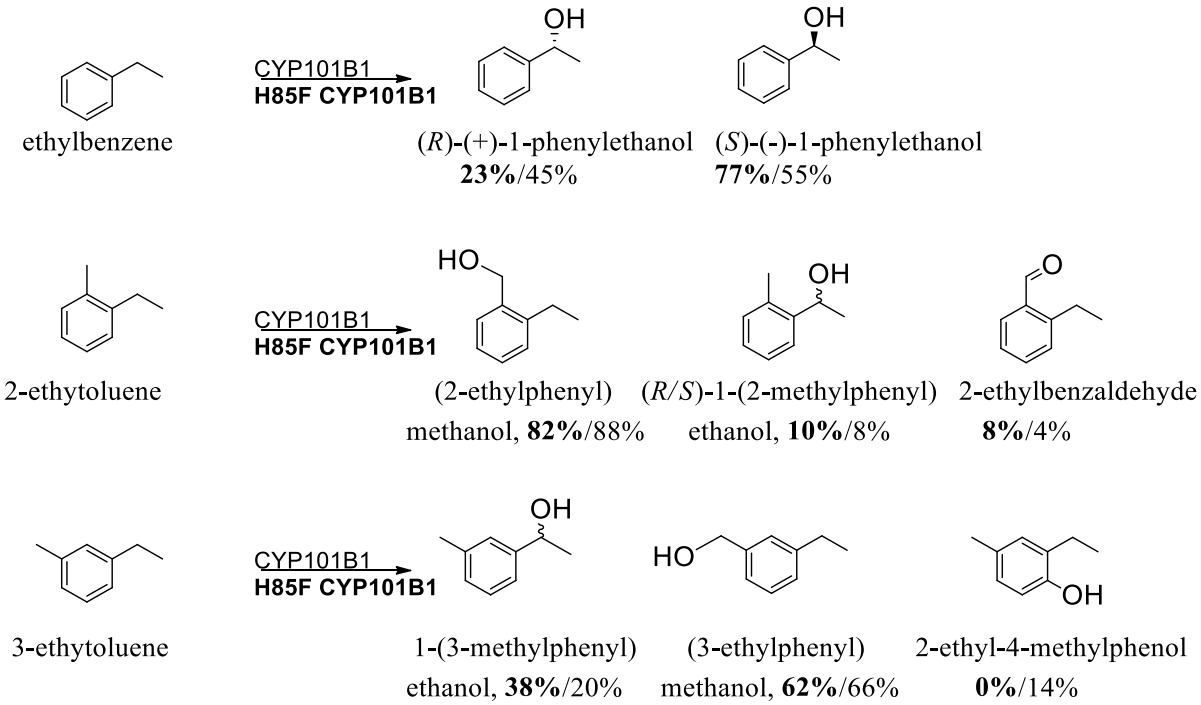

Figure 5. 16 The products identified from the CYP101B1 and H85F CYP101B1 turnovers of ethylbenzene, 2-ethyltoluene and 3-ethyltoluene [265, 272]. The product distributions are given as percentages (H85F variant in bold).

The addition of 3-ethyltoluene induced a ≤5% spin-state to the high spin form in H85F and WT enzyme (Figure 5. 17). The NADH oxidation (228 ± 5 min^{-1}) and product formation rates (100 ± 3 min^{-1}) for the H85F variant with 3-ethyltoluene were slower when compared with 2-ethyltoluene but still superior these of WT CYP101B1 (90 ± 13 min^{-1} and 15 ± 1 min^{-1}; Table 5. 3).

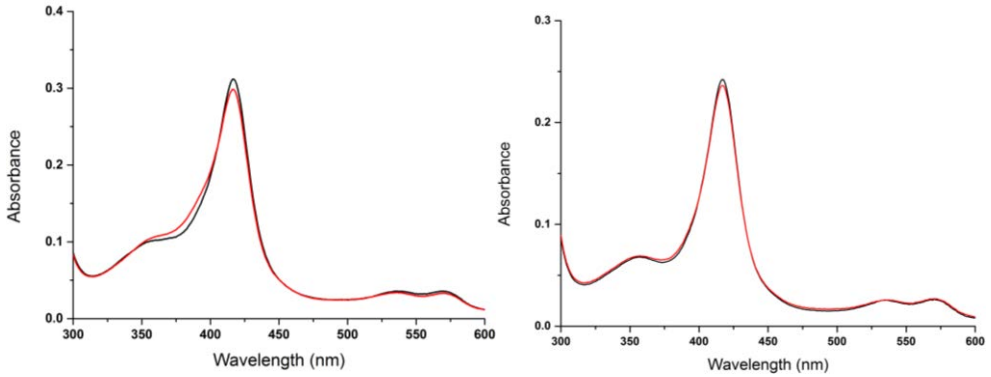

(a) (b)

Figure 5. 17 Spin-state shifts (red) of **(a)** H85F CYP101B1 and **(b)** WT CYP101B1 upon addition of 3-ethyltoluene.

The coupling efficiency was nearly 3-fold higher for the H85F variant (44%) than the WT enzyme (16%) with 3-ethyltoluene. Three metabolites were detected from the oxidation of 3-ethyltoluene by WT CYP101B1, and two products arose from the H85F mutant oxidation reactions (Figure 5. 18). These metabolites were generated by whole-cell oxidation and purified by silica column chromatography. These were characterised via analysis of their MS, NMR or coelution experiments (Figure 5. 18 and Figure 5. 16). The two products were common in both turnovers and characterised as 1-(3-methylphenyl)ethanol and (3-ethylphenyl)methanol (Based on their NMR and mass spectrum analysis; Figure 5. 16, Figure 5. 19, Figure D. 1 and Figure D. 4) [267]. The latter was formed in excess (more than 60%) in both cases (Figure 5. 16 and Figure 5. 18). The additional product found in the WT turnover (around 14% of total product) was assigned as 2-ethyl-4-methylphenol using its NMR and mass spectrum (m^+/z = 136.05; Figure 5. 16, Figure 5. 19, Figure D. 1 and Figure D. 5) [267]. Chiral GC analysis could not separate the enantiomers of 1-(3-methylphenyl)ethanol.

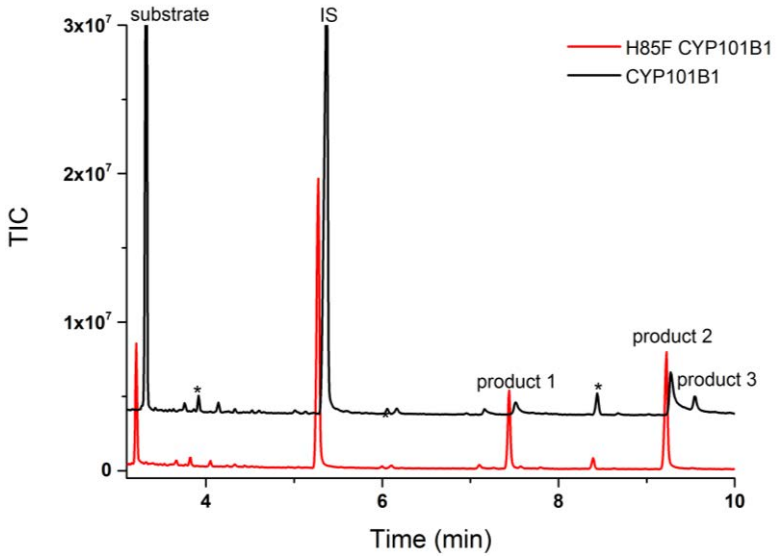

(a)

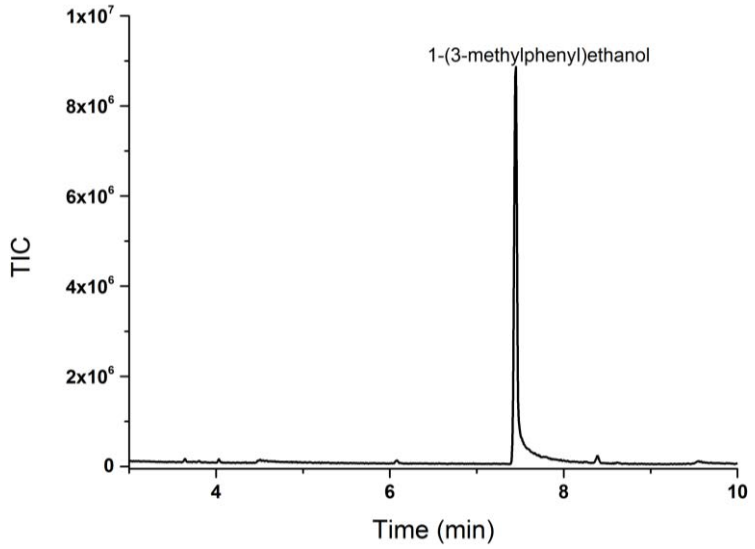

(b)

Figure 5. 18 (a) GC-MS analyses of the turnovers of 3-ethyltoluene by H85F CYP101B1 (red) and CYP101B1 (black). 3-Ethyltoluene (RT 3.48 min) and the product 1-(3-methylphenyl)ethanol (RT 7.45 min, product 1), (3-ethylphenyl)methanol (RT 9.25 min, product 2) and 2-ethyl-4-methylphenol (RT 9.45 min, product 3). **(b)** GC-MS control of 1-(3-methylphenyl)ethanol (RT 7.45 min). The chromatogram (CYP101B1) was offset along the x and y-axes for clarity. Impurities are labelled (*).

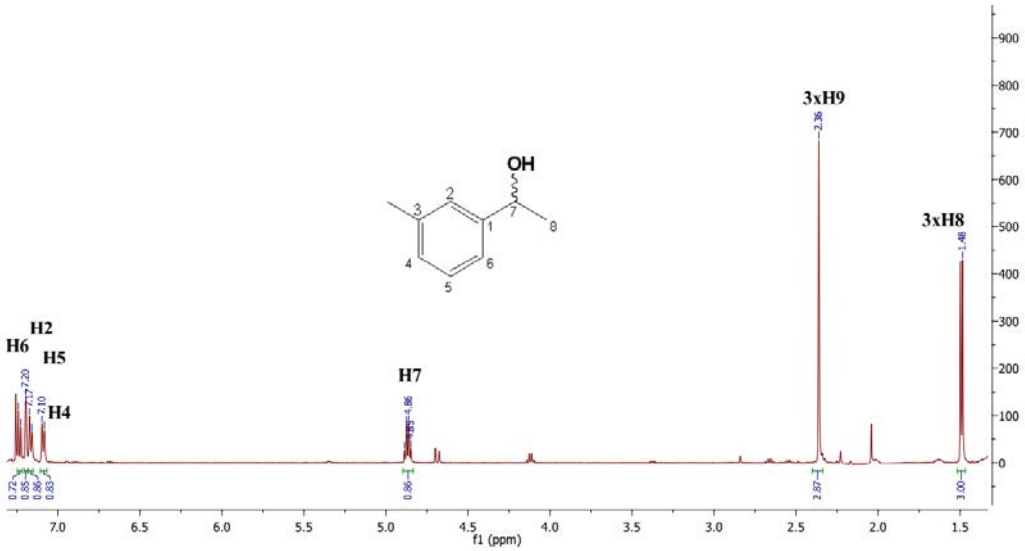

(a)

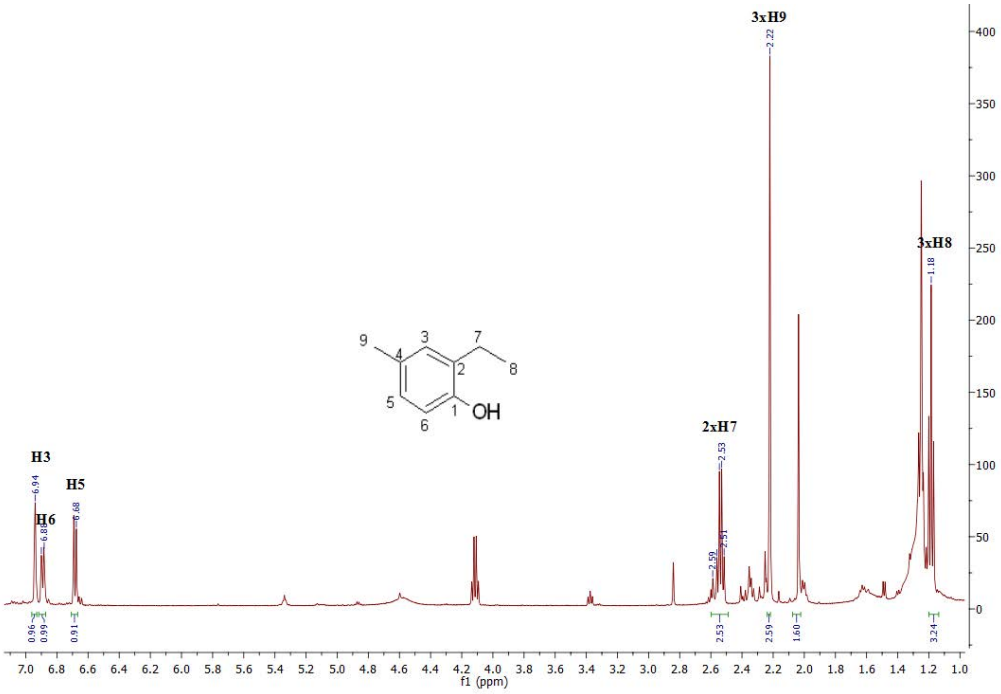

(b)

Figure 5. 19 (a) ^{1}H NMR of 1-(3-methylphenyl)ethanol. The product was assigned due to the characteristic quartet peak at 4.87 ppm, and all the benzylic and methyl protons are intact [267]. **(b)** ^{1}H NMR of 2-ethyl-4-methylphenol. The metabolite was characterised as all the proton peaks of the methyl and ethyl groups were present. The product was confirmed as 2-ethyl-4-methylphenol by comparing the NMR spectrum with the ^{1}H NMR reported in the literature [267]. There is a small amount of impurity present in the NMR sample of 2-ethyl-4-methylphenol. Full data are provided in Appendix D (Figure D. 4-D. 5).

n-Propylbenzene induced a moderate spin-state shift (30%) but showed tight binding (K_d = 0.6 ± 0.1 µM) to the H85F mutant enzyme (Figure 5. 20 and Table 5. 4). This substrate induced only a 5% spin-state shift in WT enzyme and the high dissociation constant of WT CYP101B1 (K_d = 410 ± 70 µM) indicated significantly weaker binding.

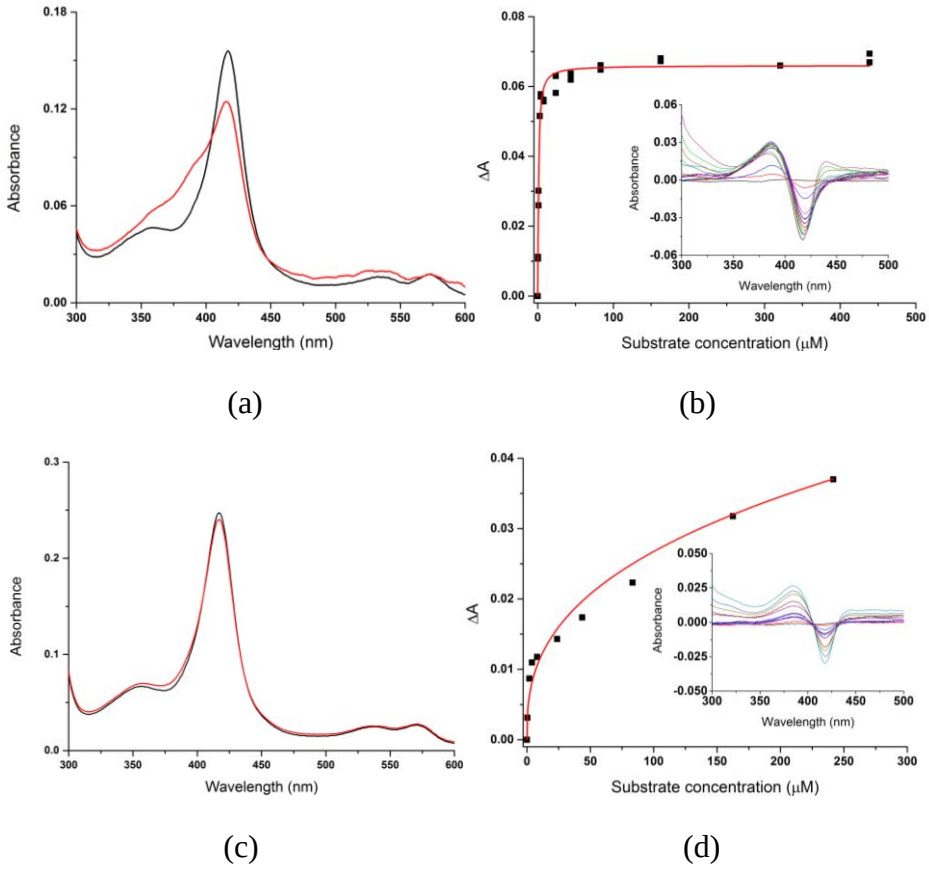

Figure 5. 20 Spin-state shifts (red) of **(a)** H85F CYP101B1 and **(c)** WT CYP101B1 after addition of *n*-propylbenzene. The dissociation constant analysis of **(b)** H85F CYP101B1 1.40 µM/K_d 0.6 µM and **(d)** WT CYP101B1 1.31 µM/K_d 410 µM. The concentration of the enzyme used in the binding assays and the dissociation constant (K_d) are provided.

The H85F mutant oxidised the *n*-propylbenzene with a NADH oxidation rate of 510 ± 13 min^{-1}, which was more than 4-fold faster compared to the WT enzyme (Table 5.4). The product formation rates were low, 44 min^{-1} and 9 min^{-1} for both the H85F mutant and WT enzyme respectively, as a result of the reduced coupling efficiencies (9% for H85F and 4% for WT CYP101B1; Table 5. 4).

Despite low product formation activity and coupling efficiency, *n*-propylbenzene was oxidised to three metabolites by both variant enzymes. Two of these were identified as 1-phenyl-1-propanol (m^+/z = 136.15) and propiophenone (m^+/z = 134.1) by GC-MS coelution with authentic standards (Figure 5. 21 and Figure D. 1). The further oxidation product propiophenone (around 70%) was formed in excess in both turnovers (Figure 5. 21). The third metabolite was identified as 1-phenylpropan-2-ol by GC-MS coelution with the product generated from the reduction of phenylacetone by $LiAlH_4$ [214]. Analysis of the mass spectrum (m^+/z = 136.10) was also in agreement with this assignment (Figure D. 1). Chiral GC and HPLC analysis of 1-phenyl-1-propanol metabolite could not separate the enantiomers. Turnover of the WT enzyme generated a 40 (*R*):60 (*S*) mixture of 1-phenylpropan-2-ol enantiomers, whereas the H85F mutant generated a 26 (*R*):74 (*S*) ratio (Figure 5. 21 and Figure 5. 19 (c)) [265].

Table 5. 4. Substrate binding, turnover and coupling efficiency data for CYP101B1 (WT and the H85F variant) with *n*-propylbenzene, isopropylbenzene, isobutylbenzene and indane. The turnover activities were measured as described in Table 5. 1. - not measured or not able to be determined accurately. The data are reported as mean ± S.D. (n = 3) and rates are given in nmol.nmol-CYP^{-1}.min^{-1}.

substrate	CYP101B1	%HS heme	K_d (μM)	N (min^{-1})	PFR (min^{-1})	C %
n-propylbenzene	WT	≤5%	410 ± 70	121 ± 6	9 ± 5	4
	H85F	**30%**	**0.6 ± 0.1**	**510 ± 13**	**44 ± 4**	**9**
isopropyl-benzene	WT	5%	-	98 ± 12	14 ± 1	12
	H85F	**20%**	**-**	**381 ± 8**	**46 ± 2**	**15**
isobutylbenzene	WT	≤5%	70 ± 20	156 ± 2	65 ± 4	42
	H85F	**20%**	**0.9 ± 0.1**	**254 ± 4**	**108 ± 3**	**43**
indane	WT	20%	99 ± 11	118 ± 21	28 ± 3	24
	H85F	**65%**	**9.5 ± 7**	**363 ± 8**	**174 ± 9**	**48**

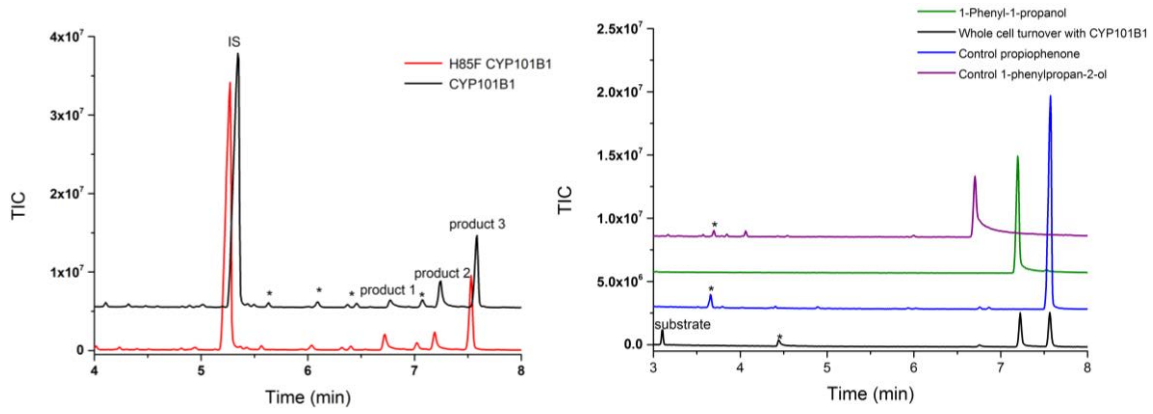

(a) (b)

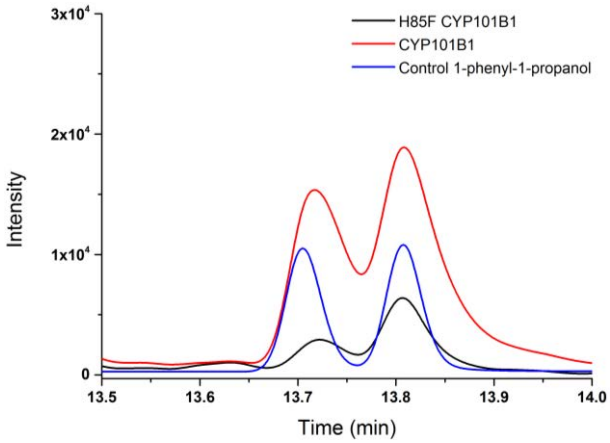

(c)

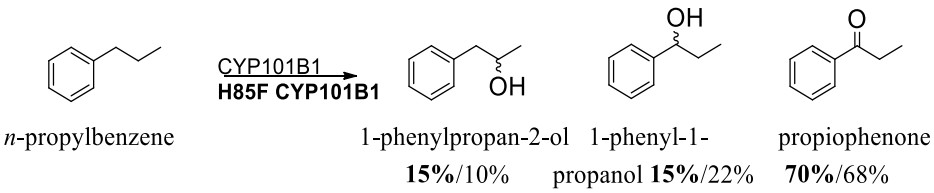

n-propylbenzene 1-phenylpropan-2-ol **15%**/10% 1-phenyl-1-propanol **15%**/22% propiophenone **70%**/68%

(d)

Figure 5. 21 (a) GC analyses of the turnovers of *n*-propylbenzene by H85F CYP101B1 (red) and CYP101B1 (black). *n*-Propylbenzene (RT 3.1 min) and the products; 1-phenylpropan-2-ol (RT 6.75 min, product 1), 1-phenyl-1-propanol (RT 7.25 min, product 2), propiophenone (RT 7.6 min, product 3) [272]. The chromatogram (CYP101B1) was offset along the x and y-axes for clarity. **(b)** GC-MS analysis of whole-cell turnover of WT CYP101B1 and products control. **(c)** Chiral GC analyses of 1-phenyl-1-propanol product region to highlight the separation of the two enantiomers (RT 13.7 min and 13.8 min). Impurities are labelled (*). **(d)** The products identified from the CYP101B1 and H85F CYP101B1 turnovers of *n*-propylbenzene. The product distributions are given as percentages (H85F variant in bold).

Addition of isopropylbenzene and isobutylbenzene shifted the heme to the high spin-state to similar levels; 20% and 5% in H85F and WT CYP101B1, respectively (Figure 5. 22 and Figure 5. 23). The H85F CYP101B1 variant exhibited higher affinity with isobutylbenzene (K_d = 0.9 ± 0.1 µM) than the WT enzyme (K_d = 70 ± 20 µM). This was consistent with the tight binding observed for *n*-propylbenzene (Table 5. 4).

The NADH oxidation and product formation rates of isobutylbenzene oxidation by the H85F CYP101B1 were 254 min^{-1} and 108 min^{-1}, respectively. Both were significantly faster than those determined with the WT system (Table 5. 4). The coupling efficiency was similar for both variants (43% versus 42%; Table 5. 4). Higher NADH oxidation (381 min^{-1}) and product formation (46 min^{-1}) rates were also observed for H85F CYP101B1 with isopropylbenzene than for the WT enzyme. The coupling efficiencies of both variants were reduced when compared with isobutylbenzene (Table 5. 4). Both enzymes catalysed the selective hydroxylation of isobutylbenzene and isopropylbenzene to a single hydroxylated metabolite which was detected in the GC-MS analysis (Figure 5. 24). The metabolites were identified as arising from hydroxylation of the alkyl substituent tertiary C-H bonds; 2-methyl-1-phenyl-2-propanol (m^+/z = 150.05) and 2-phenyl-2-propanol (m^+/z = 136.10). Both were confirmed by GC-MS coelution experiments with authentic standards (Figure 5. 24, Figure 5. 25 and Figure D. 1).

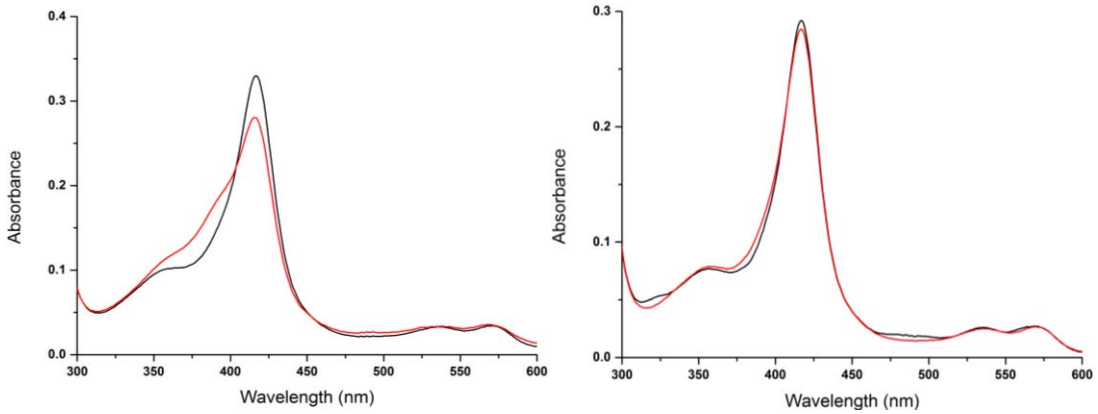

(a) (b)

Figure 5. 22 Spin-state shifts (red) of **(a)** H85F CYP101B1 and **(b)** WT CYP101B1 upon addition of isopropylbenzene.

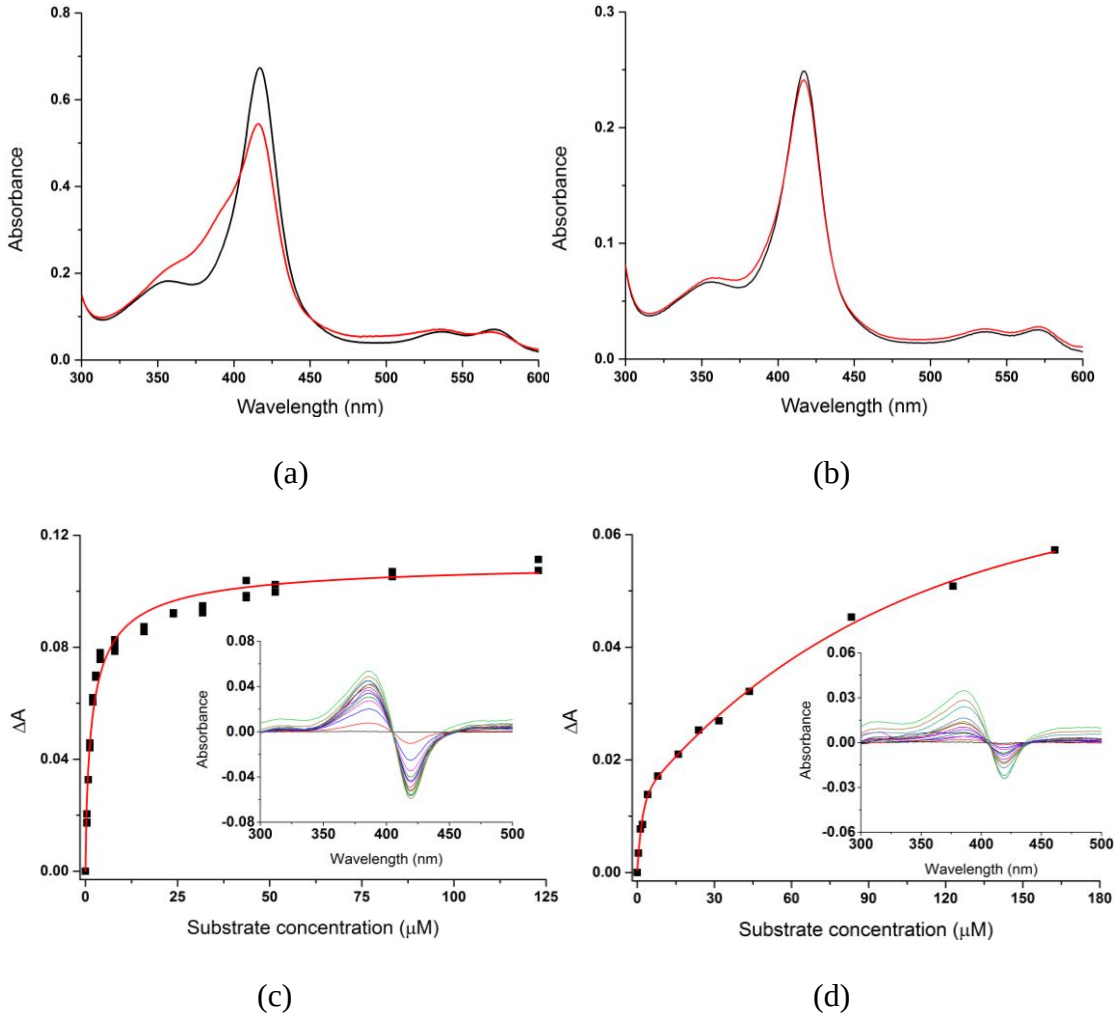

Figure 5. 23 Spin-state shifts (red) of **(a)** H85F CYP101B1 and **(b)** WT CYP101B1 upon addition of isobutylbenzene. The dissociation constant analysis of **(c)** H85F CYP101B1 1.32 μM/K_d 0.9 μM and **(d)** WT CYP101B1 1.25 μM/K_d 70 μM with isobutylbenzene. The concentration of the enzyme used in the binding analysis and the dissociation constant (K_d) are provided.

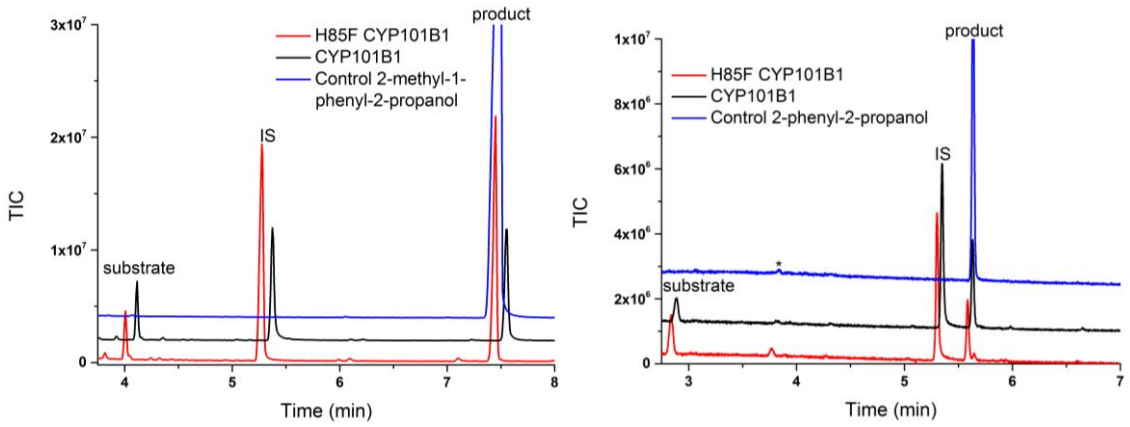

(a) (b)

Figure 5. 24 (a) GC-MS analyses of the turnovers of isobutylbenzene by H85F CYP101B1 (red) and WT CYP101B1 (black). Isobutylbenzene (RT 4.0 min) and the product; 2-methyl-1-phenyl-2-propanol (RT 7.45 min; Product control (blue)). **(b)** GC-MS analyses of the turnover of isopropylbenzene by H85F CYP101B1 (red) and CYP101B1 (black). Isopropylbenzene (RT 2.8 min) and the product; 2-phenyl-2-propanol (RT 5.6 min; Product control (blue)). The chromatograms (CYP101B1) were offset along the x and y-axes for clarity. Impurities are labelled (*).

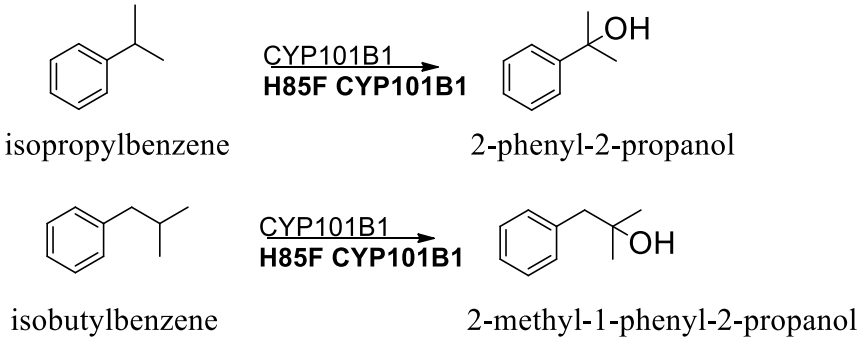

Figure 5. 25 The products identified from the CYP101B1 and H85F CYP101B1 turnovers of isopropylbenzene and isobutylbenzene [265].

The cyclic alkylbenzene indane induced a more substantial spin-state shift (65%) in the H85F variant than the WT enzyme. It also bound to the H85F variant with high affinity (K_d = 9.5 ± 7 µM; Figure 5. 26 and Table 5. 4). Indane induced only a 20% spin-state shift in WT CYP101B1 and the binding affinity to this enzyme was lower (K_d = 99 ± 11 µM; Figure 5. 26 and Table 5.

4). The NADH oxidation and product formation rates of indane oxidation by the H85F variant were 363 ± 8 min^{-1} and 174 ± 9 min^{-1}, respectively (Table 5. 4). These were significantly decreased with WT CYP101B1 (118 ± 21 min^{-1} and 28 ± 3 min^{-1}; Table 5. 4). The coupling efficiency of this oxidation reaction for the mutant enzyme was almost 2-fold superior to WT (48% versus 24%; Table 5. 4). Both variants oxidised indane into one significant product (≤95%) with another minor metabolite (Figure 5. 27). The major metabolite was identified as 1-indanol (m^+/z = 134.10) and minor product as 1-indanone (m^+/z = 132.10) by GC-MS coelution experiments with authentic standards (Figure 5. 26, Figure 5. 27 and Figure D. 1). The chiral HPLC analyses of *in vitro* turnovers of indane by both enzymes revealed that the hydroxylation proceeded with little enantioselectivity (Figure D. 21).

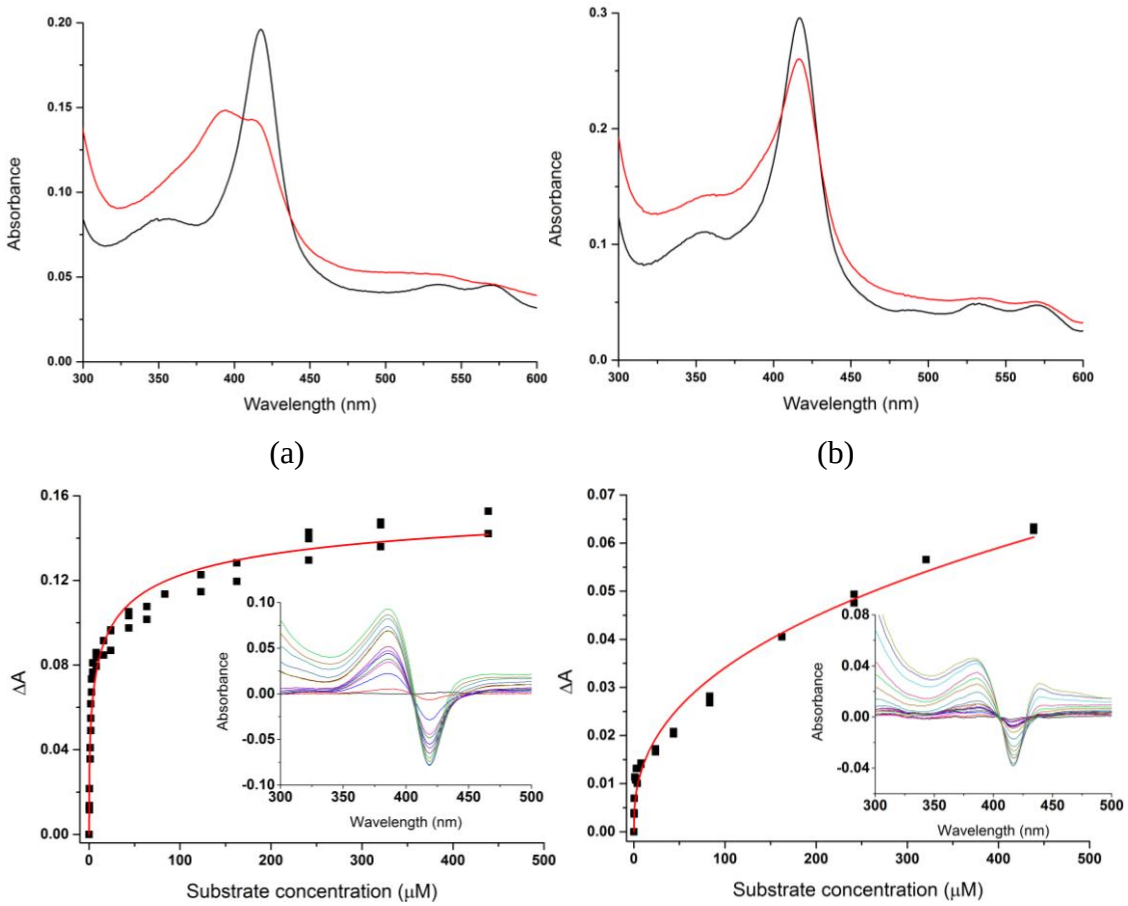

Figure 5. 26 Spin-state shifts of **(a)** H85F CYP101B1 and **(b)** WT CYP101B1 after addition of indane (red). Dissociation constant analysis of **(c)** H85F CYP101B1 1.93 μM/ K_d 9.5 μM and **(d)** WT CYP101B1 1.48 μM/K_d 99 μM. The concentration of the enzyme used in the binding assays and the dissociation constants (K_d) are provided.

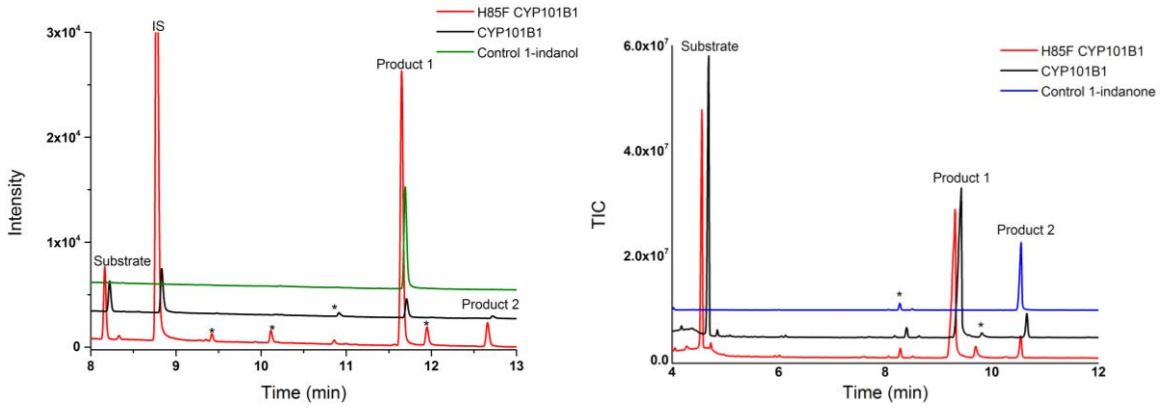

(a) (b)

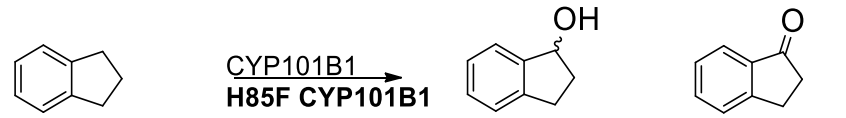

indane 1-indanol **92%**/95% 1-indanone **8%**/5%

(c)

Figure 5. 27 (a) GC analysis of the *in vitro* turnover of indane by H85F CYP101B1 (red) and CYP101B1 (black). Indane (RT 8.2 min) and the products; 1-indanol (RT 11.6 min, product 1, control; green) and 1-indanone (RT 12.7 min, product 2). **(b)** GC-MS analysis of the *in vitro* turnover of indane by H85F CYP101B1 (red) and CYP101B1 (black). Indane (RT 4.8 min) and the products; 1-indanol (product 1; RT 9.2 min) and 1-indanone (RT 10.6 min, product 2 control; blue). The chromatograms (CYP101B1) were offset along the x and y-axes for clarity. Impurities are labelled (*). **(c)** The products identified from the CYP101B1 and H85F CYP101B1 turnovers of indane [265]. The product distributions are given as percentages (H85F variant in bold).

The oxidation of styrene, 2-methylstyrene and *β*-methylstyrene were examined to see the effect of presence of an unsaturated side chain on the binding and activity of both variants. Styrene induced 5% and 10% high heme spin-state shifts of WT and H85F CYP101B1, respectively (Figure 5. 28 and Table 5. 5). Despite these low shifts, the NADH oxidation rates of both were moderately high (153 min^{-1} for H85F variant and 105 min^{-1} for WT enzyme; Table 5. 5). The H85F variant oxidised this substrate with greater product formation rate (55 min^{-1}) than the WT CYP101B1 system (Table 5. 5). The productive use of reducing equivalent to product formation was also better for H85F variant (36% versus 13%; Table 5. 5).

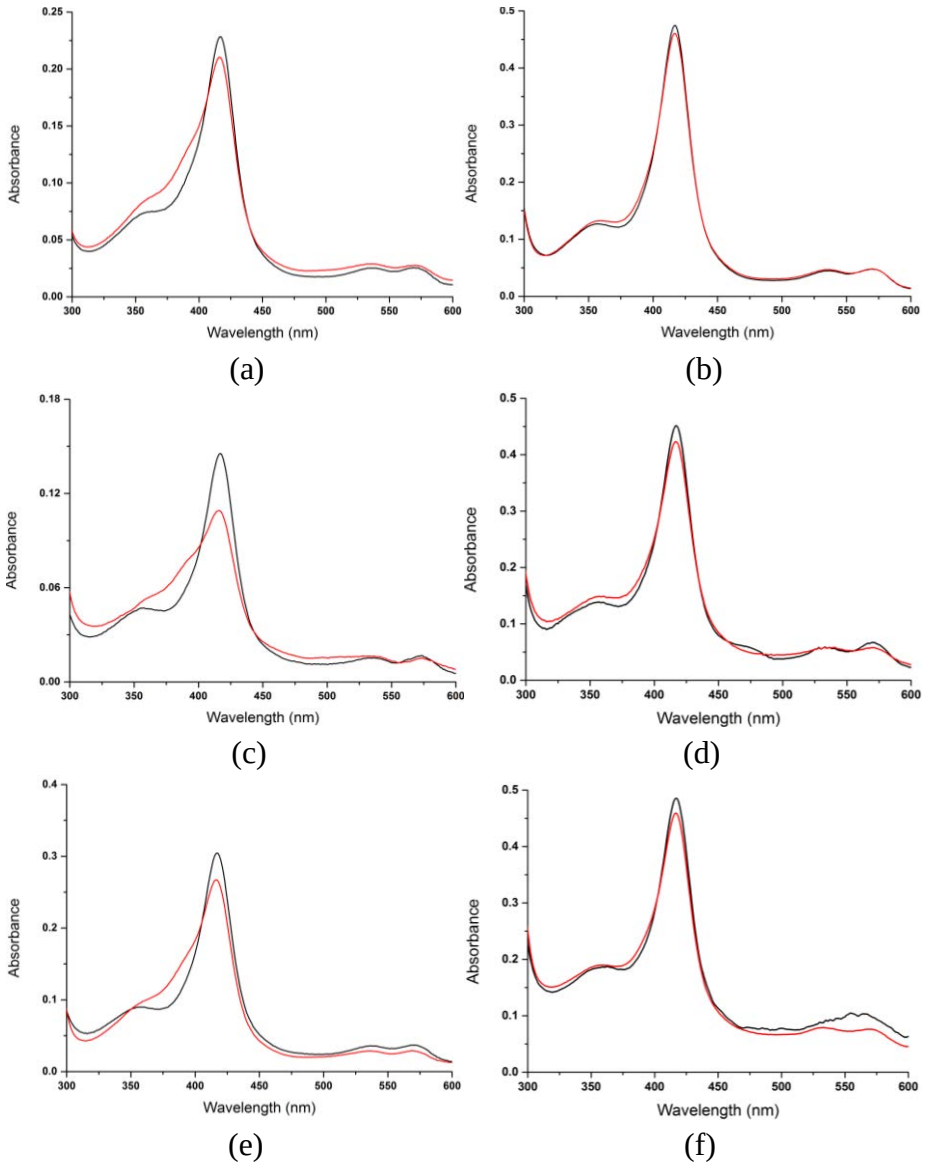

Figure 5. 28 Spin-state shifts of (left) H85F CYP101B1 and (right) WT CYP101B1. Heme spin-state changes (red) after addition of (a and b) styrene, (c and d) *β*-methylstyrene, (e and f) 2-methylstyrene.

The *in vitro* turnovers of styrene with both enzymes generated a single metabolite which was identified as phenyloxirane by GC-MS coelution (m^+/z = 120.15; Figure 5. 29, Figure 5. 33 and Figure D. 1) [272]. A minor product (less than 1%) was detected in the H85F mutant turnover, which was assigned as phenylacetaldehyde from its MS fragmentation pattern (m^+/z = 120.10; Figure 5. 29, Figure 5. 33 and Figure D. 1). Chiral GC analyses of both sets of turnovers showed the formation of a roughly equal mixture of (*S*)-(–)-phenyloxirane and (*R*)-(+)-phenyloxirane (Figure 5. 29 and Figure 5. 33).

Table 5. 5 Substrate binding, turnover and coupling efficiency data for CYP101B1 (WT and the H85F variant) with styrene, *β*-methylstyrene and 2-methylstyrene. The *in vitro* turnover activities were measured as described in Table 5. 1. -not measured or not able to be determined accurately. The data are reported as mean ± S.D. (n = 3) and rates are given in nmol.nmol-CYP^{-1}.min^{-1}.

substrate	CYP101B1	%HS heme	K_d (μM)	N (min^{-1})	PFR (min^{-1})	C %
styrene	WT	≤5%	-	105 ± 2	14 ± 10	13
	H85F	**10%**	**-**	**153 ± 7**	**55 ± 7**	**36**
2-methylstyrene	WT	5%	450 ± 70	161 ± 9	42 ± 3	26
	H85F	**20%**	**13 ± 4**	**405 ± 16**	**219 ± 17**	**54**
β-methylstyrene	WT	10%	395 ± 25	76 ± 6	54 ± 17	71
	H85F	**35%**	**1.8 ± 3**	**90 ± 1**	**33 ± 3**	**37**

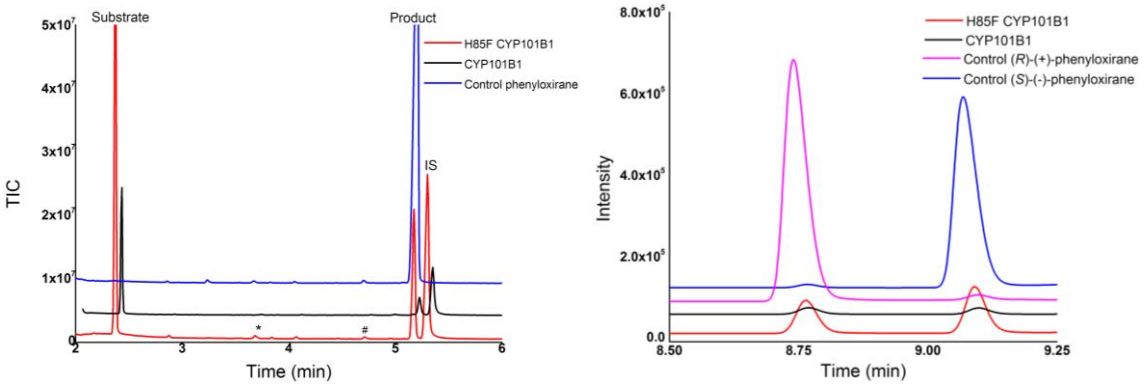

(a) (b)

Figure 5. 29 (a) GC-MS analysis of the turnover of styrene by H85F CYP101B1 (red) and CYP101B1 (black). Styrene (RT 2.4 min) and the products; #phenylacetaldehyde (RT 4.75 min) and phenyloxirane (styrene oxide; RT 5.15 min; control blue). The chromatogram (CYP101B; black) was offset along the x and y-axes for clarity. **(b)** GC chiral column analyses; styrene (RT 3.6 min) and the products control; (*S*)-(-)-phenyloxirane (blue; RT 9.2 min) and (*R*)-(+)-phenyloxirane (magenta; RT 8.75 min). Impurities are labelled (*).

The addition of 2-methylstyrene and *β*-methylstyrene in H85F CYP101B1 induced spin-state shifts to 20% and 35% high spin form, respectively. These were greater than these of WT CYP101B1 (Figure 5. 30). The H85F variant bound both these substrates with high affinity, especially in case of *β*-methylstyrene, where it exhibited very tight binding (K_d = 1.8 µM versus K_d = 13 µM; Figure 5. 30). WT CYP101B1 had a weak binding affinity with both of these substrates, as indicated by the measured dissociation constants (Figure 5. 30).

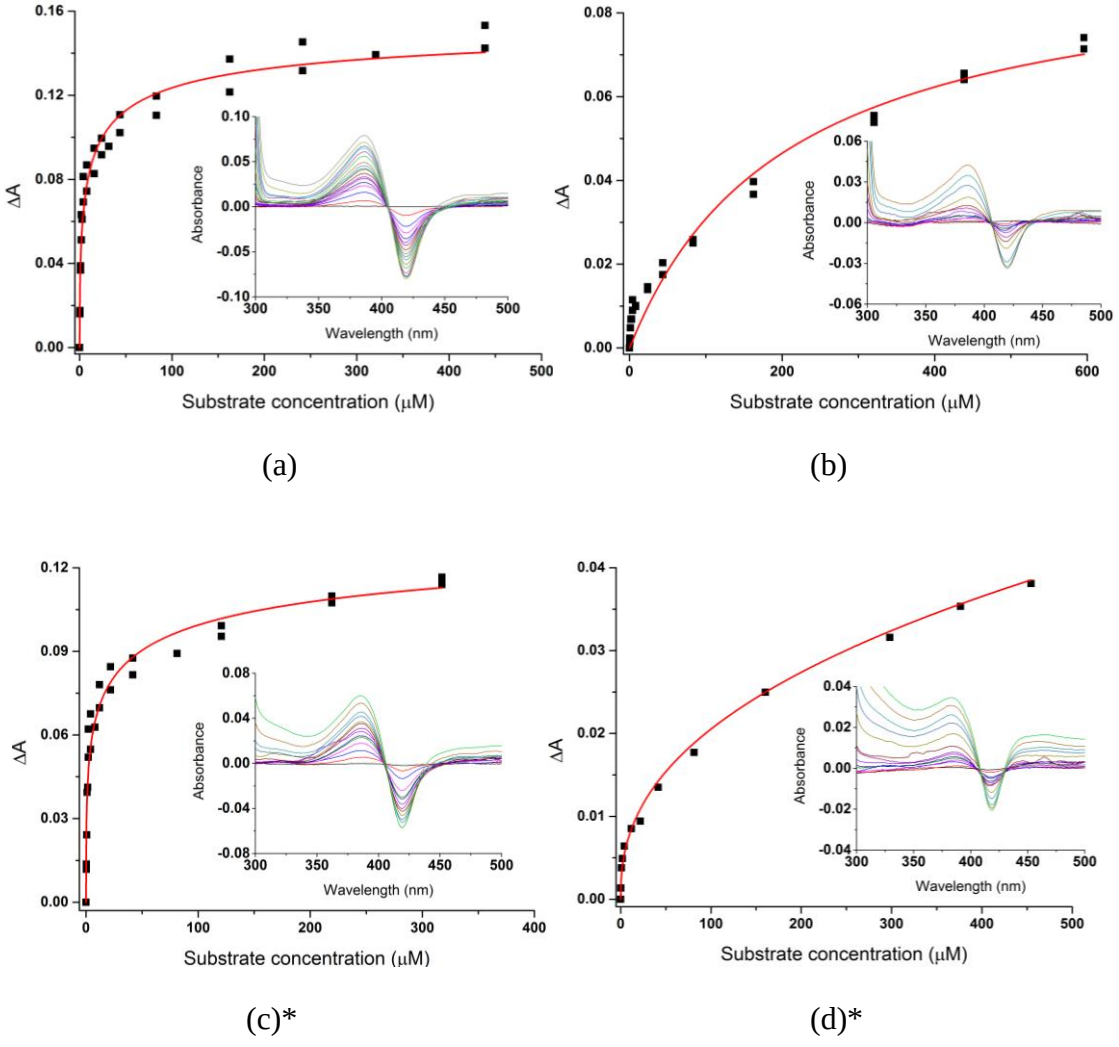

Figure 5. 30 Dissociation constant analyses of **(a)** 2-methylstyrene H85F variant 1.65 µM/K_d 13 µM, **(b)** WT 1.32 µM/K_d 450 µM and **(c)** *β*-methylstyrene H85F variant 1.83 µM/K_d 1.8 µM, **(d)** WT 1.31 µM/K_d 395 µM for the WT enzyme. *The difference between A_{420} and A_{600} nm was used due to the interference of substrate with the analysis below 400 nm. The concentration of the enzyme used in the binding investigation and the dissociation constant (K_d) are provided.

The H85F mutant exhibited significant oxidation activity with 2-methylstyrene (NADH oxidation rate 405 ± 16 min^{-1} and product formation rate 219 ± 17 min^{-1}; Table 5. 5). WT CYP101B1 had a lower coupling efficiency (26%) which resulted in a reduced product formation rate (42 ± 3 min^{-1}; Table 5. 5). A single major metabolite (95%) was detected in GC-MS analysis of the *in vitro* turnovers of 2-methylstyrene with both enzymes. This was assigned 2-(2-methylphenyl)oxirane from the mass spectrum (m^+/z = 134.05) and coelution experiment in GC-MS with the product of the reaction of 2-methylstyrene with *m*-chloroperbenzoic acid (*m*CPBA; Figure 5. 31, Figure 5. 33 and Figure D. 1) [268, 272].

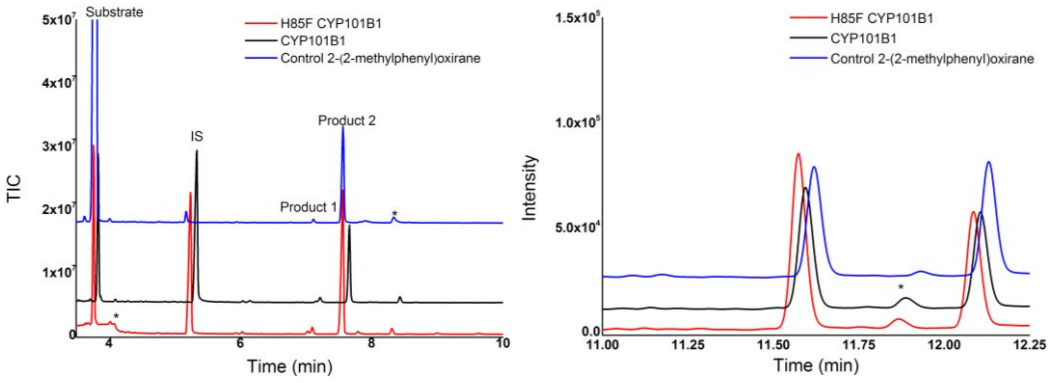

(a) (b)

Figure 5. 31 (a) GC-MS analyses of the turnover of 2-methylstyrene by H85F CYP101B1 (red), CYP101B1 (black) and 2-(2-methylphenyl)oxirane synthesised by adding *m*CPBA to 2-methylstyrene (blue). 2-Methylstyrene (RT 3.75 min) and the minor product (2-methylphenyl)acetaldehyde (RT 7.2 min, product 1) and the significant product 2-(2-methylphenyl)oxirane (RT 7.58 min, product 2). The chromatogram (CYP101B; black) was offset along the x and y-axes for clarity. **(b)** Chiral GC analyses of the *in vitro* turnovers overlaid with the racemic mixture of 2-(2-methylphenyl)oxirane (RT 11.6 min and 12.1 min). Impurities are labelled (*). The chromatograms were offset along the x and y-axes for clarity.

Chiral GC analysis confirmed that 2-(2-methylphenyl)oxirane was generated as a mixture of enantiomers (WT (60:40) and H85F (55:45); Figure 5. 31 and Figure 5. 33). The minor product was assigned as (2-methylphenyl)acetaldehyde (m^+/z = 134.05) based on its MS fragmentation pattern (Figure 5. 31, Figure 5. 33 and Figure D. 1).

β-Methylstyrene was oxidised by H85F and wild-type CYP101B1 with NADH oxidation rates of 90 min^{-1} and 76 min^{-1}, respectively. These were lower than those of 2-methylstyrene and styrene. Unusually the product formation rate was reduced for the mutant enzyme compared to the WT (33 min^{-1} versus 54 min^{-1}; Table 5. 5). The coupling efficiency for the oxidation of *β*-methylstyrene by the WT enzyme was greater (71%) than the H85F variant, 37% (Table 5. 5). *β*-Methylstyrene oxidation by both variants generated two metabolites (Figure 5. 32 and Figure 5. 33). The major product was identified as 3-phenyl-2-propen-1-ol (m^+/z = 134.0) by coeluting with an authentic standard in both GC and GC-MS (Figure 5. 32, Figure 5. 33 and Figure D. 1) [272]. The second metabolite was confirmed as the epoxide, 2-methyl-3-phenyloxirane (m^+/z = 134.0) by analysing the mass spectrum and a coelution experiment with the epoxide of *β*-methylstyrene synthesised using *m*CPBA (Figure 5. 32, Figure 5. 33 and Figure D.1) [268]. Chiral GC analyses showed that an almost equal mixture of the two stereoisomers, (*R*, *R*)- and (*S*, *S*)-2-methyl-3-phenyloxirane, were formed in the turnovers of H85F variant but for WT the ratio was 58:42 (Figure 5. 32 and Figure 5. 33).

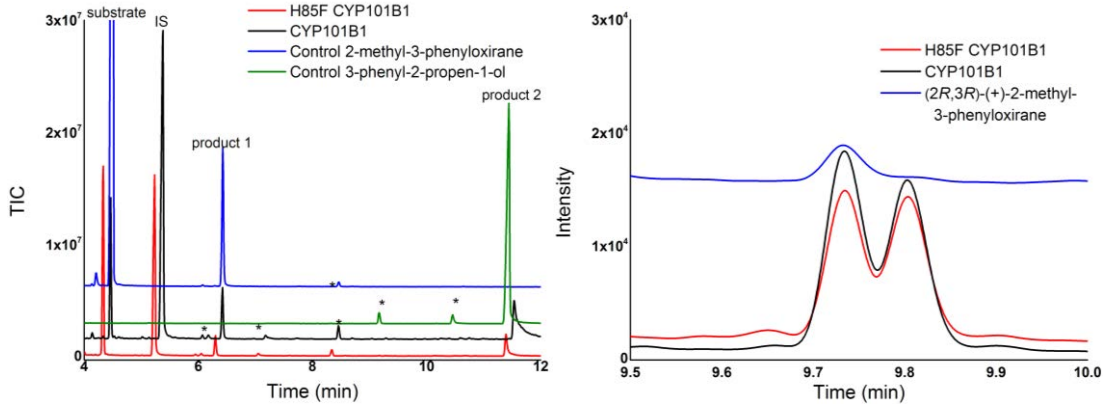

(a) (b)

Figure 5. 32 (a) GC-MS analyses of the turnovers of *β*-methylstyrene by H85F CYP101B1 (red), CYP101B1 (black), and the product 2-methyl-3-phenyloxirane formed by the reaction of the substrate with *m*CPBA (blue). *β*-Methylstyrene (RT 4.3 min) and the products; 2-methyl-3-phenyloxirane (RT 6.3 min, product 1) and 3-phenyl-2-propen-1-ol (11.45 min, product 2 control; green). The chromatogram (CYP101B; black) was offset along the x and y-axes for clarity. **(b)** Chiral GC analyses of both *in vitro* turnovers and highlighted the region of the metabolites and product control (2*R*, 3*R*)-(+)-2-methyl-3-phenyloxirane (blue). Impurities are labelled (*).

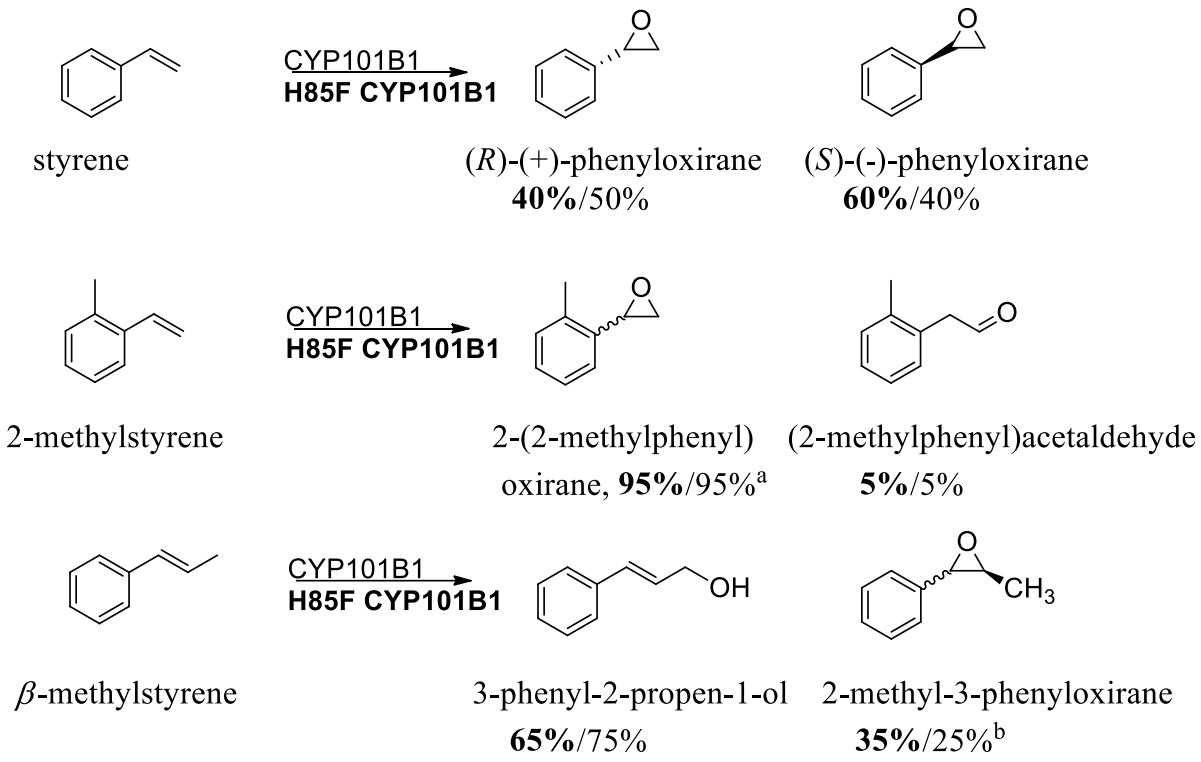

Figure 5. 33 The products identified from the CYP101B1 and H85F CYP101B1 turnovers of the styrene, 2-methylstyrene and *β*-methylstyrene. The product distributions are given as percentages (H85F variant in bold). [a] WT and the H85F variant generated a 60:40 and 55:45 mixture of each enantiomer, respectively. [b] Both the WT and H85F variants generated a 58(*R*):42 and 50:50 mixture of each enantiomer, respectively.

5.3.2 The oxidation of naphthalene derivatives and related molecules by WT and H85F CYP101B1

The H85F variant of CYP101B1 showed an improved oxidation activity with alkylbenzene substrates over the WT enzyme. The cyclic alkylbenzene indane resulted in the greatest spin-state shift to the high spin form in H85F variant, indicative of a suitable substrate fit in the active site of the enzyme. To expand the substrate range towards larger aromatic substrates, both variants were investigated with naphthalene derivatives and related molecules (Figure 5. 34). A series of substituted naphthalenes, bicyclic and tricyclic compounds were selected for binding and activity assays with WT and H85F CYP101B1 (Figure 5. 34).

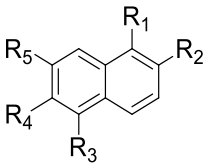

R_1 & R_2 = Me, R_3, R_4 & R_5 = H, 1, 2-dimethylnaphthalene
R_1 & R_3 = Me, R_2, R_4 & R_5 = H, 1, 5-dimethylnaphthalene
R_2 & R_4 = Me, R_1, R_3 & R_5 = H, 2, 6-dimethylnaphthalene
R_2 & R_5 = Me, R_1, R_3 & R_4 = H, 2, 7-dimethylnaphthalene
R_2, R_3, R_4 & R_5 = H, R_1 = Me, 1-methylnaphthalene
R_1, R_3, R_4 & R_5 = H, R_2 = Me, 2-methylnaphthalene

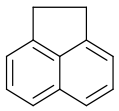

acenaphthene

Figure 5. 34 The naphthalene derivatives and related substrates screened with WT CYP101B1 and H85F CYP101B1.

The addition of 1-methylnaphthalene in H85F and WT CYP101B1, induced the spin-state shift to the high spin form of 60% versus 50%, respectively (Figure 5. 35) [265, 266]. The substrate binding assays showed that H85F variant bound with this substrate more tightly than the WT (K_d = 3.3 ± 0.4 µM versus K_d = 63 ± 9 µM; Figure 5. 36) [265, 266]. As with the alkylbenzenes, 1-methylnaphthalene oxidation occurred with higher NADH oxidation (453 min^{-1}) and product formation (161 min^{-1}) rates with the H85F system compared to the WT (Table 5. 6). The coupling efficiency was also better (36% versus 16%; Table 5. 6). Both variants selectively oxidised 1-methylnaphthalene to a single metabolite (Table 5. 6). This was identified as 1-naphthylmethanol (m^+/z = 158.05) by coeluting with an authentic standard in GC-MS (Figure 5. 37 and Figure D. 1) [265, 266].

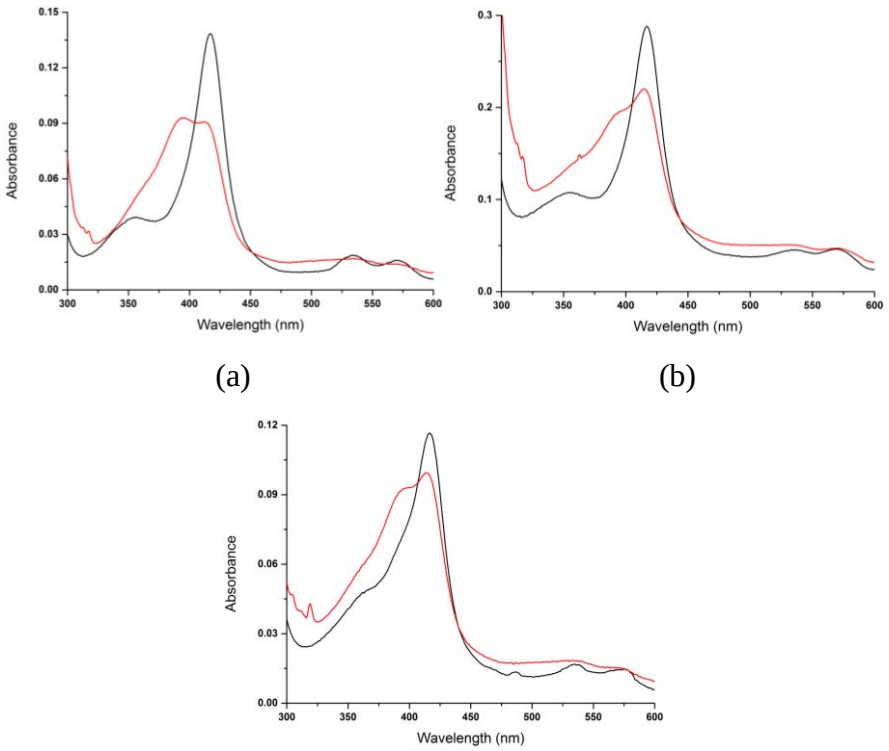

Figure 5. 35 Spin-state shifts (red) of H85F variant after addition of **(a)** 1-methylnaphthalene, **(c)** 2-methylnaphthalene and spin-state shifts of WT CYP101B1 after addition of **(b)** 1-methylnaphthalene.

Table 5. 6 Substrate binding, turnover and coupling efficiency data for CYP101B1 (WT and the H85F variant) with 1- and 2-methylnaphthalene. The *in vitro* turnover activities were measured as described in Table 5. 1. The data are reported as mean ± S.D. (n = 3) and rates are given in nmol.nmol-CYP^{-1}.min^{-1}.

substrate	CYP101B1	%HS heme	K_d (μM)	N (min^{-1})	PFR (min^{-1})	C %
1-methylnaphthalene	WT [266]	50%	63 ± 9	240 ± 17	38 ± 10	16
	H85F	**60%**	**3.3 ± 0.4**	**453 ± 25**	**161 ± 13**	**36**
2-methylnaphthalene	WT [266]	30%	140 ± 10	212 ± 24	57 ± 18	26
	H85F	**50%**	**16 ± 6**	**158 ± 13**	**32 ± 3**	**20**

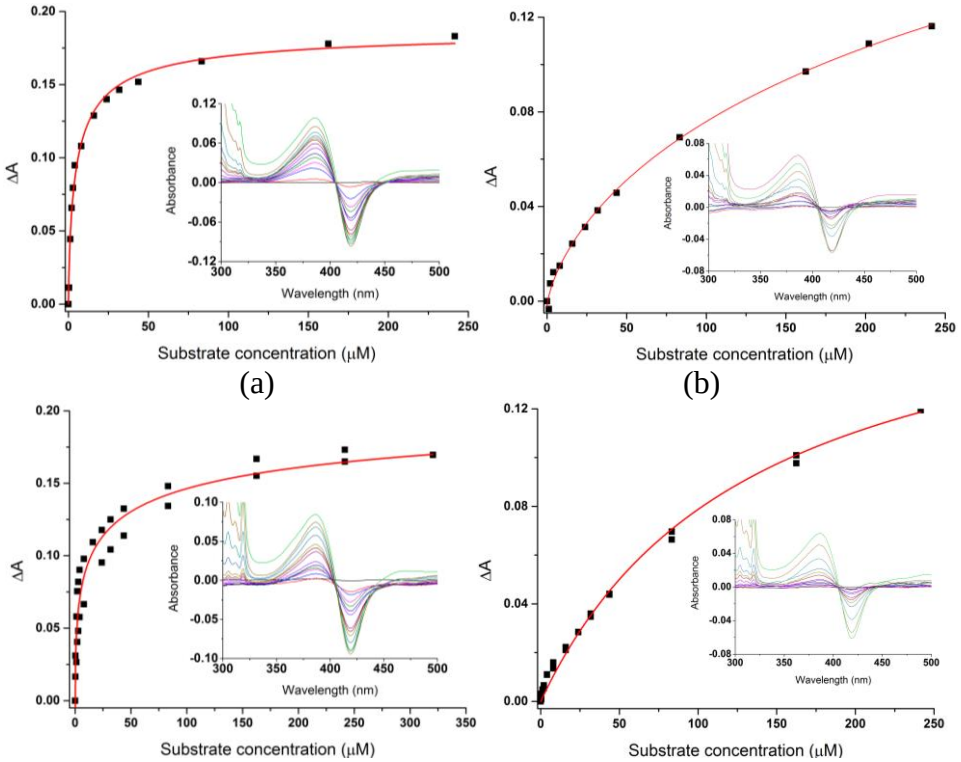

Figure 5. 36 Dissociation constant analysis of **(a)** H85F 1.49 μM/K_d 3.3 μM, **(b)** WT CYP101B1 1.76 μM/K_d 63 μM with 1-methylnaphthalene, and **(c)** H85F 1.84 μM/K_d 16 μM, **(d)** WT CYP101B1 1.84 μM/K_d 140 μM with 2-methylnaphthalene. The concentration of the enzyme used in the binding analyses and the dissociation constants (K_d) are provided.

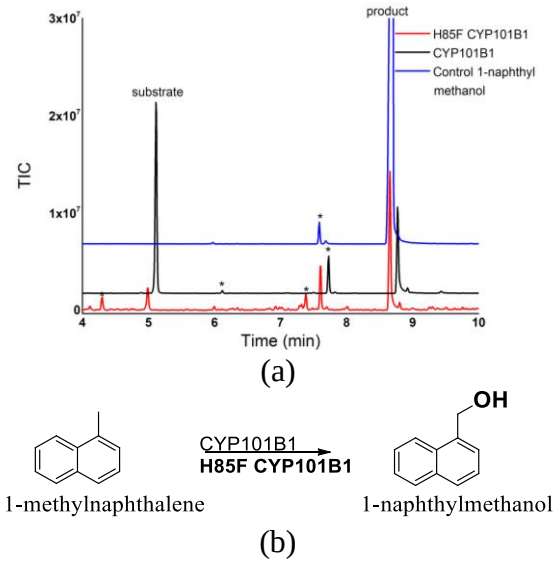

Figure 5. 37 (a) GC-MS analyses of the turnovers of 1-methylnaphthalene by H85F CYP101B1 (red) and CYP101B1 (black). 1-Methylnaphthalene (RT 4.9 min) and the product; 1-naphthylmethanol (blue; RT 8.7 min) [265, 266]. Impurities are labelled (*). The chromatogram (CYP101B1) was offset along the x and y-axes for clarity. **(b)** The product identified from the CYP101B1 and H85F CYP101B1 turnovers of the 1-methylnaphthalene [265, 266].

2-Methylnaphthalene induced a spin-state shift of 50% in H85F variant and 30% in WT enzyme (Figure 5. 35). The H85F mutant bound the substrate nearly 9-fold more tightly (K_d = 16 ± 6 µM) than the WT (K_d = 140 ± 10 µM; Figure 5. 36). However, there was no clear relationship between binding affinity and oxidation activity in the case of 2-methylnaphthalene as the NADH oxidation (212 min^{-1}) and product formation (57 min^{-1}) rates of the WT system with this substrate were faster than those of the mutant (Table 5. 6). The coupling efficiency was also found to be higher with WT CYP101B1 (26% versus 20%; Table 5. 6). The GC-MS analyses of the *in vitro* turnovers of 2-methylnaphthalene showed that a single monooxygenase metabolite was formed by both variants (Figure 5. 38). The product was confirmed as 2-naphthylmethanol (m^+/z = 158.15) by GC-MS coelution experiment with an authentic standard (Figure 5. 38 and Figure D. 1) [265, 266].

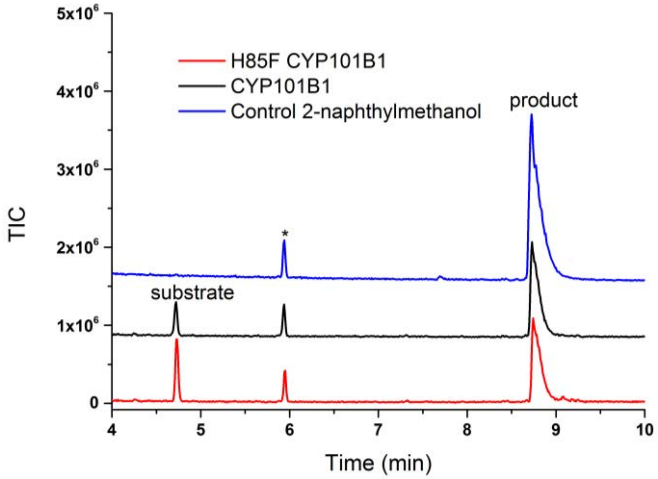

(a)

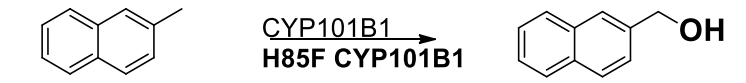

2-methylnaphthalene 2-naphthylmethanol

(b)

Figure 5. 38 (a) GC-MS analyses of the turnovers of 2-methylnaphthalene by H85F CYP101B1 (red) and CYP101B1 (black). 2-Methylnaphthalene (RT 4.8 min) and the product; 2-naphthylmethanol (RT 8.9 min; standard blue) [265, 266]. Impurities are labelled (*). **(b)** The product identified from the CYP101B1 and H85F CYP101B1 turnovers of the 2-methylnaphthalene [265, 266].

The disubstituted naphthalene derivative 1,2-dimethylnaphthalene induced a 40% spin-state shift in H85F variant (Figure 5. 39). This was lower than 1-and 2-methylnaphthalene induced spin-state alterations with this variant (Figure 5. 39). The WT CYP101B1 had a slightly higher spin-state shift, but the binding affinity of the H85F variant was nearly 8-fold tighter (Figure 5. 39).

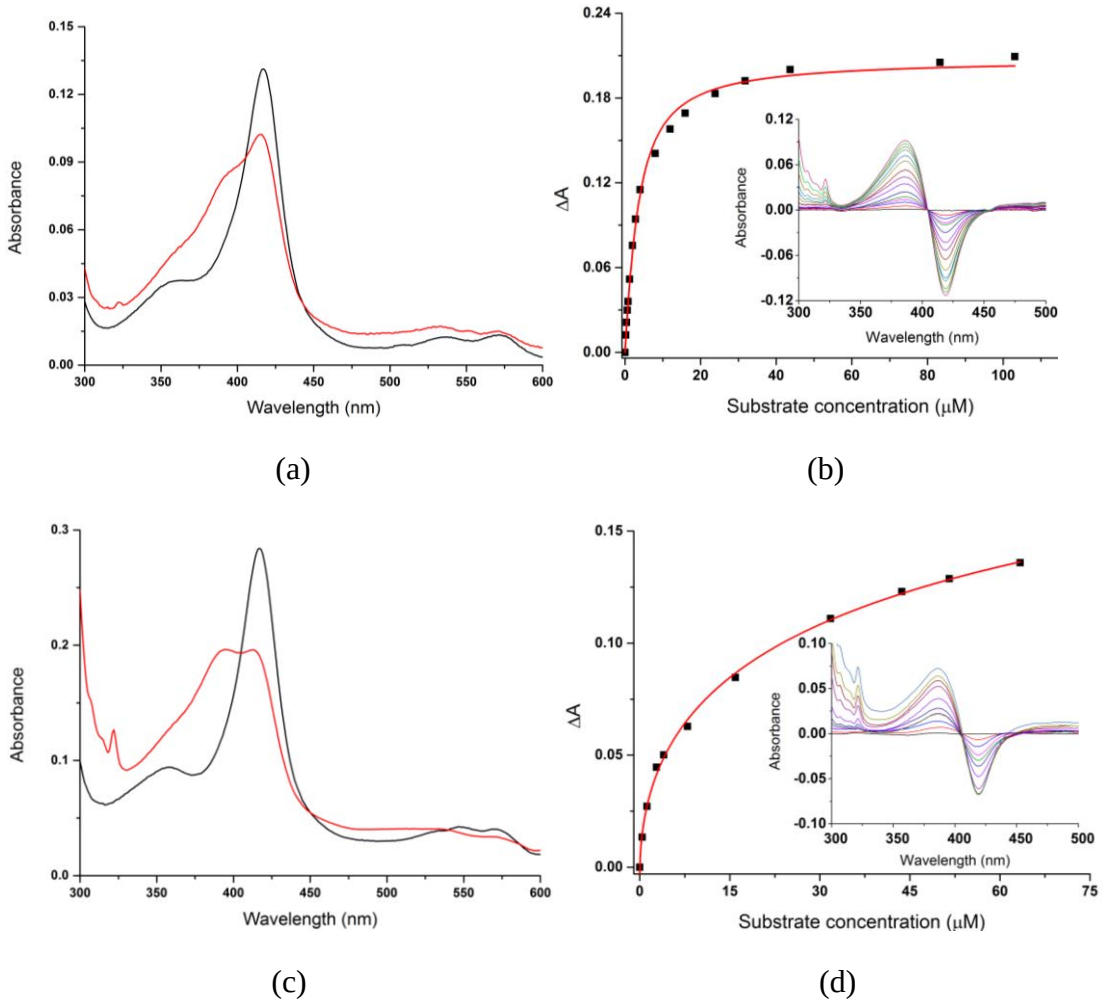

Figure 5. 39 Spin-state shifts (red) after addition of 1,2-dimethylnaphthalene to **(a)** H85F CYP101B1 and **(c)** WT CYP101B1. Dissociation constant analysis of **(b)** H85F 1.93 μM/K_d 2.4 μM and **(d)** WT CYP101B1 1.57 μM/K_d 20 μM with 1,2-dimethylnaphthalene. The concentration of the enzyme used in the binding assays and the dissociation constants (K_d) are provided.

The NADH oxidation rate (242 min^{-1} versus 136 min^{-1}) and coupling efficiency (24% versus 19%) were also higher for the H85F mutant than these of the WT with 1,2-dimethylnaphthalene, resulting in an increased rate of product formation (84 min^{-1} versus 17

min^{-1}; Table 5. 7). A single metabolite was detected in the *in vitro* turnovers of both variants. GC-MS analyses indicated it was a monooxygenase metabolite (m^+/z = 172.05; Figure 5. 40 and Figure D. 1). This metabolite was generated on a larger scale using whole-cell biotransformation system, and it was separated in a pure form (~8 mg) by silica column chromatography. The metabolite was confirmed as (1-methyl-2-naphthyl)methanol by comparing the NMR spectrum to that published previously (Figure 5. 40, Figure 5. 43 and Figure D. 6-D. 8) [265, 315]. The ^{1}H NMR spectrum showed a distinct 2H peak at 4.91 ppm, which indicated that hydroxylation occurs at one of the methyl groups (Figure 5. 40). The correlation of H8 (7.72 ppm) with the H11 (2.71 ppm) in gCOSY NMR spectrum enabled identification of 1-methyl-2-naphthyl)methanol not (2-methyl-1-naphthyl)methanol (Figure 5. 40 and Figure D. 6-D. 8).

Table 5. 7. Substrate binding, turnover and coupling efficiency data for the CYP101B1 (WT and the H85F variant) with alkyl substituted naphthalenes [265, 266]. The turnover activities were measured as described in Table 5. 1. - not measured or not able to be determined accurately. The data are reported as mean ± S.D. (n = 3) and rates are given in nmol.nmol-CYP^{-1}.min^{-1}.

substrate	CYP101B1	%HS heme	K_d (μM)	N (min^{-1})	PFR (min^{-1})	C %
1,2-dimethyl naphthalene	WT	55%	20 ± 4	136 ± 13	25 ± 2	19
	H85F	**40%**	**2.4 ± 0.1**	**242 ± 8**	**57 ± 2**	**24**
1,5-dimethyl naphthalene	WT	55%	28 ± 3	135 ± 5	17 ± 1	13
	H85F	**80%**	**2.6 ± 0.2**	**355 ± 30**	**84 ± 12**	**24**
2,6-dimethyl naphthalene	WT [266]	10%	-	113 ± 5	23 ± 1	21
	H85F	**20%**	**-**	**76 ± 13**	**3 ±1**	**4**
2,7-dimethyl naphthalene	WT [266]	30%	-	448 ± 44	79 ± 10	18
	H85F	**25%**	**-**	**87 ± 25**	**6 ±1**	**7**
acenaphthene	WT	30%	20 ± 4	165 ± 24	42 ± 7	25
	H85F	**60%**	**5.9 ± 0.6**	**513 ± 16**	**245 ± 12**	**48**

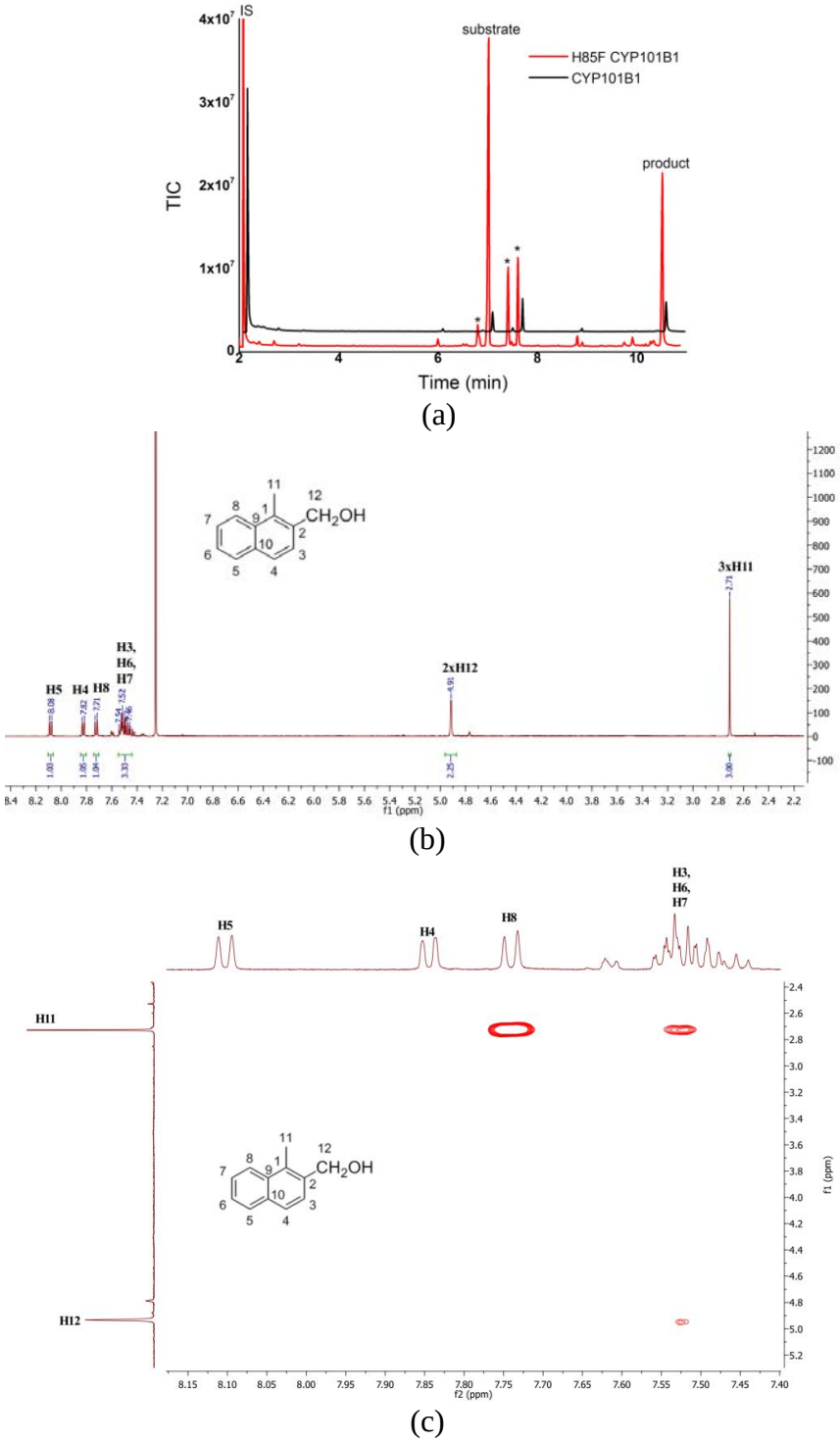

Figure 5. 40 (a) GC-MS analyses of the turnovers of 1,2-dimethylnaphthalene by H85F (red) and WT (black) CYP101B1. 1,2-Dimethylnaphthalene (RT 7.0 min) and the product (1-methyl-2-naphthyl)methanol (RT 10.5 min) [265]. Impurities are labelled (*). The chromatogram (CYP101B1; black) was offset along the x and y-axes for clarity. **(b)** ^{1}H NMR spectrum of (1-methyl-2-naphthyl)methanol. **(c)** Zoomed in gCOSY NMR spectrum to highlight the interaction of H11 and H12. Full data in Appendix D (Figure D. 6-D. 8).

The addition of 1,5-dimethylnaphthalene induced a substantial spin-state shift of 80% to the high spin form in the H85F mutant (Figure 5. 41). The H85F mutant exhibited a strong binding affinity with this substrate (K_d = 2.6 ± 0.2 µM; Figure 5. 41 and Table 5. 7). The WT enzyme showed a lower affinity than that of the H85F variant (K_d = 28 ± 3 µM; Figure 5. 41 and Table 5. 7). The H85F variant catalysed the oxidation of 1,5-dimethylnaphthalene at a faster NADH oxidation activity (355 min^{-1}) and product formation rate (84 min^{-1}) than the WT and the reaction was more tightly coupled to the use of the reducing equivalent (24% versus 13%; Table 5. 7).

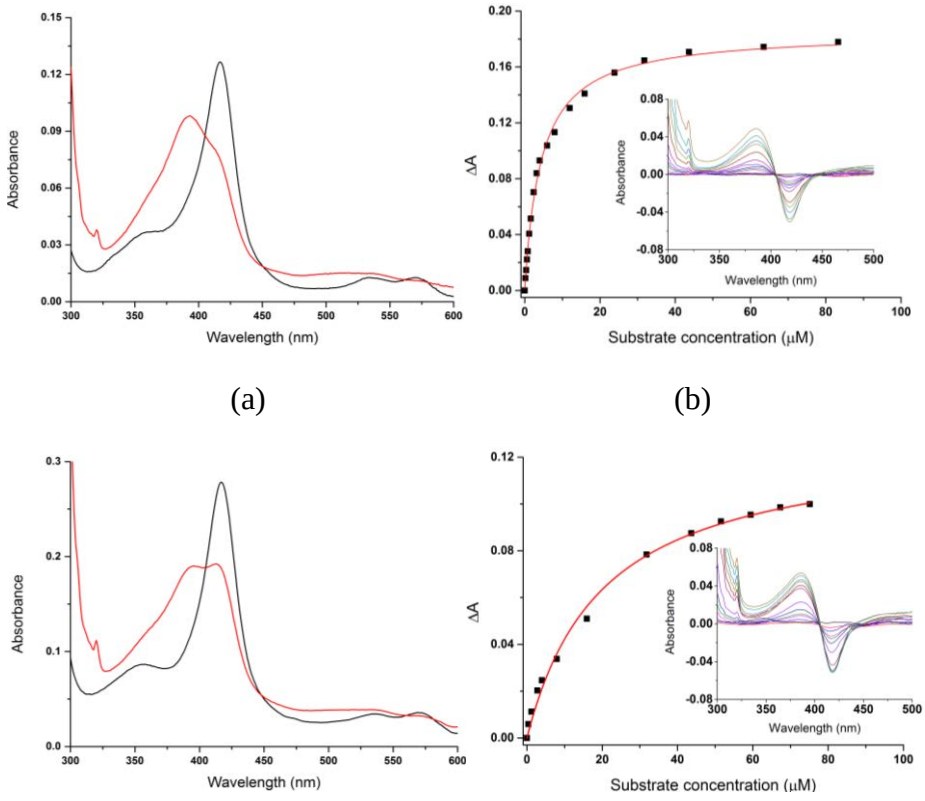

Figure 5. 41 Spin-state shifts (red) of **(a)** H85F variant and **(c)** WT CYP101B1 after addition of 1,5-dimethylnaphthalene. Dissociation constant analysis of **(b)** H85F CYP101B1 1.70 µM/K_d 2.6 µM and **(d)** WT CYP101B1 1.31 µM/K_d 28 µM. The concentration of the enzyme used in the binding studies and the dissociation constants (K_d) are provided.

Turnovers of 1,5-dimethylnaphthalene with both H85F and WT CYP101B1 formed a sole metabolite (m^+/z = 172.1; Figure 5. 42 and Figure D. 1). Whole-cell biotransformation of 1,5-dimethylnaphthalene was used to generate this in sufficient yield and it was purified (~10 mg)

and identified as (5-methyl-1-naphthyl)methanol by NMR analysis (Figure 5. 42, Figure 5. 43 and Figure D. 8-D. 9). The ^{1}H NMR spectrum had a characteristic multiplet peak at 5.15-5.11 ppm (m, 2H, 2xH11) enabling characterisation of (5-methyl-1-naphthyl)methanol (Figure 5. 42 and Figure D. 8-D. 9).

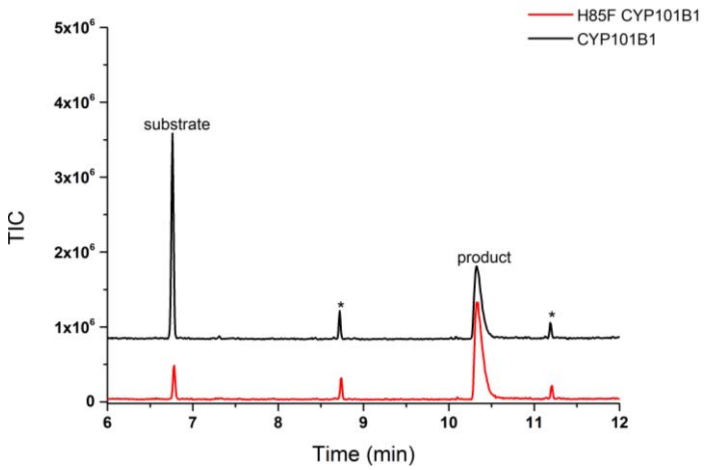

(a)

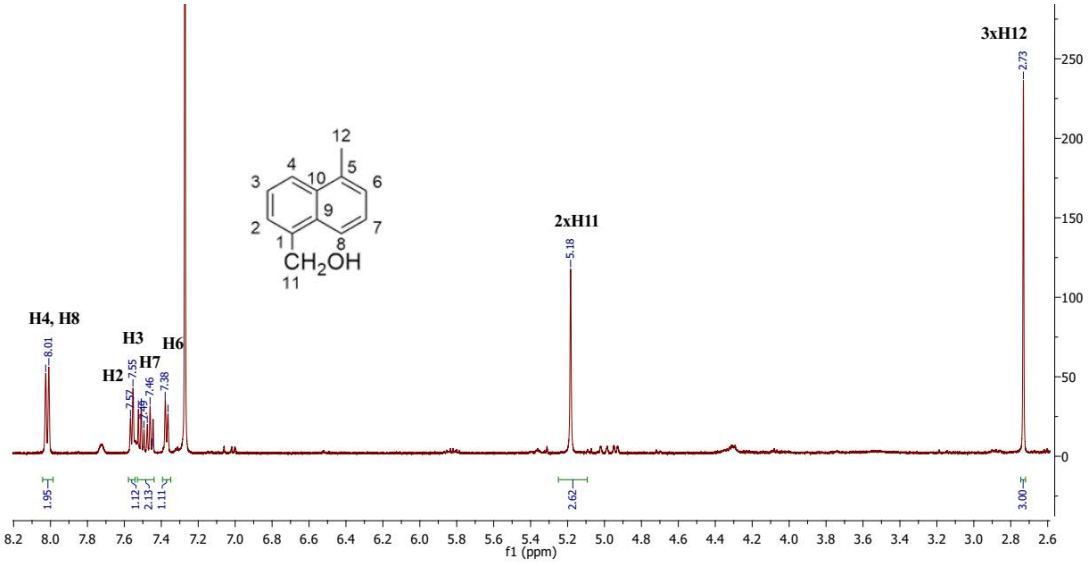

(b)

Figure 5. 42 (a) GC-MS analyses of the turnovers of 1,5-dimethylnaphthalene by both variants. 1,5-Dimethylnaphthalene (RT 6.8 min) and the product (5-methyl-1-naphthyl)methanol (RT 10.4 min). Impurities are labelled (*). **(b)** ^{1}H NMR spectrum of (5-methyl-1-naphthyl)methanol. Full data are in Appendix D (Figure D. 8-D. 9).

Compared to 1,2 and 1,5-dimethylnaphthalene, 2,6-dimethylnaphthalene induced a lower spin-state shift in both variants (20% and 10%; Figure 5. 44 and Table 5. 7). The dissociation

constant for 2,6-dimethylnaphthalene could not be determined due to low solubility and response of the spin-state shift to the addition of the substrate, suggesting weak binding.

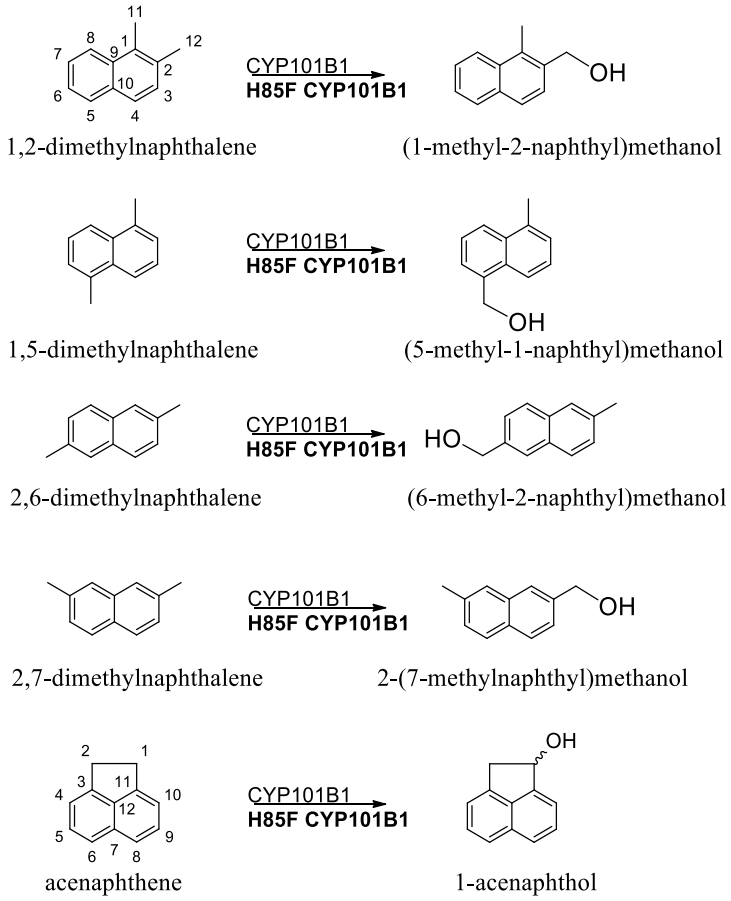

Figure 5. 43 The products identified from the WT and H85F CYP101B1 turnovers with alkylnaphthalenes [265, 266].

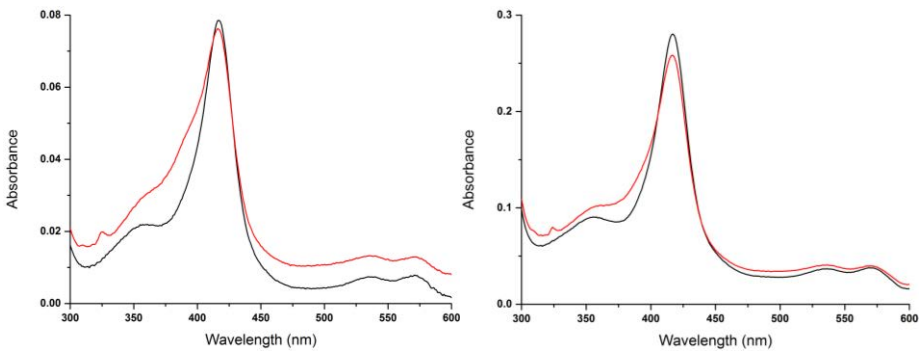

(a) (b)

Figure 5. 44 Spin-state shifts (red) of **(a)** H85F and **(b)** WT variant after addition of 2,6-dimethylnaphthalene.

The product formation activity and coupling efficiency of the H85F variant with this substrate were low (3 min^{-1} and 4%; Table 5. 7). Better activity was observed with the WT CYP101B1 due to greater coupling efficiency (21% versus 4%). The oxidation of 2,6-dimethylnaphthalene by both variants formed one monooxygenase metabolite (m^+/z = 172.2; Figure 5. 45, Figure D. 1). A larger scale *in vivo* turnover of WT CYP101B1 was used to generate the metabolite in enough yield for characterisation. The product was extracted and purified (~21 mg) using silica column chromatography and analysed by NMR (Figure 5. 45 and Figure D. 10-D. 13). The presence of a single 3H benzylic peak and a characteristic 2H peak at 4.85 ppm in the ^{1}H NMR spectrum indicated a methyl hydrogen was abstracted and this was the site of hydroxylation (Figure 5. 45, Figure 5. 43, and Figure D. 10-D. 13). The product was assigned as (6-methyl-2-naphthyl)methanol (Figure 5. 43 and Figure D. 10-D. 13).

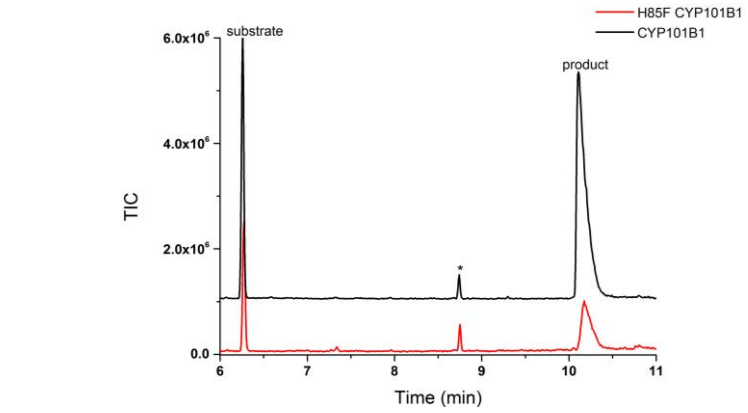

(a)

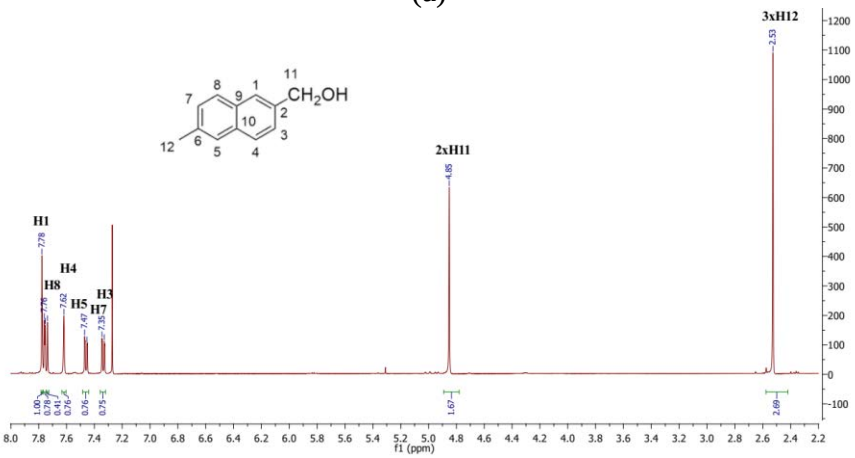

(b)

Figure 5. 45 (a) GC-MS analyses of the turnovers of 2,6-dimethylnaphthalene by H85F CYP101B1 (red) and CYP101B1 (black). 2,6-Dimethylnaphthalene (RT 6.4 min) and the product (6-methyl-2-naphthyl)methanol (RT 10.3 min). Impurities are labelled (*). **(b)** ^{1}H NMR spectrum of (6-methyl-2-naphthyl)methanol. Full data in Appendix D (Figure D. 10-D. 13).

2,7-Dimethylnaphthalene has been shown to induce a 30% high spin-state shift upon addition to WT CYP101B1 [266]. This was slightly reduced in the H85F variant (25%; Figure 5. 46). The NADH oxidation activity (87 ± 25 min^{-1}) and product formation rate (6 min^{-1}) of the H85F mutant enzyme were also slower than the WT enzyme which were in agreement with the lower spin-state shift observed (Table 5. 7) [266].

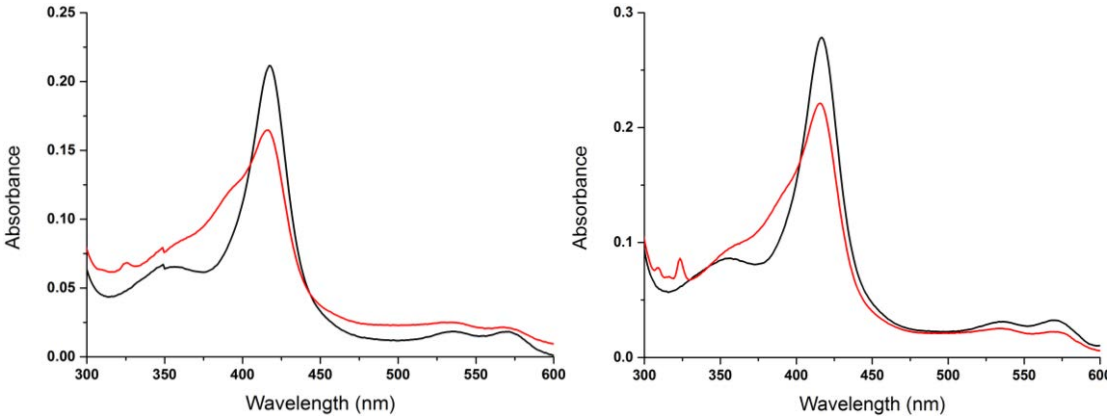

(a) (b)

Figure 5. 46 Spin-state shifts (red) of **(a)** H85F and **(b)** WT CYP101B1 after addition of 2,7-dimethylnaphthalene.

The *in vitro* turnover of 2,7-dimethylnaphthalene with H85F variant generated a single metabolite (Figure 5. 47). That was confirmed as 2-(7-methylnaphthyl)methanol via GC-MS coelution with the *in vitro* turnover metabolite of WT CYP101B1, which was previously characterised by Emma A. Hall using NMR spectrum analysis (m^+/z = 172.15; Figure 5. 43 and Figure 5. 47, Figure D. 1, Figure D. 14) [233, 266].

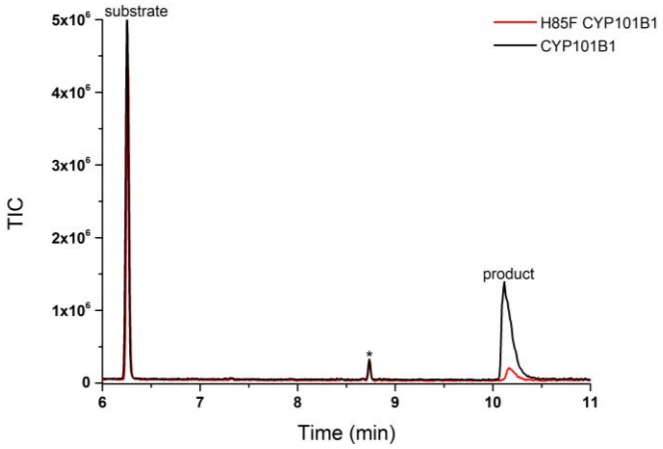

Figure 5. 47 GC-MS analysis of the turnover of 2,7-dimethylnaphthalene by H85F CYP101B1 (red) and CYP101B1 (black). 2,7-Dimethylnaphthalene (RT 6.3 min) and the product 2-(7-methylnaphthyl)methanol (RT 10.2 min). Impurities are labelled (*).

Acenaphthene is found in tobacco smoke and broiled food [269, 270]. This substrate induced the heme spin to 60% high spin-state in the H85F variant but only 30% in the WT (Figure 5. 48). H85F variant bound acenaphthene with a higher affinity compared to the WT (K_d = 5.9 ± 0.6 µM versus K_d = 20 ± 4 µM; Figure 5. 48). The NADH oxidation rate (531 min^{-1} versus 165 min^{-1}) and product formation activity (245 min^{-1} versus 42 min^{-1}) were also significantly greater for the H85F variant as was the coupling efficiency (48% versus 25%; Table 5. 7).

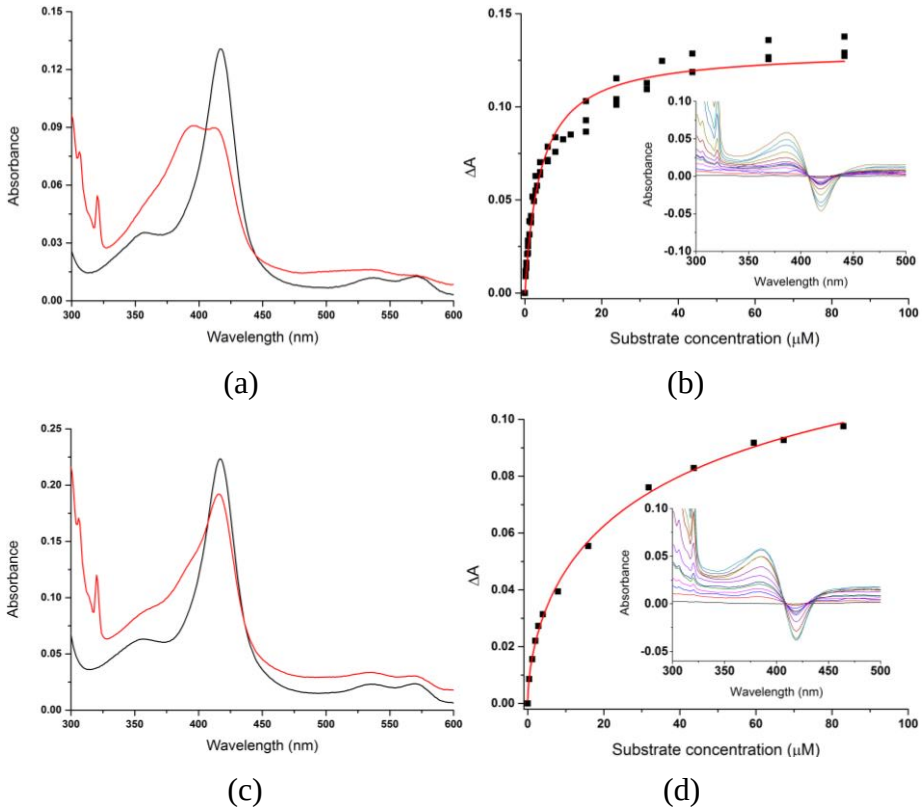

Figure 5. 48 Spin-state shifts (left) and dissociation constants (right) of H85F and WT CYP101B1 with acenaphthene. Spin-state shifts (red) of **(a)** H85F CYP101B1 and **(c)** WT CYP101B1. The dissociation constants of **(b)** H85F 1.44 µM/K_d 5.9 µM and **(d)** WT CYP101B1 1.32 µM/K_d 20 µM. The concentration of the enzyme used in the binding assays and the dissociation constant (K_d) are provided.

WT and H85F CYP101B1 mediated oxidation of acenaphthene resulted in a single metabolite. The H85F variant catalysed the oxidation with significantly higher yield, and the mass spectrum was indicative of a monooxygenase metabolite (m^+/z = 170.0, Figure 5. 49 and Figure D. 1). The metabolite was generated in a sufficient amount by whole-cell oxidation system. This was purified (~16 mg) and characterised by NMR spectrum analysis (Figure 5. 43, Figure

5. 49 and Figure D. 16-D. 19). The ^{1}H NMR spectrum displayed a distinct doublet peak at 5.75 ppm, suggested hydroxylation occurred in the ethylene bridge connecting positions 1 and 8 of the naphthalene. Therefore, the product was identified as 1-acenaphthol (Figure 5. 43, Figure 5. 49 and Figure D. 16-D. 19) [271]. The enantioselectivity of the metabolite was investigated by chiral HPLC (Figure 5. 49). The WT and the H85F CYP101B1 generated a 70:30 and 60:40 ratios of the enantiomers, respectively (Figure 5. 49).

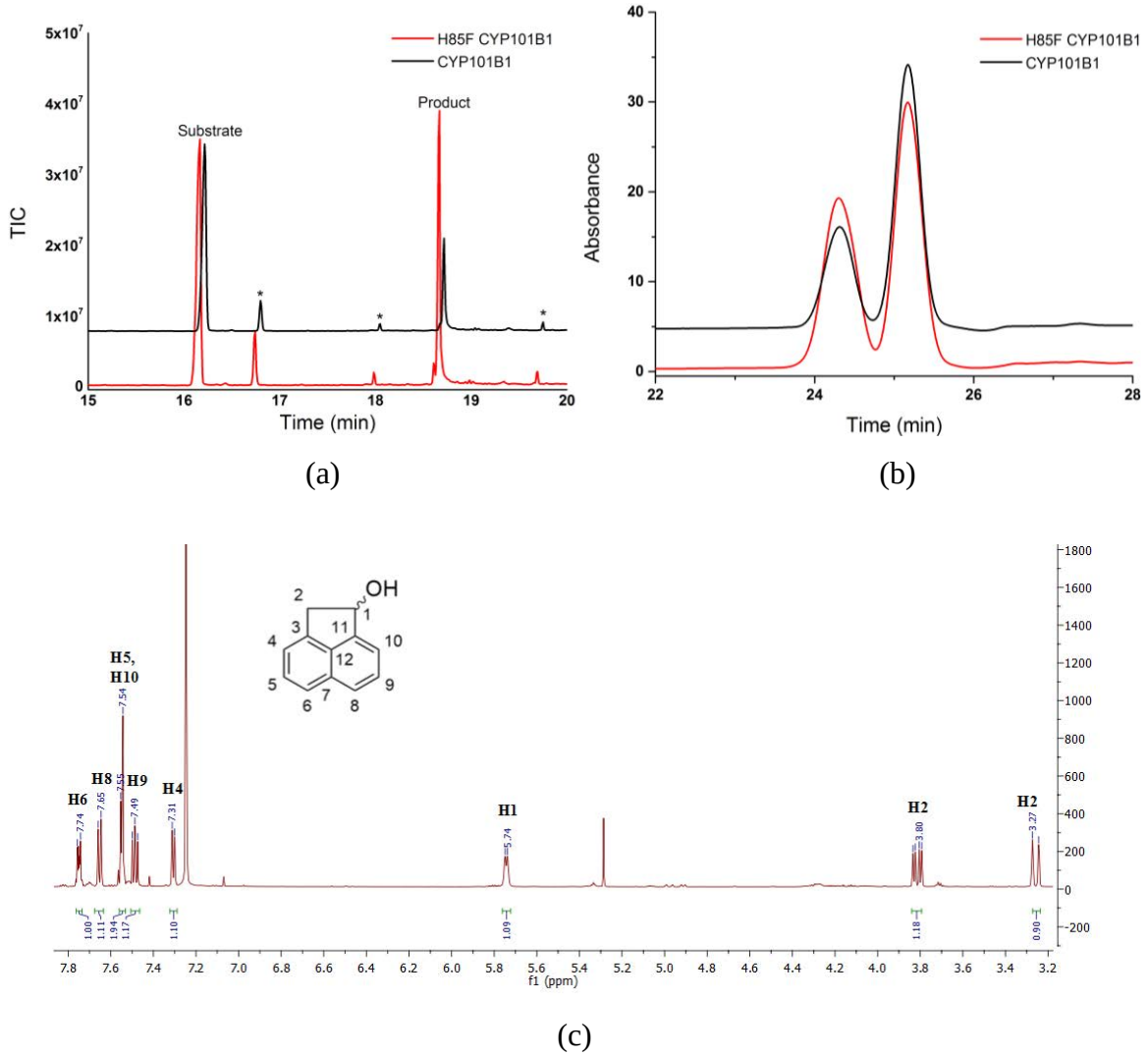

Figure 5. 49 (a) GC-MS analyses of the *in vitro* turnovers of acenaphthene by H85F (red) and WT (black) CYP101B1. Acenaphthene (RT 16.2 min) and the product; 1-acenaphthol (RT 18.8 min). The chromatogram (CYP101B1; black) was offset along the x and y-axes for clarity **(b)** Chiral HPLC analysis of the *in vitro* turnover of acenaphthene by H85F CYP101B1 (red) and CYP101B1 (black), and a mixture of enantiomer of 1-acenaphthol was detected. Impurities are labelled (*). **(c)** ^{1}H NMR spectrum of 1-acenaphthol. Full data are in Appendix D (Figure D. 16-D. 19).

WT CYP101B1 has been shown to have moderate activity for the oxidation of methyl biphenyl compounds and phenylcyclohexane [266]. Phenylcyclohexane induced a similar spin-state shift in both variants of CYP101B1, but the oxidation activity for H85F variant was slower than the WT (Figure 5. 50 and Table 5. 8). The NADH oxidation (106 min^{-1} versus 293 min^{-1}) and product formation rates (22 min^{-1} versus 141 min^{-1}) were significantly reduced (Table 5. 8). The mutant also generated a lower level of oxidised metabolite (Figure 5. 51). A single product was observed in the turnover of phenylcyclohexane with both variants (Figure 5. 51). The metabolite has been identified as *trans*-4-phenylcyclohexanol, which was confirmed by GC-MS coelution experiment with the turnover of WT CYP101B1 (m^+/z = 176.15; Figure 5. 51, Figure 5. 55 and Figure D. 1) [175, 266].

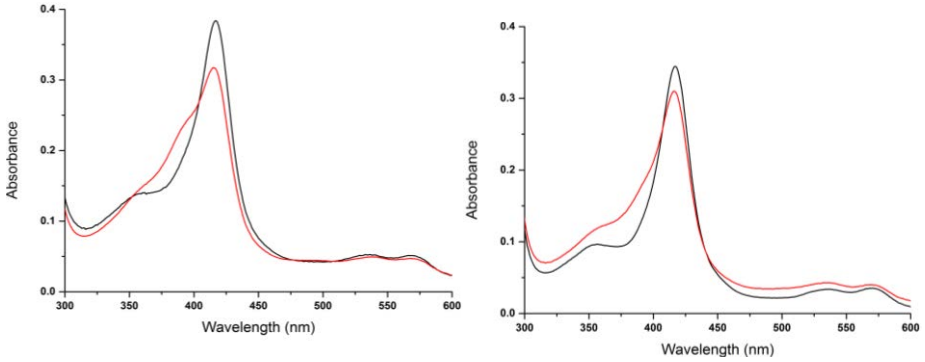

(a) (b)

Figure 5. 50 Spin-state shifts (red) of **(a)** H85F and **(b)** WT variants after addition of phenylcyclohexane.

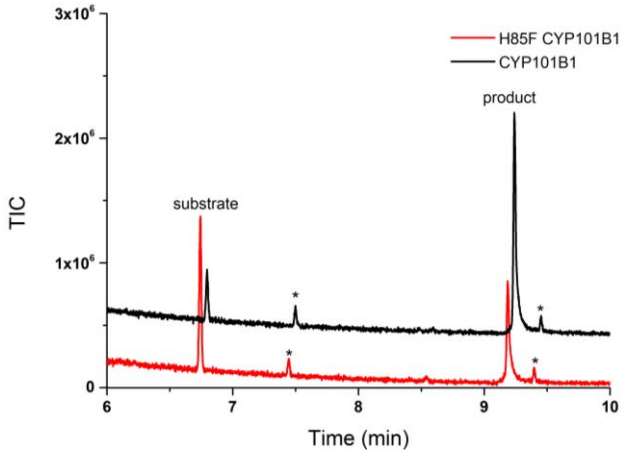

Figure 5. 51 GC-MS analyses of the turnovers of phenylcyclohexane by H85F (red) and WT (black) CYP101B1. Phenylcyclohexane (RT 6.9 min) and the product *trans*-4-phenylcyclohexanol (RT 9.2 min) [175, 266]. Impurities are labelled (*). The chromatogram (CYP101B1; black) was offset along the x and y-axes for clarity.

A higher spin-state shift (20%) and comparably slower NADH oxidation rate were measured for H85F mutant enzyme upon addition of biphenyl than the WT (Figure 5. 52 and Table 5. 8). However, this variant oxidised biphenyl with a higher product formation rate (23 min^{-1}) and coupling efficiency (16%) than these of the WT enzyme (Table 5. 8). Both variants oxidised biphenyl into single monooxygenase metabolite that was identified as 4-phenylphenol by coeluting with an authentic standard in GC-MS (m^+/z = 170.15; Figure 5. 52, Figure 5. 55 and Figure D. 1) [266].

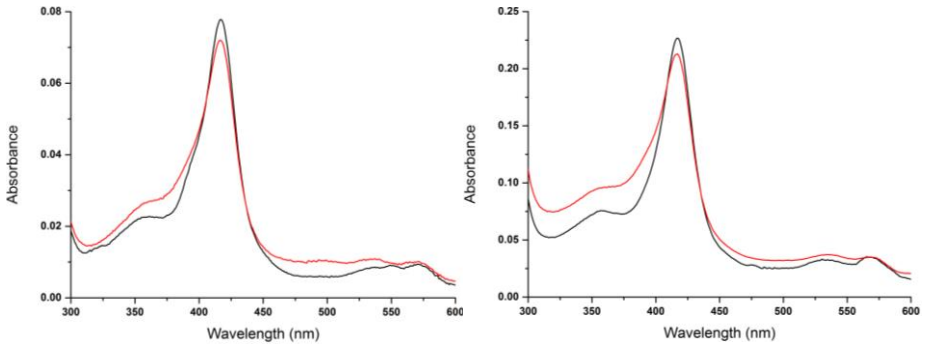

(a) (b)

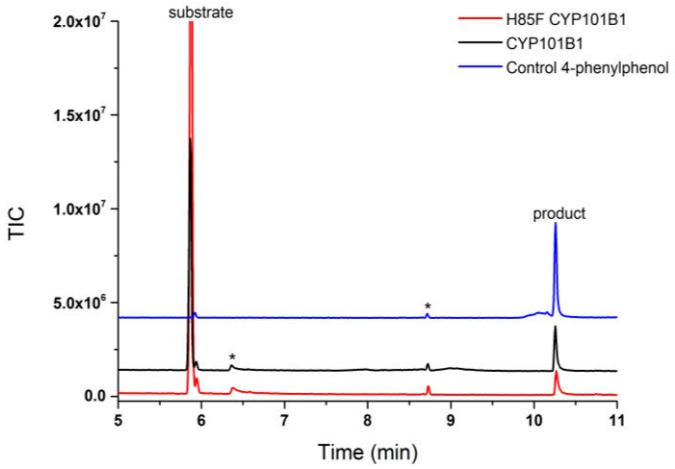

(c)

Figure 5. 52 Spin-state shifts (red) of **(a)** H85F CYP101B1 and **(b)** WT CYP101B1 after addition of biphenyl. **(c)** GC-MS analyses of the turnovers of biphenyl by H85F CYP101B1 (red) and CYP101B1 (black). Biphenyl (RT 5.9 min) and the product 4-phenylphenol (RT 10.25 min; authentic standard: blue). Impurities are labelled (*).

Methylbiphenyls with the substituent at the 2-, 3- and 4-positions were also investigated with the H85F mutant enzyme. All these substituted biphenyls induced a small type I spin-state shift

(≤30%) upon addition in the H85F mutant (Figure 5. 53). However, in all instances, the NADH oxidation and product formation rates were reduced for the H85F mutant versus the WT enzyme. The coupling efficiencies with the mutant were also lower (Table 5. 8).

Both variants selectively oxidised 2- and 3-methylbiphenyl into a single metabolite arising from the benzylic C-H bond hydroxylation (Figure 5. 54). 2-Biphenylmethanol was confirmed by HPLC and GC-MS coelution experiments with an authentic standard (m^+/z = 184.05; Figure 5. 54, Figure 5. 55 and Figure D. 1).

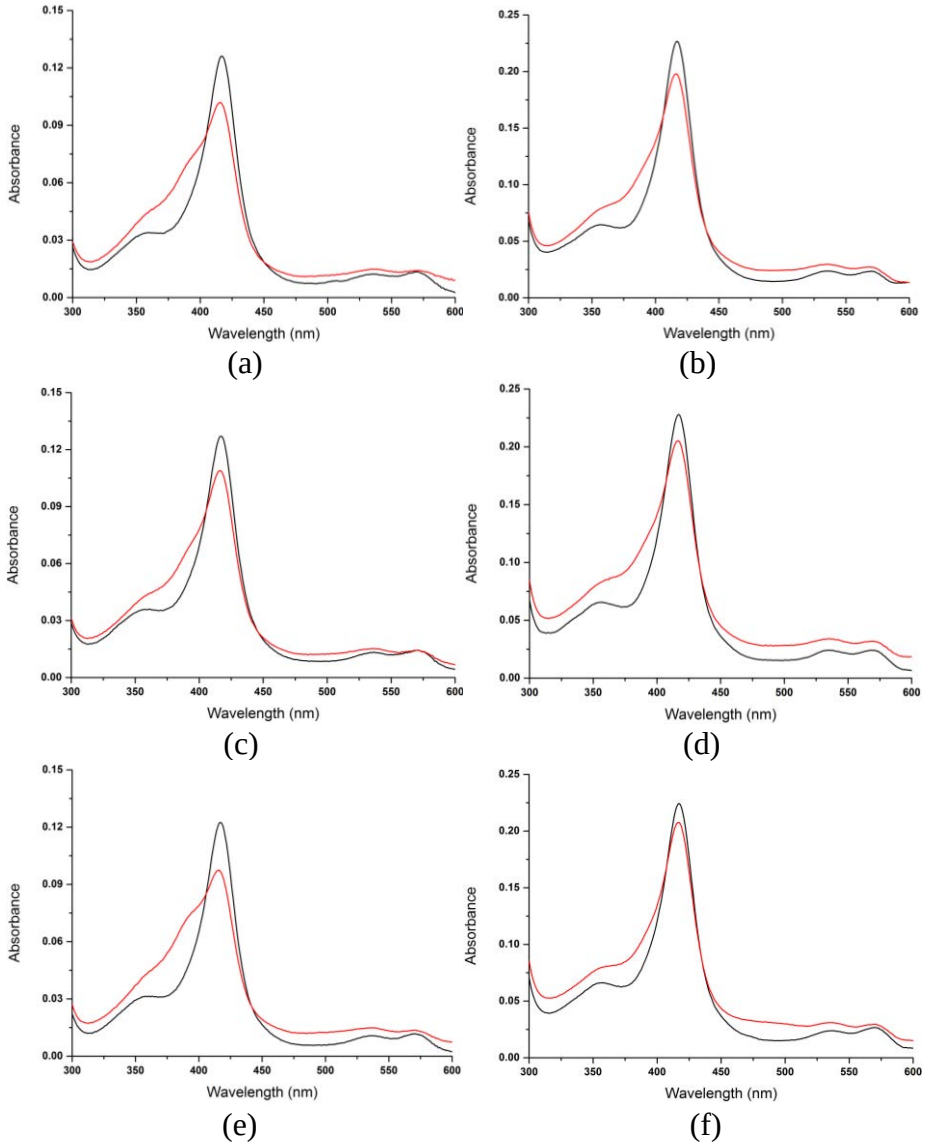

Figure 5. 53 (left) Spin-state shifts (red) of H85F CYP101B1 after addition of **(a)** 2-methylbiphenyl, **(c)** 2-methylbiphenyl, **(e)** 4-methylbiphenyl, and **(right)** spin-state shifts (red) of WT CYP101B1 with **(b)** 2-methylbiphenyl, **(d)** 2-methylbiphenyl and **(f)** 4-methylbiphenyl.

Table 5. 8 Substrate binding, turnover and coupling efficiency data for CYP101B1 (WT and the H85F variant) with phenylcyclohexane, biphenyl and substituted biphenyls [266]. The *in vitro* turnover activities were measured as described in Table 5. 1. The data are reported as mean ± S.D. (n = 3) and rates are given in nmol.nmol-CYP^{-1}.min^{-1}.

Substrate	CYP101B1	%HS heme	N (min^{-1})	PFR (min^{-1})	C %
phenylcyclohexane	WT [175, 266]	20	293 ± 9	141 ± 17	48
	H85F	**20**	**106 ± 5**	**22 ± 1**	**21**
biphenyl	WT [266]	15	200 ± 10	8 ± 2	7
	H85F	**20**	**154 ± 5**	**23 ± 1**	**16**
2-methylbiphenyl	WT [266]	20	257 ± 9	35 ± 8	14
	H85F	**30**	**102 ± 9**	**17 ± 1**	**17**
3-methylbiphenyl	WT [266]	20	127 ± 10	30 ± 12	23
	H85F	**20**	**81 ± 3**	**7 ± 0.5**	**8**
4-methylbiphenyl	WT [266]	20	176 ± 10	39 ± 7	22
	H85F	**30**	**72 ± 8**	**5 ± 1**	**6**

The oxidised metabolite of 3-methylbiphenyl was generated in a larger amount via the whole-cell oxidation system, purified using silica column chromatography and identified by NMR analysis (Figure D. 15) [266]. The characteristic 2H signal at 4.77 ppm (C**H**$_2$OH) and the presence of nine hydrogens signals of the aromatic region in ^{1}H NMR spectrum, allowed characterisation of the product as 3-biphenylmethanol (Figure D. 15) [266]. The mass spectrum analysis was also in agreement with this assignment (m^+/z = 184.10; Figure 5. 54, Figure 5. 55, and Figure D. 1) [233, 266].

GC-MS analysis showed that two metabolites were formed in the turnovers of 4-methylbiphenyl by H85F CYP101B1. The products were identified by coelution experiment in GC-MS and HPLC with the *in vitro* turnover metabolites of WT CYP101B1 which were previously reported (Figure 5. 54 and Figure 5. 55) [233, 266]. The H85F variant favoured the generation of 4-biphenylmethanol (95%), whereas WT generated 4′-(4-methylphenyl)phenol (70%) as a significant product (Both m^+/z = 184.1; Figure 5. 54, Figure 5. 55 and Figure D. 1) [266].

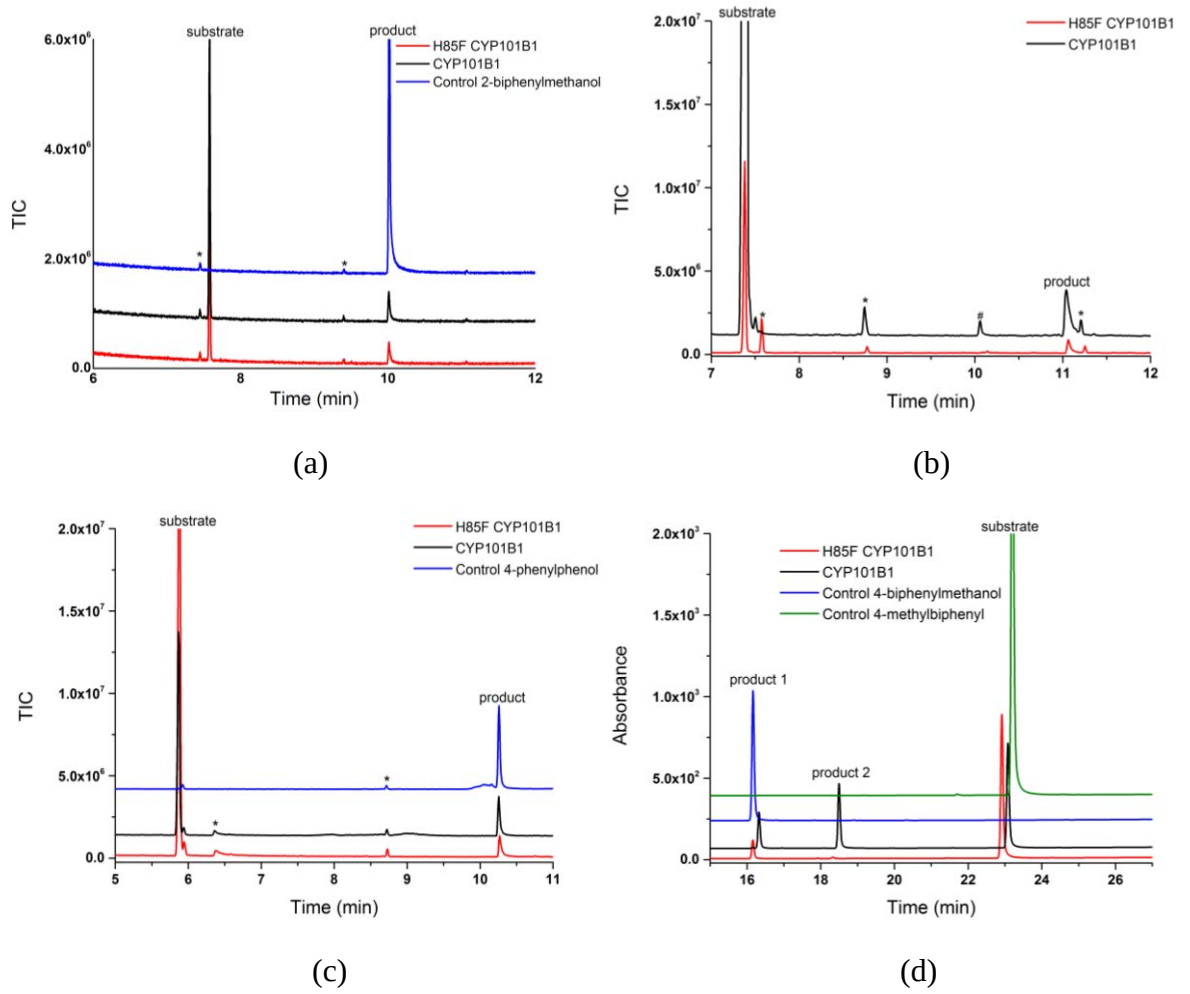

Figure 5. 54 (a) GC-MS analyses of the turnovers of 2-methylbiphenyl by H85F (red) and WT (black) CYP101B1. 2-Methylbiphenyl (RT 7.6 min) and the product; 2-biphenylmethanol (RT 10.0 min). **(b)** GC-MS analyses of the turnovers of 3-methylbiphenyl by H85F (red) and WT (black) CYP101B1. 3-Methylbiphenyl (RT 8.3 min) and the products; #3-phenylbenzaldehyde (RT 10.1 min) and 3-biphenylmethanol (RT 11.0 min). **(c)** GC-MS analyses of the turnovers of biphenyl by H85F (red) and WT (black) CYP101B1. Biphenyl (RT 5.9 min) and the product; 4-phenylphenol (RT 10.25 min). **(d)** HPLC analysis of the turnover of 4-methylbiphenyl by H85F (red) and WT (black) CYP101B1. 4-Methylbiphenyl (RT 23.0 min) and the products; 4-biphenylmethanol (RT 16.1 min, product 1) and 4´-(4-methylphenyl)phenol (RT 18.2 min, product 2) [233, 266]. The chromatograms (products control and CYP101B1) were offset along the x and y-axes for clarity. Impurities are labelled (*).

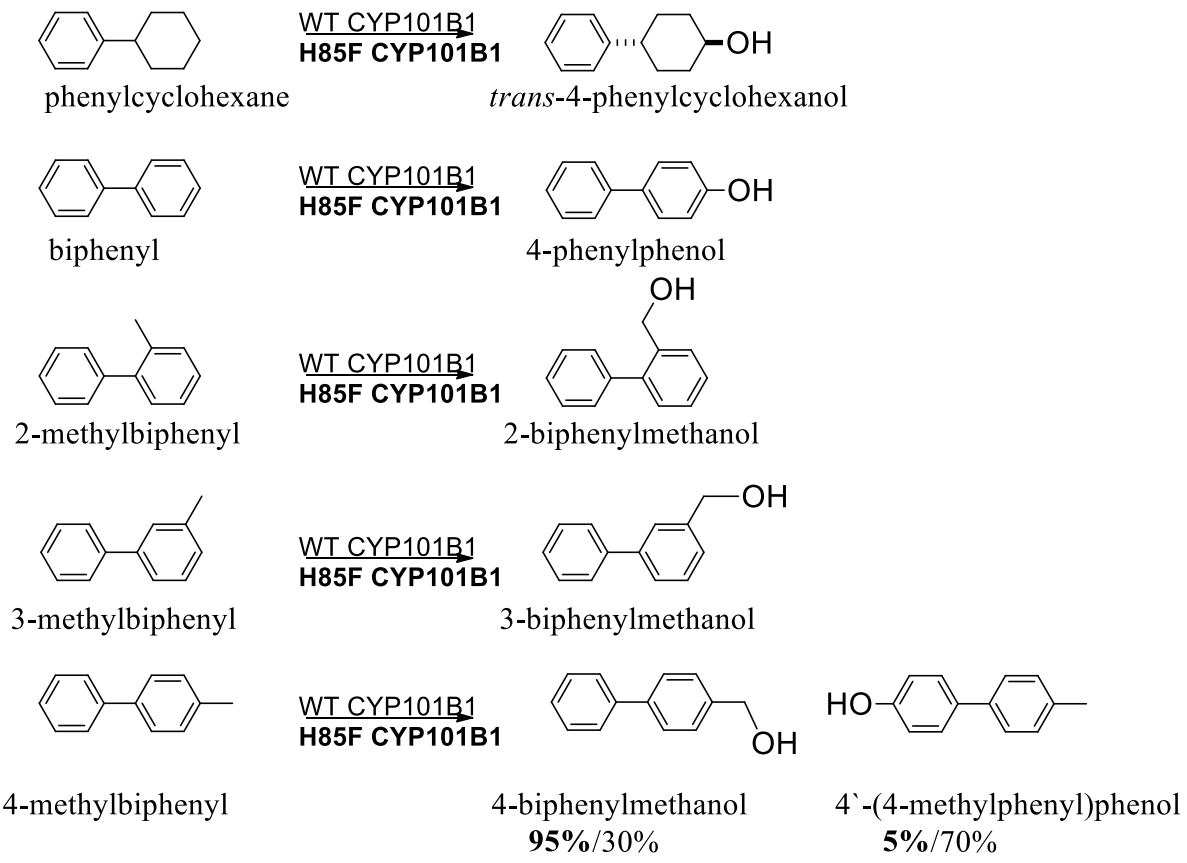

Figure 5. 55 The products generated from the CYP101B1 and H85F CYP101B1 turnovers with phenylcyclohexane and biphenyl substrates [265, 266].

5.4. Discussion

The results indicated that alkylbenzenes and certain methylnaphthalenes were better accommodated in the active site of the H85F mutant of CYP101B1. Many of these compounds induced a greater spin-state shift in the H85F mutant indicative of a better active site/substrate fit. In most instances, the H85F variant displayed a higher binding affinity with these substrates than the WT. Many of the hydroxylation reactions of these substrates were selective. Products were generated with higher catalytic activity with the H85F variant than they were with the WT enzyme. However, longer substrates including biphenyls and phenylcyclohexane displayed poor binding and lower activities with the H85F variant.

The coupling efficiencies and product formation rates for most of the tested alkyl substituted benzenes were higher with the H85F variant. In some occasions, this was despite a lower spin-state shift. This suggests that the gating mechanism in CYP101B1 may be less stringent than is observed in other systems such as CYP101A1, which is in agreement with results obtained for other CYP101 family enzymes [47, 250, 273]. Changes in the regio- and stereoselectivity of product formation were observed in certain substrate oxidations with the H85F mutant enzyme. In the oxidation of *β*-ionone, H85F variant was 90% selective for hydroxylation at the allylic C-H bond, generating 4-hydroxy-*β*-ionone in contrast to the WT enzyme which formed 3-hydroxy-*β*-ionone in excess (90%). These selectivity changes indicate that the histidine 85 residue of CYP101B1 must be in the active site or the access channel of CYP101B1, and that it interacts with the norisoprenoid substrate to control its binding orientation [175]. The oxidation of ethylbenzene, alkylnaphthalenes, acenaphthene and indane were selective, and hydroxylation occurred at a benzylic C-H bond. The presence of substituents on the benzene ring altered the selectivity with the observation of competition between two alkyl substituents. The enzymatic oxidation of 2- and 3-ethyltoluene generated metabolites from oxidation at the less reactive methyl substituent which was consistent with the reactivity observed with *p*-cymene, suggesting a preference for oxidation at benzylic methyl groups over longer and more branched chain alkyl groups. The oxidation of styrene resulted in epoxidation which was also consistent in other substituted styrenes. However, oxidation of *β*-methylstyrene to generate 3-phenyl-2-propen-1-ol (cinnamyl alcohol) suggests that the allylic methyl group of *β*-methylstyrene must be located significantly closer to the heme iron than the more reactive alkene. The increased flexibility and longer chain substrates such as *n*-propylbenzene resulted in preferential hydroxylation at the benzylic position though the major metabolite was the ketone further oxidation product. Isobutylbenzene hydroxylation was shifted to the tertiary *β*-carbon, and the branching in the alkyl chain must alter the binding orientation of substrate in the vicinity of the heme iron. When incorporated into whole-cell biotransformation system, with the physiological electron transfer partners, ArR/Arx and the CYP101B1 H85F variant was capable of synthesising the oxidised metabolites of alkylbenzenes and naphthalenes in good yields for characterisation (18-33 mg of purified naphthalene metabolites were generated from 200 ml of culture after a 16 h reaction performed as described in the experimental section) [265].

The oxidation of *o*-, *m*- and *p*-xylene occurred without any observation of products arising from a 1,2-shift, and the oxidation of the longer alkylbenzene substrates displayed minimal

desaturation activity (<1%). There was also little or no oxidation at the aromatic ring. All of these reactions were observed with CYP102A1 [267, 274, 275]. The ability of WT and H85F variant of CYP101B1 to favour hydroxylation at less reactive positions in certain substrates may make it a useful for future synthetic applications. Longer substrates such as phenylcyclohexane and biphenyls were poor substrates for the H85F variant which suggests that this mutation may result in less available space for substrate binding or difficult to accommodate into the binding pocket. H85A and H85G variants of CYP101B1 have also been investigated with different hydrophobic substrates, but they also exhibited lower binding affinity and oxidation activity compared to WT CYP101B1 with biphenyls [264]. Mutations at other residues in the active site of CYP101B1 could be used to generate variants that could bind and oxidise these longer aromatic substrates efficiently. The active site of CYP101A1 has been modified, for example, glutamine 234 and isoleucine 237 of CYP101B1 align with leucine 244 and valine 247 which have been altered to increase the activity of CYP101A1 for unnatural substrates [143]. These mutagenesis experiments could be expanded to enable the development of biocatalytic routes to synthesise fine chemicals arising from the oxidation of aromatic substrates [265].

Chapter 6

6. The Selective Oxidation of Alkyl Substituted Cubanes Using CYP101B1 Enzyme

6.1. Introduction

Cubane (C_8H_8) is comprised of eight methine (CH) units arrayed in a cubic formation, resulting in a compact approximately, spherical molecular entity (Figure 6. 1) [276]. The unnatural and unique geometry of cubane makes it highly strained in nature (SE = 161.5 kcal mol^{-1}) and thermodynamically unstable (ΔH_f = 144 kcal mol^{-1}) [276-278]. However, cubane and its derivatives are kinetically stable [276, 278-280].

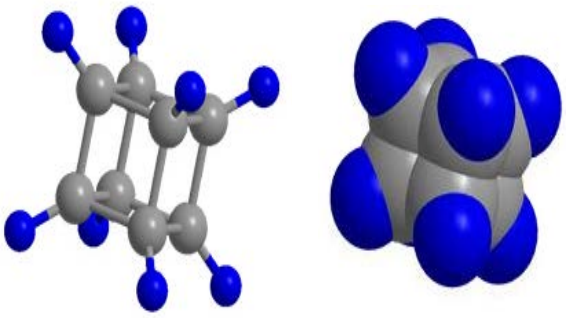

Figure 6. 1 Three-dimensional views of cubane [281].

Cubane has been hypothesised as a bioisostere for benzene due to its similar size and shape, and subsequently, several groups have reported that it can be used to develop new drug molecules with improved characteristics over existing candidates [282-284]. Some cubane analogues have shown improved bioactivity than their benzene counterparts (Figure 6. 2) [277, 284, 285]. For example, different benzene containing drug derivatives and their cubane analogues were investigated to compare their activity (Figure 6. 2). Subacube and cubocaine performed identically to SAHA (suberoylanilide hydroxamic acid) and benzocaine, respectively (Figure 6. 2). Diflucuburon also showed better bioactivity over its benzene counterparts (Figure 6. 2) [277]. One advantage of using cubane rather than benzene is that it would be less prone to phase I drug metabolism by cytochrome P450 enzymes, due to its strong C-H bond (BDE = 104 kcal mol^{-1}; Table 6. 1) [276, 277, 286]. The metabolism of cubane by P450 hydroxylation is decreased

due to the hindrance of tertiary C-H bonds and its high *s* orbital character [277, 285, 287]. The oxidation of a phenyl ring by P450s proceeds via the addition of hydroxyl to the electron-rich π-moiety [287]. For example, $P450_{cam}$ mediated oxidation of *tert*-butylcubane and *tert*-butylbenzene generated only one metabolite (hydroxylation of the methyl group of *tert*-butylcubane) and two metabolites (hydroxylation of the methyl and aromatic ring), respectively [277]. This is one of the proposed explanations for the better activity of diflucuburon over diflubenzuron [277]. The presence of the eight-membered cubane cage also increases the lipophilicity of the drug molecule that allows easier transport across cell membranes [276]. Furthermore, cubane is considered as a candidate for novel synthesis of fuels, propellants and explosives [276, 281].

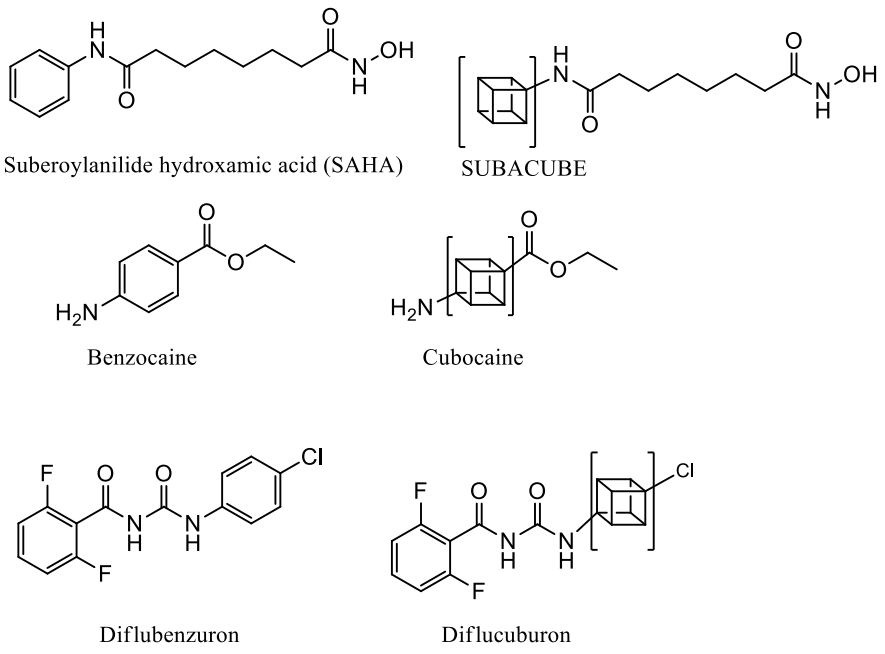

Figure 6. 2 Cubane as a bioisostere for benzene [277, 285]. The names for the cubane derivatives were based on the hypothetical brand name [277].

The main drawback regarding the use of cubane was the availability of suitable cubane precursors to enable synthesis [277]. This problem has been overcome by the discovery of large-scale synthesis of dimethyl cubane-1,4-dicarboxylate, which can be generated on a kilogram scale [277]. Recently several cubane drug derivatives were synthesised from the dimethyl cubane-1,4-dicarboxylate precursor, using a wide range of organic chemistry methodologies and conditions to which the cubane core proved to be tolerant [277]. Another disadvantage of using

cubane is functional-group placement and manipulation. New methods for functionalising of cubane substrates are required to synthesise potential biologically active pharmacophores and agrochemical molecules [277, 283, 288].

Table 6. 1 C-H Bond Dissociation Energies (BDE) and s orbital character of different substrates [289-293].

Substrate	BDE (kcal mol^{-1})	% of S Character
Cubane	104	30
Benzene	111	33.3
Cyclopropane	106.3	32
Cyclobutane	99.8	27
Cyclopentane	95.5	25
Cyclohexane	100.0	25
Cyclooctane	95.7	25
Cyclononane	96.3	25
Methane	104.3	25
Ethane	101.2	25

Stability of a bond is linked to the amount of s character as increasing this leads to stronger C-H bonds [293, 294, 232]. Cubane hydrogens (ca. 30% s character) are more readily abstracted by *t*-butoxyl radicals than those of cyclopropane (ca. 32% s character) and surprisingly the hydrogens of the methyl group in methylcubane [295-297]. Several groups have also reported oxidation of cubane using methyl(trifluoromethyl)dioxirane, and the selective halogenation of cubane by polyhalomethanes as halogen sources under phase-transfer (PT) conditions [298, 299]. However, there are no reports of efficient and selective oxidation at the primary C-H bonds of the methyl group in methylcubane derivatives.

Methylcubanes show interesting reactivity. Mammalian P450-mediated oxidation of methylcubanes generated a mixture of cubylmethanol, methylcubanols and other cationic rearrangement metabolites [84, 297]. In principle, it can be oxidised at two types of C-H bonds either the methyl group or a C-H of the cube [84, 296, 297, 300]. Radical intermediates would be formed during hydroxylation if a hydrogen atom is abstracted. The cubylcarbinyl radical can

rearrange rapidly to form different products (Figure 6. 3). If a cationic intermediate (4) is formed a distinct rearrangement to 1-homocubanol (5) would be possible (Figure 6. 3) [282]. The rapid nature of the initial *β*-scission step ($k = 2 \times 10^{10}\ s^{-1}$) of the methylcubane derived radical (cubylcarbinyl), is one of the fastest reported radical reactions and enables methylcubane to be used as a radical clock [84, 177, 297, 298]. The distinct radical and cation rearrangement metabolites, enable methylcubane to be used as a mechanistic probe for the identification of radical or cationic intermediates formed during the C-H oxidation reaction of P450s (Figure 6. 3) [84, 177, 296, 297, 300].

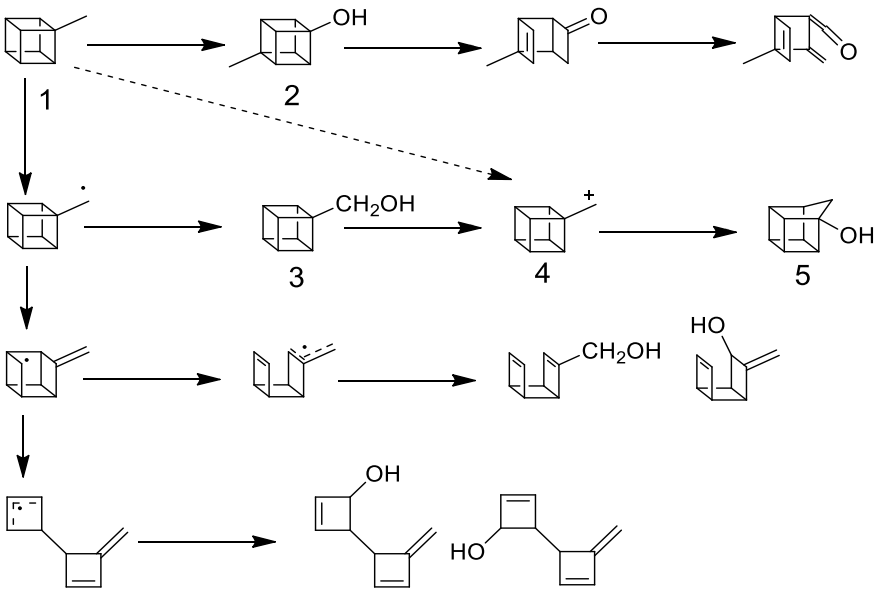

Figure 6. 3 Potential radical and cationic rearrangement products which could arise from P450 oxidation reactions [282].

For example, the methane monooxygenase (MMO) from *Methylococcus capsulatus* oxidised methylcubane to cubylmethanol and MMO from *Methylosinus trichosporium* OB3b gave rise to a mixture of metabolites such as cubylmethanol, methylcubanols and a radical rearrangement product (Figure 6. 4) [177, 297]. The accurate and detailed analysis of the products was hampered due to the low rate, yield and selectivity of the reactions, the fragile nature of methylcubanols and the volatile nature of the substrate and products (Figure 6. 4) [301-303]. The different metabolites observed in methylcubane oxidation by P450 and MMO systems have been rationalised via their reactive intermediates (heme versus non-heme) and substrate specificities [84, 177, 297].

There is strong evidence that P450 enzyme hydroxylation occurs via iron(IV)oxo species (Compound I) through a radical rebound mechanism (Figure 1. 6) [2, 38, 73, 304]. In certain studies products arising from cationic intermediates have been rationalised using a two-state model of P450 reactivity. Rather than using a second oxidant, such as hydroperoxo complex, Cpd 0 the precursor to Cpd I, the two-state model hypothesises that the reactive intermediate (compound I) can be present in doublet and quartet states (Figure 1. 6) [25, 84, 87, 101, 103].

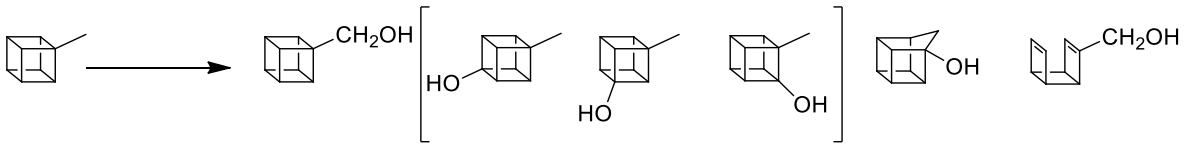

MMO *Me. tri.*	40%	18% total methylcubanols			0%	42%
MMO *M. cap.*[a]	100%	0% total methylcubanols			0%	0%
CYP2B1 Choi[a]	22%	38%	29%	13%	nr	nr
CYP2B1 Newcomb[a]	54-78%	9-17%	6-19%	5-17%	<1%	0%
CYP2E1[a]	42-71%	1-13%	7-20%	10-20%	6-14%	0%

Figure 6. 4 The reactions of various methane monooxygenase (MMO) and cytochrome P450 (CYP) enzymes with methylcubane and their product distributions. [a] Reported as the acetate derivatives. The total yield of product in most instances was low (<25 μmoles product or <1% yield reported for the CYP reactions and that of MMO *M. cap*.) [301-303]. Higher yields were reported with MMO *Me. tri*. (A yield of 5% was estimated) [301-303]. *Me. tri*. *Methylosinus trichosporium*; *M. cap. Methylococcus capsulatus*.

The selectivity and activity of CYP101B1 can be improved by the addition of carbonyl directing groups [176, 182]. For example, CYP101B1 can regioselectively oxidise *β*-ionone, isobornyl acetate and 2-adamantyl acetate at a C-H bond on the opposite side of the cyclic ring system to the carbonyl-containing substituent [176, 182]. In order to assess whether CYP101B1 could be used to efficiently and selectively introduce a hydroxyl group at the methyl substituent of a methylcubane derivative, a series of cubane derivatives were designed and evaluated (Figure 6. 5).

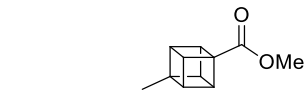

4-methylcubane-1-methoxy carbonyl

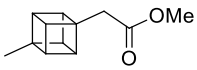

4-methylcubane-1-acetic acid methyl ester

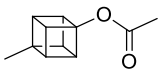

4-methylcuban-1-yl acetate

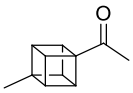

4-methylcubane-1-methyl ketone

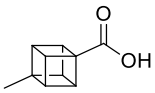

4-methylcubane-1-carboxylic acid

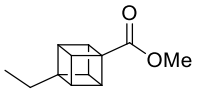

4-ethylcubane-1-methoxy carbonyl

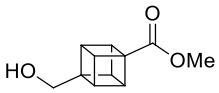

4-hydroxymethylcubane-1-methoxy carbonyl

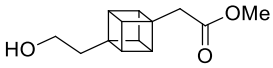

4-(2-hydroxyethyl)-cubane-1-methoxy carbonyl

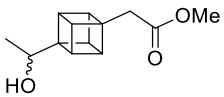

4-(1-hydroxyethyl)-cubane-1-methoxy carbonyl

Figure 6. 5 Cubane derivatives used in this study with CYP101B1. All these cubane derivatives were synthesised and supplied by Sevan D. Houston (University of Queensland) using standard synthetic methods described in Appendix E.

6.2. Results

Addition of 4-methylcubane-1-methoxy carbonyl induced a 50% heme spin-state shift in CYP101B1 to the high spin form (Figure 6. 6). The NADH oxidation and product formation rates were determined to measure the catalytic activity. The NADH turnover rate was 438 ± 5 min^{-1} (Table 6. 2). The amount of product was quantitated by calibrating the GC-MS detector response of 4-hydroxymethyl-cubane-1-methoxy carbonyl, and the product formation rate was 155 min^{-1} (Table 6. 2). CYP101B1 system displayed a coupling efficiency of 36% for the oxidation of the 4-methylcubane-1-methoxy carbonyl (Table 6. 2).

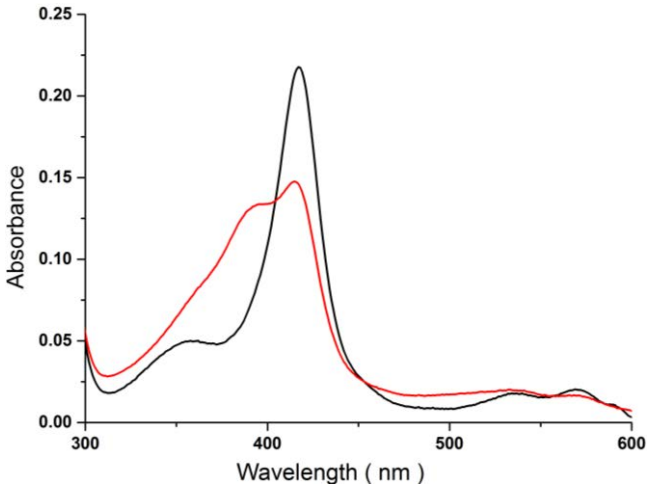

Figure 6. 6 Spin-state shift of CYP101B1 with 4-methylcubane-1-methoxy carbonyl (red).

GC (BID detector) and GC-MS analysis revealed that a single major product was generated in the small-scale *in vitro* turnovers of CYP101B1 with 4-methylcubane-1-methoxy carbonyl (Figure 6. 7 (a)). A larger scale turnover was also carried out with excess NADH (~4 mM) in order to generate enough metabolite for NMR analysis (Figure 6. 7 (b)). GC-MS analyses of these large-scale turnovers indicated that very little or no substrate remained. The same main product was detected in both small and large-scale turnovers by GC-MS. This was identified as 4-hydroxymethylcubane-1-methoxy carbonyl by GC-MS coelution experiment with an authentic standard (m^+/z = 192.35; Figure 6. 7, Figure 6. 8 and Figure E. 7).

The ^{1}H NMR spectrum of turnover product (4-hydroxymethylcubane-1-methoxy carbonyl without purification) has two distinctive signals for the six hydrogens of the *para*-substituted cubane (in the range 3.70-4.16 ppm). In addition, there is also a 2H signal peak for the hydroxymethyl substituent at 3.76-3.78 (m, 2H, 2xH11), confirming the product identified by GC-MS coelution experiment (Figure 6. 8, Figure 6. 9 and Figure E. 8-E. 9). In the larger-scale turnovers, several minor metabolites were observed which could be assigned by MS analysis and/or coelution experiments. The small peak in GC-MS analysis at RT 5.4 min was confirmed as a 4-methylcubane-1-carboxylic acid via MS and coelution experiment with an authentic standard, which arises from ester hydrolysis of the substrate (m^+/z = 162.0; Figure 6. 7 (b) and Figure 6. 7 (c)). Another minor peak at RT 8.16 min was labelled as the further oxidation product of 4-hydroxymethylcubane-1-methoxy carbonyl (m^+/z = 190.15; Figure 6. 7 (b) and Figure 6. 7 (c)). The peak at 9.45 min in the larger-scale turnover has a MS and retention time

consistent with hydrolysis of the product ester (4-hydroxymethylcubane-1-carboxylic acid; Figure 6. 7 (b) and Figure 6. 7 (c)). Importantly the ^{1}H NMR spectrum of the turnover product indicated no radical or cation rearrangement product or hydroxylation on the cubane C-H bonds (Figure 6. 7 and Figure E. 8-E. 9).

Table 6. 2 Substrate binding, turnover and coupling efficiency data for the CYP101B1 with 4-methylcubane-1-methoxy carbonyl, 4-methylcubane-1-acetic acid methyl ester, 4-ethylcubane-1-methoxy carbonyl, 4-methylcuban-1-yl acetate, 4-methylcubane-1-methyl ketone and 4-methylcubane-1-carboxylic acid. The *in vitro* turnover activities were measured using a ArR:Arx:CYP101B1 concentration ratio of 1:10:1 (0.5 μM CYP enzyme, 50 mM Tris, pH 7.4). N is the NADH oxidation rate, PFR the product formation rate and C is the coupling efficiency, which is the percentage of NADH utilised for the formation of products. The data are reported as mean ± S.D. (n = 3). Rates are given in nmol.nmol-CYP^{-1}.min^{-1}. [a] Measured by a single experiment. n.d not determined due to lack of product formation.

CYP101B1 Substrate	**%HS heme**	**N (min^{-1})**	**PFR (min^{-1})**	**C %**
4-methylcubane-1-methoxy carbonyl	50	438 ± 5	155 ± 39	36
4-ethylcubane-1-methoxy carbonyl	70	690 ± 28	298 ± 32	43
4-methylcubane-1-acetic acid methyl ester	85	468 ± 7	189 ± 35	41
4-methylcuban-1-yl acetate	60	374 ± 10	<10	<2.5
4-methylcubane-1-methyl ketone	30	251 ± 10	<10	<5
4-methylcubane-1-carboxylic acid	<5	39[a]	n.d.	n.d

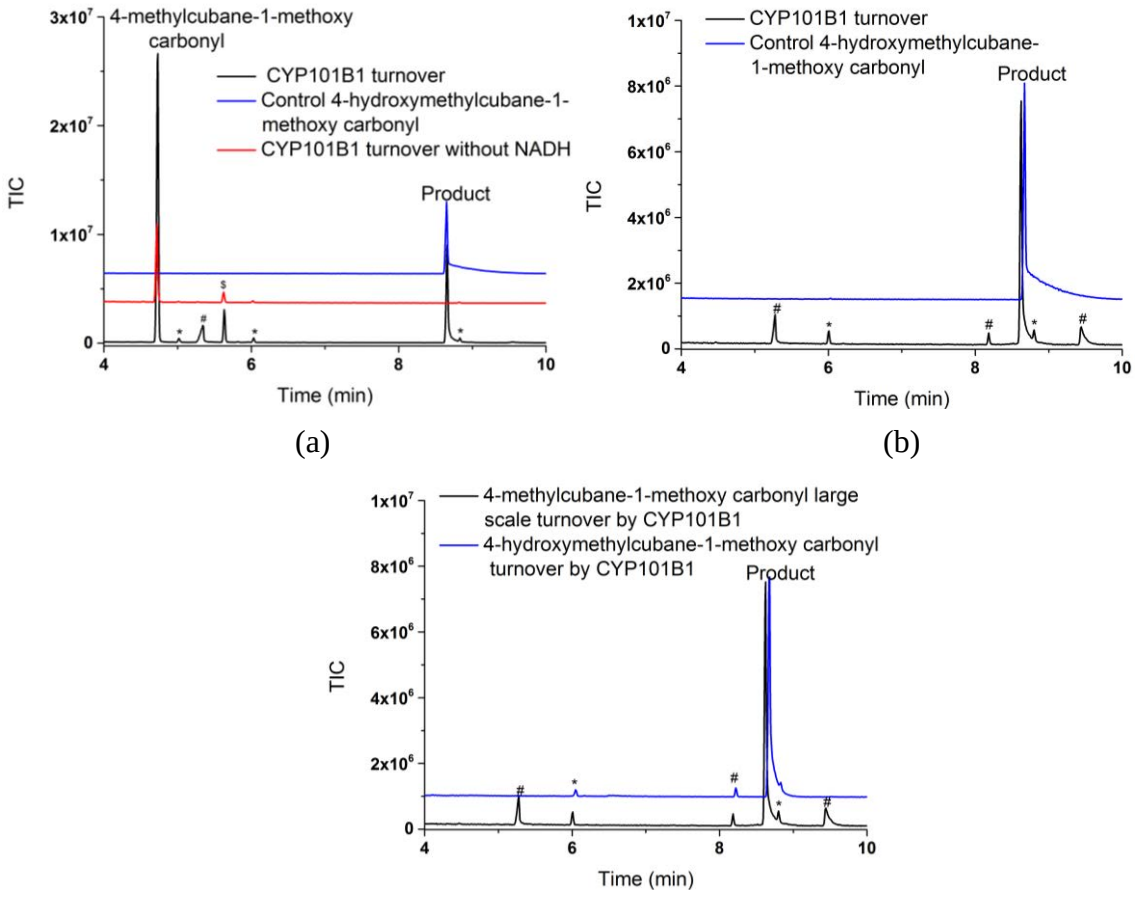

Figure 6. 7 (a) GC-MS analysis of the *in vitro* turnover of 4-methylcubane-1-methoxy carbonyl by CYP101B1. The turnover is shown in black, the product control (4-hydroxymethylcubane-1-methoxy carbonyl) in blue and a control turnover where no NADH was added in red. Impurities have been labelled (*), as have [#]4-methylcubane-1-carboxylic acid (RT 5.4 min), and an additional impurity[$] in the no NADH turnover. **(b)** GC-MS analysis of the *in vitro* larger scale turnover of 4-methylcubane-1-methoxy carbonyl by CYP101B1 using excess NADH. The large-scale turnover is overlaid with the product (4-hydroxymethyl-cubane-1-methoxy carbonyl, blue) control. **(c)** The same larger scale turnover overlaid with a CYP101B1 turnover (blue) of the product control (4-hydroxymethylcubane-1-methoxy carbonyl), highlighting the formation of the further oxidation product labelled [#] (RT 8.16 min). 4-Methylcubane-1-carboxylic acid (RT 5.4 min, #) was identified by MS and a coelution experiment with an authentic standard. It arises from ester hydrolysis of the substrate. The peak at 9.45 minutes[#] in the larger-scale turnover appears after all the substrate has been oxidised and has a MS and retention time consistent with hydrolysis of the product ester (4-hydroxy-methylcubane-1-carboxylic acid). The chromatograms (b and c) have been offset along the x and y-axes for clarity.

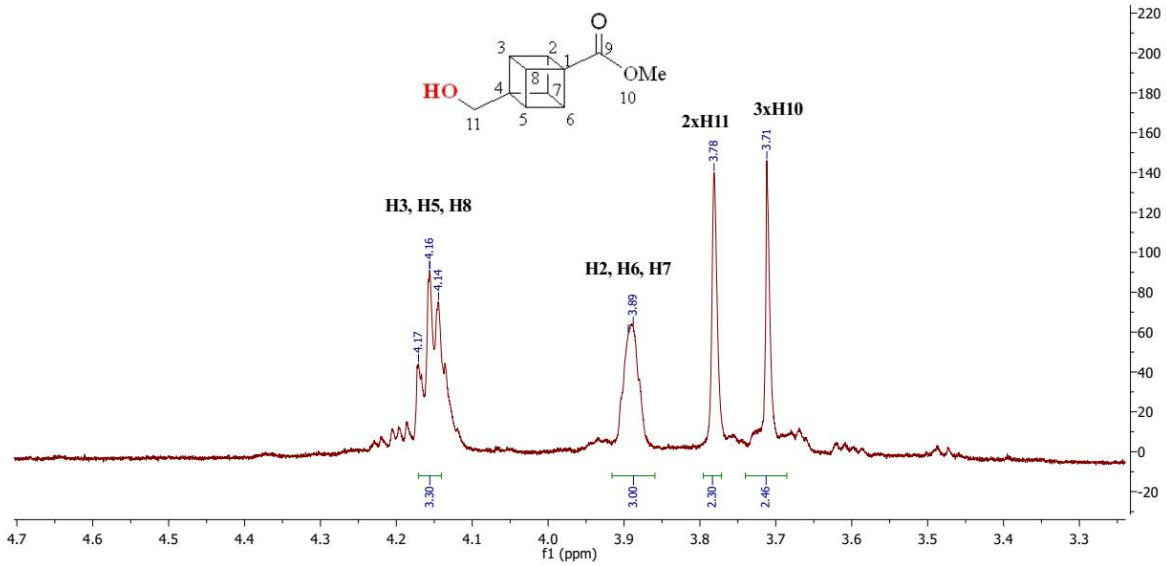

Figure 6. 8 ^{1}H NMR spectrum of 4-hydroxymethylcubane-1-methoxy carbonyl (4-methylcubane-1-methoxy carbonyl turnover). The NMR experiment was performed without purification due to the low quantity of metabolite and available substrate. Full data are presented in Appendix E (Figure E. 8-E. 9).

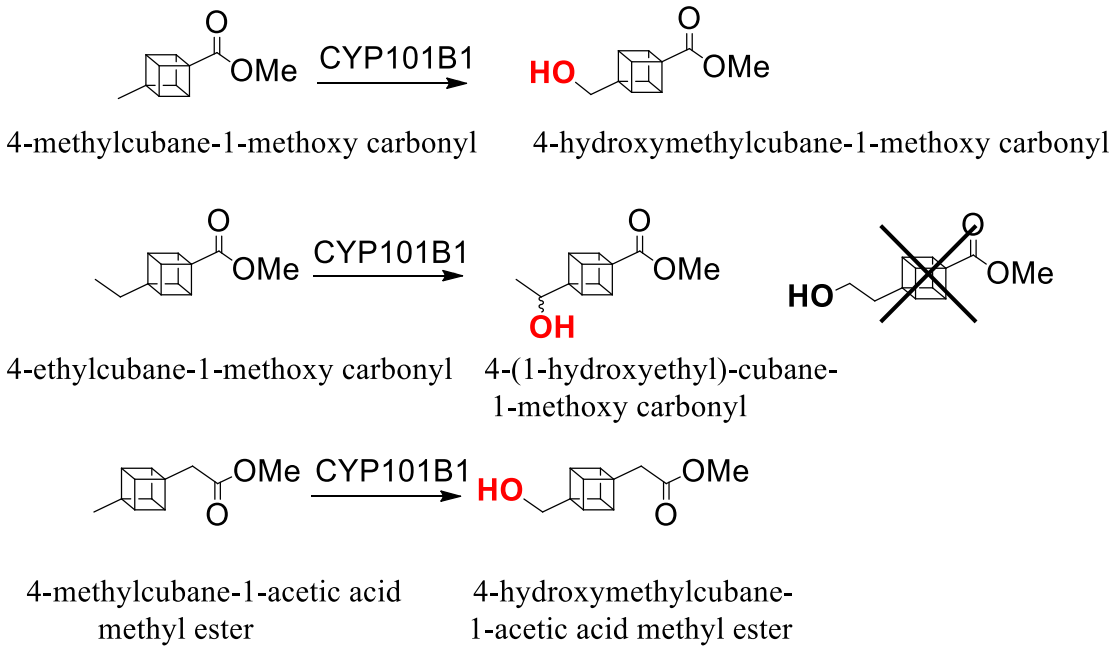

Figure 6. 9 Products identified after the oxidation of the substrates 4-methylcubane-1-methoxy carbonyl, 4-ethylcubane-1-methoxy carbonyl and 4-methylcubane-1-acetic acid methyl ester by CYP101B1.

The replacement of the methyl group with an ethyl substituent in 4-ethylcubane-1-methoxy carbonyl, induced slightly higher heme spin-state shift upon addition in CYP101B1 (% HS ~ 70%; Figure 6. 10). The oxidation activity of CYP101B1 was also increased for this substrate with a faster NADH oxidation activity (690 min^{-1} versus 438 min^{-1}), product formation rate (298 min^{-1} versus 155 min^{-1}) and higher coupling efficiency (43% versus 36%) (Table 6. 2).

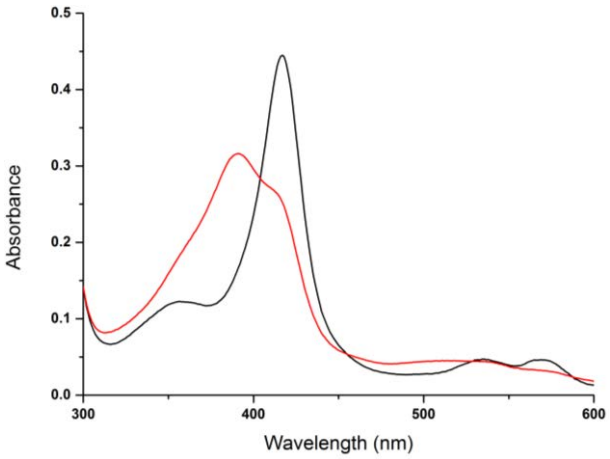

Figure 6. 10 Spin-state shift of CYP101B1 with the 4-ethylcubane-1-methoxy carbonyl (red).

The *in vitro* oxidation of 4-ethylcubane-1-methoxy carbonyl by CYP101B1 was found to give a single product (Figure 6. 11). The metabolite was identified as 4-(1-hydroxyethyl)-cubane-1-methoxy carbonyl by GC/GC-MS coelution experiment with an authentic standard (m^+/z = 206.45; Figure 6. 9, Figure 6. 11 and Figure E. 7). The MS fragmentation pattern of this turnover product indicated that the cubane structure remained intact (some important fragmentations 206.45, 191 (-CH_3), 175 (-OH); Figure E. 7).

There was no 2-hydroxyethyl product detected in these turnovers. The chiral GC analysis of the *in vitro* turnover of CYP101B1 and the standard 4-(1-hydroxyethyl)-cubane-1-methoxy carbonyl displayed a broad single peak at RT 23.8 min, hindering determination of the enantioselectivity of the reaction (Figure 6. 11 (b)).

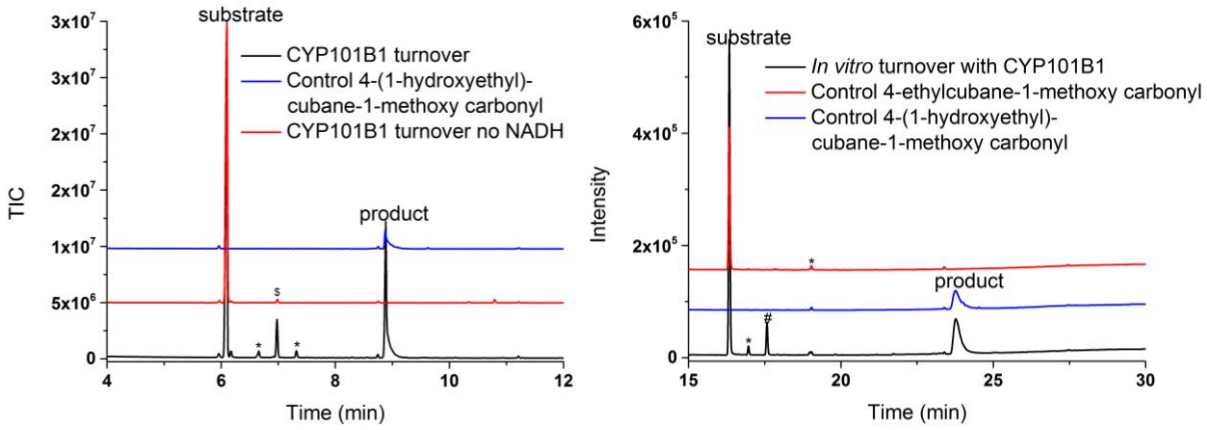

(a) (b)

Figure 6. 11 (a) GC-MS analysis of the *in vitro* turnover of 4-ethylcubane-1-methoxy carbonyl by CYP101B1 in black and a control turnover where no NADH was added in red. The substrate: 4-ethylcubane-1-methoxy carbonyl (RT 6.05 min); the product: 4-(1-hydroxyethyl)-cubane-1-methoxy carbonyl (RT 8.95 min). A peak with an MS consistent with $4-ethylcubane-1-carboxylic acid was observed in the turnovers with or without NADH (RT 6.95 min; m^+/z = 175.2). Other impurities have been labelled (*). **(b)** Chiral GC analysis of the turnover of 4-ethylcubane-1-methoxy carbonyl by CYP101B1. 4-Ethylcubane-1-methoxy carbonyl (RT 16.3 min); a peak consistent with that of the hydrolysed substrate has been tagged, # 4-ethylcubane-1-carboxylic acid (RT 17.6 min), and the product: 4-(1-hydroxyethyl)-cubane-1-methoxy carbonyl (RT 23.8 min). Impurities have been marked *.

The addition of the 4-methylcubane-1-acetic acid methyl ester to CYP101B1 resulted in a more extensive shift than the 4-methylcubane-1-methoxy carbonyl, indicating a good substrate/active site fit (85% versus 50%; Figure 6. 13 and Table 6. 2). CYP101B1 catalysed the turnover of this substrate with a faster NADH turnover (468 ± 7 min^{-1}) and product formation (189 ± 35 min^{-1}) rates than those of 4-methylcubane-1-methoxy carbonyl and 4-ethylcubane-1-methoxy carbonyl (Table 6. 2). The coupling efficiency was also improved (41%; Table 6. 2).

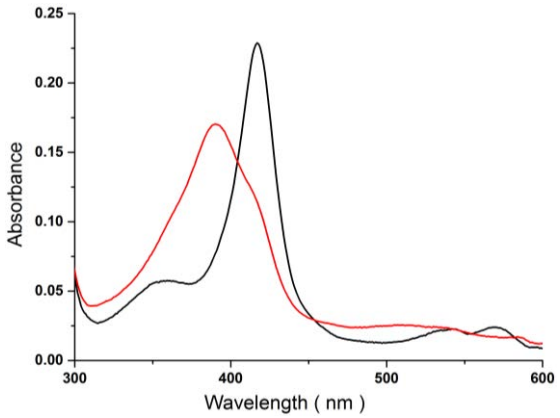

Figure 6. 12 The spin-state shift of CYP101B1 with 4-methylcubane-1-acetic acid methyl ester (red).

A single major product was detected by GC-MS and GC analysis of the *in vitro* turnovers of CYP101B1 with the 4-methylcubane-1-acetic acid methyl ester (m^+/z = 206.35; Figure 6. 13 (a) and Figure E. 7). A larger scale *in vitro* turnover was carried out with an excess NADH to generate the metabolite in a sufficient yield for NMR characterisation (Figure 6. 13 (b) and Figure 6. 9). GC-MS analysis of this large-scale turnover displayed that very little or no substrate remained and that the same significant product observed in the smaller-scale turnover was present. Some minor metabolite peaks were detected which were assigned as the ester hydrolysis of the substrate, product and further oxidation of the initial product (Figure 6. 13 (b)). Mass fragmentation patterns of the main product (m^+/z = 206.35, 190.95 (-OH), 175.0 (-CH_3), 131.05 (-COO)) and minor products indicated that the cubane structure remained intact (Figure E. 7). The NMR spectrum of the extracted large-scale turnovers showed that the main product had two distinctive signals for six *para*-substituted hydrogens of cubane (in the range 3.83-3.88 ppm and 3.71-3.76 ppm; Figure 6. 14 and Figure E. 10-E. 13). In addition, a 2H peak was present as expected for the hydroxymethyl substituent, δ 3.79-3.76 (m, 2H, 2xH12; Figure 6. 14 and Figure E. 10-E. 13). The NMR spectrum for 4-methylcubane-1-acetic acid methyl ester turnover displayed no signals in the vinyl region or other signals that would indicate radical or cation rearrangement product(s) (cyclobutenes have distinctive peaks above 6 ppm) or hydroxylation on the cubane C-H bonds (Figure 6. 14 and Figure E. 10-E. 13).

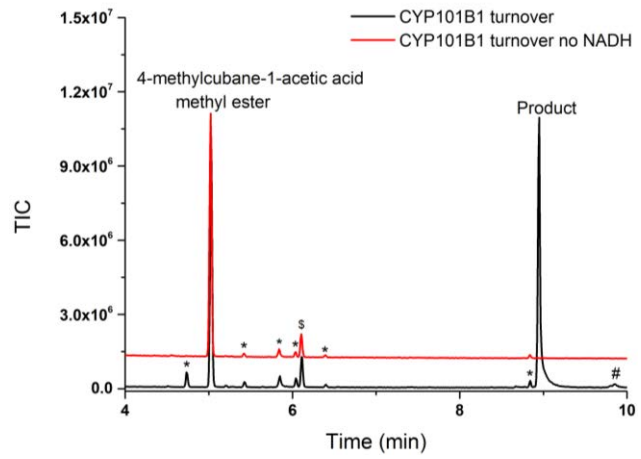

(a)

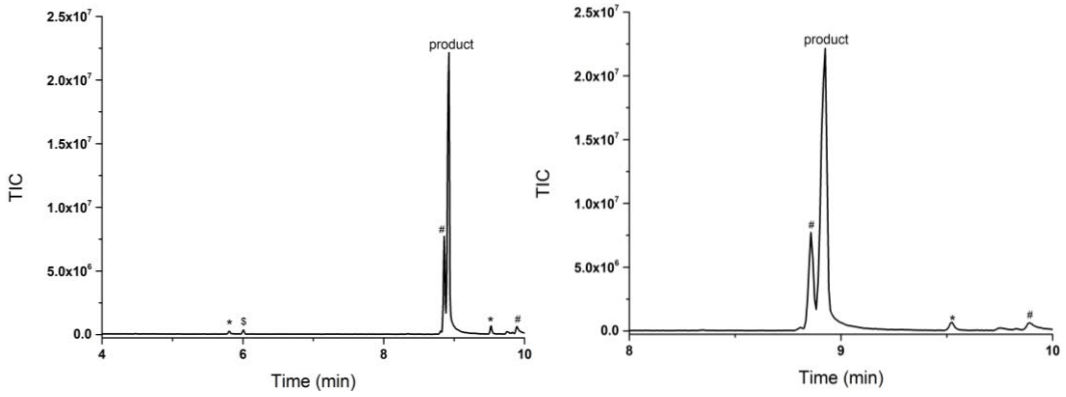

(b)

Figure 6. 13 (a) The GC-MS analysis of the small-scale turnover of 4-methylcubane-1-acetic acid methyl ester by CYP101B1. The turnover is shown in black, the control (the turnover without NADH) in red. The substrate 4-methylcubane-1-acetic acid methyl ester (RT 5.1 min); and the product 4-hydroxymethylcubane-1-acetic acid methyl ester (RT 9.0 min). A minor metabolite (RT 6.2 min; m^+/z = 176.15; labelled, $) arising from the possible hydrolysis of the ester (4-methylcubane-1-acetic acid). **(b)** The GC-MS analysis of a large-scale *in vitro* turnover of 4-methylcubane-1-acetic acid methyl ester. All the substrate has been transformed into product. The minor product (RT 8.95 min #; m^+/z = 204.0) has an MS consistent with an aldehyde further oxidation product and is only detected when all the substrate has been converted. Other possible minor peaks arising from hydrolysis of the ester (substrate and product) have been labelled, 6.0 min $ and 9.8 min #. Impurities are marked (*).

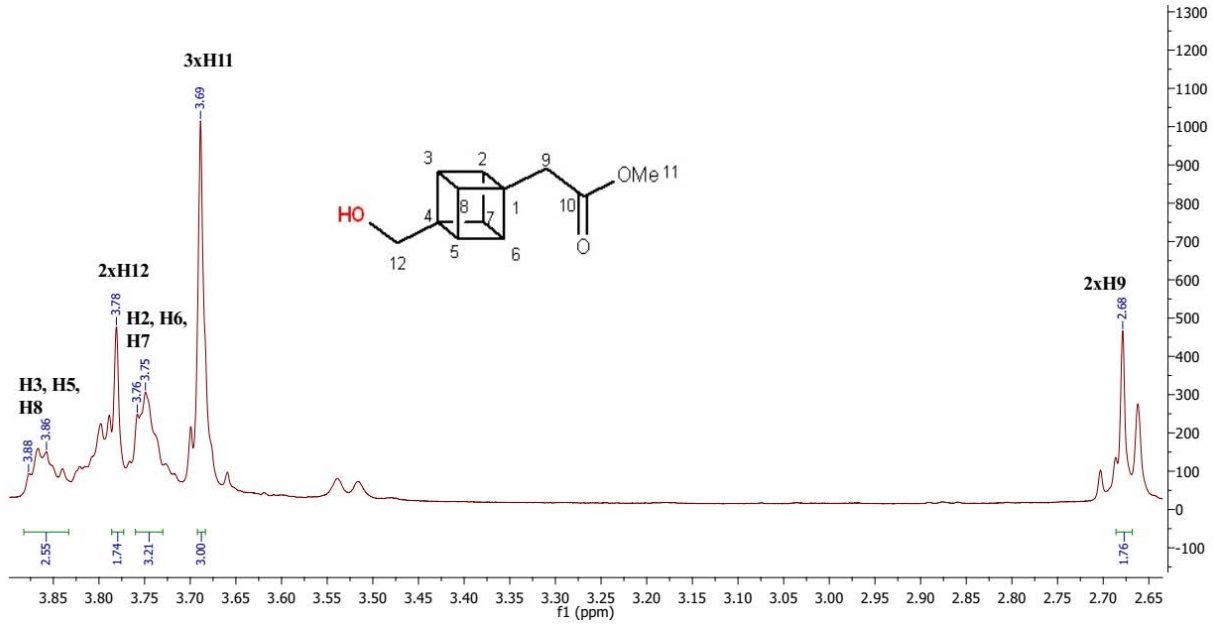

Figure 6. 14 ^{1}H NMR spectrum of 4-hydroxymethylcubane-1-acetic acid methyl ester (4-methylcubane-1-acetic acid methyl ester). The NMR experiment was performed without purification due to the low quantity of metabolite and available substrate. Some impurities were present in the NMR sample including the starting material, the aldehyde, further oxidation product, and hydrolysed product/starting material. Full data are provided in Appendix E (Figure E. 10-E. 13).

4-Methylcuban-1-yl acetate induced a 60% shift of CYP101B1 to the high spin form (Figure 6. 15 and Table 6. 2). 4-Methylcubane-1-methyl ketone effected a lower spin-state change (30%), while 4-methylcubane-1-carboxylic acid did not alter the spin-state (≤5%) significantly (Figure 6. 15 and Table 6. 2). The NADH turnovers with 4-methylcuban-1-yl acetate (374 min^{-1}) and 4-methylcubane-1-methyl ketone (251 min^{-1}) were found to be slower than the substrates described previously, and the rate was lowest for 4-methylcubane-1-carboxylic acid (39 min^{-1}). Little or no product could be detected by GC-MS analysis after CYP101B1 mediated oxidation of 4-methylcubane-1-methyl ketone and 4-methylcubane-1-carboxylic acid and more surprisingly with 4-methylcuban-1-yl acetate (Table 6. 2, Figure 6. 16 and Figure E. 7).

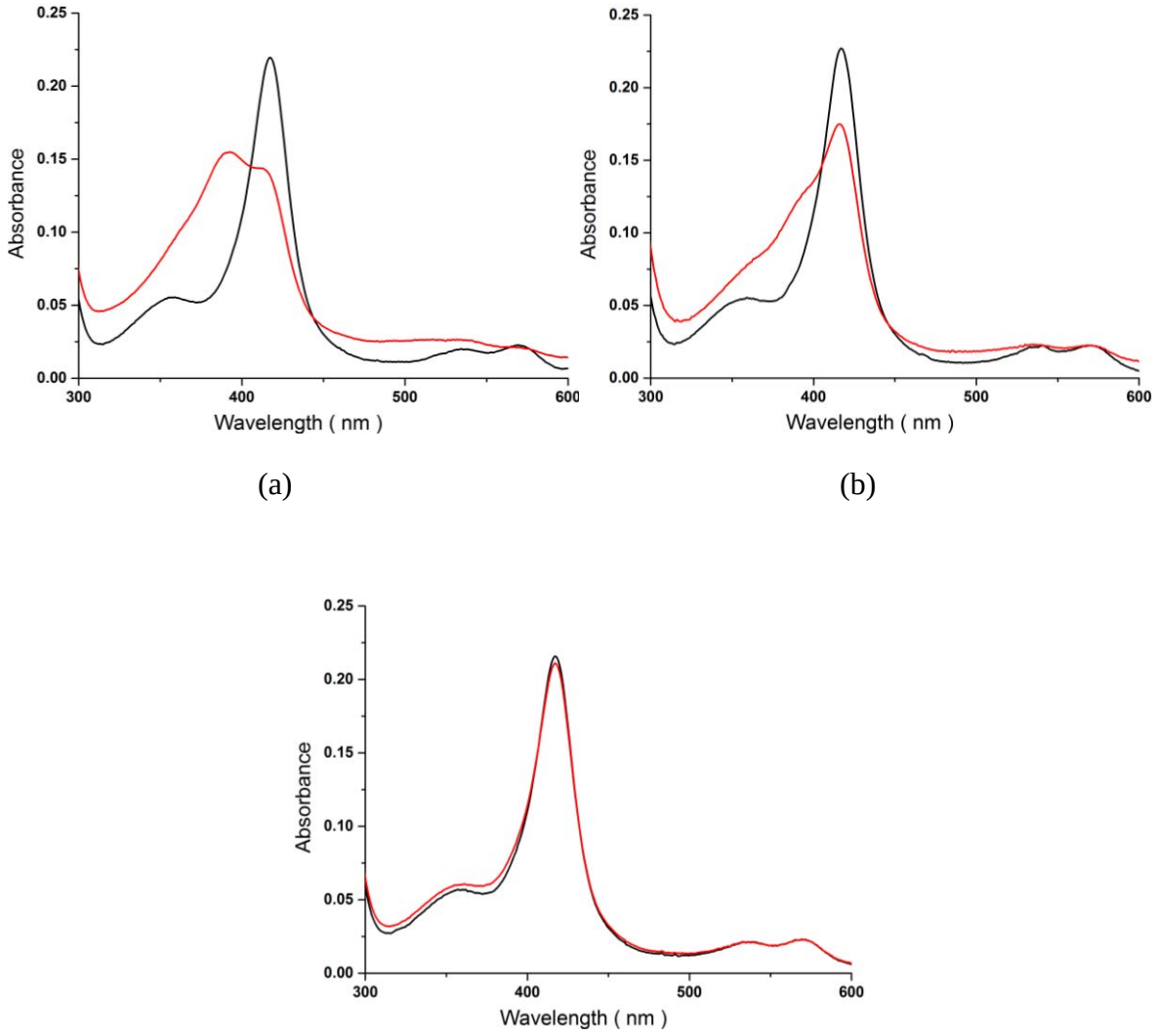

(a) (b)

(c)

Figure 6. 15 Spin-state shifts (red) of CYP101B1 with **(a)** 4-methylcuban-1-yl acetate, **(b)** 4-methylcubane-1-methyl ketone and **(c)** 4-methylcubane-1-carboxylic acid.

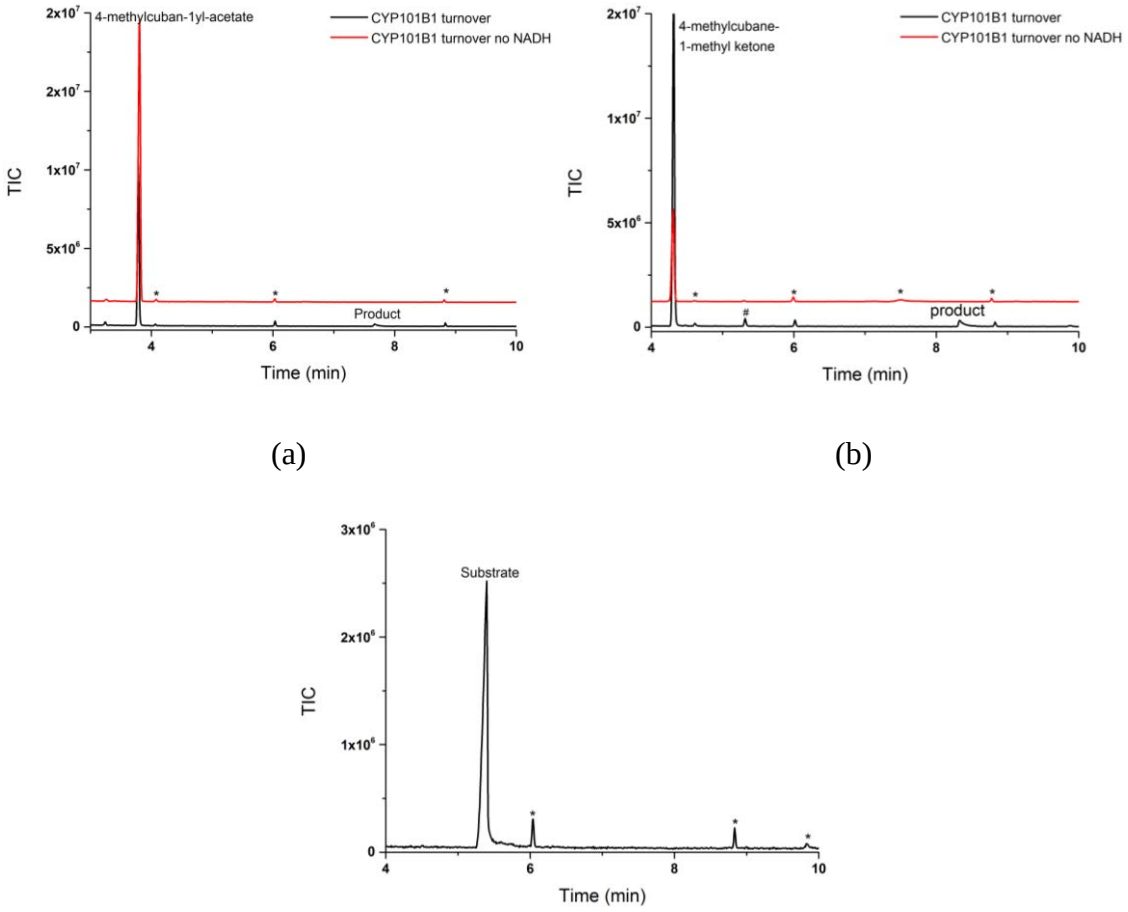

Figure 6. 16 (a) GC-MS analysis of the turnover of 4-methylcuban-1-yl-acetate by CYP101B1. 4-Methylcuban-1-yl-acetate (RT 3.9 min). There was a small amount of a possible hydroxy metabolite at RT 7.7 min (m^+/z = 191.00). **(b)** GC-MS analysis of the turnover of 4-methylcubane-1-methyl ketone by CYP101B1. 4-Methylcubane-1-methyl ketone (RT 4.2 min). There is a small peak of a potential product at RT 8.35 min (m^+/z = 175.25), and an unidentified metabolite at RT 5.3 min has been labelled as (#). **(c)** GC-MS analysis of the turnover of 4-methylcubane-1-carboxylic acid by CYP101B1. 4-Methylcubane-1-carboxylic acid (RT 5.4 min). No metabolites arising from oxidation were detected. Impurities have been marked (*).

6.3. Discussion

CYP101B1 efficiently oxidised the methyl C-H bonds of certain cubane derivatives. Unexpectedly that no rearrangement products were detected. This may be due to significantly faster radical rebound than radical rearrangement. The rearrangement may be slower in these substituted cubane systems, or the substituted cubanes are not able to rearrange in the environment of the CYP101B1 active site. To address the question of the radical rearrangement rate, derivatives of the methoxycarbonyl substrate have been synthesised which could undergo Barton decarboxylation reactions (thiohydroxamate ester) and Barton-McCombie deoxygenation (imidazole thiocarbamate ester) (Figure 6. 17 and full data in Appendix E).

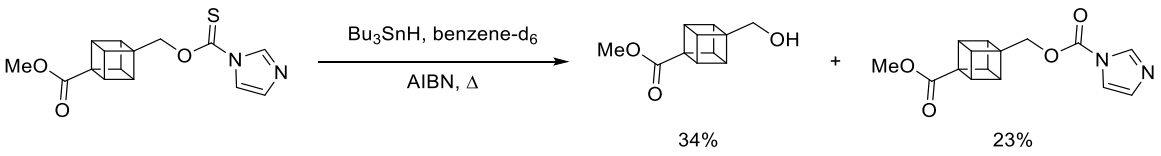

imidazole carbamate ester

4-hydroxymethylcubane-1-methoxy carbonyl and imidazole carbamate ester (3:2 inseparable mixture)

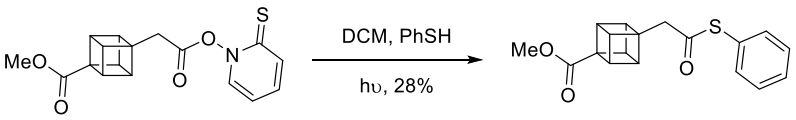

thiohydroxamate ester

thiophenol ester

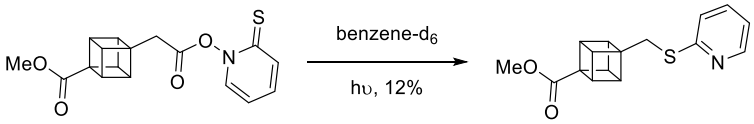

thiohydroxamate ester

thiopyridine ether

Figure 6. 17 Barton-McCombie deoxygenations and Barton decarboxylation to monitor radical rearrangement. No evidence of homocubane, and no significant alkene signals from a radical rearrangement product. All this synthetic work was performed by Sevan D. Houston (University of Queensland) using standard methods described completely in Appendix E.

The synthesised imidazole thiocarbamate ester was treated with the radical initiator azobisisobutyronitrile (AIBN) and Bu_3SnH to yield 4-hydroxymethylcubane-1-methoxy carbonyl (34%) and an imidazole carbamate ester, 23% with a mixture of other unidentified products (Figure 6. 17 and Full data in Appendix E) [305]. Irradiation of the thioxhydroxamate ester in the presence of thiophenol in anhydrous DCM, generated thiophenol ester (28%) and other impurities [306]. Irradiation in deuterated benzene yielded a thiopryidine ether 12% (Full data in Appendix E) [306]. All of the starting material was converted in this turnover and the other products formed could not be identified. Importantly, there was no evidence of homocubane, no significant alkene signals from a radical rearrangement product (potentially less than 5%) and no generation of the 4-methylcubane-1-methoxy carbonyl. Barton decarboxylation was used to synthesise 4-ethylcubane-1-methoxy carbonyl from the reaction of 4-methoxycarbonylcuban-1-yl propanoic acid with oxalyl chloride, in which a radical at the *β*-carbon would be generated [307]. The reaction proceeded smoothly, yielding the product in 91% yield (Figure 6. 18 and Full data in Appendix E).

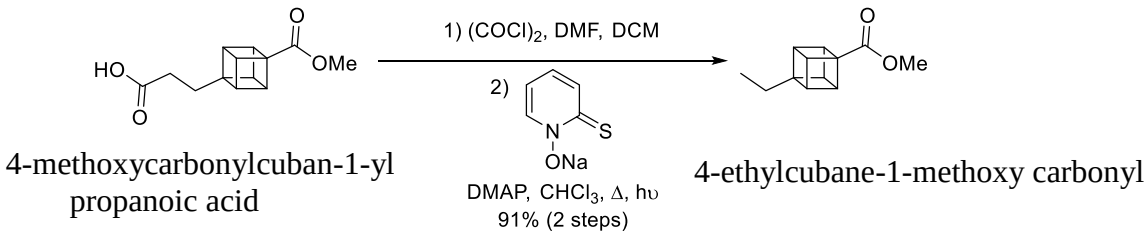

Figure 6. 18. Barton decarboxylation approach to synthesise 4-ethylcubane-1-methoxy carbonyl (described fully in Appendix E) [307].

Minimal radical rearrangement products from these chemical reactions were observed. The cubylcarbinyl radical from the substituted cubane derivatives in these reactions may decompose to undetectable products. Alternatively, this could be because of the slower rate of radical rearrangement or greater instability of the radical or the radical rearrangement products of the tested cubane derivative. These chemical reactions indicated the substituted cubane framework is stable to radical conditions and the cubylcarbinyl radical is difficult to form compared to a typical alkyl radical.

However, the P450 enzyme CYP101B1 is able to efficiently and selectively hydroxylate the substrates at the *α*-carbon C-H bonds in high yield with little or no rearrangement product arising from a radical or cationic intermediate.

The mechanism of action of this enzyme is best explained by hydrogen abstraction to generate a radical intermediate (Figure 6. 19) [85]. It is hypothesised the lifetime of this intermediate will vary depending on the spin-state of the Cpd I reactive intermediate [98, 308-310]. Longer radical lifetimes (intermediates) are expected on pathways proceeding via the quartet state, on the other hand, the trajectory of doublet state is calculated to proceed in a barrier-less fashion via a short-lived transition state [311]. This could explain why radical rearrangement products after the enzymatic turnover are not observed. An alternative explanation could be that the enzyme active site sterically prevents the rearrangement pathway. However, CYP101B1 is capable of tightly binding and efficiently oxidising larger substrates than those tested here, e.g. 2-adamantyl isobutyrate [182].

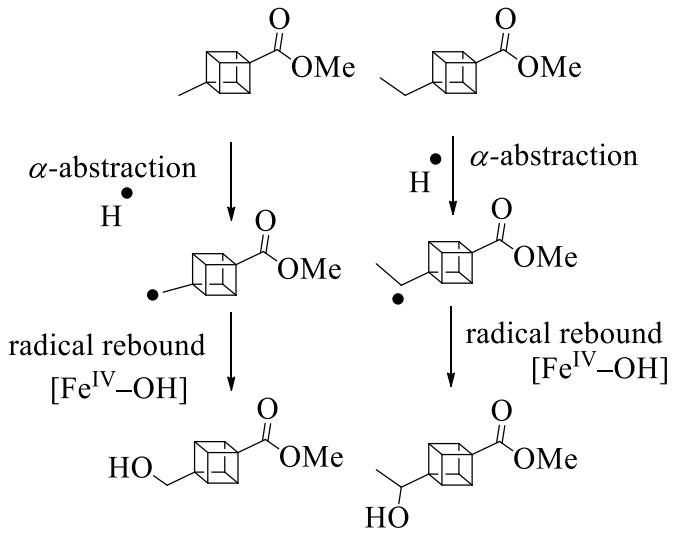

Figure 6. 19 The proposed mechanism of the hydroxylation reactions of CYP101B1 with the 4-methylcubane-1-methoxy carbonyl and 4-ethylcubane-1-methoxy carbonyl.

Another alternative explanation is that of the cage effect proposed by Groves and coworkers. This involves the proximity of the substrate radical and metal centre in the confined space of P450 active site, which is hypothesised to affect the rates of rearrangement of monooxygenases [38]. After the initial hydrogen abstraction, a caged radical pair (Fe^{IV}-OH ·R) can form containing the substrate radical (·R) and a reduced iron hydroxide (Fe^{IV}-OH; Figure 6. 20) [38, 312]. If a water molecule or any protein functional group can insert or interfere with close proximity of the substrate radical and metal-centre (Fe-OH···H_2O ·R), a rearranged product could arise (Figure 6. 20) [38, 312]. Overall, the radical formed during P450 catalysed hydroxylation seems to possess

the characteristics of both an intermediate (cage escape) and a transition state (oxygen rebound without rearrangement) depending on the system.

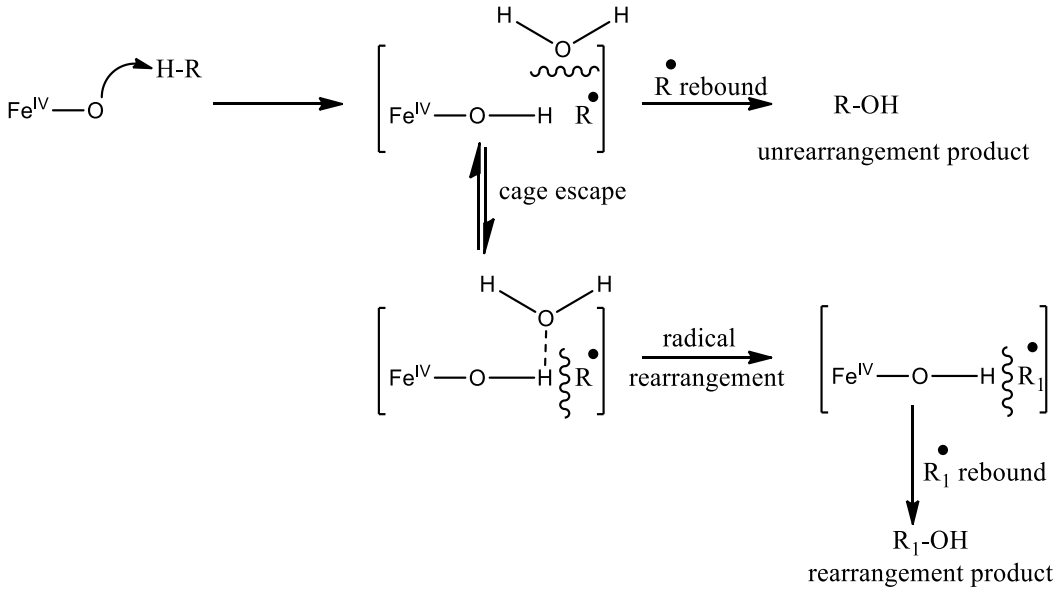

Figure 6. 20 An overview of the in-cage radical recombination and diffusive case escape [38, 312].

In summary, CYP101B1 was shown to be an efficient catalyst for the hydroxylation of cubane derivatives which have been designed to fit into the substrate binding pocket of the enzyme. The presence of an ester or ketone substituent on the cube promoted selective oxidation at the position opposite to the functional group. The directing group could place the methyl group close to the reactive iron-oxo species, resulting in hydroxylation solely at the methylcubyl group. This is notoriously difficult to achieve using chemical methodologies. Little or no methylcubanol or rearrangement metabolites were observed in these turnovers. These results support the kinetics of a putative radical rebound mechanism and argue against the involvement of any carbocation based mechanism in these oxidations. Further work is required to fully assess the nature of radical intermediates formed during the monooxygenase catalysed C-H hydroxylations of these and other cubane derivatives.

Chapter 7

7. Futile Redox Cycling in Cytochrome P450 Electron Transfer Systems Induced by Oxygenated Aromatics

7.1. Introduction

P450 enzyme-mediated oxidation depends on several successive steps including electron transport and oxygen activation [313]. P450s accept two electrons sequentially from NAD(P)H via redox partner(s) (Figure 1. 3). Instead of the productive utilisation of these reducing equivalents, they can be diverted to unproductive (futile) reactions which can generate cytotoxic reactive oxygen species (ROS). This phenomenon is called uncoupling which mainly arises from events at the P450 active site during oxygen activation by the heme centre (Figure 1. 3) [71]. Unproductive loss of the reducing equivalent can also occur between the electron transfer proteins. For example, the slow leaking of electrons in mitochondrial electron transfer system in the absence of substrate and the P450 enzyme has been reported [77, 78].

Cytochrome P450s are one of the major classes of enzyme involved in the metabolism of different toxic chemicals [80]. Many compounds including polycyclic aromatic hydrocarbons, arylamines, quinones, nitrofurantoin and naphthoquinones have been described to show enzyme-catalysed redox cycles in biological systems [81, 83, 314]. Most of these substrates convert to reactive intermediates by accepting one electron and are able to transfer the electron to molecular oxygen to form a toxic superoxide anion radical [81, 83, 314]. This superoxide anion radical can dismutate to form hydrogen peroxide and singlet oxygen [81]. Most of these compounds induce oxidative stress and DNA damage which are the leading cause of cytotoxicity, mutagenicity, and carcinogenicity [81, 316-318]. However, many anticancer drugs and antitumor therapies are effective through a redox cycling mechanism [319, 320]. Studies have demonstrated that many of these substrates can inhibit and inactivate the function of mammalian P450s [80, 81-83]. For example, they impede the enzyme activity by facilitating the uncoupling process through redox cycling in microsomal cytochrome P450 reductase and cytochrome b5 reductase [81-83]. NADPH cytochrome P450 reductase is the enzyme that transfers electrons to the microsomal P450 enzymes. It can initiate a futile redox cycle by donating an

electron to a quinone, a process that interferes with the electron flow to the P450s and inhibits monooxygenase activity [83, 321]. NADH cytochrome b5 reductase, an electron transfer protein of cytochrome b5, also displayed a similar type of activity in the presence of redox-active chemicals [83].

Most bacterial P450s get the reducing equivalents for catalysis from NAD(P)H through a flavin-containing reductase (ferredoxin reductase) and iron-sulfur protein (ferredoxin) [46, 47]. The mitochondrial P450s use a similar system consisting of an adrenodoxin reductase and adrenodoxin in which only adrenodoxin is soluble, and the reductase and P450 enzyme are bound with the membrane (Figure 1. 5) [44, 46, 47]. Ferredoxin/adrenodoxin reductase first receives two electrons from NAD(P)H and transfer the electrons one at a time from the flavin cofactor to the iron-sulfur clusters of ferredoxin/adrenodoxin. This then acts as a carrier and delivers the electrons one at a time to the active site of the P450.

Exogenous substrates which can mediate uncoupling during the transfer of electrons from nicotinamide cofactors to the P450, have not been described in detail with bacterial or mitochondrial electron transfer systems [71, 322-324]. In the present study, the ability of bacterial P450 electron transfers system containing ferredoxin [2Fe–2S] to catalyse the redox cycling with different oxygenated aromatics including naphthalene and naphthoquinone derivatives, were investigated (Figure 7. 1). The investigation of these aromatic compounds with bacterial and mitochondrial P450 systems and their electron transfer partners could enable to determine if this process interferes with electron flow from NAD(P)H to P450s. This is likely to have an important implication for understanding how this class of compounds inhibit the activity of bacterial and mitochondrial P450 systems.

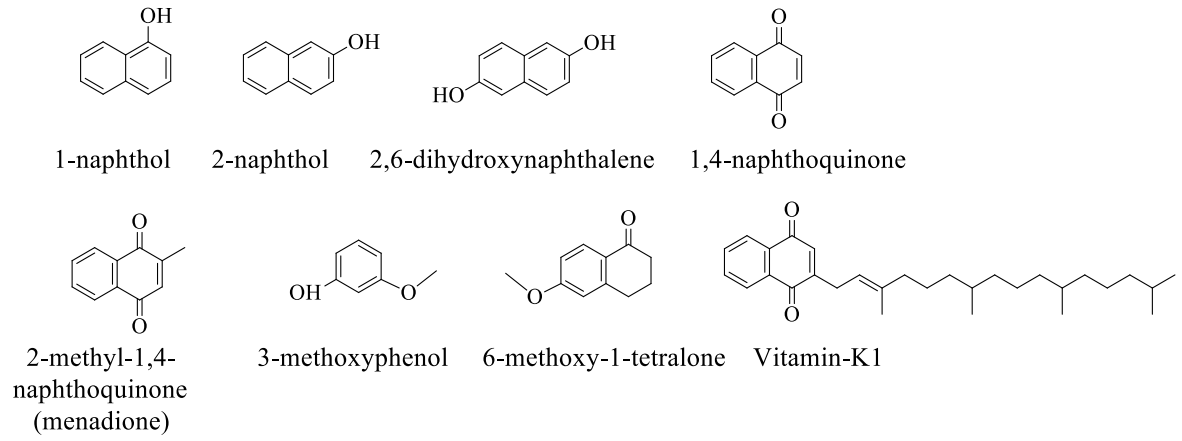

Figure 7. 1 Oxygenated aromatics used in the current study.

7.2. Results

The reaction of CYP101B1 system with naphthalene has previously been described [233]. Naphthalene did not induce a significant spin-state shift (20%) on binding to CYP101B1. However, the NADH turnover rate was reasonably fast (90 min^{-1}) and increased over the course of the reaction (Figure 7. 2) [233, 266]. Minimal levels of naphthol metabolites or any others were detected in GC/GC-MS analysis (Figure 7. 2) [266]. CYP101B1, therefore, oxidised naphthalene with a low product formation rate and coupling efficiency. Even when an excess of NADH (~4 to 6 mM) was added, only low levels of 1-naphthol were detected [233, 266].

To investigate the cause of the increasing NADH oxidation rate over time in the presence of naphthalene, both naphthols were screened as substrates. Addition of 1-naphthol and 2-naphthol shifted the spin-state of CYP101B1 to the high spin form: 60% and 40%, respectively [266]. The binding affinities were also determined and reported by Emma A. Hall (Dissociation constants; 165 µM and 195 µM, respectively) [266]. The NADH oxidation rate of a fully constituted CYP101B1/ArR/Arx system with 1-naphthol was four-fold higher than 2-naphthol (2090 versus 560 nmol. nmol. $P450^{-1}$ min^{-1}; Figure 7. 3).

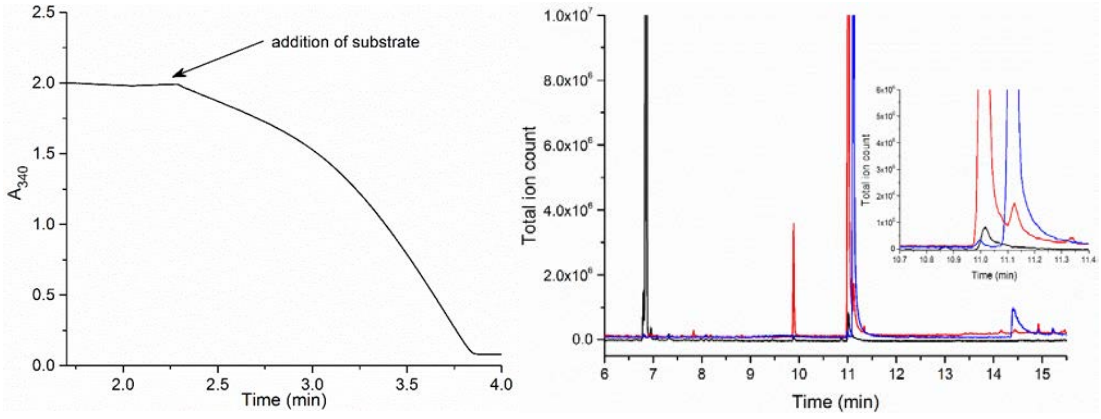

(a) (b)

Figure 7. 2 (a) UV-Vis NADH oxidation assay of CYP101B1 with naphthalene. **(b)** GC-MS analysis of turnover of naphthalene by CYP101B1 using excess NADH (black) overlaid with the turnover of 1-naphthol (red) and 2-naphthol (blue) [233, 266]. The inset shows a more detailed view of the region where 1- and 2-naphthol elute (RT 11.0 min and RT 11.15 min).

No metabolites were detected in the GC-MS analysis of these *in vitro* turnovers of 1-naphthol and 2-naphthol. However, with excess NADH (~ 4 mM) low levels of metabolites were detected in GC-MS analyses of both substrates (Figure 7. 4) [266]. The oxidation of 1-naphthol by CYP101B1 generated one metabolite which was assigned as 1,4-naphthoquinone via mass spectrometry and GC-MS coelution with an authentic commercial standard [233, 266]. CYP101B1 oxidised 2-naphthol into 2,6-dihydroxynaphthalene which was identified by a GC-MS coelution experiment and analysis of the mass spectrum (Figure 7. 4). No evidence of 2-naphthol or 2,6-dihydroxynaphthalene was detected in the turnovers of naphthalene by CYP101B1. The quantities of unreacted naphthalene and naphthol substrates remained high in turnovers with excess NADH (~4 mM). Therefore, other oxidation products, such as those arising from oxidative aryl coupling also do not seem to appear in a significant amount [325-327].

Control turnovers without the CYP101B1 enzyme were also carried out. The NADH oxidation rate in the presence of just the electron transfer proteins ArR and Arx with 1-naphthol (1 mM) was 1560 min^{-1}, and 2-naphthol (1 mM) was 871 min^{-1} (Table 7. 1 and Figure 7. 3). The NADH oxidation activity was dramatically reduced in the absence of both Arx and CYP101B1 (Figure 7. 3). The assays indicated that the NADH rate acceleration observed in the naphthalene turnovers might arise from transfer of electrons from ferredoxin, Arx, to the oxygenated substrates (or an impurity present in these substrates).

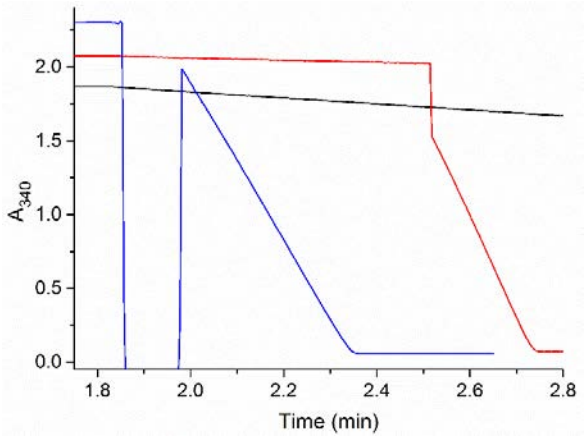

Figure 7. 3 NADH oxidation assays of CYP101B1 with 1-naphthol (red), 1-naphthol no P450 control (blue) and 1-naphthol, no Arx and P450 control (black) [233, 266].

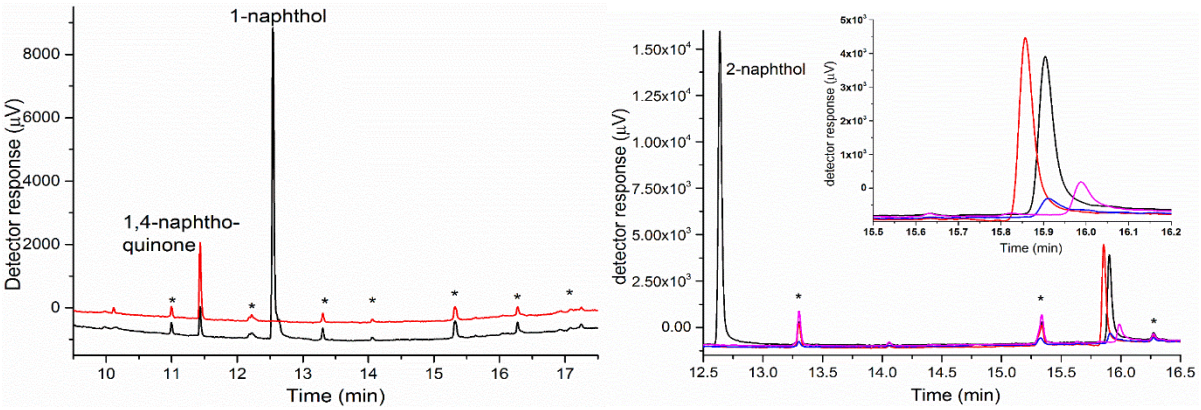

(a) (b)

Figure 7. 4 (a) GC analysis of the turnover of 1-naphthol (black) and a control of 1,4-naphthoquinone (red) [233, 266]. **(b)** GC analysis of the turnover of 2-naphthol (black) and controls of 1,7-dihydroxynaphthalene (red), 2,6-dihydroxynaphthalene (blue) and 2,7-dihydroxynaphthalene (magenta) [233, 266]. Emma A. Hall did these analyses. Repeating these experiments showed similar activity and product formation. The inset shows the region where the products elute in more detail. Impurities are labelled (*).

Table 7. 1 The NADH oxidation rates of CYP101B1/Arx/ArR system and only Arx/ArR with naphthalene, 1-naphthol and 2-naphthol. The *in vitro* turnovers were measured using a ArR:Arx:CYP101B1 concentration ratio of 1:10:1 (0.5 µM CYP enzyme, 50 mM Tris, pH 7.4). [a] The P450 enzyme was omitted in the turnover. Rates are given in nmol. nmol. $P450^{-1}$ min^{-1} in the presence of P450 enzyme (Note for ease of comparison the NADH oxidation rates provided in the main text in the absence of the P450 enzyme are given in the same units as if the P450 enzyme was present) [233, 266]. [b] The initial rate of NADH oxidation as the rate increased over time.

Substrate	NADH oxidation rate [266]	NADH oxidation rate [a]
naphthalene	90 [b]	-
1-naphthol	2090	1560
2-naphthol	560	871

1,4-Naphthoquinone was screened as a substrate, which induced a rapid NADH oxidation rate in CYP101B1 system at 0.5 mM concentration (2334 min^{-1}; Table 7. 2). The addition of 1,4-naphthoquinone also resulted in very fast NADH oxidation rate in the absence of CYP101B1. This occurred even when this substrate was present in very low concentration (~4 µM of substrate; 1305 min^{-1}, 50 nM; 321 min^{-1}; Table 7. 2). Analysis of these turnovers by GC-MS showed no product arising from the monooxygenase activity of CYP101B1. The majority of the reducing equivalents in both systems containing the P450 and/or electron transfer proteins ended up as hydrogen peroxide (as measured by the standard procedure described in the experimental chapter; Table 7. 2) [181].

The high NADH oxidation rate upon addition of 1,4-naphthoquinone suggested that the acceleration of the NADH oxidation rate in the case of naphthalene in CYP101B1/ArR/Arx turnover could be due to the presence or generation of a small amount of 1,4-naphthoquinone. CYP101B1 first oxidised the naphthalene to 1-naphthol followed by further oxidation to the 1,4-naphthoquinone. The presence of 1,4-naphthoquinone either as an impurity or oxidation product of 1-naphthol turnovers may be the reason for the acceleration of the NADH oxidation rate. Instead of acting as a substrate or promoting established P450 uncoupling pathways, 1,4-naphthoquinone receives electrons from ferredoxin (Arx) and converts to the semiquinone form. This can then donate an electron to molecular oxygen to form superoxide with the semiquinone reverting to the parent quinone [328]. The cytotoxic superoxide could spontaneously dismutate to hydrogen peroxide and singlet dioxygen. These steps would inhibit the productive activity of P450 by removing the reducing equivalents from the monooxygenase enzyme (Figure 7. 5) [81, 83, 328]. This activity was similar to that reported for NADPH cytochrome P450 reductase (FAD/FMN cofactors) discussed above (Figure 7. 5) [77, 81]. Overall, this resulted in low levels of product formation despite high NADH consumption rates.

Table 7. 2 The NADH oxidation rates of CYP101B1/Arx/ArR system and only Arx/ArR with 1,4-naphthoquinone. The rates were measured and reported same as described in Table 7. 1. The added NADH concentration (μM), NADH oxidation rate and hydrogen peroxide concentration (μM) are given. [a] The turnovers containing CYP101B1 are provided in the brackets. The P450 enzyme was omitted in all other turnovers. In certain instances, the detected levels of hydrogen peroxide were higher than the theoretical maximum value. This is most likely due to the substrate or any impurity interfering with the H_2O_2 assays.

1,4-naphthoquinone conc. (μM)	NADH conc. (μM)	NADH oxidation rate	H_2O_2 conc. (μM)
500	344	3180	462
	(328) [a]	**(2334) [a]**	**(413) [a]**
50	336	2572	486
	(323) [a]	**(2186) [a]**	**(517) [a]**
8	326	2755	486
4	303	1305	407
0.5	314	321	279
0.2	317	128	187
0.1	309	125	231
0.05	306	122	182

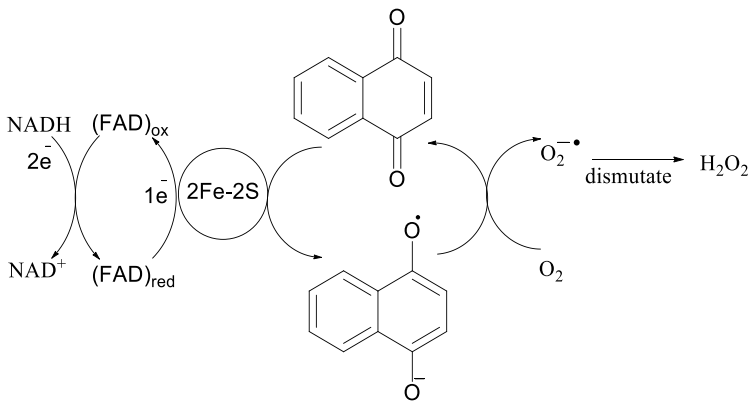

Figure 7. 5 Enzymes mediated futile redox cycling [83, 329, 330].

In order to investigate how this futile redox cycle inhibits the product formation activity of CYP101B1, 2-adamantyl acetate and 1-naphthol were used together in fully reconstituted CYP101B1 turnovers. Addition of 1-naphthol and 2-adamantyl acetate induced the spin-state shift to 60% and 90% high spin form in CYP101B1, respectively. 2-Adamantyl acetate bound very tightly with CYP101B1, and 1-naphthol displayed a weaker binding affinity (K_d = 1.9 µM versus K_d = 165 µM) [182, 266]. CYP101B1 oxidised 2-adamantyl acetate with a NADH oxidation rate of 1170 min^{-1}, product formation rate of 877 min^{-1} and a high coupling efficiency of 75% (Table 7. 3) [182]. However, in the presence of 1-naphthol (1000 µM) the product formation diminished to 264 min^{-1} and a coupling efficiency reduced to 15% despite rapid NADH oxidation rate (1723 min^{-1}). A minimal amount of 1,4-naphthoquinone was observed either as an oxidation product of 1-naphthol or impurity. CYP101B1 turnovers with 2-adamantyl acetate showed progressively higher product formation activities and coupling efficiencies as the concentration of 1-naphthol was decreased (Table 7. 3 and Figure 7. 6).

Table 7. 3 The NADH oxidation rates of CYP101B1 with 2-adamantyl acetate in the presence of 1-naphthol. The rates were measured using a ArR:Arx:CYP101B1 concentration ratio of 1:10:1 (0.5 µM CYP enzyme, 50 mM Tris, pH 7.4). 2-Adamantyl acetate concentration was used 1000 µM in all turnovers. Rates are given in nmol. nmol. $P450^{-1}$ min^{-1}.

1-naphthol conc. (µM)	NADH oxidation rate (CYP101B1)	Product formation rate	Coupling efficiency (%)
1000	1723	264	15
500	1550	281	18
125	1061	490	46
62.5	814	456	56
31	813	448	55
15	798	547	67
0	1170	877	75

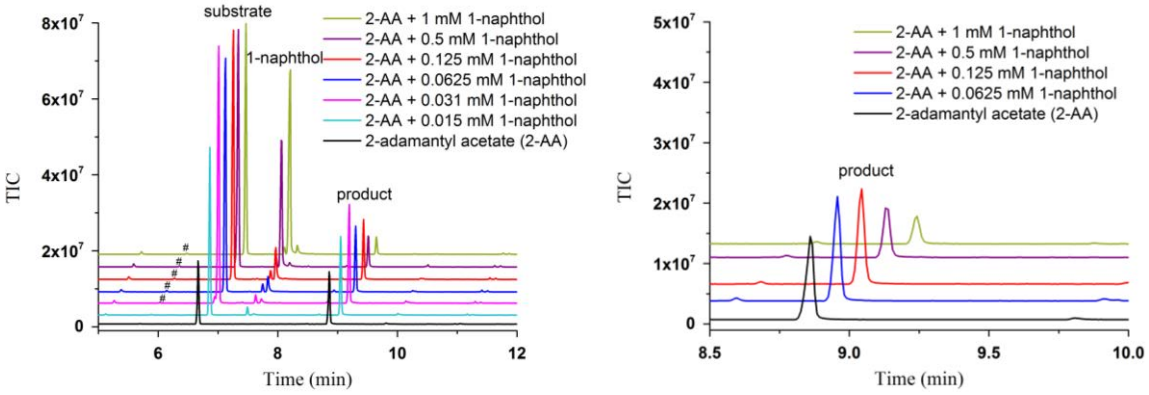

Figure 7. 6 (a) GC-MS analyses of the *in vitro* turnovers of 2-adamantyl acetate with CYP101B1/ArR/Arx system in the presence of different concentrations of 1-naphthol. The internal standard; *p*-cresol, RT 2.10 min (not shown); 1,4-naphthoquinone[#], RT 6.2 min; 2-adamantyl acetate, RT 6.8 min, 1-naphthol, RT 7.3 min and the product; 5-hydroxy-2-adamantyl acetate, RT 8.9 min [182]. The internal standard was added to 0.2 mM in all cases, and the product concentration was determined via the procedure described in the experimental chapter. **(b)** Zoom of the 8.5 to 10 min region to highlight the product peaks. For clarity, the chromatograms (a and b) were offset along the x and y-axes.

To assess the effect of 1,4-naphthoquinone on the inhibition of CYP101B1/Arx/ArR monooxygenase activity, this substrate was investigated with 2-adamantyl acetate. When 1,4-naphthoquinone (0.1 mM) and 1-adamantyl acetate (1.0 mM) were added together to the CYP101B1/Arx/ARr system, the product formation activity diminished to ~4 min^{-1} (Table 7. 4). This was despite a fast NADH oxidation activity of 2032 min^{-1} (Table 7. 4 and Figure 7. 7). Overall the productive utilisation of the NADH reducing equivalents decreased from 75% to 0.17%. The product formation rates and use of reducing equivalents (coupling efficiency) of CYP101B1 were low even when minimal amounts (~1 µM) of 1,4-naphthoquinone were used. The concentration of 1,4-naphthoquinone and the product formation activity of CYP101B1 system with 2-adamantyl acetate exhibited a linear relationship. Increasing the 1,4-naphthoquinone level in the system decreased the product formation activity (Table 7. 4 and Figure 7. 7). In all cases the NADH consumption rates were rapid, and these suggested that the naphthoquinone interferes with the transfer of reducing equivalents from Arx to CYP101B1.

Table 7. 4 The NADH oxidation rates of CYP101B1 with 2-adamantyl acetate in the presence of 1,4-naphthoquinone. The rates were determined using a ArR:Arx:CYP101B1 concentration ratio of 1:10:1 (0.5 µM CYP enzyme, 50 mM Tris, pH 7.4). The 2-adamantyl acetate concentration was used 1000 µM in all the turnovers. Rates are given in nmol. nmol. $P450^{-1}$ min^{-1}. No metabolites of 1,4-naphthoquinone were detected.

1,4-naphthoquinone conc. (µM)	NADH oxidation rate (CYP101B1)	Product formation rate	Coupling efficiency (%)
100	2032	4	0.17
20	1807	37	2
5	916	222	24
2	704	269	38
1	633	279	44

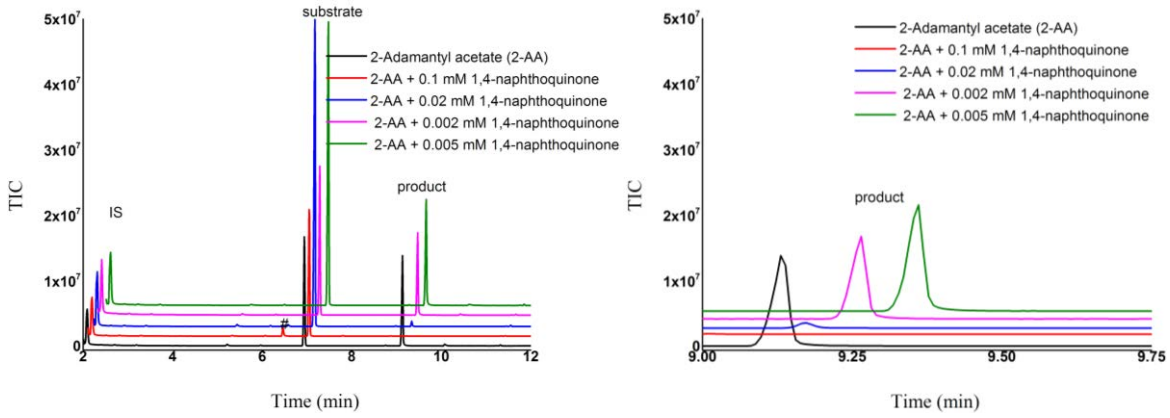

Figure 7. 7 (a) GC-MS analyses of *in vitro* turnovers of 2-adamantyl acetate with the CYP101B1/ArR/Arx system in the presence of different concentrations of 1,4-naphthoquinone. The internal standard; *p*-cresol, RT 2.15 min; 1,4-naphthoquinone[#], RT 6.3 min; 2-adamantyl acetate, RT 6.9 min, and the product; 5-hydroxy-2-adamantyl acetate, RT 9.1 min [182]. The chromatograms were slightly shifted due to GC-MS method change. The internal standard was added to 0.2 mM in all cases, and the product concentration was determined via the procedure described in the experimental chapter. **(b)** Zoomed in version of the 9 to 9.75 min region to highlight the product peaks. For clarity, the chromatograms (a and b) were offset along the x and y-axes.

2-Methyl-1,4-naphthoquinone, also known menadione or vitamin K3, is a toxic quinone usually used to investigate the mechanisms underlying oxidative injury [83, 329, 331-333]. Menadione acts as a potent inhibitor of different P450 mediated metabolism [329, 334]. For example, in the presence of menadione, quinone redox cycling inhibited the reduction of cytochrome b5 by cytochrome b5 reductase and this activity together with generating the cytotoxic reactive oxygen species might be the leading cause of tissue injury in the presence of this substrate [83]. Addition of menadione (500 µM) to CYP101B1 *in vitro* turnover system induced a fast NADH oxidation rate (2350 min^{-1}) similar to that observed with 1,4-naphthoquinone. The control turnover without P450 showed a similarly high NADH oxidation rate (2360 min^{-1}). The rapid oxidation of NADH occurred at concentrations as low as 5 µM (296 min^{-1}; Table 7. 5). No menadione metabolite was detected in GC-MS analyses of any of the turnovers containing the P450. Large amounts of reducing equivalents ended up as hydrogen peroxide due to futile redox cycling in the absence and presence of CYP101B1 (Table 7. 5).

Table 7. 5 The NADH oxidation rates of CYP101B1/Arx/ArR system and only Arx/ArR with menadione. The rates were measured and reported same as described in Table 7. 1. [a] The NADH oxidation concentration, NADH oxidation rate and hydrogen peroxide concentration in the presence of CYP101B1 are provided in the brackets. The P450 enzyme was omitted in all the other turnovers.

Menadione conc. (µM)	NADH conc. (µM)	NADH oxidation rate	H_2O_2 conc. (µM)
500	314	2360	298
	(305) [a]	(2350) [a]	(268) [a]
200	306	2357	274
50	314	2000	311
20	307	2026	328
5	307	1113	273
2	331	1119	233
0.5	320	296	103
0.2	344	97	10

Menadione was also screened in the presence of the substrate 2-adamantyl acetate to investigate how this quinone inhibits the monooxygenase activity of the CYP101B1/Arx/ArR system. Addition of 100 µM of menadione significantly diminished the productive activity of this system with the product formation rate (2-adamantyl acetate) decreasing from 877 min^{-1} to ~ 5 min^{-1} (Table 7. 6). Product formation activity of this P450 system remained low in the presence of menadione even at a concentration of 5 µM despite the relative fast NADH oxidation rates observed in each turnover (Table 7. 6 and Figure 7. 8). Results of the current study indicate that menadione can also act as an electron acceptor from Arx (Figure 7. 8) [335]. Thus the metabolism of 2-adamantyl acetate by CYP101B1 is decreased due to the interruption of electron transfer from NAD(P)H to CYP101B1 via Arx/ArR system [335]. A similar type of inhibition by menadione has also been reported for P450s including CYP1A2, CYP2B6 and CYP3A4 mediated metabolism of parathion and aniline hydroxylase that catalysed the hydroxylation of *p*-aniline [329, 335, 336]. Menadione inhibits the activity of these mammalian enzymes through the NADPH-Cytochrome P450 reductase-mediated futile redox cycling, which preferentially uses the electrons from NADPH instead of delivering to the active site of the enzymes [329, 335, 336]. In this process, the reduction of oxygen also leads to the formation of reactive oxygen species (ROS) [328, 337].

Table 7. 6 The NADH oxidation rates of CYP101B1 with 2-adamantyl acetate in the presence of menadione. The oxidation rates were determined using a ArR:Arx:CYP101B1 concentration ratio of 1:10:1 (0.5 µM CYP enzyme, 50 mM Tris, pH 7.4). The concentration of 2-adamantyl acetate was used 1000 µM in all turnovers. Rates are given in nmol. nmol. $P450^{-1}$ min^{-1}. No metabolite of 2-methyl-1,4-naphthoquinone (menadione) was detected.

Menadione conc. (µM)	NADH oxidation rate (CYP101B1)	Product formation rate	Coupling efficiency (%)
100	2064	4.5	0.22
20	1860	0.3	0.016
10	1476	10.4	0.71
5	1254	77.4	6.2
0.1	839	357	42.5

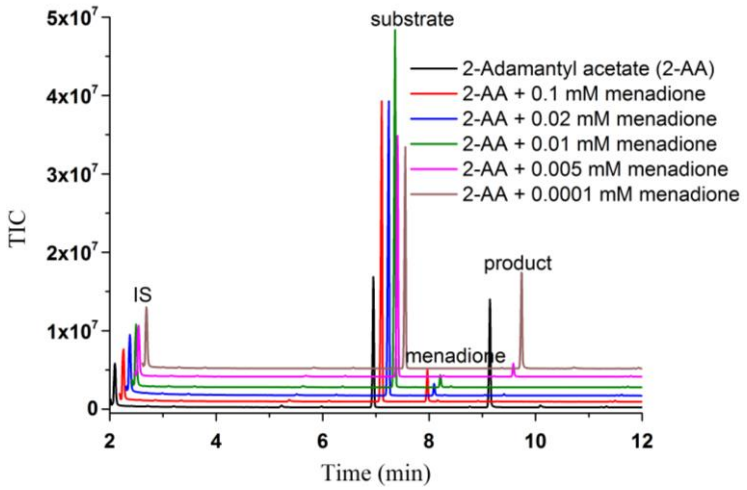

(a)

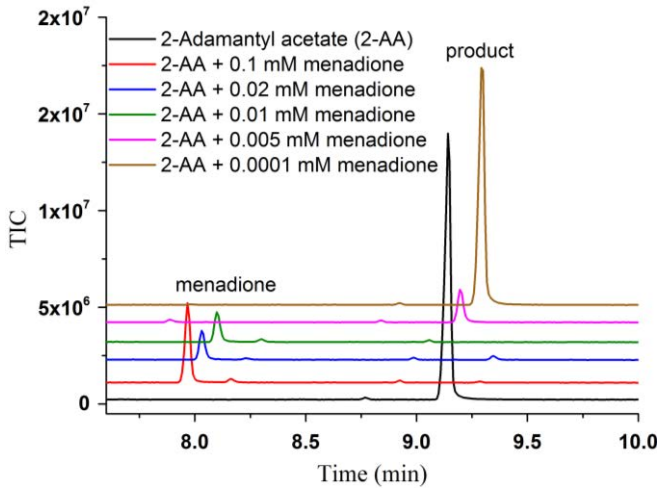

(b)

Figure 7. 8 (a) GC-MS analyses of the *in vitro* turnovers of 2-adamantyl acetate with CYP101B1/ArR/Arx system in the presence of different concentrations of menadione. The internal standard; *p*-cresol, RT 2.15 min; 2-adamantyl acetate, RT 6.9 min, menadione, RT 7.8 min; and the product; 5-hydroxy-2-adamantyl acetate, RT 9.1 min [182]. The internal standard was added to 0.2 mM in all cases. **(b)** Zoomed in 7.5 to 10.0 min region to highlight the product peaks. For clarity, the chromatograms (a and b) were offset along the x and y-axes.

Vitamin K1 (Phytonadione) shares the quinone backbone of menadione and 1,4-naphthoquinone. Addition of vitamin K1 (250 µM) to the CYP101B1 system induced a lower NADH oxidation rate (103 min^{-1}) than either menadione or 1,4-naphthoquinone (Table 7. 7). This could potentially be due to lower solubility of vitamin K1 in aqueous solution. GC-MS analysis of the *in vitro* turnovers showed that CYP101B1 generated no metabolite. Most of the

reducing equivalents were again converted to H_2O_2 as a result of futile redox cycling. Assays were performed without the P450, and the NADH oxidation rate was similar to that described above. Most of the reducing equivalents were diverted to hydrogen peroxide. When the concentration of vitamin K1 was decreased to 100 µM, the NADH oxidation rate was reduced, but high levels of hydrogen peroxide were still detected. Overall, these results show that vitamin K1 is also capable of accepting electrons from NAD(P)H via Arx and involved in the futile redox cycling [335].

Table 7. 7 The NADH oxidation rates of CYP101B1/Arx/ArR system and only Arx/ArR with vitamin K1. The rates were measured and reported same as described in Table 7. 1. [a] The NADH oxidation concentration, NADH oxidation rate and hydrogen peroxide concentration in the presence of CYP101B1 are provided in the brackets. The P450 enzyme was omitted in all the other turnovers.

Vitamin K1 conc. (µM)	NADH conc. (µM)	NADH oxidation rate	H_2O_2 conc. (µM)
250	314	84	298
	(306) [a]	(103) [a]	(268) [a]
100	306	52	294

CYP101B1 oxidised 2-naphthol to generate 2,6-dihydroxynaphthalene (Figure 7. 4 (b)) [266]. Therefore, this diol was also examined as a substrate of CYP101B1 and to asses if this metabolite also could inhibit the catalytic activity of this enzyme system. 2,6-Dihydroxynaphthalene induced a NADH oxidation rate of 1045 min^{-1} in the turnover of CYP101B1 system (Table 7. 8). GC-MS analysis showed no detectable product arose from this turnover. The NADH oxidation rate was greater when 2,6-dihydroxynaphthalene was added to a turnover where P450 was omitted (Table 7. 8). Hydrogen peroxide assays showed that most of the reducing equivalents ended up as hydrogen peroxide. However, it should be noted that in certain instances the detected levels of hydrogen peroxide were higher than expected. This is most likely due to the phenolic substrate interfering with the H_2O_2 assays which also use phenol as a substrate.

Table 7. 8 The NADH oxidation rates of CYP101B1/Arx/ArR system and only Arx/ArR with 2,6-dihydroxynaphthalene. The rates were measured and reported same as described in Table 7. 1. [a] The turnover with the presence of CYP101B1 was shaded. The P450 was omitted in all the other turnovers. Rates are given in nmol. nmol. $P450^{-1}$ min^{-1}. -not determined. - detected levels of hydrogen peroxide were higher than expected (not shown).

2,6-dihydroxynaphthalene conc. (µM)	NADH conc. (µM)	NADH oxidation rate	H_2O_2 conc. (µM)
500 [a]	**301 [a]**	**1045 [a]**	**243 [a]**
250	302	1704	255
100	-	1611	-
50	-	1518	-
10	-	1405	-
5	-	1138	-
0.5	-	360	-

To determine whether 2,6-dihydroxynaphthalene is also an inhibitor of CYP101B1-mediated metabolism of 2-adamantyl acetate, this diol (1000 µM) and 2-adamantyl acetate (1000 µM) was added together in the CYP101B1/Arx/ArR system, the amount of product formation decreased 44-fold. Only 1% substrate was converted to product whereas in the normal turnover the conversion was 44% (Figure 7. 9). When the concentration of the diol reduced to 100 µM in the CYP101B1 turnover assay, the product formation activity was diminished to 198 min^{-1} from 877 min^{-1}, despite a fast NADH oxidation rate (855 min^{-1}). The product formation activity was nearly 3-fold lower when the concentration of 2,6-dihydroxynaphthalene was reduced to 20 µM than the normal 2-adamantyl acetate turnover without 2,6-dihydroxynaphthalene (Figure 7. 9). 2,6-Dihydroxynaphthalene induced fast NADH oxidation rates in the absence of CYP101B1 and generated excessive amounts of hydrogen peroxide in each turnover. Addition of this substrate facilitates futile redox cycling in the turnovers, and this may be due to the presence of small amounts of 2,6-naphthoquinone. Further study with 2,6-naphthoquinone could be attempted to fully understand the futile redox cycle and intermediates formed in the 2,6-dihydroxynaphthalene turnovers.

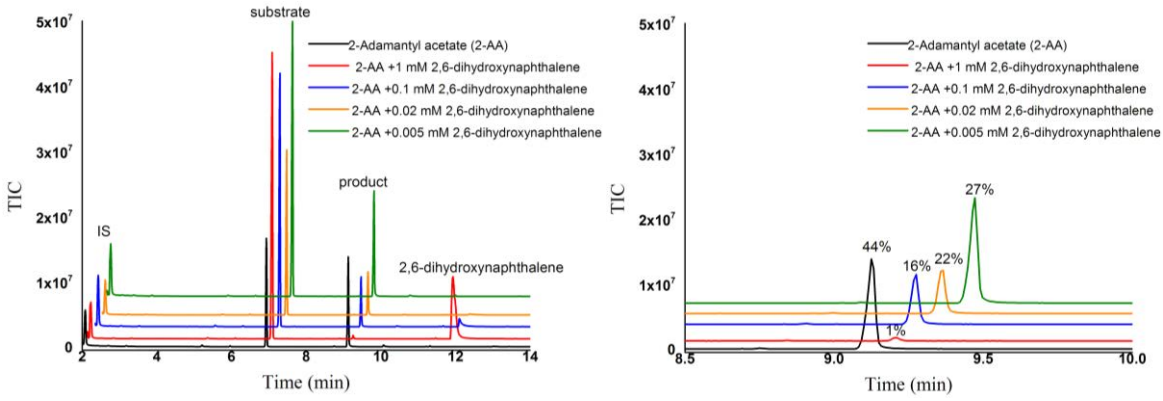

(a) (b)

Figure 7. 9 (a) GC-MS analyses of the *in vitro* turnovers of 2-adamantyl acetate with the complete CYP101B1 system in the presence of different concentrations of 2,6-dihydroxynaphthalene. The internal standard; *p*-cresol, RT 2.15 min; 2-adamantyl acetate, RT 6.9 min, the product; 5-hydroxy-2-adamantyl acetate, RT 9.1 min, and 2,6-dihydroxynaphthalene, RT 11.8 min [182]. The internal standard was added to 0.2 mM in all cases. **(b)** Zoomed in 7.5 to 10.0 min region to highlight the product peaks. The percentage of total amount of substrate (2-adamantyl acetate) converted to product in the presence or absence of 2,6-dihydroxynaphthalene were also given. For clarity, the chromatograms (a and b) were offset along the x- and y-axes.

Phenolic compounds such as alkylmethoxy phenols, flavonoids and catechin have been shown to inhibit the activity of P450 by forming cytotoxic quinoid and/or quinone methides species through redox cycling [330, 338-341]. In the current study, 3-methoxyphenol was investigated. Addition of 3-methoxyphenol (2000 µM) in the turnover mixture without CYP101B1 induced a high NADH oxidation rate (1814 min^{-1}; Table 7. 9). The NADH oxidation rates were fast at different concentrations without P450, and a high amount of hydrogen peroxide was detected in all cases (Table 7. 9). These NADH oxidation rates and a large amount of hydrogen peroxide without the presence of CYP101B1 indicated 3-methoxyphenol or an impurity in the sample could also act as a redox active chemical.

6-Methoxy-1-tetralone is a bicyclic aromatic hydrocarbon. The NADH oxidation rates were lower with 6-methoxy-1-tetralone in Arx/ArR system with no CYP101B1 than the 3-methoxyphenol. However, again, high levels of hydrogen peroxide were generated in these

turnovers (Table 7. 9). The findings suggest that these substrates may accept electrons from redox proteins and convert to a radical anion. This unstable intermediate donates electron to the molecular oxygen to generate superoxide which then dismutates to hydrogen peroxide. However, further study is required to fully determine the reason of futile redox cycling in the presence of these substrates. Other substrates including phenylphenols, biphenylmethanols or naphthylmethanols have been screened with this system previously, but a minimal activity of this type was detected [266].

Table 7. 9 The NADH oxidation rates of Arx/ArR with 3-methoxyphenol and 6-methoxy-1-tetralone. The rates were measured and reported same as described in Table 7. 1. n.d. Not determined. In certain instances, the detected levels of hydrogen peroxide were higher than the theoretical value this is most likely due to interference of the phenolic substrates with the H_2O_2 assays.

Substrate	Substrate conc. (µM)	NADH conc. (µM)	NADH oxidation rate (min^{-1})	H_2O_2 conc. (µM)
3-methoxyphenol	2000	314	1814	541
	1500	314	1704	534
	1000	306	1158	438
	500	306	373	195
	250	317	232	213
	100	331	119	n.d.
	50	338	80	n.d.
	25	305	74	n.d.
6-methoxy-1-tetralone	1000	338	547	213
	500	299	286	190

Oxygenated aromatics redox cycling by mitochondrial P450s electron transfer partners

Adrenodoxin (Adx) is an iron-sulfur protein of the broad family of [2Fe-2S]-ferredoxins [342]. It supplies reducing equivalents from NADPH dependent adrenodoxin reductase (AdR) to the active site of mitochondrial P450s [52, 342]. This system was also tested with the oxygenated aromatics to investigate if adrenodoxin is a mediator of futile redox cycling of these substrates as observed for the bacterial ferredoxin system.

Different concentrations of 1-naphthol (2500 to 10 µM) were added in Adx/AdR system, and NADPH oxidation rates were monitored (Table 7. 10). The rates were lower when compared to Arx/ArR system (Table 7. 10). The hydrogen peroxide assays displayed that a significant amount of reducing equivalents was converted to hydrogen peroxide.

Table 7. 10 The NADPH oxidation rates of Adx/AdR system with 1-naphthol. The oxidation rates were measured using a AdR:Adx system (0.1 µM AdR and 1 µM Adx). The original concentration of both enzymes were Adx; 374 µM and AdR; 34 µM. Rates are given same as P450 system (CYP101B1/Arx/ArR) for ease of comparison. - not determined.

1-naphthol conc. (µM)	NADPH conc. (µM)	NADPH oxidation rate	H_2O_2 conc. (µM)
2500	320	145	-
2000	354	209	-
1500	320	177	225
1000	352	200	255
500	324	189	219
200	318	193	-
100	313	150	231
50	325	143	-
20	320	121	316
10	312	113	-

The turnovers assays of Adx and AdR (without any P450 enzyme) with 1,4-naphthoquinone (250 µM) and menadione (250 µM), showed a NADPH consumption rate of 165 min^{-1} and 151 min^{-1}, respectively (Table 7. 11). For phenolic compounds, 2,6-dihydroxynaphthalene and 3-methoxyphenol also induced similar NADPH oxidation rates with this system (Table 7. 11). A large amount of hydrogen peroxide was detected in each turnover assay (Table 7. 11).

Table 7. 11 The NADPH oxidation rates of Adx/AdR system with different oxygenated aromatics. The rates were measured using a AdR:Adx concentration ratio of (0.1 µM AdR and 1 µM Adx). Rates are given same as CYP101B1/Arx/ArR system for ease of comparison.

Concentration (µM)	Substrate	NADPH conc. (µM)	NADPH oxidation rate (min^{-1})	H_2O_2 conc. (µM)
250	1,4- naphthoquinone	294	165	264
100	1,4-naphthoquinone	318	169	261
250	menadione	267	151	267
100	menadione	261	137	261
250	2,6-dihydroxynaphthalene	312	140	292
250	3-methoxy phenol	301	148	298
100	3-methoxy phenol	310	138	304

Cytochrome P450 reductase (CPR) is an enzyme which transfers reducing equivalents from NADPH to human P450s [343, 344]. The enzyme (FAD/FMN cofactors) have been reported to reduce many quinone derivatives and under the suitable condition and capable of initiate redox cycling [333, 345, 346]. The enzyme was screened with 1-naphthol. Upon addition of 2000 µM of 1-naphthol, the enzyme showed a NADPH turnover rate 418 min^{-1}. The rate of NADPH oxidation decreased as the concentration of the substrate was lowered (Table 7. 12). A high level of H_2O_2 was noticed in these turnovers. A similar type of activity has also been described for this enzyme with various redox active substrates such as menadione and parathion [314, 329, 334, 347]. CPR has been reported to reduce the substrate to the radical anion, and this anion reduced the molecular oxygen to superoxide anion that rapidly dismutates to hydrogen peroxide [314, 329, 334, 347]. In the current study, CPR catalysed the futile redox cycling with the 1-naphthol (1,4-naphthoquinone) and generated a significant amount of hydrogen peroxide in the turnover

assays presumably via a similar mechanism. It is assumed that this is the same process which occurs with the other redox partners assessed here.

Table 7. 12 The NADPH oxidation rates of CPR system with 1-naphthol. The oxidation rates were measured using a human P450 reductase system (0.2 µM CPR). The original concentration of enzyme was 11.5 µM. Rates are given same as CYP101B1/Arx/ArR system for ease of comparison. n.d. not determined.

1-naphthol conc. (µM)	NADPH conc. (µM)	NADPH oxidation rate	H_2O_2 conc. (µM)
2000	315 ± 15	418 ± 28	277
1500	314 ± 3	366 ± 39	300
1000	326 ± 16	322 ± 34	274
500	-	248 ± 1	n.d
200	-	169 ± 11	n.d
100	-	100 ± 6	n.d
50	-	39 ± 6	n.d

7.3. Discussion

The oxidation of naphthalene by CYP101B1/Arx/ArR system proceeds with a NADH oxidation rate that increased over time. Minimal amounts of naphthols or other metabolites were observed despite a moderately high NADH oxidation rate. We hypothesised that the metabolite(s) which form in the turnovers of naphthalene could be the reason for the increase in the NADH oxidation rate over time. To test the hypothesis, 1-naphthol and 2-naphthol were screened as substrates in the CYP101B1 system, which generated a minimal amount of metabolite 1,4-naphthoquinone and 2,6-dihydroxynaphthalene, respectively, despite very fast NADH oxidation rates. Both 1- and 2-naphthol were tested with only Arx/ArR system, and no P450 was added in the turnovers. The turnovers of ArR/Arx system with naphthols without the CYP101B1 enzyme, even exceeds the rate of NADH oxidation than the fully reconstituted CYP101B1 system, indicated a small amount 1,4-naphthoquinone might be already present as

an impurity with 1-naphthol. A large amount of hydrogen peroxide was detected in each turnover with or without P450 enzyme. To check 1,4-naphthoquinone is most likely the primary cause of rapid NADH oxidation, different concentrations of this substrate were added in the turnover assays with or without the P450 enzyme. In spite of very high NADH oxidation rates, no detectable product was observed in the turnovers of CYP101B1. Hydrogen peroxide assays of all turnovers containing either the complete P450 system or only the redox partners revealed that the majority of the reducing equivalents were converted to H_2O_2. This indicated that the bacterial ferredoxin (Arx) could reduce 1,4-naphthoquinone to semiquinone and catalyse redox cycling (Figure 7. 10). Hence a large quantity of hydrogen peroxide was detected in the turnovers without P450. This type of exogenous oxygenated aromatic mediated uncoupling pathway in bacterial electron transfer systems containing ferredoxin would be an additional form uncoupling. The presence of menadione and vitamin K1 in the CYP101B1/Arx/ArR or only Arx/ArR system displayed similar effect to 1,4-naphthoquinone. The dihydroxylated naphthalene, 3-methoxyphenol and 6-methoxy-1-tetralone also induced high NADH oxidation with the ArR/Arx system and formed a large quantity of hydrogen peroxide suggesting this ArR/Arx system was capable of catalysing futile redox cycle to these substrates [338-340].

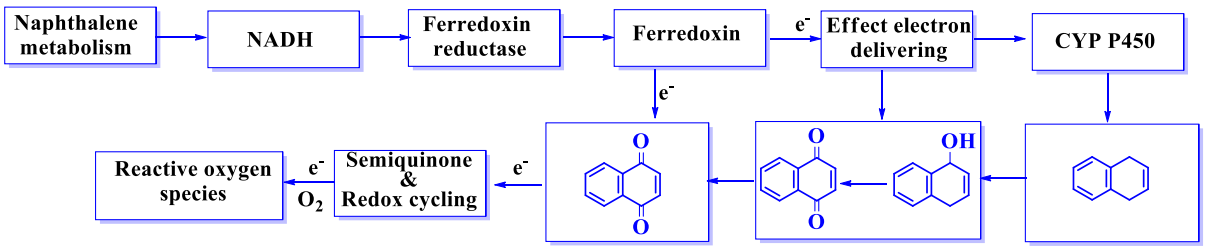

Figure 7. 10 An overview of how 1,4-naphthoquinone could interrupt the electron transfer to P450 during naphthalene or 1-naphthol metabolism.

The effect of 1,4-naphthoquinone, menadione and 2,6-dihydroxynaphthalene in the CYP101B1 catalysed oxidation of 2-adamantyl acetate were examined combining both substrates in the assays. This demonstrated that these substrates were each potent inhibitors of CYP101B1 metabolism. In the presence of these redox active substrates the yield of 5-hydroxy-2-adamantyl acetate was dramatically reduced, and in certain instances, no product was formed.

These redox active chemicals were seen to inhibit the activity of CYP101B1 by interfering with the electron transfer.

The investigation of mitochondrial P450s redox partners Adx/Adr and cytochrome P450 reductase (CPR) with 1-naphthol and 1,4-naphthoquinone indicated that they also catalysed the futile redox cycling with these substrates. This type of activity was in agreement with the previously reported activities of CPR enzyme [314, 329, 334, 347]. However, further study is required with other oxygenated substrates to fully assess these systems.

This form of uncoupling in electron transfer partners would make these P450 systems unsuitable biocatalysts for the oxidation of substrates which can accept electrons from the redox partners or that generate metabolite(s) which can do this. Electron transport proteins mediated futile redox cycling interferes with the function of the P450, and in mitochondrial P450 system which can lead to inhibit the biosynthesis of steroid and drug metabolism [323]. This is most likely the primary cause of toxicity of these substrates. In these instances using an alternate system such as peroxygenases may be more effective [266].

Further investigation is required to find out the exact mechanism of the transfer of the electrons from the ferredoxin (Adx and Arx) to the naphthoquinones, and other related substrates like dihydroxybenzene, alkylpolyphenols, menaquinone and aromatic nitro compounds which results in the subsequent generation of hydrogen peroxide [81, 266]. It would also be essential to determine if this uncoupling behaviour is generic across all class I electron transfer systems including Fdx having iron–sulfur-cluster of [3Fe–4S] and [4Fe–4S] type [44, 56, 348]. To understand the thermodynamics of the electron transfer process and structural features of the substrates which can inhibit with the electron transfer process in this way further studies could be attempted, e.g. redox potential determination [324, 342, 349]. The quantification and detection of any superoxide and the ROS such as hydroxyl radical formation in this process will be valuable. The superoxide can be quantified using several standard methods and chemicals, e.g. nitroblue tetrazolium, epinephrine, superoxide dismutase (assayed after superoxide dismutation to H_2O_2) and spin-traps with ESR spectroscopic equipment [323, 350, 351]. These results are essential when considering the toxicity of polyaromatic substrates and their oxygenated metabolites [266, 319, 352].

Chapter 8

Conclusion and Future Direction

General Conclusion:

The investigations detailed herein describe efforts towards developing novel C-H functionalisation reactions using biocatalysts. This study concentrates on the application of the cytochrome P450 enzymes in the biocatalytic oxidation of a wide range of substrates including alicyclic compounds, adamantanes, aromatic substrates and cubanes. The oxidation activity of CYP101B1 and CYP101C1 enzymes was investigated with different sized cyclic alkanes and ketones as well as the esters of cyclic alcohol and cyclohexylacetic acid in order to fully explore the substrate range of these enzymes. A comparative study between CYP101B1 and CYP101C1 with these cyclic and linear compounds provided insight into their catalytic activity, regio and stereoselectivity patterns.

Adamantane derivatives are used as building blocks for many complex drug molecules and polymers. CYP101B1 oxidised adamantane based substrates but at low product formation activity and selectivity. We envisioned that introduction of an ester directing group to adamantanols, which would mimic the butenone side chain of β-ionone, could improve the enzyme monooxygenase activity. This substrate engineering approach was effective, and the oxidation of these engineered adamantyl esters proceeded more efficiently and was highly regioselective.

The oxidation of hydrophobic aromatic compounds including alkylbenzenes, styrenes, substituted naphthalenes were investigated with CYP101B1. The binding affinity and oxidation activity of CYP101B1 with these hydrophobic substrates were low. Protein engineering of the active-site of CYP101B1 was undertaken. The H85F variant exhibited higher binding affinities and resulted in greater metabolite yields with certain aromatic substrates.

Methylcubane was used to investigate the mechanistic pathways of P450 hydroxylation. To probe the product-determining step a series of cubane derivatives were designed and screened. These are capable of distinguishing between radical or carbocation intermediates formed during the oxidation.

Several electron transfer proteins including bacterial (Arx/ArR) and mitochondrial (Adx/AdR) were investigated to assess futile redox cycling with oxygenated aromatics. The high NADH oxidation rates in the absence of P450 enzyme and the significant quantity of hydrogen peroxide observed in these turnovers indicated that these enzymes facilitate the uncoupling in the presence of certain oxygenated aromatics.

Chapter 3: The binding and kinetic properties of CYP101B1 and CYP101C1 were determined with a range of cycloalkanes. However, most of the reactions proceed at low product formation activity. The addition of a ketone group to these cyclic compounds improved the binding affinity and activity. CYP101C1 showed different regioselectivity for cycloalkanones, and it hydroxylated these substrates at the C-2 position. CYP101B1 catalysed the oxidation of these cyclic ketones with higher product formation rates than the CYP101C1 system. However, the selectivity was often reduced for CYP101B1, e.g. in the case of cycloundecanone hydroxylation occurred at the 2-, 5- and 6-positions. CYP101B1 also generated cyclisation metabolites with cyclononanone and cyclodecanone. The regioselectivity enhanced for larger cycloalkanones like cyclododecanone and cyclopentadecanone, where the hydroxylation occurs predominantly on the remote site of the ring to the ketone moiety to form C-7 (96%) and C-8 (90%) hydroxy products, respectively. The majority of the cycloalkanols (cyclohexanol and cyclooctanol) investigated with both enzymes did not show any activity. The exception was cyclododecanol which was metabolised by both enzymes. The esters derivatives of the cycloalkanols did bind tightly with CYP101B1. The productive oxidation rates of the CYP101B1 enzyme were 2 to 25-fold faster than these of the CYP101C1. The coupling efficiencies of the CYP101B1 with these substrates were also significantly improved. Both enzymes catalysed the selective oxidation of these cyclic esters, and the hydroxylation occurs solely on the other side of the ring to the ester directing group.

CYP101C1 oxidised *α*-terpinyl acetate with a high product formation rate and coupling efficiency, whereas, CYP101B1 did not show any activity with this substrate. CYP101B1 and CYP101C1 catalysed the oxidation of linear substrates including 2-nonanone, 2-undecanone, linalyl acetate and citronellyl acetate. CYP101C1 exhibited higher biocatalytic activities with linalyl acetate and citronellyl acetate. The ability to catalyse the oxidation of a range of cyclic and linear compounds highlighted the potential of these two enzymes to functionalise inert C-H bonds.

Overall, cyclic ketones and esters were good substrates for CYP101B1 and CYP101C1. The presence of a ketone or an ester carbonyl group significantly improved the activity. The work on CYP101B1 clearly shows that the enzyme must hold the substrate in a way that selective C-H bond abstraction occurs on the opposite side of the ring to the carbonyl functionality. There is also a good correlation with the substrate binding parameters and the activity. This trend can be observed when comparing for example cyclodecanone versus cyclooctanone and cycloctyl acetate versus cyclooctanol. It is however important to note that better binding does not always result in improved activity or total turnover number and we hypothesis that this is related to the solubility of the substrate for example cyclododecyl acetate versus cyclooctyl acetate. There is currently no structural data for the CYP101B1 enzyme to help explain why the substrates are bound in this manner. The use of a homology model to direct mutagenesis was found not to be as successful as related studies with $P450_{cam}$ (Chapter 5). Crystal structure data are available for the related enzymes CYP101A1 ($P450_{cam}$), CYP101D1, CYP101D2 and CYP101C1 [47, 49, 248, 250, 264, 265]. While the first three share some similarities as well as important differences are observed [47, 175, 248, 250]. Of relevance here is that the CYP101C1 structure is significantly different to the others [47]. It contains additional loops and short helices and has a distinctive active site [47]. This is in line with the altered substrate range of this enzyme. CYP101B1 is functionally different from all of the above-mentioned enzymes (dissimilar substrate range) which suggests that its structure (especially around the active site) will not closely resemble the others. However based on the CYP101C1 structure, we would predict that the butenone side chain of the norisoprenoids (and the carbonyl moiety of the ketones or esters) will interact with residues near the entrance of the substrate binding pocket and hold the opposite side of the ring system close to the heme iron to allow selective C-H bond abstraction.

Further investigation of larger (>C15) and smaller (<C6) cyclic and linear compounds with ketone and ester moieties would be valuable to expand their substrate range. Lactones and lactams, e.g. *ε*-caprolactone, *ε*-caprolactam, pentadecanolide and 16-hexadecanolide, which have received attention because of their chemical versatility, could be investigated with these monooxygenase enzymes. Crystal structures of substrate-bound CYP101B1 would enable to determine the amino acids of the active site of CYP101B1 which interact with the ketone oxygen. Protein engineering of both enzymes could be a useful approach to improve the binding affinity and selectivity further.

Chapter 4: Tricyclic adamantane derivatives were studied with CYP101B1, and the enzyme showed low affinity for adamantane and adamantanols. Low product formation activity and selectivity were also observed in these turnovers. Substrate engineering was used to enhance the binding affinity and activity of CYP101B1 for this class of substrates. The introduction of ester protecting groups (acetate and isobutyrate) to the adamantanols, significantly improved the binding affinity of CYP101B1 when compared to parent alcohols. The enzyme oxidised these compounds with fast product formation activities and high regio- and stereoselectivity. The enzyme predominantly oxidised 1-adamantyl acetate/isobutyrate and 2-adamantyl acetate/isobutyrate at the C-4 and C-5 position, respectively. All the 4-hydroxy metabolites are confirmed as having a *trans* arrangement of the alcohol and ester. The same approach was also applied where an acetamide moiety was used to replace the amine moiety of 1-adamantylamine. The acetamide was metabolised by CYP101B1 whereas the amine was not. Significant quantities of metabolites were generated using a whole-cell system which indicated that CYP101B1 could be used to synthesise these products on a larger scale. These observations demonstrate that the substrate engineering strategy using ester and amide protecting groups could be useful for this class of substrates and other.

The yield of hydroxylated metabolites could be significantly improved using higher density cell cultures in a fermentor with more control of the pH and nutrients, when combined with a substrate feeding/product removal regime. Further investigation could be undertaken with other adamantane derivatives found in pharmaceutical compositions such as adamantane-1-carboxamide, adamantyl-alkylamines, *n*-[1-(adamantan-1-yl)ethyl]acetamide and tromantadine [237].

Chapter 5: CYP101B1 was shown to catalyse the oxidation of aromatic substrates including alkylbenzenes, styrenes, alkyl substituted naphthalenes and the tricyclic acenaphthene. However, the binding affinity and activity were low. Replacement of histidine (H85) residue, from the active site by a hydrophobic phenylalanine residue altered the functional properties of the enzyme. Variations in the binding affinity and selectivity were observed when *β*-ionone was screened with each variant. The H85F variant of CYP101B1 exhibited tighter binding affinities and gave higher metabolite yields with the majority of the hydrophobic aromatic substrates tested including naphthalene derivatives. Studies were also carried out with biphenyl and substituted biphenyls. However, the activity of H85F variant with these longer hydrophobic compounds was not significantly improved over the WT enzyme. Other variants of CYP101B1 such as H85A and H85G have also been investigated with different hydrophobic substrates, but they also showed lower binding affinity and oxidation activity compared to WT CYP101B1 with biphenyls [264]. The productivity may be enhanced towards larger aromatic compounds by altering other active site residues, for example, I237 and Q234. Solving the crystal structure would be valuable for this enzyme to facilitate further mutagenesis studies and makes the enzyme truly efficient and practical towards a wide range of aromatic substrates particularly biphenyls.

Chapter 6: CYP101B1 was studied with substituted methylcubanes, and these reactions were used to probe the mechanism of hydroxylation in P450. Most of the methylcubane derivates were oxidised with high activity and selectively. The cubane skeleton remained intact after all the turnovers. The enzyme abstracted one of the protons from the methyl group and little or no rearrangement product was detected. This is most likely due to the faster radical rebound compared to radical rearrangement. The metabolites which arise from the oxidation of CYP101B1 supported the absence of any involvement of a carbocation-based intermediate during the oxidation of methyl C-H bond. This could be further investigated to determine the nature of radical intermediates formed. Additional studies with other related mechanistic probes are required in order to verify the current findings and more precisely define the hydroxylation mechanism of this enzyme.

Chapter 7: The NAD(P)H oxidation activities of both bacterial and mitochondrial P450 electron transfer proteins were found to be fast in the presence of different oxygenated aromatics but in the absence of the monooxygenase enzyme. Assays showed that most of the

reducing equivalents in these turnovers were converted into H_2O_2. The likely mechanism for this H_2O_2 formation in the turnovers is that the redox partner proteins catalyse the reduction of naphthoquinones to the corresponding semiquinones. These unstable semiquinones donate an electron to molecular oxygen, generating superoxide anions which then dismutate to hydrogen peroxide and O_2. This type of uncoupling of reducing equivalents without the presence of P450 enzyme highlighted the ability of ferredoxin or adrenodoxin iron-sulfur proteins to catalyse this futile redox cycling which should be considered an additional form of uncoupling in these systems.

Overall, this futile redox cycling significantly reduces the catalytic performance of CYP101B1 by impairing the electron transfer from physiological redox partners to the heme of the enzyme. For illustration, the presence of any of these naphthoquinones in the fully reconstituted CYP101B1 system, significantly reduced the P450 mediated metabolism of 2-adamantyl acetate. The cytochrome P450 reductase (CPR) was also studied with oxygenated aromatics and shown to catalyse this futile redox cycle.

More work is necessary to elucidate the exact mechanism of electron transfer during redox cycling reactions, and how these redox active chemicals interact with the electron transfer proteins. The investigation of redox cycle in cell would be useful to find out the physiological significances of a small quantity of quinone on P450 activity *in vivo*, e.g. ESR detection and *in vivo* spin traps would be used to determine the mechanism of futile redox cycling.

Chapter 9

References

1. P. R. O. De Montellano, *Cytochrome P450: structure, mechanism, and biochemistry*, Springer Science & Business Media, 2005.
2. T. L. Poulos, *Chemical Reviews*, 2014, 114, 3919-3962.
3. D. Garfinkel, *Archives of Biochemistry and Biophysics*, 1958, 77, 493-509.
4. M. Klingenberg, *Archives of Biochemistry and Biophysics*, 1958, 75, 376-386.
5. T. Omura and R. Sato, *Journal of Biological Chemistry*, 1964, 239, 2370-2378.
6. J. H. Dawson and M. Sono, *Chemical Reviews*, 1987, 87, 1255-1276.
7. S. Yoshioka, S. Takahashi, H. Hori, K. Ishimori and I. Morishima, *European Journal of Biochemistry*, 2001, 268, 252-259.
8. D. R. Nelson, *Biochimica et Biophysica Acta (BBA)-Proteins and Proteomics*, 2018, 1866, 141-154.
9. F. P. Guengerich, in *Cytochrome P450*, Springer, 2015, pp. 523-785.
10. K. J. McLean and A. W. Munro, *Drug Metabolism Reviews*, 2008, 40, 427-446.
11. M. A. Schuler and D. Werck-Reichhart, *Annual Review of Plant Biology*, 2003, 54, 629-667.
12. J. Park, S. Lee, J. Choi, K. Ahn, B. Park, J. Park, S. Kang and Y.-H. Lee, *BMC Genomics*, 2008, 9, 402.
13. F. P. Guengerich, *Chemical Research in Toxicology*, 2001, 14, 611-650.
14. D. R. Nelson, *Biochimica et Biophysica Acta (BBA)-Proteins and Proteomics*, 2011, 1814, 14-18.
15. D. R. Nelson, in *Cytochrome P450 Protocols*, Springer, 1998, pp. 15-24.
16. D. R. Nelson, T. Kamataki, D. J. Waxman, F. P. Guengerich, R. W. Estabrook, R. Feyereisen, F. J. Gonzalez, M. J. Coon, I. C. Gunsalus and O. Gotoh, *DNA and Cell Biology*, 1993, 12, 1-51.
17. D. R. Nelson, L. Koymans, T. Kamataki, J. J. Stegeman, R. Feyereisen, D. J. Waxman, M. R. Waterman, O. Gotoh, M. J. Coon and R. W. Estabrook, *Pharmacogenetics*, 1996, 6, 1-42.
18. D. Nelson, CytochromeP450. html, (http://drnelson. utmem. edu), 2004.

19. D. W. Nebert, K. Wikvall and W. L. Miller, *Philosophical Transactions of the Royal Society B: Biological Sciences*, 2013, 368, 20120431.

20. D. E. Kelly, N. Kraševec, J. Mullins and D. R. Nelson, *Fungal Genetics and Biology*, 2009, 46, S53-S61.

21. Y. Miura and A. J. Fulco, *Journal of Biological Chemistry*, 1974, 249, 1880-1888.

22. R. S. Hare and A. J. Fulco, *Biochemical and Biophysical Research Communications*, 1975, 65, 665-672.

23. P. P. Ho and A. J. Fulco, *Biochimica et Biophysica Acta (BBA)-Lipids and Lipid Metabolism*, 1976, 431, 249-256.

24. M. Correia and P. O. de Montellano, *Inhibition of cytochrome P450 enzymes, PR Ortiz de Montellano. Kluwer/Plenum, New York, NY*, 2005, 247-322.

25. B. Meunier, S. P. de Visser and S. Shaik, *Chemical Reviews*, 2004, 104, 3947-3980.

26. R. a. Chao, Thesis (M.Phil.)--University of Adelaide, School of Physical Sciences 2016.

27. A. E. Rettie, M. Boberg, A. Rettenmeier and T. A. Baillie, *Journal of Biological Chemistry*, 1988, 263, 13733-13738.

28. Y. Seto and F. Guengerich, *Journal of Biological Chemistry*, 1993, 268, 9986-9997.

29. A. B. Carmichael and L. L. Wong, *European Journal of Biochemistry*, 2001, 268, 3117-3125.

30. S. G. Bell, W. Yang, J. A. Yorke, W. Zhou, H. Wang, J. Harmer, R. Copley, A. Zhang, R. Zhou and M. Bartlam, *Acta Crystallographica Section D: Biological Crystallography*, 2012, 68, 277-291.

31. L.-H. Xu, H. Ikeda, L. Liu, T. Arakawa, T. Wakagi, H. Shoun and S. Fushinobu, *Applied Microbiology and Biotechnology*, 2015, 99, 3081-3091.

32. T. L. Poulos and R. Raag, *The FASEB Journal*, 1992, 6, 674-679.

33. I. C. Gunsalus and G. C. Wagner, in *Methods in enzymology*, Elsevier, 1978, vol. 52, pp. 166-188.

34. T. L. Poulos, B. Finzel, I. Gunsalus, G. C. Wagner and J. Kraut, *Journal of Biological Chemistry*, 1985, 260, 16122-16130.

35. T. M. Makris, I. Denisov, I. Schlichting and S. G. Sligar, in *Cytochrome P450*, Springer, 2005, pp. 149-182.

36. J. Rittle and M. T. Green, *Science (New York, N.Y.)*, 2010, 330, 933-937.

37. F. P. Guengerich and A. W. Munro, *Journal of Biological Chemistry*, 2013, jbc. R113. 462275.

38. X. Huang and J. T. Groves, *JBIC Journal of Biological Inorganic Chemistry*, 2017, 22, 185-207.

39. P. J. Mak and I. G. Denisov, *Biochimica et Biophysica Acta (BBA)-Proteins and Proteomics*, 2017.

40. S. Shaik, D. Kumar, S. P. de Visser, A. Altun and W. Thiel, *Chemical Reviews*, 2005, 105, 2279-2328.

41. H. Hirao, D. Kumar, W. Thiel and S. Shaik, *Journal of the American Chemical Society*, 2005, 127, 13007-13018.

42. S. Shaik, H. Hirao and D. Kumar, *Natural Product Reports*, 2007, 24, 533-552.

43. L. Waskell and J. J. P. Kim, *Electron transfer partners of cytochrome P450*, 2015.

44. F. Hannemann, A. Bichet, K. M. Ewen and R. Bernhardt, *Biochimica et Biophysica Acta (BBA)-General Subjects*, 2007, 1770, 330-344.

45. T. Omura, E. Sanders, R. Estabrook, D. Cooper and O. Rosenthal, *Archives of Biochemistry and Biophysics*, 1966, 117, 660-673.

46. L. Waskell and J.-J. P. Kim, in *Cytochrome P450*, Springer, 2015, pp. 33-68.

47. M. Ma, S. G. Bell, W. Yang, Y. Hao, N. H. Rees, M. Bartlam, W. Zhou, L. L. Wong and Z. Rao, *Chembiochem*, 2011, 12, 88-99.

48. S. G. Bell and L.-L. Wong, *Biochemical and Biophysical Research Communications*, 2007, 360, 666-672.

49. S. G. Bell, A. Dale, N. H. Rees and L.-L. Wong, *Applied Microbiology and Biotechnology*, 2010, 86, 163-175.

50. W. Yang, G. Stephen, H. Wang, W. Zhou, N. Hoskins, A. Dale, M. Bartlam, L. L. Wong and Z. Rao, *Journal of Biological Chemistry*, 2010, jbc. M110. 118349.

51. T. Omura and K.-i. Morohashi, *The Journal of Steroid Biochemistry and Molecular Biology*, 1995, 53, 19-25.

52. T. Omura, *Chemico-biological Interactions*, 2006, 163, 86-93.

53. M. J. Paine, N. S. Scrutton, A. W. Munro, A. Gutierrez, G. C. Roberts and C. R. Wolf, in *Cytochrome P450*, Springer, 2005, pp. 115-148.

54. R. Bernhardt, *Journal of Biotechnology*, 2006, 124, 128-145.

55. M. Ramachandra, R. Seetharam, M. Emptage and F. Sariaslani, *Journal of Bacteriology*, 1991, 173, 7106-7112.

56. M. K. Trower, M. H. Emptage and F. S. Sariaslani, *Biochimica et Biophysica Acta (BBA)-Protein Structure and Molecular Enzymology*, 1990, 1037, 281-289.

57. M. Trower, R. Lenstra, C. Omer, S. Buchholz and F. Sariaslani, *Molecular Microbiology*, 1992, 6, 2125-2134.

58. I. Hanukoglu, in *Advances in molecular and cell biology*, Elsevier, 1996, vol. 14, pp. 29-56.

59. P. A. Williams, J. Cosme, V. Sridhar, E. F. Johnson and D. E. McRee, *Molecular cell*, 2000, 5, 121-131.

60. D. R. Davydov, *Expert opinion on drug metabolism & toxicology*, 2011, 7, 543-558.

61. D. B. Hawkes, G. W. Adams, A. L. Burlingame, P. R. O. de Montellano and J. J. De Voss, *Journal of Biological Chemistry*, 2002, 277, 27725-27732.

62. L. O. Narhi and A. J. Fulco, *Journal of Biological Chemistry*, 1986, 261, 7160-7169.

63. E. L. Rylott, R. G. Jackson, J. Edwards, G. L. Womack, H. M. Seth-Smith, D. A. Rathbone, S. E. Strand and N. C. Bruce, *Nature Biotechnology*, 2006, 24, 216.

64. H. M. Seth-Smith, S. J. Rosser, A. Basran, E. R. Travis, E. R. Dabbs, S. Nicklin and N. C. Bruce, *Applied and Environmental Microbiology*, 2002, 68, 4764-4771.

65. L. O. Narhi and A. J. Fulco, *Journal of Biological Chemistry*, 1987, 262, 6683-6690.

66. A. Daiber, H. Shoun and V. Ullrich, *Journal of Inorganic Biochemistry*, 2005, 99, 185-193.

67. W. G. Zumft, *Microbiology and Molecular Biology Reviews*, 1997, 61, 533-616.

68. H. Shoun and T. Tanimoto, *Journal of Biological Chemistry*, 1991, 266, 11078-11082.

69. I. G. Denisov and S. G. Sligar, in *Cytochrome P450*, Springer, 2015, pp. 69-109.

70. N. Shakunthala, *Expert opinion on drug metabolism & toxicology*, 2010, 6, 1-15.

71. D. Holtmann and F. Hollmann, *ChemBioChem*, 2016, 17, 1391-1398.

72. P. J. Loida and S. G. Sligar, *Biochemistry*, 1993, 32, 11530-11538.

73. I. G. Denisov, T. M. Makris, S. G. Sligar and I. Schlichting, *Chemical Reviews*, 2005, 105, 2253-2278.

74. R. Bernhardt and V. B. Urlacher, *Applied Microbiology and Biotechnology*, 2014, 98, 6185-6203.

75. R. Fasan, *Curr. Opin. Biotechnol*, 2011, 22, 809-817.

76. E. O'Reilly, V. Köhler, S. L. Flitsch and N. J. Turner, *Chemical Communications*, 2011, 47, 2490-2501.

77. I. Hanukoglu, R. Rapoport, L. Weiner and D. Sklan, *Archives of Biochemistry and Biophysics*, 1993, 305, 489-498.

78. R. Rapoport, D. Sklan and I. Hanukoglu, *Archives of Biochemistry and Biophysics*, 1995, 317, 412-416.

79. G. Gilardi, Y. T. Meharenna, G. E. Tsotsou, S. J. Sadeghi, M. Fairhead and S. Giannini, *Biosensors and Bioelectronics*, 2002, 17, 133-145.

80. S. Rendic and F. P. Guengerich, *Chemical research in toxicology*, 2012, 25, 1316-1383.

81. H. Kappus, *Biochem. Pharmacol*, 1986, 35, 1-6.

82. R. Docampo and S. N. Moreno, *Free Radicals in Biology*, 1984, 6, 243-288.

83. J. T. Szilagyi, K. C. Fussell, Y. Wang, Y.-H. Jan, V. Mishin, J. R. Richardson, D. E. Heck, S. Yang, L. M. Aleksunes and D. L. Laskin, *Toxicology and Applied pharmacology*, 2018, 359, 102-107.

84. M. Newcomb, R. Shen, S.-Y. Choi, P. H. Toy, P. F. Hollenberg, A. D. Vaz and M. J. Coon, *Journal of the American Chemical Society*, 2000, 122, 2677-2686.

85. M. J. Cryle, P. R. Ortiz de Montellano and J. J. De Voss, *The Journal of Organic Chemistry*, 2005, 70, 2455-2469.

86. M. Newcomb and P. H. Toy, *Accounts of Chemical Research*, 2000, 33, 449-455.

87. M. Newcomb, M.-H. Le Tadic-Biadatti, D. L. Chestney, E. S. Roberts and P. F. Hollenberg, *Journal of the American Chemical Society*, 1995, 117, 12085-12091.

88. P. H. Toy, M. Newcomb and P. F. Hollenberg, *Journal of the American Chemical Society*, 1998, 120, 7719-7729.

89. F. Lichtenberger, W. Nastainczyk and V. Ullrich, *Biochemical and Biophysical Research Communications*, 1976, 70, 939-946.

90. J. T. Groves and G. A. McClusky, *Journal of the American Chemical Society*, 1976, 98, 859-861.

91. J. T. Groves, G. A. McClusky, R. E. White and M. J. Coon, *Biochemical and Biophysical Research Communications*, 1978, 81, 154-160.

92. J. T. Groves and D. V. Adhyam, *Journal of the American Chemical Society*, 1984, 106, 2177-2181.

93. S. Y. Choi, P. E. Eaton, M. Newcomb and Y. C. Yip, *Journal of the American Chemical Society*, 1992, 114, 6326-6329.

94. M. J. Cryle and J. J. De Voss, *ChemBioChem*, 2008, 9, 261-266.

95. W. D. Kerber, B. Ramdhanie and D. P. Goldberg, *Angewandte Chemie International Edition*, 2007, 46, 3718-3721.

96. R. Davydov, R. Perera, S. Jin, T.-C. Yang, T. A. Bryson, M. Sono, J. H. Dawson and B. M. Hoffman, *Journal of the American Chemical Society*, 2005, 127, 1403-1413.

97. S. Shaik, *Special Publication-Royal Society of Chemistry*, 2006, 304, 233-248.

98. S. P de Visser, C. S Porro, M. G Quesne, M. A Sainna and A. W Munro, *Current Topics in Medicinal Chemistry*, 2013, 13, 2218-2232.

99. C. Li, L. Zhang, C. Zhang, H. Hirao, W. Wu and S. Shaik, *Angewandte Chemie International Edition*, 2007, 46, 8168-8170.

100. M. J. Park, J. Lee, Y. Suh, J. Kim and W. Nam, *Journal of the American Chemical Society*, 2006, 128, 2630-2634.

101. F. Ogliaro, S. P. de Visser, S. Cohen, P. K. Sharma and S. Shaik, *Journal of the American Chemical Society*, 2002, 124, 2806-2817.

102. S. Jin, T. M. Makris, T. A. Bryson, S. G. Sligar and J. H. Dawson, *Journal of the American Chemical Society*, 2003, 125, 3406-3407.

103. S. P. de Visser, F. Ogliaro, N. Harris and S. Shaik, *Journal of the American Chemical Society*, 2001, 123, 3037-3047.

104. T. M. Makris, R. Davydov, I. G. Denisov, B. M. Hoffman and S. G. Sligar, *Drug Metabolism Reviews*, 2002, 34, 691-708.

105. R. Fasan, *ACS Catalysis*, 2012, 2, 647-666.

106. D. W. Nebert and D. W. Russell, *The Lancet*, 2002, 360, 1155-1162.

107. K. Hayashi, K. Yasuda, H. Sugimoto, S. Ikushiro, M. Kamakura, A. Kittaka, R. L. Horst, T. C. Chen, M. Ohta and Y. Shiro, *The FEBS Journal*, 2010, 277, 3999-4009.

108. T. Sakaki, M. Akiyoshi-Shibata, Y. Yabusaki, K. Manabe, H. Murakami and H. Ohkawa, *Pharmacogenetics*, 1991, 1, 86-93.

109. J. A. Labinger and J. E. Bercaw, *Nature*, 2002, 417, 507.

110. B. D. Dangel, J. A. Johnson and D. Sames, *Journal of the American Chemical Society*, 2001, 123, 8149-8150.

111. L. V. Desai, K. L. Hull and M. S. Sanford, *Journal of the American Chemical Society*, 2004, 126, 9542-9543.

112. A. R. Dick, K. L. Hull and M. S. Sanford, *Journal of the American Chemical Society*, 2004, 126, 2300-2301.

113. L. Gómez, I. Garcia-Bosch, A. Company, J. Benet-Buchholz, A. Polo, X. Sala, X. Ribas and M. Costas, *Angewandte Chemie International Edition*, 2009, 48, 5720-5723.

114. D. K. Romney and S. J. Miller, *Organic Letters*, 2012, 14, 1138-1141.

115. M. S. Chen and M. C. White, *Science*, 2007, 318, 783-787.

116. B. R. Cook, T. J. Reinert and K. S. Suslick, *Journal of the American Chemical Society*, 1986, 108, 7281-7286.

117. S. Das, C. D. Incarvito, R. H. Crabtree and G. W. Brudvig, *Science*, 2006, 312, 1941-1943.

118. S. Das, G. W. Brudvig and R. H. Crabtree, *Journal of the American Chemical Society*, 2008, 130, 1628-1637.

119. J. F. Hartwig and M. A. Larsen, *ACS Central Science*, 2016, 2, 281-292.

120. M. Lee and M. S. Sanford, *Journal of the American Chemical Society*, 2015, 137, 12796-12799.

121. T. W. Lyons and M. S. Sanford, *Chemical Reviews*, 2010, 110, 1147-1169.

122. R. E. Maleczka, F. Shi, D. Holmes and M. R. Smith, *Journal of the American Chemical Society*, 2003, 125, 7792-7793.

123. M. Girhard, P. J. Bakkes, O. Mahmoud and V. B. Urlacher, in *Cytochrome P450*, Springer, 2015, pp. 451-520.

124. M. Arroyo, I. de la Mata, J.-L. García and J.-L. Barredo, in *Biotechnology of Microbial Enzymes*, Elsevier, 2017, pp. 451-473.

125. M. Landwehr, L. Hochrein, C. R. Otey, A. Kasrayan, J.-E. Bäckvall and F. H. Arnold, *Journal of the American Chemical Society*, 2006, 128, 6058-6059.

126. T. Furuya and K. Kino, *Applied Microbiology and Biotechnology*, 2010, 85, 1861-1868.

127. A. Rühlmann, D. Antovic, T. J. Müller and V. B. Urlacher, *Advanced Synthesis & Catalysis*, 2017, 359, 984-994.

128. E. M. Gillam, *Chemical Research in Toxicology*, 2007, 21, 220-231.

129. E. M. Gillam, *Clinical and Experimental Pharmacology and Physiology*, 2005, 32, 147-152.

130. F. P. Guengerich, *Nature Reviews Drug Discovery*, 2002, 1, 359.

131. H. M. Girvan and A. W. Munro, *Current opinion in Chemical Biology*, 2016, 31, 136-145.

132. I. Watanabe, F. Nara and N. Serizawa, *Gene*, 1995, 163, 81-85.

133. T. Sakaki, *Biological and Pharmaceutical Bulletin*, 2012, 35, 844-849.

134. M. Litzenburger and R. Bernhardt, *Applied Microbiology and Biotechnology*, 2016, 100, 4447-4457.

135. T. Sakaki and E. Munetsuna, *Applied Microbiology and Biotechnology*, 2010, 88, 23-30.

136. R. Shinkyo, T. Sakaki, M. Ohta and K. Inouye, *Archives of Biochemistry and Biophysics*, 2003, 409, 180-187.

137. J. A. Bumpus, M. Tien, D. Wright and S. D. Aust, *Science (New York, N.Y.)*, 1985, 228, 1434-1436.

138. K. Auclair and V. Polic, in *Monooxygenase, Peroxidase and Peroxygenase Properties and Mechanisms of Cytochrome P450*, Springer, 2015, pp. 209-228.

139. M. K. Julsing, S. Cornelissen, B. Bühler and A. Schmid, *Current Opinion in Chemical Biology*, 2008, 12, 177-186.

140. T. Seng Wong, F. H. Arnold and U. Schwaneberg, *Biotechnology and Bioengineering*, 2004, 85, 351-358.

141. C. R. Otey, G. Bandara, J. Lalonde, K. Takahashi and F. H. Arnold, *Biotechnology and Bioengineering*, 2006, 93, 494-499.

142. V. B. Urlacher, A. Makhsumkhanov and R. D. Schmid, *Applied Microbiology and Biotechnology*, 2006, 70, 53-59.

143. S. G. Bell, W. Yang, A. Dale, W. Zhou and L.-L. Wong, *Applied Microbiology and Biotechnology*, 2013, 97, 3979-3990.

144. S. G. Bell, D. A. Rouch and L.-L. Wong, *Journal of Molecular Catalysis B: Enzymatic*, 1997, 3, 293-302.

145. K. Nakamura, M. V. Martin and F. P. Guengerich, *Archives of Biochemistry and Biophysics*, 2001, 395, 25-31.

146. B. M. van Vugt-Lussenburg, E. Stjernschantz, J. Lastdrager, P. Vermeulen and J. N. Commandeur, *Journal of Medicinal Chemistry*, 2007, 50, 455-461.

147. N. N. Rosic, W. Huang, W. A. Johnston, J. J. DeVoss and E. M. Gillam, *Gene*, 2007, 395, 40-48.

148. G. Braunegg, A. De Raadt, S. Feichtenhofer, H. Griengl, I. Kopper, A. Lehmann and H. J. Weber, *Angewandte Chemie International Edition*, 1999, 38, 2763-2766.

149. A. De Raadt, H. Griengl and H. Weber, *Chemistry–A European Journal*, 2001, 7, 27-31.

150. S. Li, M. R. Chaulagain, A. R. Knauff, L. M. Podust, J. Montgomery and D. H. Sherman, *Proceedings of the National Academy of Sciences*, 2009, 106, 18463-18468.

151. A. Ménard, C. Fabra, Y. Huang and K. Auclair, *ChemBioChem*, 2012, 13, 2527-2536.

152. D. F. Münzer, P. Meinhold, M. W. Peters, S. Feichtenhofer, H. Griengl, F. H. Arnold, A. Glieder And A. De Raadt, *Chemical Communications*, 2005, 2597-2599.

153. A. T. Larsen, E. M. May and K. Auclair, *Journal of the American Chemical Society*, 2011, 133, 7853-7858.

154. H. S. Shin and J. T. Slattery, *Journal of Pharmaceutical Sciences*, 1998, 87, 390-393.

155. J. C. Lewis, S. Bastian, C. S. Bennett, Y. Fu, Y. Mitsuda, M. M. Chen, W. A. Greenberg, C.-H. Wong and F. H. Arnold, *Proceedings of the National Academy of Sciences*, 2009, pnas. 0908954106.

156. J. K. Yano, M. R. Wester, G. A. Schoch, K. J. Griffin, C. D. Stout and E. F. Johnson, *Journal of Biological Chemistry*, 2004.

157. A. W. Munro, D. G. Leys, K. J. McLean, K. R. Marshall, T. W. Ost, S. Daff, C. S. Miles, S. K. Chapman, D. A. Lysek and C. C. Moser, *Trends in Biochemical Sciences*, 2002, 27, 250-257.

158. J.-D. Zhang, A.-T. Li, H.-L. Yu, T. Imanaka and J.-H. Xu, *Journal of Industrial Microbiology & Biotechnology*, 2011, 38, 633-641.

159. K. Seelbach, B. Riebel, W. Hummel, M.-R. Kula, V. I. Tishkov, A. M. Egorov, C. Wandrey and U. Kragl, *Tetrahedron Letters*, 1996, 37, 1377-1380.

160. F. Hollmann, I. W. Arends and K. Buehler, *ChemCatChem*, 2010, 2, 762-782.

161. H. Zhao and W. A. Van Der Donk, *Current Opinion in Biotechnology*, 2003, 14, 583-589.

162. R. B. Vail, M. J. Homann, I. Hanna and A. Zaks, *Journal of Industrial Microbiology and Biotechnology*, 2005, 32, 67-74.

163. K. Vuorilehto, S. Lütz and C. Wandrey, *Bioelectrochemistry*, 2004, 65, 1-7.

164. W. A. Van Der Donk and H. Zhao, *Current Opinion in Biotechnology*, 2003, 14, 421-426.

165. C. Wong, D. G. Drueckhammer and H. M. Sweers, *Journal of the American Chemical Society*, 1985, 107, 4028-4031.

166. C.-H. Wong and G. M. Whitesides, *Journal of the American Chemical Society*, 1981, 103, 4890-4899.

167. A. Chefson and K. Auclair, *Molecular BioSystems*, 2006, 2, 462-469.

168. S. Kochius, J. van Marwijk, A. Ebrecht, D. Opperman and M. Smit, *Catalysts*, 2018, 8, 531.

169. F. Hollmann, B. Witholt and A. Schmid, *Journal of Molecular Catalysis B: Enzymatic*, 2002, 19, 167-176.

170. J. Fredrickson, F. Brockman, D. Workman, S. Li and T. Stevens, *Applied and Environmental Microbiology*, 1991, 57, 796-803.

171. J. Fredrickson, D. Balkwill, G. Drake, M. Romine, D. Ringelberg and D. White, *Applied and Environmental Microbiology*, 1995, 61, 1917-1922.

172. S. G. Bell and L. L. Wong, *Biochemical and Biophysical Research Communications*, 2007, 360, 666-672.

173. M. H. Gelb, D. C. Heimbrook, P. Malkonen and S. G. Sligar, *Biochemistry*, 1982, 21, 370-377.

174. T. J. McMurry, J. T. Groves and P. R. O. de Montellano, 1986.

175. E. A. Hall and S. G. Bell, *RSC Advances*, 2015, 5, 5762-5773.

176. E. A. Hall, M. R. Sarkar, J. H. Z. Lee, S. D. Munday and S. G. Bell, *Acs Catalysis*, 2016, 6, 6306-6317.

177. Y. Jin and J. D. Lipscomb, *Biochemistry*, 1999, 38, 6178-6186.

178. L. Michaelis and M. Menten, *Zeitschrift*, 1913, 49, 333-369.

179. G. E. Briggs and J. B. S. Haldane, *Biochemical Journal*, 1925, 19, 338.

180. J. W. Williams and J. F. Morrison, in *Methods in Enzymology*, Elsevier, 1979, vol. 63, pp. 437-467.

181. F. Xu, S. G. Bell, Z. Rao and L.-L. Wong, *Protein Engineering, Design & Selection*, 2007, 20, 473-480.

182. M. R. Sarkar, E. A. Hall, S. Dasgupta and S. G. Bell, *ChemistrySelect*, 2016, 1, 6700-6707.

183. AF Thomas, G Ohloff - *US Patent* 3,993,604, 1976.

184. Q. Cheng, S. Thomas and P. Rouviere, *Applied Microbiology and Biotechnology*, 2002, 58, 704-711.

185. P. Morgan and R. J. Watkinson, in *Biochemistry of Microbial Degradation*, ed. C. Ratledge, Springer Netherlands, Dordrecht, 1994, DOI: 10.1007/978-94-011-1687-9_1, pp. 1-31.

186. K. Kostichka, S. M. Thomas, K. J. Gibson, V. Nagarajan and Q. Cheng, *Journal of Bacteriology*, 2001, 183, 6478-6486.

187. H. Iwaki, S. Wang, S. Grosse, H. Bergeron, A. Nagahashi, J. Lertvorachon, J. Yang, Y. Konishi, Y. Hasegawa and P. C. Lau, *Applied and Environmental Microbiology*, 2006, 72, 2707-2720.

188. P. Trudgill, *Terpenoid metabolism by Pseudomonas*, Sokatch, JR, Ornston, LN,(ed.-in-chief), 1986.

189. A. E. Shilov and G. B. Shul'pin, *Chemical Reviews*, 1997, 97, 2879-2932.

190. F. Kakiuchi and S. Murai, in *Activation of Unreactive Bonds and Organic Synthesis*, Springer, 1999, pp. 47-79.

191. J. M. Brown, S. Murai, H. Alper, P. Dixneuf, S. Murai, A. Furstner, R. Gossage, V. Grushin, L. Hegedus and M. Hidai, *Activation of unreactive bonds and organic synthesis*, Springer Science & Business Media, 1999.

192. C. Jia, T. Kitamura and Y. Fujiwara, *Accounts of Chemical Rresearch*, 2001, 34, 633-639.

193. J. Long, H. Liu, S. Wu, S. Liao and Y. Li, *ACS Catalysis*, 2013, 3, 647-654.

194. A. D. Aloise, M. E. Layton and M. D. Shair, *Journal of the American Chemical Society*, 2000, 122, 12610-12611.

195. T. Seiser, O. A. Roth and N. Cramer, *Angewandte Chemie*, 2009, 121, 6438-6441.

196. R. Curci, L. D'Accolti and C. Fusco, *Accounts of Chemical Research*, 2006, 39, 1-9.

197. K. I. Goldberg and A. S. Goldman, *Activation and functionalization of CH bonds*, American Chemical Society Washington, DC, 2004.

198. B. Meunier, *Biomimetic oxidations catalyzed by transition metal complexes*, Imperial College Press, 2000.

199. P. J. Figiel, A. M. Kirillov, M. F. C. G. da Silva, J. Lasri and A. J. Pombeiro, *Dalton Transactions*, 2010, 39, 9879-9888.

200. P. J. Figiel, A. M. Kirillov, Y. Y. Karabach, M. N. Kopylovich and A. J. Pombeiro, *Journal of Molecular Catalysis A: Chemical*, 2009, 305, 178-182.

201. M. V. Kirillova, Y. N. Kozlov, L. S. Shul'pina, O. Y. Lyakin, A. M. Kirillov, E. P. Talsi, A. J. Pombeiro and G. B. Shul'pin, *Journal of Catalysis*, 2009, 268, 26-38.

202. M. V. Kirillova, A. M. Kirillov, M. L. Kuznetsov, J. A. Silva, J. J. F. da Silva and A. J. Pombeiro, *Chemical Communications*, 2009, 2353-2355.

203. A. M. Kirillov, M. V. Kirillova, L. S. Shul'pina, P. J. Figiel, K. R. Gruenwald, M. F. C. G. da Silva, M. Haukka, A. J. Pombeiro and G. B. Shul'pin, *Journal of Molecular Catalysis A: Chemical*, 2011, 350, 26-34.

204. K. Kamata, K. Yonehara, Y. Nakagawa, K. Uehara and N. Mizuno, *Nature Chemistry*, 2010, 2, 478.

205. R. G. Bergman, *Nature*, 2007, 446, 391.

206. U. Schuchardt, W. A. Carvalho and E. V. Spinacé, *Synlett*, 1993, 1993, 713-718.

207. T. J. Collins, *Accounts of Chemical Research*, 2002, 35, 782-790.

208. M. J. Ashton, A. S. Bailey and E. R. Jones, *Journal of the Chemical Society, Perkin Transactions 1*, 1974, 1665-1669.

209. G. S. Fonken, M. E. Herr, H. C. Murray and L. M. Reineke, *Journal of the American Chemical Society*, 1967, 89, 672-675.

210. E. G. Funhoff, U. Bauer, I. García-Rubio, B. Witholt and J. B. van Beilen, *Journal of Bacteriology*, 2006, 188, 5220-5227.

211. M. B. Fisher, Y.-M. Zheng and A. E. Rettie, *Biochemical and Biophysical Research Communications*, 1998, 248, 352-355.

212. U. Scheller, T. Zimmer, D. Becher, F. Schauer and W.-H. Schunck, *Journal of Biological Chemistry*, 1998, 273, 32528-32534.

213. E. Weber, A. Seifert, M. Antonovici, C. Geinitz, J. Pleiss and V. B. Urlacher, *Chemical Communications*, 2011, 47, 944-946.

214. M. Ishihara, T. Tsuneya, H. Shiota, M. Shiga and K. Nakatsu, *The Journal of Organic Chemistry*, 1986, 51, 491-495.

215. J. R. Hanson and A. Parvez, *ChemInform*, 1995, 26, no-no.

216. E. Friedrich and W. Lutz, *Chemischer Informationsdienst*, 1980, 11, no-no.

217. G. A. Molander and J. A. McKie, *The Journal of Organic Chemistry*, 1993, 58, 7216-7227.

218. G. Kräme, A. Oehlhof and H. Meier, *Zeitschrift für Naturforschung B*, 2009, 64, 847-850.

219. W. Chai, A. Takeda, M. Hara, S.-J. Ji and C. A. Horiuchi, *Tetrahedron*, 2005, 61, 2453-2463.

220. S. Matsubara, K. Takai and H. Nozaki, *Bulletin of the Chemical Society of Japan*, 1983, 56, 2029-2032.

221. E. Friedrich and W. Lutz, *Chemische Berichte*, 1980, 113, 1245-1263.

222. L. Yu, X. Li, S. Liu, G. Xu and Y. Liang, *Journal of Separation Science*, 2009, 32, 3457-3465.

223. M. Hatano, S. Kamiya, K. Moriyama and K. Ishihara, *Organic Letters*, 2010, 13, 430-433.

224. H. S. Whang and A. Tonelli, *Journal of Inclusion Phenomena and Macrocyclic Chemistry*, 2008, 62, 127-134.

225. E.-B. Goh, E. E. Baidoo, J. D. Keasling and H. R. Beller, *Applied and Environmental Microbiology*, 2012, 78, 70-80.

226. P. A. Claon and C. C. Akoh, *Enzyme and Microbial Technology*, 1994, 16, 835-838.

227. A. T. Peana, P. S. D'Aquila, F. Panin, G. Serra, P. Pippia and M. D. L. Moretti, *Phytomedicine*, 2002, 9, 721-726.

228. H. L. Holland, A. Kohl, B. G. Larsen, P. Andreana and J.-X. Gu, *Journal of Molecular Catalysis B: Enzymatic*, 1997, 2, L253-L255.

229. T. Yagi, T. Hatano, F. Fukui and S. Fukui, *Journal of Fermentation and Bioengineering*, 1992, 74, 218-221.

230. M. Bezard, A.-T. Karlberg, J. Montelius and J.-P. Lepoittevin, *Chemical Research in Toxicology*, 1997, 10, 987-993.

231. L. Hagvall, *Chemical Analysis, Structure Elucidation and Experimental Sensitization Studies. Doctoral Thesis, University of Gothenburg, Gothenburg, Sweden*, 2009.

232. M. Sköld, L. Hagvall and A. T. Karlberg, *Contact Dermatitis*, 2008, 58, 9-14.

233. E. A. Hall, Thesis (M.Phil.)--University of Adelaide, School of Physical Sciences, 2015.

234. T. S. Zhuk, M. Goldmann, J. Hofmann, J. C. Pohl and H. Zorn, *Journal of Molecular Catalysis B: Enzymatic*, 2015, 122, 87-92.

235. T. P. Stockdale and C. M. Williams, *Chemical Society Reviews*, 2015, 44, 7737-7763.

236. K. A. Agnew-Francis and C. M. Williams, *Advanced Synthesis & Catalysis*, 2016, 358, 675-700.

237. G. Lamoureux and G. Artavia, *Current Medicinal Chemistry*, 2010, 17, 2967-2978.

238. T. Furuya, T. Kanno, H. Yamamoto, N. Kimoto, A. Matsuyama and K. Kino, *Journal of Molecular Catalysis B: Enzymatic*, 2013, 94, 111-118.

239. K. Mitsukura, H. Sakamoto, H. Kubo, T. Yoshida and T. Nagasawa, *Journal of Bioscience and Bioengineering*, 2010, 109, 550-553.

240. R. E. White, M.-B. McCarthy, K. D. Egeberg and S. G. Sligar, *Archives of Biochemistry and Biophysics*, 1984, 228, 493-502.

241. M. E. Herr, R. A. Johnson, H. C. Murray, L. M. Reineke and G. S. Fonken, *The Journal of Organic Chemistry*, 1968, 33, 3201-3207.

242. P. D. Bailey, S. D. Higgins, C. H. Ridyard, S. M. Roberts, G. M. Rosair, R. A. Whittaker and A. J. Willetts, *Chemical Communications*, 1996, 1833-1834.

243. H. Leonov, P. Astrahan, M. Krugliak and I. T. Arkin, *Journal of the American Chemical Society*, 2011, 133, 9903-9911.

244. K. Spilovska, F. Zemek, J. Korabecny, E. Nepovimova, O. Soukup, M. Windisch and K. Kuca, *Current Medicinal Chemistry*, 2016, 23, 3245-3266.

245. K. Rosenthal, M. Sokol, R. Ingram, R. Subramanian and R. Fort, *Antimicrobial Agents and Chemotherapy*, 1982, 22, 1031-1036.

246. W. Yang, S. G. Bell, H. Wang, W. Zhou, M. Bartlam, L.-L. Wong and Z. Rao, *Biochemical Journal*, 2011, 433, 85-93.

247. S. Vohra, M. Musgaard, S. G. Bell, L. L. Wong, W. Zhou and P. C. Biggin, *Protein Science*, 2013, 22, 1218-1229.

248. T. L. Poulos, B. C. Finzel and A. J. Howard, *Journal of Molecular Biology*, 1987, 195, 687-700.

249. M. Katagiri, B. Ganguli and I. Gunsalus, *Journal of Biological Chemistry*, 1968, 243, 3543-3546.

250. W. Yang, S. G. Bell, H. Wang, W. Zhou, N. Hoskins, A. Dale, M. Bartlam, L.-L. Wong and Z. Rao, *Journal of Biological Chemistry*, 2010, 285, 27372-27384.

251. C. Andrew, *Journal of the Chemical Society, Chemical Communications*, 1994, 2761-2762.

252. W. M. Atkins and S. Sligar, *Journal of Biological Chemistry*, 1988, 263, 18842-18849.

253. S. G. Bell, C. F. Harford-Cross and L.-L. Wong, *Protein Engineering*, 2001, 14, 797-802.

254. B. D. Fleming, Y. Tian, S. G. Bell, L.-L. Wong, V. Urlacher and H. A. O. Hill, *European Journal of Biochemistry*, 2003, 270, 4082-4088.

255. P. A. England, C. F. Harford-Cross, J.-A. Stevenson, D. A. Rouch and L.-L. Wong, *FEBS Letters*, 1998, 424, 271-274.

256. S. M. Fowler, P. A. England, A. C. G. Westlake, D. R. Rouch, D. P. Nickerson, C. Blunt, D. Braybrook, S. West, L.-L. Wong and S. L. Flitsch, *Journal of the Chemical Society, Chemical Communications*, 1994, DOI: 10.1039/C39940002761, 2761-2762.

257. S. K. Manna and S. Mazumdar, *Dalton Transactions*, 2010, 39, 3115-3123.

258. P. P. Kelly, A. Eichler, S. Herter, D. C. Kranz, N. J. Turner and S. L. Flitsch, *Beilstein Journal of Organic Chemistry*, 2015, 11, 1713.

259. S. G. Bell, N. Hoskins, C. J. C. Whitehouse and L. L. Wong, in *The Ubiquitous Roles of Cytochrome P450 Proteins*, John Wiley & Sons, Ltd, 2007, DOI: 10.1002/9780470028155.ch14, pp. 437-476.

260. P. A. England, D. A. Rouch, A. C. G. Westlake, S. G. Bell, D. P. Nickerson, M. Webberley, S. L. Flitsch and L.-L. Wong, *Chemical Communications*, 1996, DOI: 10.1039/CC9960000357, 357-358.

261. J.-A. Stevenson, A. C. Westlake, C. Whittock and L.-L. Wong, *Journal of the American Chemical Society*, 1996, 118, 12846-12847.

262. K. Arnold, L. Bordoli, J. Kopp and T. Schwede, *Bioinformatics*, 2006, 22, 195-201.

263. M. Biasini, S. Bienert, A. Waterhouse, K. Arnold, G. Studer, T. Schmidt, F. Kiefer, T. G. Cassarino, M. Bertoni and L. Bordoli, *Nucleic Acids Research*, 2014, 42, W252-W258.

264. J. H. Z. Lee, Thesis (M.Phil.)--University of Adelaide, School of Physical Sciences, 2018.

265. M. R. Sarkar, J. H. Z. Lee and S. G. Bell, *Chembiochem*, 2017, 18, 2119-2128.

266. E. A. Hall, M. R. Sarkar and S. G. Bell, *Catalysis Science & Technology*, 2017, 7, 1537-1548.

267. S. D. Munday, S. Dezvarei, I. C. K. Lau and S. G. Bell, *ChemCatChem*, 2017, 9, 2512-2522.

268. E. Corey and M. Sodeoka, *Tetrahedron Letters*, 1991, 32, 7005-7008.

269. M. Nadal, M. Schuhmacher and J. Domingo, *Environmental Pollution*, 2004, 132, 1-11.

270. N. Grova, C. Feidt, C. Crépineau, C. Laurent, P. E. Lafargue, A. Hachimi and G. Rychen, *Journal of Agricultural and Food Chemistry*, 2002, 50, 4640-4642.

271. J. Pothuluri, J. Freeman, F. Evans and C. Cerniglia, *Applied and Environmental Microbiology*, 1992, 58, 3654-3659.

272. S. D. Munday, S. Dezvarei and S. G. Bell, *ChemCatChem*, 2016, 8, 2789-2796.

273. A. M. Colthart, D. R. Tietz, Y. Ni, J. L. Friedman, M. Dang and T. C. Pochapsky, *Scientific Reports*, 2016, 6, 22035.

274. C. J. Whitehouse, S. G. Bell and L. L. Wong, *Chemistry-A European Journal*, 2008, 14, 10905-10908.

275. C. J. Whitehouse, N. H. Rees, S. G. Bell and L. L. Wong, *Chemistry-A European Journal*, 2011, 17, 6862-6868.

276. K. F. Biegasiewicz, J. R. Griffiths, G. P. Savage, J. Tsanaktsidis and R. Priefer, *Chemical Reviews*, 2015, 115, 6719-6745.

277. B. A. Chalmers, H. Xing, S. Houston, C. Clark, S. Ghassabian, A. Kuo, B. Cao, A. Reitsma, C. E. P. Murray and J. E. Stok, *Angewandte Chemie*, 2016, 128, 3644-3649.

278. R. J. Doedens, P. E. Eaton and E. B. Fleischer, *European Journal of Organic Chemistry*, 2017, 2017, 2627-2630.

279. Z. Li and S. L. Anderson, *The Journal of Physical Chemistry A*, 2003, 107, 1162-1174.

280. M. Maslov, D. Lobanov, A. Podlivaev and L. Openov, *Physics of the Solid State*, 2009, 51, 645-648.

281. F. Agapito, R. C. Santos, R. M. Borges dos Santos and J. A. Martinho Simoes, *J Phys Chem A*, 2015, 119, 2998-3007.

282. P. E. Eaton, *Angewandte Chemie International Edition in English*, 1992, 31, 1421-1436.

283. J. Wlochal, R. D. Davies and J. Burton, *Organic Letters*, 2014, 16, 4094-4097.

284. Y. P. Auberson, C. Brocklehurst, M. Furegati, T. C. Fessard, G. Koch, A. Decker, L. La Vecchia and E. Briard, *ChemMedChem*, 2017, 12, 590-598.

285. A. S. Sklyarova, V. N. Rodionov, C. G. Parsons, G. Quack, P. R. Schreiner and A. A. Fokin, *Medicinal Chemistry Research*, 2013, **22**, 360-366

286. Q. L. Zhang and B. Z. Chen, *Journal of Physical Organic Chemistry*, 2011, 24, 147-154.

287. W. Adcock, M. J. Brunger, I. E. McCarthy, M. T. Michalewicz, W. von Niessen, F. Wang, E. Weigold and D. A. Winkler, *Journal of the American Chemical Society*, 2000, 122, 3892-3900.

288. S. Plunkett, K. J. Flanagan, B. Twamley and M. O. Senge, *Organometallics*, 2015, 34, 1408-1414.

289. M. Hare, T. Emrick, P. E. Eaton and S. R. Kass, *Journal of the American Chemical Society*, 1997, 119, 237-238.

290. D. F. McMillen and D. M. Golden, *Annual Review of Physical Chemistry*, 1982, 33, 493-532.

291. Z. Tian, A. Fattahi, L. Lis and S. R. Kass, *Journal of the American Chemical Society*, 2006, 128, 17087-17092.

292. Y.-R. Luo, *Handbook of bond dissociation energies in organic compounds*, CRC press, 2002.

293. K. B. Wiberg, *PATAI'S Chemistry of Functional Groups*, 2009.

294. A. Streitwieser Jr, R. A. Caldwell and W. R. Young, *Journal of the American Chemical Society*, 1969, 91, 529-529.

295. T.-Y. Luh and L. M. Stock, *Journal of the American Chemical Society*, 1974, 96, 3712-3713.

296. E. W. Della, N. J. Head, P. Mallon and J. C. Walton, *Journal of the American Chemical Society*, 1992, 114, 10730-10738.

297. S.-Y. Choi, P. E. Eaton, P. F. Hollenberg, K. E. Liu, S. J. Lippard, M. Newcomb, D. A. Putt, S. P. Upadhyaya and Y. Xiong, *Journal of the American Chemical Society*, 1996, 118, 6547-6555.

298. C. Annese, L. D'Accolti, C. Fusco, R. Gandolfi, P. E. Eaton and R. Curci, *Org Lett*, 2009, 11, 3574-3577.

299. A. A. Fokin, O. Lauenstein, P. A. Gunchenko and P. R. Schreiner, *Journal of the American Chemical Society*, 2001, 123, 1842-1847.

300. M. Newcomb, *Tetrahedron*, 1993, 49, 1151-1176.

301. S. Y. Choi, P. E. Eaton, P. F. Hollenberg, K. E. Liu, S. J. Lippard, M. Newcomb, D. A. Putt, S. P. Upadhyaya and Y. S. Xiong, *J. Am. Chem. Soc.*, 1996, 118, 6547-6555.

302. M. Newcomb, R. Shen, S. Y. Choi, P. H. Toy, P. F. Hollenberg, A. D. N. Vaz and M. J. Coon, *J. Am. Chem. Soc.*, 2000, 122, 2677-2686.

303. Y. Jin and J. D. Lipscomb, *Biochemistry*, 1999, 38, 6178-6186.

304. P. R. O. de Montellano, *Cytochrome P450: Structure, mechanism, and biochemistry, fourth edition*, 2015.

305. E. L. Sauer and L. Barriault, *Organic Letters*, 2004, 6, 3329-3332.

306. P. E. Eaton and Y. C. Yip, *Journal of the American Chemical Society*, 1991, 113, 7692-7697.

307. E. J. Ko, G. P. Savage, C. M. Williams and J. Tsanaktsidis, *Organic Letters*, 2011, 13, 1944-1947.

308. H. Hirao, D. Kumar, L. Que Jr and S. Shaik, *Journal of the American Chemical Society*, 2006, 128, 8590-8606.

309. C. Li, W. Wu, D. Kumar and S. Shaik, *Journal of the American Chemical Society*, 2006, 128, 394-395.

310. S. Shaik, S. Cohen, S. P. de Visser, P. K. Sharma, D. Kumar, S. Kozuch, F. Ogliaro and D. Danovich, *European Journal of Inorganic Chemistry*, 2004, 2004, 207-226.

311. J. C. Schöneboom, S. Cohen, H. Lin, S. Shaik and W. Thiel, *Journal of the American Chemical Society*, 2004, 126, 4017-4034.

312. R. N. Austin, K. Luddy, K. Erickson, M. Pender-Cudlip, E. Bertrand, D. Deng, R. S. Buzdygon, J. B. van Beilen and J. T. Groves, *Angewandte Chemie*, 2008, 120, 5310-5312.

313. T. L. Poulos, *Philosophical Transactions of the Royal Society of London A: Mathematical, Physical and Engineering Sciences*, 2005, 363, 793-806.

314. Y. Wang, J. P. Gray, V. Mishin, D. E. Heck, D. L. Laskin and J. D. Laskin, *Free Radical Biology and Medicine*, 2008, 44, 1169-1179.

315. D. Garcia, F. Foubelo and M. Yus, *Tetrahedron*, 2008, 64, 4275-4286.

316. T. Shimada, D. Kim, N. Murayama, K. Tanaka, S. Takenaka, L. D. Nagy, L. M. Folkman, M. K. Foroozesh, M. Komori and H. Yamazaki, *Chemical Research in Toxicology*, 2013, 26, 517-528.

317. T. M. Cho, R. L. Rose and E. Hodgson, *Drug Metabolism and Disposition*, 2005.

318. M. Bagchi, D. Bagchi, J. Balmoori, X. Ye and S. Stohs, *Free Radical Biology and Medicine*, 1998, 25, 137-143.

319. H. Kappus and H. Sies, *Experientia*, 1981, 37, 1233-1241.

320. J. W. Lown, *Molecular and Cellular Biochemistry*, 1983, 55, 17-40.

321. J. T. Szilagyi, V. Mishin, D. E. Heck, Y.-H. Jan, L. M. Aleksunes, J. R. Richardson, N. D. Heindel, D. L. Laskin and J. D. Laskin, *Toxicological Sciences*, 2016, 151, 150-159.

322. P. R. e. Ortiz de Montellano, *Cytochrome P450 Structure, Mechanism, and Biochemistry*, Springer International Publishing : Imprint: Springer, 4th ed. 2015. edn., 2015.

323. I. Hanukoglu, *Drug Metabolism Reviews*, 2006, 38, 171-196.

324. J. Marcinkeviciene, N. Cenas, J. Kulys, S. Usanov, N. Sukhova, I. Selezneva and V. Gryazev, *Biomedica Biochimica Acta*, 1990, 49, 167-172.

325. N. Misawa, M. Nodate, T. Otomatsu, K. Shimizu, C. Kaido, M. Kikuta, A. Ideno, H. Ikenaga, J. Ogawa and S. Shimizu, *Applied Microbiology and Biotechnology*, 2011, 90, 147-157.

326. O. Shoji, C. Wiese, T. Fujishiro, C. Shirataki, B. Wünsch and Y. Watanabe, *Journal of Biological Inorganic Chemistry*, 2010, 15, 1109-1115.

327. E. M. Gillam, L. M. Notley, H. Cai, J. J. De Voss and F. P. Guengerich, *Biochemistry*, 2000, 39, 13817-13824.

328. X. Gong, R. Gutala and A. K. Jaiswal, *Vitamins & Hormones*, 2008, 78, 85-101.

329. Y.-H. Jan, J. R. Richardson, A. A. Baker, V. Mishin, D. E. Heck, D. L. Laskin and J. D. Laskin, *Toxicology and Applied Pharmacology*, 2015, 288, 114-120.

330. T. M. Penning, M. E. Burczynski, C.-F. Hung, K. D. McCoull, N. T. Palackal and L. S. Tsuruda, *Chemical Research in Toxicology*, 1999, 12, 1-18.

331. G. Xing, C. J. Miller, A. N. Pham, A. M. Jones and T. D. Waite, *Journal of Inorganic Biochemistry*, 2018, 188, 38-49.

332. P. F. Smith, D. W. Alberts and G. F. Rush, *Biochemical Pharmacology*, 1987, 36, 3879-3884.

333. G. Cohen and M. d. A. Doherty, *The British journal of cancer. Supplement*, 1987, 8, 46.

334. H. Nishibayashi-Yamashita and R. SATO, *The Journal of Biochemistry*, 1970, 67, 199-210.

335. A. Jaiswal, O. W. McBride, M. Adesnik and D. Nebert, *Journal of Biological Chemistry*, 1988, 263, 13572-13578.

336. M. Floreani and F. Carpenedo, *Toxicology and Applied Pharmacology*, 1990, 105, 333-339.

337. L. M. Nutter, E. Ngo, G. Fisher and P. Gutierrez, *Journal of Biological Chemistry*, 1992, 267, 2474-2479.

338. M. Y. Moridani, H. Scobie, P. Salehi and P. J. O'Brien, *Chemical Research in Toxicology*, 2001, 14, 841-848.

339. D. C. Thompson, K. Perera, E. Krol and J. L. Bolton, *Chemical Research in Toxicology*, 1995, 8, 323-327.

340. J. L. Bolton, E. Comeau and V. Vukomanovic, *Chemico-biological Interactions*, 1995, 95, 279-290.

341. C. Rice-Evans, *Free Radical Biology and Medicine*, 2004, 7, 827-828.

342. A. V. Grinberg, F. Hannemann, B. Schiffler, J. Müller, U. Heinemann and R. Bernhardt, *Proteins: Structure, Function, and Bioinformatics*, 2000, 40, 590-612.

343. A. Gutierrez, A. Grunau, M. Paine, A. Munro, C. Wolf, G. Roberts and N. Scrutton, *Journal*, 2003.

344. D. S. Riddick, X. Ding, C. R. Wolf, T. D. Porter, A. V. Pandey, Q.-Y. Zhang, J. Gu, R. D. Finn, S. Ronseaux and L. A. McLaughlin, *Drug Metabolism and Disposition*, 2013, 41, 12-23.

345. I. Yamazaki, M. Tamura, R. Nakajima and M. Nakamura, *Environmental Health Perspectives*, 1985, 64, 331.

346. M. G. Miller, A. Rodgers and G. M. Cohen, *Biochemical Pharmacology*, 1986, 35, 1177-1184.

347. Y. Wang, J. P. Gray, V. Mishin, D. E. Heck, D. L. Laskin and J. D. Laskin, *Molecular Cancer Therapeutics*, 2010, 1535-7163. MCT-1509-1098.

348. A. J. Green, A. W. Munro, M. R. Cheesman, G. A. Reid, C. von Wachenfeldt and S. K. Chapman, *Journal of Inorganic Biochemistry*, 2003, 93, 92-99.

349. I. Martsinkiavichene, N. Chenas, I. Kulis and S. Usanov, *Biokhimiia (Moscow, Russia)*, 1990, 55, 1624-1631.

350. R. Rapoport, I. Hanukoglu and D. Sklan, *Analytical Biochemistry*, 1994, 218, 309-313.

351. G. R. Buettner and R. P. Mason, in *Methods in Enzymology*, Elsevier, 1990, vol. 186, pp. 127-133.

352. P. J. Thornalley, M. d. A. Doherty, M. T. Smith, J. V. Bannister and G. M. Cohen, *Chemico-biological Interactions*, 1984, 48, 195-206.

353. H. E. Gottlieb, V. Kotlyar and A. Nudelman, *J. Org. Chem.*, 1997, 62, 7512-7515.

354. W. L. F. Armarego and C. L. L. Chai, *Purification of Laboratory Chemicals*, Elsevier, Oxford, 6 edn.

355. J. Tsanaktsidis and P. E. Eaton, *Tetraheron Lett.*, 1989, 30, 6967-6968.

356. J. R. Griffiths, J. Tsanaktsidis, G. P. Savage and R. Priefer, *Thermochim. Acta*, 2010, 499, 15-20.

357. P. E. Eaton, J. C. Li and S. P. Upadhyaya, *J. Org. Chem.*, 1995, 60, 966-968.

358. P. E. Eaton, *Angew. Chem. Int. Ed.* , 1992, 31, 1421-1436.

359. A. J. H. Klunder and B. Zwanenburg, *Tetrahedron*, 1975, 31, 1419-1426.

360. P. E. Eaton and Y. C. Yip, *J. Am. Chem. Soc.*, 1991, 113, 7692-7697.

361. E. J. Ko, G. P. Savage, C. M. Williams and J. Tsanaktsidis, *Org. Lett.*, 2011, 13, 1944-1947.

362. A. E. McGonagle and G. P. Savage, *Aust. J. Chem.*, 2009, 62, 145-149.

363. P. W. Moore, P. M. Mirzayans and C. M. Williams, *Chem. Eur. J.*, 2015, 21, 3567-3571.

364. E. L. O. Sauer and L. Barriault, *Org. Lett.*, 2004, 6, 3329-3332.

365. D. C. Harrowven and I. L. Guy, *Chem. Commun.*, 2004, DOI: 10.1039/B406041E, 1968-1969.

366. C.-Z. Zhu, K. Wang, M.-h. Zhang, D.-Y. Zhang, Y.-C. Wu, X.-M. Wu and W.-Y. Hua, *Synthesis*, 2014, 46, 2574-2578.

367. Y. Jin and J. D. Lipscomb, *Faseb Journal*, 1997, 11, A1305-A1305.

368. L. B. Romanova, L. S. Barinova, V. V. Zakharov, L. T. Eremenko, G. G. Aleksandrov and I. L. Eremenko, *Russ. Chem. Bull.*, 2010, 59, 1051-1055.

369. M. R. Sarkar, S. Dasgupta, S. Pike and S. G. Bell, *Chemical Communications*, 2019.

370. S. Li, L. M. Podust and D. H. Sherman, *Journal of the American Chemical Society*, 2007, 129, 12940-12941.

371. A. R. Narayan, G. Jimenez-Oses, P. Liu, S. Negretti, W. Zhao, M. M. Gilbert, R. O. Ramabhadran, Y. F. Yang, L. R. Furan, Z. Li, L. M. Podust, J. Montgomery, K. N. Houk and D. H. Sherman, *Nat. Chem.*, 2015, 7, 653‑660.

372. P. Le-Huu, D. Rekow, C. Krüger, A. Bokel, T. Heidt, S. Schaubach, B. Claasen, S. Hölzel, W. Frey and S. Laschat, *Chemistry–A European Journal*, 2018, 24, 12010-12021.

373. P. Le-Huu, T. Heidt, B. Claasen, S. Laschat and V. B. Urlacher, *ACS Catalysis*, 2015, 5, 1772-1780.

Appendix

Appendix A Supplementary Data for Chapter 2

Figure A. 1 ^{1}H NMR of 1-adamantyl acetate.....270
Figure A. 2 ^{13}C NMR of 1-adamantyl acetate. 270
Figure A. 3 gCOSY NMR of 1-adamantyl acetate. 271
Figure A. 4 HSQC NMR of 1-adamantyl acetate. 271
Figure A. 5 ^{1}H NMR of 2-adamantyl acetate.....272
Figure A. 6 ^{13}C NMR of 2-adamantyl acetate. 273
Figure A. 7 gCOSY NMR of 2-adamantyl acetate. 273
Figure A. 8 HSQC NMR of 2-adamantyl acetate. 274
Figure A. 9 ^{1}H NMR of 1-adamantyl isobutyrate. 275
Figure A. 10 gCOSY NMR of 1-adamantyl isobutyrate. 276
Figure A. 11 ^{1}H NMR of 2-adamantyl isobutyrate. 277
Figure A. 12 ^{13}C NMR of 2-adamantyl isobutyrate. 278
Figure A. 13 gCOSY NMR of 2-adamantyl isobutyrate. 278
Figure A. 14 HSQC NMR of 2-adamantyl isobutyrate. 279
Figure A. 15 ^{1}H NMR of cyclohexyl isobutyrate. 280
Figure A. 16 ^{1}H NMR of cyclooctyl acetate 281
Figure A. 17 ^{1}H NMR of cyclooctyl isobutyrate. 282
Figure A. 18 ^{1}H NMR of cyclododecyl acetate. 283

NMR of 1-adamantyl acetate [182]:

^{1}H NMR (500 MHz, $CDCl_3$) δ 2.18-2.13 (m, 3H, H3, H5 & H7), 2.11-2.08 (m, 6H, 2xH2, 2xH9 & 2xH10), 1.96 (s, 3H, 3xH12), 1.70-1.61 (m, 6H, 2xH4, 2xH6 & 2xH8).

^{13}C NMR (126 MHz, $CDCl_3$) δ 172.92 (C11), 82.65 (C1), 43.68 (C2, C9 & C10), 38.65 (C4, C6 & C8), 33.31 (C3, C5 & C7), 25.47 (C12).

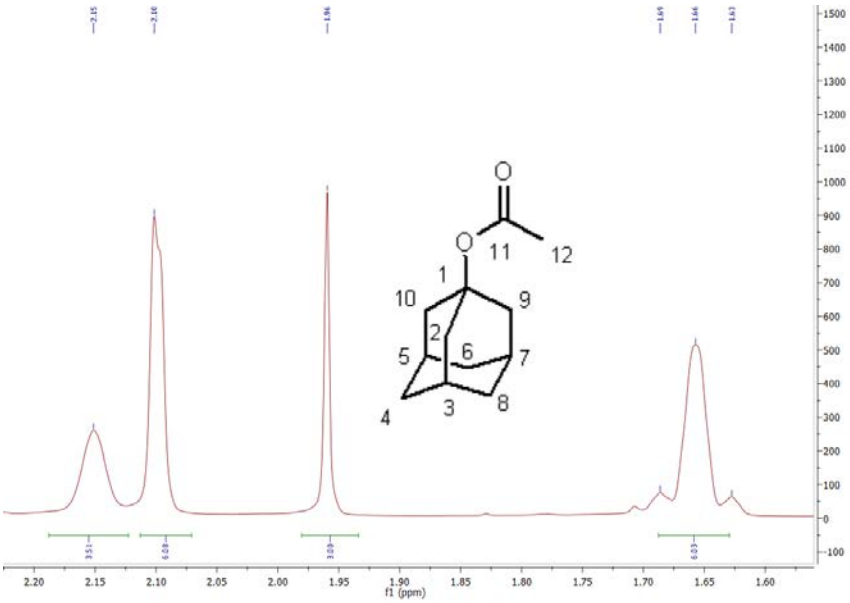

Figure A. 1 ^{1}H NMR spectrum of 1-adamantyl acetate.

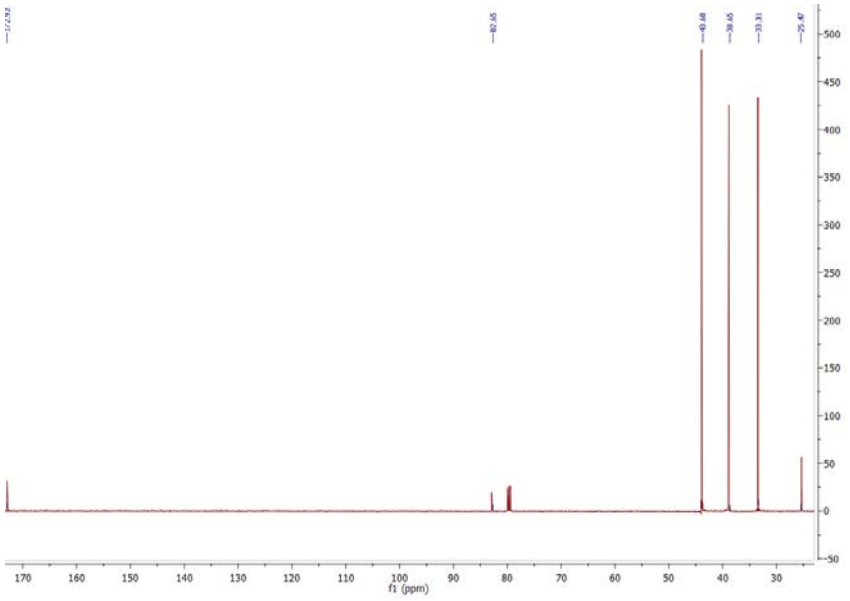

Figure A. 2 ^{13}C NMR spectrum of 1-adamantyl acetate.

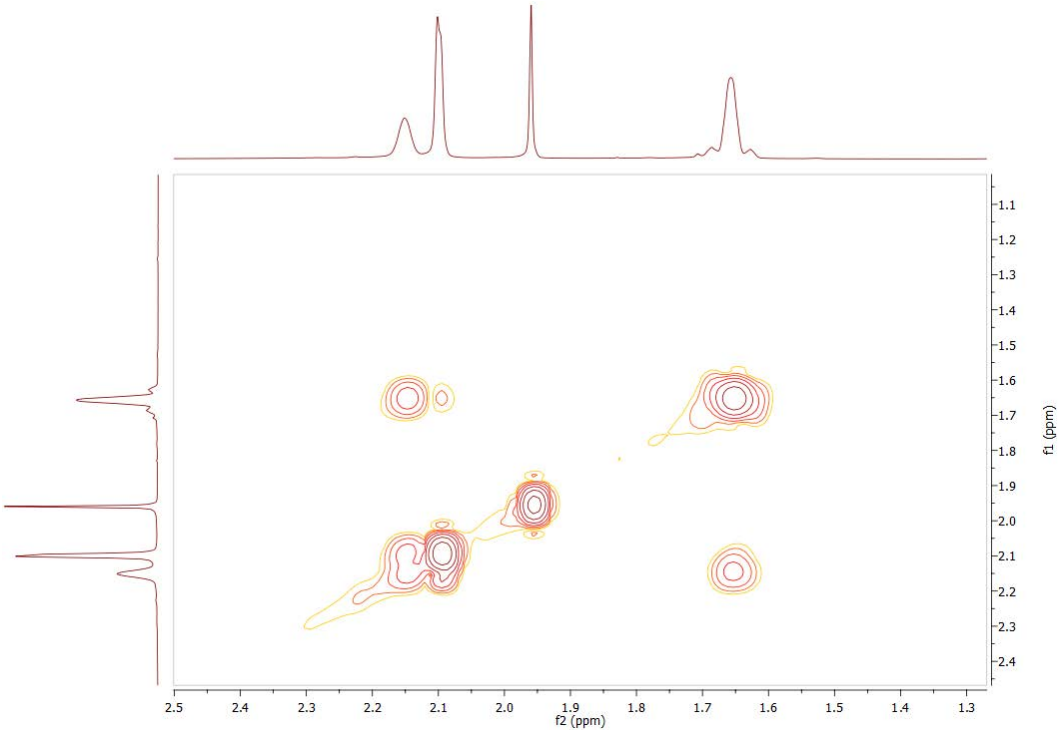

Figure A. 3 gCOSY NMR spectrum of 1-adamantyl acetate.

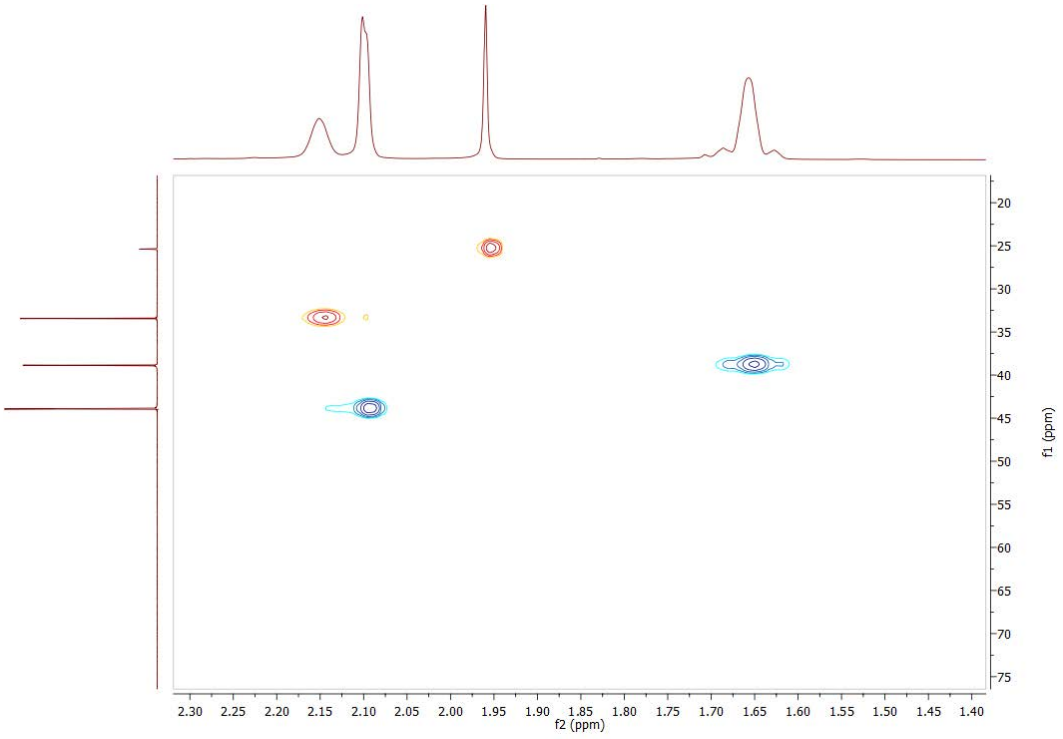

Figure A. 4 HSQC NMR spectrum of 1-adamantyl acetate.

NMR data for 2-adamantyl acetate [182]:

^{1}H NMR (500 MHz, $CDCl_3$) δ 4.96-4.83 (m, 1H, H2), 2.07 (s, 3H, 3xH12), 2.05-1.97 (m, 4H, H1, H3, H8 & H10), 1.88-1.82 (m, 4H, H4, H5, H7 & H9), 1.80-1.73 (m, 4H, H4, 2xH6 & H9), 1.56 (d, J = 10.6 Hz, 2H, H8 & H10).

^{13}C NMR (126 MHz, $CDCl_3$) δ 173.50 (C11), 79.54 (C2), 40.04 (C6), 39.01 (C4 & C9), 34.65 (C1 & C3), 34.37 (C8 & C10), 29.88/29.69 (C5/C7), 24.23 (C12).

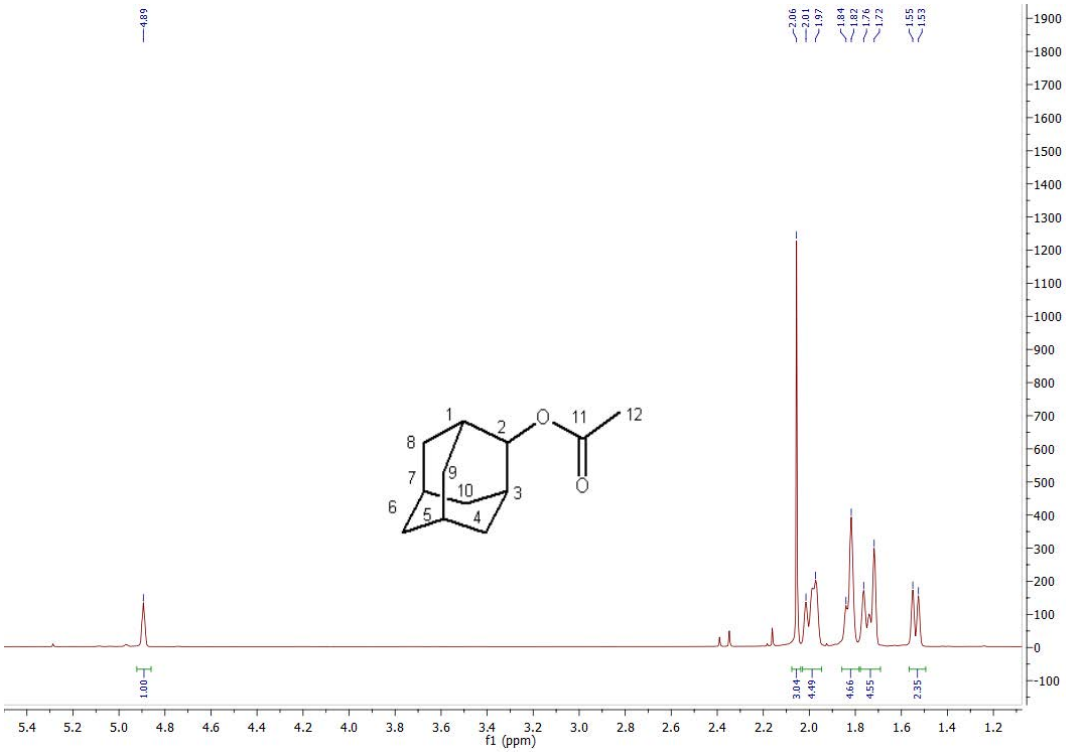

Figure A. 5 ^{1}H NMR spectrum of 2-adamantyl acetate.

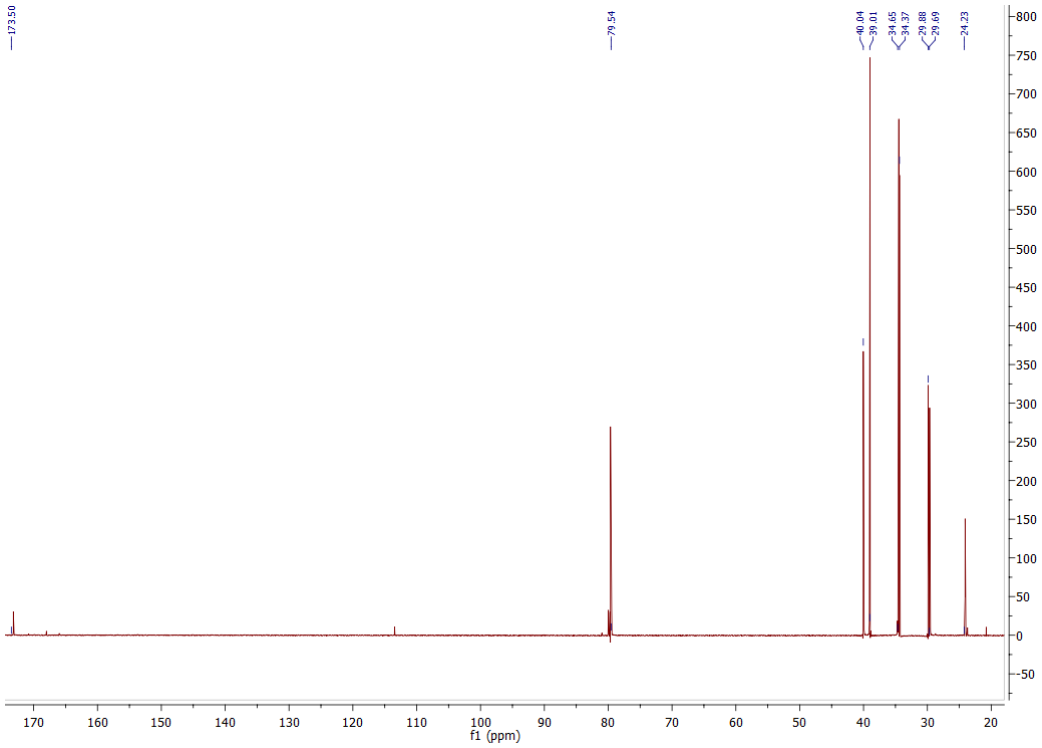

Figure A. 6 ^{13}C NMR spectrum of 2-adamantyl acetate.

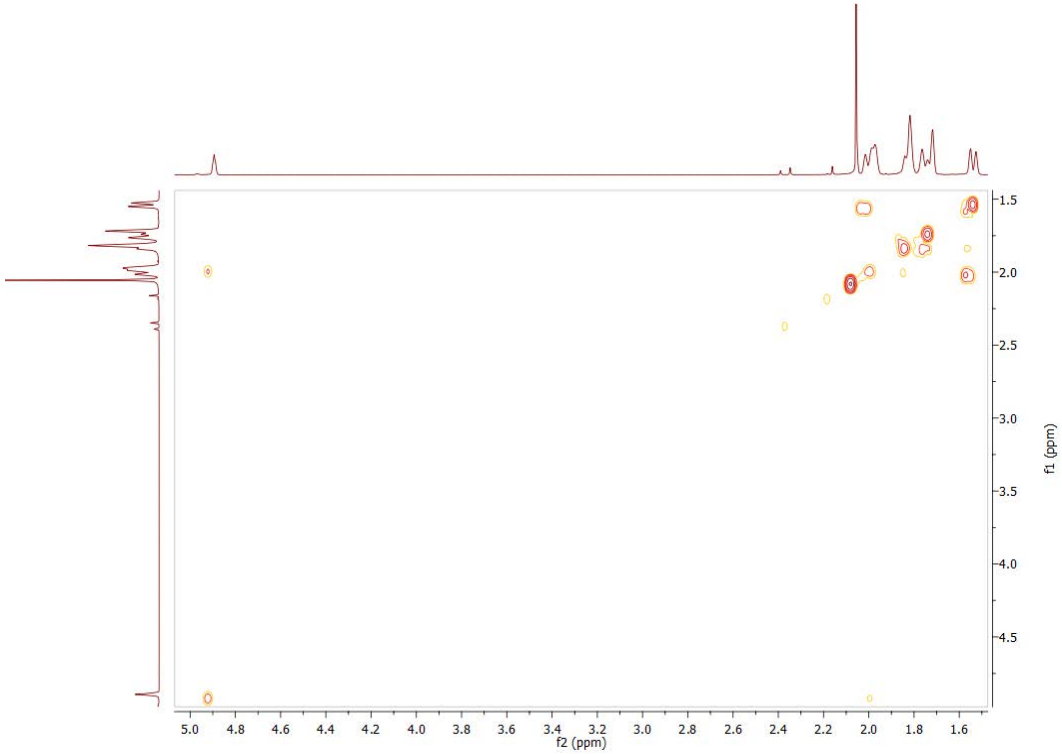

Figure A. 7 gCOSY NMR spectrum of 2-adamantyl acetate.

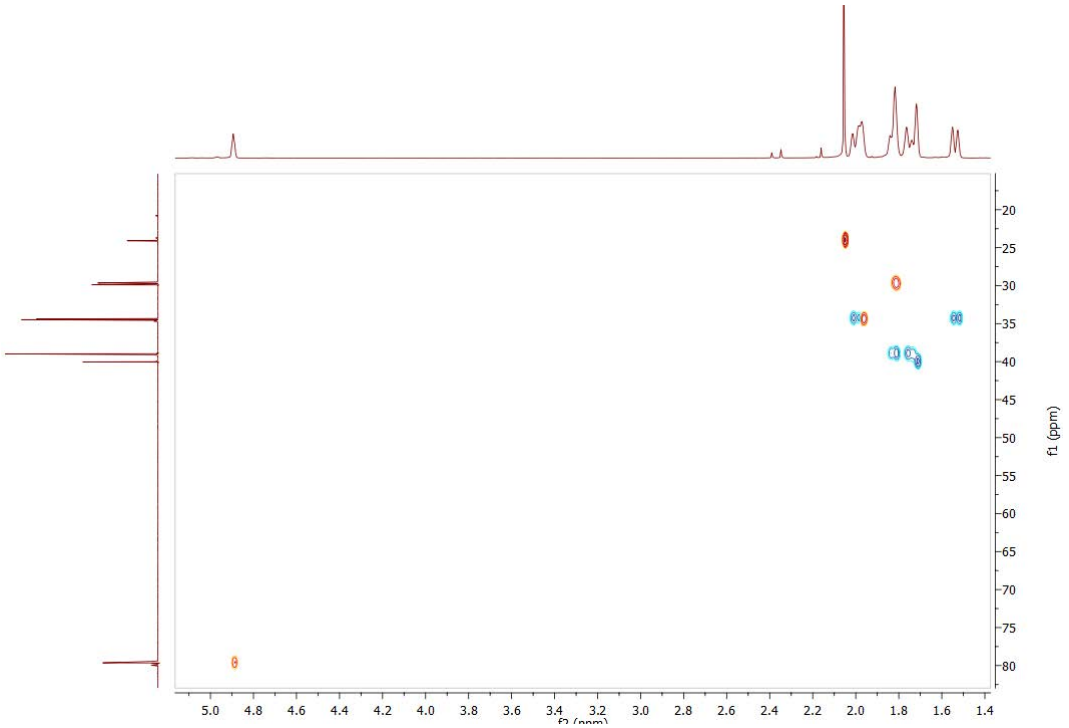

Figure A. 8 HSQC NMR spectrum of 2-adamantyl acetate.

NMR data for 1-adamantyl isobutyrate [182]:

^{1}H NMR (500 MHz, $CDCl_3$) δ 2.43 (*sept*, J = 7.0 Hz, 1H, H12), 2.19-2.14 (m, 3H, H3, H5 & H7), 2.13-2.05 (m, 6H, 2xH2, 2xH9 & 2xH10), 1.72-1.63 (m, 6H, 2xH4, 2xH6 & 2xH8), 1.11 (d, J = 7.0 Hz, 6H, 3xH13 & 3xH14).

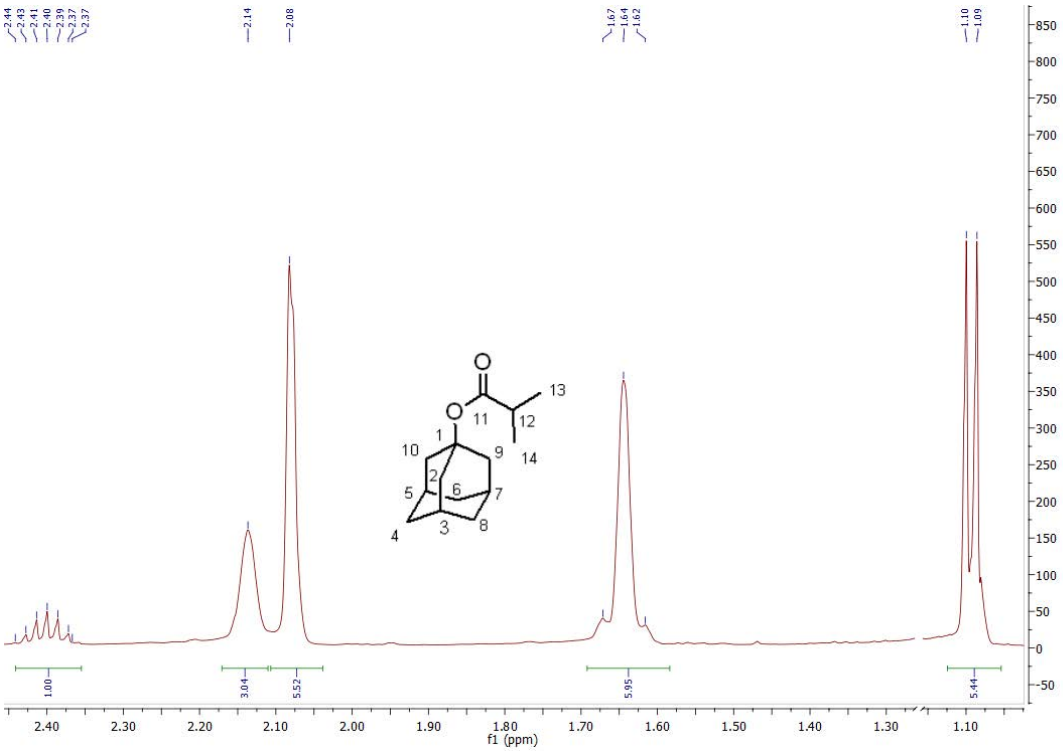

Figure A. 9 ^{1}H NMR spectrum of 1-adamantyl isobutyrate.

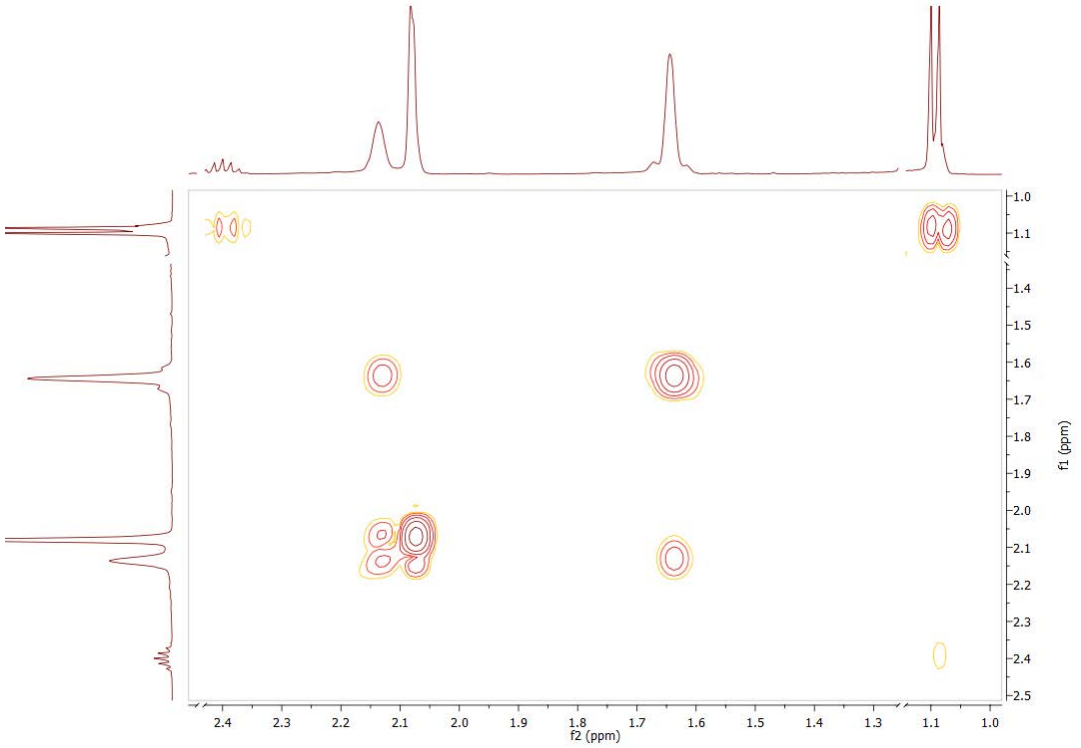

Figure A. 10 gCOSY spectrum NMR of 1-adamantyl isobutyrate.

NMR for 2-adamantyl isobutyrate [182]:

^{1}H NMR (500 MHz, $CDCl_3$) δ 4.93-4.87 (m, 1H, H2), 2.57 (*sept*, J = 7.0 Hz, 1H, H12), 2.05-1.96 (m, 4H, H1, H3, H8 & H10), 1.87-1.81 (m, 4H, H4, H5, H7 & H9), 1.79-1.41 (m, 4H, H4, 2xH6 & H9), 1.56 (d, J = 11.9 Hz, 2H, H8 & H10), 1.19 (d, J = 7.0 Hz, 6H, 3xH13 & 3xH14).

^{13}C NMR (126 MHz, $CDCl_3$) δ 179.0 (C11), 79.04 (C2), 40.04 (C6), 38.98 (C4 & C9), 37.06 (C12), 34.49 (C1 & C3), 34.44 (C8 & C10), 29.91/29.66 (C5/C7), 21.70 (C13 & C14).

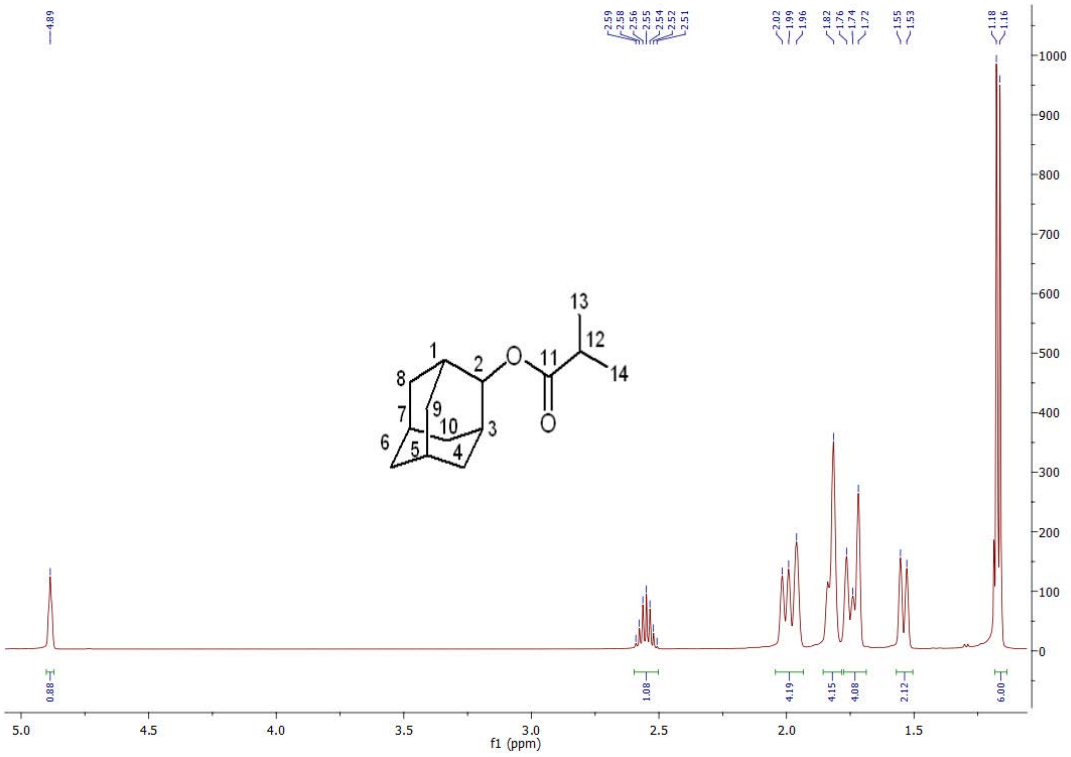

Figure A. 11 ^{1}H NMR spectrum of 2-adamantyl isobutyrate.

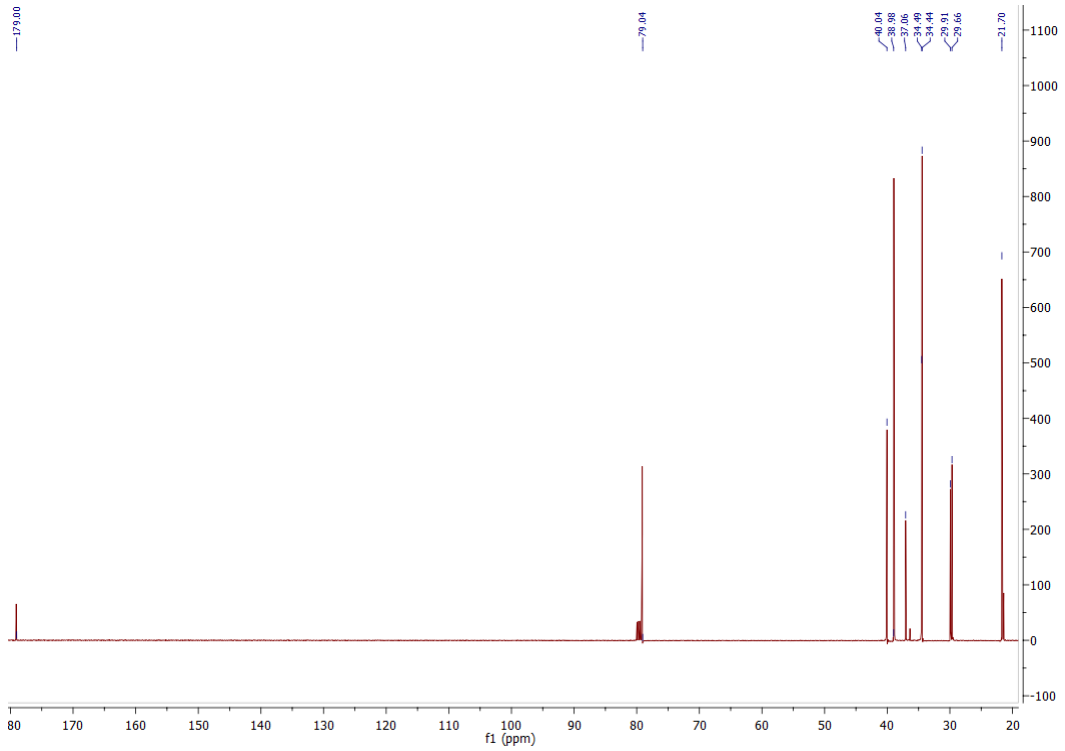

Figure A. 12 ^{13}C NMR spectrum of 2-adamantyl isobutyrate.

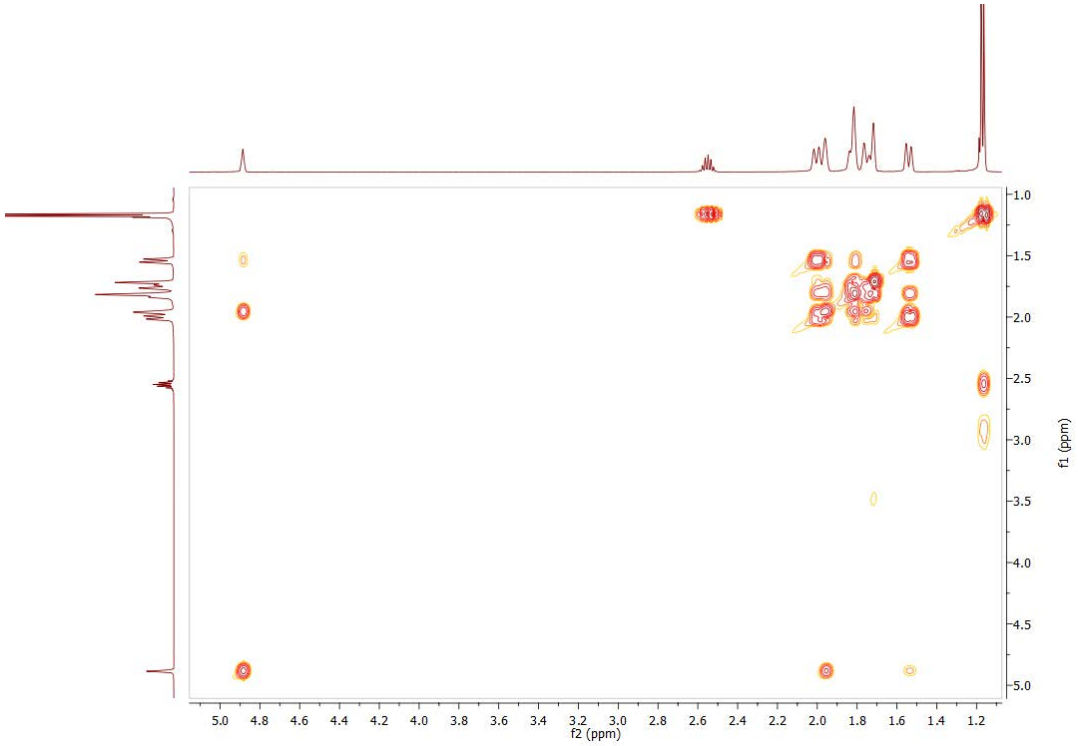

Figure A. 13 gCOSY NMR spectrum of 2-adamantyl isobutyrate.

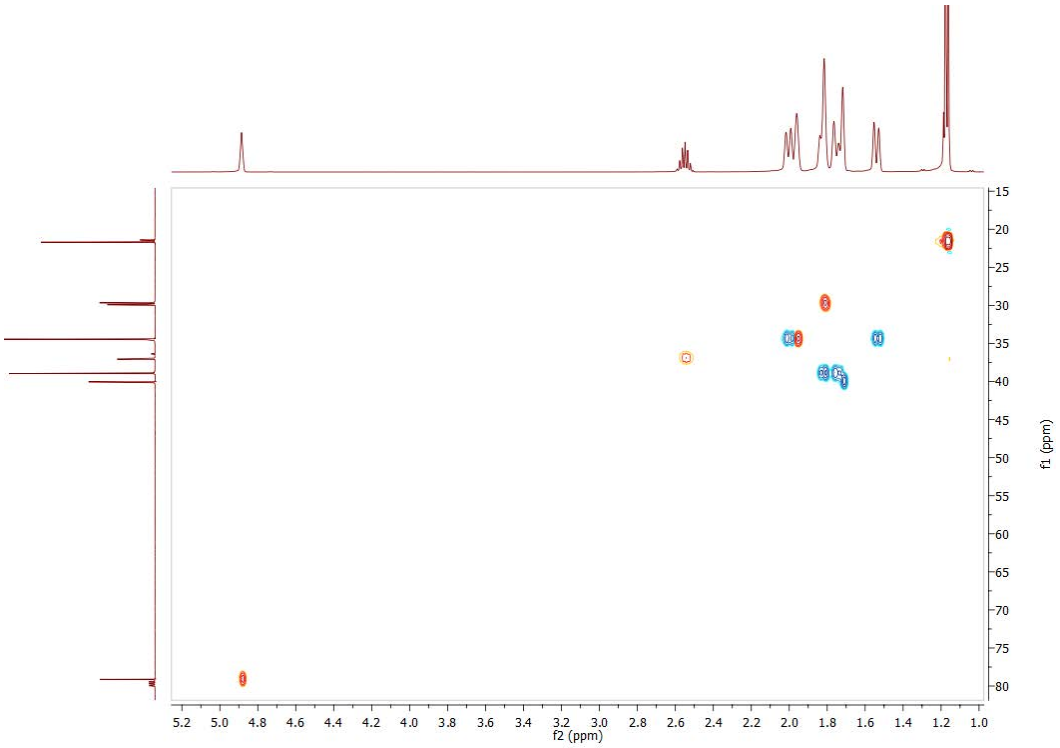

Figure A. 14 HSQC NMR spectrum of 2-adamantyl isobutyrate.

NMR data for cyclohexyl isobutyrate:

^{1}H NMR (500 MHz, $CDCl_3$) δ 4.82-4.66 (m, 1H, H1), 2.52 (*septet*, *J* = 7.0 Hz, 1H, H8), 1.88-1.66 (m, 10H), 1.16 (d, *J* = 7.0 Hz, 6H, 3xH9 & 3xH10).

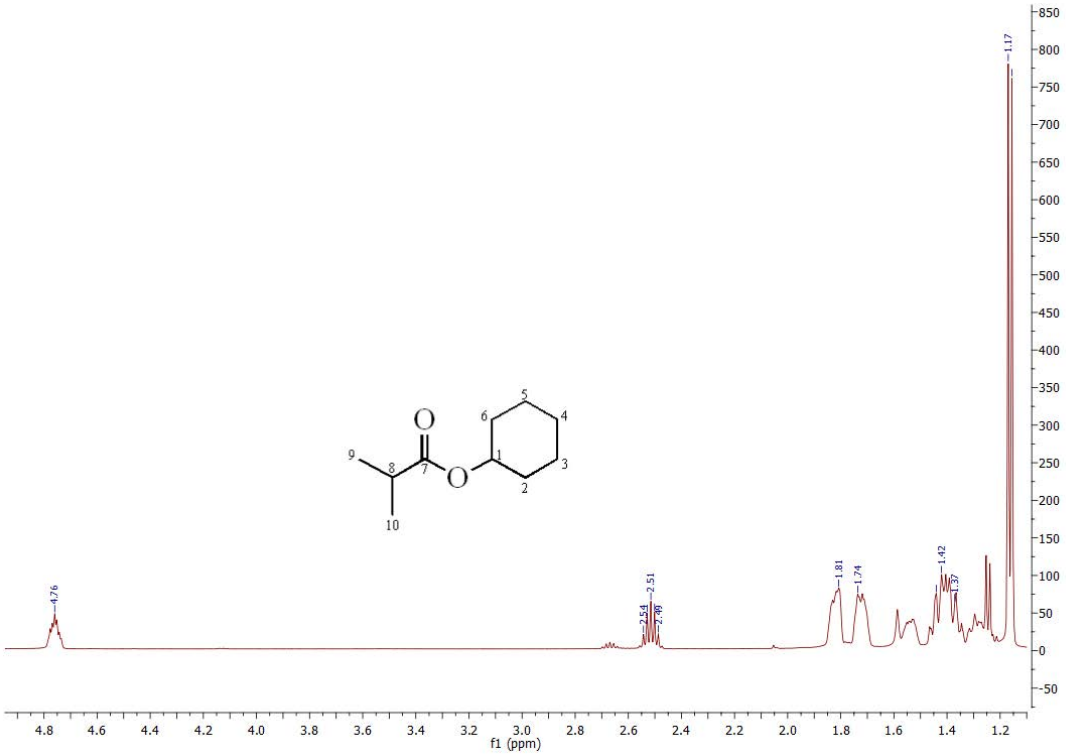

Figure A. 15 ^{1}H NMR spectrum of cyclohexyl isobutyrate.

NMR data for cyclooctyl Acetate

^{1}H NMR (500 MHz, $CDCl_3$) δ 4.95-4.85 (m, 1H, H1), 1.99 (s, 3H, 3xH10), 1.83-1.42 (m, 14H).

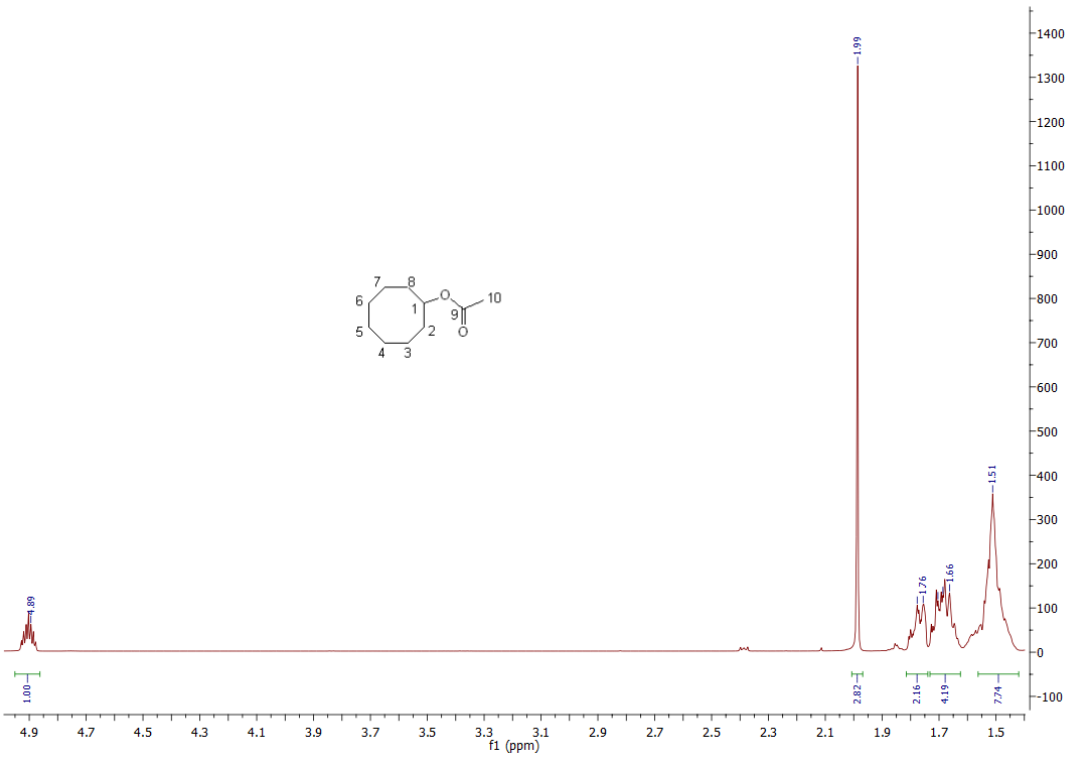

Figure A. 16 ^{1}H NMR spectrum of cyclooctyl acetate

NMR data for cyclooctyl isobutyrate

^{1}H NMR (500 MHz, $CDCl_3$) δ 4.99-4.84 (m, 1H, H1), 2.49 (*septet*, J = 7.0 Hz, 1H, H10), 1.85-1.43 (m, 14H), 1.15 (d, J = 7.0 Hz, 6H, 3xH11 & 3xH12).

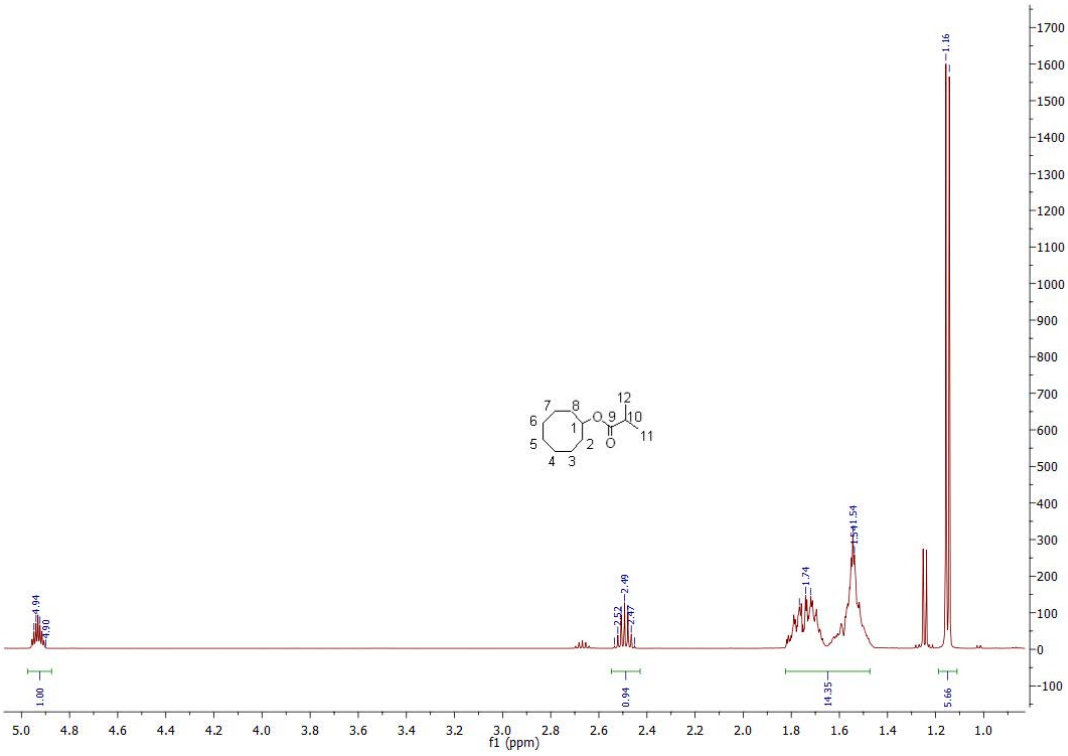

Figure A. 17 ^{1}H NMR spectrum of cyclooctyl isobutyrate.

NMR data for cyclododecyl acetate

^{1}H NMR (500 MHz, $CDCl_3$) δ 5.05-4.95 (m, 1H, H1), 2.03 (s, 3H, 3xH14), 1.76-1.63 and 1.53-1.26 (m, 22H).

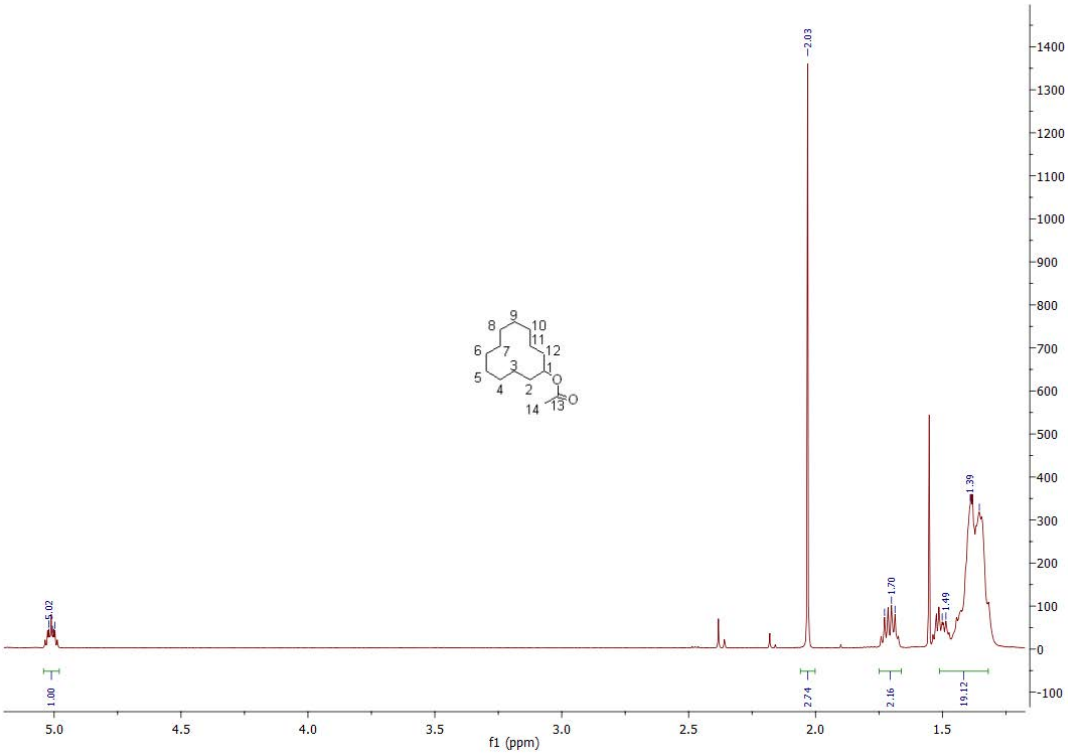

Figure A. 18 ^{1}H NMR spectrum of cyclododecyl acetate.

Appendix B Supplementary Data for Chapter 3

Figure B. 1 Mass Spectra Analysis **289**
Figure B. 2 ^{1}H NMR of a mixture of 1,7-cyclododecanediol, 1,6-cyclododecanediol and 1,4-cyclododecanediol or diastereomer of 1,6-cyclododecanediol. 311
Figure B. 3 ^{13}C NMR of a mixture of 1,7-cyclododecanediol, 1,6-cyclododecanediol and 1,4-cyclododecanediol or diastereomer of 1,6-cyclododecanediol 312
Figure B. 4 gCOSY NMR of a mixture of cyclododecanediol products 312
Figure B. 5 HSQC NMR of a mixture of cyclododecanediol products 313
Figure B. 6 Zoomed in HMBC NMR of a mixture of cyclododecanediol products..... 313
Figure B. 7 ^{1}H NMR of 2-hydroxycyclononanone 314
Figure B. 8 ^{13}C NMR of 2-hydroxycyclononanone. 315
Figure B. 9 gCOSY NMR of 2-hydroxycyclononanone..... 316
Figure B. 10 HSQC NMR of 2-hydroxycyclononanone..... 316
Figure B. 11 ^{1}H NMR of 1-hydroxy-10-oxabicyclo[4.3.1]decane 317
Figure B. 12 ^{13}C NMR of 1-hydroxy-10-oxabicyclo[4.3.1]decane 318
Figure B. 13 gCOSY NMR of 1-hydroxy-10-oxabicyclo[4.3.1]decane..... 318
Figure B. 14 HSQC NMR of 1-hydroxy-10-oxabicyclo[4.3.1]decane 319
Figure B. 15 Zoomed in HMBC NMR of 1-hydroxy-10-oxabicyclo[4.3.1]decane 319
Figure B. 16 HMBC NMR of 1-hydroxy-10-oxabicyclo[4.3.1]decane..... 320
Figure B. 17 ^{1}H NMR of 2-hydroxycyclodecanone 321
Figure B. 18 ^{13}C NMR of 2-hydroxycyclodecanone 322
Figure B. 19 gCOSY NMR of 2-hydroxycyclodecanone 322
Figure B. 20 HSQC NMR of 2-hydroxycyclodecanone 323
Figure B. 21 ^{1}H NMR of 1-oxabicyclo[5.3.1]undecan-1-ol. 324
Figure B. 22 ^{13}C NMR of 1-oxabicyclo[5.3.1]undecan-1-ol. 325
Figure B. 23 gCOSY NMR of 1-oxabicyclo[5.3.1]undecan-1-ol. 325
Figure B. 24 HSQC NMR of 1-oxabicyclo[5.3.1]undecan-1-ol 326
Figure B. 25 Zoomed in version of HMBC NMR of 1-oxabicyclo[5.3.1]undecan-1-ol 327
Figure B. 26 HMBC NMR of 1-oxabicyclo[5.3.1]undecan-1-ol..... 328
Figure B. 27 ^{1}H NMR of 1-oxabicyclo[6.3.1]undecan-1-ol and 6-hydroxycyclodecanone mixture 329
Figure B. 28 ^{13}C NMR of 1-oxabicyclo[6.3.1]undecan-1-ol 330

Figure B. 29 gCOSY NMR of 1-oxabicyclo[6.3.1]undecan-1-ol and 6-hydroxycyclodecanone mixture 331
Figure B. 30 HSQC NMR of 1-oxabicyclo[6.3.1]undecan-1-ol and 6-hydroxycyclodecanone mixture 331
Figure B. 31 Zoomed in version of HMBC NMR of 1-oxabicyclo[6.3.1]undecan-1-ol and 6-hydroxycyclodecanone mixture 332
Figure B. 32 Zoomed in gCOSY NMR to highlight the interactions 333
Figure B. 33 ^{1}H NMR of 2-hydroxycycloundecanone 334
Figure B. 34 ^{13}C NMR of 2-hydroxycycloundecanone..... 334
Figure B. 35 gCOSY NMR of 2-hydroxycycloundecanone. 335
Figure B. 36 HSQC NMR of 2-hydroxycycloundecanone 336
Figure B. 37 Zoomed in HSQC NMR to highlight the correlations. 336
Figure B. 38 Zoomed in HMBC NMR of 2-hydroxycycloundecanone. 337
Figure B. 39 HMBC NMR of 2-hydroxycycloundecanone. 338
Figure B. 40 ^{1}H NMR of 5-hydroxycycloundecanone. 339
Figure B. 41 ^{13}C NMR of 5-hydroxycycloundecanone. 340
Figure B. 42 gCOSY NMR of 5-hydroxycycloundecanone..... 340
Figure B. 43 HSQC NMR of 5-hydroxycycloundecanone. 341
Figure B. 44 HMBC NMR of 5-hydroxycycloundecanone. 342
Figure B. 45 ^{1}H NMR of 6-hydroxycycloundecanone 343
Figure B. 46 ^{13}C NMR of 6-hydroxycycloundecanone. 343
Figure B. 47 gCOSY NMR of 6-hydroxycycloundecanone. 344
Figure B. 48 HSQC NMR of 6-hydroxycycloundecanone. 344
Figure B. 49 HMBC NMR of 6-hydroxycycloundecanone. 345
Figure B. 50 ^{1}H NMR of 2-hydroxycyclododecanone 346
Figure B. 51 ^{1}H NMR of 2-hydroxycyclododecanone (standard). 346
Figure B. 52 ^{13}C NMR of 2-hydroxycyclododecanone. 347
Figure B. 53 gCOSY NMR of 2-hydroxycyclododecanone 347
Figure B. 54 HSQC NMR of 2-hydroxycyclododecanone 348
Figure B. 55 HMBC NMR of 2-hydroxycyclododecanone. 349
Figure B. 56 ^{1}H NMR of 7-hydroxycyclododecanone 350
Figure B. 57 ^{13}C NMR of 7-hydroxycyclododecanone. 351
Figure B. 58 gCOSY NMR of 7-hydroxycyclododecanone. 351

Figure B. 59 HSQC NMR of 7-hydroxycyclododecanone 352
Figure B. 60 HMBC NMR of 7-hydroxycyclododecanone.....353
Figure B. 61 ^{1}H NMR of 8-hydroxycyclopentadecanone.....354
Figure B. 62 ^{13}C NMR of 8-hydroxycyclopentadecanone.....355
Figure B. 63 gCOSY NMR of 8-hydroxycyclopentadecanone. 356
Figure B. 64 Zoomed in HSQC NMR of 8-hydroxycyclopentadecanone.....356
Figure B. 65 HSQC NMR of 8-hydroxycyclopentadecanone 357
Figure B. 66 Zoomed in HMBC NMR of 8-hydroxycyclopentadecanone.....357
Figure B. 67 Zoomed in HMBC NMR of 8-hydroxycyclopentadecanone which highlighted the correlations of C1with H2, H3, H14 and H15. 358
Figure B. 68 HMBC NMR of 8-hydroxycyclopentadecanone. 358
Figure B. 69 ^{1}H NMR of *trans*-4-hydroxycyclohexyl acetate. 359
Figure B. 70 ^{13}C NMR of *trans*-4-hydroxycyclohexyl acetate.....360
Figure B. 71 gCOSY NMR of *trans*-4-hydroxycyclohexyl acetate.....360
Figure B. 72 HSQC NMR of *trans*-4-hydroxycyclohexyl acetate.....361
Figure B. 73 HMBC NMR of *trans*-4-hydroxycyclohexyl acetate. 361
Figure B. 74 ROESY NMR of *trans*-4-hydroxycyclohexyl acetate. 362
Figure B. 75 ^{1}H NMR of *trans*-4-hydroxycyclohexyl butyrate. 363
Figure B. 76 ^{13}C NMR of *trans*-4-hydroxycyclohexyl butyrate.....364
Figure B. 77 gCOSY NMR of trans-4-hydroxycyclohexyl butyrate.....364
Figure B. 78 HSQC NMR of *trans*-4-hydroxycyclohexyl butyrate.....365
Figure B. 79 ROESY NMR of *trans*-4-hydroxycyclohexyl butyrate.. 366
Figure B. 80 ^{1}H NMR of *trans*-4-hydroxycyclohexyl isobutyrate. 367
Figure B. 81 ^{13}C NMR of *trans*-4-hydroxycyclohexyl isobutyrate. 368
Figure B. 82 gCOSY NMR of *trans*-4-hydroxycyclohexyl isobutyrate.....368
Figure B. 83 HSQC NMR of *trans*-4-hydroxycyclohexyl isobutyrate.....369
Figure B. 84 ^{1}H NMR of 4-(1-hydroxy-2-methylpropan-2-yl)cyclohexyl acetate.....370
Figure B. 85 The ^{1}H NMR of mixture of *cis* and *trans* 4-*tert*-butylcyclohexyl acetate. 371
Figure B. 86 ^{13}C NMR of 4-(1-hydroxy-2-methylpropan-2-yl)cyclohexyl acetate.....372
Figure B. 87 gCOSY NMR of 4-(1-hydroxy-2-methylpropan-2-yl)cyclohexyl acetate 372
Figure B. 88 HSQC NMR of 4-(1-hydroxy-2-methylpropan-2-yl)cyclohexyl acetate…… 373
Figure B. 89 ^{1}H NMR of methyl-2-(*trans*-4-hydroxycyclohexyl)acetate.....374
Figure B. 90 ^{13}C NMR of methyl-2-(*trans*-4-hydroxycyclohexyl)acetate. 375

Figure B. 91 gCOSY NMR of methyl-2-(*trans*-4-hydroxycyclohexyl)acetate. 375
Figure B. 92 HSQC NMR of methyl-2-(*trans*-4-hydroxycyclohexyl)acetate. 376
Figure B. 93 HMBC NMR of methyl-2-(*trans*-4-hydroxycyclohexyl)acetate. 376
Figure B. 94 Zoomed in ROESY NMR of methyl-2-(*trans*-4-hydroxycyclohexyl)acetate. 377
Figure B. 95 Zoomed in ROESY NMR of methyl-2-(*trans*-4-hydroxycyclohexyl)acetate .377
Figure B. 96 ^{1}H NMR of ethyl-*trans*-2-(4-hydroxycyclohexyl)acetate.....378
Figure B. 97 ^{13}C NMR of ethyl-*trans*-2-(4-hydroxycyclohexyl)acetate.....379
Figure B. 98 gCOSY NMR of ethyl-*trans*-2-(4-hydroxycyclohexyl)acetate. 379
Figure B. 99 HSQC NMR of ethyl-*trans*-2-(4-hydroxycyclohexyl)acetate. 380
Figure B. 100 HMBC NMR of ethyl-*trans*-2-(4-hydroxycyclohexyl)acetate. 380
Figure B. 101 Zoomed in ROESY NMR of ethyl-*trans*-2-(4-hydroxycyclohexyl)acetate ..381
Figure B. 102 Zoomed in ROESY NMR of ethyl-*trans*-2-(4-hydroxycyclohexyl)acetate ..381
Figure B. 103 ^{1}H NMR of 5-hydroxycyclooctyl acetate. 382
Figure B. 104 ^{13}C NMR of 5-hydroxycyclooctyl acetate.. 383
Figure B. 105 gCOSY NMR of 5-hydroxycyclooctyl acetate 383
Figure B. 106 HSQC NMR of 5-hydroxycyclooctyl acetate 384
Figure B. 107 HMBC NMR of 5-hydroxycyclooctyl acetate. 384
Figure B. 108 ROESY NMR of 5-hydroxycyclooctyl acetate.....385
Figure B. 109 ^{1}H NMR of 5-hydroxycyclooctyl isobutyrate. 386
Figure B. 110 ^{13}C NMR of 5-hydroxycyclooctyl isobutyrate. 387
Figure B. 111 gCOSY NMR of 5-hydroxycyclooctyl isobutyrate. 387
Figure B. 112 HSQC NMR of 5-hydroxycyclooctyl isobutyrate. 388
Figure B. 113 HMBC NMR of 5-hydroxycyclooctyl isobutyrate. 388
Figure B. 114 ROESY NMR of 5-hydroxycyclooctyl isobutyrate.. 389
Figure B. 115 ^{1}H NMR of 7-hydroxycyclododecyl acetate 390
Figure B. 116 ^{13}C NMR of 7-hydroxycyclododecyl acetate. 391
Figure B. 117 gCOSY NMR of 7-hydroxycyclododecyl acetate. 392
Figure B. 118 HSQC NMR of 7-hydroxycyclododecyl acetate 393
Figure B. 119 ^{1}H NMR of 5-hydroxycyclododecyl acetate. 394
Figure B. 120 ^{13}C NMR highlighted the carbon peaks of 5-hydroxycyclododecyl acetate..394
Table B. 1 The carbon signals detected in the ^{13}C NMR of different metabolites of cyclododecyl acetate…….....394
Figure B. 121 gCOSY NMR of 5-hydroxycyclododecyl acetate. 395

Figure B. 122 HMBC NMR of 5-hydroxycyclododecyl acetate.. 396
Figure B. 123 ^{1}H NMR of 7-hydroxycyclododecyl acetate 396
Figure B. 124 ^{1}H NMR of 3-cyclohexene-1-methanol, 5-hydroxy-*α*,*α*,4-trimethyl-,*α*-acetate (CYP101C1). 397
Figure B. 125 gCOSY NMR of 3-cyclohexene-1-methanol, 5-hydroxy-*α*,*α*,4-trimethyl-,*α*-acetate 398
Figure B. 126 Zoomed in gCOSY NMR region to highlight the interactions. 398
Figure B. 127 NMR of 3-cyclohexene-1-methanol, 5-hydroxy-*α*,*α*,4-trimethyl-,*α*-acetate. 399
Figure B. 128 HSQC NMR of 3-cyclohexene-1-methanol, 5-hydroxy-*α*,*α*,4-trimethyl-,*α*-acetate 400
Figure B. 129 HMBC NMR of 3-cyclohexene-1-methanol, 5-hydroxy-*α*,*α*,4-trimethyl-,*α*-acetate 400
Figure B. 130 Zoomed in HMBC NMR of 3-cyclohexene-1-methanol, 5-hydroxy-*α*,*α*,4-trimethyl-,*α*-acetate. 401
Figure B. 131 Zoomed in HMBC NMR of 3-cyclohexene-1-methanol, 5-hydroxy-*α*,*α*,4-trimethyl-,*α*-acetate to highlight the minor product signals. 402
Figure B. 132 ^{1}H NMR of 8-hydroxy-2-nonanone 403
Figure B. 133 ^{13}C NMR of 8-hydroxy-2-nonanone 404
Figure B. 134 gCOSY NMR of 8-hydroxy-2-nonanone 404
Figure B. 135 HSQC NMR of 8-hydroxy-2-nonanone 405
Figure B. 136 HMBC NMR of 8-hydroxy-2-nonanone 405
Figure B. 137 ^{1}H NMR of 8-hydroxy-2-undecanone 406
Figure B. 138 ^{13}C NMR of 8-hydroxy-2-undecanone. 407
Figure B. 139 gCOSY NMR of 8-hydroxy-2-undecanone 408
Figure B. 140 HSQC NMR of 8-hydroxy-2-undecanone 408
Figure B. 141 HMBC NMR of 8-hydroxy-2-undecanone 409
Figure B. 142 Zoomed in the HMBC NMR to highlight the C-H interactions of minor metabolites. 410

Figure B. 1 Mass Spectra Analysis

MS analysis of cyclooctane products

MS analysis of cyclooctanone RT 6.6 min (m^+/z = 126.05)

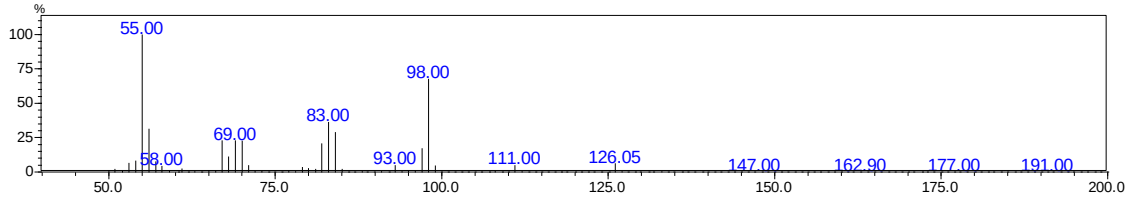

MS analysis of cyclooctanol RT 6.9 min (m^+/z = 128.05)

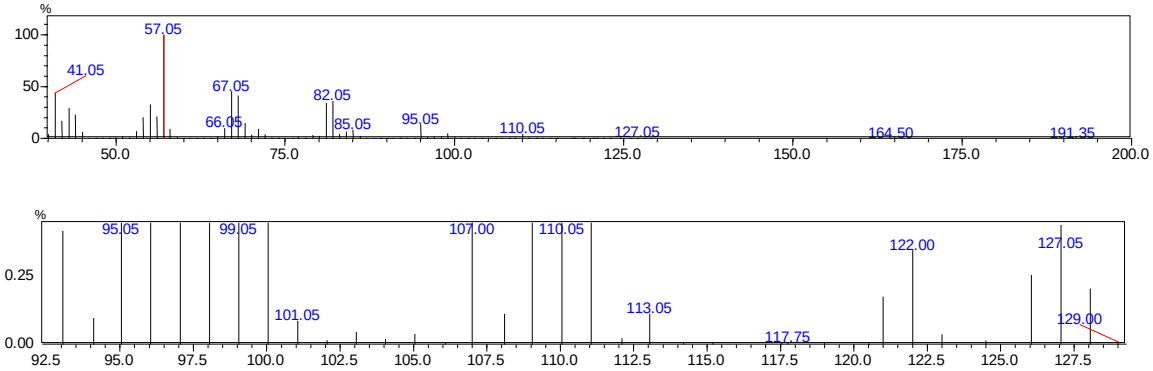

zoomed in version

MS analysis of cyclodecane and its products

MS analysis of cyclodecanone RT 9.7 min (m^+/z = 154.20)

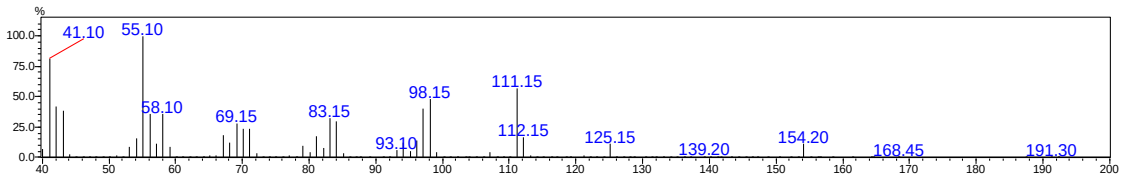

MS analysis of cyclodecanol RT 10.45 min (m^+/z = 156.20)

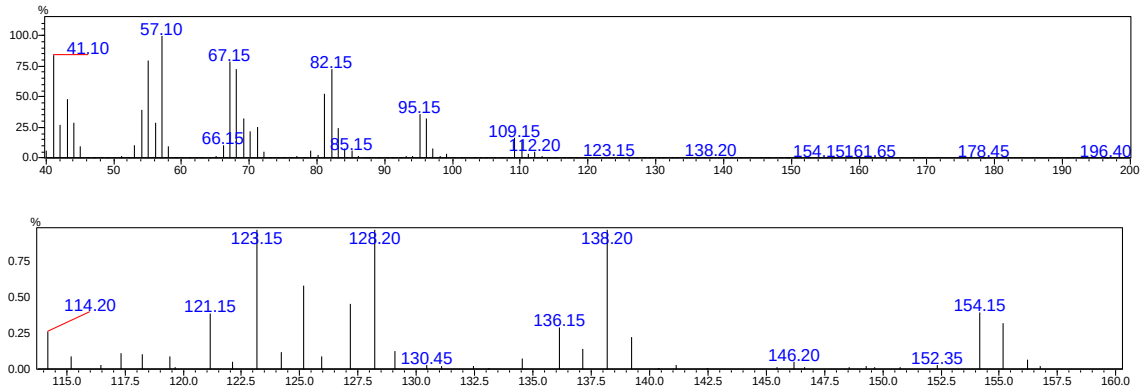

zoomed in version

MS analysis of cyclododecane, cyclododecanol and their products

MS analysis of cyclododecane RT 6.8 min (m^+/z = 168.20)

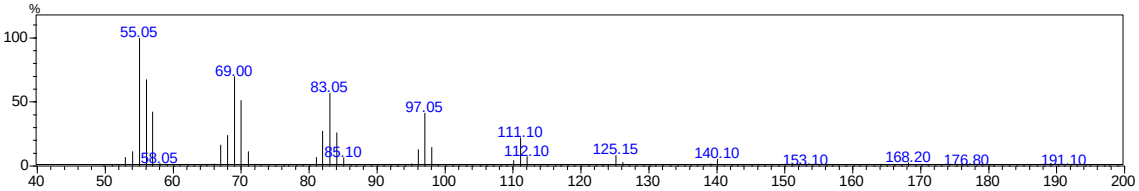

MS analysis of 1,7-cyclododecanediol RT 12.9 min (m^+/z = 200.10)

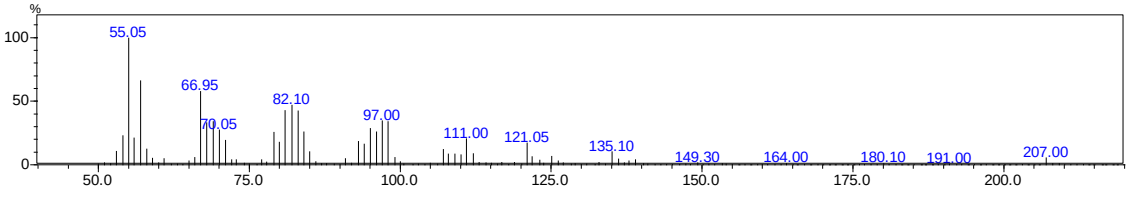

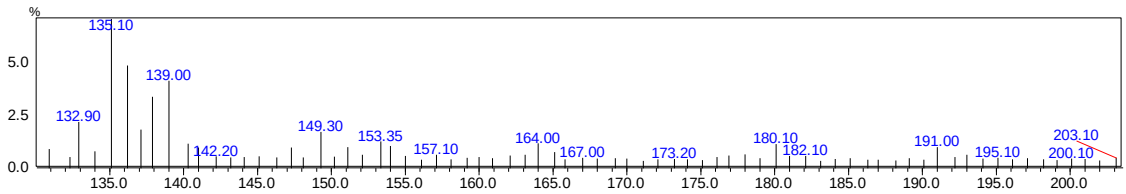

zoomed in version

MS analysis of cyclododecanone RT 7.6 min (m^+/z = 182.15)

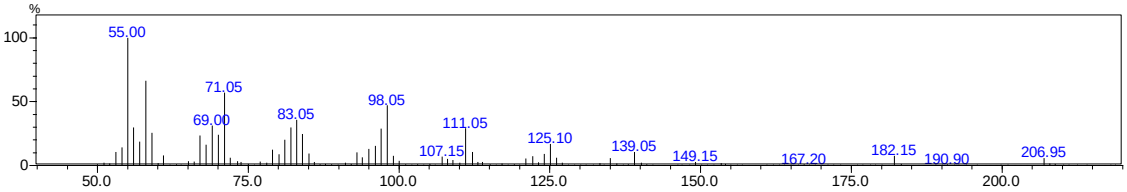

MS analysis of cyclododecanol RT 7.9 min (m^+/z = 184.2)

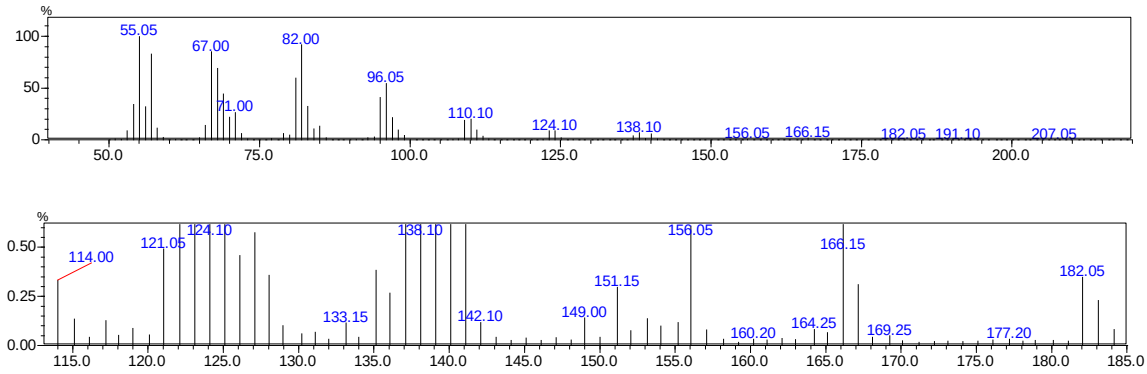

zoomed in version

MS analysis of cyclononanone and its products

MS analysis of cyclononanone RT 9.1 min (m^+/z = 140.15; CYP101B1)

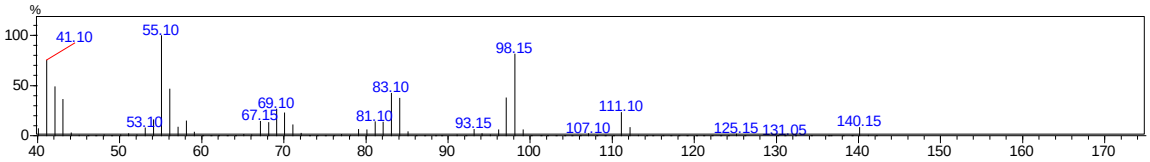

MS analysis of 1-hydroxy-10-oxabicyclo[4.3.1]decane RT 11.2 min (m^+/z = 156.15) [217].

Experimental m^+/z = 156.15, 138.15, 120.15, 113.10, 97.15, 94.10, 81.10, 71.10, 69.15, 68.15, 67.15, 55.10, 43.10.

Reported [217] m^+/z = 156 (17), 113 (64), 110 (66), 97 (81), 71 (63), 69 (84), 68 (97), 55 (100).

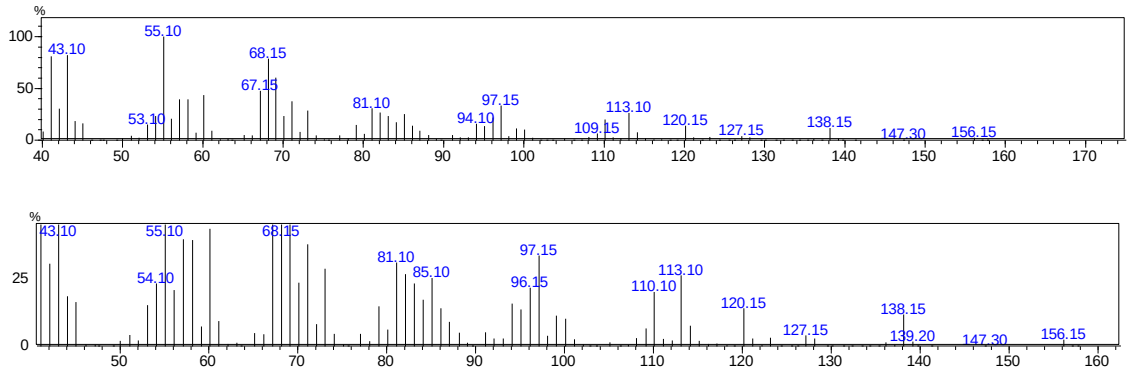

zoomed in version

MS analysis of 2-hydroxycyclononanone RT 12.2 min (m^+/z = 156.15; CYP101C1) [221].

Experimental m^+/z = 156.15, 138.15, 120.15, 110.15, 95.15, 94.10, 82.10, 67.15, 57.10, 41.10.

Reported m^+/z = 156, 138, 120, 110, 95, 95, 82, 67, 57, and 41 (WSS: Spectral data were obtained from Wiley Subscription Services, Inc. (US)).

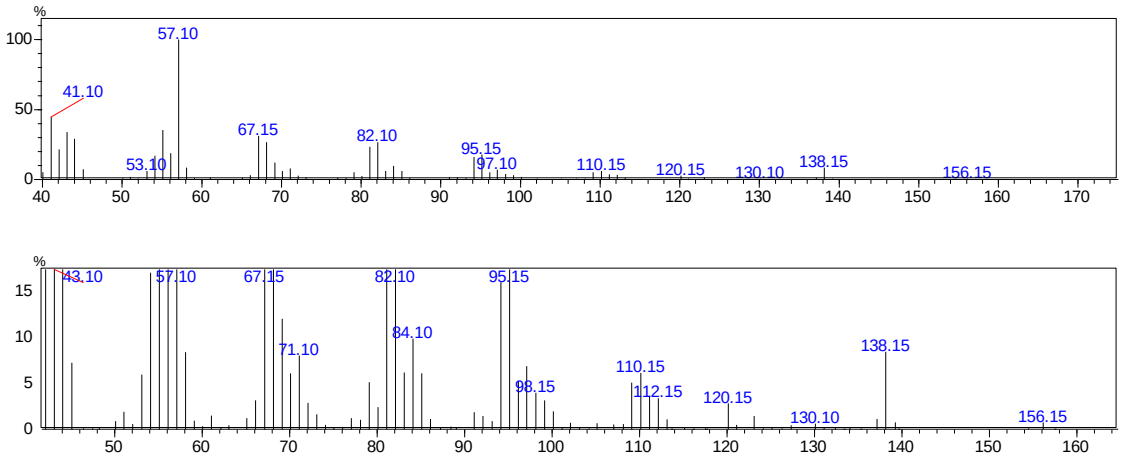

zoomed in version

MS analysis of cyclodecanone and its products

MS analysis of cyclodecanone RT 7.5 min (m^+/z = 154.20; GC-FID RT 2.9 min).

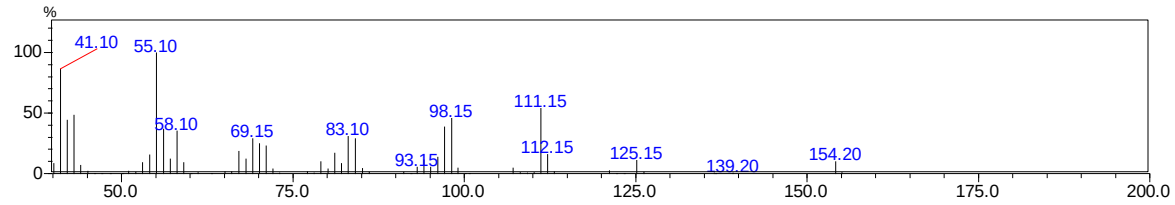

MS analysis of 2-hydroxycyclodecanone RT 10.6 min (m^+/z = 170.2; CYP101C1; GC-FID RT 7.2 min).

Experimental m^+/z = 170.2, 152.20, 134.2, 111.1, 108.15, 98.1, 96.10, 95.15, 82.15, 81.10, 67.15, 57.10 and 41.10.

Reported [219] m^+/z = 170, 152, 134, 111, 98, 81, 57 and 41.

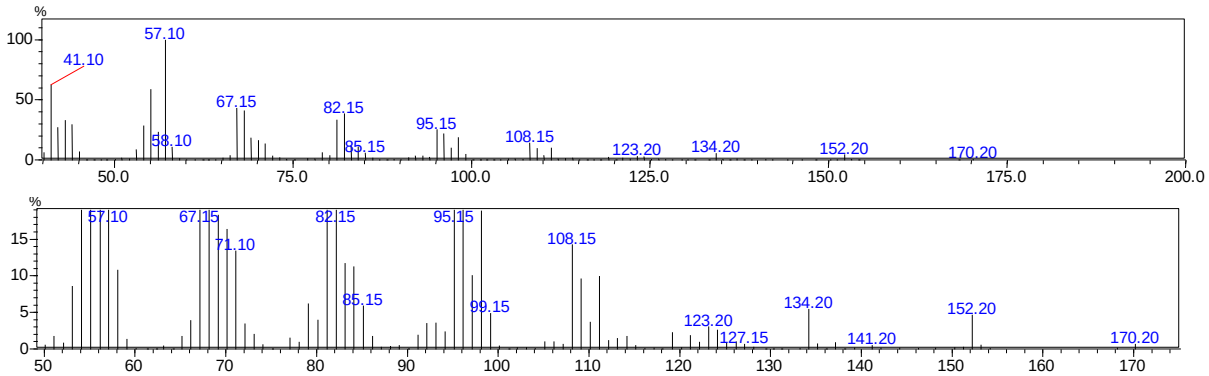

zoomed in version

MS analysis of 1-oxabicyclo[5.3.1]undecan-1-ol and 5-hydroxycyclodecanone RT 13.4 min (m^+/z = 170.20; CYP101B1; GC-FID RT 10.0 min) [218].

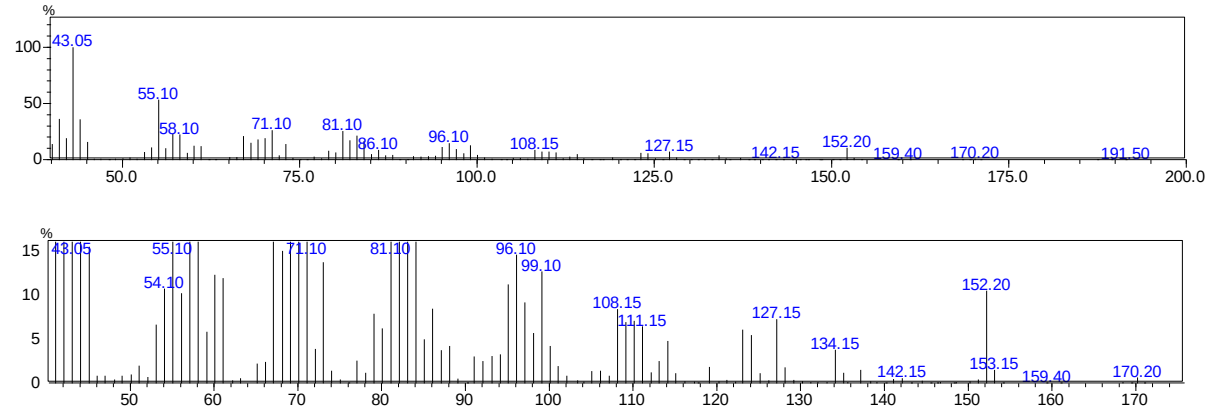

zoomed in version

MS analysis of 1-oxabicyclo[6.3.1]undecan-1-ol and 6-hydroxycyclodecanone RT 13.7 min (m^+/z = 170.1; CYP101B1; GC-FID RT 10.9 min).

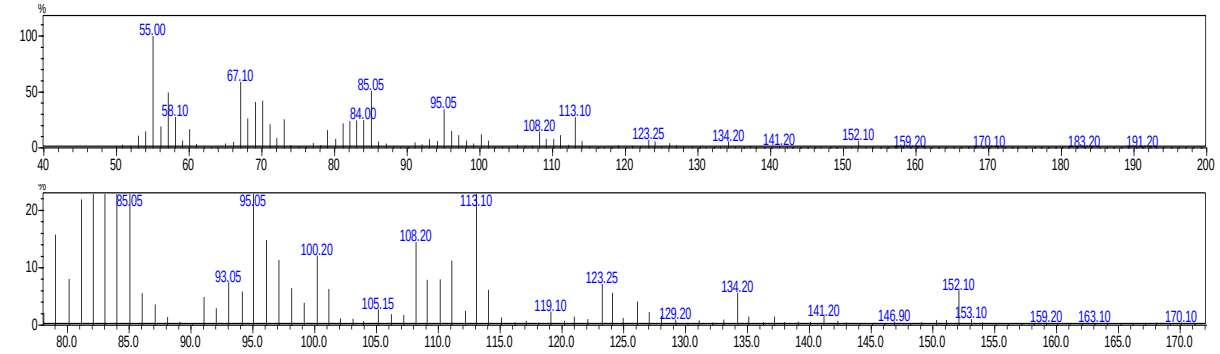

zoomed in version

MS analysis of cycloundecanone and its products

MS analysis of cycloundecanone RT 6.4 min (m^+/z = 168.20).

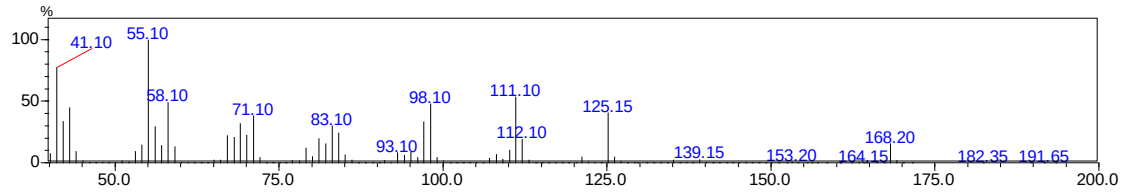

MS analysis of 2-hydroxycycloundecanone RT 8.4 min (m^+/z = 184.40; CYP101C1).

Experimental m^+/z = 184.40, 166.20, 148.20, 138.15, 133.15, 122.20, 119.15, 111.15, 98.15, 95.15, 82.10, 81.15, 68.10, 67.15, 57.10, 55.15 and 41.10.

Reported [220] m^+/z = 184, 119, 111, 98, 85, 81, 68 and 55.

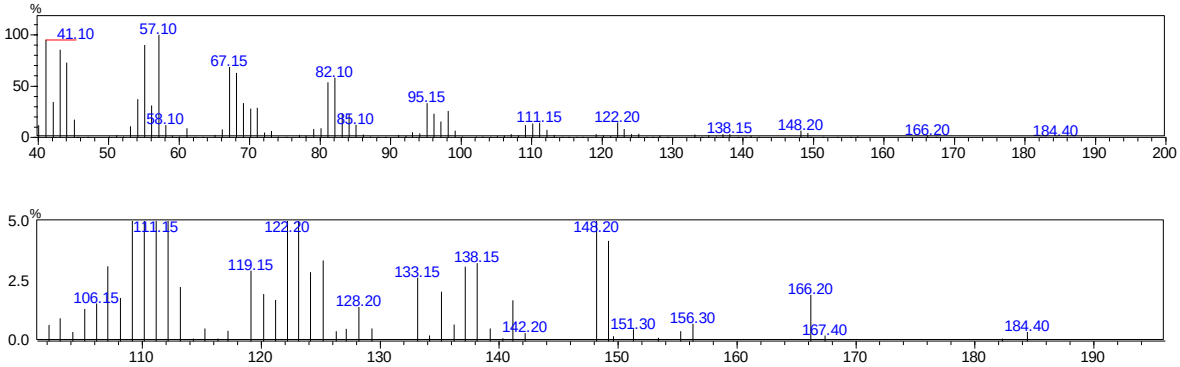

zoomed in version

MS analysis of further oxidation product of CYP101B1 turnover at RT 8.8 min (m^+/z = 182.30).

Experimental m^+/z = 182.30, 166.10, 155.55, 148.10, 137.35, 133.50, 109.20, 98.10, 95.10, 83.10, 67.10, 58.10, 55.0 and 43.10.

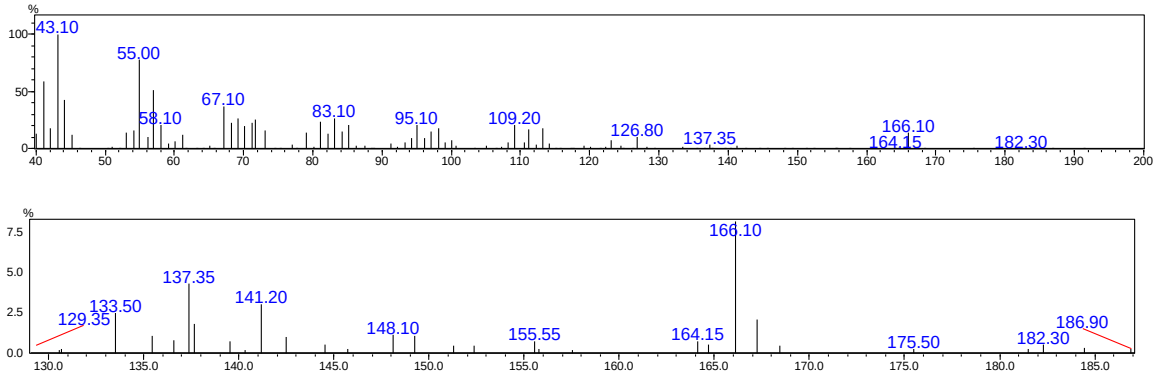

zoomed in version

MS analysis of product 5-hydroxycycloundecanone RT 9.3 min (m^+/z = 184.3; CYP101B1).

Experimental m^+/z = 184.3, 166.20, 148.15, 137.15, 128.15, 127.15, 123.15, 113.15, 109.10, 81.10, 71.10, 67.15, 55.10 and 41.10.

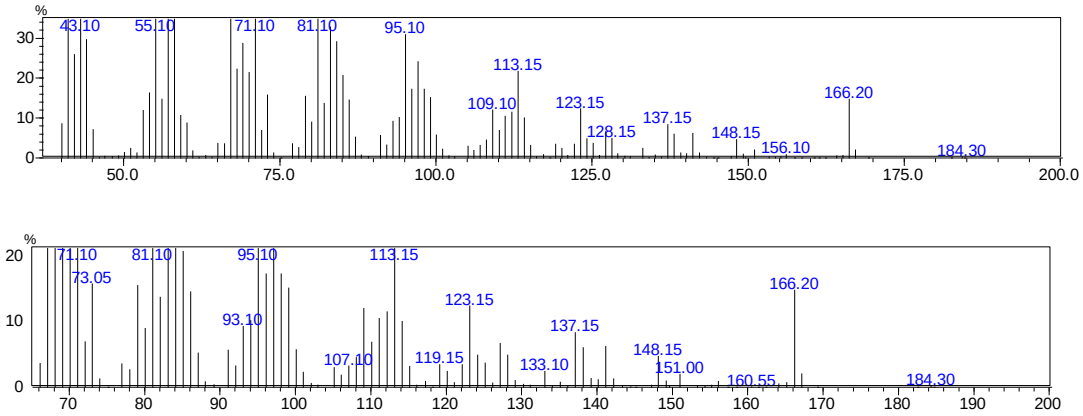

zoomed in version

MS analysis of product 6-hydroxycycloundecanone RT 9.45 min (m^+/z = 184.2; CYP101B1).

Experimental m^+/z = 184.2, 166.20, 148.20, 137.15, 127.15, 123.15, 113.15, 109.10, 98.15, 95.15, 85.10, 81.15, 67.15, 58.10, 55.10 and 41.10.

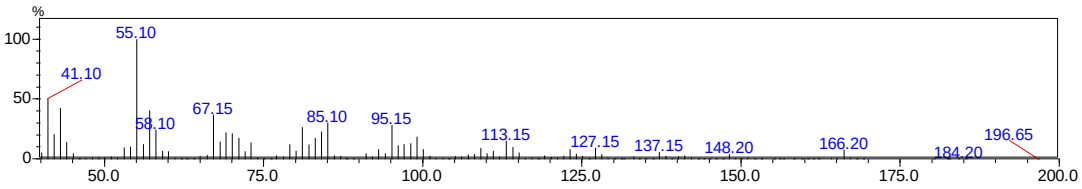

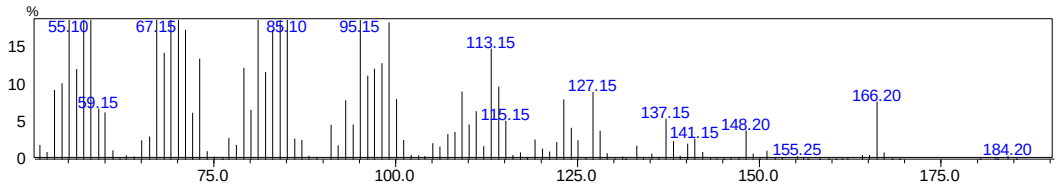

zoomed in version

MS analysis of cyclododecanone and its products

MS analysis of cyclododecanone RT 12.1 min (m^+/z = 182.2).

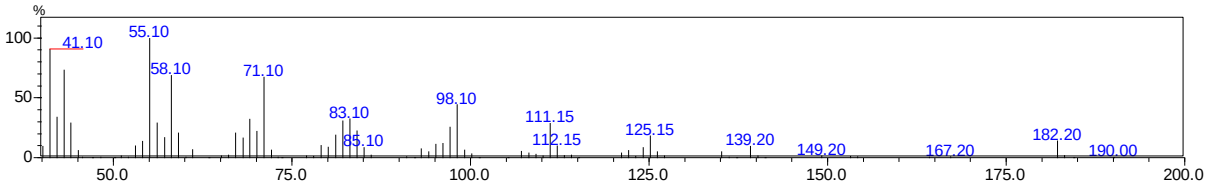

MS analysis of 2-hydroxycyclododecanone RT 15.5 min (m^+/z = 198.25; CYP101C1) [219, 220].

Experimental m^+/z = 198.25, 180.25, 170.15, 162.20, 149.25, 136.10, 133.20, 124.10, 123.10, 133.20, 121.20, 111.10, 109.15, 98.15, 95.15, 82.15, 81.10, 68.10, 67.15, 57.10, 55.10 and 41.10.

Reported [2] m^+/z = 198, 180, 136, 124, 111, 98, 96, 95, 82, 81, 68, 67 and 57.

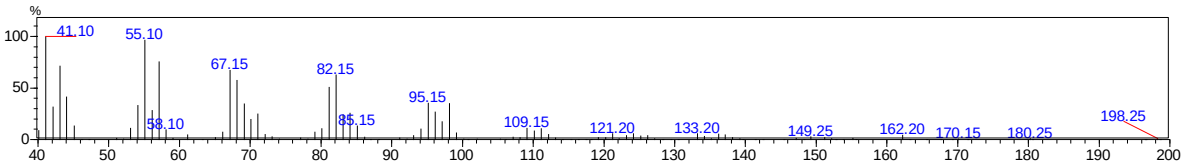

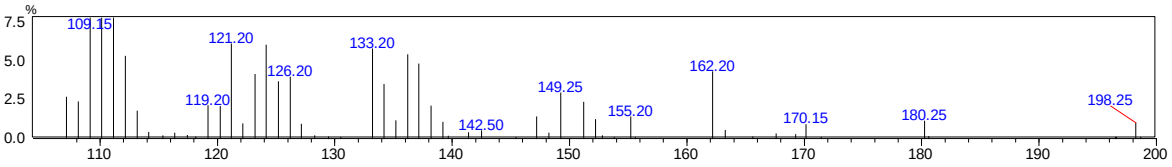

zoomed in version

MS analysis of 2-hydroxycyclododecanone standard (m^+/z = 198.15).

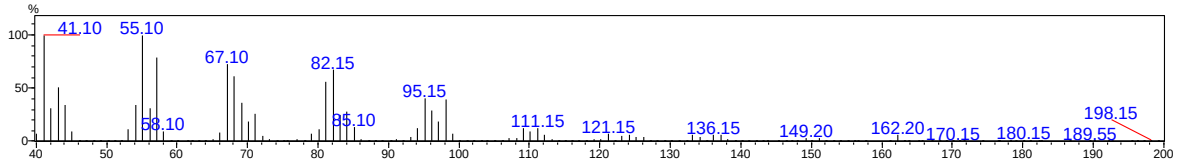

MS analysis of minor unidentified product at RT 16.9 min (m^+/z = 198.35; CYP101B1).

Experimental m^+/z = 198.35, 180.35, 162.30, 155.35, 151.25, 137.25, 127.55, 111.20, 98.20, 81.20, 71.05, 67.15. 55.15 and 43.15

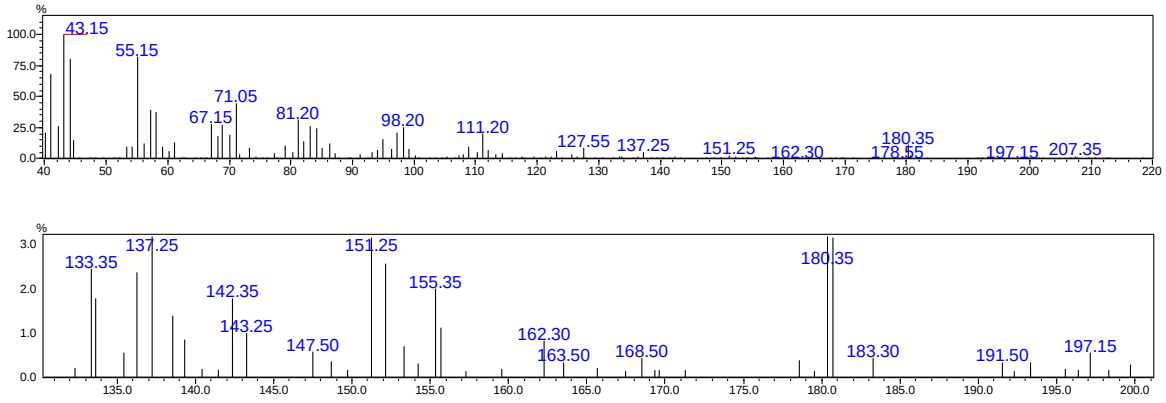

zoomed in version

MS analysis of 7-hydroxycyclododecanone RT 17.7 min (m^+/z = 198.50; CYP101B1) [208].

Experimental m^+/z = 198.05, 180.05, 162.10, 151.05, 137.1, 123.05, 113.1, 95.05, 84.05, 84.05, 81.10, 67.05. 55.00 and 41.10

Reported [208] m^+/z = 198, 180, 109, 81 and 55.

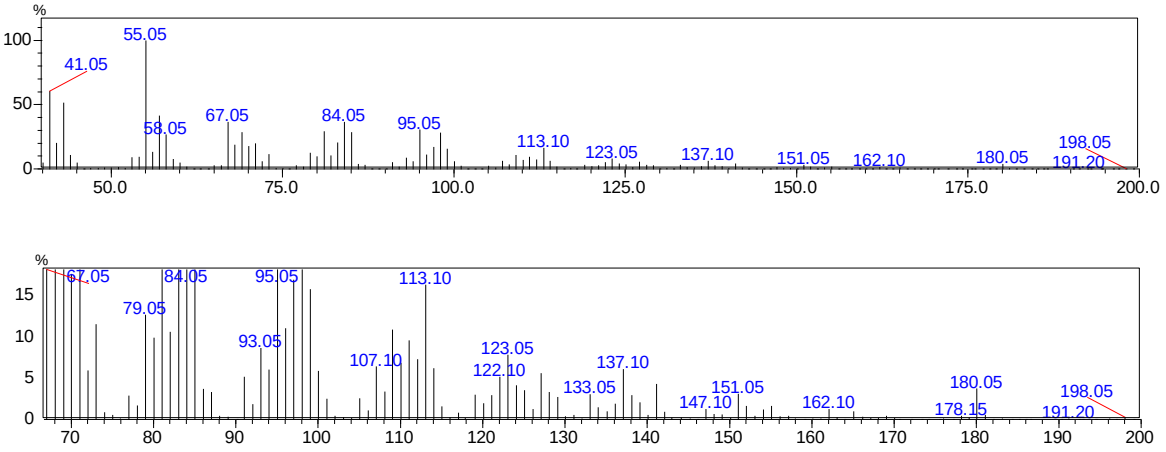

zoomed in version

MS analysis of cyclopentadecanone and its products

MS analysis of cyclopentadecanone RT 13.1 min (m^+/z = 224.25).

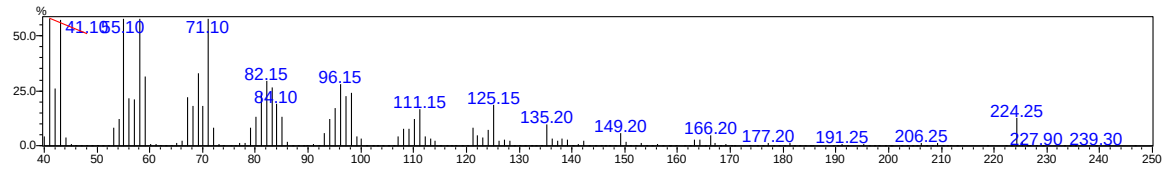

MS analysis of 2-hydroxycyclopentadecanone RT 14.6 min (m^+/z = 240.25; CYP101C1) [219, 222].

Experimental m^+/z = 240.25, 222.25, 166.25, 152.10, 149.15, 135.15, 124.10, 123.20, 110.10, 109.15, 96.15, 82.10, 67.10, 55.10 and 41.10.

Reported [219, 222] m^+/z = 240, 222, 166, 152, 138, 124, 110, 96, 82 and 55.

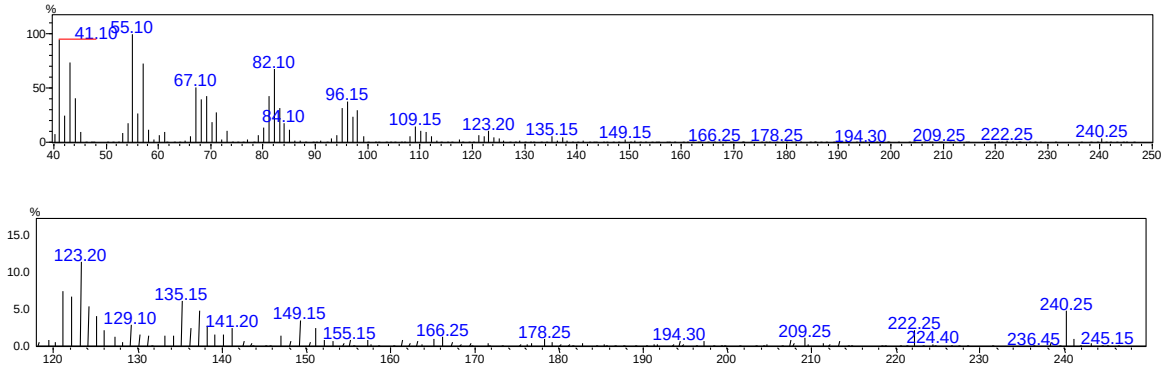

zoomed in version

MS analysis of 8-hydroxycyclopentadecanone RT 15.6 min (m^+/z = 240.25; CYP101B1) [208].

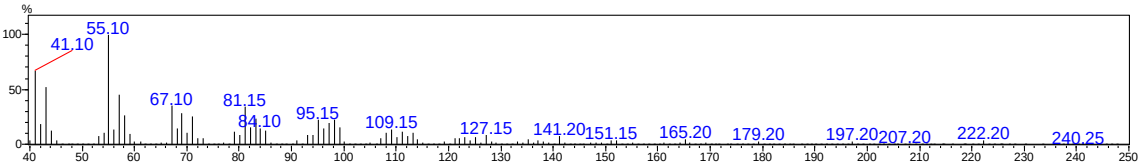

MS analysis of cyclopentadecanone minor product (cyclopentadecane-1,8-dione) CYP101B1 RT 15.1 min (m^+/z = 238.20; CYP101B1) [208].

Experimental m^+/z = 238.20, 220.20, 181.20, 125.15, 112.10, 111.15, 98.15, 84.15, 83.10, 69.10, 55.10 and 43.10.

Reported [208] m^+/z = 238, 181, 126, 112, 111, 98 and 84.

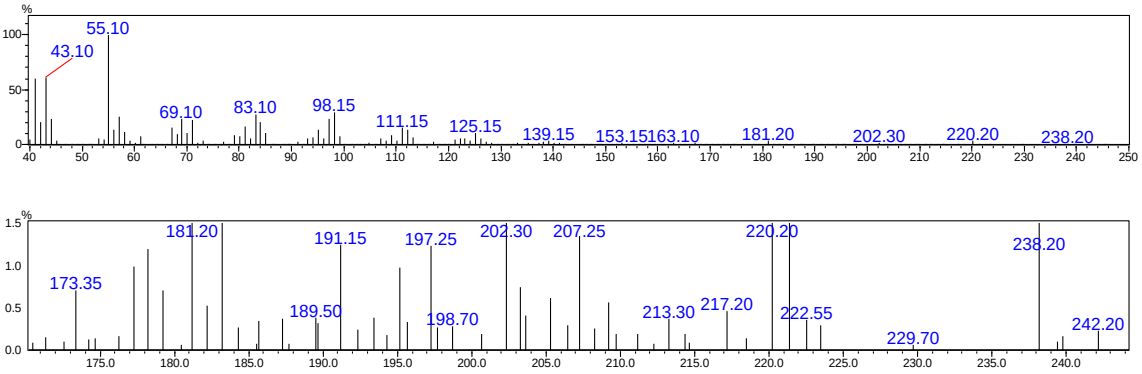

zoomed in version

MS analysis of cyclohexyl acetate product

MS analysis of *trans*-4-hydroxycyclohexyl acetate RT 10.6 min (m^+/z = 158.00)

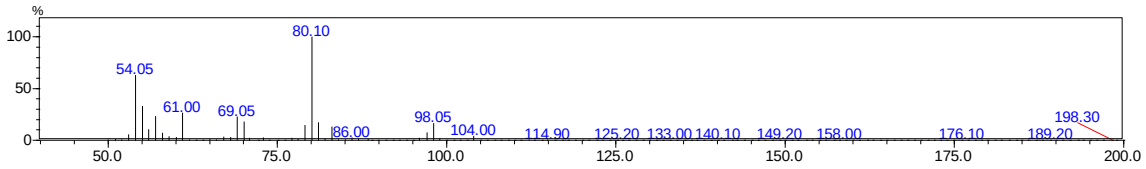

MS analysis of cyclohexyl butyrate product

MS analysis of *trans*-4-hydroxy cyclohexyl butyrate RT 8.5 min (m^+/z = 186.20)

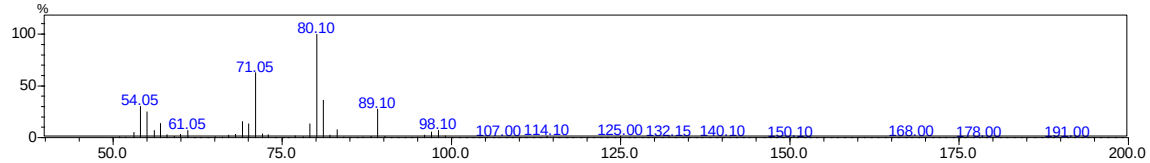

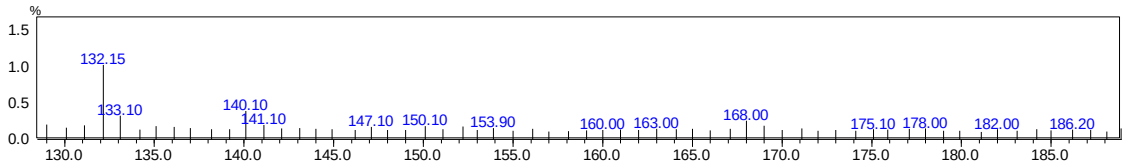

zoomed in version

MS analysis of cyclohexyl isobutyrate product

MS analysis of *trans*-4-hydroxycyclohexyl isobutyrate RT 7.9 min (m^+/z =186.0)

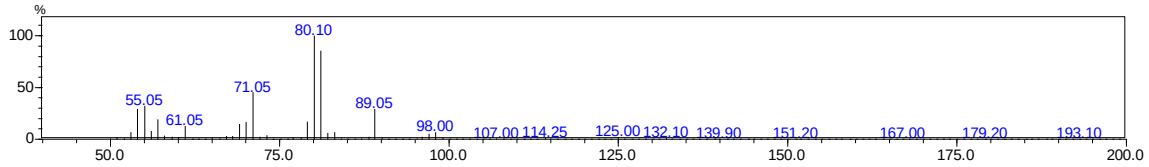

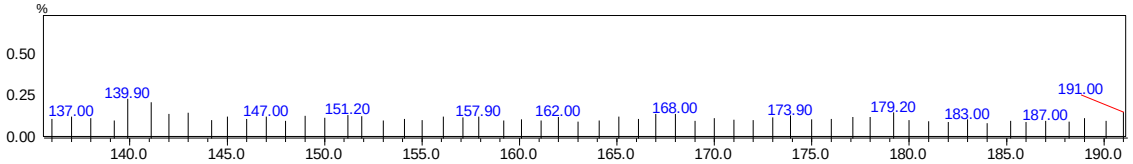

zoomed in version

MS analysis of *cis/trans*-4-*tert*-butylcyclohexyl acetate substrate and its product

MS analysis of *cis/trans* 4-*tert*-butylcyclohexyl acetate RT 10.45 min (m^+/z = 198.30).

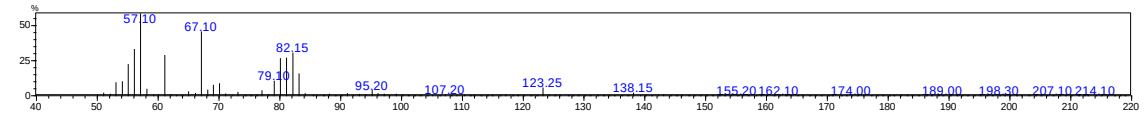

MS analysis of *cis/trans* 4-*tert*-butylcyclohexyl acetate RT 10.9 min (m^+/z = 198.10).

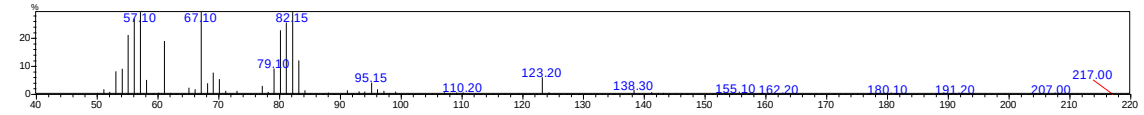

MS analysis of proposed *cis*-4-(1-hydroxy-2-methylpropan-2-yl) cyclohexyl acetate RT 13.2 min (m^+/z = 214.10; CYP101B1).

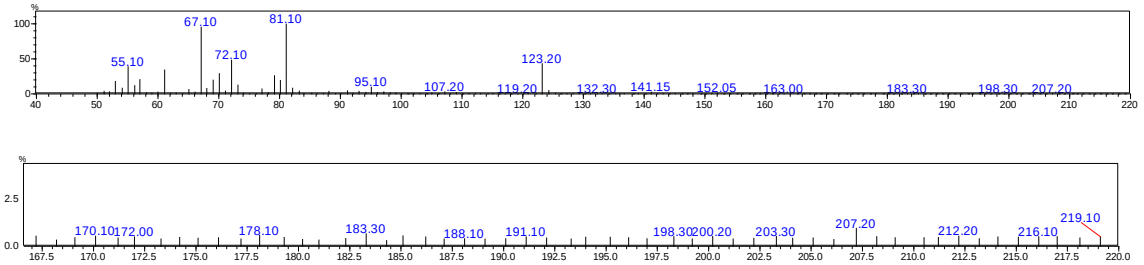

MS analysis of *trans*-4-(1-hydroxy-2-methylpropan-2-yl) cyclohexyl acetate RT 14.1 min (m^+/z = 214.20; *trans*).

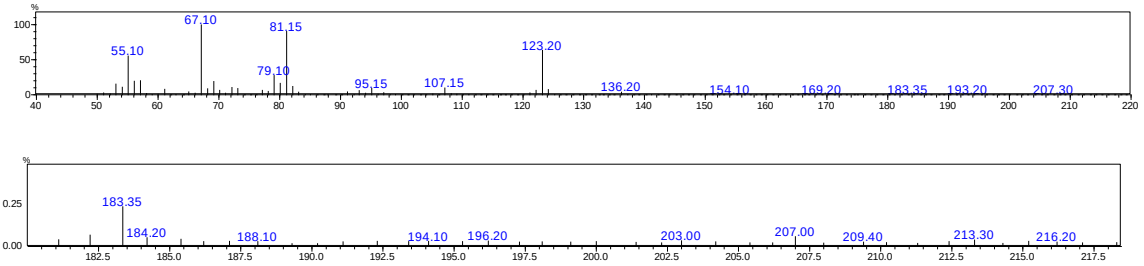

MS analysis of methyl cyclohexylacetate product

MS analysis of methyl-2-(*trans*-4-hydroxycyclohexyl)acetate RT 9.9 min (m^+/z = 172.0; RT 18.5 min in GC-FID).

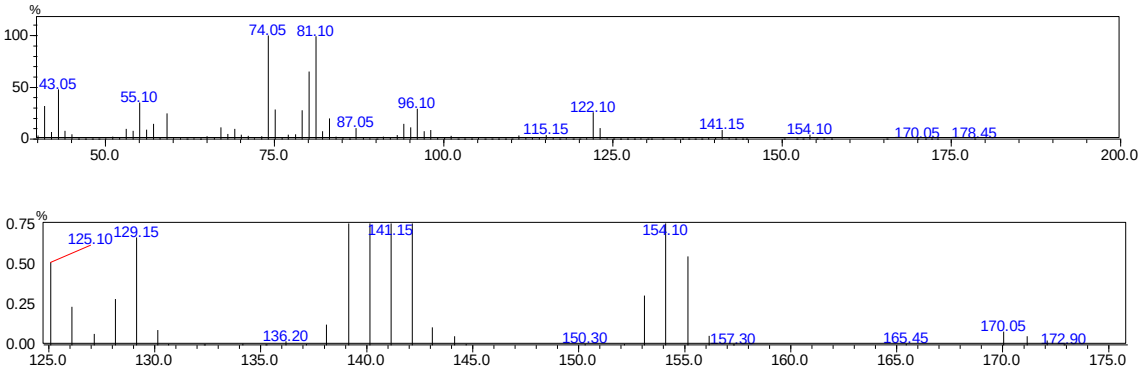

zoomed in version

MS analysis of ethylcyclohexyl acetate products

MS analysis of ethyl-*trans*-2-(4-hydroxycyclohexyl)acetate RT 7.0 min (m^+/z = 186.15; RT 20.1 min in GC-FID).

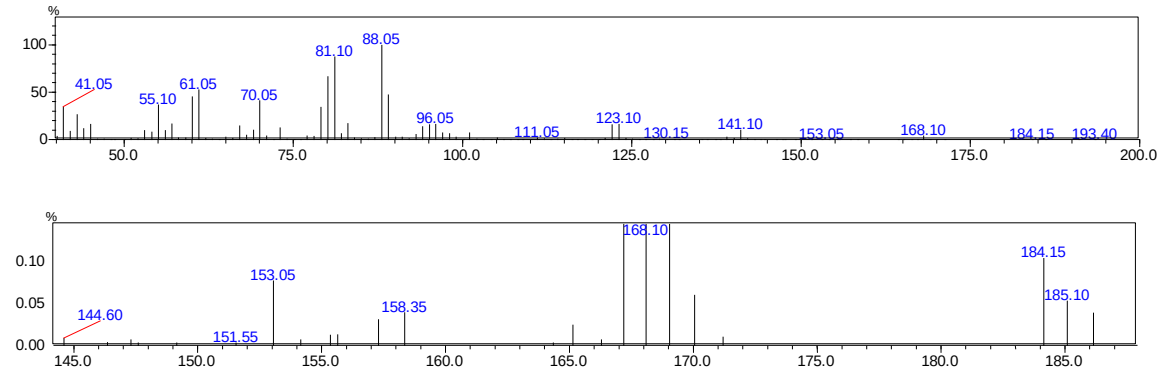

zoomed in version

MS analysis of further oxidation product RT 6.9 min (m^+/z = 184.25).

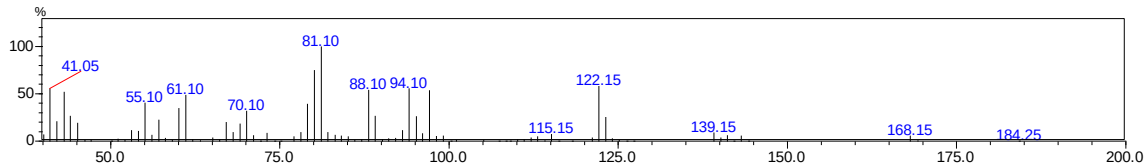

MS analysis of cyclooctyl acetate and its products

MS analysis of cyclooctyl acetate RT 6.5 min (m^+/z = 170.10).

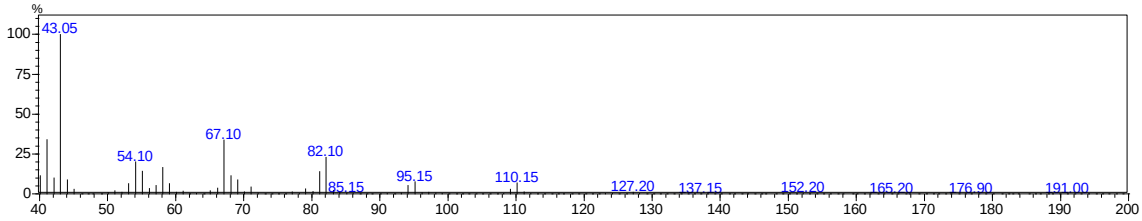

MS analysis of further oxidation product cyclooctyl acetate RT 8.8 min (m^+/z = 184.10; CYP101C1)

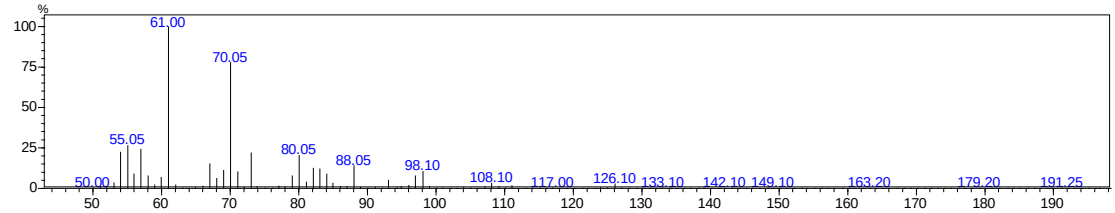

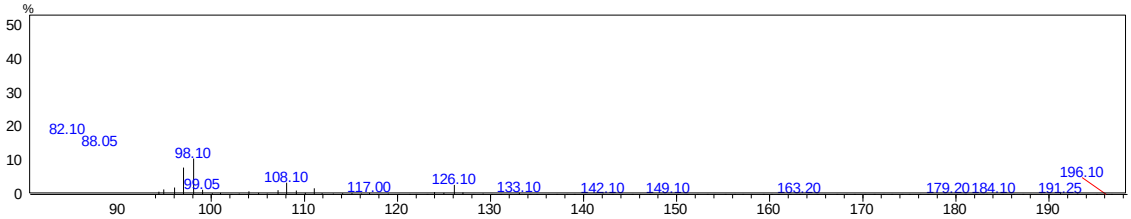

zoomed in version

MS analysis of 5-hydroxycyclooctyl acetate RT 8.95 min (m^+/z = 186.20).

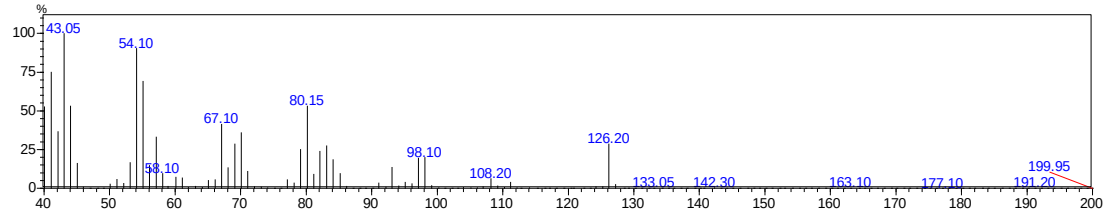

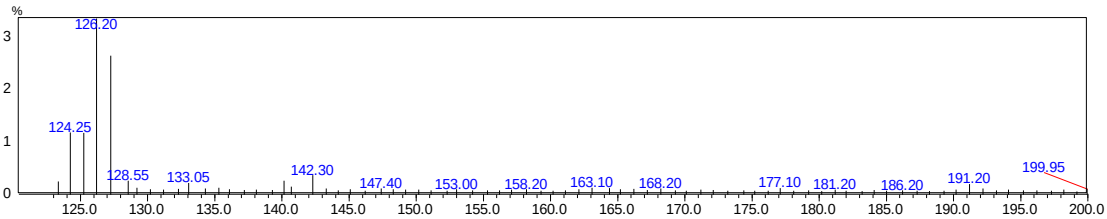

zoomed in version

MS analysis of cyclooctyl isobutyrate and its products

MS analysis of cyclooctyl isobutyrate RT 8.0 min (m^+/z = 198.05).

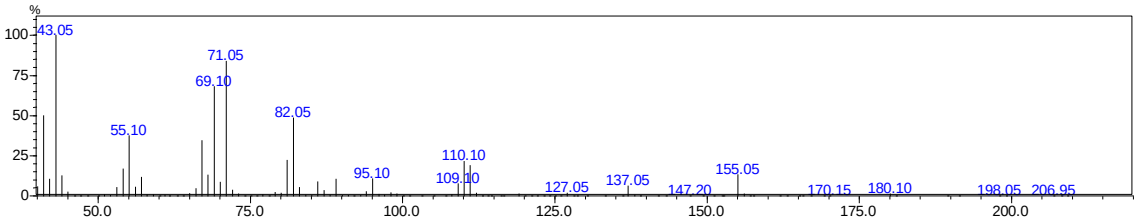

MS analysis of 5-hydroxycyclooctyl isobutyrate RT 10.2 min (m^+/z = 214.9).

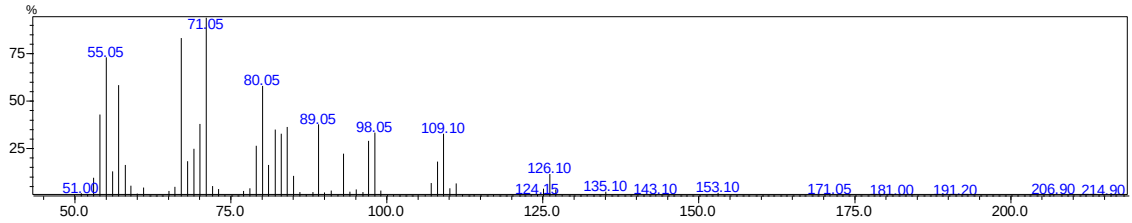

MS analysis of further oxidation product of cyclooctyl isobutyrate RT 10.1 min (m^+/z = 212.15).

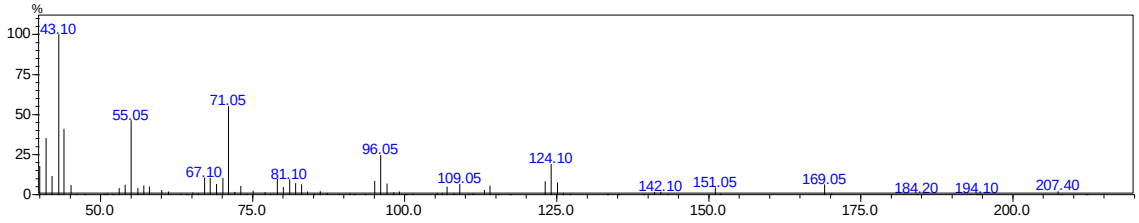

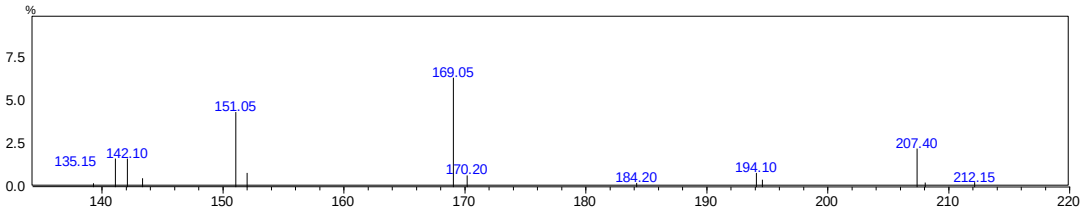

zoomed in version

MS analysis of cyclododecyl acetate and its products

MS analysis of cyclododecyl acetate RT 9.6 min GC-MS (m^+/z = 226.15; RT 5.6 min in GC).

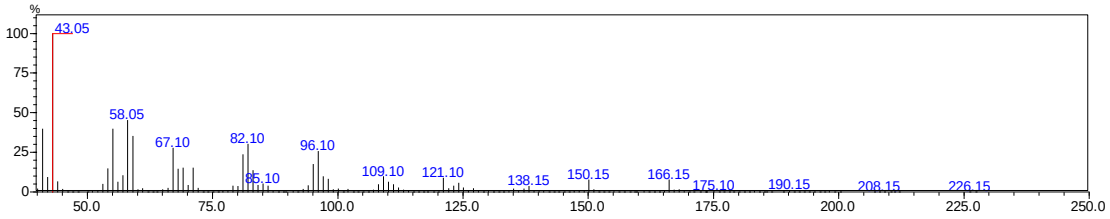

MS analysis of 7-hydroxycyclododecyl acetate (*cis*) RT 12.8 min GC-MS (m^+/z = 242.0; CYP101C1; RT 16.5 min in GC).

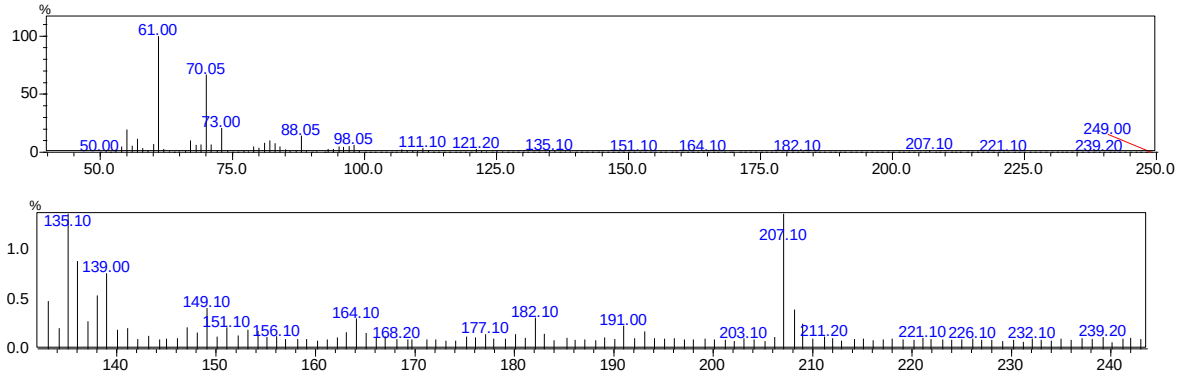

zoomed in version

MS analysis of 7-hydroxycyclododecyl acetate (*trans*) RT 13.6 min (m^+/z = 242.10; CYP101B1; RT 17.3 min in GC).

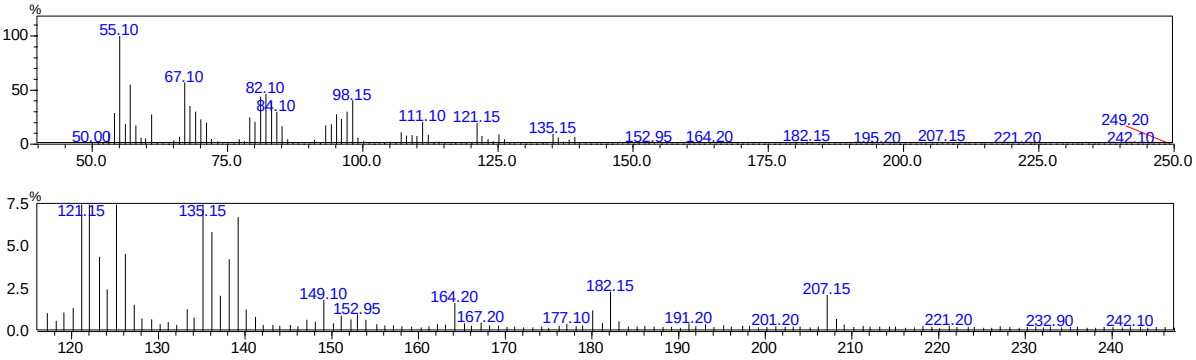

zoomed in version

MS analysis of 5-hydroxycyclododecyl acetate RT 12.4 min (RT 16.2 min GC).

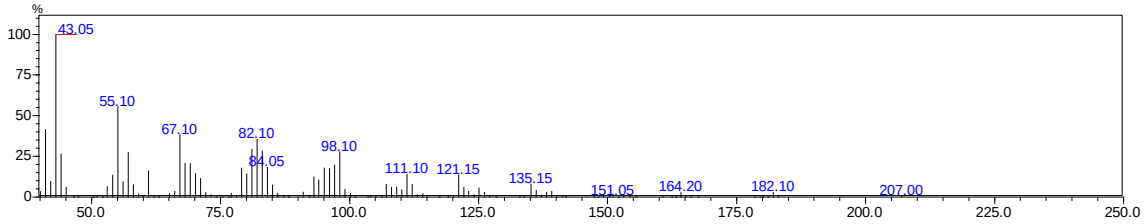

MS analysis of *α*-terpinyl acetate and its products

MS analysis of *α*-terpinyl acetate RT 12.6 min (m^+/z = 196.25).

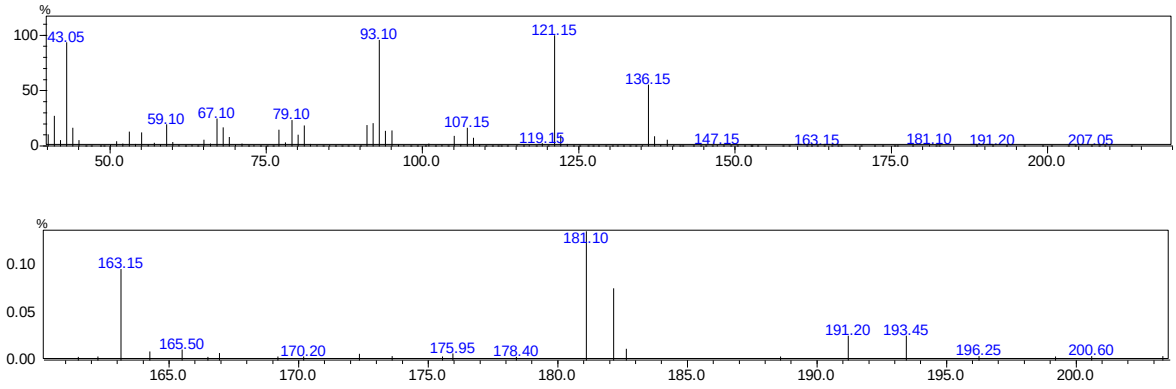

zoomed in version

MS analysis of 3-cyclohexene-1-methanol, 5-hydroxy-*α*,*α*,4-trimethyl-,*α*-acetate at RT 17.4 min (m^+/z = 212.10; CYP101C1).

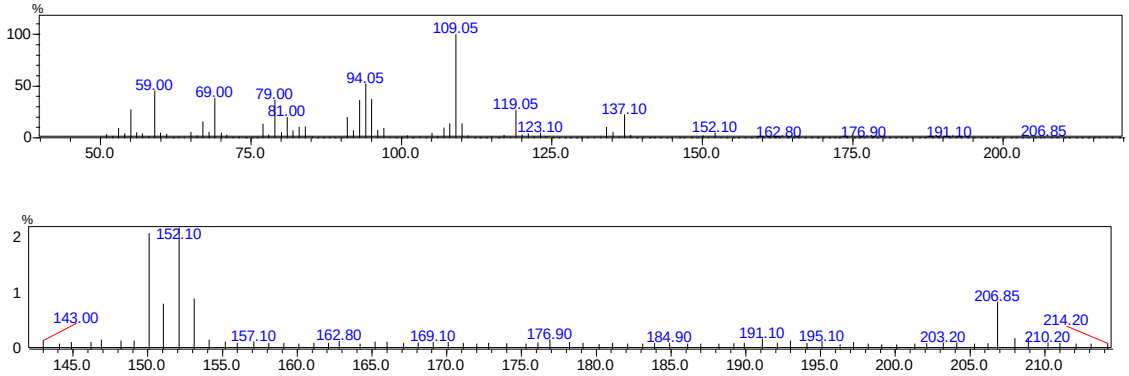

zoomed in version

MS analysis of 3-cyclohexene-1-methanol, 5-hydroxy-*α*,*α*,4-trimethyl-,*α*-acetate (other diastereomer) at RT 17.0 min (m^+/z = 212.10; CYP101C1).

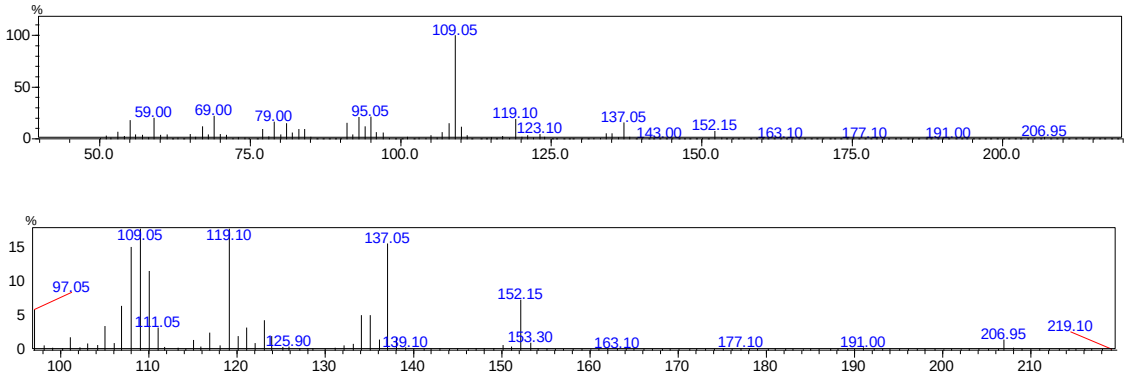

zoomed in version

MS analysis of 2-nonanone and its products

MS analysis of 2-nonanone RT 5.8 min (m^+/z = 142.05).

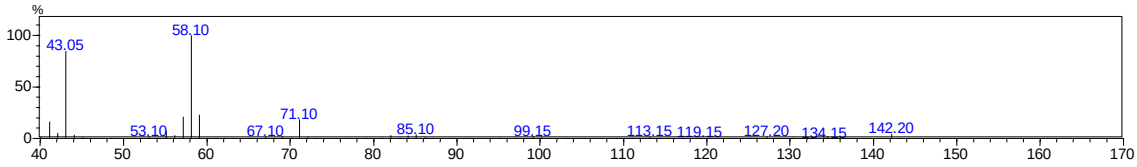

MS analysis of 3-hydroxy-2-nonanone RT 8.5 min (m^+/z = 158.65; CYP101C1).

Experimental m^+/z = 158.65, 115.15, 97.15, 85.10, 74.05, 71.15, 69.15, 55.10, 43.10.

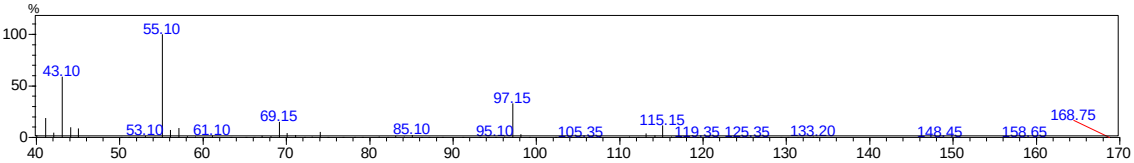

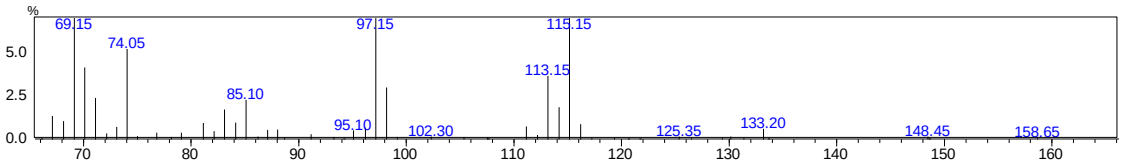

zoomed in version

MS analysis of 8-hydroxy-2-nonanone RT 11.25 min (m^+/z = 158.20; CYP101B1).

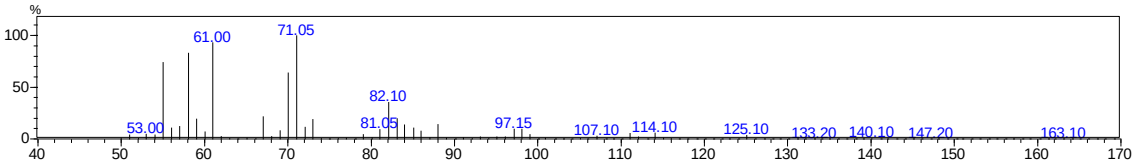

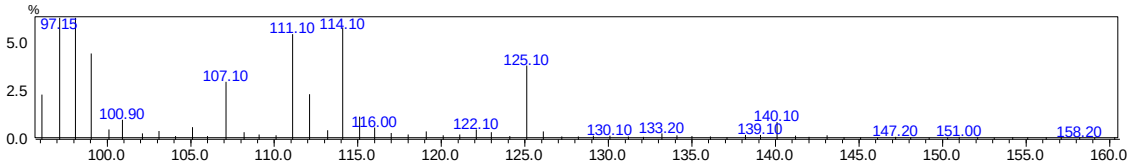

zoomed in version

MS analysis of 2-undecanone and its products

MS analysis of 2-undecanone RT 6.2 min (m^+/z = 170.25).

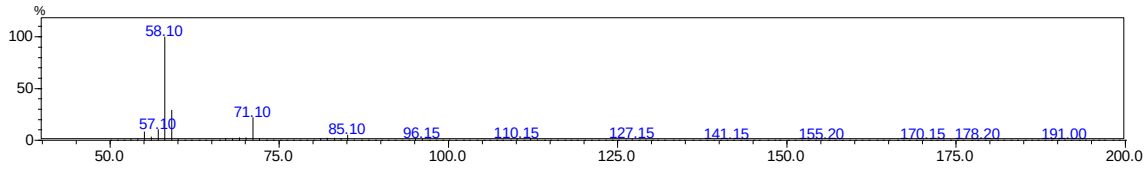

MS analysis of 3-hydroxy-2-undecanone RT 11.5 min (m^+/z = 186.25; CYP101C1) [219].

Experimental m^+/z = 186.25, 143.20, 125.25, 111.50, 97.15, 83.10, 69.15, 55.10, 43.05.

Reported [219] m^+/z = 186, 143, 125, 111, 97, 83, 69, 55 and 43.

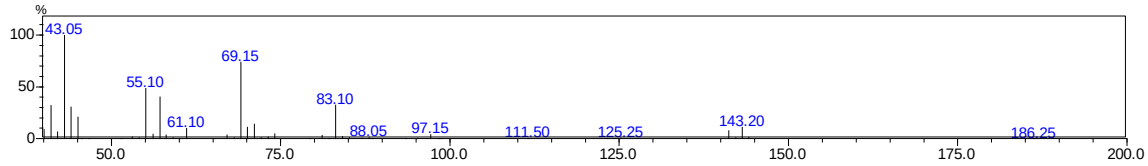

MS analysis of 8-hydroxy-2-undecanone RT 14.95 min (m^+/z = 186.20; CYP101B1).

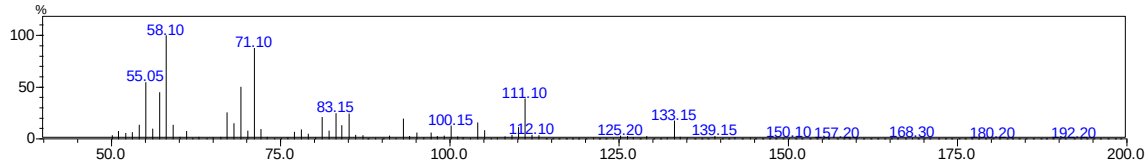

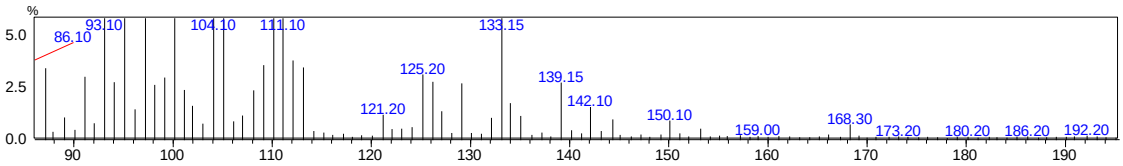

zoomed in version

MS analysis of a mixture of unidentified metabolites of CYP101B1 turnovers at RT 15.2 min and 15.9 min.

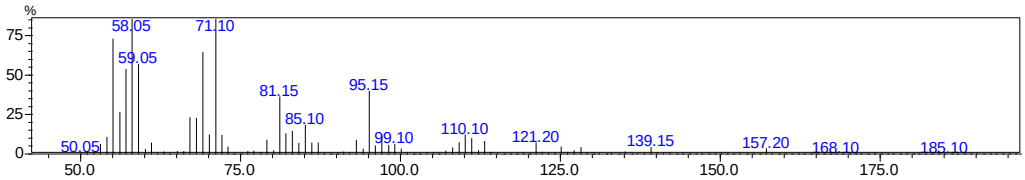

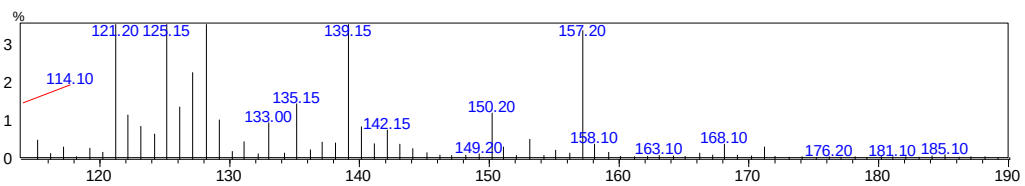

zoomed in version

MS analysis of citronellyl acetate and its product

MS analysis of citronellyl acetate RT 12.7 min (m^+/z = 198.40).

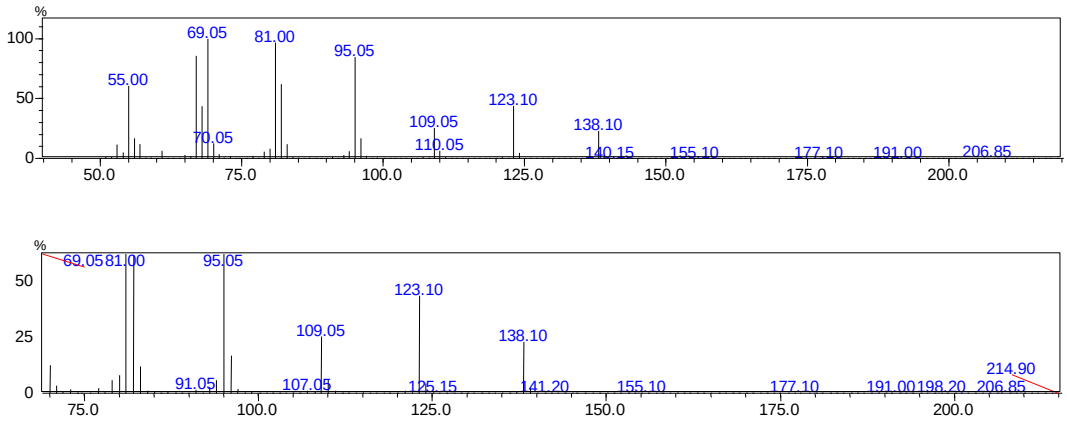

zoomed in version

MS analysis of citronellyl acetate epoxide RT 15.5 min (m^+/z = 214.60).

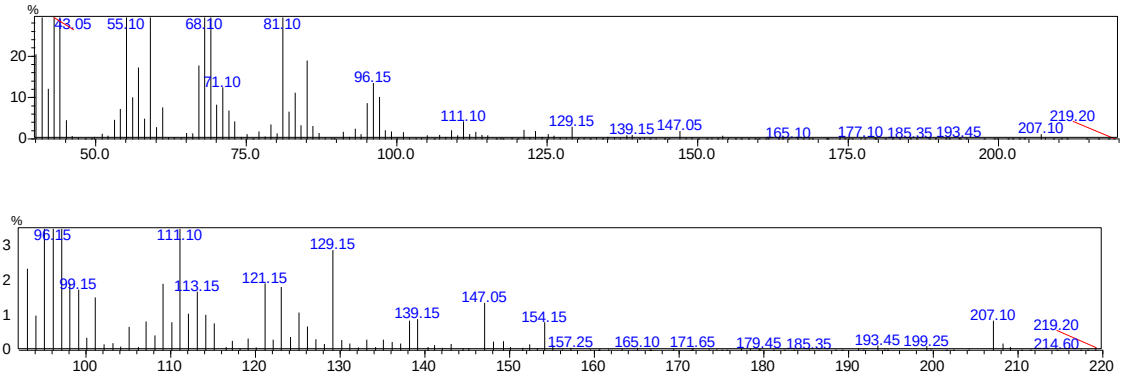

zoomed in version

MS analysis of citronellyl acetate epoxide synthesised using *m*CPBA RT 15.5 min (m^+/z = 214.35).

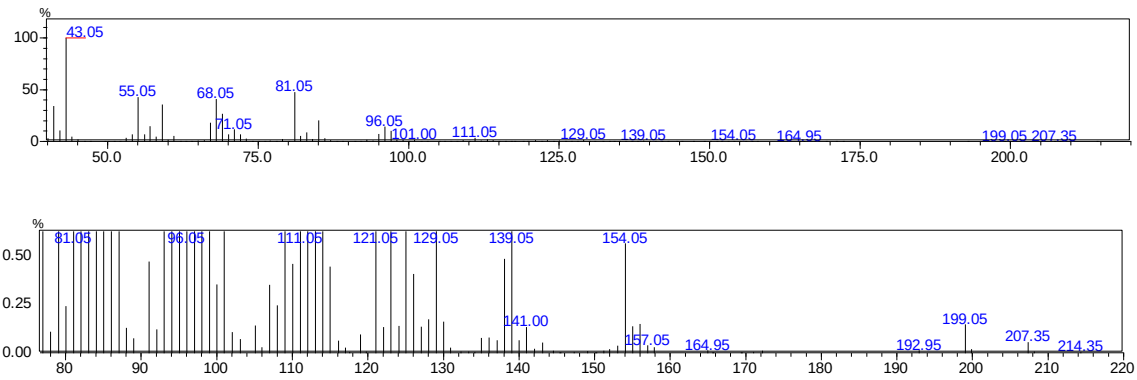

zoomed in version

MS analysis of linalyl acetate and its products

MS analysis of linalyl acetate RT 9.9 min (m^+/z = 196.0)

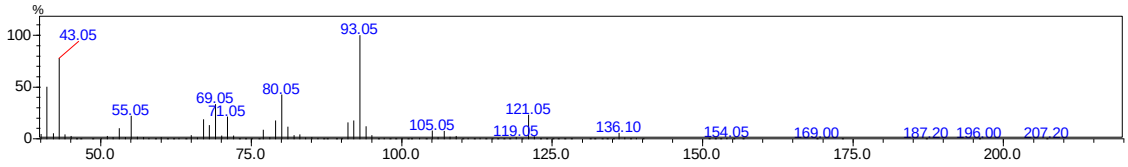

MS analysis of 6,7-epoxy-3,7-dimethyl-1-octen-3-yl acetate at RT 12.5 min (CYP101C1) [232].

Experimental m^+/z = 152.10, 147.10, 137.15, 121.15, 119.10, 109.10, 95.10, 94.10, 93.15, 81.10, 79.10, 69.15, 68.10, 67.10, 59.10, 55.10, 53.15 and 43.05.

Reported [232] m^+/z = 152.1(22), 137.1(17), 119.1(20), 109.1(45), 96.05(19), 95.1(23), 93.1(21), 91.1(28), 82.1(28), 81.1(100), 79.1(79), 77.1(24), 71.1(36), 69.1(22), 68.1(71), 67.1(83), 55.1(49), 53.1(32).

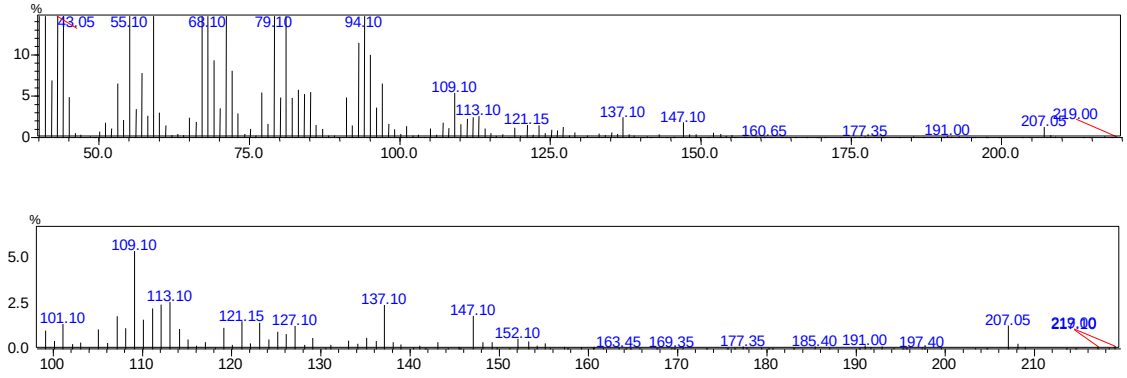

zoomed in version

MS analysis of 6,7-epoxy-3,7-dimethyl-1-octen-3-yl acetate synthesised using *m*CPBA (RT 12.5 min) [232].

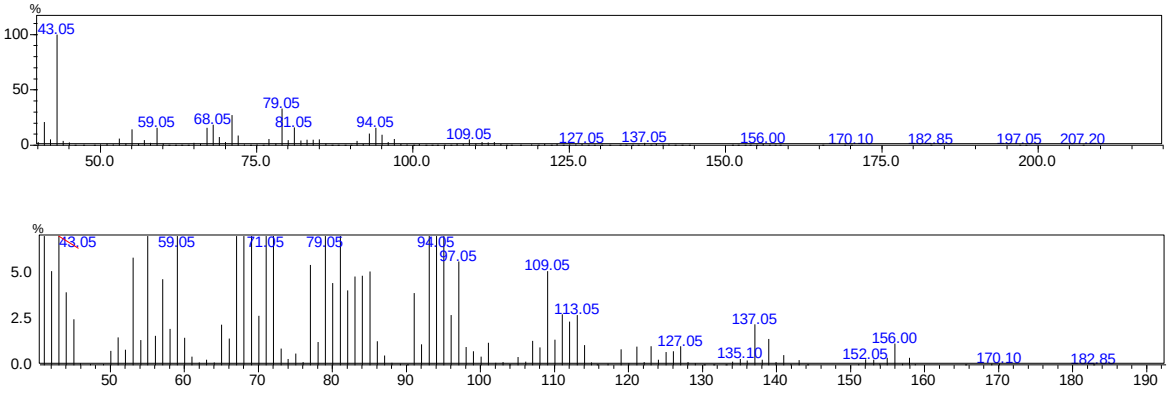

zoomed in version

MS analysis of 1,2-epoxy-3,7-dimethyl-6-octen-3-yl acetate at RT 12.6 min (CYP101C1).

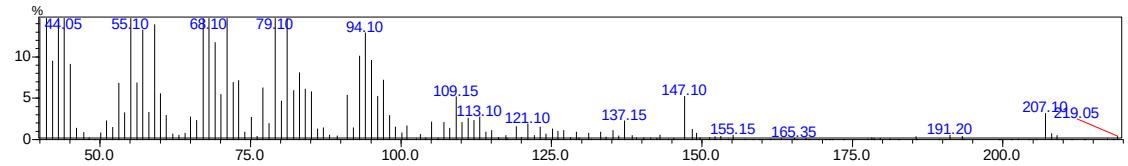

MS analysis of 1,2-Epoxy-3,7-dimethyl-6-octen-3-yl acetate synthesised using *m*CPBA (RT 12.6 min).

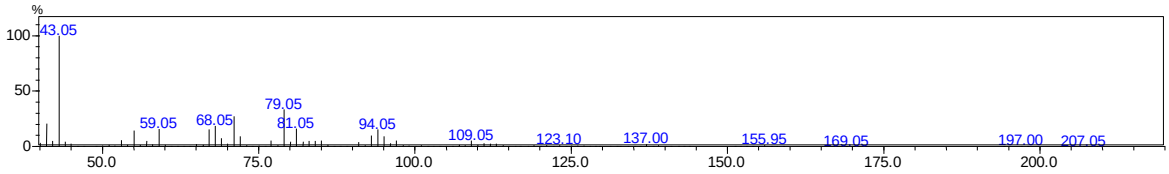

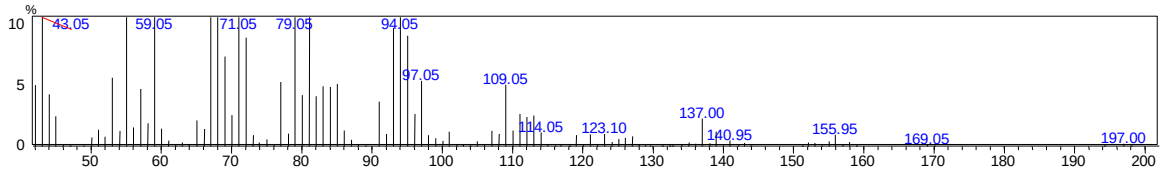

zoomed in version

NMR analysis of the generated products by the CYP101B1 and CYP101C1

NMR of mixture of 1,7-cyclododecanediol, 1,6-cyclododecanediol and 1,4-cyclododecanediol or diastereomer of 1,6-cyclododecanediol:

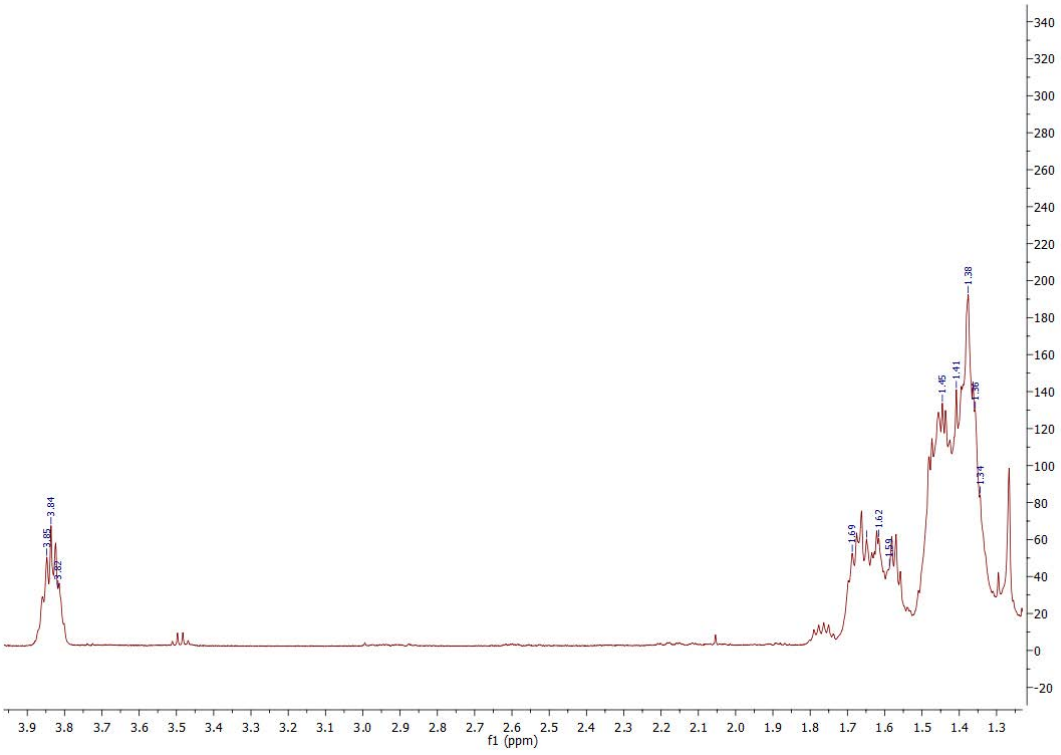

Figure B. 2 ^{1}H NMR spectrum of mixture of 1,7-cyclododecanediol, 1,6-cyclododecanediol and 1,4-cyclododecanediol or diastereomer of 1,6-cyclododecanediol (CYP101B1). The metabolites were assigned using carbon signal intensities.

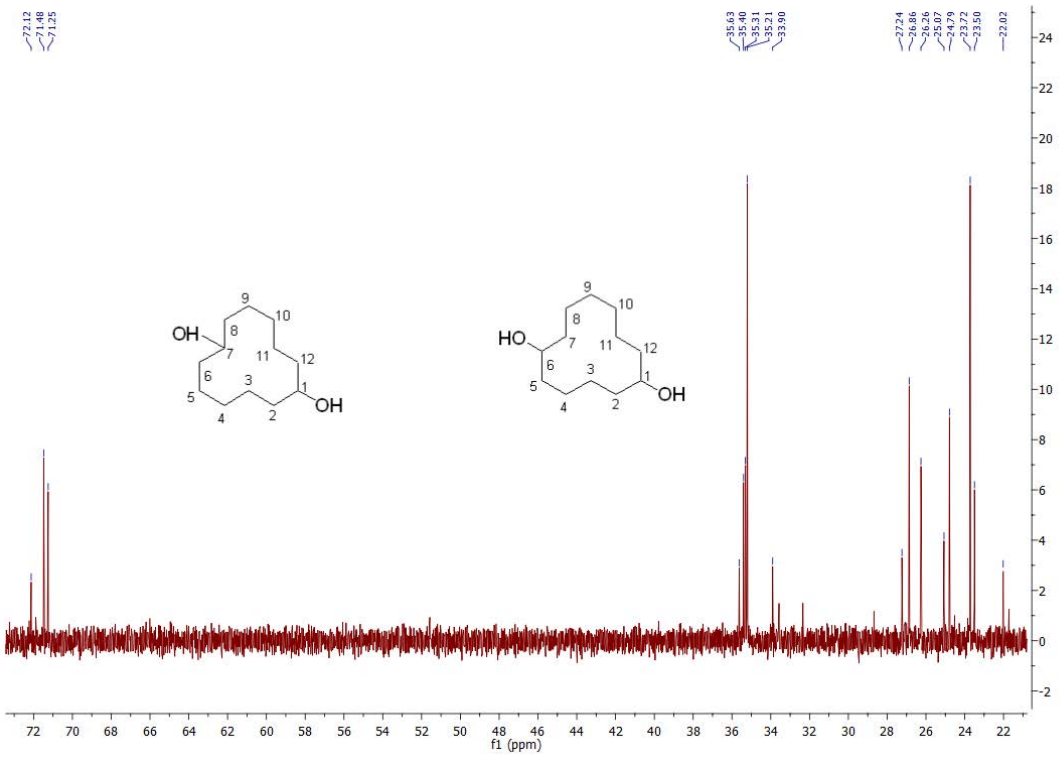

Figure B. 3 ^{13}C NMR spectrum of mixture of 1,7-cyclododecanediol, 1,6-cyclododecanediol and 1,4-cyclododecanediol or diastereomer of 1,6-cyclododecanediol (CYP101B1). The metabolites were assigned using the carbon signal intensities given Table 3. 2.

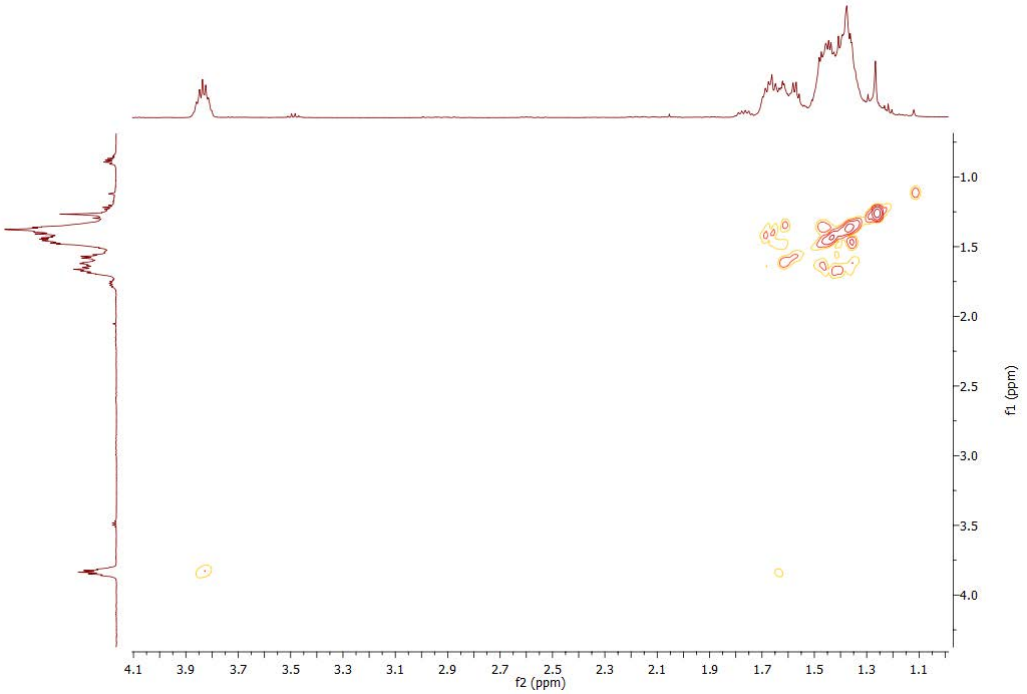

Figure B. 4 gCOSY NMR spectrum of a mixture of cyclododecanediol products (CYP101B1).

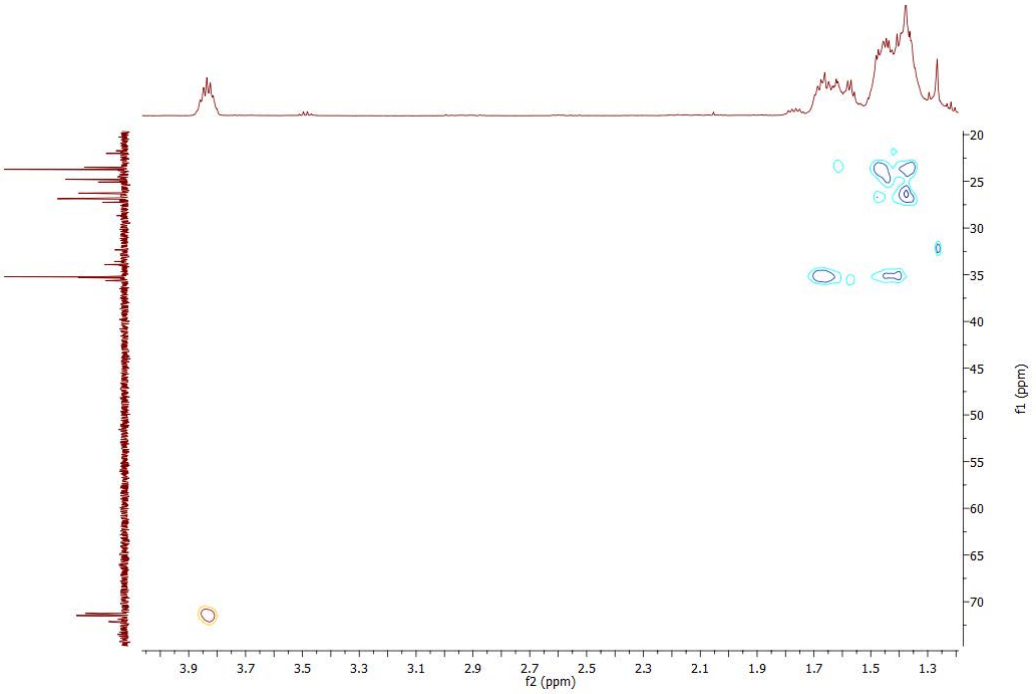

Figure B. 5 HSQC NMR spectrum of a mixture of cyclododecanediol products (CYP101B1).

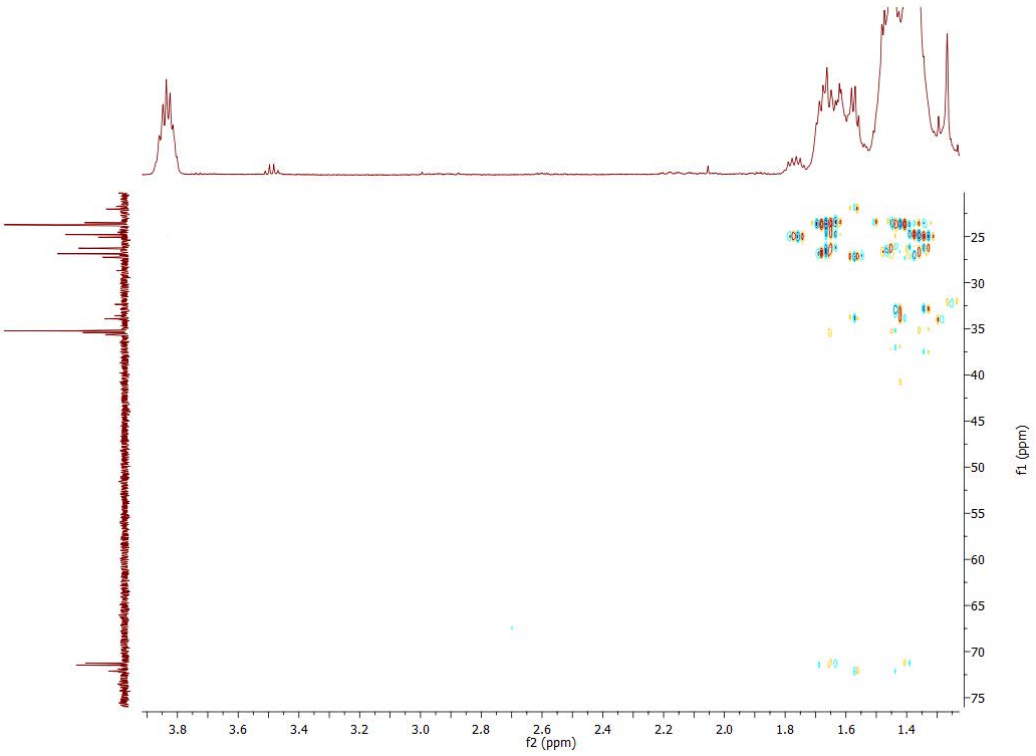

Figure B. 6 Zoomed in HMBC NMR spectrum of a mixture of cyclododecanediol products (CYP101B1).

Data for 2-hydroxycyclononanone [221]:

^{1}H NMR (500 MHz, $CDCl_3$) δ 4.28-4.21 (m, 1H, H2), 3.7-3.72 (m, 1H, O**H** (C2)), 2.83-2.73 (m, 1H, H9), 2.37-2.22 (m, 2H, H3 & H9), 2.12-2.01 (m, 1H, H3), 1.89-1.81 (m, 2H, H6 & H8), 1.68-1.57 (m, 3H, H4, H7 & H8), 1.49-1.42 (m, 3H, H4, H6 & H7), 1.39-1.32 (m, 1H, H5), 1.31-1.25 (m, 1H, H5).

^{13}C NMR (126 MHz, $CDCl_3$) δ 219.16 (C1), 79.86 (C2), 39.81 (C9), 31.16 (C3), 27.91 (C4), 27.42 (C6), 27.33 (C8), 26.64 (C5), 23.14 (C7).

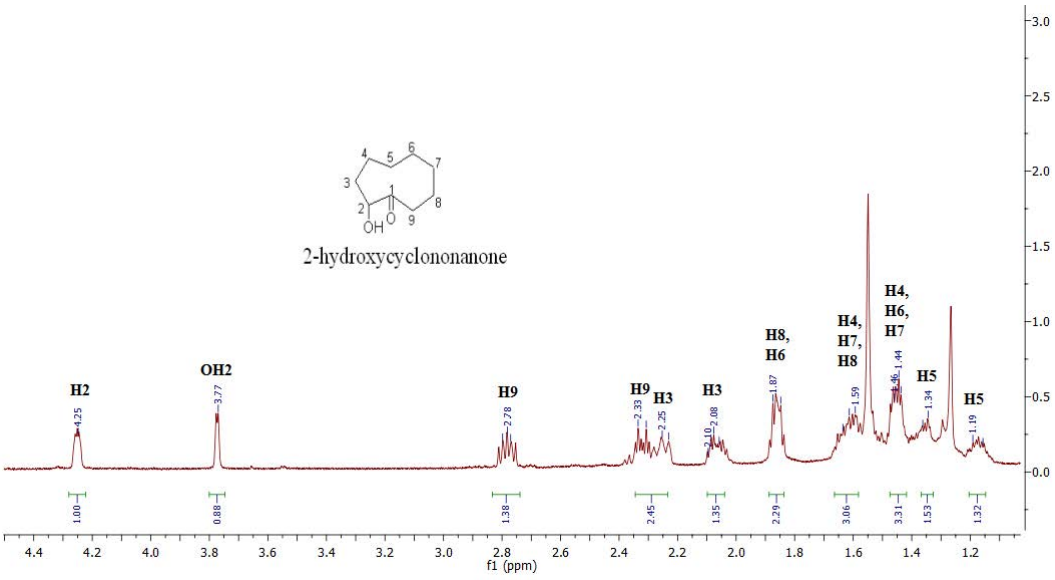

Figure B. 7 ^{1}H NMR spectrum of 2-hydroxycyclononanone (CYP101C1) [221].

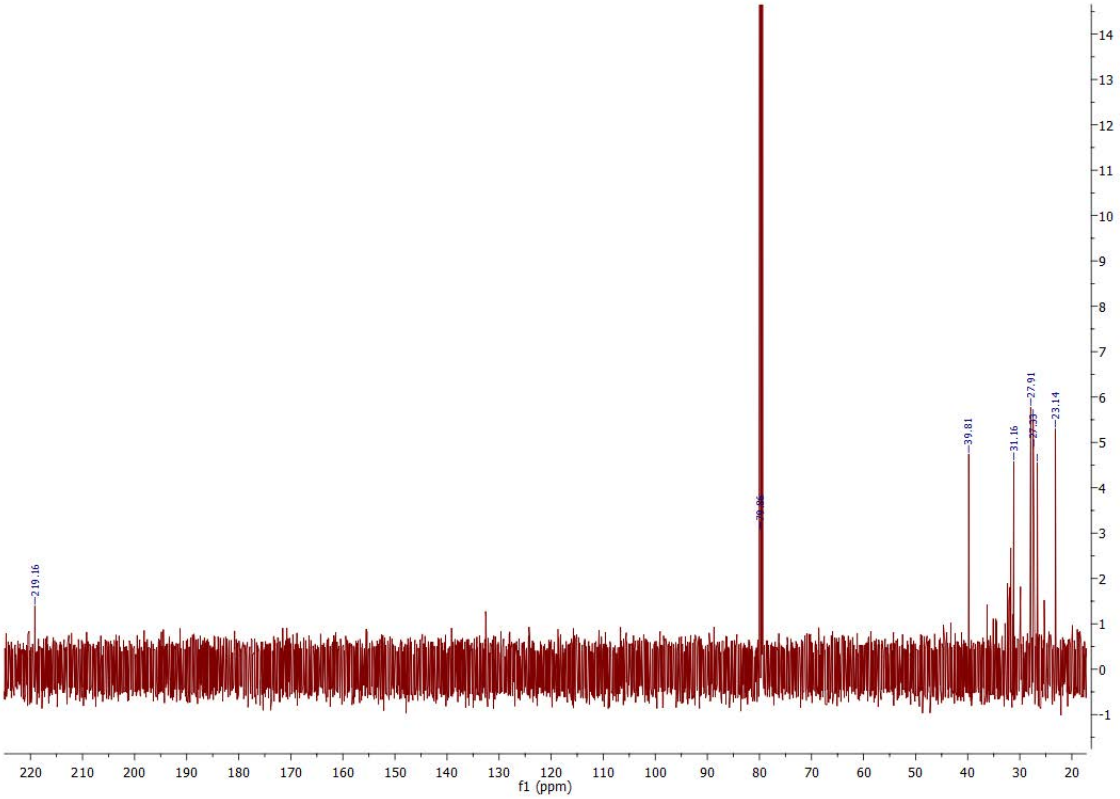

(a)

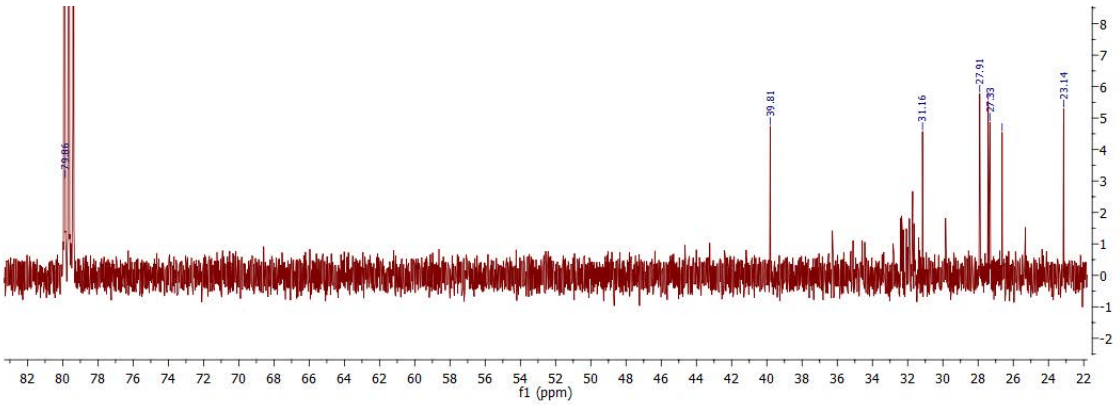

(b)

Figure B. 8 (a) ^{13}C NMR spectrum of 2-hydroxycyclononanone. **(b)** Zoomed in version of the 20 to 80 ppm region to highlight the carbon peaks.

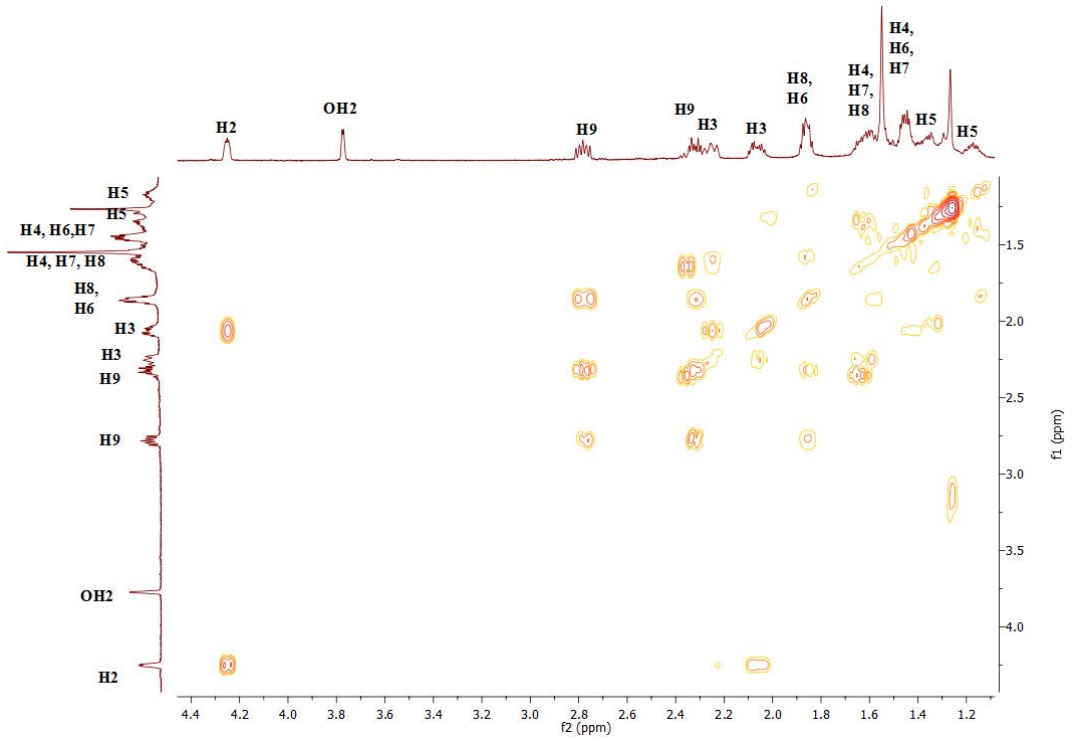

Figure B. 9 gCOSY NMR spectrum of 2-hydroxycyclononanone.

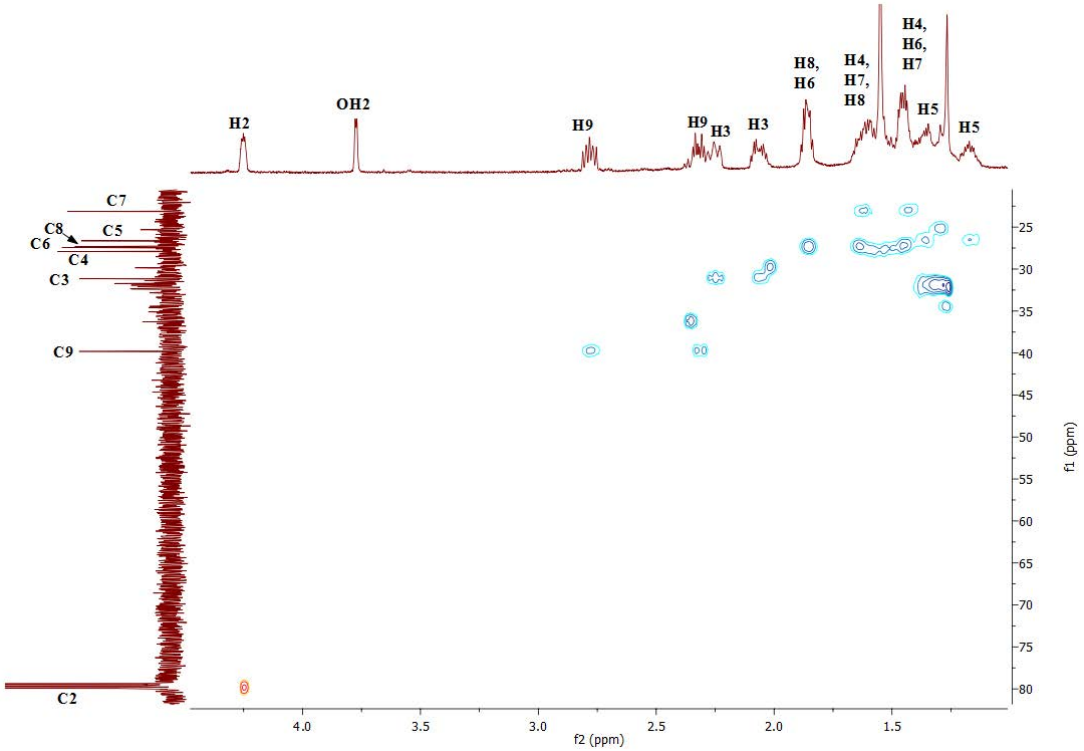

Figure B. 10 HSQC NMR spectrum of 2-hydroxycyclononanone.

NMR for 1-hydroxy-10-oxabicyclo[4.3.1]decane [217, 218]:

^{1}H NMR (600 MHz, $CDCl_3$) δ 4.15-4.02 (m, 1H, H5), 2.42 (br s, 1H, O**H**1 (C1)), 2.13-2.03 (m, 1H, H9), 1.95-1.85 (m, 3H, H2, H3 & H8), 1.82-1.70 (m, 4H, H3, H4, H6 & H7), 1.70-1.61 (m, 3H, H6, H7 & H9), 1.55-1.46 (m, 2H, H2 & H8), 1.40-1.34 (m, 1H, H4).

^{13}C NMR (151 MHz, $CDCl_3$) δ 100.36 (C1), 75.11 (C5), 39.22 (C2), 38.48 (C9), 32.85 (C6), 30.26 (C4), 23.92 (C7), 22.60 (C8), 20.21 (C3).

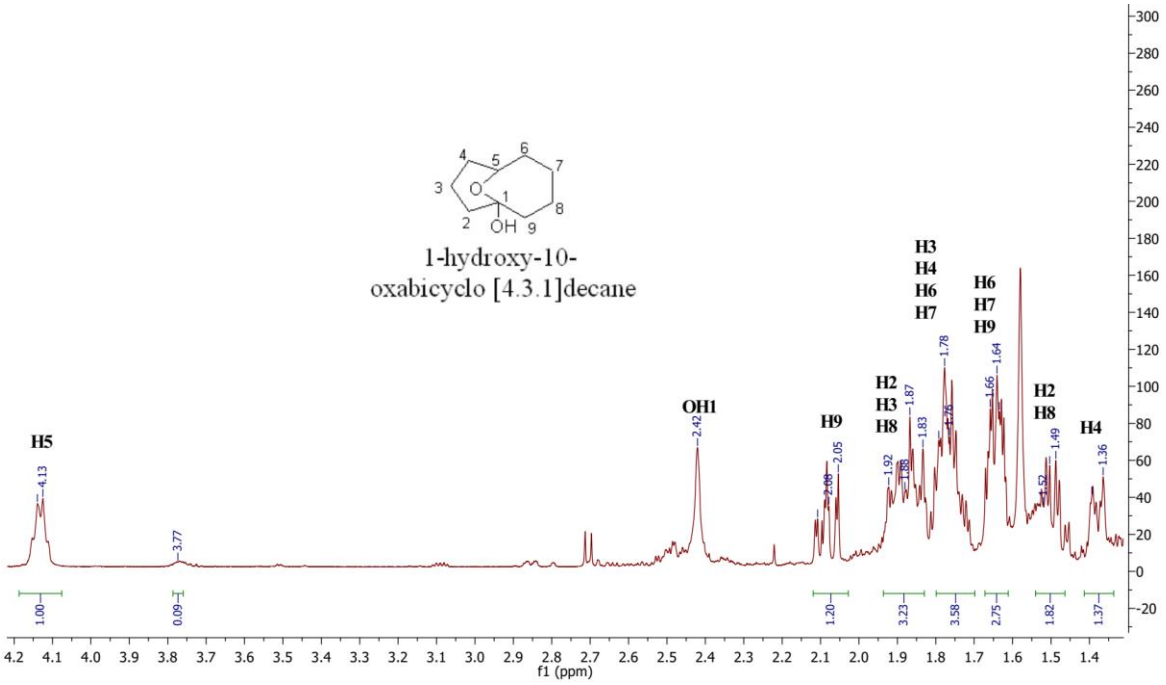

Figure B. 11 ^{1}H NMR spectrum of 1-hydroxy-10-oxabicyclo[4.3.1]decane (cyclononanone; CYP101B1) [217, 218].

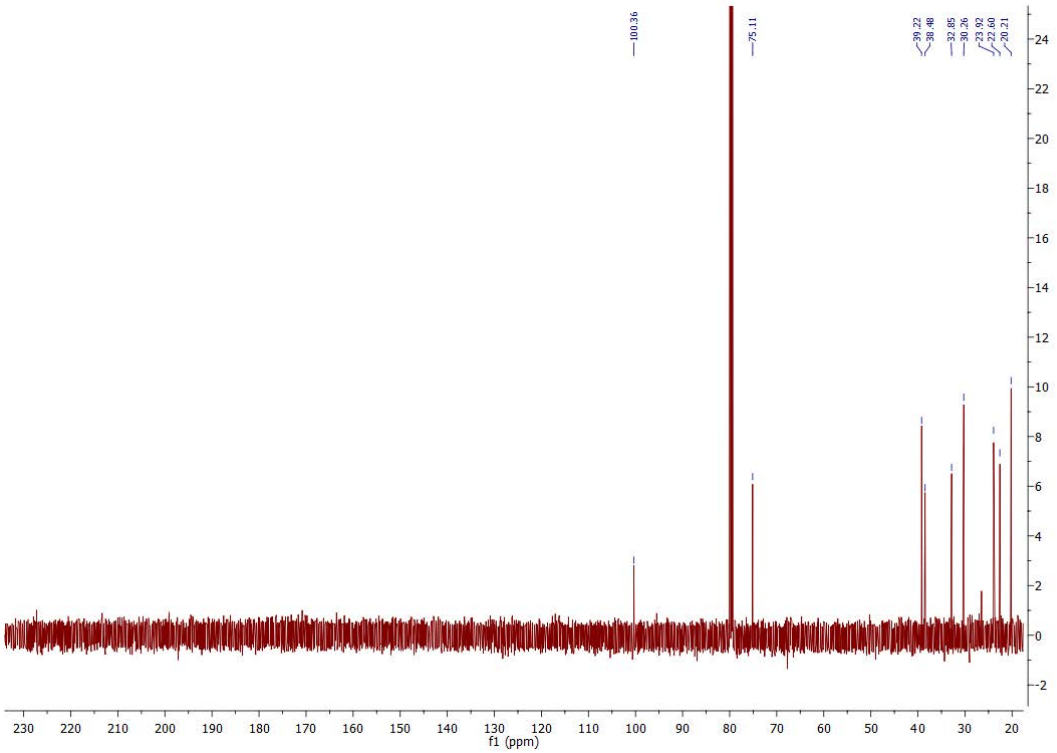

Figure B. 12 ^{13}C NMR spectrum of 1-hydroxy-10-oxabicyclo[4.3.1]decane (cyclononanone; CYP101B1) [217, 218].

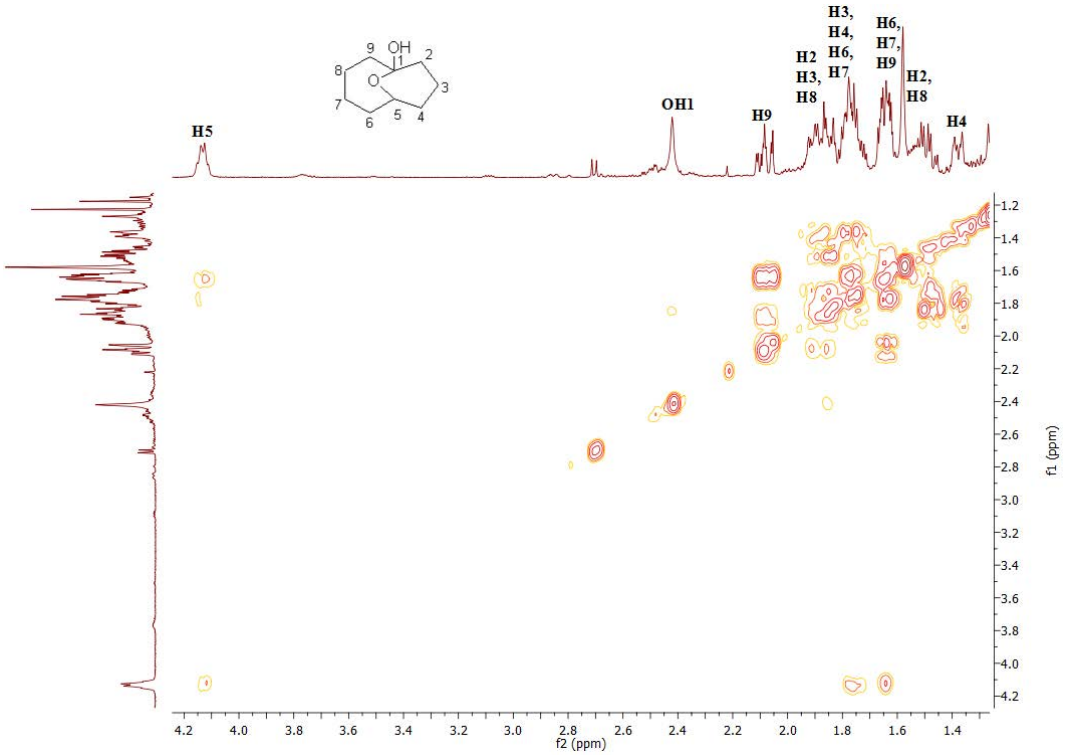

Figure B. 13 gCOSY NMR spectrum of 1-hydroxy-10-oxabicyclo[4.3.1]decane (cyclononanone; CYP101B1).

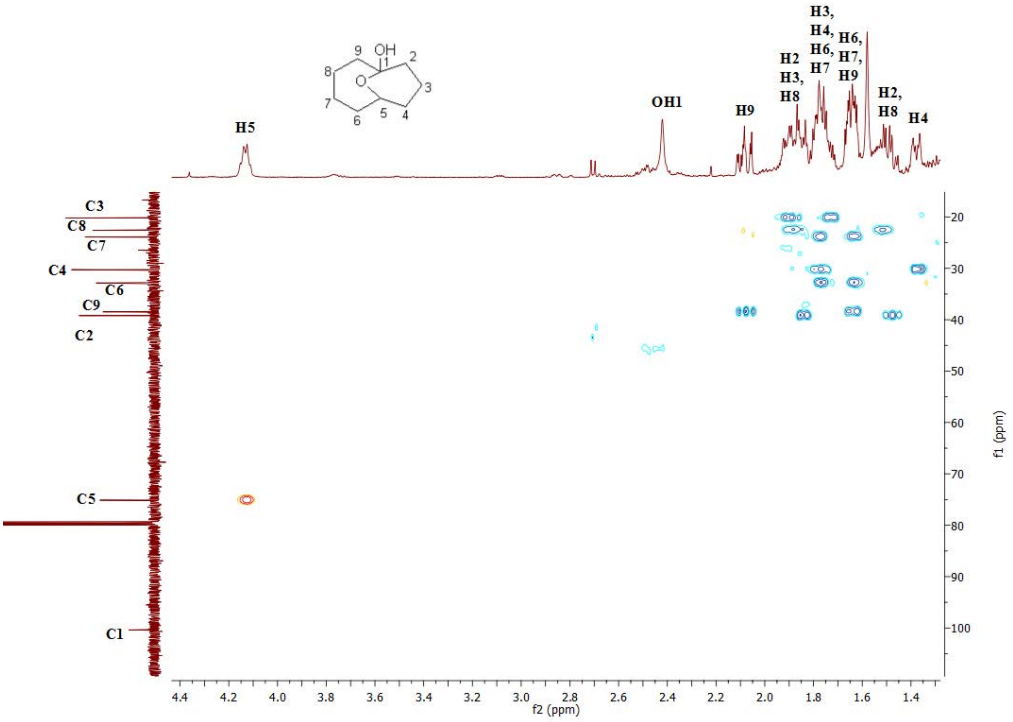

Figure B. 14 HSQC NMR spectrum of 1-hydroxy-10-oxabicyclo[4.3.1]decane (cyclononanone; CYP101B1).

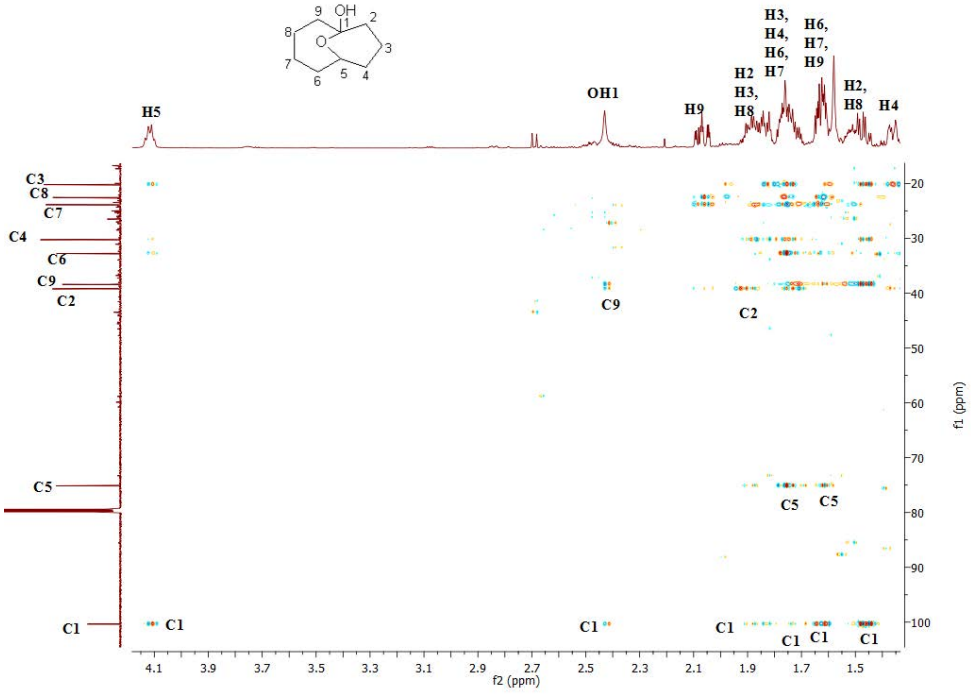

Figure B. 15 Zoomed in HMBC NMR spectrum of 1-hydroxy-10-oxabicyclo[4.3.1]decane to highlight the C-H interactions in 18 to 108 ppm region (cyclononanone; CYP101B1).

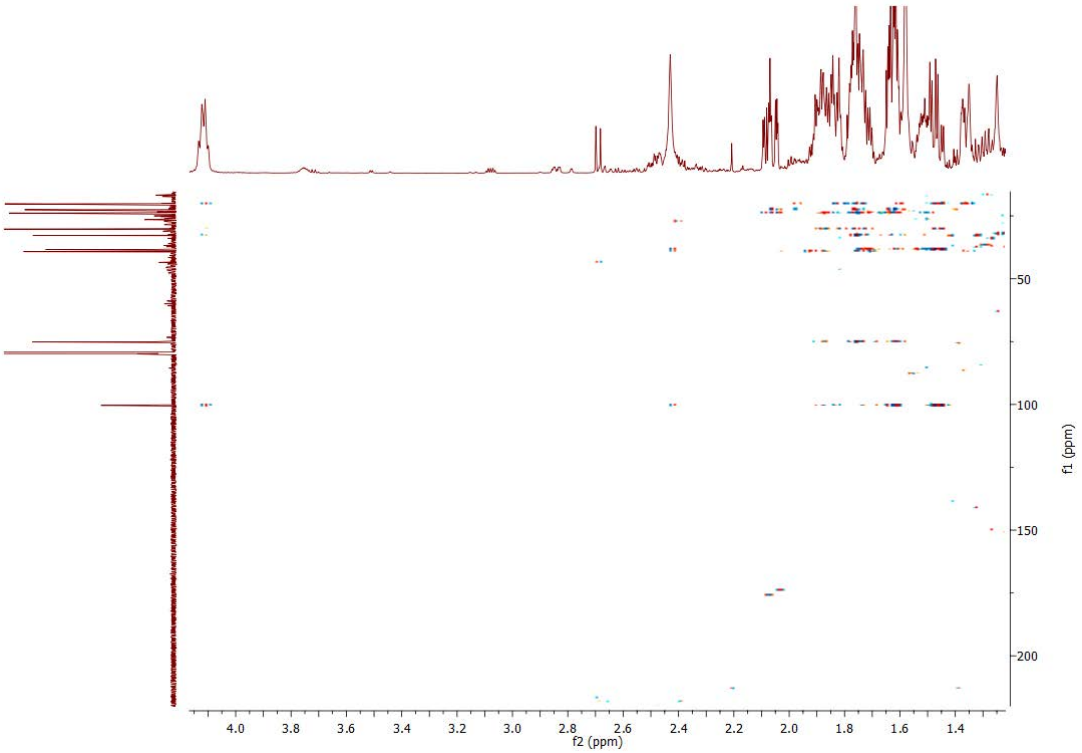

Figure B. 16 HMBC NMR spectrum of 1-hydroxy-10-oxabicyclo[4.3.1]decane (cyclononanone; CYP101B1).

Data for 2-hydroxycyclodecanone [219]:

^{1}H NMR (500 MHz, $CDCl_3$) δ 4.29-4.17 (m, 1H, H2), 3.88-3.76 (m, 1H, O**H**2 (C2)), 3.24-3.11 (m, 1H, H10), 2.32-2.06 (m, 4H, 2xH3, H9, H10), 1.74-1.59 (m, 3H, H5, H6 & H9), 1.55-1.47 (m, 1H, H4), 1.46-1.31 (m, 6H, H4, H5, H6, 2xH7 & H8), 1.12-0.99 (m, 1H, H8).

^{13}C NMR (126 MHz, $CDCl_3$) δ 216.62 (C1), 79.11 (C2), 37.67 (C10), 31.73 (C3), 28.84 (C4), 27.55 (C8), 25.73 (C7), 25.45 (C5), 25.37 (C9), 23.12 (C6).

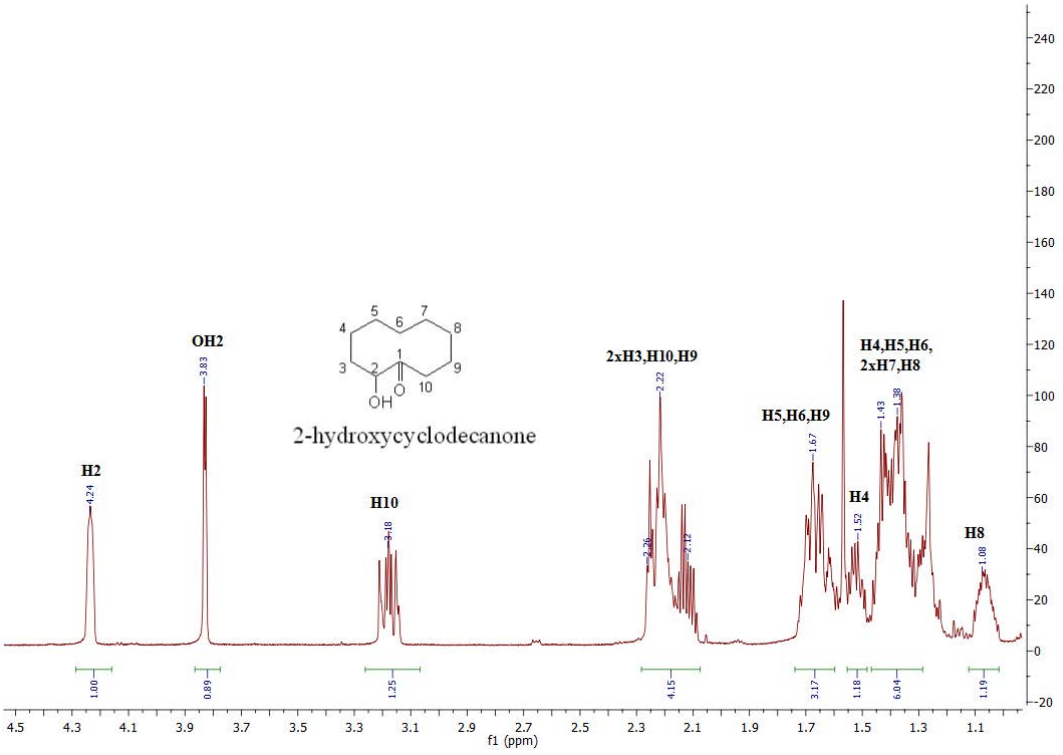

Figure B. 17 ^{1}H NMR spectrum of 2-hydroxycyclodecanone (CYP101C1).

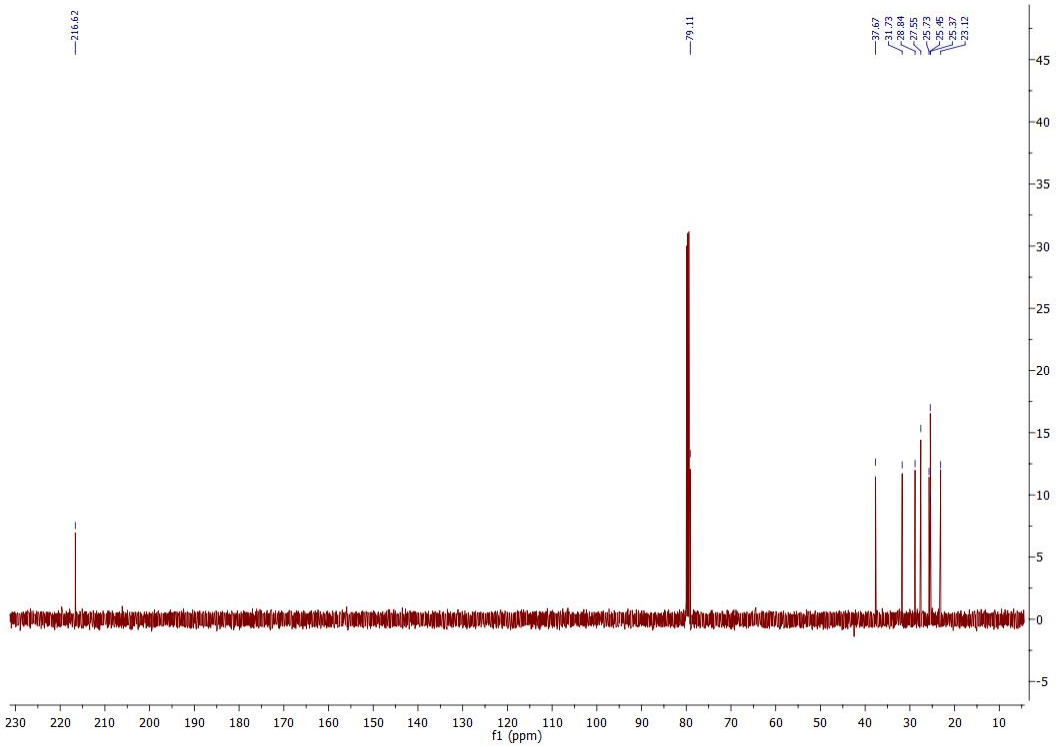

Figure B. 18 ^{13}C NMR spectrum of 2-hydroxycyclodecanone (CYP101C1).

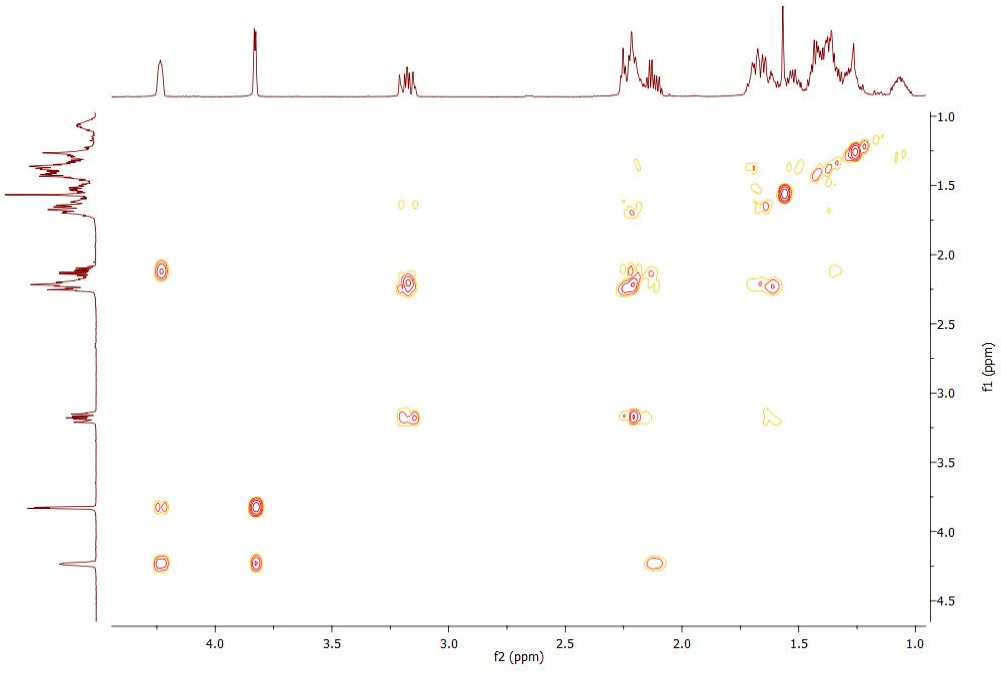

Figure B. 19 gCOSY NMR spectrum of 2-hydroxycyclodecanone (CYP101C1).

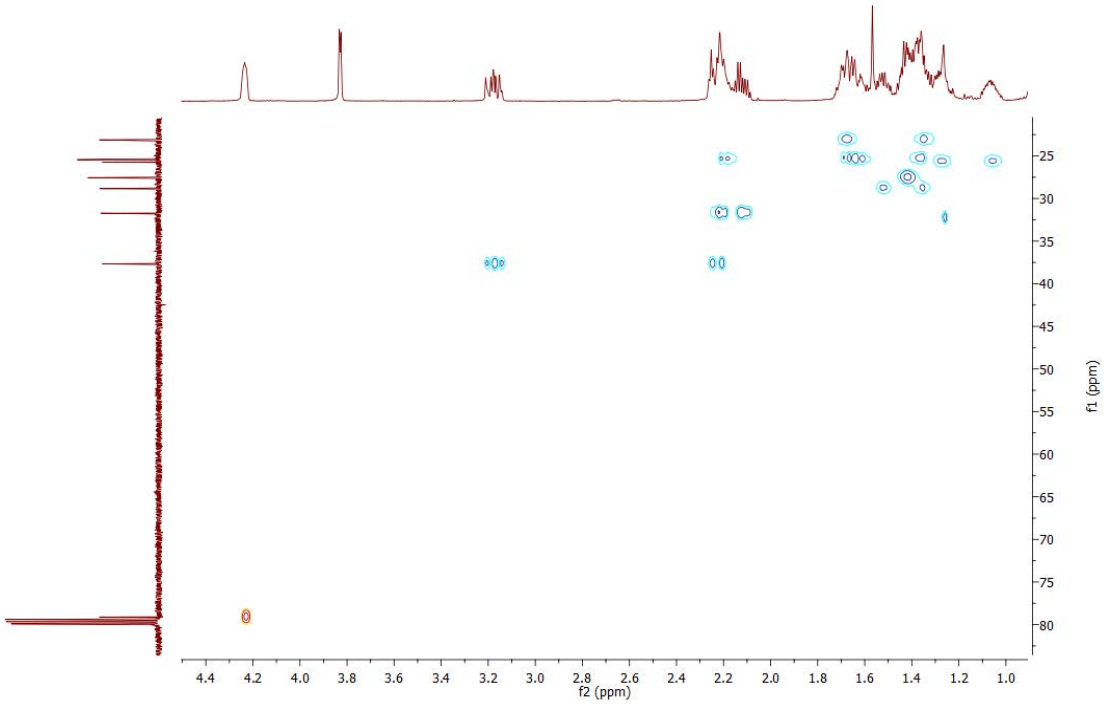

Figure B. 20 HSQC NMR spectrum of 2-hydroxycyclodecanone (CYP101C1).

NMR for 1-oxabicyclo[5.3.1]undecan-1-ol [218] :

^{1}H NMR (500 MHz, $CDCl_3$) δ 4.07-4.97 (m, 1H, H5), 2.50-2.43 (m, 1H, O**H1**(C1)), 1.92-1.72 (m, 8H, H2, H3, H6, H7, H8, H9 & 2xH10), 1.71-1.61 (m, 4H, H2, H4, H7 & H8), 1.60-1.47 (m, 3H, H2, H4 & H9), 1.40-1.33 (m, 1H, H3), 1.2-1.15 (m, 1H, H6).

^{13}C NMR (126 MHz, $CDCl_3$) δ 98.85 (C1), 76.33 (C5), 40.33 (C2), 39.95 (C10), 35.24 (C6), 34.74 (C4), 30.48 (C3), 27.70 (C9), 24.42 (C8), 19.94 (C7).

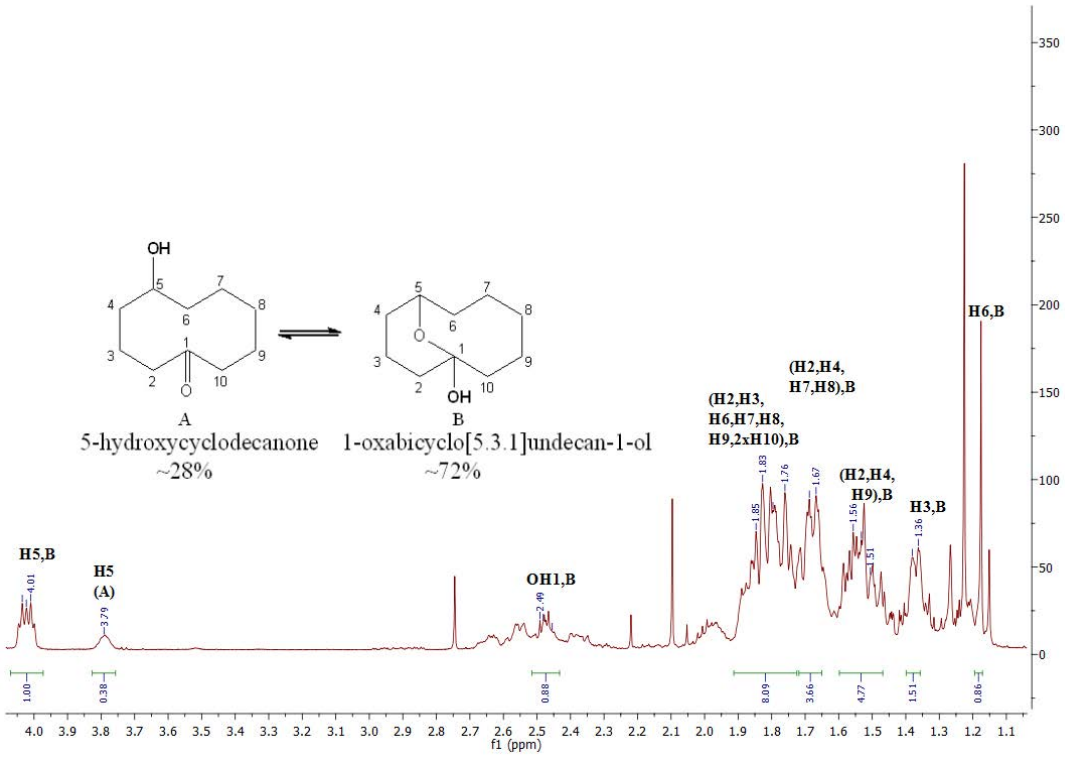

Figure B. 21 ^{1}H NMR spectrum of 1-oxabicyclo[5.3.1]undecan-1-ol (72%; B; CYP101B1). The other minor product 5-hydroxycyclodecanone (A) was also present (28%) in the NMR. The H5 (A) peak of 5-hydroxycyclodecanone at 3.79 ppm was observed (Table 3. 4) [218].

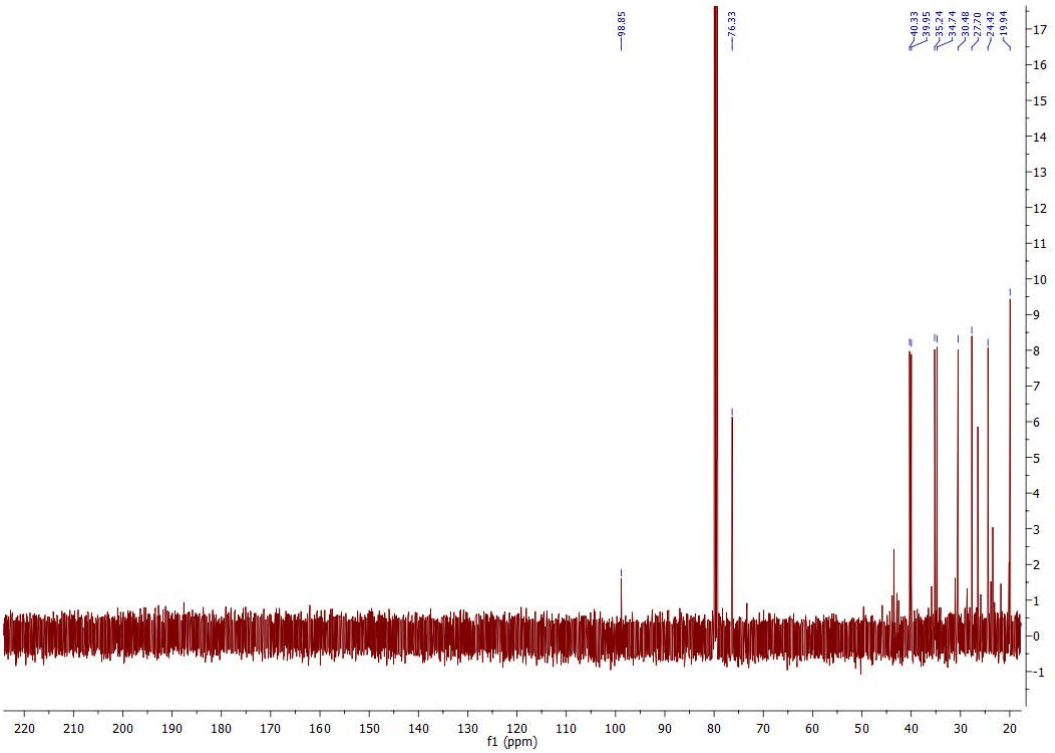

Figure B. 22 ^{13}C NMR spectrum of 1-oxabicyclo[5.3.1]undecan-1-ol (CYP101B1) [218].

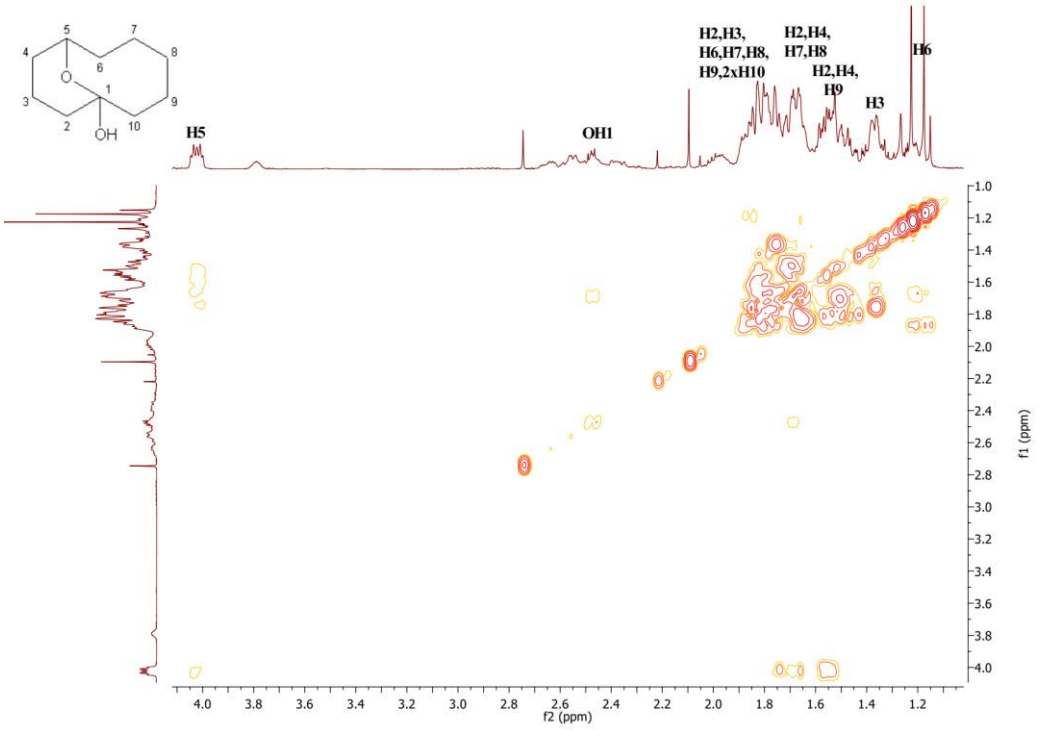

Figure B. 23 gCOSY NMR spectrum of 1-oxabicyclo[5.3.1]undecan-1-ol (CYP101B1).

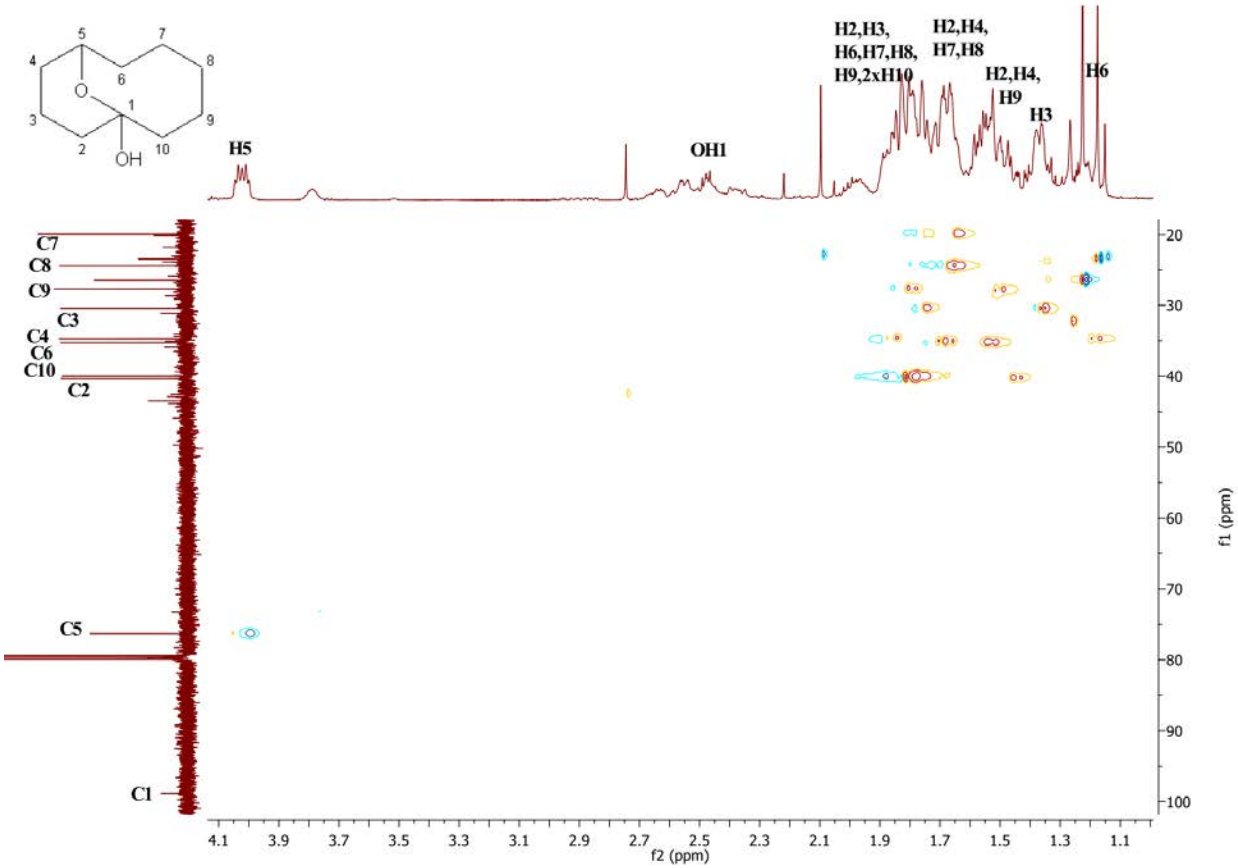

Figure B. 24 HSQC NMR spectrum of 1-oxabicyclo[5.3.1]undecan-1-ol (CYP101B1).

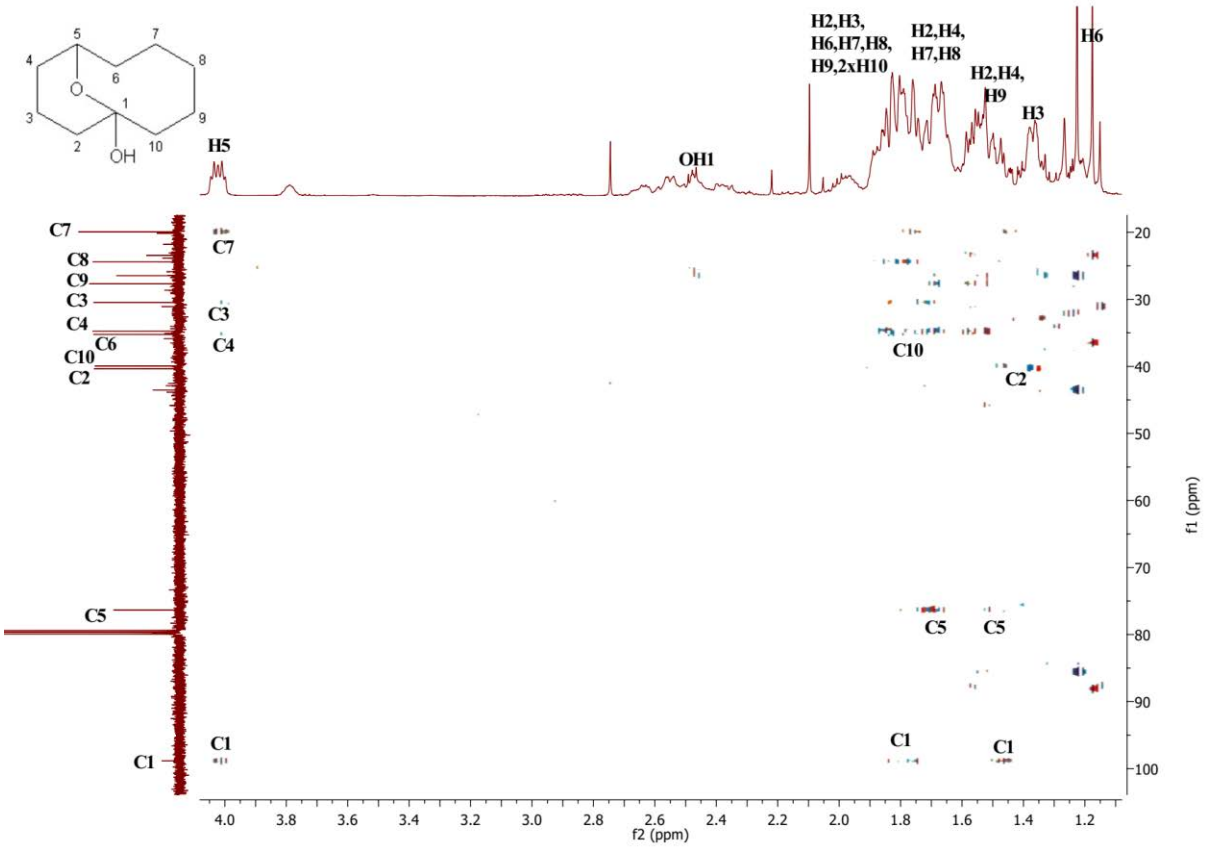

Figure B. 25 Zoomed in (18 ppm to 104 ppm region) version of HMBC NMR spectrum of 1-oxabicyclo[5.3.1]undecan-1-ol to highlight the C-H interactions in this region (CYP101B1). The product was confirmed oxabicycloalkanols as ^{13}C and HMBC NMR had no C=O peak. Instead of C=O peak, a characteristic signal of C1 was observed at 98.85 ppm which displayed a correlation with H5 (3.97-4.07 ppm) in HMBC NMR. The product was further confirmed by comparing the NMR spectrum with the reported NMR in the literature [218].

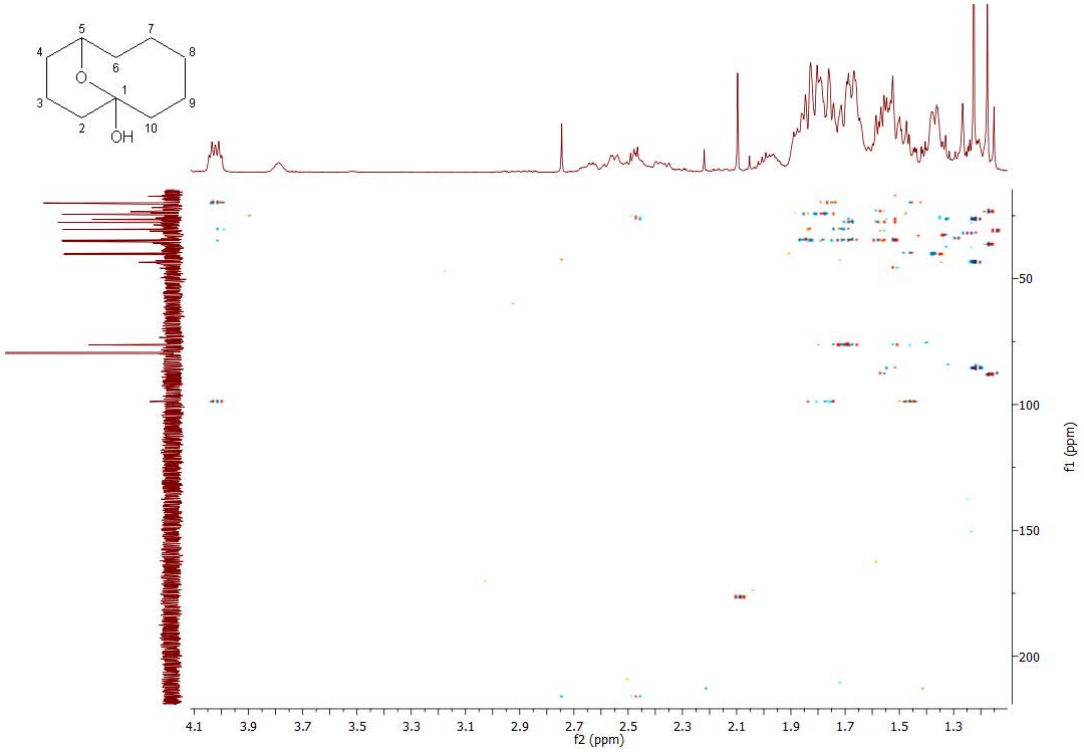

Figure B. 26 HMBC NMR spectrum of 1-oxabicyclo[5.3.1]undecan-1-ol (CYP101B1).

NMR for 1-oxabicyclo[6.3.1]undecan-1-ol and and 6-hydroxycyclodecanone mixture [218]:

^{1}H NMR (600 MHz, $CDCl_3$) δ 4.13-4.01 (m, 1H, H6; B), 3.9-3.79 (m, 1H, H6; A), 2.70-1.59 (m, 2H, 2xH2; A), 2.41-2.33 (m, 2H, 2xH10; A), 2.01-1.87 (m, 4H, 2xH2; B & 2xH3; A), 1.80-1.72 (m, 8H, 2xH5; B, 2xH7; B, 2xH10; B & 2xH9; A), 1.7-1.61 (m, 4H, 2xH4; B & 2xH8; B), 1.63-1.46 (m, 12H, 2xH3; B, 2xH9; B, 2xH4; A, 2xH5; A, 2xH7; A & 2xH8; A)

^{13}C NMR (151 MHz, $CDCl_3$) δ 217.20 (C1; A), 105.08 (C1; B), 78.08 (C6; B), 72.20 (C6; A), 44.54 (C2 & C10; A), 43.18 (C2 & C10; B), 36.47 (C5 & C7; A&B), 27.57 (C4 & C8; B), 25.93 (C3 & C9; A), 25.36 (C4 & C8; A, C3 & C9; B).

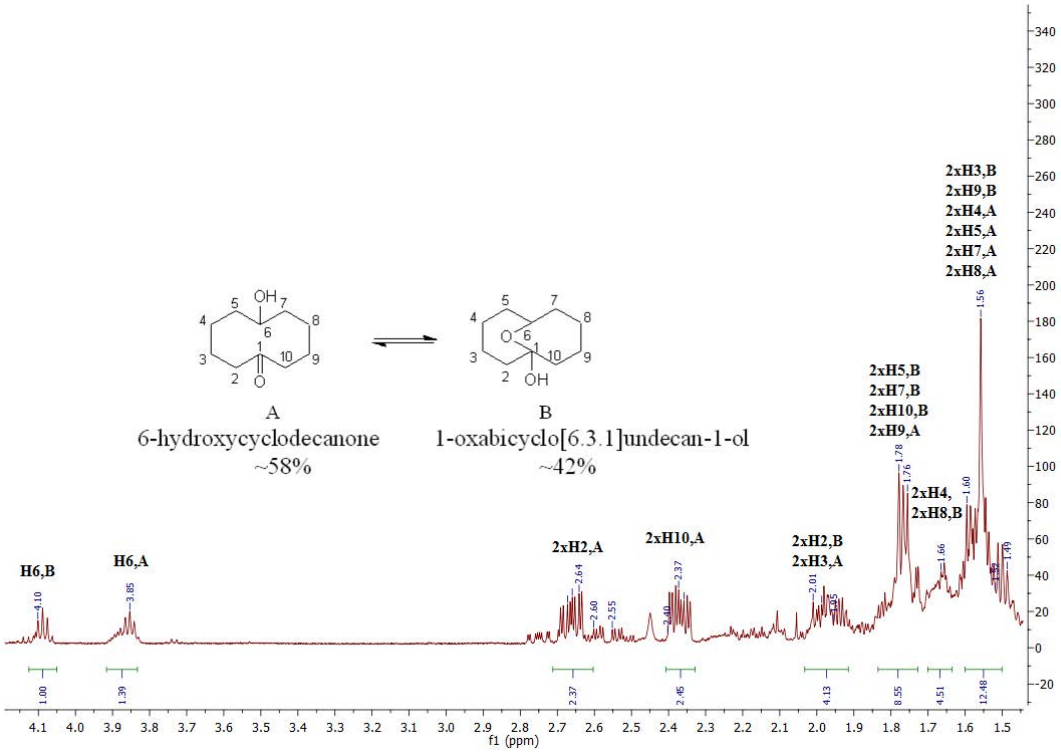

Figure B. 27 ^{1}H NMR spectrum of 1-oxabicyclo[6.3.1]undecan-1-ol and 6-hydroxycyclodecanone mixture (CYP101B1). The H6; B and H6; A was confirmed by comparing the reported ^{1}H NMR in literature (Table 3. 4) [218].

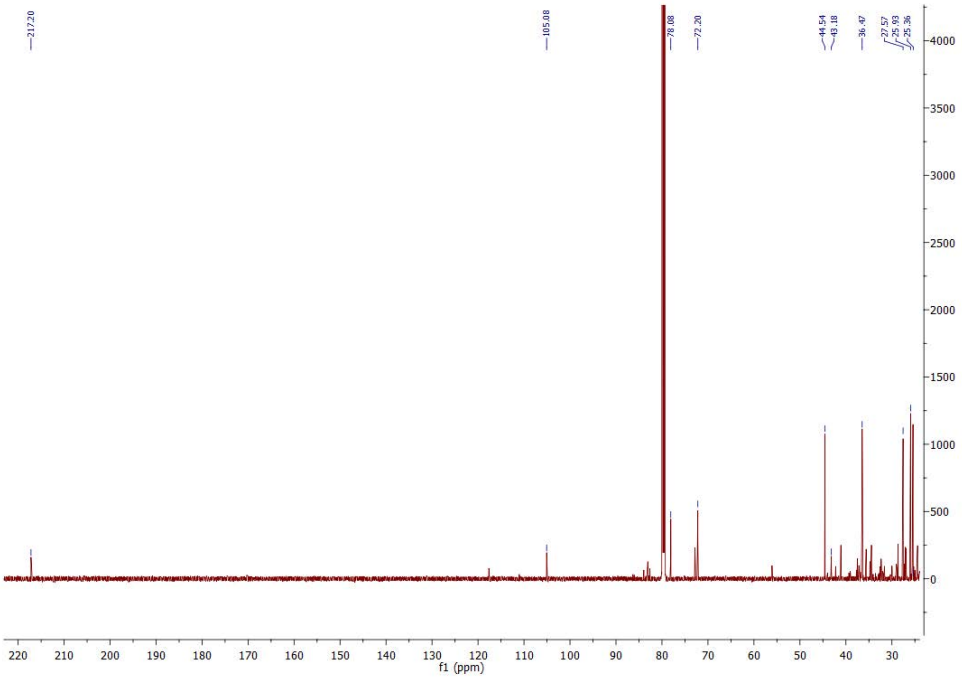

(a)

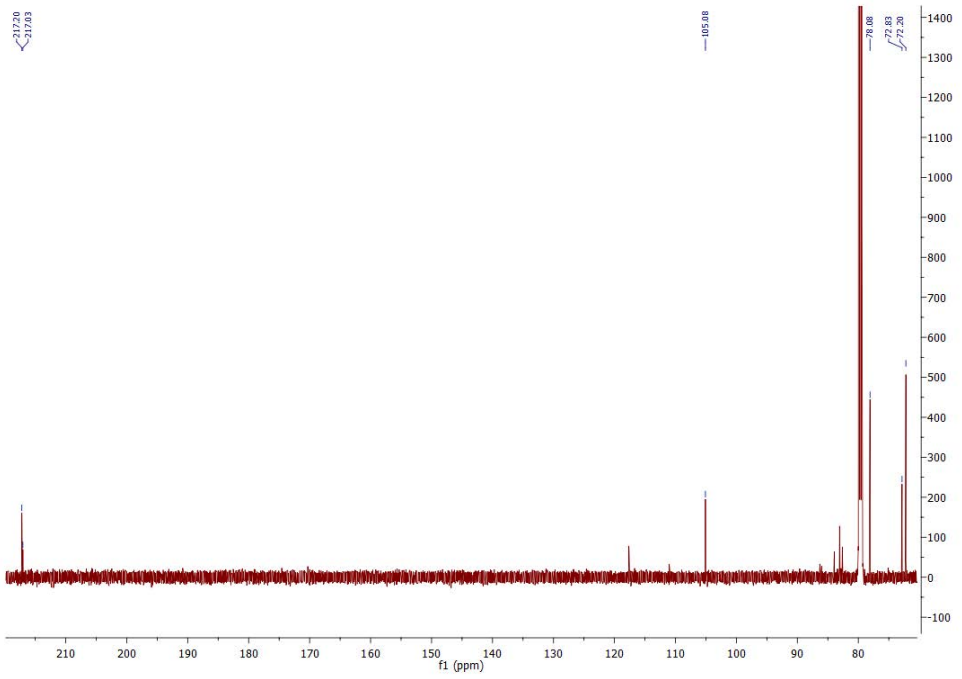

(b)

Figure B. 28 (a) ^{13}C NMR spectrum of 1-oxabicyclo[6.3.1]undecan-1-ol and 6-hydroxycyclodecanone mixture (CYP101B1) [218]. **(b)** Zoomed in version of ^{13}C NMR spectrum (70 ppm to 220 ppm region) to highlight the minor metabolite signals that was assigned as 4-hydroxy via the HMBC NMR below.

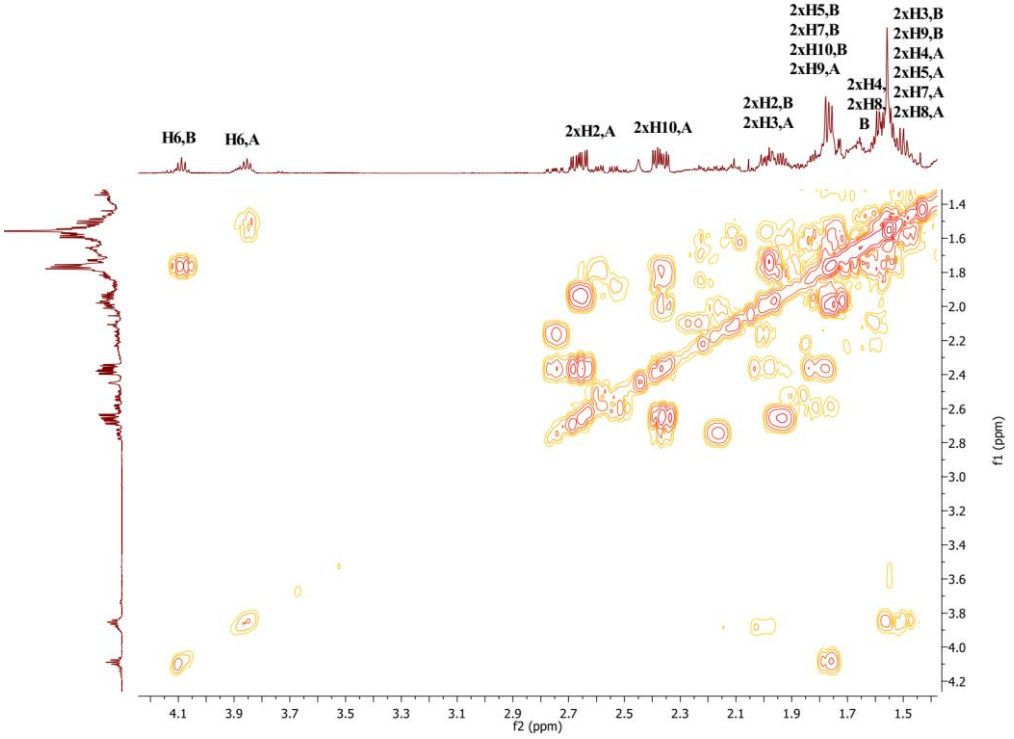

Figure B. 29 gCOSY NMR spectrum of 1-oxabicyclo[6.3.1]undecan-1-ol and 6-hydroxycyclodecanone mixture (CYP101B1).

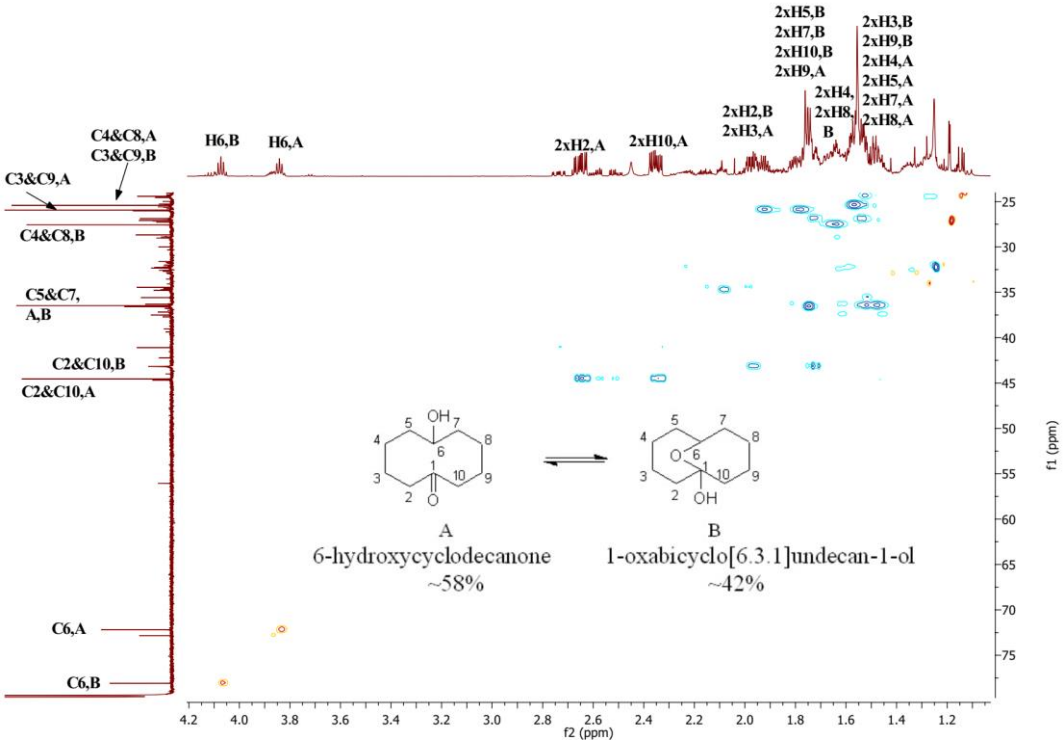

Figure B. 30 HSQC NMR spectrum of 1-oxabicyclo[6.3.1]undecan-1-ol and 6-hydroxycyclodecanone mixture (CYP101B1).

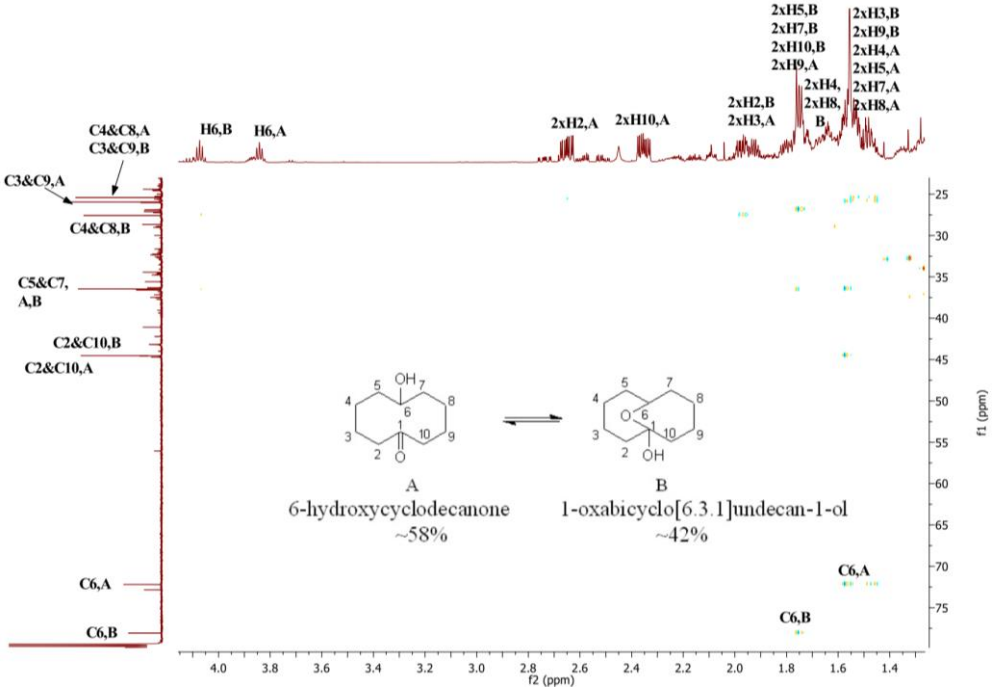

(a)

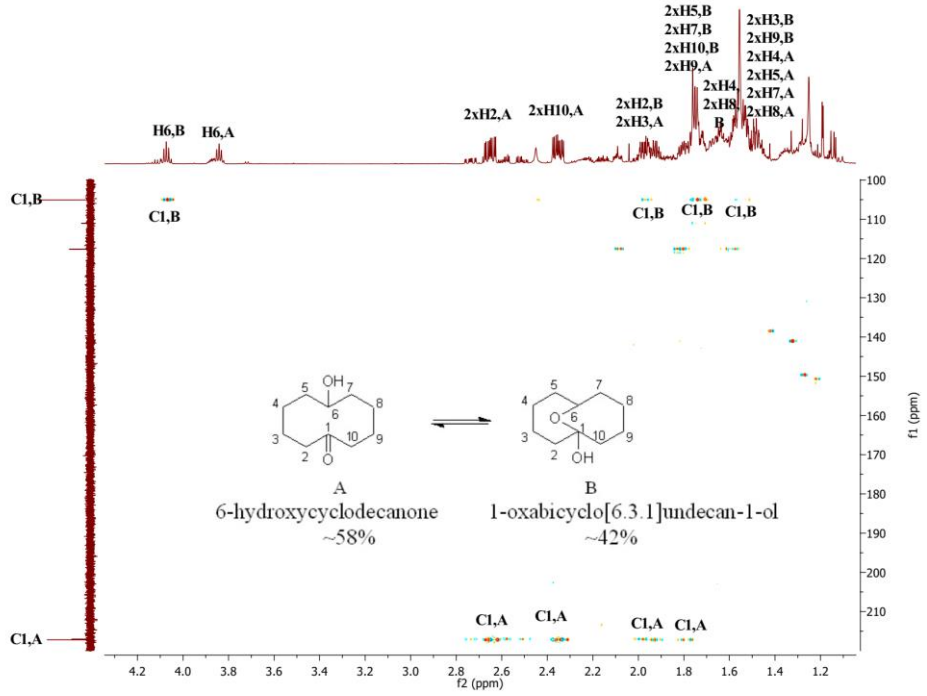

(b)

Figure B. 31 (a) Zoomed in (20 ppm to 80 ppm region) version of HMBC NMR spectrum of 1-oxabicyclo[6.3.1]undecan-1-ol and 6-hydroxycyclodecanone mixture to highlight the interactions of C-H in this region (CYP101B1). **(b)** Zoomed in (100 ppm to 220 ppm region) version of the HMBC NMR of 1-oxabicyclo[6.3.1]undecan-1-ol and 6-hydroxycyclodecanone (CYP101B1) which highlighted the correlations of C1,A and C1,B with the protons.

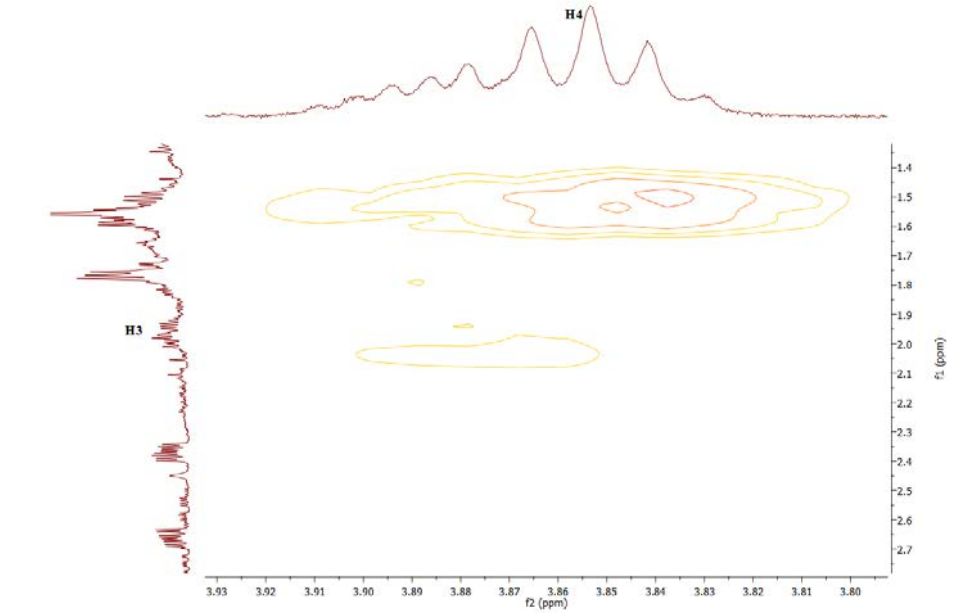

(a)

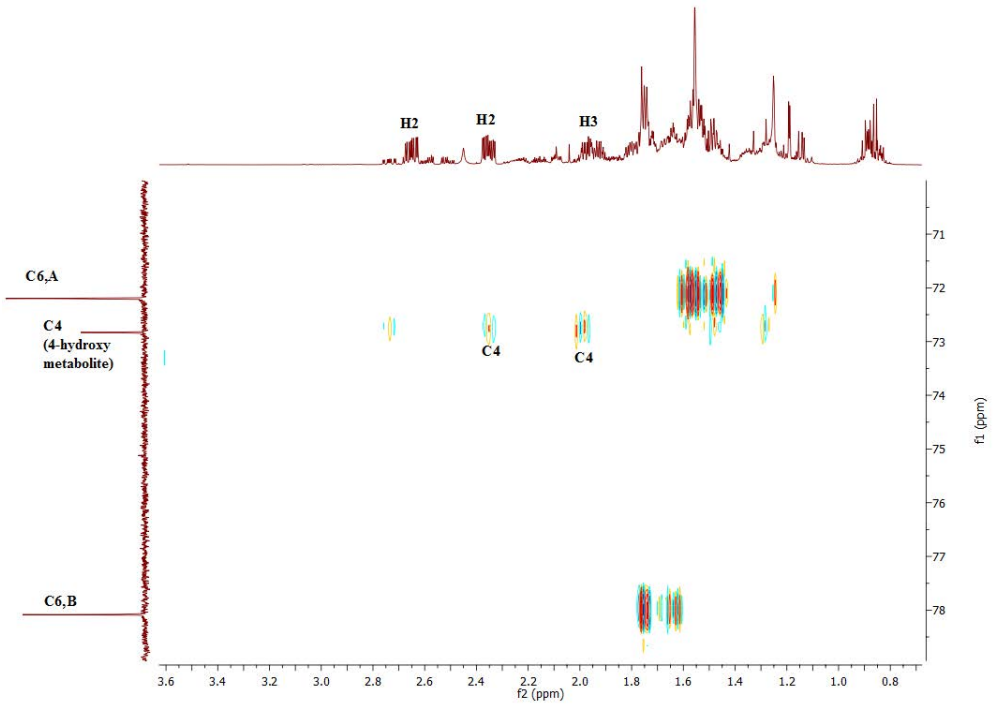

(b)

Figure B. 32 (a) Zoomed in gCOSY NMR spectrum to highlight the interaction of H4 with H3. **(b)** Zoomed in version of HMBC NMR to highlight the peak of 4-hydroxy metabolite that confirmed by the correlations of C4 (72.83) with the protons of 2.41-2.33 ppm and 2.01-1.87 ppm. The product was not fully characterised due to noise and low yield.

NMR for 2-hydroxycycloundecanone [216, 220, 221] :

^{1}H NMR (500 MHz, $CDCl_3$) δ 4.30-4.24 (m, 1H, H2), 3.6-3.44 (m, 1H, O**H2** (C2)), 2.96-2.75 (m, 1H, H11), 2.37-2.25 (m, 1H, H11), 2.13-1.95 (m, 2H, H3 & H10), 1.79-1.5 (m, 4H, H4, H8, H9 & H10), 1.42-1.10 (m, 10H, H3, H4, 2xH5, 2xH6, 2xH7, H8 & H9).

^{13}C NMR (126 MHz, $CDCl_3$) δ 216.74 (C1), 79.19 (C2), 39.90 (C11), 32.22 (C3), 29.45 (C7), 29.36 (C9), 29.01 (C8), 28.83 (C5), 26.38 (C6), 24.72 (C10), 23.40 (C4).

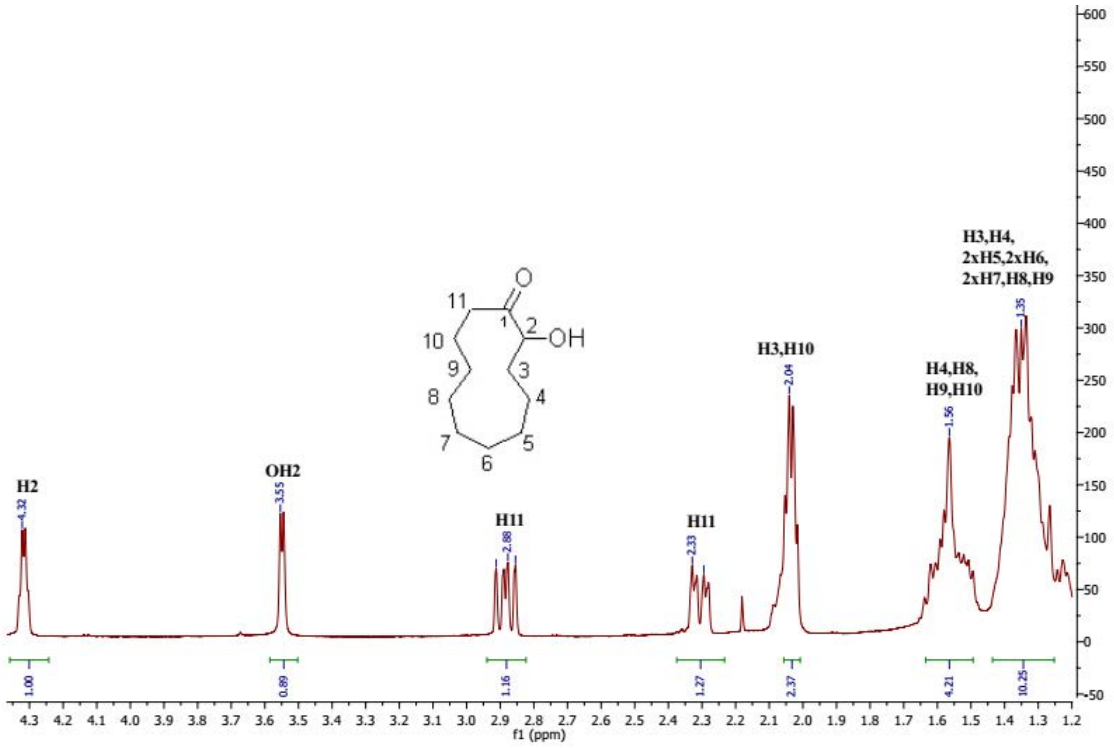

Figure B. 33 ^{1}H NMR spectrum of 2-hydroxycycloundecanone (CYP101C1).

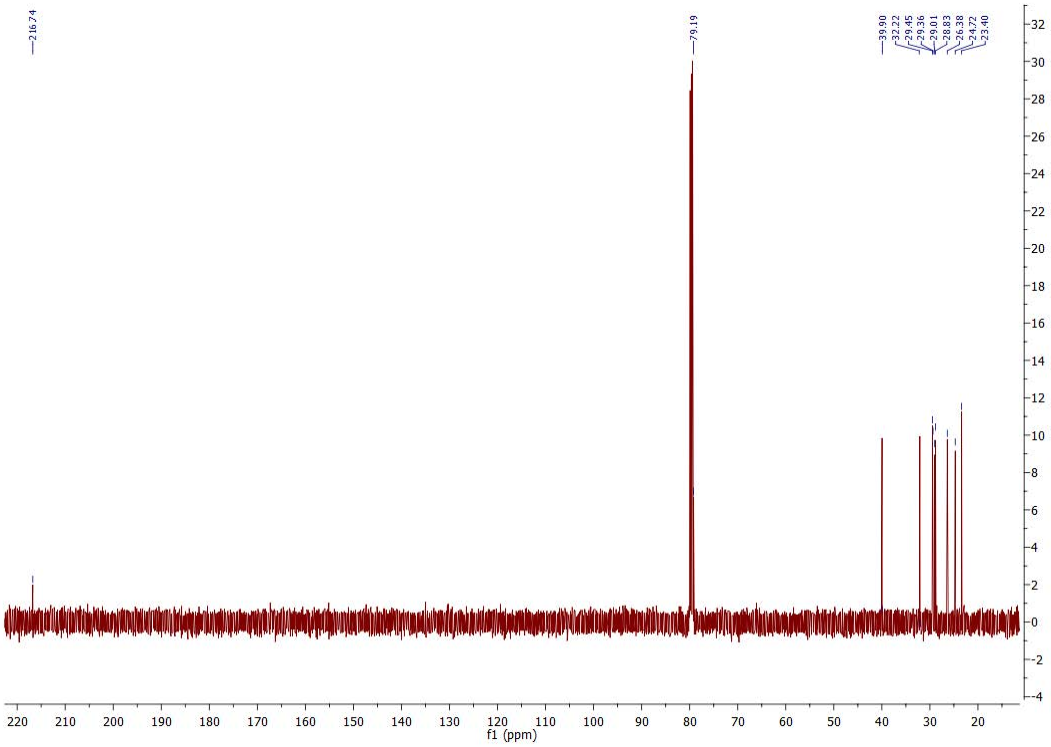

Figure B. 34 ^{13}C NMR spectrum of 2-hydroxycycloundecanone (CYP101C1).

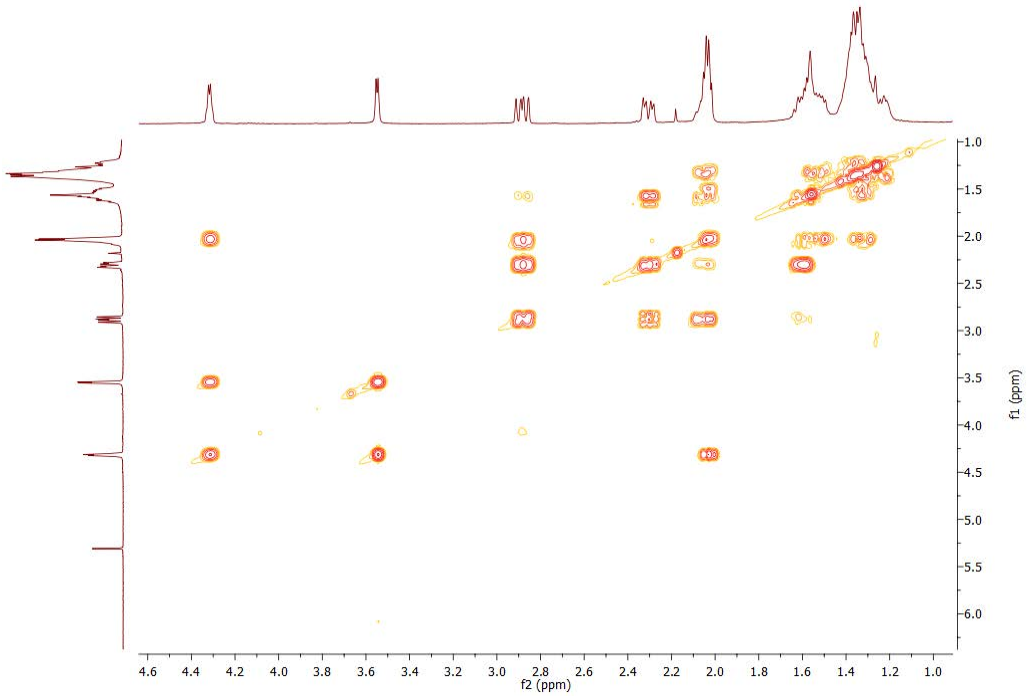

Figure B. 35 gCOSY NMR spectrum of 2-hydroxycycloundecanone (CYP101C1).

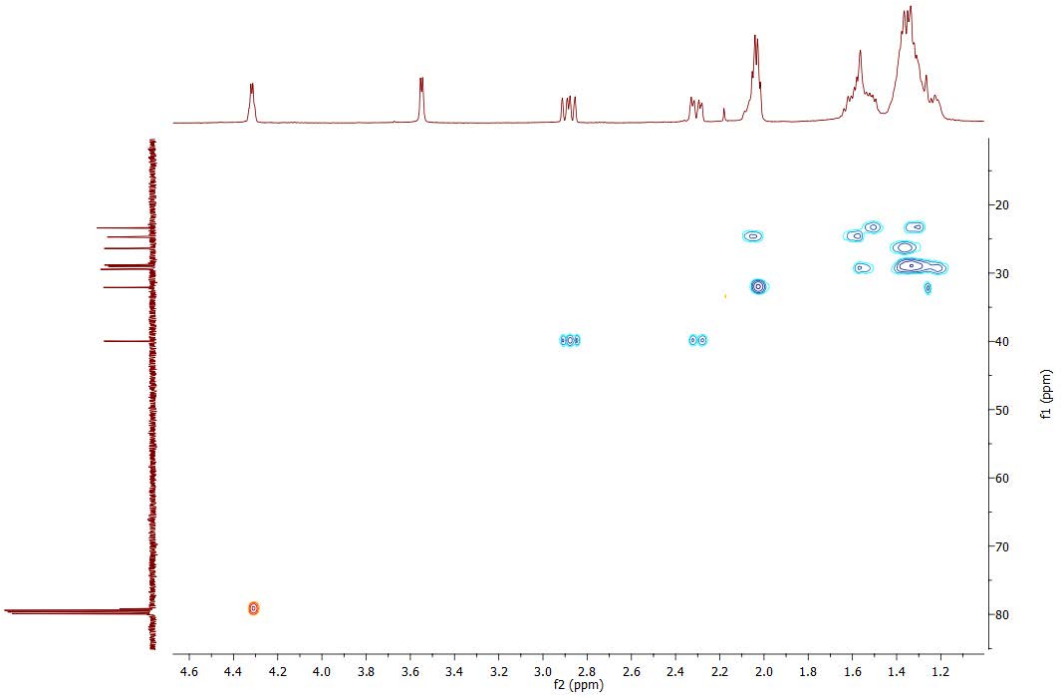

Figure B. 36 HSQC NMR spectrum of 2-hydroxycycloundecanone (CYP101C1).

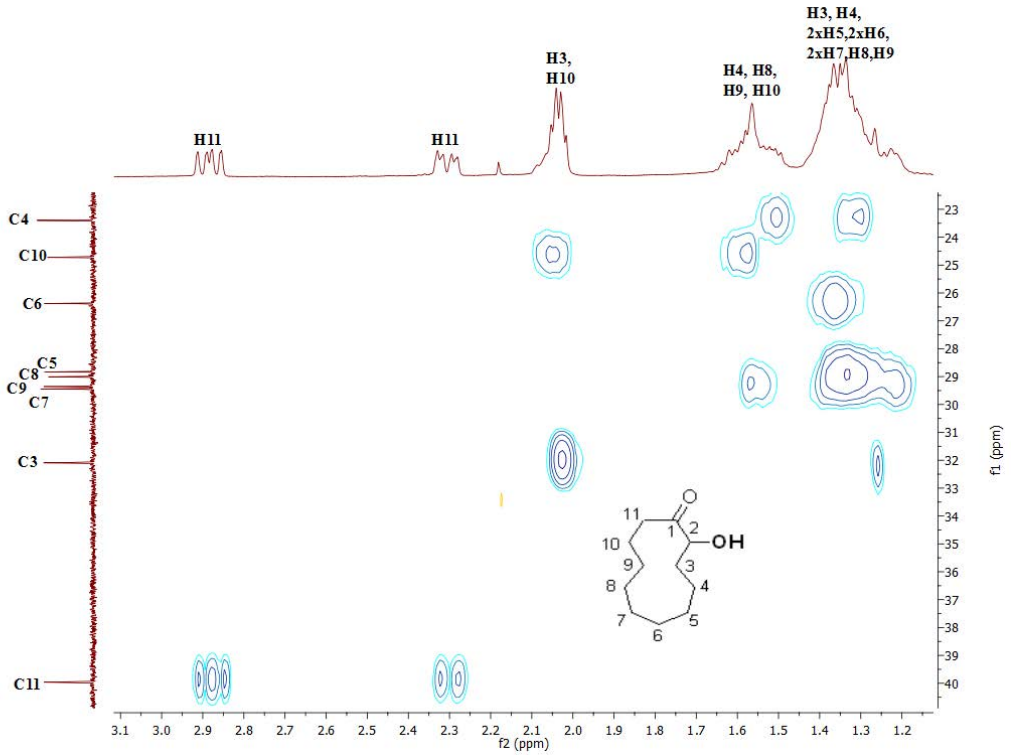

Figure B. 37 Zoomed in HSQC NMR spectrum to highlight the C-H correlations in 20-40 ppm region.

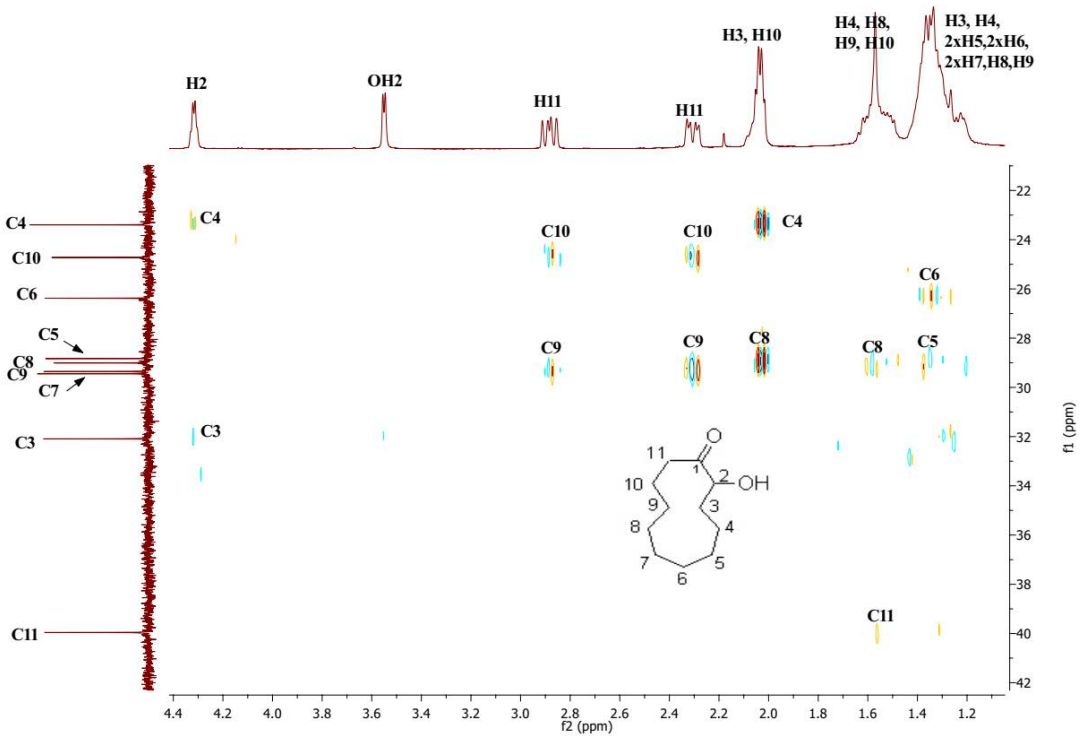

Zoomed in 20-80 ppm region (HMBC NMR)

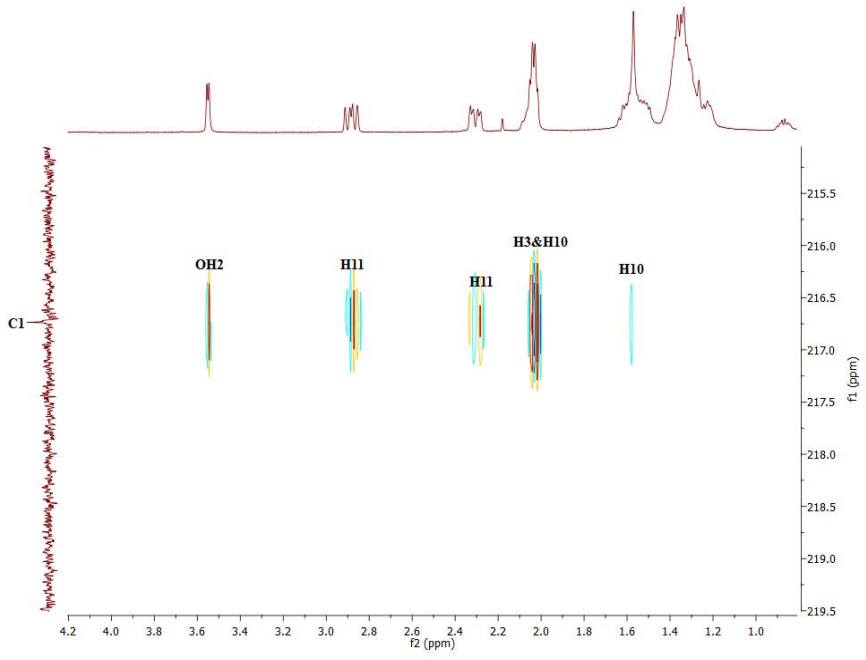

Zoomed in C=O region of HMBC NMR spectrum. The product was confirmed as 2-hydroxy metabolite as C1 showed strong connections with H2, O**H2**, H3, H10 and H11.

Figure B. 38 Zoomed in HMBC NMR spectrum of 2-hydroxycycloundecanone.

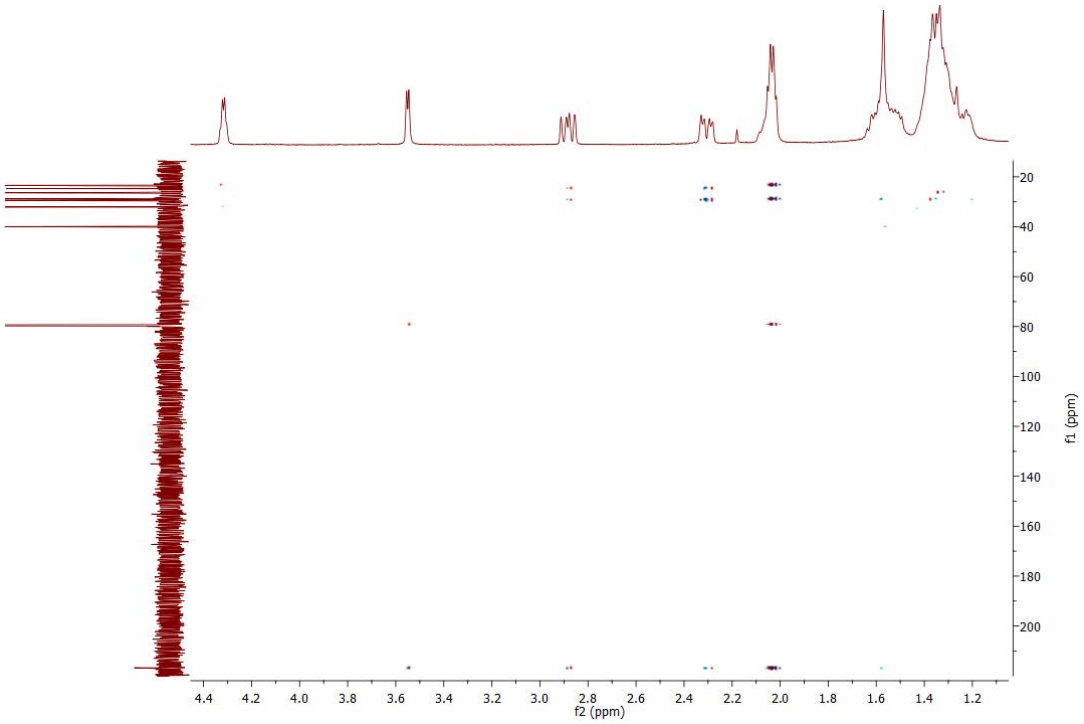

Figure B. 39 HMBC NMR spectrum of 2-hydroxycycloundecanone (CYP101C1).

NMR for 5-hydroxycycloundecanone:

^{1}H NMR (600 MHz, $CDCl_3$) δ 3.76-3.70 (m, 1H, H5), 2.55-2.42 (m, 4H, 2xH2 & 2xH11), 1.89-1.82 (m, 2H, 2xH3), 1.81-1.74 (m, 1H, H10), 1.73-1.63 (m, 2H, H4 & H10), 1.61-1.55 (m, 1H, H4), 1.54-1.50 (m, 2H, H6 & H9), 1.48-1.42 (m, 1H, H6), 1.40-1.33 (m, 3H, H7, H8 & H9), 1.31-1.26 (m, 2H, H7 & H8).

^{13}C NMR (151 MHz, $CDCl_3$) δ 216.69 (C1), 72.36 (C5), 45.02 (C11), 44.97 (C2), 37.77 (C4), 36.57 (C6), 28.68 (C9), 27.71 (C8), 25.0 (C10), 24.85 (C7), 22.33 (C3).

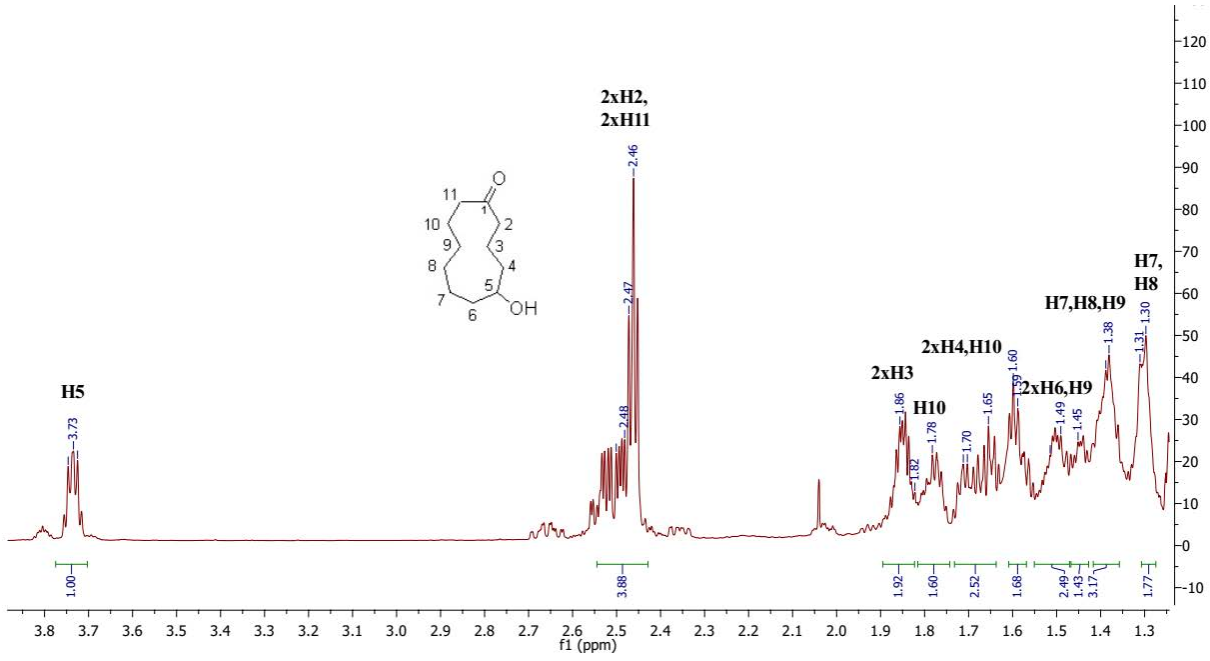

Figure B. 40 ^{1}H NMR spectrum of 5-hydroxycycloundecanone (CYP101B1; GC-MS RT 9.25 min).

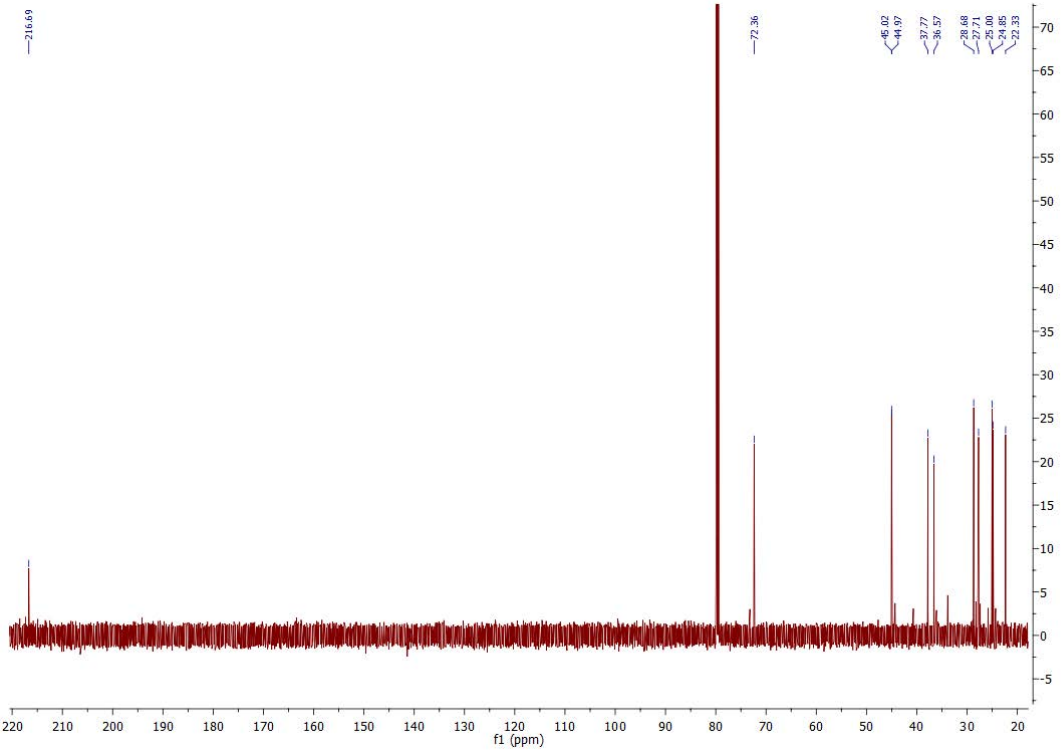

Figure B. 41 ^{13}C NMR spectrum of 5-hydroxycycloundecanone.

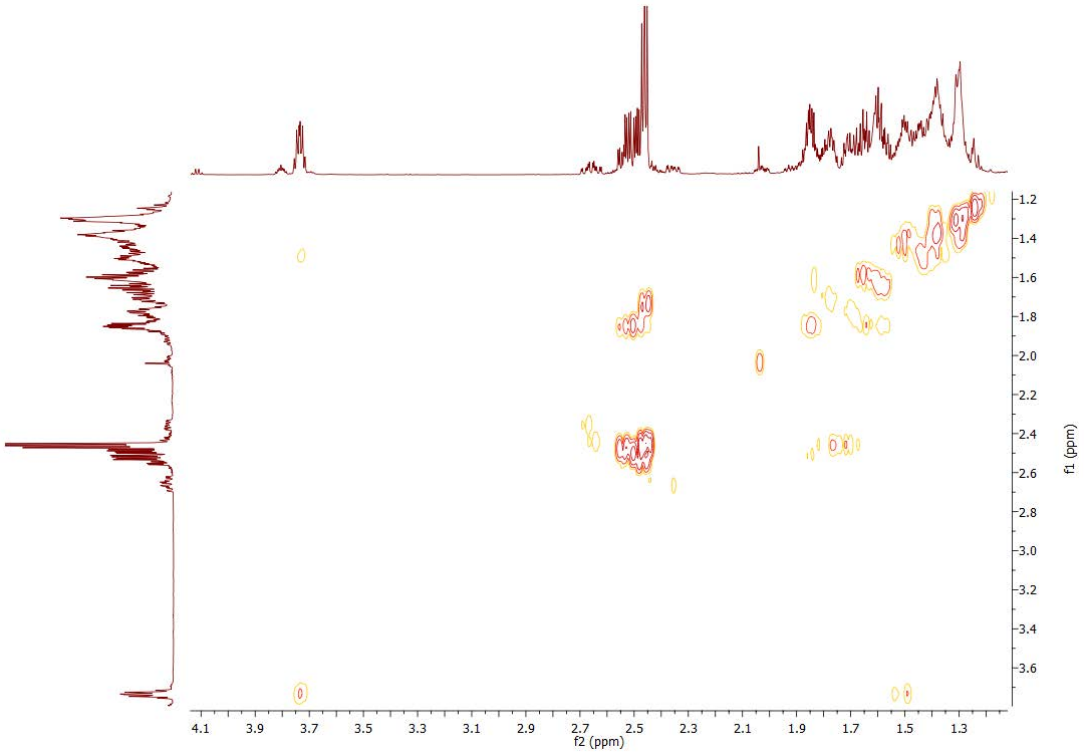

Figure B. 42 gCOSY NMR spectrum of 5-hydroxycycloundecanone.

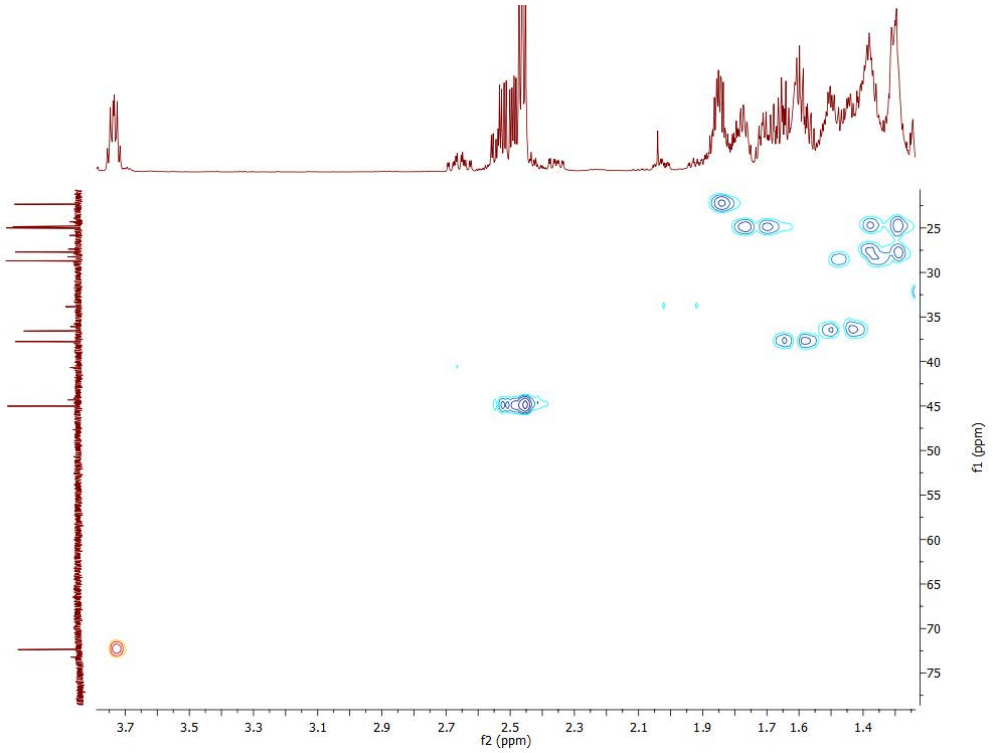

Figure B. 43 HSQC NMR spectrum of 5-hydroxycycloundecanone.

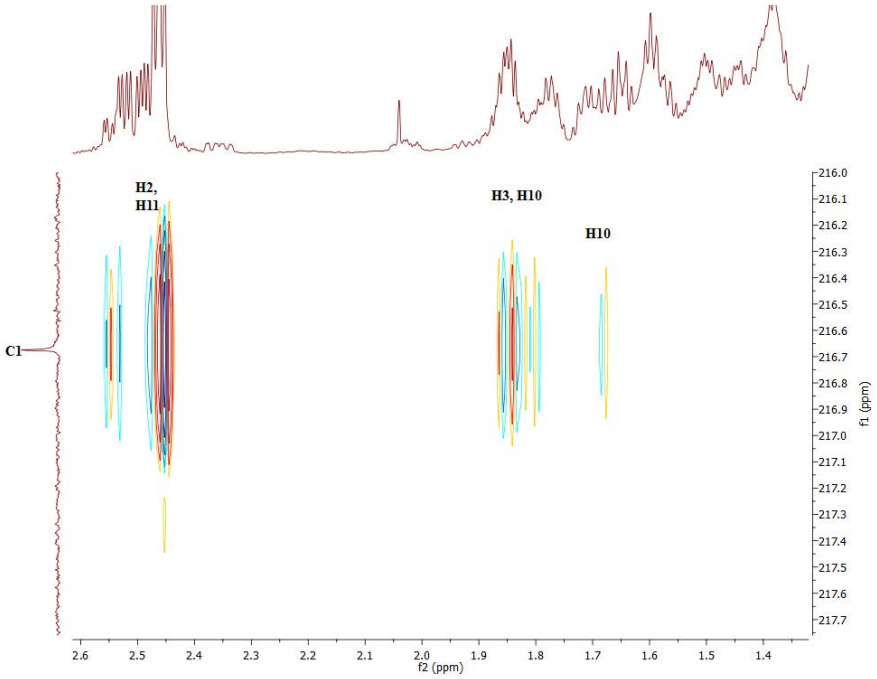

Zoomed in C=O region of HMBC NMR spectrum to highlight the C1 correlations with the H2, H3, H10 and H11.

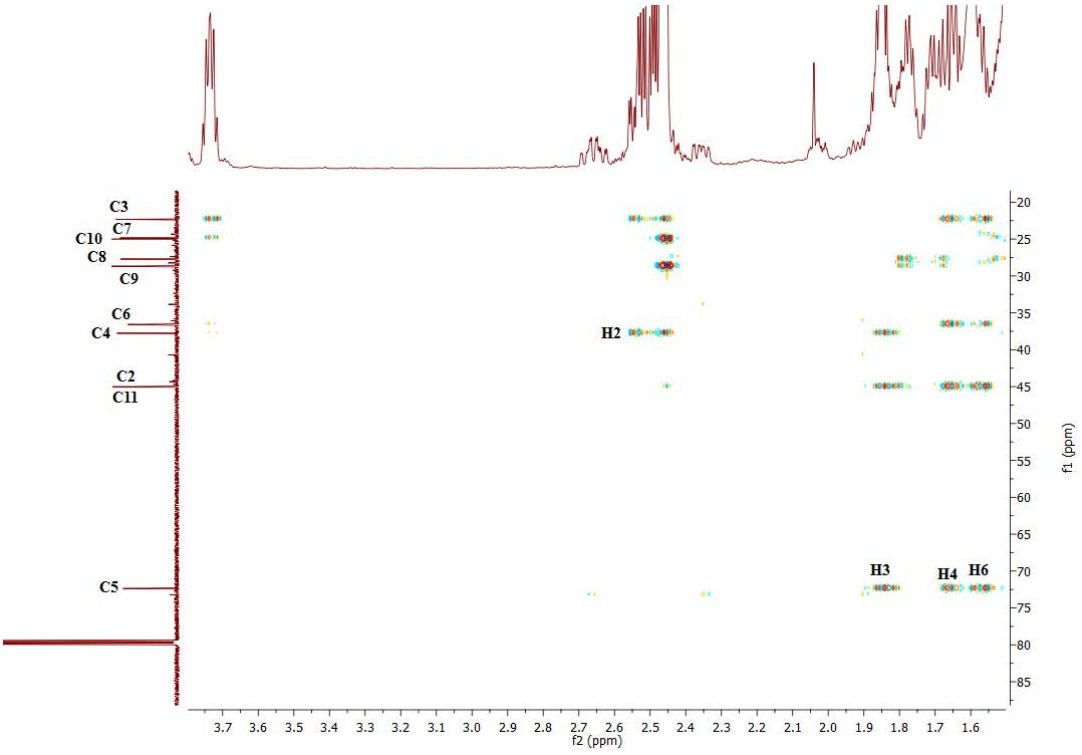

Zoomed in HMBC NMR to highlight the C-H interactions in 25 to 90 ppm region. The product was assigned as 5-hydroxycycloundecanone as C5 have strong correlations with H3, H4 and H6. H4 was confirmed by the interaction between C4 with H2 peak in the HMBC NMR.

Figure B. 44 HMBC NMR spectrum of 5-hydroxycycloundecanone (CYP101B1).

NMR for 6-hydroxycycloundecanone:

^{1}H NMR (600 MHz, $CDCl_3$) δ 3.72-3.66 (m, 1H, H6), 2.60-2.36 (m, 4H, 2xH2 & 2xH11), 1.84-1.72 (m, 4H, 2xH3, 2xH10), 1.63-1.56 (m, 2H, 2xH5), 1.54-1.48 (m, 1H, H9), 1.47-1.42 (m, 3H, H4 & 2xH7), 1.41-1.33 (m, 4H, H4, 2xH8 & H9).

^{13}C NMR (151 MHz, $CDCl_3$) δ 216.91 (C1), 72.73 (C6), 44.71 (C2), 44.17 (C11), 35.81 (C7), 34.79 (C5), 29.23 (C9), 25.18 (C10), 25.0 (C3), 24.42 (C4), 23.89 (C8).

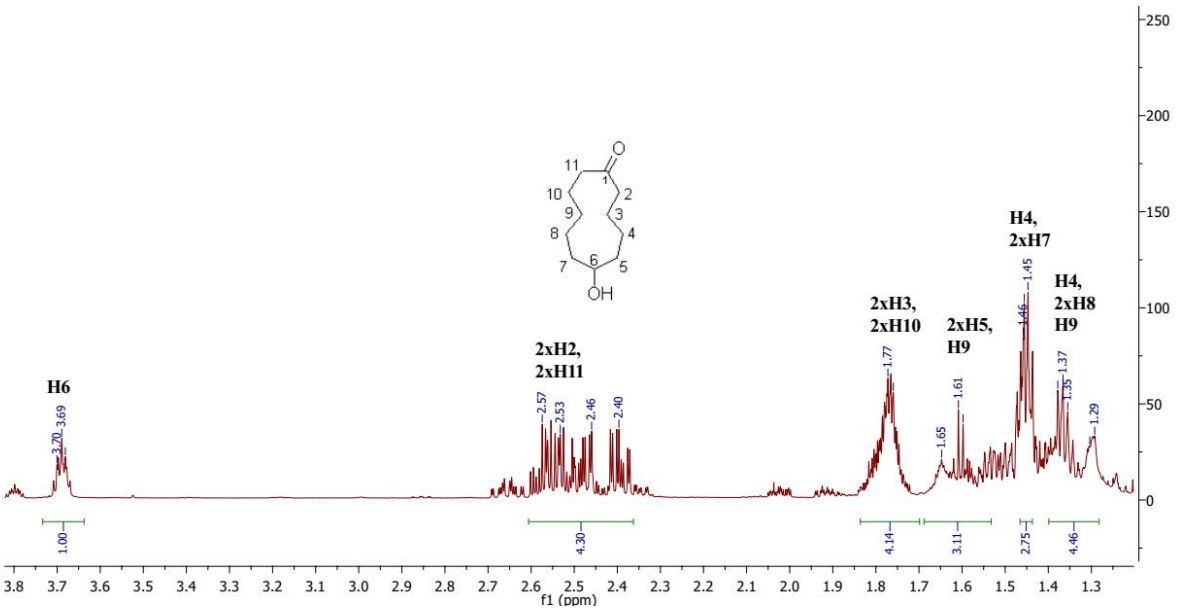

Figure B. 45 ^{1}H NMR spectrum of 6-hydroxycycloundecanone (CYP101B1).

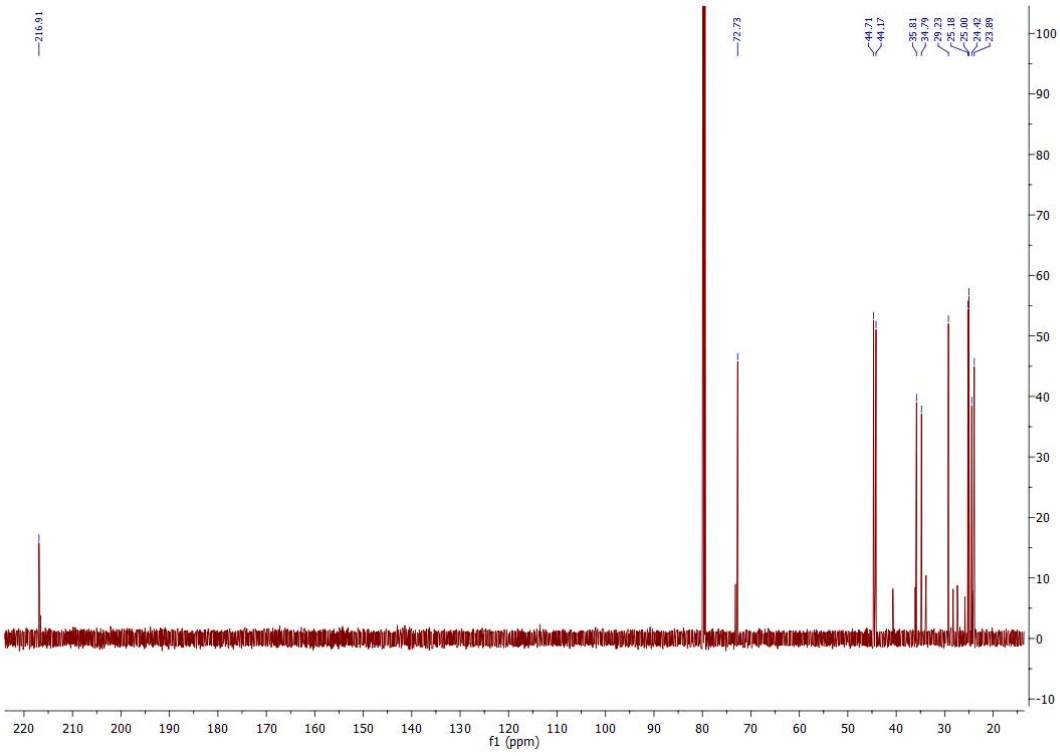

Figure B. 46 ^{13}C NMR spectrum of 6-hydroxycycloundecanone.

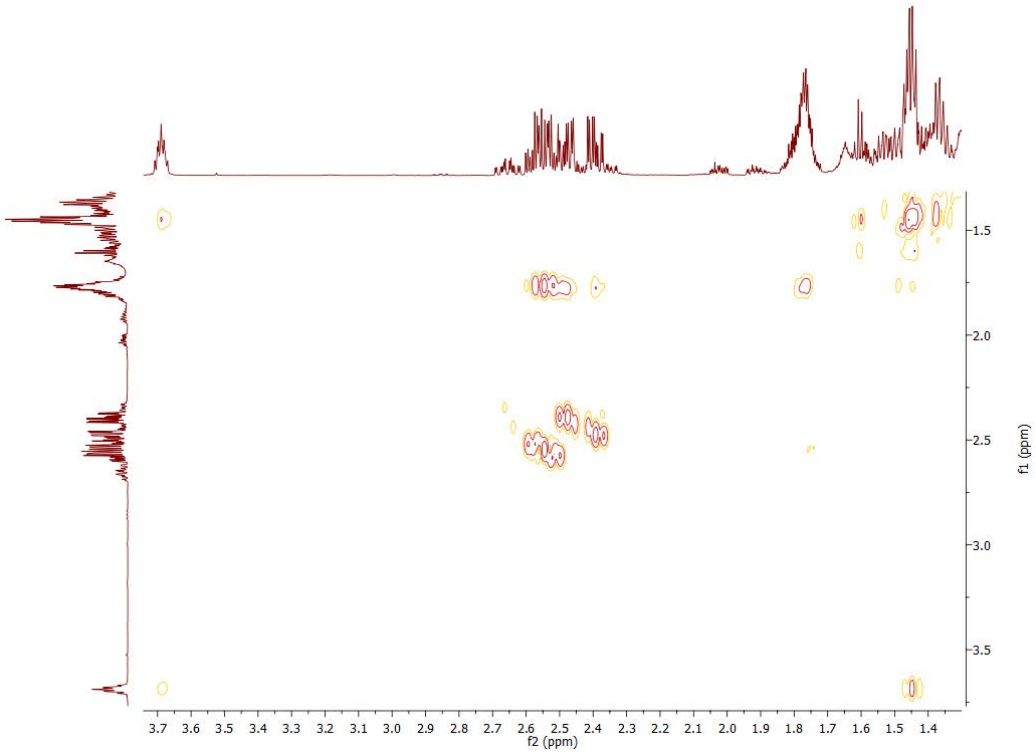

Figure B. 47 gCOSY NMR spectrum of 6-hydroxycycloundecanone.

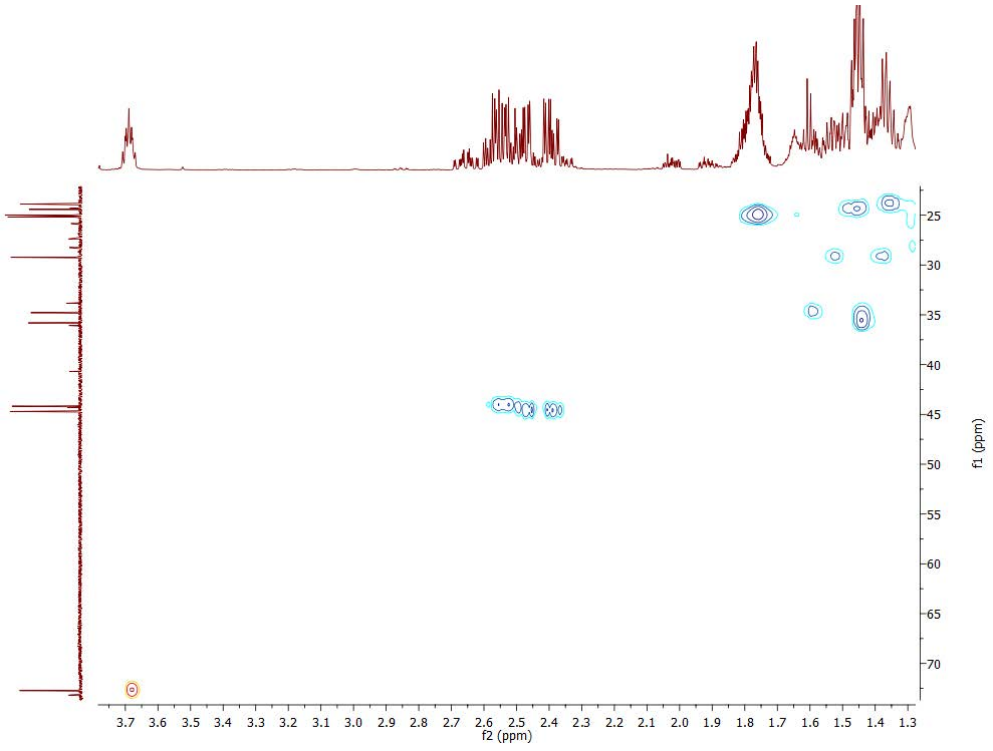

Figure B. 48 HSQC NMR spectrum of 6-hydroxycycloundecanone.

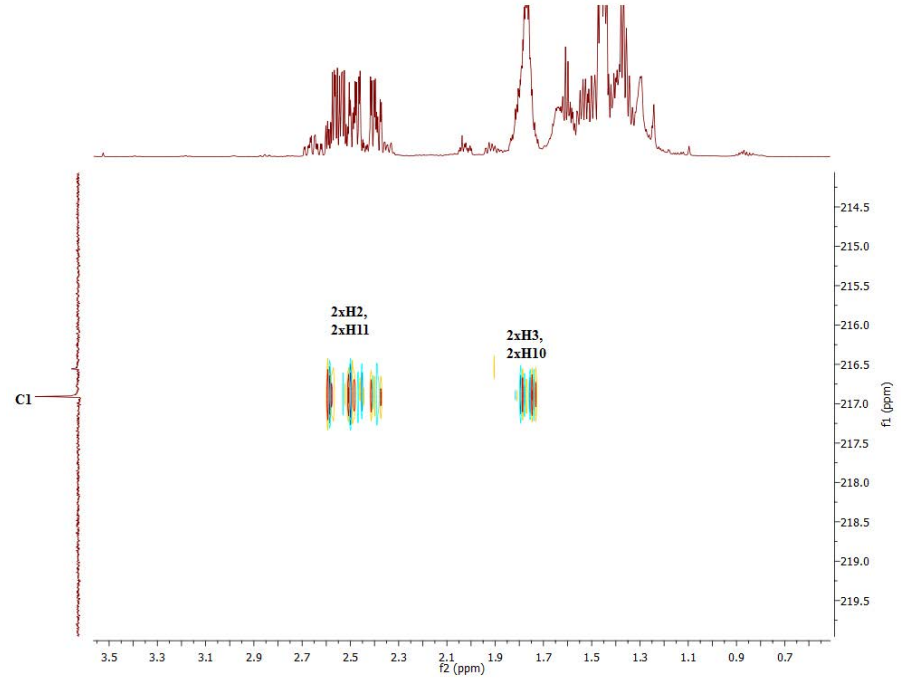

Zoomed in C=O region, which highlights the correlations of C1 with the H2, H11, H3 and H10.

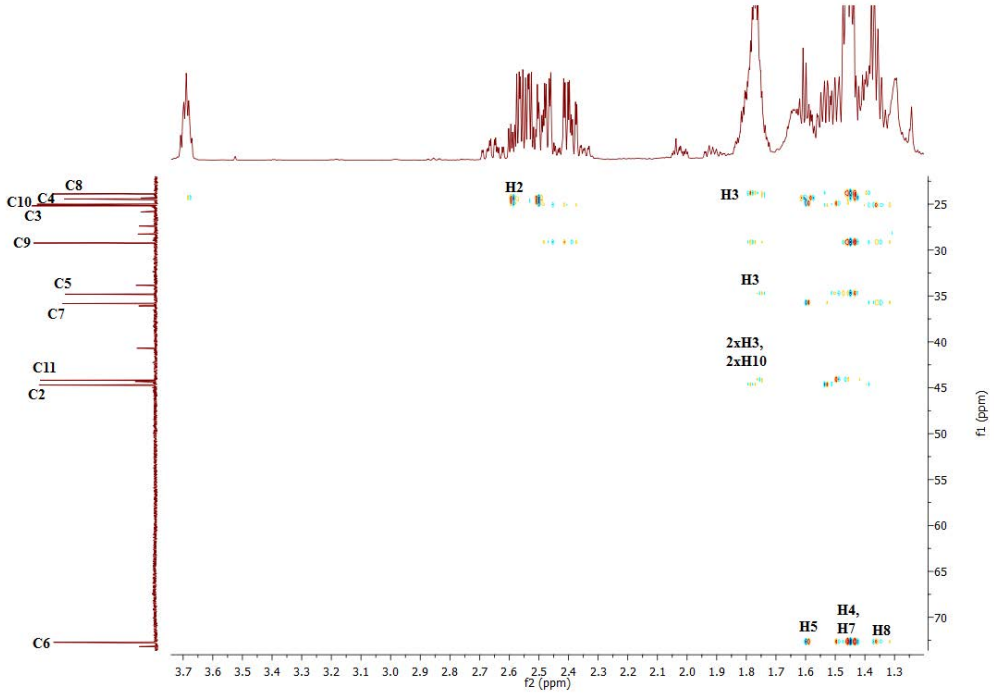

Zoomed in HMBC NMR to highlight the C-H interactions in 20 to 80 ppm region. The product was confirmed 6-hydroxycycloundecanone as C6 showed correlations with H4, H5, H7 and H8. C4 and C5 were assigned due to the interactions with H2 and H3, respectively. The H4 and H5 proton peaks in ^{1}H NMR were identified using the HSQC NMR.

Figure B. 49 HMBC NMR spectrum of 6-hydroxycycloundecanone.

NMR for 2-hydroxycyclododecanone [208, 216, 219, 220]:

^{1}H NMR (500 MHz, $CDCl_3$) δ 4.44-4.34 (m, 1H, H2), 3.58-3.50 (m, 1H, O**H2** (C2)), 3.01-2.96 (m, 1H, H12), 2.26-2.18 (m, 1H, H10), 2.17-2.1 (m, 1H, H12), 1.99-1.87 (m, 2H, 2xH3), 1.60-1.50 (m, 1H, H4), 1.21-1.46 (m, 13H, 2xH5, 2xH6, 2xH7, 2xH8, 2xH9, H10 & 2xH11), 0.77-0.93 (m, 1H, H4).

^{13}C NMR (126 MHz, $CDCl_3$) δ 215.55 (C1), 79.18 (C2), 36.93 (C12), 33.39 (C3), 28.76 (C5), 28.72 (C11), 26.60, 25.34 (C8 & C9), 25.11 (C6), 24.73 (C7), 24.05 (C10), 21.35 (C4).

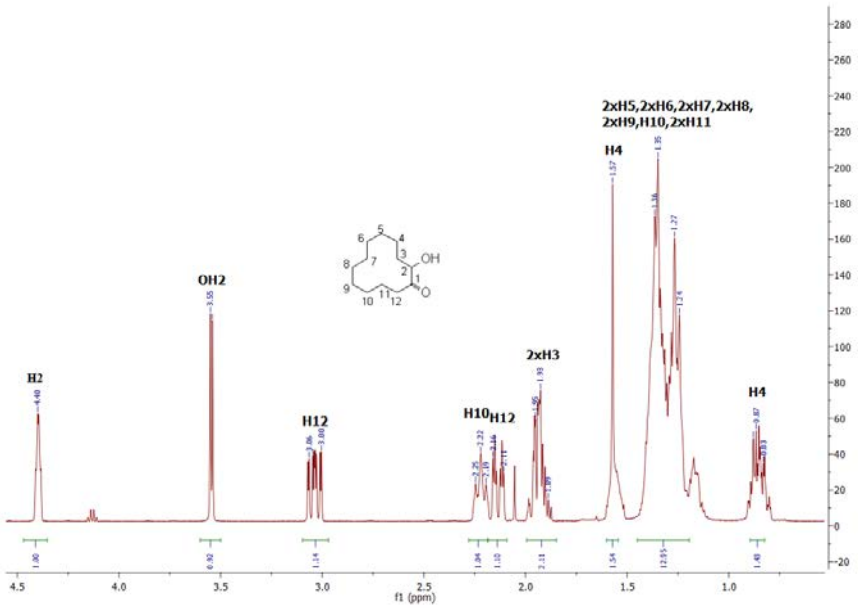

Figure B. 50 ^{1}H NMR spectrum of 2-hydroxycyclododecanone (CYP101C1).

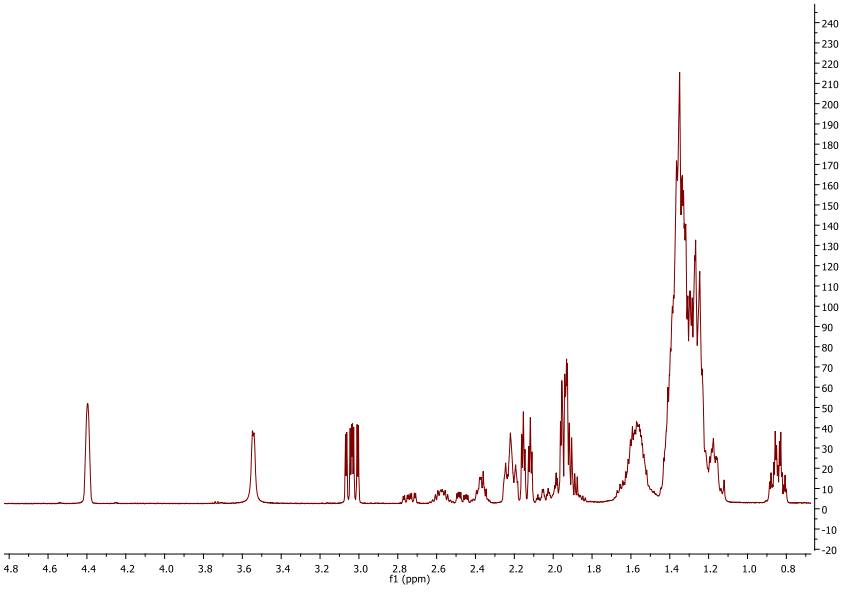

Figure B. 51 ^{1}H NMR spectrum of 2-hydroxycyclododecanone (standard).

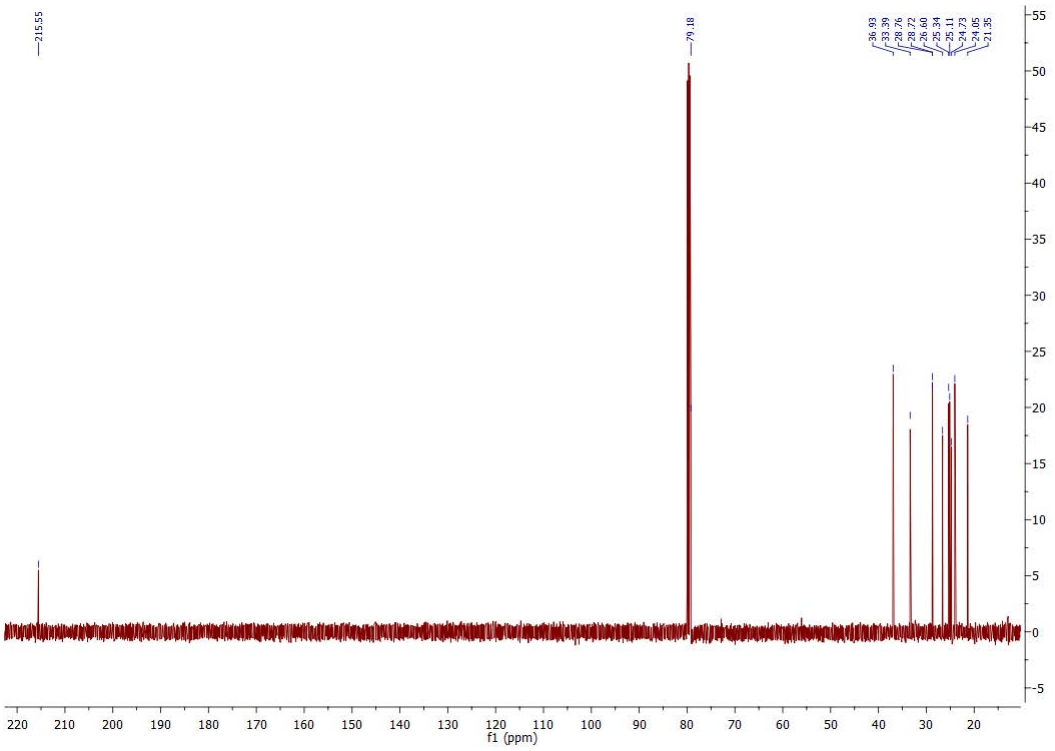

Figure B. 52 ^{13}C NMR spectrum of 2-hydroxycyclododecanone (CYP101C1).

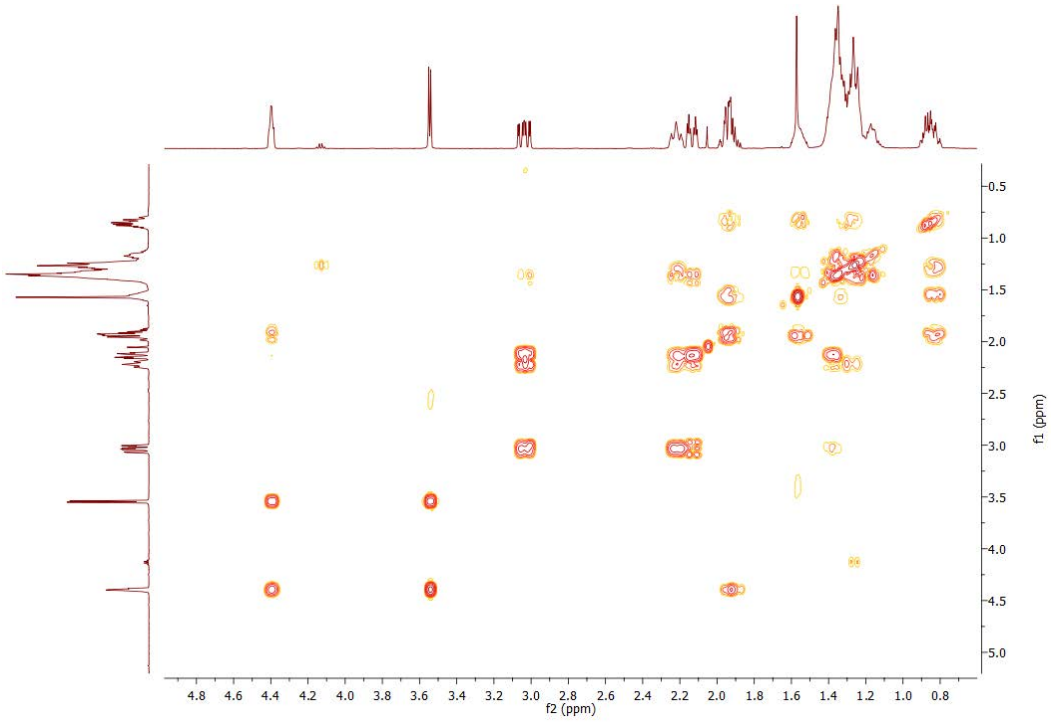

Figure B. 53 gCOSY NMR spectrum of 2-hydroxycyclododecanone (CYP101C1).

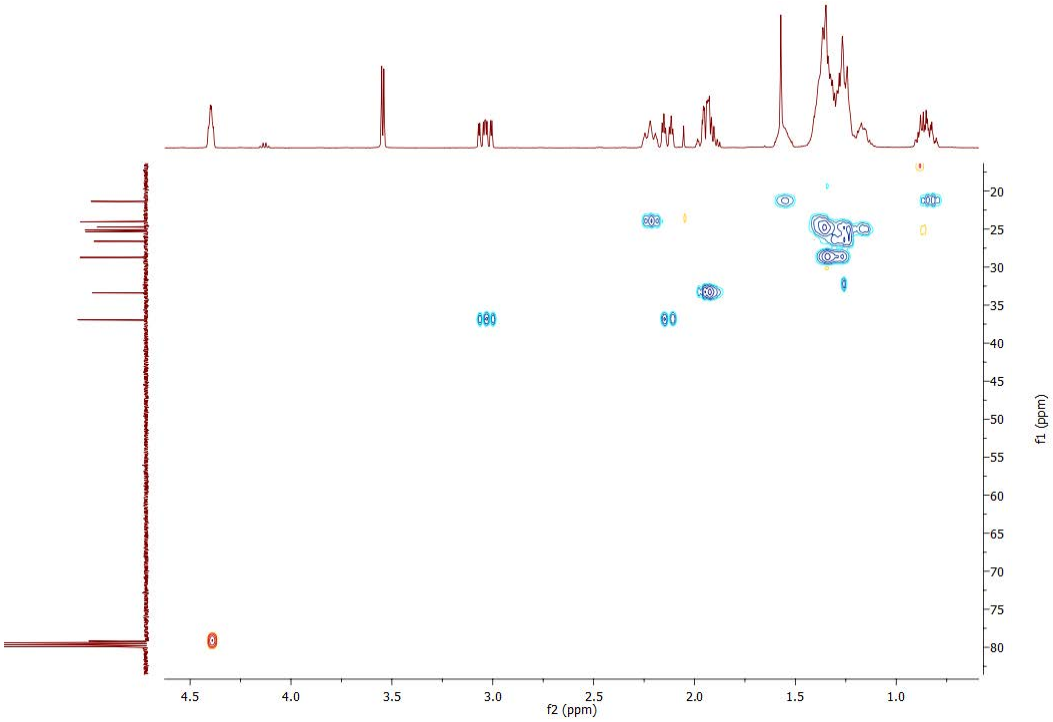

Figure B. 54 HSQC NMR spectrum of 2-hydroxycyclododecanone (CYP101C1).

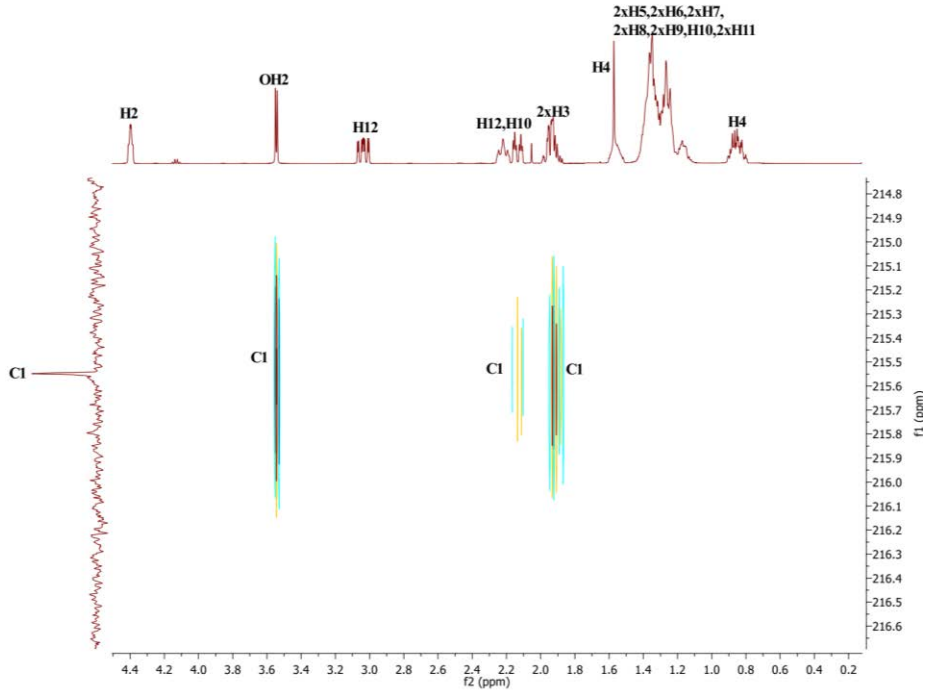

Zoomed in HMBC NMR spectrum to highlight the interactions of the C=O region. The product was confirmed 2-hydroxy due to the correlations of C1 (215.55 ppm) with O**H2** (3.58-3.50 ppm), H12 (3.01-2.96 ppm), H12 (2.17-2.1 ppm) and H3 (1.99-1.87 ppm).

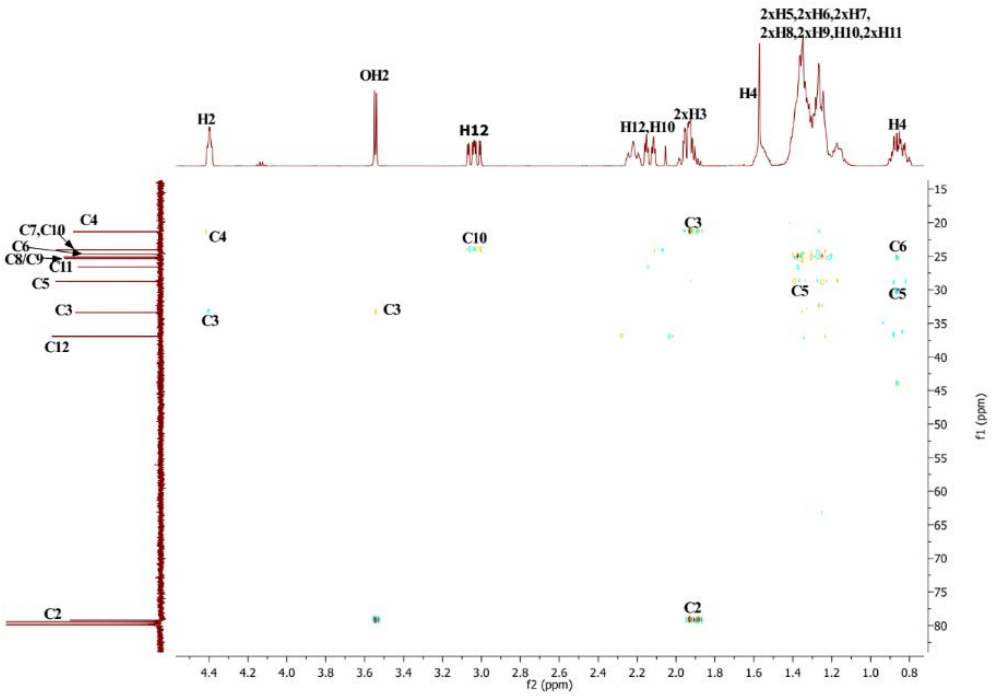

Zoomed in the region 15-80 ppm to highlight the interactions of C4 and C3 with H2 (4.44-4.34 ppm).

Figure B. 55 HMBC NMR spectrum of 2-hydroxycyclododecanone (CYP101C1).

Data for 7-hydroxycyclododecanone [208]:

^{1}H NMR (500 MHz, $CDCl_3$) δ 3.75-3.65 (m,1H, H7), 2.81-2.68 (m, 2H, H2 & H12), 2.25-2.11 (m, 2H, H2 & H12), 1.92-1.8 (m, 2H, H3 & H11), 1.68-1.51 (m, 4H, H3, H6, H8 & H11), 1.49-1.39 (m, 6H, H4, H5, H6, H8, H9 & H10), 1.37-1.29 (m, 2H, H5 & H9), 1.27-1.17 (m, 2H, H4 & H10).

^{13}C NMR (126 MHz, $CDCl_3$) δ 215.27 (C1), 71.43 (C7), 42.96 (C2 & C12), 36.62 (C6 & C8), 27.58 (C4 & C10), 25.37 (C5 & C9), 25.0 (C3 & C11).

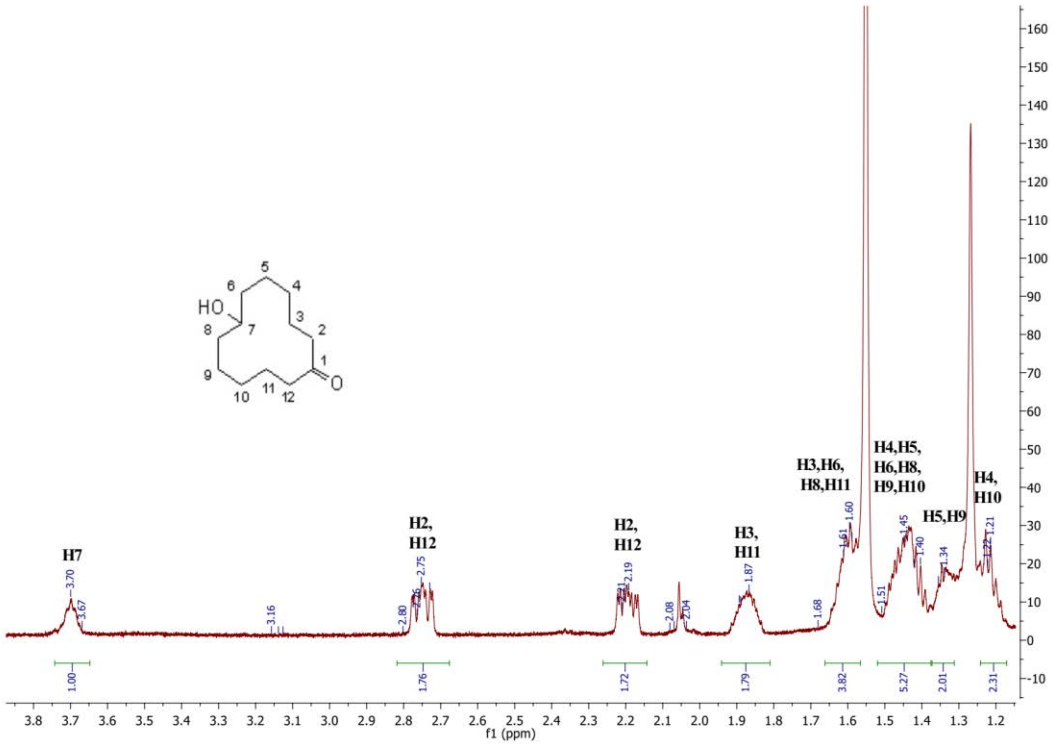

Figure B. 56 ^{1}H NMR spectrum of 7-hydroxycyclododecanone (CYP101B1).

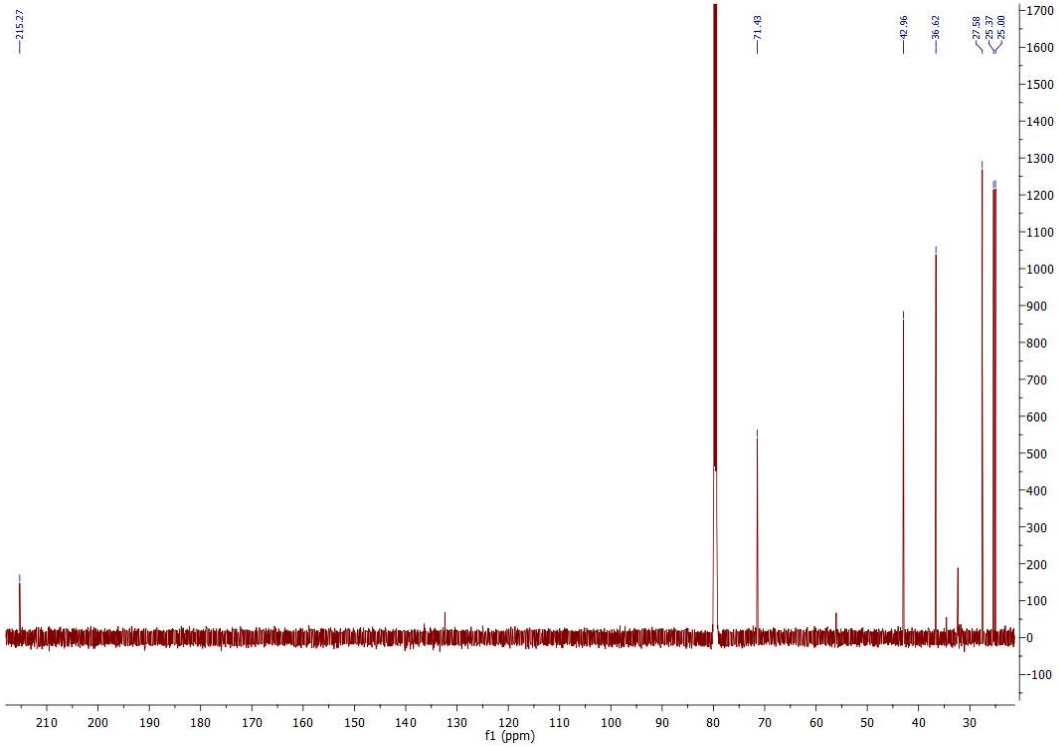

Figure B. 57 ^{13}C NMR spectrum of 7-hydroxycyclododecanone.

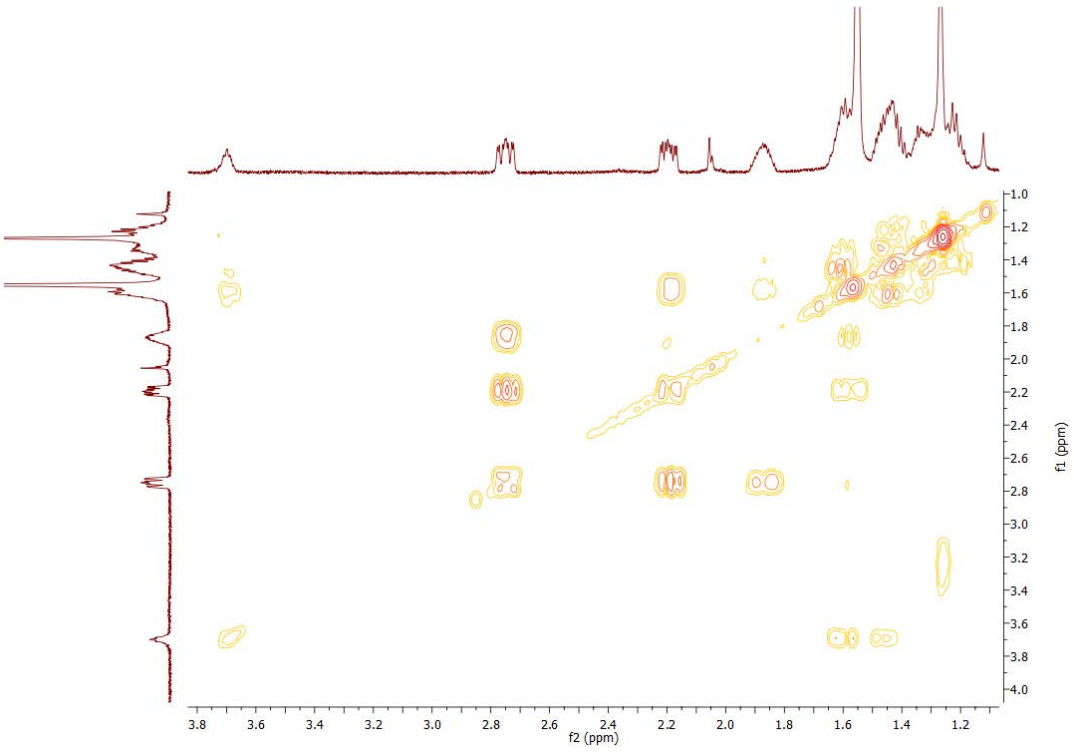

Figure B. 58 gCOSY spectrum NMR of 7-hydroxycyclododecanone.

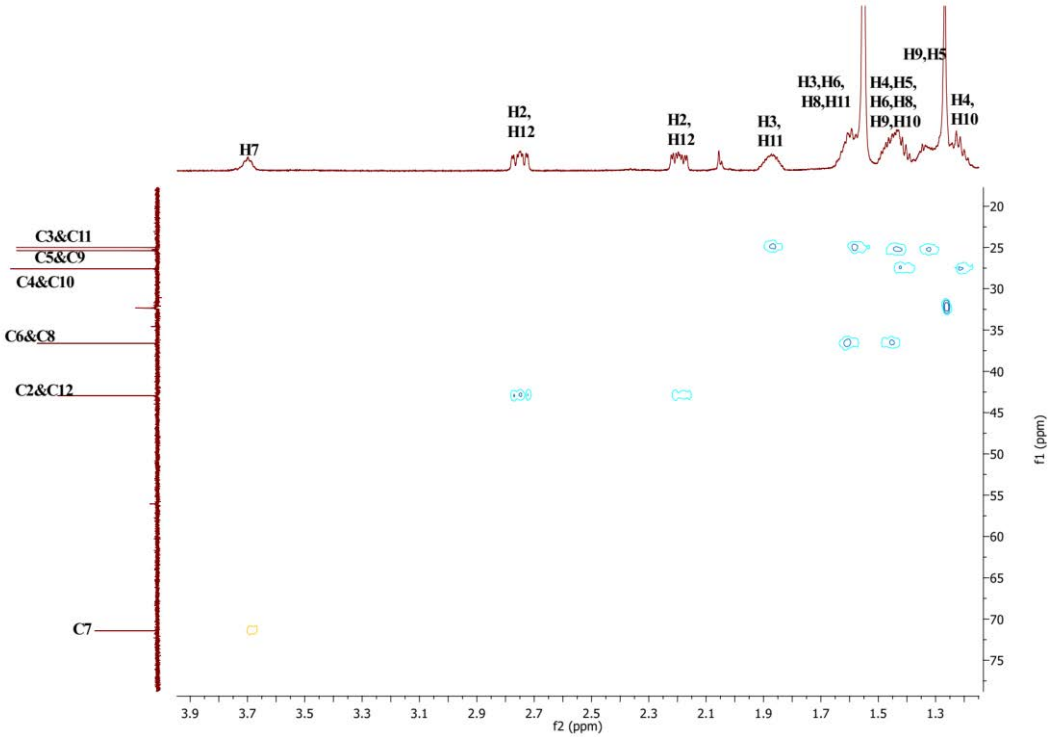

Figure B. 59 HSQC NMR spectrum of 7-hydroxycyclododecanone (CYP101B1).

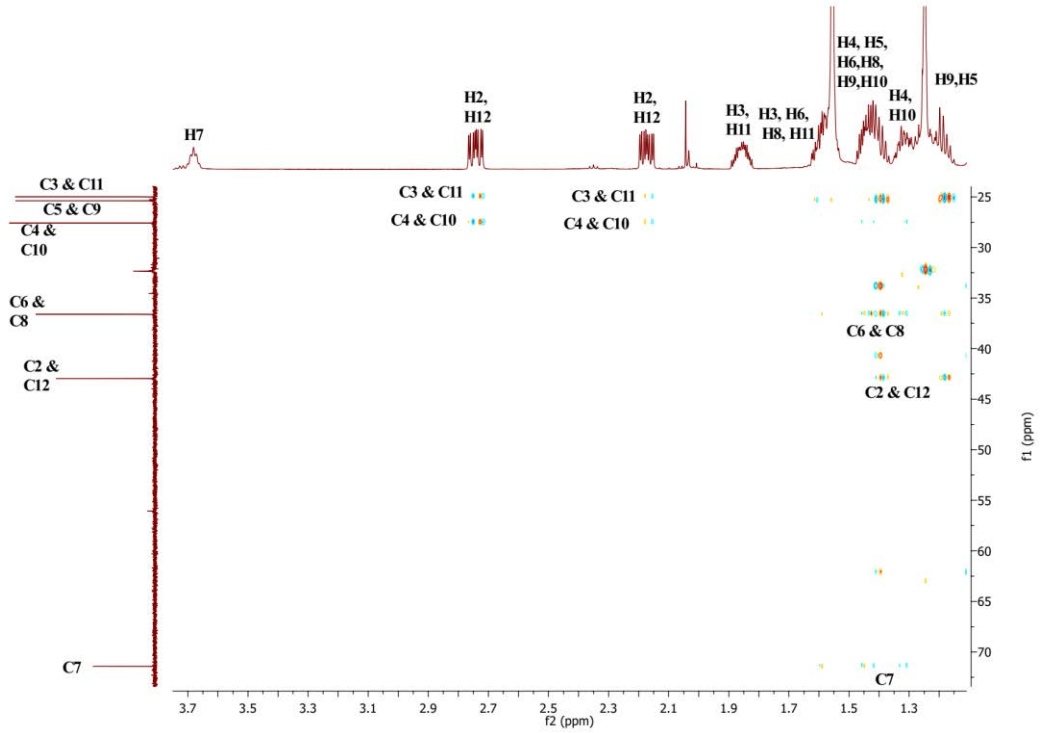

Zoomed in the 20 to 76 ppm region, which highlighted the C-H correlations

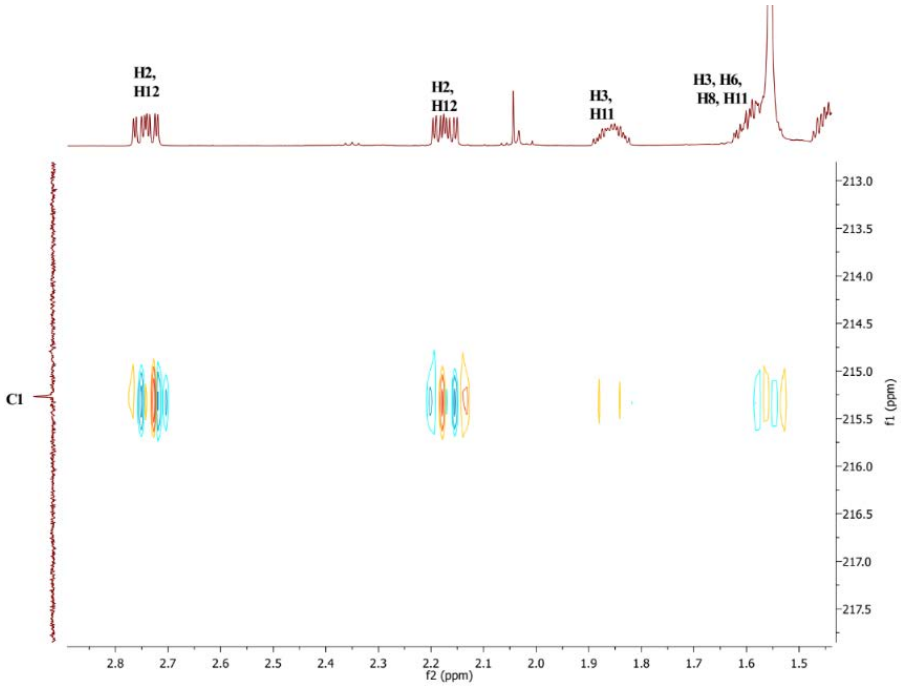

Zoomed in the HMBC NMR C=O region to highlight the interactions of C1 (215.27 ppm) with H2 and H12 (2.81-2.68 ppm & 2.25-2.11 ppm) and with H3 and H11 (1.92-1.8 ppm & 1.68-1.51 ppm).

Figure B. 60 HMBC NMR spectrum of 7-hydroxycyclododecanone (CYP101B1).

NMR for 8-hydroxycylopentadecanone [208]:

^{1}H NMR (600 MHz, $CDCl_3$) δ 3.71-3.64 (m, 1H, H8), 2.47-2.33 (m, 4H, 2xH2 & 2xH15), 1.74-1.60 (m, 4H, 2xH3 & 2xH14), 1.58-1.43 (m, 4H, 2xH7 & 2xH9), 1.40-1.25 (m, 14H, 2xH4, 2xH5, 2xH6, 2xH10, 2xH11, 2xH12 & 2xH13).

^{13}C NMR (151 MHz, $CDCl_3$) δ 215.30 (C1), 72.70 (C8), 44.86 (C2), 44.56 (C15), 37.35 (C7), 37.30 (C9), 30.18 (C5), 30.16 (C13), 29.64 (C4), 29.63 (C11), 29.51 (C12), 26.26 (C3), 25.90 (C6), 25.70 (C14), 25.45 (C10).

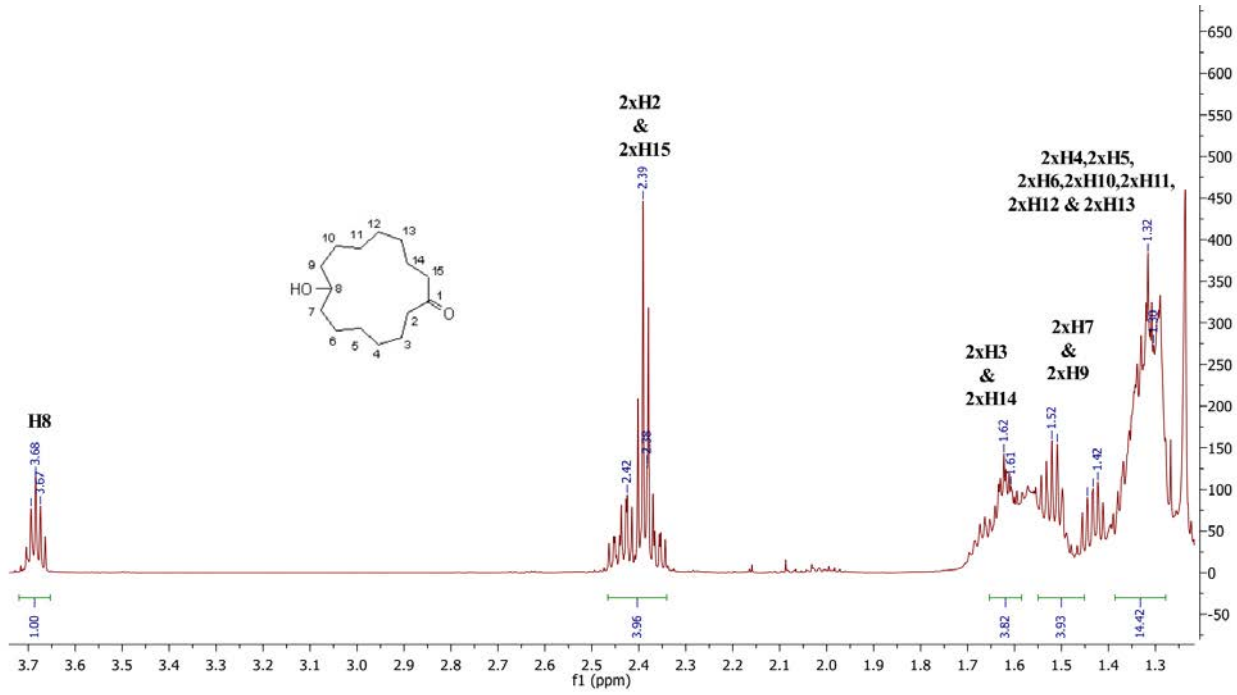

Figure B. 61 ^{1}H NMR spectrum of 8-hydroxycyclopentadecanone (CYP101B1).

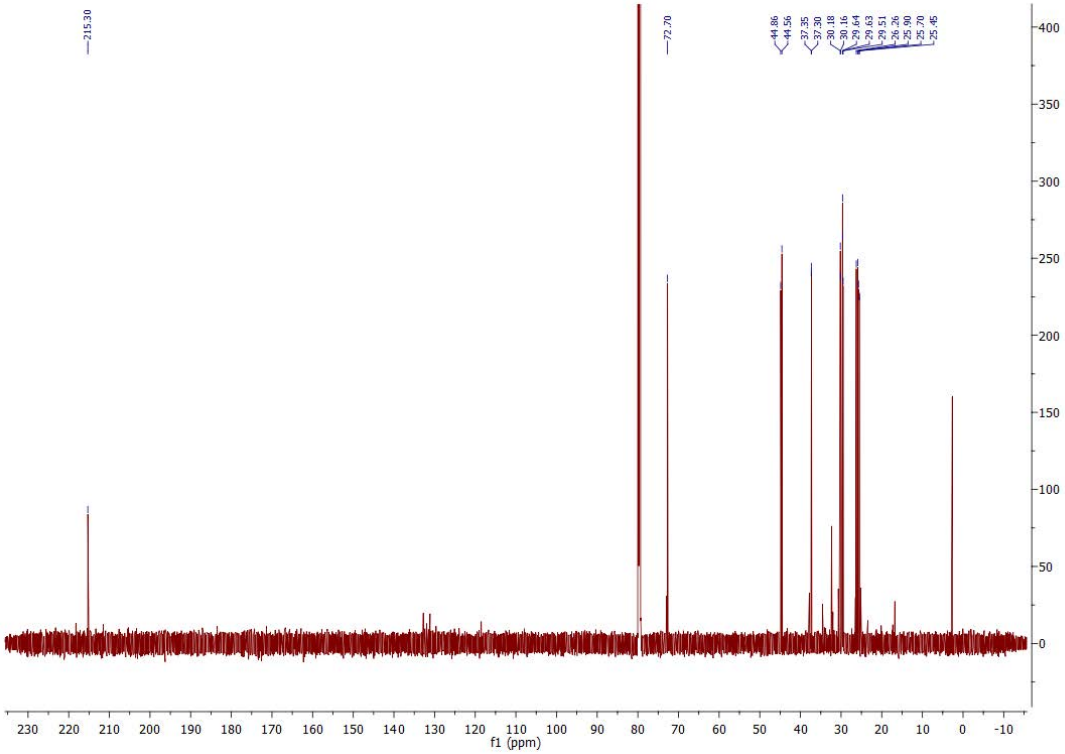

(a)

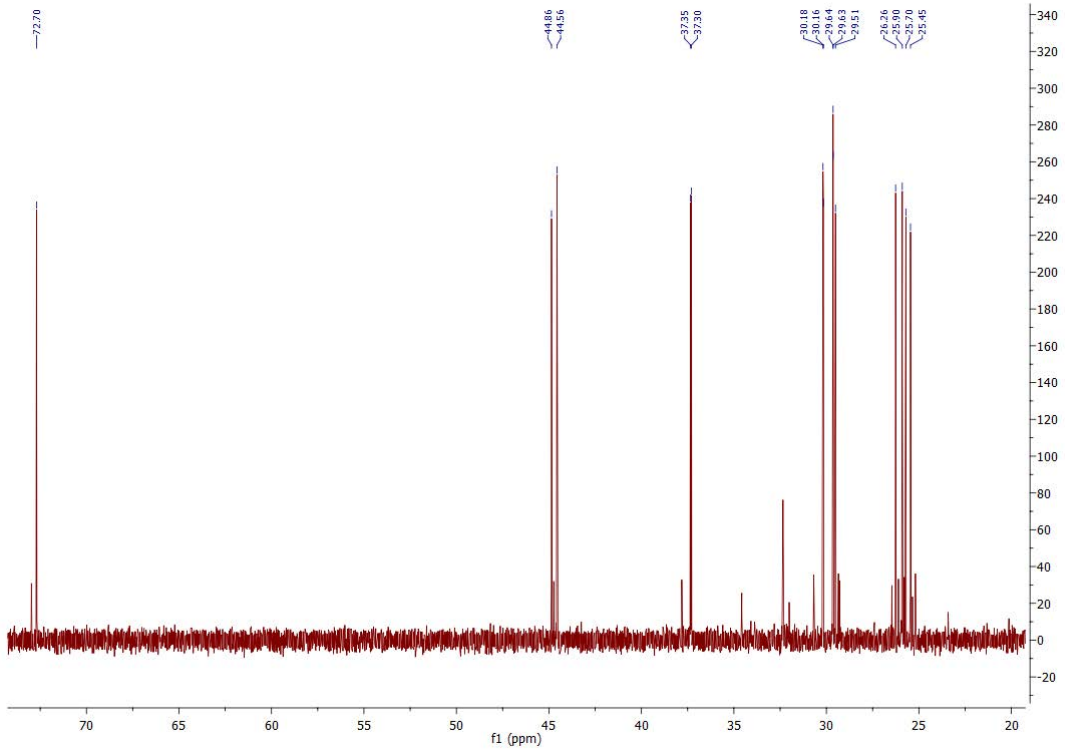

(b)

Figure B. 62 (a) ^{13}C NMR spectrum of 8-hydroxycyclopentadecanone and some minor peaks were also observed indicating one or two minor metabolites (5%) might present. **(b)** Zoomed in ^{13}C NMR spectrum of 8-hydroxycyclopentadecanone from the 25 to 73 ppm region.

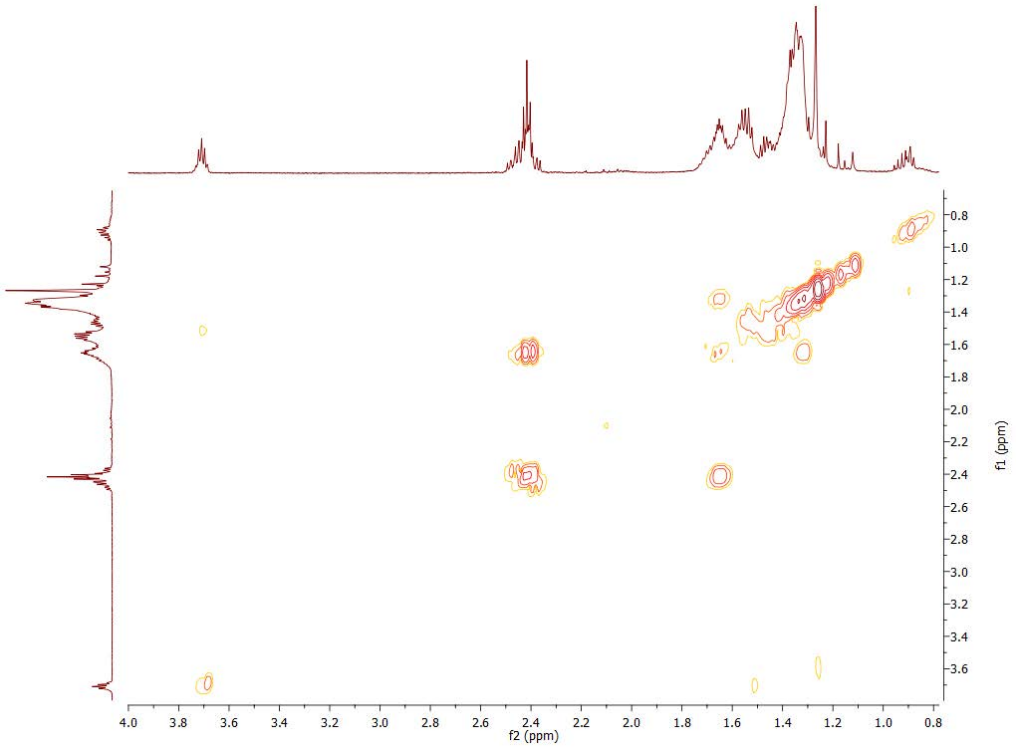

Figure B. 63 gCOSY NMR spectrum of 8-hydroxycyclopentadecanone (CYP101B1).

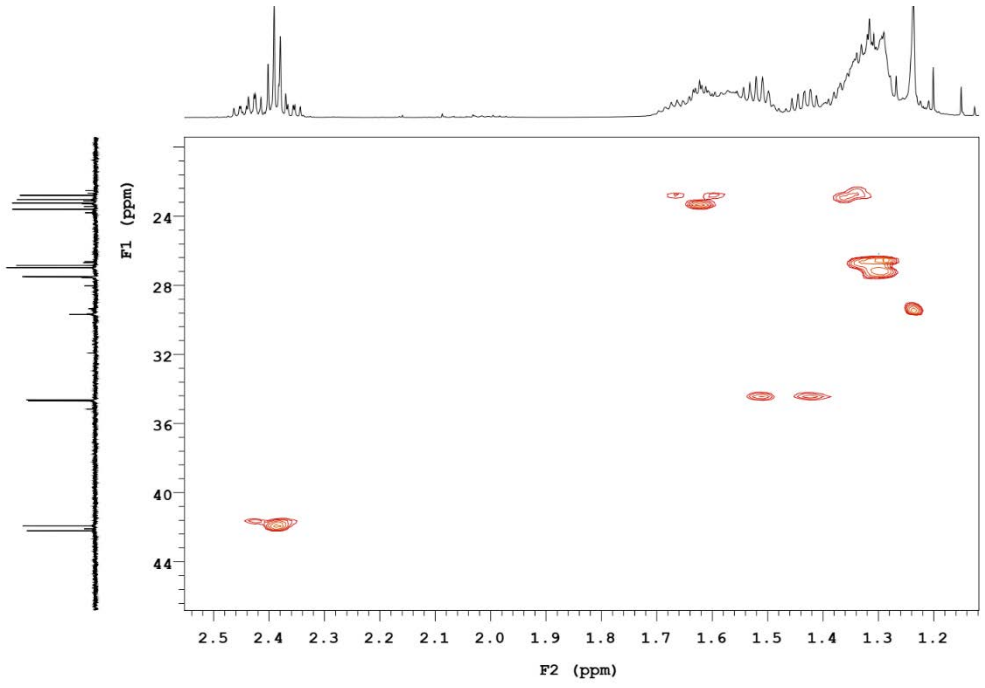

Figure B. 64 Zoomed in (20 to 50 ppm region) HSQC NMR spectrum of 8-hydroxycyclopentadecanone (CYP101B1).

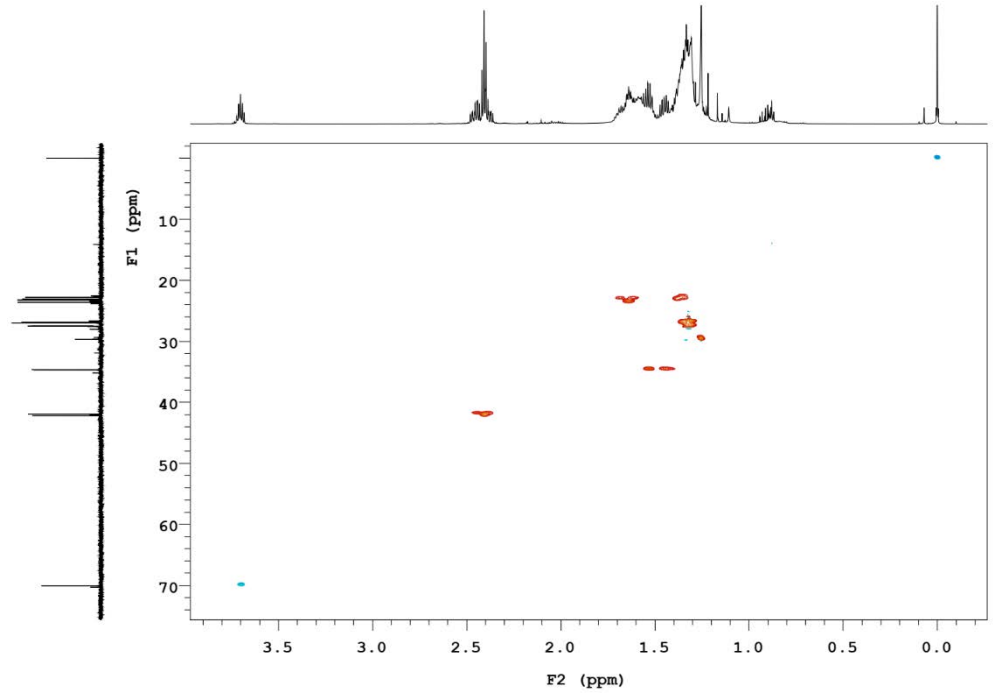

Figure B. 65 HSQC NMR spectrum of 8-hydroxycyclopentadecanone (CYP101B1).

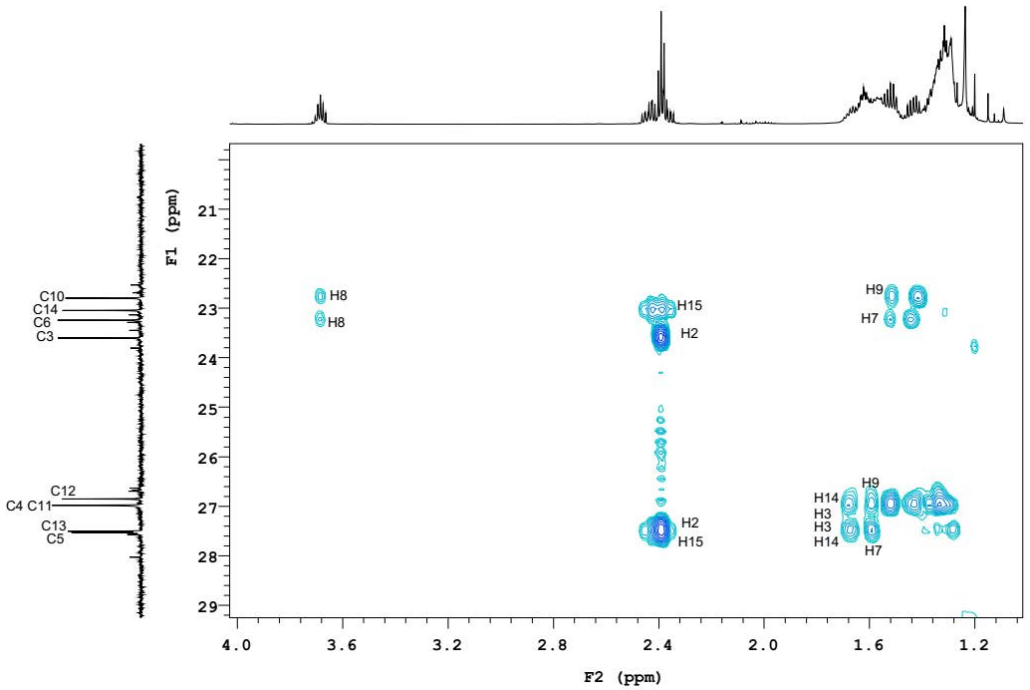

Figure B. 66 Zoomed in (20 to 30 ppm region) HMBC NMR spectrum of 8-hydroxycyclopenta- decanone which highlighted the correlations of carbons with the protons.

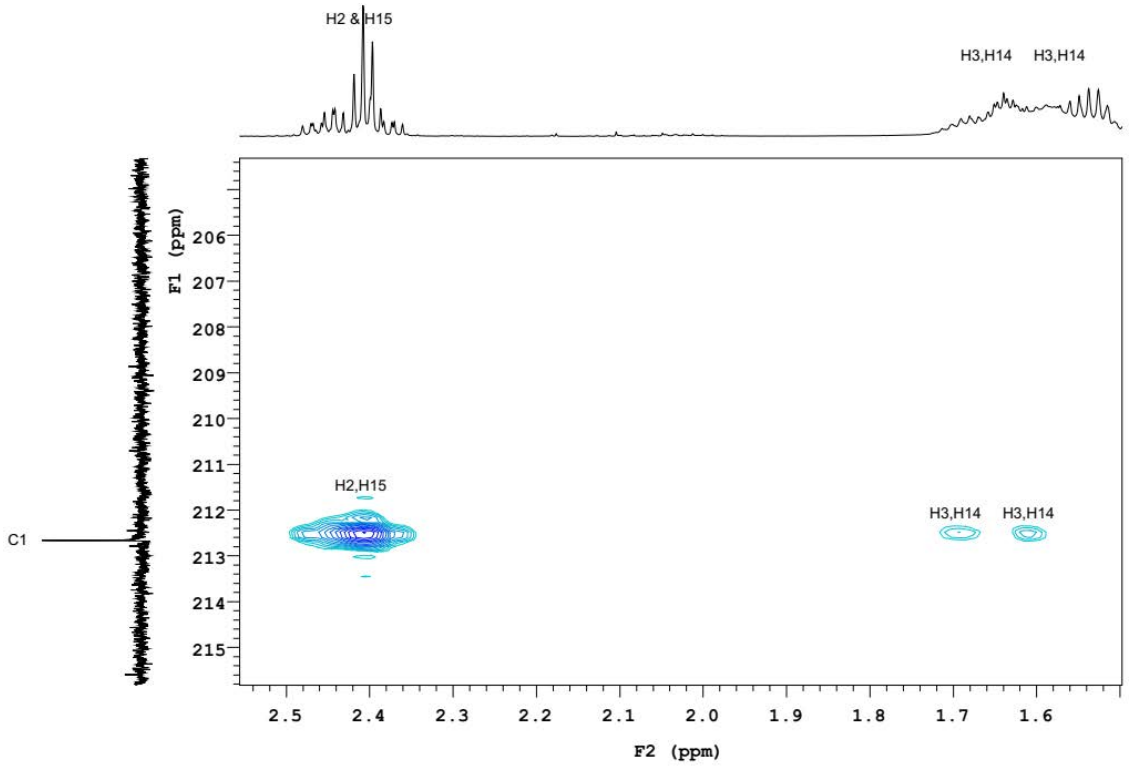

Figure B. 67 Zoomed in C=O (215.30 ppm) region of HMBC NMR spectrum of 8-hydroxycyclopenta- decanone which highlighted the correlations of C1 (215.30 ppm) with H2, H3, H14 and H15.

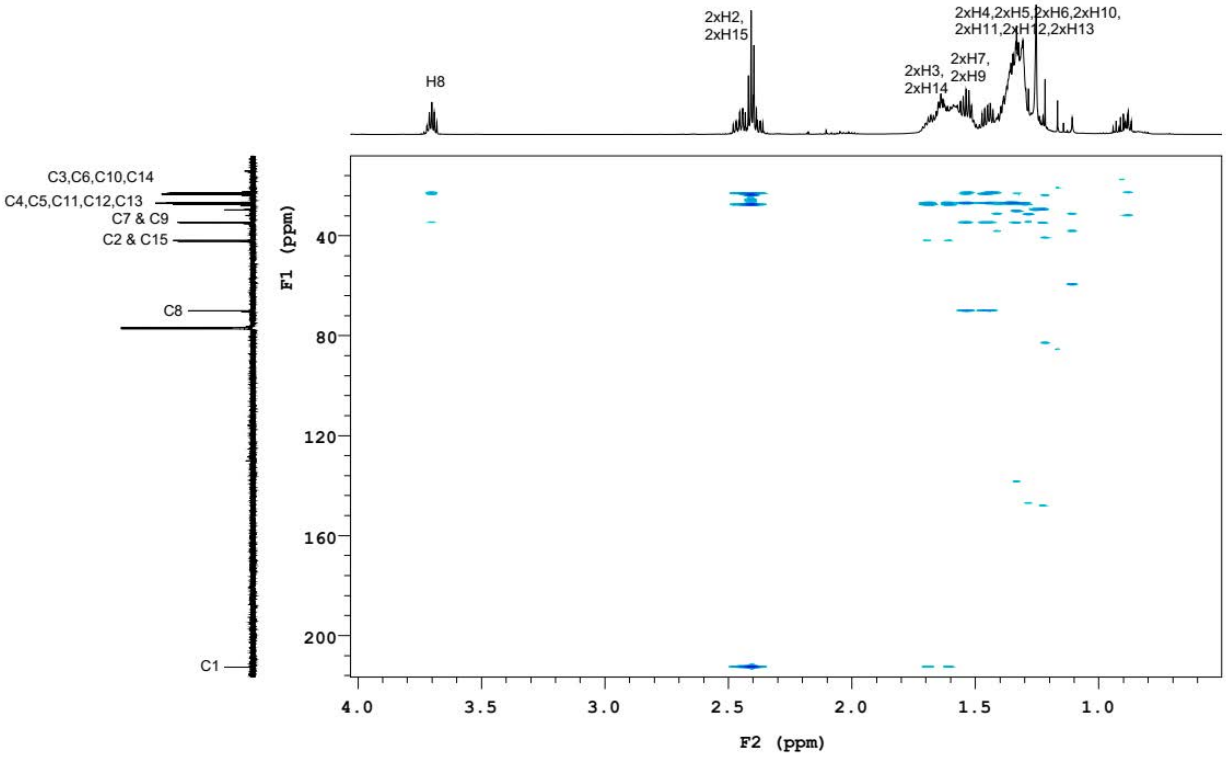

Figure B. 68 HMBC NMR spectrum of 8-hydroxycyclopentadecanone.

NMR data for *trans*-4-hydroxycyclohexyl acetate:

^{1}H NMR (500 MHz, $CDCl_3$) δ 4.77-4.70 (m, 1H, H1), 3.76-3.68 (m, 1H, H4), 2.04 (s, 3H, 3xH8), 2.02-1.93 (m, 4H, $H2_{eq}$, $H3_{eq}$, $H5_{eq}$ & $H6_{eq}$), 1.54-1.36 (m, 4H, $H2_{ax}$, $H3_{ax}$, $H5_{ax}$ & $H6_{ax}$).

^{13}C NMR (126 MHz, $CDCl_3$) δ 173.27 (C7), 74.38 (C1), 71.66 (C4), 34.94 (C3 & C5), 31.27 (C2 & C6), 24.01 (C8).

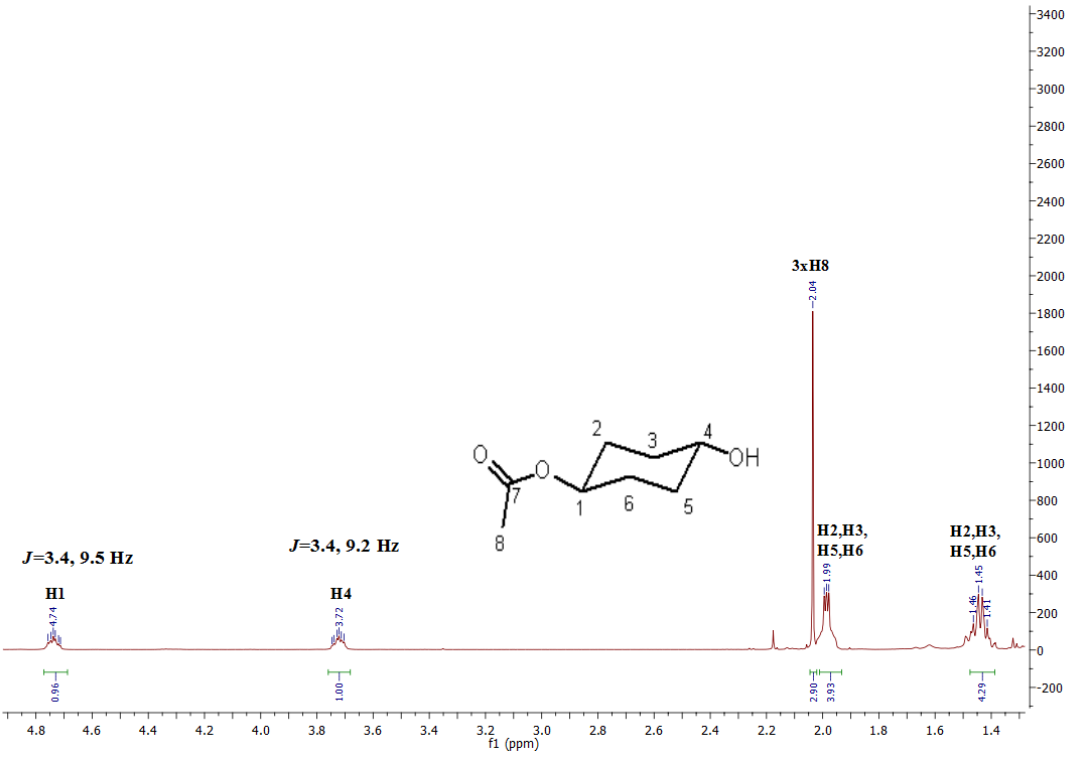

Figure B. 69 ^{1}H NMR spectrum of *trans*-4-hydroxycyclohexyl acetate (cyclohexyl acetate).

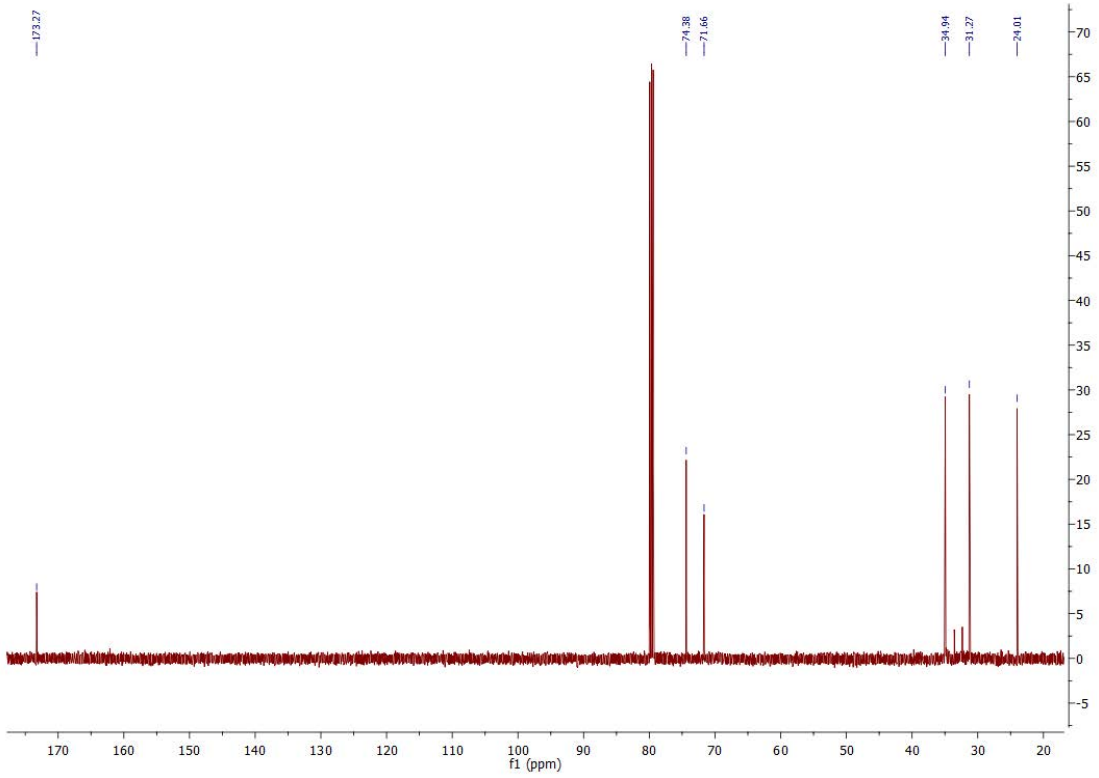

Figure B. 70 ^{13}C NMR spectrum of *trans*-4-hydroxycyclohexyl acetate (cyclohexyl acetate).

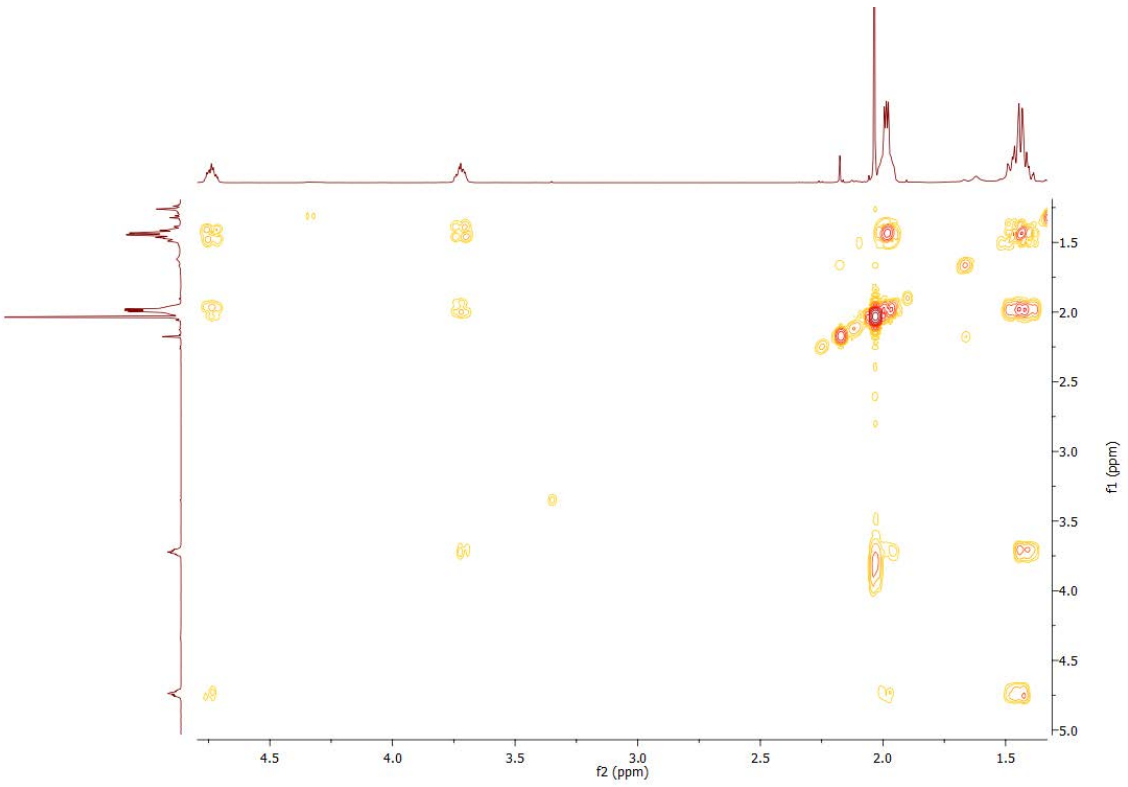

Figure B. 71 gCOSY NMR spectrum of *trans*-4-hydroxycyclohexyl acetate (cyclohexyl acetate).

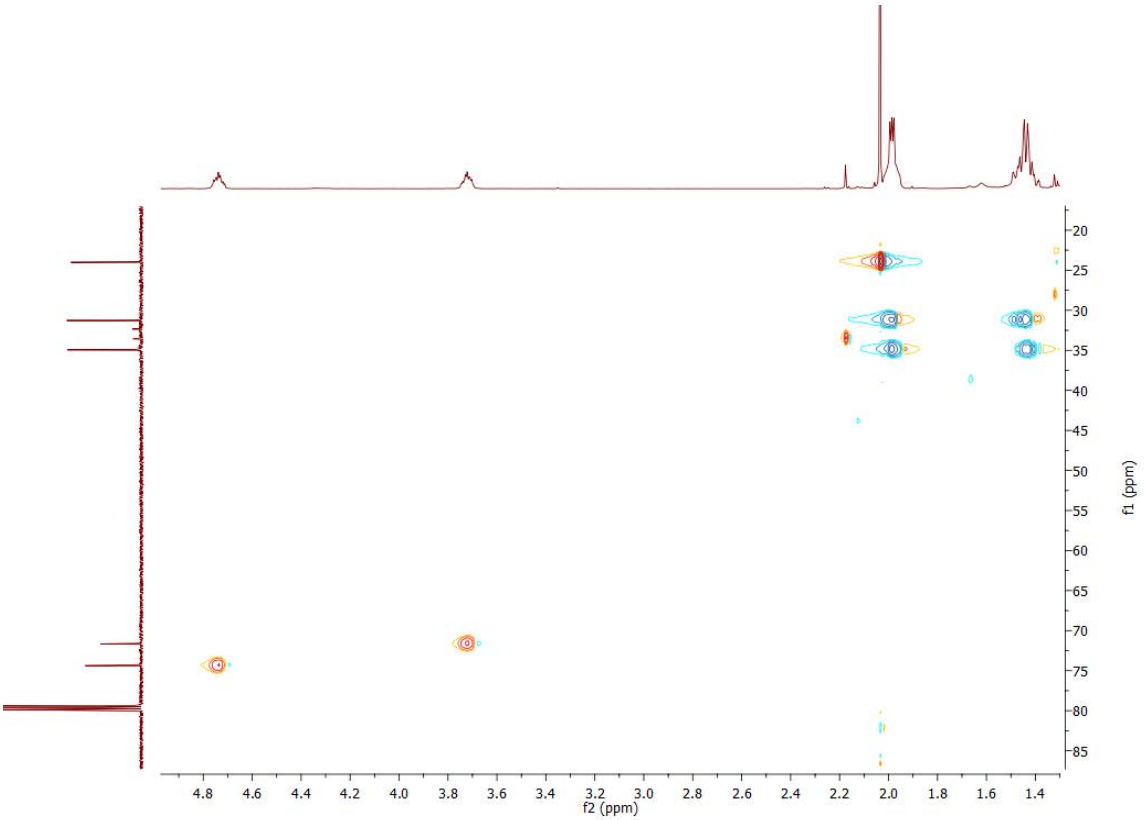

Figure B. 72 HSQC NMR spectrum of *trans*-4-hydroxycyclohexyl acetate (cyclohexyl acetate).

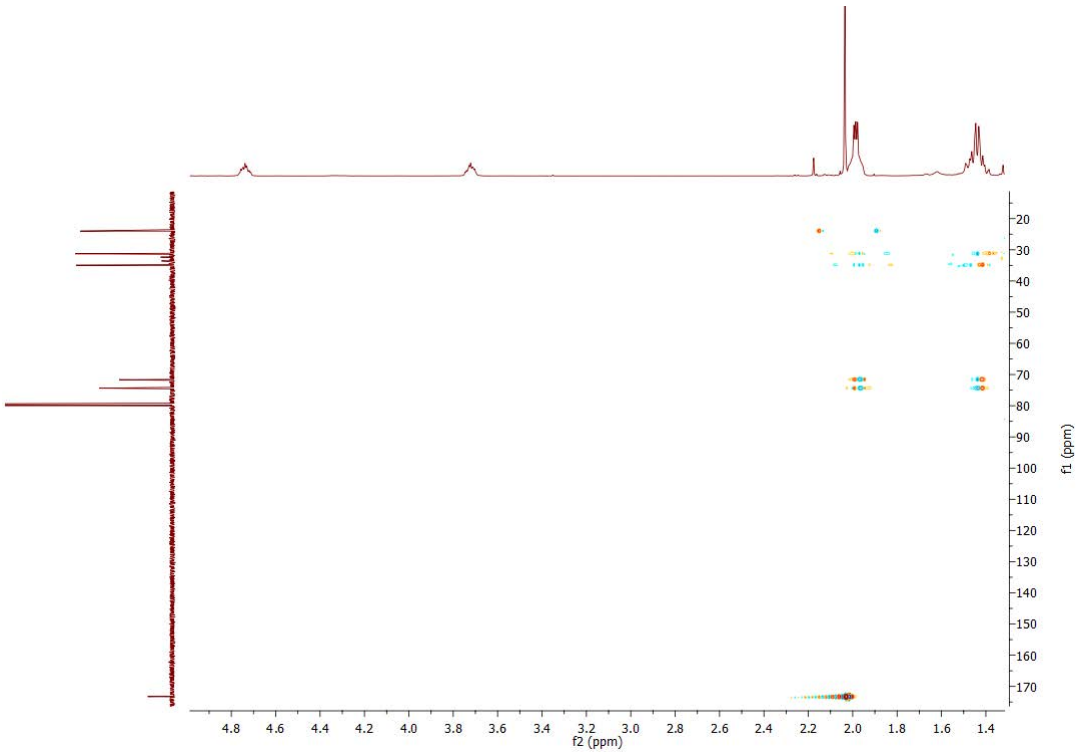

Figure B. 73 HMBC NMR spectrum of *trans*-4-hydroxycyclohexyl acetate (cyclohexyl acetate).

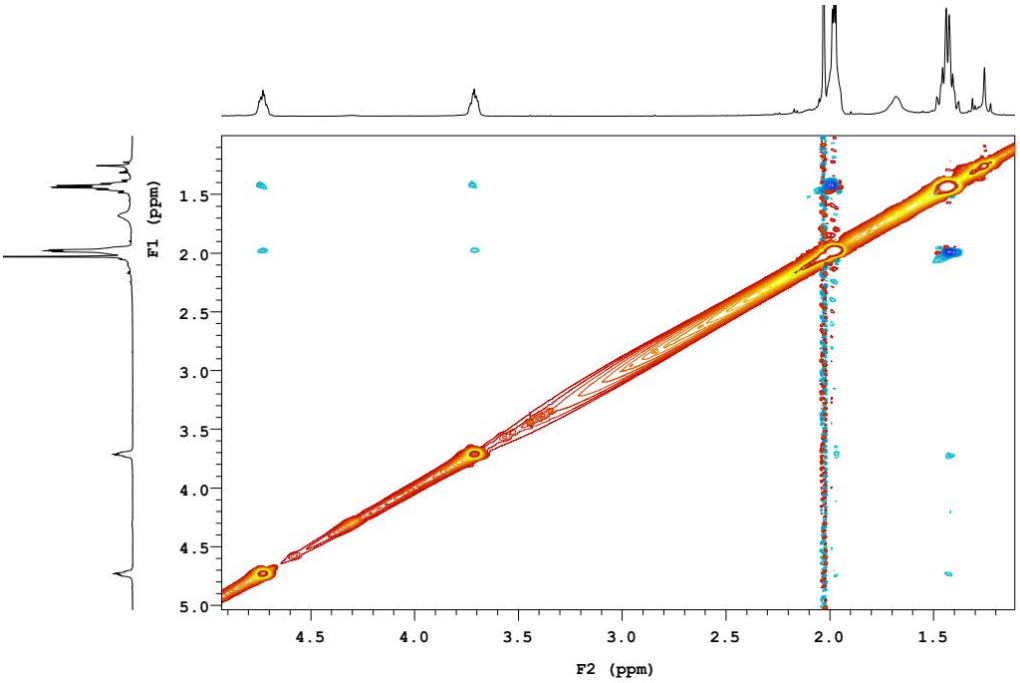

(a)

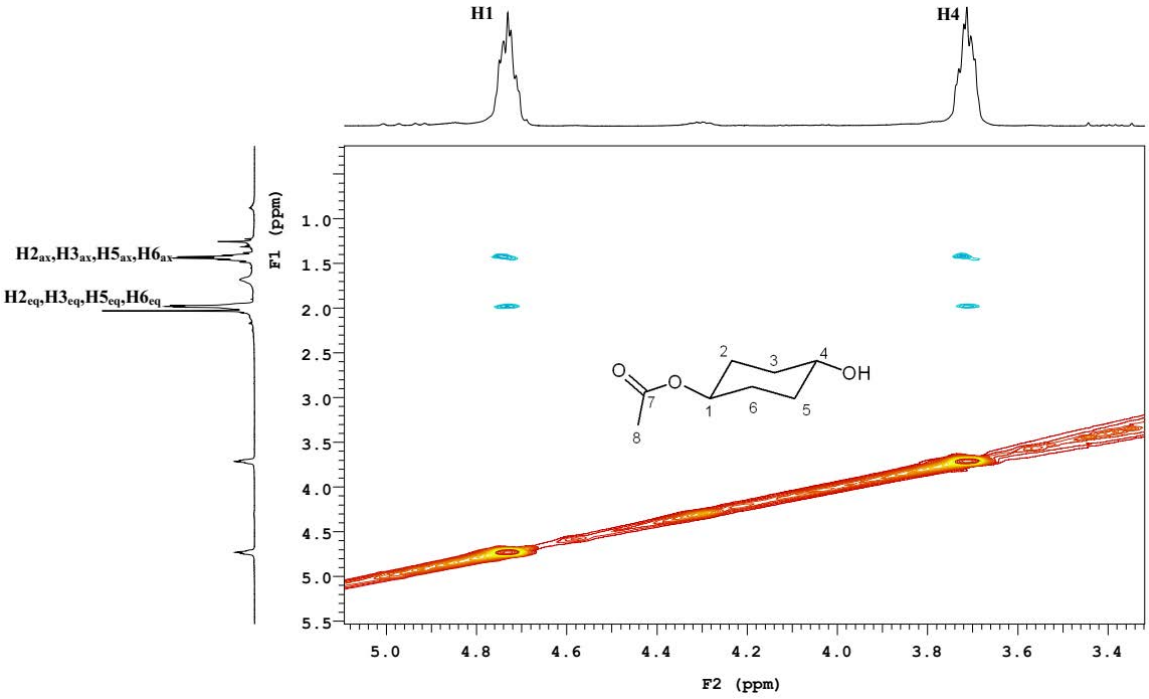

(b)

Figure B. 74 (a) ROESY NMR spectrum of *trans*-4-hydroxycyclohexyl acetate. **(b)** Zoomed in ROESY NMR highlighted the interactions of H1 (4.77-4.70 ppm) and H4 (3.76-3.72 ppm) with the protons of 2.02-1.93 ppm and 1.54-1.36 ppm region.

Data for *trans*-4-hydroxycyclohexyl butyrate:

^{1}H NMR (500 MHz, $CDCl_3$) δ 4.78-4.66 (m, 1H, H1), 3.71-3.60 (m, 1H, H4), 2.22 (*t*, *J* = 7.4 Hz, 2H, 2xH8), 1.99-1.88 (m, 4H, $H2_{eq}$, $H3_{eq}$, $H5_{eq}$ & $H6_{eq}$), 1.61 (*sextet*, *J* = 7.4 Hz, 2H, 2xH9), 1.47-1.33 (4H, $H2_{ax}$, $H3_{ax}$, $H5_{ax}$ & $H6_{ax}$), 0.91 (*t*, *J* = 7.4 Hz, 3H, 3xH10)

^{13}C NMR (126 MHz, $CDCl_3$) δ 175.93 (C7), 74.11 (C1), 71.47 (C4), 39.17 (C8), 34.80 (C3 & C5), 31.25 (C2 & C6), 21.16 (C9), 16.22 (C10).

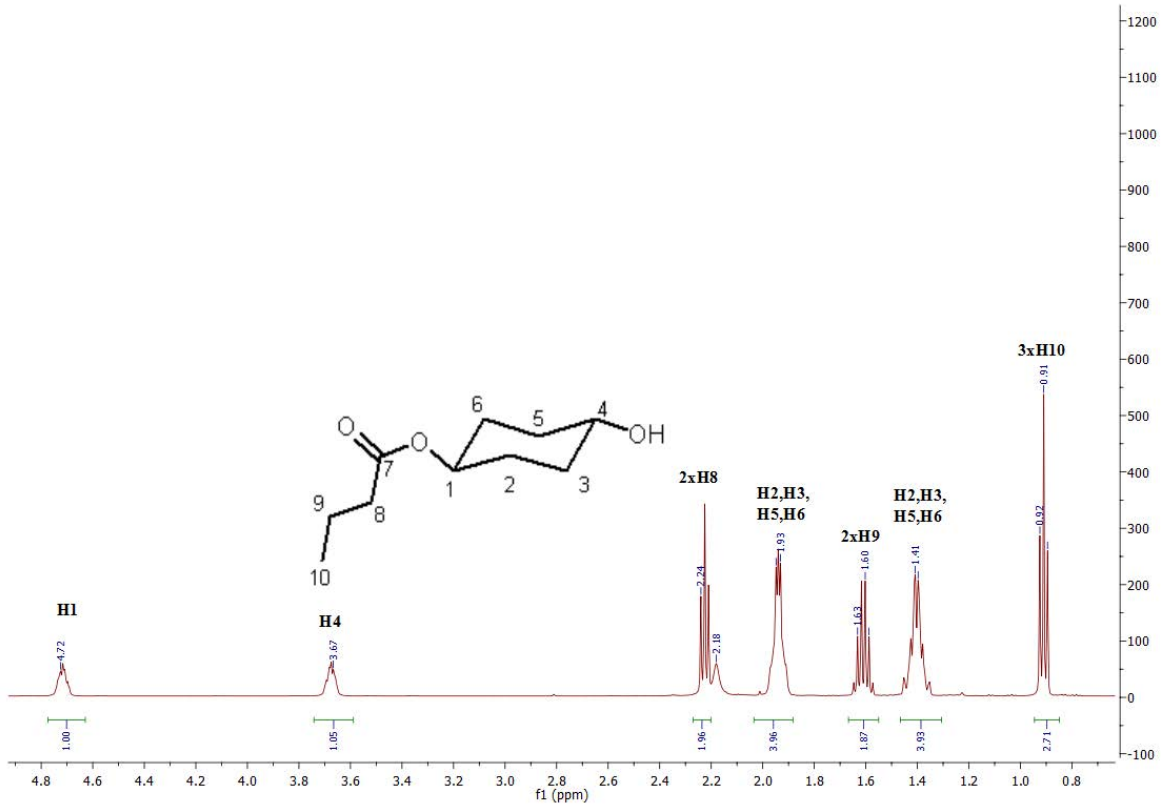

Figure B. 75 ^{1}H NMR spectrum of *trans*-4-hydroxycyclohexyl butyrate (cyclohexyl butyrate).

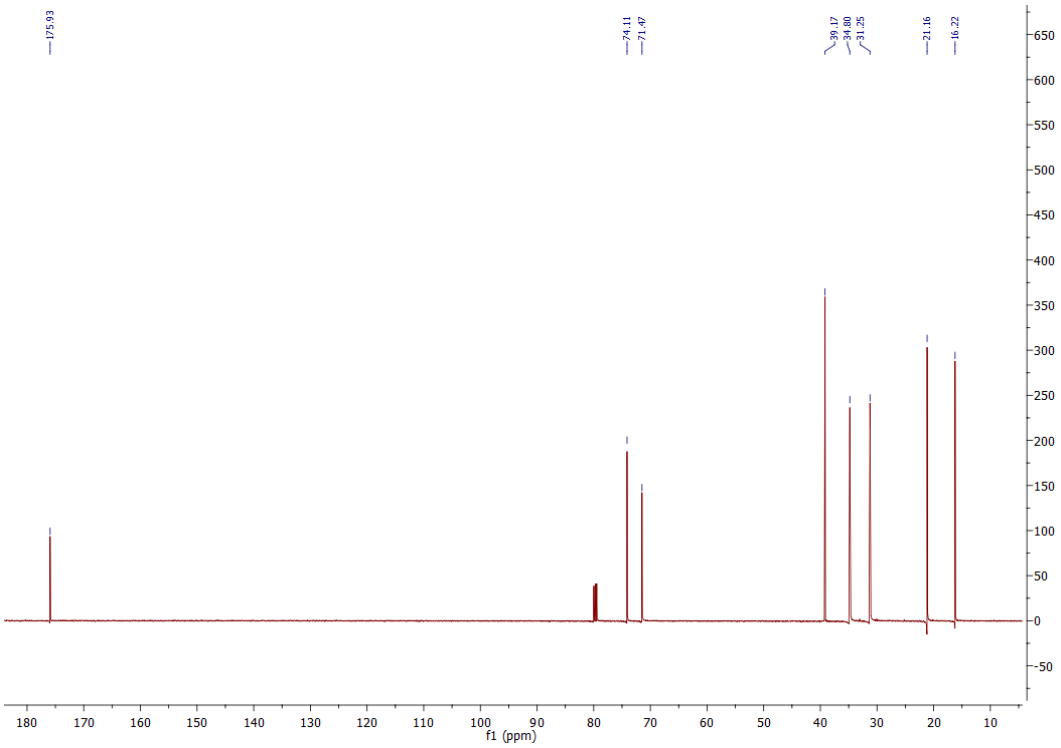

Figure B. 76 ^{13}C NMR spectrum of *trans*-4-hydroxycyclohexyl butyrate (cyclohexyl butyrate).

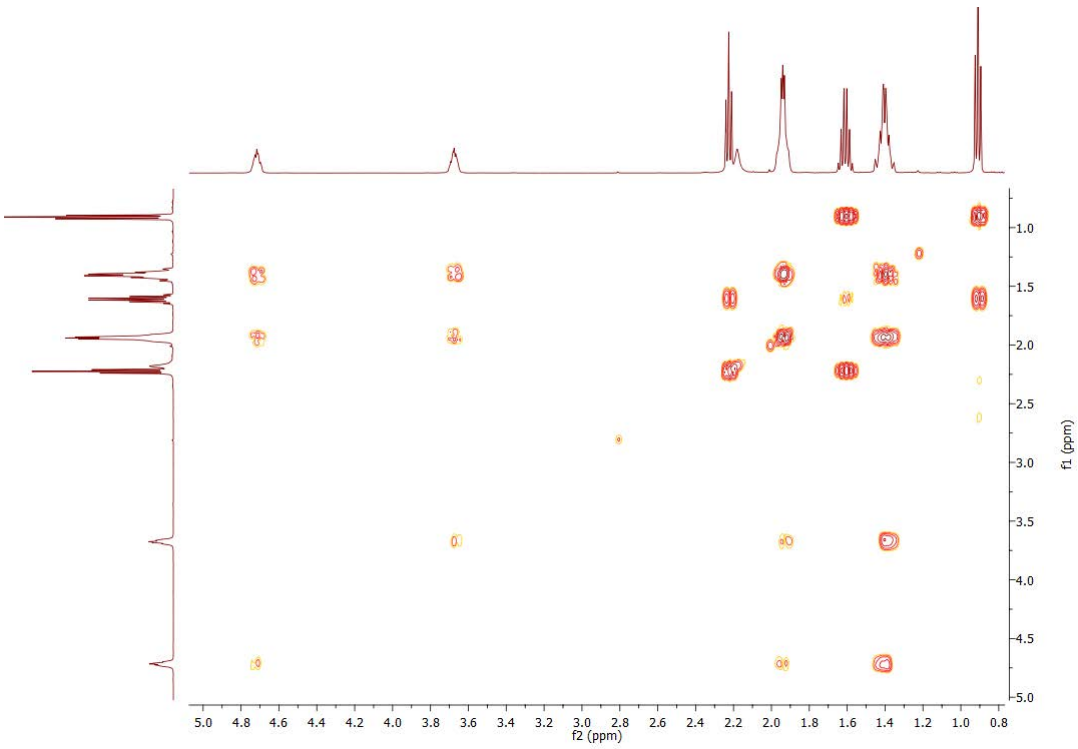

Figure B. 77 gCOSY NMR spectrum of *trans*-4-hydroxycyclohexyl butyrate (cyclohexyl butyrate).

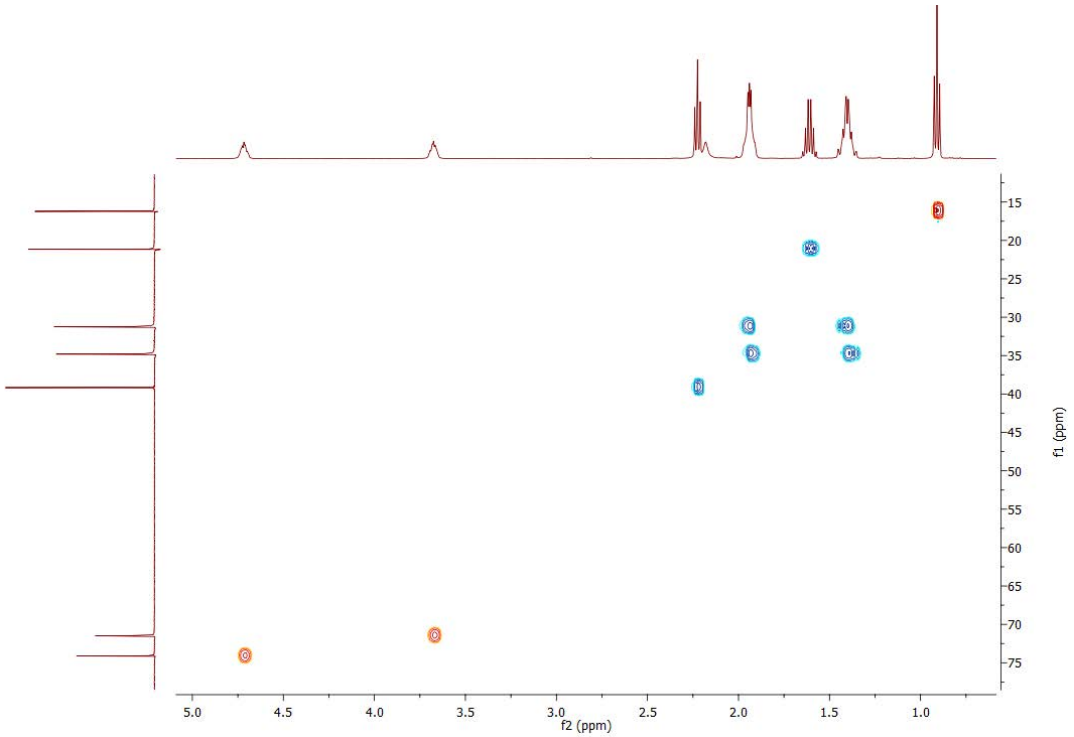

Figure B. 78 HSQC NMR spectrum of *trans*-4-hydroxycyclohexyl butyrate (cyclohexyl butyrate).

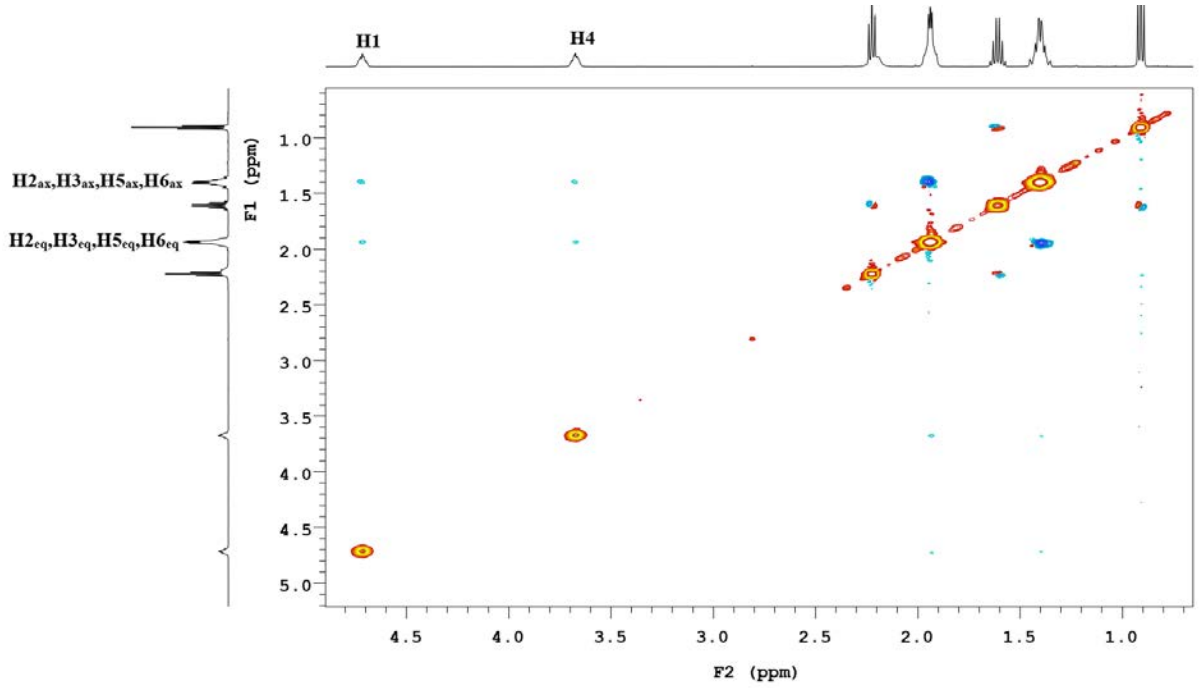

(a)

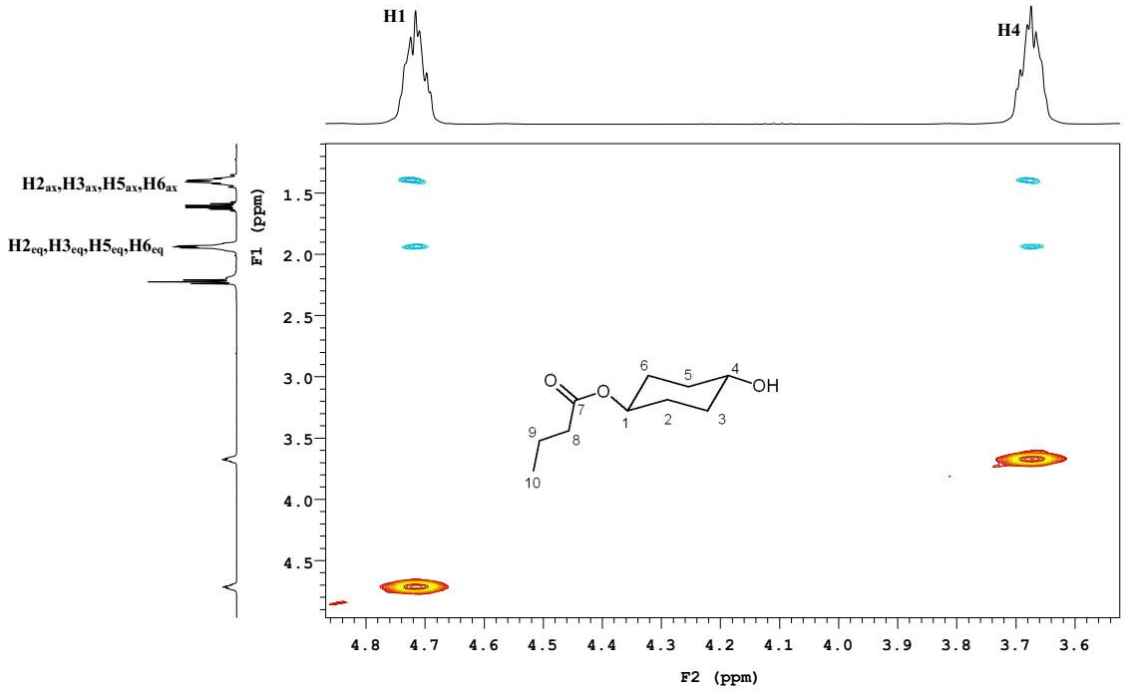

(b)

Figure B. 79 (a) ROESY NMR spectrum of *trans*-4-hydroxycyclohexyl butyrate. **(b)** Zoomed in ROESY NMR which highlighted the interactions of H1 (4.78-4.66 ppm) and H4 (3.71-3.60 ppm) with the protons of 1.99-1.88 ppm and 1.47-1.33 ppm region.

NMR for *trans*-4-hydroxycyclohexyl isobutyrate:

^{1}H NMR (500 MHz, $CDCl_3$) δ 4.78-4.69 (m, 1H, H1), 3.78-3.7 (m, 1H, H4), 2.51 (*septet*, J = 7 Hz, 1H, H8), 2.04-1.89 (m, 4H, $H2_{eq}$, $H3_{eq}$, $H5_{eq}$ & $H6_{eq}$), 1.51-1.43 (m, 4H, $H2_{ax}$, $H3_{ax}$, $H5_{ax}$ & $H6_{ax}$), 1.16 (d, J = 7.0 Hz, 6H, 3xH9 & 3xH10)

^{13}C NMR (126 MHz, $CDCl_3$) δ 179.33(C7), 73.82(C1),71.6 (C3), 36.83 (C8), 34.75 (C3 & C5), 31.04 (C2 & C6), 21.64 (C9 & C10).

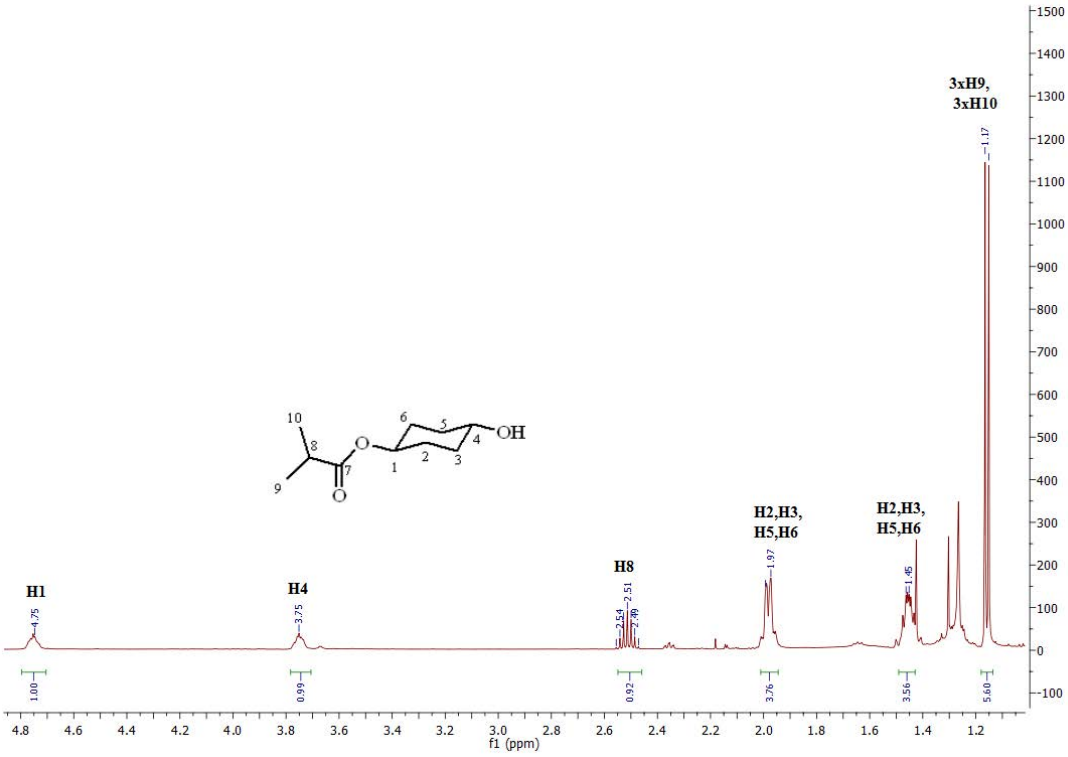

Figure B. 80 ^{1}H NMR spectrum of *trans*-4-hydroxycyclohexyl isobutyrate (cyclohexyl isobutyrate).

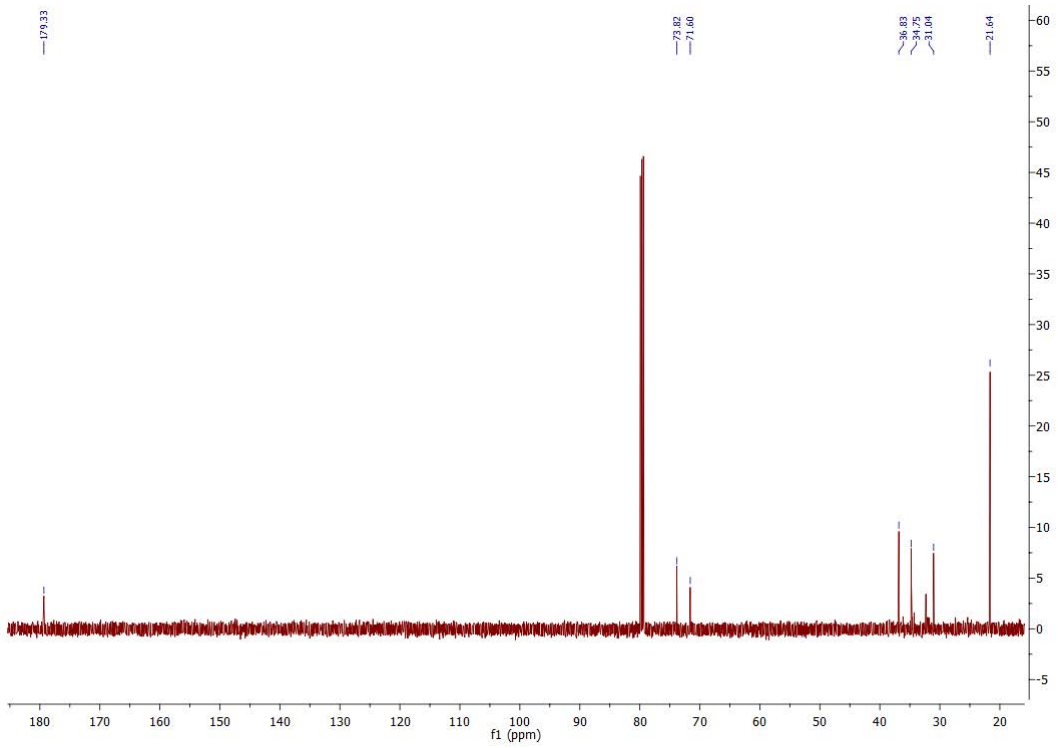

Figure B. 81 ^{13}C NMR spectrum of *trans*-4-hydroxycyclohexyl isobutyrate (cyclohexyl isobutyrate).

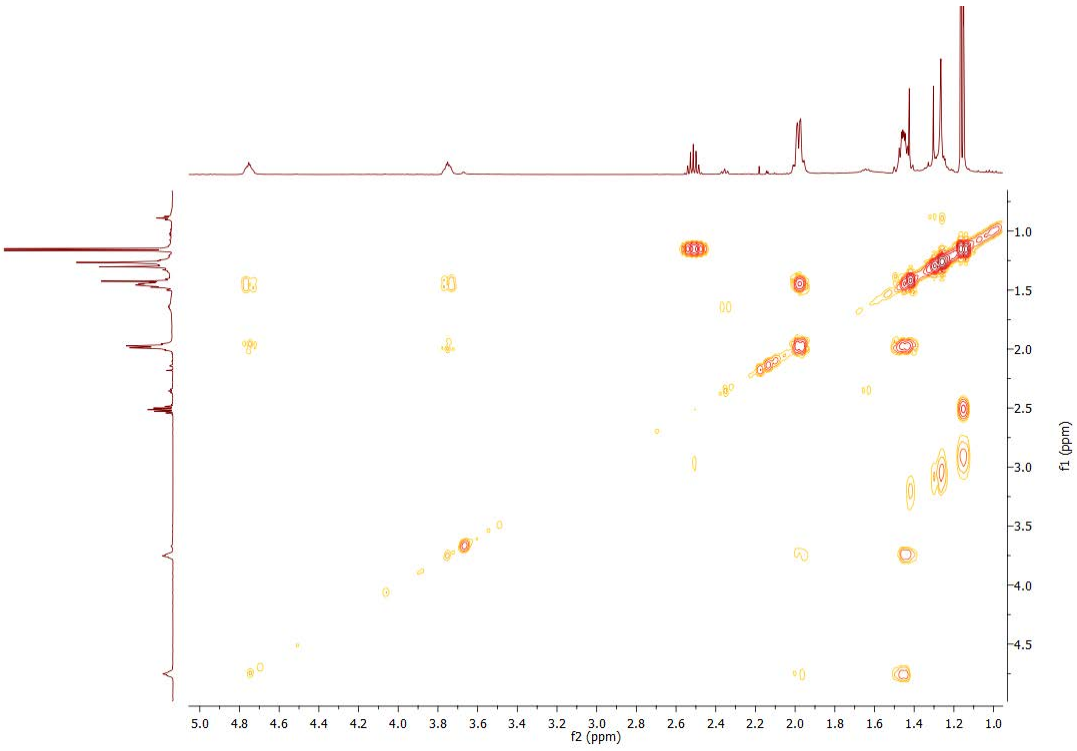

Figure B. 82 gCOSY NMR spectrum of *trans*-4-hydroxycyclohexyl isobutyrate (cyclohexyl isobutyrate).

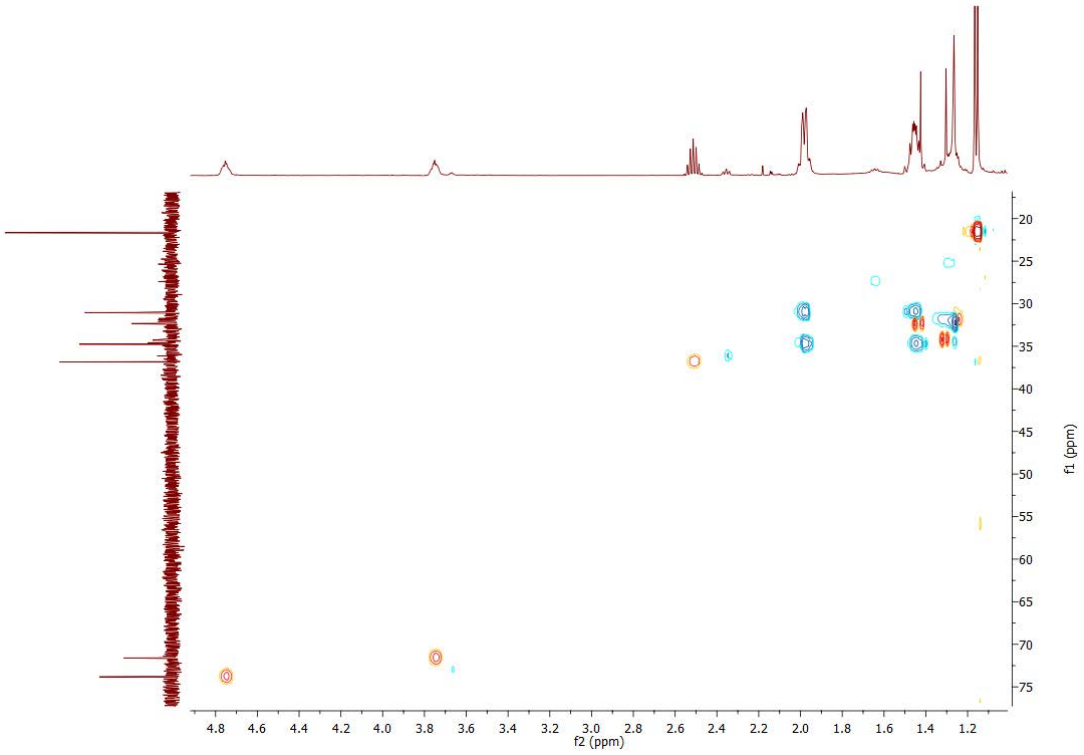

Figure B. 83 HSQC NMR spectrum of *trans*-4-hydroxycyclohexyl isobutyrate (cyclohexyl isobutyrate).

NMR for 4-(1-hydroxy-2-methylpropan-2-yl)cyclohexyl acetate:

^{1}H NMR (500 MHz, $CDCl_3$) δ 4.66-4.56 (m, 1H, H1), 3.39 (s, 2H, 2xH8), 2.06-1.95 (m, 5H, H2, H6, 3xH12), 1.81-1.72 (m, 2H, H3, H5), 1.35-1.27 (m, 3H, H2, H4, H6), 1.2-1.13 (m, 2H, H3, H5), 0.84 (s, 6H, 3xH9, 3xH10).

^{13}C NMR (126 MHz, $CDCl_3$) δ 173.39 (C11), 76.18 (C1), 73.38 (C8), 44.57 (C4), 34.68 (C2 & C6), 27.73 (C3 & C5), 24.39 (C12), 24.11 (C7).

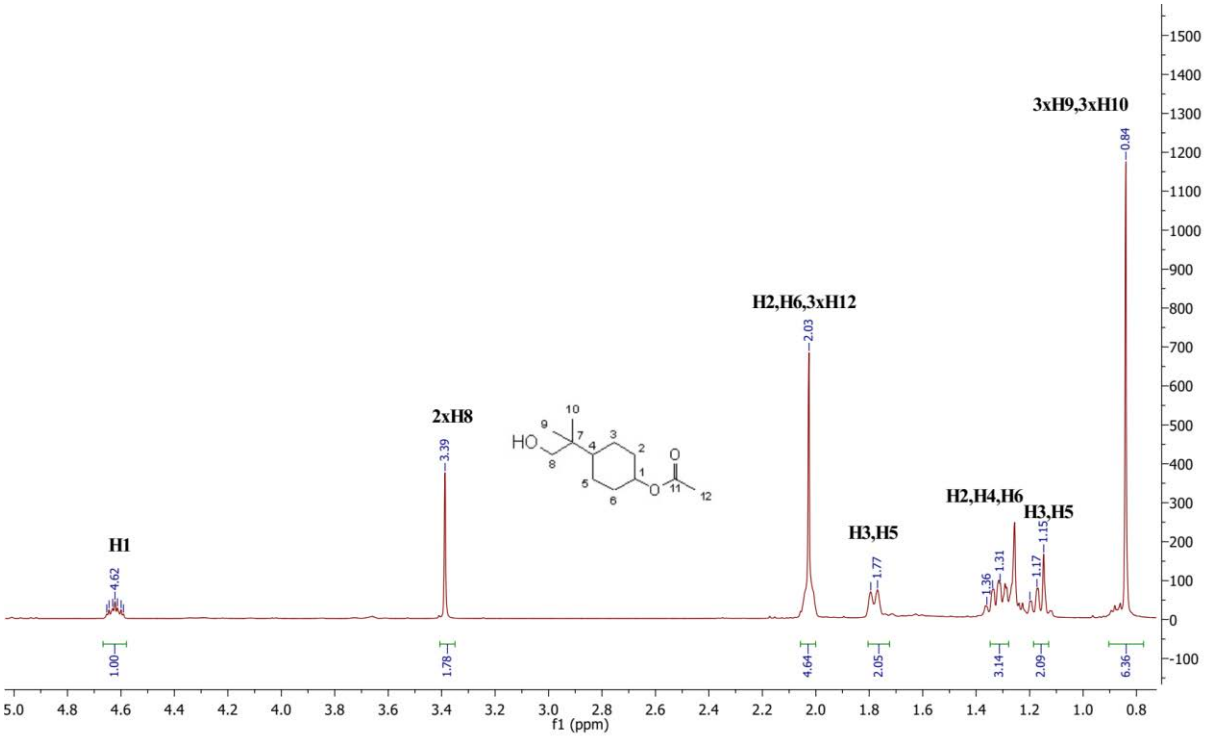

Figure B. 84 ^{1}H NMR spectrum of 4-(1-hydroxy-2-methylpropan-2-yl)cyclohexyl acetate (4-*tert*-butylcyclohexyl acetate). The coupling constants of H1 peak J = 4.2, 11.3 Hz indicated it's a *trans* isomer of 4-*tert*-butylcyclohexyl acetate (Figure B. 85).

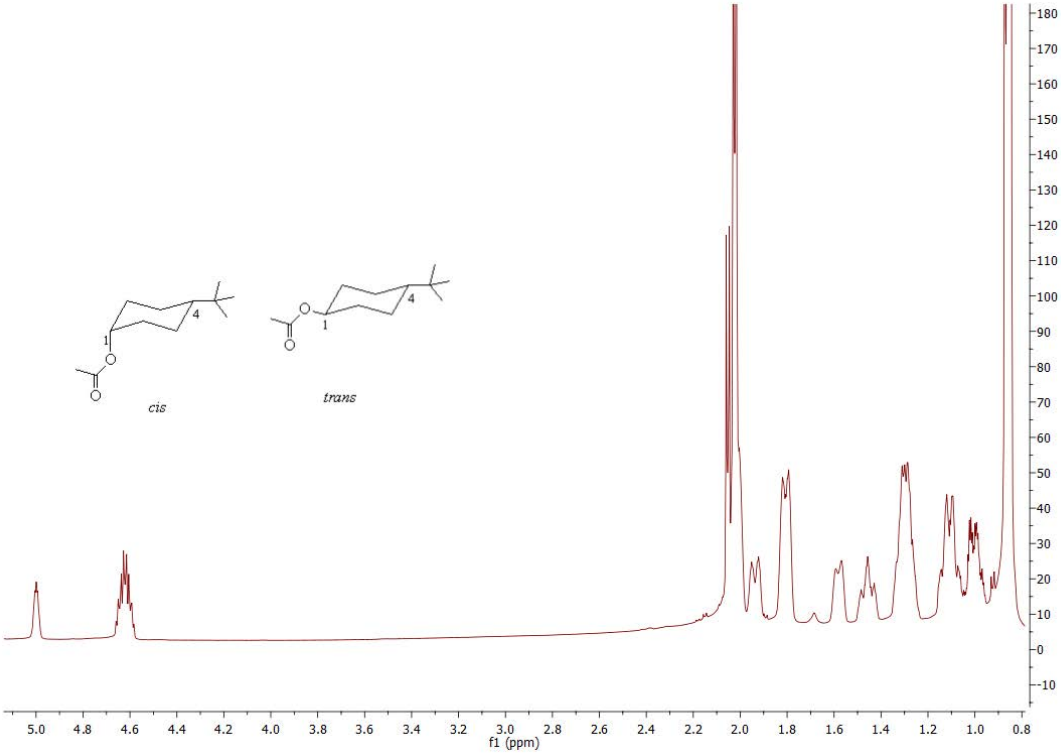

(a)

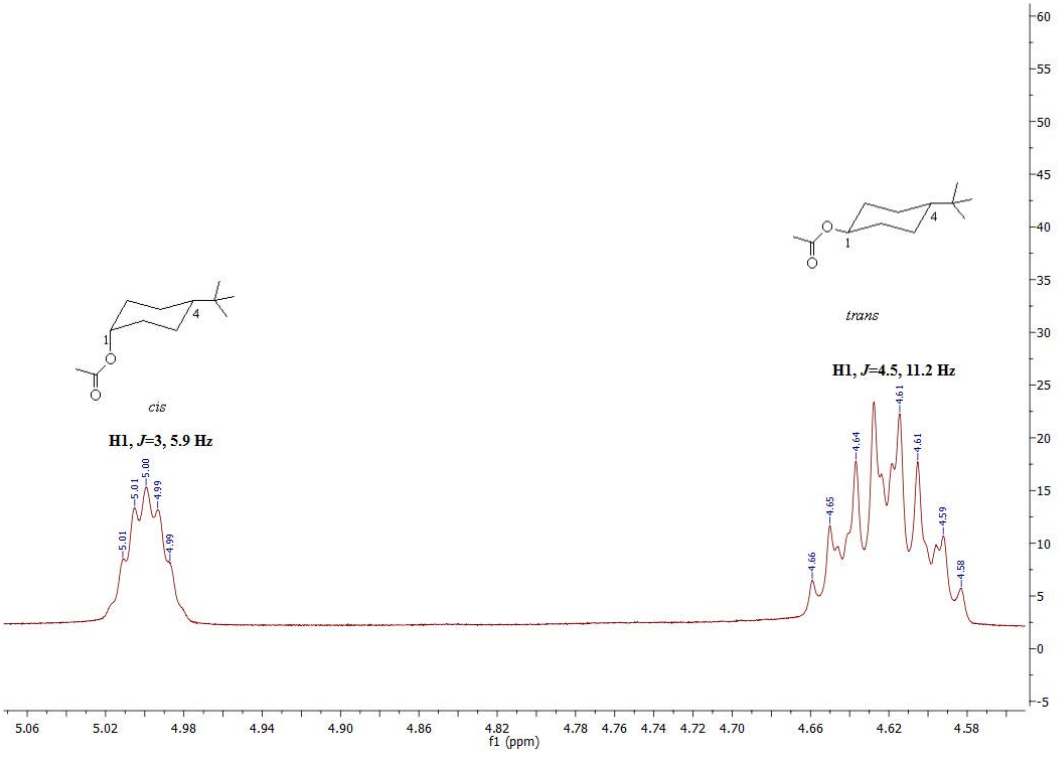

(b)

Figure B. 85 (a) The ^{1}H NMR spectrum of a mixture of *cis* and *trans* 4-*tert*-butylcyclohexyl acetate (substrate). **(b)** Zoomed in ^{1}H NMR spectrum of the substrate to highlight the H1 peaks and from the coupling constants of both peak *cis* and *trans* isomers were assigned.

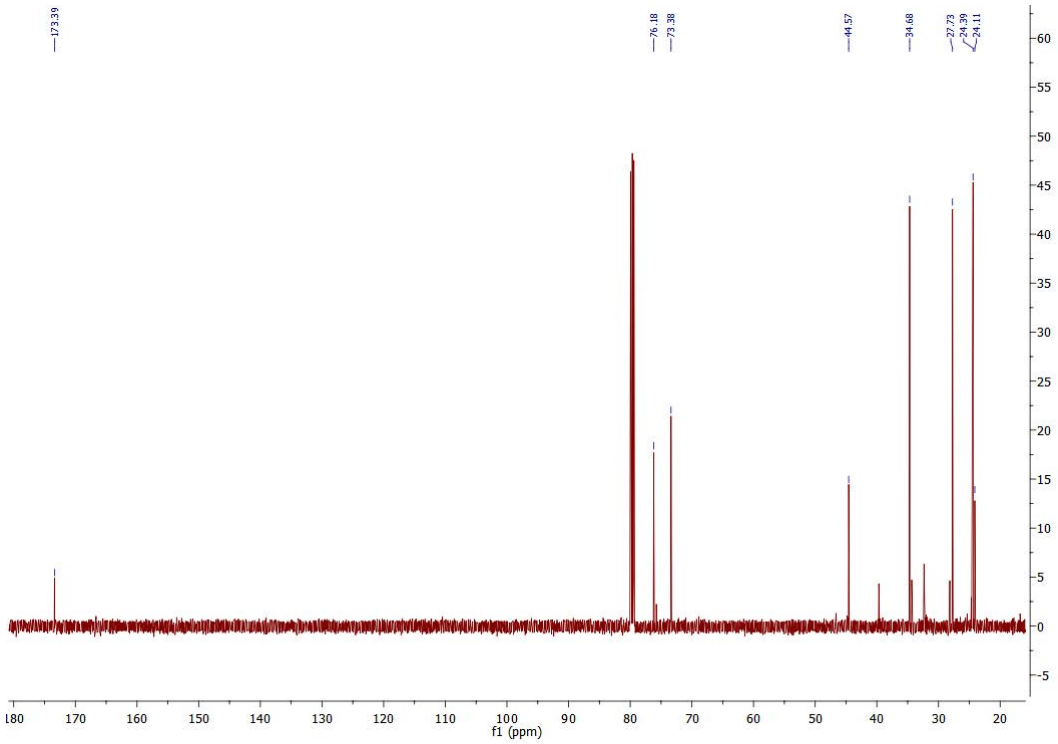

Figure B. 86 ^{13}C NMR spectrum of 4-(1-hydroxy-2-methylpropan-2-yl)cyclohexyl acetate (4-*tert*-butylcyclohexyl acetate).

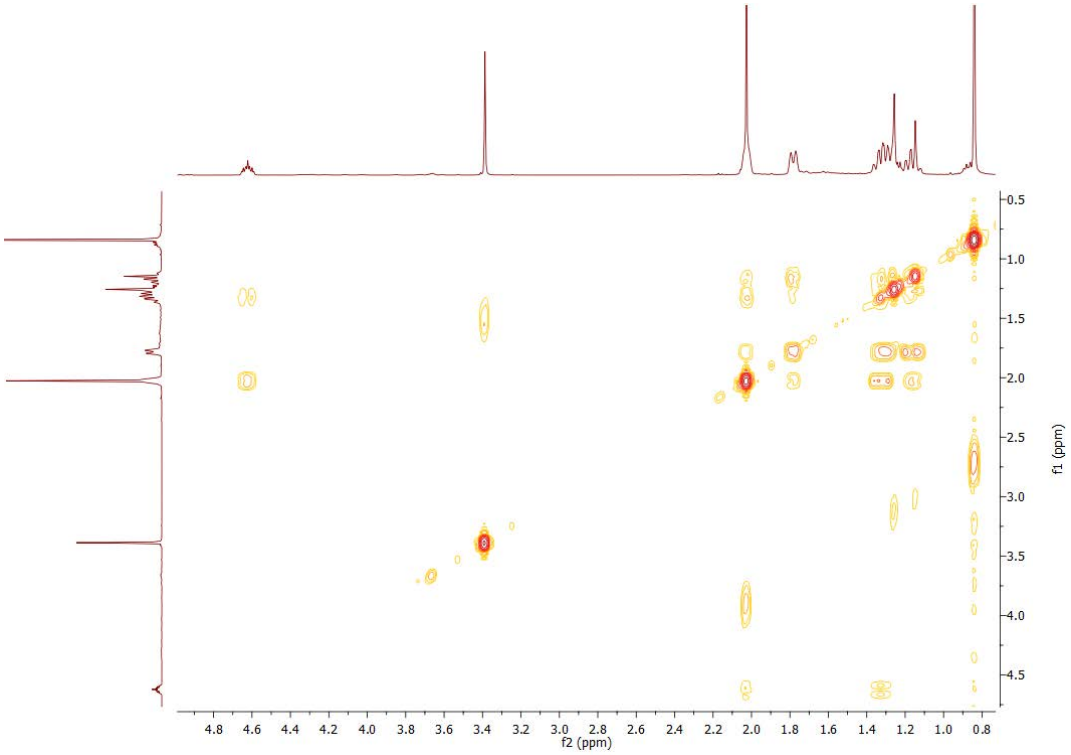

Figure B. 87 gCOSY NMR spectrum of 4-(1-hydroxy-2-methylpropan-2-yl)cyclohexyl acetate (4-*tert*-butylcyclohexyl acetate).

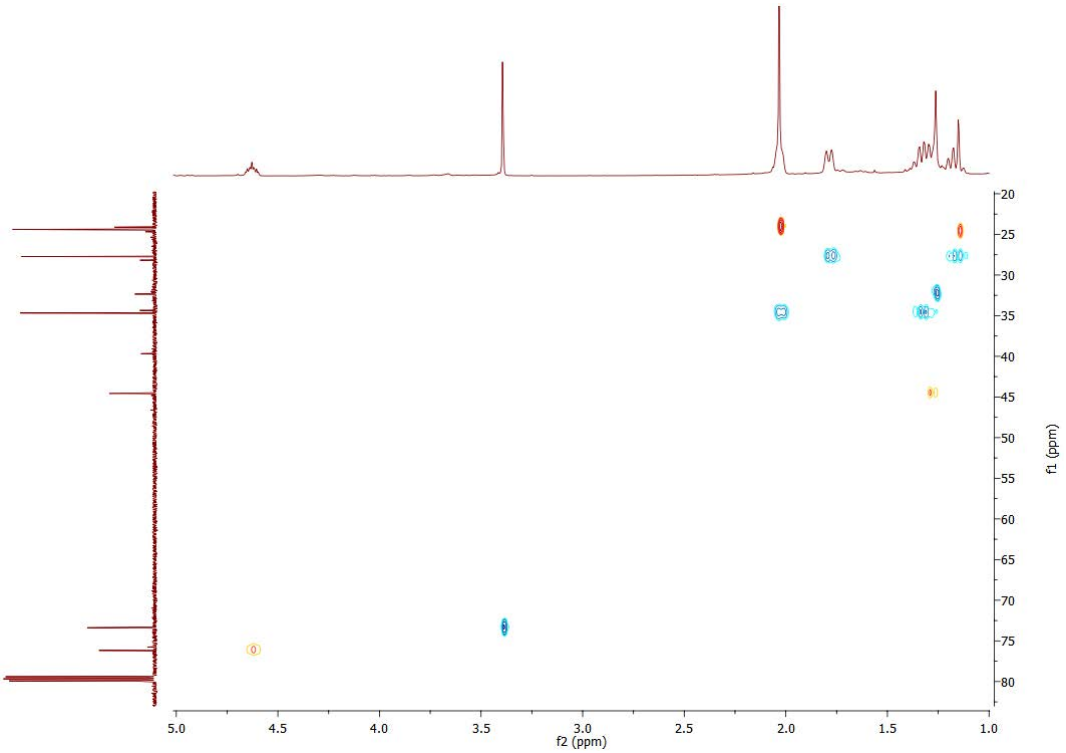

Figure B. 88 HSQC NMR spectrum of 4-(1-hydroxy-2-methylpropan-2-yl)cyclohexyl acetate (4-*tert*-butylcyclohexyl acetate).

NMR data for methyl-2-(*trans*-4-hydroxycyclohexyl)acetate:

^{1}H NMR (500 MHz, $CDCl_3$) δ 3.68 (s, 3H, 3xH9), 3.59-3.52 (m, 1H, H4), 2.21 (d, J = 6.8 Hz, 2H, 2xH7), 2.02-1.94 (m, 2H, $H3_{eq}$ & $H5_{eq}$), 1.84-1.74 (m, 3H, H1, $H2_{eq}$ & $H6_{eq}$), 1.36-1.28 (m, 2H, $H3_{ax}$ & $H5_{ax}$), 1.12-1.00 (m, 2H, $H2_{ax}$ & $H6_{ax}$).

^{13}C NMR (126 MHz, $CDCl_3$) δ 175.94 (C8), 73.25 (C4), 54.10 (C9), 43.71 (C7), 37.86 (C3 & C5), 36.51 (C1), 33.61 (C2 & C6).

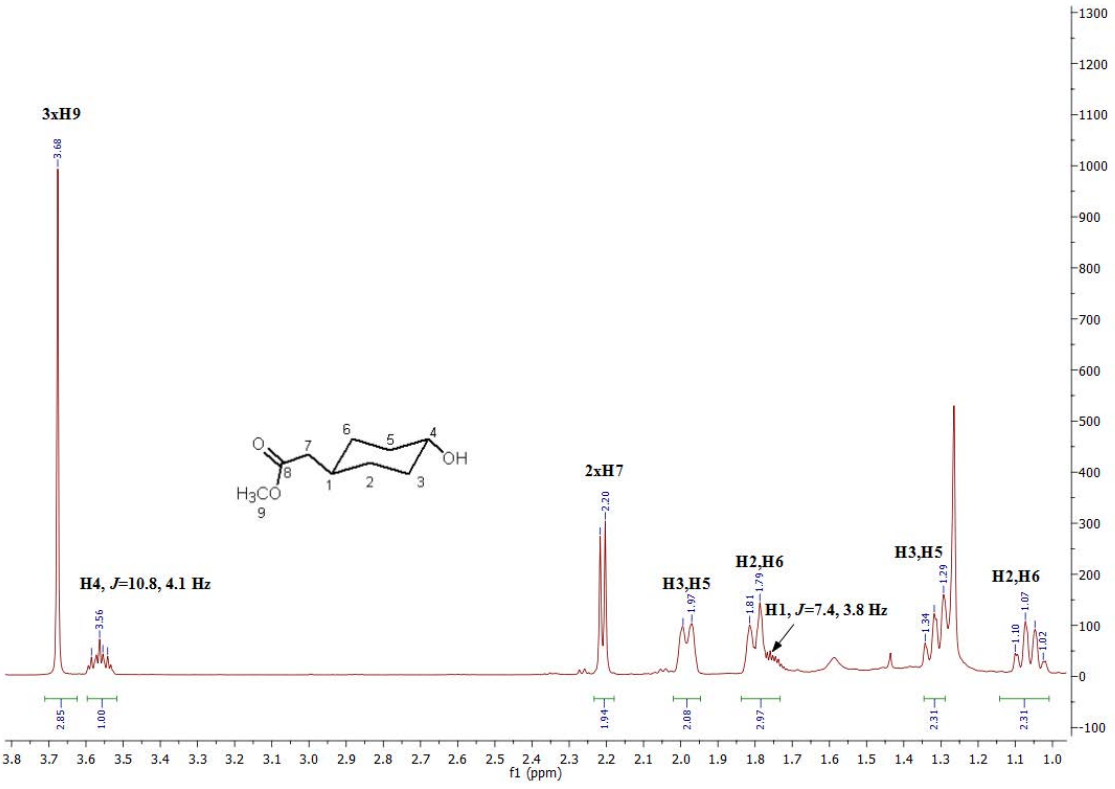

Figure B. 89 ^{1}H NMR spectrum of methyl-2-(*trans*-4-hydroxycyclohexyl)acetate (methylcyclohexyl acetate). The coupling constants of H4 and H1 indicated their axial orientation and therefore the metabolite was assigned as a *trans* isomer.

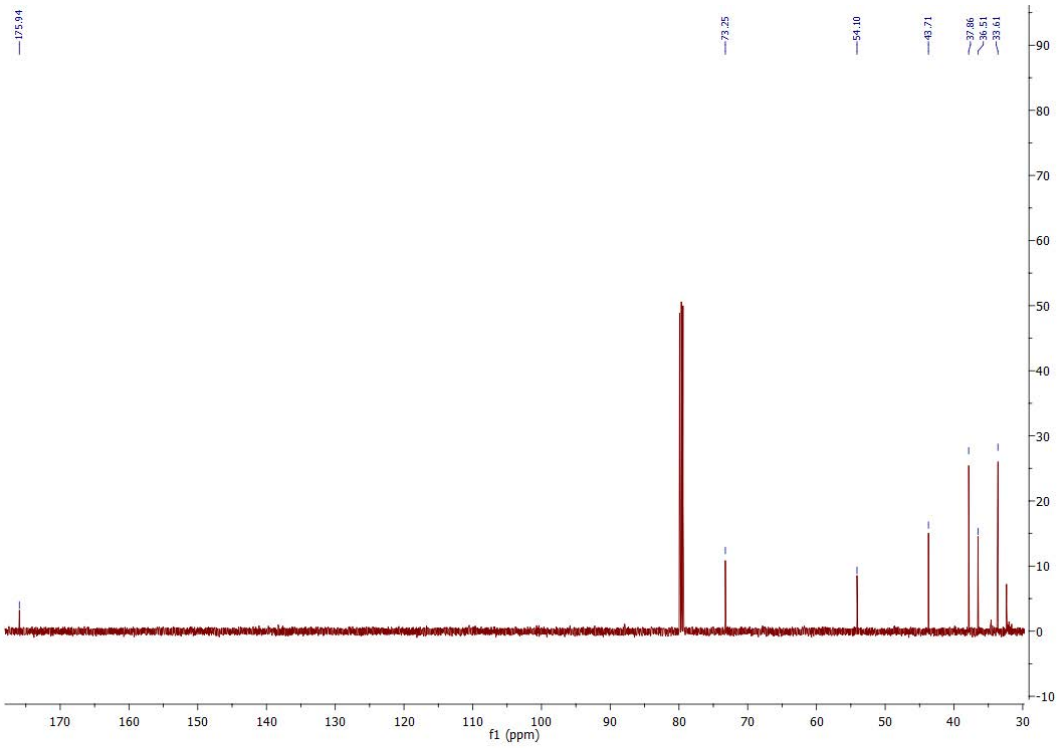

Figure B. 90 ^{13}C NMR spectrum of methyl-2-(*trans*-4-hydroxycyclohexyl)acetate.

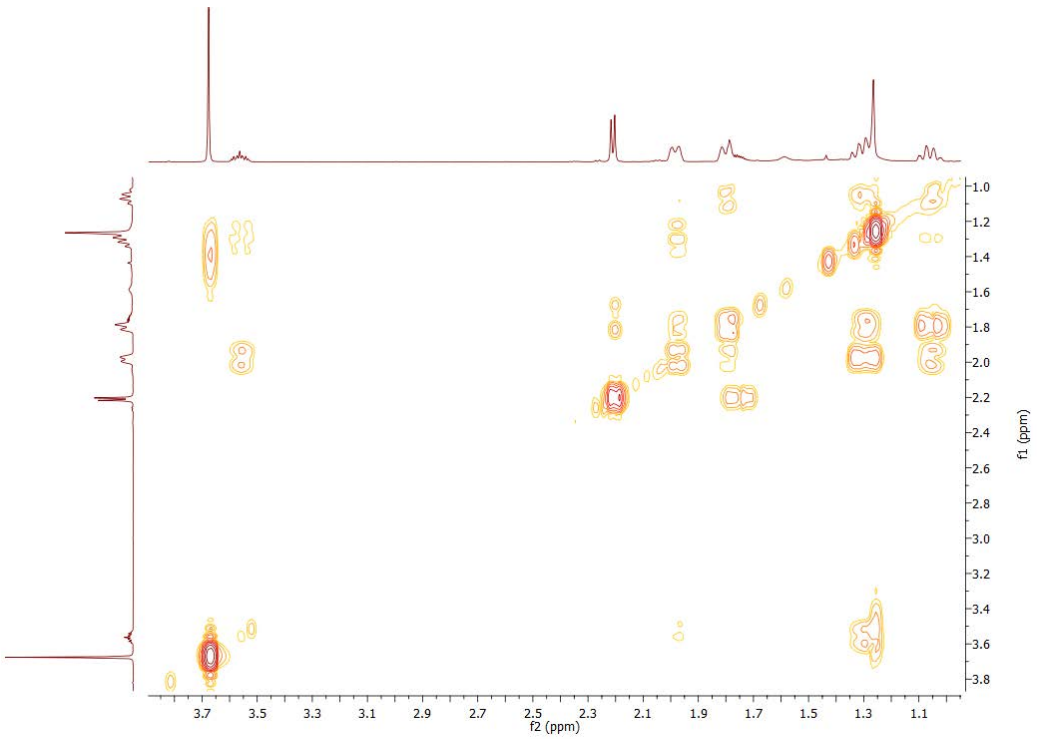

Figure B. 91 gCOSY NMR spectrum of methyl-2-(*trans*-4-hydroxycyclohexyl)acetate.

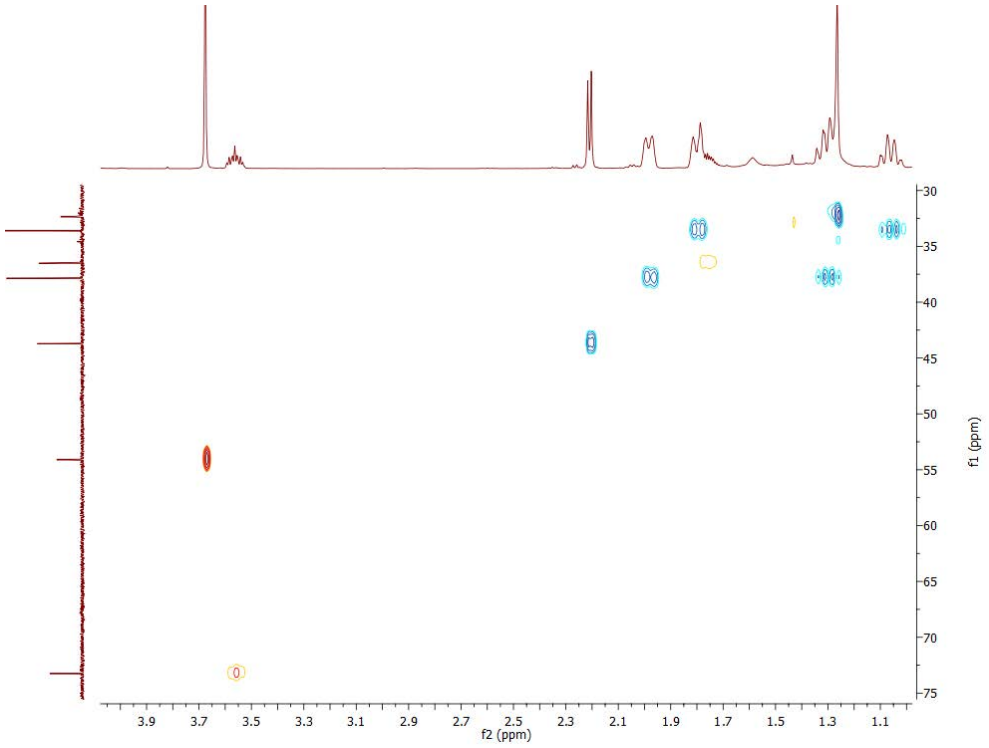

Figure B. 92 HSQC NMR spectrum of methyl-2-(*trans*-4-hydroxycyclohexyl)acetate.

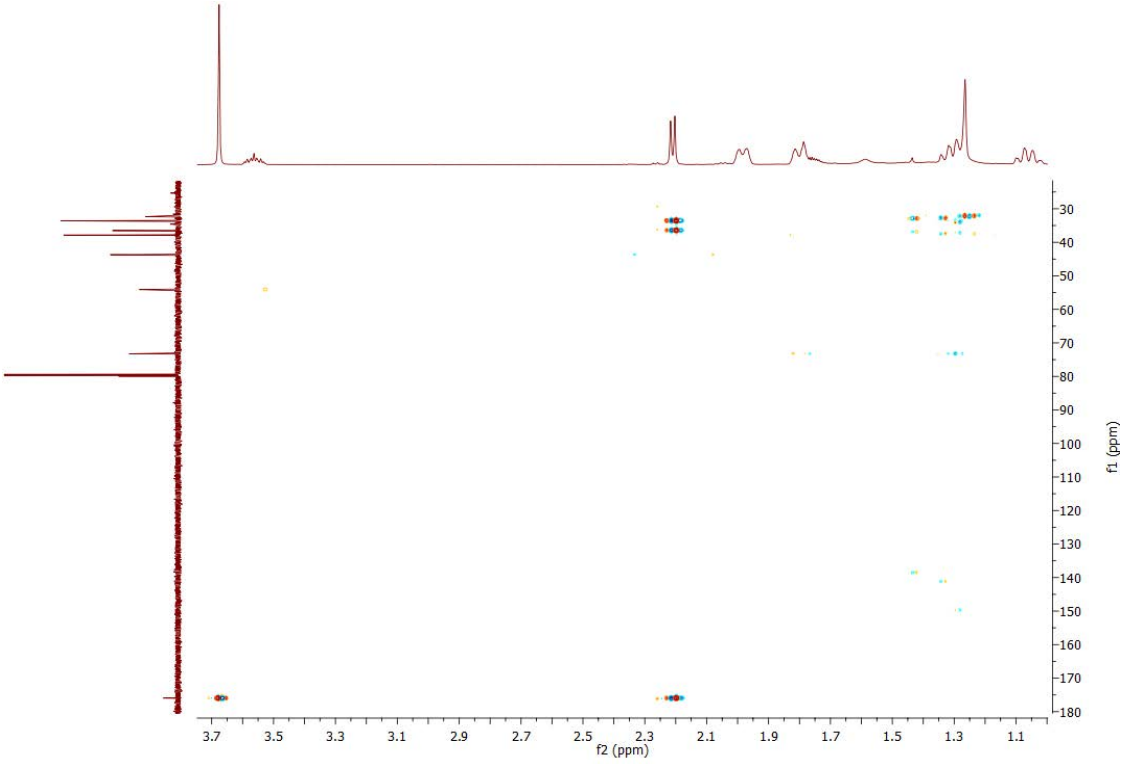

Figure B. 93 HMBC NMR spectrum of methyl-2-(*trans*-4-hydroxycyclohexyl)acetate.

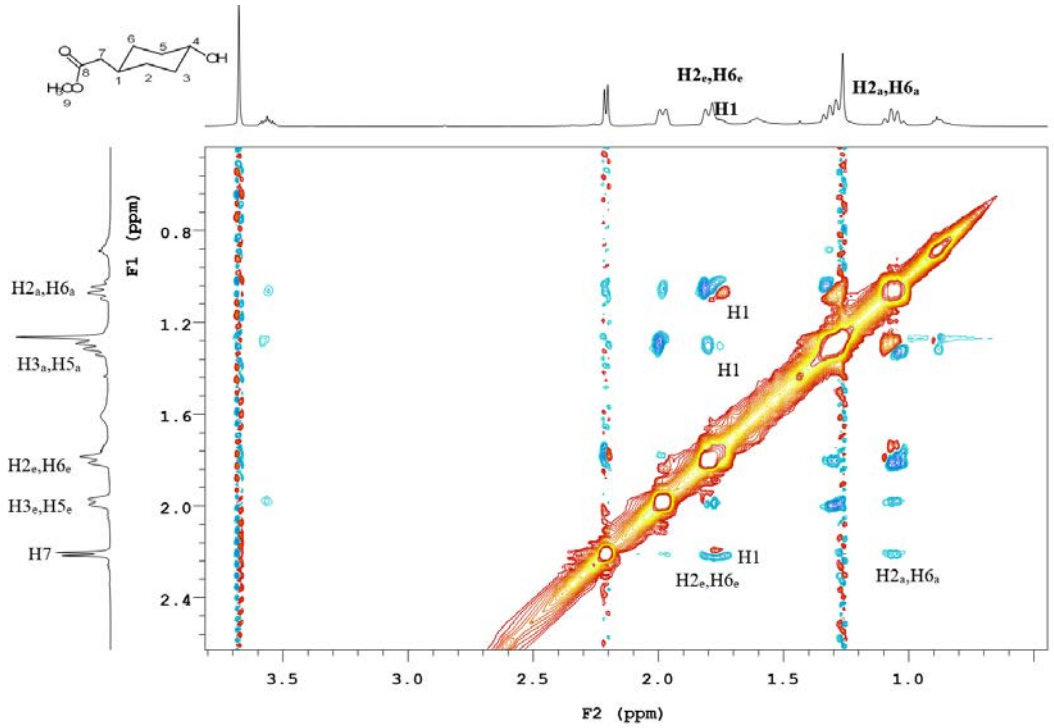

Figure B. 94 Zoomed in ROESY NMR of methyl-2-(*trans*-4-hydroxycyclohexyl)acetate which highlighted the interactions of H7 (equatorial side chain) with the $H6_{ax/eq}$ protons.

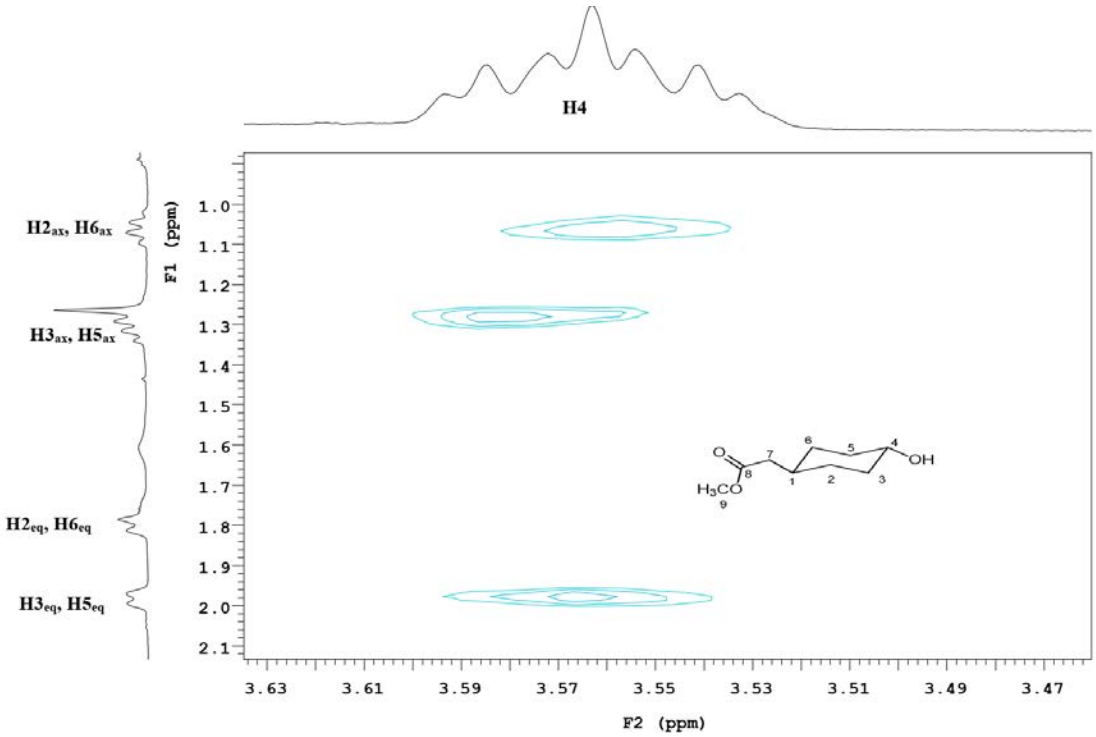

Figure B. 95 Zoomed in ROESY NMR spectrum of methyl-2-(*trans*-4-hydroxycyclohexyl)acetate which highlighted the interactions of H4 (axial) with the protons $H_{2/6ax}$ at 1.12-1.00 ppm.

NMR data for ethyl-*trans*-2-(4-hydroxycyclohexyl)acetate:

^{1}H NMR (500 MHz, $CDCl_3$) δ 4.13 (*q*, *J* = 7.1 Hz, 2H, 2xH9), 3.59-3.50 (m, 1H, H4), 2.19 (d, *J* = 6.7 Hz, 2H, 2xH7), 2.02-1.91 (m, 2H, $H3_{eq}$ & $H5_{eq}$), 1.84-1.71 (m, 3H, H1, $H2_{eq}$ & $H6_{eq}$), 1.3-1.23 (m, 5H, $H3_{ax}$, $H5_{ax}$ & 3xH10), 1.11-1.01 (m, 2H, $H2_{ax}$ & $H6_{ax}$).

^{13}C NMR (126 MHz, $CDCl_3$) δ 175.52 (C8), 73.26 (C4), 62.86 (C9), 43.98 (C7), 37.87 (C3 & C5), 36.54 (C1), 33.59 (C2 & C6), 16.62 (C10).

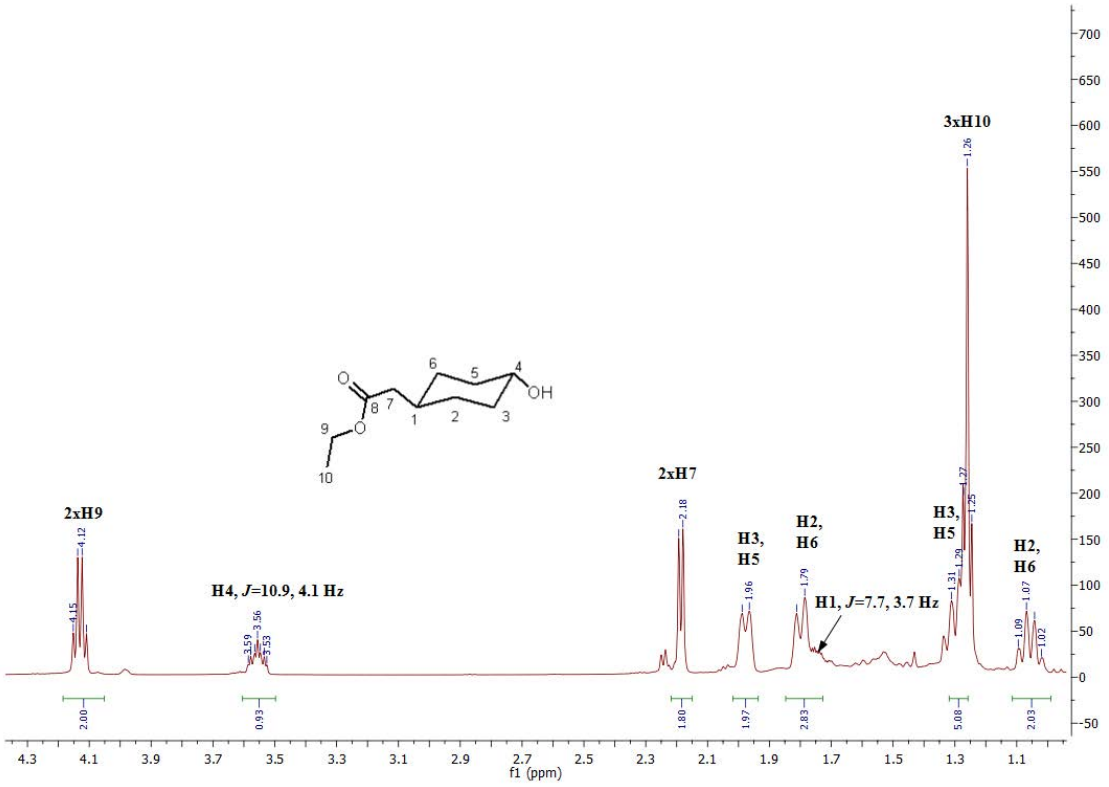

Figure B. 96 ^{1}H NMR spectrum of ethyl-*trans*-2-(4-hydroxycyclohexyl)acetate (ethylcyclohexyl acetate). The coupling constants of H1 and H4 indicated their axial orientation and therefore the metabolite was assigned as a *trans* isomer.

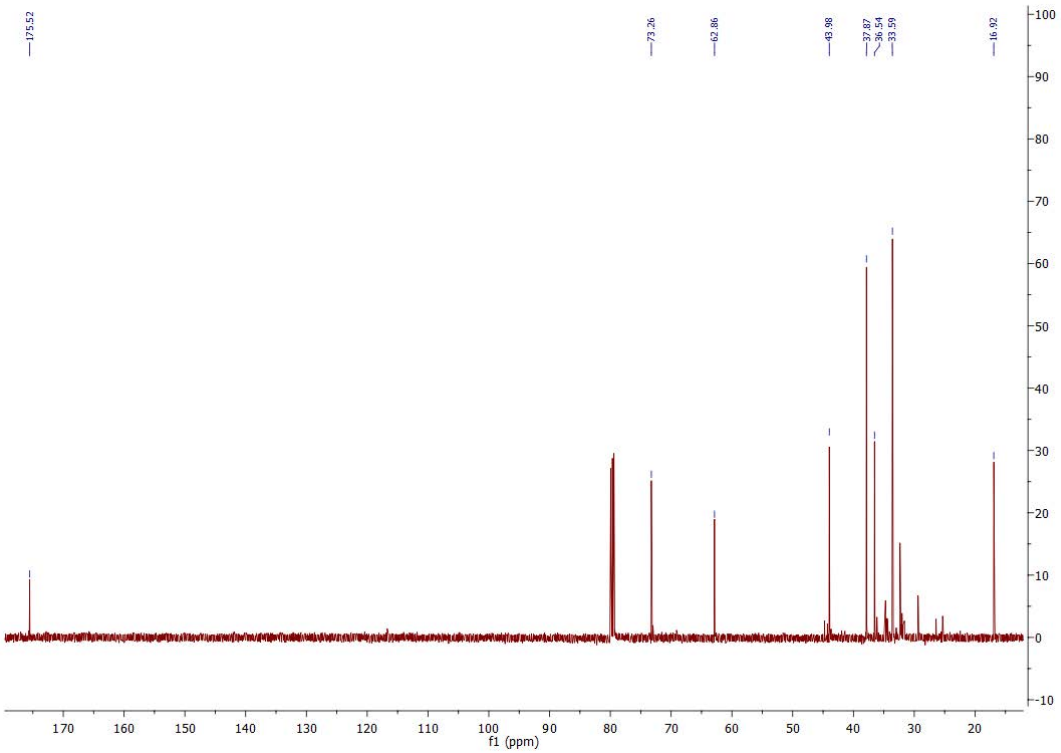

Figure B. 97 ^{13}C NMR spectrum of ethyl-*trans*-2-(4-hydroxycyclohexyl)acetate.

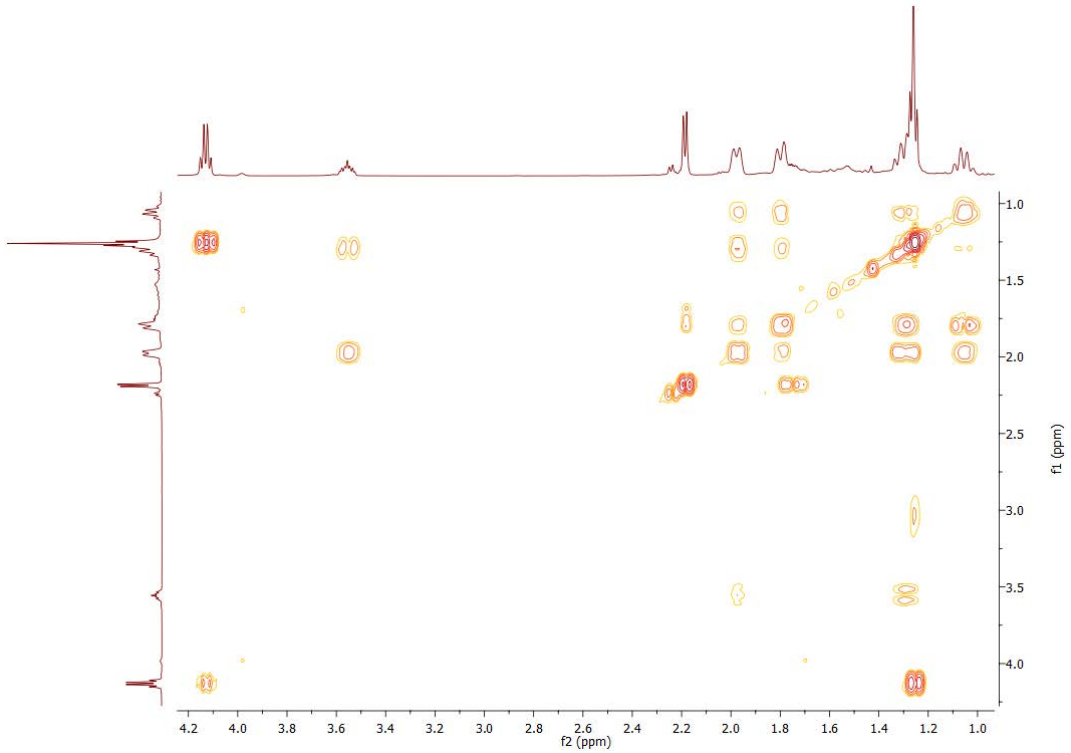

Figure B. 98 gCOSY NMR spectrum of ethyl-*trans*-2-(4-hydroxycyclohexyl)acetate.

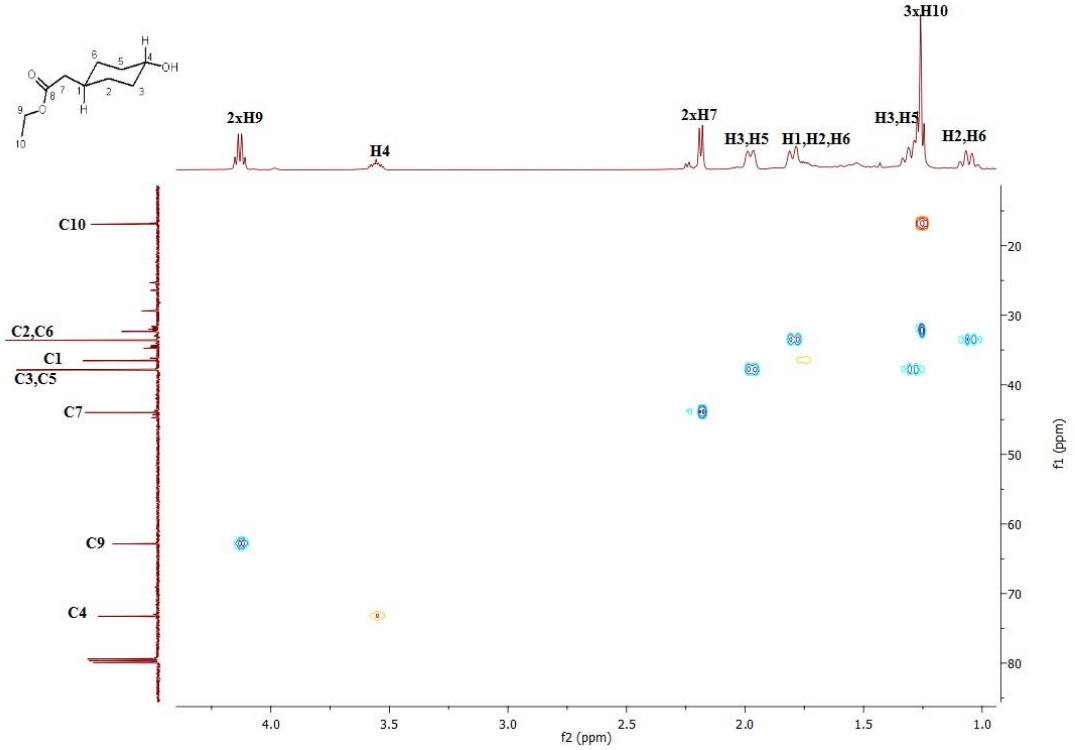

Figure B. 99 HSQC NMR spectrum of ethyl-*trans*-2-(4-hydroxycyclohexyl)acetate.

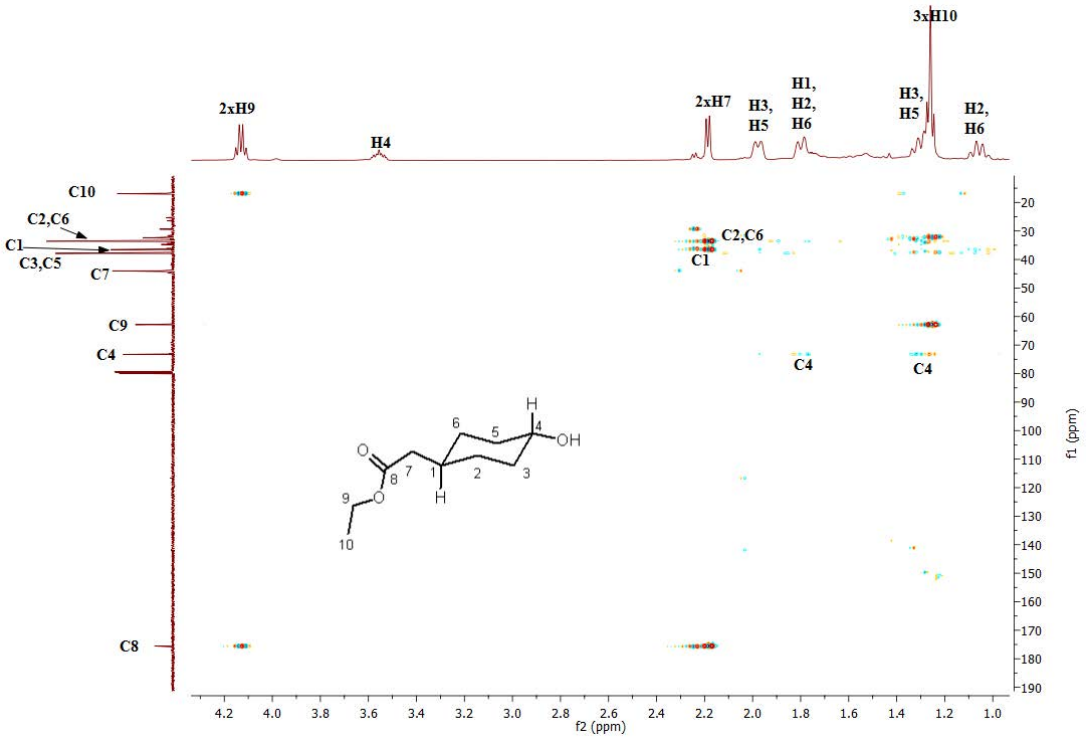

Figure B. 100 HMBC NMR spectrum of ethyl-*trans*-2-(4-hydroxycyclohexyl)acetate.

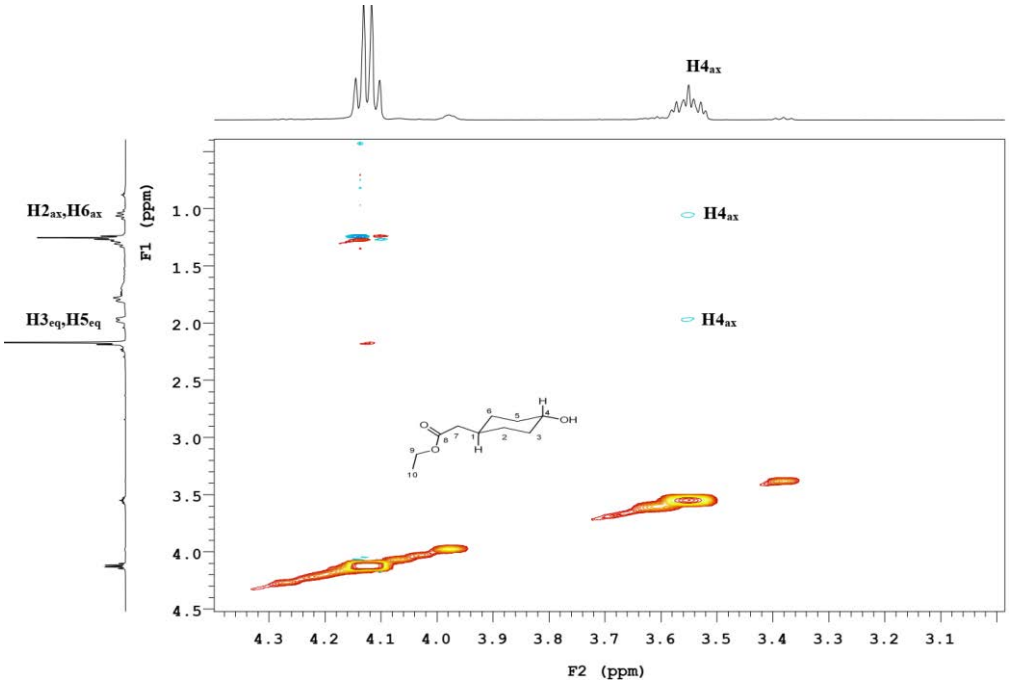

Figure B. 101 Zoomed in ROESY NMR spectrum of ethyl-*trans*-2-(4-hydroxycyclohexyl)acetate which highlighted the interactions of H4 (3.59-3.50 ppm; axial) with the protons $H_{2/6ax}$ at 1.11-1.01 ppm.

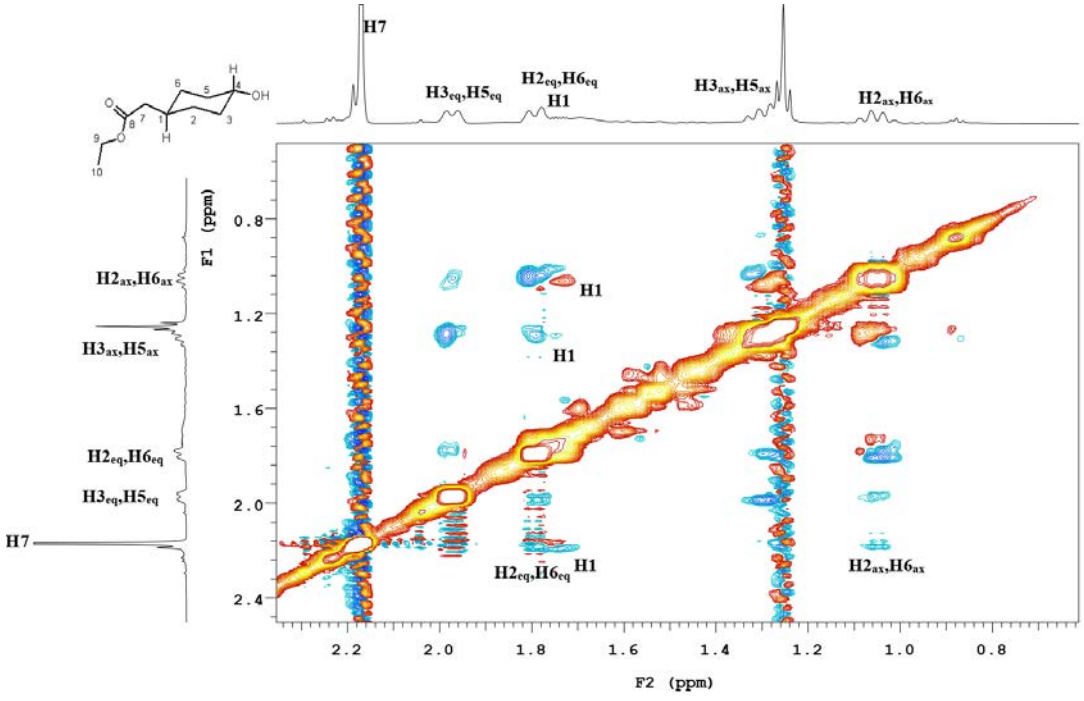

Figure B. 102 Zoomed in ROESY NMR spectrum of ethyl-*trans*-2-(4-hydroxycyclohexyl)acetate which displayed the interactions of H7 (equatorial side chain) with the $H6_{ax/eq}$ protons.

NMR for 5-hydroxycyclooctyl acetate:

^{1}H NMR (500 MHz, $CDCl_3$) δ 4.93-4.85 (m, 1H, H1), 3.87-3.78 (m, 1H, H5), 2.01 (s, 3H, 3xH10), 1.90-1.77 (m, 4H, H2, H4, H6 & H8), 1.75-1.59 (m, 8H, H2, 2xH3, H4, H6, 2xH7 & H8).

^{13}C NMR (126 MHz, $CDCl_3$) δ 173.0 (C9), 76.61 (C1), 73.88 (C5), 37.87 (C4 & C6), 34.93 (C2 & C8), 24.13 (C10), 21.55 (C3 & C7).

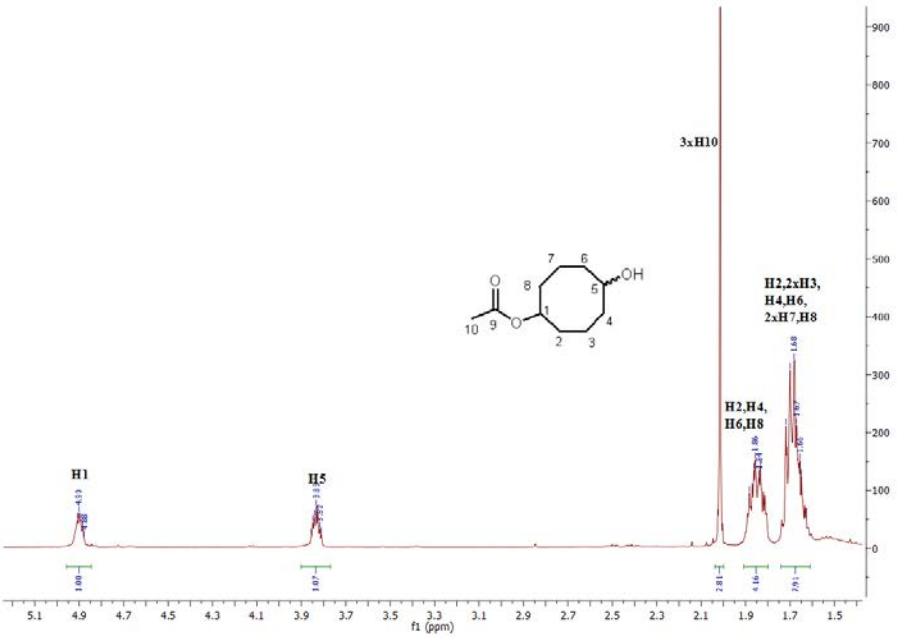

(a)

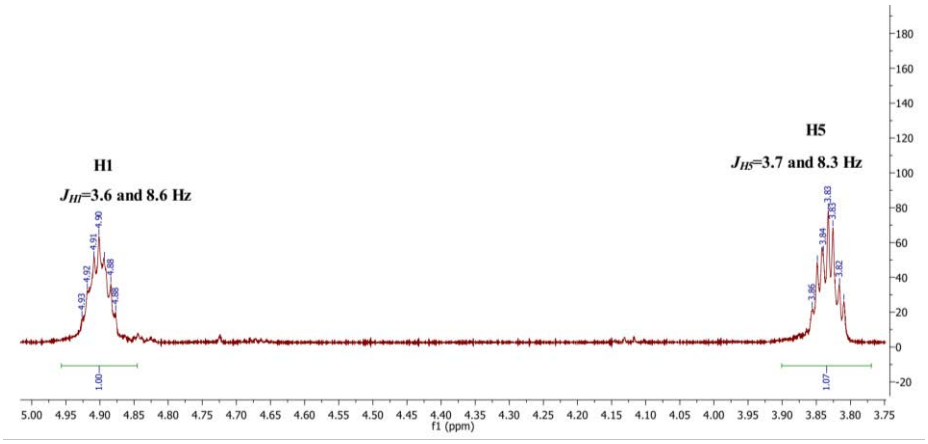

(b)

Figure B. 103 (a) ^{1}H NMR spectrum of 5-hydroxycyclooctyl acetate. **(b)** Zoomed in ^{1}H NMR to highlight the H1 and H5 peaks splitting patterns. The coupling constants of H1 (3.6 and 8.6 Hz) and H5 (3.7 and 8.3) nearly similar indicated their similar orientation (both axial). Hence, the metabolite is presumed to be a *trans* isomer.

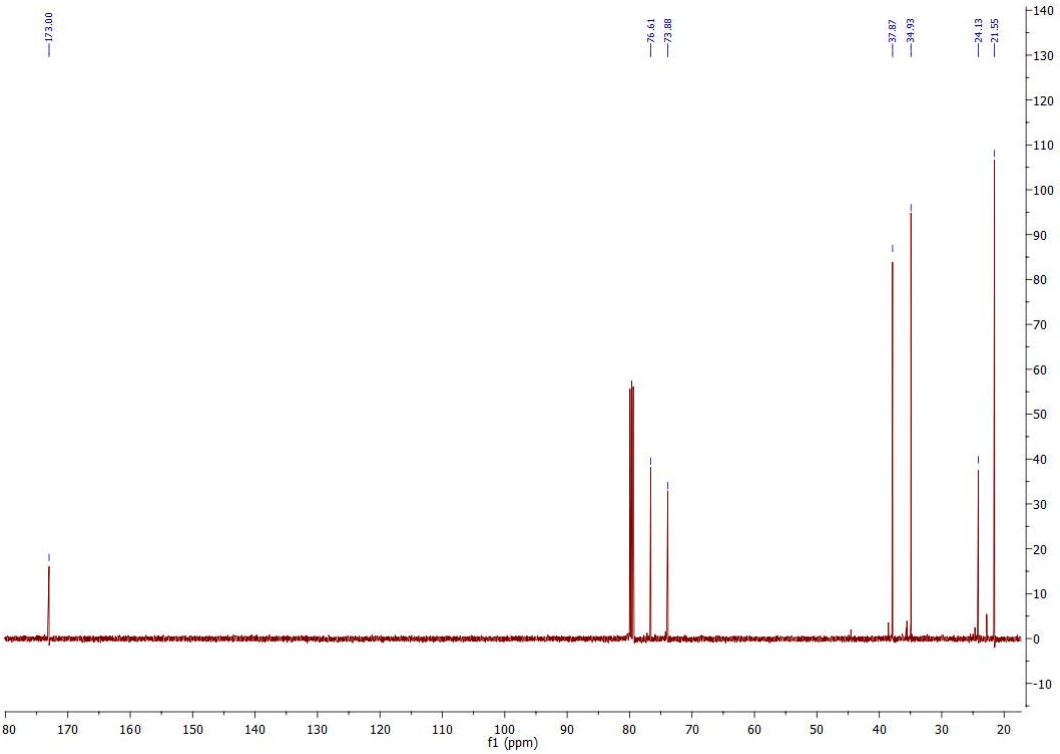

Figure B. 104 ^{13}C NMR of 5-hydroxycyclooctyl acetate. Minor signals indicated the presence of other diastereomer of 5-hydroxycyclooctyl acetate (77.19, 74.25, 38.53, 35.58, 24.68, 22.79 ppm). But full characterisation of this minor metabolite was not possible due to low yield.

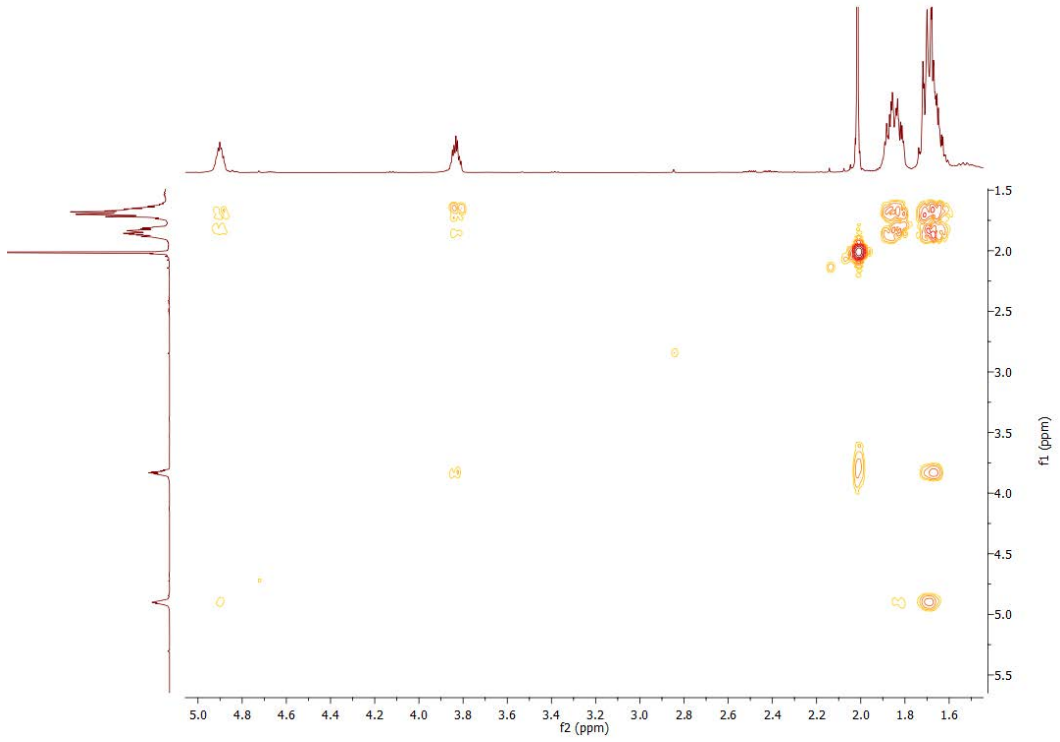

Figure B. 105 gCOSY NMR spectrum of 5-hydroxycyclooctyl acetate.

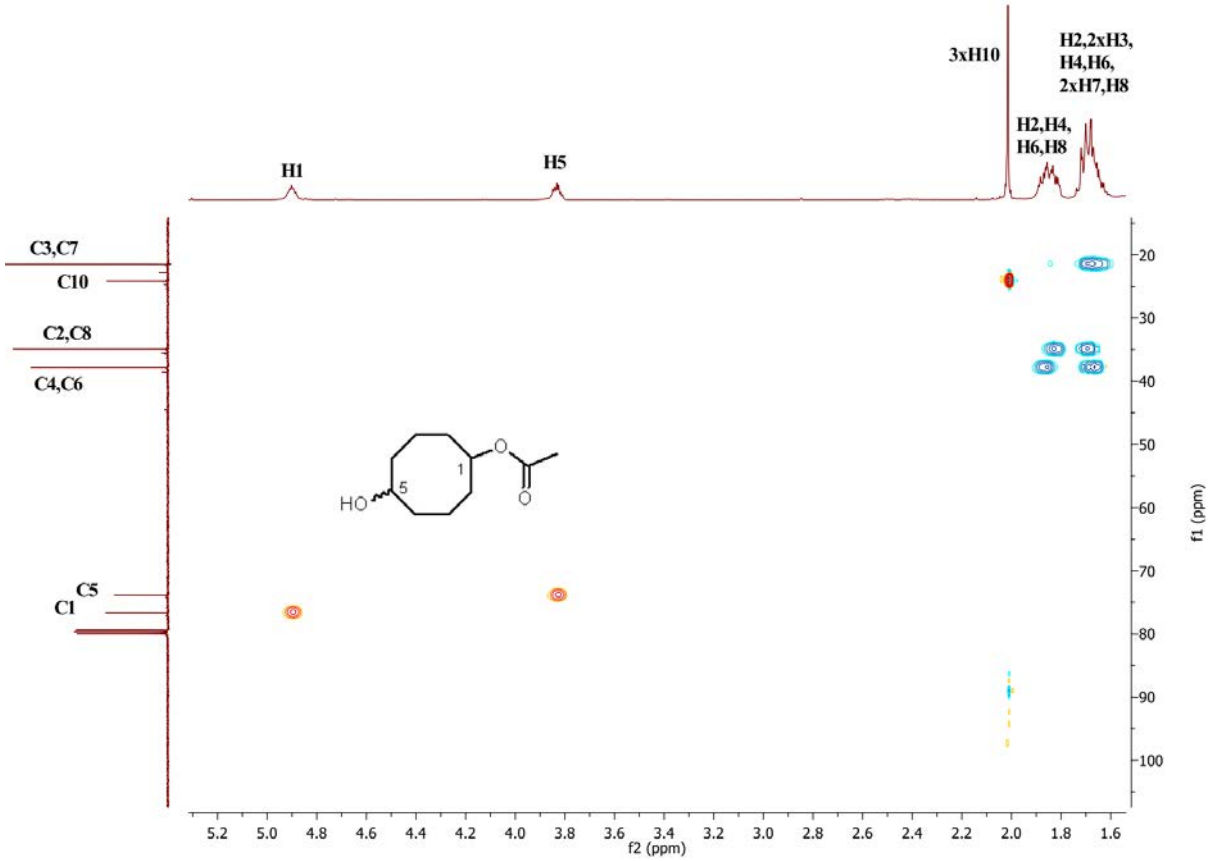

Figure B. 106 HSQC NMR spectrum of 5-hydroxycyclooctyl acetate.

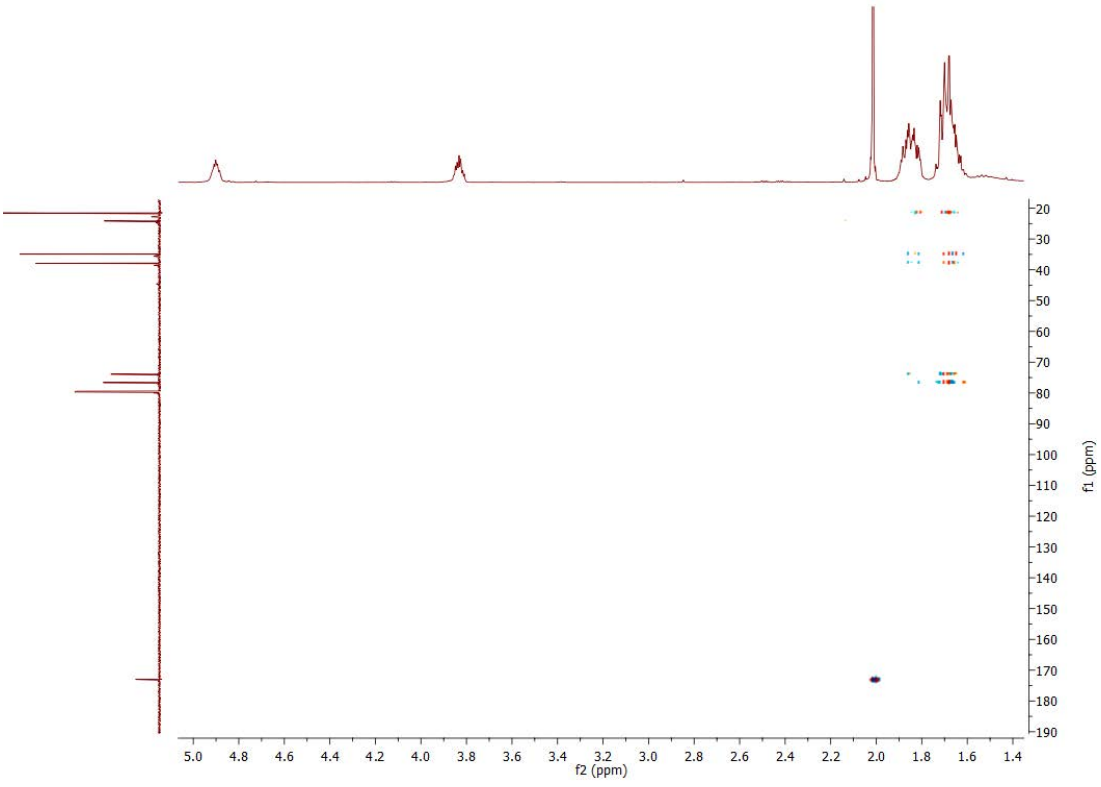

Figure B. 107 HMBC NMR spectrum of 5-hydroxycyclooctyl acetate.

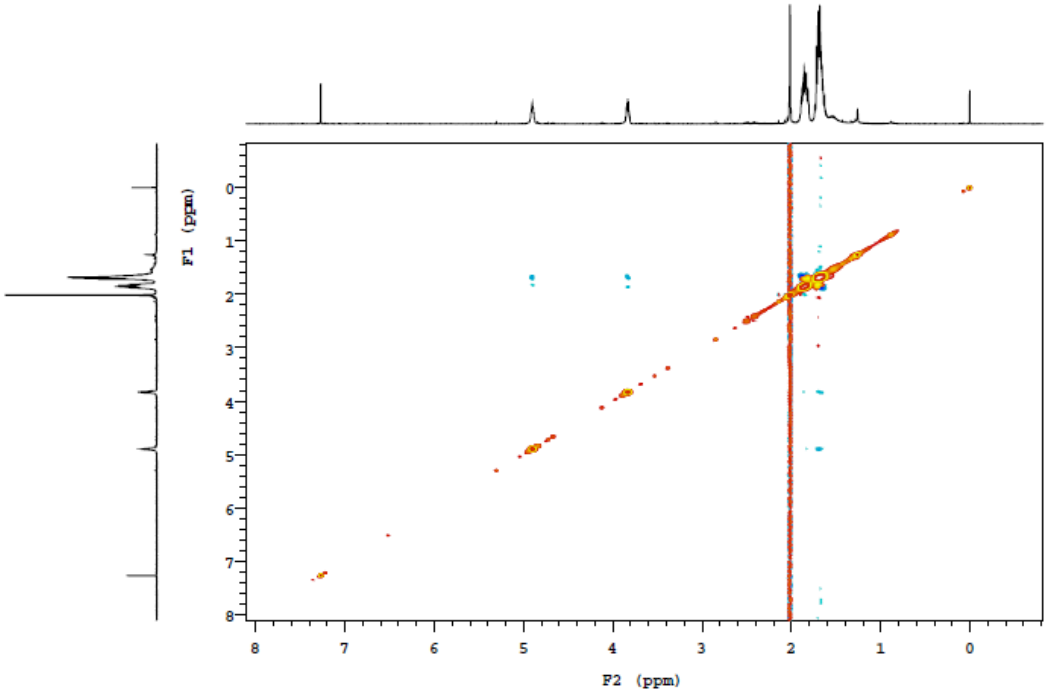

(a)

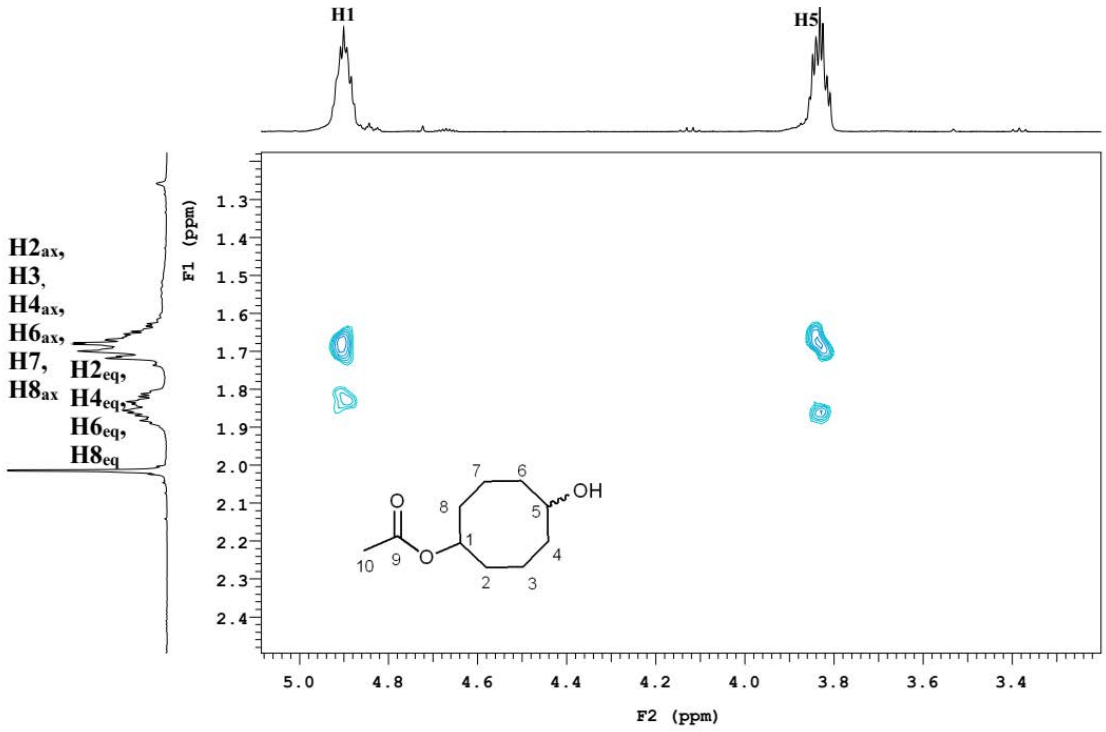

(b)

Figure B. 108 (a) ROESY NMR spectrum of 5-hydroxycyclooctyl acetate. **(b)** Zoomed in ROESY NMR to highlight the strong interactions of H1 and H5 with the other protons.

NMR for 5-hydroxycyclooctyl isobutyrate:

^{1}H NMR (500 MHz, $CDCl_3$) δ 4.95-4.89 (m, 1H, H1), 3.88-3.74 (m, 1H, H5), 2.48 (*septet*, J = 7.0 Hz, 1H, H10), 1.94-1.88 (m, 2H, H4, H6), 1.82-1.76 (m, 2H, 2H, H2 & H8), 1.76-1.56 (m, 8H, H2, 2xH3, H4, H6, 2xH7 & H8), 1.13 (d, J = 7.0 Hz, 6H, 3xH11 & 3xH12).

^{13}C NMR (126 MHz, $CDCl_3$) δ 179.06 (C9), 76.10 (C1), 73.92 (C5), 37.85 (C4 & C6), 36.81 (C10), 34.92 (C2 & C8), 21.59 (C3, C7), 21.53 (C11 & C12).

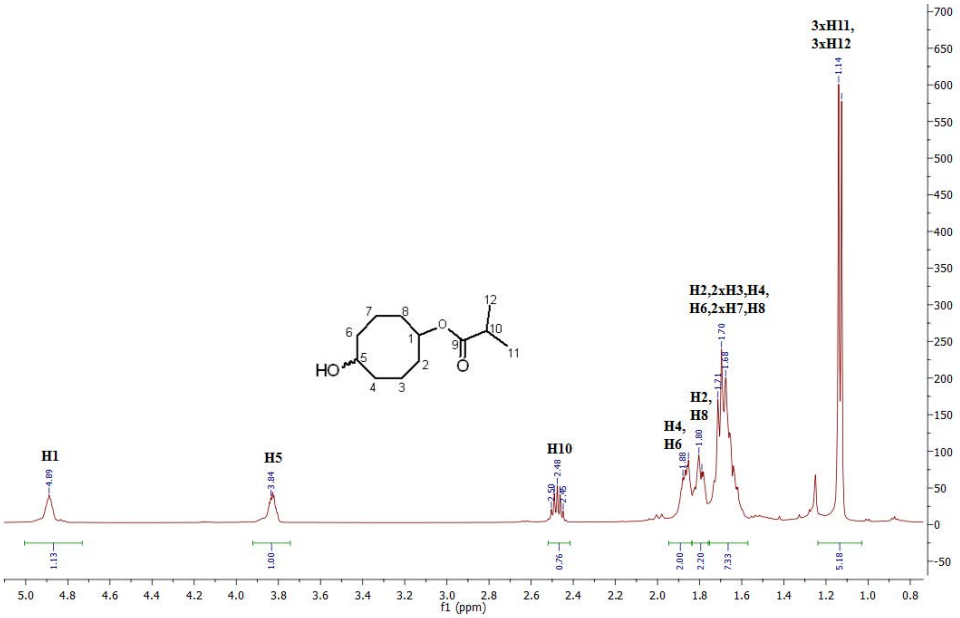

(a)

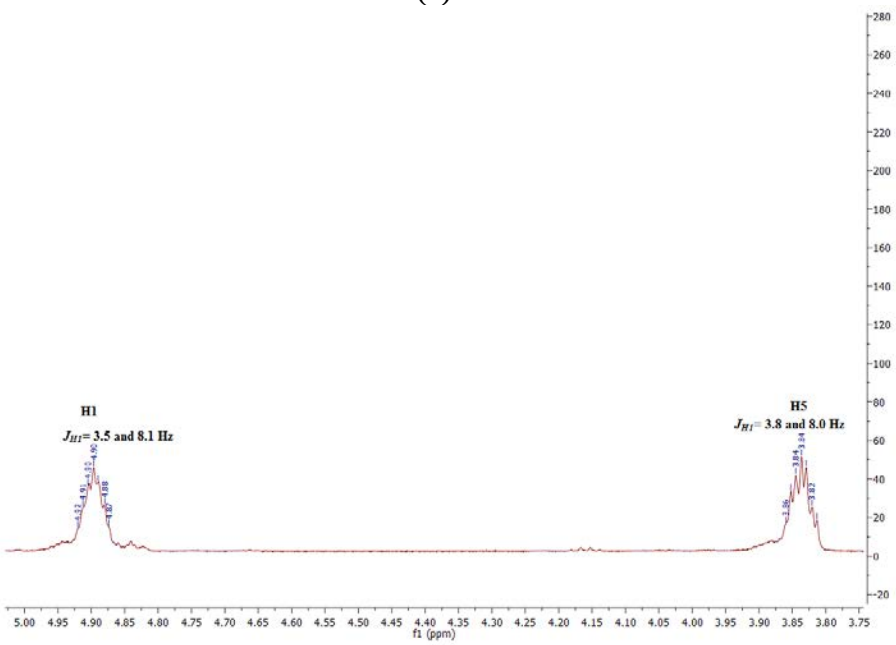

(b)

Figure B. 109 (a) ^{1}H NMR of 5-hydroxycyclooctyl isobutyrate. **(b)** The coupling constants of H1 and H5 were similar to each other suggested their similar orientation (both axial), therefore the metabolite is presumed to be a *trans* isomer of 5-hydroxycyclooctyl isobutyrate.

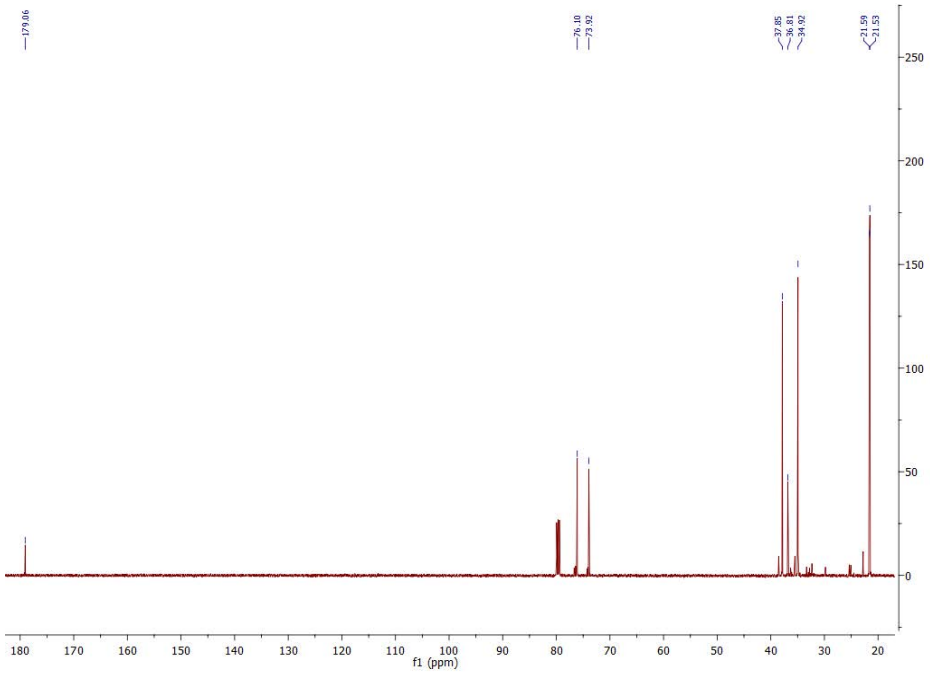

Figure B. 110 ^{13}C NMR spectrum of 5-hydroxycyclooctyl isobutyrate. The minor carbon signals: 76.78, 76.40, 74.22, 74.07, 38.53, 36.86, 36.30, 35.50, 33.32, 32.78, 32.33, 29.81, 25.36, 25.07 and 22.77. Minor signals indicated the presence of other diastereomer of 5-hydroxycyclooctyl isobutyrate and a minor unidentified metabolite. But fully characterisation of these metabolites were not possible due to low yield.

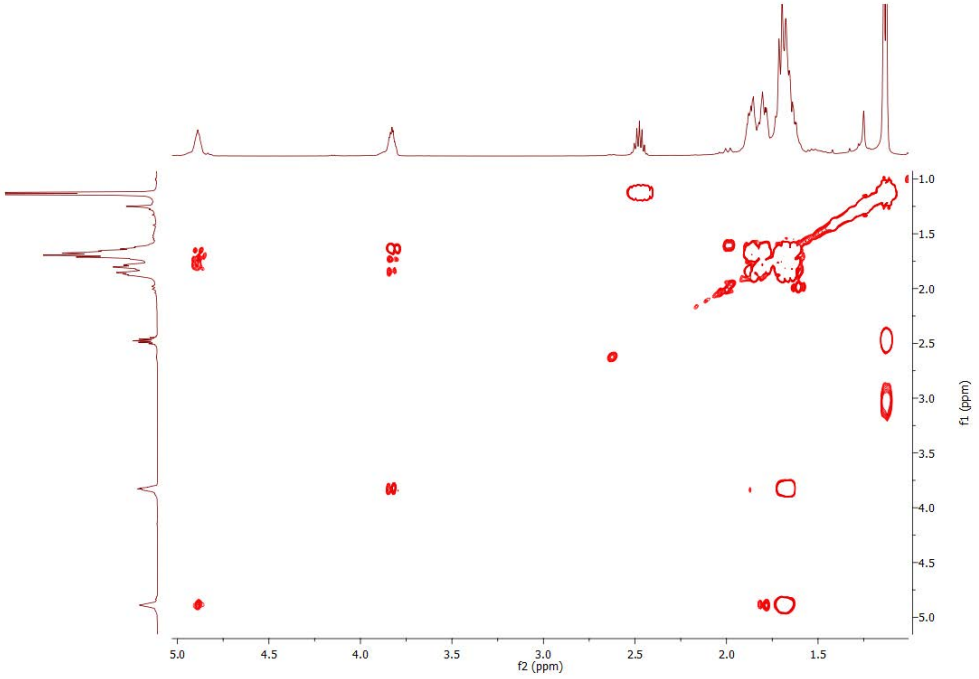

Figure B. 111 gCOSY NMR spectrum of 5-hydroxycyclooctyl isobutyrate.

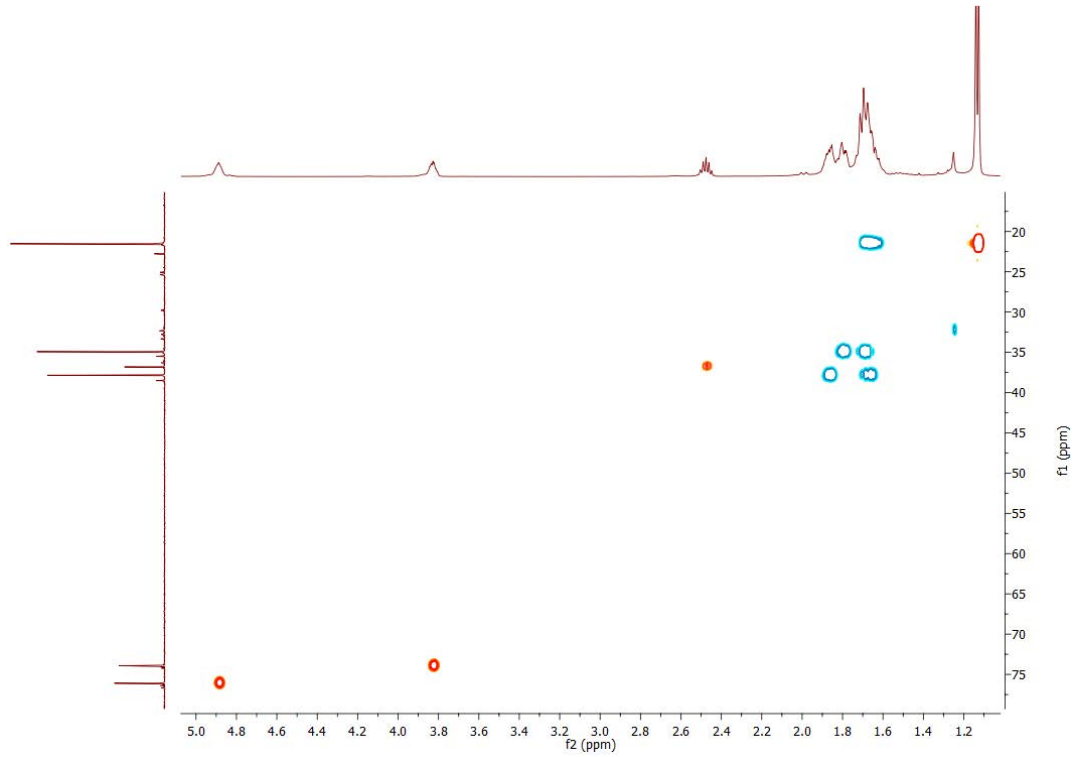

Figure B. 112 HSQC NMR spectrum of 5-hydroxycyclooctyl isobutyrate.

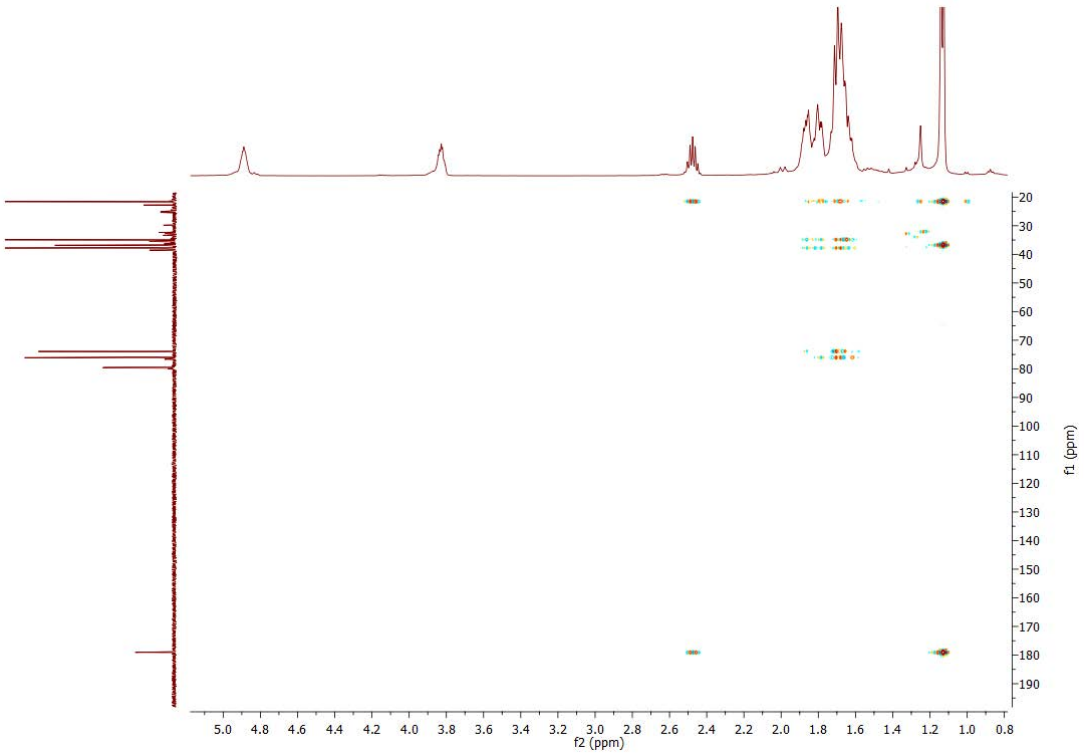

Figure B. 113 HMBC NMR spectrum of 5-hydroxycyclooctyl isobutyrate.

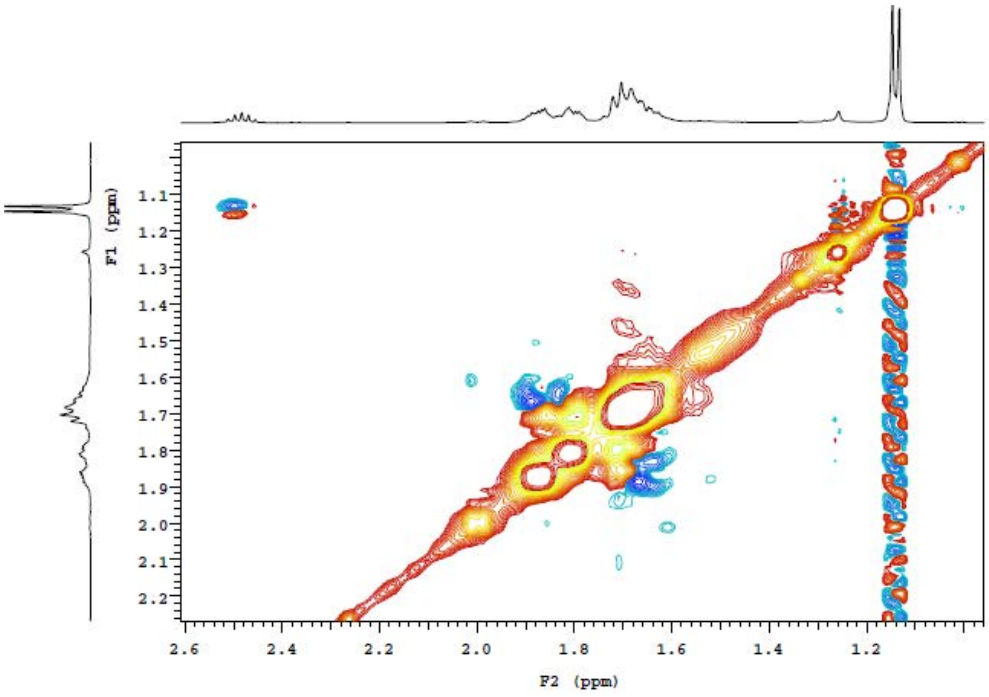

(a)

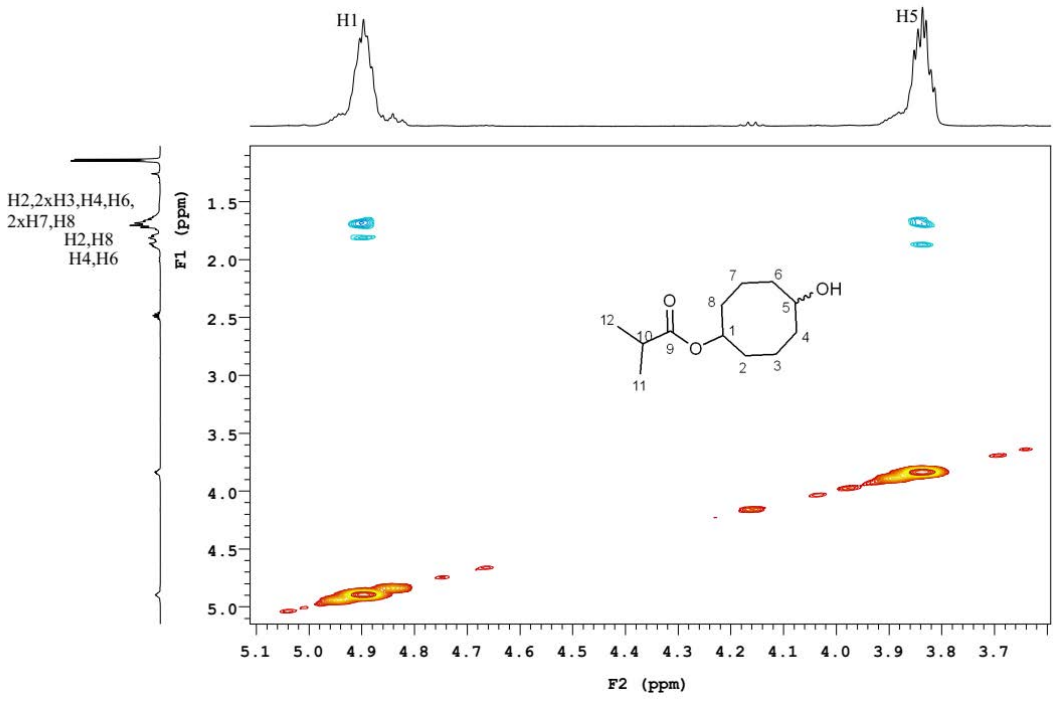

(b)

Figure B. 114 (a) ROESY NMR spectrum of 5-hydroxycyclooctyl isobutyrate. **(b)** Zoomed in ROSEY NMR to highlight the strong interactions of H1 and H5 with adjacent protons.

NMR for 7-hydroxycyclododecyl acetate [150] (CYP101B1):

^{1}H NMR (500 MHz, $CDCl_3$) δ 4.91 (*t*, *J* = 8.1 Hz, 1H, H1), 3.89-3.80 (m, 1H, H7), 2.02 (s, 3H, 3xH14), 1.73-1.61 (m, 4H, H2, H6, H8 & H12), 1.57-1.50 (m, 4H, H2, H6, H8 & H12), 1.48-1.32 (m, 12H, 2xH3, 2xH4, 2xH5, 2xH9, 2xH10 & 2xH11).

^{13}C NMR (126 MHz, $CDCl_3$) δ 170.57 (C13), 73.61 (C1), 70.83 (C7), 30.83 (C2 & C12), 27.53 (C6 & C8), 25.88 (C3 & C11), 21.36 (C14), 19.14 (C5 & C9), 18.97 (C4 & C10).

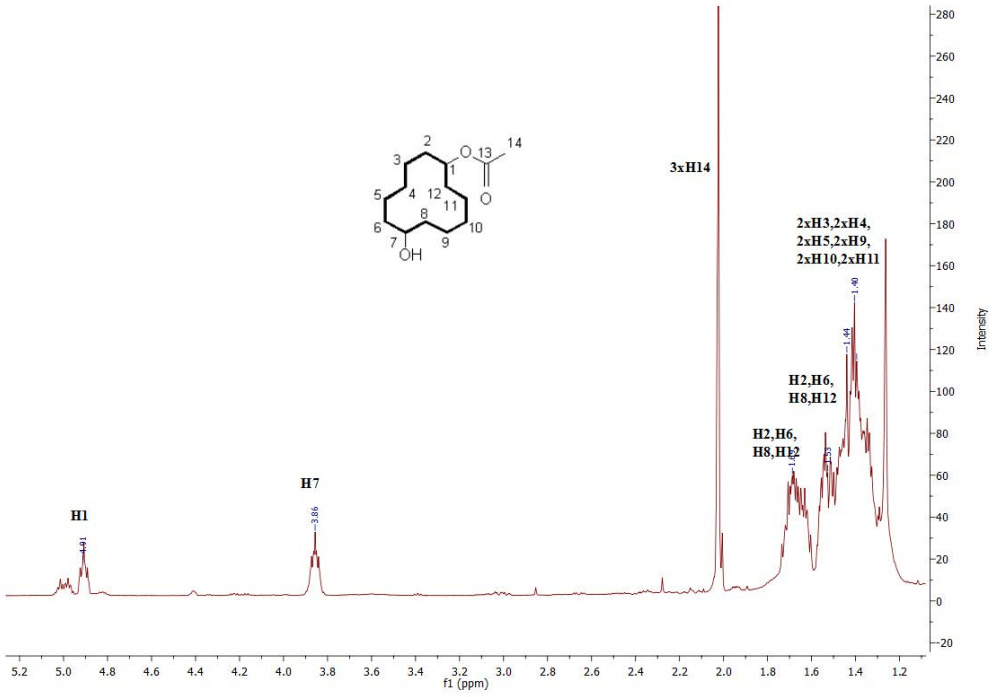

(a)

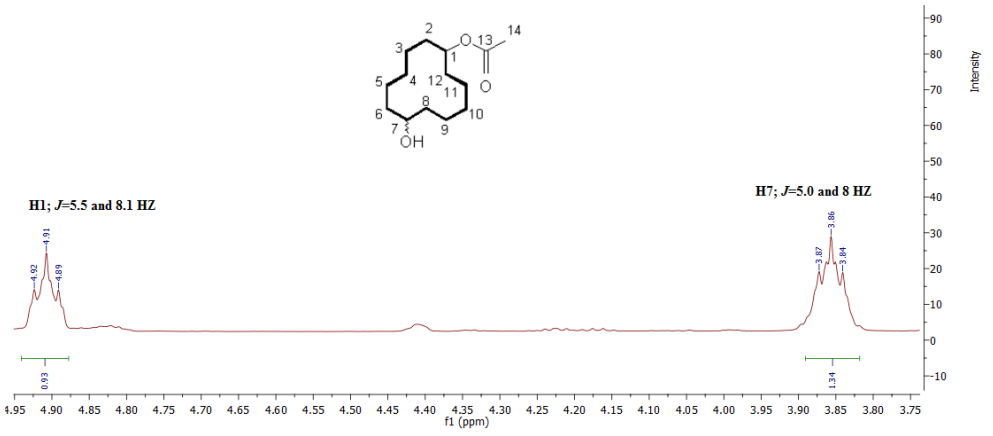

(b)

Figure B. 115 (a) ^{1}H NMR spectrum of 7-hydroxycyclododecyl acetate [150]. **(b)** Zoomed in proton NMR to highlight the H1 and H7 peaks. The H1 and H7 peaks and their coupling constants J_{H1} = 5.5, 8.1 Hz and J_{H7} = 5.0, 8.0 Hz are almost similar, suggested both protons are in the same orientation (both axial). The product therefore assigned as a *trans* isomer.

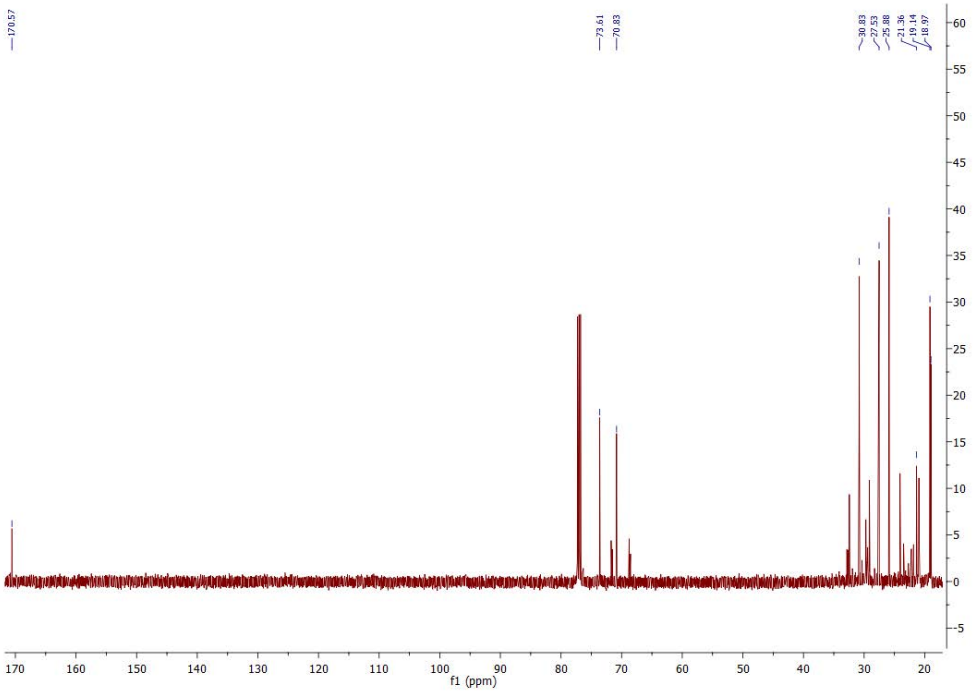

(a)

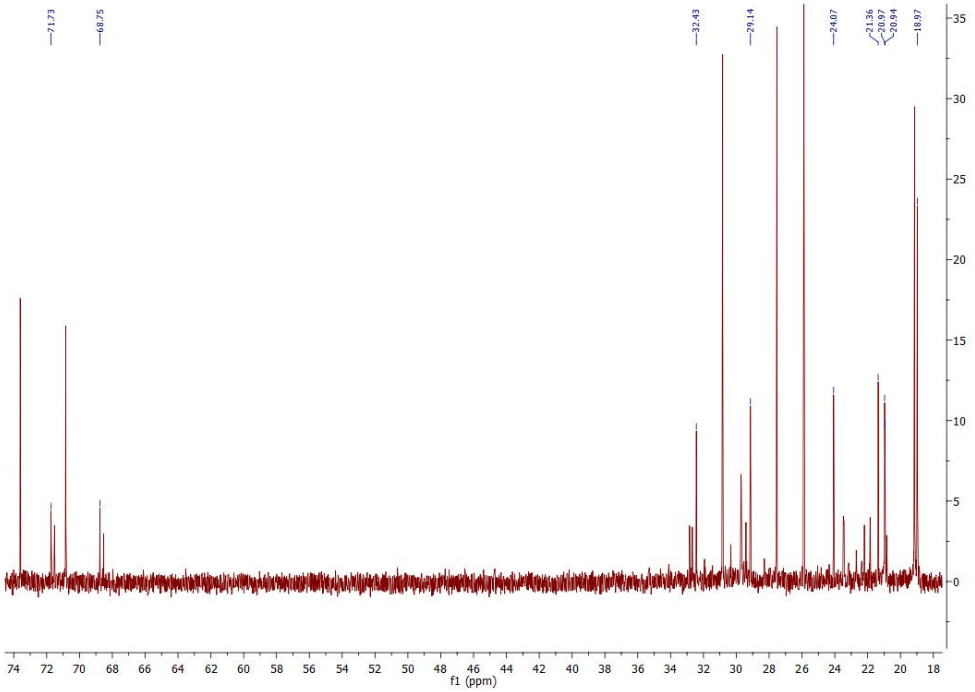

(b)

Figure B. 116 (a) ^{13}C NMR spectrum of 7-hydroxycyclododecyl acetate (*trans*; RT 17.3 min in GC) [150]. The product was assigned as 7-hydroxy as in ^{13}C showed symmetrical carbon peaks of the cyclic ring. **(b)** The NMR highlighted the minor carbon signals of 7-hydroxycyclododecyl acetate (*cis*; RT 16.5 min) [150]. The ^{13}C NMR also had additional minor product signals, that product was presumed to be another alcohol or the other diastereomer of 5-hydroxycyclododecyl acetate (RT 16.4 min; see below Table B. 1).

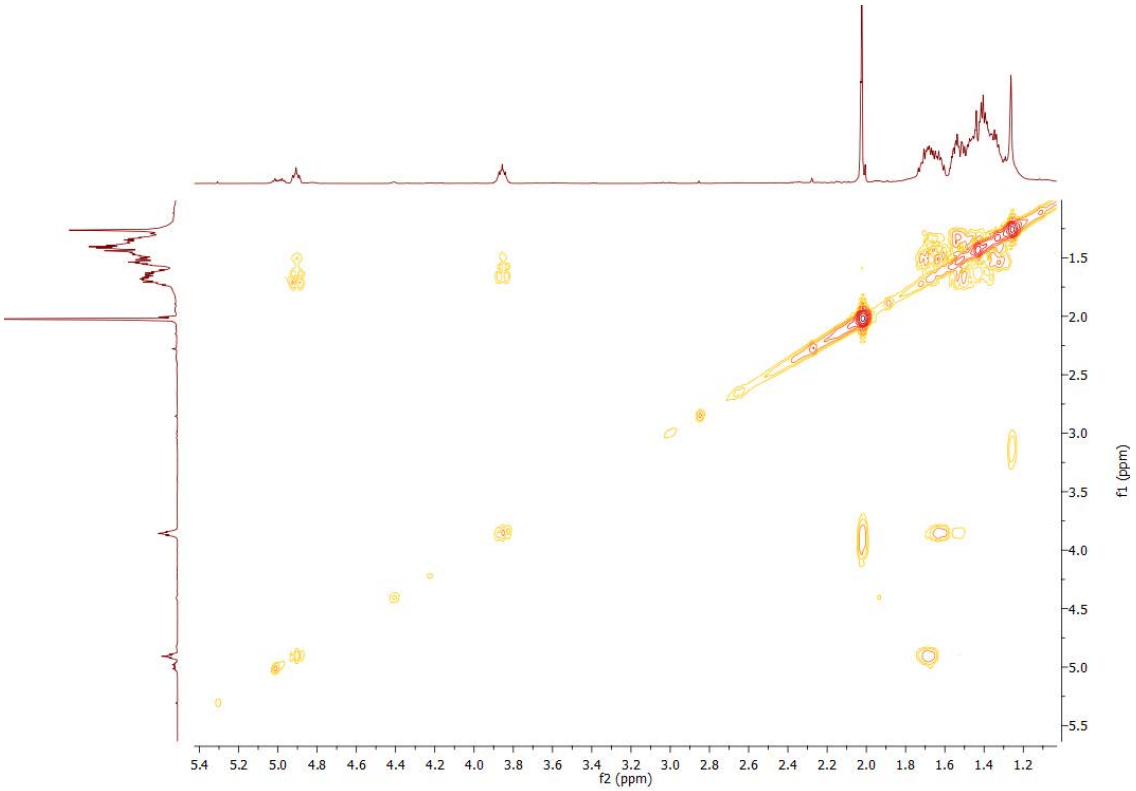

Figure B. 117 gCOSY NMR spectrum of 7-hydroxycyclododecyl acetate.

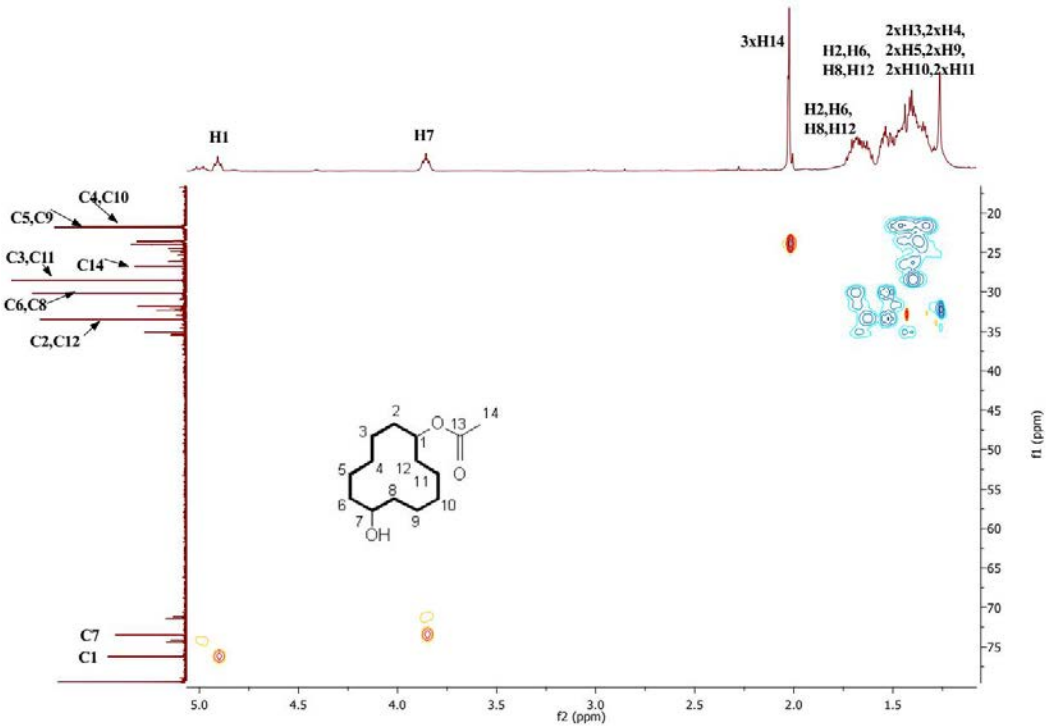

(a)

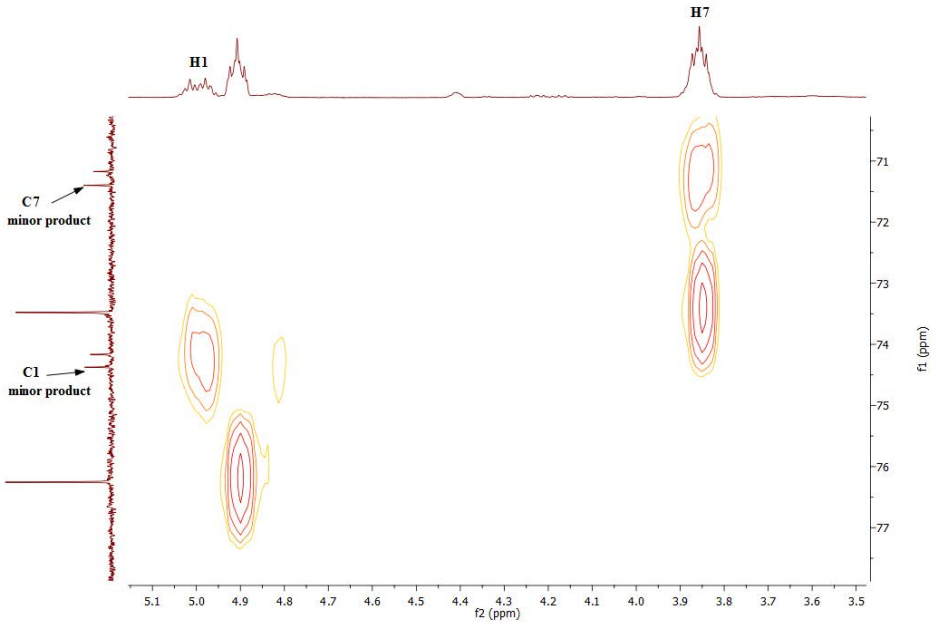

(b)

Figure B. 118 (a) HSQC NMR of 7-hydroxycyclododecyl acetate (*trans*). **(b)** Zoomed in the HSQC NMR in 65 to 80 ppm region to highlight the interactions of minor product C1 and C7 signals with the proton of 5.04-4.99 ppm and 3.9-3.81 ppm regions, which was assigned as other diastereomer of 7-hydroxy cyclododecyl acetate (*cis*; RT 16.5 min in GC; Table B. 1) [150].

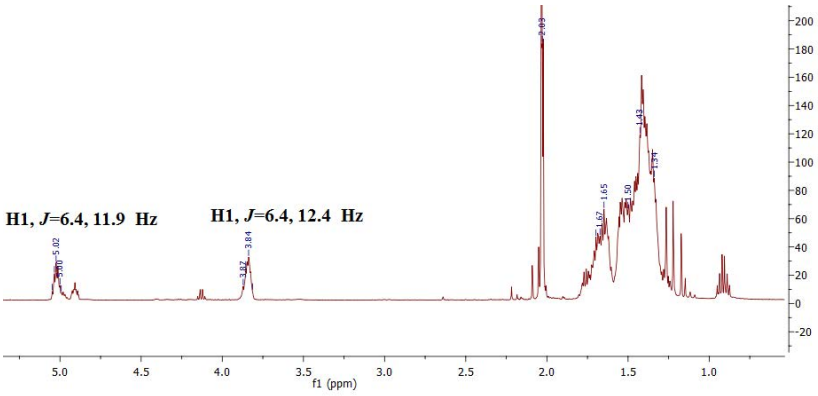

Figure B. 119 ^{1}H NMR spectrum of 5-hydroxycyclododecyl acetate (RT 16.2 min in GC).

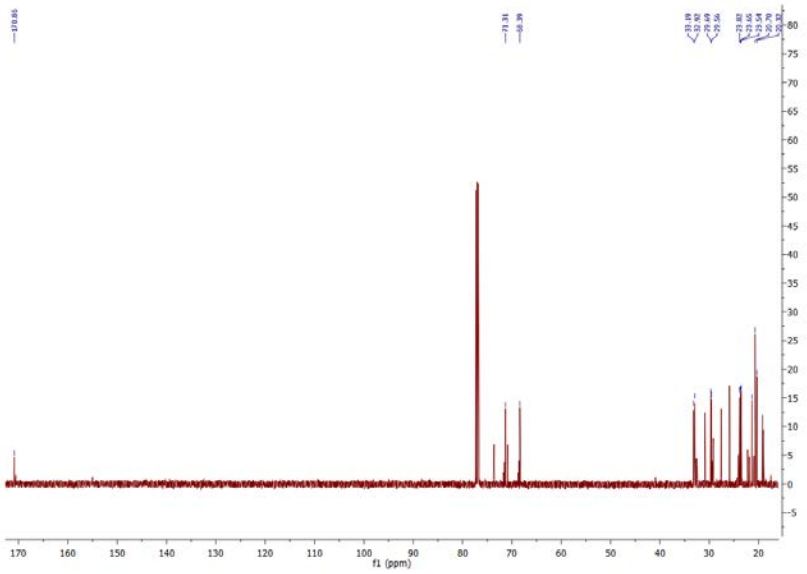

Figure B. 120 ^{13}C NMR highlighted the carbon signals of 5-hydroxycyclododecyl acetate.

Table B. 1 The carbon signals detected in the ^{13}C NMR of different metabolites of cyclododecyl acetate (in $CDCl_3$).

Products	**^{13}C NMR signals**
5-hydroxycyclododecyl acetate (RT 16.2 min in GC)	170.86, 71.31, 68.39, 33.19, 32.92, 30.88, 29.69, 29.56, 23.82, 23.63, 23.54, 21.36, 20.70, 20.32
Unidentified metabolite: another alcohol or other diastereomer of 5-hydroxycyclododecyl acetate, Signals observed in ^{13}C NMR of 5-hydroxycyclododecyl acetate (RT 16.4 min)	71.54, 68.55, 32.88, 32.71, 29.44, 23.51, 23.46, 22.22, 21.87, 21.36, 20.99, 20.96, 20.87, C=O peak not detected
trans-7-hydroxycyclododecyl acetate [150]	170.57, 73.61, 70.83, 30.83, 27.53, 25.88, 21.36, 19.14, 18.97
cis-7-hydroxycyclododecyl acetate [150]	71.73, 68.75, 32.43, 29.14, 24.07, 21.36, 20.97, 20.94, 18.97, C=O peak not detected

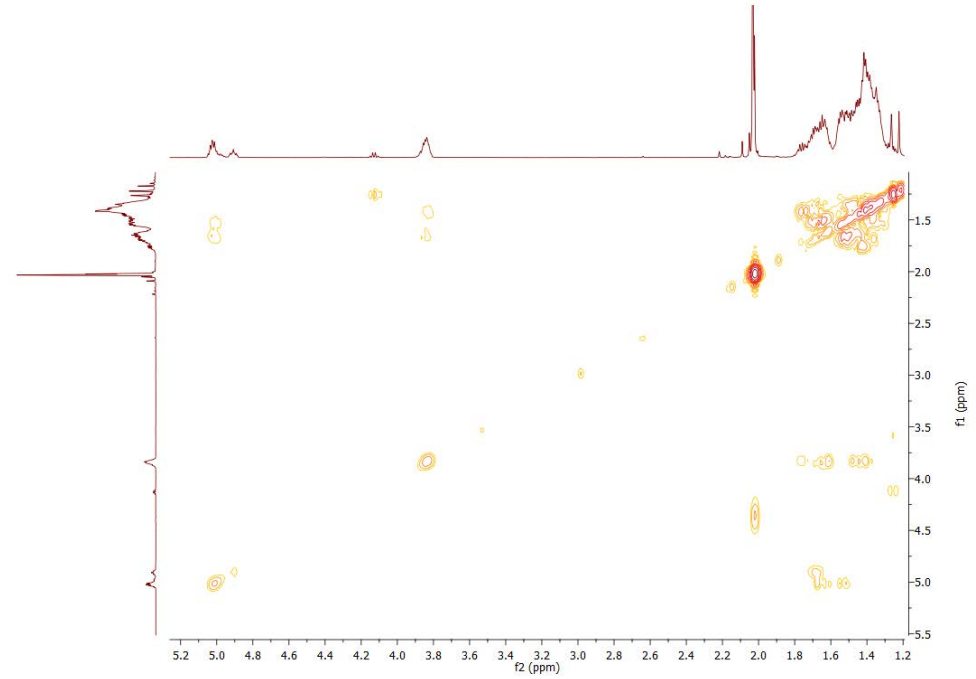

(a)

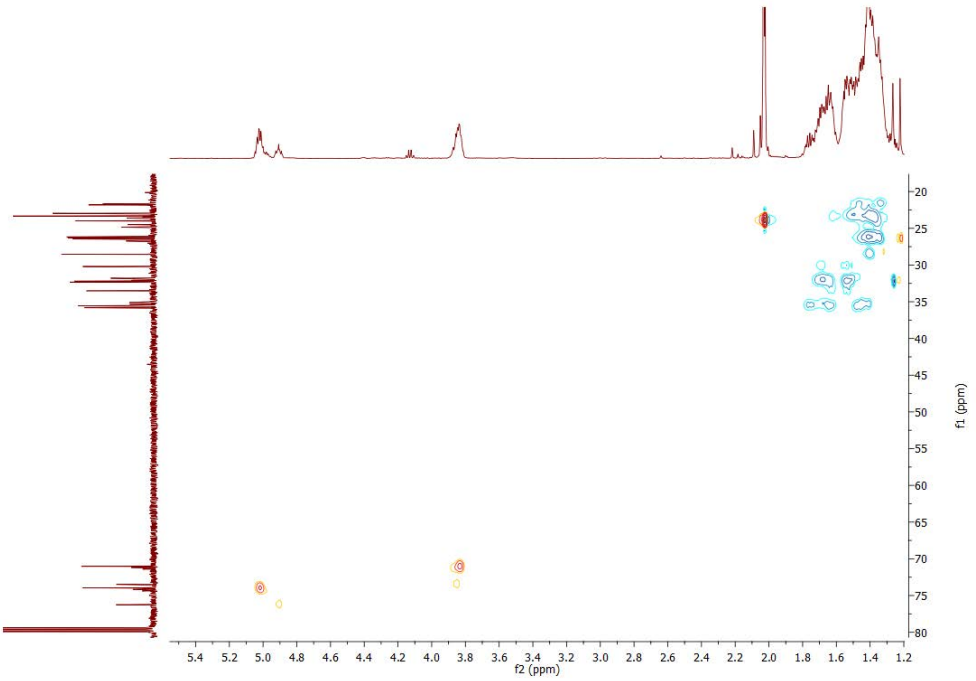

(b)

Figure B. 121 (a) gCOSY NMR spectrum of 5-hydroxycyclododecyl acetate. **(b)** HSQC NMR spectrum of 5-hydroxycyclododecyl acetate.

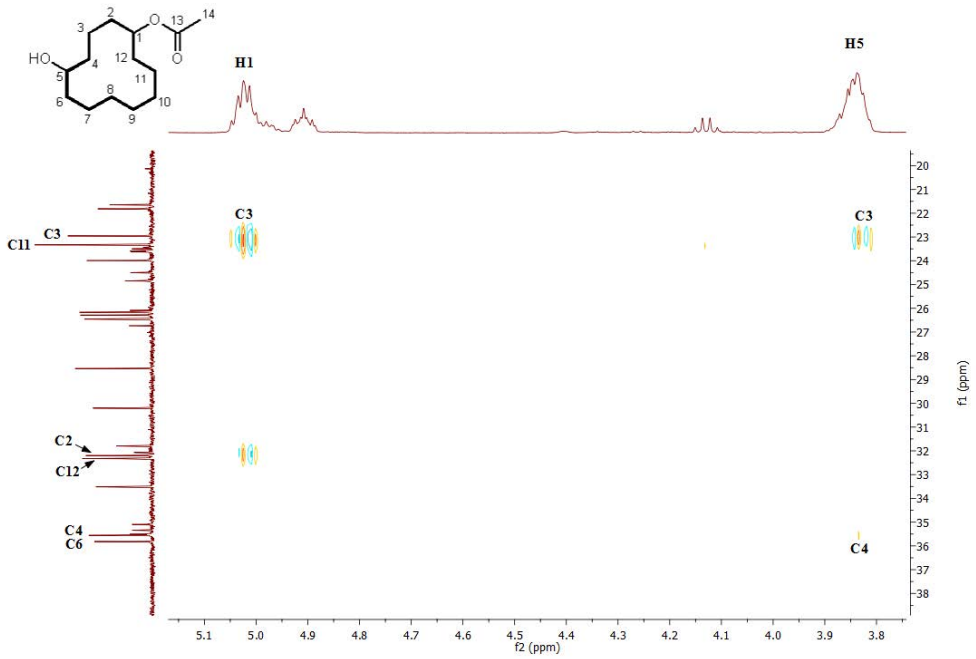

Figure B. 122 HMBC NMR spectrum of 5-hydroxycyclododecyl acetate. The metabolite was confirmed 5-hydroxy metabolite as both H1 and H5 showed strong interactions with C3.

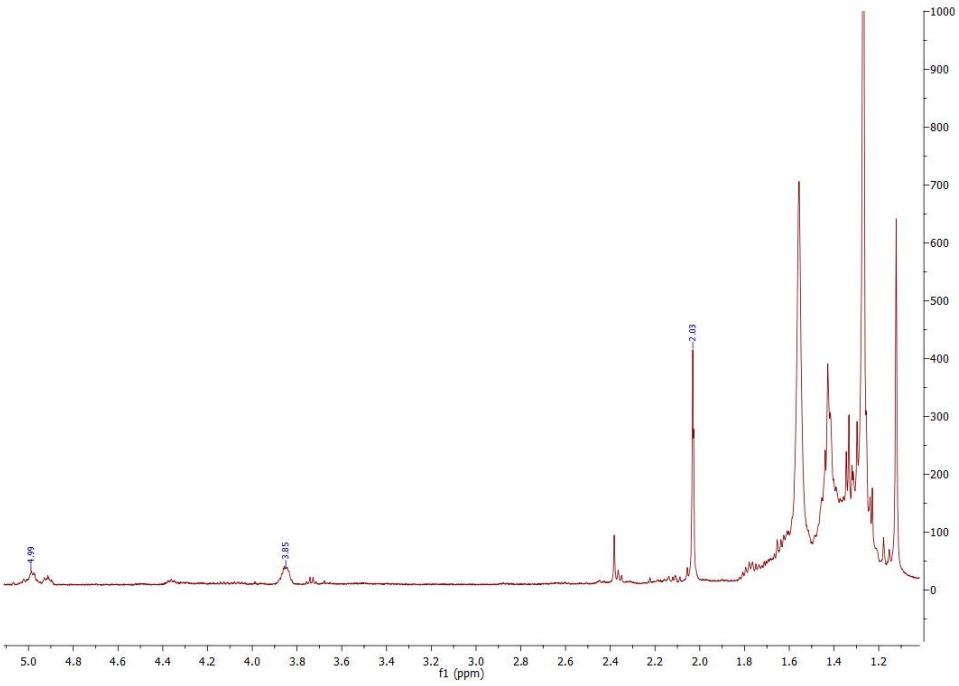

Figure B. 123 ^{1}H NMR spectrum of 7-hydroxycyclododecyl acetate (*cis*; CYP101C1). But this product was not generated in enough yield for characterisation by NMR. The peak of H1 (5.04-4.99 ppm) and GC coelution experiment with the metabolite of CYP101B1, enabled confirmation as 7-hydroxycyclododecyl acetate (*cis*) [150].

NMR for 3-cyclohexene-1-methanol, 5-hydroxy-*α*,*α*,4-trimethyl-,*α*-acetate:

^{1}H NMR (500 MHz, $CDCl_3$) δ 5.52-5.41 (m, 1H, H3), 4.20 (brd s, 1H, H5), 2.28-2.19 (m, 1H, H1), 2.19-2.13 (m, 1H, H6), 2.02-1.97 (m, 4H, H2 & 3xH12), 1.92-1.85 (m, 1H, H2), 1.76 (s, 3H, 3xH7), 1.48-1.41 (2s, 6H, 3xH9 & 3xH10), 1.35-1.20 (m, 1H, H6).

^{13}C NMR (126 MHz, $CDCl_3$) δ C11 (173.12), C4 (139.06), C3 (126.18), C8 (86.64), C5 (73.78), C1 (44.56), C6 (36.97), C2 (29.36), C9/C10 (25.97), C9/C10 (25.64), C12 (25.08), C7 (21.26).

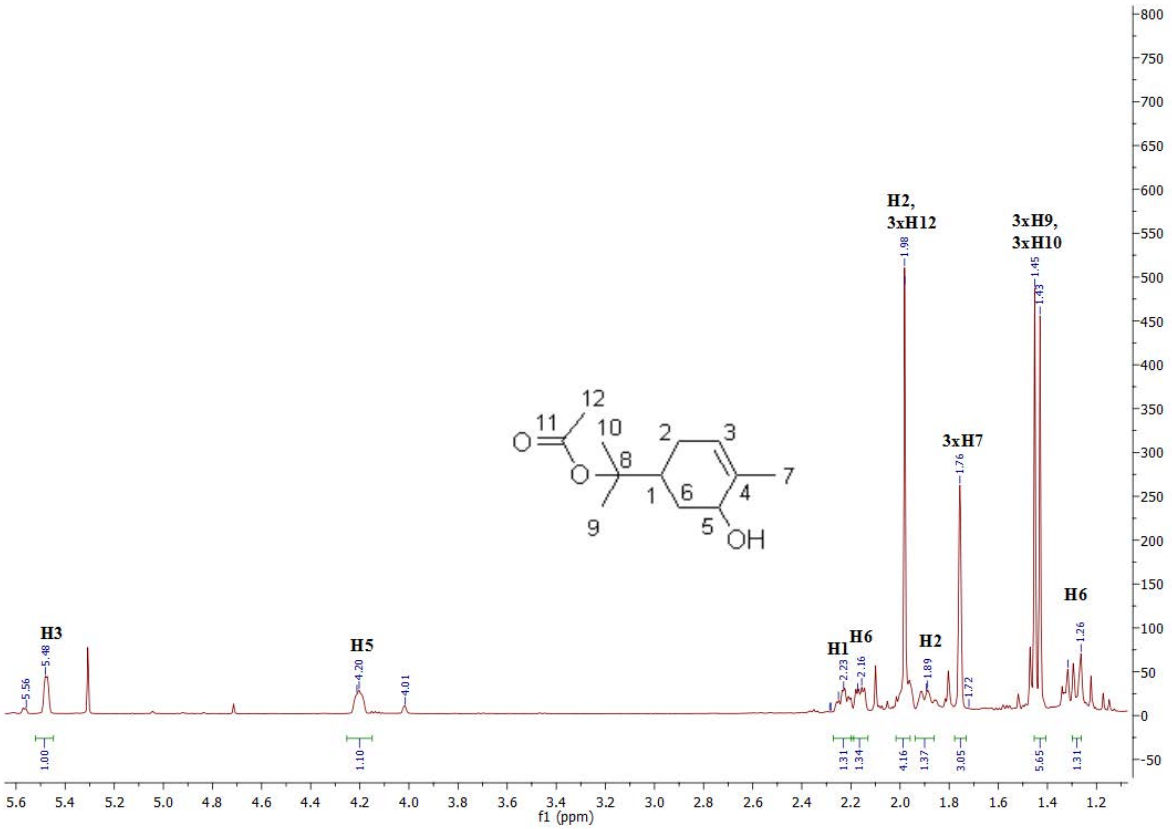

Figure B. 124 ^{1}H NMR spectrum of 3-cyclohexene-1-methanol, 5-hydroxy-*α*,*α*,4-trimethyl-,*α*-acetate (CYP101C1). The minor peaks at 5.56 ppm and 4.01 ppm indicated the presence of other diastereomer of 3-cyclohexene-1-methanol, 5-hydroxy-*α*,*α*,4-trimethyl-,*α*-acetate (Figure B. 131).

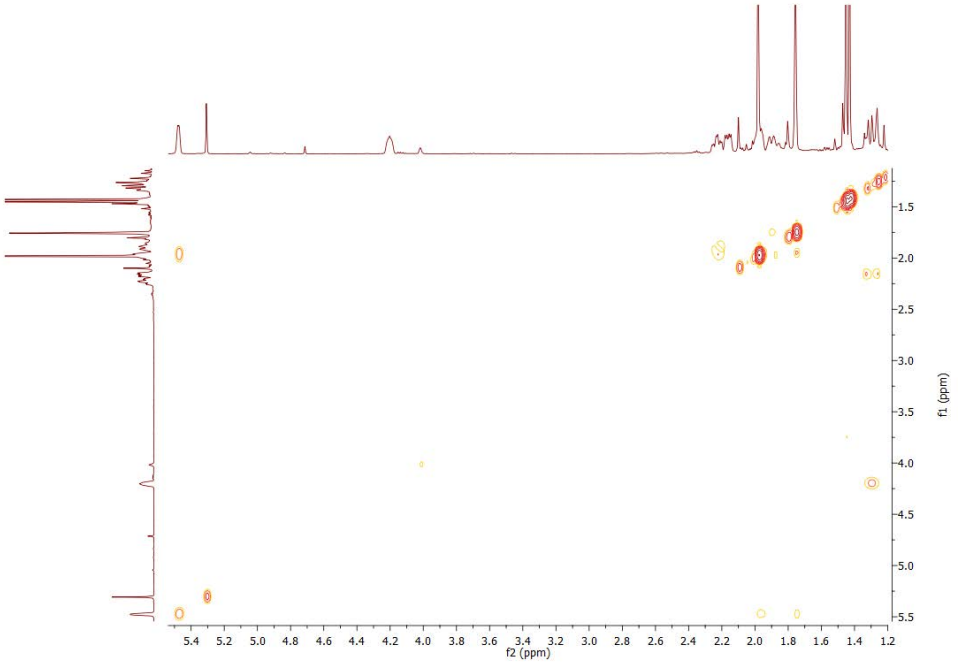

Figure B. 125 gCOSY NMR spectrum of 3-cyclohexene-1-methanol, 5-hydroxy-*α*,*α*,4-trimethyl-,*α*-acetate (CYP101C1).

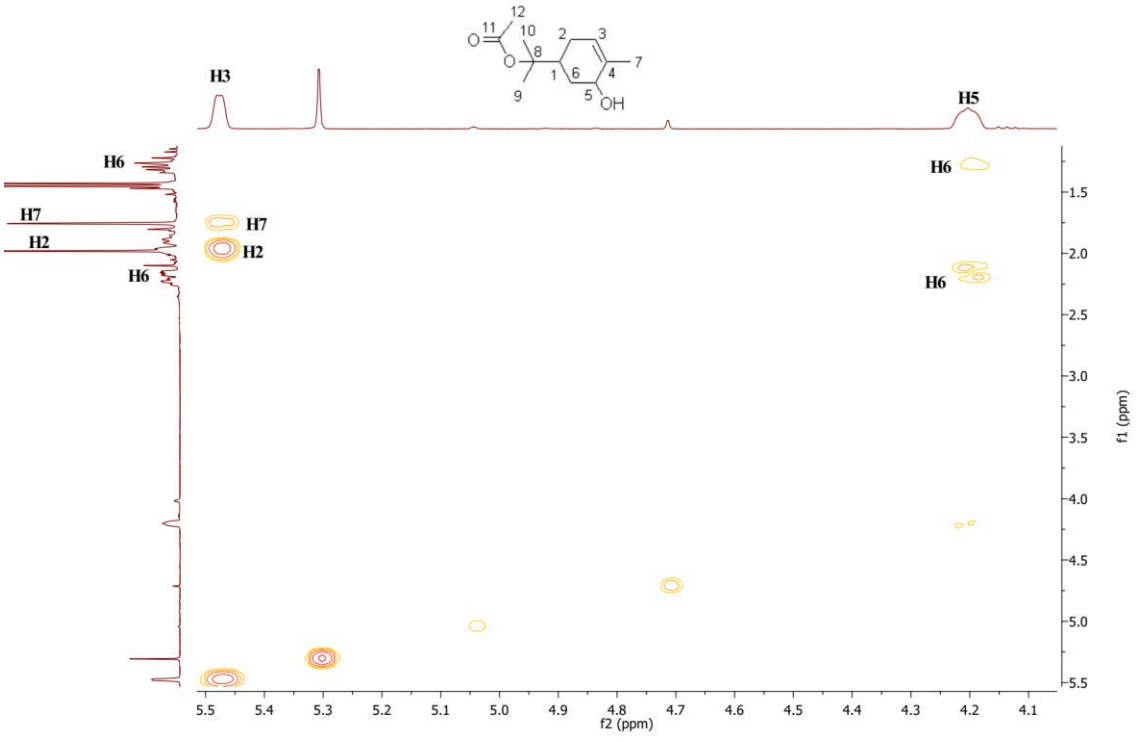

Figure B. 126 Zoomed in gCOSY NMR spectrum region of 4.1 ppm to 5.55 ppm to highlight the interactions. The product was confirmed due to strong coupling of H5 (4.21 ppm) with H6 (2.19-2.13 ppm) and H6 (1.35-1.20). H3 showed strong coupling with H2 and a weak coupling with the H7.

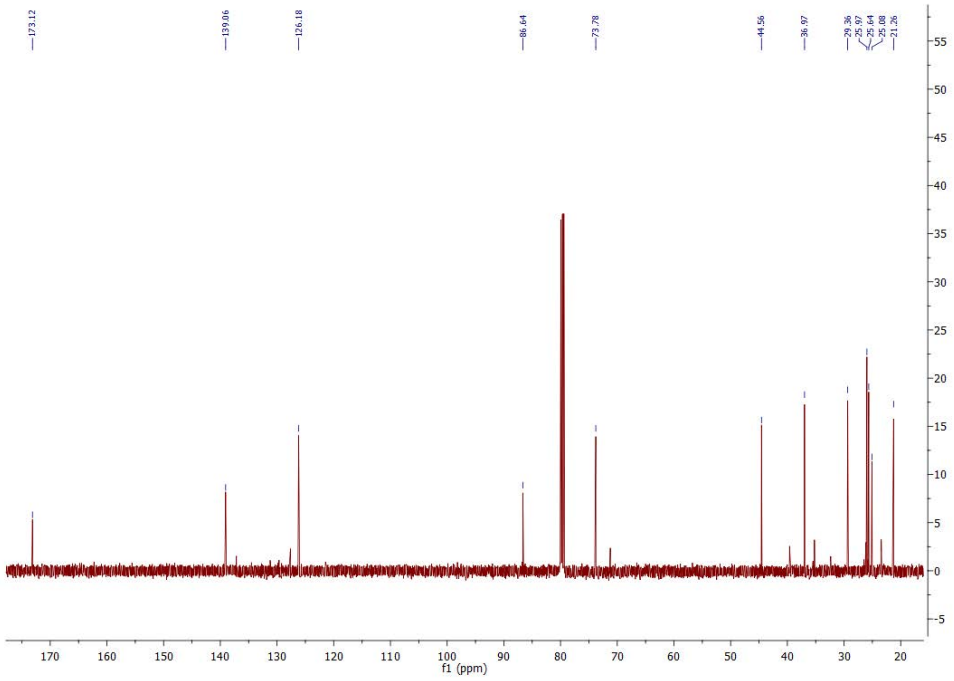

(a)

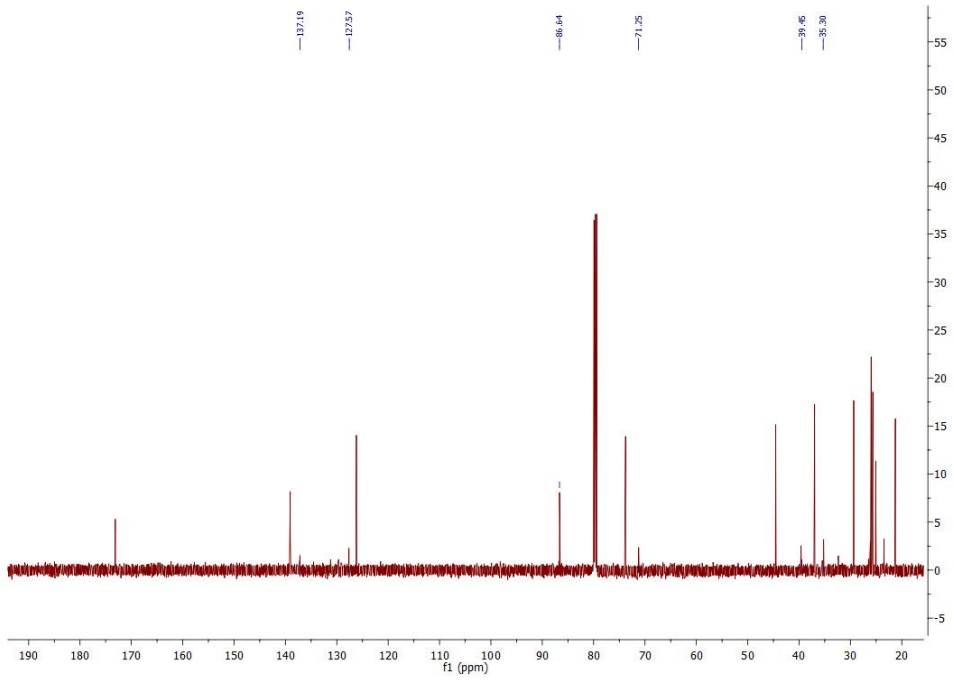

(b)

Figure B. 127 (a) ^{13}C NMR of 3-cyclohexene-1-methanol, 5-hydroxy-*α*,*α*,4-trimethyl-,*α*-acetate (CYP101C1). **(b)** Highlighted the signals of minor product which was assigned as the other diastereomer of 3-cyclohexene-1-methanol, 5-hydroxy-*α*,*α*,4-trimethyl-, *α*-acetate.

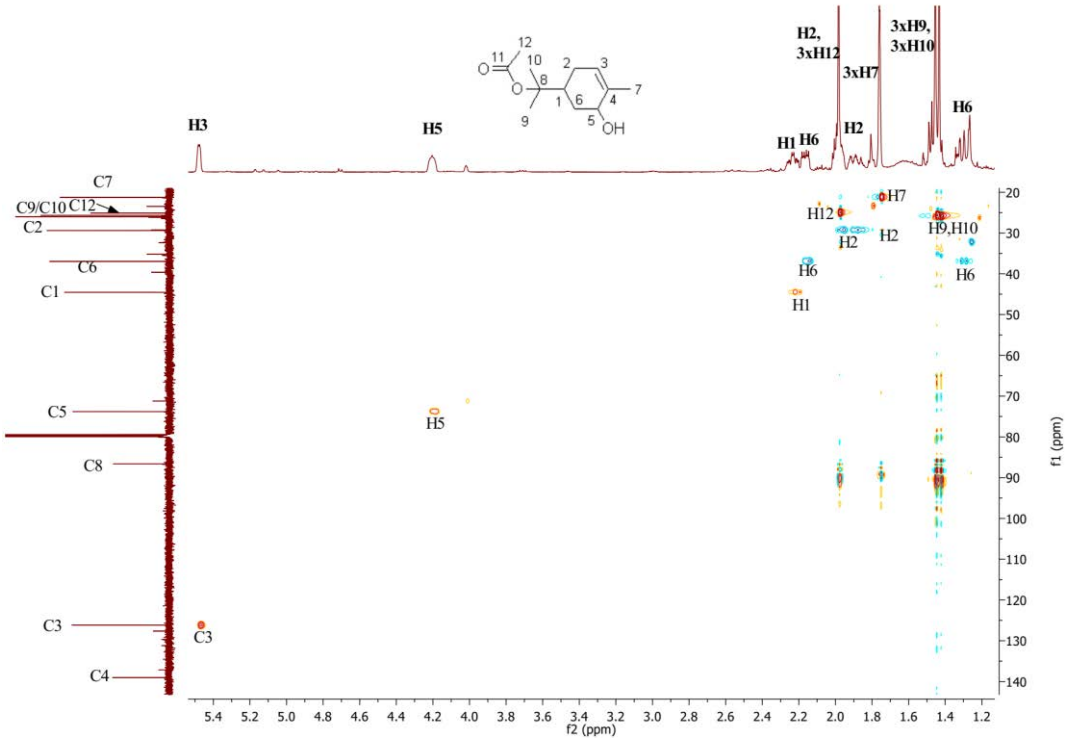

Figure B. 128 HSQC NMR spectrum of 3-cyclohexene-1-methanol, 5-hydroxy-*α*,*α*,4-trimethyl-,*α*-acetate (CYP101C1), highlighted the C-H interactions.

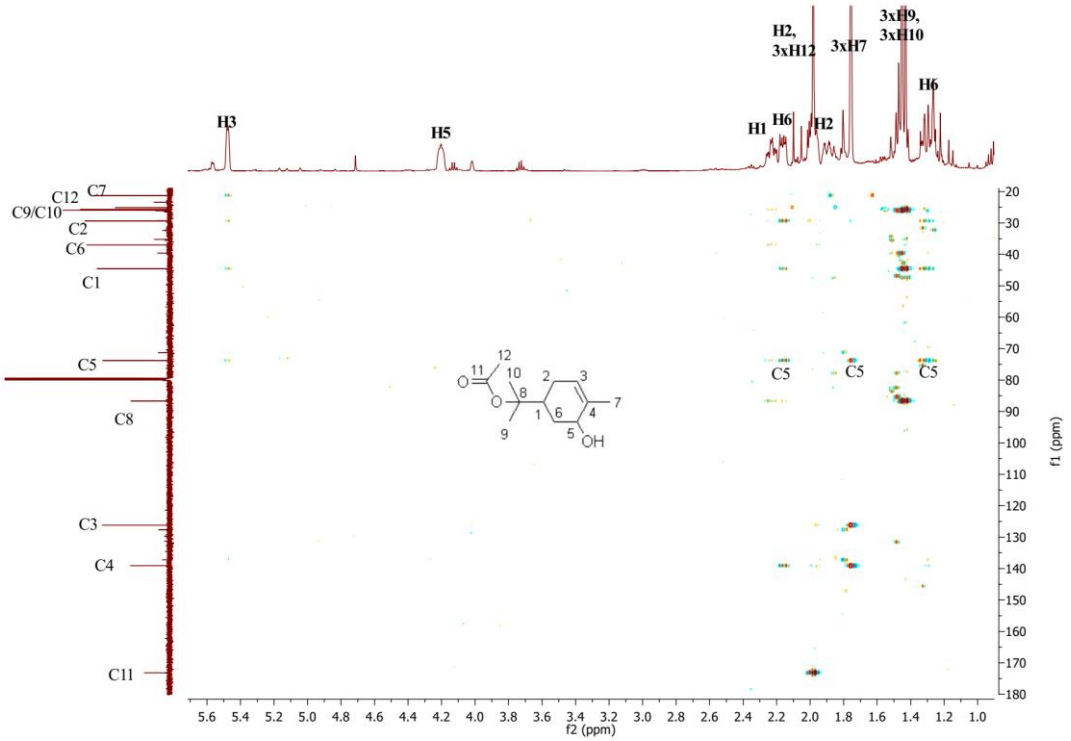

Figure B. 129 HMBC NMR spectrum of 3-cyclohexene-1-methanol, 5-hydroxy-*α*,*α*,4-trimethyl-,*α*-acetate (CYP101C1).

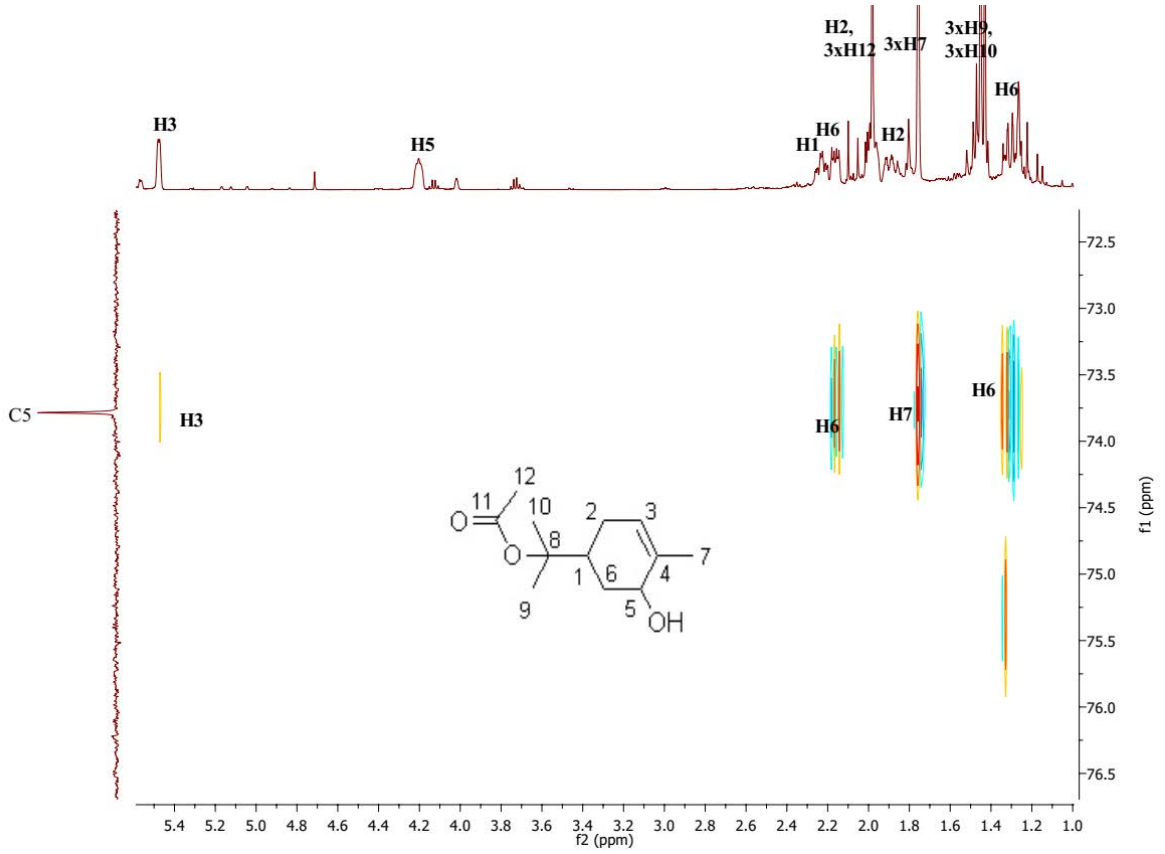

Figure B. 130 HMBC NMR spectrum of 3-cyclohexene-1-methanol, 5-hydroxy-*α*,*α*,4-trimethyl-,*α*-acetate (CYP101C1), highlighted the correlations of C5 with H3, H6 and H7.

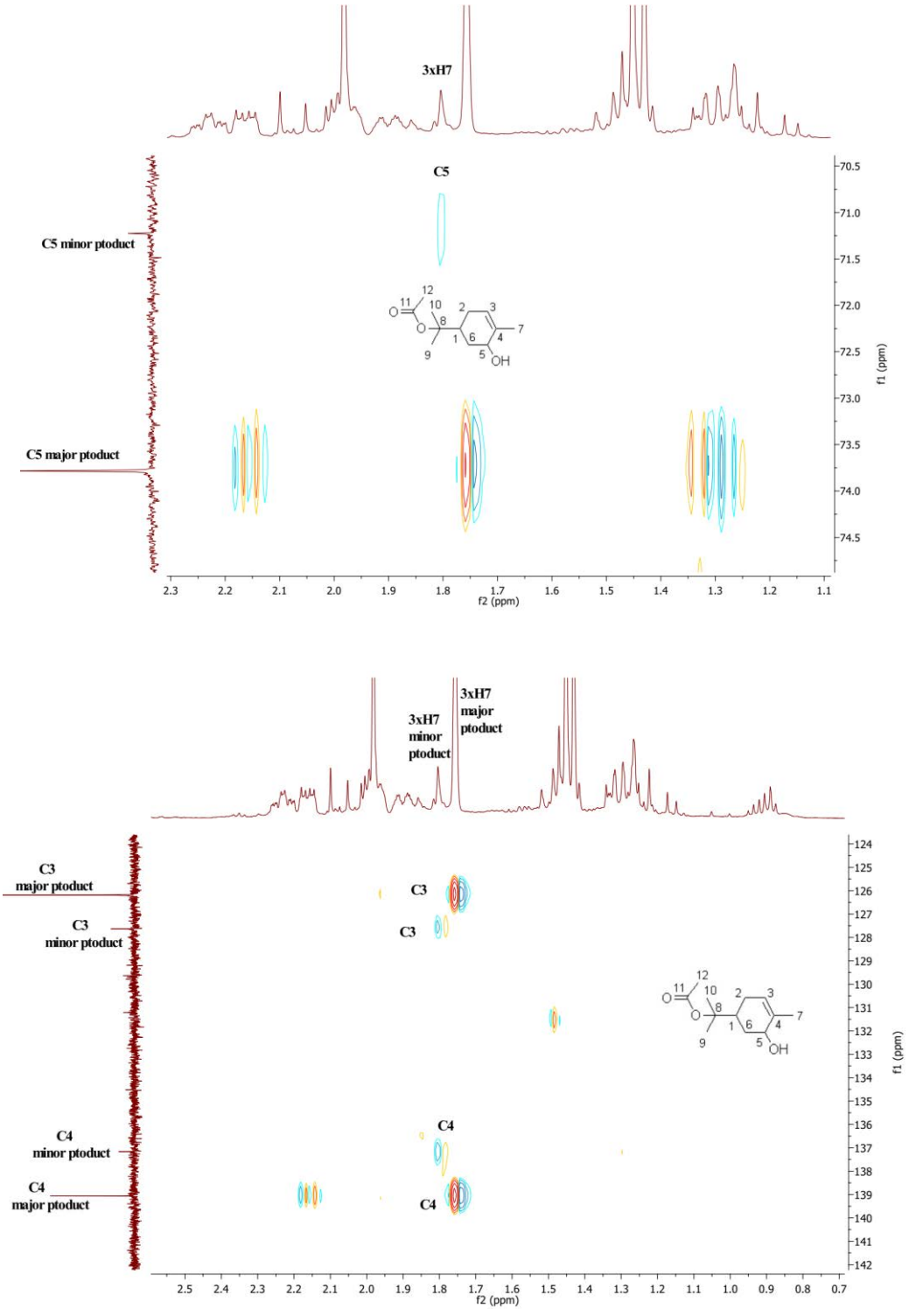

Figure B. 131 Zoomed in HMBC NMR spectrum of major product (3-cyclohexene-1-methanol, 5-hydroxy-α,α,4-trimethyl-,α-acetate) to highlight the minor product signals. The minor product was presumed to be diastereomer of the main product as C5 signal showed a correlation with H7 as well as the presence of two alkene carbons peaks at 120 to 140 ppm region in the ^{13}C NMR.

NMR for 8-hydroxy-2-nonanone:

^{1}H NMR (500 MHz, $CDCl_3$) δ 3.86-3.73 (m, 1H, H8), 2.44 (*t*, *J* = 7.4 Hz, 2H, 2xH3), 2.14 (s, 3H, 3xH1), 1.69-1.59 (m, 2H, 2xH4), 1.48-1.39 (m, 3H, H6 & 2xH7), 1.37-1.29 (m, 3H, 2xH5 & H6), 1.19 (d, *J* = 6.2 Hz, 3H, 3xH9).

^{13}C NMR (126 MHz, $CDCl_3$) δ 211.86 (C2), 70.71 (C8), 46.30 (C3), 41.73 (C7), 32.54 (C1), 31.77 (C5), 28.17 (C6), 26.38 (C4), 26.21 (C9).

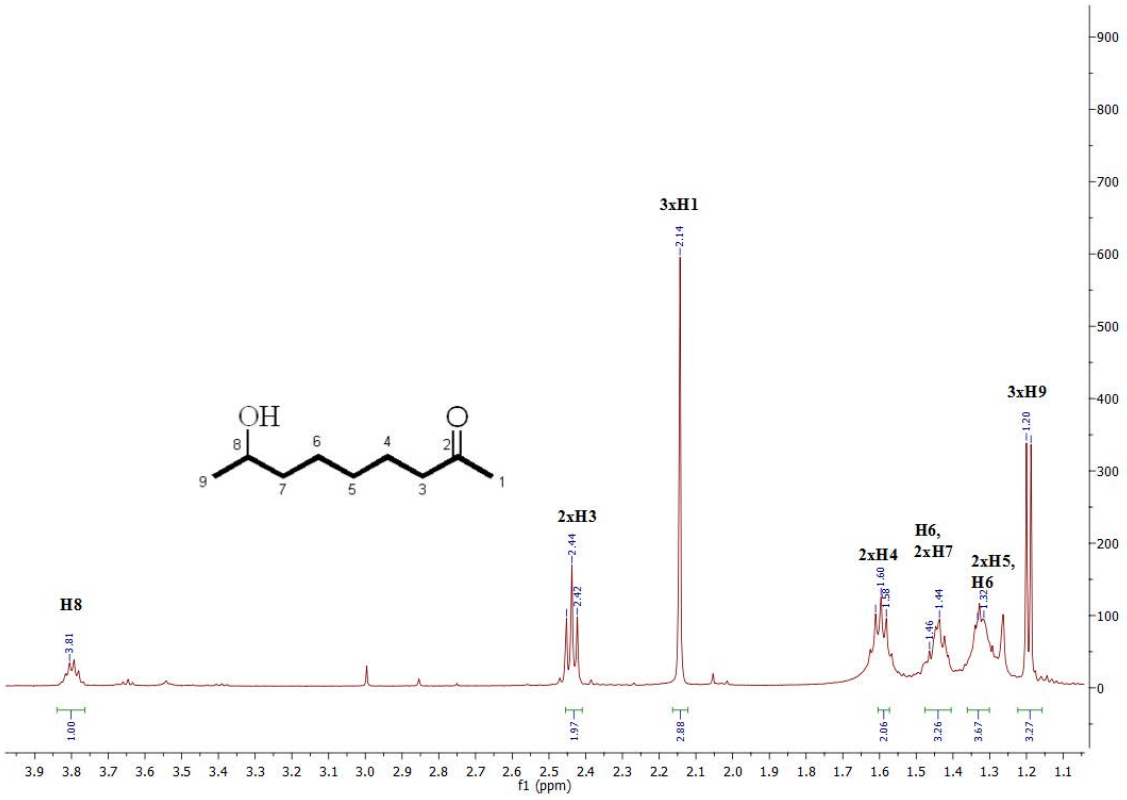

Figure B. 132 ^{1}H NMR spectrum of 8-hydroxy-2-nonanone (CYP101B1).

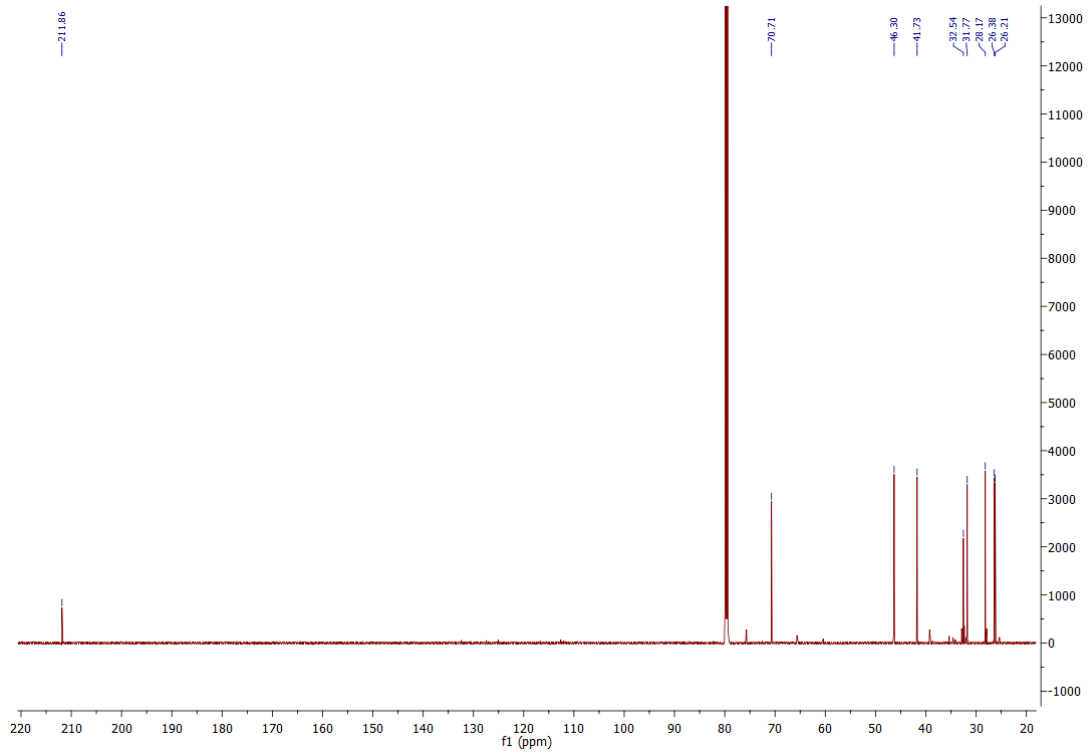

Figure B. 133 ^{13}C NMR spectrum of 8-hydroxy-2-nonanone (CYP101B1).

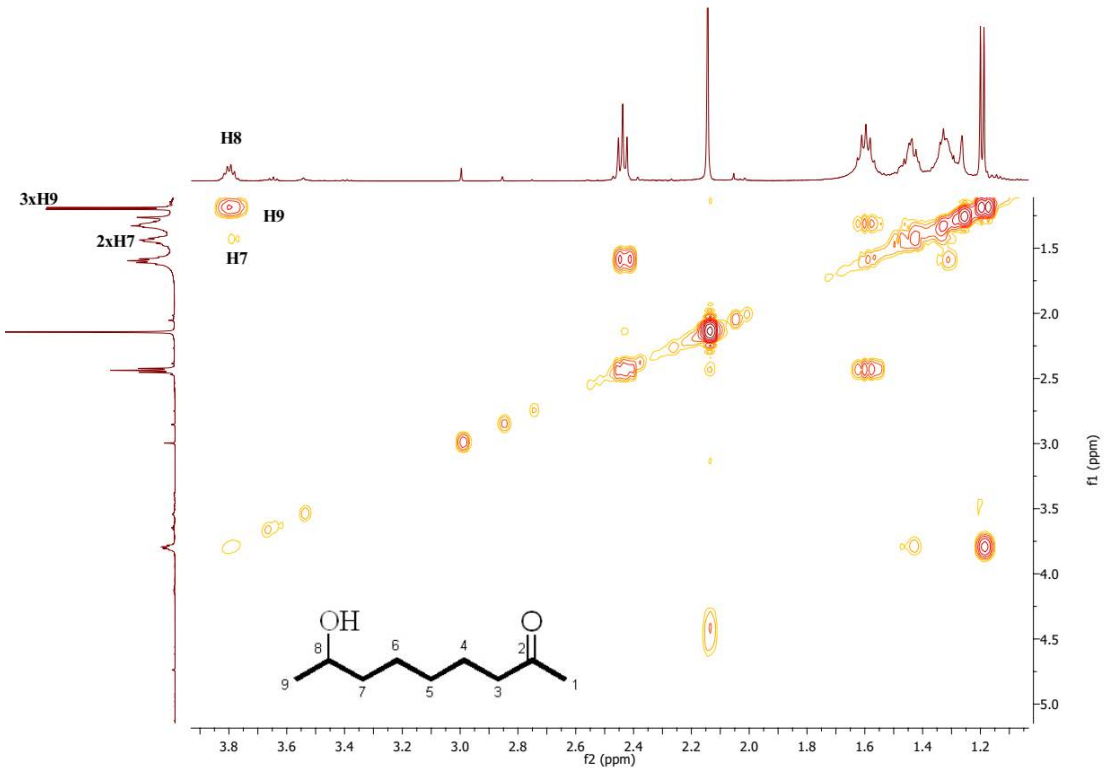

Figure B. 134 gCOSY NMR spectrum of 8-hydroxy-2-nonanone (CYP101B1).

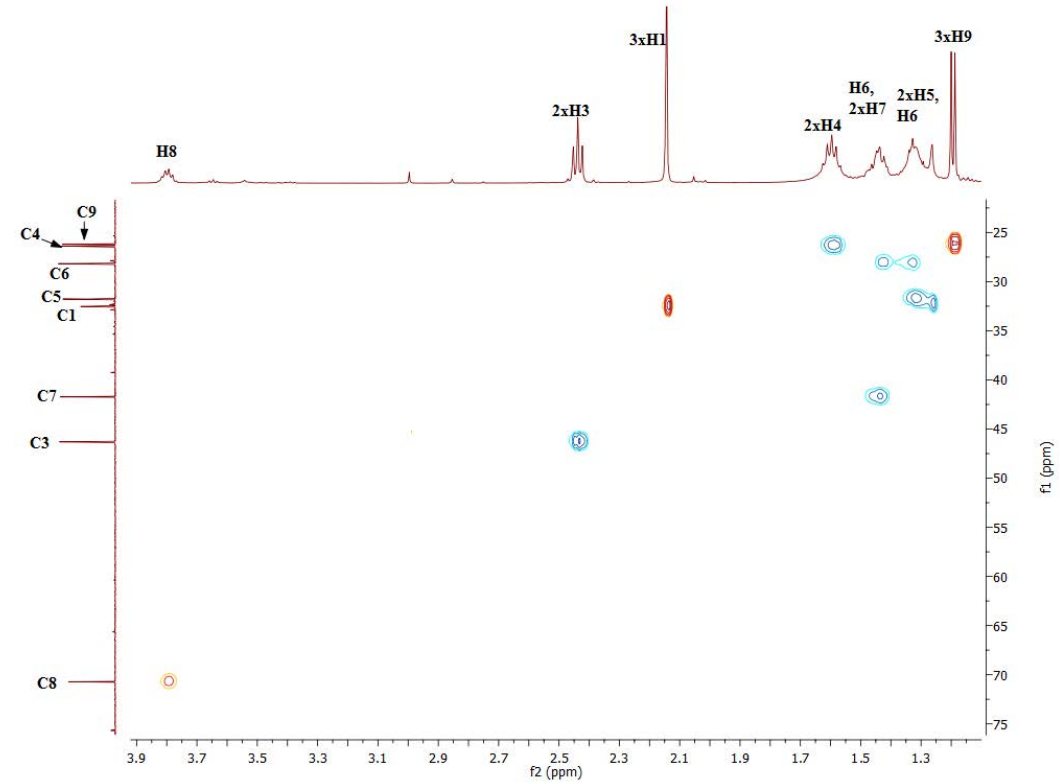

Figure B. 135 HSQC NMR spectrum of 8-hydroxy-2-nonanone (CYP101B1).

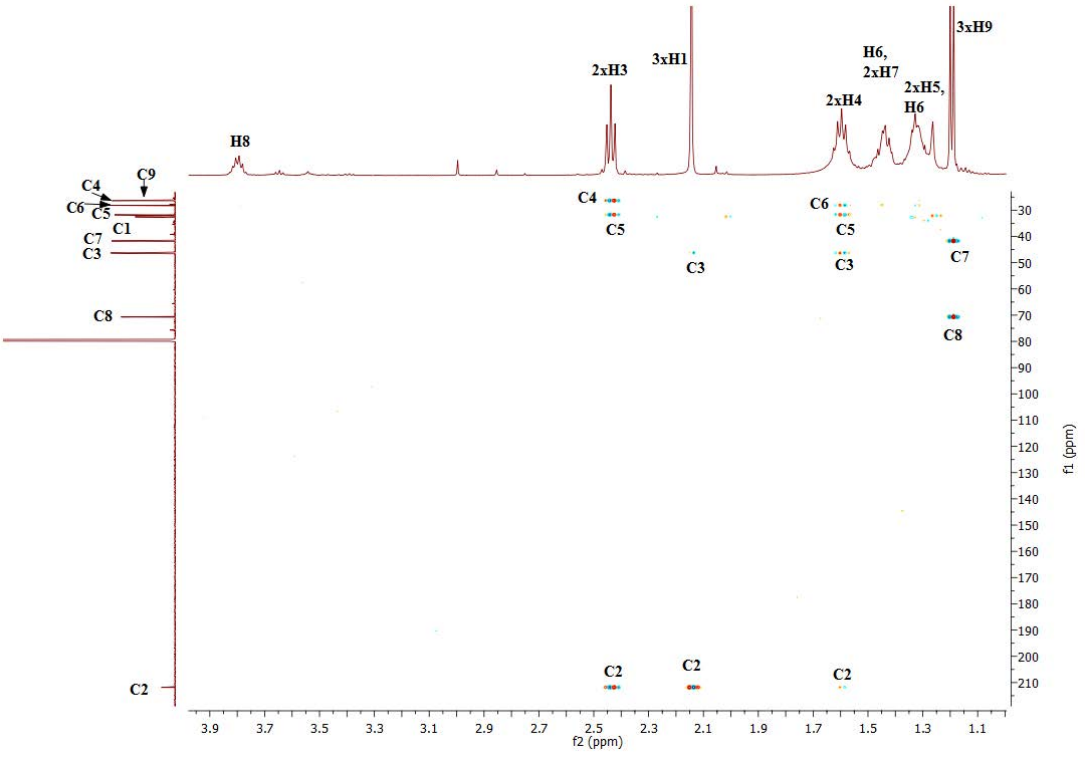

Figure B. 136 HMBC NMR spectrum of 8-hydroxy-2-nonanone (CYP101B1).

NMR for 8-hydroxy-2-undecanone:

^{1}H NMR (500 MHz, $CDCl_3$) δ 3.63-3.53 (quintet, 1H, H8), 2.44 (dd, J = 15.5, 7.8 Hz, 2H, 2xH3), 2.14 (s, 3H, 3xH1), 1.65-1.53 (m, 2H, 2xH4), 1.52-1.37 (m, 6H, H6, 2xH7, 2xH9 & H10), 1.36-1.28 (m, 4H, 2xH5, H6 & H10), 0.96-0.88 (m, 3H, 3xH11).

^{13}C NMR (126 MHz, $CDCl_3$) δ C2 (211.83), C8 (74.26), C3 (46.32), C9 (42.38), C7 (39.90), C1 (32.50), C5 (31.84), C6 (28.06), C4 (26.42), C10 (21.53), C11 (16.78).

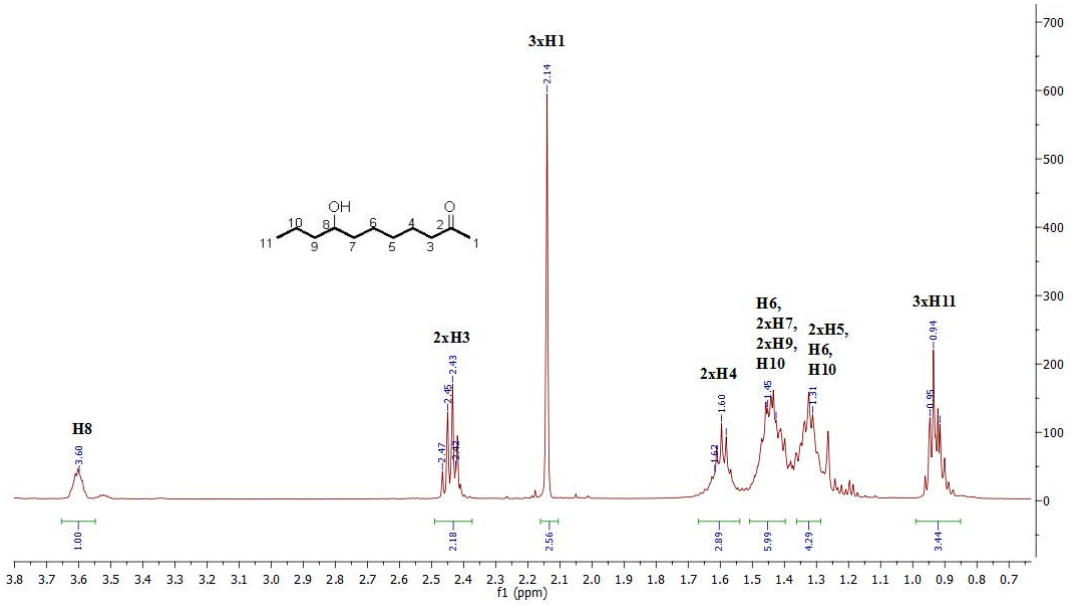

Figure B. 137 ^{1}H NMR spectrum of 8-hydroxy-2-undecanone (CYP101B1).

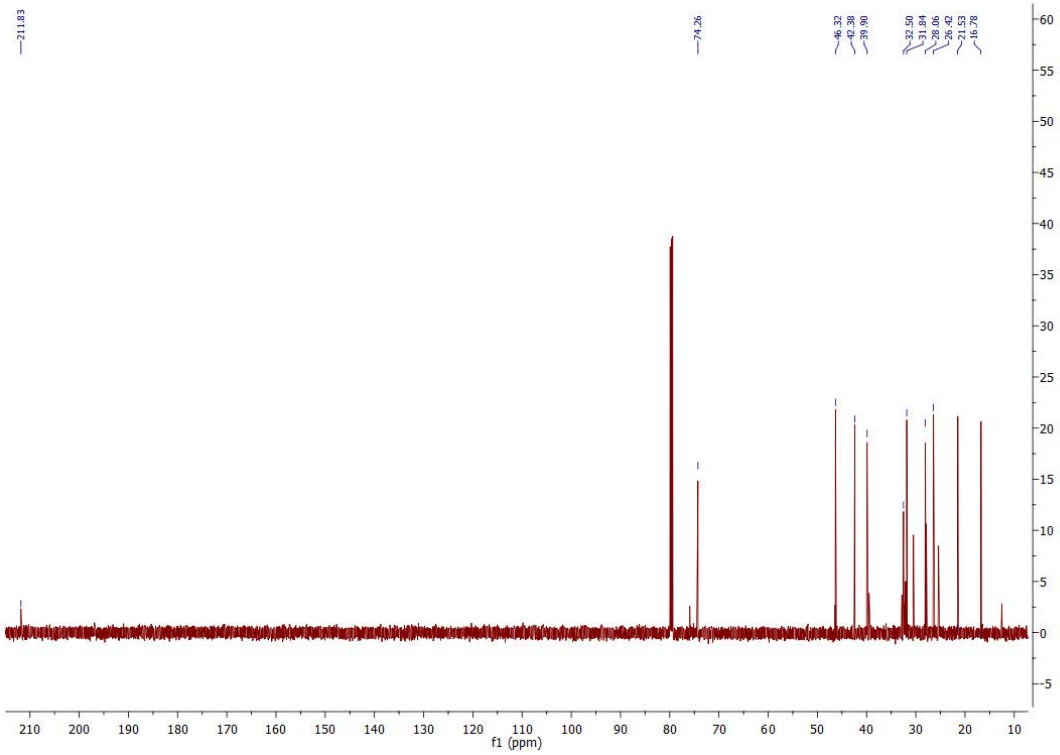

(a)

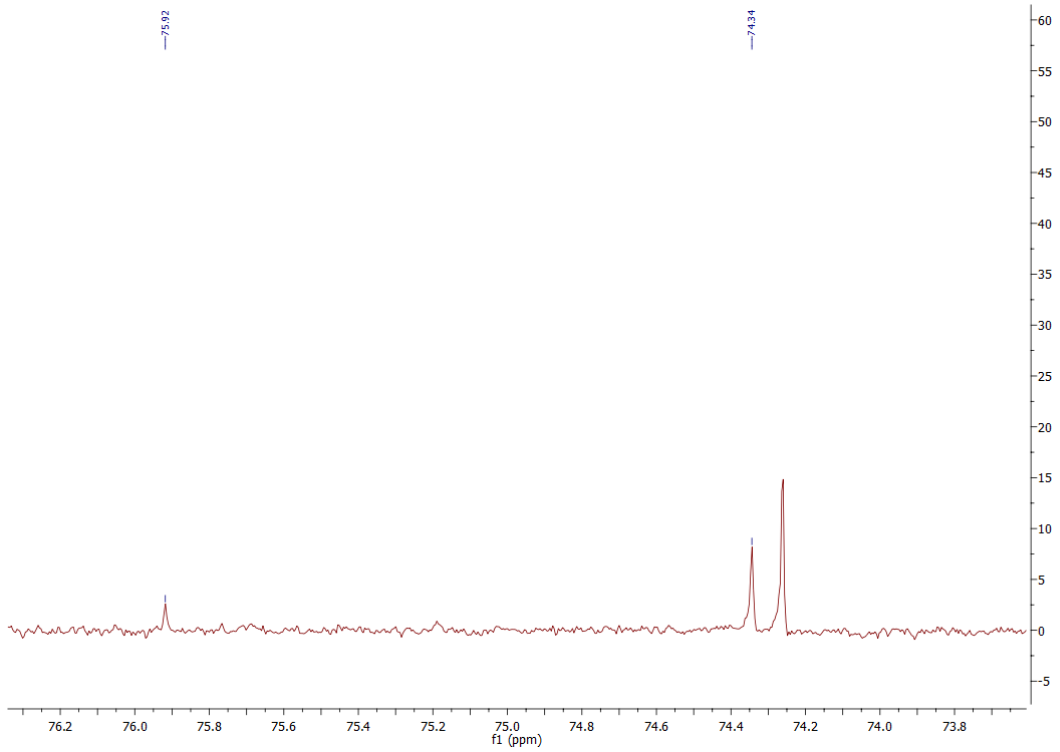

(b)

Figure B. 138 (a) ^{13}C NMR spectrum of 8-hydroxy-2-undecanone. **(b)** The zoomed in ^{13}C NMR of the region 70-76 ppm to highlight the carbon peaks of minor metabolites.

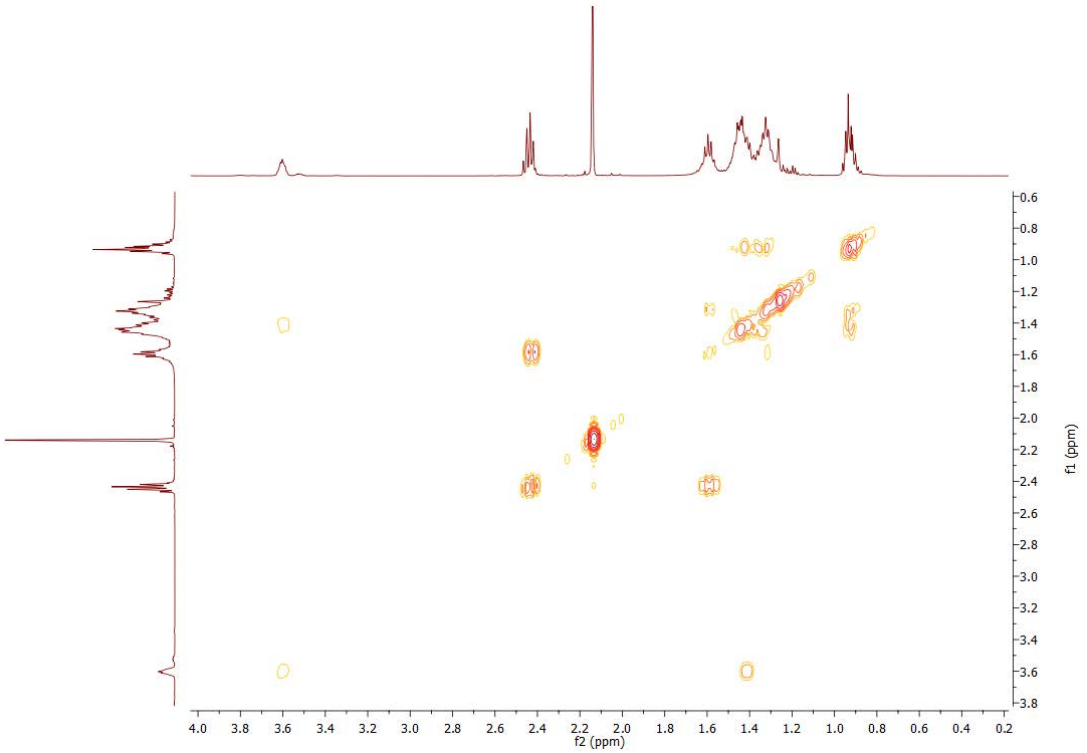

Figure B. 139 gCOSY NMR spectrum of 8-hydroxy-2-undecanone (CYP101B1).

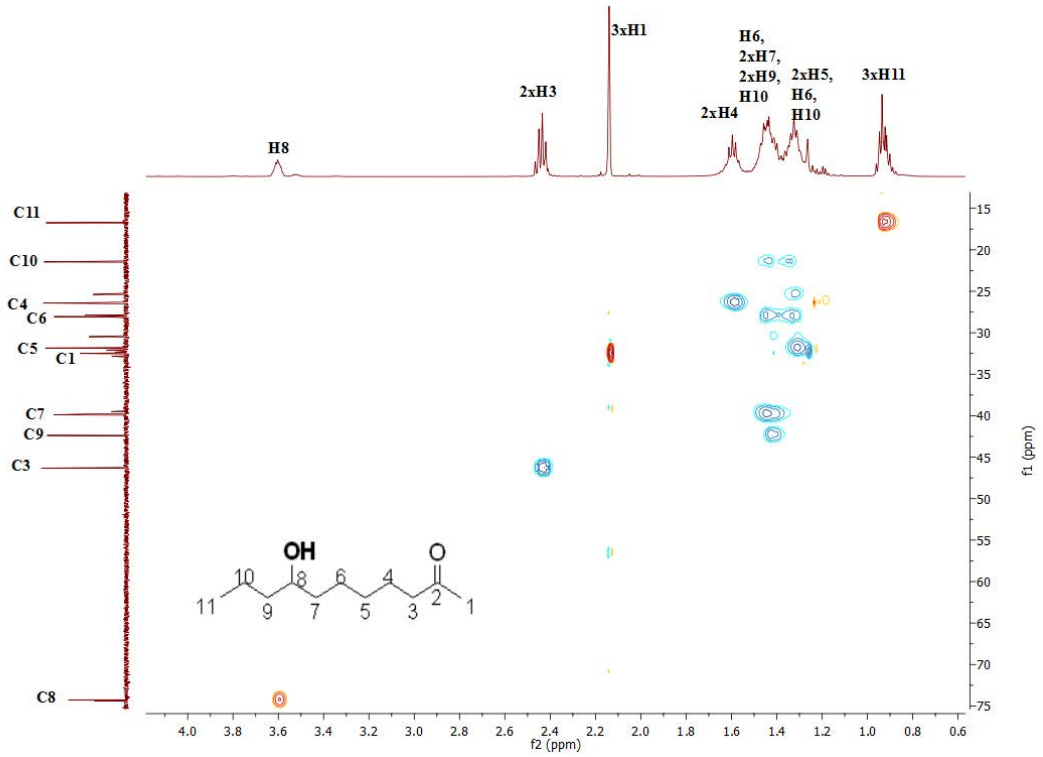

Figure B. 140 HSQC NMR spectrum of 8-hydroxy-2-undecanone (CYP101B1).

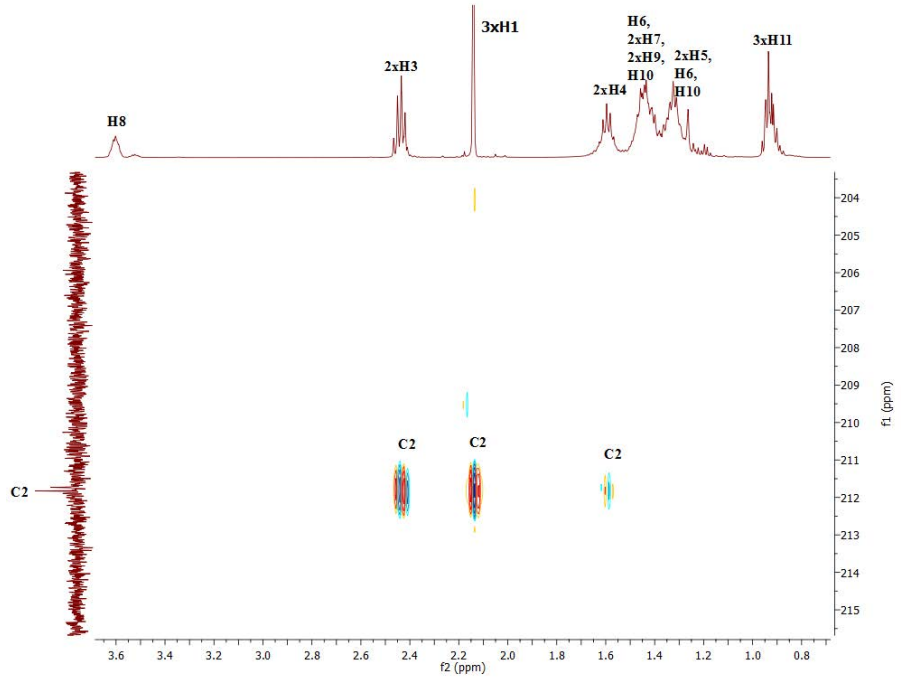

(a)

Zoomed in version of HMBC NMR to highlight the interactions of C2 with H3, H1 and H4.

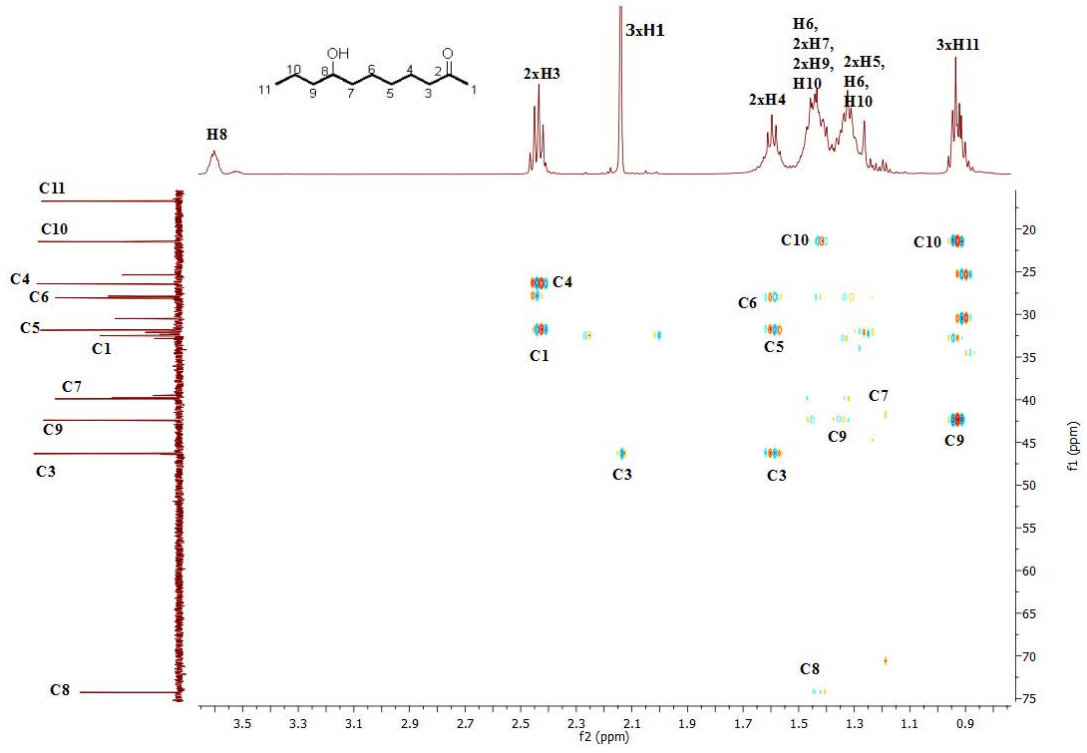

(b)

Figure B. 141 (a and b) HMBC NMR spectrum of 8-hydroxy-2-undecanone (CYP101B1). **(b)** The product was confirmed 8-hydroxy-2-undecanone as carbon signal (74.26 ppm) showed correlations with the protons H6, H7, H9 and H10 (1.52-1.37 ppm).

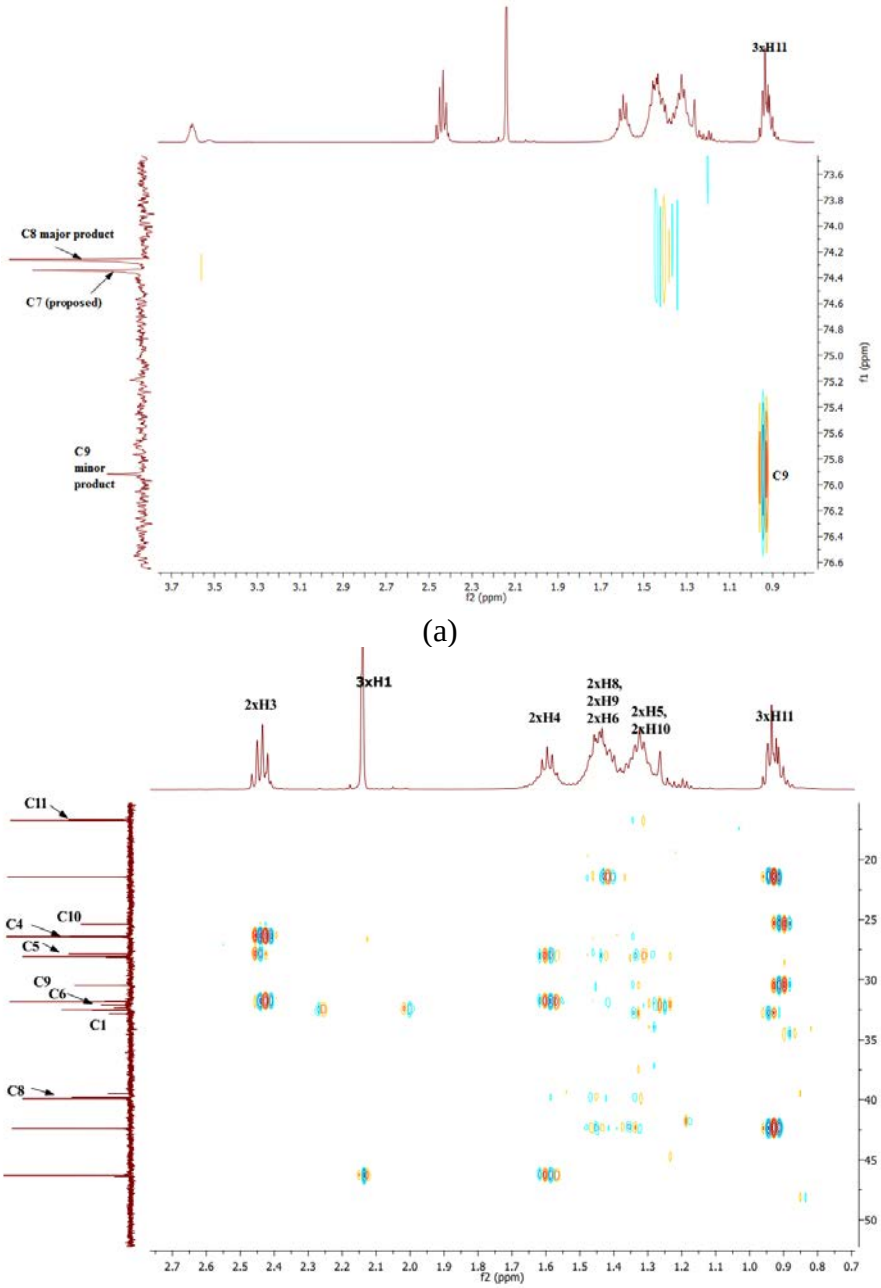

Figure B. 142 (a) Zoomed in the HMBC NMR spectrum of 8-hydroxy-2-undecanone to highlight the C-H interactions of minor metabolites. The peak at 75.94 ppm showed a strong correlation with H11 protons and this product was assigned as a 9-hydroxy metabolite. The minor signal at 74.34 ppm displayed the interaction with the protons at 1.52-1.28 ppm. Other carbon signals C1, C4, C5, C6, C8, C9, C10, C11 of this metabolite were identified using the C-H correlations in the HMBC NMR **(b)**. Hydroxylation did not occur at C3 as 74.34 ppm carbon signal has no correlation with H4 peak. Therefore the product was presumed to be a 7-hydroxy metabolite. However, full characterisation of these metabolites were not possible due to noise and low yield.

Appendix C Supporting information for Chapter 4

Figure C. 1 Mass Spectra Analysis **413**
Figure C. 2 ^{1}H NMR of *trans*-4-hydroxy-1-adamantylmethyl ketone. 417
Figure C. 3 ^{13}C NMR of *trans*-4-hydroxy-1-adamantylmethyl ketone. 418
Figure C. 4 gCOSY NMR of *trans*-4-hydroxy-1-adamantylmethyl ketone. 418
Figure C. 5 HSQC NMR of *trans*-4-hydroxy-1-adamantylmethyl ketone. 419
Figure C. 6 HMBC NMR of *trans*-4-hydroxy-1-adamantylmethyl ketone. 420
Figure C. 7 Zoomed in ROESY NMR of *trans*-4-hydroxy-1-adamantylmethyl ketone to highlight the interactions of H4 with H5 and H10. 421
Figure C. 8 ROESY NMR of *trans*-4-hydroxy-1-adamantylmethyl ketone. 421
Figure C. 9 ^{1}H NMR of 3-hydroxy-1-adamantylmethyl ketone. 422
Figure C. 10 ^{13}CNMR of 3-hydroxy-1-adamantylmethyl ketone. 423
Figure C. 11 gCOSY NMR of 3-hydroxy-1-adamantylmethyl ketone. 423
Figure C. 12 HSQC NMR of 3-hydroxy-1-adamantylmethyl ketone. 424
Figure C. 13 Zoomed in HMBC NMR of 3-hydroxy-1-adamantylmethyl ketone to highlight the interactions of carbons with protons. 425
Figure C. 14 ^{1}H NMR of methyl-2-(*trans*-4-hydroxy-1-adamantyl) acetate. 426
Figure C. 15 ^{13}C NMR of methyl-2-(*trans*-4-hydroxy-1-adamantyl) acetate. 427
Figure C. 16 gCOSY NMR of methyl-2-(*trans*-4-hydroxy-1-adamantyl) acetate. 427
Figure C. 17 HSQC NMR of methyl-2-(*trans*-4-hydroxy-1-adamantyl) acetate. 428
Figure C. 18 Zoomed in ROESY NMR of methyl-2-(*trans*-4-hydroxy-1-adamantyl) acetate highlighting the interactions of H4 with H5 and H10. 428
Figure C. 19 ROESY NMR of methyl-2-(*trans*-4-hydroxy-1-adamantyl) acetate. 429
Figure C. 20 ^{1}H NMR of methyl-2-(3-hydroxy-1-adamantyl) acetate. 430
Figure C. 21 ^{13}C NMR of methyl-2-(3-hydroxy-1-adamantyl) acetate. 431
Figure C. 22 gCOSY NMR of methyl-2-(3-hydroxy-1-adamantyl) acetate. 431
Figure C. 23 HSQC NMR of methyl-2-(3-hydroxy-1-adamantyl) acetate. 432
Figure C. 24 ^{1}H NMR of *trans*-4-hydroxy-1-adamantyl acetate. 433
Figure C. 25 ^{13}C NMR of *trans*-4-hydroxy-1-adamantyl acetate. 434
Figure C. 26 gCOSY NMR of *trans*-4-hydroxy-1-adamantyl acetate. 434
Figure C. 27 HSQC of NMR of *trans*-4-hydroxy-1-adamantyl acetate. 435
Figure C. 28 HMBC NMR of *trans*-4-hydroxy-1-adamantyl acetate. 435

Figure C. 29 Zoomed in ROESY NMR of *trans*-4-hydroxy-1-adamantyl acetate.....436
Figure C. 30 ROESY NMR of *trans*-4-hydroxy-1-adamantyl acetate. 436
Figure C. 31 ^{1}H NMR of 3-hydroxy-1-adamantyl acetate.....437
Figure C. 32 ^{1}H NMR of *trans*-4-hydroxy-1-adamantyl isobutyrate. 438
Figure C. 33 ^{13}C NMR of *trans*-4-hydroxy-1-adamantyl isobutyrate 439
Figure C. 34 gCOSY NMR of *trans*-4-hydroxy-1-adamantyl isobutyrate.....439
Figure C. 35 HSQC NMR of *trans*-4-hydroxy-1-adamantyl isobutyrate.....440
Figure C. 36 HMBC NMR of *trans*-4-hydroxy-1-adamantyl isobutyrate.....440
Figure C. 37 Zoomed in ROESY NMR of *trans*-4-hydroxy-1-adamantyl isobutyrate 441
Figure C. 38 ROESY NMR of *trans*-4-hydroxy-1-adamantyl isobutyrate. 441
Figure C. 39 ^{1}H NMR of 5-hydroxy-2-adamantyl acetate.....442
Figure C. 40 ^{13}C NMR of 5-hydroxy-2-adamantyl acetate. 443
Figure C. 41 gCOSY NMR of 5-hydroxy-2-adamantyl acetate. 443
Figure C. 42 HSQC NMR of 5-hydroxy-2-adamantyl acetate. 444
Figure C. 43 HMBC NMR of 5-hydroxy-2-adamantyl acetate. 444
Figure C. 44 ^{1}H NMR of 5-hydroxy-2-adamantyl isobutyrate..... 446
Figure C. 45 ^{13}C NMR of 5-hydroxy-2-adamantyl isobutyrate.....446
Figure C. 46 gCOSY NMR of 5-hydroxy-2-adamantyl isobutyrate. 446
Figure C. 47 HSQC NMR of 5-hydroxy-2 adamantyl isobutyrate.....447
Figure C. 48 HMBC NMR of 5-hydroxy-2 adamantyl isobutyrate.....447
Figure C. 49 ^{1}H NMR of 4-hydroxy-N-(1-adamantyl)acetamide.....449
Figure C. 50 ^{13}C NMR of 4-hydroxy-N-(1-adamantyl)acetamide. 450
Figure C. 51 gCOSY NMR of 4-hydroxy-N-(1-adamantyl)acetamide. 450
Figure C. 52 HSQC NMR of 4-hydroxy-N-(1-adamantyl)acetamide. 451
Figure C. 53 HMBC NMR of 4-hydroxy-N-(1-adamantyl)acetamide. 451
Figure C. 54 Zoomed in ROESY NMR of 4-hydroxy-N-(1-adamantyl)acetamide. 452
Figure C. 55 ROESY NMR of 4-hydroxy-N-(1-adamantyl)acetamide.....452
Figure C. 56 ^{1}H NMR of 3-hydroxy-N-(1-adamantyl)acetamide.....453
Figure C. 57 gCOSY NMR of 3-hydroxy-N-(1-adamantyl)acetamide. 453

Figure C. 1 Mass Spectra Analysis

MS analysis of 1-adamantylmethyl ketone products

MS analysis of 3-hydroxy-1-adamantylmethyl ketone (m^+/z = 194.05) RT 9.2 min.

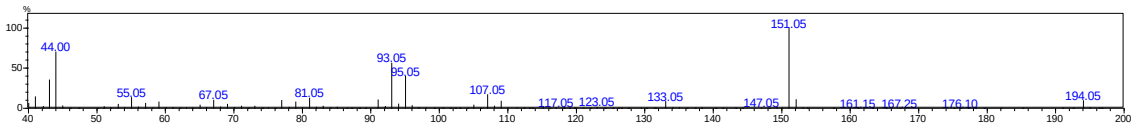

MS analysis of *trans*-4-hydroxy-1-adamantylmethyl ketone (m^+/z = 194.05) RT 10.2 min.

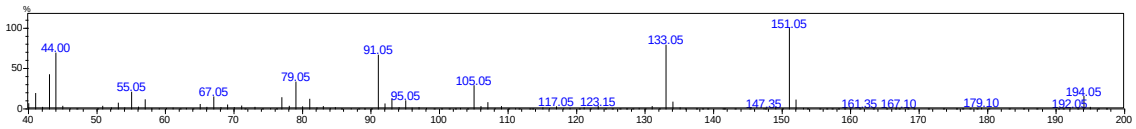

MS analysis of methyl-2-(1-adamantyl acetate)

MS analysis of methyl-2-(*trans*-4-hydroxy-1-adamantyl) acetate (m^+/z = 224.05) RT 15.6 min.

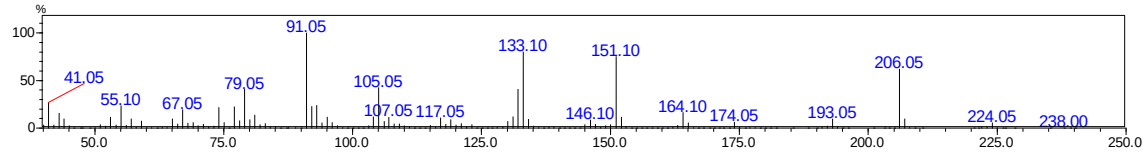

MS analysis of methyl-2-(3-hydroxy-1-adamantyl) acetate (m^+/z = 224.05) RT 14.8 min.

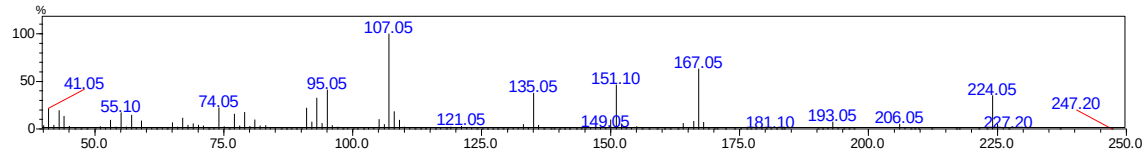

MS analysis of 1-adamantyl acetate

MS analysis of 3-hydroxyl-1-adamantyl acetate (m^+/z = 210.0) RT 8.9 min

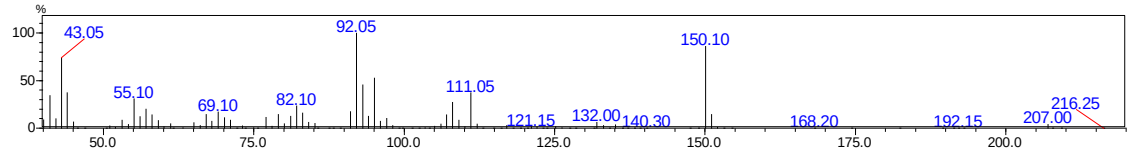

MS analysis of *trans*-4-hydroxyl-1-adamantyl acetate (m^+/z = 210.10) RT 9.9 min

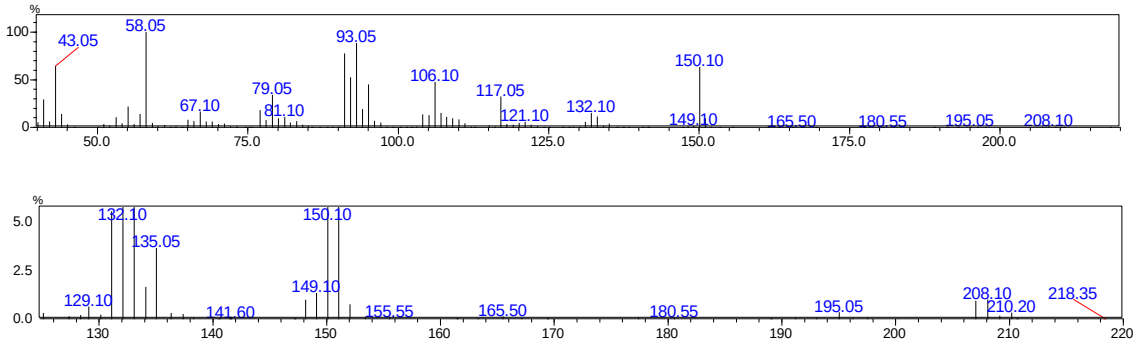

Zoomed in

MS analysis of 1-adamantyl isobutyrate

MS analysis of *trans*-4-hydroxy-1-adamantyl isobutyrate (m^+/z = 238.05) RT 11.5 min

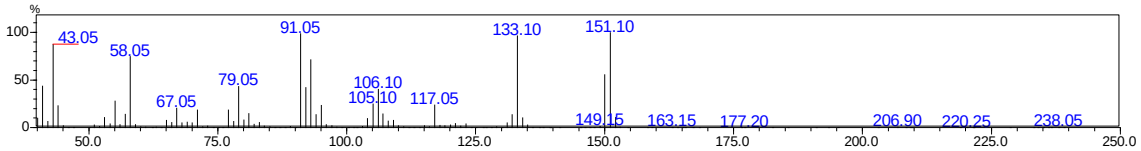

MS analysis of a minor product from 1-adamantyl isobutyrate turnover (m^+/z = 238.05) RT 10.6 min

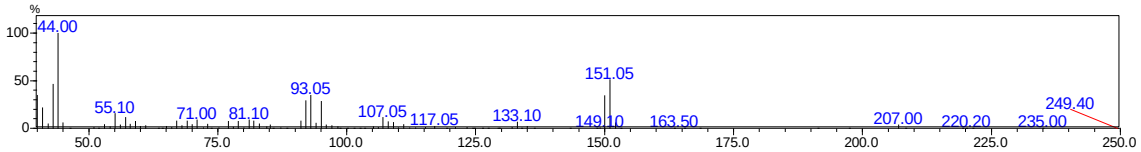

MS analysis of 2-adamantyl acetate

MS analysis of 5-hydroxy-2-adamantyl acetate (m^+/z = 210.1) RT 9.4 min

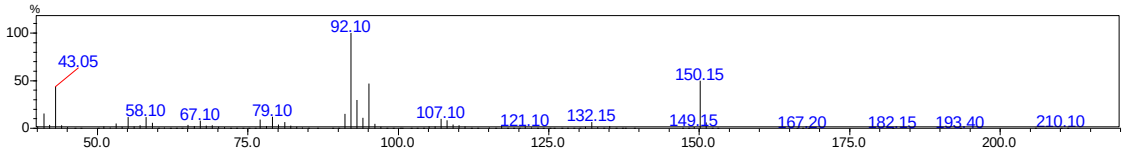

MS analysis of a minor product from 2-adamantyl acetate turnover RT 10.1 min (m^+/z = 210.20)

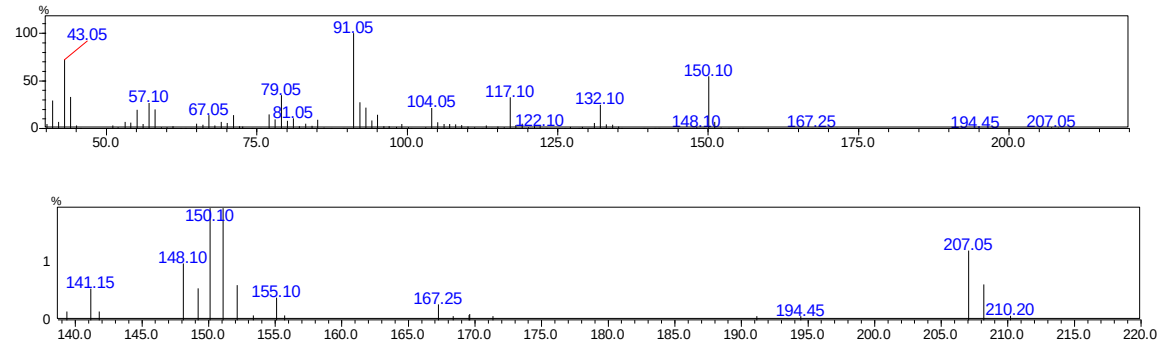

Zoomed in version

MS analysis of 2-adamantyl isobutyrate

MS analysis of 5-hydroxy-2-adamantyl isobutyrate (m^+/z = 238.10) RT 11.1 min.

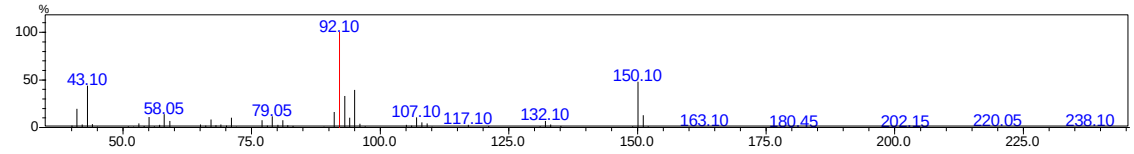

MS analysis of minor product from 2-adamantyl isobutyrate (m^+/z = 238.25) RT 11.4 min

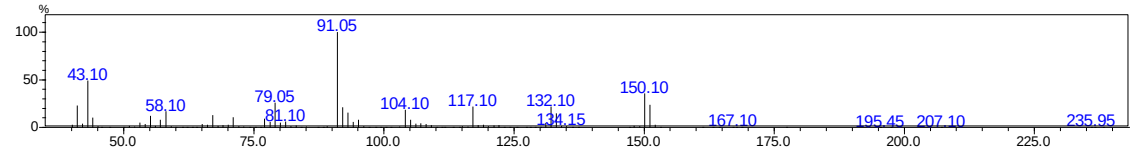

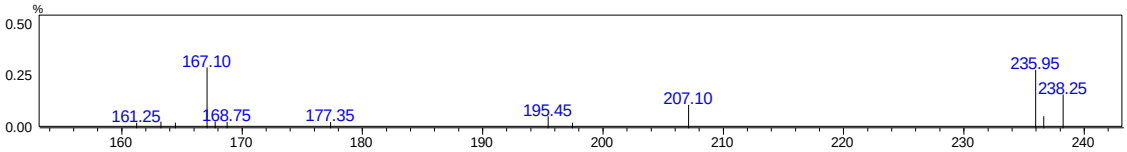

Zoomed in

MS analysis of N-(1-adamantyl)acetamide

MS analysis of 3-hydroxy-N-(1-adamantyl)acetamide (m^+/z = 209.1) RT 11.8 min.

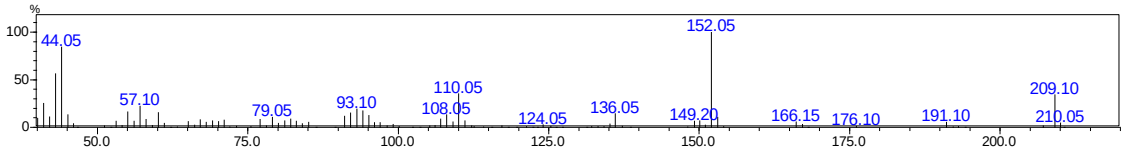

MS analysis of 4-hydroxy-N-(1-adamantyl)acetamide (m^+/z = 209.1) RT 12.8 min.

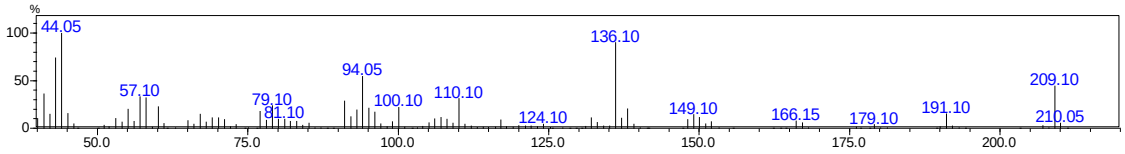

NMR Analysis

Data for *trans*-4-hydroxy-1-adamantylmethyl ketone (~31 mg) [182]:

^{1}H NMR (500 MHz, $CDCl_3$) δ 3.88-3.84 (m, 1H, H4), 2.14-2.06 (m, 5H, H6, H8 & 3xH12), 2.02-1.95 (m, 3H, H3, H5 & H7), 1.90-1.83 (m, 2H, H2 & H10), 1.82-1.75 (m, 4H, H2, 2xH9 & H10), 1.45 (d, J = 12.6 Hz, 2H, H6 & H8).

^{13}C NMR (126 MHz, $CDCl_3$) δ 216.17 (C11), 76.15 (C4), 48.34 (C1), 40.94 (C9), 39.93 (C2 & C10), 36.68 (C3 & C5), 32.62 (C6 & C8), 29.86 (C7), 27.18 (C12).

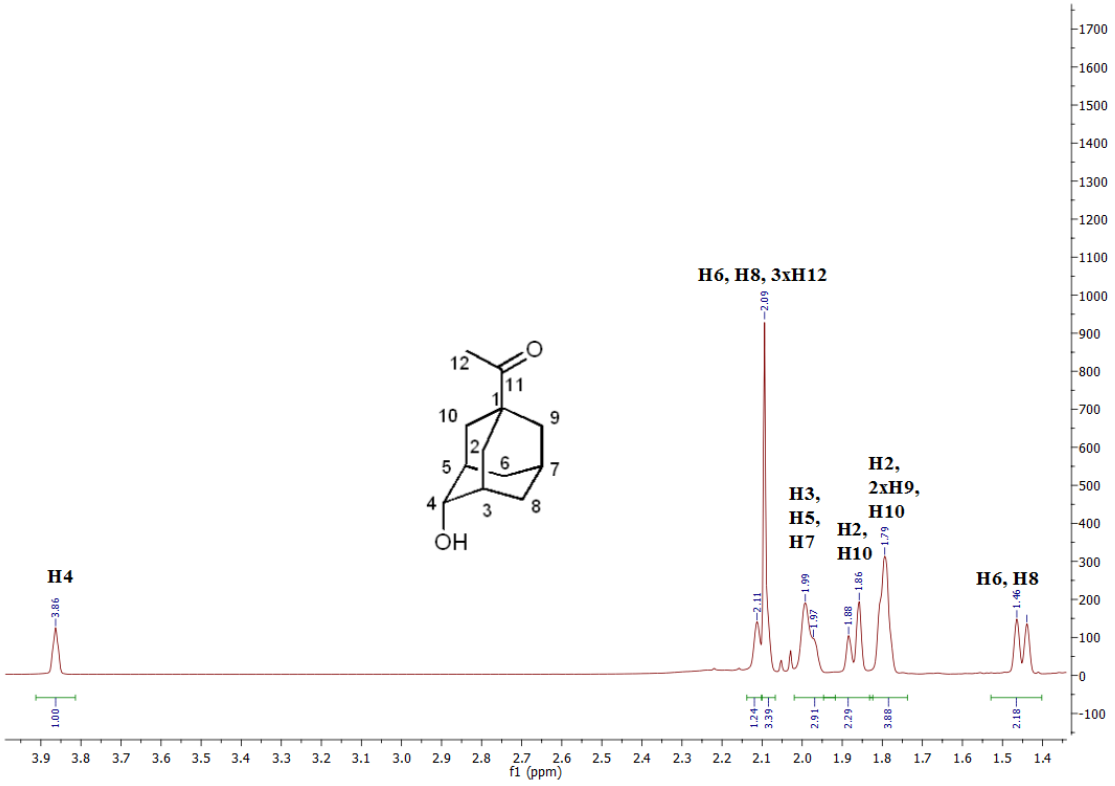

Figure C. 2 ^{1}H NMR spectrum of *trans*-4-hydroxy-1-adamantylmethyl ketone.

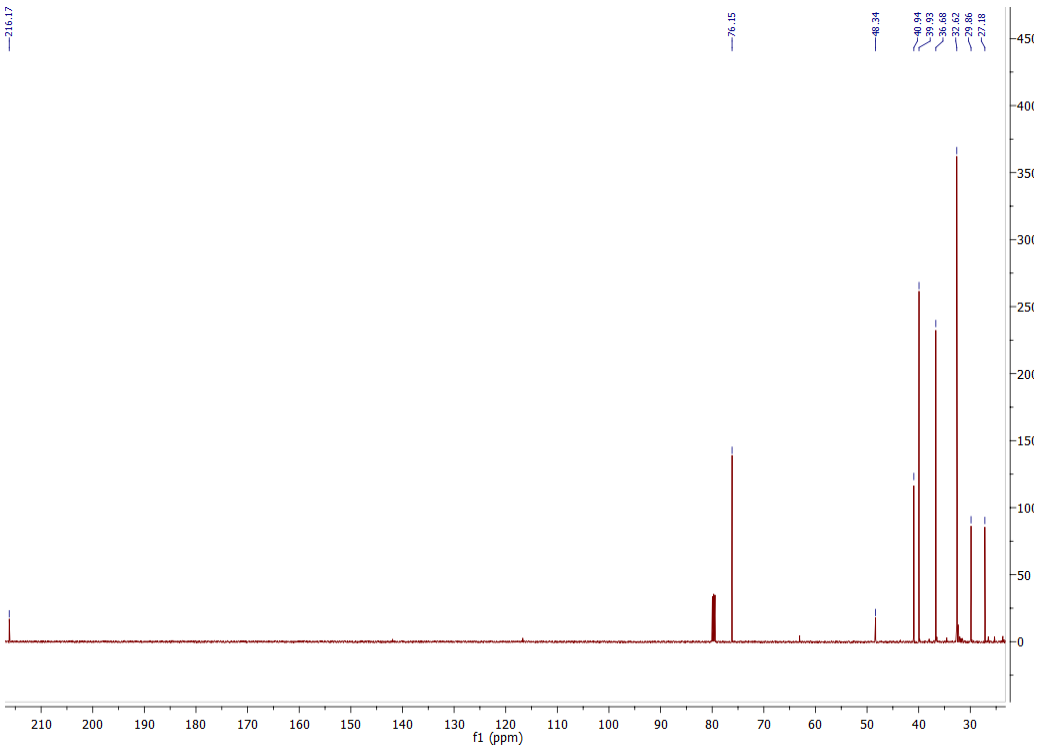

Figure C. 3 ^{13}C NMR spectrum of *trans*-4-hydroxy-1-adamantylmethyl ketone.

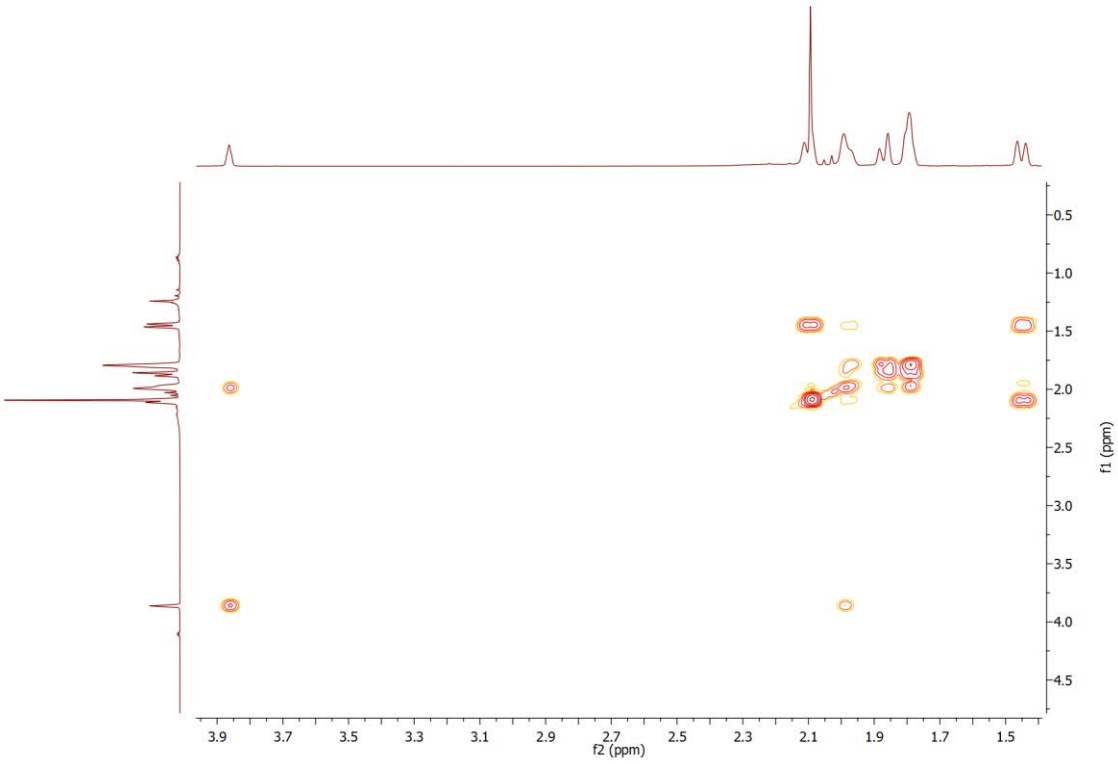

Figure C. 4 gCOSY NMR spectrum of *trans*-4-hydroxy-1-adamantylmethyl ketone.

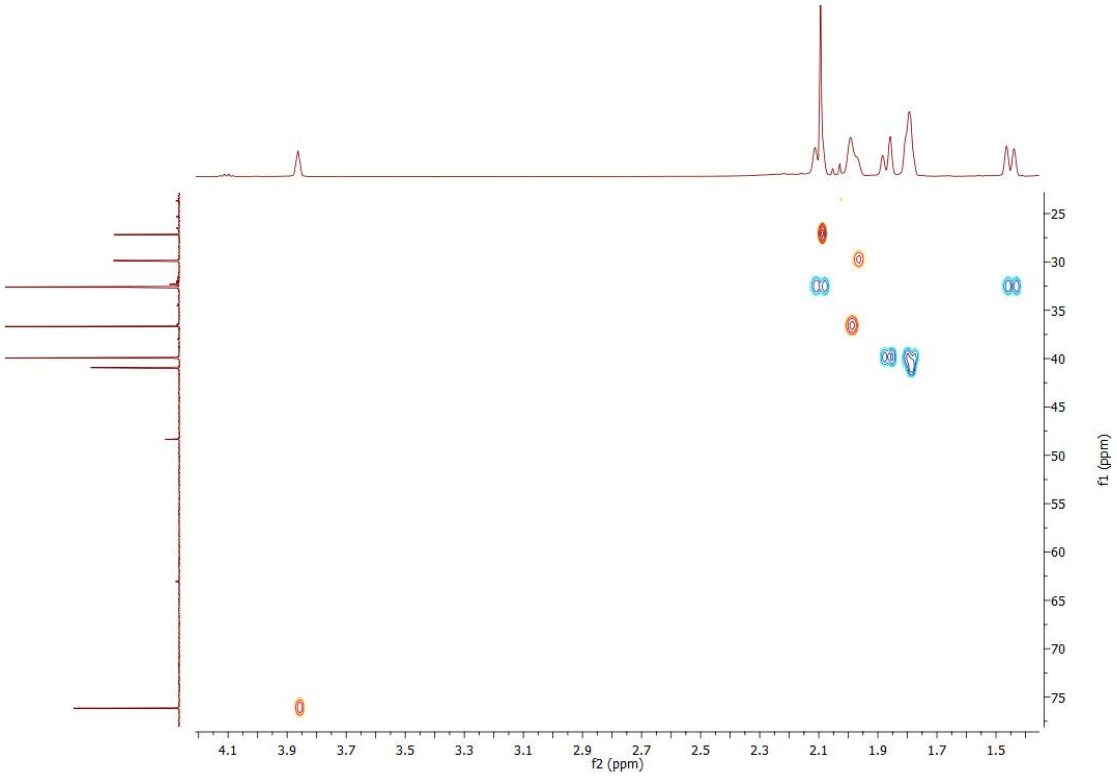

Figure C. 5 HSQC NMR spectrum of *trans*-4-hydroxy-1-adamantylmethyl ketone.

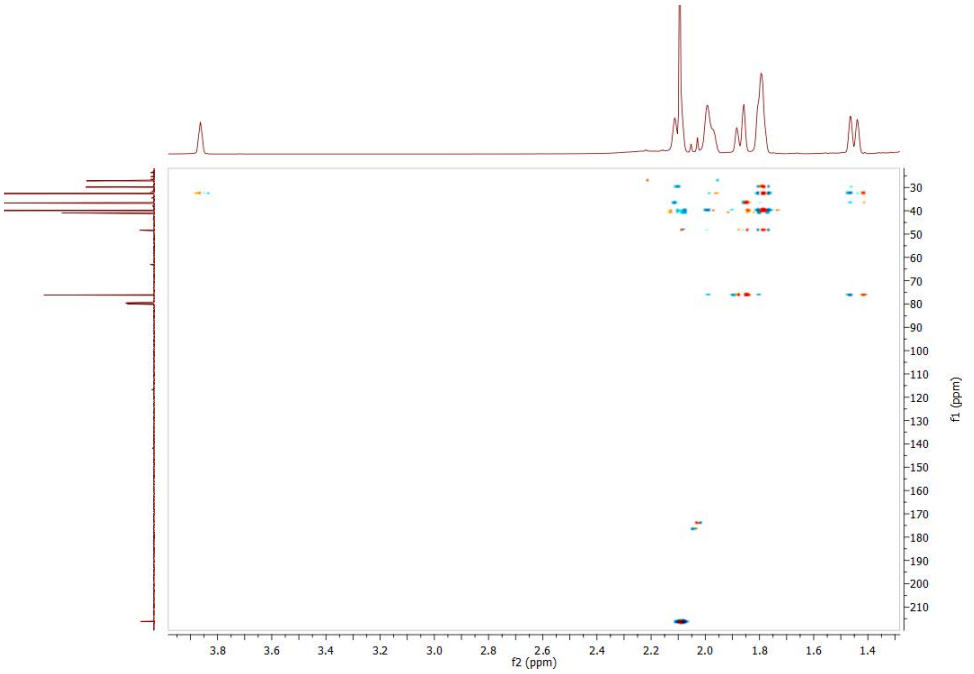

(a)

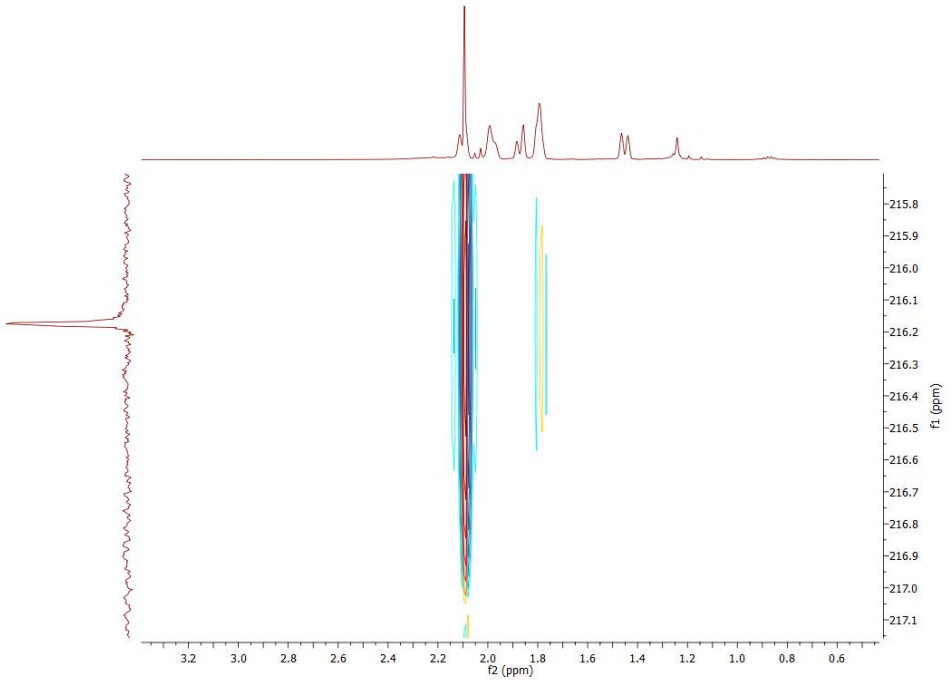

(b)

Figure C. 6 (a) HMBC NMR spectrum of *trans*-4-hydroxy-1-adamantylmethyl ketone. **(b)** Zoomed in C=O region to highlight the interactions of C11 with H2, H9 and H10.

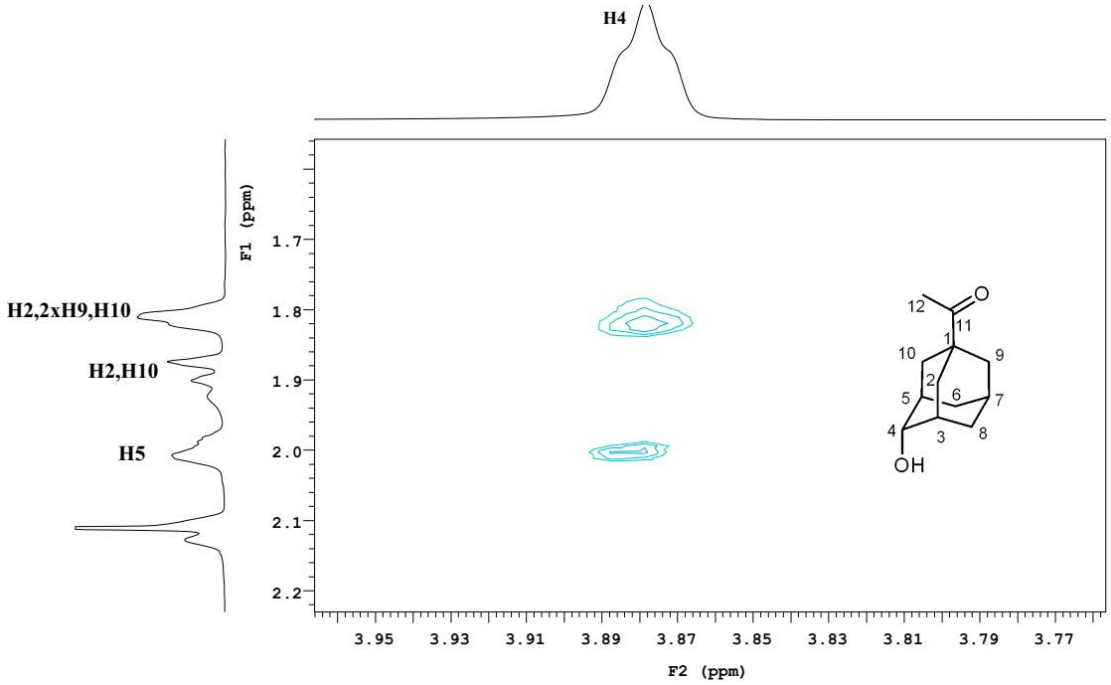

Figure C. 7 Zoomed in ROESY NMR spectrum of *trans*-4-hydroxy-1-adamantylmethyl ketone to highlight the interactions of H4 with H2, H5 and H10.

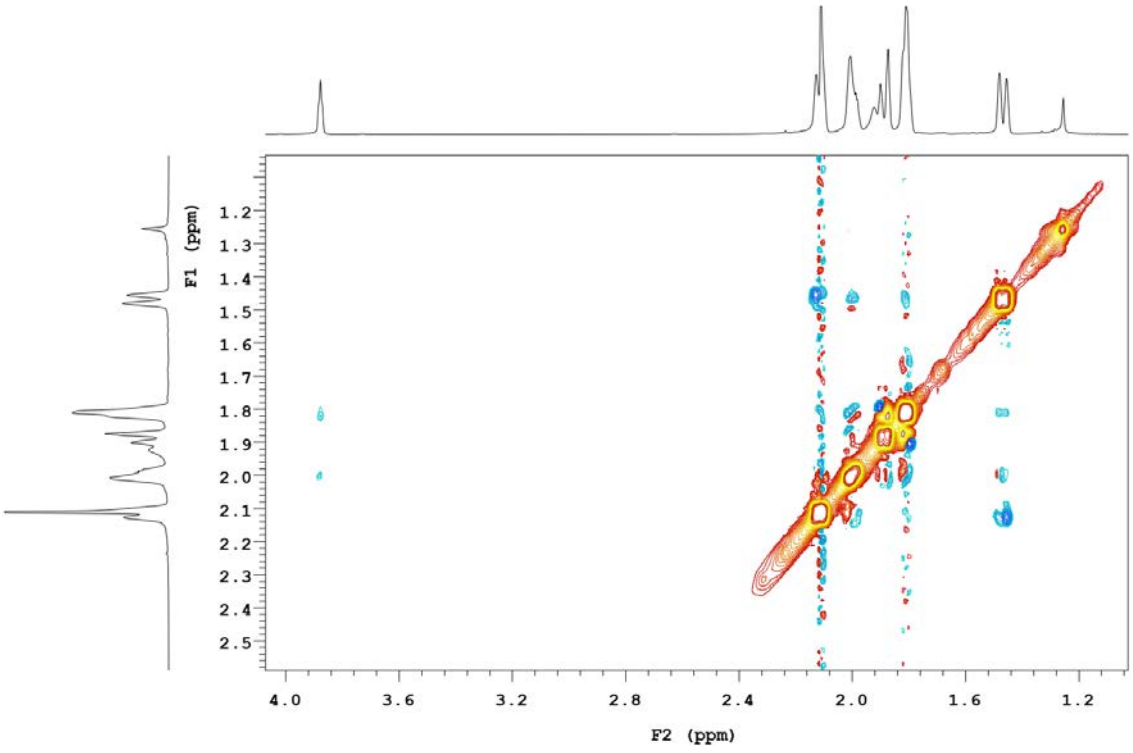

Figure C. 8 ROESY NMR spectrum of *trans*-4-hydroxy-1-adamantylmethyl ketone.

Data for 3-hydroxy-1-adamantylmethyl ketone (~20 mg) [182]:

^{1}H NMR (500 MHz, $CDCl_3$) δ 2.34-2.27 (m, 2H, H5 & H7), 2.12 (s, 3H, 3xH12), 1.78-1.74 (m, 2H, 2xH2), 1.73-1.67 (m, 8H, 2xH4, 2xH8, 2xH9 & 2xH10), 1.63-1.59 (m, 2H, 2xH6).

^{13}C NMR (126 MHz, $CDCl_3$) δ 214.87 (C11), 71.21 (C3), 52.65 (C1), 48.42 (C2), 47.03 (C4 & C8), 39.76 (C9 & C10), 37.70 (C6), 32.92 (C5 & C7), 27.22 (C12).

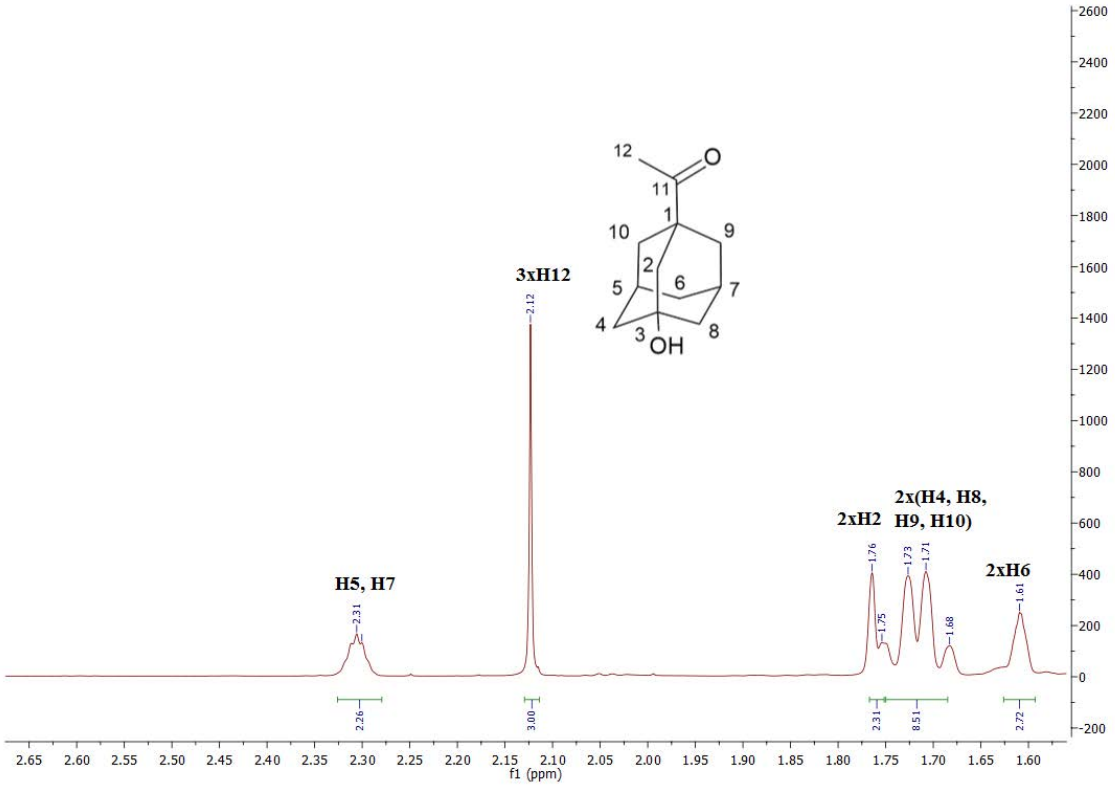

Figure C. 9 ^{1}H NMR spectrum of 3-hydroxy-1-adamantylmethyl ketone.

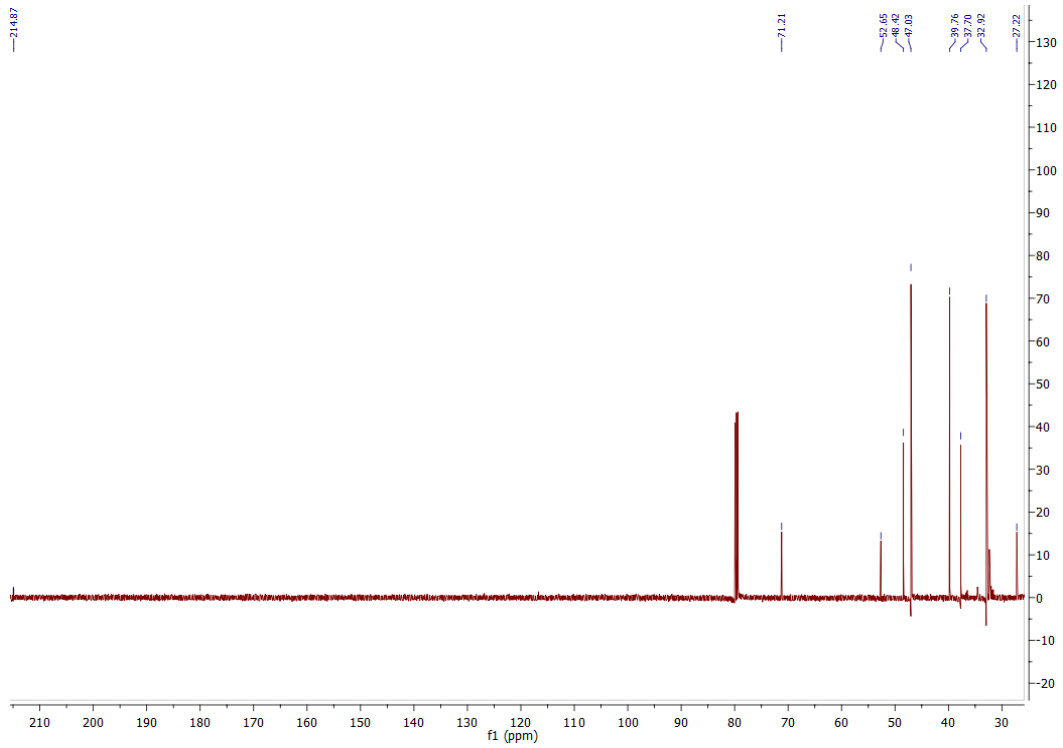

Figure C. 10 ^{13}CNMR spectrum of 3-hydroxy-1-adamantylmethyl ketone.

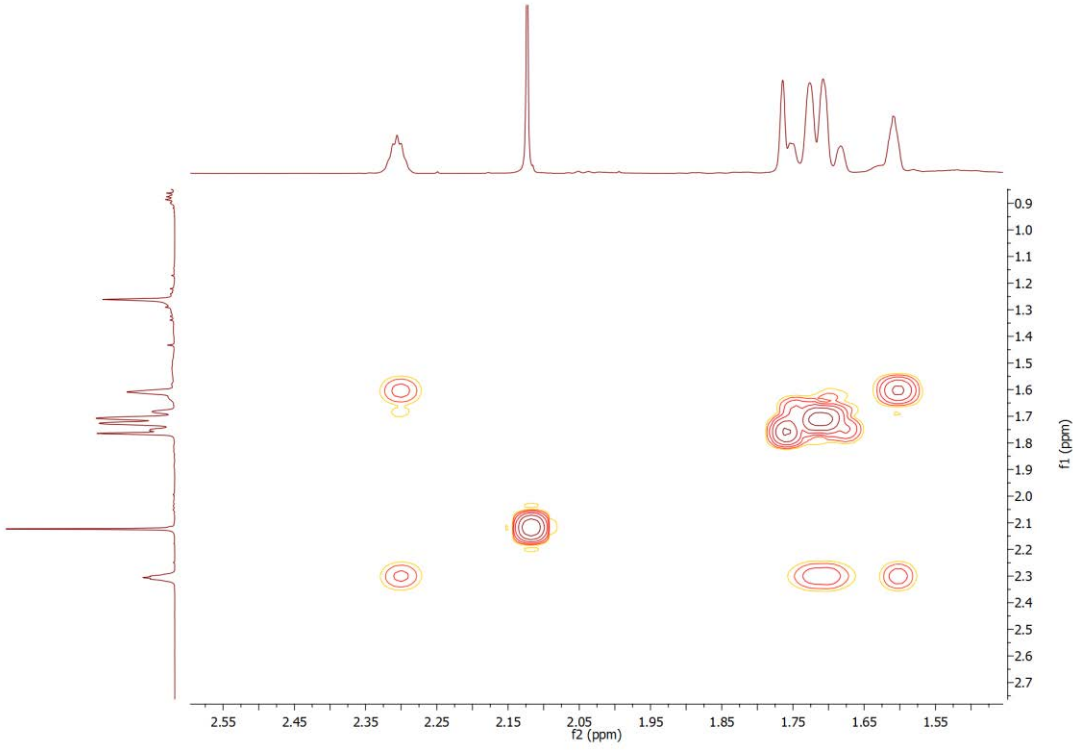

Figure C. 11 gCOSY NMR spectrum of 3-hydroxy-1-adamantylmethyl ketone.

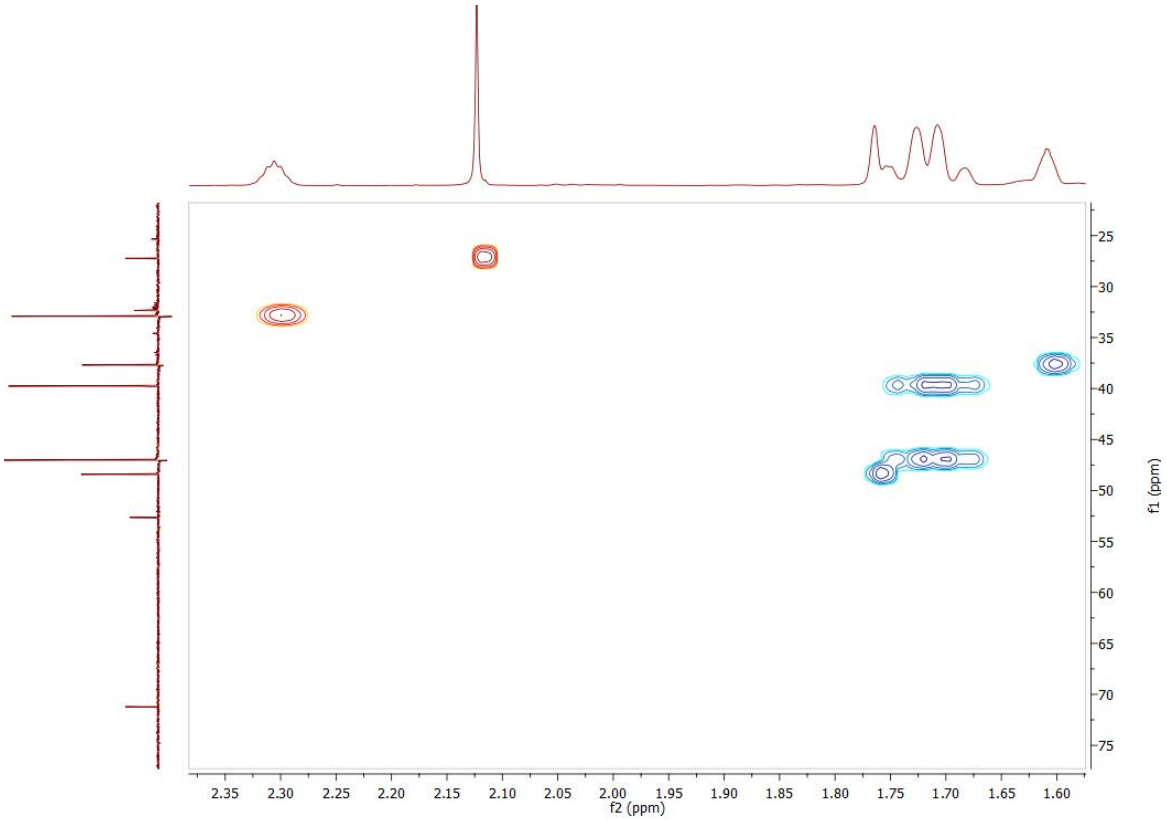

Figure C. 12 HSQC NMR spectrum of 3-hydroxy-1-adamantylmethyl ketone.

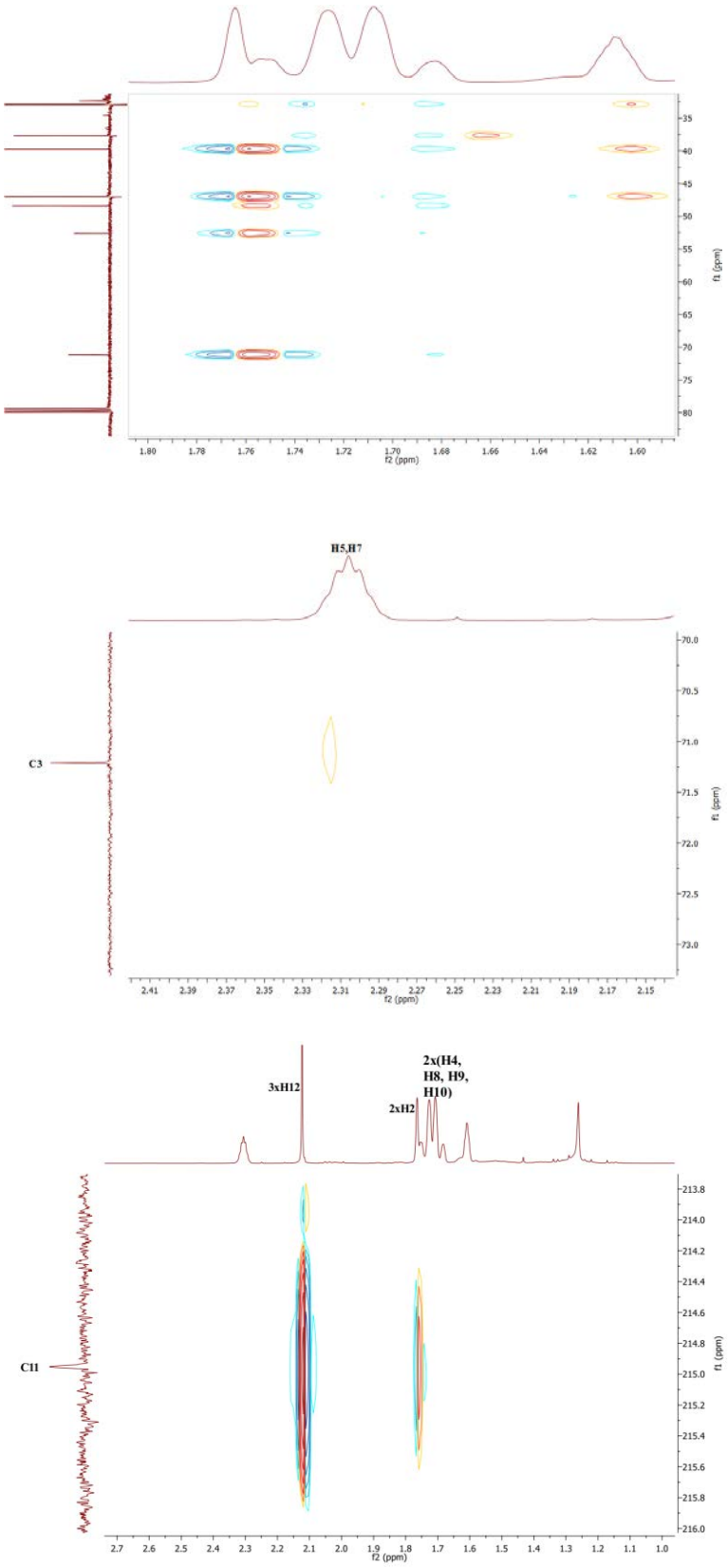

Figure C. 13 Zoomed in HMBC NMR spectrum of 3-hydroxy-1-adamantylmethyl ketone to highlight the interactions of carbons (35-80 ppm, 70-73 ppm, 213-217 ppm) with protons.

Data for methyl-2-(*trans*-4-hydroxy-1-adamantyl) acetate (~25 mg):

^{1}H NMR (500 MHz, $CDCl_3$) δ 3.88-3.83 (m,1H, H4), 3.65 (s, 3H, 3xH13), 2.10 (s, 2H, 2xH11), 2.08-2.04 (m, 2H, H6 & H8), 1.96-1.88 (m, 3H, H3, H5 & H7), 1.72-1.66 (m, 2H, H2 & H10), 1.65-1.59 (m, 4H, H2, 2xH9 & H10), 1.43 (d, J = 11.9 Hz, 2H, H6 & H8);

^{13}C NMR (126 MHz, $CDCl_3$) δ 174.75 (C12), 76.63 (C4), 53.80 (C13), 50.35 (C11), 44.91 (C9), 43.73 (C2 & C10), 37.27 (C3 & C5), 34.60 (C1), 32.77 (C6 & C8), 30.47 (C7).

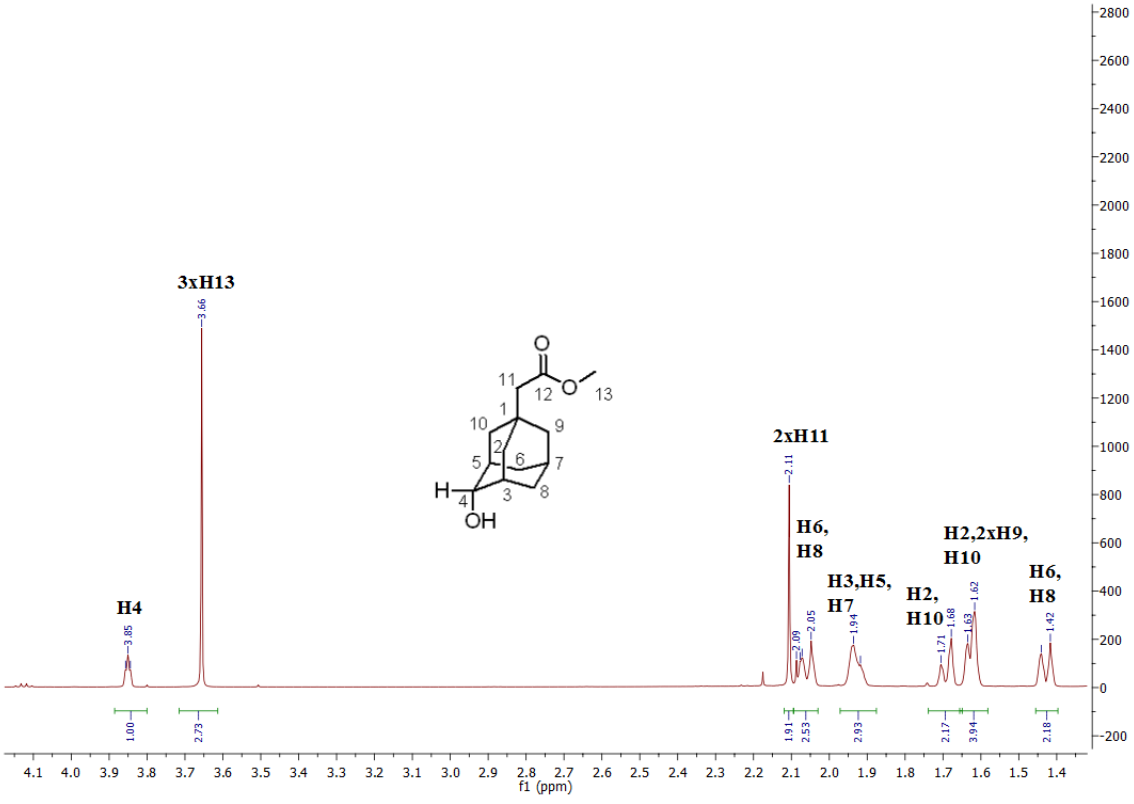

Figure C. 14 ^{1}H NMR spectrum of methyl-2-(*trans*-4-hydroxy-1-adamantyl) acetate.

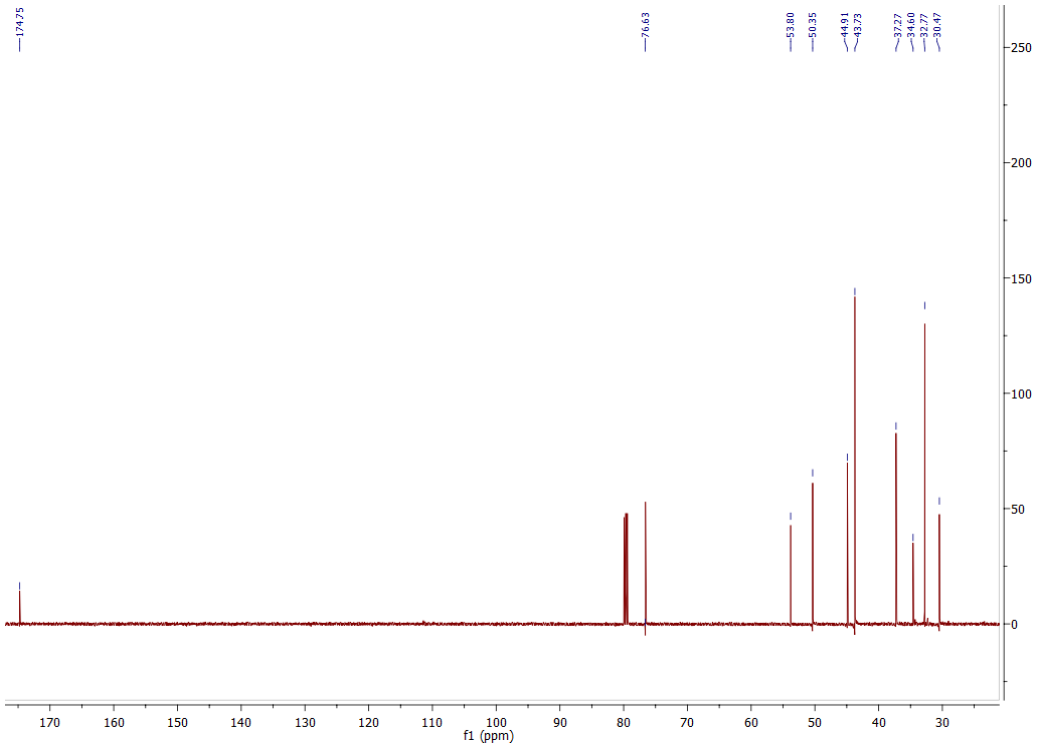

Figure C. 15 ^{13}C NMR spectrum of methyl-2-(*trans*-4-hydroxy-1-adamantyl) acetate.

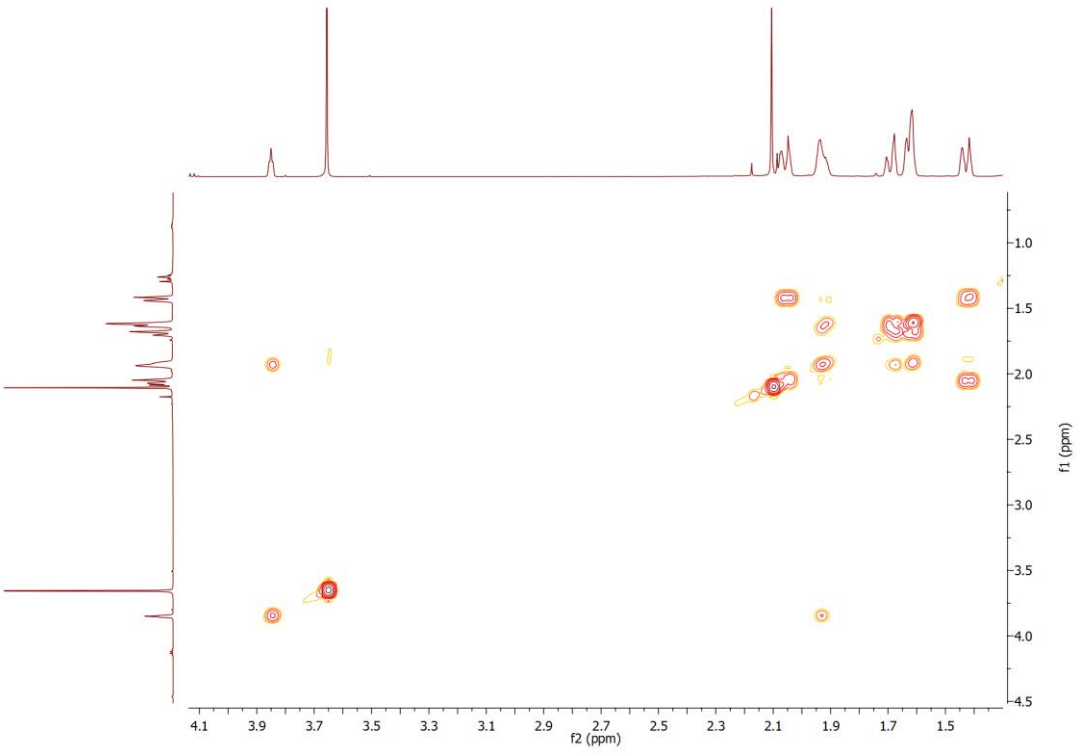

Figure C. 16 gCOSY NMR spectrum of methyl-2-(*trans*-4-hydroxy-1-adamantyl) acetate.

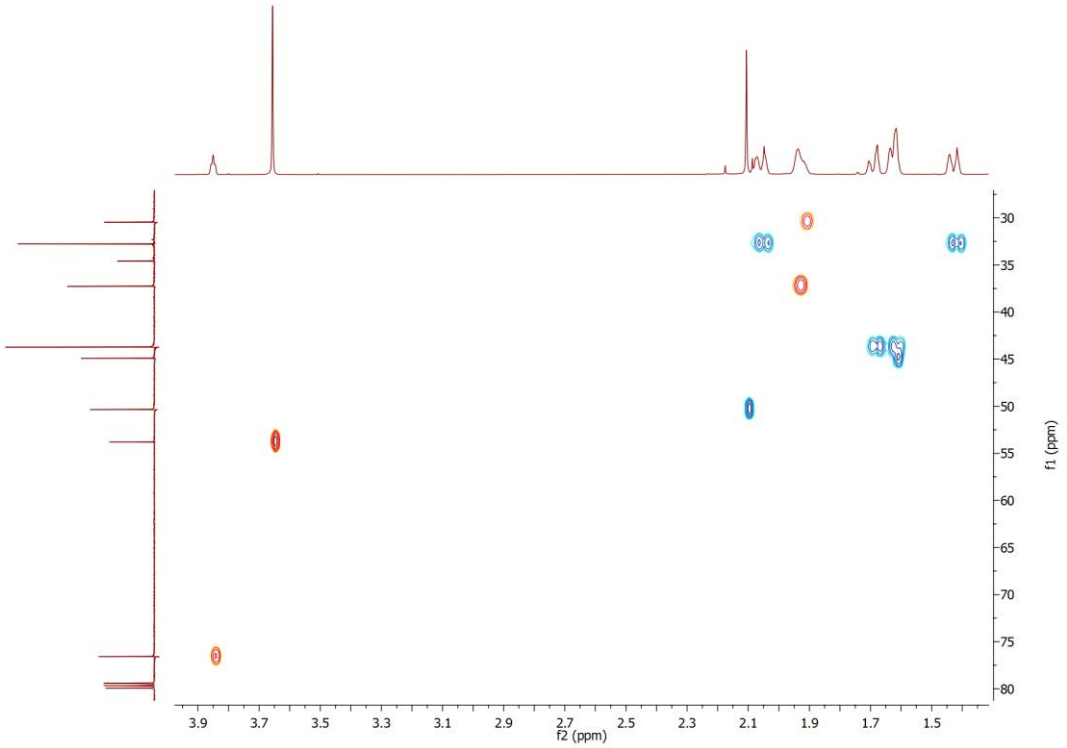

Figure C. 17 HSQC NMR spectrum of methyl-2-(*trans*-4-hydroxy-1-adamantyl) acetate.

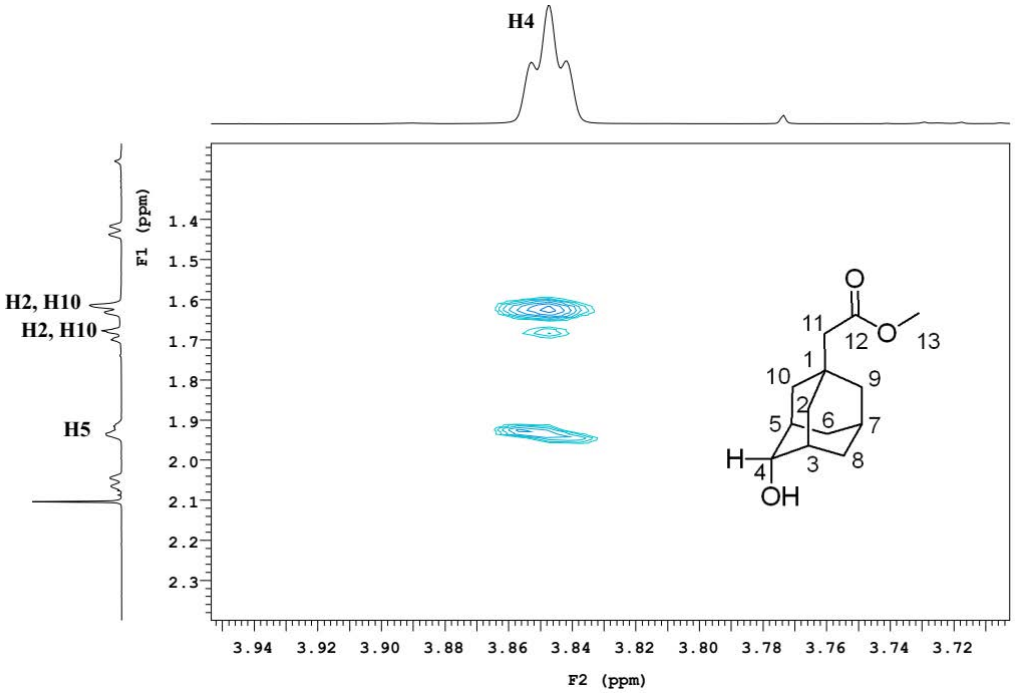

Figure C. 18 Zoomed in ROESY NMR spectrum of methyl-2-(*trans*-4-hydroxy-1-adamantyl) acetate highlighting the interactions of H4 with H2, H5 and H10.

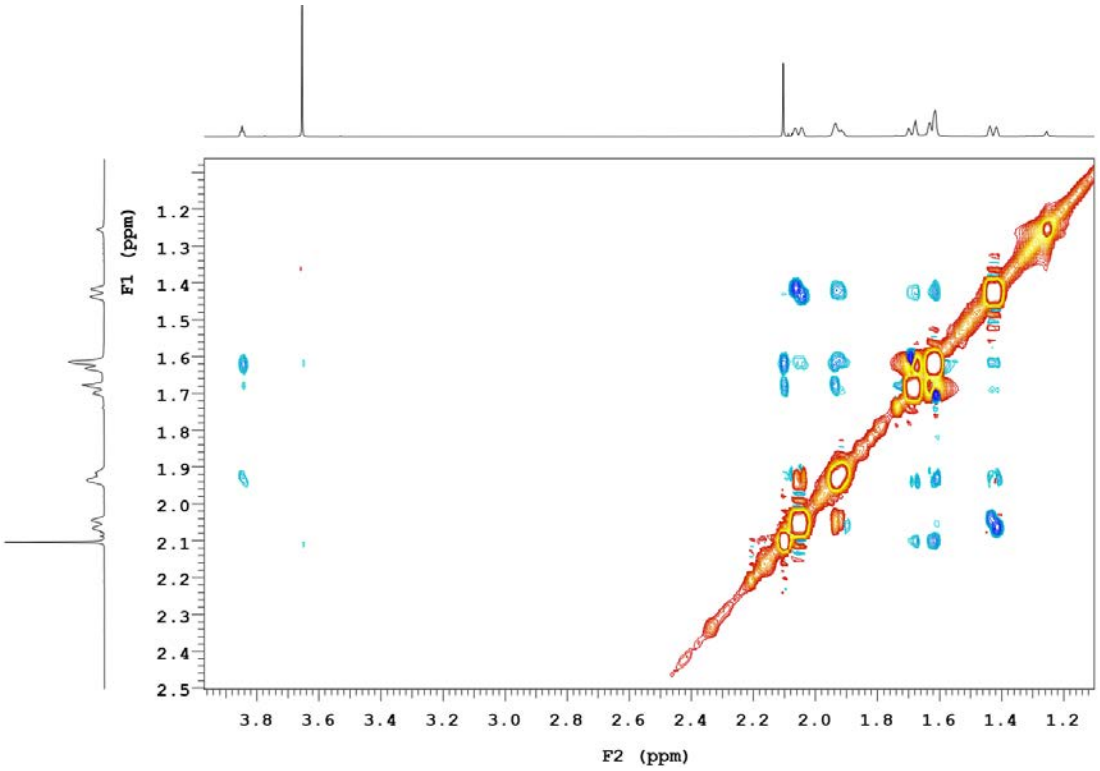

Figure C. 19 ROESY NMR spectrum of methyl-2-(*trans*-4-hydroxy-1-adamantyl) acetate.

Data for methyl-2-(3-hydroxy-1-adamantyl) acetate (~5 mg):

^{1}H NMR (500 MHz, $CDCl_3$) δ 3.65 (s, 3H, 3xH13), 2.24-2.19 (m, 2H, H5, H7), 2.17 (s, 2H, 2xH11), 1.71-1.61 (m, 4H, 2xH4 & 2xH8), 1.56-1.50 (m, 8H, 2xH2, 2xH6, 2xH9 & 2xH10).

^{13}C NMR (126 MHz, $CDCl_3$) δ 174.90 (C12), 71.34 (C3), 53.85 (C13), 52.53 (C2), 50.29 (C11), 47.09 (C4 & C8), 43.60 (C9 & C10), 38.60 (C1), 37.82 (C6), 33.24 (C5 & C7).

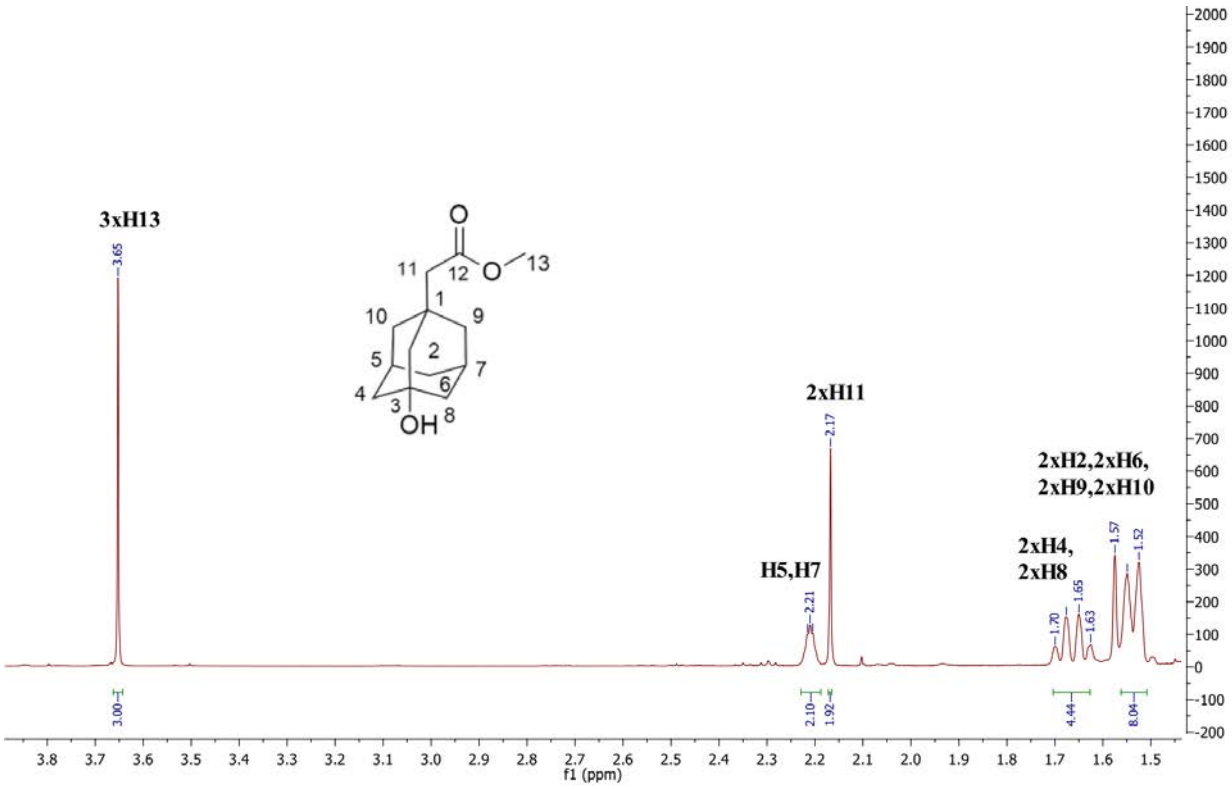

Figure C. 20 ^{1}H NMR spectrum of methyl-2-(3-hydroxy-1-adamantyl) acetate.

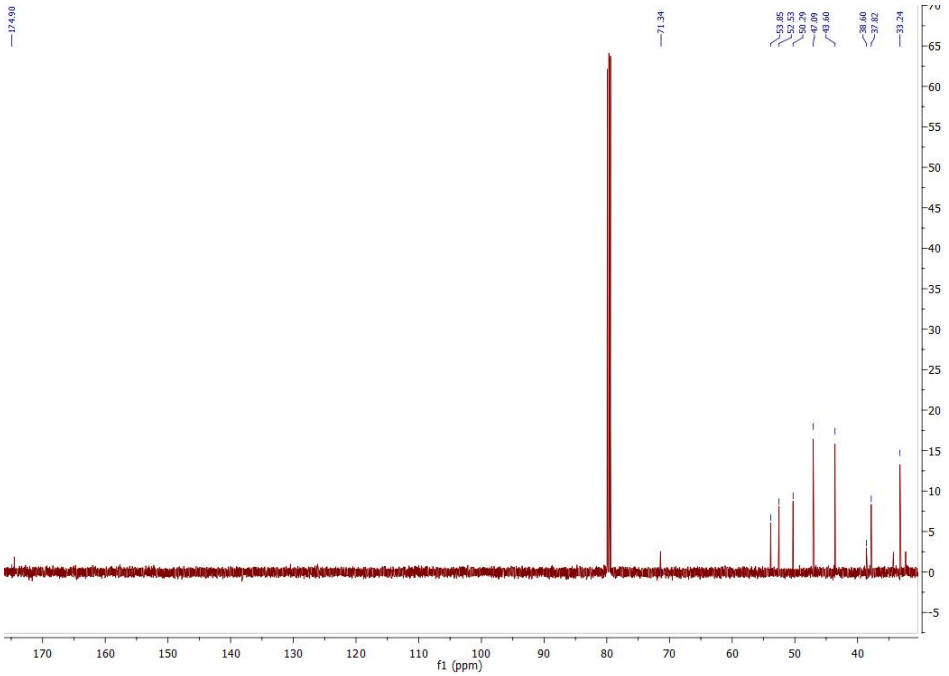

Figure C. 21 ^{13}C NMR spectrum of methyl-2-(3-hydroxy-1-adamantyl) acetate. The product was confirmed 3-hydroxy as the carbon signals at 47.09 (C4 & C8), 43.60 (C9 & C10), 33.24 (C5 & C7) displayed double the intensity than other peaks, suggesting the hydroxylation at symmetrical C3.

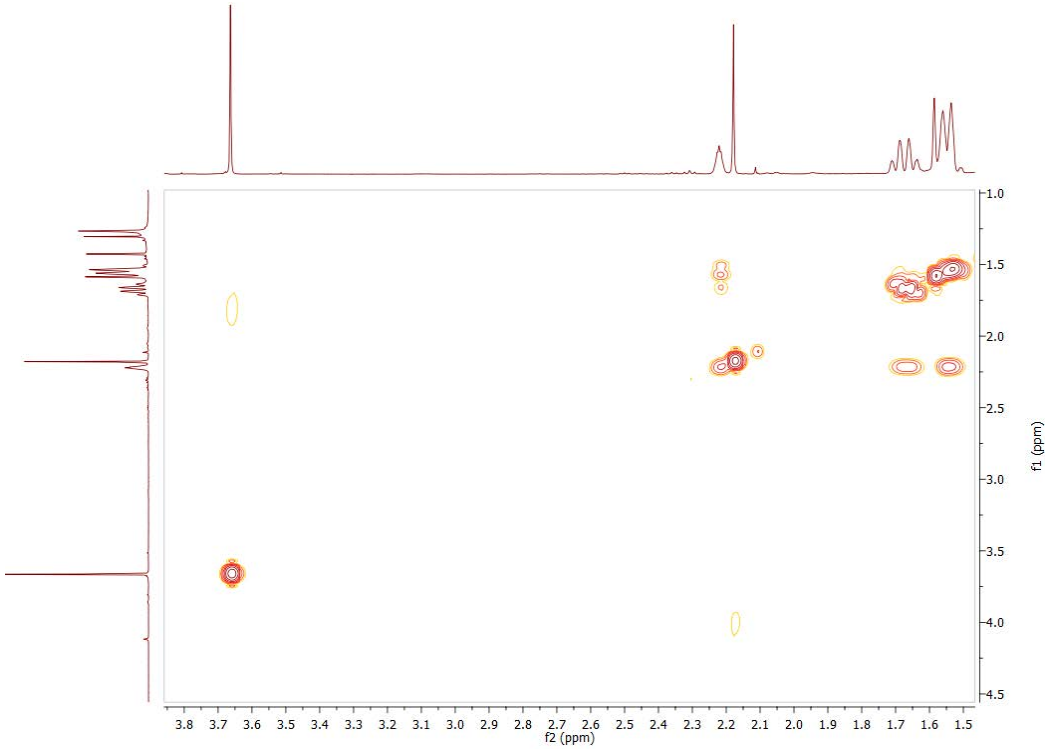

Figure C. 22 gCOSY NMR spectrum of methyl-2-(3-hydroxy-1-adamantyl) acetate.

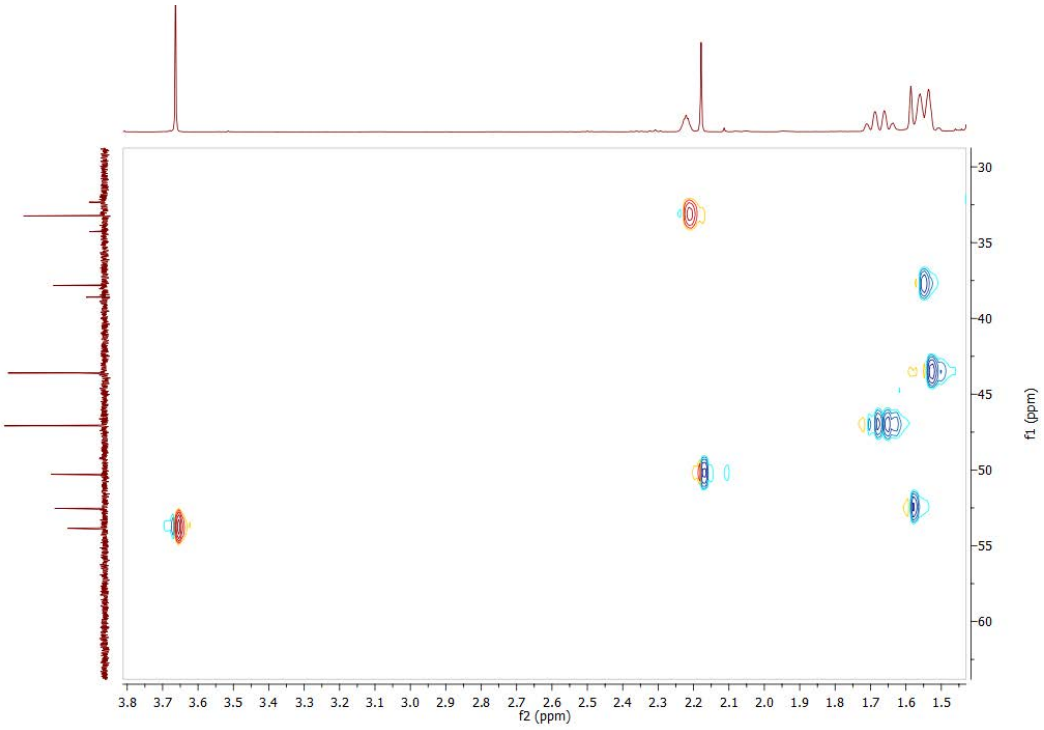

Figure C. 23 HSQC NMR spectrum of methyl-2-(3-hydroxy-1-adamantyl) acetate.

Data for *trans*-4-hydroxy-1-adamantyl acetate (~26 mg) [182]:

^{1}H NMR (500 MHz, $CDCl_3$) δ 3.96-3.92 (m, 1H, H4), 2.16-2.09 (m, 7H, 2xH2, H7, 2xH9 & 2xH10), 2.09-2.01 (m, 4H, H3, H5, H6 & H8), 1.96 (s, 3H, 3xH12),1.45 (d, J = 12.1 Hz, 2H, H6 & H8).

^{13}C NMR (126 MHz, $CDCl_3$) δ 173.0 (C11), 81.76 (C1), 75.74 (C4), 43.93 (C9), 42.21 (C2 & C10), 38.93 (C3 & C5), 32.60 (C7), 32.34 (C6 & C8), 25.25 (C12).

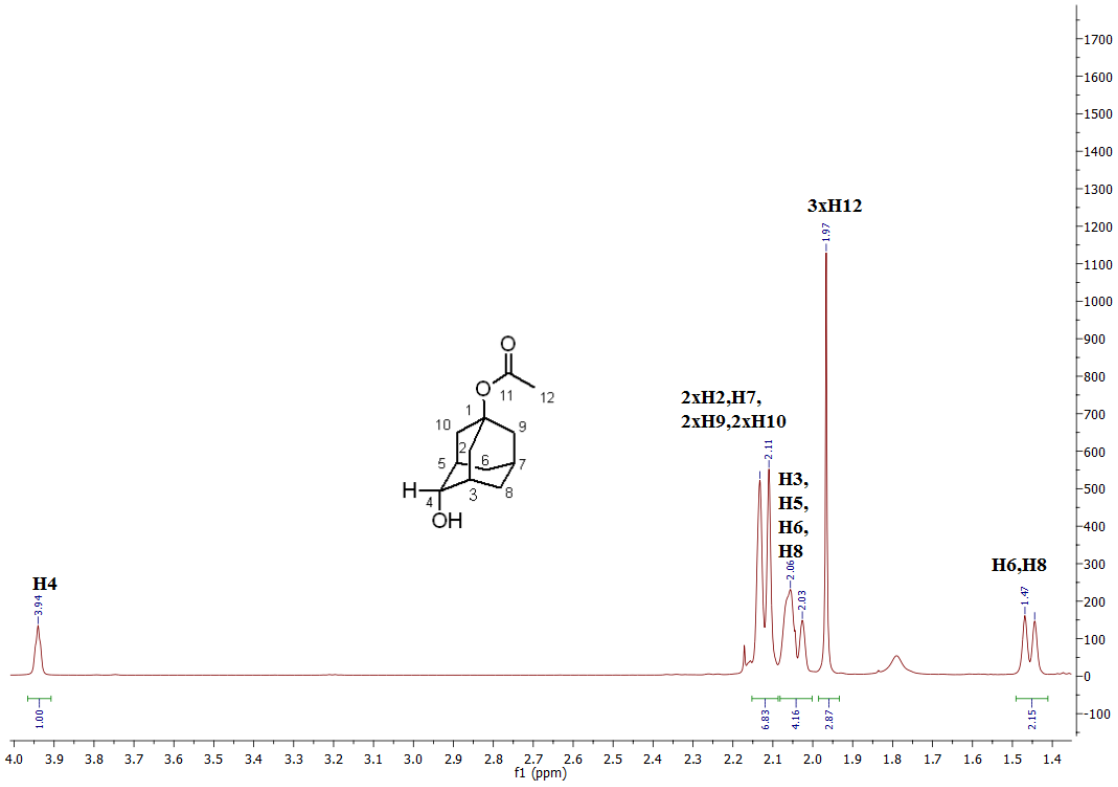

Figure C. 24 ^{1}H NMR spectrum of *trans*-4-hydroxy-1-adamantyl acetate.

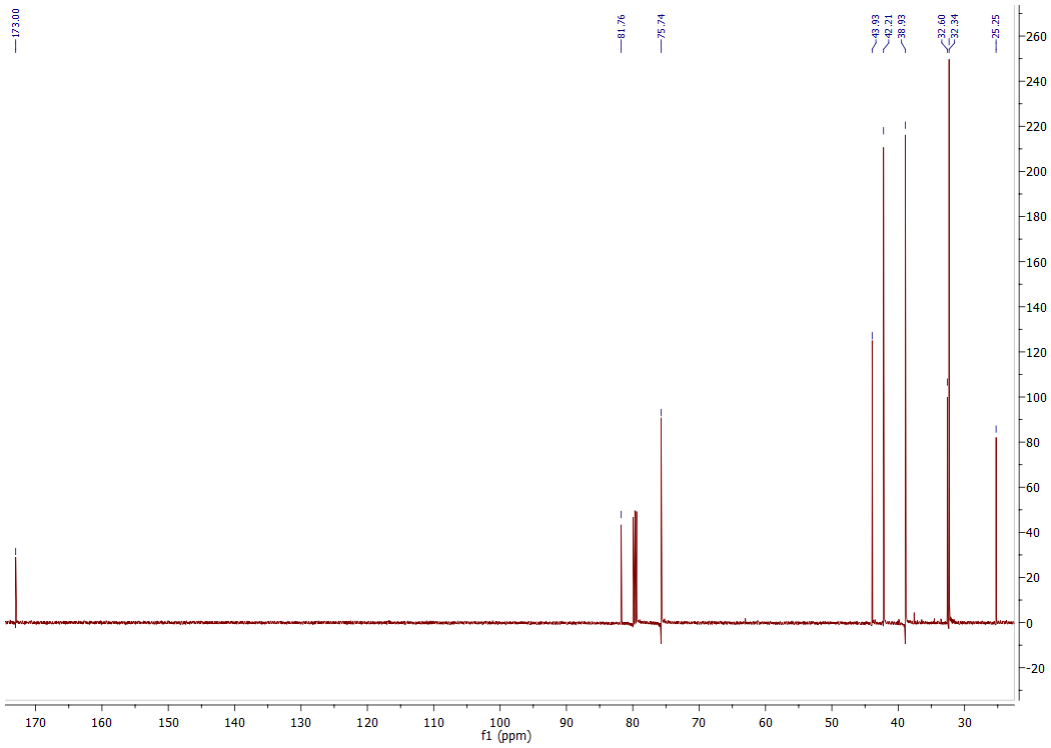

Figure C. 25 ^{13}C NMR spectrum of *trans*-4-hydroxy-1-adamantyl acetate.

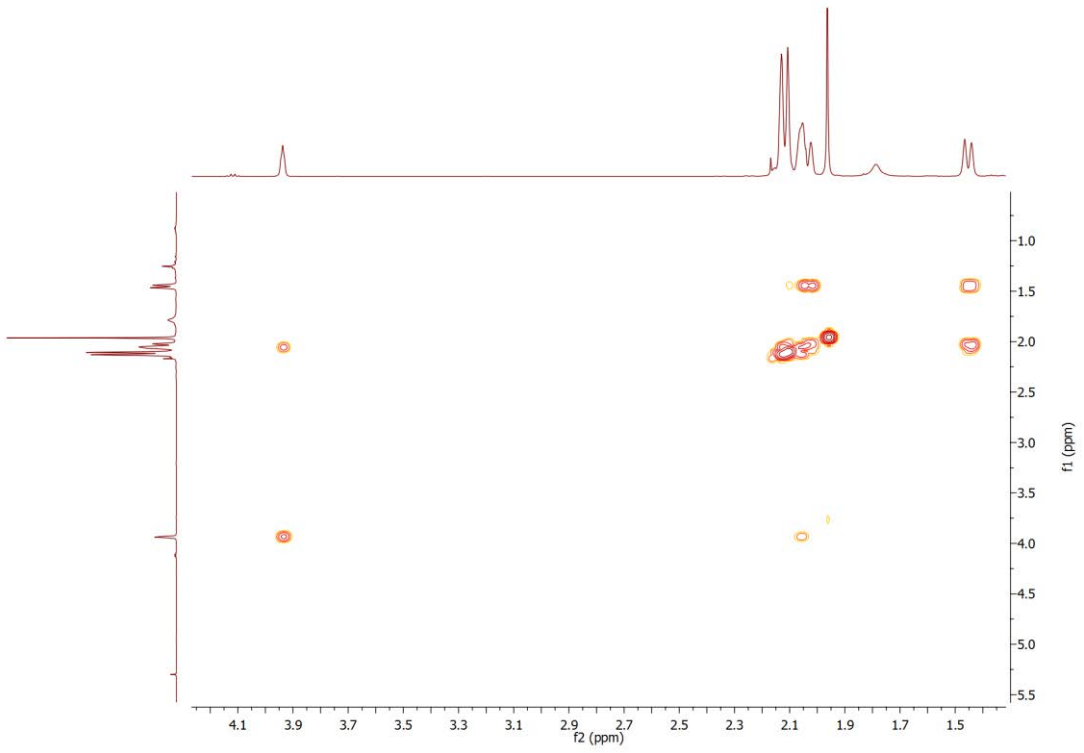

Figure C. 26 gCOSY spectrum NMR of *trans*-4-hydroxy-1-adamantyl acetate.

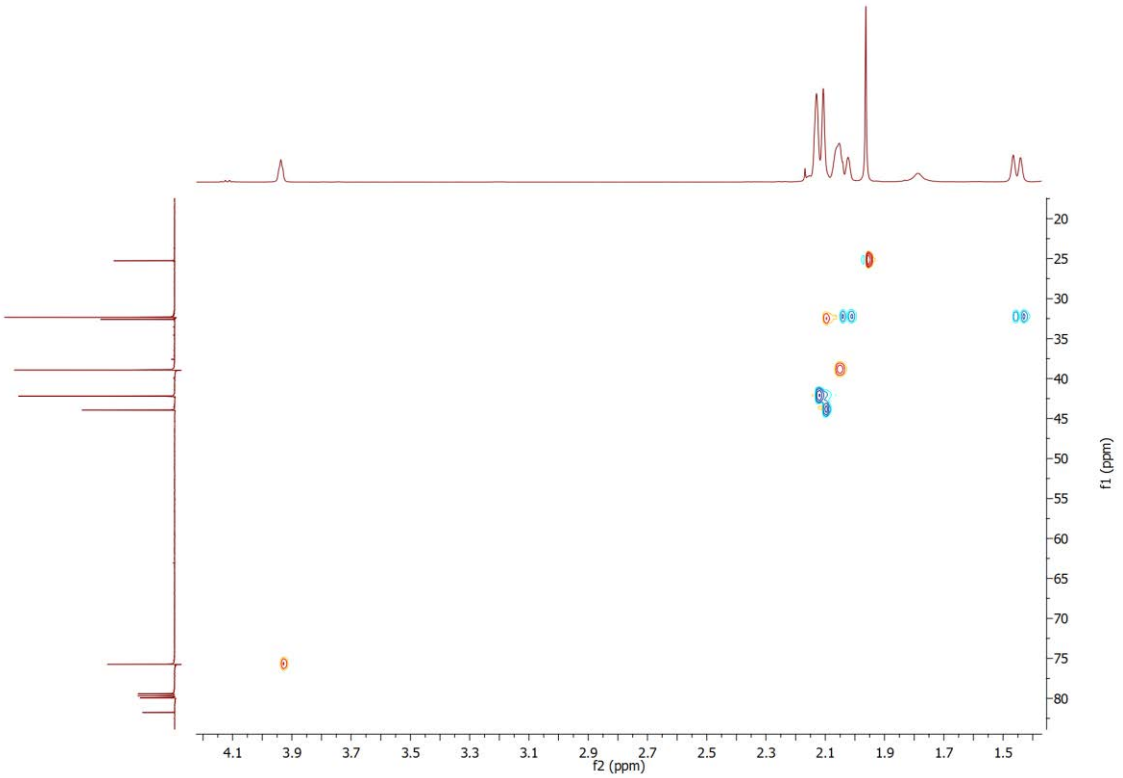

Figure C. 27 HSQC of NMR spectrum of *trans*-4-hydroxy-1-adamantyl acetate.

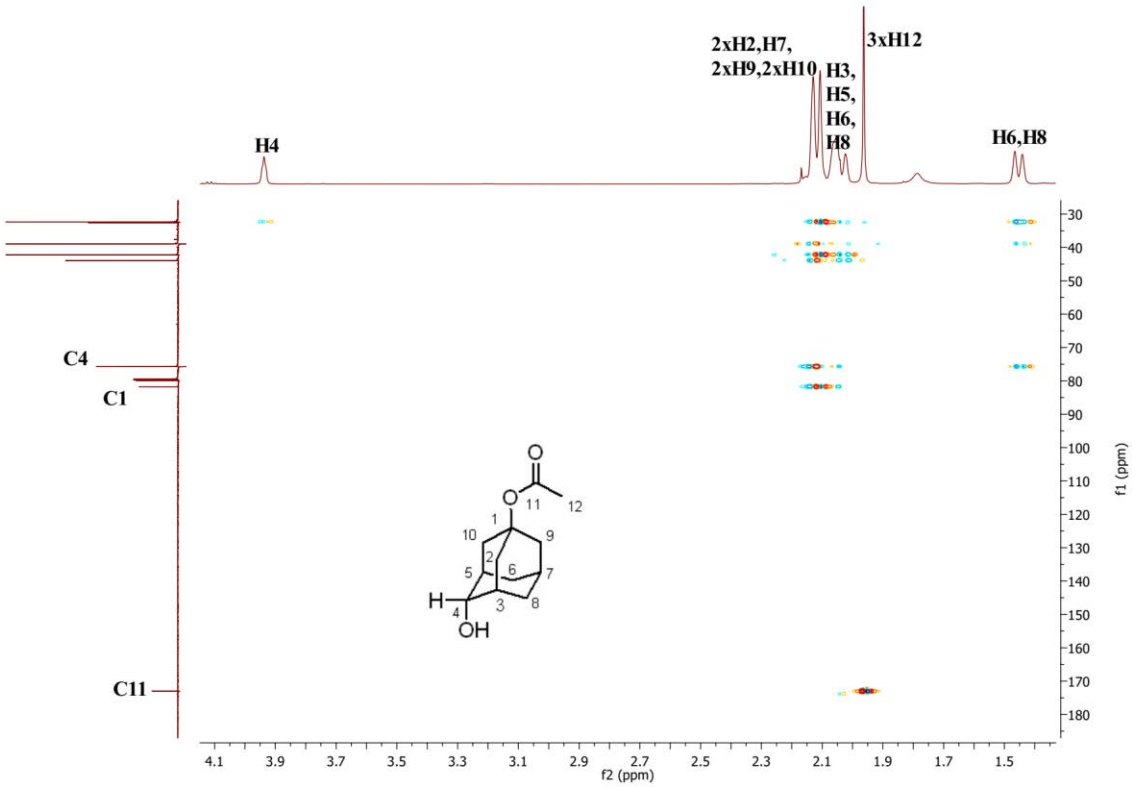

Figure C. 28 HMBC NMR spectrum of *trans*-4-hydroxy-1-adamantyl acetate.

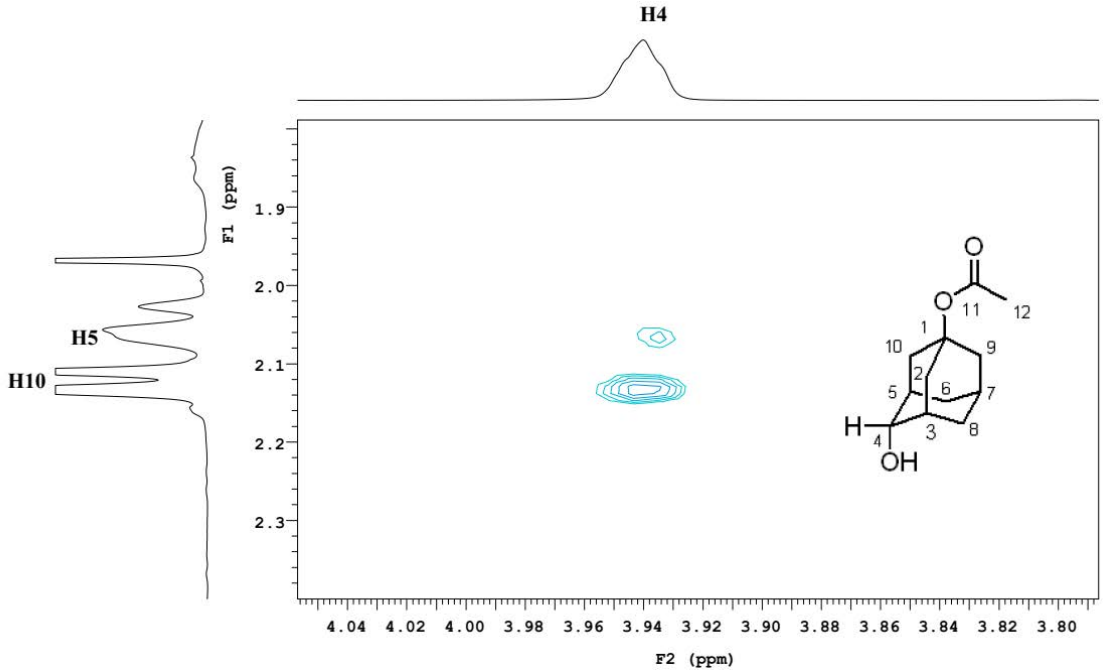

Figure C. 29 Zoomed in ROESY NMR spectrum of *trans*-4-hydroxy-1-adamantyl acetate highlighting the interactions of the H4 with H5 and H10.

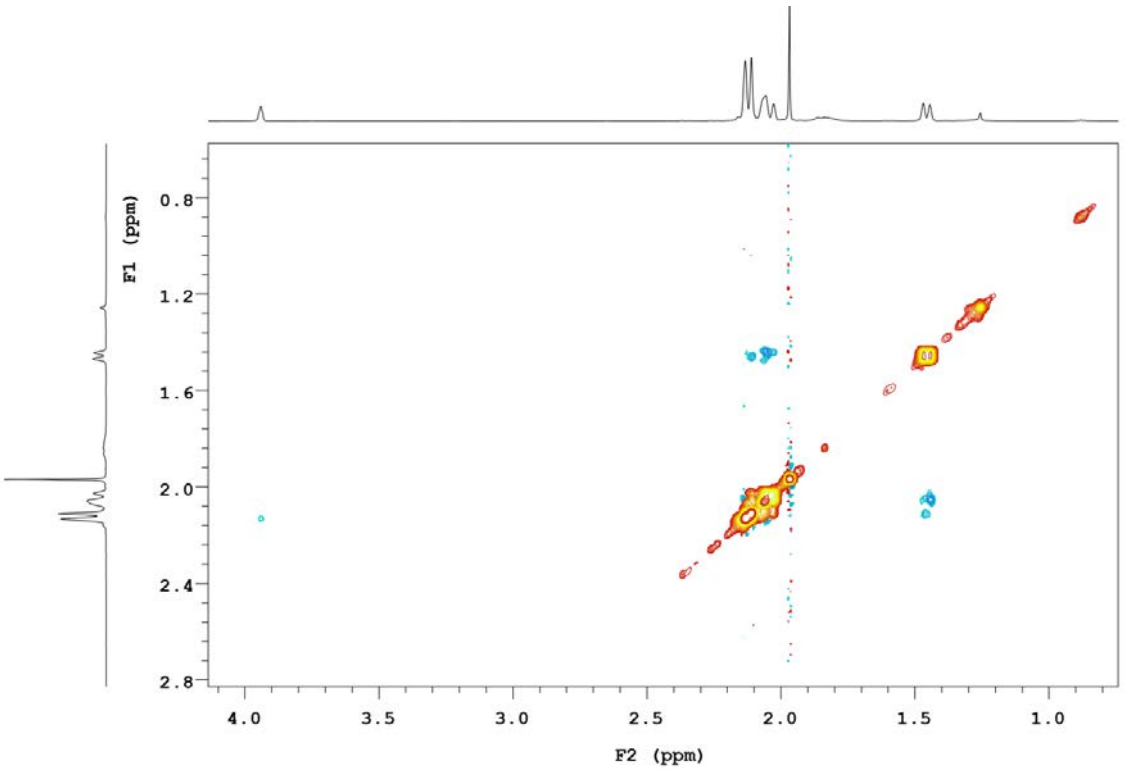

Figure C. 30 ROESY NMR spectrum of *trans*-4-hydroxy-1-adamantyl acetate.

Data for 3-hydroxy-1-adamantyl acetate (~2 mg) [182]:

^{1}H NMR (500 MHz, $CDCl_3$) δ 2.36-2.29 (m, 2H), 2.14-2.04 (m, 6H), 1.99 (s, 3H, 3xH12), 1.74-1.65 (m, 6H).

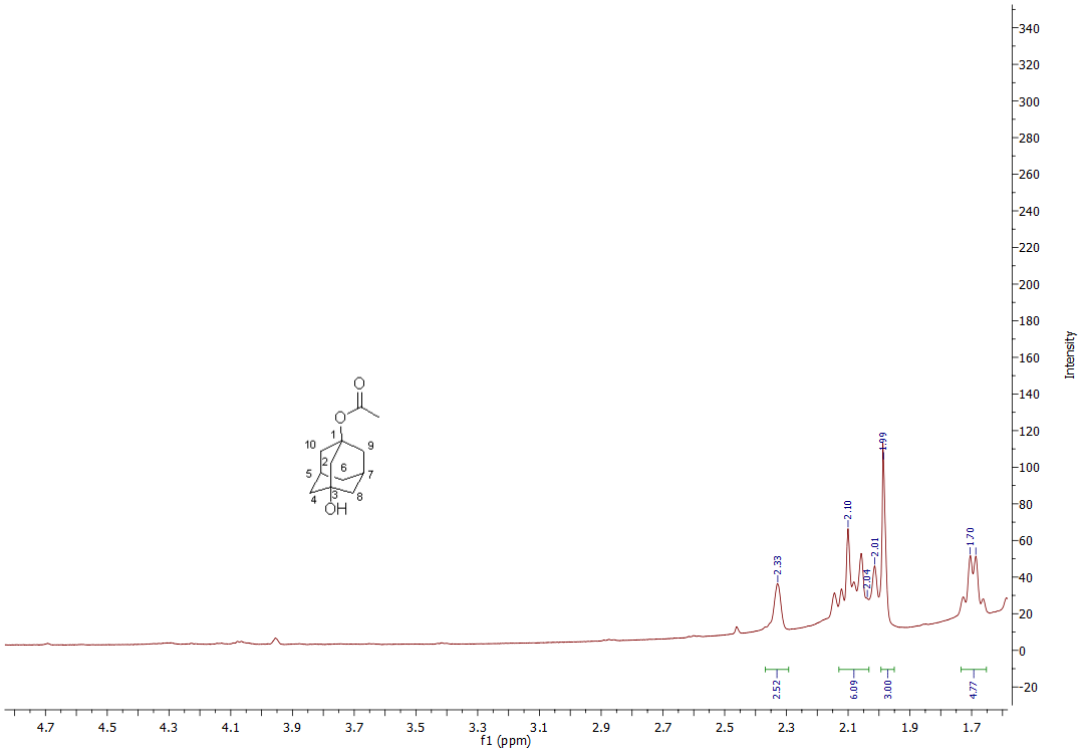

Figure C. 31 ^{1}H NMR spectrum of 3-hydroxy-1-adamantyl acetate.

Data for *trans*-4-hydroxy-1-adamantyl isobutyrate (~35 mg) [182]:

^{1}H NMR (500 MHz, $CDCl_3$) δ 3.96-3.92 (m, 1H, H4), 2.42 (*sept*, J = 7.0 Hz, 1H, H12), 2.17-2.09 (m, 7H, 2xH2, H7, 2xH9 & 2xH10), 2.08-2.01 (m, 4H, H3, H5, H6 & H8), 1.44 (d, J = 14.7 Hz, 2H, H6 & H8), 1.11 (d, J = 7.0 Hz, 6H, 3xH13 & 3xH14).

^{13}C NMR (126 MHz, $CDCl_3$) δ 179.19 (C11), 81.20 (C1), 75.82 (C4), 43.94 (C9), 42.21 (C2 & C10), 38.94 (C3 & C5), 37.57 (C12), 32.60 (C7), 32.38 (C6 & C8), 21.69 (C13 & C14).

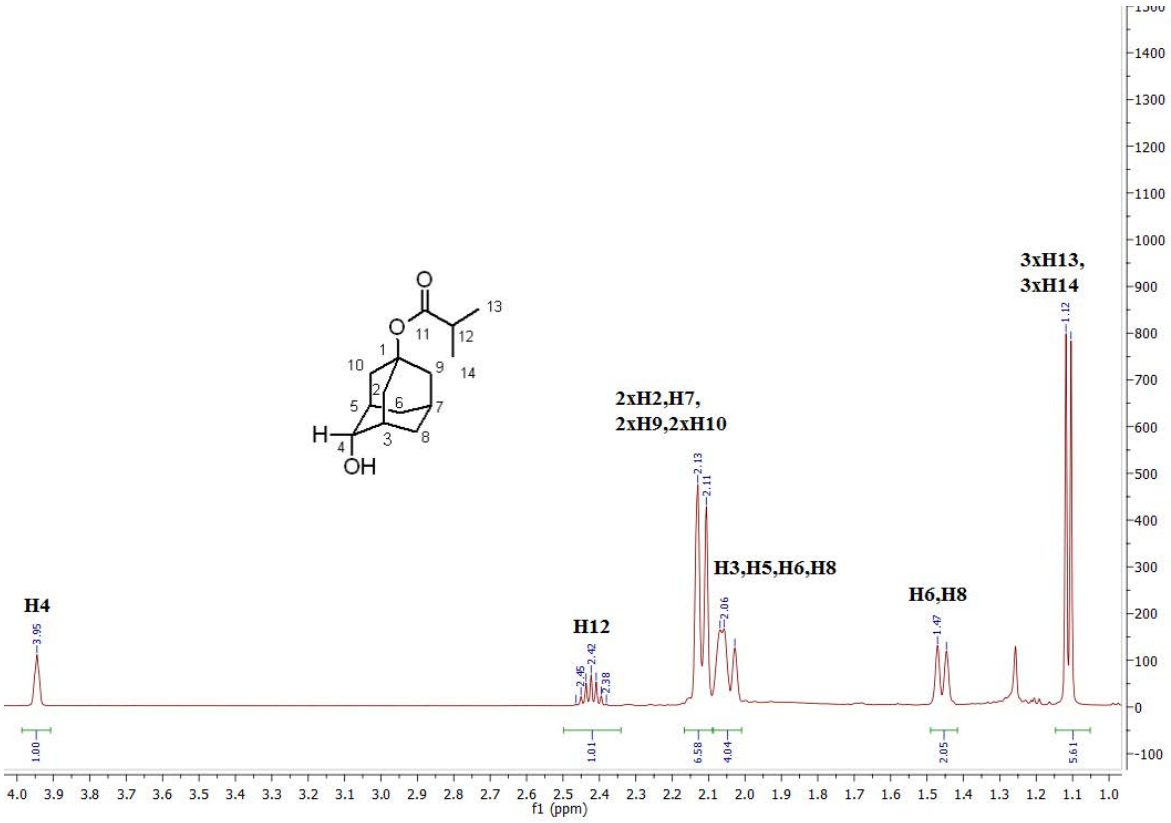

Figure C. 32 ^{1}H NMR spectrum of *trans*-4-hydroxy-1-adamantyl isobutyrate.

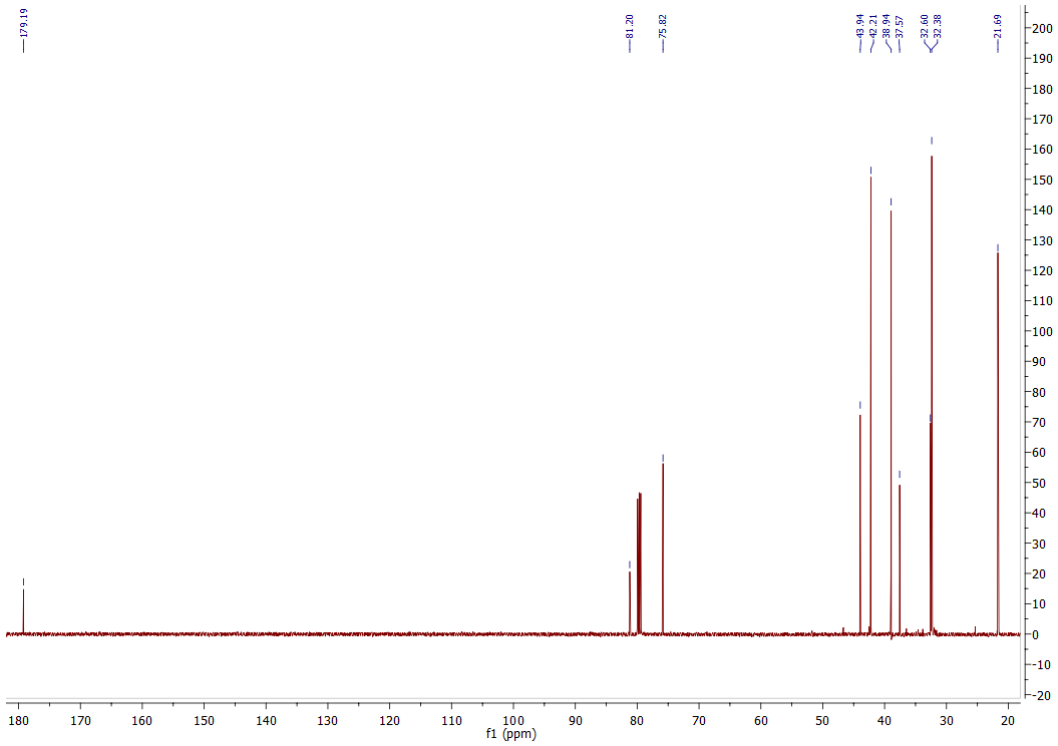

Figure C. 33 ^{13}C NMR spectrum of *trans*-4-hydroxy-1-adamantyl isobutyrate

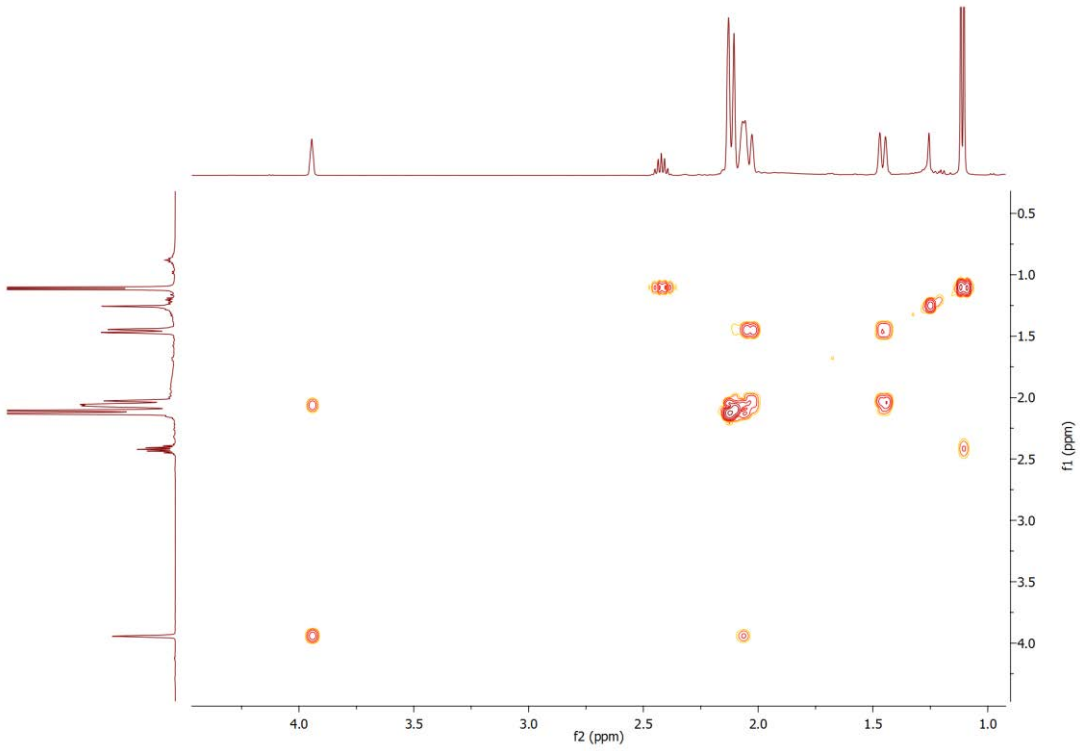

Figure C. 34 gCOSY NMR spectrum of *trans*-4-hydroxy-1-adamantyl isobutyrate.

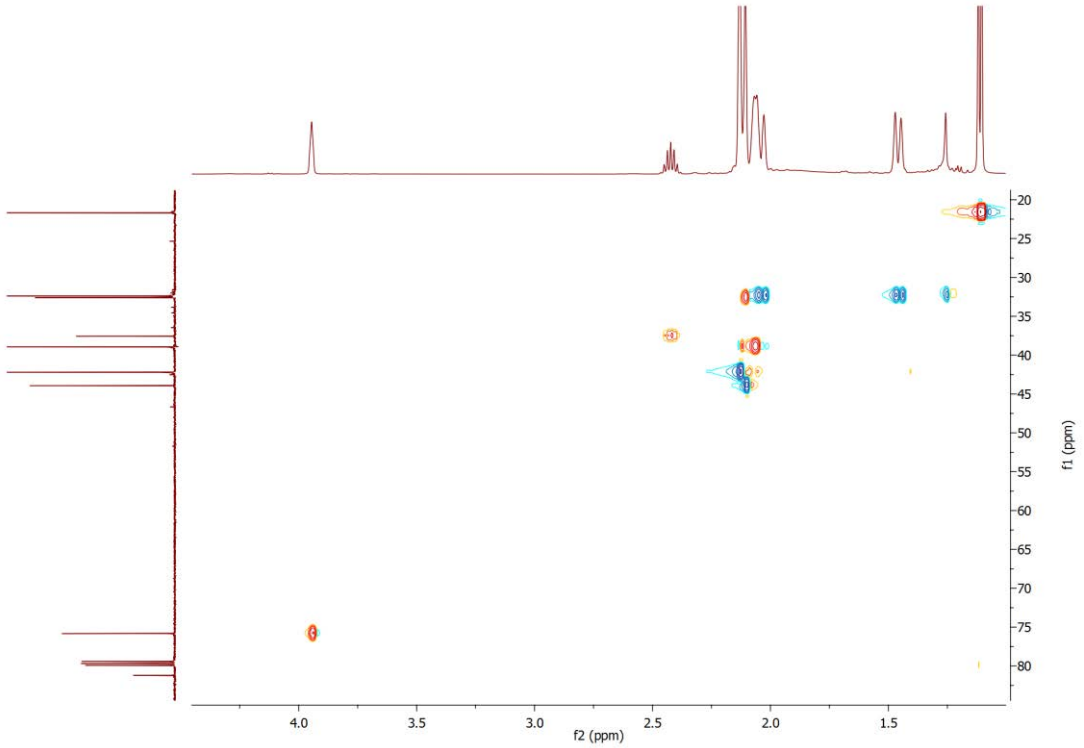

Figure C. 35 HSQC NMR spectrum of *trans*-4-hydroxy-1-adamantyl isobutyrate.

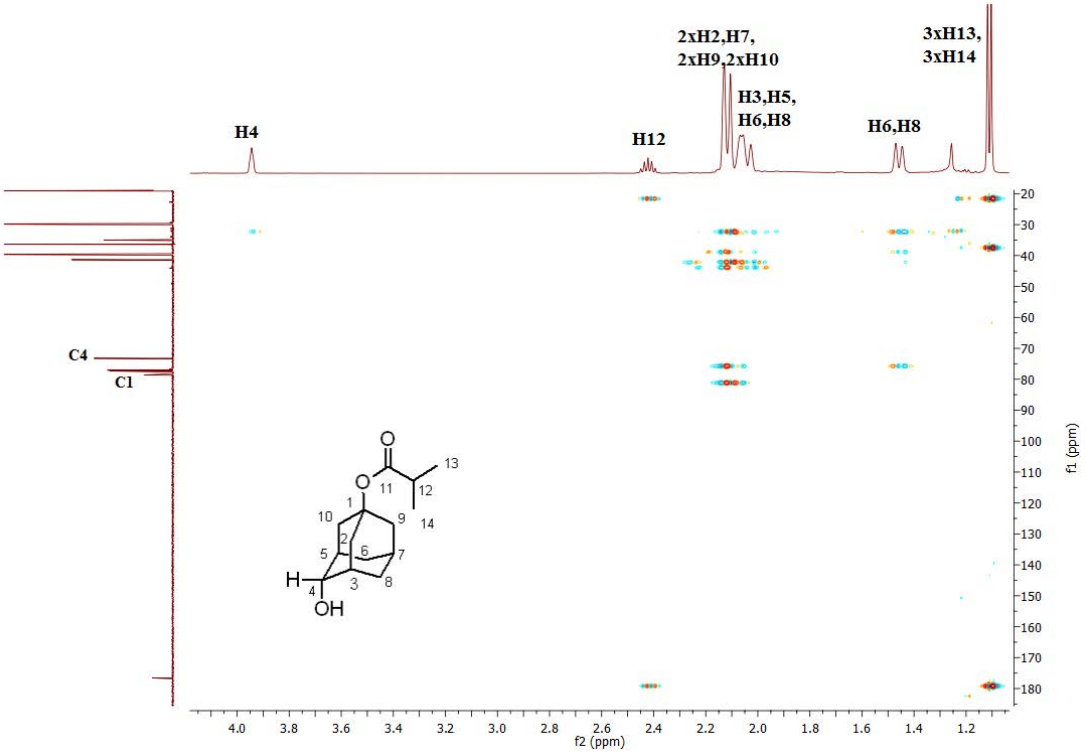

Figure C. 36 HMBC NMR spectrum of *trans*-4-hydroxy-1-adamantyl isobutyrate.

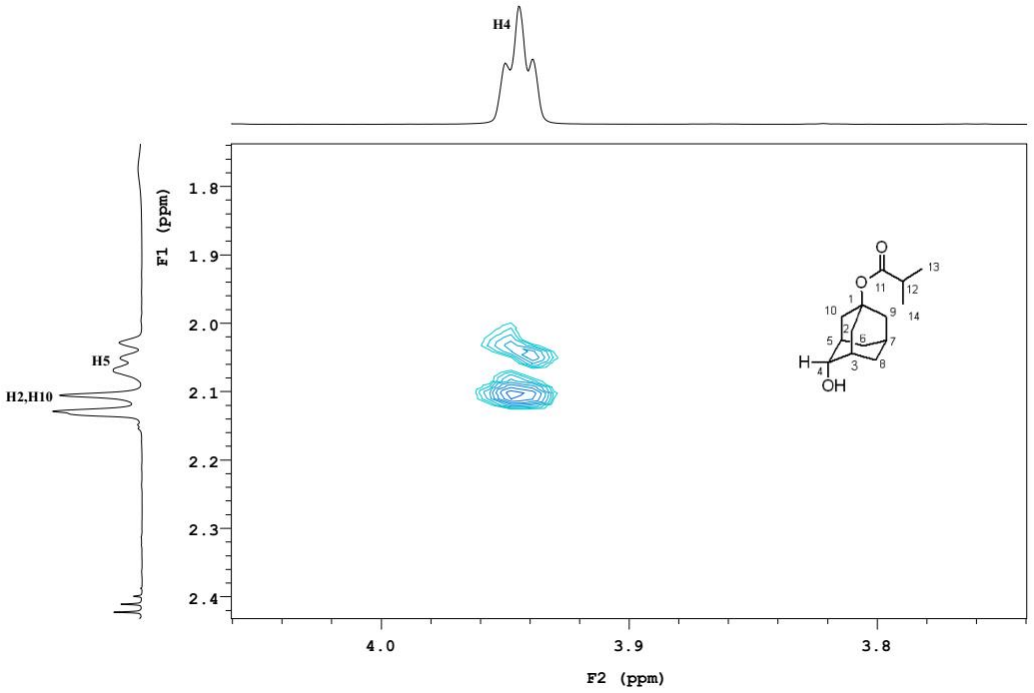

Figure C. 37 Zoomed in ROESY NMR spectrum of *trans*-4-hydroxy-1-adamantyl isobutyrate highlighting the interactions of the H4 hydrogen with H2, H5 and H10.

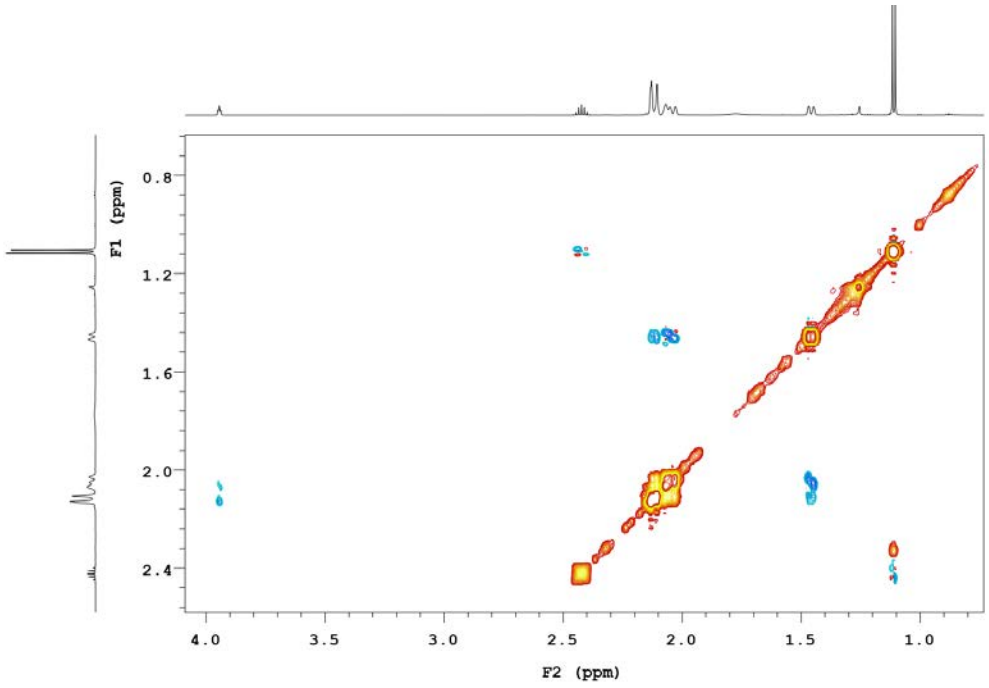

Figure C. 38 ROESY NMR spectrum of *trans*-4-hydroxy-1-adamantyl isobutyrate.

Data for 5-hydroxy-2-adamantyl acetate (~25 mg) [182]:

^{1}H NMR (500 MHz, $CDCl_3$) δ 4.89-4.86 (m, 1H, H2), 2.21-2.10 (m, 3H, H1, H3 & H7), 2.08 (s, 3H, 3xH12), 1.95 (d, J = 12.8 Hz, 2H, H8 & H10), 1.86-1.80 (m, 2H, H4 & H9), 1.78-1.70 (m, 4H, H4, 2xH6 & H9), 1.43 (d, J = 12.3 Hz, 2H, H8 & H10).

^{13}C NMR (126 MHz, $CDCl_3$) δ 173.21 (C11), 78.25 (C2), 70.12 (C5), 47.81 (C6), 46.03 (C4 & C9), 36.20 (C1 & C3), 32.99 (C8 & C10), 32.26 (C7), 24.06 (C12).

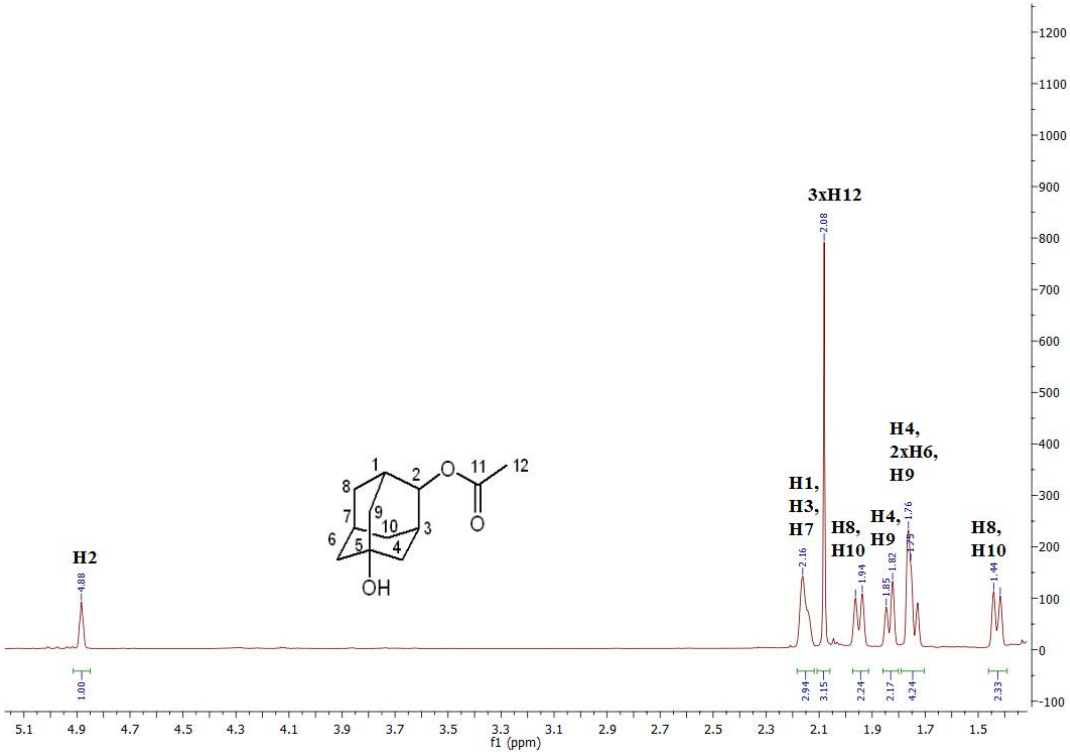

Figure C. 39 ^{1}H NMR spectrum of 5-hydroxy-2-adamantyl acetate.

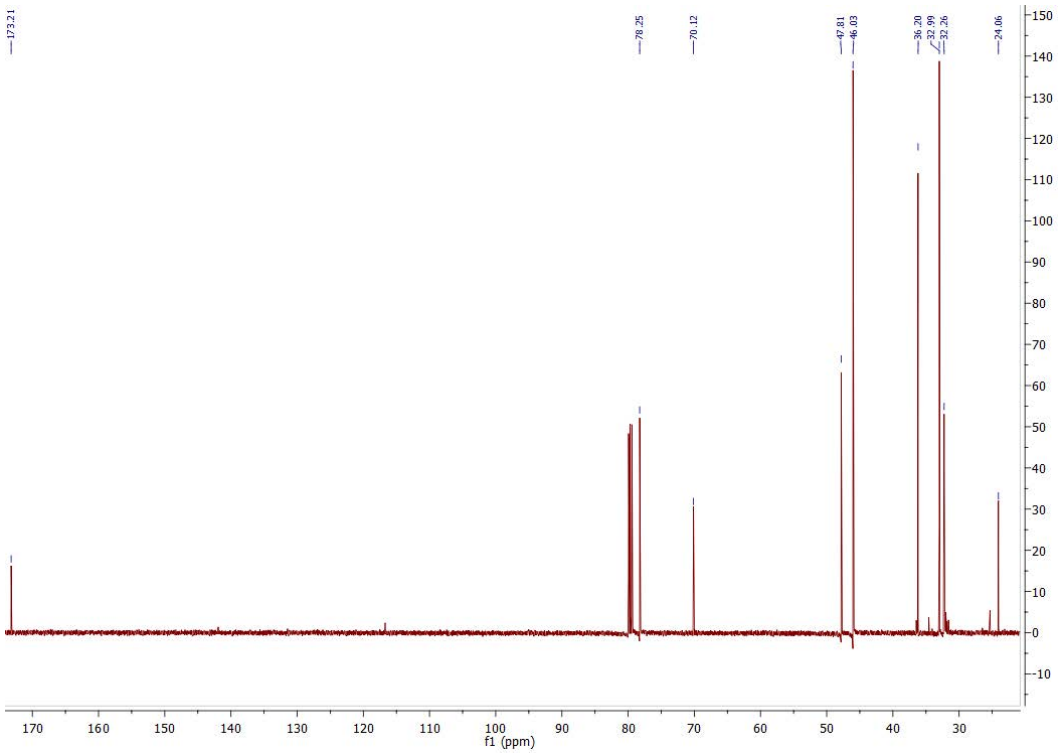

Figure C. 40 ^{13}C NMR spectrum of 5-hydroxy-2-adamantyl acetate.

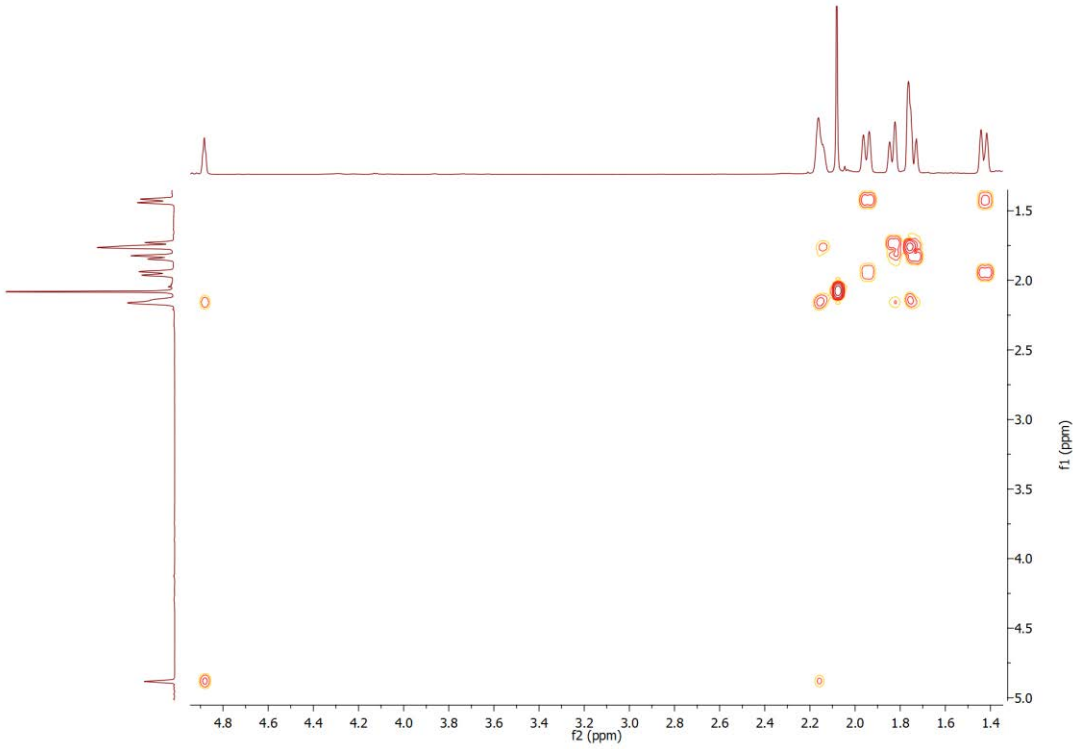

Figure C. 41 gCOSY NMR spectrum of 5-hydroxy-2-adamantyl acetate.

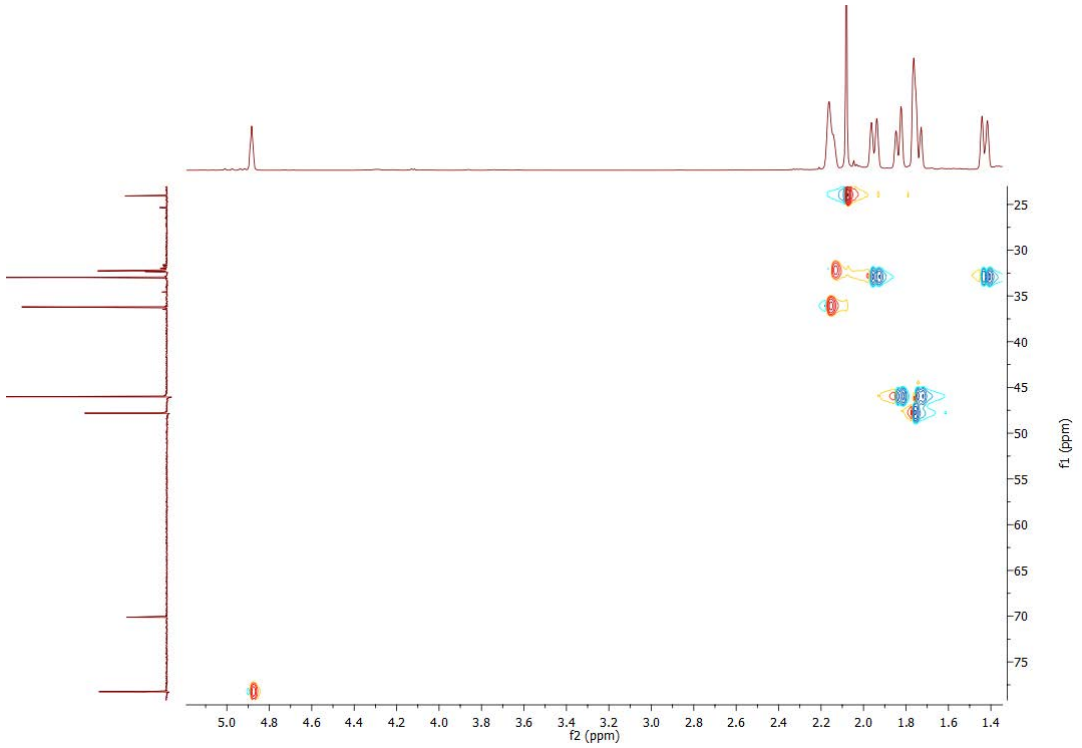

Figure C. 42 HSQC NMR spectrum of 5-hydroxy-2-adamantyl acetate.

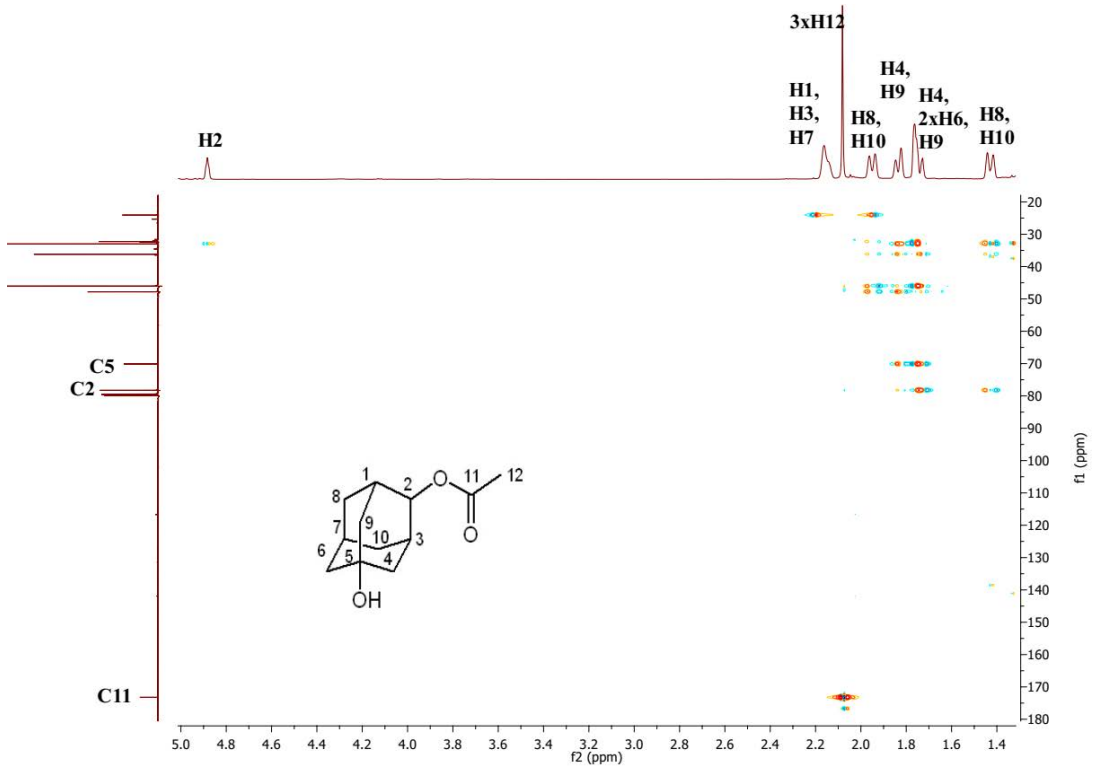

Figure C. 43 HMBC NMR spectrum of 5-hydroxy-2-adamantyl acetate.

Data for 5-hydroxy-2-adamantyl isobutyrate (40 mg) [182]:

^{1}H NMR (500 MHz, $CDCl_3$) δ 4.90-4.84 (m, 1H, H2), 2.62-2.52 (*sept*, J = 7.0 Hz, 1H, H12), 2.20-2.10 (m, 3H, H1, H3 & H7), 1.94 (d, J = 12.7 Hz, 2H, H8 & H10), 1.84 (d, J = 11.9 Hz, 2H, H4 & H9), 1.79-1.69 (m, 4H, H4, 2xH6 & H9), 1.43 (d, J = 12.5 Hz, 2H, H8, H10), 1.19 (d, J = 7.0 Hz, 6H, 3xH13 & 3xH14).

^{13}C NMR (126 MHz, $CDCl_3$) δ 179.11 (C11), 77.76 (C2), 70.15 (C5), 47.74 (C6), 45.96 (C4 & C9), 37.02 (C12), 36.20 (C1 & C3), 33.04 (C8 & C10), 32.27 (C7), 21.69 (C13 & C14).

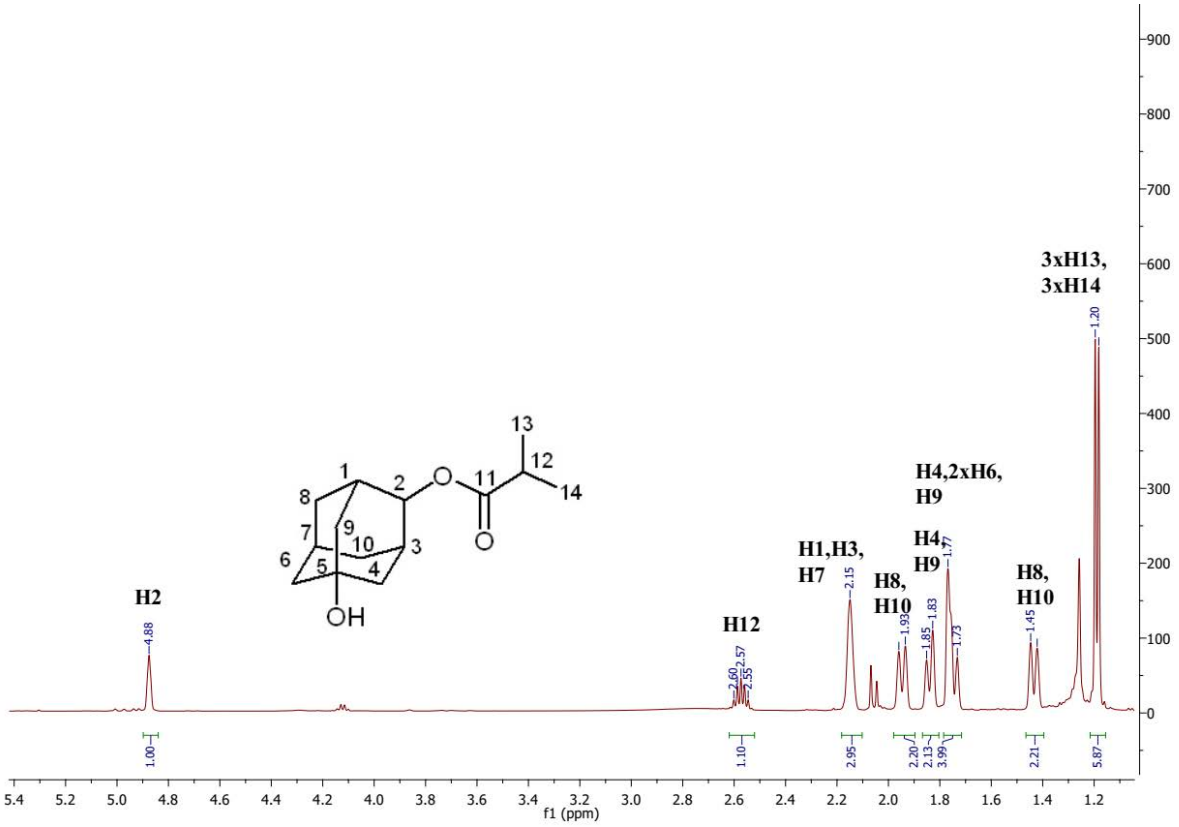

Figure C. 44 ^{1}H NMR spectrum of 5-hydroxy-2-adamantyl isobutyrate.

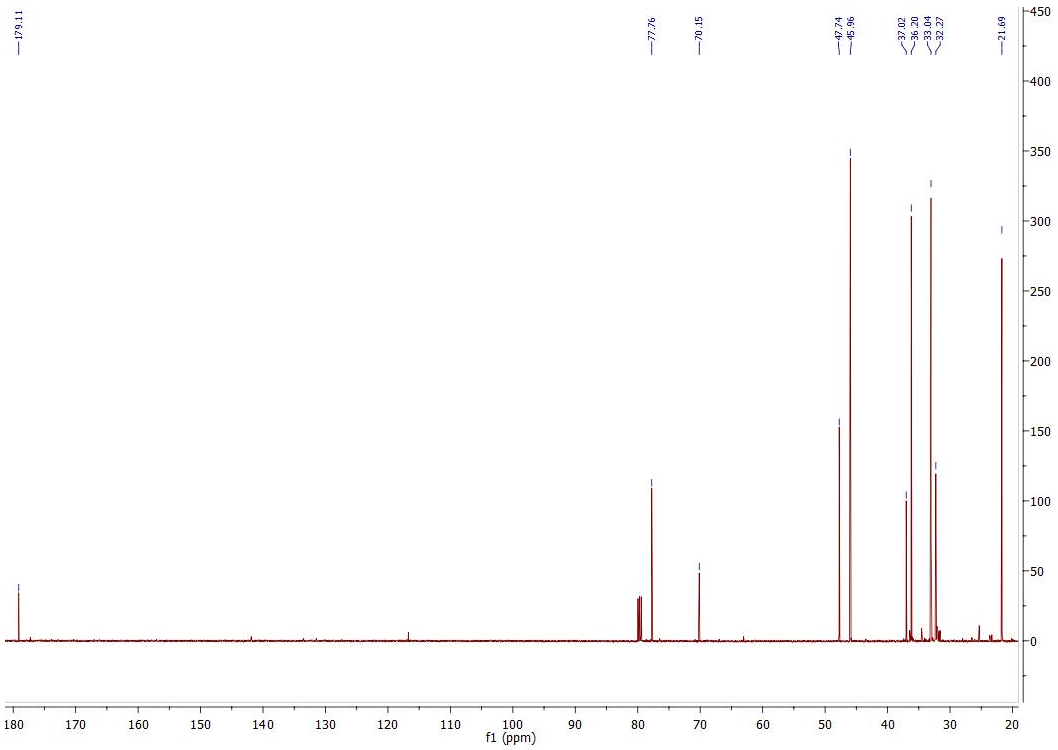

Figure C. 45 ^{13}C NMR spectrum of 5-hydroxy-2-adamantyl isobutyrate.

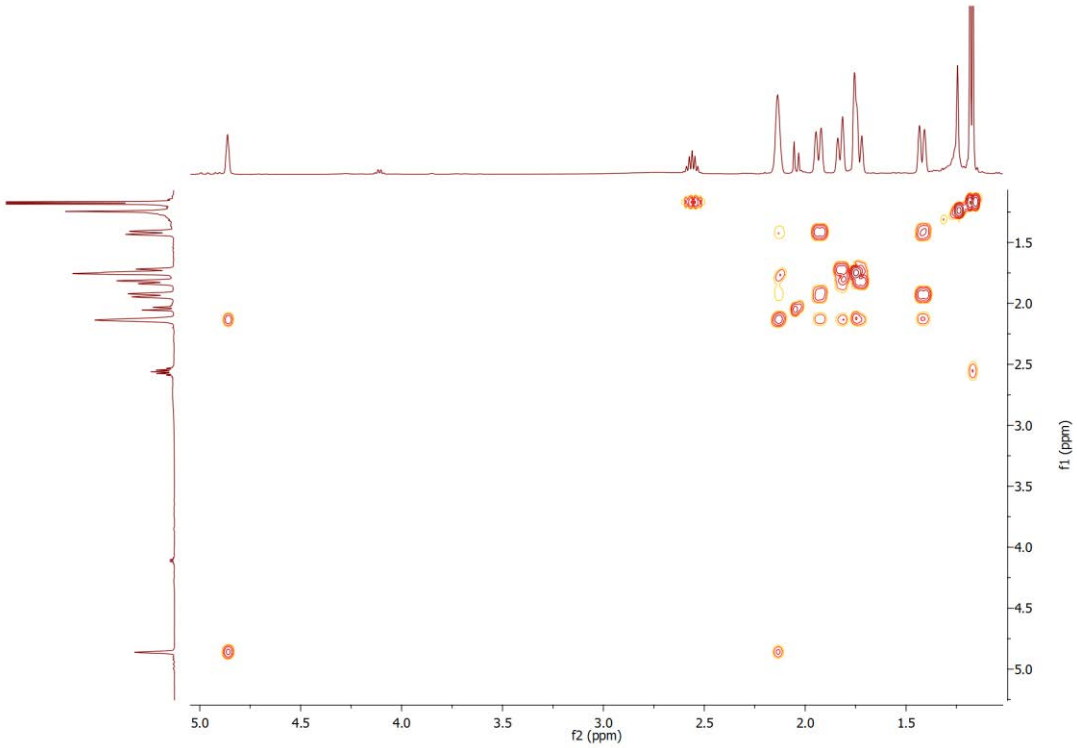

Figure C. 46 gCOSY NMR spectrum of 5-hydroxy-2-adamantyl isobutyrate.

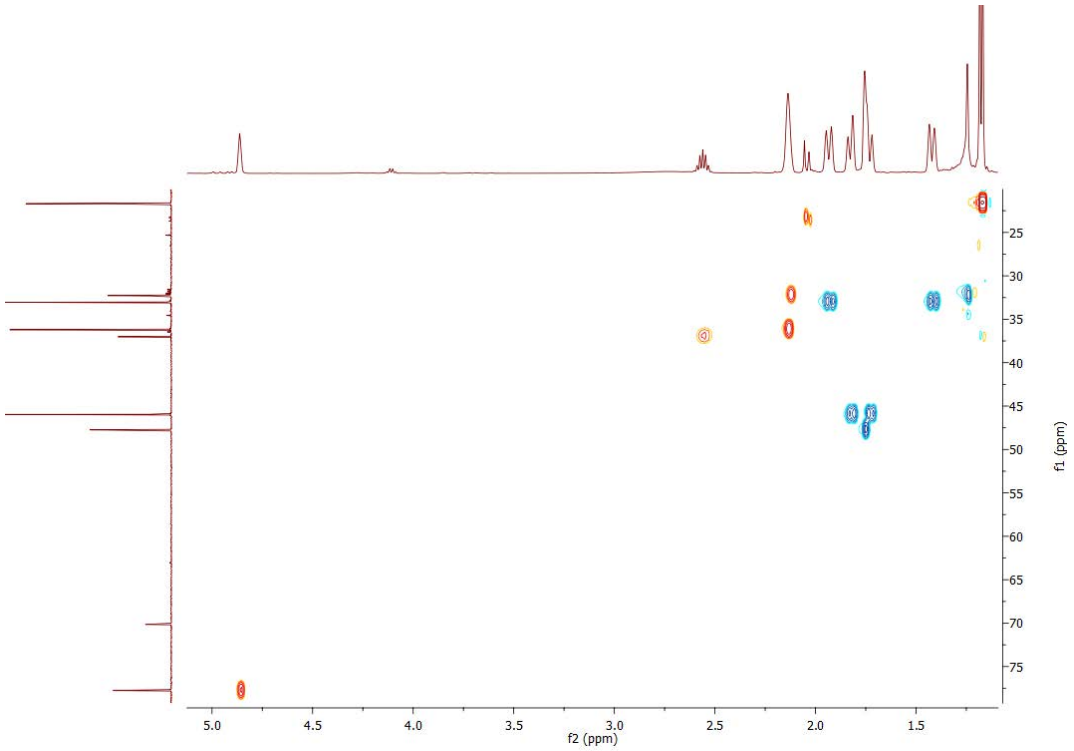

Figure C. 47 HSQC NMR spectrum of 5-hydroxy-2 adamantyl isobutyrate.

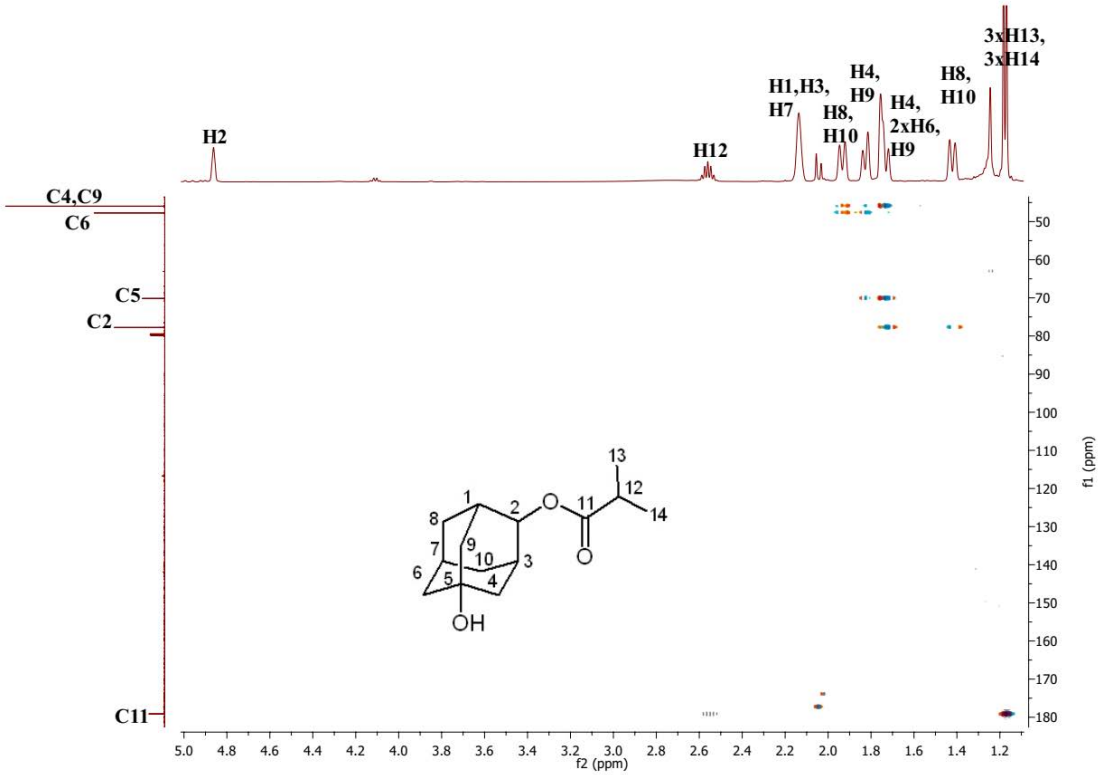

(a)

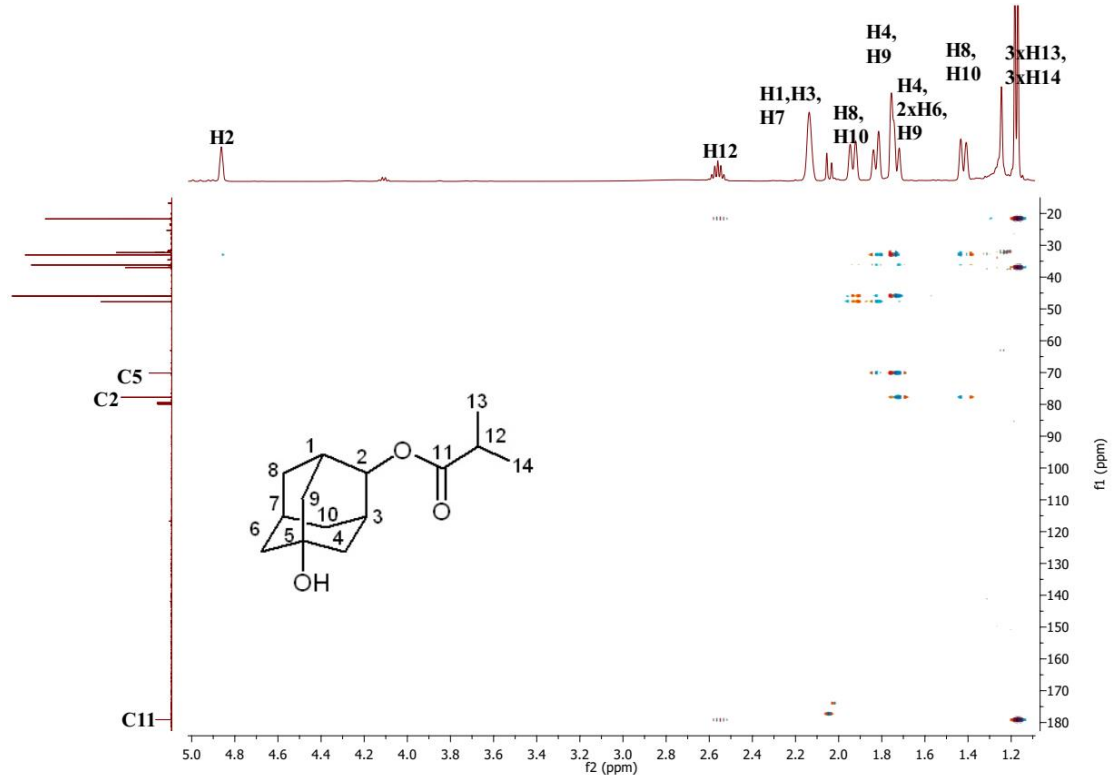

(b)

Figure C. 48 (a) Zoomed in HMBC NMR spectrum (40 to 180 ppm region) of 5-hydroxy-2-adamantyl isobutyrate. **(b)** HMBC NMR spectrum of 5-hydroxy-2-adamantyl isobutyrate.

Data for 4-hydroxy-N-(1-adamantyl)acetamide (~15 mg) [182]:

^{1}H NMR (500 MHz, $CDCl_3$) δ 5.15 (s, 1H, N**H11**), 3.98-3.84 (m, 1H, H4), 2.10-1.94 (m, 11H, 2.10-1.96, 2xH2 & 2xH10; 2.07-1.96, H3 & H5; 2.01-1.97, H7; 2.01-1.96, H6 & H8; 1.98-1.93, 2xH9), 1.91 (s, 3H, 3xH13), 1.47 (d, J = 12.2 Hz, 2H, H6 & H8).

^{13}C NMR (126 MHz, $CDCl_3$) δ 172.09 (C12), 75.98 (C4), 53.76 (C1), 44.42 (C9), 42.68 (C2 & C10), 37.89 (C3 &C5), 32.47 (C6 & C8), 31.30 (C7), 27.29 (C13).

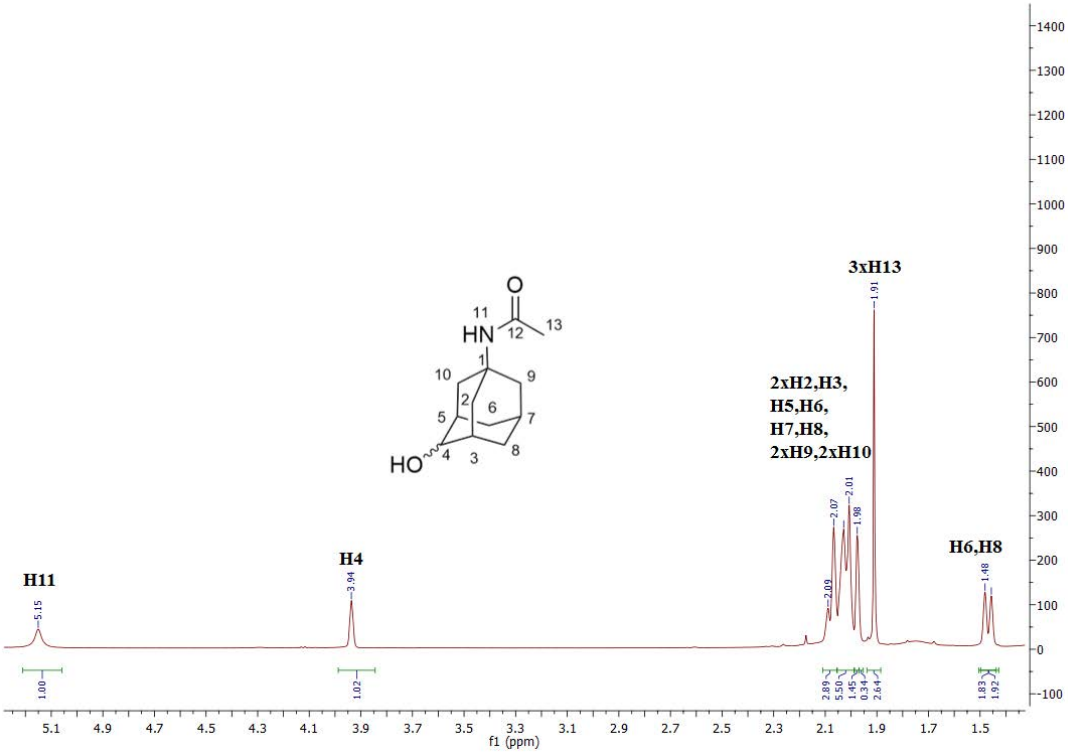

Figure C. 49 ^{1}H NMR spectrum of 4-hydroxy-N-(1-adamantyl)acetamide.

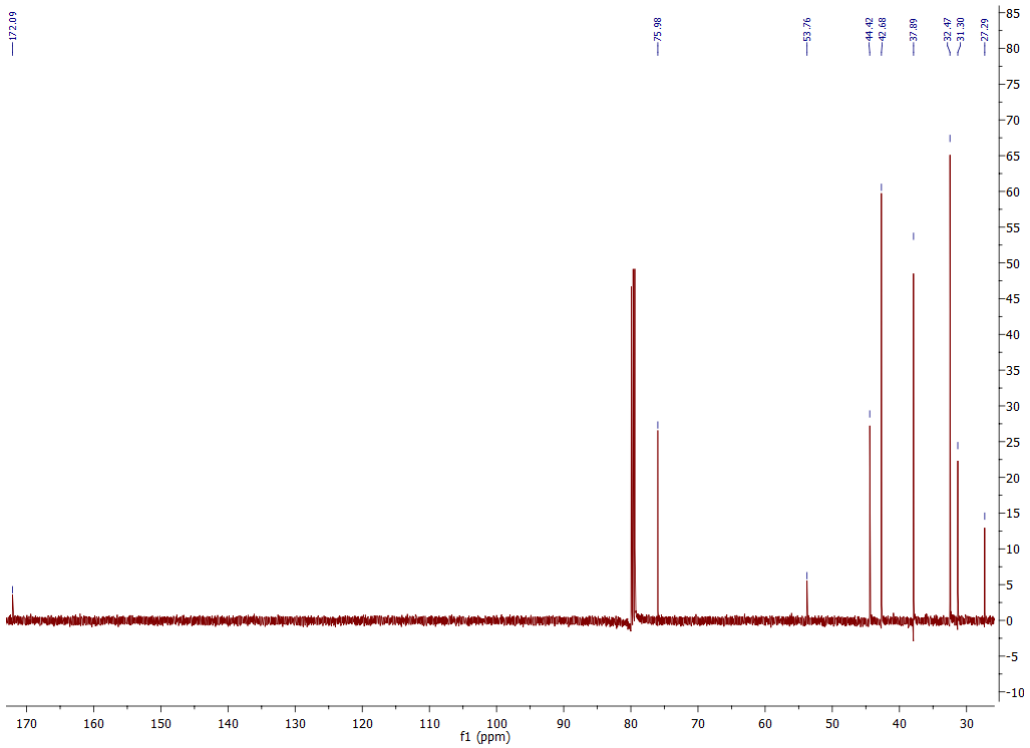

Figure C. 50 ^{13}C NMR spectrum of 4-hydroxy-N-(1-adamantyl)acetamide.

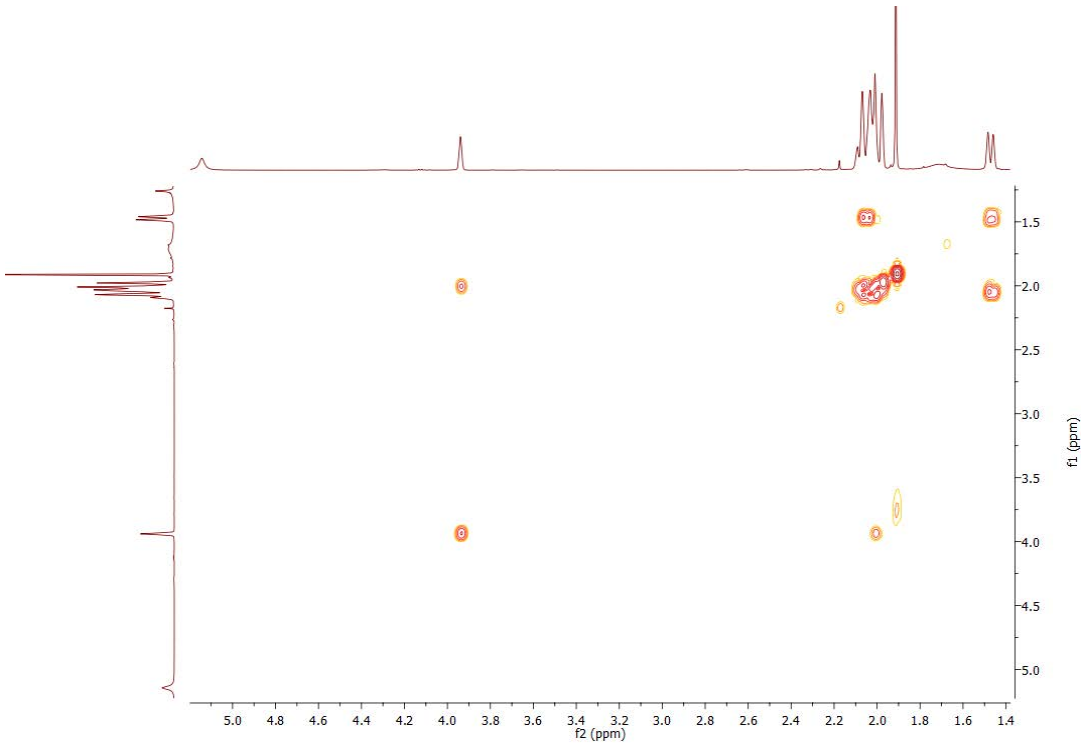

Figure C. 51 gCOSY NMR spectrum of 4-hydroxy-N-(1-adamantyl)acetamide.

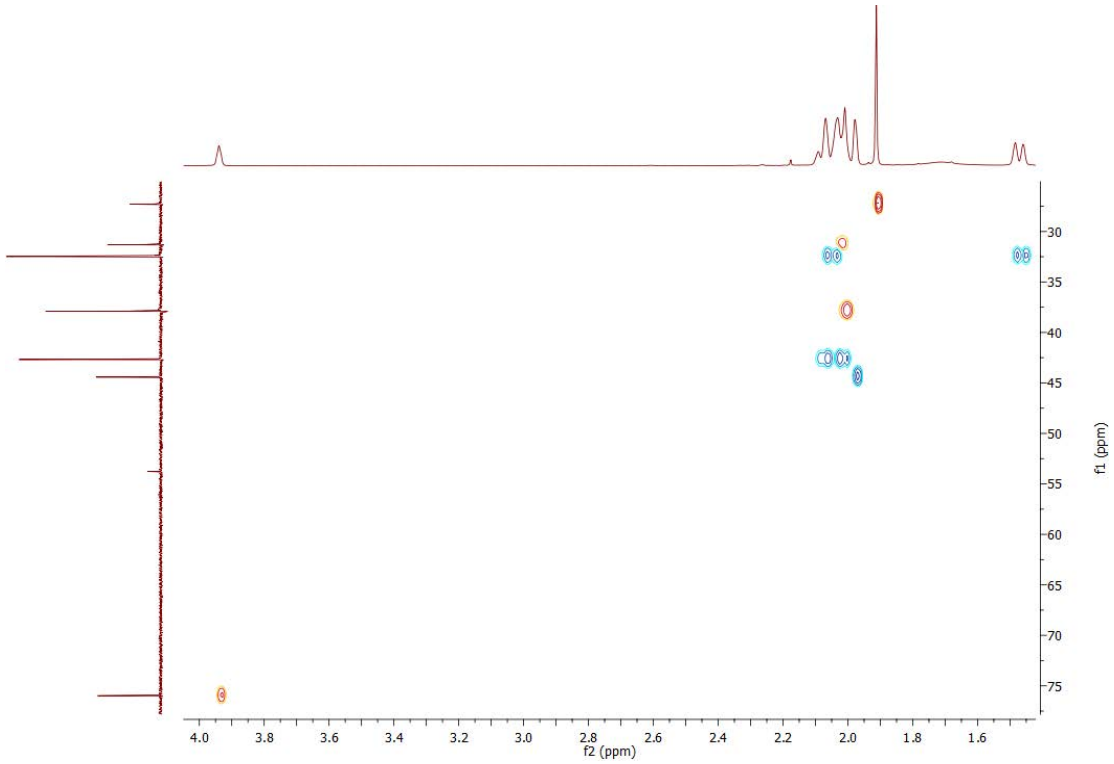

Figure C. 52 HSQC NMR spectrum of 4-hydroxy-N-(1-adamantyl)acetamide.

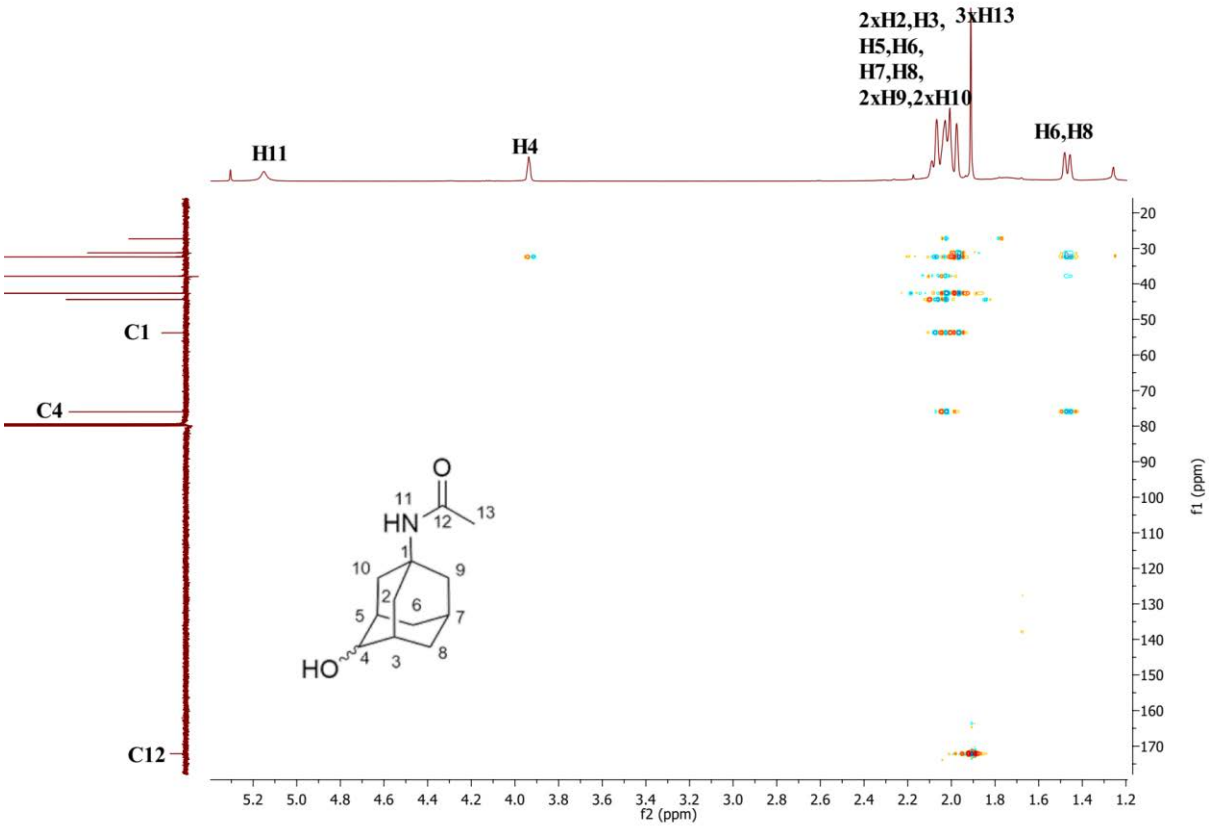

Figure C. 53 HMBC NMR spectrum of 4-hydroxy-N-(1-adamantyl)acetamide.

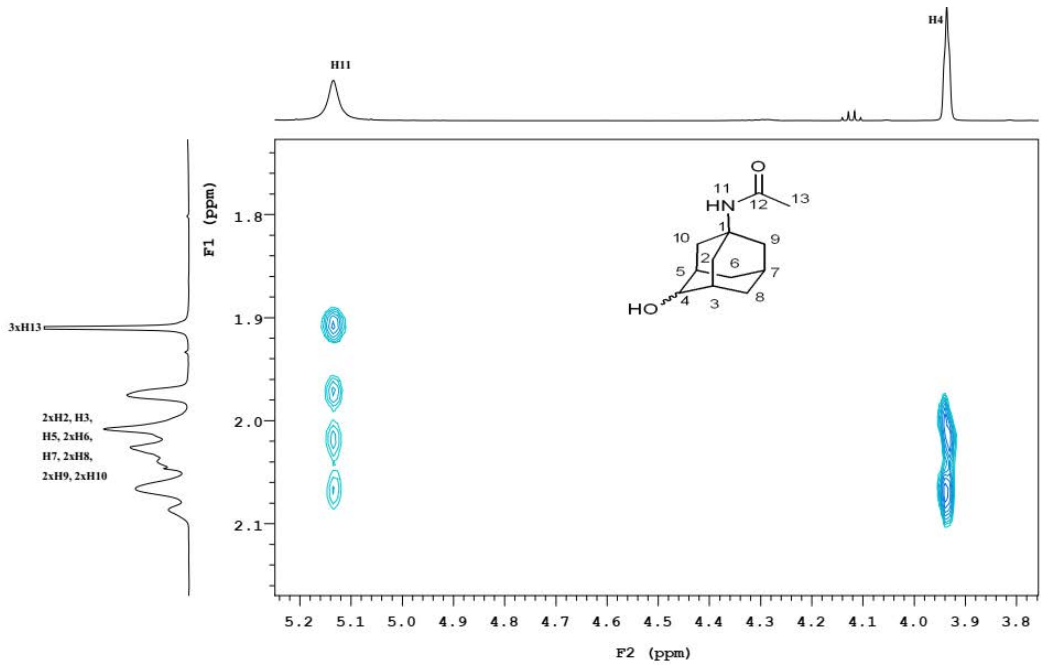

Figure C. 54 Zoomed in ROESY NMR spectrum of 4-hydroxy-N-(1-adamantyl)acetamide. This highlights the potential interactions between the H4 hydrogen and those on C2 and C10, which would indicate the *trans*-isomer consistent with the previous studies though we can not definitively assign the stereochemistry.

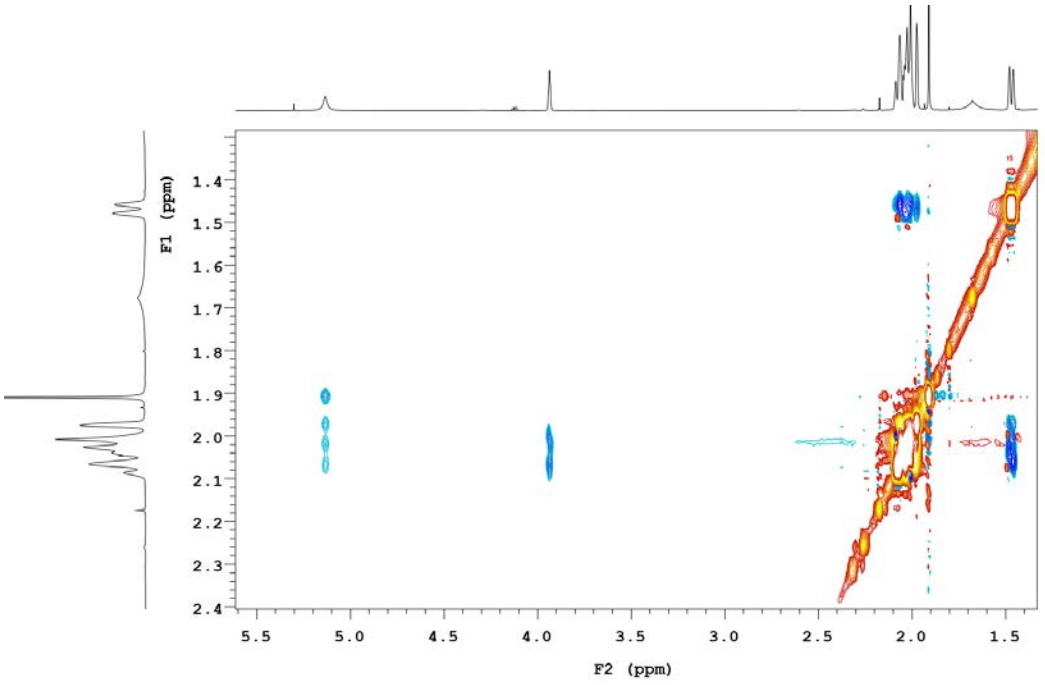

Figure C. 55 ROESY NMR spectrum of 4-hydroxy-N-(1-adamantyl)acetamide.

Data for 3-hydroxy-N-(1-adamantyl)acetamide (~2 mg) [182]:

^{1}H NMR (500 MHz, $CDCl_3$) δ 5.19 (s, 1H, N**H11**), 2.33-2.22 (m, 2H, H5, H7), 1.99 (s, 2H, 2xH2), 1.94-1.89 (m, 5H, 3xH13 & 2xH6), 1.74-1.65 (m, 4H, 2xH9 & 2xH10 or 2xH4 & 2xH8), 1.58-1.56 (m, 4H, 2xH9 & 2xH10 or 2xH4 & 2xH8).

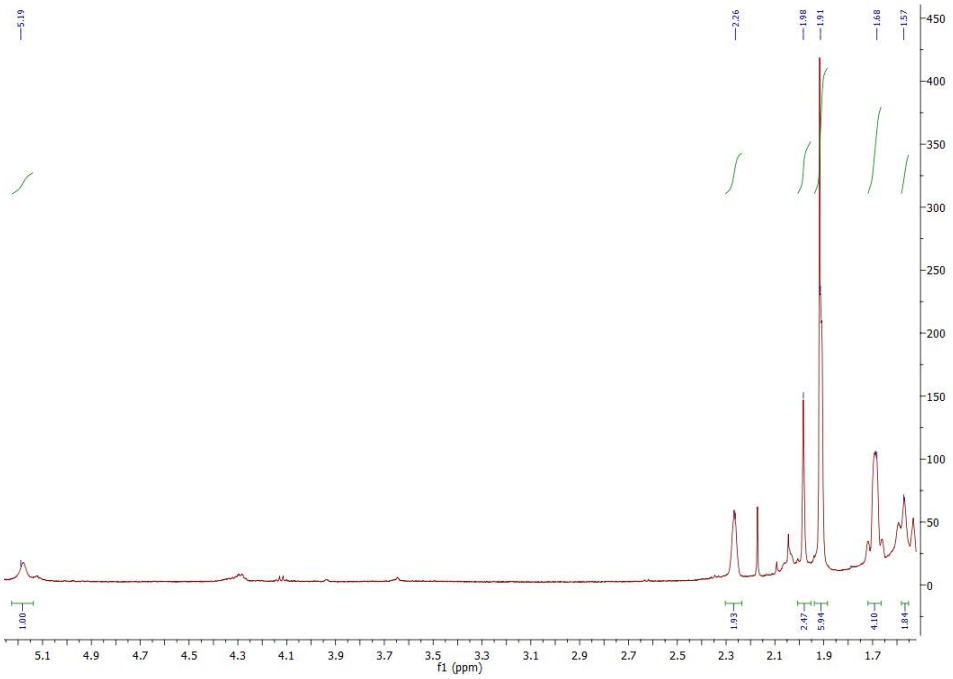

Figure C. 56 ^{1}H NMR spectrum of 3-hydroxy-N-(1-adamantyl)acetamide.

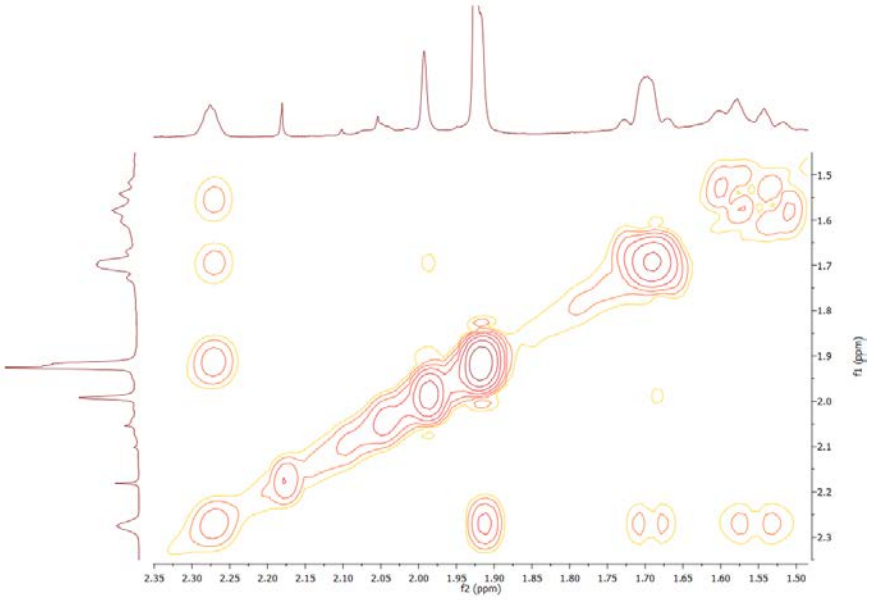

Figure C. 57 gCOSY NMR spectrum of 3-hydroxy-N-(1-adamantyl)acetamide.

Appendix D Supporting information for Chapter 5

Figure D. 1 MS analysis of products **454**
Figure D. 2 ^{1}H NMR of (2-ethylphenyl)methanol (DMSO-d_6). 463
Figure D. 3 ^{1}H NMR of (2-ethylphenyl)methanol.($CDCl_3$) 463
Figure D. 4 ^{1}H NMR of 1-(3-methylphenyl)ethanol 464
Figure D. 5 ^{1}H NMR of 2-ethyl-4-methylphenol 465
Figure D. 6 ^{1}H NMR of (1-methyl-2-naphthyl)methanol. 466
Figure D. 7 gCOSY NMR of (1-methyl-2-naphthyl)methanol 467
Figure D. 8 HSQC NMR of (1-methyl-2-naphthyl)methanol 468
Figure D. 9 ^{1}H NMR of (5-methyl-1-naphthyl)methanol. 469
Figure D. 10 gCOSY NMR of (5-methyl-1-naphthyl)methanol 470
Figure D. 11 ^{1}H NMR of (6-methyl-2-naphthyl)methanol. 471
Figure D. 12 ^{13}C NMR of (6-methyl-2-naphthyl)methanol. 472
Figure D. 13 gCOSY NMR of (6-methyl-2-naphthyl)methanol 472
Figure D. 14 HSQC NMR of (6-methyl-2-naphthyl)methanol 473
Figure D. 15 ^{1}H NMR of 2-(7-methylnaphthyl)methanol. 474
Figure D. 16 ^{1}H NMR of 1-acenaphthol. 475
Figure D. 17 ^{13}C NMR of 1-acenaphthol. 476
Figure D. 18 ^{13}C NMR of 1-acenaphthol. 476
Figure D. 19 HSQC NMR of 1-acenaphthol 477
Figure D. 20 ^{1}H NMR of 3-biphenylmethanol. 477
Figure D. 21 Chiral HPLC analysis of *in vitro* turnovers of CYP101B1 and H85F CYP101B1 with indane. 478

Figure D. 1 MS analysis of products

MS analysis of *β*-ionone products

MS analysis of 4-hydroxy-*β*-ionone (m^+/z = 208.10) RT 10.2 min

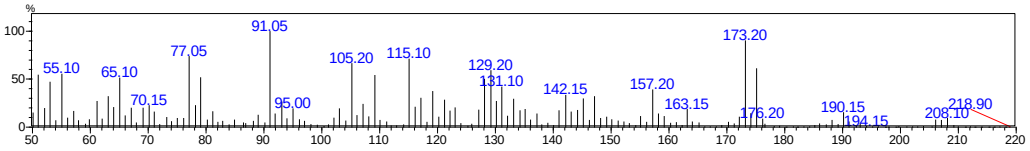

MS analysis of 3-hydroxy-*β*-ionone (m^+/z = 208.30) RT 10.3 min

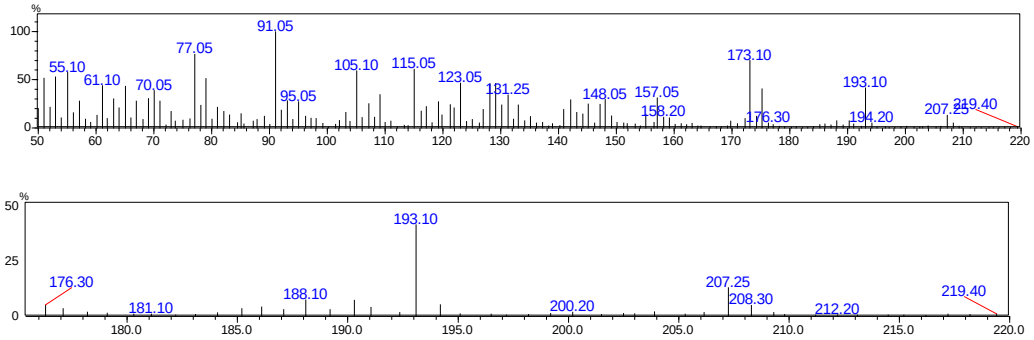

Zoomed in

MS analysis of *p*-cymene products

MS analysis of *p*-*α*,*α*-trimethylbenzyl alcohol (m^+/z = 150.2) RT 8.2 min

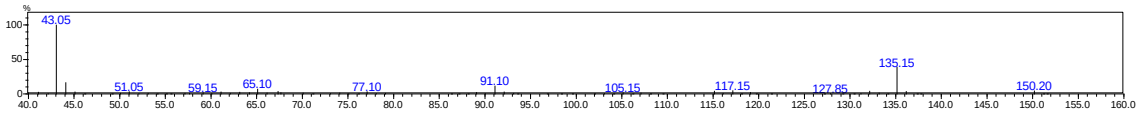

MS analysis of 4-isopropylbenzyl alcohol (m^+/z = 150.15) RT 11.1 min

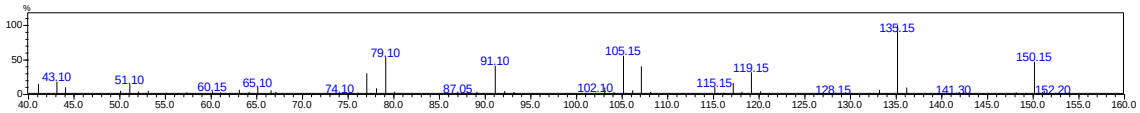

MS analysis of toluene product

MS analysis of benzyl alcohol (m^+/z = 108.10) RT 4.5 min

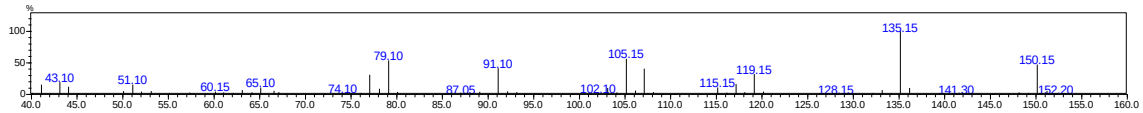

MS analysis of *o*-xylene product

MS analysis of 2-methylbenzyl alcohol (m^+/z = 122.1) RT 8.7 min

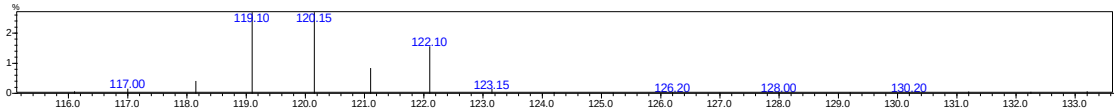

MS analysis of *p*-xylene product

MS analysis of 4-methylbenzyl alcohol (m^+/z = 122.1) RT 8.8 min

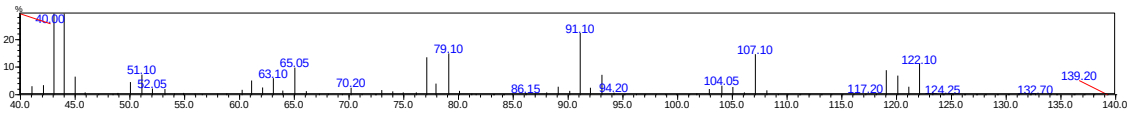

MS analysis of *m*-xylene product

MS analysis of 3-methylbenzyl alcohol (m^+/z = 122.1) RT 8.6 min

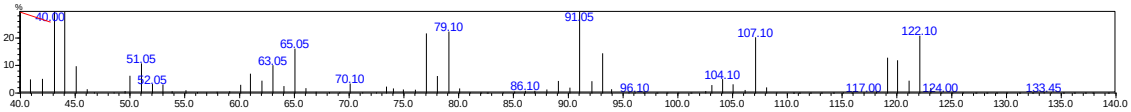

MS analysis of ethylbenzene product

MS analysis of 1-phenylethanol (m^+/z = 122.05) RT 5.05 min

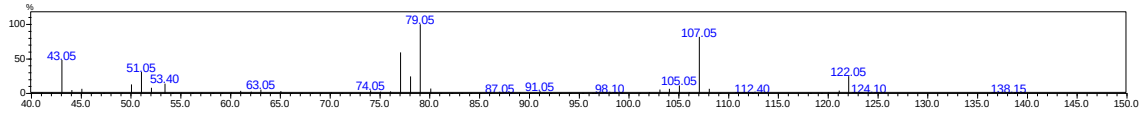

MS analysis of 2-ethyltoluene products

MS analysis of 2-ethylbenzaldehyde (m^+/z = 134.10) RT 7.10 min

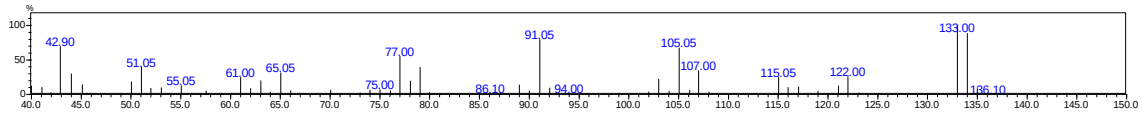

MS analysis of 1-(2-methylphenyl)ethanol (m^+/z = 136.05) RT 7.90 min

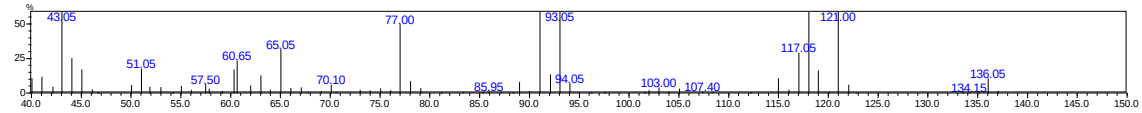

MS analysis of (2-ethylphenyl)methanol (m^+/z = 136.15) RT 9.1 min

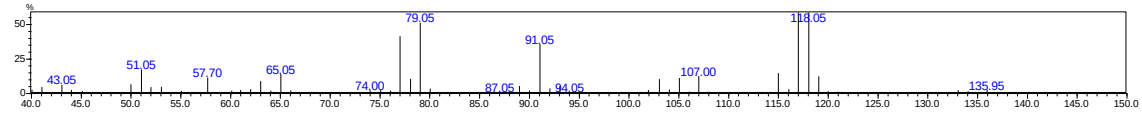

MS analysis of 3-ethyltoluene products

MS analysis of 1-(3-methylphenyl)ethanol (m^+/z = 136.05) RT 7.45 min

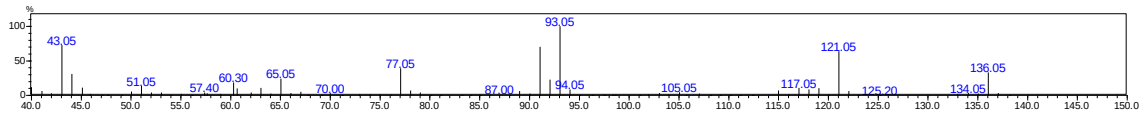

MS analysis of (3-ethylphenyl)methanol (m^+/z = 136.05) RT 9.25 min

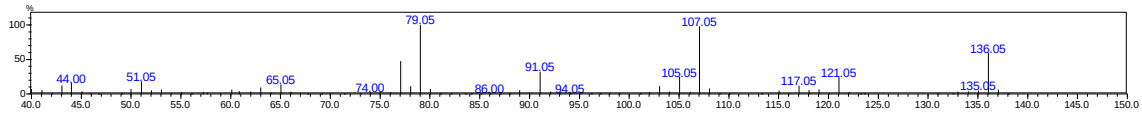

MS analysis of 2-ethyl-4-methylphenol (m^+/z = 136.05) RT 9.45 min

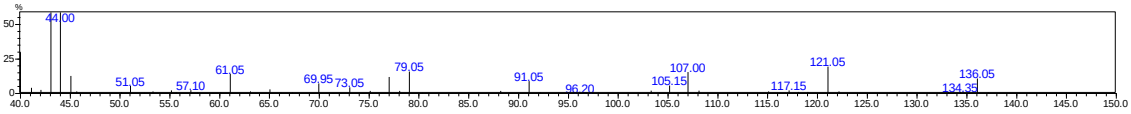

MS analysis of *n*-propylbenzene products

MS analysis of 1-phenylpropan-2-ol (m^+/z = 136.10) RT 6.75 min

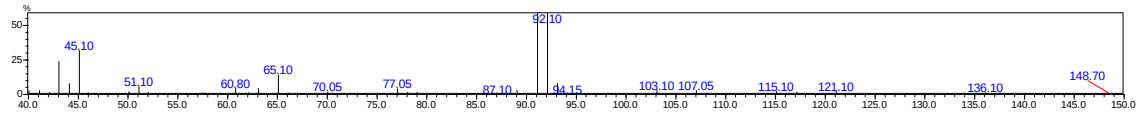

MS analysis of 1-phenyl-1-propanol (m^+/z = 136.15) RT 7.25 min

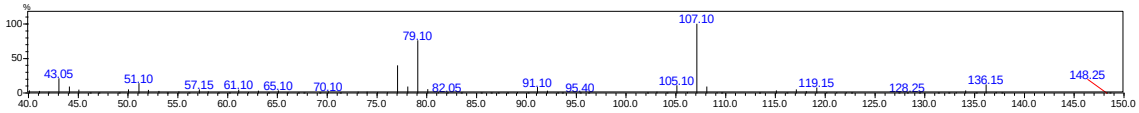

MS analysis of propiophenone (m^+/z = 134.1) RT 7.6 min

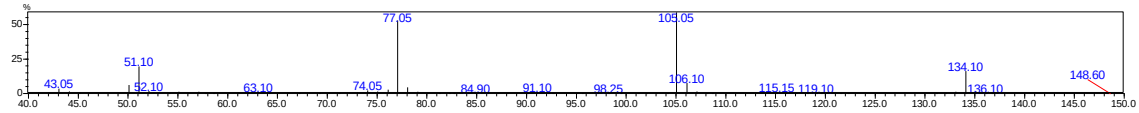

MS analysis of isopropylbenzene product

MS analysis of 2-phenyl-2-propanol (m^+/z = 136.10) RT 5.6 min

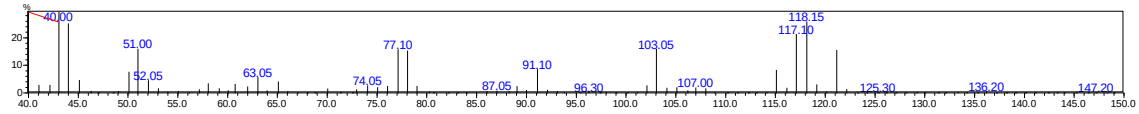

MS analysis of isobutylbenzene product

MS analysis of 2-methyl-1-phenyl-2-propanol (m^+/z = 150.05) RT 7.45 min

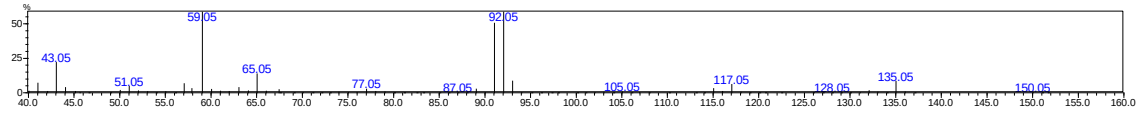

MS analysis of indane products

MS analysis of 1-indanol (m^+/z = 134.10) RT 9.2 min

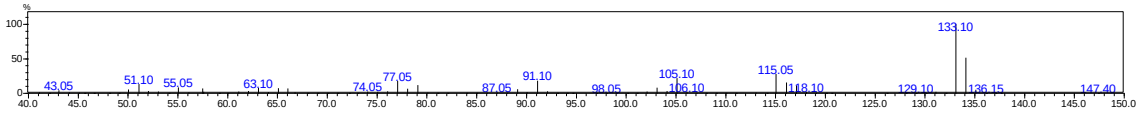

MS analysis of 1-indanone (m^+/z = 132.10) RT 10.6 min

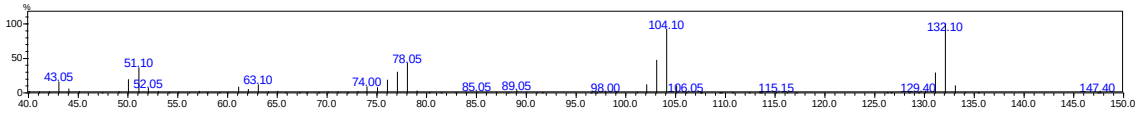

MS analysis of styrene products

MS analysis of phenylacetaldehyde (m^+/z = 120.10) RT 4.75 min

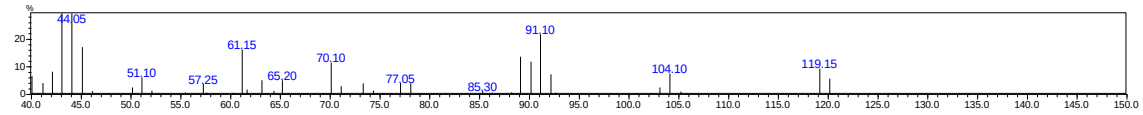

MS analysis of phenyloxirane (m^+/z = 120.15) RT 5.15 min

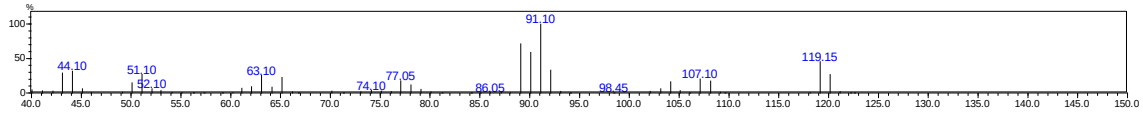

MS analysis of *β*-methylstyrene products

MS analysis of 2-methyl-3-phenyloxirane (m^+/z = 134.0) RT 6.3 min

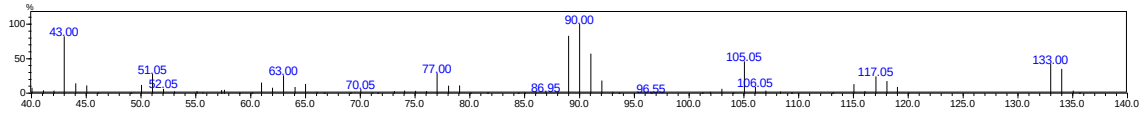

MS analysis of 3-phenyl-2-propen-1-ol (m^+/z = 134.0) RT 11.45 min

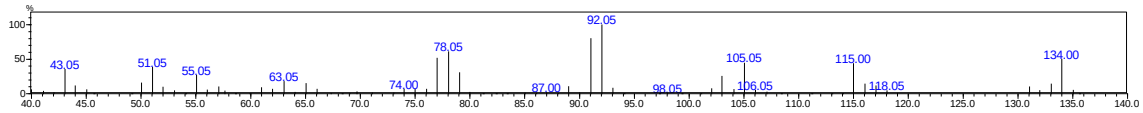

MS analysis of 2-methylstyrene products

MS analysis of minor product (2-methylphenyl)acetaldehyde (m^+/z = 134.0) RT 7.2 min

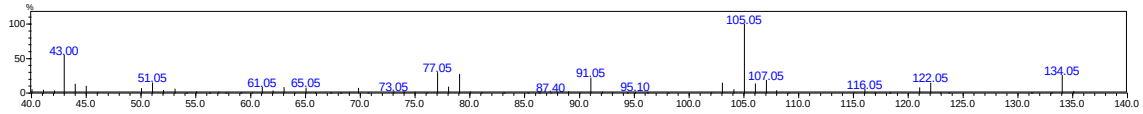

MS analysis of 2-(2-methylphenyl)oxirane (m^+/z = 134.0) RT 7.58 min

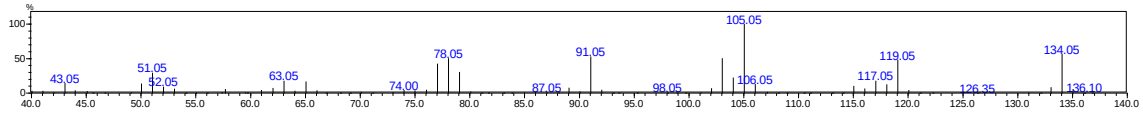

MS analysis of 1-methylnaphthalene product

MS analysis of 1-naphthylmethanol (m^+/z = 158.05) RT 8.7 min

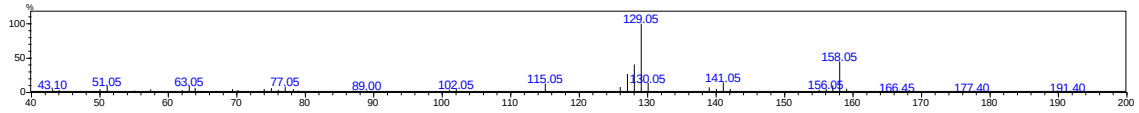

MS analysis of 2-methylnaphthalene product

MS analysis of 2-naphthylmethanol (m^+/z = 158.15) RT 8.9 min

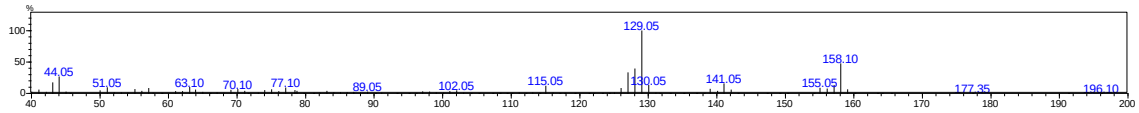

MS analysis of 1,2-dimethylnaphathlene product

MS analysis of (1-methyl-2-naphthyl)methanol (m^+/z = 172.05) RT 10.5 min

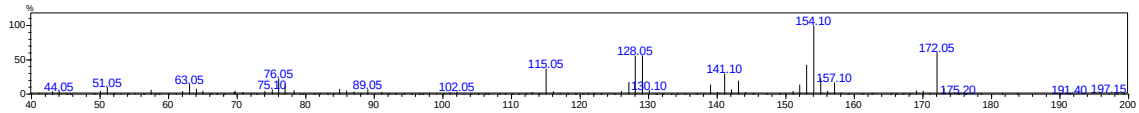

MS analysis of 1,5-dimethylnaphathlene product

MS analysis of (5-methyl-1-naphthyl)methanol (m^+/z = 172.1) RT 10.4 min

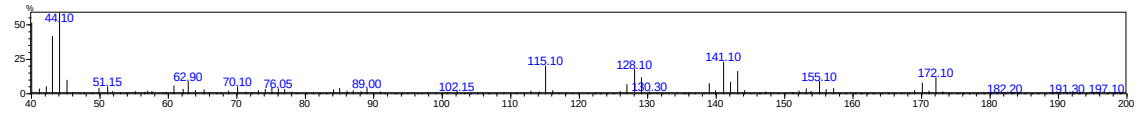

MS analysis of 2,6-dimethylnaphathlene product

MS analysis of (6-methyl-2-naphthyl)methanol (m^+/z = 172.2) RT 10.3 min

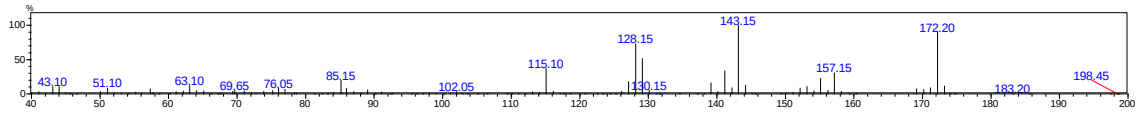

MS analysis of 2,7-dimethylnaphathlene product

MS analysis of 2-(7-methylnaphthyl)methanol (m^+/z = 172.15) RT 10.2 min

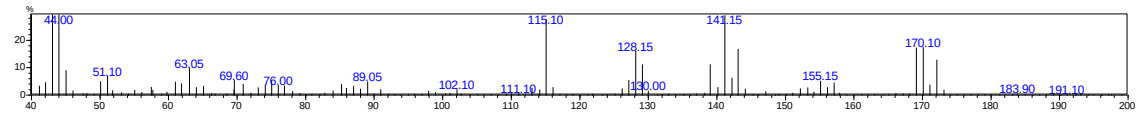

MS analysis of acenaphthene product

MS analysis of 1-acenaphthol RT 18.8 min (m^+/z = 170.0)

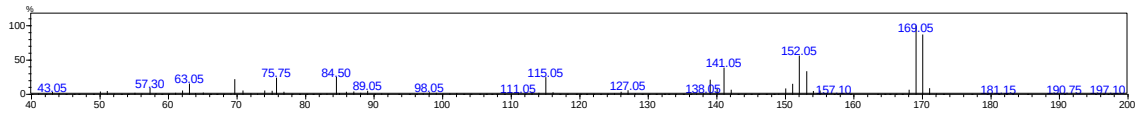

MS analysis of phenylcyclohexane product

MS analysis of *trans*-4-phenylcyclohexanol (m^+/z = 176.15) RT 9.2 min

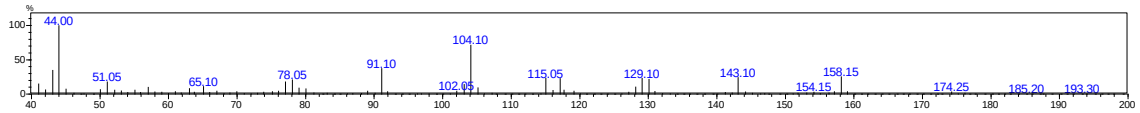

MS analysis of biphenyl product

MS analysis of 4-phenylphenol (m^+/z = 170.15) RT 10.25 min

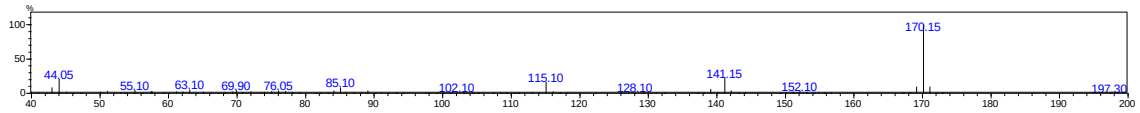

MS analysis of 2-methylbiphenyl product

MS analysis of 2-biphenylmethanol (m^+/z = 184.05) RT 10.0 min

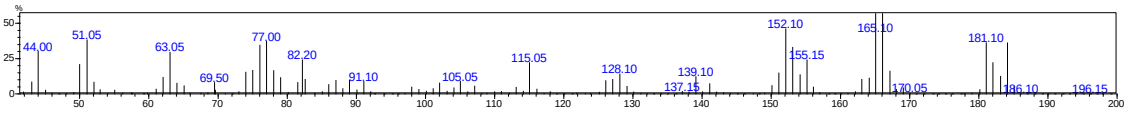

MS analysis of 3-methylbiphenyl products

MS analysis of 3-phenylbenzaldehyde (m^+/z = 182.05) RT 10.1 min

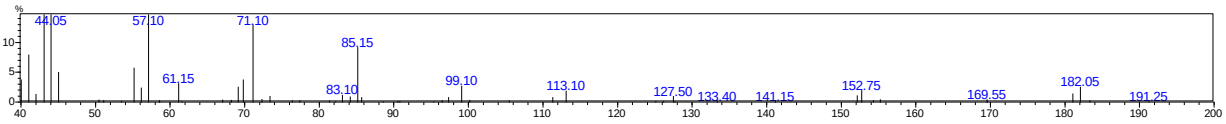

MS analysis of 3-biphenylmethanol (m^+/z = 184.10) RT 11.1 min

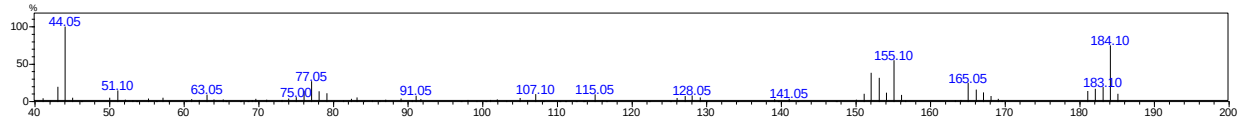

MS analysis of 4-methylbiphenyl product

MS analysis of 4-biphenylmethanol RT 11.25 min (m^+/z = 184.10; RT 16.1 in HPLC)

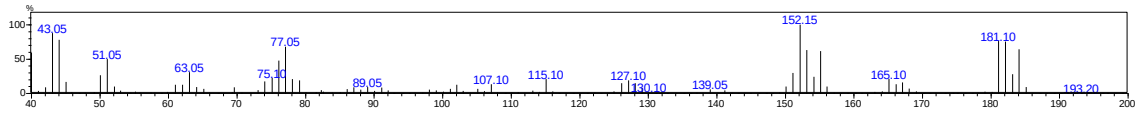

MS analysis of 4`-(4-methylphenyl)phenol RT 11.75 min (m^+/z = 184.15; RT 18.2 in HPLC)

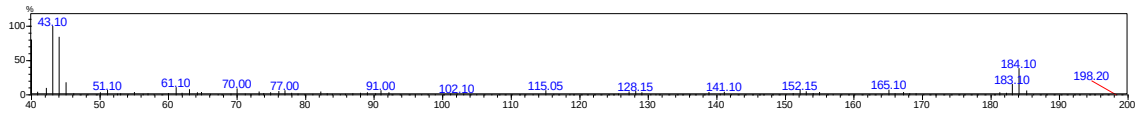

NMR Analysis

Data for (2-ethylphenyl)methanol:

^{1}H NMR (500 MHz, DMSO-d$_6$) δ 7.35 (d, J = 6.6 Hz, 1H, H6), 7.24 (d, J = 7.6 Hz, 1H, H3) 7.18-7.12 (m, 2H, H4 & H5), 4.52 (s, 2H, 2xH9), 2.60 (*q*, J = 7.9 Hz, 2H, 2xH7), 1.14 (*t*, J = 7.9 Hz, 3H, 3xH8).

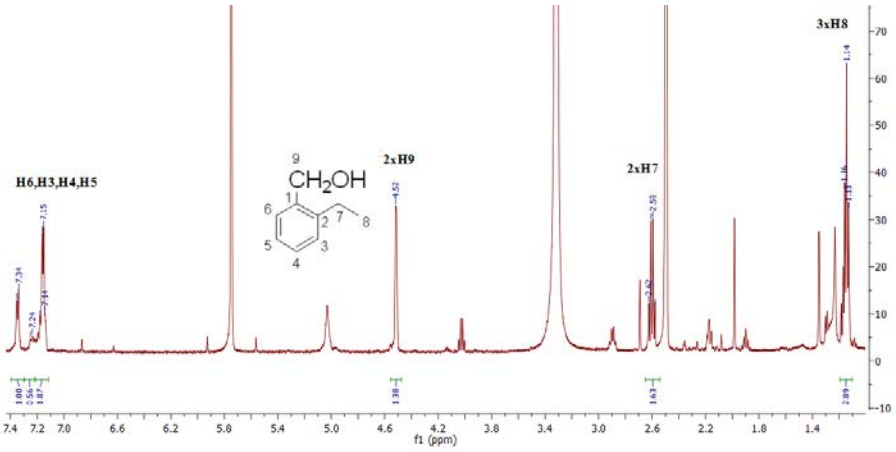

Figure D. 2 ^{1}H NMR of (2-ethylphenyl)methanol (DMSO-d$_6$). The characteristic singlet peak at 4.52 ppm indicated the hydroxylation took place at methyl group. There is a small amount of impurity also present either in the NMR sample or in the NMR solvent (DMSO).

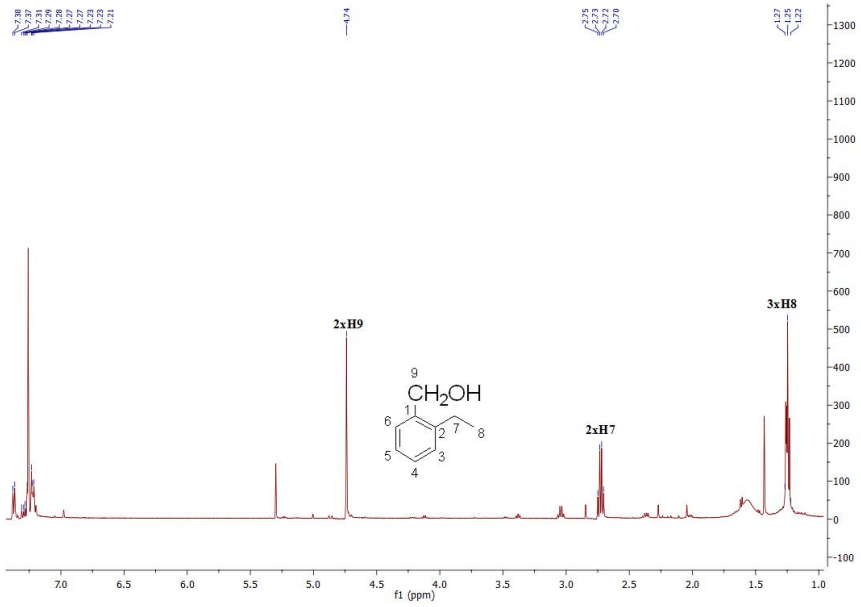

Figure D. 3 ^{1}H NMR spectrum of (2-ethylphenyl)methanol (500 MHz, CDCl$_3$). The peak at 4.74 ppm indicated hydroxylation occurred at methyl group (C9). There is a small amount of impurity present in the NMR sample.

Data for 1-(3-methylphenyl)ethanol:

^{1}H NMR (500 MHz, $CDCl_3$) δ 7.23 (d, J = 7.5 Hz, 1H, H6) 7.20 (s, 1H, H2), 7.17 (d, J = 7.5 Hz, 1H, H5), 7.09 (d, J = 7.4 Hz, 1H, H4), 4.87 (*q*, J = 6.5 Hz, 1H, H7), 2.36 (s, 3H, 3xH9), 1.49 (d, J = 6.5 Hz, 3H, 3xH8).

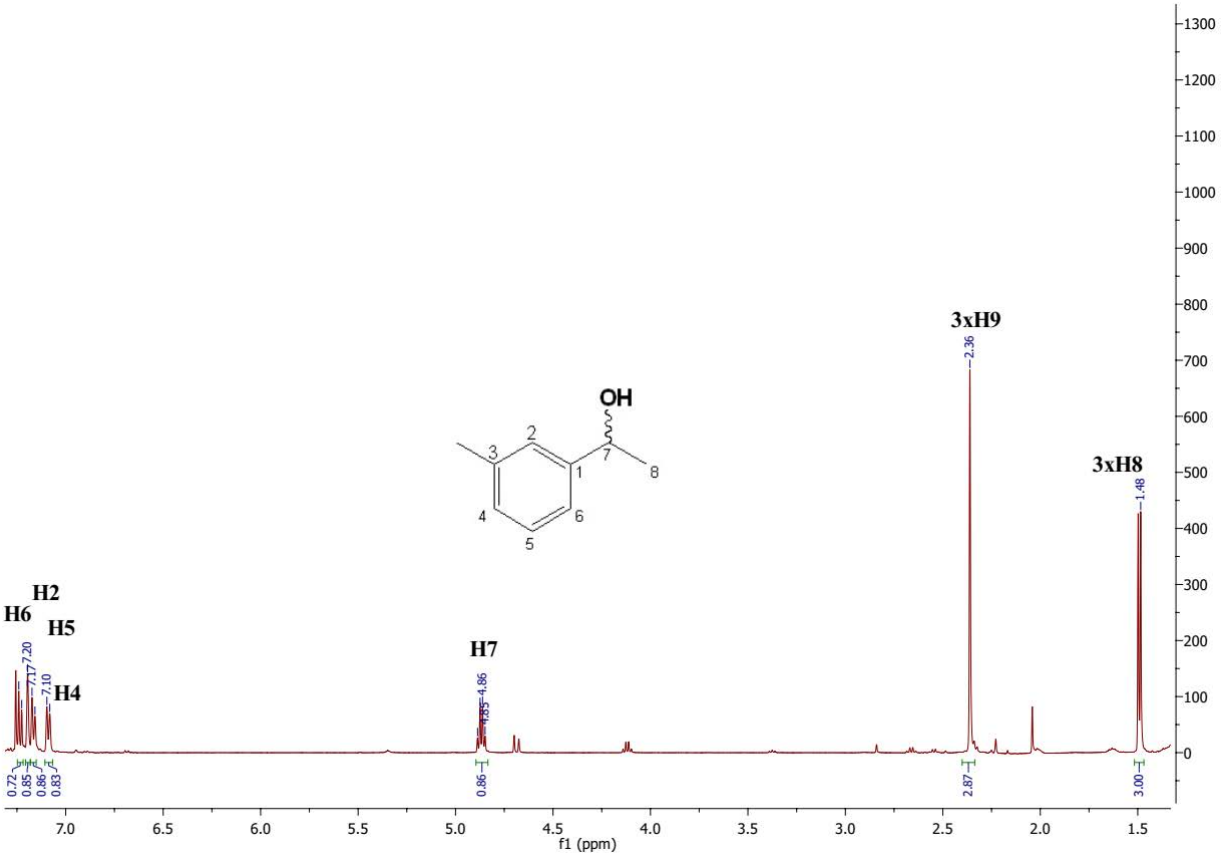

Figure D. 4 ^{1}H NMR spectrum of 1-(3-methylphenyl)ethanol [267].

Data for 2-ethyl-4-methylphenol:

^{1}H NMR (500 MHz, $CDCl_3$) δ 6.94 (s, 1H, H3), 6.89 (d, J = 8.1 Hz, 1H, H6), 6.68 (d, J = 8.1 Hz, 1H, H5), 2.54 (q, J = 7.6 Hz, 2H, 2xH7), 2.22 (s, 3H, 3xH9), 1.18 (t, J = 7.6 Hz, 3H, 3xH8).

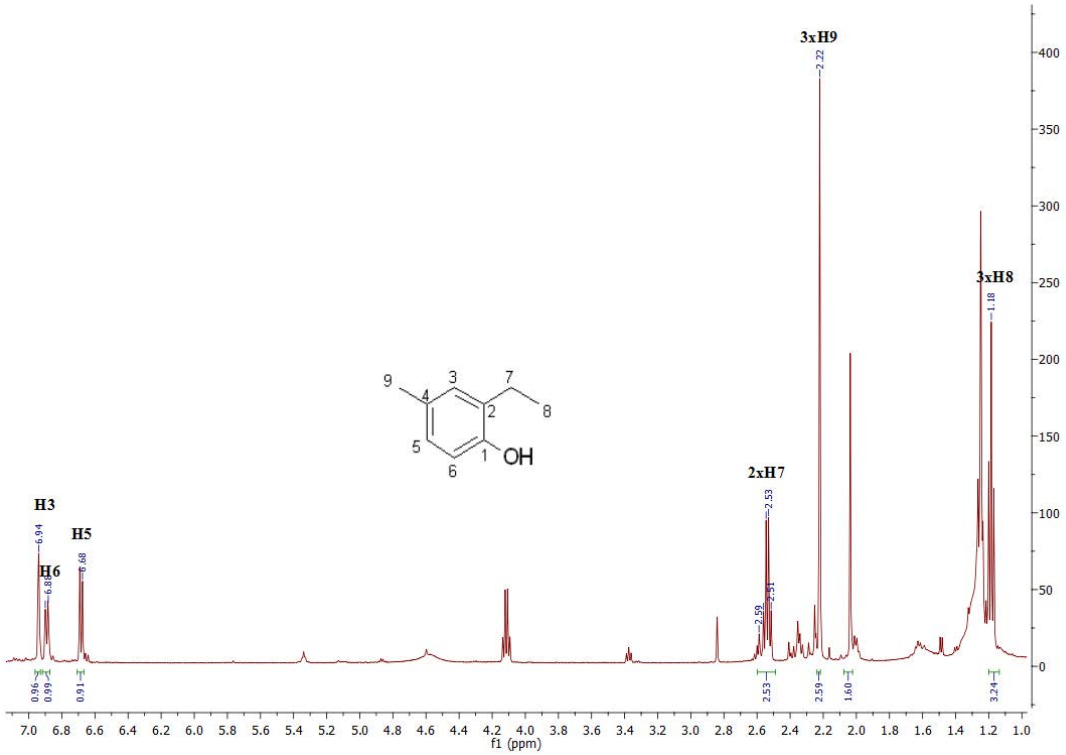

Figure D. 5 ^{1}H NMR spectrum of 2-ethyl-4-methylphenol [267]. A small amount of impurity was also present in the NMR sample.

Data for (1-methyl-2-naphthyl)methanol:

^{1}H NMR (500 MHz, $CDCl_3$) δ 8.08 (d, J = 8.6 Hz, 1H, H5), 7.83 (d, J = 8.8 Hz, 1H, H4), 7.72 (d, J = 8.4 Hz, 1H, H8), 7.54-7.45 (m, 3H, H3, H6 & H7), 4.91 (s, 2H, 2xH12), 2.71 (s, 3H, 3xH11).

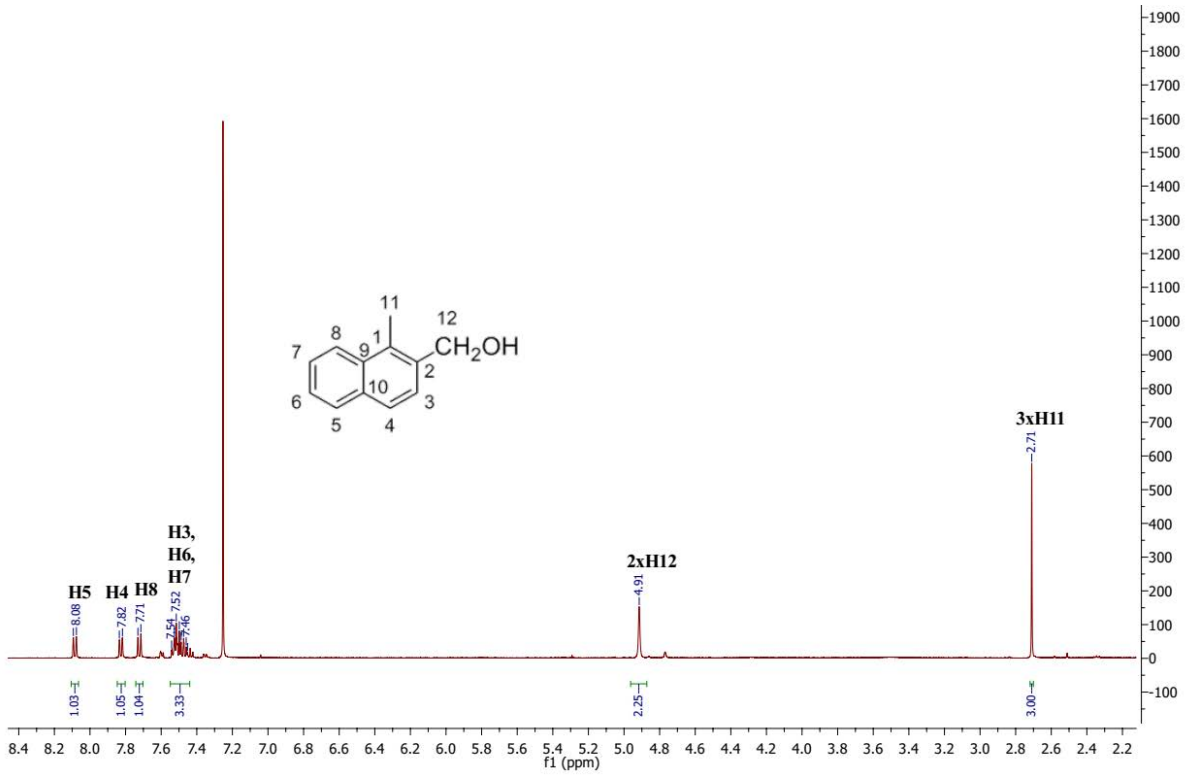

Figure D. 6 ^{1}H NMR spectrum of (1-methyl-2-naphthyl)methanol [315].

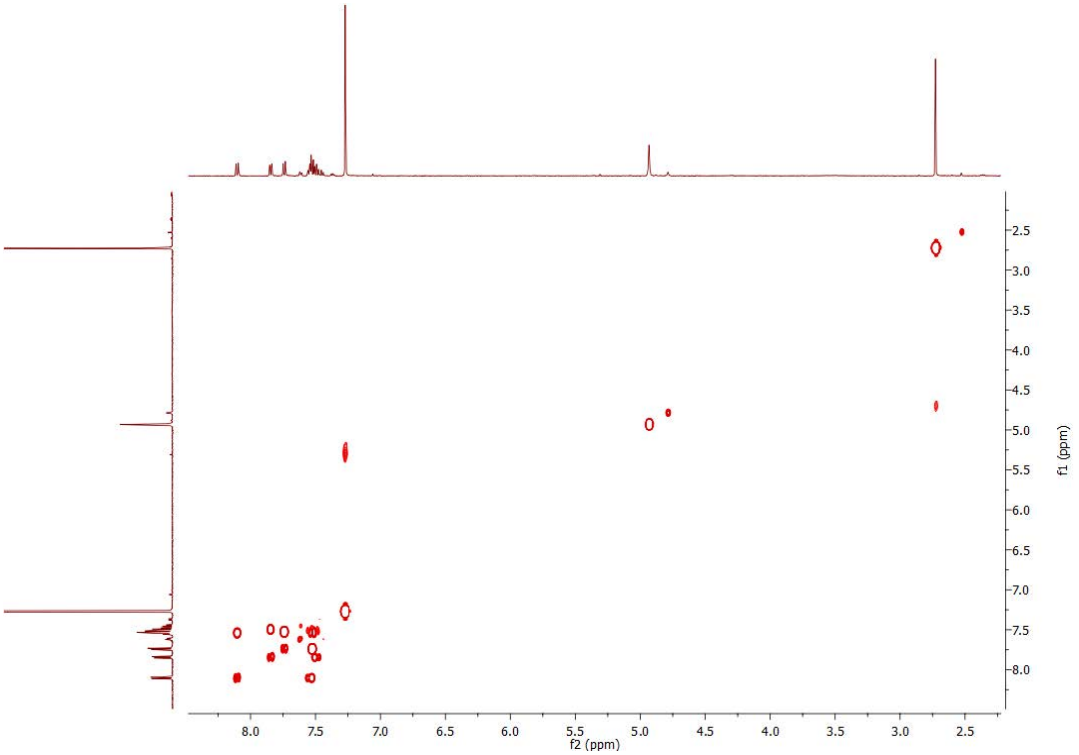

(a)

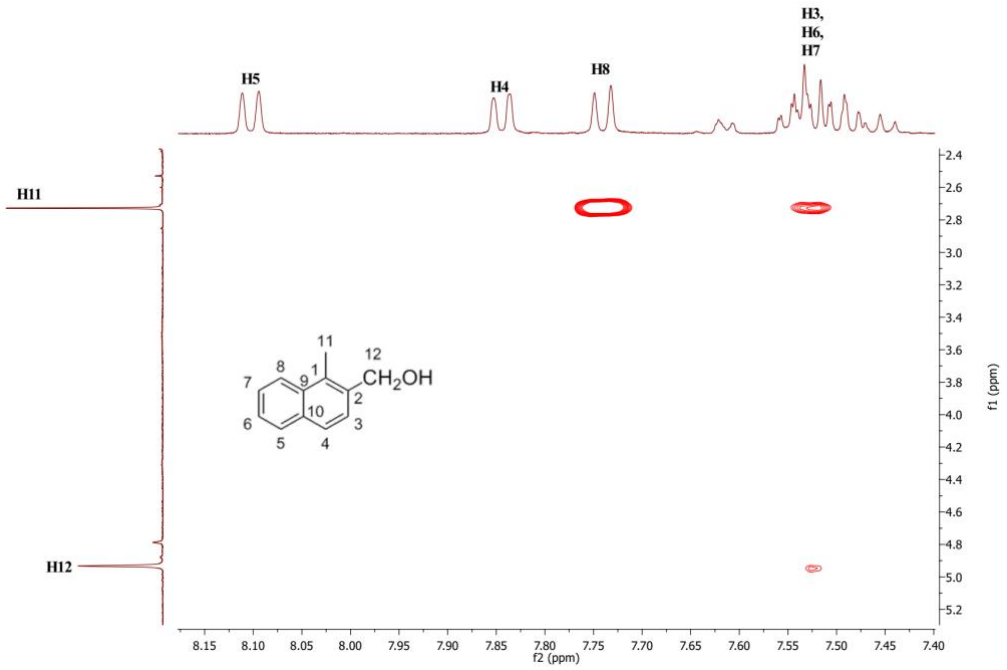

(b)

Figure D. 7 (a) gCOSY NMR spectrum of (1-methyl-2-naphthyl)methanol. **(b)** Zoomed in gCOSY NMR spectrum to highlight the interaction of H11 with H8.

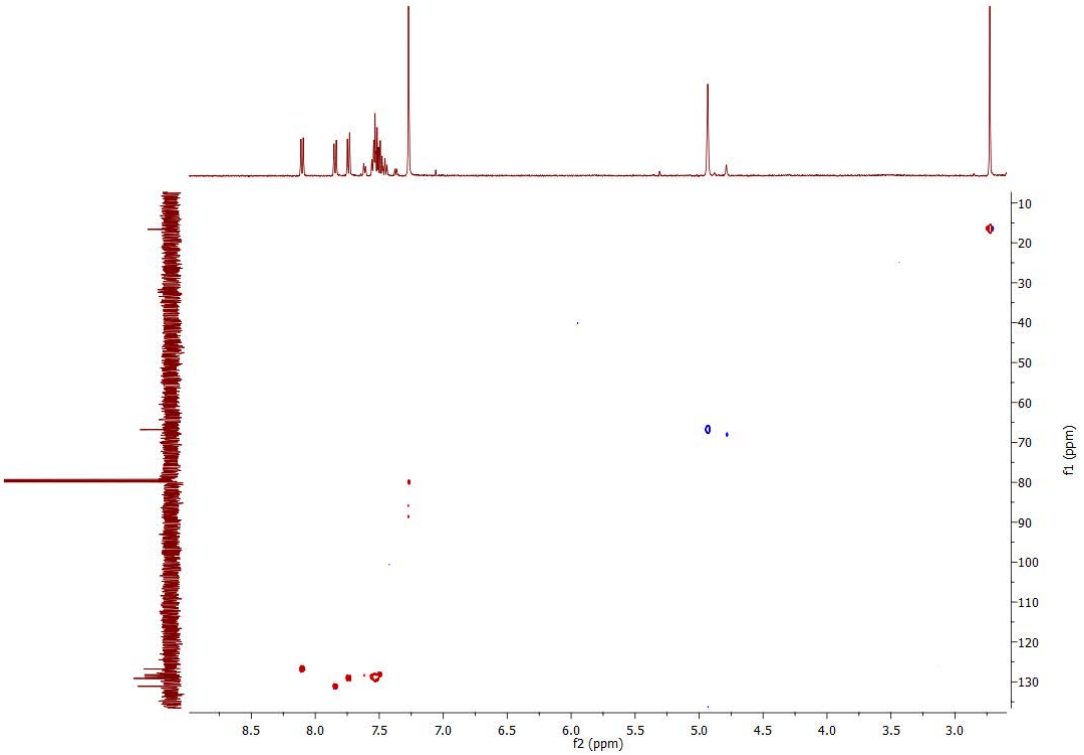

Figure D. 8 HSQC NMR spectrum of (1-methyl-2-naphthyl)methanol.

Data for (5-methyl-1-naphthyl)methanol:

^{1}H NMR (500 MHz, $CDCl_3$) δ 8.02 (d, J = 8.5 Hz, 2H, H4 & H8), 7.56 (d, J = 6.9 Hz, 1H, H2), 7.53-7.43 (m, 2H, H3 & H7), 7.37 (d, J = 7.6 Hz, 1H, H6), 5.18 (s, 2H, 2xH11), 2.73 (s, 3H, 3xH12).

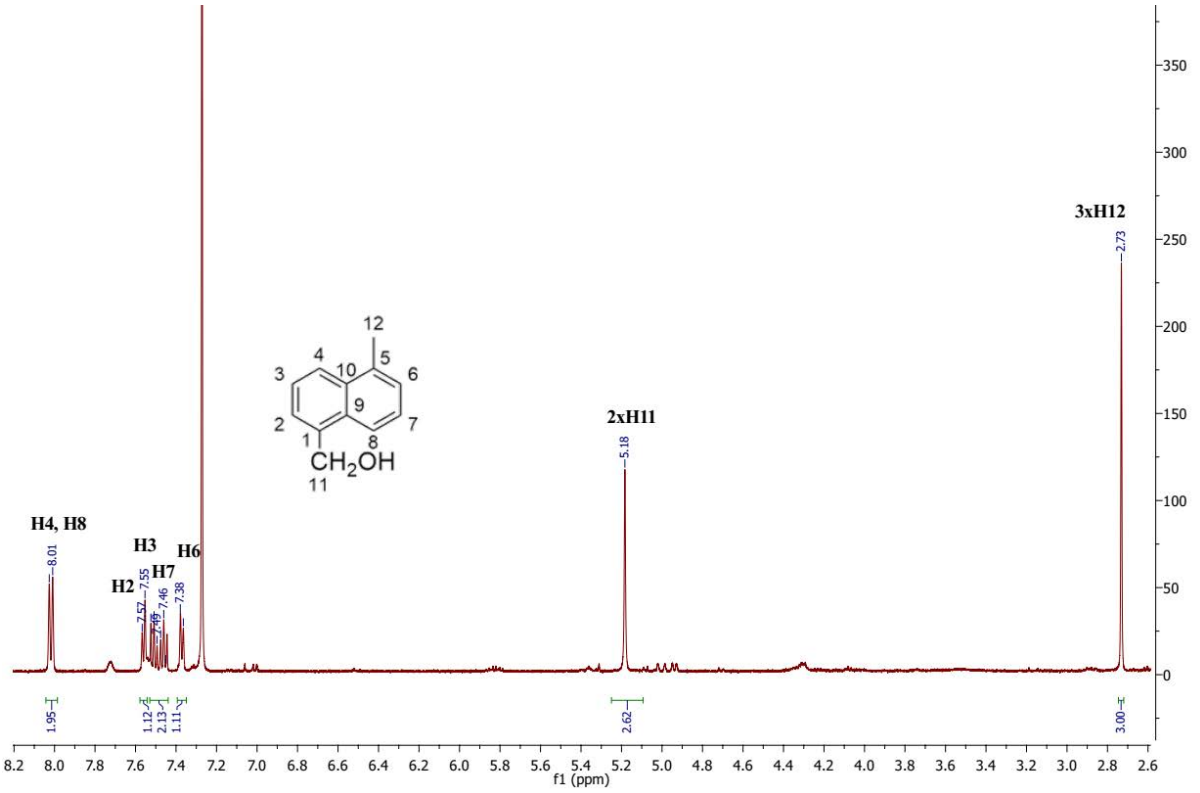

Figure D. 9 ^{1}H NMR spectrum of (5-methyl-1-naphthyl)methanol.

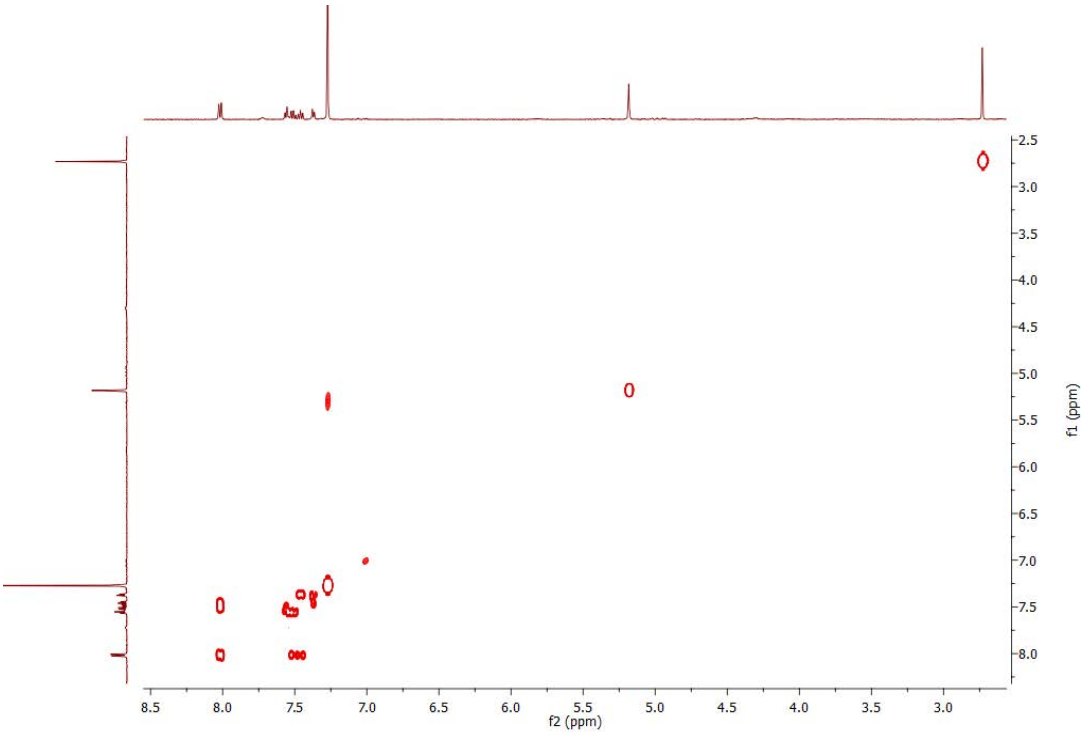

Figure D. 10 gCOSY NMR spectrum of (5-methyl-1-naphthyl)methanol.

Data for (6-methyl-2-naphthyl)methanol:

^{1}H NMR (500 MHz, $CDCl_3$) δ 7.78 (s, 1H, H1), 7.76 (*d*, *J* = 3.1 Hz, 1H, H8), 7.75-7.73 (m, 1H, H4), 7.62 (s, 1H, H1, H5), 7.46 (*dd*, *J* = 8.3, 1.6 Hz, 1H, H7), 7.34 (*dd*, *J* = 8.3, 1.5 Hz, 1H, H3), 4.85 (m, 2H, 2xH11), 2.53 (s, 3H, 3xH12).

^{13}C NMR (126 MHz, $CDCl_3$) δ 140.02 (C9), 138.25 (C10), 135.83 (C2), 134.24 (C6), 131.13 (C3), 130.37 (C8), 130.33 (C4), 129.36 (C5), 127.98 (C7), 127.92 (C1), 68.27 (C11), 24.36 (C12).

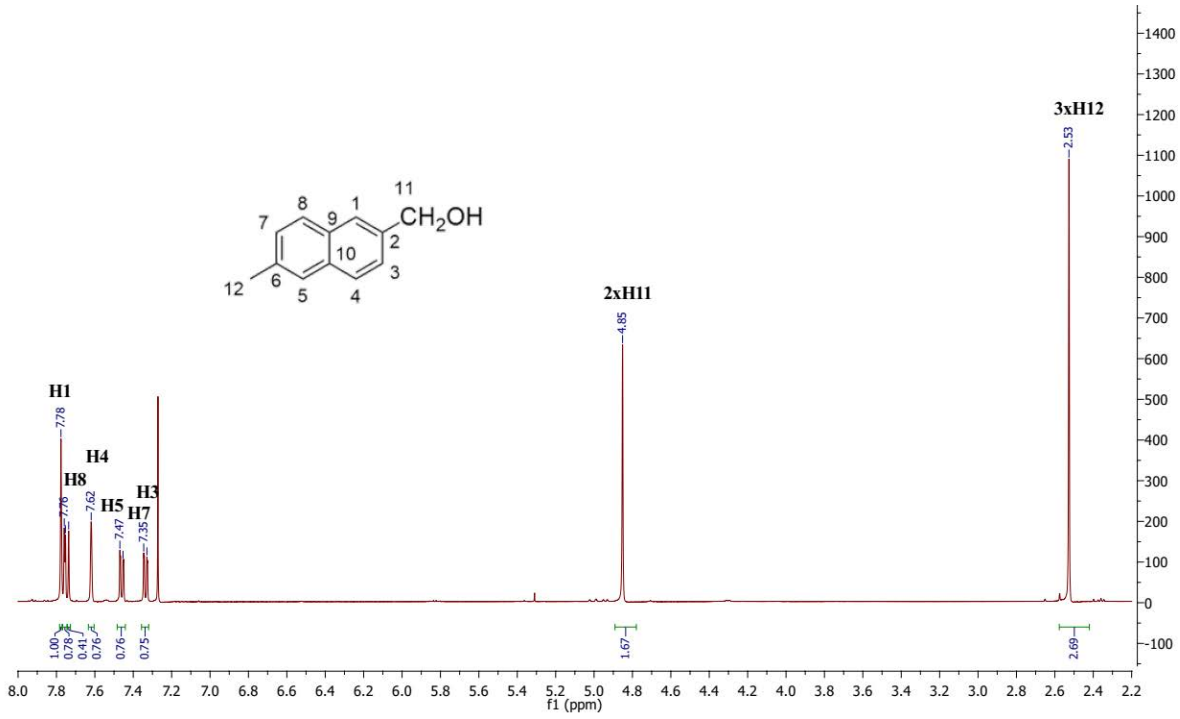

Figure D. 11 ^{1}H NMR spectrum of (6-methyl-2-naphthyl)methanol.

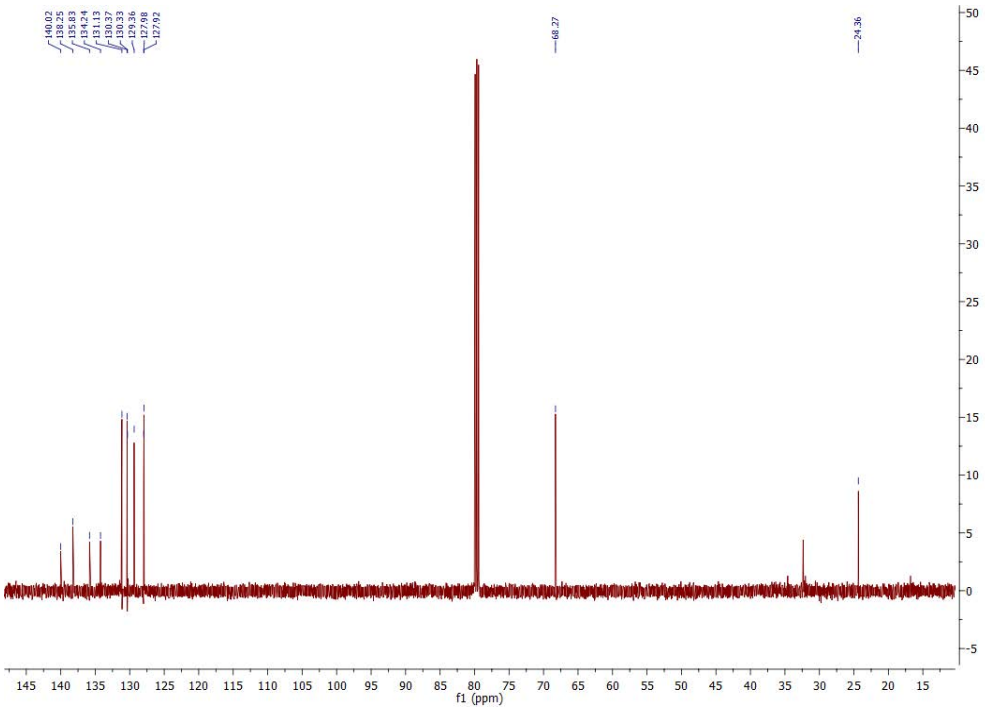

Figure D. 12 ^{13}C NMR spectrum of (6-methyl-2-naphthyl)methanol.

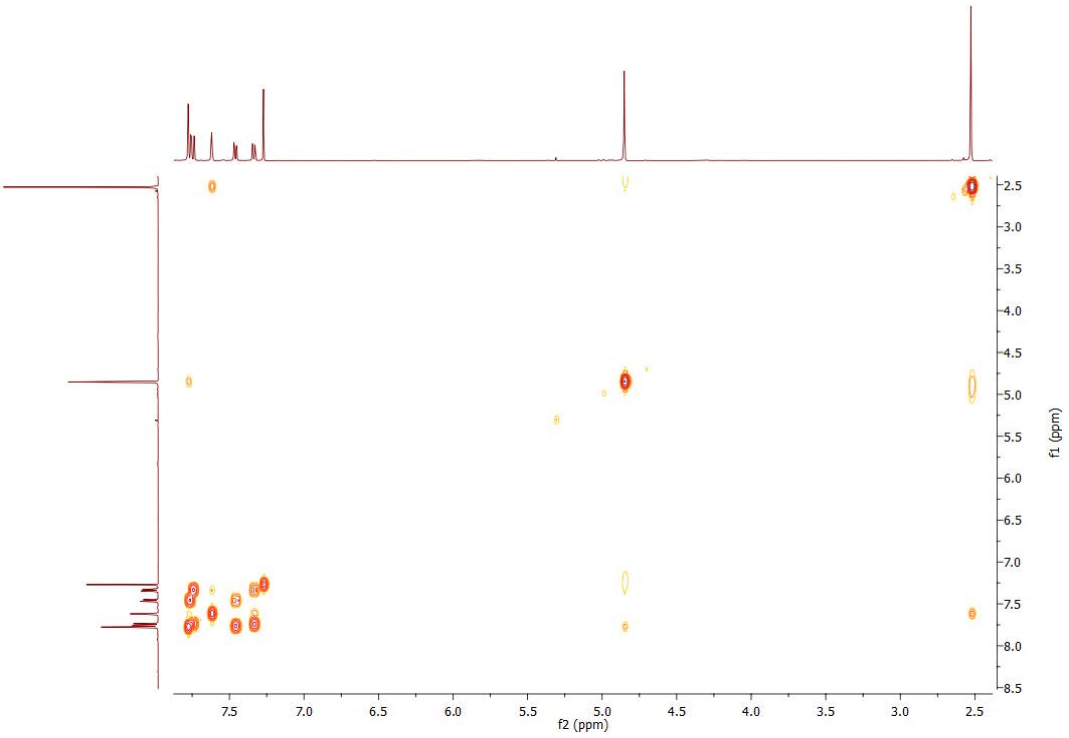

Figure D. 13 gCOSY NMR spectrum of (6-methyl-2-naphthyl)methanol.

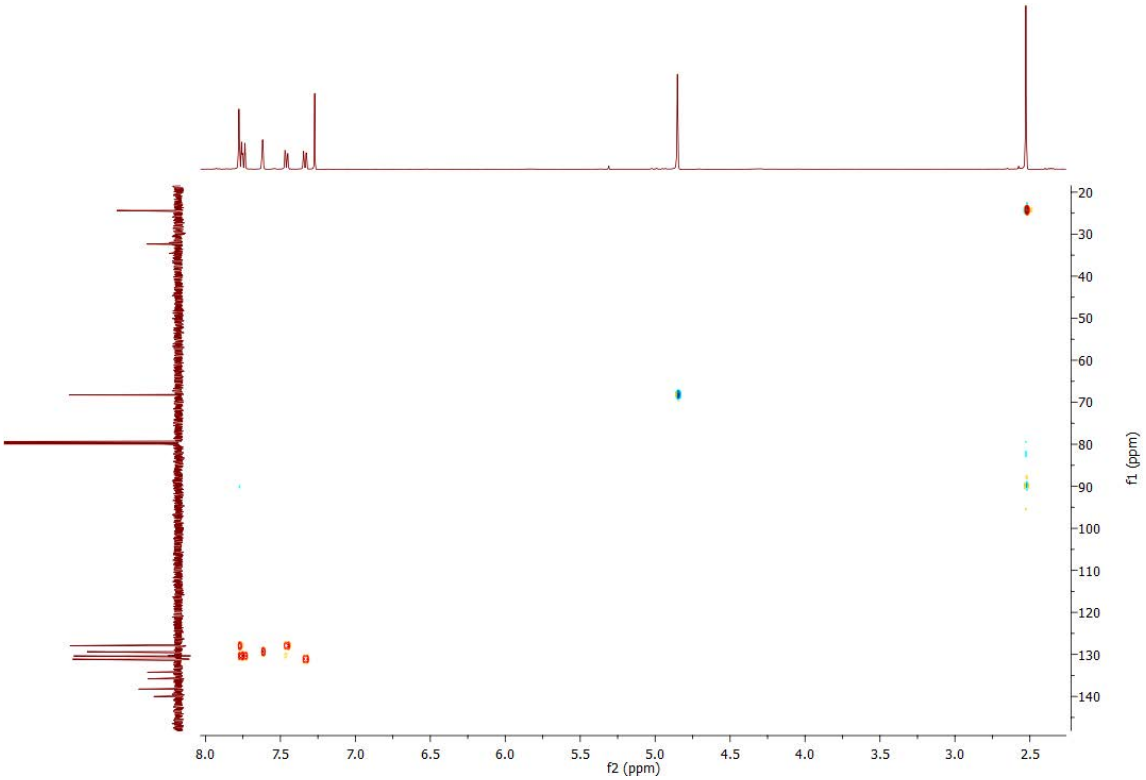

Figure D. 14 HSQC NMR spectrum of (6-methyl-2-naphthyl)methanol.

Data for 2-(7-methylnaphthyl)methanol [266]:

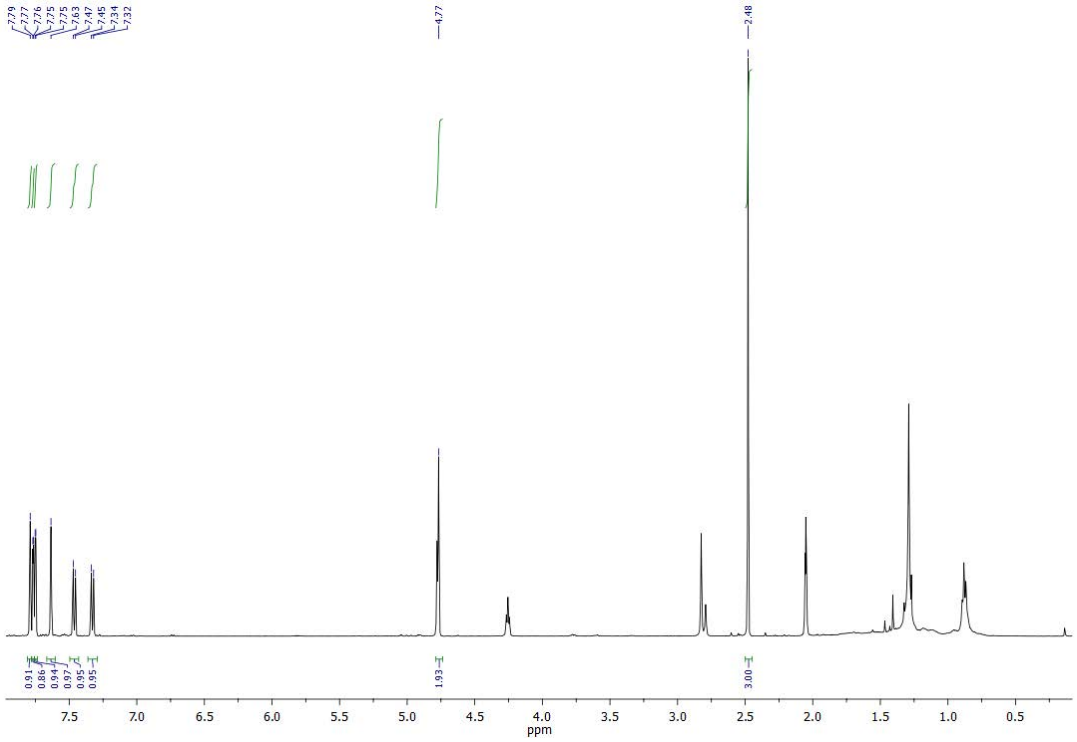

Figure D. 15 ^{1}H NMR spectrum of 2-(7-methylnaphthyl)methanol.

Data for 1-acenaphthol:

^{1}H NMR (500 MHz, $CDCl_3$) δ 7.76 -7.74 (m, 1H, H6), 7.66 (d, J = 8.2 Hz, 1H, H8), 7.58-7.53 (m, 2H, H5 & H10), 7.49 (dd, J = 15.1, 7.0 Hz, 1H, H9), 7.31 (d, J = 6.8 Hz, 1H, H4), 5.75 (d, J = 7.5 Hz, 1H, H1), 3.82 (dd, J = 17.9, 7.5 Hz, 1H, H2), 3.26 (d, J = 17.8 Hz, 1H, H2).

^{13}C NMR (126 MHz, $CDCl_3$) δ 148.34 (C11), 144.19 (C3), 139.81 (C12), 133.86 (C7), 130.88 (C9), 130.69 (C5), 127.67 (C6), 125.39 (C8), 122.95 (C10), 122.51 (C4), 77.09 (C1), 44.59 (C2).

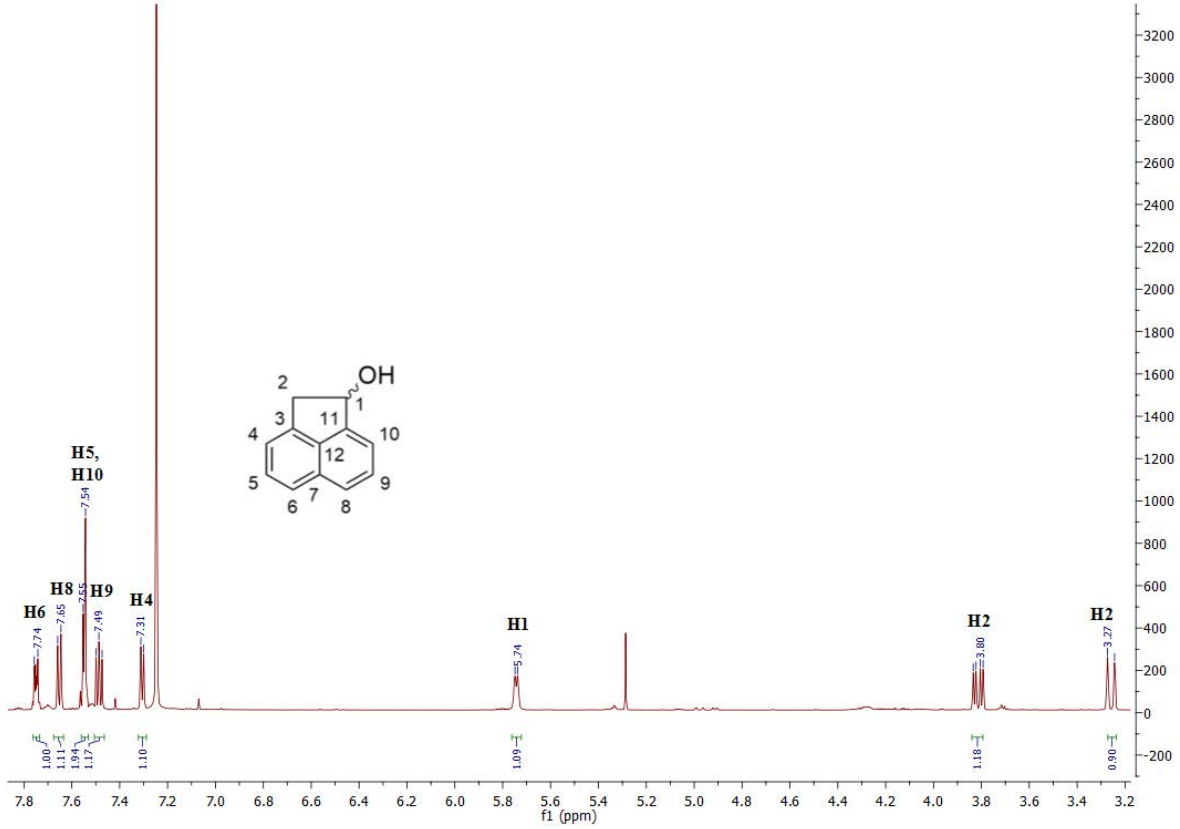

Figure D. 16 ^{1}H NMR spectrum of 1-acenaphthol.

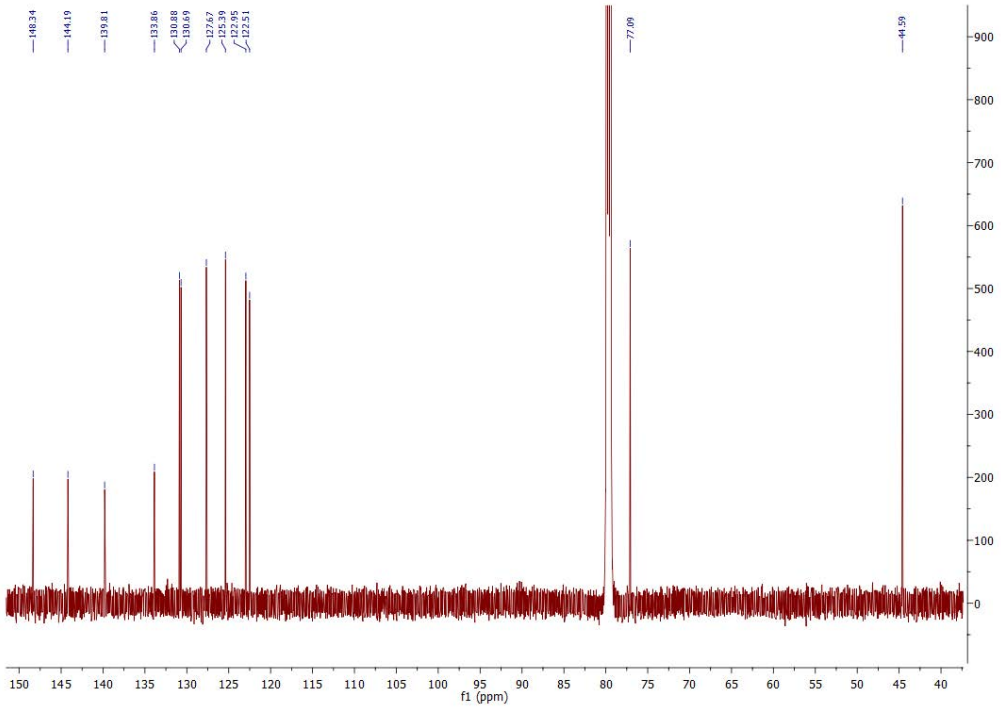

Figure D. 17 ^{13}C spectrum NMR of 1-acenaphthol.

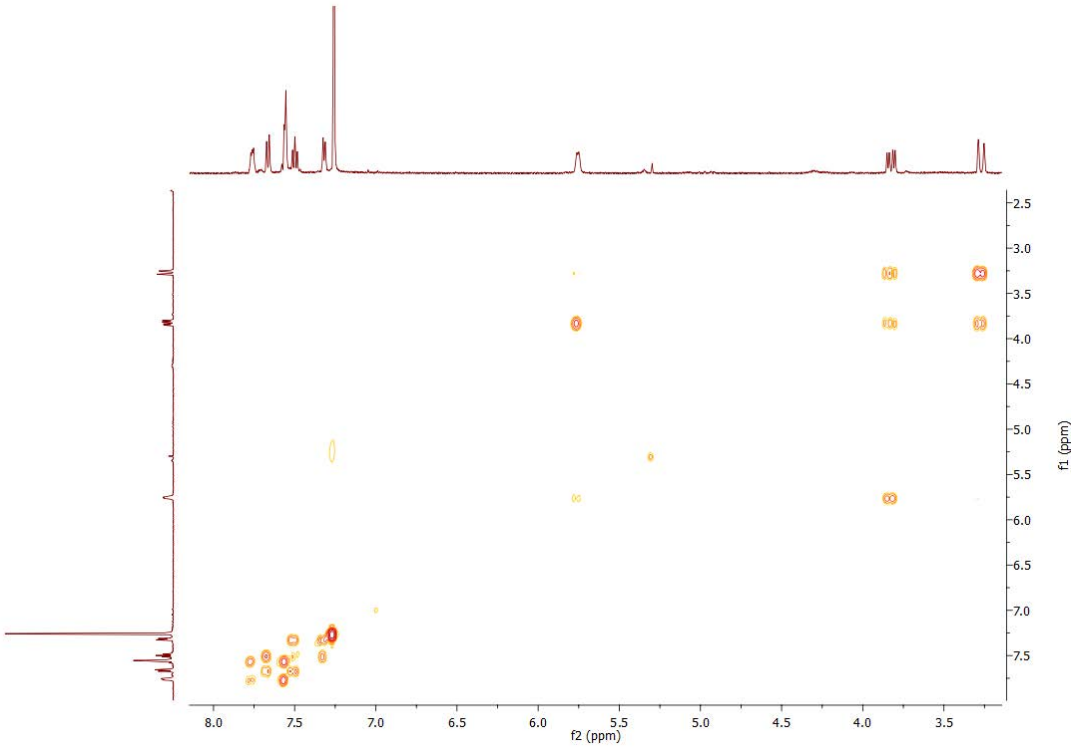

Figure D. 18 gCOSY NMR spectrum of 1-acenaphthol.

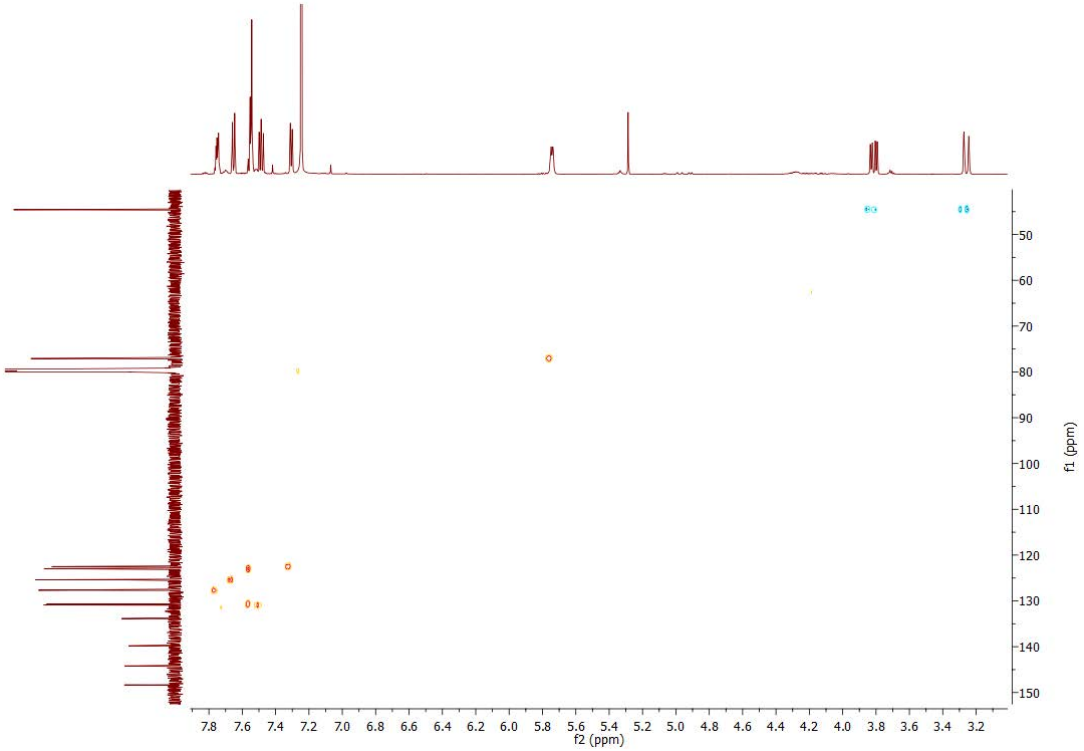

Figure D. 19 HSQC NMR spectrum of 1-acenaphthol.

Data for 3-biphenylmethanol [233, 266]:

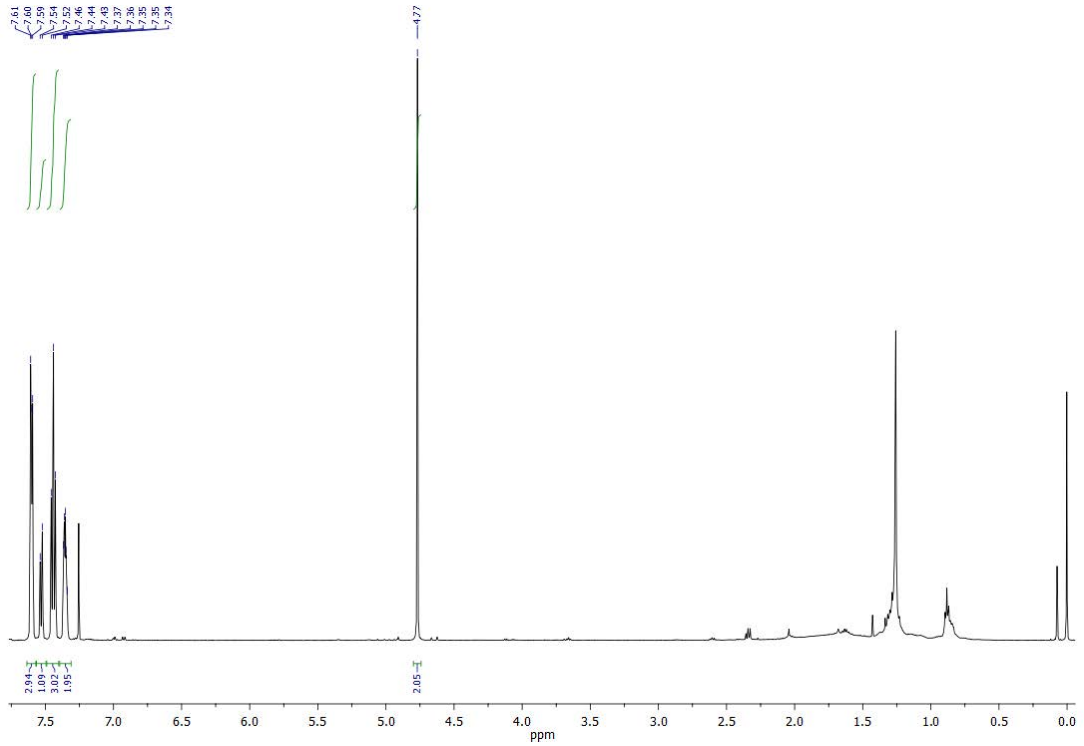

Figure D. 20 ^{1}H NMR spectrum of 3-biphenylmethanol.

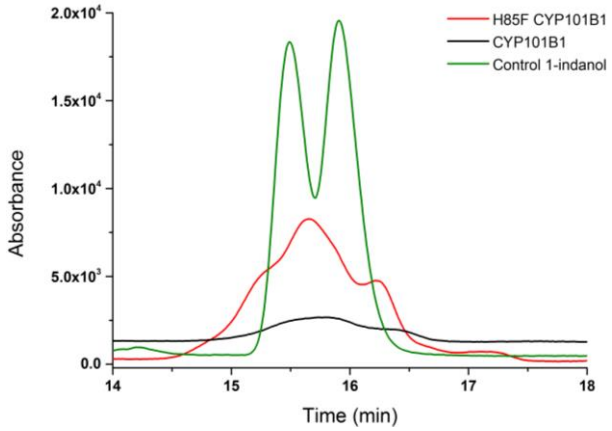

Figure D. 21 Chiral HPLC analysis of the *in vitro* turnovers of CYP101B1 and H85F CYP101B1 with indane, and a racemic mixture of enantiomers was detected.

Appendix E Supplementary Data for Chapter 6

Figure E.1 General Experimental – Synthesis 480
E. 2 Summary Schemes **481**
2.1 CYP450 Substrates 481
Scheme E.2. 1 Synthesis of 4-methylcubane CYP450 probes. 481
Scheme E.2. 2 Synthesis of 4-ethylcubane-1-methoxy carbonyl. 481
2.2 CYP450 Alcohol Standards 481
Scheme E.2. 3 Synthesis of alcohol product standards 481
2.3 Barton-McCombie Deoxygenation 481
Scheme E.2. 4 Barton-McCombie deoxygenation of imidazole thiocarbamate ester. 482
Scheme E.2. 5 Barton-McCombie deoxygenation of xanthate ester 482
Scheme E.2. 6 Barton Decarboxylation of thiohydroxamate ester. 482
E. 3 Experimental Procedures - Synthesis **482**
3.1 4-Methylcubane CYP450 Substrates 483
E. 4 Barton-McCombie Deoxygenation 493
E. 5 Barton Decarboxylation 495
Figure E. 6 The GC-MS analysis of the turnover of 4-(2-hydroxyethyl)cubane-1-methoxy carbonyl by CYP101B1. 498
Figure E. 7 MS analysis of the substrates and products of the cubanes. 498
Figure E. 8 Zoomed in (3.2 to 4.7 ppm region) ^{1}H NMR of 4-hydroxymethylcubane-1-methoxy carbonyl 504
Figure E. 9 ^{1}H NMR of 4-hydroxymethylcubane-1-methoxy carbonyl 505
Figure E. 10 Zoomed in ^{1}H NMR of 4-hydroxymethylcubane-1-acetic acid methyl ester 506
Figure E. 11 1H NMR of 4-hydroxymethylcubane-1-acetic acid methyl ester 506
Figure E. 12 13C NMR of 4-hydroxymethylcubane-1-acetic acid methyl ester 507
Figure E. 13 HSQC NMR of 4-hydroxymethylcubane-1-acetic acid methyl ester 507

Figure E.1 General Experimental – Synthesis (All this synthetic work was performed and written (Page 479-496) by Sevan D. Houston (University of Queensland)).

NMR spectra were recorded under standard conditions (unless stated otherwise) using Bruker AV 500, 400 and 300 MHz or Bruker AS 500 spectrometers and were referenced using residual monoprotic solvent peaks (e.g. $CDCl_3$, C_6D_6 etc.) [353]. Coupling constants (*J*) are quoted to the nearest 0.1 Hz. The following abbreviations are used to report multiplicities: s = singlet, d = doublet, *t* = triplet, *q* = quartet, m = multiplet, quin = quintet, sext = sextet, sep = septet, br = broad. High-resolution ESI mass spectra were recorded using a Bruker MicroTOF-Q (quadrupole-Time of Flight) with a Bruker ESI source. IR spectra were recorded using a Perkin-Elmer 400 FTIR spectrometer. Samples were run either as neat oils or solids. Melting points were determined using a Digimelt MPA 160 melting point apparatus and are reported uncorrected. Crystallographic data were collected at 190 K on an Oxford Diffraction Gemini Ultra S CCD diffractometer employing graphite monochromated Mo-Kα radiation (0.71073 Å) in the range $2 < 2\theta < 50°$. Flash column chromatography was run using Merck silica gel 60 (230–400 mesh). Fractions were initially visualised using UV irradiation and subsequently by heating TLC plates exposed to either ceric ammonium molybdate (Goofy's stain) or 10% aqueous potassium permanganate. TLC was performed with Merck silica gel plates, precoated with silica gel 60 F_{254} (0.2 mm). Unless specified otherwise, all reactions were magnetically stirred and performed in oven-dried glassware under a positive pressure of argon (4 Å mol. Sieve/silica drying tube) at ambient room temperature. Solvents were distilled to dryness prior to use based on the methods described by Amarego [354]. Unless stated otherwise commercially available chemicals were used without further purification. 2-Mercaptopyridine *N*-oxide sodium salt was concentrated to dryness, washed with ethyl acetate then dried under high vacuum for 1 h. Diazomethane was freshly prepared from Diazald® with a diazomethane distillation kit.

E. 2 Summary Schemes

2.1 CYP450 Substrates

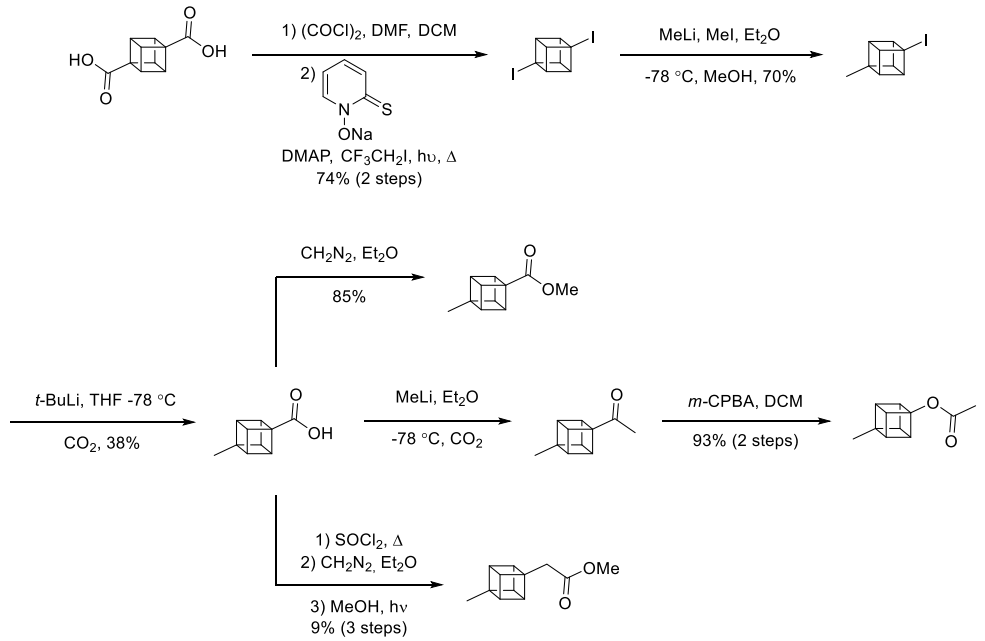

Scheme E.2. 1 Synthesis of 4-methylcubane CYP450 probes.

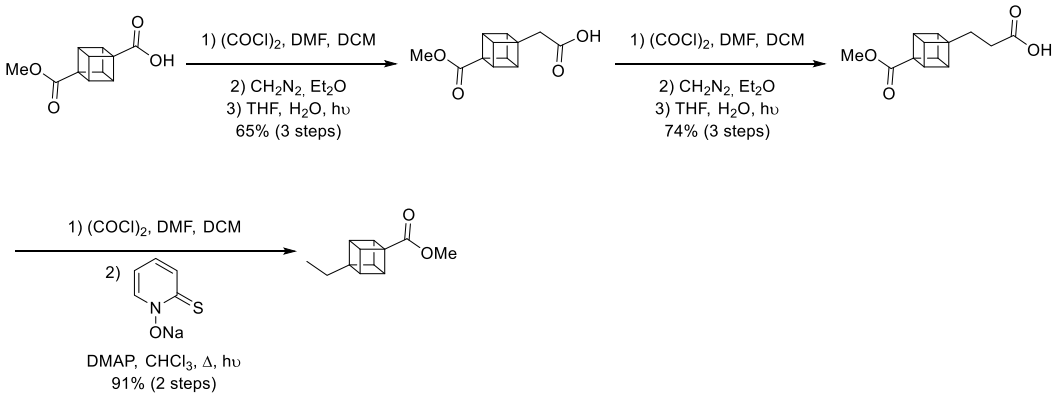

Scheme E.2. 2 Synthesis of 4-ethylcubane-1-methoxy carbonyl.

2.2 CYP450 Alcohol Standards

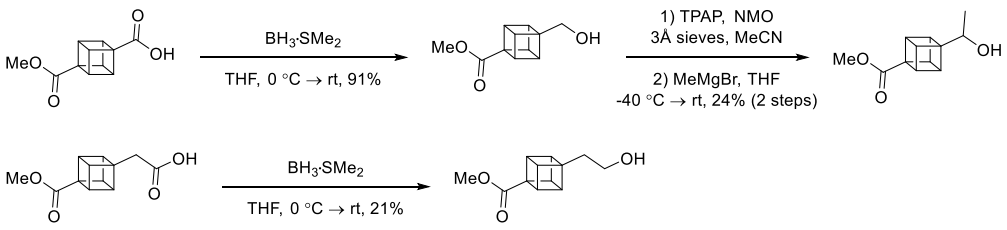

Scheme E.2. 3 Synthesis of alcohol product standards

2.3 Barton-McCombie Deoxygenation

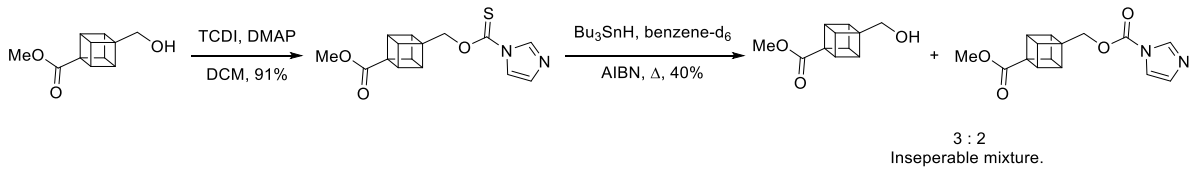

Scheme E.2. 4 Barton-McCombie deoxygenation of imidazole thiocarbamate ester.

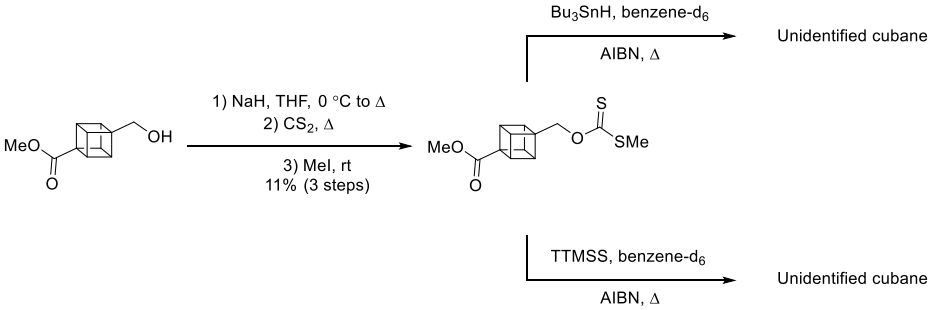

Scheme E.2. 5 Barton-McCombie deoxygenation of xanthate ester

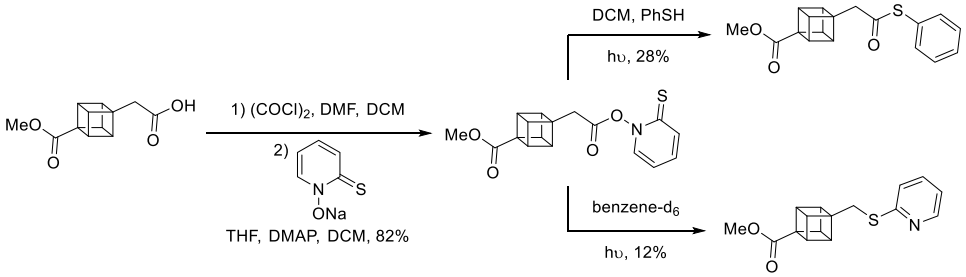

Scheme E.2. 6 Barton Decarboxylation of thiohydroxamate ester.

E. 3 Experimental Procedures - Synthesis

3.1 4-Methylcubane CYP450 Substrates

1,4-Diiodocubane

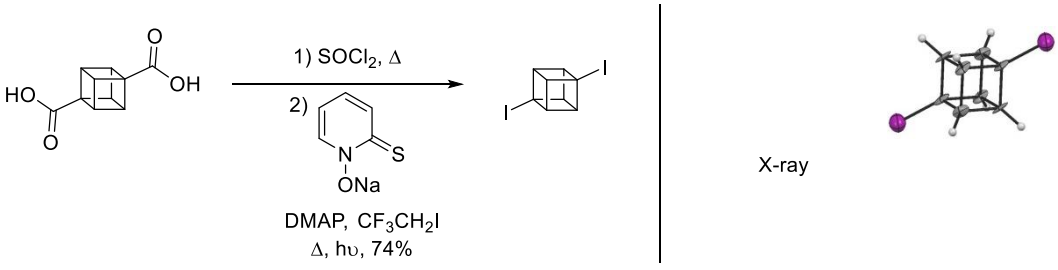

The procedure reported by Tsanaktsidis *et al* [355] was followed. Cubane-1,4-dicarboxylic acid [356] (1.000 g, 5.20 mM) was dissolved in thionyl chloride (10 mL) and heated to reflux for 1h. On cooling to r.t. the mixture was concentrated *in vacuo* and further dried under high vacuum (1 h). Separately, freshly ground 2-mercaptopyridine *N*-oxide sodium salt (2.373 g, 15.91 mM), DMAP (74 mg, 0.14 mM) and 2,2,2-trifluoroiodoethane (2.56 mL, 26.07 mM) were suspended in anhydrous DCM (25 mL) and heated to reflux whilst under irradiation from a 500-W tungsten lamp. The newly formed acid chloride was suspended in anhydrous DCM (25 mL) and added slowly to the refluxing mixture. After refluxing for 2.5 h the cooled suspension was washed with water (50 mL), hydrochloric acid (1 M, 50 mL) and brine (50 mL). The organic phase was then dried over magnesium sulphate and concentrated by distillation at atmospheric pressure. Purification of the crude material was performed by trituration with cold diethyl ether (0 °C, 5 mL), which gave the title compound (1.372 g, 74%) as an off-white solid. Data reported are consistent with Tsanaktsidis *et al.*[356].

^{1}H-NMR (300 MHz, $CDCl_3$) δ_H = 4.40 (s, 6H) ppm.

4-Methylcubane-1-iodide

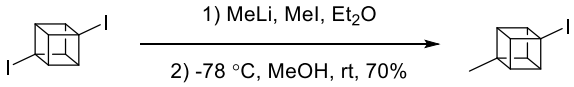

The procedure reported by Eaton *et al* [357] was followed. 1,4-Diiodocubane (1.107 g, 3.11 mM) was suspended in anhydrous diethyl ether (40 mL) together with iodomethane (3.87 mL, 62.2 mM) in a 22 °C water bath. Ethereal methyllithium (1.6 M, 38.9 mL, 62.2 mM) was slowly added dropwise and the suspension stirred for 16 h. The now homogeneous solution was cooled to -78 °C before the addition of methanol (1 mL). The solution was warmed to room temperature, and water (5 mL) was added. The organic phase was separated and washed with hydrochloric acid (1 M, 40 mL). The organic phase was then dried over magnesium sulphate and concentrated by distillation at atmospheric pressure. The crude residue was subjected to column chromatography (pentane) affording the title compound (535 mg, 70%) as a white solid.

^{1}H-NMR (300 MHz, $CDCl_3$) δ_H = 4.19-4.15 (m, 3H), 3.83-3.80 (m, 3H), 1.29 (s, 3H) ppm.

4-Methylcubane-1-carboxylic acid

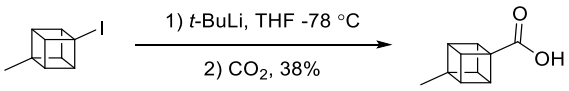

Adapted from the procedure of Eaton *et al*.[358] 4-methylcubane-1-iodide (535 mg, 2.19 mM) was suspended in anhydrous THF (50 mL) at -78 °C under an argon atmosphere. *tert*-Butyl lithium (1.2 M in pentane, 4.93 mL, 5.91 mM) was slowly added dropwise and the solution allowed to stir for 15 min. Separately, carbon dioxide (*ca* 1 L) was bubbled into anhydrous THF (100 mL) at -78 °C under an argon atmosphere. The cubyl lithium solution at -78 °C was transferred dropwise *via* cannula to the cooled carbon dioxide solution over a period of 20 min. [Note: a rapid rate of addition can result in the formation of dicubyl ketone whilst a slow rate of addition can result in decomposition of the cubyllithium]. The reaction mixture was stirred for a further 30 min before warming to room temperature over 30 min. Saturated ammonium chloride (20 mL) was added, and the THF was removed *in vacuo* on a rotary evaporator with the water bath temperature maintained at 25 °C. The remaining aqueous phase was washed with diethyl ether (2 x 20 mL), acidified to pH 1 with aqueous hydrochloric acid (10 M, 1 mL) and then extracted with diethyl ether (6 x 20 mL). The combined organic phases were dried over magnesium sulphate and concentrated *in vacuo*. The crude residue was subjected to column chromatography (50% ethyl acetate/petroleum ether v/v) to give the title compound (136 mg, 38%) as a white solid.

^{1}H-NMR (400 MHz, $CDCl_3$) δ_H = 4.14-4.11 (m, 3H), 3.68-3.65 (m, 3H), 1.28 (s, 3H) ppm.
^{13}C-NMR (100 MHz, $CDCl_3$) δ_C = 178.3, 56.3, 47.6, 46.0, 19.5 ppm.
^{1}H-NMR (500 MHz, C_6D_6) δ_H = 4.03-4.00 (m, 3H), 3.35-3.33 (m, 3H), 0.96 (s, 3H) ppm.
^{13}C-NMR (125 MHz, C_6D_6) δ_C = 179.9, 57.3, 56.6, 48.2, 46.7, 19.8 ppm.

HRMS (ESI): *m/z* calcd for $C_{10}H_{10}O_2Na$ ($[M+Na]^+$): 185.0573, found 185.0570.
FT–IR υ_{max} = 2979, 1675, 1419, 1310, 1226, 939, 734 cm^{-1}.
MP 139.7-140.4 °C.

4-Methylcubane-1-methoxy carbonyl

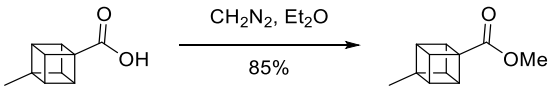

The procedure reported by Klunder *et al* [359] was followed. 4-Methylcubane-1-carboxylic acid (13 mg, 0.080 mM) was stirred in ethereal diazomethane (*ca* 1.2 mL) at r.t. for 30 min. Excess diazomethane was blown off with a stream of argon, and the remaining diethyl ether was

removed by distillation at atmospheric pressure. The crude residue was subjected to column chromatography (20% diethyl ether/pentane v/v), and the pooled fractions containing product were concentrated by distillation at atmospheric pressure to give the title compound (12 mg, 85%) as a white, sweet smelling solid.

^{1}H-NMR (400 MHz, $CDCl_3$) δ_H = 4.10-4.07 (m, 3H), 3.70 (s, 3H), 3.65-3.63 (m, 3H), 1.28 (s, 3H) ppm.
^{13}C-NMR (100 MHz, $CDCl_3$) δ_C = 173.3, 56.6, 56.2, 51.6, 47.5, 46.0, 19.5 ppm.
HRMS (ESI): *m/z* calcd for $C_{11}H_{12}O_2Na$ ($[M+Na]^+$): 199.0730, found 199.0726.
MP 63.1–64.2 °C.

4-Methylcubane-1-methyl ketone

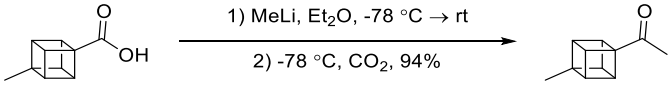

The procedure reported by Choi *et al.* [301] was followed. Methyllithium (1.6 M in diethyl ether, 0.29 mL, 0.462 mM) was added to a solution of 4-methylcubane-1-carboxylic acid (15 mg, 0.092 mM) in anhydrous diethyl ether (2 mL) at -78 °C under an argon atmosphere. The flask was from removed from the cold bath and the white suspension stirred at r.t. After 1.5 h the reaction mixture was re-cooled to -78 °C and then quenched with dry ice (*ca* 1 g). On warming to r.t. over 30 min saturated ammonium chloride (2 mL) was added. The phases were separated, and the aqueous phase washed with diethyl ether (2 x 2 mL). The combined organic phases were dried over magnesium sulphate and concentrated by distillation at atmospheric pressure. The residual oil was used for subsequent reactions without further purification. In a separate experiment, 4-methylcubane-1-carboxylic acid (13 mg, 0.80 mM) was treated in the manner described, but purified by column chromatography (10% diethyl ether/DCM v/v). The pooled fractions containing product were concentrated by distillation at atmospheric pressure to give the title compound (12 mg, 94%) as a colourless, sweet-smelling oil.

^{1}H-NMR (400 MHz, $CDCl_3$) δ_H = 4.12-4.10 (m, 3H), 3.63-3.61 (m, 3H), 2.12 (s, 3H), 1.30 (s, 3H) ppm.
^{13}C-NMR Lit:[301] ($CDCl_3$) δ_C = 207.0, 64.5, 56.4, 46.9, 54.9, 24.6, 19.4 ppm.
HRMS (ESI): *m/z* calcd for $C_{11}H_{13}O$ ($[M+H]^+$): 161.0961, found 161.0959.

4-Methylcuban-1-yl acetate

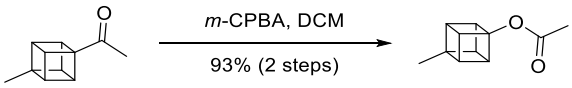

The procedure reported by Choi *et al*.[301] was followed. 4-Methylcubane-1-methyl ketone above was dissolved in DCM (1 mL) at r.t. and *m*-CPBA (77%, 45 mg, 0.18 mM) added in one portion. After 16 h the reaction mixture was diluted with DCM (4 mL) and then washed with saturated sodium carbonate (2 x 5 mL), water (5 mL) and brine (5 mL). The organic phase was dried over magnesium sulphate and concentrated by distillation at atmospheric pressure. The crude residue was subjected to column chromatography (20% diethyl ether/pentane v/v), and the pooled fractions containing product were concentrated by distillation at atmospheric pressure to give the title compound (15 mg, 93% over 2 steps) as a colourless, sweet-smelling oil.

^{1}H-NMR	(400 MHz, $CDCl_3$) δ_H 4.12-4.09 (m, 3H), 3.55-3.52 (m, 3H), 2.08 (s, 3H), 1.27 (s, 3H) ppm.
^{13}C-NMR	Lit:[301] ($CDCl_3$) δ_C = 169.3, 89.0, 55.7, 50.9, 44.1, 21.0, 19.4 ppm.
HRMS	(ESI): *m/z* calcd for $C_{11}H_{12}O_2Na$ ($[M+Na]^+$): 199.0730, found 199.0727.

4-Methylcubane-1-acetic acid methyl ester

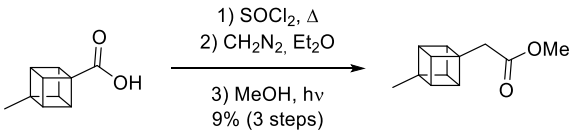

The procedure reported by Klunder *et al*. [359] was followed. 4-Methylcubane-1-carboxylic acid (23 mg, 0.14 mM) was dissolved in thionyl chloride (10 mL) and heated to reflux for 1h under an argon atmosphere. The thionyl chloride was removed *in vacuo* (70 °C, 200 torr) to leave a brown coloured oil. The remainder of this sequence should be performed behind a blast shield. To the resulting acid chloride was cautiously added ethereal diazomethane (*ca* 10 mL) dropwise. The reaction was monitored by TLC (20% diethyl ether/DCM v/v) until complete consumption of the acid chloride (R_f = 0.27) had taken place, and formation of the diazo intermediate (R_f = 0.82) was observed. The resulting solution was sealed with a rubber septum then allowed to stand at r.t. for 4 days before concentration by distillation at atmospheric pressure. The resulting yellow coloured oil was, without mechanical agitation, taken up in

degassed methanol (15 mL) and added to a Pyrex test tube with cold finger and side outlet (for pressure equalisation and inert gas) under an argon atmosphere and irradiated with a 400-W medium pressure Hanovia mercury arc lamp filtered through quartz. [Note: the Pyrex test tube had a diameter of 3.0 cm. The light source was housed in the centre of a quartz water jacket which had a diameter of 5.0 cm. The distance between the outer walls of the Pyrex test tube and the quartz water jacket was 2.0 cm. The pyrex cold finger and quartz water jacket were cooled with circulating water chilled with ice. Magnetic stirring was not required as the solution was homogenised by the resulting convection current]. After 4.5 h the methanol was removed *in vacuo* (70 °C, 325 torr) and the residue was purified by column chromatography (2.5% diethyl ether/pentane v/v). The pooled fractions containing product were concentrated by distillation at atmospheric pressure to give the title compound (2 mg, 9%) as a colourless, sweet-smelling oil.

^{1}H-NMR	(400 MHz, $CDCl_3$) δ_H = 3.67-3.65 (m, 3H), 3.53–3.51 (m, 3H), 2.65 (s, 2H), 1.27 (s, 3H) ppm.
^{13}C-NMR	(100 MHz, $CDCl_3$) δ_C = 172.2, 56.5, 55.5, 51.5, 46.7, 45.4, 38.5, 20.0 ppm.
HRMS	(ESI): *m/z* calcd for $C_{12}H_{15}O_2$ ($[M+H]^+$): 191.1067, found 191.1063.

4-Ethylcubane-1-methoxy carbonyl

4-Methoxycarbonylcuban-1-yl-acetic acid

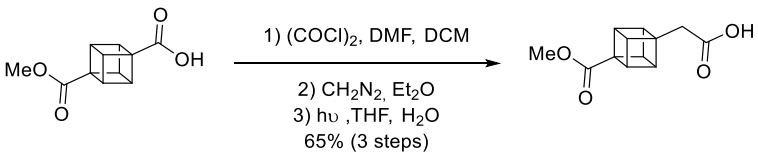

Adapted from the procedure of Eaton and Yip.[360] To a solution of 4-methoxycarbonylcubane-1-carboxylic acid (1.042 g, 5.05 mM) in anhydrous DCM (40 mL) was added oxalyl chloride (0.52 mL, 6.06 mM) and anhydrous DMF (1 drop) under an argon atmosphere. After 1 h the mixture was concentrated *in vacuo* and further dried under high vacuum (1 h). The remainder of this sequence should be performed behind a blast shield. The resulting acid chloride was suspended in diethyl ether (10 mL). Ethereal diazomethane (*ca* 60 mL) was added and the reaction monitored by TLC (ethyl acetate) until complete consumption of the acid chloride (R_f = 0.24), and formation of the diazo (R_f = 0.54) was observed. Excess diazomethane was blown off with argon, and the remaining diethyl ether was removed under reduced pressure. The resulting yellow solid was, *without mechanical agitation*, taken up in a degassed THF (40 mL)

and water (15 mL) and added to a Pyrex test tube with cold finger and side outlet (for pressure equalisation and inert gas) under an argon atmosphere and irradiated with a 400-W medium pressure Hanovia mercury arc lamp filtered through quartz. [Note: the Pyrex test tube had a diameter of 3.0 cm. The light source was housed in the centre of a quartz water jacket which had a diameter of 5.0 cm. The distance between the outer walls of the Pyrex test tube and the quartz water jacket was 2.0 cm. The Pyrex cold finger and quartz water jacket were cooled with circulating water chilled with ice. Magnetic stirring was not required as the solution was homogenised by the resulting convection current]. After 6 h the THF was removed *in vacuo,* and the remaining water was washed with DCM (3 x 20 mL). The combined organic extracts were dried over magnesium sulphate and concentrated. The crude residue was subjected to chromatography (50→100% ethyl acetate/petroleum ether v/v) to give the title compound (722 mg, 65%) as an off-white solid.

^{1}H-NMR (500 MHz, $CDCl_3$) δ_H = 4.16–4.14 (m, 3H), 3.87–3.85 (m, 3H), 3.71 (s, 3H), 2.72 (s, 2H) ppm.

^{13}C-NMR (125 MHz, $CDCl_3$) δ_C = 176.8, 172.9, 56.3, 54.6, 51.7, 46.7, 46.5, 37.7 ppm.

HRMS (ESI): *m/z* calcd for: $C_{12}H_{11}O_4$ ([M-H]$^-$): 219.0663; found: 219.0665.

FT–IR υ_{max} = 2993, 1693, 1431, 1320, 1237, 1207, 1087, 929, 842, 735 cm^{-1}.

MP 120.2–122.8 °C.

4-Methoxycarbonylcuban-1-yl-propanoic acid

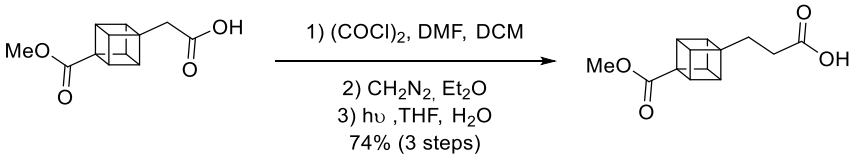

Adapted from the procedure of Eaton and Yip.[360] To a solution of 4-methoxycarbonylcuban-1-yl-acetic acid (490 mg, 2.23 mM) in anhydrous DCM (20 mL) was added oxalyl chloride (0.26 mL, 3.03 mM) and anhydrous DMF (1 drop) under an argon atmosphere. After 1 h the mixture was concentrated *in vacuo* and further dried under high vacuum (1 h). The remainder of this sequence should be performed behind a blast shield. The resulting acid chloride was suspended in diethyl ether (10 mL). Ethereal diazomethane (*ca* 20 mL) was added and the reaction monitored by TLC (ethyl acetate) until complete consumption of the acid chloride (R_f = 0.48), and formation of the diazo (R_f = 0.63) was observed. Excess diazomethane was blown off with argon, and the remaining diethyl ether was removed under reduced pressure. The

resulting yellow solid was, without mechanical agitation, taken up in a degassed THF (20 mL) and water (8 mL) and added to a Pyrex test tube with cold finger and side outlet (for pressure equalisation and inert gas) under an argon atmosphere and irradiated with a 400-W medium pressure Hanovia mercury arc lamp filtered through quartz. [Note: the Pyrex test tube had a diameter of 3.0 cm. The light source was housed in the centre of a quartz water jacket which had a diameter of 5.0 cm. The distance between the outer walls of the Pyrex test tube and the quartz water jacket was 2.0 cm. The Pyrex cold finger and quartz water jacket were cooled with circulating water chilled with ice. Magnetic stirring was not required as the solution was homogenised by the resulting convection current.] After 6 h the THF was removed *in vacuo*, and the remaining water was washed with DCM (3 x 20 mL). The combined organic extracts were dried over magnesium sulphate and concentrated. The crude residue was subjected to chromatography (50→100% ethyl acetate/petroleum ether v/v) to give the title compound (386 mg, 74%) as an off-white solid.

^{1}H-NMR (500 MHz, $CDCl_3$) δ_H = 4.10–4.08 (m, 3H), 3.75–3.73 (m, 3H), 3.69 (s, 3H), 2.33 (t, *J* = 7.6 Hz, 2H), 1.95 (t, *J* = 7.6 Hz, 2H) ppm.

^{13}C-NMR (125 MHz, $CDCl_3$) δ_C = 179.9, 173.0, 58.8, 56.5, 51.7, 46.2, 45.8, 29.1, 27.9 ppm.

HRMS (ESI): *m/z* calcd for: $C_{13}H_{14}O_4Na$ ($[M+Na]^+$): 257.0784; found: 257.0796.

FT–IR υ_{max} = 2985, 1704, 1436, 1321, 1204, 1087, 926, 840 cm^{-1}.

MP 74.8–77.6 °C.

4-ethylcubane CYP450 Substrate

4-Ethylcubane-1-methoxy carbonyl

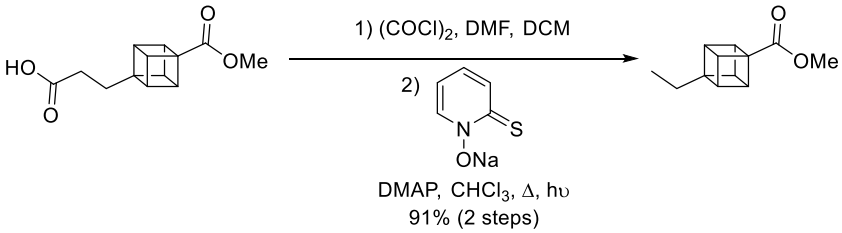

The procedure reported by Ko *et al.* [361] was followed. To a solution of 4-methoxycarbonylcuban-1-yl-propanoic acid (45 mg, 0.19 mM) in anhydrous DCM (5 mL), was added oxalyl chloride (0.03 mL, 0.35 mM) and anhydrous DMF (1 drop) under an argon atmosphere. After 1 h the mixture was concentrated *in vacuo* and further dried under high vacuum (1 h). Separately, freshly ground 2-mercaptopyridine *N*-oxide sodium salt (60 mg, 0.40

mM) and DMAP (1 mg, 0.008 mM) were suspended in anhydrous chloroform (7 mL) and heated to reflux whilst under irradiation from a 500-W tungsten lamp. [Note: the chloroform was washed with water and distilled from calcium hydride prior to use in order to remove the ethanol stabiliser]. The newly formed acid chloride was suspended in chloroform (7 mL) and added slowly over 20 min to the refluxing mixture. After reflux (2 h) the suspension was washed with water (10 mL) and brine (10 mL) then dried over magnesium sulphate and concentrated by distillation at atmospheric pressure. Purification by column chromatography (10% diethyl ether/pentane v/v) gave the title compound (33 mg, 91%) as a sweet-smelling oil.

^{1}H-NMR (500 MHz, $CDCl_3$) δ_H = 4.08-4.06 (m, 3H), 3.72-3.70 (m, 6H), 1.59 (*q*, *J* = 7.4 Hz, 2H), 0.85 (*t*, *J* = 7.4 Hz, 3H) ppm.

^{13}C-NMR (125 MHz, $CDCl_3$) δ_C = 173.3, 60.7, 56.6, 51.6, 46.1, 45.6, 25.6, 7.7 ppm.

HRMS (ESI): *m/z* calcd for: $C_{12}H_{14}O_2Na$ ($[M+Na]^+$): 213.0886; found: 213.0881.

FT–IR υ_{max} = 2966, 1727, 1435, 1320, 1290, 1208, 1087, 840 cm^{-1}.

Cubane Alcohol Standards

4-Hydroxymethylcubane-1-methoxy carbonyl

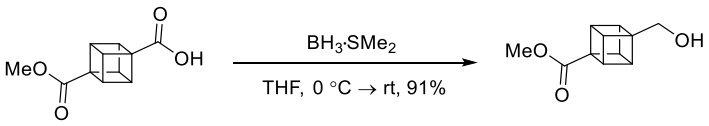

Following the procedure of McGonagle and Savage:[362] to a solution of 4-methoxycarbonylcubane-1-carboxylic acid (199 mg, 0.97 mM) in anhydrous THF (12 mL) at 0 °C under an argon atmosphere was slowly added borane dimethylsulfide complex (5 M in diethyl ether, 0.23 mL, 1.15 mM). The solution was allowed to warm to r.t. over 1 h and then water (1 mL) was cautiously added. The THF was removed *in vacuo*, and the residue was diluted with water (10 mL) then extracted with DCM (3 x 10 mL). The combined organic phases were dried over magnesium sulphate and concentrated. The crude residue was subjected to column chromatography (50% ethyl acetate/petroleum ether v/v) to give the title compound (170 mg, 91%) as a white solid.

^{1}H-NMR (500 MHz, $CDCl_3$) δ_H = 4.16-4.14 (m, 3H), 3.90-3.88 (m, 3H), 3.78-3.77 (m, 2H), 3.71 (s, 3H) ppm.

4-(1-Hydroxyethyl)-cubane-1-methoxy carbonyl

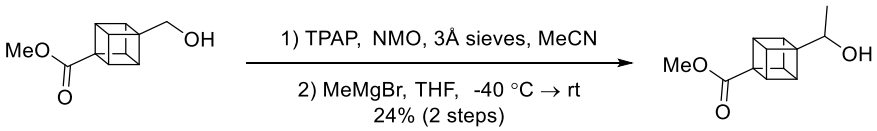

Adapted from the procedure of Moore *et al*. [363] *N*-methylmorpholine *N*-oxide (116 mg, 0.99 mM) and oven dried 3Å molecular sieves (*ca* 30 mg) were weighed into a round bottom flask and placed under high vacuum for 1 h before backflushing with argon. 4-Hydroxymethylcubane-1-methoxy carbonyl (50 mg, 0.26 mM), tetrapropylammonium perruthenate (5 mg, 0.013 mM) were added followed by anhydrous acetonitrile (2 mL). The reaction was monitored by TLC (50% ethyl acetate/petroleum ether v/v) until complete consumption of the alcohol (R_f = 0.22) and formation of the aldehyde (R_f 0.46) was observed (10 min). Water (5 mL) was added to the reaction mixture followed by extraction with pentane (3 x 5 mL). The combined organic phases were dried over magnesium sulphate (oven dried), transferred to a round bottom flask and diluted with anhydrous THF (15 mL) then cooled to -40 °C under an argon atmosphere. Methyl magnesium bromide (3 M in diethyl ether, 0.09 mL, 0.27 mM) was slowly added dropwise over 10 min. On warming to r.t. over 30 min saturated ammonium chloride (5 mL) was cautiously added. The THF was removed *in vacuo*, and the remaining aqueous phase was washed with DCM (3 x 5 mL). The combined organic phases were dried over magnesium sulphate and concentrated. The crude residue was subjected to column chromatography (20% ethyl acetate/petroleum ether v/v) to give the title compound (13 mg, 24%) as a colourless oil.

^{1}H-NMR (500 MHz, $CDCl_3$) δ_H = 4.13-4.11 (m, 3H), 3.98 (*q*, *J* = 6.4 Hz, 1H), 3.90-3.88 (m, 3H), 3.71 (s, 3H), 1.14 (d, *J* = 6.4 Hz, 3H) ppm.

^{13}C-NMR (125 MHz, $CDCl_3$) δ_C = 172.8, 67.6, 62.3, 56.6, 51.7, 46.1, 44.0, 17.0 ppm.

HRMS (ESI): *m/z* calcd for: $C_{12}H_{14}O_3Na$ ($[M+Na]^+$): 229.0835; found: 229.0841.

FT–IR υ_{max} = 3418, 2985, 1724, 1438, 1321, 1213, 1090, 1001, 600 cm^{-1}.

4-(2-Hydroxyethyl)cubane-1-methoxy carbonyl and 4-(2-hydroxyethyl)cubane-1 (hydroxymethyl)

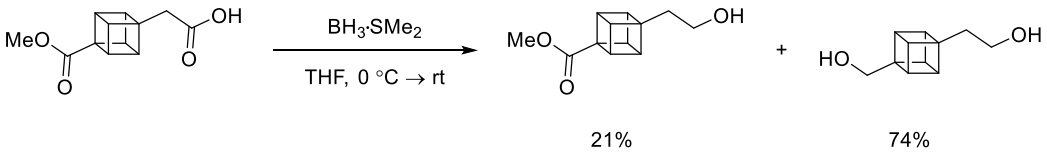

To a solution of 4-methoxycarbonylcuban-1-yl-acetic acid (15 mg, 0.068 mM) in anhydrous THF (3 mL) at 0 °C under an argon atmosphere was slowly added borane dimethylsulfide complex (5 M in diethyl ether, 0.02 mL, 0.1 mM). The solution was allowed to warm to r.t. over 1 h and then water (1 mL) was cautiously added. The THF was removed *in vacuo* and the residue diluted with water (5 mL) and extracted with DCM (3 x 5 mL). The combined organic phases were dried over magnesium sulphate and concentrated. The crude residue was subjected to column chromatography (50% ethyl acetate/petroleum ether v/v) to give the title alcohol (3 mg, 21%) and diol (9 mg, 74%) as colourless oils.

4-(2-Hydroxyethyl)cubane-1-methoxy carbonyl

^{1}H-NMR	(500 MHz, $CDCl_3$) δ_H = 4.14–4.12 (m, 3H), 3.80–3.78 (m, 3H), 3.74 (*t*, *J* = 6.7 Hz, 2H), 3.70 (s, 3H), 1.89 (*t*, *J* = 6.7 Hz, 2H) ppm.
^{13}C-NMR	(125 MHz, $CDCl_3$) δ_C = 173.1, 60.0, 57.7, 56.4, 51.6, 46.6, 46.5, 35.7 ppm.
HRMS	(ESI): *m/z* calcd for: $C_{12}H_{14}O_3Na$ ($[M+Na]^+$): 229.0835; found: 229.0832.
FT–IR	υ_{max} = 3405, 2985, 1723, 1435, 1321, 1210, 1092, 1062 cm^{-1}.

4-(2-Hydroxyethyl)cubane-1-(hydroxymethyl)

^{1}H-NMR	(500 MHz, $CDCl_3$) δ_H = 3.78–3.73 (m, 7H), 3.70–3.68 (m, 3H), 1.89 (*t*, *J* = 6.8 Hz, 2H) ppm.
^{13}C-NMR	(125 MHz, $CDCl_3$) δ_C = 64.1, 60.1, 59.3, 58.2, 45.7, 43.8, 36.2 ppm.
HRMS	(ESI): *m/z* calcd for: $C_{11}H_{14}O_2Na$ ($[M+Na]^+$): 201.0886; found: 201.0881.
FT–IR	υ_{max} = 3308, 2962, 1049, 1026, 1001, 840, 600 cm^{-1}.

E. 4 Barton-McCombie Deoxygenation

Imidazole thiocarbamate ester

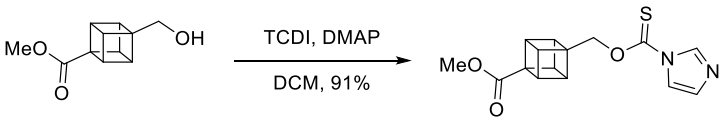

Adapted from the procedure of Sauer and Barriault.[364] To a solution of 4-hydroxymethylcubane-1-methoxy carbonyl (56 mg, 0.29 mM) in anhydrous DCM (5 mL) under an argon atmosphere was added DMAP (43 mg, 0.35 mM) and thiocarbonyldiimidazole (122 mg, 0.62 mM). The mixture was left to stir for 16 h before being concentrated. The crude residue was subjected to column chromatography (50% ethyl acetate/petroleum ether v/v) to give the title compound (80 mg, 91%) as an off-white solid.

^{1}H-NMR	(500 MHz, $CDCl_3$) δ_H = 8.31 (s, 1H), 7.60 (m, 1H), 7.04 (m, 1H), 4.83 (s, 2H), 4.24–4.22 (m, 3H), 4.01-3.99 (m, 3H), 3.71 (s, 3H) ppm.
^{13}C-NMR	(125 MHz, $CDCl_3$) δ_C = 184.6, 172.2, 136.8, 131.0, 118.0, 73.4, 56.6, 55.6, 51.8, 46.8, 45.3 ppm.
HRMS	(ESI): *m/z* calcd for: $C_{15}H_{15}N_2O_3S$ ($[M+H]^+$): 303.0798; found: 303.0797.
FT–IR	υ_{max} = 2990, 1721, 1383, 1339, 1282, 1227, 1088, 981, 656 cm^{-1}.
MP	84.1–85.2 °C.

Barton-McCombie deoxygenation

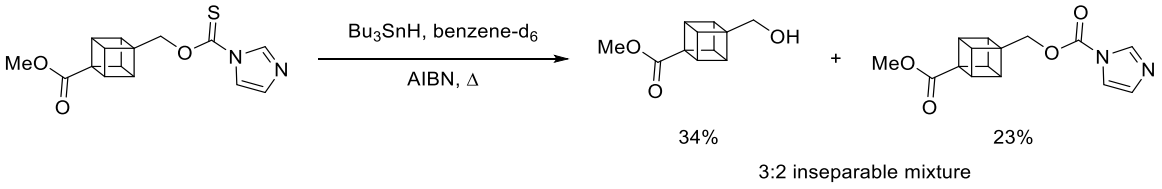

Adapted from the procedure of Sauer and Barriault. [364]. Imidazole thiocarbamate ester (14 mg, 0.046 mM) was suspended in benzene-d_6 (0. 8 mL) in an RBF and freeze-pump-thaw degassed three times. AIBN (1.6 mg, 0010 mM) and tributyltin hydride (27 µL, 0.10 mM) were added, and the mixture was heated to reflux for 11 h and then cooled to r.t. The reaction mixture was concentrated under a steam of nitrogen and purified by column chromatography (10% KF / silica w/w, [365] 5→20% ethyl acetate/petroleum ether v/v) to give a 3:2 inseparable mixture of

4-hydroxymethylcubane-1-methoxy carbonyl and imidazole carbamate ester (6 mg, 57%) as a colourless oil. ^{1}H and ^{13}C NMR data for the imidazole carbamate ester were obtained by subtraction of an authentic spectrum of 4-hydroxymethylcubane-1-methoxy carbonyl.

4-Hydroxymethylcubane-1-methoxy carbonyl

^{1}H-NMR (500 MHz, C_6D_6) δ_H = 4.05-4.03 (m, 3H), 3.57-3.55 (m, 3H), 3.41 (s, 3H), 3.29-3.28 (m, 2H) ppm.

^{13}C-NMR (125 MHz, C_6D_6) δ_C = 171.9, 63.0, 59.2, 56.9, 50.9, 46.7, 44.8 ppm.

Imidazole carbamate ester

^{1}H-NMR (500 MHz, C_6D_6) δ_H = 7.98 (s, 1H), 7.08 (m, 1H), 6.95 (m, 1H), 3.96–3.94 (m, 3H), 3.83 (s, 2H), 3.45-3.53 (m, 3H), 3.40 (s, 3H) ppm.

^{13}C-NMR (125 MHz, $CDCl_3$) δ_C = 171.4, 148.9, 137.1, 131.3, 117.1, 67.6, 56.7, 55.5, 51.1, 46.7, 45.0 ppm.

HRMS (ESI): *m/z* calcd for: $C_{15}H_{14}N_2O_4Na$ ([M+Na]$^+$): 309.0846; found: 309.0847.

Xanthate ester

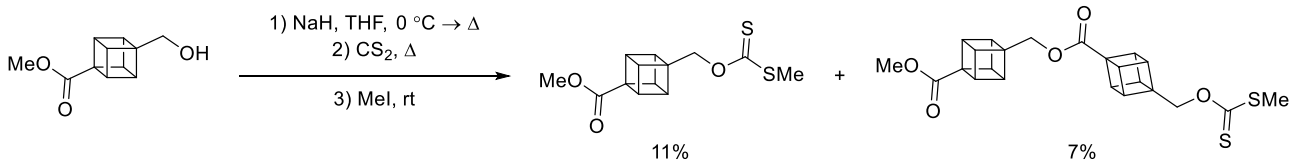

Adapted from the procedure of Zhu *et al*.[366] To a solution of 4-hydroxymethylcubane-1-methoxy carbonyl (50 mg, 0.26 mM) in anhydrous THF (10 mL) under an argon atmosphere at 0 °C was added sodium hydride (60% dispersion in mineral oil, 31 mg, 0.78 mM). The mixture was heated to reflux for 2 h, then cooled to r.t. before addition of carbon disulphide (17 µL, 0.31 mM). The mixture was heated to reflux for an additional 1 h, then again cool to r.t. before addition of methyl iodide (19 µL, 0.31 mM). After stirring for 1 h the THF was blown off with argon. The residue was taken up in saturated ammonium chloride (10 mL) and washed with DCM (3 x 10 mL). The combined organic phases were dried over magnesium sulphate and concentrated *in vacuo*. The crude residue was subjected to column chromatography (10→40% ethyl acetate/petroleum ether v/v) to give the title xanthate ester (8 mg, 11%) and transesterified xanthate ester (8 mg, 7%) as white solids.

Xanthate ester

^{1}H-NMR (500 MHz, $CDCl_3$) δ_H = 4.77 (s, 2H), 4.21–4.19 (m, 3H), 3.97–3.95 (m, 3H), 3.71 (s, 3H), 2.56 (s, 3H) ppm.

^{13}C-NMR (125 MHz, $CDCl_3$) δ_C = 216.5, 172.5, 73.8, 56.5, 56.0, 51.7, 46.8, 45.4, 19.2 ppm.

HRMS (ESI): *m/z* calcd for: $C_{13}H_{14}O_3S_2Na$ ($[M+Na]^+$): 305.0277; found: 305.0269.

FT–IR υ_{max} = 2991, 1724, 1435, 1328, 1215, 1064, 726 cm^{-1}.

MP 78.0–80.2 °C

Transesterified xanthate ester

^{1}H-NMR (500 MHz, C_6D_6) δ_H = 4.41 (s, 2H), 4.09 (s, 2H), 4.02–3.97 (m, 6H), 3.62–3.60 (m, 3H), 3.54–3.52 (m, 3H), 3.38 (s, 3H), 2.11 (s, 2H) ppm.

^{13}C-NMR (125 MHz, $CDCl_3$) δ_C = 216.7, 171.6, 171.5, 73.9, 64.1, 56.8, 56.8, 56.7, 55.8, 51.0, 47.0, 46.8, 45.4, 45.4, 19.0 ppm.

HRMS (ESI): *m/z* calcd for: $C_{23}H_{22}O_5S_2Na$ ($[M+Na]^+$): 465.0801; found: 465.0794.

FT–IR υ_{max} = 2989, 1721, 1300, 1212, 1067, 842 cm^{-1}.

MP 101.2–102.3 °C.

E. 5 Barton Decarboxylation

Thiohydroxamate ester

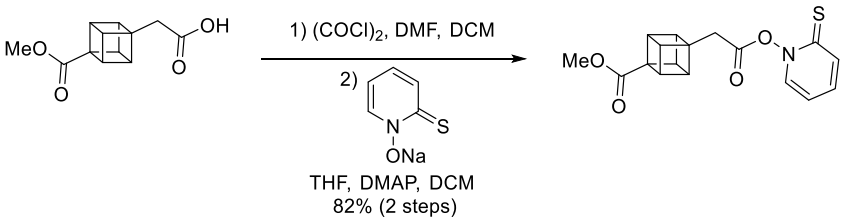

Adapted from the procedure of Eaton and Yip.[360] To a solution of 4-methoxycarbonylcuban-1-yl-acetic acid (29 mg, 0.13 mM) in anhydrous DCM (5 mL) was added oxalyl chloride (0.03 mL, 0.35 mM) and anhydrous DMF (1 drop) under an argon atmosphere. After 1 h the mixture was concentrated *in vacuo* and further dried under high vacuum (1 h). The newly formed acid chloride was taken up in anhydrous THF (5 mL) and to this was added DMAP (0.5 mg, 0.0023 mM), which turned the clear solution turbid. The reaction flask was covered in aluminium foil,

placed in a water bath at r.t. and then freshly ground 2-mercaptopyridine *N*-oxide sodium salt (36 mg, 0.24 mM) was added in two portions. The mixture was left to stir for 16 h and then filtered through glass wool. The filtrate was purified by column chromatography (dry load, silica gel *ca* 1 g, 50% ethyl acetate/petroleum ether v/v) to give the title compound (35 mg, 82%) as a yellow solid.

^{1}H-NMR	(500 MHz, C_6D_6) δ_H = 7.43–7.40 (m, 1H), 6.44–6.42 (m, 1H), 6.03–5.99 (m, 1H), 5.40–5.36 (m, 1H), 4.11–4.09 (m, 3H), 3.72–3.70 (m, 3H), 3.41 (s, 3H), 2.51 (s, 2H) ppm.
^{13}C-NMR	(125 MHz, C_6D_6) δ_C = 176.7, 171.8, 166.3, 137.6, 137.1, 132.2, 110.8, 56.5, 54.0, 51.0, 47.0, 46.8, 35.1 ppm.
HRMS	(ESI): *m/z* calcd for: $C_{17}H_{15}NO_4SNa$ ($[M+Na]^+$): 352.0614; found: 352.0616.
FT–IR	υ_{max} = 3389, 2990, 1802, 1718, 1608, 1527, 1608, 1527, 1448, 1323, 1208, 1133, 1089, 1067, 841, 755 cm^{-1}.
MP	152 °C (decomp).

Barton decarboxylation–thiophenol ester

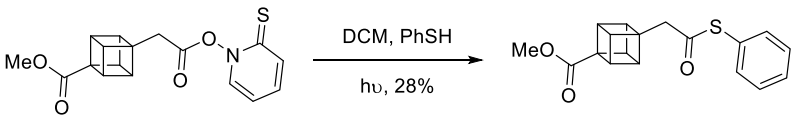

Adapted from the procedure of Eaton and Yip.[360] To a borosilicate glass microwave vessel was added thiohydroxamate ester (17.5 mg, 0.079 mM) and anhydrous DCM (2.5 mL) followed by thiophenol (12 µL, 0.12 mM). The vessel was placed in a water bath at r.t. and then irradiated with a 500-W tungsten lamp for 10 min. [Note: the borosilicate glass microwave vessel had a diameter of 1.3 cm and was placed in the centre of a water bath, which had a diameter of 11.5 cm. The distance between the outer wall of the microwave vessel and the light source was 10 cm. Magnetic stirring was not required as the solution was homogenised by the resulting convection current]. Concentration by distillation at atmospheric pressure and purification by column chromatography (25% ethyl acetate/petroleum ether v/v) gave the title compound (7 mg, 28%) as a yellow oil.

^{1}H-NMR (500 MHz, $CDCl_3$) δ_H = 7.43–7.39 (m, 5H), 4.18–4.16 (m, 3H), 3.92–3.91 (m, 3H), 3.70 (s, 3H), 3.02 (s, 2H) ppm.

^{13}C-NMR (125 MHz, $CDCl_3$) δ_C = 194.7, 172.8, 134.6, 129.6, 129.4, 127.7, 56.3, 55.2, 51.7, 47.0, 46.9, 46.7 ppm.

HRMS (ESI): *m/z* calcd for: $C_{18}H_{16}O_3SNa$ ($[M+Na]^+$): 335.0712; found: 335.0713.

FT–IR υ_{max} = 2988, 1705, 1478, 1440, 1320, 1204, 1087, 962, 747 cm^{-1}.

Barton decarboxylation – thiopyridine ether

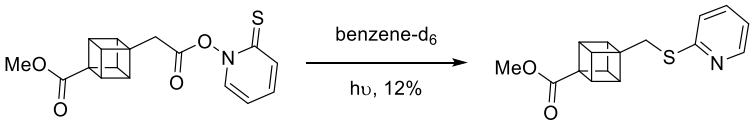

Adapted from the procedure of Eaton and Yip.[360] Thiohydroxamate ester (5 mg, 0.015 mM) was dissolved in benzene-d_6 (0.5 mL) in a round bottom flask. The solution was freeze-pump-thaw degassed three times with argon and then transferred to a borosilicate glass NMR tube. The NMR tube was placed in a water bath at r.t. and irradiated with a 500-W tungsten lamp for 5 min. [Note: the borosilicate glass NMR tube had a diameter of 5 mm and was placed in the centre of a water bath, which had a diameter of 11.5 cm. The distance between the outer wall of the NMR tube and the light source was 10 cm. Magnetic stirring was not required as the solution was homogenised by the resulting convection current]. Concentration by distillation at atmospheric pressure and purification by column chromatography (20% ethyl acetate/petroleum ether v/v) gave the title compound (0.5 mg, ca 12%). Further attempts to purify the title compound using HPLC were unsuccessful.

^{1}H-NMR (500 MHz, C_6D_6) δ_H = 8.21 (ddd, *J* = 4.9, 1.9, 1.0 Hz, 1H), 6.87 (dt, *J* = 8.1, 1.0 Hz, 1H), 6.74 (ddd, *J* = 8.1, 7.3, 1.9 Hz, 1H), 6.37 (ddd, *J* = 7.3, 4.9, 1.1 Hz, 1H), 4.03-4.01 (m, 3H), 3.63-3.61 (m, 3H), 3.50 (s, 2H), 3.36 (s, 3H) ppm.

^{13}C-NMR (175 MHz, $CDCl_3$) δ_C = 171.9, 159.3, 149.4, 135.6, 122.6, 119.2, 58.1, 56.9, 50.9, 46.4, 46.3, 32.3 ppm.

HRMS (ESI): *m/z* calcd for: $C_{16}H_{16}NO_2S$ ($[M+H]^+$): 286.0896; found: 286.0905.

Figure E. 6 The GC-MS analysis of the turnover of 4-(2-hydroxyethyl)cubane-1-methoxy carbonyl by CYP101B1. 4-(2-hydroxyethyl)cubane-1-methoxy carbonyl, (RT 9.95 min).

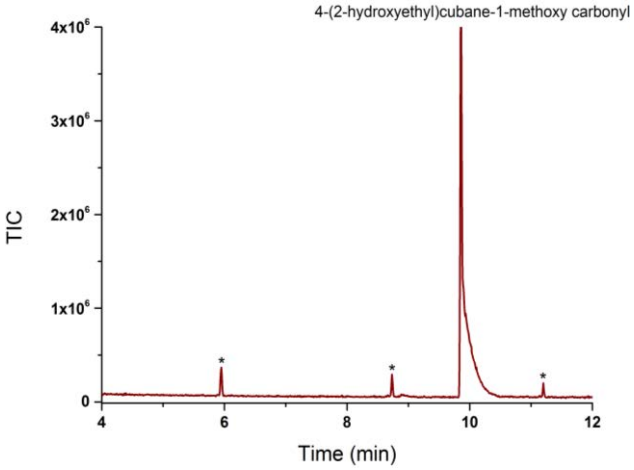

Figure E. 7 MS analysis of the substrates and products of the cubanes.

4-methylcubane-1-methoxy carbonyl

4-methylcubane-1-methoxy carbonyl RT 4.75 min (m^+/z = 176.00)

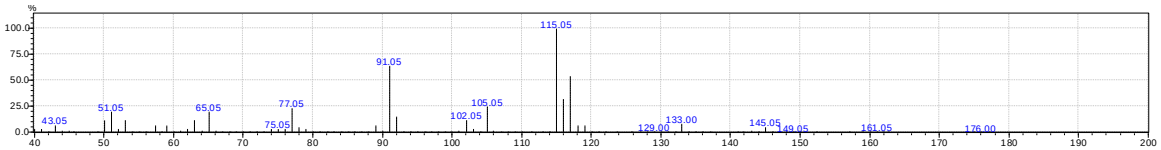

4-methylcubane-1-carboxylic acid RT 5.4 min (m^+/z = 162.15) – see MS of standard later

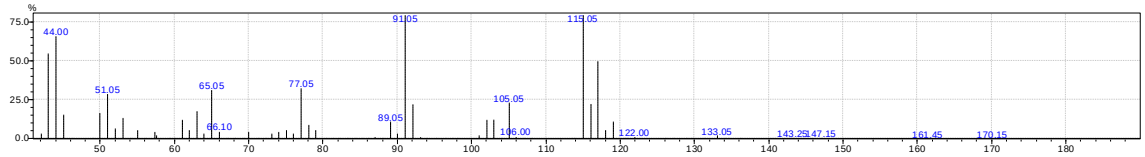

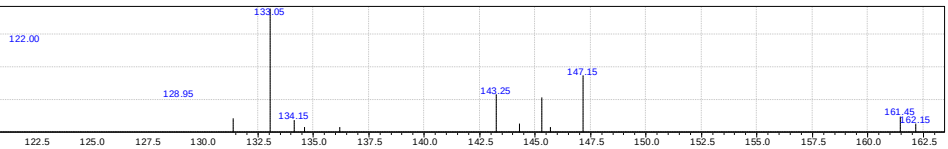

Zoomed in version

4-methylcubane-1-methoxy carbonyl product: 4-hydroxymethylcubane-1-methoxy carbonyl

Product RT 8.65 min (m^+/z = 192.35)

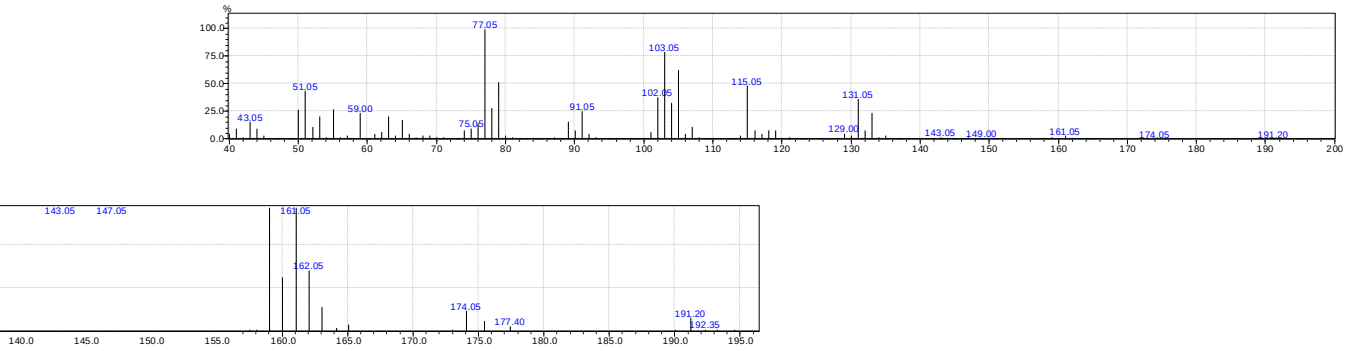

zoomed in version

MS of synthesised standard of 4-hydroxymethylcubane-1-methoxy carbonyl

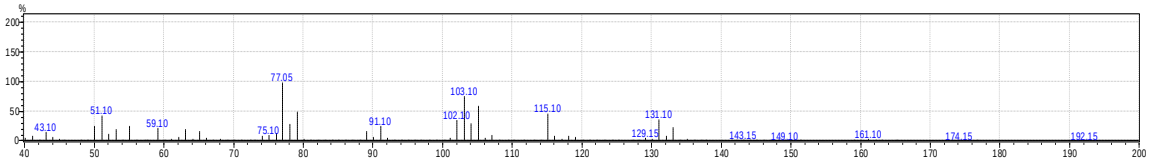

Product RT 8.16 min aldehyde further oxidation product (m^+/z = 190.15)

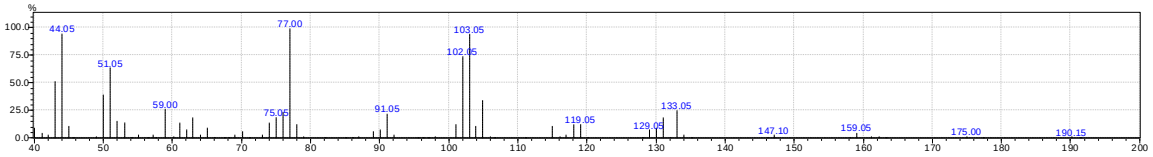

Product RT 9.45 min–ester hydrolysis of product (m^+/z = 177.5)

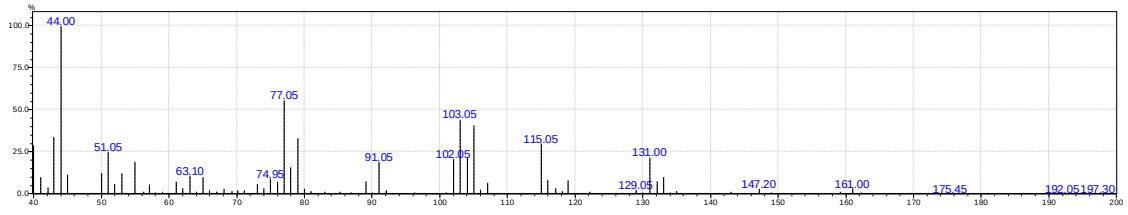

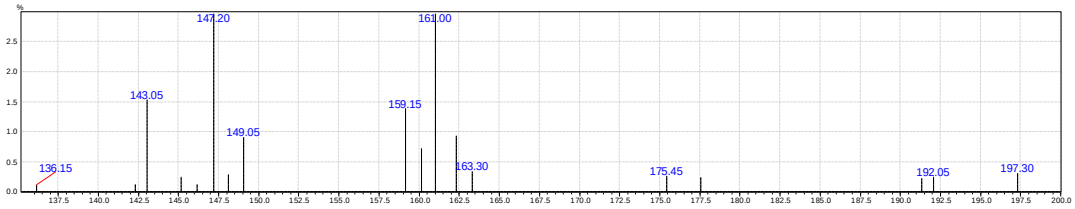

zoomed in version

4-methylcubane-1-acetic acid methyl ester

MS analysis of 4-methylcubane-1-acetic acid methyl ester RT 5.1 min (m^+/z = 190.05)

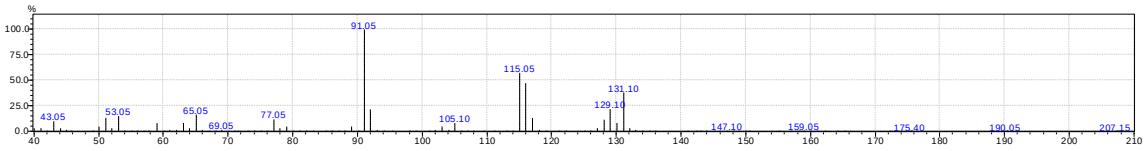

MS analysis of 4-methylcubane-1-acetic acid methyl ester RT 6.13 min (m^+/z = 176.15) possibly hydrolysis to carboxylic acid

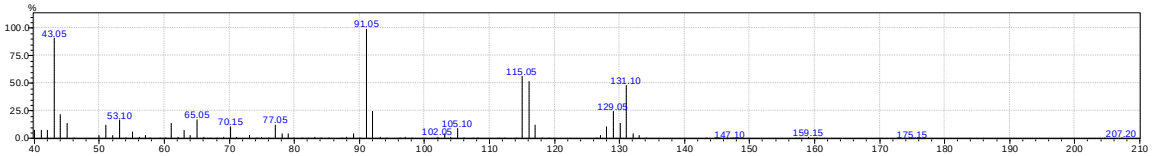

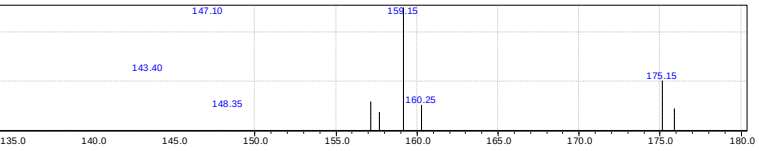

zoomed in version

Product: 4-hydroxymethylcubane-1-acetic acid methyl ester RT 9.0 min (m^+/z = 206.35)

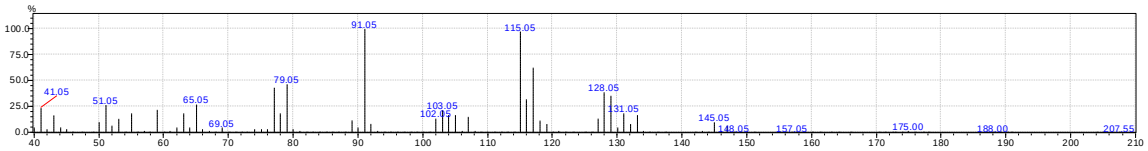

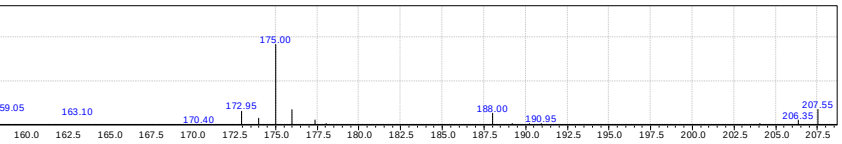

zoomed in version

Product: RT 8.95 min; m^+/z = 204.00 (aldehyde - only found large-scale turnover after all the product has been consumed).

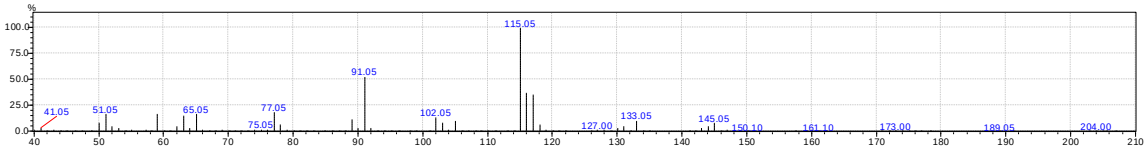

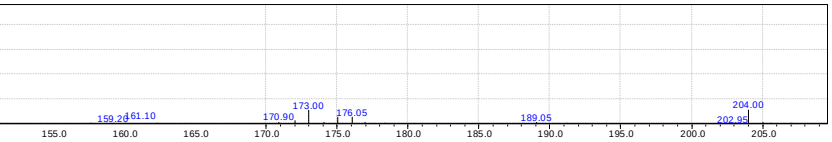

zoomed in version

4-methylcuban-1-yl acetate

substrate RT 3.9 min (m^+/z = 175.35)

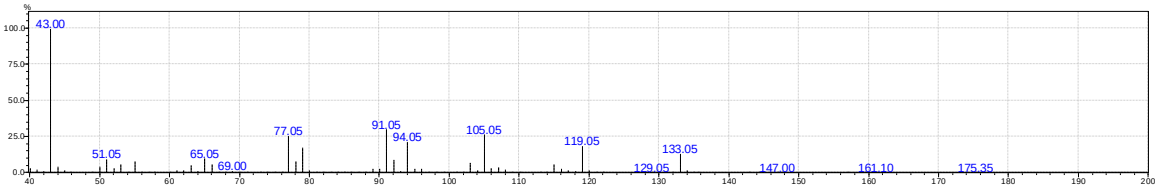

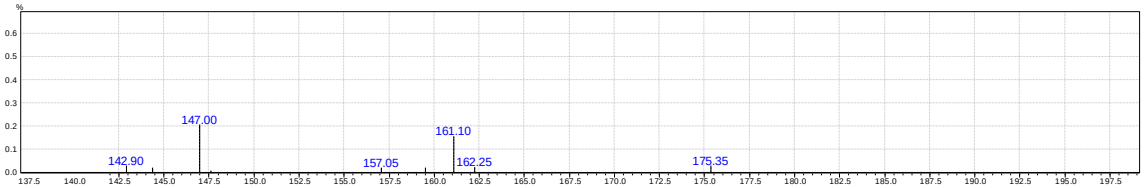

zoomed in version

product 7.7 min (m^+/z = 191.00)

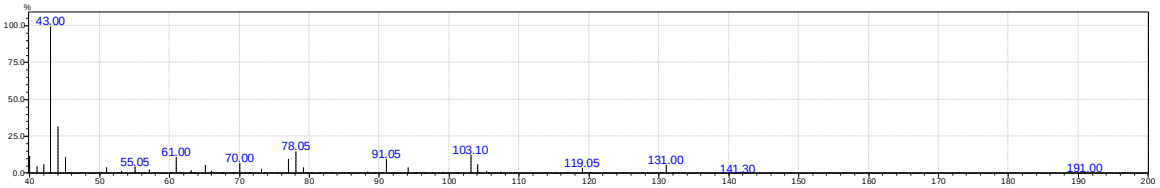

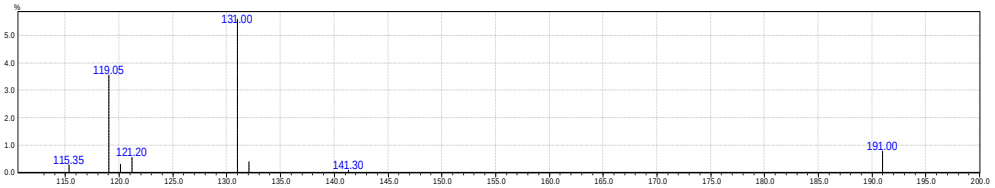

zoomed in version

4-methylcubane-1-methyl ketone

MS analysis of substrate RT 4.2 min (m^+/z = 160.05)

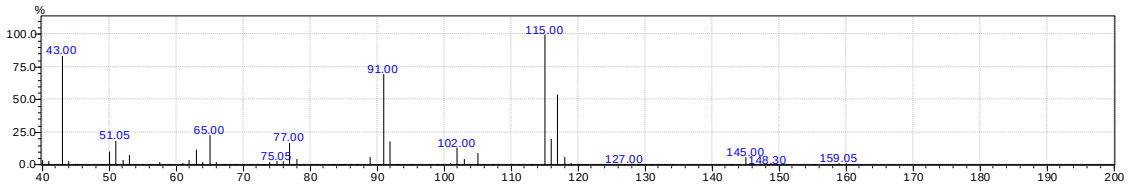

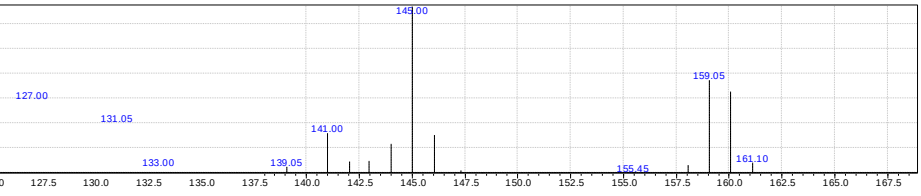

zoomed in version

MS analysis of possible 4-methylcubane-1-methyl ketone product RT 8.35 min (m^+/z = 175.25)

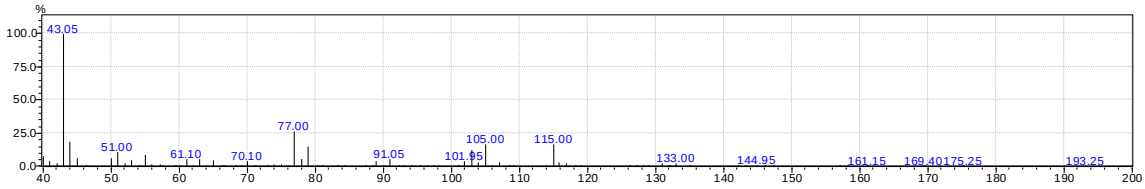

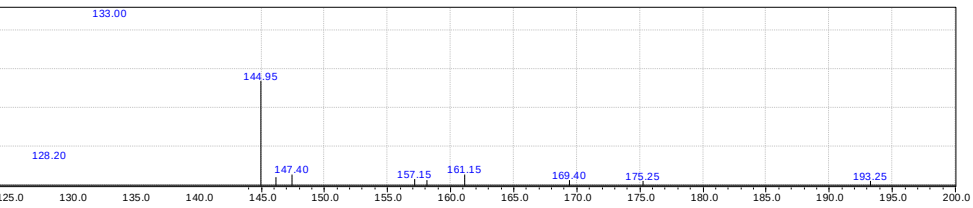

zoomed in version

4-ethylcubane-1-methoxy carbonyl

4-ethylcubane-1-methoxycarbonyl RT 6.05 min (m^+/z = 190.20)

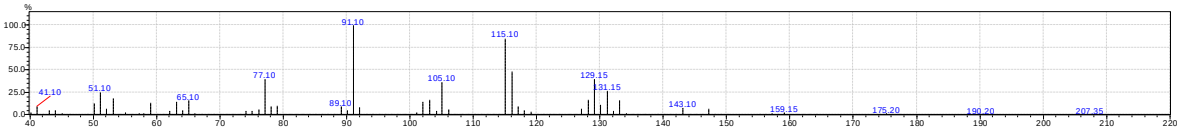

4-ethylcubane-1-carboxylic acid RT 6.95 min (m^+/z = 175.20)

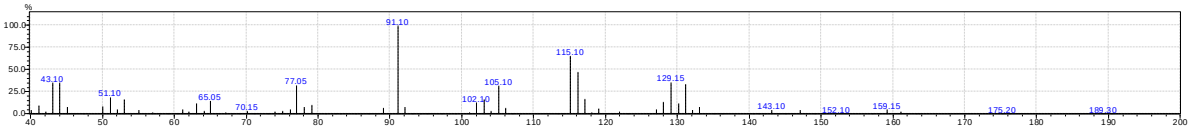

4-(1-hydroxyethyl)-cubane-1-methoxy carbonyl, from enzyme turnover, RT 8.95 min (m^+/z = 206.45)

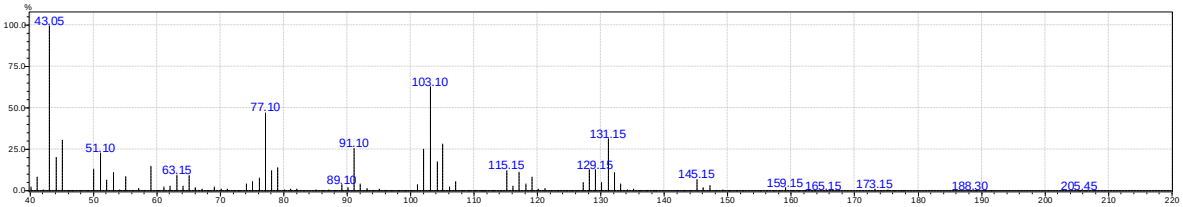

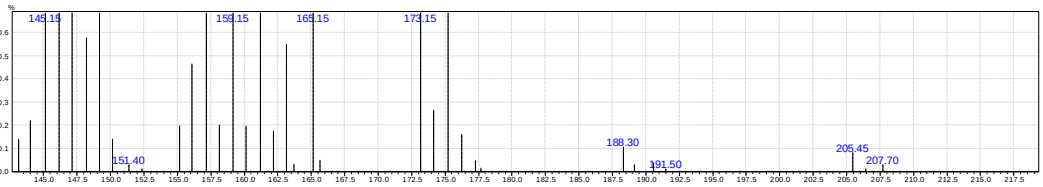

zoomed in version

4-(1-hydroxyethyl)-cubane-1-methoxy carbonyl RT 8.95 min synthesised control GC-MS

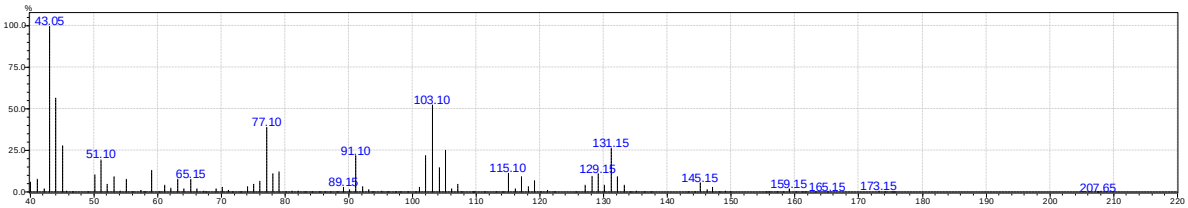

4-(2-hydroxyethyl)-cubane-1-methoxy carbonyl RT 9.95 min (m^+/z = 206.30)

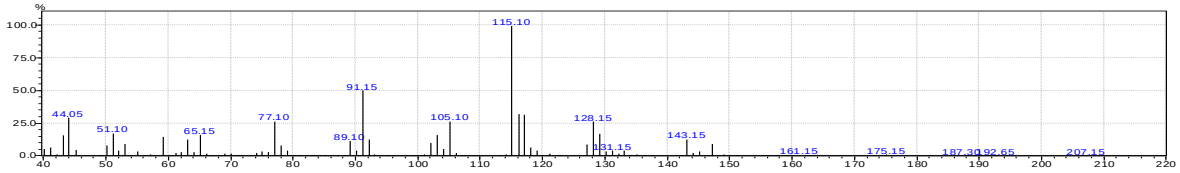

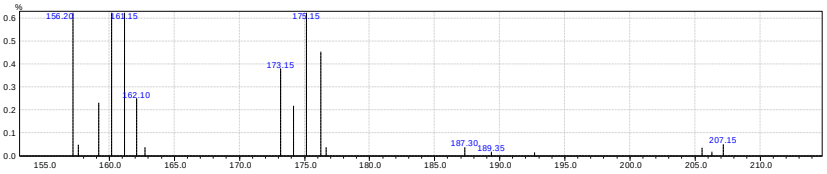

zoomed in version

4-methylcubane-1-carboxylic acid RT 5.4 min (m^+/z = 162.0)

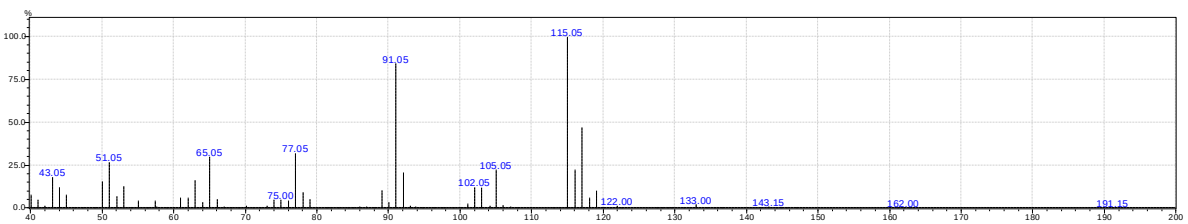

NMR Analysis

4-hydroxymethylcubane-1-methoxy carbonyl

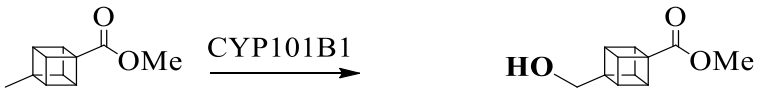

4-methylcubane-1-methoxy carbonyl 4-hydroxymethylcubane-1-methoxy carbonyl

Note there is a small amount of impurity in the NMR but nothing in the vinyl region (radical rearrangement) or in the region expected for the cation rearrangement product. Possible Minor products from ester hydrolysis and potentially starting material (GC-MS and the NMR combined seems to rule out oxidation on cube C-Hs) [301-303, 367, 368].

4-hydroxymethylcubane-1-methoxy carbonyl (500 MHz, $CDCl_3$): δ 4.16-4.13 (m, 3H, H3, H5 & H8), 3.91-3.87 (m, 3H, H2, H6 & H7), 3.78 (m, 2H, 2xH11), 3.71 (s, 3H, 3xH10).

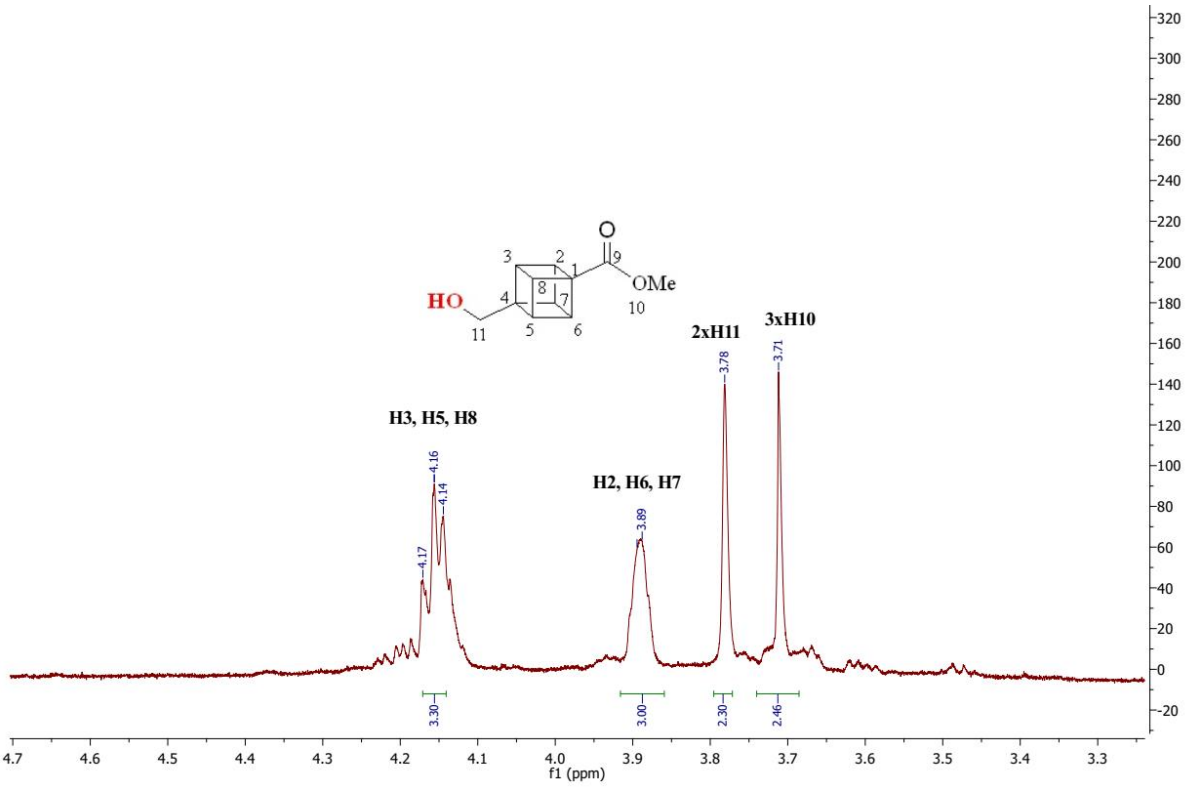

Figure E. 8 Zoomed in (3.2 to 4.7 ppm region) version of ^{1}H NMR spectrum of 4-hydroxymethylcubane-1-methoxy carbonyl (4-Methylcubane-1-methoxy carbonyl; CYP101B1).

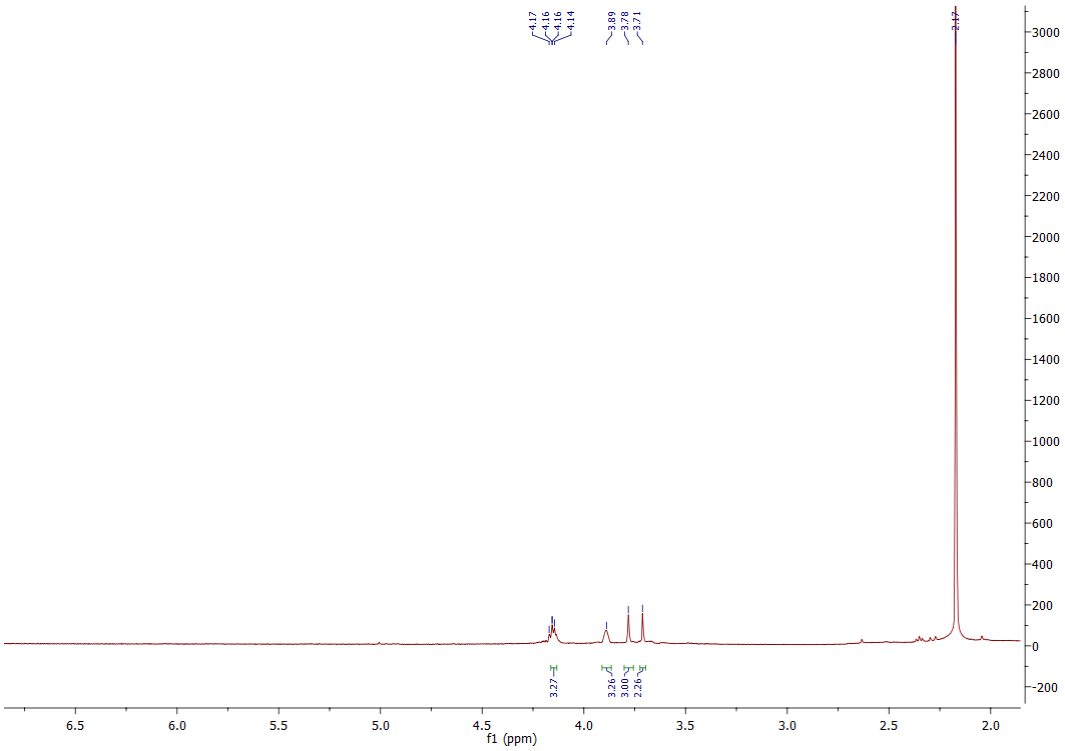

Figure E. 9 ^{1}H NMR spectrum of 4-hydroxymethylcubane-1-methoxy carbonyl (4-Methylcubane-1-methoxy carbonyl; CYP101B1). The large peak at 2.17 is acetone.

4-hydroxymethylcubane-1-acetic acid methyl ester

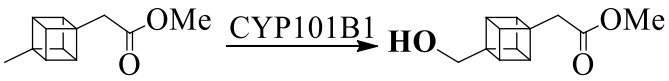

4-methylcubane-1-acetic acid methyl ester

4-hydroxymethylcubane-1-acetic acid methyl ester

Overoxidation to the aldehyde is suggested by a peak at 9.76 ppm and peaks from the cubane structure at above 4 ppm. Also, there is a small EtOH impurity, and ester hydrolysis of the substrate and product interfere with the signals as well. However for all the impurities, the cube seems intact, and there is no evidence for other products from GC-MS [301-303, 367].

Impurities – starting material

aldehyde, further oxidation product

hydrolysed product or starting material

4-hydroxymethylcubane-1-acetic acid methyl ester (600 MHz, $CDCl_3$) δ 3.88-3.83 (m, 3H, H3, H5 & H8), 3.79-3.76 (m, 2H, 2xH12), 3.75-3.70 (m, 3H, H2, H6 & H7), 3.69 (s, 3H, 3xH11), 2.68 (s, 2H, 2xH9).

^{13}C NMR (151 MHz, $CDCl_3$) δ 174.48 (C10), 66.48 (C12), 54.03 (C11), 48.46 (C2, C6 & C7), 46.56 (C3, C5 & C8), 40.67 (C9), 25.33 (C4), 16.76 (C1).

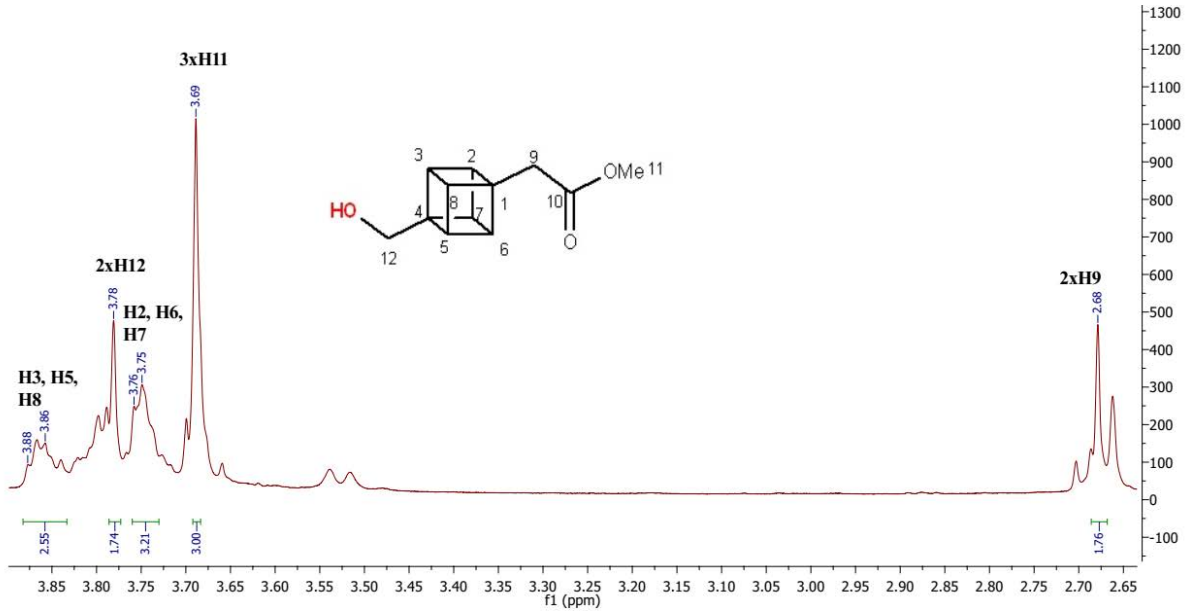

Figure E. 10 Zoomed in (2.65 to 3.9 ppm region) ^1H NMR of 4-hydroxymethylcubane-1-acetic acid methyl ester (4-Methylcubane-1-acetic acid methyl ester; CYP101B1).

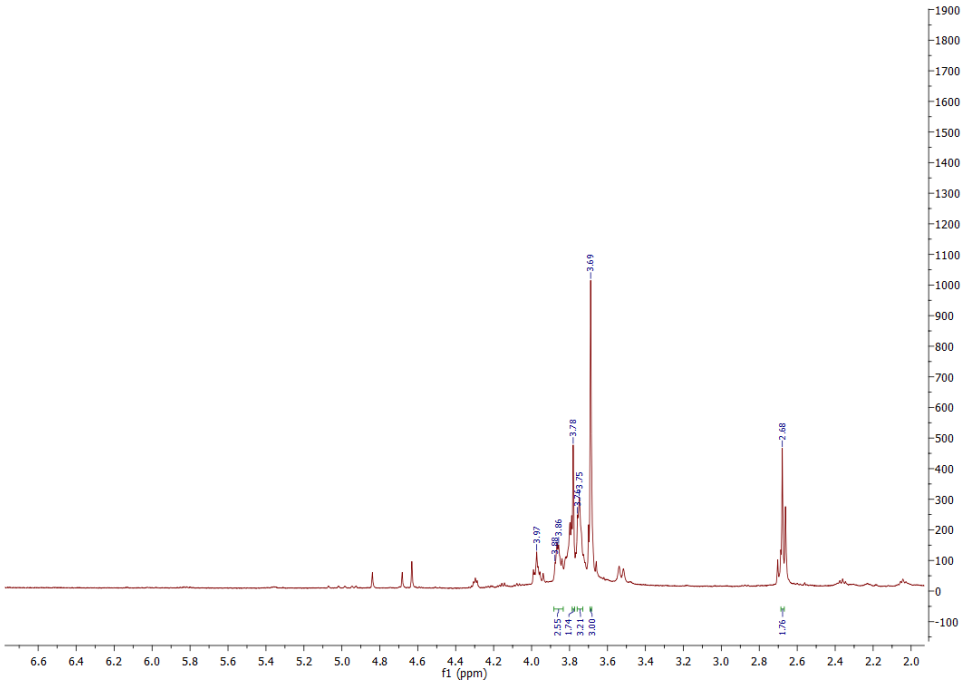

Figure E. 11 ^1H NMR spectrum of 4-hydroxymethylcubane-1-acetic acid methyl ester (4-Methylcubane-1-acetic acid methyl ester; CYP101B1).

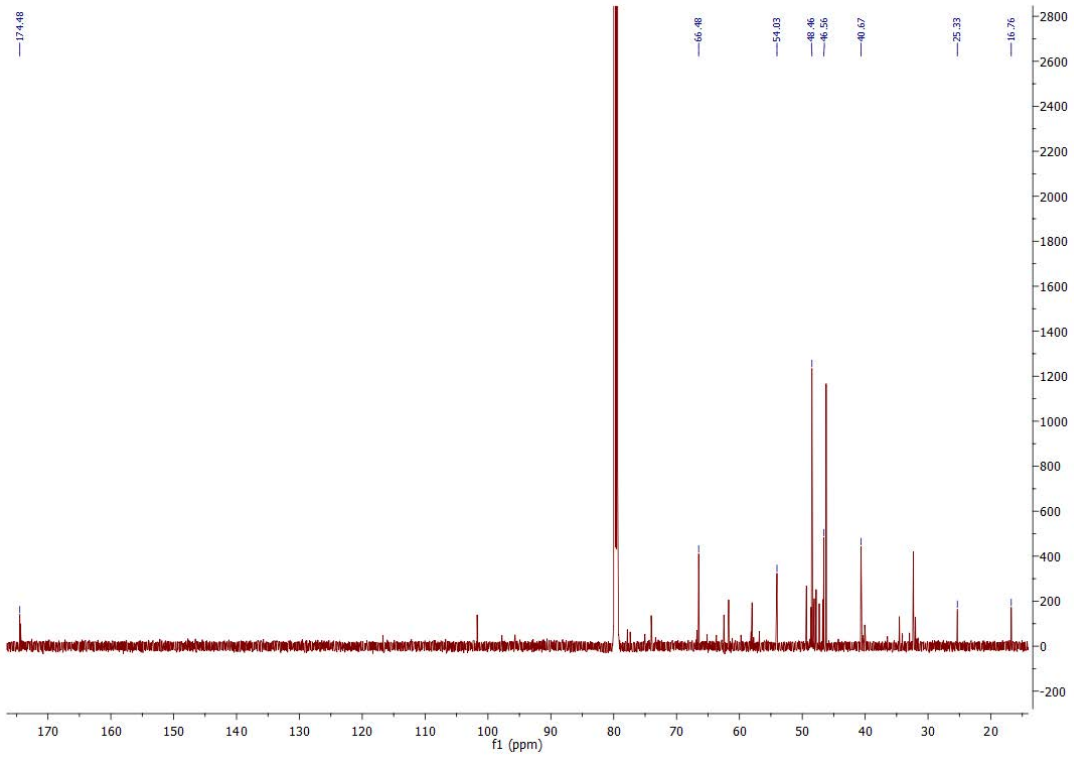

Figure E. 12 ^{13}C NMR spectrum of 4-hydroxymethylcubane-1-acetic acid methyl ester (4-Methylcubane-1-acetic acid methyl ester; CYP101B1).

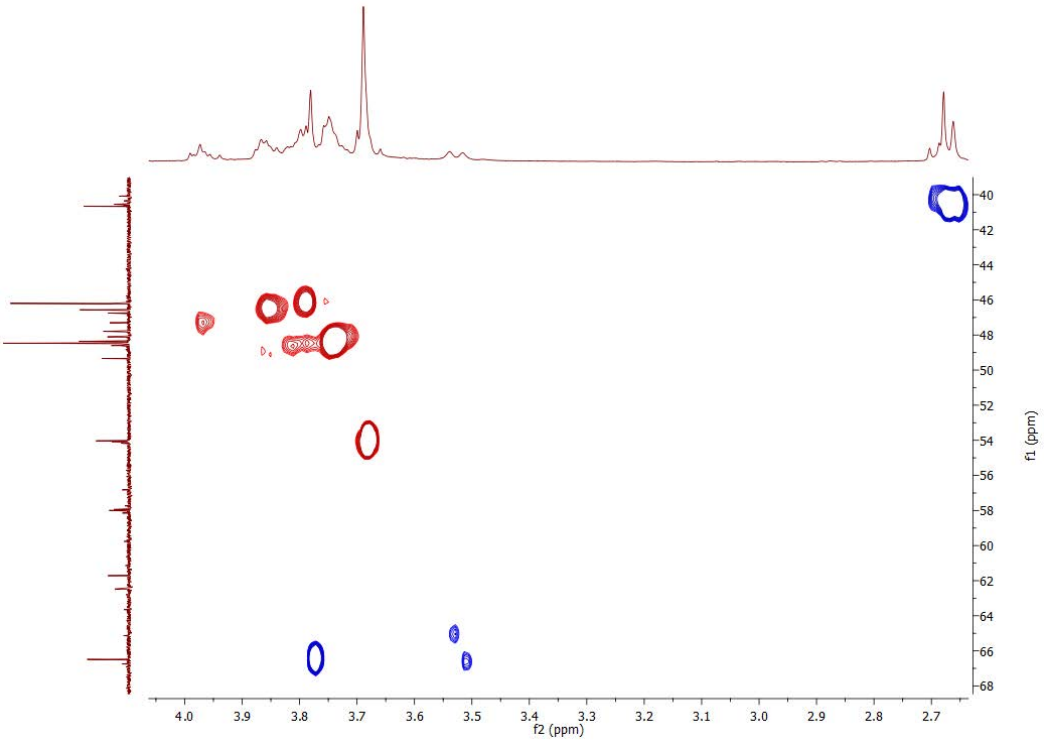

Figure E. 13 HSQC NMR spectrum of 4-hydroxymethylcubane-1-acetic acid methyl ester (4-Methylcubane-1-acetic acid methyl ester; CYP101B1).

List of Publications Arising From This Thesis

This thesis is based on the following publications during the period of my PhD candidature:

1. (182) M. R. Sarkar, E. A. Hall, S. Dasgupta and S. G. Bell (2016). "The Use of Directing Groups Enables the Selective and Efficient Biocatalytic Oxidation of Unactivated Adamantyl C-H Bonds." ChemistrySelect 1(21): 6700-6707.

2. (265) M. R. Sarkar, J. H. Lee and S. G. Bell (2017). "The oxidation of hydrophobic aromatic substrates by using a variant of the P450 monooxygenase CYP101B1." ChemBioChem 18(21): 2119-2128.

3. (266) E. A. Hall, M. R. Sarkar and S. G. Bell (2017). "The selective oxidation of substituted aromatic hydrocarbons and the observation of uncoupling via redox cycling during naphthalene oxidation by the CYP101B1 system." Catalysis Science & Technology 7(7): 1537-1548.

4. (176) E. A. Hall, M. R. Sarkar, J. H. Lee, S. D. Munday and S. G. Bell (2016). "Improving the monooxygenase activity and the regio-and stereoselectivity of terpenoid hydroxylation using ester directing groups." ACS Catalysis 6(9): 6306-6317.

5. (369) M. R. Sarkar, S. Dasgupta, S. Pike, and S. G. Bell (2019). "Selective biocatalytic hydroxylation of unactivated methylene C-H bonds in cyclic alkyl substrates." Chemical Communications, 2019, DOI: 10.1039/C9CC02060H.